Luca Saba · U. Rajendra Acharya
Stefano Guerriero · Jasjit Suri *Editors*

Ovarian Neoplasm Imaging

Springer

Ovarian Neoplasm Imaging

Luca Saba • U. Rajendra Acharya
Stefano Guerriero • Jasjit Suri
Editors

Ovarian Neoplasm Imaging

Springer

Editors
Luca Saba
Department of Radiology
University of Cagliari
Cagliari
Italy

U. Rajendra Acharya
Ngee Ann Polytechnic
Singapore

Stefano Guerriero
University of Cagliari
Cagliari
Italy

Jasjit S. Suri
Department of Biomedical Engineering
CTO, Global Biomedical Technologies
Roseville, CA
USA

Department of Biomedical Engineering
Idaho State University (Aff.)
Pocatello, ID
USA

ISBN 978-1-4614-8632-9 ISBN 978-1-4614-8633-6 (eBook)
DOI 10.1007/978-1-4614-8633-6
Springer New York Heidelberg Dordrecht London

Library of Congress Control Number: 2013957808

Printed on acid-free paper

Springer is part of Springer Science+Business Media (www.springer.com)

Contents

Part V New Prospectives

Part I

General Concepts

Epidemiology of Epithelial Ovarian Carcinoma

Anna Maria Paoletti, Bruno Piras, Monica Pilloni, Maria Francesca Marotto, Marisa Orrù, Valentina Corda, and Gian Benedetto Melis

Abstract

Epithelial ovarian cancer is the fifth to sixth most common cancer in women, causing more annual deaths than any other gynecological malignancies in women worldwide. In the majority of cases, a good prognosis cannot be made at the diagnosis because clinical presentation of the disease occurs at an advanced stage. In the United States, approximately one-half of ovarian cancer-afflicted women die of this disease.

Several environmental factors can interfere on the risk of ovarian cancer, and the different interferences of some risk factors on the histologic type of tumor lead to hypothesize a different mechanism of carcinogenesis.

In this view, the epithelial ovarian cancer seems to recognize a proper oncogenetic mechanism in which genetic factors, reproductive factors, and some lifestyle factors play an important role.

Keywords

Epidemiology • Epithelial ovarian cancer • Oncogenetic mechanism • Prevalence • Incidence

Introduction

Epithelial ovarian cancer is the fifth to sixth most common cancer in women, causing more annual deaths than any other gynecological malignancies in women worldwide [1]. In the majority of cases, a good prognosis cannot be made at the diagnosis because clinical presentation of the disease occurs at an advanced stage [2]. In the United States, approximately one-half of ovarian cancer-afflicted women die of this disease [3]. One group of tumors is represented by endometrioid, mucinous, and low-grade serous carcinomas. They are discovered in the substance of the ovary, and likely they proceed in a gradual fashion from benign to malignant. In the second group, there are the serous carcinomas that appear on the ovarian surface with the involvement of fallopian tubes, mesentery, and omentum. This latter group are the most lethal form of epithelial ovarian cancer [4, 5].

In the absence of current screening methods of the disease, the evaluation of risk factors seems to play a key role to do an adequate prevention.

A.M. Paoletti (✉)
Clinica Ginecologica Ostetrica e di Fisiopatologia della Riproduzione Umana, Dipartimento di Scienze Chirurgiche, Università degli Studi di Cagliari, Azienda Ospedaliero Universitaria di Cagliari, Cagliari, Italy

Dipartimento Chirurgico Materno Infantile e di Scienze delle Immagini, Sezione di Clinica Ginecologica Ostetrica e di Fisiopatologia della Riproduzione Umana, Università di Cagliari, Via Ospedale 54, I-09124, Cagliari, Italy
e-mail: gineca.annapaoletti@tiscali.it

B. Piras • M. Pilloni • M.F. Marotto • M. Orrù
V. Corda • G.B. Melis
Clinica Ginecologica Ostetrica e di Fisiopatologia della Riproduzione Umana, Dipartimento di Scienze Chirurgiche, Università degli Studi di Cagliari, Azienda Ospedaliero Universitaria di Cagliari, Cagliari, Italy

L. Saba et al. (eds.), *Ovarian Neoplasm Imaging*,
DOI 10.1007/978-1-4614-8633-6_1,

Serous Epithelial Ovarian Carcinoma

Family History

A family history of epithelial ovarian cancer confers an increased risk. Women with one first-degree relative with epithelial ovarian cancer have an approximately 5 % lifetime risk for developing ovarian cancer, whereas the risk is 1.6 % in the general population and it is higher (7 %) in women with two first-degree relatives with ovarian cancer [6].

Mutations of BRCA1 and BRCA2 Genes

In the last years, the molecular genetic basis of hereditary predisposition to epithelial ovarian cancer has been largely evaluated. Prat et al. [7] reported that patients with a family history of ovarian cancer are classified in three groups: (1) site-specific ovarian cancer, (2) breast and ovarian cancer syndrome, and (3) hereditary nonpolyposis colorectal cancer (HNPCC, Lynch II syndrome).

The first two groups are associated with germ line mutations in the BRCA1 and BRCA2 tumor suppressor genes. BRCA1 gene was identified and cloned in 1994 [8]. The BRCA2 gene was isolated in 1995 [9]. BRCA1 and BRCA2 are large suppressor genes located on chromosomes 17q21 and 13q12-13, respectively. BRCA1 and BRCA2 play a key role in the protection from tumor origin and progression. Through the interaction with regulatory proteins, they provide to DNA repair [10], transcriptional regulation of gene expression, and cell cycle control [10]. In the absence of BRCA1 or BRCA2 function, DNA repair does not occur, with changes in the function of p53 leading to progressive proliferation and accumulation of DNA damage with increased frequency of malignancy [7].

In the majority of women afflicted by hereditary ovarian carcinomas, there are mutations in BRCA1 and BRCA2 genes. Two studies in North America demonstrated that 13–15 % of women with invasive ovarian carcinoma are carrier of BRCA1/BRCA2 mutations [11, 12]. Risch et al. [13] reported that in women with invasive ovarian cancer, 7 % are carriers of BRCA1 mutations and 4 % of BRCA2 mutations. In women with BRCA1 mutations, the ovarian cancer is diagnosed at an average age of 51.2 years, whereas in those with mutations in BRCA2 gene, the disease is diagnosed in a higher average age (57.5 years). BRCA1 mutations represented 83 % of the mutations found in women who were diagnosed under 50 years of age, and BRCA2 mutations represented 60 % of those diagnosed after 60 years age [14]. The BRCA-associated cancers are not usually found in women younger than 30 years and are rarely diagnosed in those younger than 40 years [15]. Several studies found that Jewish women with ovarian cancer are carrier of BRCA1/BRCA2 mutations in a higher percentage varying between 29 and 45 % [16–19].

The lifetime risk of developing ovarian cancer is 40 % for women carrier mutations in BRCA1, lower for those carrier of BRCA2 mutations [20].

Serous histology characterizes the ovarian cancer in carriers of BRCA mutations, with only few cases of clear cells or endometrioid tumors. Unfortunately, the majority of BRCA-related ovarian cancers show moderate or poor differentiation and present at an advanced surgical stage [17, 21]. In the screening program using serial Ca125 levels and abdominal ultrasound, observational cohort studies have shown that neither Ca125 nor ultrasound demonstrated to be sensitive for detecting stage I and stage II ovarian cancer [22–26]. Since 1995, the prophylactic oophorectomy for high-risk women at age 35 years and/or after the completion of childbearing is recommended by a consensus panel of the National Institute of Health (NIH) [27]. Thereafter, many reports agree with the efficacy of prophylactic oophorectomy in the prevention of epithelial ovarian cancer [28–32]. The study of Rebbeck et al. [29] was performed in 551 women with disease-associated germ line BRCA1 or BRCA2 mutations. The incidence of ovarian cancer was determined in 259 who underwent prophylactic oophorectomy (PO) and in 292 matched controls who were not oophorectomized, but submitted to a screening follow-up. Among the controls, 19.9 % ovarian cancer was diagnosed after a mean follow-up of 8.8 years, whereas 2.3 % of women submitted to prophylactic oophorectomy received the diagnosis of stage I ovarian cancer at the time of procedure, and two women (0.8 %) received a diagnosis of papillary serous peritoneal carcinoma 3.8 and 8.6 years after prophylactic oophorectomy. The study of Kauff et al. [31] was performed in 890 women with BRCA1 and BRCA2 mutations. Prophylactic ovariectomy decreased the risk of ovarian cancer in both BRCA1 carriers with a HR 0.13 (95 % CI 0.04–0.46, $p<0.002$) and BRCA2 carriers (HR 0.0, no ovarian cancer events were observed in BRCA2 carriers following PO). The study of Finch et al. [32] examined 1838 women BRCA1/BRCA2 carriers from 32 centers. With a median follow-up time of 3.5 years, prophylactic oophorectomy was associated with a significant reduction in ovarian cancer, with a multivariate relative risk of 0.20 (95 % CI 0.07–0.58, $p<0.03$). In the majority of cases, prophylactic oophorectomy is associated with bilateral salpingectomy. The detailed analyses of the fallopian tubes have shown that tubal lesions are present in up to 100 % of cases of early serous cancers associated with familial BRCA mutations and strongly suggest that the fallopian tube cells may play an important role in the genesis of BRCA-associated high-grade serous ovarian carcinoma [33]. The presence of proliferative multilayered tubal epithelium and tubal intraepithelial carcinomas suggests a model of progression from premalignant to invasive malignant disease [34]. It is thought that cancer cells are implanted on the surface of the ovary and/or the peritoneum to induce ovarian or primary peritoneal carcinomas.

Therefore, a common origin can be hypothesized for tubal, ovarian, and peritoneal carcinoma. According to Crum et al. [35], the distal fallopian tube can be a new model for pelvic serous carcinogenesis. However, the old concepts on the epithelial origin of the serous epithelial ovarian cancer cannot be excluded [36].

With these concepts in mind, environmental factors and reproductive factors can interfere in the process of malignant degeneration and in the progression of the disease, either in women genetically predisposed or in sporadic epithelial cancers that represent a high percentage of epithelial ovarian cancer [37].

Reproductive Factors and Ovarian Carcinoma

Reproductive hormones are thought to be involved in the etiology of epithelial ovarian cancer. Mainly, the "incessant ovulation" and the "gonadotropin hypothesis" have been linked with the ovarian carcinogenesis.

The "incessant ovulation" hypothesis suggests that the risk of epithelial ovarian cancer increases with the number of ovulations, because the traumatized epithelium of ruptured follicles is recurrently repaired and exposed to estrogen-rich follicular fluid. Thereafter, the growth factors (GFs) involved in the postovulatory repair and impaired regulation of GFs are hypothesized as promoters of malignant transformation. In accordance with this hypothesis, it has been demonstrated that epithelial growth factor (EGF) stimulates growth in several human ovarian cancer cell lines capable of secreting EGF whose receptors have been frequently expressed in their surface [38–40].

The "gonadotropin hypothesis" suggests that high gonadotropin levels stimulate the ovarian surface epithelium. In animal studies, the suppression of gonadotropin secretion obtained with a GnRH analog treatment inhibits the genesis of tumor in mice genetically predisposed to the development of ovarian tumor [41]. The presence of gonadotropin receptors in ovarian surface is demonstrated only by some studies [42, 43], whereas other authors did not confirm them [44]. Both hypotheses can explain the epidemiologic studies showing a reduced risk of epithelial ovarian cancer in women with increasing parity, who are breastfeeding, and using oral contraceptives. During pregnancy, there is a natural hormonal contraception with the loss of gonadotropin secretion as a consequence of the negative feedback of steroid hormones and the inhibition of ovulation. The full-term pregnancy has been demonstrated to reduce up to 30–40 % the risk of epithelial ovarian cancer [45–47], and each pregnancy after the first induces a further 14–20 % risk reduction [47, 48]. There are conflicting data about the relationship between the age at the first pregnancy and the protection of epithelial ovarian cancer, with some authors identifying a protection factor at first full-term pregnancy at late age [45, 47, 49], whereas others did not show association between these factors [46, 50, 51]. The lactation is also a period of natural anovulation dependent on the suckling-induced hyperprolactinemia that leads to neuroendocrine mechanisms causing the reduction of GnRH and gonadotropin secretion. The majority of the studies shows a decreased risk of epithelial ovarian cancer with lactation [47, 50, 52], with the evidence that the lactation during the initial months after delivery offers the major protection [52].

In this context, it is important to know epidemiological data on the relationship between the use of pharmacological-induced anovulation and pharmacological-induced hyperovulation.

As above reported, the use of oral contraceptives is associated with a reduced risk of ovarian cancer. The study of Hannaford et al. [53] clearly demonstrates that compared to never oral contraceptive users, the ever oral contraceptive users have a significant reduced risk of epithelial ovarian cancer (relative risk, 0.54; CI, 95 %, 0.40–0.71). The onset of the Royal College of General Practitioners' oral contraceptive study [53] was since 1968, and at the end of the study, at 2004, it examined 744,717 women years of observation for ever oral contraceptive users and 339,349 women years for never oral contraceptive users. The number of women with epithelial ovarian cancer was 96 in ever oral contraceptive user women and 93 in never oral contraceptive user women, with an observed rate and standardized rate of 12.57 and 13.23, respectively, in ever users versus 26.54 and 24.66 in never users [53]. In addition, it has been demonstrated that the greater reduction in ovarian cancer risk is associated with a longer oral contraceptives use [54]. The reduced risk persists for more than 30 years after the interruption of oral contraceptive use, with an attenuation proportional to years by the oral contraceptive cessation [54]. In the conclusion of their study, the authors suggest that the oral contraceptive use prevented 200,000 ovarian cancer and 100,000 deaths for this disease [54].

On the contrary, the exposition to multiple folliculogenesis or superovulation, induced by the use of clomiphene citrate [55] or of human menopausal gonadotropins (hMG) [56], has been reported as a risk factor of ovarian cancer [55, 56]. These drugs are used in women affected by infertility, and it is unclear if infertility is "per se" a promoter risk factor for ovarian cancer or if the drugs used to induce superovulation can play a role throughout a higher stimulation of epithelial ovarian cells. Although some authors agree with this last mechanism [55–59], numerous studies showed a higher incidence of epithelial ovarian cancer in infertile women compared with controls independent of the use of drugs capable of inducing superovulation. Contrasting data are reported about the role of infertility "per se" on ovarian cancer risk. Some authors report a similar incidence of ovarian cancer in

fertile and infertile women followed for 10 years [60–63], whereas other studies show an increased risk of ovarian cancer in infertile women [55, 64–66]. The hypothesis that nulliparity dependent on infertility could be the real risk factor of epithelial ovarian cancer instead of infertility has been investigated [67–69]. Nevertheless, all the case–control studies demonstrate only a nonsignificant increased risk of epithelial ovarian cancer in nulliparous versus parous women with a history of infertility [67–69]. In their analysis, Ness et al. [67] and Whittemore et al. [68] reported that the years of nulliparity are directly related with an increased risk of epithelial ovarian cancer. These epidemiological studies reinforce the hypothesis that incessant ovulation is an important risk factor of epithelial ovarian cancer.

The relationship between increased epithelial ovarian cancer risk and the cause of infertility has been also evaluated. Endometriosis seems to be a common risk factor either for infertility or for epithelial ovarian cancer [64]. The infertility dependent on endometriosis seems to not interfere on the risk of ovarian cancer through the mechanism of incessant ovulation, as suggested for the association between nulliparity and epithelial ovarian cancer risk. Melin et al. [70] show that the risk of epithelial ovarian cancer is increased independently on the parity. The link of endometriosis and ovarian cancer could be the increased activation of immune system, with phenomena of angiogenesis and neurogenesis interfering in the multiplication of endometriosis cells. In accordance with these mechanisms, it is also known that endometrioid and clear cell ovarian cancers show a higher incidence in women with endometriosis in comparison with control subjects [71]. Other known factors of infertility, such as the polycystic ovary syndrome in lean women, do not seem to be a risk factor of epithelial ovarian cancer [72]. In polycystic ovary syndrome-affected women with a high body mass index, the demonstrated increase of epithelial ovarian cancer risk [72] could depend on other than polycystic ovary syndrome factors, such as the presence of excessive adipose tissues or disorders of insulin metabolism, as suggested by studies on the relationship between body mass index and ovarian cancer risk [73].

In accordance with the hypothesis that epithelial ovarian cancer could derive from epithelial cells of distal tubes [35], the tubal ligation has been reported to protect from ovarian cancer [49, 50, 67, 74–76]. Nevertheless, the mechanism involved in protection on epithelial ovarian cancer by tubal ligation could be the reduction of ovarian blood flow, as consequence of the ligation of ovarian branches of the uterine arteries that run parallel to the tubes. The same mechanism could explain the reported protective effect of hysterectomy on epithelial ovarian cancer [74–76].

In conclusion, tubal ligation and a persistent time with the absent insult on epithelial ovarian cells, such as that obtained with the use of oral contraceptives or with multiparity, seem to be the major factors involved in the protection of epithelial ovarian cancer. In the context of factors impairing the woman's fertility, endometriosis has been recognized the major factor risk, mainly of the endometrioid and clear cells ovarian cancer.

Obesity, Anthropometric Measures, and Ovarian Carcinoma

It has been demonstrated that obesity is a risk factor for many gynecological cancers, with a strong evidence for breast cancer and endometrial cancer [77].

As suggested for the increased breast cancer risk in obese women, the mechanism through which the excessive adipose tissue could favor ovarian cancer risk seems to depend on the secretive factors deriving from the adipose cells. In addition to aromatase enzyme, involved in the synthesis of estrogens by androgen precursors, adipose cells secrete leptin, interleukins, such as tumor necrosis factor α (TNFα) and interleukin-6 that directly favor the mitosis of epithelial cells and, through their action on pancreatic β-cells stimulate the secretion of insulin and insulin growth factors. These last factors concur to potentiate the mitotic activity on epithelial cells [78]. In accordance with this hypothesis, a reduced survival to ovarian cancer has been reported in women with major expression of leptin receptors in ovarian epithelial cells in comparison with those with lower expression of the above receptors [79]. A pooled analysis of primary data from 12 prospective cohort studies from North America and Europe examined the association of height, body mass index, and ovarian cancer risk [80]. A total of 531,583 women was the study population, with 2,036 women diagnosed with epithelial ovarian cancer. In the subjects with height >1.70 m, the relative risk of ovarian cancer was higher than in women with height <1.60 m (relative risk, 1.38; 95 % confidence interval, 1.16–1.65). The relative risk showed to be higher in premenopausal than in postmenopausal women. As for the relationship of ovarian cancer risk and body mass index, the same study [80] reports that women with a body mass index >30 compared to women with a body mass index ranged from 18.5 to 23 had a significant higher risk of ovarian cancer, but only in the group of premenopausal women (RR, 1.72; 95 % confidence interval, 0.87–1.33) [80].

In an epidemiologic study on 226,798 women evaluated throughout 8.9 years, 611 cases of epithelial ovarian carcinoma have been diagnosed. The relative risk was significantly higher in women with a body mass index >30 in comparison than those with a body mass index <25 (relative risk, 1.33; 95 % confidence interval, 1.05–1.68; $p=0.02$) [73]. On the contrary of the above reported study [80], the relative risk was higher in postmenopausal (relative risk, 1.59; 95 % confidence interval, 1.20–2.10) than in premenopausal women (relative risk, 1.16; 95 % confidence interval, 0.65–2.06; $p=0.65$). Adipose tissue distribution did not show to be

related with the risk of ovarian. In fact, no significant increase of relative risk of ovarian cancer has been found in women with a higher waist to hip ratio, marker of a central distribution of adipose tissue known for its secretory pattern of inflammatory factors [78].

Nutrition Factors, Physical Exercise, and Ovarian Cancer

The link of adipose tissue with an increased risk of ovarian carcinoma induces to hypothesize that similar to other gynecological cancers, a fat-rich diet and/or a reduced physical activity could favor ovarian carcinoma risk, whereas a fruit-rich diet could exert an opposite effect on the ovarian carcinoma risk, as suggested by Kolahdooz et al. [81] and by Bidoli et al. [82]. A case–control study in which 455 cases of ovarian cancer were compared with 1,385 age-matched controls showed that the high consumption of meat increases the risk of ovarian cancer (relative risk, 1.6; 95 % confidence interval, 1.2–2.12) and a parallel decreased risk was calculated in women assuming a diet rich in whole-grain bread and pasta [83]. A larger study in the United States performed in more than 29,000 women demonstrated a higher carcinoma ovarian risk in women assuming a diet rich in carbohydrate, eggs, and dairy and a reduced risk in those assuming a diet with a high quantity of vegetables [84]. However, the same study did not confirm the association of increased ovarian cancer risk and a high meat intake [84]. A sugar-rich diet has also been associated with an increased ovarian carcinoma risk [85]. According with these studies, a change in diet has been hypothesized the factor involved in the increase of ovarian cancer incidence in women migrants from Japan to the United States [86]. A very interesting study has been published by Aschebrook-Kilfoy et al. [87] on the exposure to diet containing nitrate and nitrite. These compounds were studied in relationship to their role as precursors of the endogenous synthesis of N-nitroso compounds which have been demonstrated to induce tumors in animals [88]. Nitrite and nitrate are present in many nutrients, commonly used in industrialized nations, as some vegetables. They are present as contaminant in drinking water, and as additive in some meat, ham, and bacon to prevent the growth of bacteria. The study of Aschebrook-Kilfoy et al. [87], promoted by the National Institutes of Health (NIH)-AARP Diet and Health Study, included 151,316 women aged 50–61 years and evaluated the frequency of nitrate and nitrite intake through a validated questionnaire. At the end of the study, the authors found that a nitrate-rich diet significantly increases the risk of epithelial ovarian cancer [87].

Although numerous studies on diet and ovarian carcinoma risk have been published so far, up to now no conclusive data have been produced on some nutrients, whereas there is agreement on a relationship between increased ovarian carcinoma risk and excessive assumption of fat, meat, and sugar. Physical exercise seems to protect from ovarian carcinoma [89, 90], but strenuous exercise is directly related with increased risk of ovarian carcinoma [90]. It is possible to hypothesize that moderate exercise potentiates the caloric expenditure with a decreased adipose tissue and their inflammatory growth factors, whereas strenuous exercise induces an opposite mechanism with the purpose to defend the body by excessive stress factors deriving from the continuous loss of energy. Further studies are needed to demonstrate these hypotheses, but it is confirmed that diet rich in nutrient known for their role in reducing the oxidative stress, such as the tea [91], is associated with a reduced mortality in women with ovarian carcinoma [92]. The study of Zhang et al. [92] comprised a cohort of 254 patients with epithelial ovarian cancer which were followed for at least 3 years. The survival of the patients was higher in green tea drinker than in non-drinker patients [92]. The comparison between drinkers and nondrinkers showed that the survival is directly related to the quantity of green tea consumed every day [92]. The loss of high consumption of tea in China and other countries of Asia, associated with increased intake of fat nutrients, could be the cause of increased ovarian risk, likely of other tumors, in migrant women from Asia to the United States and other western countries. In addition to its antioxidative effect, green tea could act through its polyphenolic compounds that have demonstrated anticarcinogenic properties in studies in vitro and in animal studies [93]. The study showing that the tea component, theanine, potentiates the antitumor activity of some chemotherapeutic agents [94], induces also to its useful in clinical chemotherapy in association with the chemotherapeutic drugs [95]. Other nutrient factors related to a protective role in ovarian cancer are fibers, carotene, vitamin C, vitamin E, and retinol [96].

A very important role could be also exerted by a lifestyle: an increased sun exposure induces the production of vitamin D by the ultraviolet (UV)-B radiation in sunlight that converts 7-dehydrocholesterol to vitamin D3 in the skin. Vitamin D is also contained in some foods, such as some fish, with small amounts present in beef liver, cheese, and egg yolks [97, 98].

In the study of Lefkowitz and Garland [99], the ovarian cancer mortality was reported higher in women with a low regional sunlight exposure. More convincing data on the protective role of vitamin D in ovarian cancer are given by the demonstration that in animal model, vitamin D and its synthetic analogs are capable of both inhibiting the growth and inducing the apoptosis of ovarian cells [100, 101]. The receptors of vitamin D have been found in human ovarian tumor cells [100, 102–104]. A systematic literature review on this topic has been published by Cook et al. [105]. After the revision of all papers on vitamin D and ovarian cancer, the authors report the results of 20 full-text articles. These articles included 10 ecologic studies conducted in various

countries [99, 106–114], 6 case–control studies [82, 115–119], and 4 cohort studies [84, 120–122]. Unfortunately, after the evaluation of all studies, Cook et al. [105] conclude that there are no strong evidences on the protective role of vitamin D in ovarian cancer incidence and mortality [105]. The meta-analysis of Yin et al. [123] on the circulating vitamin D and ovarian cancer incidence examines 10 longitudinal studies included in 4 articles [121, 124–126] and comprises a total of 2,488 subjects including 883 cases of ovarian cancer. The summary relative risk between circulating vitamin D levels over 20 ng/ml and a reduction of ovarian cancer incidence is 0.83 (95 % confidence interval, 0.63–1.08), showing only a weak, but not significant ($p=0.160$), inverse association between circulating vitamin D levels and ovarian cancer risk [123]. The no conclusive epidemiological studies on vitamin D and ovarian cancer protection could depend on the difference in the vitamin D receptor in the studied populations. In fact, the functional polymorphism rs2228570 in the vitamin D receptor has been found higher in the younger than in older women with ovarian carcinoma by the examination of five studies within the ovarian cancer association consortium [127].

Other lifestyle factors studied to evaluate their connection with ovarian cancer risk are alcohol drinking and smoking exposure. Alcohol has been hypothesized to be a risk factor of ovarian cancer in relation to their known mechanisms of both induction of oxidative products acting as cocarcinogenic factors and depletion of folate and other nutrients [128]. Several studies have been published on this topic with contrasting findings. The meta-analysis published by Bagnardi et al. [129] examined a total of 235 studies including over 117,000 cases. In this study, there is no correlation between ovarian cancer risk and a low alcohol intake (25 g/day) (relative risk, 1.11; 95 % confidence interval, 1.00–1.24), but the relative risk increases up to 1.53 (95 % confidence interval, 1.03–2.32) in women assuming a higher daily alcohol intake (100 g/day). On the contrary, the study of Webb et al. [130] conducted in Australian population women showed that wine drink, but not beer or sherry/spirit drinks, is associated with a significant reduction of ovarian cancer risk in drinkers 1 wine glass/day versus nondrinkers, with a relative risk of 0.56 (95 % confidence interval, 0.33–0.93). In the conclusion of their work, the authors think that this protective effect could depend on the antioxidant factors present in the wine, mainly in the red wine [130]. Another study did not evidence correlations between the ovarian carcinoma risk and alcohol drink [131]. Similarly, a recent systematic review and meta-analysis do not provide evidences of an increased or reduced risk of ovarian carcinoma in women who are heavy drinkers [132]. The study examined 23 case–control studies and 4 cohort studies. The authors found an overall relative risk of 1.00 (95 % confidence interval, 0.95–1.05) [132]. The relationship between ovarian cancer and smoking emerged in 2009 when the International Agency for Research and Cancer added the rare form of ovarian cancer, the mucinous ovarian tumor, in the list of tobacco-related cancer [133]. With the purpose to know whether smoking could be a risk factor for other ovarian cancer subtypes, the study of Collaborative Group on Epidemiological Studies of Ovarian Cancer examined 51 epidemiological studies with data for 28,114 women with and 94,942 women without ovarian cancer [134]. The study confirms the significant ($p=0.0001$) higher risk of mucinous ovarian cancer in current versus never smoker women (relative risk, 1.79; 95 % confidence interval, 1.60–2.00), but does not show a significant relationship between smoking and serous ovarian cancer (relative risk, 0.99; 95 % confidence interval, 0.93–1.06; $p=0.8$). Endometrioid and clear cell ovarian cancers were not directly but inversely correlated with smoking (endometrioid tumor, relative risk is 0.81; 95 % confidence interval, 0.72–0.92; $p=0.001$. Clear cell tumor, relative risk is 0.80; 95 % confidence interval, 0.65–0.97; $p=0.03$) [134]. The opposite effects of smoking on mucinous ovarian tumor and on endometrioid and clear cells ovarian tumors associated with a neutral effect on serous ovarian cancer are interpreted by the authors as a "substantial no effect of smoking on the overall ovarian cancer risk....and that the different subtypes of ovarian cancer recognize a different mechanism of carcinogenesis" [134].

In conclusion, many environmental factors can interfere on the risk of ovarian cancer, and the different interferences of some risk factors on the histologic type of tumor lead to hypothesize a different mechanism of carcinogenesis. In this view, the epithelial ovarian cancer seems to recognize a proper oncogenetic mechanism in which genetic factors, reproductive factors, and some lifestyle factors play an important role.

References

1. Jemal A, Siegel R, Xu J, Ward E. Cancer statistics 2010. CA Cancer J Clin. 2010;60:277–300.
2. Cannistra SA. Cancer of the ovary. N Engl J Med. 2004;351:2519–29.
3. Quirk JT, Natarajan N, Mettlin CJ. Age-specific ovarian cancer incidence rate patterns in the United States. Gynecol Oncol. 2005;99:248–50.
4. Rabban JT, Bell DA. Current issues in the pathology of ovarian cancer. J Reprod Med. 2005;50:467–74.
5. Singer G, Stöhr R, Cope L, Dehari R, Hartmann A, Cao DF, Wang TL, Kurman RJ, Shih IM. Patterns of p53 mutations separate ovarian serous borderline tumors and low- and high-grade carcinomas and provide support for a new model of ovarian carcinogenesis: a mutational analysis with immunohistochemical correlation. Am J Surg Pathol. 2005;29:218–24.
6. Werness BA, Eltabbakh GH. Familial ovarian cancer and early ovarian cancer: biologic, pathologic, and clinical features. Int J Gynecol Pathol. 2001;20:48–63.
7. Prat J, Ribé A, Gallardo A. Hereditary ovarian cancer. Hum Pathol. 2005;36:861–70.

8. Miki Y, Swensen J, Shattuck-Eidens D, Futreal PA, Harshman K, Tavtigian S, Liu Q, Cochran C, Bennett LM, Ding W, et al. A strong candidate for the breast and ovarian cancer susceptibility gene BRCA1. Science. 1994;266:66–71.
9. Wooster R, Bignell G, Lancaster J, Swift S, Seal S, Mangion J, Collins N, Gregory S, Gumbs C, Micklem G. Identification of the breast cancer susceptibility gene BRCA2. Nature. 1995;378: 789–92.
10. Scully R, Livingston DM. In search of the tumour-suppressor functions of BRCA1 and BRCA2. Nature. 2000;408:429–32.
11. Zhang S, Royer R, Li S, McLaughlin JR, Rosen B, Risch HA, Fan I, Bradley L, Shaw PA, Narod SA. Frequencies of BRCA1 and BRCA2 mutations among 1,342 unselected patients with invasive ovarian cancer. Gynecol Oncol. 2011;121:353–7.
12. Pal T, Permuth-Wey J, Betts JA, Krischer JP, Fiorica J, Arango H, LaPolla J, Hoffman M, Martino MA, Wakeley K, Wilbanks G, Nicosia S, Cantor A, Sutphen R. BRCA1 and BRCA2 mutations account for a large proportion of ovarian carcinoma cases. Cancer. 2005;104:2807–16.
13. Risch HA, McLaughlin JR, Cole DE, Rosen B, Bradley L, Kwan E, Jack E, Vesprini DJ, Kuperstein G, Abrahamson JL, Fan I, Wong B, Narod SA. Prevalence and penetrance of germline BRCA1 and BRCA2 mutations in a population series of 649 women with ovarian cancer. Am J Hum Genet. 2001;68:700–10.
14. Narod SA, Boyd J. Current understanding of the epidemiology and clinical implications of BRCA1 and BRCA2 mutations for ovarian cancer. Curr Opin Obstet Gynecol. 2002;14:19–26.
15. Lakhani SR, Manek S, Penault-Llorca F, et al. Pathology of ovarian cancers in BRCA1 and BRCA 2 carriers. Clin Cancer Res. 2004;10:2473–81.
16. Modan B, Hartge P, Hirsh-Yechezkel G, Chetrit A, Lubin F, Beller U, Ben-Baruch G, Fishman A, Menczer J, Struewing JP, Tucker MA, Wacholder S, National Israel Ovarian Cancer Study Group. Parity, oral contraceptives, and the risk of ovarian cancer among carriers and noncarriers of a BRCA1 or BRCA2 mutation. N Engl J Med. 2001;345:235–40.
17. Moslehi R, Chu W, Karlan B, Fishman D, Risch H, Fields A, Smotkin D, Ben-David Y, Rosenblatt J, Russo D, Schwartz P, Tung N, Warner E, Rosen B, Friedman J, Brunet JS, Narod SA. BRCA1 and BRCA2 mutation analysis of 208 Ashkenazi Jewish women with ovarian cancer. Am J Hum Genet. 2000;66: 1259–72.
18. Levy-Lahad E, Catane R, Eisenberg S, Kaufman B, Hornreich G, Lishinsky E, Shohat M, Weber BL, Beller U, Lahad A, Halle D. Founder BRCA1 and BRCA2 mutations in Ashkenazi Jews in Israel: frequency and differential penetrance in ovarian cancer and in breast-ovarian cancer families. Am J Hum Genet. 1997;60: 1059–67.
19. Hirsh-Yechezkel G, Chetrit A, Lubin F, Friedman E, Peretz T, Gershoni R, Rizel S, Struewing JP, Modan B. Population attributes affecting the prevalence of BRCA mutation carriers in epithelial ovarian cancer cases in Israel. Gynecol Oncol. 2003;89: 494–8.
20. Ford D, Easton DF, Stratton M, Narod S, Goldgar D, Devilee P, Bishop DT, Weber B, Lenoir G, Chang-Claude J, Sobol H, Teare MD, Struewing J, Arason A, Scherneck S, Peto J, Rebbeck TR, Tonin P, Neuhausen S, Barkardottir R, Eyfjord J, Lynch H, Ponder BA, Gayther SA, Zelada-Hedman M, et al. Genetic heterogeneity and penetrance analysis of the BRCA1 and BRCA2 genes in breast cancer families. The Breast Cancer Linkage Consortium. Am J Hum Genet. 1998;62:676–89.
21. Boyd J, Sonoda Y, Federici MG, Bogomolniy F, Rhei E, Maresco DL, Saigo PE, Almadrones LA, Barakat RR, Brown CL, Chi DS, Curtin JP, Poynor EA, Hoskins WJ. Clinicopathologic features of BRCA-linked and sporadic ovarian cancer. JAMA. 2000;283: 2260–5.
22. Liede A, Karlan BY, Baldwin RL, Platt LD, Kuperstein G, Narod SA. Cancer incidence in a population of Jewish women at risk of ovarian cancer. J Clin Oncol. 2002;20:1570–7.
23. Jacobs IJ, Skates SJ, MacDonald N, Menon U, Rosenthal AN, Davies AP, Woolas R, Jeyarajah AR, Sibley K, Lowe DG, Oram DH. Screening for ovarian cancer: a pilot randomized control trial. Lancet. 1999;363:1207–10.
24. Gaarenstroom KN, van der Hiel B, Tollenaar RA, et al. Efficacy of screening women at high risk of hereditary ovarian cancer: results of an 11-year cohort study. Int J Gynecol Cancer. 2006;16 Suppl 1:54–9.
25. Oei AL, Massuger LF, Bulten J, Ligtenberg MJ, Hoogerbrugge N, de Hullu JA. Surveillance of women at high risk for hereditary ovarian cancer is inefficient. Br J Cancer. 2006;94:814–9.
26. Olivier RI, Lubsen-Brandsma MA, Verhoef S, van Beurden M. CA125 and transvaginal ultrasound monitoring in high-risk women cannot prevent the diagnosis of advanced ovarian cancer. Gynecol Oncol. 2006;100:20–6.
27. NIH Consensus Development Panel on Ovarian Cancer. Ovarian cancer screening, treatment and follow-up. JAMA. 1995;273: 491–7.
28. Piver MS. Prophylactic oophorectomy: reducing the U.S. death rate from epithelial ovarian cancer. A continuing debate. Oncologist. 1996;1:326–30.
29. Rebbeck TR, Lynch HT, Neuhausen SL, Narod SA, Van't Veer L, Garber JE, Evans G, Isaacs C, Daly MB, Matloff E, Olopade OI, Weber BL, Prevention and Observation of Surgical End Points Study Group. Prophylactic oophorectomy in carriers of *BRCA1* or *BRCA2* mutations. N Engl J Med. 2002;346:1616–22.
30. Kauff ND, Satagopan JM, Robson ME, Scheuer L, Hensley M, Hudis CA, Ellis NA, Boyd J, Borgen PI, Barakat RR, Norton L, Castiel M, Nafa K, Offit K. Risk-reducing salpingo-oophorectomy in women with a BRCA1 or BRCA2 mutation. N Engl J Med. 2002;346:1609–15.
31. Kauff ND, Domchek SM, Friebel TM, Robson ME, Lee J, Garber JE, Isaacs C, Evans DG, Lynch H, Eeles RA, Neuhausen SL, Daly MB, Matloff E, Blum JL, Sabbatini P, Barakat RR, Hudis C, Norton L, Offit K, Rebbeck TR. Risk-reducing salpingo-oophorectomy for the prevention of BRCA1- and BRCA2-associated breast and gynecologic cancer: a multicenter, prospective study. J Clin Oncol. 2008;26:1331–7.
32. Finch A, Beiner M, Lubinski J, Lynch HT, Moller P, Rosen B, Murphy J, Ghadirian P, Friedman E, Foulkes WD, Kim-Sing C, Wagner T, Tung N, Couch F, Stoppa-Lyonnet D, Ainsworth P, Daly M, Pasini B, Gershoni-Baruch R, Eng C, Olopade OI, McLennan J, Karlan B, Weitzel J, Sun P, Narod SA, Hereditary Ovarian Cancer Clinical Study Group. Salpingo-oophorectomy and the risk of ovarian, fallopian tube, and peritoneal cancers in women with a BRCA1 or BRCA2 Mutation. JAMA. 2006;296:185–92.
33. Finch A, Shaw P, Rosen B, Murphy J, Narod SA, Colgan TJ. Clinical and pathologic findings of prophylactic salpingo-oophorectomies in 159 BRCA1 and BRCA2 carriers. Gynecol Oncol. 2006;100:58–64.
34. Kindelberger DW, Lee Y, Miron A, Hirsch MS, Feltmate C, Medeiros F, Callahan MJ, Garner EO, Gordon RW, Birch C, Berkowitz RS, Muto MG, Crum CP. Intraepithelial carcinoma of the fimbria and pelvic serous carcinoma: evidence for a causal relationship. Am J Surg Pathol. 2007;31:161–9.
35. Crum CP, Drapkin R, Miron A, Ince TA, Muto M, Kindelberger DW, Lee Y. The distal fallopian tube: a new model for pelvic serous carcinogenesis. Curr Opin Obstet Gynecol. 2007;19:3–9.
36. Hamilton TC. Ovarian cancer, part I: biology. Curr Probl Cancer. 1992;16:1–57.
37. Narod SA, Madlensky L, Bradley L, Cole D, Tonin P, Rosen B, Risch HA. Hereditary and familial ovarian cancer in Southern Ontario. Cancer. 1994;74:2341–6.

38. Berchuck A, Rodriguez GC, Kamel A, Dodge RK, Soper JT, Clarke-Pearson DL, Bast RC. Epidermal growth factor receptor expression in normal ovarian epithelium and ovarian cancer. Am J Obstet Gynecol. 1991;164:669–74.
39. Rodriguez CG, Berchuck A, Whitaker RS, Schlossman D, Clarke-Pearson DL, Bast Jr RC. Epidermal growth factor receptor expression in normal ovarian epithelium and ovarian cancer. II. Relationship between receptor expression and response to epidermal growth factor. J Obstet Gynecol. 1991;164:745–50.
40. Ilekis JV, Connor JP, Prins GS, Ferrer K, Niederberger C, Scoccia B. Expression of epidermal growth factor and androgen receptors in ovarian cancer. Gynecol Oncol. 1997;66:250–4.
41. Blaakaer J, Backsted M, Micic S, Albreetsen P, Rygaard J, Bock J. Gonadotropin-releasing hormone agonist suppression of ovarian tumorigenesis in mice of the W^x/W^v genotype. Biol Reprod. 1995;53:775–9.
42. Kammerman S, Demopoulos RI, Raphael C, Ross J. Gonadotropic hormone binding to human ovarian tumors. Hum Pathol. 1981;12:886–90.
43. Rajaniemi H, Kauppila A, Rönnberg L, Selander K, Pystynen P. LH (hCG) receptor in benign and malignant tumor of human ovary. Acta Obstetrica et Gynecologica Scandinavica Supplement. 1981;101:83–6.
44. Stouffer FL, Grodin MS, Davis JR, Surwit EA. Investigation of binding sites for follicle-stimulating hormone and chorionic gonadotropin in human ovarian cancers. J Clin Endocrinol Metab. 1984;59:441–6.
45. Negri E, Franceschi S, Tzonou A, Booth M, La Vecchia C, Parazzini F, Beral V, Boyle P, Trichopoulos D. Pooled analysis of 3 European case–control studies. I. Reproductive factors and risk of epithelial ovarian cancer. Int J Cancer. 1991;49:50–6.
46. Chen Y, Wu PC, Lang JH, Ge WJ, Hartge P, Brinton LA. Risk factors for epithelial ovarian cancer in Beijing, China. Int J Epidemiol. 1992;21:23–9.
47. Whittemore AS, Harris R, Itnyre J, the Collaborative Ovarian Cancer Group. Characteristics relating to ovarian cancer risk: collaborative analysis of 12 US case–control studies: II. Invasive epithelial ovarian cancers in white women. Am J Epidemiol. 1992;136:1184–203.
48. Adami HO, Hsieh CC, Lambe M, Trichopoulos D, Leon D, Persson I, Ekbom A, Janson PO. Parity, age at first childbirth, and risk of ovarian cancer. Lancet. 1994;344:1250–4.
49. Purdie D, Green A, Bain C, Siskind V, Ward B, Hacker N, Quinn M, Wright G, Russell P, Susil B, Survey of Women's Health Study Group. Reproductive and other factors and risk of epithelial ovarian cancer: an Australian case–control study. Int J Cancer. 1995;62:678–84.
50. Risch HA, Marrett LD, Howe GR. Parity, contraception, infertility, and the risk of epithelial ovarian cancer. Am J Epidemiol. 1994;140:585–97.
51. Hankinson SE, Colditz GA, Hunter DJ, Willett WC, Stampfer MJ, Rosner B, Hennekens CH, Speizer FE. A prospective study of reproductive factors and risk of epithelial ovarian cancer. Cancer. 1995;76:284–90.
52. Rosenblatt KA, Thomas DB, the WHO Collaborative Study of Neoplasia and Steroid Contraceptives. Lactation and the risk of epithelial ovarian cancer. Int J Epidemiol. 1993;22:192–7.
53. Hannaford PC, Selvaraj S, Elliott AM, Angus V, Iversen L, Lee AJ. Cancer risk among users of oral contraceptives: cohort data from the Royal College of General Practitioner's oral contraception study. BMJ. 2007;335:651.
54. Collaborative Group on Epidemiological Studies of Ovarian Cancer, Beral V, Doll R, Hermon C, Peto R, Reeves G. Ovarian cancer and oral contraceptives: collaborative reanalysis of data from 45 epidemiological studies including 23,257 women with ovarian cancer and 87,303 controls. Lancet. 2008;371:303–14.
55. Rossing MA, Daling JR, Weiss NS, Moore DE, Self SG. Ovarian tumors in a cohort of infertile women. N Engl J Med. 1994;331:771–6.
56. Shushan A, Paltiel O, Iscovich J, Elchalal U, Peretz T, Schenker JG. Human menopausal gonadotropin and the risk of epithelial ovarian cancer. Fertil Steril. 1996;65:13–8.
57. Bamford PN, Steele SJ. Uterine and ovarian carcinoma in a patient receiving gonadotrophin therapy. A case report. Br J Obstet Gynaecol. 1982;89:962–4.
58. Bristow RE, Karlan BY. Ovulation induction, infertility, and ovarian cancer risk. Fertil Steril. 1996;66:499–507.
59. Fishel S, Jackson P. Follicular stimulation for high tech pregnancies: are we playing it safe? Br Med J. 1989;299:309–11.
60. Brinton LA, Melton III LJ, Malkasian Jr GD, Bond A, Hoover R. Cancer risk after evaluation for infertility. Am J Epidemiol. 1989;129:712–22.
61. Modan B, Ron E, Lerner-Geva L, Blumstein T, Menczer J, Rabinovici J, Oelsner G, Freedman L, Mashiach S, Lunenfeld B. Cancer incidence in a color of infertile women. Am J Epidemiol. 1998;147:1038–42.
62. Patashnik G, Lerner-Geva L, Genkin LI, Chetrit A, Lunenfeld E, Porath A. Fertility drugs and the risk of breast and ovarian cancers: results of a long follow-up study. Fertil Steril. 1999;71:853–9.
63. Venn A, Watson L, Bruinsma F, Giles G, Healy D. Risk of cancer after use of fertility drugs with in-vitro fertilization. Lancet. 1999;354:1586–90.
64. Brinton LA, Lamb EJ, Moghissi KS, Scoccia B, Althuis MD, Mabie JE, Westhoff CL. Ovarian cancer risk associated with varying causes of infertilità. Fertil Steril. 2004;82:405–14.
65. Harlow BL, Weiss NS, Roth GS, Chu J, Dalling JR. Case–control study of borderline ovarian tumors: reproductive history and exposure to exogenous female hormones. Cancer Res. 1988;48:5849–52.
66. Tworoger SS, Fairfield KM, Colditz GA, Rosner BA, Hankinson SE. Association of oral contraceptive use, other contraceptive methods, and infertility with ovarian cancer risk. Am J Epidemiol. 2007;166:894–901.
67. Whittemore A, Harris R, Intyre J. Characteristics relating to ovarian cancer risk: collaborative analysis of 12 US case–control studies. II. Invasive epithelial ovarian cancers in white women. Collaborative Ovarian Cancer Group. Am J Epidemiol. 1992;136:1184–203.
68. Ness RB, Cramer DW, Goodman MT, Kjaer SK, Mallin K, Mosgaard BJ, Purdie DM, Risch HA, Vergona R, Wu AH. Infertility, fertility drugs, and ovarian cancer: a pooled analysis of case–control studies. Am J Epidemiol. 2002;155:217–24.
69. Rossing MA, Tang MT, Flagg EW, Weiss LK, Wicklund KG. A case–control study of ovarian cancer in relation to infertility and the use of ovulation induction drugs. Am J Epidemiol. 2004;160:1070–8.
70. Melin A, Sparen P, Bergquist A. The risk of cancer and the role of parity among women with endometriosis. Hum Reprod. 2007;22:3021–6.
71. Vercellini P, Parazzini F, Bolis G, Carinelli S, Dindelli M, Vendola N, Luchini L, Crosignani PG. Endometriosis and ovarian cancer. Am J Obstet Gynecol. 1993;169:181–2.
72. Schildkraut JM, Schwingl PJ, Bastos E, Evanoff A, Hughes C. Epithelial ovarian cancer risk among women with polycystic ovary syndrome. Obstet Gynecol. 1996;88:554–9.
73. Lahmann PH, Cust AE, Friedenreich CM, Schulz M, Lukanova A, Kaaks R, Lundin E, Tjønneland A, Halkjaer J, Severinsen MT, Overvad K, Fournier A, Chabbert-Buffet N, Clavel-Chapelon F, Dossus L, Pischon T, Boeing H, Trichopoulou A, Lagiou P, Naska A, Palli D, Grioni S, Mattiello A, Tumino R, Sacerdote C, Redondo ML, Jakszyn P, Sánchez MJ, Tormo MJ, Ardanaz E, Arriola L, Manjer J, Jirström K, Bueno-de-Mesquita HB, May AM,

Peeters PH, Onland-Moret NC, Bingham S, Khaw KT, Allen NE, Spencer E, Rinaldi S, Slimani N, Chajes V, Michaud D, Norat T, Riboli E. Anthropometric measures and epithelial ovarian cancer risk in the European Prospective Investigation into Cancer and Nutrition. Int J Cancer. 2010;125:2404–15.
74. Hankinson SE, Hunter DJ, Colditz GA, Willett WC, Stampfer MJ, Rosner B, Hennekens CH, Speizer FE. Tubal ligation, hysterectomy and risk of ovarian cancer, a prospective study. JAMA. 1993;270:2813–8.
75. Irwin KL, Weiss NS, Lee LC, Peterson HB. Tubal sterilization, hysterectomy and the subsequent occurrence of epithelial ovarian cancer. Am J Epidemiol. 1991;134:362–9.
76. Rosenblatt KA, Thomas DB, the WHO collaborative Study of Neoplasia and Steroid Contraceptives. Reduced risk of ovarian cancer in women with a tubal ligation or hysterectomy. Cancer Epidemiol Biomarkers Prev. 1996;5:933–5.
77. Calle EE, Kaaks R. Overweight, obesity and cancer epidemiological evidence and proposed mechanisms. Nat Rev Cancer. 2004;4:579–91.
78. Macciò A, Madeddu C, Mantovani G. Adipose tissue as target organ in the treatment of hormone-dependent breast cancer: new therapeutic perspectives. Obes Rev. 2009;10(6):660–70.
79. Uddin S, Bu R, Ahmed M, Abubaker J, Al-Dayel F, Bavi P, Al-Kuraya KS. Overexpression of leptin receptor predicts an unfavorable outcome in Middle Eastern ovarian cancer. Mol Cancer. 2009;8:74. doi:10.1186/1476-4598-8-74. Published online 2009 September 18.
80. Schouten LJ, Rivera C, Hunter DJ, Spiegelman D, Adami HO, Arslan A, Beeson WL, van den Brandt PA, Buring JE, Folsom AR, Fraser GE, Freudenheim JL, Goldbohm RA, Hankinson SE, Lacey Jr JV, Leitzmann M, Lukanova A, Marshall JR, Miller AB, Patel AV, Rodriguez C, Rohan TE, Ross JA, Wolk A, Zhang SM, Smith-Warner SA. Height, body mass index, and ovarian cancer: a pooled analysis of 12 cohort studies. Cancer Epidemiol Biomarkers Prev. 2008;17:902–12.
81. Kolahdooz F, Ibiebele TI, van der Pols JC, Webb PM. Dietary patterns and ovarian cancer risk. Am J Clin Nutr. 2009;89:297–304.
82. Bidoli E, La Vecchia C, Talamini R, Negri E, Parpinel M, Conti E, Montella M, Carbone MA, Franceschi S. Micronutrients and ovarian cancer: a case–control study in Italy. Ann Oncol. 2001;12:1589–93.
83. La Vecchia C, Decarli A, Negri E, Parazzini F, Gentile A, Cecchetti G, Fasoli M, Franceschi S. Dietary factors and the risk of epithelial ovarian cancer. J Natl Cancer Inst. 1987;79:663–9.
84. Kushi LH, Mink PJ, Folsom AR, Anderson KE, Zheng W, Lazovich D, Sellers TA. Prospective study of diet and ovarian cancer. Am J Epidemiol. 1999;149:21–31.
85. Nagle CM, Kolahdooz F, Ibiebele TI, Olsen CM, Lahmann PH, Green AC, Webb PM, Australian Cancer Study (Ovarian Cancer) and the Australian Ovarian Cancer Study Group. Carbohydrate intake, glycemic load, glycemic index, and risk of ovarian cancer. Ann Oncol. 2011;22:1332–8.
86. Herrinton LJ, Stanford JL, Schwartz SM, Weiss NS. Ovarian cancer incidence among Asian migrants to the United States and their descendants. J Natl Cancer Inst. 1994;86:1336–9.
87. Aschebrook-Kilfoy B, Ward MH, Gierach GL, Schatzkin A, Hollenbeck AR, Sinha R, Cross AJ. Epithelial ovarian cancer and exposure to dietary nitrate and nitrite in the NIH-AARP diet and Health study. Eur J Cancer Prev. 2012;21:65–72.
88. Bogovski P, Bogovski S. Animal species in which N-nitroso compounds induce cancer. Int J Cancer. 1981;27:471–4.
89. Biesma RG, Schouten LJ, Dirx MJ, Goldbohm RA, van den Brandt PA. Physical activity and the risk of ovarian cancer: results from the Netherlands Cohort Study. Cancer Causes Control. 2006;17:109–15.
90. Bertone ER, Bertone ER, Willett WC, Rosner BA, Hunter DJ, Fuchs CS, Speizer FE, Colditz GA, Hankinson SE, Nurses' Health Study. Prospective study of recreational physical activity and ovarian cancer. J Natl Cancer Inst. 2001;93:942–8.
91. Phipps RP. The second International scientific symposium on tea and human health, September 14th 1998. Nutrition. 1999;15:968–71.
92. Zhang M, Lee AH, Binns CW, Xie X. Green tea consumption enhances survival of epithelial ovarian cancer. Int J Cancer. 2004;112:465–9.
93. Suganuma M, Okabe S, Sueoka N, Sueoka E, Matsuyama S, Imai K, Nakachi K, Fujiki H. Green tea and cancer chemoprevention. Mutat Res. 1999;428:339–44.
94. Sugiyama T, Sadzuka Y. Combination of theanine with doxorubicin inhibits hepatic metastasis of M5076 ovarian sarcoma. Clin Cancer Res. 1999;5:413–6.
95. Mukhtar H, Ahmad N. Tea polyphenols: prevention of cancer and optimizing health. Am J Nutr. 2000;71:1698S–702.
96. Zhang M, Lee AH, Binns CW. Reproductive and dietary risk factors for epithelial ovarian cancer in China. Gynecol Oncol. 2004;92:320–6.
97. Holick MF. Vitamin D, deficiency. N Engl J Med. 2007;357:266–81.
98. Institute of Medicine. Dietary supplement fact sheet: vitamin D. 2009. Available at: http://www.ods.od.nih.gov/factsheets/vitamind.asp. Accessed 1 Sept 2009.
99. Lefkowitz ES, Garland CF. Sunlight, vitamin D, and ovarian cancer mortality rates in US women. Int J Epidemiol. 1994;23:1133–6.
100. Saunders DE, Christensen C, Wappler NL, Schultz JF, Lawrence WD, Malviya VK, Malone JM, Deppe G. Inhibition of c-myc in breast and ovarian carcinoma cells by 1,25-dihydroxyvitamin D3, retinoic acid and dexamethasone. Anticancer Drugs. 1993;4:201–8.
101. Jiang F, Bao J, Li P, Nicosia SV, Bai W. Induction of ovarian cancer cell apoptosis by 1,25-dihydroxyvitamin D3 through the down-regulation of telomerase. J Biol Chem. 2004;279:53213–21.
102. Ahonen MH, Zhuang YH, Aine R, Ylikomi T, Tuohimaa P. Androgen receptor and vitamin D receptor in human ovarian cancer: growth stimulation and inhibition by ligands. Int J Cancer. 2000;86:40–6.
103. Villena-Heinsen C, Meyberg R, Axt-Fliedner R, Reitnauer K, Reichrath J, Friedrich M. Immunohistochemical analysis of 1,25-dihydroxyvitamin-D3-receptors, estrogen and progesterone receptors and Ki-67 in ovarian carcinoma. Anticancer Res. 2002;22:2261–7.
104. Saunders DE, Christensen C, Lawrence WD, Malviya VK, Malone JM, Williams JR, Deppe G. Receptors for 1,25-dihydroxyvitamin D3 in gynecologic neoplasms. Gynecol Oncol. 1992;44:131–6.
105. Cook LS, Neilson HK, Lorenzetti DL, Lee RC. A systematic literature review of vitamin D and ovarian cancer. Am J Obstet Gynecol. 2010;203:70.e1–8.
106. Pinto JA. The epidemiology of ovarian cancer in the United States: an ecological analysis (cohort analysis, geographic patterns). Berkeley: University of California, Berkeley; 1984.
107. Decarli A, La Vecchia C. Environmental factors and cancer mortality in Italy: correlational exercise. Oncology. 1986;43:116–26.
108. Mizoue T. Ecological study of solar radiation and cancer mortality in Japan. Health Phys. 2004;87:532–8.
109. Grant WB. The likely role of vitamin D from solar ultraviolet-B irradiance in increasing cancer survival. Anticancer Res. 2006;26(4A):2605–14.
110. Grant WB. An ecologic study of cancer mortality rates in Spain with respect to indices of solar UVB irradiance and smoking. Int J Cancer. 2007;120:1123–8.

111. Boscoe FP, Schymura MJ. Solar ultraviolet-B exposure and cancer incidence and mortality in the United States, 1993–2002. BMC Cancer. 2006;6:264.
112. Garland CF, Mohr SB, Gorham ED, Grant WB, Garland FC. Role of ultraviolet B irradiance and vitamin D in prevention of ovarian cancer. Am J Prev Med. 2006;31:512–4.
113. Waltz P, Chodick G. Assessment of ecological regression in the study of colon, breast, ovary, non-Hodgkin's lymphoma, or prostate cancer and residential UV. Eur J Cancer Prev. 2008; 17:279–86.
114. Grant WB, Garland CF. The association of solar ultraviolet B (UVB) with reducing risk of cancer: multifactorial ecologic analysis of geographic variation in age-adjusted cancer mortality rates. Anticancer Res. 2006;26(4A):2687–99.
115. Freedman DM, Dosemeci M, McGlynn K. Sunlight and mortality from breast, ovarian, colon, prostate, and non-melanoma skin cancer: a composite death certificate based case–control study. Occup Environ Med. 2002;59:257–62.
116. Cramer DW, Kuper H, Harlow BL, Titus-Ernstoff L. Carotenoids, antioxidants and ovarian cancer risk in pre- and postmenopausal women. Int J Cancer. 2001;94:128–34.
117. Bertone ER, Hankinson SE, Newcomb PA, Rosner B, Willet WC, Stampfer MJ, Egan KM. A population-based case–control study of carotenoid and vitamin A intake and ovarian cancer (United States). Cancer Causes Control. 2001;12:83–90.
118. Salazar-Martinez E, Lazcano-Ponce EC, Gonzalez Lira-Lira G, Escudero-De los Rios P, Hernandez-Avila M. Nutritional determinants of epithelial ovarian cancer risk: a case–control study in Mexico. Oncology. 2002;63:151–7.
119. Goodman MT, Wu AH, Tung KH, McDuffie K, Kolonel LN, Nomura AM, Terada K, Wilkens LR, Murphy S, Hankin JH. Association of dairy products, lactose, and calcium with the risk of ovarian cancer. Am J Epidemiol. 2002;156:148–57.
120. Koralek DO, Bertone-Johnson ER, Leitzmann MF, Sturgeon SR, Lacey Jr JV, Schairer C, Schatzkin A. Relationship between calcium, lactose, vitamin D, and dairy products and ovarian cancer. Nutr Cancer. 2006;56:22–30.
121. Tworoger SS, Lee IM, Buring JE, Rosner B, Hollis BW, Hankinson SE. Plasma 25-hydroxyvitamin D and 1,25-dihydroxyvitamin D and risk of incident ovarian cancer. Cancer Epidemiol Biomarkers Prev. 2007;16:783–8.
122. Genkinger JM, Hunter DJ, Spiegelman D, Anderson KE, Arslan A, Beeson WL, Buring JE, Fraser GE, Freudenheim JL, Goldbohm RA, Hankinson SE, Jacobs Jr DR, Koushik A, Lacey Jr JV, Larsson SC, Leitzmann M, McCullough ML, Miller AB, Rodriguez C, Rohan TE, Schouten LJ, Shore R, Smit E, Wolk A, Zhang SM, Smith-Warner SA. Dairy products and ovarian cancer: a pooled analysis of 12 cohort studies. Cancer Epidemiol Biomarkers Prev. 2006;15:364–72.
123. Yin L, Grandi N, Raum E, Haug U, Arndt V, Brenner H. Meta-analysis: circulating vitamin D and ovarian cancer risk. Gynecol Oncol. 2011;121:369–75.
124. Arslan AA, Clendenen TV, Koenig KL, Hultdin J, Enquist K, Agren A, Lukanova A, Sjodin H, Zeleniuch-Jacquotte A, Shore RE, Hallmans G, Toniolo P, Lundin E. Circulating vitamin D and risk of epithelial ovarian cancer. J Oncol. 2009;2009:672492.
125. Toriola AT, Surcel HM, Agborsangaya C, Grankvist K, Tuohimaa P, Toniolo P, Lukanova A, Pukkala E, Lehtinen M. Serum 25-hydroxyvitamin D and the risk of ovarian cancer. Eur J Cancer. 2010;46:364–9.
126. Zheng W, Danforth KN, Tworoger SS, Goodman MT, Arslan AA, Patel AV, McCullough ML, Weinstein SJ, Kolonel LN, Purdue MP, Shu XO, Snyder K, Steplowski E, Visvanathan K, Yu K, Zeleniuch-Jacquotte A, Gao YT, Hankinson SE, Harvey C, Hayes RB, Henderson BE, Horst RL, Helzlsouer KJ. Circulating 25-hydroxyvitamin D and risk of epithelial ovarian cancer: Cohort Consortium Vitamin D Pooling Project of Rarer Cancers. Am J Epidemiol. 2010;172:70–80.
127. Lurie G, Wilkens LR, Thompson PJ, Carney ME, Palmieri RT, Pharoah PD, Song H, Hogdall E, Kjaer SK, DiCioccio RA, McGuire V, Whittemore AS, Gayther SA, Gentry-Maharaj A, Menon U, Ramus SJ, Goodman MT, Ovarian Cancer Association Consortium. Vitamin D receptor rs2228570 polymorphism and invasive ovarian carcinoma risk: pooled analysis in five studies within the Ovarian Cancer Association Consortium. Int J Cancer. 2011;128:936–43.
128. Poschl G, Seitz HK. Alcohol and cancer. Alcohol Alcohol. 2004;39:155–65.
129. Bagnardi V, Blangiardo M, La Vecchia C, Corrao G. A meta-analysis of alcohol drinking and cancer risk. Br J Cancer. 2001;85:1700–5.
130. Webb PM, Purdie DM, Bain CJ, Green AC. Alcohol, wine, and risk of epithelial ovarian cancer. Cancer Epidemiol Biomarkers Prev. 2004;13:592–9.
131. Genkinger JM, Hunter DJ, Spiegelman D, Anderson KE, Buring JE, Freudenheim JL, Goldbohm RA, Harnack L, Hankinson SE, Larsson SC, Leitzmann M, McCullough ML, Marshall J, Miller AB, Rodriguez C, Rohan TE, Schatzkin A, Schouten LJ, Wolk A, Zhang SM, Smith-Warner SA. Alcohol intake and ovarian cancer risk: a pooled analysis of 10 cohort studies. Br J Cancer. 2006;94:757–62.
132. Rota M, Pasquali E, Scotti L, Pelucchi C, Tramacere I, Islami F, Negri E, Boffetta P, Bellocco R, Corrao G, La Vecchia C, Bagnardi V. Alcohol drinking and epithelial ovarian cancer risk. a systematic review and meta-analysis. Gynecol Oncol. 2012;125: 758–63.
133. Secretan B, Straif K, Baan R, Grosse Y, El Ghissassi F, Bouvard V, Benbrahim-Tallaa L, Guha N, Freeman C, Galichet L, Cogliano V, WHO International Agency for Research on Cancer Monograph Working Group. A review of human carcinogens – part E: tobacco, areca nut, alcohol, coal smoke, and salted fish. Lancet Oncol. 2009;10:1033–4.
134. Collaborative Group on Epidemiological Studies of Ovarian Cancer. Ovarian cancer and smoking: individual participant meta-analysis including 28114 women with ovarian cancer from 51 epidemiological studies. Lancet Oncol. 2012;13:936–45.

Histopathology

Giuseppina Parodo, Clara Gerosa, and Silvia Soddu

Abstract

The histology of ovarian tumors exhibits a wide variety of histological features. The World Health Organization (WHO) histological classification subdivides ovarian tumors according to histogenetic principles as epithelial tumors arising from surface müllerian epithelium, sex cord-stromal tumors, germ cell tumors, and metastatic tumors. Gross and microscopic findings and immunohistochemical features are reported for each group.

Keywords

Histology • Pathology • Ovarian neoplasm • Epithelial tumors • Sex cord-stromal tumors • Germ cell tumors • Metastatic tumors

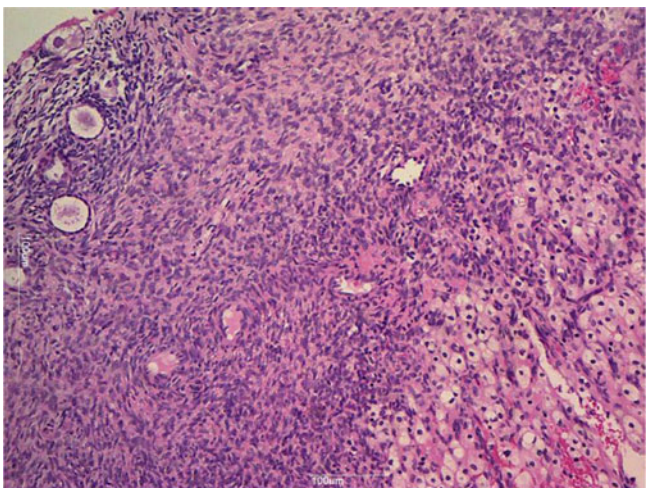

G. Parodo, MD (✉) • C. Gerosa, MD • S. Soddu, MD
Division of Pathology,
Department of Surgical Sciences,
University of Cagliari, Cagliari 09124, Italy
e-mail: giusiparodo@tiscali.it

Nonneoplastic Lesion of the Ovary

Cysts of Follicular Origin

During prepuberal and reproductive years, the functional follicle cysts and corpus luteum cysts measuring 3–10 cm in diameter are, by definition, benign. These lesions are often completely asymptomatic; most resolve spontaneously but may cause acute abdominal pain secondary to rupture and hemoperitoneum or torsion.

The cysts of follicular origin are solitary and fluid-filled. At microscopy follicular cysts are lined by granulosa cells, with a surrounding layer of theca cells (Fig. 1); both layers may show luteinization; corpus luteum cysts commonly contain intracystic hemorrhage, show a yellow rim of variable thickness, and are lined by a thick undulating layer of granulosa and theca cells, with prominent luteinization.

Differential Diagnosis

- Cystic granulosa cell tumor
- Surface epithelial cystoadenoma

L. Saba et al. (eds.), *Ovarian Neoplasm Imaging*,
DOI 10.1007/978-1-4614-8633-6_2, © Springer Science+Business Media New York 2013

Pregnancy Luteoma

It can mimic an ovarian neoplasia both grossly and microscopically. These tumorlike lesions, more common in black women, are composed of luteinized cells occurring during pregnancy secondary to hormonal stimulations. Macroscopically, pregnancy luteoma presents as one or multiple (30 % are bilateral, 50 % are multiple) solid masses with multiple circumscribed nodules that show a red-brown cut surface. At microscopy, nodules are well-circumscribed and luteinized cells show abundant eosinophilic cytoplasm, central and regular nuclei and prominent nucleoli (Fig. 2). Mitoses could be up to 7/10 HPFs. Necrotic and degenerative changes may be present. Usually pregnancy luteoma regresses after delivery.

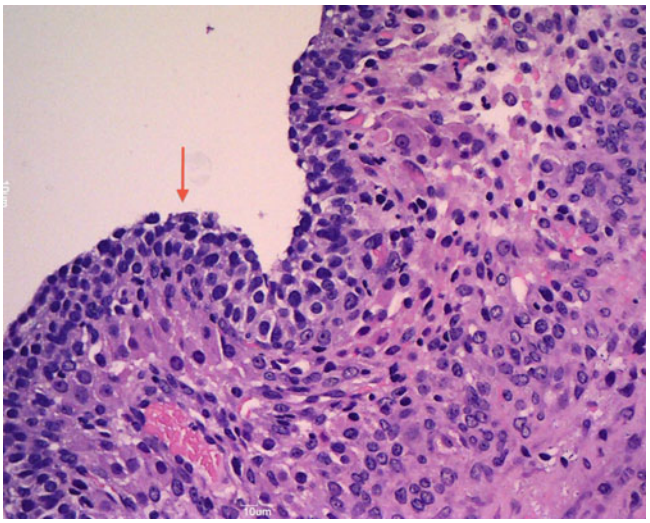

Fig. 1 Follicular cyst is lined by several layers of granulosa cells (*arrow*)

Differential Diagnosis

- Steroid cell tumor
- Leydig cell tumor
- Thecoma

Endometrioma (Endometriotic Cyst)

Ovarian endometriosis is a common finding and frequently gives to cystic masses (endometriomas): it is often bilateral and usually presents during the reproductive age. The macroscopic appearance is that of a large cystic mass (usually < 15 cm) with a thick wall that often replaces the ovary completely. Frequently, the ovarian surface is covered by dense fibrous adhesions. The intracystic material is dense and brown ("chocolate cyst"). The variable microscopic appearance is due to the different ectopic endometrial glands and stromal response to the hormonal milieu of the menstrual cycle. Endometrial glands surrounded by endometrial-type stroma may show inactive or proliferative, secretory, or

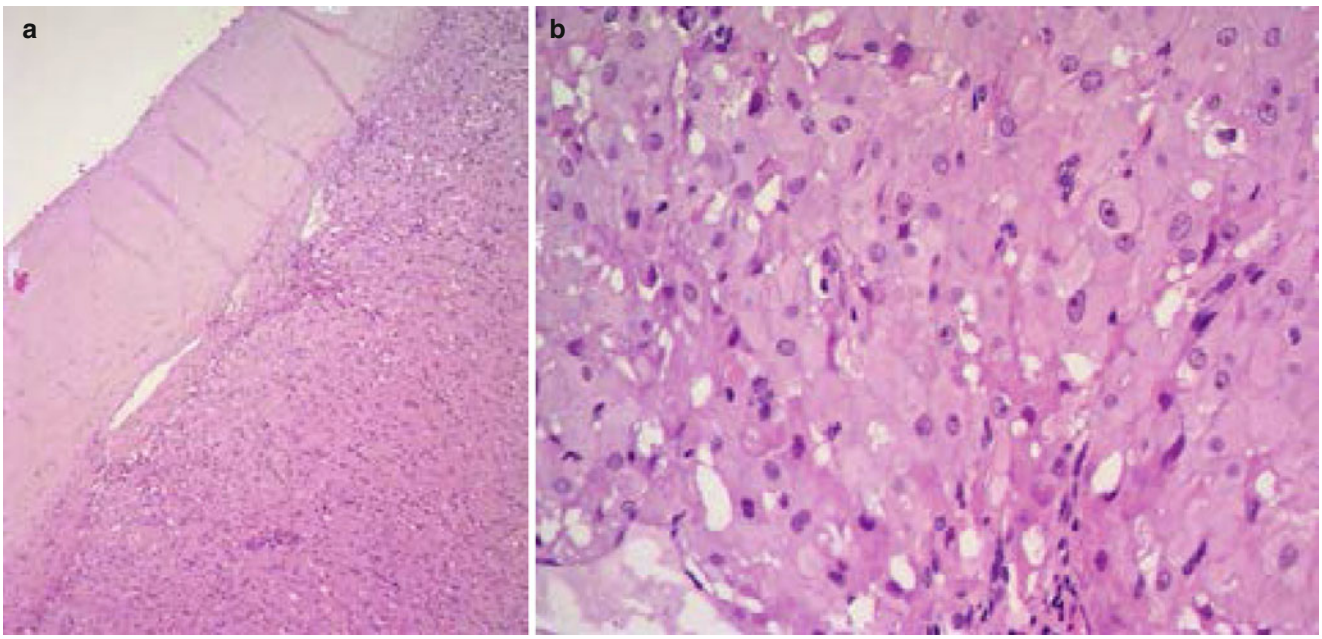

Fig. 2 Pregnancy luteoma is composed of luteinized cells with abundant eosinophilic cytoplasm (**a**); central and regular nuclei and prominent nucleoli are present (**b**)

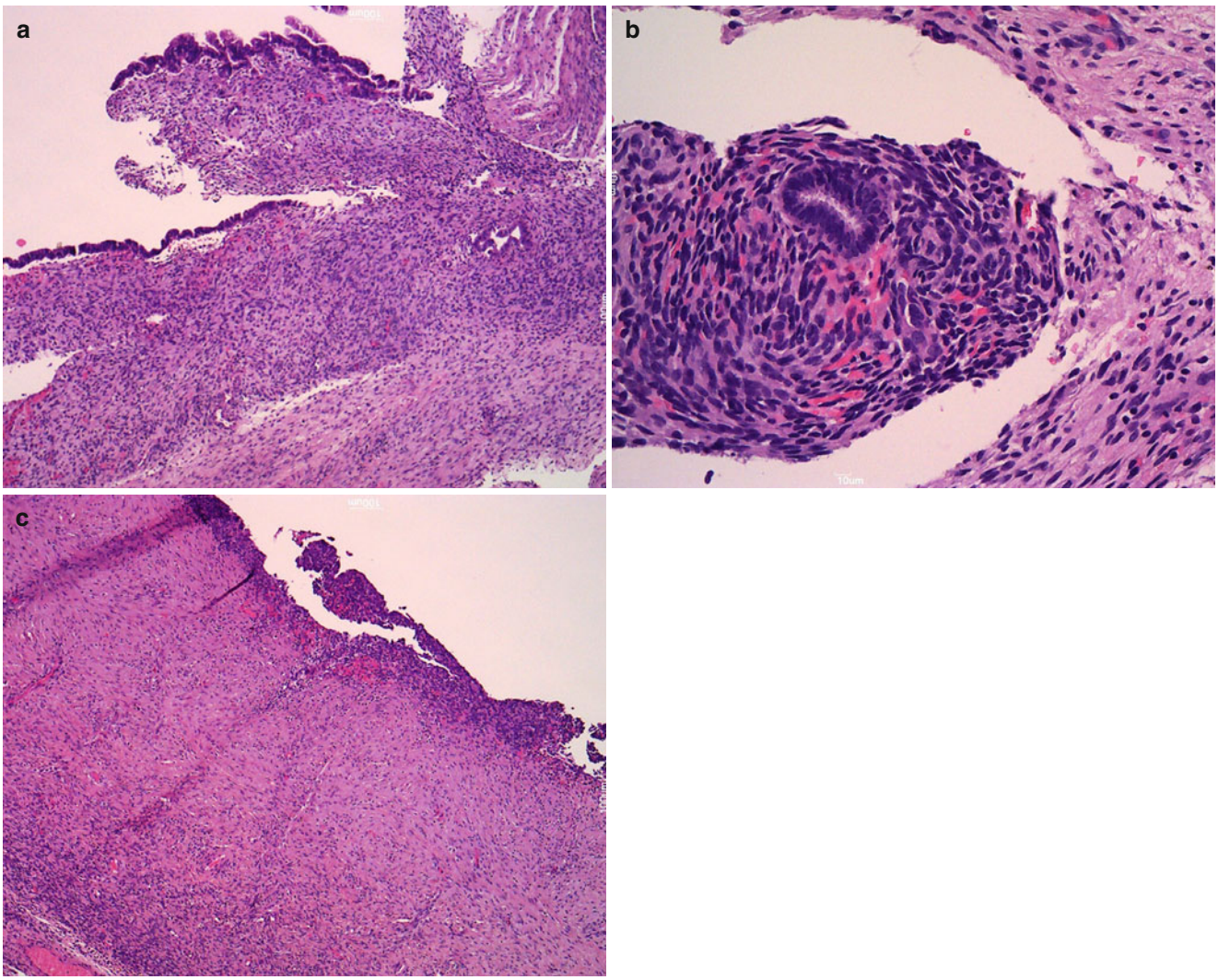

Fig. 3 Endometriosis. Endometriotic cyst is lined by endometrial-type epithelium (**a**); endometrioid gland is surrounded by endometrial-type stroma (**b**); atrophic changes of epithelium (**c**)

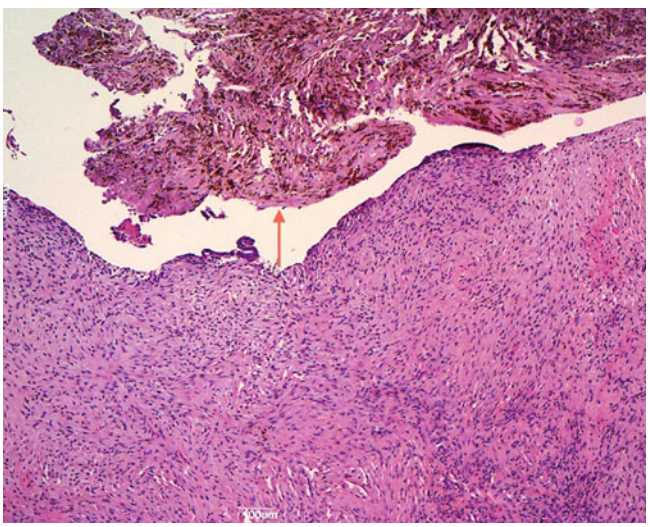

Fig. 4 Granulation tissue macrophages and siderophages (*arrow*) in endometrioma

atrophic changes (Fig. 3). Fibrosis and inflammation also interfere with macro- and microscopic features. Often, in non-recent cases, where we cannot find a well-defined glandular or stromal structure, the histological diagnosis is suggested by indirect signs including granulation tissue, macrophages, and siderophages (Fig. 4). Foci with epithelial atypia are often detected (atypical endometriosis), but they should not be mistaken for malignant transformation. Ancillary immunohistochemical studies may help to detect endometrial stroma and glandular structures.

Differential Diagnosis

- Benign hemorrhagic cyst of follicular origin
- Chronic tubo-ovarian abscesses
- Cystoadenomas
- Unilocular granulosa cell tumors
- Secondary neoplasm (clear cell or endometrioid carcinoma)

Ovarian Tumors

Ovarian tumors, according to the WHO classification (2003), can be primary or secondary (metastatic). Primary ovarian tumors arise from surface müllerian epithelium or from sex cord-stroma or from germ cells.

Surface Epithelial Tumors of the Ovary

Surface epithelial tumors are the most common neoplasms of the ovary. They may arise from the surface epithelium, from the fallopian tube epithelium, or from preexistent ovarian endometriosis. Surface epithelial tumors are classified into serous (46 %), mucinous (36 %), endometrioid (8 %), clear cells (3 %), transitional (2 %), undifferentiated (2 %), and mixed (3 %) on the basis of their different cell type. Histological features allow us to subclassify these tumors as benign, borderline and malignant. By definition, the borderline tumors lack destructive stromal invasion but show other histological features of malignancy (nuclear atypia, cellular stratification, mitotic activity). Their clinical behavior is mostly benign but, caveat, as far as serous borderline surface tumors are concerned, they are frequently associated with extraovarian disease and present a clinical behavior intermediate between benign tumors and invasive serous carcinomas.

Tumor stage, according to FIGO, is the most important prognostic factor; stage can only be assigned after completion of a proper surgical staging procedure. Tumor grading is done on the basis of architectural and cytologic atypia; mitotic count is another prognostic factor, but its prognostic value and reproducibility remain to be determined.

Serous Surface Epithelial Tumors

Serous Cystoadenoma, Cystoadenofibroma, and Adenofibroma

It is the most common serous benign ovarian neoplasm (50 %), occurs in the reproductive age, is composed of varying amounts of fibrous stroma and cysts and is subclassified by the WHO in serous cystoadenoma, cystoadenofibroma, and adenofibroma. These tumors range in size from 1 to 10 cm and are bilateral in 20 % of the cases. Smooth-walled unilocular or multilocular cysts are lined by nonstratified tubal-type epithelium. Epithelial cells do not show nuclear atypia, mitoses and necrosis. Torsion, rupture, and infection are the most common complications.

Differential Diagnosis

- Epithelial inclusion cyst
- Ovarian rete cyst
- Endometriotic cyst
- Struma ovarii
- Serous borderline tumor
- Mucinous cystoadenoma

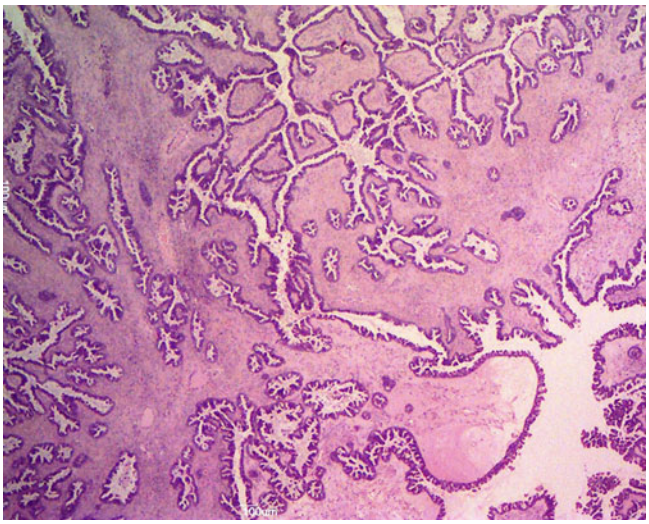

Fig. 5 Serous borderline tumor: the inner layer of the cyst is composed of large and small confluent papillae with complex hierarchical branching

Serous Borderline Tumor (Serous Tumor of Low Malignant Potential)

Serous borderline tumors occur more frequently during the fourth and fifth decades and usually in the reproductive age. They form bilateral (30–40 %) large cystic or solid and cystic masses with surface papillary epithelial structures. The inner layer of the cyst is composed of large and small confluent papillae with complex hierarchical branching (Fig. 5). The lining cells are tall to columnar with stratification, mild–moderate atypia, and sparse mitoses (Fig. 6). Psammoma bodies can be present. Foci of stromal microinvasion (<10 mm^2) do not warrant a diagnosis of carcinoma. Extraovarian peritoneal and lymph node implants may be present at the time of detection. The extraovarian serous implants are classified according to the WHO as invasive or noninvasive, epithelial or desmoplastic, on the basis of the interface between the implant and normal tissue. The micropapillary variant of serous borderline tumors is more frequently associated with bilaterality, ovarian surface involvement and extraovarian implants, some of which may be invasive. The course of disease is indolent. Tumor stage is an important prognostic factor; invasive extraovarian implants confer a comparatively poor prognosis. Serous borderline tumor cells are immunoreactive for CK7, EMA, WT1, CA125 while are CK20 negative. Point mutations in BRAF or K-RAS are frequently associated with serous borderline tumors, but no association with germ line or somatic BRCA1/BRCA2 mutations has been reported.

Differential Diagnosis

- Serous borderline tumor with focal proliferation
- Serous adenocarcinoma
- Well-differentiated papillary mesothelioma
- Struma ovarii
- Mucinous borderline tumor, endocervical type

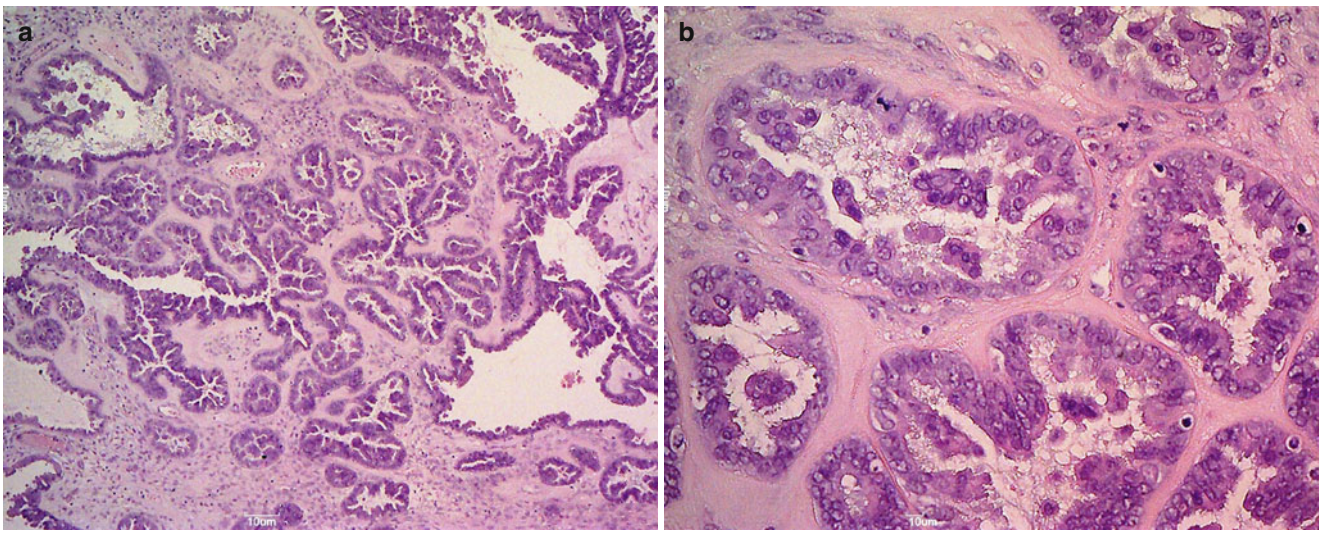

Fig. 6 Serous borderline tumor: the lining cells are tall to columnar with stratification (**a**); mild–moderate atypia and sparse mitosis are present (**b**)

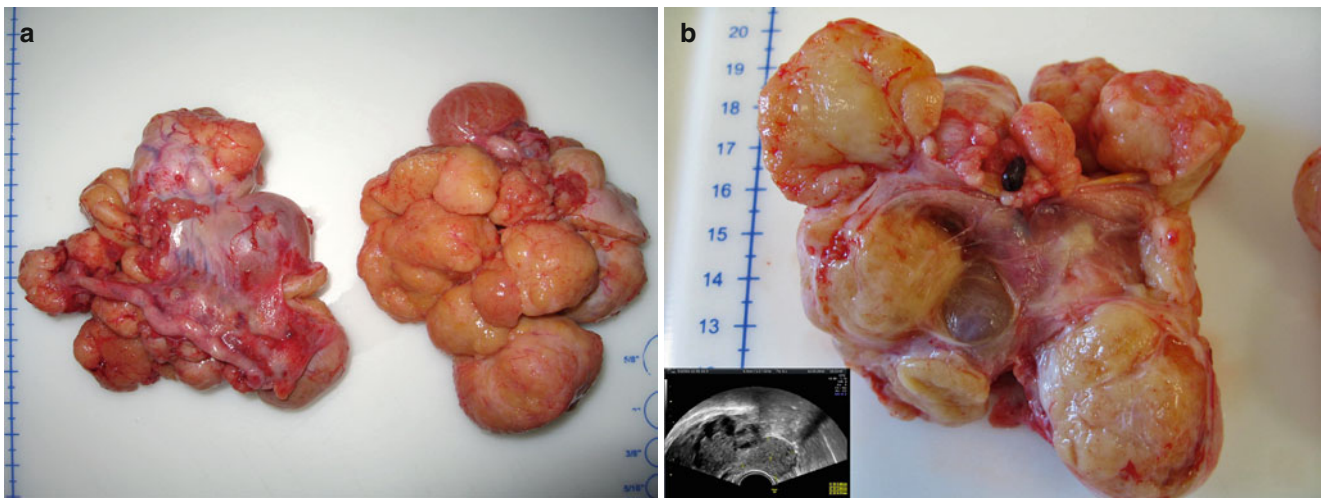

Fig. 7 Bilateral serous adenocarcinoma: solid masses replace both ovaries (**a**); cut surface shows also areas of necrosis; perfect concordance with the transvaginal scan (**b**)

Serous Adenocarcinoma

Serous carcinoma comprises 35 % of all ovarian tumors, the incidence peak being in the sixth to seventh decades. At the time of diagnosis, pelvic ovarian masses, peritoneal spread and ascites are present. Serous carcinoma forms solid and cystic masses (Fig. 7) that frequently show areas of necrosis and hemorrhage. At microscopy, complex papillae, glands with malignant cellular stratification, and psammoma bodies are observed. The immunohistochemical profile is similar to that typically found in benign and borderline serous tumors. Grading, from 1 to 3 according to the WHO, is based on architectural features and nuclear atypia (Fig. 8). Molecular studies show somatic or germ line abnormalities of BRCA1/BRCA2 genes in high-grade tumors. In contrast, low-grade serous carcinoma shows a molecular profile similar to that of serous borderline tumors (BRAF or K-RAS mutation).

Differential Diagnosis

- Serous borderline tumor
- Endometrioid adenocarcinoma
- Clear cell carcinoma
- Transitional cell carcinoma
- Primary peritoneal serous carcinoma
- Peritoneal papillary mesothelioma
- Metastatic serous carcinoma of endometrium
- Metastatic breast carcinoma

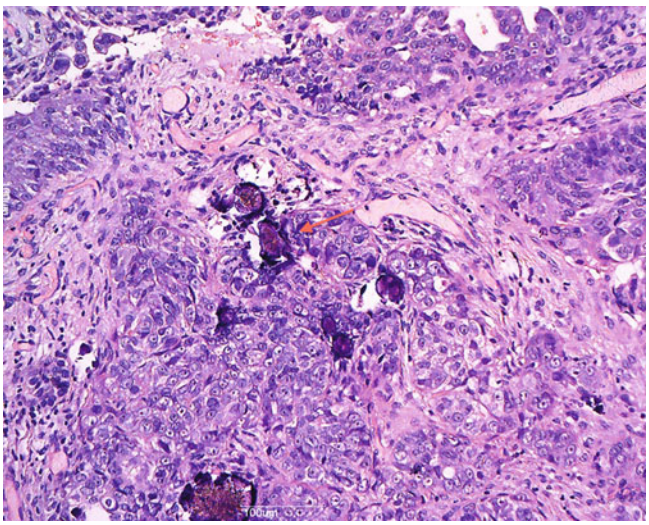

Fig. 8 High-grade serous carcinoma: solid growth with marked cytologic atypia and psammoma bodies (*arrow*)

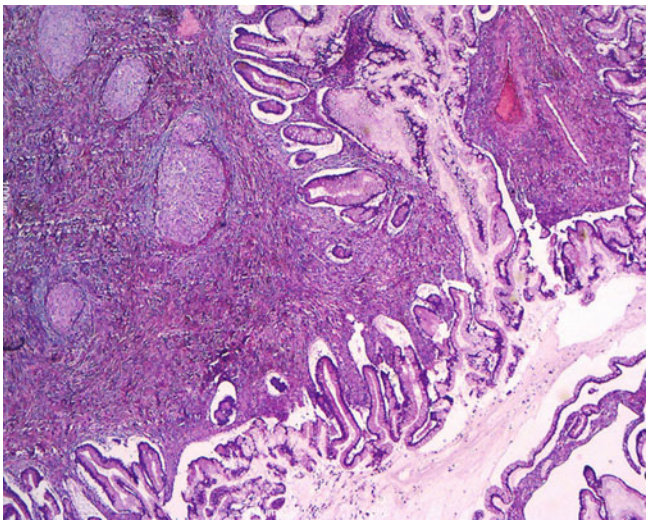

Fig. 9 Mixed tumor: mucinous borderline tumor, intestinal type, and benign Brenner tumor

Mucinous Surface Epithelial Tumors

Primary ovarian mucinous tumors include cystoadenomas, borderline or low malignant potential tumors, and carcinomas (intraepithelial and invasive). Cystoadenomas and borderline tumors are, by definition, noninvasive and are distinguished by their degree of complexity and epithelial proliferation. Frequently, in the same tumor there is a morphologic spectrum of epithelial proliferations which include benign, borderline, and malignant features; therefore, an appropriate histological sampling is very important for a correct diagnosis. Mucinous tumors with the same histological features can also occur in extraovarian sites; ovarian metastases from tumors of gastrointestinal and biliary tract can simulate primary ovarian mucinous carcinoma. Even with the aid of ancillary immunohistochemical techniques, and in expert hands, distinction of primary from metastatic mucinous carcinoma may be very difficult. Mucinous epithelial tumors may coexist with Brenner tumors (Fig. 9): it has been suggested that the majority of intestinal-type mucinous tumors arise from Brenner tumors or transitional cell nests.

Benign Mucinous Tumors (Cystoadenoma, Cystoadenofibroma, and Adenofibroma)

Benign mucinous tumors are composed of intestinal-type or endocervical-like mucinous epithelium. They account for the majority of mucinous ovarian tumors (80 %). They are unilocular or multilocular tumors of variable size, ranging from a few to over 30 cm. They are typically unilateral; the capsula is thick and white with a smooth outer surface. Mucinous cysts contain gelatinous material and are composed of glands and cysts lined by columnar, pale-staining epithelium; stratification and atypia are absent (Fig. 10).

Mucinous Borderline Tumor (Mucinous Tumor of Low Malignant Potential)

Two histological types of mucinous borderline tumors are distinguished: intestinal type and endocervical-like. The first type (Fig. 11) is a large, multicystic and unilateral (>95 %) tumor lined by stratified intestinal-type epithelium with papillary intraglandular growth, mild to moderate nuclear atypia, and rare mitoses. Stromal invasion is absent (Fig. 12). Intestinal-type mucinous borderline tumors at immunohistochemistry are CEA positive, CA125 negative, CK7 and CK20 positive. At presentation, most of them are stage I and have a benign clinical course. Patients with associated peritoneal implants, foci of intraepithelial carcinoma, or stromal microinvasion have an excellent prognosis (100 % survival). Recent studies show that advanced stage intestinal-type mucinous borderline tumors with adverse outcome represent in fact metastases from occult extraovarian primary tumors.

Differential Diagnosis

- Mucinous cystoadenoma with focal proliferation
- Mucinous adenocarcinoma
- Metastatic adenocarcinoma (appendix, colon, stomach, pancreatobiliary tract, cervix, lung)

In contrast to intestinal-type mucinous borderline tumors, endocervical-like neoplasms are less common, usually smaller, frequently bilateral and associated with endometriosis. Tumor cells are CK7 positive and CK20 negative. These tumors are often admixed with a component of serous borderline tumor.

Differential Diagnosis

- Serous borderline tumor
- Mucinous borderline tumor, intestinal type

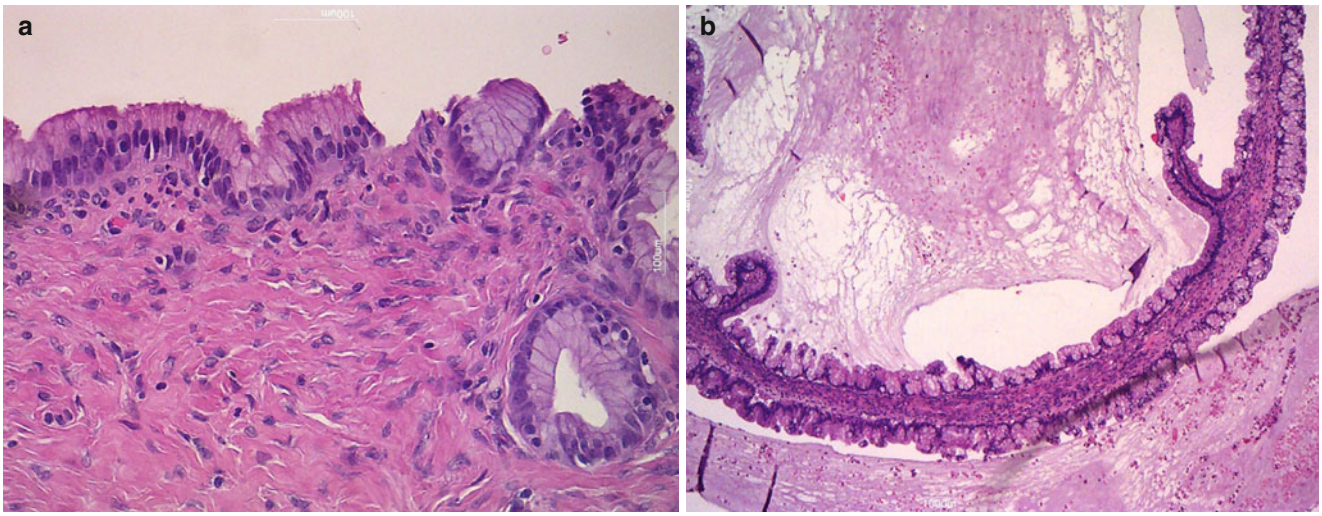

Fig. 10 Mucinous cystoadenoma. The cysts are lined by simple nonstratified mucinous epithelium (**a**) and contain thick gelatinous material (**b**)

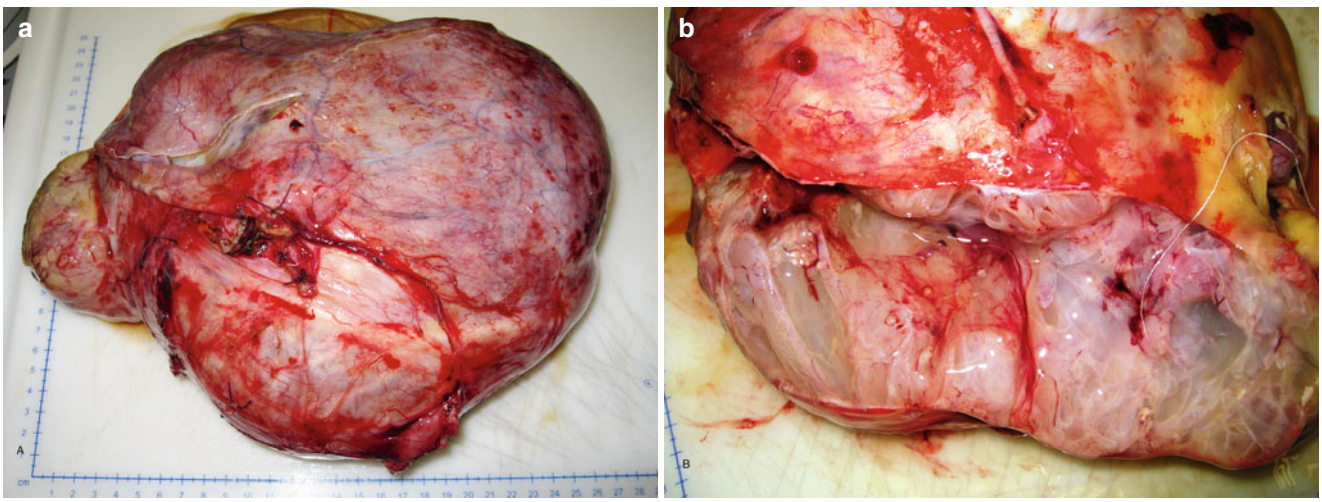

Fig. 11 Mucinous borderline tumor, intestinal type: large ovarian mass (**a**); multiloculated cysts contain mucoid material (**b**)

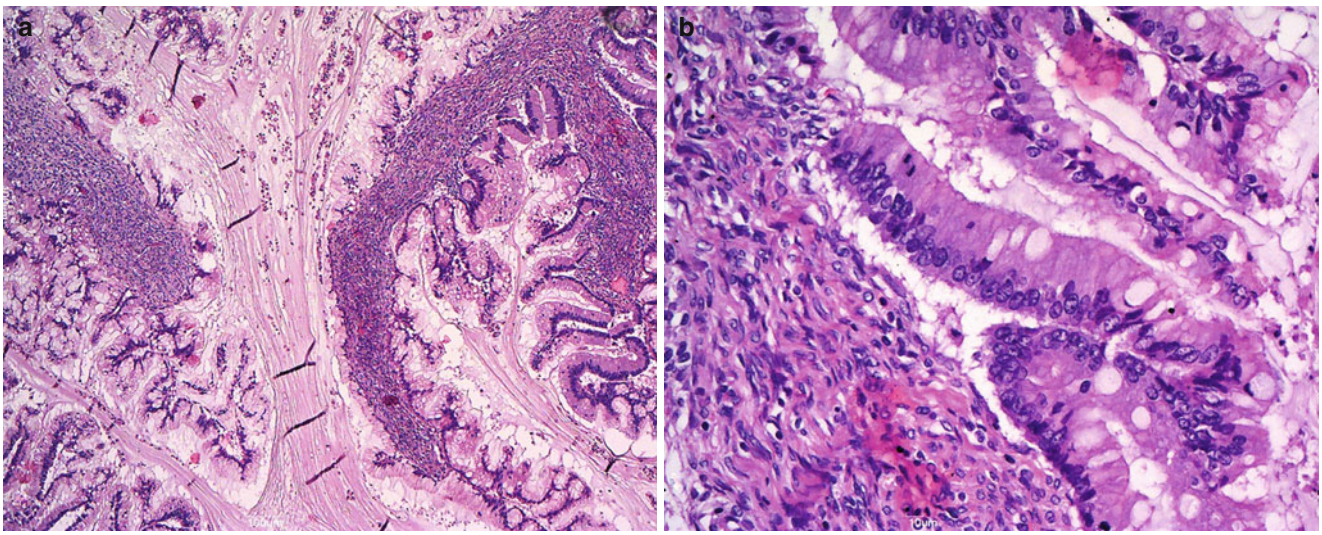

Fig. 12 Mucinous borderline tumor, intestinal type: complex papillary folds (**a**); intestinal-type epithelium with goblet cells, mild to moderate cytologic atypia, and focal mitoses (**b**)

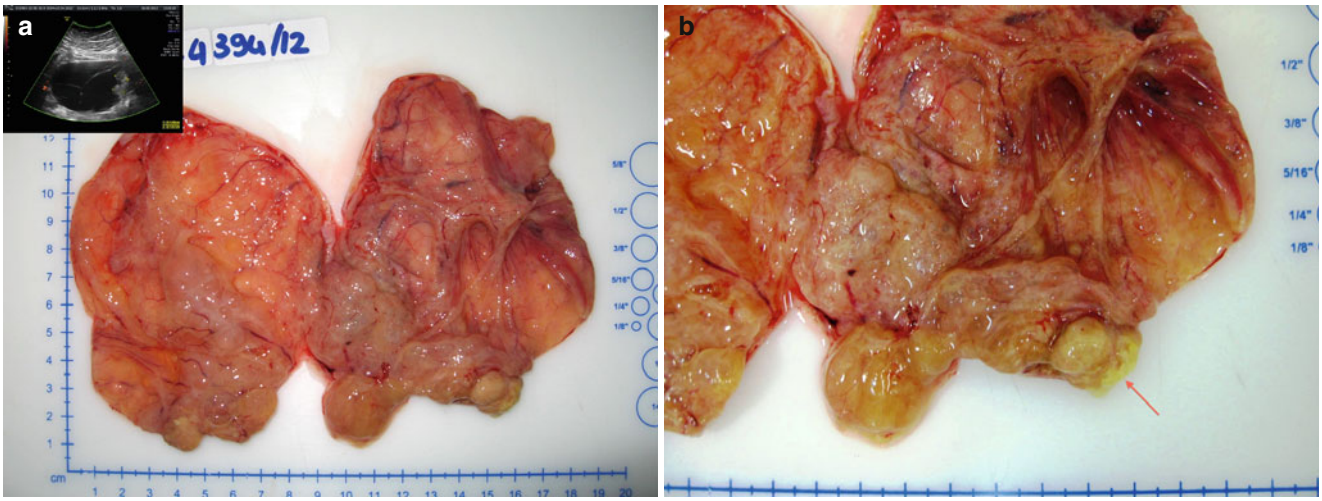

Fig. 13 Mucinous carcinoma: on cut surface the tumor is partly cystic multiloculated filled with mucoid material (perfect concordance with the transvaginal scan) (**a**) partly solid with areas of necrosis (*arrow*) (**b**)

Mucinous Adenocarcinoma

Mucinous adenocarcinomas are <15 % of all mucinous ovarian tumors and most of them are stage I at presentation. The tumoral masses are solid and cystic and may contain foci of necrosis and hemorrhage (Fig. 13). Ovarian surface involvement is rare but large tumors may present capsular rupture. Different patterns of stromal invasion can be recognized in intestinal-type adenocarcinoma: (1) confluent or expansile pattern (complex, crowded, confluent glands with cytologic atypia and little stroma) (Fig. 14); (2) infiltrative and destructive pattern (Fig. 15), more frequent in metastatic tumors. Areas of benign, borderline, and invasive mucinous carcinoma coexist in the same tumor (Fig. 16). Immunohistochemical profile is similar to that of borderline tumors (CK7+, CK20+, CEA+). The stage is the most important prognostic factor. Grading of mucinous carcinomas has not been precisely defined yet, but the nuclear features are the best discriminator; tumors with glandular and papillary architecture are low grade.

Differential Diagnosis

- Metastatic adenocarcinoma (appendix, colon, stomach, pancreatobiliary tract, cervix, lung)
- Mucinous borderline tumor

Mucinous Tumors Associated with Pseudomyxoma Peritonei (PMP)

Mucoid noninvasive nodules adherent to peritoneal surface characterize PMP. Low-grade neoplastic mucinous epithelium with pools of extracellular mucin and fibrosis is their typical morphologic appearance. Many studies show that all cases of PMP derive from low-grade mucinous tumors of the appendix and that ovarian involvement is secondary ("metastatic mucinous tumor").

Endometrioid Surface Epithelial Tumors

The majority of endometrioid ovarian tumors are carcinomas (75 %). Benign and borderline endometrioid tumors are uncommon. Many of them arise from malignant transformation of ovarian endometriosis (Fig. 17). Endometrioid carcinomas are associated with synchronous low-grade endometrioid carcinoma of the endometrium in 15–20 % of cases. Borderline tumors and carcinomas may be monolateral or bilateral; they can be cystic with intracystic solid nodules. Areas of hemorrhage and necrosis are found in carcinomas. Endometrioid tumors are composed of endometrial-type glands and stroma. Endometrioid borderline tumors, according to the WHO classification, are composed of atypical endometrioid-type glands in a dense stroma without stromal invasion. Ovarian endometrioid adenocarcinoma is usually comparable to FIGO grade 1 or 2 endometrioid endometrial carcinoma (Fig. 18) and grading system is the same as for endometrial carcinoma; squamous metaplasia is common. At immunohistochemistry, endometrioid tumors are positive for CK7, ER and PR, negative for CK20, alpha-inhibin and calretinin. The most common genetic abnormalities in sporadic ovarian endometrioid carcinoma are somatic mutations of beta-catenin and PTEN.

Differential Diagnosis

- Serous adenocarcinoma
- Sex cord-stromal tumors
- Carcinoid tumor
- Metastatic colorectal or endometrial carcinoma
- Polypoid endometriosis
- Diffuse granulosa cell tumor
- High-grade carcinoma

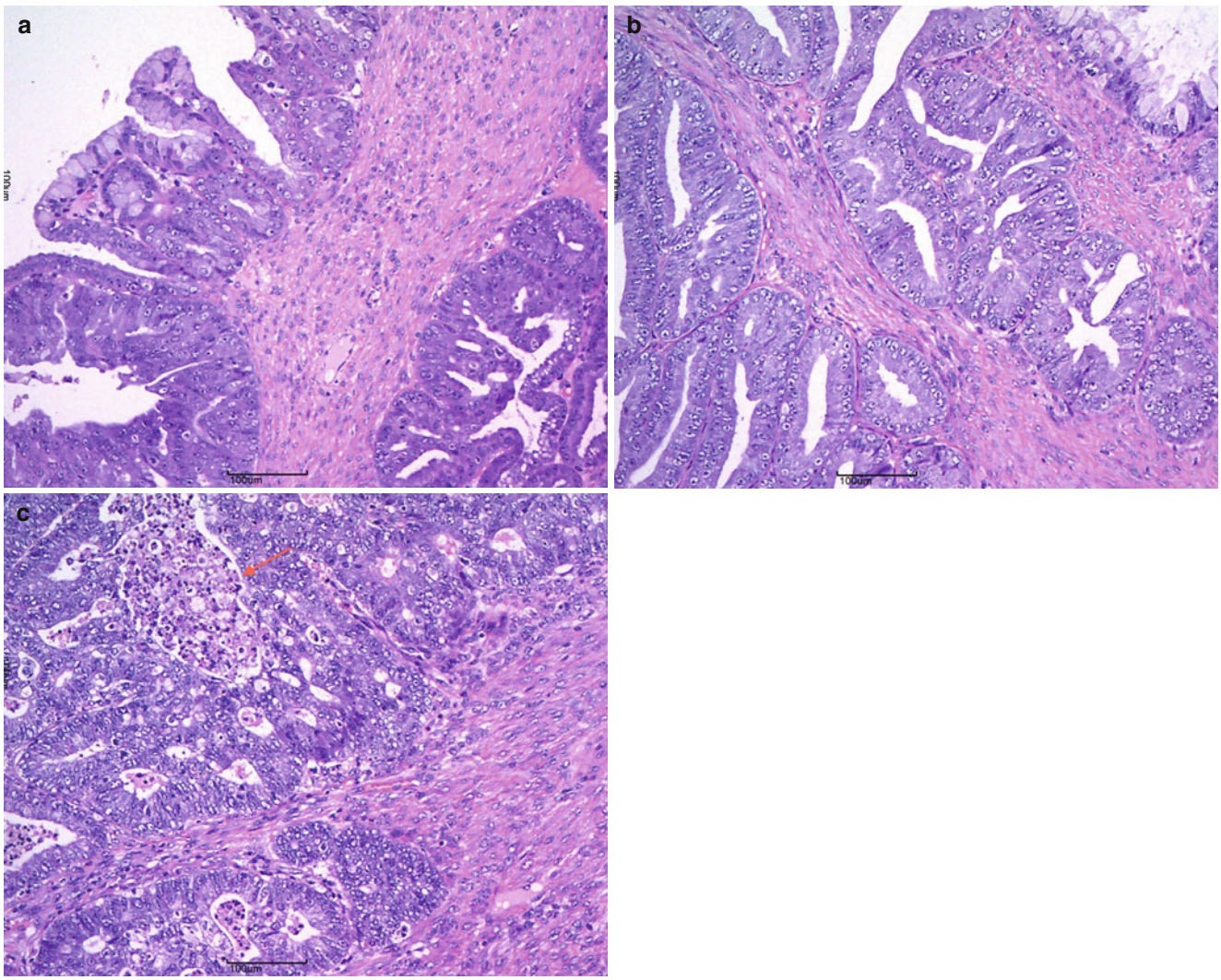

Fig. 14 Mucinous carcinoma: expansile pattern of invasion (**a**); complex interconnecting neoplastic glands (**b**); cribriform pattern with marked cytologic atypia and necrotic debris in gland lumens (*arrow*) (**c**)

Clear Cell Surface Epithelial Tumors

The vast majority of clear cell surface epithelial tumors are malignant (99 %). Benign and borderline clear cell adenofibromatous tumors are very rare and are composed of firm tissue with small cysts (Fig. 19), showing, on cut surface, a fine honeycomb appearance. Clear cell carcinomas present frequently as a unilocular cyst containing a solid mass with foci of necrosis and hemorrhage (Fig. 20). Clear cell carcinomas are frequently associated with endometriosis (70–80 %), and one-fourth of cases arise in endometriotic cysts as a single fleshy nodule. Tumor architecture is usually an admixture of tubulocystic, papillary, and solid patterns. At microscopy clear cell tumors are composed of epithelial cells with abundant glycogen-rich cytoplasm and hobnail cells with scant cytoplasm and nuclei protruding into the lumens of cystic spaces (Fig. 21). All clear cell carcinomas are considered high grade.

Differential Diagnosis

- Yolk sac tumor
- Metastatic renal carcinoma
- Endometrioid carcinoma
- Serous adenocarcinoma
- Juvenile granulose cell tumor

Transitional Cell Surface Epithelial Tumors

Transitional cell tumors are composed of transitional (urothelial)-type epithelium and comprise 2 % of all surface epithelial tumor of the ovary. Ninety-nine percent of them are benign (Brenner tumor). Transitional borderline and malignant tumors are very uncommon (<1 %). Malignant tumors can be diagnosed only if associated with benign and borderline Brenner tumors or transitional cell carcinomas (non-Brenner type). Many benign Brenner tumors are microscopic incidental findings at laparotomy for other

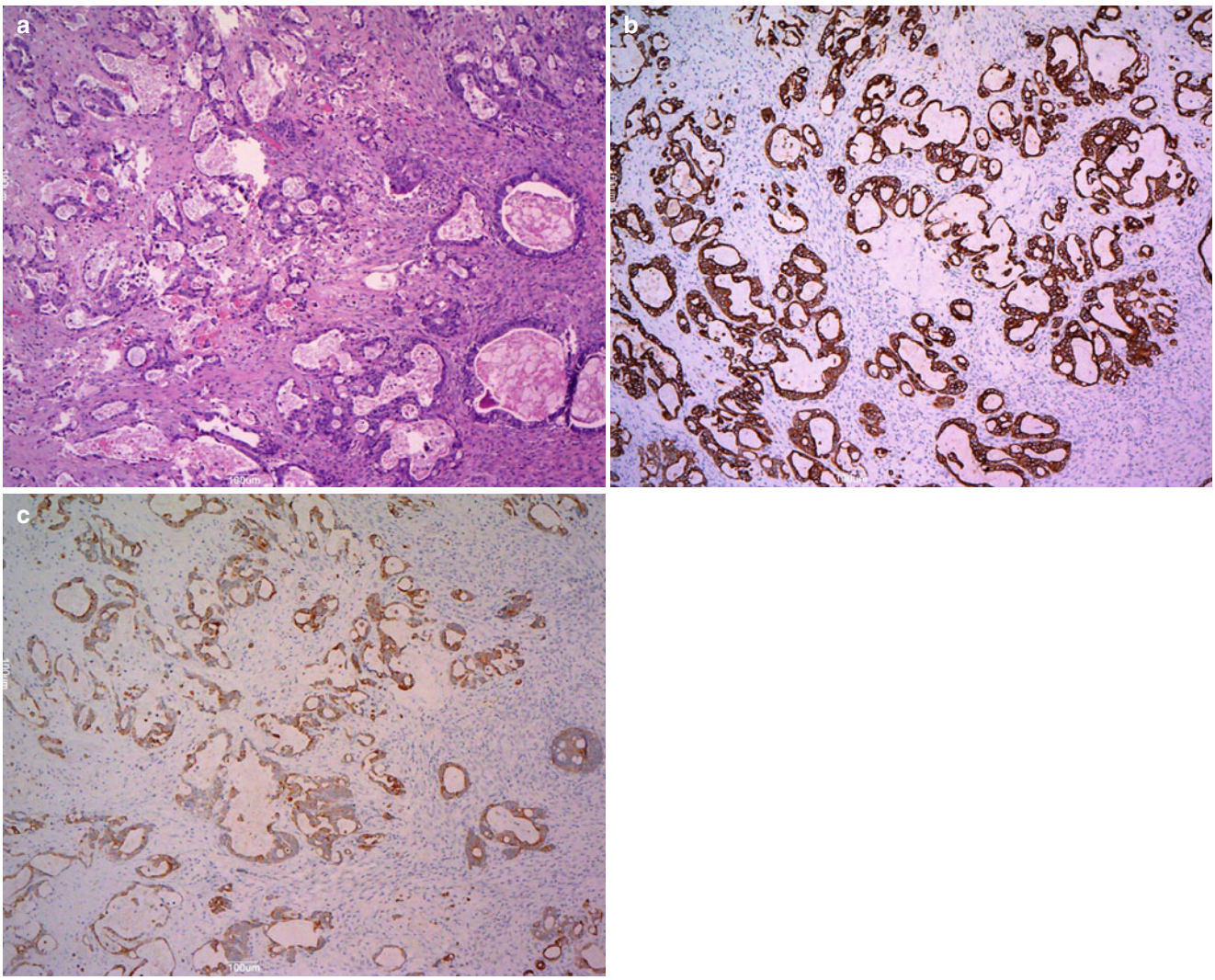

Fig. 15 Mucinous carcinoma: infiltrative pattern of stromal invasion (**a**); the tumor cells show strong and diffuse positivity for CK20 (**b**) and CK7 (**c**)

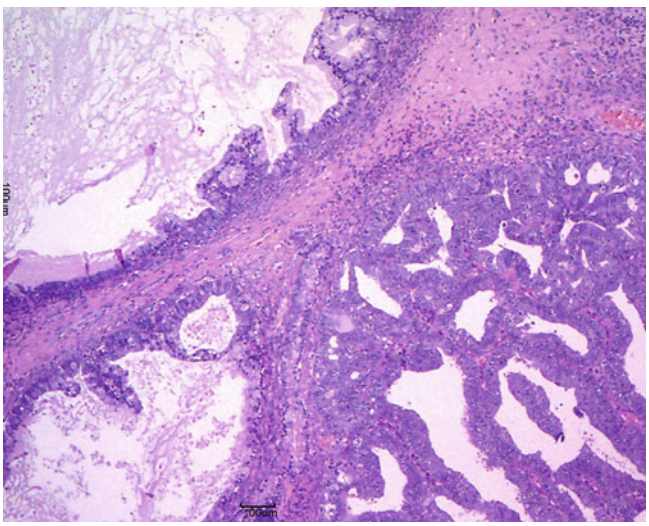

Fig. 16 Mucinous carcinoma: areas of borderline tumor adjacent to areas of carcinoma

pathological conditions; tumor size may vary from <2 up to 20 cm. They are well-circumscribed solid masses of yellow or white tissue comprising small cysts and dystrophic calcifications. At microscopy, nests of transitional cells, often with nuclear grooves (coffee bean), are enmeshed in a prominent fibromatous stroma (Fig. 22). Borderline tumors are larger solid and cystic masses, with endophytic or exophytic nodules in the cystic wall. Malignant Brenner tumors have similar histological features but areas of necrosis and hemorrhage are also present. Benign and borderline tumors may be associated with a mucinous cystic tumor. At immunohistochemistry, transitional cell tumors express cytokeratin, CK7, EMA and WT1; CK20 is negative, whereas transitional cell tumors of the urinary tract are CK7 and CK20 positive.

Differential Diagnosis

- Benign Brenner tumor d.d. with endometrioid adenofibroma

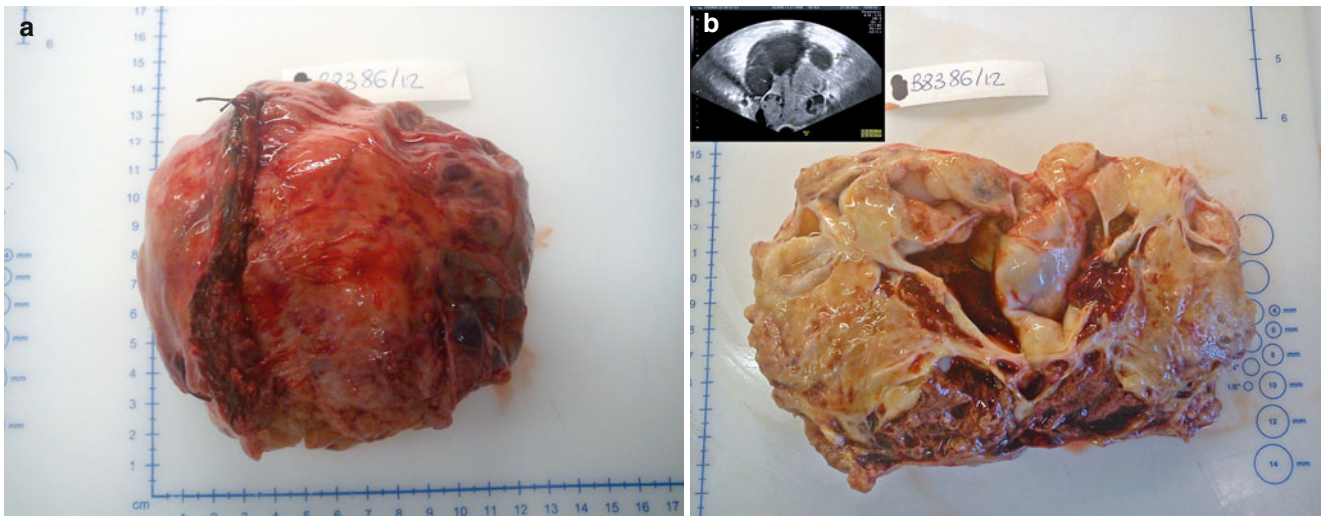

Fig. 17 Endometrioid adenocarcinoma: large unilateral ovarian mass with capsule rupture (**a**); on cut surface the tumor shows cystic and solid areas, hemorrhage and necrosis; the transvaginal scan shows the same large ovarian multilocular-solid tumor (**b**)

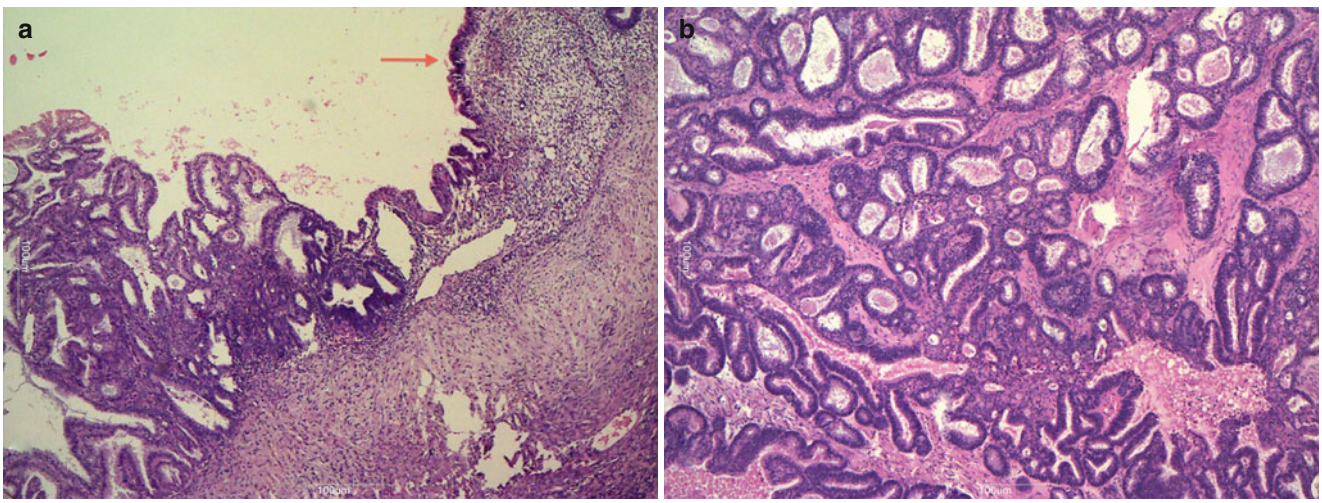

Fig. 18 Endometrioid adenocarcinoma associated with endometriosis (*arrow*) (**a**); FIGO grade 1 endometrioid carcinoma (**b**)

- Borderline Brenner tumor d.d. with benign and malignant Brenner tumor and metastatic papillary urothelial carcinoma
- Malignant Brenner d.d. with metastatic papillary urothelial carcinoma, undifferentiated carcinoma, granulosa cell tumors and serous carcinoma

Undifferentiated Surface Epithelial Tumors

Undifferentiated surface epithelial tumors are high-grade carcinomas lacking histological features of a specific müllerian cell type. They are frequently bilateral and advanced stage at presentation. At microscopic examination, they show a solid growth pattern. The neoplastic cells are pleomorphic; they have a high mitotic index; necrosis and hemorrhage are present.

Mixed Surface Epithelial Tumors

Mixed surface epithelial tumors are prevalently malignant tumors (90 %). They have at least a 10 % component of one or more types of müllerian differentiation. Only 10 % are borderline tumors and benign tumors are uncommon (1 %).

Sex Cord-Stromal Tumors of the Ovary

According to the WHO classification (2003) these tumors are divided into four groups: (1) granulosa stromal cell tumors composed of various combination of granulosa cells, theca cells and fibroblasts; (2) Sertoli stromal cell tumors composed of testicular-type cells; (3) sex cord-stromal

tumors of mixed cell types; (4) steroid cell tumors. These tumors may be associated with estrogenic or androgenic manifestations.

Granulosa Stromal Cell Tumors

Granulosa stromal cell tumors are classified, on the basis of different combinations of granulosa cells, theca cells, and fibroblasts, in granulosa cell tumors (adult or juvenile), thecoma, fibroma, and other very rare tumors.

- Adult granulosa cell tumor (AGCT) is the most frequent (95 %) and accounts for 2–3 % of all primary ovarian tumors. Estrogen production by tumor cells causes frequently menometrorrhagia, postmenopausal bleeding due to endometrial hyperplasia or adenocarcinoma, or prepuberal patients' isosexual pseudoprecocity. The majority of AGCT are unilateral and range in size from few up to 30 cm. They are solid or solid and cystic, with a yellow to white cut surface and cystic hemorrhagic areas. The neoplastic cells have scant cytoplasm and round or oval nuclei with grooves. These cells are enmeshed in a fibrothecomatous background and may show, within the same tumor, different growth patterns: diffuse, trabecular, microfollicular (Call–Exner bodies), and insular. The cytologic atypia is usually mild, and mitotic activity is low (Fig. 23). The immunohistochemical profile of neoplastic cells shows inhibin, calretinin, vimentin, WT1 and CD99 positivity, and EMA and CK7 negativity. Other markers show variable positivity. Tumor stage is the most important prognostic factor, but tumor rupture, size, and mitotic activity may have prognostic value.

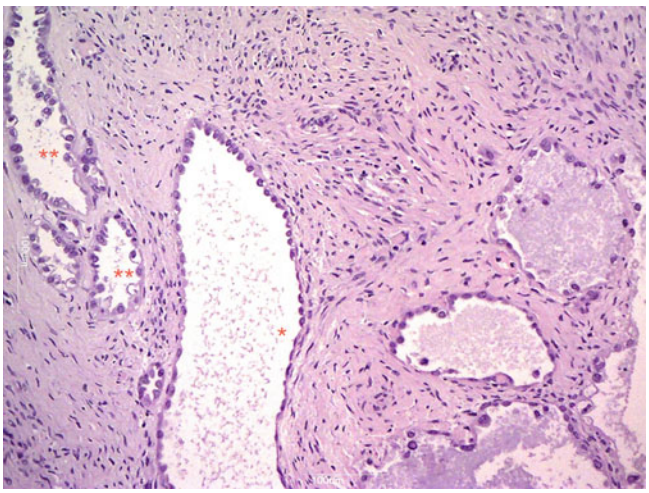

Fig. 19 Borderline clear cell adenofibroma: cystic glands, separated by fibromatous stroma, are lined by flat (*) or hobnail cells with clear cytoplasm (**)

Differential Diagnosis

- Endometrial stromal sarcoma (primary or metastatic)
- Undifferentiated carcinoma
- Endometrioid adenocarcinoma with sex cord-like differentiation
- Carcinoid tumor
- Thecoma
- Metastatic breast carcinoma

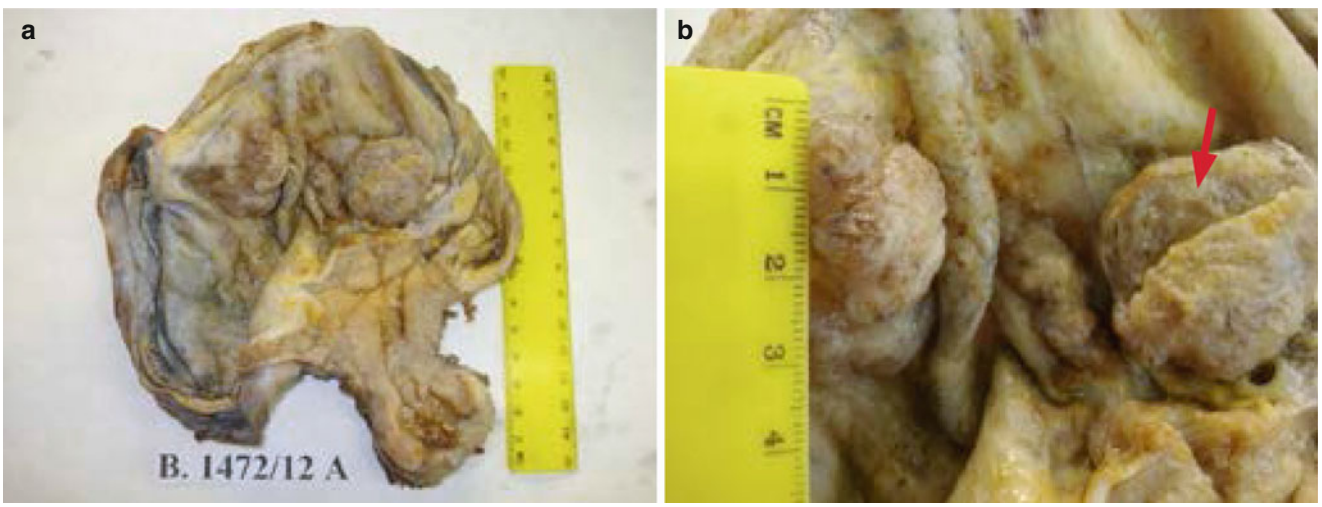

Fig. 20 Clear cell carcinoma associated with endometriosis: fleshy nodules in an endometriotic cyst with capsular adhesion to the uterus (**a**); the cut surface of nodules (*arrow*) shows microcystic appearance (**b**)

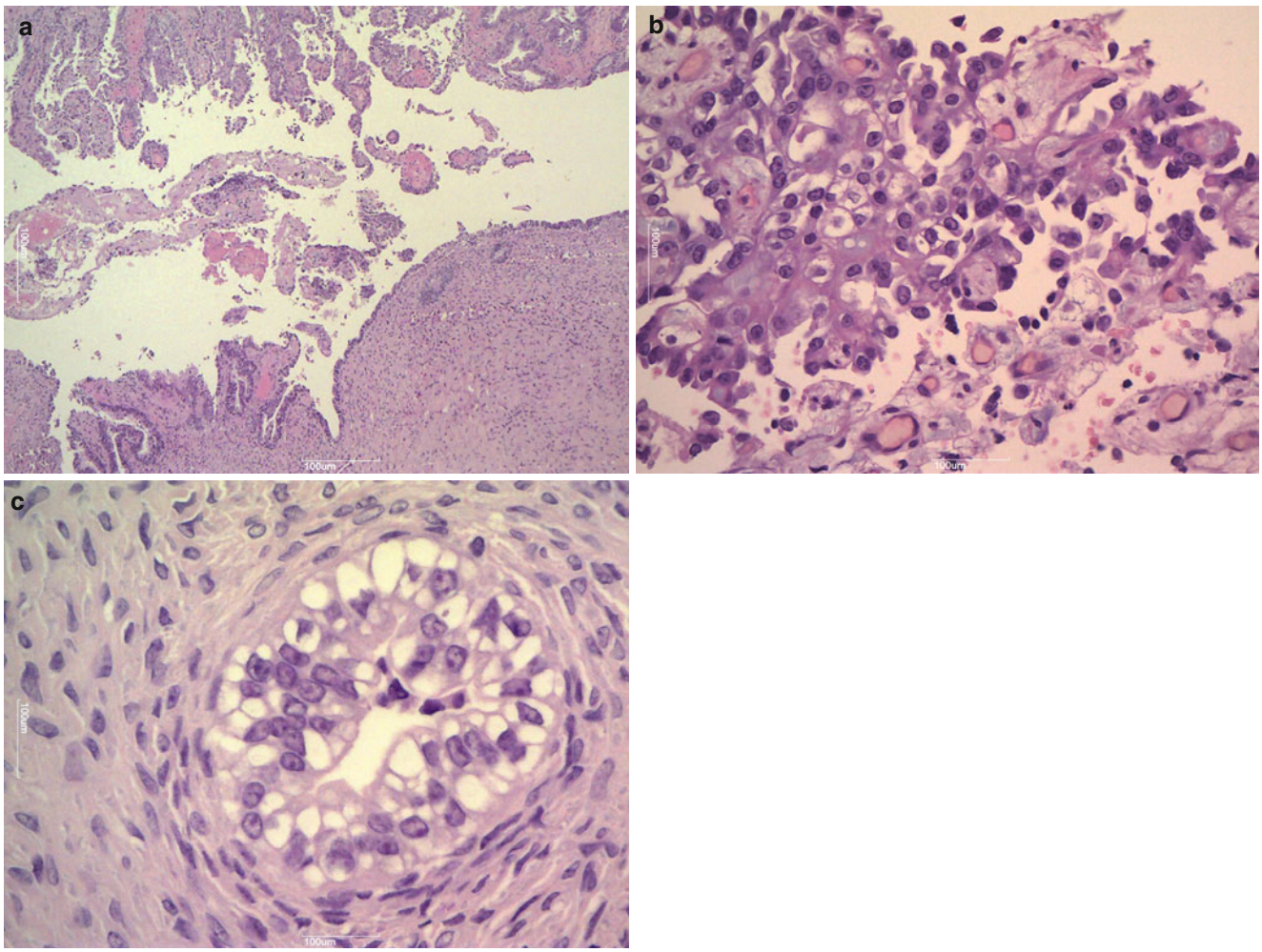

Fig. 21 Clear cell carcinoma: tubulocystic and papillary architecture (**a**); nuclear pleomorphism (**b**); polyhedral cells with abundant clear cytoplasm (**c**)

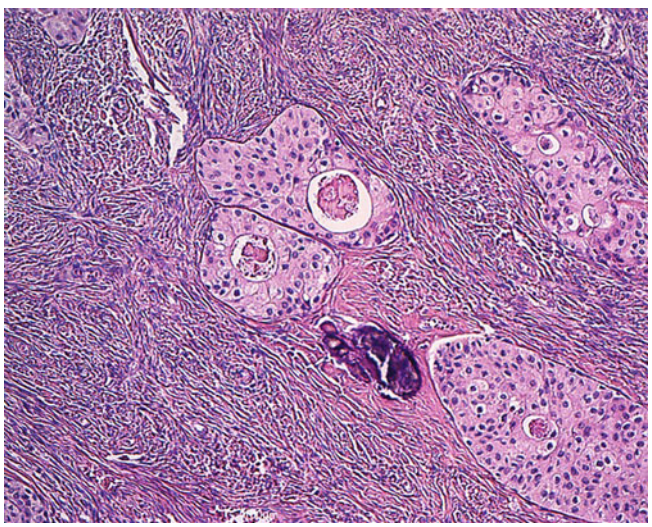

Fig. 22 Benign Brenner tumor: nests of transitional cells are enmeshed in prominent fibromatous stroma; small cysts and dystrophic calcifications are present

- Juvenile Granulosa Cell Tumor (JGCT). The majority (97 %) of JGCT are found before 30 years, and 40 % of them are diagnosed in prepuberal patients. The tumor is a unilateral mass (98 %), and tumor stage is the most important prognostic factor. Most recurrences are found within 3 years from initial surgery, and high-stage tumors are often fatal. The tumors are solid and cystic and have a lobulated, gray-white to tan-yellow cut surface. Hemorrhage and necrosis may be present. At microscopy, diffuse or nodular proliferation of granulosa cells in a myxoid or edematous background is observed. These cells form irregular follicle-like spaces, and the tumor nodules are frequently hyalinized. The immunohistochemical profile is similar to that found in AGCT.

Differential Diagnosis

– AGCT
– Thecoma
– Yolk sac tumor

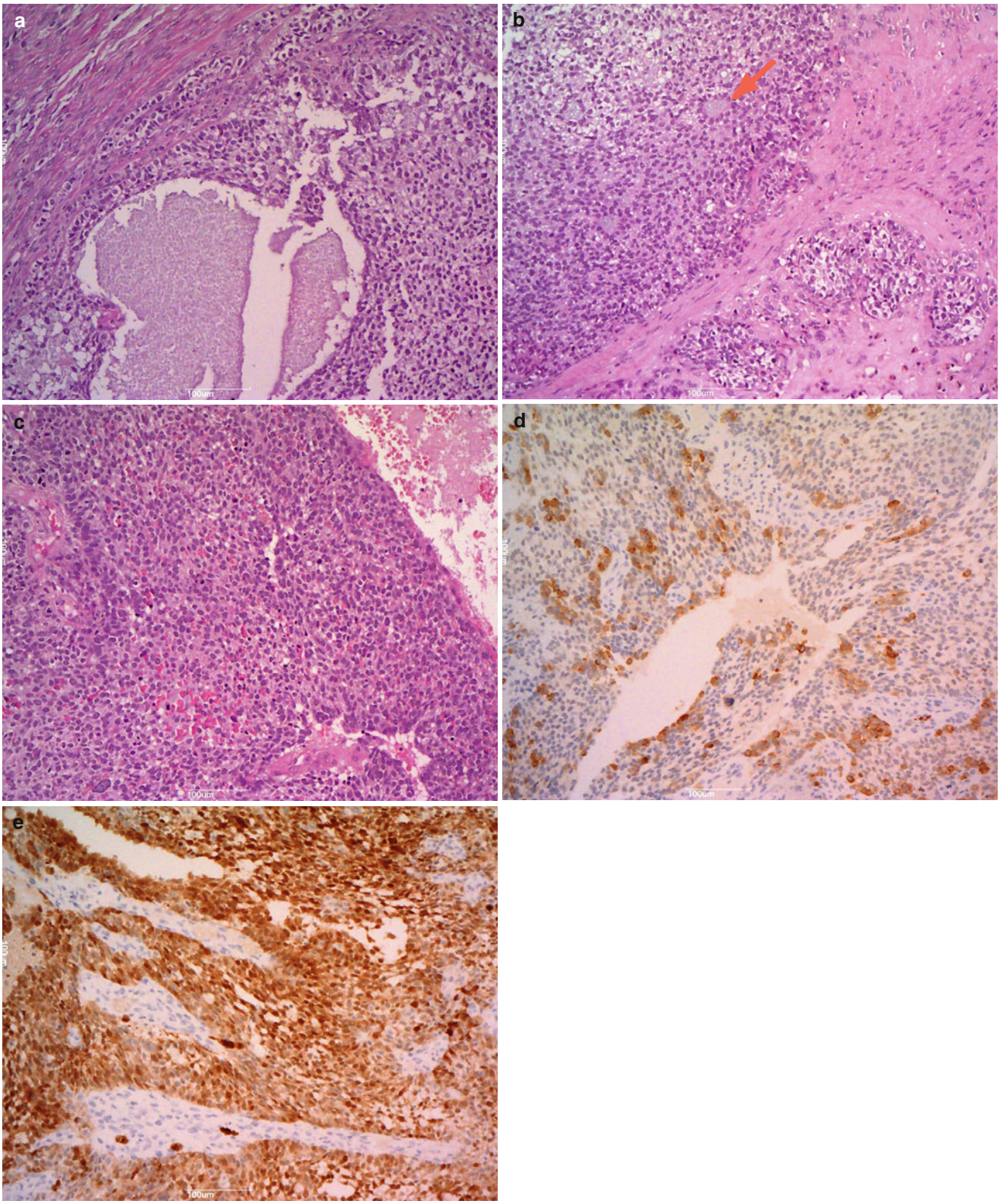

Fig. 23 Adult granulosa cell tumor: the neoplastic cells have a diffuse and macrofollicular growth pattern (**a**) or solid and microfollicular (Call–Exner bodies, *arrow*) pattern (**b**) and show mild atypia and low mitotic activity (**c**). Tumor cells exhibit inhibin (**d**) and calretinin (**e**) expression

  - Small cell carcinoma of hypercalcemic type
  - Clear cell carcinoma
  - Metastatic and primary melanoma
- Thecomas occur mostly in postmenopausal women and are commonly estrogenic. Most women present abnormal vaginal bleeding and 20 % of them develop endometrial adenocarcinoma. These tumors are unilateral and solid masses, have a lobulated, tan-yellow cut surface, and sometimes show cystic changes; hemorrhage and necrosis are present. At microscopy, thecomas are composed of nodular aggregates of oval to round cells with abundant pale to vacuolated cytoplasm, alternating with spindled cells and hyaline plaques. Focal lutein cells can be present. Thecoma is a benign tumor. Malignant transformation occurs very rarely.
- Fibroma is benign and is the most common sex cord-stromal tumor (70 %). Fibromas are usually unilateral and range in size from microscopic up to 20 cm. These tumors are well-circumscribed solid masses and have a white to yellow cut surface. At histology, fibromas are composed of spindle cells organized in intersecting fascicles or in a storiform pattern with a variable edematous and fibromatous component. There is minimal cytologic atypia and mitotic activity is rare.

Fibrosarcoma, stromal tumor with minor sex cord elements, sclerosing stromal tumor, and signet-ring stromal tumor are the other very rare granulosa stromal cell tumors.

Sertoli Stromal Cell Tumors

Sertoli stromal cell tumors are composed of testicular-type cells. This category includes:

(a) Sertoli–Leydig cell tumors (well differentiated, intermediate differentiation, poorly differentiated, retiform with heterologous elements). They account for <1 % of ovarian tumors and occur in reproductive-age women. Typically they have a solid yellow cut surface, but the retiform variant shows a spongy cut surface.

(b) Sertoli cell tumors represent approximately 4 % of Sertoli stromal cell tumors and are usually nonfunctioning. Most are benign and can be associated with the Peutz–Jeghers syndrome. At microscopy, the tumor cells show a tubular growth pattern. The tubules are lined by cuboidal to columnar cells with abundant pale or eosinophilic cytoplasm. Diffuse or nodular growth pattern can be also observed. The stroma is fibromatous but may be hyalinized. The neoplastic cells are typically inhibin, vimentin, and keratin 8–18 positive, CK7 and EMA negative; calretinin and WT1 are frequently positive.

Differential Diagnosis

- Endometrioid carcinoma
- Well-differentiated Sertoli–Leydig cell tumor
- Carcinoid
- Tubular Krukenberg tumor

Sex Cord-Stromal Tumors of Mixed or Unclassified Cell Type and Steroid Cell Tumors

Sex cord-stromal tumors of mixed or unclassified cell type and steroid cell tumors are very rare ovarian sex cord-stromal tumors.

Germ Cell Tumors of the Ovary

These tumors arise from primordial germ cells that migrate from the yolk sac to the primitive gonadal ridge. They account for 30 % of primary ovarian tumors; 95 % are benign, mature cystic teratomas, whereas 5 % are malignant. Germ cell tumors occur in the first two decades of life and one-third of cases in this age group are malignant.

According to the WHO classification 2003, ovarian germ cell tumors are subclassified into dysgerminoma, yolk sac tumor, embryonal carcinoma, polyembryoma, choriocarcinoma, teratomas, and mixed germ cell tumors.

Dysgerminomas

Dysgerminomas are more common in the second and third decade; 10–20 % are diagnosed in pregnancy; they represent 50 % of all malignant germ cell tumors and 1 % of all malignant ovarian tumors. These tumors are morphologically identical to testicular seminoma and to extragonadal germinomas. They are large, solid, capsulated, unilateral masses which show homogeneous, lobulated, white to gray cut surface (Fig. 24). Areas of hemorrhage and necrosis can be present. At microscopy dysgerminoma is composed of a monotonous proliferation of polygonal cells with abundant cytoplasm and uniform nuclei with brisk mitotic activity that grow in islands and sheets. Variable amounts of fibrous stroma containing many lymphocytes are present (Fig. 25). Foci of other more aggressive germinal cell tumors may be found. Dysgerminoma cells (Fig. 26) typically show strong cytoplasmic and membrane immunostaining for PLAP and c-kit (CD117). They are negative for EMA, CEA, LCA, and AFP.

Differential Diagnosis

- Yolk sac tumor with solid pattern
- Embryonal carcinoma with solid pattern
- Large cell lymphoma
- Clear cell carcinoma with diffuse pattern

Yolk Sac Tumor

Yolk sac tumor represents 10–20 % of all malignant germ cell tumors, the majority being found in young women (I–II decades). The most common sign at presentation is a rapidly enlarging pelvic–abdominal mass; extraovarian diffusion is frequent. The macroscopic appearance (Fig. 27) is of a unilateral large mass (usually > 15 cm) with a smooth capsule, sometimes ruptured. The tumor shows a solid, fleshy, or cystic ("honeycomb appearance") yellow-gray cut surface.

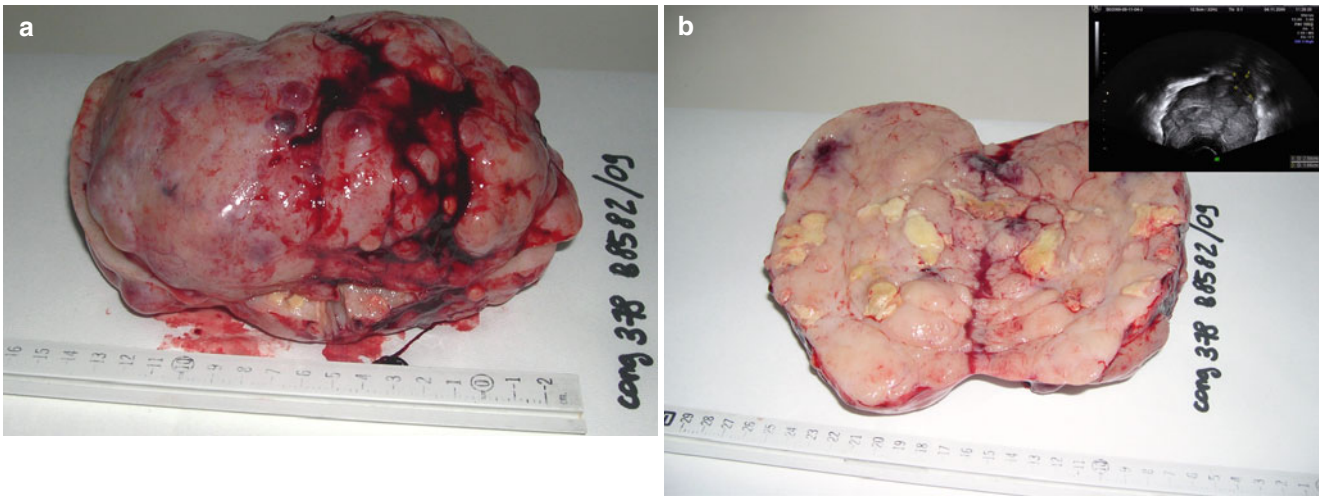

Fig. 24 Dysgerminoma: large, solid, capsulated mass (**a**), cut surface is lobulated, white to gray, with areas of hemorrhage and necrosis (perfect concordance with the transvaginal scan) (**b**)

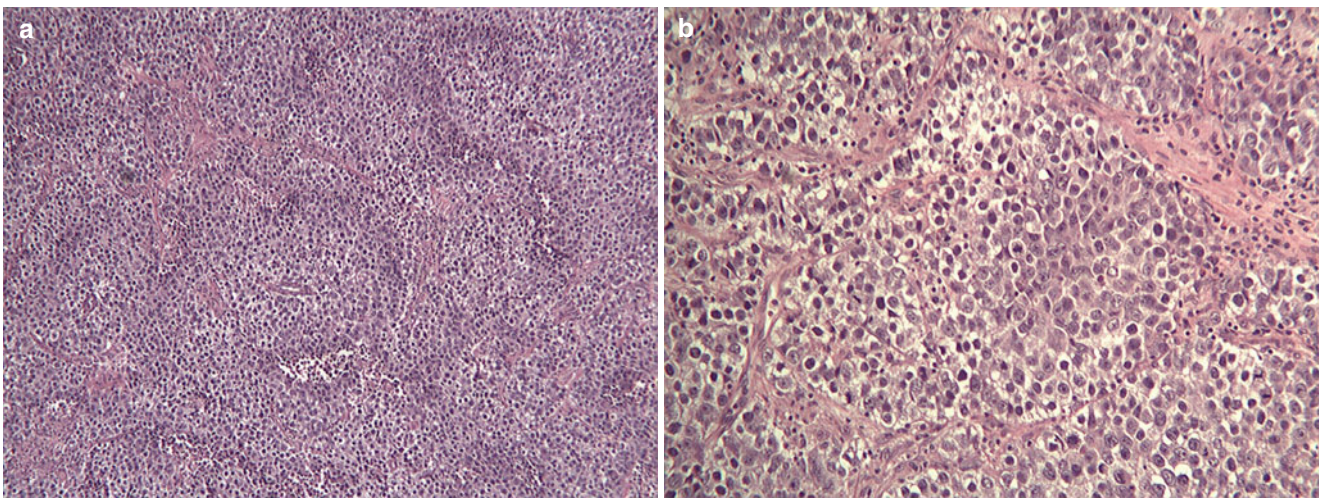

Fig. 25 Dysgerminoma: the tumor is composed of large aggregates of uniform cells (**a**); nests of tumor cells are separated by fibrous septa containing numerous lymphocytes (**b**)

Large necrotic and hemorrhagic areas are found. The neoplastic cells show in the same tumor an admixture of different growth patterns: reticular (most common), microcystic, pseudopapillary, solid, and multivesicular (Fig. 28). The neoplastic cells display clear cytoplasm and large hyperchromatic irregular nuclei with prominent nucleoli and brisk mitotic activity. The most characteristic feature is the presence of Schiller–Duval bodies (found in only one-third of tumors) and of intracytoplasmic and extracellular hyaline globules (PAS-positive diastase resistant). The tumor cells are AFP (Fig. 29), cytokeratin and CD34 positive, EMA and CK7 negative. No difference in survival rates between different histological patterns has been reported. Death occurs within 2 years from clinical presentation.

Differential Diagnosis

- Clear cell carcinoma
- Endometrioid carcinoma, secretory variant
- Dysgerminoma
- Sertoli–Leydig cell tumor, retiform variant

Embryonal Carcinoma

Embryonal carcinoma is a very rare ovarian tumor (2–3 % of malignant germ cell tumors). The neoplastic cells reproduce the primitive stage of somatic and extraembryonic differentiation. The incidence peak is in the first and second decades. The patients present with an abdominal or a pelvic mass with endocrine manifestations including

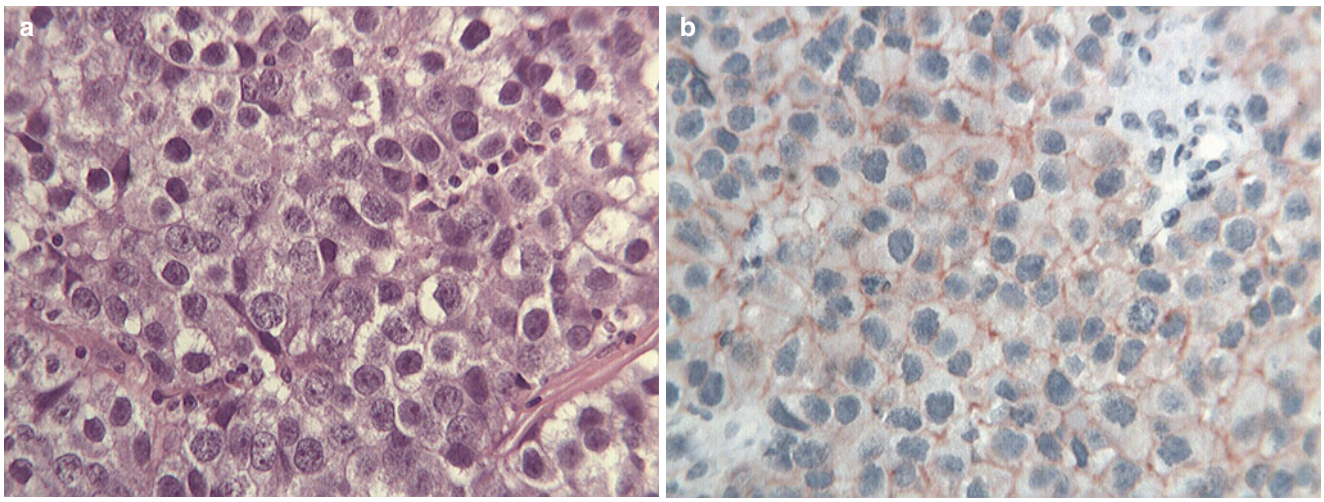

Fig. 26 Dysgerminoma: the neoplastic cells have abundant clear cytoplasm, large central nuclei, and prominent nucleoli (**a**) and show membrane staining for c-kit (CD117) (**b**)

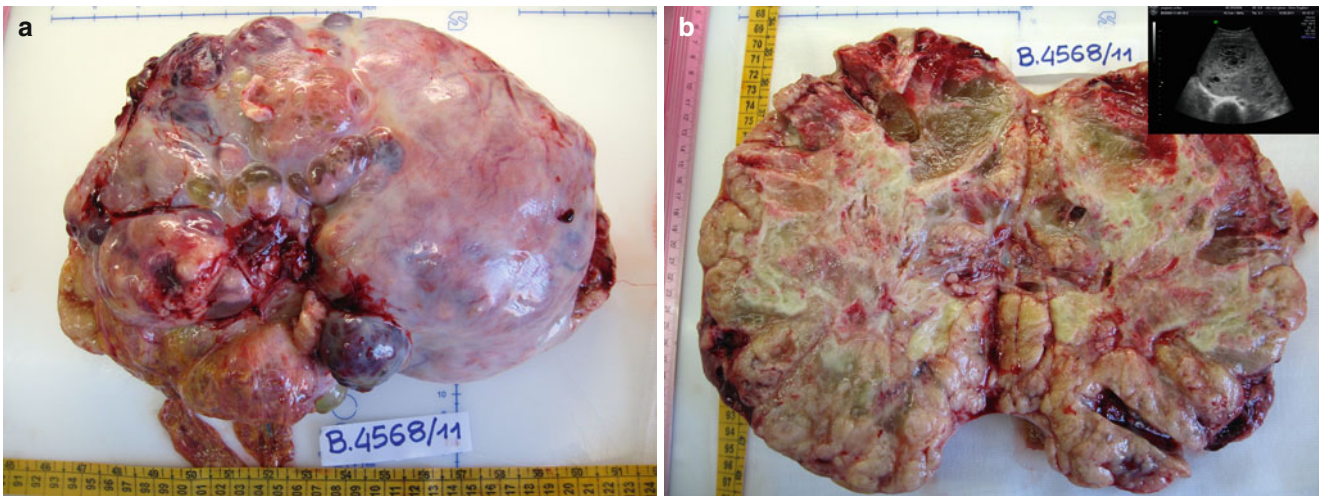

Fig. 27 Yolk sac tumor: a large mass with smooth breaking capsule and small cystic appearance (**a**); cut surface is mainly solid with cystic spaces containing gelatinous fluid (perfect concordance with the transvaginal scan) (**b**)

isosexual precocity, abnormal uterine–vaginal bleeding, amenorrhea, hirsutism, and symptoms of pseudopregnancy secondary to elevated levels of β-HCG. At the time of presentation, peritoneal diffusion is present in 50 % of cases. Embryonal carcinoma shows good response to multiagent chemotherapy after surgical conservative debulking. Grossly, the tumor is a solid, unilateral mass with many areas of necrosis and hemorrhage. At histology, tumor cells are highly pleomorphic and immunoreactive for PLAP, cytokeratins and CD30; EMA, CEA and vimentin are negative. Syncytiotrophoblast cells (β-hCG positive) are found.

Differential Diagnosis

- Dysgerminoma with solid pattern
- Yolk sac tumor with solid pattern
- Poorly differentiated carcinoma

Choriocarcinoma

Choriocarcinoma, as pure primary ovarian tumor of germ cell origin, is extremely rare (<1 % of malignant germ cell tumors). It is a highly malignant germ cell tumor and shows extraembryonic trophoblastic differentiation; it occurs only in children and young women under 20 years of age. Choriocarcinoma presents as a unilateral large abdominal or

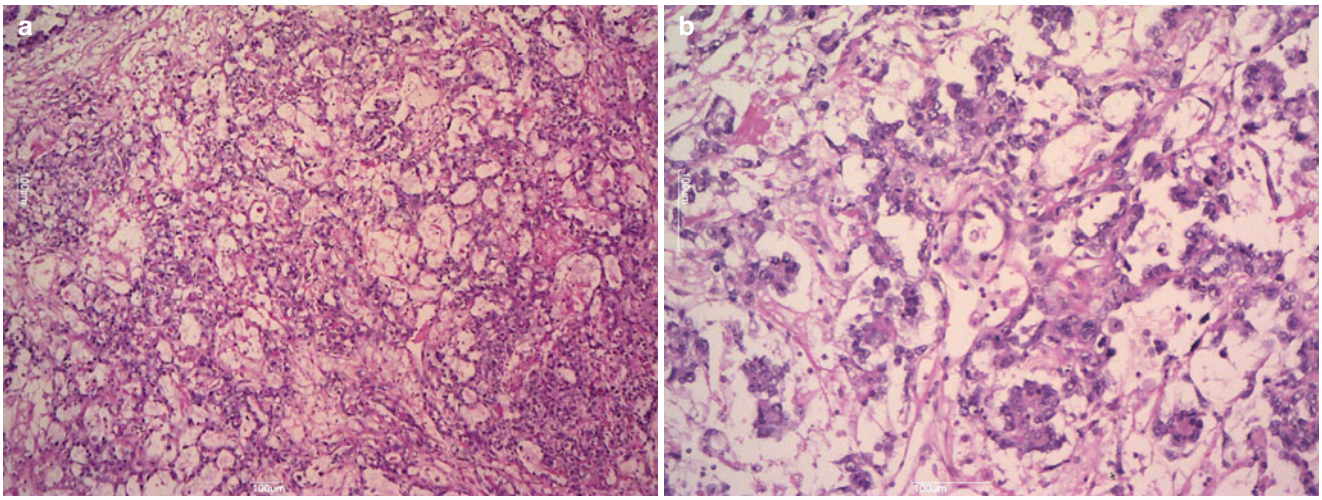

Fig. 28 Yolk sac tumor: the tumor shows an admixture of different growth patterns: reticular and microcystic patterns (**a**); glandular pattern (**b**)

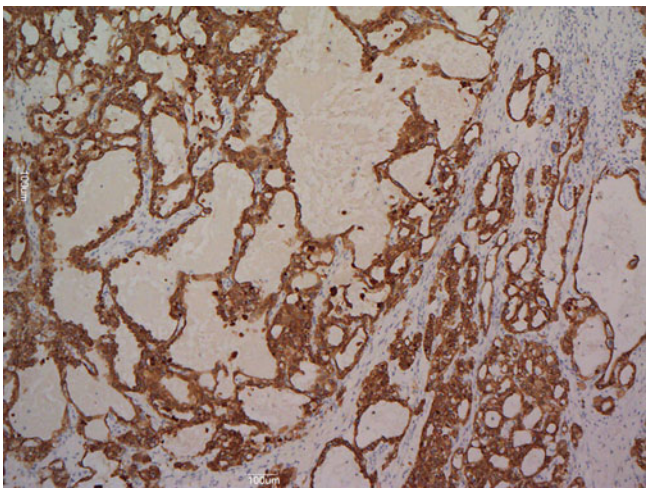

Fig. 29 Yolk sac tumor: neoplastic cells show diffuse immunoreactivity for α-fetoprotein

pelvic mass with a hemorrhagic and necrotic cut surface. Microscopically, it is defined by the presence of syncytiotrophoblast cells admixed with cytotrophoblast or intermediate trophoblast cells. By definition, chorionic villi are absent. Vascular invasion is common and extensive hemorrhage and necrosis may obscure the tumor cells. Immunohistochemical stains show strong positivity for cytokeratins in all tumoral cells. Only the syncytiotrophoblast is positive for β-HCG and inhibin, whereas intermediate trophoblast is immunoreactive for HPL. These tumors are rapidly fatal if not treated, and β-HCG levels are important to monitoring recurrences.

Differential Diagnosis

- Gestational choriocarcinoma
- Mixed germ cell tumor

Teratomas

Teratomas are classified as mature cystic (dermoid cyst); mature solid (fetiform teratoma); immature; monodermal teratomas (struma ovarii, carcinoid, neuroectodermal tumor, sebaceous tumor).

Mature Teratoma

Mature cystic teratoma (dermoid cyst) accounts for >95 % of germ cell tumors and for 20–40 % of all ovarian tumors. This tumor contains a varied mixture of mature tissue derived from one or more of the embryonic germ layers (ectoderm, mesoderm, endoderm). These teratomas have a wide age distribution; most are found in women between 20 and 50 years of age. Up to 10 % of cases are bilateral. Mature teratoma is a benign tumor that can be treated conservatively. The most common complications are torsion and rupture; malignant transformation rarely occurs. The average diameter is <10 cm, but very small or very large tumors can be found. These tumors typically have a smooth external surface and are unilocular or multilocular cysts on cut surface containing abundant hair and sebaceous material (Fig. 30). There is usually a solid white nodule arising from the cyst wall and projecting into the cavity, containing bone or teeth, called the dermoid mamilla (Rokitansky protuberance). Foci of soft gray-tan tissue resembling brain or brown thyroid tissue are also commonly seen. Rare mature teratomas are completely solid and can be differentiated from immature teratomas at microscopy. Mature teratomas are commonly composed of ectodermal derivate such as skin, hair follicles and sebaceous and sweat glands (Fig. 31); glial tissue, choroid plexus, peripheral nerve and dental structure may also be present (Fig. 32). Endodermal tissues most frequently found are gastrointestinal and respiratory epithelium, renal and thyroid tissue. The most frequent

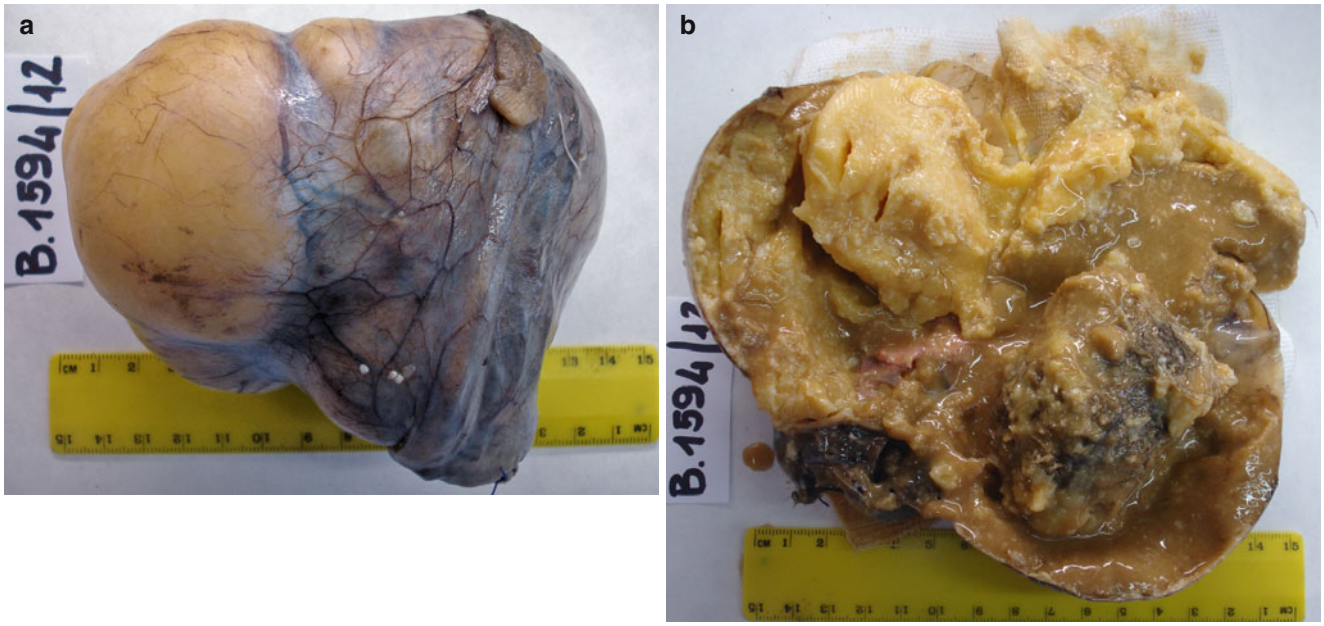

Fig. 30 Mature cystic teratoma: smooth external surface (**a**), multilocular cystic on cut surface with abundant hair and sebaceous material (**b**)

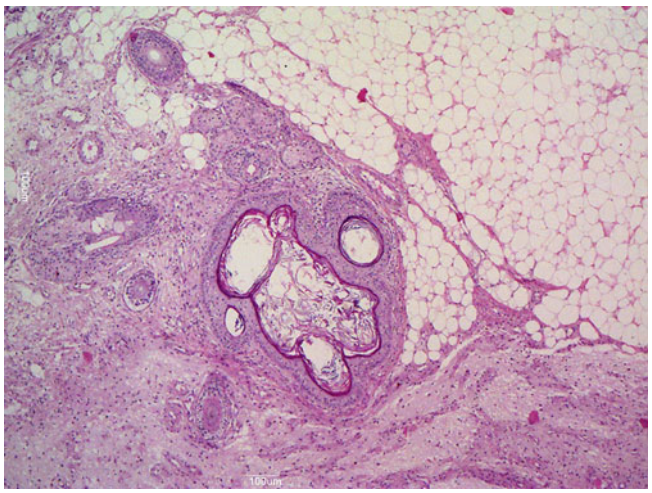

Fig. 31 Mature cystic teratoma: ectodermal derivate such as skin, hair follicles and adipose tissue

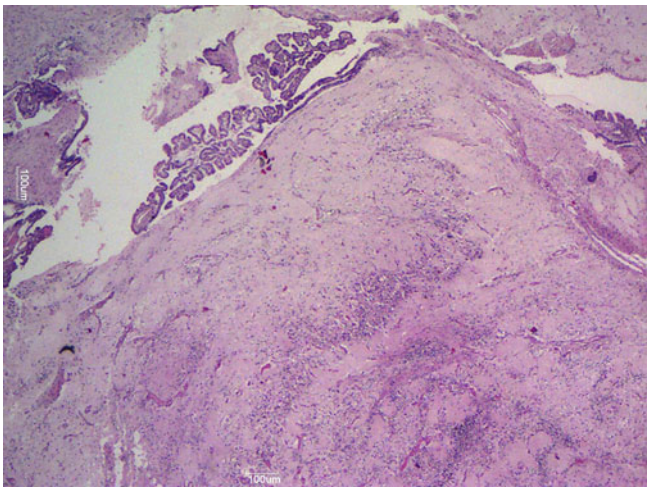

Fig. 32 Mature cystic teratoma: glial tissue and choroid plexus

mesodermal derivates are adipose tissue, smooth or striated muscle, bone and cartilage. Other elements are rarely identified. Frequently, a foreign body-type granulomatous reaction is seen, caused by disruption of the epithelium with a prominent lipogranulomatous response in the wall of the cyst and in the surrounding ovarian tissue. Malignant transformation of a mature cystic teratoma is rare (2 %), commonly with the development of an invasive squamous cell carcinoma. It is typically seen in postmenopausal women and should be suspected when a rapid growth of the dermoid cyst occurs. In 5–10 % of the cases, the association with a malignant germ cell tumor is found, usually yolk sac tumor or immature teratoma, either in the same or in the opposite ovary.

Immature Teratoma

Immature teratoma is the third most common malignant germ cell tumors of the ovary. It is more common in the first two decades. The clinical presentation is nonspecific. A painful palpable abdominal mass and elevated AFP serum levels are present. Immature teratoma spreads mainly by implantation on the pelvic and abdominal peritoneum and the omentum. By the time of the diagnosis, capsular rupture is present in 50 % of cases. Most tumors are large and solid

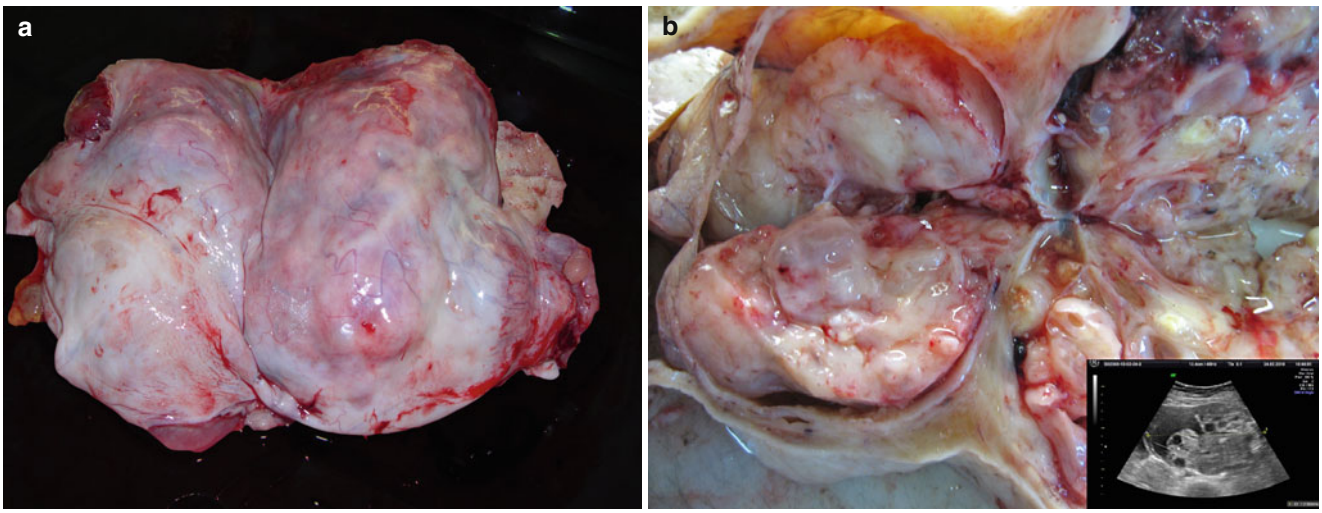

Fig. 33 Immature teratoma: large and solid mass (**a**), cut surface is gray-white and small cysts containing areas of necrotic and hemorrhagic material are present (concordance with the transvaginal scan of the pelvic mass) (**b**)

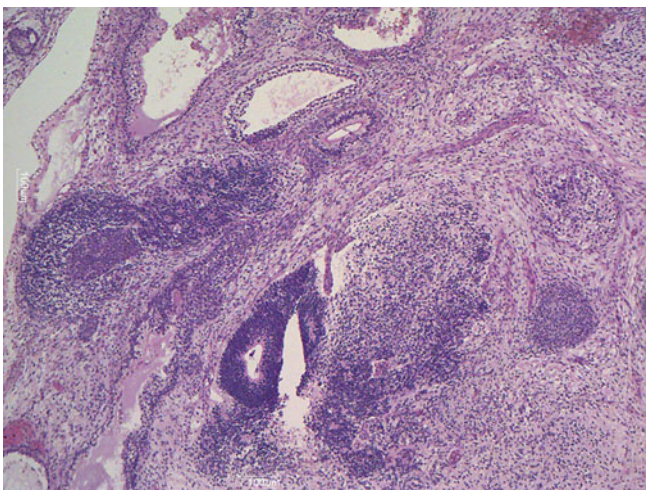

Fig. 34 Immature teratoma: variable admixture of mature and immature neural tissue

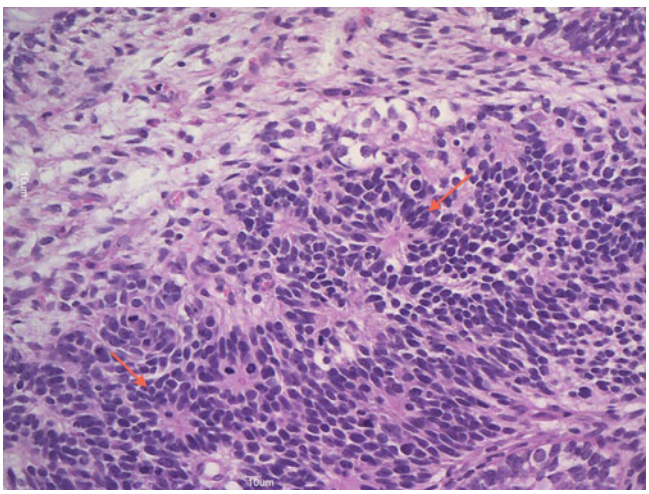

Fig. 35 Immature teratoma. Immature elements of neuroepithelium: neuroepithelial rosettes (*arrows*)

masses, fleshy, brown-pink or gray-white on cut surface, often with cystic areas containing necrotic and hemorrhagic material (Fig. 33). At microscopy, tissues derived from the three germ cell layers are identified with a variable admixture of mature and immature tissues (Fig. 34). The presence of immature tissue establishes the diagnosis of immature teratoma. The most common immature element is the neuroepithelium, with neuroepithelial rosettes and tubules (Fig. 35). Immature mesenchymal stroma and immature endodermal tissues are less commonly found. Grading system of immature teratoma is based on the amount of immature neuroepithelium. Therefore, it is very important to make an extensive sampling (one section per centimeter of tumor) in order to identify immature neuroectodermal tissues. Immunohistochemistry plays a limited role in the diagnosis of immature teratoma. Neural markers (GFAP, S100, NSE) may help to distinguish immature neural tissue from other immature nonneural tissues with overlapping morphology.

Differential Diagnosis

- Mature solid teratoma
- Yolk sac tumor
- Malignant neuroectodermal tumor
- Malignant mixed mesodermal tumor

Monodermal Teratomas

Struma Ovarii

Struma ovarii is a monodermal teratoma predominantly composed of thyroid tissue. It comprises 1–3 % of benign

ovarian teratomas. More common in the fifth decade, it is usually asymptomatic, less commonly presenting as a palpable mass or with signs and symptoms of hyperthyroidism. Struma ovarii is a circumscribed tumor, with average diameter of 5–10 cm, solid or focally cystic and red-brown on cut surface. Microscopically, it is composed of normal thyroid follicles; degenerative changes such as fibrosis, calcification, and aggregates of hemosiderin-laden macrophages may be present. Any type of thyroid cancer can arise in struma ovarii.

Carcinoid

Carcinoid is a rare ovarian tumor (<1 % of all ovarian teratomas): it is classified as monodermal teratoma composed of neuroendocrine cells similar to those found in neuroendocrine tumors in the gastrointestinal tract. One-third of patients present with a carcinoid syndrome. Carcinoids are solid yellow masses of variable size or solid nodules in the wall of a mature cystic teratoma. The tumor is composed of round or cuboidal neuroendocrine uniform cells which show different growth patterns: insular, trabecular, stromal, in a fibromatous or hyalinized stroma. Useful immunohistochemical stains are chromogranin and synaptophysin, but many other peptide hormones can be detected in carcinoid cells.

Malignant Mixed Germ Cell Tumors

Malignant mixed germ cell tumors are very rare tumors. *Gonadoblastoma* arises almost exclusively in abnormal gonads and contains an admixture of germ cells and sex cord cells. *Polyembryoma* is extremely rare and composed of embryoid bodies.

Other Rare Tumors of the Ovary

Small Cell Carcinoma

Small cell carcinoma (of hypercalcemic type) is an aggressive tumor of uncertain histogenesis. It occurs in young women. The clinical presentation is nonspecific, presenting with abdominal pain or as a palpable abdominal mass usually unilateral. About two-thirds of patients have hypercalcemia. Small cell carcinoma is a solid nodular tumor with an average diameter of 15 cm. On cut surface, small cysts and areas of hemorrhage and necrosis can be found. Microscopically, tumor cells are small with scant cytoplasm and oval to round nuclei showing brisk mitotic activity. Follicle-like spaces filled with eosinophilic fluid are present. At immunohistochemistry, the tumor cells are positive for low-molecular-weight cytokeratins (CK8/18), variably positive for EMA, CD10, WT1 and calretinin. Inhibin, chromogranin, CD99, and TTF-1 are typically negative.

Differential Diagnosis

- Juvenile granulosa cell tumor
- Small cell carcinoma, pulmonary type
- Small round blue cell tumors (lymphoma, rhabdomyosarcoma)
- Metastatic melanoma

Desmoplastic Small Round Cell Tumor

Desmoplastic small round cell tumor is a rare malignant tumor that occurs in young females, arising in the peritoneal cavity, rarely clinically presenting as a primary ovarian tumor. Histogenesis is unknown. Tumor cells exhibit a reciprocal translocation t(11;22) resulting in a fusion of the EWS and WT1 genes. By the time of diagnosis, an extensive intra-abdominal tumor growth is common. Tumor cells are small with uniform, round, hyperchromic nuclei and scanty amount of cytoplasm. Tumor cells grow in nests and sheets separated by sclerotic fibrous stroma and are polyphenotypic, expressing cytokeratins, desmin, NSE, and WT1.

Female Adnexal Tumor of Probable Wolffian Origin

Female adnexal tumor of probable Wolffian origin usually occurs in the broad ligament or mesosalpinx, but rare cases have arisen in the ovary. The tumors range from 2 to 20 cm in diameter. The tumor cells grow in diffuse, trabecular, tubular or microcystic pattern and are immunoreactive for vimentin and cytokeratin but not for EMA. Most of these tumors are benign, but rare malignant cases may occur.

Adenomatoid Tumors

Adenomatoid tumors are circumscribed, not encapsulated, benign tumors of mesothelial derivation. They are solid nodules, less than 2 cm in diameter. At microscopy, they are similar to the more frequent adenomatoid tumors in other sites.

Metastatic Tumors of the Ovary

Metastatic tumors involving the ovary comprise 5–10 % of all malignant ovarian tumors, and they vary in appearance depending on the primary site. Ovarian spread may occur by direct local extension from adjacent sites or from distant extragenital sites or from peritoneal tumors. It is often difficult to differentiate metastatic endometrial adenocarcinoma in the ovary from synchronous primary endometrioid adenocarcinomas of the endometrium and ovary. Ovarian metastases often occur in women with a history of an extraovarian cancer, usually from the colon or rectum, but some patients have no history of a primary extraovarian tumor. Characteristic gross findings of metastases in the ovaries are bilateral involvement and size that is often

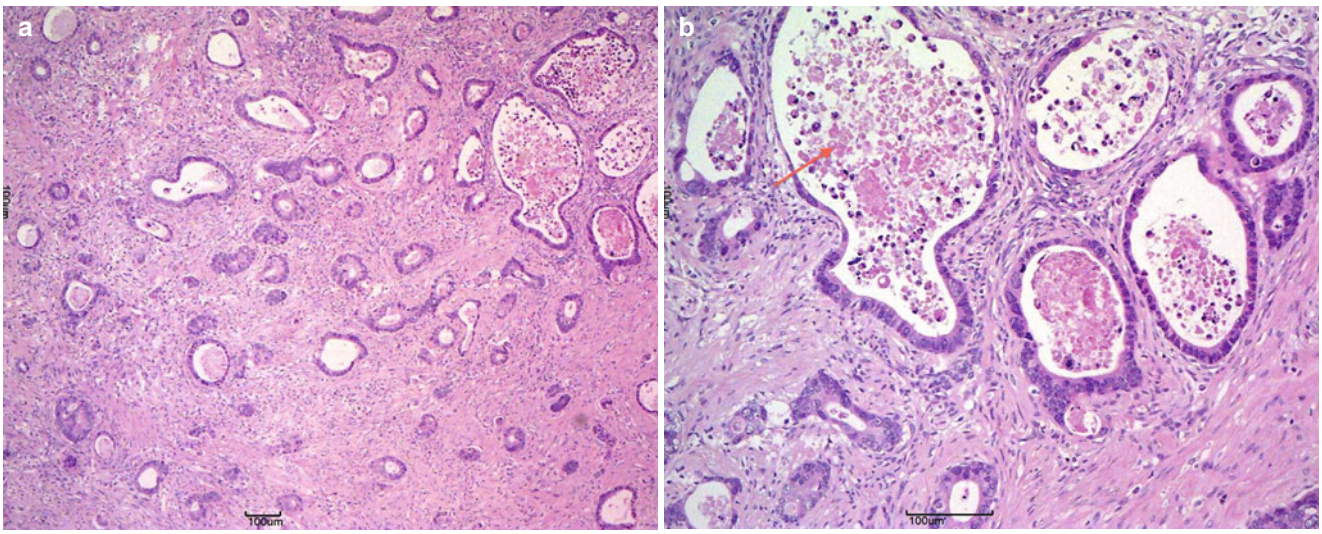

Fig. 36 Metastatic carcinoma from the colon. Neoplastic glands are lined by atypical columnar cells (**a**); there is extensive dirty necrosis (*arrow*) (**b**)

<10 cm. The growth pattern is nodular, solid and/or cystic; surface implants may be found. Microscopy shows metastatic carcinoma in lymphatic spaces of the hylus and mesovarium.

Metastases from Nongynecologic Sites

Metastases from Colorectal Adenocarcinoma

Metastases from colorectal adenocarcinoma often simulate a primary ovarian adenocarcinoma. It occurs in 2–13 % of women with a history of colorectal carcinoma. Time lapse between surgery for the primary tumor and detection of the ovarian metastases ranges from few months up to 5 years. When a patient with a history of colorectal cancer develops a new pelvic mass, a diagnosis of metastatic adenocarcinoma is likely, but benign or primary malignant ovarian tumors can be discovered. The typical colorectal adenocarcinoma, with rare or absent goblet cells, can simulate primary endometrioid tumors of the ovary, but the degree of nuclear atypia is higher and there is no squamous metaplasia. Metastatic tumors form large complex glands and cysts that contain necrotic debris, often termed "dirty" necrosis (Fig. 36). When goblet cells are numerous and there is abundant mucin production, metastatic colorectal adenocarcinoma mimics primary ovarian mucinous tumor. Metastatic adenocarcinoma from the pancreas or biliary tract grows as a mucinous adenocarcinoma, and a differential diagnosis is very important. Sometimes, it may be necessary to compare the microscopic features of the metastases with the primary tumor. Immunohistochemical studies may help in the differential diagnosis: metastatic colorectal carcinoma shows diffuse and strong positivity for CK20 and CDX2 and is negative for CK7 (Fig. 37). Primary ovarian mucinous carcinomas are diffusely and strongly positive for CK7; they may be immunoreactive for CK20, but staining is typically weak and focal.

Differential Diagnosis

- Endometrioid and mucinous tumors of the ovary
- Synchronous colonic and ovarian tumors (Lynch syndrome)

Metastases from Carcinoma of the Breast

Breast carcinoma is the second most frequent (12 %) metastatic tumor of the ovary. A history of primary breast carcinoma is known in most of the cases, but sometimes the ovarian metastases are the first clinical manifestation. In two-thirds of patients, metastases are bilateral, and ovarian enlargement is solid nodular or diffuse. At microscopy, ductal carcinoma (Fig. 38) with papillary, cribriform, diffuse growth pattern or lobular carcinoma (Fig. 39) with trabecular, single file, diffuse growth pattern may be seen. Neoplastic cells are typically positive for CK7 and negative for CK20. Variable expression of estrogen and progesterone receptors is often observed.

Differential Diagnosis

- Ovarian serous and endometrioid carcinoma
- Carcinoid tumor
- Adult granulosa cell tumor
- Lymphoma

Metastases from Carcinoma of the Stomach

Most patients have symptoms related to an adnexal mass, and only 25 % of cases have a history of a prior gastric

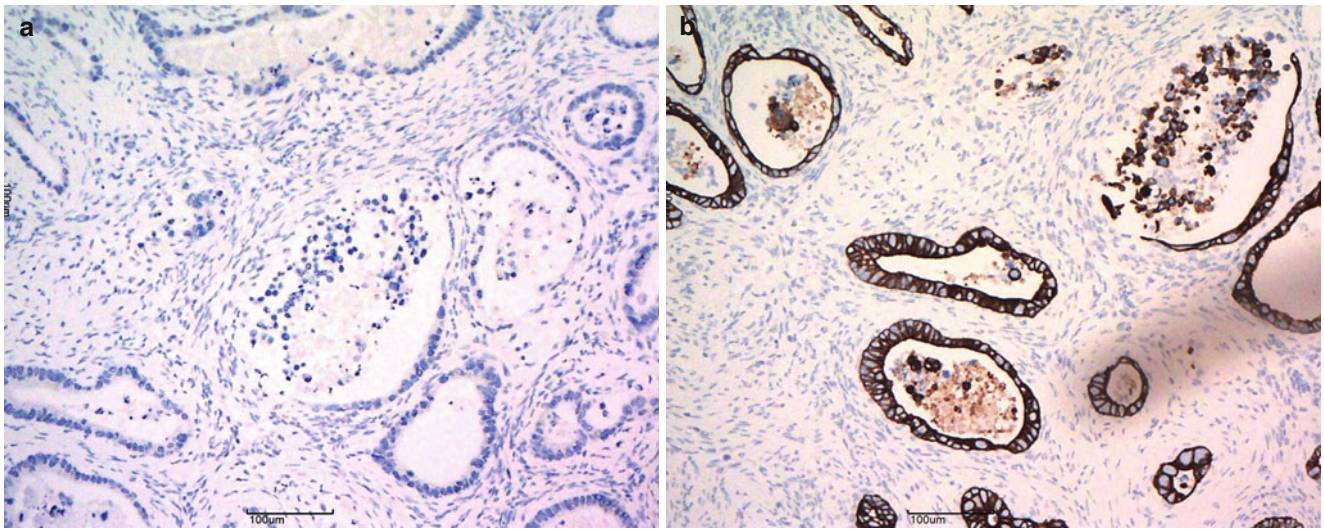

Fig. 37 Metastatic carcinoma from the colon. The tumor lacks CK7 expression (**a**) but diffusely expresses CK20 (**b**)

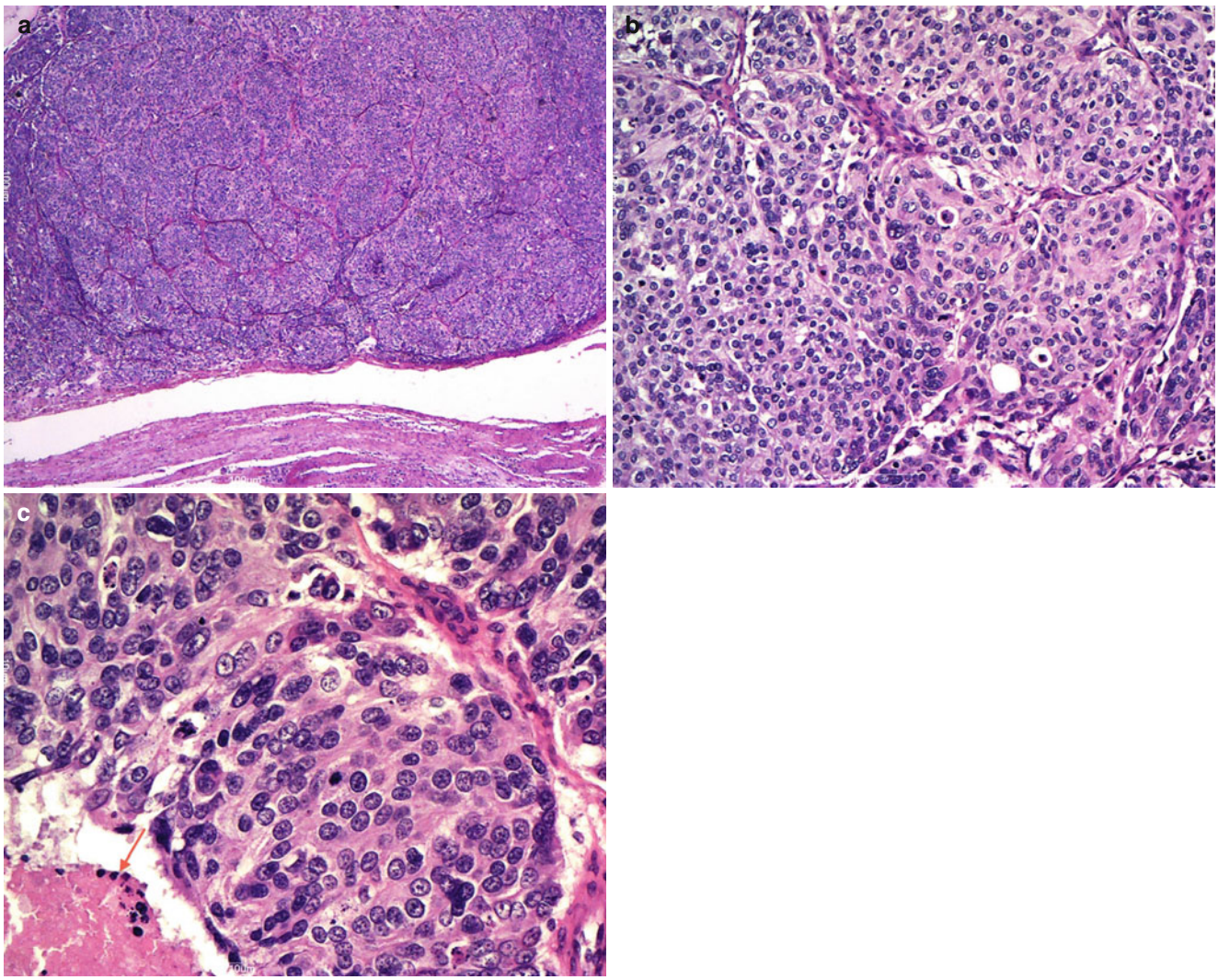

Fig. 38 Metastatic breast carcinoma, ductal type. The tumor is composed of solid nodules (**a**); nests of monotonous tumor cells with pale to eosinophilic cytoplasm and round to oval nuclei (**b**); focal central necrosis is present (*arrow*) (**c**)

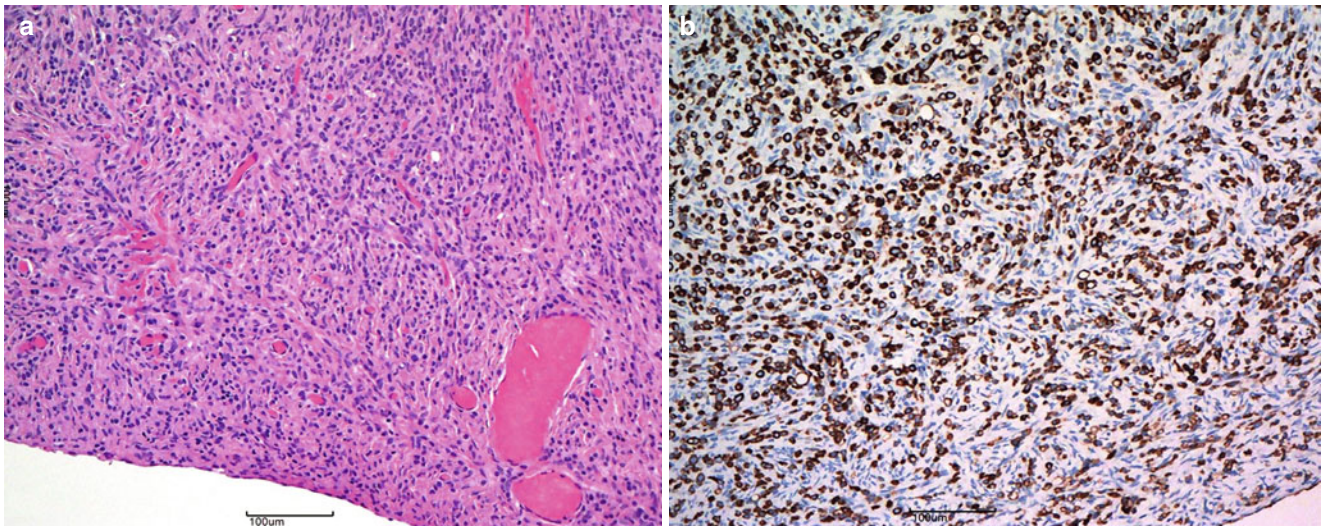

Fig. 39 Metastatic breast carcinoma, lobular type. Neoplastic cell growth in trabeculae or single file (**a**); CK7 identifies single neoplastic cells in small ovarian masses (**b**)

cancer. The tumor is a solid bilateral (80 %) mass, measuring up to 18 cm in diameter, with a lobulated white or yellow cut surface. Histologically, metastatic gastric cancer is usually a signet-ring cell carcinoma, composed of single cells or clusters growing in a hypercellular stroma (Krukenberg tumor). Abundant extracellular mucin may be present. Metastatic gastric adenocarcinoma is rare. Tumor cells frequently express CK7, CK20 and CDX2.

Differential Diagnosis

- Cellular fibroma
- Fibrothecoma
- Sclerosing stromal tumor
- Primary mucinous carcinoid

Metastases from Carcinoma of the Appendix

Metastases from carcinoma of the appendix present as a pelvic mass, almost always bilateral, 10 cm in average diameter, often larger than the primary tumor in the appendix. Histologically, they may show Krukenberg features, intestinal type, or mixed patterns. Neoplastic cells diffusely express CK20; CK7 expression, if present, is weak, focal or diffuse.

Ovarian metastases by low-grade mucinous adenocarcinoma of the appendix with pseudomyxoma peritonei is an uncommon condition. Implants are almost always bilateral on the surface of the ovaries. They are composed of abundant extracellular mucin with foci of fibrosis and granulation tissue. Mucinous epithelium is scant, composed of incomplete glands embedded in a pool of extracellular mucin. Similar to primary appendiceal mucinous tumors, ovarian metastases show diffuse positivity for CK20 and are usually negative for CK7.

Differential Diagnosis

- Borderline mucinous tumor, intestinal type
- Mucinous cystoadenoma
- Mucinous adenocarcinoma

Metastases from Carcinoma of the Pancreas

Metastases from carcinoma of the pancreas are bilateral with or without ovarian surface involvement. Frequently, at diagnosis of adnexal masses or diffuse carcinomatosis, the primary pancreatic cancer may be undetected, and clinical impression in many patients is that of a primary ovarian carcinoma. Neoplastic glands, variable in size and shape, with minimal to marked nuclear atypia, show mucinous, endometrioid-like or secretory features and haphazardly infiltrate a desmoplastic stroma. The immunoprofile of metastatic pancreatic carcinoma is the same of primary ovarian mucinous tumors (CK7 diffusely positive, CK20 focally positive).

Differential Diagnosis

- Primary mucinous borderline tumor or mucinous carcinoma of the ovary
- Metastatic gallbladder or bile duct carcinoma

Metastases from Carcinoma of the Gallbladder, Bile Ducts and Ampulla of Vater

They constitute 1 % of all clinically apparent metastatic ovarian tumors. Grossly they present as large (>10 cm), bilateral masses (75 %) with nodular surface and solid or cystic cut surface. At microscopy, metastases may show a variety of growth patterns including glandular, cribriform, villoglandular and mucinous with goblet cell differentiation (Fig. 40). Similar to metastatic pancreatic carcinoma, these metastases may mimic primary mucinous tumors of the

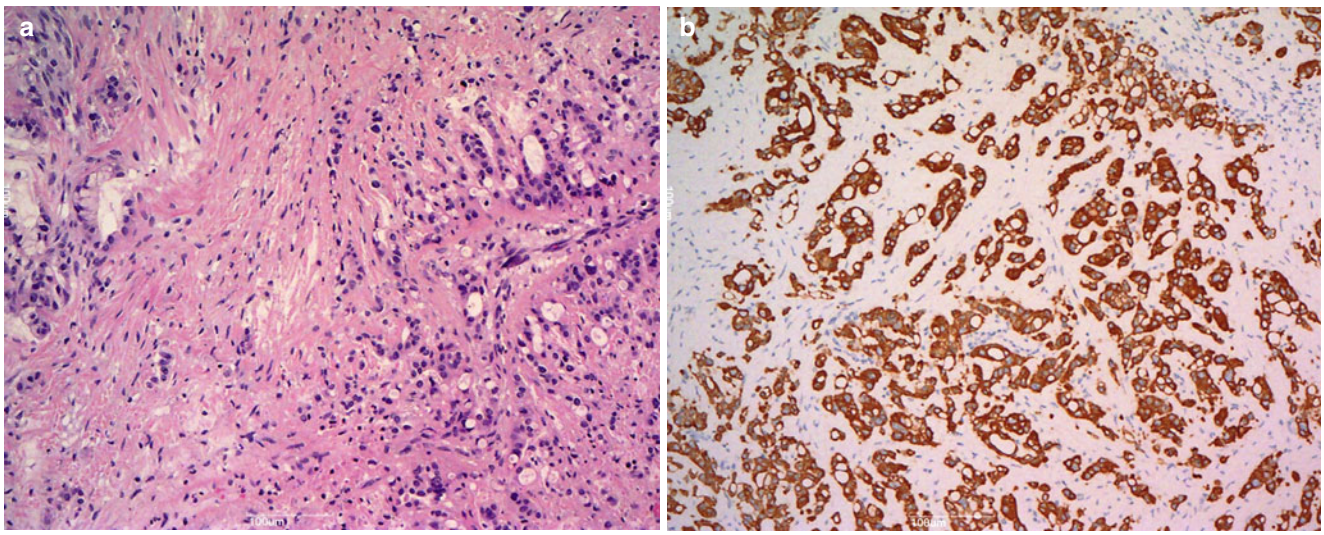

Fig. 40 Metastatic gallbladder adenocarcinoma. Neoplastic cells show glandular pattern, and are surrounded by a prominent stromal reaction (**a**). The tumor exhibits diffuse CK7 expression (**b**)

ovary; also the immunophenotype (CK7 diffusely positive and variable expression of CK20) is very similar. Bilaterality, surface involvement, and nodularity highly support a metastatic tumor.

Metastases from Carcinoma of the Lung

Small cell carcinoma is the most frequent histological subtype that metastasizes to the ovary. Commonly it presents as a unilateral smooth mass with lobulated white to yellow cut surface. Foci of hemorrhage and necrosis are present. Tumor cells may be arranged in sheets, trabeculae or nests; at immunohistochemistry, they are positive for low-molecular-weight cytokeratins, TTF-1, chromogranin A, and synaptophysin.

Differential Diagnosis

- Primary ovarian pulmonary-type small cell carcinoma

Lymphoma

Many types of lymphoma can involve the ovary; secondary non-Hodgkin lymphoma (50 % bilateral) should be distinguished from primary disease that most commonly is unilateral.

Differential Diagnosis

- Granulocytic sarcoma
- Undifferentiated carcinoma
- Small cell carcinoma
- Dysgerminoma
- Adult granulosa cell tumor.

A panel of immunohistochemical markers is usually necessary to provide the correct diagnosis.

Metastases from Melanoma

Ovarian metastases from melanoma represent 1 % of all metastases from nongynecologic primary tumor and are usually detected during follow-up for a prior cutaneous melanoma. In one-third of cases, metastases are bilateral; grossly solid and cystic, sometimes they show dark pigmentation on cut surface. The tumor cells, most frequently large epithelioid, less commonly small or spindle, are positive for S-100, HMB-45, and Melan A.

Metastases from Carcinoma of the Urinary Bladder

Metastases from carcinoma of the urinary bladder are rare and unilateral: the most common histological type is transitional cell carcinoma.

Differential Diagnosis

- Primary ovarian transitional cell carcinoma
- Malignant Brenner tumor

Metastases from Carcinoma of the Kidney

They are very rare tumors (<1 % of all metastases) and may be bilateral and solid with a cystic component. Clear cell carcinoma is the most common histological subtype of renal cell carcinoma that metastasizes to the ovary, but other histological subtypes as chromophobe cell carcinoma (Fig. 41) may be found. Immunohistochemical features may help to reach a correct diagnosis.

Differential Diagnosis

- Clear cell carcinoma of the ovary
- Steroid cell tumor
- Dysgerminoma
- Yolk sac tumor

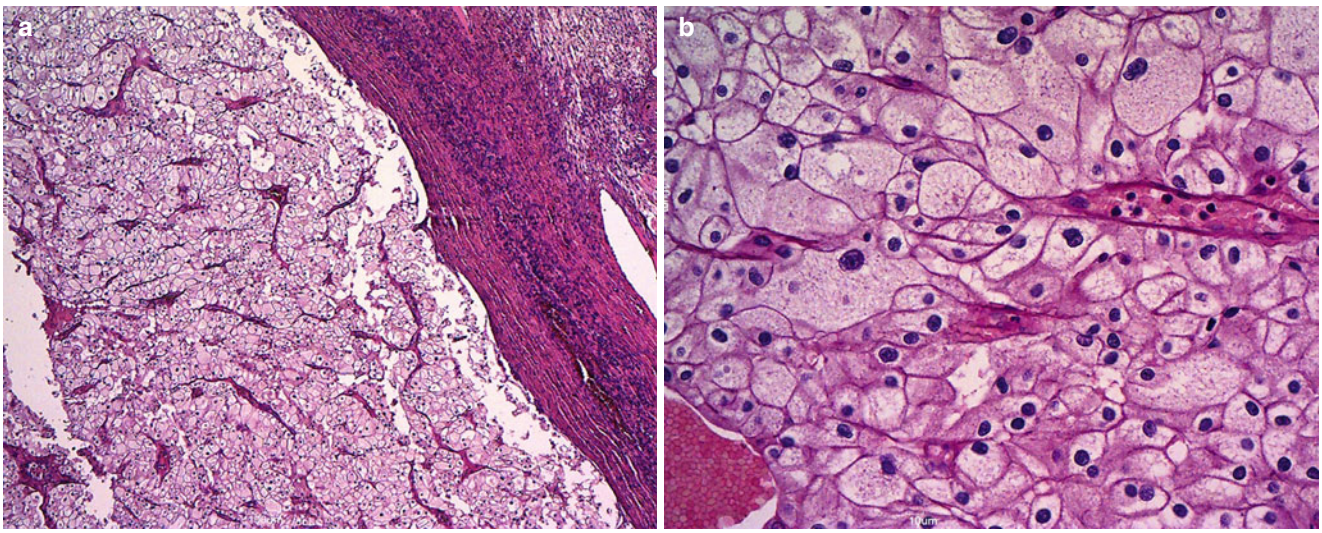

Fig. 41 Metastatic renal cell carcinoma, chromophobe cell type. Solid growth pattern of large polygonal cells, arranged along vascular channels (**a**); the neoplastic cells show prominent cell membranes, typical granular cytoplasm, and irregular nuclei; some cells are binucleated and show perinuclear halos (**b**)

Secondary Involvement by Malignant Mesothelioma

Secondary ovarian involvement by malignant mesothelioma comprises <1 % of ovarian metastases, involves both ovarian surface and parenchyma with diffuse abdominal implants. Tubulopapillary or solid patterns are the typical histological features. The most important differential diagnosis is serous carcinoma of the ovary. Expression of calretinin, CK5/6, and h-caldesmon, combined with negativity for B72.3, MOC-31, ER, and Ber-EP4, supports the diagnosis of malignant mesothelioma.

Metastases from Extraovarian Carcinoid Tumor

Metastases from extraovarian carcinoid tumor comprise about 5 % of all metastases from nongynecologic primary tumors and are histologically similar to primary ovarian carcinoids.

Metastases from Small Round Blue Cells Sarcomas

Metastases from small round blue cells sarcomas comprise <1 % of all metastases. They usually occur in pediatric age and present as a unilateral or bilateral abdominal or pelvic mass. The tumors may be solid or cystic and histological appearance is variable. Small round blue cells sarcomas include rhabdomyosarcoma, neuroblastoma, Ewing's sarcoma, and desmoplastic small round blue cell tumor. A panel of immunohistochemical markers is usually necessary to provide the correct diagnosis.

Metastases from Gynecologic Sites

Metastases from Uterine Cervix and Endometrium

Metastases from uterine cervix and endometrium comprise about 10 % of all clinically apparent ovarian metastases. The most common (78 %) are metastases from adenocarcinoma or squamous cell carcinoma of the uterine cervix. These metastases frequently present as unilateral masses up to 30 cm in diameter and appear to be HPV-related. Endometrial carcinoma may also metastasize to the ovary, but metastases are usually bilateral.

Differential Diagnosis

- Primary mucinous and endometrioid ovarian tumor
- Synchronous ovarian and endometrial tumors of similar histological type

Metastases from Mesenchymal Tumor of the Uterine Corpus

Metastases from mesenchymal tumor of the uterine corpus are very rare. More frequently are bilateral, lobulated, or nodular masses, and their cut surface is solid with areas of hemorrhage and necrosis. Endometrial stromal sarcoma is more common than leiomyosarcoma, and the tumor cells resemble their uterine counterpart.

Differential Diagnosis

- Endometrioid stromal sarcoma of the ovary
- Cellular fibroma

- Adult granulosa cell tumor
- Leiomyosarcoma of the ovary
- Secondary involvement by gastrointestinal stromal tumor (GIST)

Suggested Reading

Abu-Rustm N, Barakat RR, Curtin JP. Ovarian and uterine disease in women with colorectal cancer. Obstet Gynecol. 1997;89:85–7.

Albee Jr RB, Sinervo K, Fisher DT. Laparoscopic excision of lesions suggestive of endometriosis or otherwise atypical in appearance: relationship between visual findings and final histologic diagnosis. J Minim Invasive Gynecol. 2008;15:32–7.

Birnkrant A, Sampson J, Sugarbaker PH. Ovarian metastasis from colorectal cancer. Dis Colon Rectum. 1986;29:767–71.

Blamey SL, McDermott FT, Pihl E, et al. Resected ovarian recurrence from colorectal adenocarcinoma: a study of 13 cases. Dis Colon Rectum. 1981;24:272–5.

Clement PB. The pathology of endometriosis: a survey of the many faces of a common disease emphasizing diagnostic pitfalls and unusual and newly appreciated aspects. Adv Anat Pathol. 2007;14:241–60.

Dabbs DJ, editor. Diagnostic immunohistochemistry. 2nd ed. London: Churchill Livingstone; 2006. p. 637–98.

Fletcher C, editor. Diagnostic histopathology of tumors. 2nd ed. London: Churchill Livingstone; 2000. p. 567–642.

Kurman RJ, Ellenson LH, Ronnett BM, editors. Blaunstein's pathology of the female genital tract. 6th ed. New York: Springer; 2011. p. 579–997.

Nucci MR, Oliva E, editors. Gynecologic pathology. London, Elsevier: Churchill Livingstone; 2009. p. 367–613.

Ronnett BM, Kurman RJ, Zahn CM, et al. Pseudomyxoma peritonei in women: a clinicopathologic analysis of 30 cases with emphasis on site of origin, prognosis, and relationship to ovarian mucinous tumors of low malignant potential. Hum Pathol. 1995a;26: 509–24.

Ronnett BM, Yan H, Kurman RJ, et al. Patients with pseudomyxoma peritonei associated with disseminated peritoneal adenomucinosis have a significantly more favorable prognosis than patients with peritoneal mucinous carcinomatosis. Cancer. 2001;92:85–91.

Ronnett BM, Zahn CM, Kurman RJ. Disseminated peritoneal adenomucinosis and peritoneal mucinous carcinomatosis. A clinicopathologic analysis of 109 cases with emphasis on distinguishing pathologic features, site of origin, prognosis, and relationship to "pseudomyxoma peritonei". Am J Surg Pathol. 1995b;19: 1390–408.

Scully RE, Young RH, Clement PB. Atlas of tumor pathology. Tumors of the ovary, maldeveloped gonads, fallopian tube, and broad ligament. 3rd ed. Washington, DC: AFIP; 1998.

Soslow RA, Tornos C, editors. Diagnostic pathology of ovarian tumors. New York: Springer; 2011.

Tavassoli F, Devilee P. Pathology and genetics of tumours of the breast and female genital organs. In: Kleihues P, Sobin LH, editors. World Health Organization classification of tumours, vol. 5. Lyon: IARC Press; 2003.

Ulbright TM, Roth LM, Stehman FB. Secondary ovarian neoplasia. A clinicopathologic study of 35 cases. Cancer. 1984;53:1164–74.

Young RH, Scully RE. Metastatic tumors in the ovary: a problem-oriented approach and review of the recent literature. Semin Diagn Pathol. 1991;8:250–76.

Part II

Non Neoplastic Lesions of the Ovary

Cysts of Follicular Origin and Pregnancy Luteoma

Bianka K. Freiwald-Chilla, Nik Hauser, and Rahel A. Kubik-Huch

Abstract

Normal ovarian changes and functional cysts of follicular origin should not be confused with cystic neoplasm. The day-to-day changes in the appearance of the female reproductive organs are the major challenge of women's imaging. This chapter aims to describe the normal imaging appearance of the ovaries, its anatomic variants, and physiological changes, with focus on cross-sectional imaging.

Keywords

Cyst • Follicular luteoma • Imaging • Ultrasound • Computed tomography • Magnetic resonance

Focus Point

A number of different physiological conditions in women cause morphological alterations of the ovary. Ovarian appearance changes not only with respect to patient age, but for women of childbearing age, it is also dependent on the menstrual cycle and the presence or absence of pregnancy. These day-to-day changes in the hormonal status and thus of the appearance of the female reproductive organs, including the ovaries, are one of the major challenges of effectively imaging the adnexa and its associated structures. Similarly, the complexity of female pelvic anatomy and the wide spectrum of differential diagnoses in assessing cystic ovarian lesions can prove problematic in the interpretation and determination of the appropriate care. Accordingly, normal ovarian changes with functional cysts of follicular origin related to the menstrual cycle should not be confused with cystic neoplasms. In order to correctly recognize a pathologic adnexal lesion, it is therefore of outmost importance for radiologist and clinicians alike to be familiar with the normal physiological changes and findings associated with ovarian cysts.

Adnexal Anatomy

Normal Anatomy of the Ovaries

The female reproductive system includes the uterus and its associated organs and body parts, collectively known as the adnexa. In general, the adnexa comprise a woman's ovaries, fallopian tubes, blood vessels, supporting ligaments, and peritoneal folds of the lateral pelvis.

The paired ovaries are typically located within the ovarian fossae on the lateral wall of the pelvis and, in a position

B.K. Freiwald-Chilla, MD (✉) • R.A. Kubik-Huch
Institute of Radiology, Kantonsspital Baden AG,
Im Ergel 1, CH – 5404 Baden-Dättwil, Switzerland
e-mail: bianka.freiwald@ksb.ch

N. Hauser
Department of Gynecology and Obstetrics,
Kantonsspital Baden AG, Baden, Switzerland

L. Saba et al. (eds.), *Ovarian Neoplasm Imaging*,
DOI 10.1007/978-1-4614-8633-6_3,

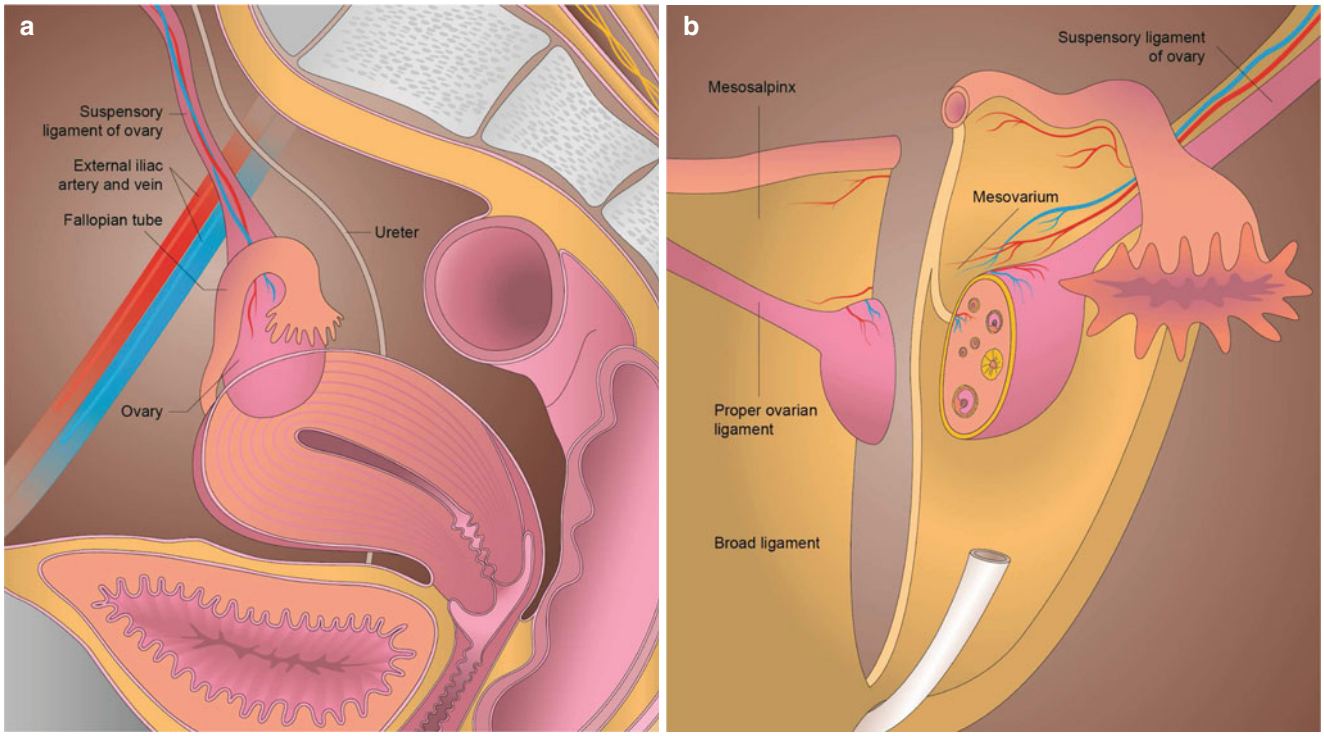

Fig. 1 (**a**) Sagittal overview shows the normal topography of the ovarian fossa at the posterolateral pelvic sidewall. The ureter is located posteriorly and the external iliac artery and vein superiorly. The ovary is anchored by the suspensory ligament to the posterolateral wall of the pelvis (Drawing by W. Herzig). (**b**) Graphic coronal overview of the ovary and its associated ligaments. The suspensory ligament extends from the superolateral part of the ovary and the broad ligament to the pelvic sidewall. The medially located proper ovarian ligament is enclosed between the two peritoneal layers of the broad ligament and extends to the laterocranial surface of the uterus (Drawing by W. Herzig)

posterolateral to the corpus uteri, anterior and medial to the ureter, posterior to the round ligament, and medial or posteromedial to the external iliac vessels. In nulliparous women sitting or standing in the upright position, the long axis of the ovaries is vertical, with each ovary held in position by three ligaments, as shown in Fig. 1 [1]. The location of the ovaries is variable in parous women, because they are displaced during pregnancy and do not subsequently return to their original position. In addition position may change in response to such factors as intestinal activity or filling of the bladder; ovaries can be further displaced from typical positioning by mass lesions of adjacent organs (e.g., subserous myoma) or by pregnancy.

Age and hormonal status coalesce to influence ovarian size and appearance, with the typical ovary measuring 3 mm in length in neonates and 3–5 cm in women of childbearing age; in general, ovarian size begins to decrease starting at age 30, with the length of a typical ovary shrinking to 2 cm in postmenopausal women [2–4]. Pregnancy leads to further variation in ovarian size, as does the use of hormone replacement therapy [3]. Later in this chapter we discuss such variances that must be taken into consideration during diagnostic imaging.

Congenital Abnormalities

Ovarian anomalies are unusual, with ovarian agenesis being quite rare. The condition, in which one or both ovaries are missing, is most frequently associated with a more serious disorder in which an ipsilateral tube and a same-side kidney are also missing. Ovarian duplication is a considerably more common finding than ovarian agenesis, with imaging or histology confirming the presence of small accessory ovaries located near the normal ovarian tissue or, on occasion, in ectopic locations [2].

Abnormal development or fusion of the paramesonephric (Müllerian) and the mesonephric (Wolffian) ducts may prevent ovaries from becoming correctly positioned in the true pelvis [5] found that there is an increased incidence of incomplete ovarian descent defined as an upper ovarian pole at or above the level of the iliac artery bifurcation on MRI in women with Müllerian duct abnormalities, with this correlation being greatest in women with uterine agenesis and various fusion abnormalities.

Effective Methods of Ovarian Imaging

A number of imaging modalities to detect and analyze the adnexa and its associated ovarian tissues are available in today's clinical settings.

Even in postmenopausal women, the majority of detected adnexal cysts will be benign [3], but effective imaging remains key to distinguishing benign cysts from malignant cysts. We describe the most common and preferred options for examining cystic disorders of the adnexa.

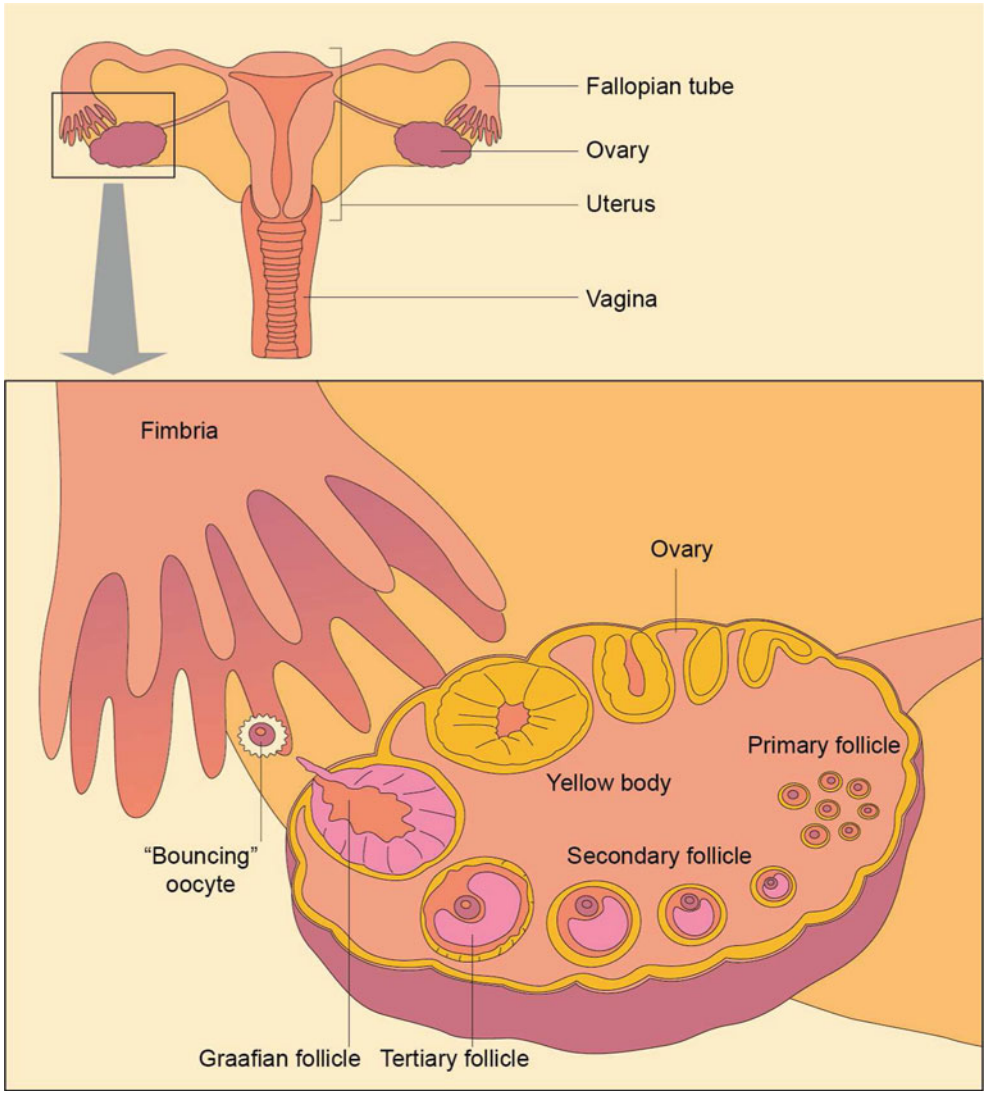

Fig. 2 Ovarian cycle. Yellow body: corpus luteum (Drawing by W. Herzig)

Ultrasound Imaging (Sonography)

External transabdominal sonography (TAS) and internal transvaginal sonography (TVS) can be used together or separately to effectively image the ovaries and the adnexal regions, with TVS proving especially efficacious for pinpointing specific areas of concern and visualizing ovarian tissues. Furthermore, Doppler ultrasonography can be used to easily distinguish ovarian abnormalities (e.g., cysts) from other structures [3, 6].

In recent years, TVS has become an increasingly common adjunct to physical examination of the vagina, cervix, uterus, and ovaries. It is the first-line method of choice for ovarian imaging, especially for distinguishing cystic from cystic-solid and solid lesions. Although its field of view is limited compared with that of TAS, TVS achieves higher-resolution diagnostic imaging than TAS partly because of the transducer's proximity to the imaged tissue and its use of a higher frequency (5–12 MHz). For TAS, the transducer is positioned externally, and the distance to the targeted tissues is larger; the transducer's frequency is also considerably lower (2–7 MHz) in TAS [6].

Magnetic Resonance Imaging (MRI)

A number of physiological conditions, e.g., corpus luteum cysts, are capable of causing morphological changes in the ovarian tissues of women of childbearing age. In the majority of premenopausal women, the ovaries can be easily identified by magnetic resonance imaging (MRI). The visualization can be accomplished relatively easily through MRI-based diffusion-weighted imaging, with the functional ovarian cysts being easily depicted because of their T2-shine-through effect (Figs. 2 and 3).

Normal ovaries contain multiple physiological small cysts of high signal intensity on T2-weighted images, including follicles at various stages of development. These cysts, which vary in size and number during the menstrual cycle, are

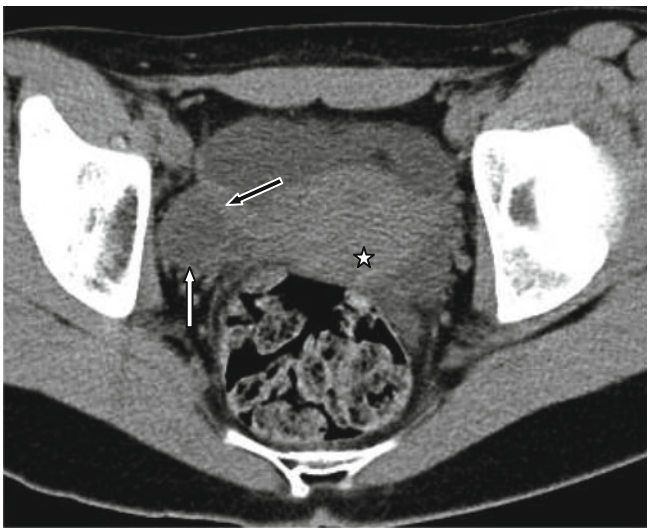

Fig. 3 Axial contrast-enhanced CT shows a normal attenuated myometrium (*white star*) and a follicle cyst in the right ovary with typical fluid density (*white arrow*) enclosed by normal ovarian parenchyma (*black arrow*)

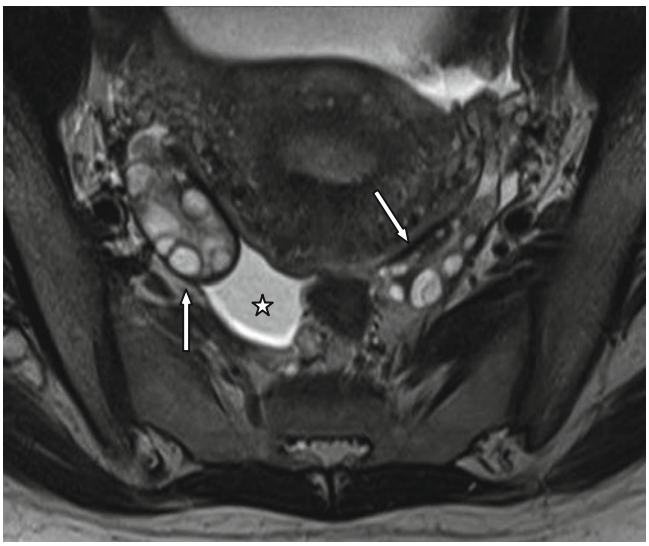

Fig. 4 Transverse T2-weighted TIRM MR image with normal appearance of left and right ovaries (*white arrows*) and a small, physiological amount of free fluid in the pelvis (*white star*)

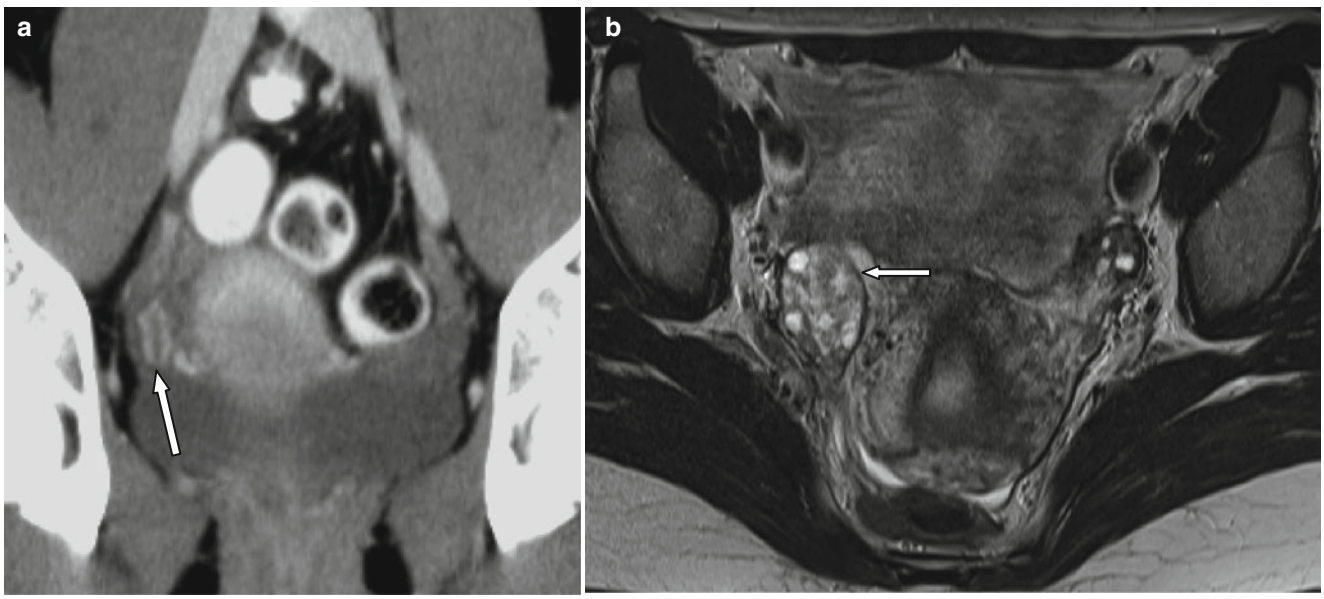

Fig. 5 (**a**) Corpus luteum. Coronary contrast-enhanced CT image demonstrates enhancement of the wall of a right corpus luteum (*arrow*). (**b**) Right ovary with small follicles and a typical appearance of a corpus luteum at T2-weighted TSE MR images. Corpus luteum presents as a lesion with a thick convoluted wall and a small amount of fluid in the central part (*arrow*). Physiological fluid is shown in the pelvis

embedded in the cortex, showing a T2-weighted lower intensity signal than the central medulla (Fig. 4) [7]. In the preovulatory period, the dominant follicle can increase to 15–17 mm in diameter, while the diameter of the postovulation follicular remnant (i.e., corpus luteum) is as small as 2–5 mm [7, 8]. Figure 5 shows T2-weighted images of this remnant. In postmenopausal women, the ovaries can be seen as oval structures of homogenous low signal intensity on T2-weighted images.

In addition to its relatively easy visualization of ovarian tissues, MRI offers multiplanar imaging capabilities and high contrast and spatial resolution. MRI permits visualization of the ovaries in both the axial and coronal planes, which can be particularly useful when seeking to examine ovarian tissues or the parametrial structures and any associated lesions or multiplanar parametrial structures [4, 6].

MRI has been found to be especially helpful in the characterization of adnexal lesions, as it permits the accurate

differentiation of indeterminate adnexal masses and helps to distinguish between benign and malignant ovarian masses [3, 9]. For these reasons MRI is the first-line imaging modality to evaluate congenital abnormalities of the female genital organs [10].

Yet, despite these proven benefits, MRI is not appropriate for every patient. Electronic medical apparatuses such as cochlear implants and cardiac devices are contraindicated for MRI. When MRI is contraindicated, computed tomography (CT) may be used alternatively. CT is also widely used by clinicians to stage malignant ovarian carcinoma.

Computed Tomography

CT recognition of the ovaries is facilitated by the radiologist's understanding of the structures' morphological features and of the relationship of the ovary to the ureter, the course of the ovarian and iliac arteries and veins, and the ligamentous attachments of the ovaries. The majority of ovaries in women of childbearing age can be identified by CT, but postmenopausal ovaries are small and thus difficult to visualize using this imaging modality. The ovarian parenchyma surrounding cysts has a uniform soft-tissue attenuation that results in a low-density appearance on CT scans; this is especially when the ovarian tissues contain numerous cystic follicles that are too small to be easily resolved from the ovarian parenchyma (Fig. 3) [11].

CT offers fast data acquisition with high spatial resolution and impressive post-processing capabilities and can be performed over the entire body. Both CT and MRI are well suited to the evaluation of pelvic organs, although MRI provides higher soft-tissue contrast than CT and is more capable of differentiating congenital ovarian abnormalities from normal tissues or evaluating normal ovarian tissues [5, 12]. Additional disadvantages of CT are associated with patients' exposure to relatively high levels of ionizing radiation; this concern is especially important in young women of childbearing age and during pregnancy [13].

Cysts of Follicular Origin

There are different cystic ovarian lesions of follicular origin: normal follicles, follicular cysts, corpus luteum cysts, hemorrhagic functional cysts, and theca lutein cysts. The imaging modalities described previously can be used for visualization and diagnostics. These imaging tools can also be used to differentiate cysts from nonneoplastic adnexal structures, such as hydrosalpinx, paraovarian cysts or ectopic pregnancies, or mimics of those cysts (e.g., bowel loops) as well as neoplastic ovarian lesions [6].

The following chapter addresses the physiological characteristics, imaging-specific findings, and differential diagnoses of cystic ovarian lesions. In addition, we discuss the luteoma of pregnancy, which is not an ovarian cyst per se but is a tumorlike mass of the adnexa with cyst-like properties.

Follicular Cyst

In women of childbearing age, simple cysts with a diameter of up to 3 cm are considered physiologically normal. The simplest ovarian cysts are known as follicular cysts; these growths are caused by a failure of the follicle to ovulate and tend to have a diameter of 3–8 cm. These growths are most frequently found in the adnexa of premenopausal women, but postmenopausal women have also been known to develop follicular cysts [6, 7, 14].

As described by Liang et al. (2012), the American College of Radiology Appropriateness Criteria concluded in their 2009 update on adnexal masses that physiological cysts should resolve spontaneously in asymptomatic premenopausal women. Furthermore, as benign-appearing simple cysts, endometriomas, dermoids, and hydrosalpinges (each <6 cm in diameter) remain unchanged during long-term follow-up, they should be managed noninvasively with follow-up US rather than other imaging modalities or even surgical intervention.

The following year, the Society of Radiologists in Ultrasound published a detailed consensus statement that set forth specific cyst-management guidelines for premenopausal women, women in early menopause, and postmenopausal women. A major concern was management of simple-appearing cysts that were not physiological or functional. The panelists concurred with published findings that adnexal cysts up to 10 cm are highly likely to be benign and that up to 84 % of these lesions are histologically benign serous cystadenomas [15].

MRI Findings

Follicular cysts typically display on MRI as a simple cyst with high signal intensity on T2-weighted images and low signal intensity on T1-weighted images. In cases in which the cyst is affected by hemorrhage and does not contain simple fluid, the T1-weighted images will show increased signal intensity [6, 7].

CT Findings

CT of follicular cysts typically reveals a thin-walled, fluid-filled sac. As with MRI, the administration of contrast media may further enhance imaging of the cyst [6]. A small amount of free fluid in the rectouterine pouch (i.e., pouch of Douglas) is a physiological finding in reproductive women and should not be mistaken for pathological ascites (Fig. 6).

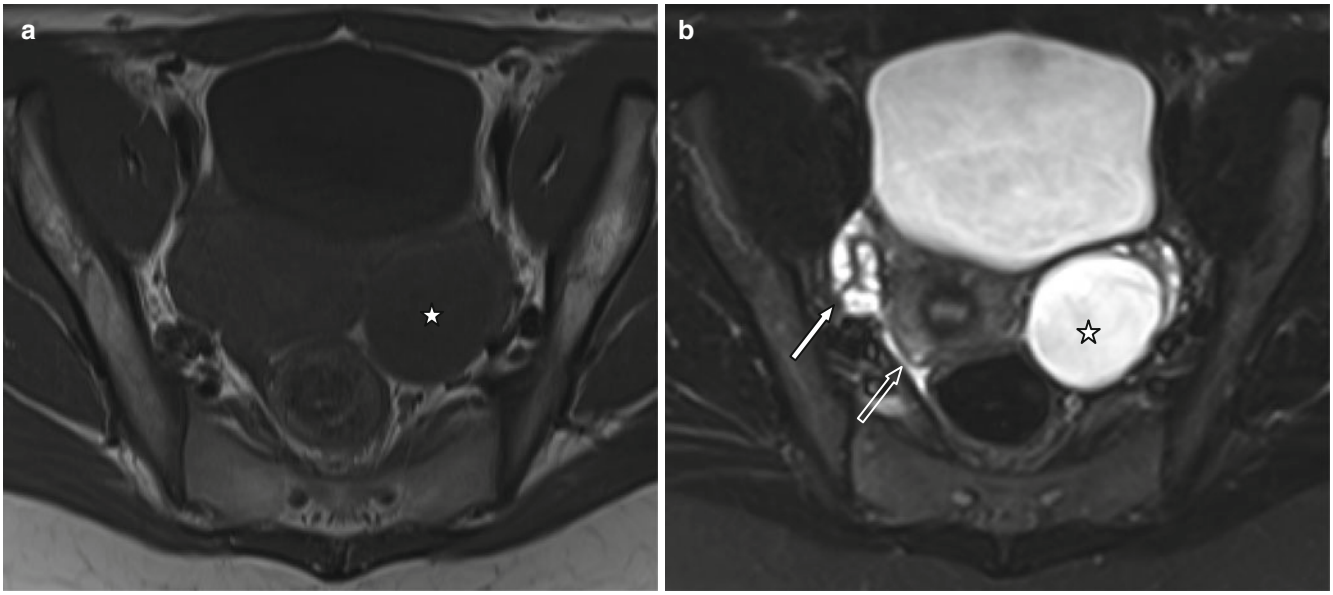

Fig. 6 A 32-year-old patient with a follicular cyst in the left ovary that resolved after two menstrual cycles followed up by transvaginal ultrasound. (**a**) T1-weighted TSE MR image with a hypointense, cystic lesion in the left ovary (*white star*). (**b**) T2-weighted STIR MR image shows the same cystic lesion in the left ovary with a hyperintense signal (*white star*). Good depiction of the right ovary containing many small follicles (*white arrow*). A small amount of physiological fluid is shown in the pouch of Douglas (*transparent arrow*)

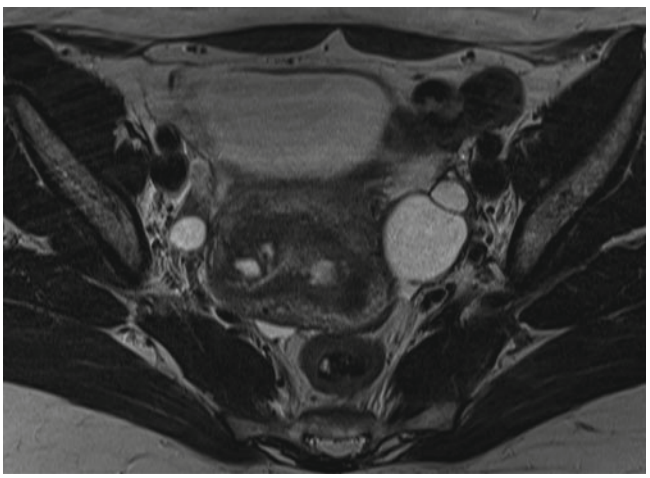

Fig. 7 A 50-year-old patient with a polyloculated, cystic change at the left ovary. The lesion did not resolve over time, resulting in the patient undergoing laparoscopy. A small cystadenoma was subsequently diagnosed histologically

Differential Diagnosis

Clinicians must consider a serous cystadenoma as an important differential diagnosis, especially if the lesion does not disappear over time (Fig. 7) [6]. An additional potential differential diagnosis for a follicular cyst is an endometrioma. On MRI, however, the so-called T2-shading in a T1-hyperintense ovarian lesion is a distinguishing feature of endometrioma. The phenomenon may involve the entire cyst, and the degree of shading can vary from faint to complete signal loss [16].

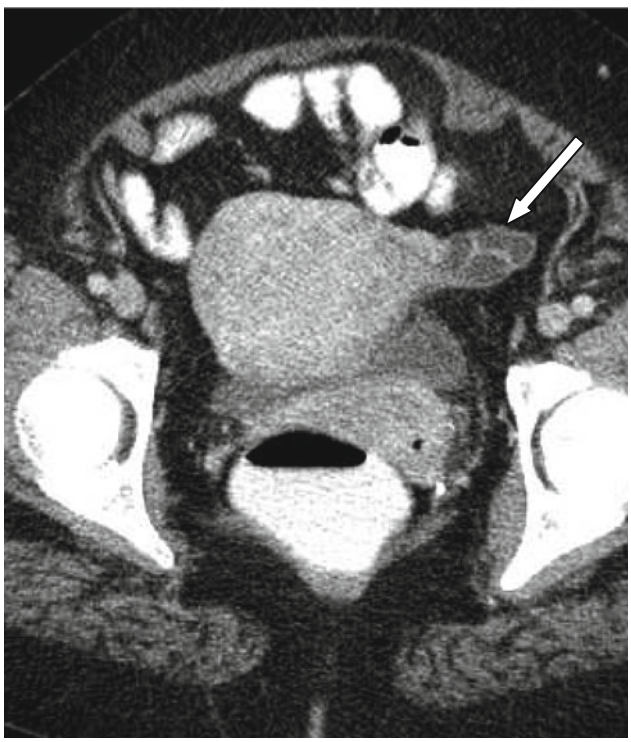

Fig. 8 Hydrosalpinx on the left side mimics polycystic structure on an axial contrast-enhanced CT image (*arrow*), which could be misinterpreted as an ovary with multiple small cysts

Further structures like hydrosalpinx (Fig. 8), paraovarian cyst (Fig. 9) or peritoneal inclusion cyst (Fig. 10), lymphocele, ascites, bowel, pelvic varices, diverticulum, or iliac aneurysm can be misinterpreted as a follicular cyst.

Corpus Luteum Cysts

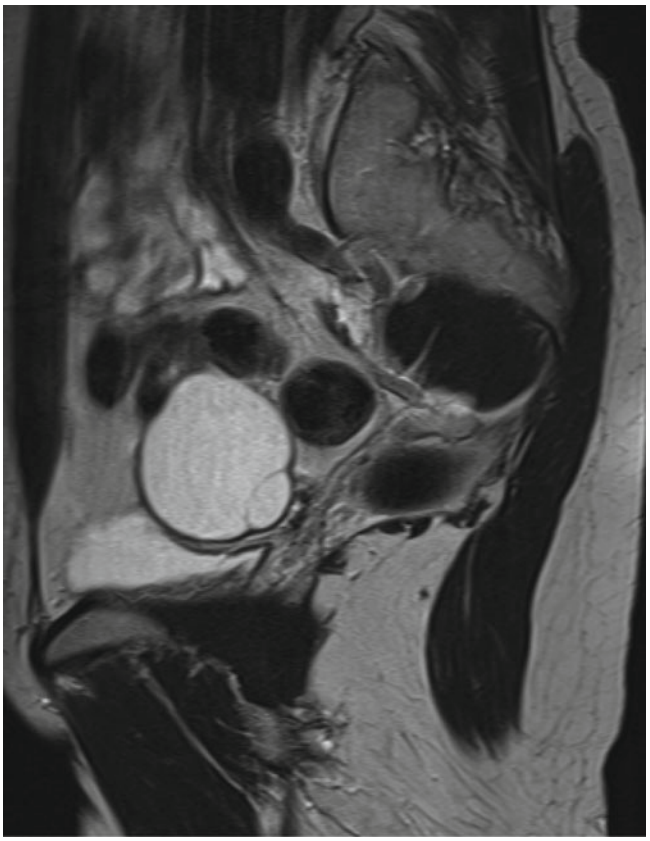

Fig. 9 Sagittal T2-weighted TSE MR image. A 40-year-old patient showed on TVS follow-up examinations a persistent, cystic change in the left ovarian fossa. The patient thus underwent an MRI examination to better analyze the lesion as well as the origin of the change. The lesion in the left ovarian fossa with typical fluid intensity on T1- and T2-weighted images was round and well circumscribed. The change did not resolve over time, resulting in the patient undergoing laparoscopy. A paraovarian cyst was subsequently diagnosed histologically

Corpus luteum cysts should not be mistaken for disease. Typically, the corpus luteum breaks down and dissolves if conception does not occur. However, in some cases, the corpus luteum fails to regress following ovulation, resulting in a late luteal-phase cyst that can potentially persist for several weeks and into the second trimester of a pregnancy. These growths tend to vary between 2.5 and 6 cm in diameter and rarely present as multiple cysts [6, 7]. In the majority of cases, corpus luteum cysts remain symptomless and do not move beyond the ovarian tissue, but they may be accompanied by a small amount of fluid in the pouch of Douglas.

MRI Findings

On MRI, corpus luteum cysts display as round or oval masses and have thicker walls than those of follicular cysts. Reflecting the associated increased vascularity, the cystic wall may have slightly increased intensity on T1-weighted images and relatively lower signal intensity on T2-weighted images and may show intense and early wall enhancement after the intravenous administration of a gadolinium-based contrast agent. The signal intensity of the cyst is variable and corresponds to its hemorrhagic share (i.e., low to high signal intensity on both T1- and T2-weighted images), as shown in Fig. 11 [6, 7, 17].

In rare cases, abdominal pain caused by hemoperitoneum may result from massive bleeding arising from a corpus luteum cyst [7, 17]. Hemorrhagic ascites is visualized as free pelvic fluid of high intensity on T1-weighted images. In this case, an accurate pregnancy test is crucial for diagnosis, as a corpus luteum cyst accompanied by hemoperitoneum clinically presents as a ruptured ectopic pregnancy [7].

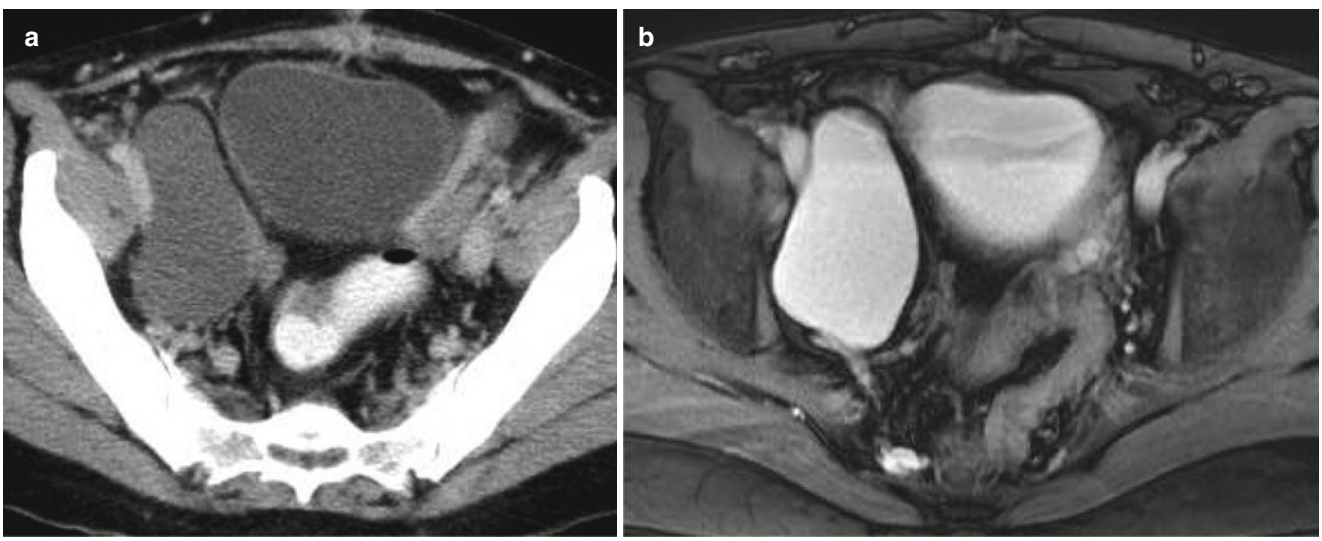

Fig. 10 (**a**) A 30-year-old patient with a well-circumscribed fluid collection in the region of the right ovarian fossa. The image shows low attenuation on contrast-enhanced CT, which is typical for a cystic lesion. (**b**) The same lesion on a T2-weighted TRUFI MR image. The image shows homogeneous high-signal-intensity fluid collection at the left pelvic wall. No septations or mural nodules were identified

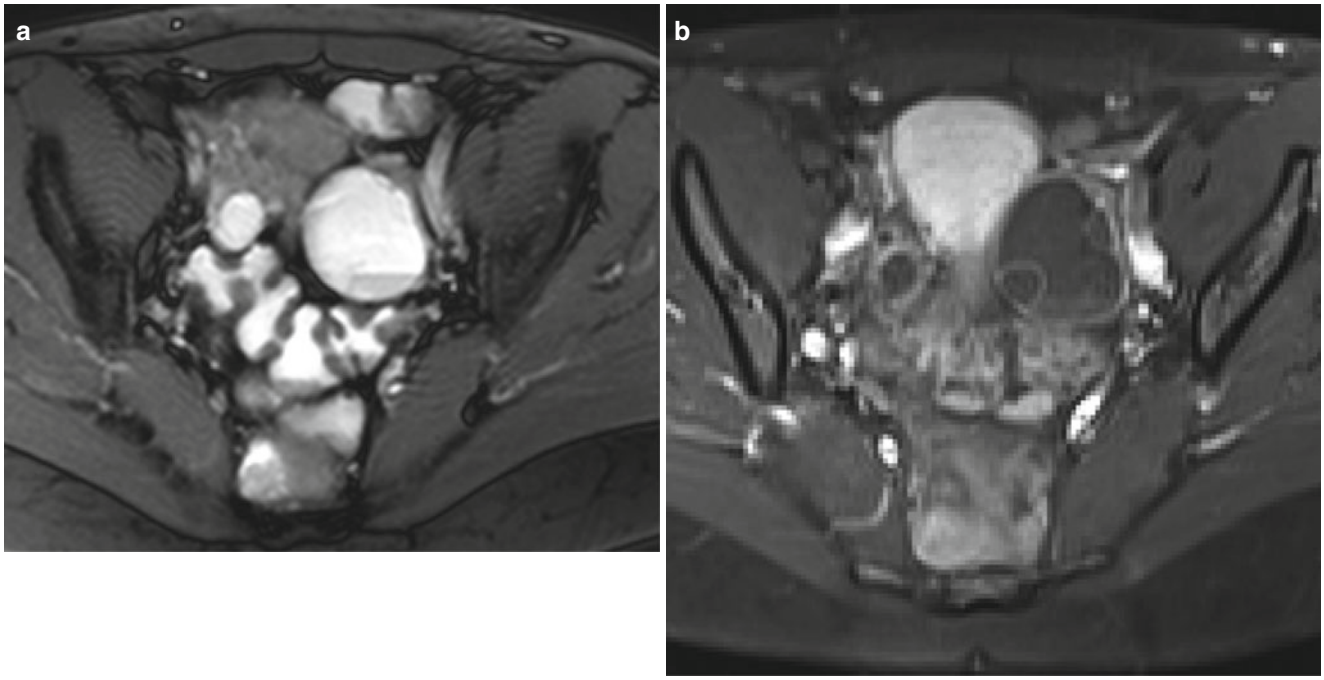

Fig. 11 (**a**) Hemorrhagic corpus luteum cyst in a 41-year-old patient. Axial T2-weighted TRUFI MR image shows a complex cyst with high signal intensity in the left ovary. There are intracystic septations and sedimentation in the posterior aspect of the cyst. (**b**) Axial T1-weighted TSE MR image with fat saturation and contrast administration shows low signal intensity of the cyst with enhancement of the intracystic septa

CT Findings

Corpus luteum cysts have a thicker wall than do follicular cysts, and this wall is mostly irregular in thickness and structure because of accompanying factors such as a recent cystic rupture or adherent blood clots. The cyst wall can be enhanced to a limited extent by the use of axial contrast-enhanced CT, which also shows the presence of free fluid adjacent to the cyst [6, 7].

Differential Diagnosis

The complex intracystic characteristics of corpus luteum cysts may mimic an endometrioma or even solid tumors such as epithelial tumors, sex-cord stromal tumors, or germ cell tumors.

Hemorrhagic Functional Cysts

A round or ovoid hemorrhagic cyst forms when a Graafian follicle, follicular cyst, or corpus luteum bleeds. Typically, such cysts are located within the ovary or in the ovarian cortex. These cysts can reach a diameter of up to 10 cm. In typical cases involving a cyst with a diameter of less than 5 cm, short-term follow-up is recommended for women of childbearing age as well as for postmenopausal women; MRI evaluation of these cysts is generally recommended if the cyst does not resolve within 3 months or if its diameter exceeds 5 cm [6, 14].

MRI Findings

The majority of hemorrhagic cysts are hyperintense on T1-weighted sequences because of early staging of the hemorrhage. Signal intensity typically stays high on T1-weighted images with fat suppression [17], and these growths typically display as partially hyperintense or heterogeneously intense on T2-weighted images. The intravenous administration of a gadolinium-based contrast agent may provide somewhat greater enhancement of the cystic wall, but the presence of an internal nodule (i.e., blood clot) cancels out this potential enhancement [6].

CT Findings

A hemorrhagic ovarian cyst displays on CT as a heterogeneous ovarian mass with some contrast enhancement of the cystic wall. The central cystic region shows high attenuation representing blood.

Differential Diagnosis

Endometrioma as a differential diagnosis to hemorrhagic ovarian cysts is more homogeneous and shows hyperintense intensity on T1-weighted images with and without fat suppression or after intravenous gadolinium administration. As discussed previously, in addition to clinical symptoms and patient history, the typical shading shown on T2-weighted images helps to distinguish these cysts from other blood-containing ovarian lesions (e.g., hemorrhagic ovarian cyst, hemorrhagic corpus luteum cyst). Glastonbury [16] found

these cysts to have an MRI sensitivity of 90–92 %, a specificity of 91–98 %, and a diagnostic accuracy of 91–96 %.

Endometriomas involve in 30–50 % both ovaries and are accompanied by clinical symptoms such as recurrent dysmenorrhea, pain, dyspareunia, irregular bleeding, and infertility. The presence of small, hyperintense endometrial implants together with tethered bowel loops and low signal intensity in the adhesive bands associated with ovarian tissues may also prove helpful in MRI-aided diagnosis of hemorrhagic functional cysts. In addition, the use of T1-weighted fat-saturation imaging sequences is similarly effective [6].

Ectopic pregnancy can sometimes mimic the appearance of hemorrhagic functional cysts on imaging, and an elevated hCG level makes these findings strongly suggestive of an ectopic ovarian gestation. A negative hCG makes a hemorrhagic cyst most likely [7]. Further possibilities for differential diagnoses include ovarian torsion or a degenerating leiomyoma or dermoid cyst.

Theca Lutein Cysts

A theca lutein cyst (or hyperreactio luteinalis) is a subtype of functional ovarian cyst found in women of childbearing age; these lesions develop as a result of an excessive response to β-hCG and other circulating gonadotropins. Theca lutein cysts are rarely observed in normal pregnancies and are typically asymptomatic, although they have been shown to cause nausea, vomiting, and abdominal distension and, on occasion, abdominal pain resulting from hemorrhage, rupture, or torsion of the cyst [6, 7, 18]. Theca lutein cysts typically present multifocally and bilaterally.

MRI Findings

The typical MRI of these cysts displays varying signal intensity due to the similar variance in cystic blood content [6, 7]. Enhanced visualization of the bilaterally enlarged, cyst-containing ovaries can be attained by the administration of contrast media, as these cysts mimic enhanced septations [6, 7].

CT Findings

As with MRI, CT of theca lutein cysts also typically displays bilaterally enlarged ovaries with multiple, variably sized cystic lesions appearing as a multiloculated cystic mass. Cystic density may vary significantly based on hemorrhagic complications. The cystic walls are similar to very thin septations, and in contrast to corpus luteum cysts, there are no wall irregularities or nodularities [6, 19].

Differential Diagnosis

The multiple cysts present in hyperreactio luteinalis may resemble cystic ovarian neoplasm with septations (e.g., mucinous cystic tumors, granulosa cell tumors). For accurate diagnosis of this condition, radiologic findings must be correlated with the patient's clinical history.

Luteomas of Pregnancy

Luteoma of pregnancy is a rare, tumorlike mass that emerges during pregnancy and regresses spontaneously following delivery and is always benign. Luteomas result from the hormone-dependent proliferation of luteinized ovarian stroma cells. They may occur uni- or bilaterally in multiparous women, most often in the third and fourth decades. An increased prevalence of this condition can be found in the African-American population [20]. Luteomas vary widely in size, ranging from microscopic lesions to greater than 20 cm in diameter, with multiple lesions developing at the same time within the same ovary. Ovaries and serum testosterone typically return to normal size and levels, respectively, 2–3 weeks after delivery. Recurrence of luteomas with subsequent pregnancy is rare [20, 21].

MRI Findings

MRI of luteomas displays results similar to that of other cystic tumors or tumorlike lesions found in ovarian tissue. In many cases, luteomas present bilaterally as multilocular cystic, complex heterogeneous masses with thickened internal septa. These lesions can be highly vascularized [22]. Luteomas show intermediate to high signal on T1-weighted images, and the administration of contrast media results in marked enhancement of luteoma structures on T2-weighted images. Luteomas do not typically progress to malignancy, and no secondary signs of malignancy are generally seen on MRI [22, 23].

CT Findings

CT examination in pregnancy is contraindicated because of the ionizing radiation produced by this imaging modality. Instead, ultrasound (sonography) and MRI are typically used to evaluate adnexal masses during pregnancy.

Differential Diagnosis

Differential diagnoses for luteomas include benign and malignant tumors, with benign tumors being much more common than malignant ones.

Despite the relative rarity of maternal virilization during pregnancy, the most common cause of this condition is a luteoma of pregnancy [24].

Biography Dr. Freiwald-Chilla studied medicine in Zurich from 1992 to 2000. From 2000 to 2001, she was an assistant physician at the Surgical Clinic of Triemli City Hospital. She was then an assistant physician at the Institute for Diagnostic Radiology at Zurich University Hospital from 2002 to 2006, with rotations in radiology at the Orthopaedic Balgrist University Clinic and the Institute for Neuroradiology at the Zurich University Hospital. She continued her training from 2004 to 2006 at the Institute for Medical Radiology and Nuclear Medicine at Waid City Hospital in Zurich. Since 2006, she has worked at the Institute for Radiology at the Baden Canton Hospital in Switzerland, initially as an assistant physician. After receiving her Medical Specialist Certification in 2007, she became a senior physician at the institute. Since 2009 she has been acting senior physician at the Institute for Radiology at the Baden Canton Hospital, and on January 9, 2012, she was named senior physician.

Dr. Hauser studied chemistry at the University of Basel in Switzerland, followed by doctoral studies in biochemistry at the University of Bern and the Biocenter in Basel until 1995. After receiving his PhD, Dr. Hauser worked as a postdoctoral fellow and scientific group leader in the Department of Medical Biochemistry at the University of Cologne in Germany and the Department of Rheumatology at the University of Zürich in Switzerland. During that time, he also studied medicine at the University of Basel. Dr. Hauser's clinical career includes training in surgery at the University of Basel, followed by specialist training in gynecology and obstetrics until 2007 at the University of Ulm in Germany. Since 2007, Dr. Hauser has worked in the Department of Gynecology and Obstetrics at the Baden Canton Hospital in Switzerland as a senior physician and vice head of the department.

Rahel Kubik-Huch earned her medical degree and doctorate from the University of Zurich in 1991 and her titular professorship for diagnostic radiology in 2005. In 2006, she completed her interuniversity postgraduate studies of public health at the Universities of Zürich, Berne, and Basel (Master of Public Health, MPH). Following her medical studies, she spent 1 year at Rockefeller University Hospital in New York, USA. She completed her residency in diagnostic radiology at the University Hospital of Zürich, Switzerland, where she subsequently worked as senior physician. Since 2002 she has worked at the Kantonsspital Baden AG in Switzerland, where she was appointed head of the Institute of Radiology and the Department of Medical Services in 2005. In 2010, she also became a member of the executive board of the hospital.

She is a member and former president of the Executive Board of the Swiss Society of Radiology SGR-SSR; deputy editor for the journal European Radiology; member of the organizing committee of the School of MRI, ESMRMB; course organizer for "Advanced Breast and Pelvis MR Imaging"; and satellite course advisor for breast imaging at the International Diagnostic Course in Davos (IDKD). She has received several scientific awards, including the Anniversary Award ("Jubiläumspreis") from the Swiss Society of Radiology. She is author and coauthor of numerous scientific publications and book chapters.

Her specialist focus is magnetic resonance tomography (particularly of the abdominal region as well as the female breast and pelvis) and breast imaging allowing for minimal invasive interventions.

References

1. Thurmond A, Jones M, Cohen D. Adnexa. In: Gynecologic, obstetric and breast radiology. 1st ed. London: Blackwell Science; 1997.
2. Cohen D. Ovary and adnexa. In: Abdominal-pelvic MRI. 2nd ed. Hoboken: Wiley; 2006.
3. Chilla B, Hohl M, Kubik R. Raumforderungen der Adnexe – Bildgebung und Differential diagnosen. Radiologie up2date. 2008;4:335–55.
4. Kubik R. Female pelvis. Eur Radiol. 1999;9:1715–21.
5. Steinkeler J, Woodfield C, Lazarus E, Hillstrom M. Female infertility: a systematic approach to radiologic imaging and diagnosis. Radiographics. 2009;29:1353–70.
6. Hricak H. Pelvis. In: Diagnostik imaging: gynecology. 1st ed. Salt Lake City: Amirsys; 2007.
7. Tamai K, Koyoma T, Saga T. MRI features of physiologic and benign conditions of the ovary. Eur Radiol. 2006;16:2700–11.
8. Fleischer AC, Daniell JF, Rodier J, Lindsay AM, James Jr AE. Sonographic monitoring of ovarian follicular development. J Clin Ultrasound. 1981;9(6):275–80.
9. Spencer JA, Forstner R, Cunha TM, Kinkel K. ESUR guidelines for MR imaging of the sonographically indeterminate adnexal mass: an algorithmic approach. Eur Radiol. 2010;20(1):25–35. http://www.ncbi.nlm.nih.gov/pubmed/20069737.
10. Lidle A, Davies A. Pelvic congestion syndrome: chronic pelvic pain caused by ovarian and internal iliac varices. Phlebology. 2007;22:100–4.
11. Saksouk FA, Johnson SC. Recognition of the ovaries and ovarian origin of the pelvic masses with CT. Radiographics. 2004;24:133–46.
12. Jared A, Seth C, Mayuree K, Cary S. Incidence of ovarian maldescent in women with mullerian duct anomalies: evaluation by MRI. AJR Am J Roentgenol. 2012;198(4):381–5.
13. Taupiz M, Rogalia P. MR and CT techniques. In: MRI and CT of the female pelvis. 1st ed. Berlin/Heidelberg: Springer; 2009.
14. Brown D, Dudiak K, Laing F. Adnexal masses: US characterization and reporting. Radiology. 2010;254:342–54.
15. Laing FC, Allison SJ. US of the ovary and adnexa. To worry or not to worry? Radiographics. 2012;32:1621–39.
16. Glastonbury CM. The shading sign. Radiology. 2002;224(1):199–201.
17. Togashi K. MR imaging of the ovaries: normal appearance and benign disease. Radiol Clin North Am. 2003;41(4):799–811. http://dx.doi.org/10.1148/radiol.2241010361.
18. Ghossain MA, Buy JN, Ruiz A. Hyperreactio luteinalis in a normal pregnancy: sonographic and MRI findings. J Magn Reson Imaging. 1998;8:1203–6.
19. Jung SE, Byun JY, Lee JM, Rha SE, Kim H, Choi BG, Hahn ST. MR imaging of maternal diseases in pregnancy. AJR Am J Roentgenol. 2001;177:1293–300.
20. Choi JR, Levine D, Finberg H. Luteoma of pregnancy: sonographic findings in two cases. J Ultrasound Med. 2000;19:877–81.
21. Van Slooten AJ, Rechner SF, Dodds WG. Recurrent maternal virilization during pregnancy caused by benign androgen producing ovarian lesions. Am J Obstet Gynecol. 1992;167:5.
22. Masarie K, Katz VK, Baldeerston K. Pregnancy luteomas: clinical presentations and management strategies. Obstet Gynecol Surv. 2010;65(9):575–82.
23. Hung-Wen K, Ching-Jiunn W, Kuo-Teng C. MR imaging of pregnancy luteoma: a case report and correlation with clinical features. Korean J Radiol. 2005;6:44–6.
24. Whitecar P, Turner S, Higby K. Adnexal masses in pregnancy: a review of 130 cases undergoing surgical management. Am J Obstet Gynecol. 1999;181:19–24.

The Ovarian Endometrioma: Clinical Setting and Ultrasound Findings

Stefano Guerriero, Silvia Ajossa, Cristina Peddes, Maura Perniciano, Bruna Soggiu, Jasjit S. Suri, Luca Saba, and Gian Benedetto Melis

Abstract

Ovarian endometrioma is defined as a pseudocyst arising from growth of ectopic endometrial tissue. The typical features of endometriomas are diffuse low-level internal echoes ("ground glass") in the absence of particular neoplastic features and with a clear demarcation from ovarian parenchyma. Several studies report very high values of specificity with values of sensitivity usually ranging from 87 to 77 %.

Keywords

Endometriosis • Endometrioma • Ovarian neoplasm • Imaging • Ultrasound • Flow chart • Ovarian mass

Ovarian endometrioma is often defined as a pseudocyst arising from growth of ectopic endometrial tissue, which progressively invaginates the ovarian cortex [1]. This kind of cyst is more frequent in the premenopausal women. As a matter of fact, Alcázar et al. [2] report in a series of adnexal masses submitted to surgery an incidence of 35 % (546/1,540) in premenopausal patients and only 2 % in postmenopause (12/606). Also Van Holsbeke et al. [3] comparing premenopausal and postmenopausal patients found only 30 endometriomas (2 %) out of 1,377 adnexal masses in the postmenopausal group and 683 endometriomas (32 %) out of 2,134 adnexal masses in the premenopausal group of the 3,511 patients included in the IOTA studies [3]. Other studies report that the incidence of endometriomas among ovarian masses in premenopausal populations ranged from 29 to 31 % when functional cysts were included and from 45 to 58 % when functional cysts were excluded [4, 5]. Data from IOTA study report that patients with an endometrioma were younger than those with other benign (median age 34 vs. 45 years) or malignant (median age 56 years) tumors [3]. Among women with unilateral ovarian endometrioma, a left cyst was found more frequently than a right cyst [6, 7].

The presence of an endometrioma is frequently associated with pelvic pain [8]. In fact this pathology is found in 32 % of women with pelvic pain and within the age range of 20–45 years [9]. Recent studies demonstrate that pelvic pain in women with ovarian endometrioma is mostly associated with coexisting peritoneal lesions and/or deep endometriosis [10, 11]. The presence of endometrioma is also related to the

S. Guerriero, MD (✉)
Department of Obstetrics and Gynecology, University of Cagliari, Cagliari, Italy

Dipartimento Chirurgico Materno Infantile e di Scienze delle Immagini, Università di Cagliari, Via Ospedale 46, I-09124 Cagliari, Italy
e-mail: gineca.sguerriero@tiscali.it

S. Ajossa, MD • C. Peddes • M. Perniciano
B. Soggiu • G.B. Melis
Department of Obstetrics and Gynecology, University of Cagliari, Cagliari, Italy

J.S. Suri, PhD, MBA, Fellow AIMBE
CTO, Global Biomedical Technologies, Roseville, CA, USA

Department of Biomedical Engineering, Idaho State University (Aff.), Pocatello, ID, USA

L. Saba, MD
Department of Radiology, University of Cagliari, Cagliari, Italy

L. Saba et al. (eds.), *Ovarian Neoplasm Imaging*,
DOI 10.1007/978-1-4614-8633-6_4, © Springer Science+Business Media New York 2013

infertility. Two of the mechanisms proposed for this interference are the association with dense pelvic adhesions [33], frequently present with endometriomas, and the reduction of follicular numbers and activity associated with microscopic stromal implants [12]. On the contrary the presence of ovarian endometrioma in a controlled ovarian hyperstimulation cycle for IVF treatment is not associated with a reduced number of oocytes retrieved from the affected ovary [13]. New evidences are present in the literature about the necessity of surgical removal in infertile patients due to the lower ovarian reserve after surgery. Additionally, a reduced response of the ovaries to gonadotropins has been described in different studies after surgical removal of endometriomas, and the quality of the oocytes retrieved in IVF cycles is not improved after surgery [14].

Two conflicting theories on the origin of ovarian endometriomas are reported. The first, called the "colonization theory," was formulated in 1946 by McLeod [15] and was recently confirmed by Nezhat and colleagues with a laparoscopic study [16]. This states that endometrioma develops in a functional cyst that has been invaded by superficial ovarian cortex endometriosis. Recently Vercellini et al. [17] demonstrate that bleeding from a corpus luteum appears to be a critical event in the development of endometriomas confirming this theory [17]. Using serial ultrasonographic scans, these authors demonstrate the transition to an endometriotic cyst from hemorrhagic corpus luteum. The second theory, the "invagination theory," formulated by Hughesdon [18] and also laparoscopically confirmed by Brosens and Puttemans [19], refused the previous theory and reported that in most cases the endometrioma is formed by invagination of cortex and that active implant is located at the site of invagination [19]. This theory is the basis of the definition of endometriomas as pseudocyst. The inflammation around these intracystic endometrial foci, associated with cyst wall exudation and congestion of vessels, instead of shedding of the ectopic endometrium, produces the chocolate-colored fluid [20] responsible for the content of the cyst and consequently for the ultrasonographic imaging.

Ultrasonographic Findings and Use of Color Doppler

The spectrum of transabdominal sonographic findings in endometrioma is wide [21], because of the difficulty in accurately determining the presence or otherwise of hematic content with the low frequencies used by the transabdominal probe. In fact, in the largest series of endometriomas presented in the literature [21], the majority of cysts were predominantly anechoic.

In contrast, using B-mode transvaginal ultrasonography, Kupfer and colleagues [22] showed, in a retrospective study, the presence in 82 % of cases of a homogeneous hypoechoic "carpet" of low-level echoes. Endometriomas may exhibit a variety of sonographic appearances. The typical features of endometriomas are diffuse low-level internal echoes ("ground glass") and hypoechoic focal lesion in the wall in the absence of particular neoplastic features and with a clear demarcation from ovarian parenchyma [23–26] (Figs. 1, 2, and 3). Also the IOTA [3] study confirms that 73 % of the endometriomas had cyst fluid with ground glass echogenicity vs. 6 % of the

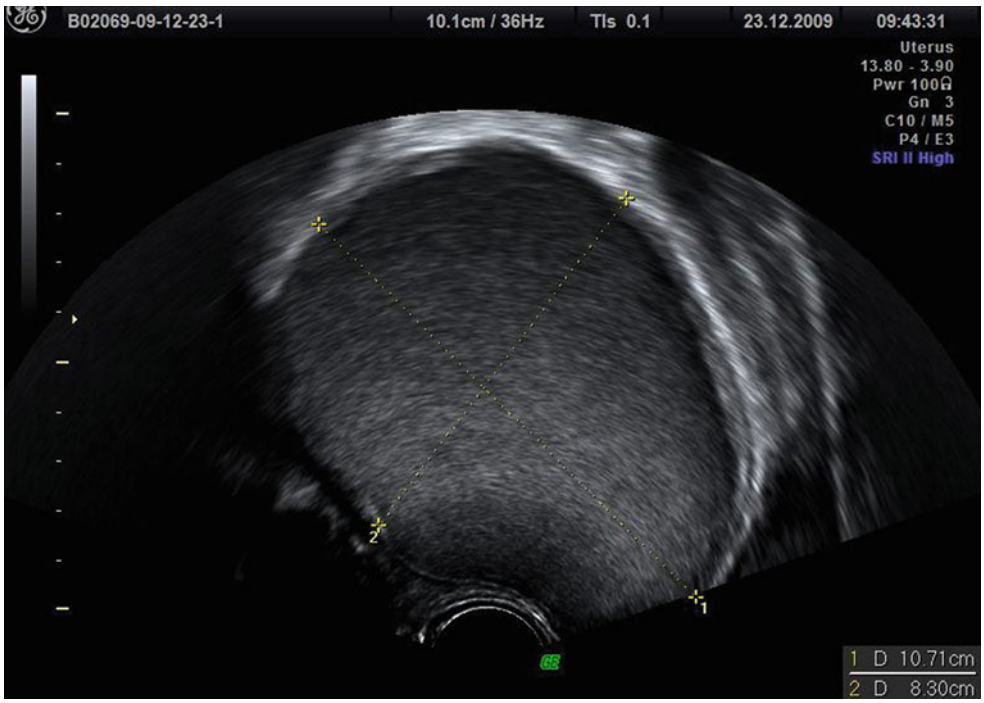

Fig. 1 The typical features of endometriomas: diffuse low-level internal echoes ("ground glass") and hypoechoic focal lesion in the wall in the absence of particular neoplastic features

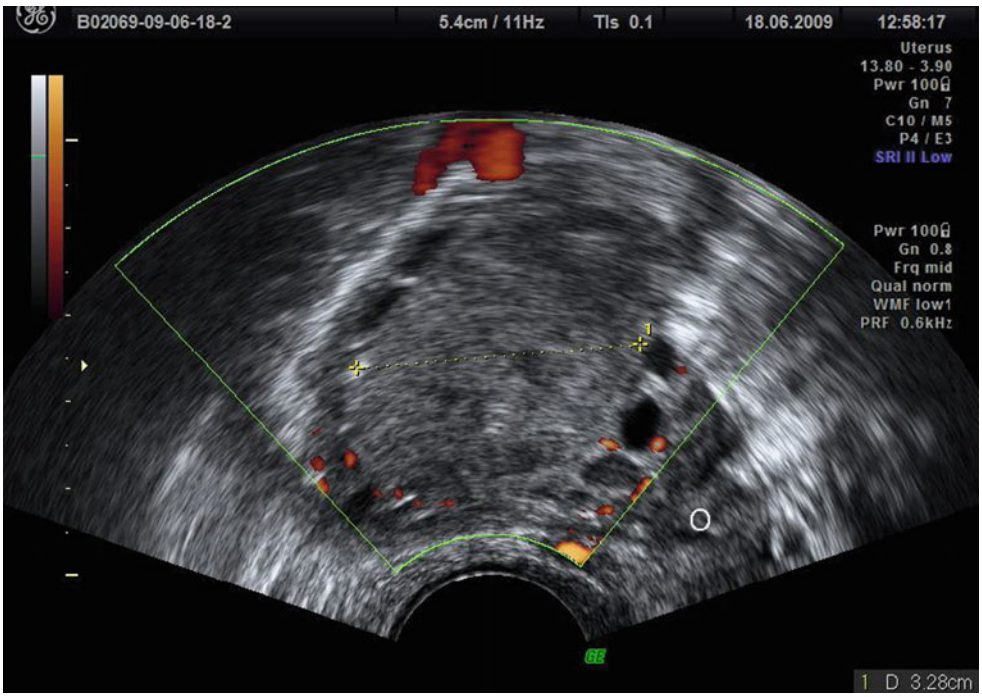

Fig. 2 Diffuse low-level internal echoes ("ground glass") cyst with a clear demarcation from ovarian parenchyma (*O*)

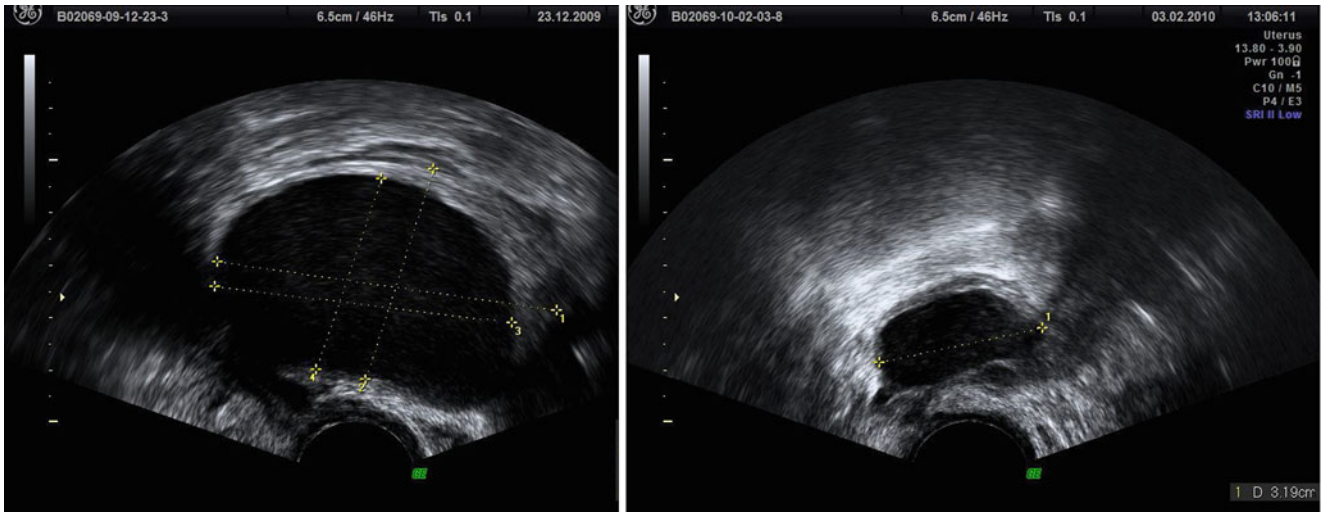

Fig. 3 Less frequent content in two endometriomas: less intense hypoechoic and homogeneous diffuse low-level internal echoes

other benign tumors. Based on IOTA study [3], anechoic content was very rare and present in the 3 % of endometriomas in premenopausal women.

Ovarian endometriosis may be unilocular or multilocular (Fig. 4) (appearing as multiple cysts separated by septations) and is often multiple or bilateral. Van Holsbeke et al. [3] found that only 51 % of the endometriomas were unilocular cysts with ground glass echogenicity of the cyst fluid. These characteristics were found less often among other benign tumors or malignancies or among the small set of endometriomas (4 %) that were found in postmenopausal patients. In fact the endometriomas in the postmenopausal patients were less often unilocular cysts (40 % vs. 66 %), and they present ground glass echogenicity in only 40 % of cases (vs. 74 %) [3].

Patel et al. [23] demonstrate that hyperechoic wall foci (Fig. 5) in a mass with low-level echoes with the absence of neoplastic features are strongly predictive of an endometrioma although the pathologic basis of these hyperechoic wall foci has not been established. Patel et al. [23] suggest that these foci may contain cholesterol, perhaps from the breakdown of cell membranes. In fact they are similar in appearance to hyperechoic wall foci seen in the gallbladder wall in patients with hyperplastic cholecystosis, due to the presence of cholesterol within polyps.

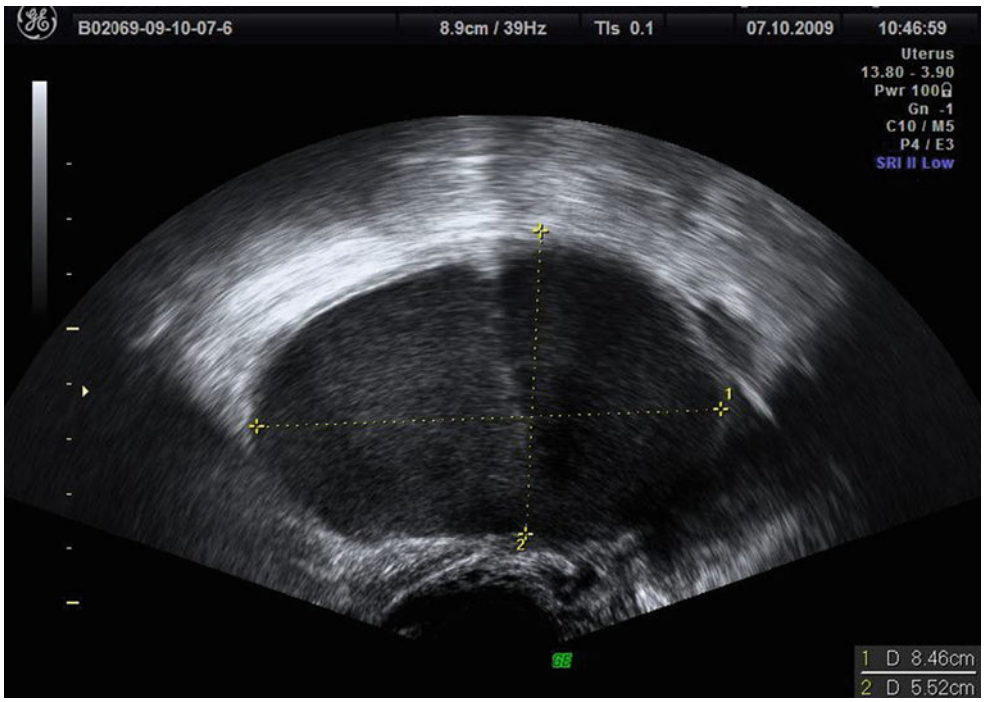

Fig. 4 Bilocular endometrioma

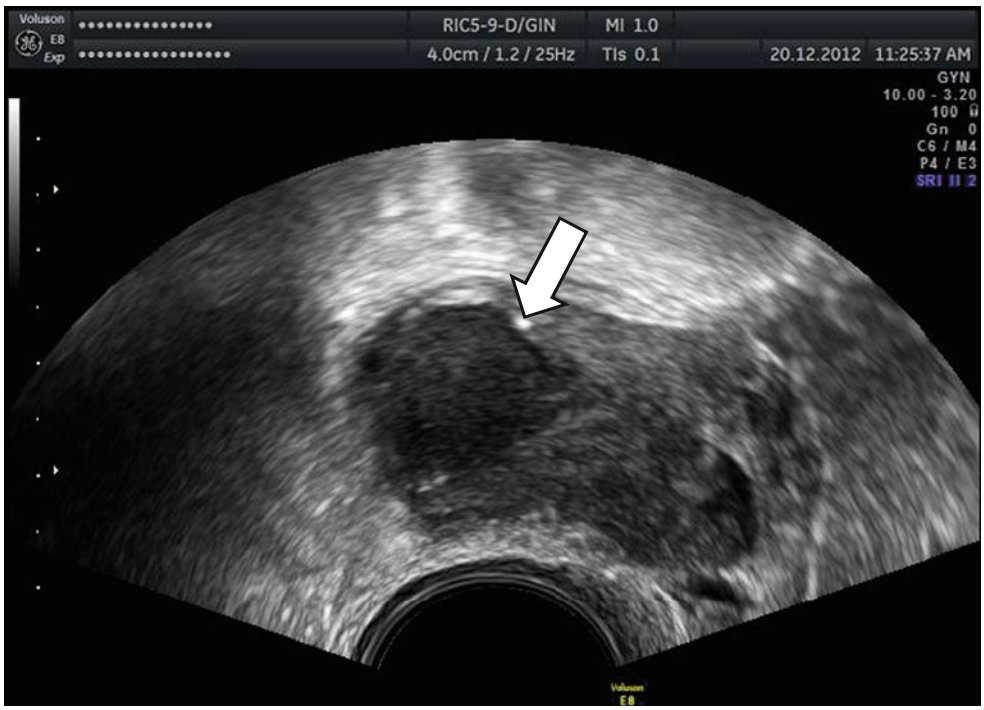

Fig. 5 Hyperechoic wall foci (see *arrow*) in a mass with low-level echoes

Ash and Levine [27] report that in the 10 % of cases, the endometriomas were described as hemorrhagic cysts. A small percentage of endometriomas have less typical US features such as a fluid-fluid level. These authors [27] suggest that in an endometrioma, the supernatant fluid layer should be hypoechoic, with a hyperechoic dependent layer representing blood. On the contrary in a dermoid, the supernatant layer will be echogenic, representing fat.

Atypical endometriomas included cases with retracted clots that appeared solid but without blood flow (Figs. 6 and 7). As correctly discussed by Brown et al. [28], endometriomas may contain a small solid area in 4–20 % of cases, and these can simulate the mural nodule of malignant neoplasm [23, 26]. Based on IOTA study [3], an irregular wall can present in the 26 % of endometriomas in premenopausal women, and in the 10 % of these, a papillary projection was present.

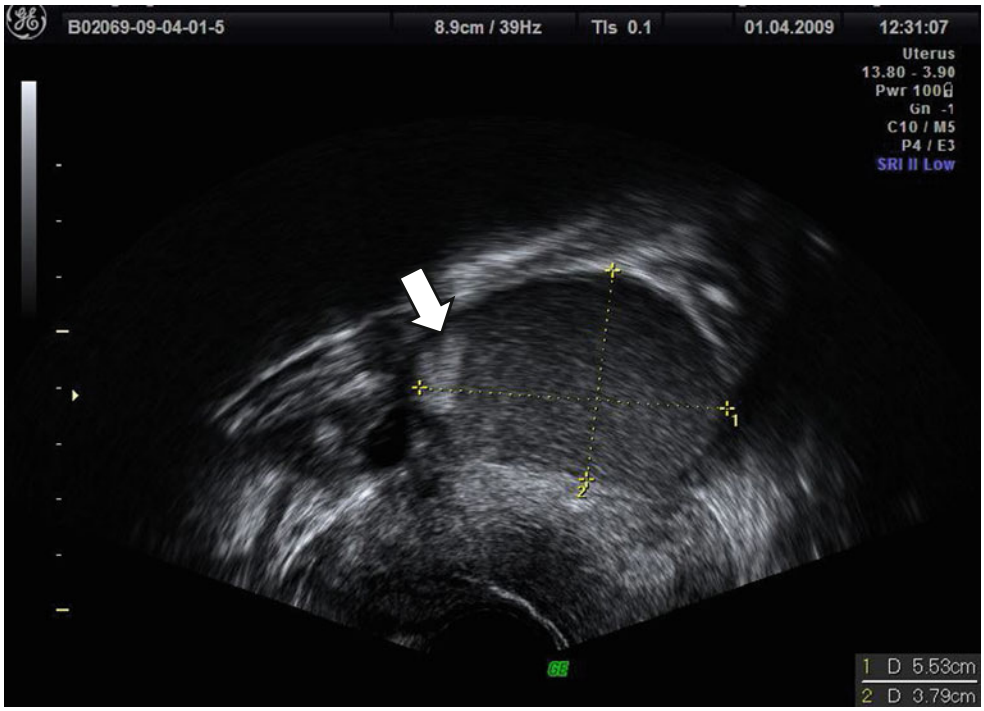

Fig. 6 Atypical endometriomas with irregular wall due to retracted clots (see *arrow*)

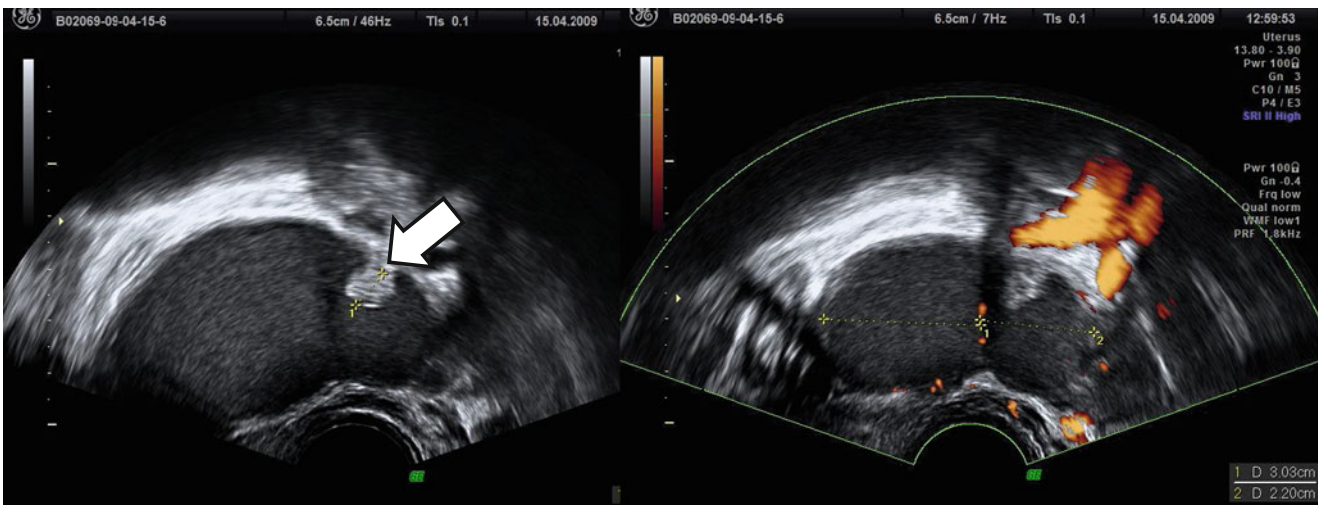

Fig. 7 Another atypical endometriomas with a small solid area that can simulate the mural nodule of malignant neoplasm but without blood flow (see *arrow*)

The Van Holsbeke study [3] reports a proportion of "atypical" endometriomas higher than in any other in the literature [2, 22–27]. In particular Guerriero et al. [29] found that the 83 % of endometriomas in premenopausal patients demonstrated the typical appearance of a unilocular cyst with ground glass echogenicity of cyst fluid [29] vs. only 53 % in IOTA study [3]. The causes of this difference are unknown.

To evaluate these "atypical" endometriomas, Guerriero et al. [29] propose to use color Doppler. Usually endometrioma showed an absent or scanty peripheral vascularization at color Doppler (Fig. 8). In the IOTA study [3], the proportion of masses with color score 1 or 2 (absent to minimal) was 78 %. The use of color Doppler as a secondary test permits to diagnose the presence of endometrioma also in case of "atypical" endometriomas in which no flow is detected in the echogenic portion due to the presence of a clot and enables them to be differentiated from an intracystic vegetation. On the contrary, this simple color Doppler imaging flow chart (Fig. 9), based on the localization of vessels and intensity of arterial flow, permits exclusion of ground glass appearance but "rich vascularization" frequently associated with the presence of corpus luteum cysts or mucinous cystadenoma [29].

Alcázar reports that vascularization of ovarian endometriomas in patients presenting with pelvic pain is higher than

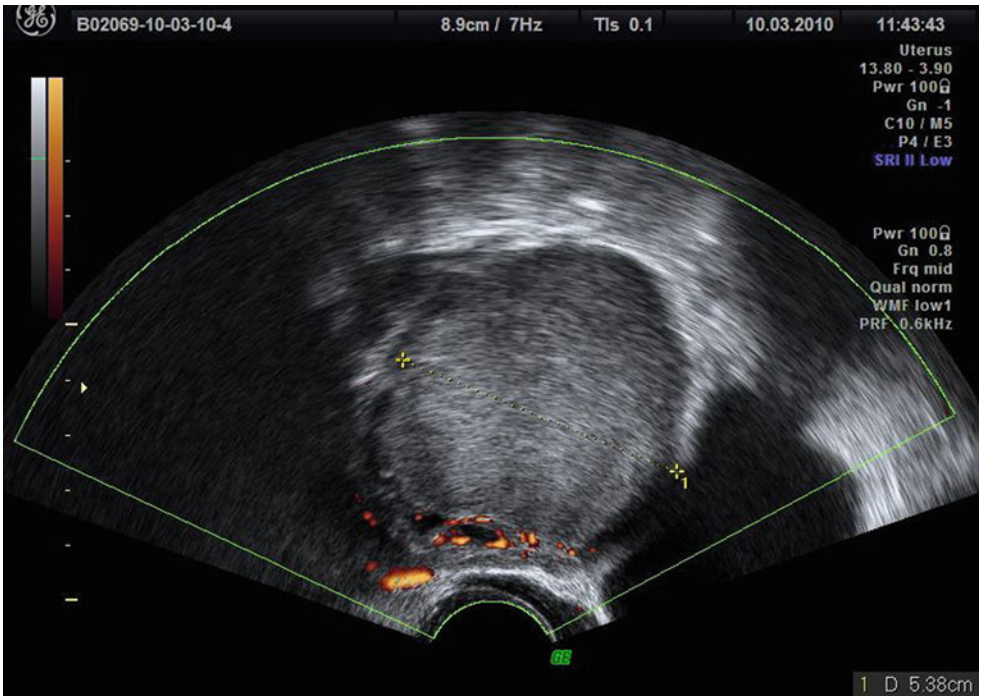

Fig. 8 The typical scanty peripheral vascularization at color Doppler of endometrioma

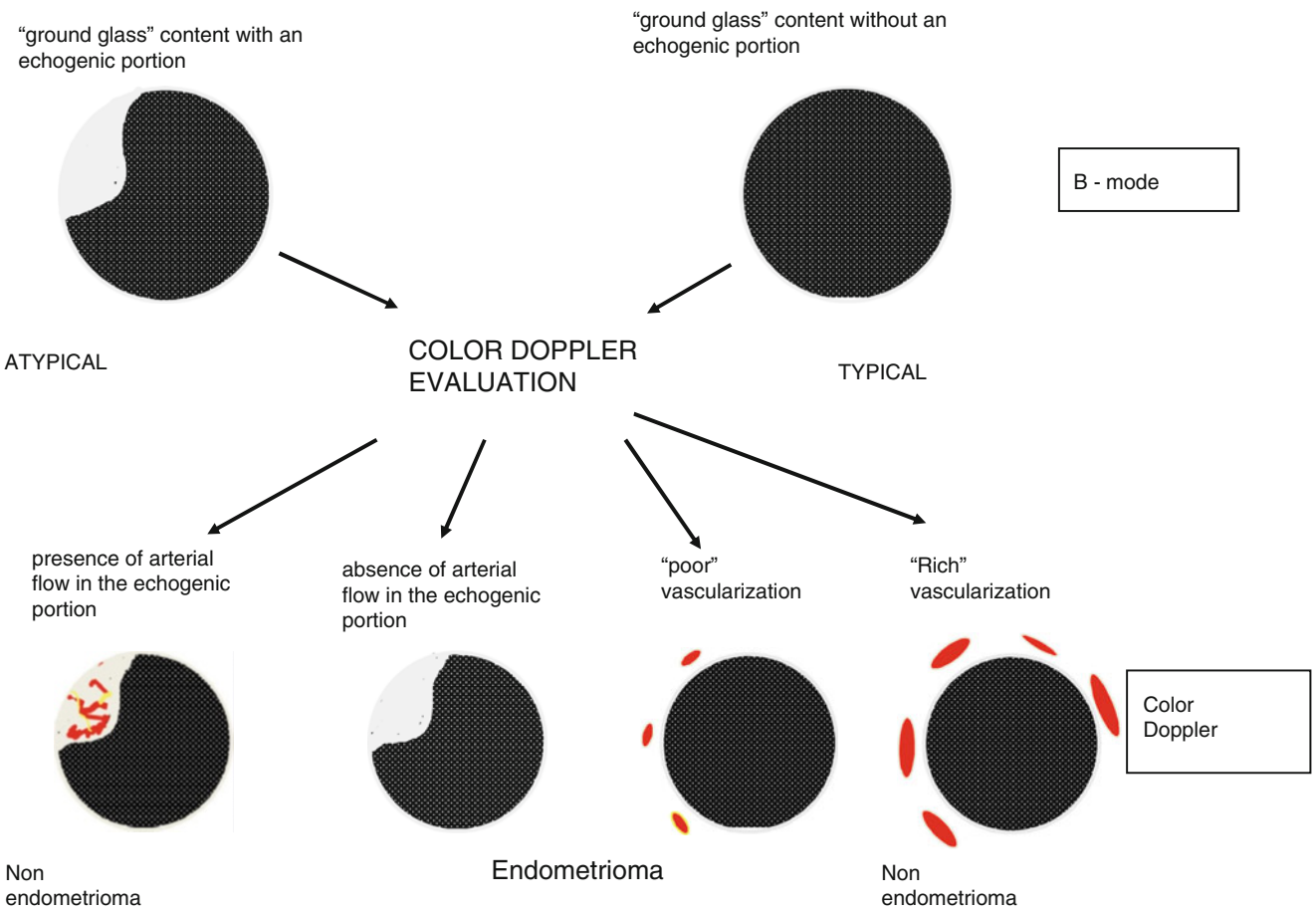

Fig. 9 The flow chart proposed by Guerriero et al. [29] using color Doppler (see text)

in asymptomatic patients. This could be an indicator of endometriosis activity [30]. From anecdotal point of view (because without any clinical value), Aleem et al. [31] evaluating pulsed Doppler analysis found that mean of the resistance index (RI) and pulsatility index (PI) for the endometriomas were 0. and 0.95, respectively. All endometriomas showed an RI of >0.5 with a range of 0.5–0.74, while the PI was 0.59–1.59.

The reproducibility of ultrasonographic B-mode findings is high [32]. Guerriero et al. [32] performed a study to evaluate the reproducibility and the accuracy of B-mode ultrasonographic features of ovarian endometrioma ("ground glass appearance"). They used digitally stored B-mode sonographic images of 98 women submitted to surgery for the presence of an adnexal mass performing an evaluation by five different examiners with different degrees of experience.

Table 1 The diagnostic accuracy of ultrasonography in the diagnosis of endometrioma

Reference	Sensitivity (%)	Specificity (%)
Mais et al. [24]	84	90
Kurjak and Kupesic [33]	84	97
Volpi et al. [34]	82	98
Guerriero et al. [35]	84	95
Alcázar et al. [26]	89	91
Guerriero et al. [29]	81	96
Sokalska et al. [36]	77	98
Van Holsbeke et al. [3]	68	98
Alcázar et al. [2]	89	96

The intraobserver agreement was good or very good for all examiners. Also the interobserver agreement was good for all experts (kappa = 0.66–0.78). Interobserver agreement between experts and highly experienced operators was good or very good (kappa = 0.70–0.83) [32].

The diagnostic value of transvaginal B-mode ultrasonography is well established. In Table 1 the diagnostic performance of B-mode ultrasonography among the most important studies published in the literature [2, 3, 24, 26, 29, 33–36] is reported. Several studies report very high values of specificity with values of sensitivity usually ranging from 87 to 77 % (Table 1). Only the IOTA study [3], for unknown reason, reports a value of sensitivity of 68 %. Alcázar et al. [2], analyzing pre- and postmenopausal women separately, found that diagnostic performance is different. As a matter of fact, transvaginal ultrasound is more sensitive for diagnosing endometrioma in premenopausal women in comparison with postmenopausal population (89 % vs. 67 %). A possible explanation for this, in the case of endometrioma, is that ultrasound appearance of this kind of cyst may change from premenopause to postmenopause because bleeding within the lesion would stop in menopausal women and cyst mucosa will become atrophic as also suggested by Van Holsbeke et al. [3] that observe the increase of anechoic content in this latter population. The different prevalence of endometrioma in premenopausal and postmenopausal women may be also an explanation because examiner's knowledge of different prevalence may bias his/her impression [2].

The differential diagnosis should be performed by mainly considering hemorrhagic cysts (Fig. 10), teratomas, and

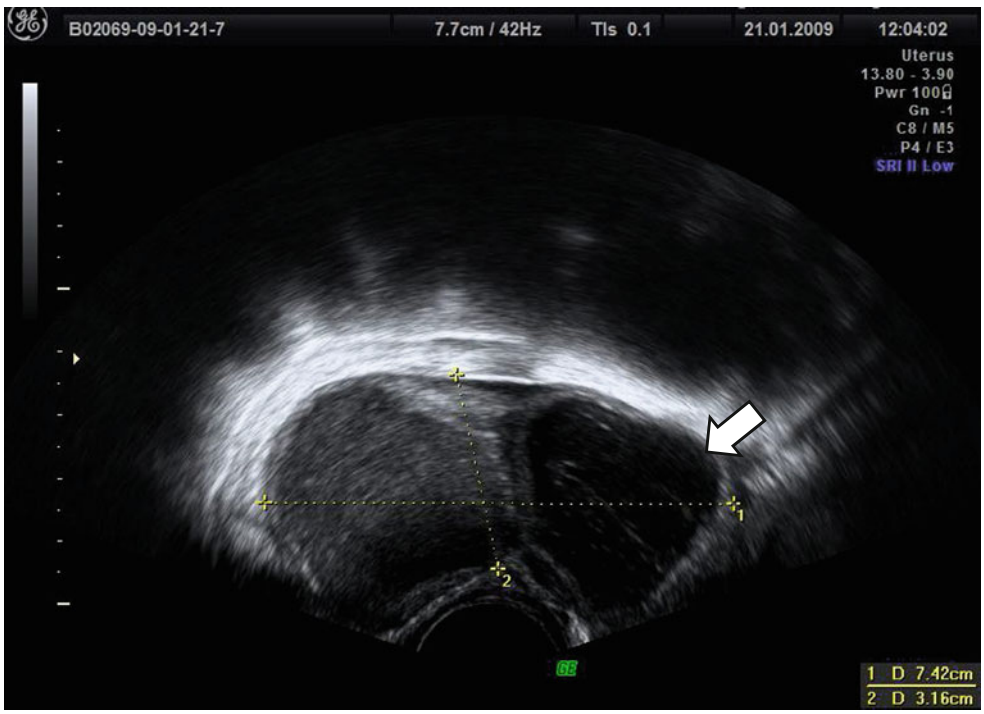

Fig. 10 The hemorrhagic cysts (see *arrow*) are often associated with endometrioma

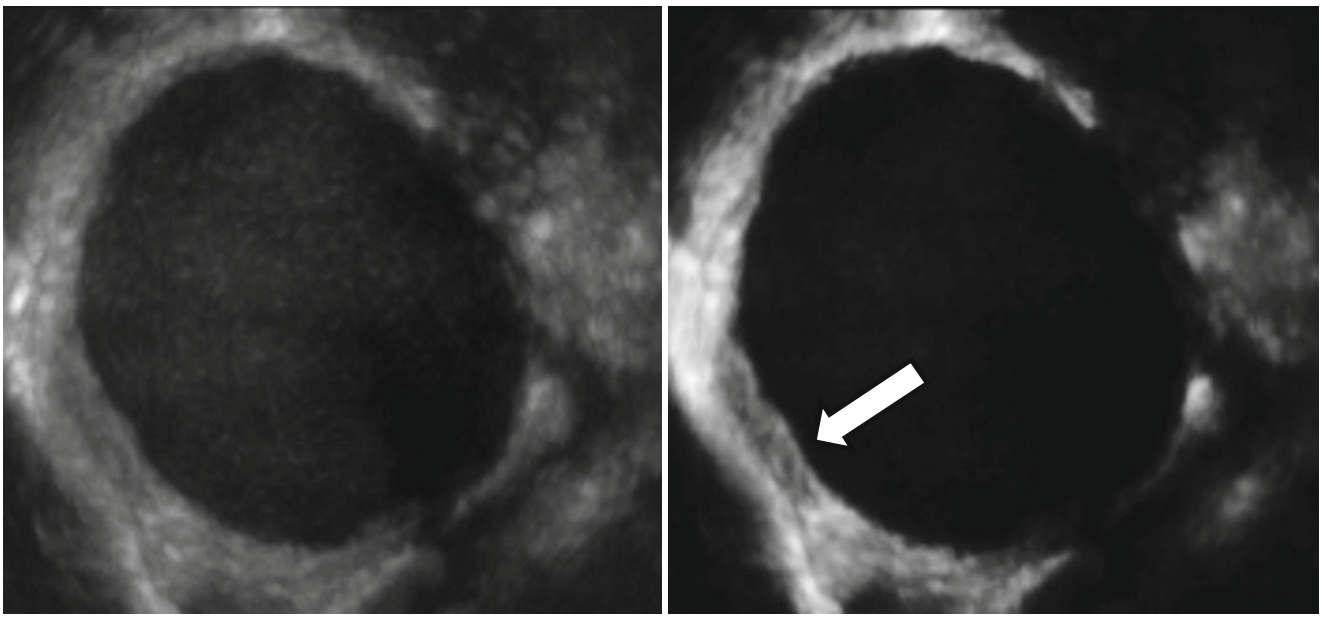

Fig. 11 Using three-dimensional ultrasonography and speckle reduction, the thickened fibrotic capsule is well defined (see *arrow*)

malignant neoplasms. An appropriate anamnesis focused on symptoms and gynecologic history of the patient may be helpful, in fact usually hemorrhagic cysts have often a more acute symptomatology which generally resolves in 4–6 weeks. Alcázar et al. [2] confirm that the main source of false-positive cases in premenopausal population (29/42, 69 %) was the hemorrhagic cysts. In this large series of more than 2,000 adnexal masses, no cases of malignancy were erroneously suspected to be endometriomas in both populations. On the contrary Van Holsbeke et al. [3] observe that a large proportion of masses with ground glass echogenicity in postmenopausal patients are malignant (34/77, 44.2 %). These authors [3], in contrast with Alcázar et al. [2], conclude that masses in postmenopausal women whose cystic contents have a ground glass appearance have a high risk of malignancy and should be observed with caution. We agree with this latter authors due to the very low incidence of endometrioma in postmenopausal population previously reported [2, 3].

Regarding false-negative cases in the 40 % (25/61), a malignant lesion was suspected due to the high rate of irregular walls and presence of papillations previously described [2].

Some additional features have been proposed to reduce the number of false positive and negative. Although promising after first studies [37], the absence of acoustic streaming (defined as movement of particles inside the cyst fluid during gray-scale and/or color Doppler examination provided that the probe had been held still for two seconds to ensure that the movement of the particles was not caused by movement of the probe or the patient) in endometrioma seems unable to discriminate reliably between these masses and other adnexal lesions, in an IOTA study performed on more than 400 adnexal masses [38].

To further reduce the number of false positive and negative, the use of color Doppler has been proposed. Guerriero et al. [29] using the flow chart previously described (Fig. 9) obtain a specificity of 97 % associated with a very high sensitivity of 90 %.

Very few data are present in the literature about three-dimensional (3D) ultrasonographic characteristics of endometrioma. Few studies explore the potential of this new technology in the field of endometriosis [39–42]. Raine-Fenning et al. [39] suggest that some features such as the texture and homogeneity of the endometriotic material within the body of the cyst and the thickened fibrotic capsule and echodense nodules within the wall of the cyst can also be seen on a conventional two-dimensional image but are more apparent when some 3D modalities such as speckle reduction imaging are used to enhance the contrast between different interfaces (Figs. 11 and 12). Rendering can also be used to display Doppler information within a three-dimensional dataset in different formats. The vascular tree can also be seen as a separate entity through subtraction of the gray-scale information, allowing an immediate impression of the vessel pattern in terms of its distribution and progressive branching. At 3D the endometrioma wall is generally well perfused, and the vessels often appear to have a short course, with minimal variation in their diameter, that surrounds the cyst in a uniform manner; Raine-Fenning et al. suggest to call this pattern "bird's nest" appearance [39] (Fig. 13). This technology can be also used for teaching purpose using stored three-dimensional volume for "virtual navigation" [43].

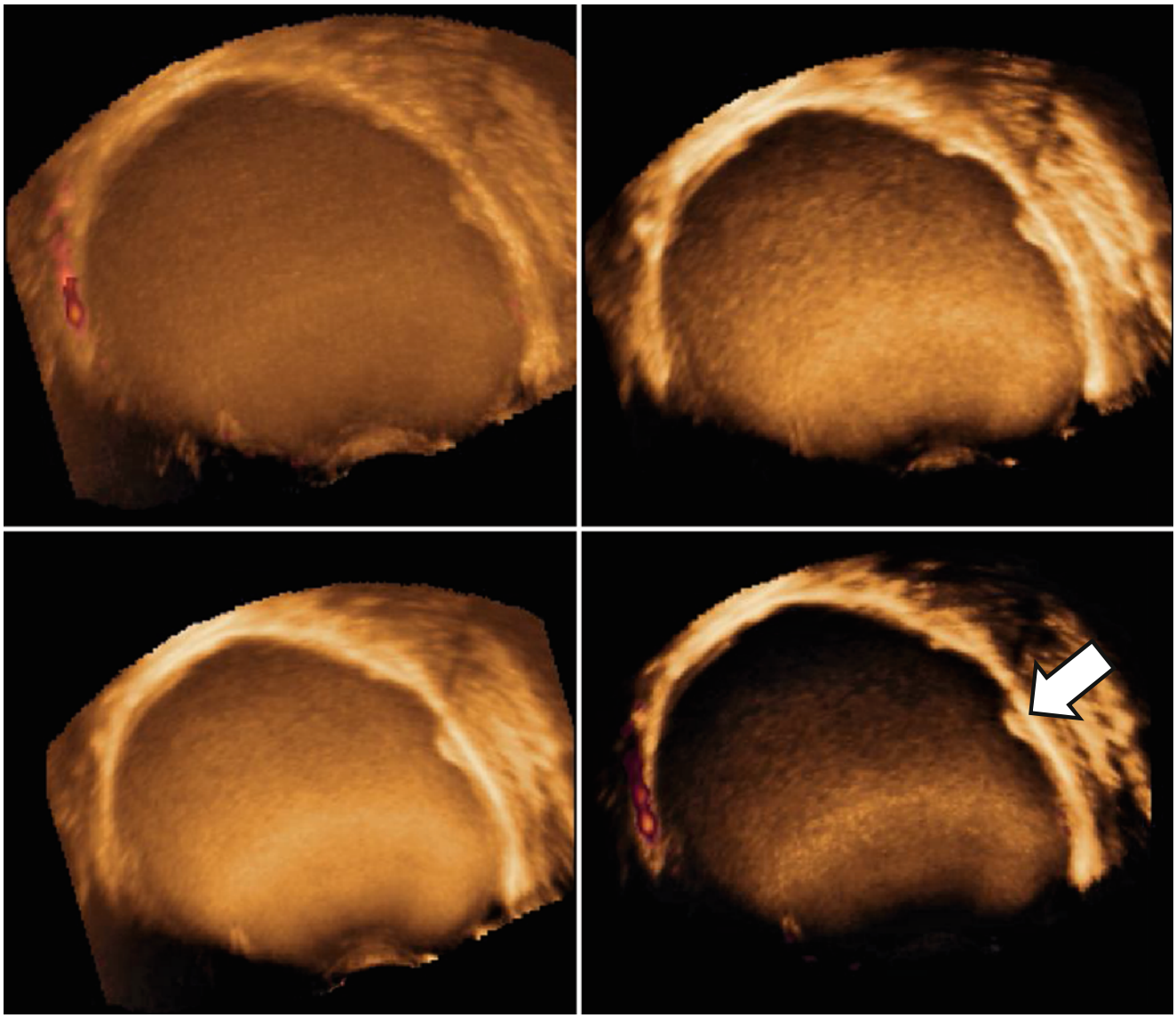

Fig. 12 Another cases of the use of three-dimensional ultrasonography and speckle reduction used to improve the visualization of echodense nodules within the wall of the cyst (see *arrow*)

Recently Alcázar et al. [44] found that three-dimensional ultrasonography mean gray value (MGV) that represents the mean intensity of gray-scale voxels (the smallest unit of volume) within a region of interest can discriminate ovarian endometriomas from other unilocular ovarian cysts in premenopausal women [40]. From a conceptual point of view, this is quite similar to the Hounsfield Unit (HU) values that are used in computed tomography (CT) to analyze the tissue properties and composition. MGV of cysts content is significantly higher in ovarian endometrioma (Fig. 14) when compared with all other kinds of cyst. The receiver-operating characteristics curve shows that using an MGV cutoff ≥ 15.560 had a sensitivity of 85 % and a specificity of 76.5 % for diagnosing ovarian endometrioma (area under the curve, 0.831; 95 % CI, 0.718–0.944). These figures are similar to those for B-mode diagnosis (sensitivity, 90 %; specificity, 82 %). Combining B-mode and MGV gives a sensitivity of 80 % and a specificity of 91 % [44].

Use of Tumor Markers

In the diagnosis of endometrioma, the use of cancer antigen 125, or carbohydrate antigen 125 (CA-125), has been proposed. CA-125, a 220 kD cell surface glycoprotein, is present in more than 80 % of non-mucinous epithelial ovarian carcinomas [45] but is also increased in several benign conditions, such as superficial and deep endometriosis [45],

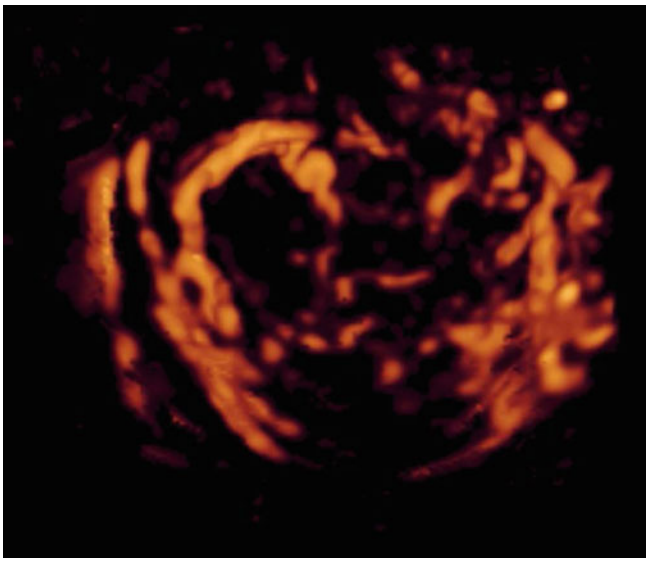

Fig. 13 At 3D a well-perfused wall with vessels with "bird's nest" appearance

ovarian cysts [46], pelvic inflammatory disease [45], resolution of ovarian torsion [47], and uterine fibroids [45], or in physiological conditions such as menstruation and early pregnancy [48].

In the literature controversial results [46, 49] are present using CA-125 alone in the diagnosis of endometrioma. Some authors [46] found 100 % of endometriomas with CA-125 higher than 20 U ml and 100 % of non-endometriomas with CA-125 lower than 20 U ml. On the contrary, using a different cutoff level, other authors [49] reported a sensitivity of 36 % and specificity of 87 % in the diagnosis of endometrioma. Further studies confirmed the presence of a significant difference between the values of CA-125 in endometrioic and non-endometrioic cysts [4, 35]; the use of CA-125 alone in the differential diagnosis of endometrioma is associated with very poor agreement also in combination with another tumor marker as carbohydrate antigen 19–9 (CA19-9) [35].

Recently Alcázar et al. [50] in a large series of cases found that the median CA-125 level was significantly higher in endometrioma (71.9 IU/mL; range: 5–2,620 IU/mL) compared to all other tumor types ($P<.001$). The CA-125 level was 35 IU/mL or higher in 74 % of endometriomas. In the diagnosis of endometrioma, the positive likelihood ratio for sonography plus CA-125 (55.0; 95 % confidence interval, 27.5–109.9) was significantly higher than for sonography alone (19.2; 95 % confidence interval, 13.6–27.1). For these reasons from the clinical point of view, an elevated CA-125 level (although not routinely suggested) associated with the presence of typical ultrasonographic findings significantly increases the probability of such lesion.

Furthermore using the previously described flow chart (Fig. 9), Guerriero et al. [29] found that, when color Doppler imaging evaluation is positive and serum CA-125 concentration is >25 IU/ml, the probability of the presence of an endometrioma is very high (95.6 %).

Ultrasonography and Malignant Transformation of Endometriomas

Although malignant transformation is a rare complication of endometriosis (<1 % of cases), it is very important to follow the disease. Several studies have found an increased overall cancer incidence in women with endometriosis, and many retrospective and epidemiologic studies have reported an increased rate of endometriosis in women with ovarian cancer, especially endometrioid and clear cell histologies showing that endometriosis is correlated to an increased risk of developing ovarian cancer [51, 52]. Luckily it represents an uncommon complication, and considering that the overall frequency of endometrioma in the general population may range from 1 to 10 % and combining this data with the incidence of ovarian cancer in the general population (10 cases per 100,000 person per year), we can assert that most of ovarian endometrioma does not develop ovarian cancer [51, 52].

Testa et al. [53], in 2011, demonstrated in their study, for the first time, the excellent diagnostic value of TVUS in the discrimination of benign vs. malignant ovarian masses arising in endometrioid cysts and demonstrated also that these masses might not represent a specifically difficult category of ovarian masses (compared with the general population of ovarian masses) if the assessment is conducted by an expert US examiner. Women with malignant findings (borderline ovarian tumors and cancers) were older (median age 52 (range, 28–79) years) than those with benign endometrioid cysts (median age 34 (range, 18–76) years) ($P<0.0001$), and the prevalence of postmenopausal status was significantly higher in malignant cases. All (15/15) malignant tumors vs. 16 % (50/309) of benign tumors were characterized by the presence of solid tissue ($P<0.0001$).

Testa et al. [53] suggest that the presence of a vascularized solid component and differences in ultrasound-assessed fluidity of endometriomas (low percentage of ground glass appearance in malignancies because of the dilution of thick hemorrhagic fluid by tumor secretions or its enlargement) can be used to discriminate benign vs. malignant ovarian masses. In addition the presence of "ovarian crescent sign" – a rim of normal ovarian tissue seen adjacent to an ipsilateral adnexal mass – as a sonographic feature to discriminate between benign and malignant adnexal masses is frequently present in endometriomas [54].

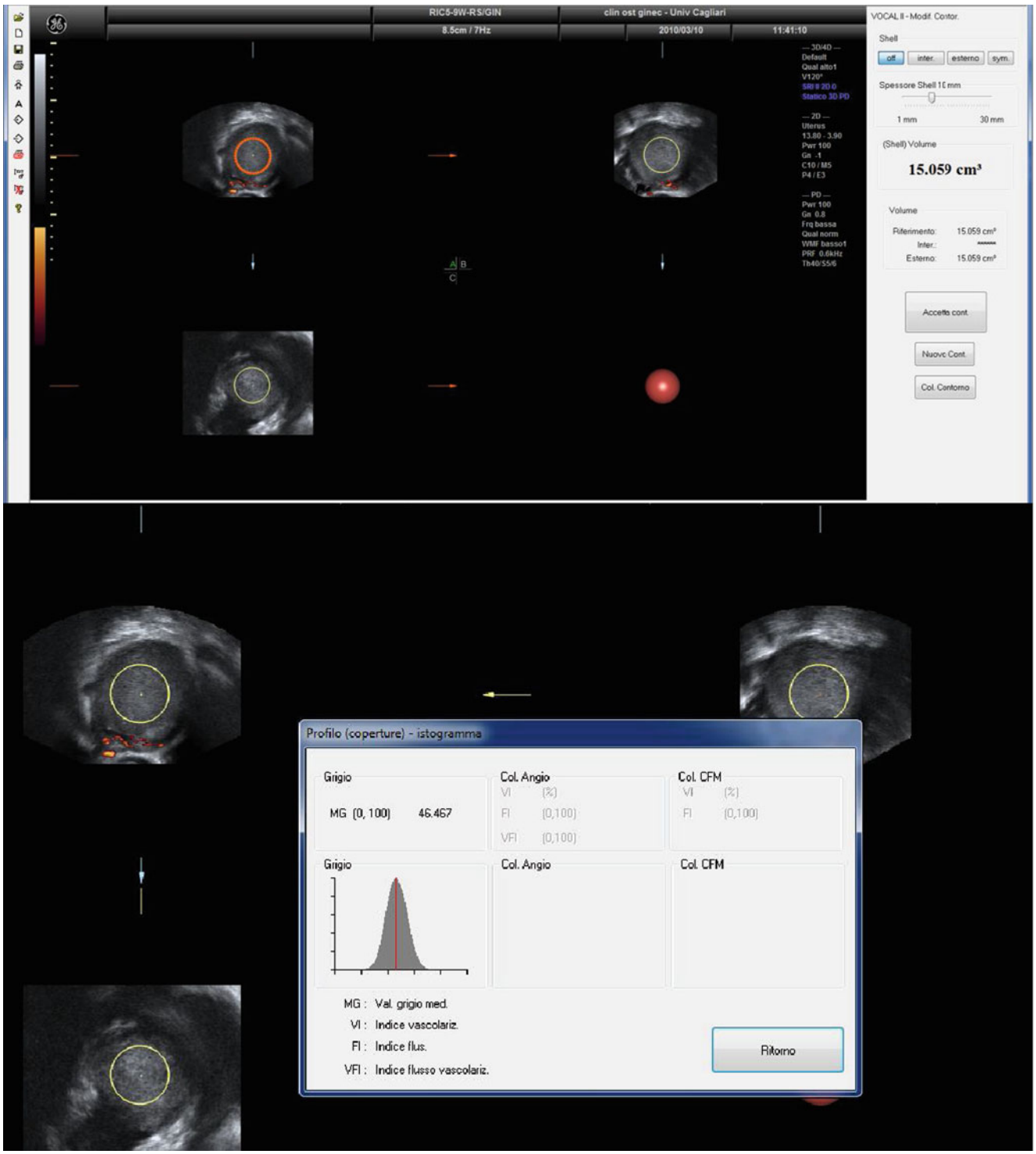

Fig. 14 Three-dimensional ultrasonography mean gray value (MGV) of an endometrioma

It is fundamental to know that some modifications of endometrioma during pregnancy can simulate malignancy. As a matter of fact, pregnancy-related modifications of an ovarian endometrioma leading to the rapid development of vascularized intracystic excrescences are an uncommon but possible event called decidualization. An expectant management and serial monitoring should first be envisaged in these cases provided that other features of malignancy, such as septations or free fluid, are absent [55, 56].

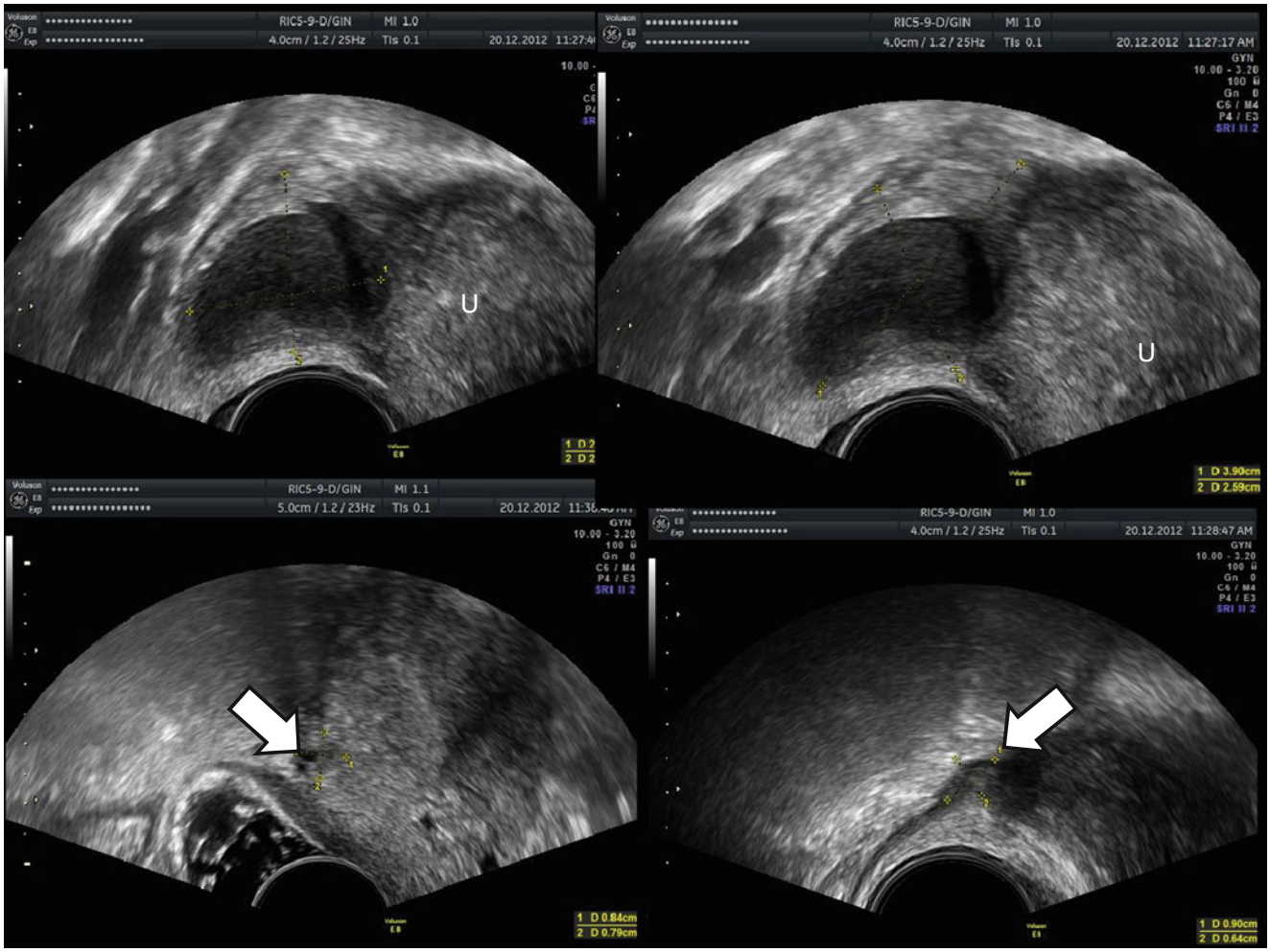

Fig. 15 An endometrioma adherent to the uterus (*U*) as a sign of the presence of severe adhesions and deep endometriosis (see *arrows*)

Ultrasonography in the Management of Endometrioma

While some years ago the removal of endometrioma was mandatory, recent studies criticized this approach [57]. A meta-analysis of Raffi et al. [58], obtained pooling a total of 237 patients, suggests a negative impact of excision of endometriomas on ovarian reserve as evidenced by a significant postoperative fall in circulating AMH, a marker of ovarian reserve. Ultrasonography is used to monitor the ovary after surgery because ovarian stripping for the surgical removal of endometriomas is associated with a significant decrease in residual ovarian volume easily evaluated by ultrasonography which may result in diminished ovarian reserve and function [59]. Ultrasonography is widely used as first-line technique in the follow-up of patients submitted to surgery to found recurrence [60].

Ultrasonography can be used also for the therapy. Although previous studies showed that aspiration alone and aspiration associated with medical treatment are inadequate [20, 61], recent data reported that the repetitive aspiration of endometriomas is an effective therapeutic option in patients with endometriosis also using sclerotherapy with 95 % ethanol [62, 63].

Ultrasonography can be used in the expectant management of adnexal masses. In a recent study [64] patients with several kind of cysts were followed up for some years using ultrasonography. In particular the authors followed-up 72 cysts with the ultrasonographic appearance of endometrioma (72/192 in total, 37 %). Of these, 30 % spontaneously disappeared and 29 % remains unchanged after years of follow-up. Based on these studies, the expectant management of endometriomas seems feasible also because of the previously described risks of impact of excision of ovarian endometrioma on ovarian reserve in infertile patients.

The ultrasonography can be used to evaluate associated disease as severe pelvic adhesions and/or deep endometriosis [65–69]. As a matter of fact in patients with endometriomas,

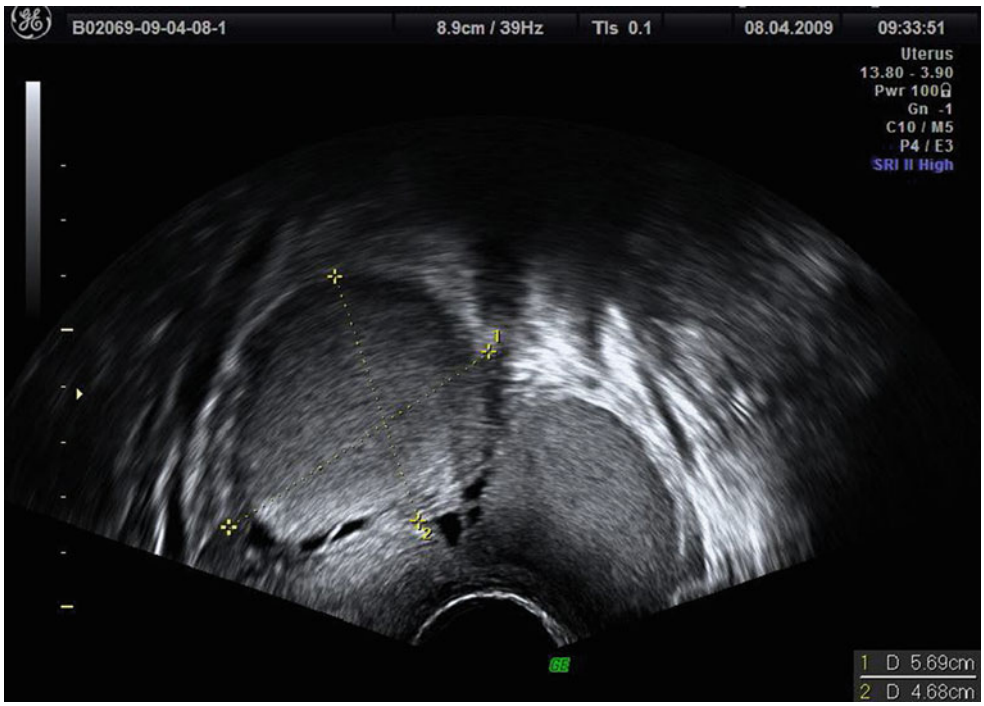

Fig. 16 The so-called "kissing ovaries" sign characterized by the closing up of ovaries containing endometriomas

the presence of adhesions should be suspected when the endometrioma is adherent to the uterus with a high degree of accuracy [70] (Fig. 15). Another useful finding related to the presence of associated pelvic adhesions and/or deep endometriosis is the so-called "kissing ovaries" sign characterized by the closing up of ovaries [71] (Fig. 16).

Ultrasonographic findings such as the presence of ovarian endometriomas and other associated sonographic markers (anatomic sites and their relation to abdomino-vaginal palpation, adhesions, deep or infiltrating nodules) can predict pelvic extension and stage of endometriosis and associated pouch of Douglas occlusion [72–75]. New evidences show that in women with a right endometrioma, incidence of the pouch of Douglas obliteration is higher and the endometriosis tends to be more severe compared to women with a left endometrioma [7].

In conclusion transvaginal ultrasonography is an accurate method for the diagnosis of endometrioma and must be used carefully in the management of this kind of adnexal masses so frequent in premenopausal women.

References

1. Hachisuga T, Kawarabayashi T. Histopathological analysis of laparoscopically treated ovarian endometriotic cysts with special reference to loss of follicles. Hum Reprod. 2002;17(2):432–5.
2. Alcázar JL, Guerriero S, Laparte C, Ajossa S, Ruiz-Zambrana A, Melis GB. Diagnostic performance of transvaginal gray-scale ultrasound for specific diagnosis of benign ovarian cysts in relation to menopausal status. Maturitas. 2011;68(2):182–8.
3. Van Holsbeke C, Van Calster B, Guerriero S, Savelli L, Paladini D, Lissoni AA, Czekierdowski A, Fischerova D, Zhang J, Mestdagh G, Testa AC, Bourne T, Valentin L, Timmerman D. Endometriomas: their ultrasound characteristics. Ultrasound Obstet Gynecol. 2010;35(6):730–40.
4. Guerriero S, Mais V, Ajossa S, Paoletti AM, Angiolucci M, Melis GB. Transvaginal ultrasonography combined with CA-125 plasma levels in the diagnosis of endometrioma. Fertil Steril. 1996; 65(2):293–8.
5. Mais V, Guerriero S, Ajossa S, Angiolucci M, Paoletti AM, Melis GB. Transvaginal ultrasonography in the diagnosis of cystic teratoma. Obstet Gynecol. 1995;85(1):48–52.
6. Al-Fozan H, Tulandi T. Left lateral predisposition of endometriosis and endometrioma. Obstet Gynecol. 2003;101(1):164–6.
7. Ulukus M, Yeniel AÖ, Ergenoglu AM, Mermer T. Right endometrioma is related with more extensive obliteration of the Douglas pouch. Arch Gynecol Obstet. 2012;285(5):1483–6.
8. Vercellini P. Endometriosis: what a pain it is. Semin Reprod Endocrinol. 1997;15:251–6.
9. Koninckx PR, Meuleman C, Demeyere S, Lesaffre E, Cornillie FJ. Suggestive evidence that pelvic endometriosis is a progressive disease, whereas deeply infiltrating endometriosis is associated with pelvic pain. Fertil Steril. 1991;55(4):759–65.
10. Khan KN, Kitajima M, Fujishita A, Hiraki K, Matsumoto A, Nakashima M, Masuzaki H. Pelvic pain in women with ovarian endometrioma is mostly associated with coexisting peritoneal lesions. Hum Reprod. 2013;28(1):109–18.
11. Chapron C, Santulli P, de Ziegler D, Noel JC, Anaf V, Streuli I, Foulot H, Souza C, Borghese B. Ovarian endometrioma: severe pelvic pain is associated with deeply infiltrating endometriosis. Hum Reprod. 2012;27(3):702–11.
12. Maneschi F, Marasá L, Incandela S, Mazzarese M, Zupi E. Ovarian cortex surrounding benign neoplasms: a histologic study. Am J Obstet Gynecol. 1993;169(2 Pt 1):388–93.
13. Almog B, Shehata F, Sheizaf B, Tan SL, Tulandi T. Effects of ovarian endometrioma on the number of oocytes retrieved for in vitro fertilization. Fertil Steril. 2011;95(2):525–7.

14. Ruiz-Flores FJ, Garcia-Velasco JA. Is there a benefit for surgery in endometrioma-associated infertility? Curr Opin Obstet Gynecol. 2012;24(3):136–40.
15. Macleod D. Endometriosis; a surgical problem. Br J Surg. 1946;34(134):109–16.
16. Nezhat F, Nezhat C, Allen CJ, et al. Clinical and histologic classification of endometriomas. Implications for a mechanism of pathogenesis. J Reprod Med. 1992;37:771–6.
17. Vercellini P, Somigliana E, Vigano P, Abbiati A, Barbara G, Fedele L. 'Blood On The Tracks' from corpora lutea to endometriomas. BJOG. 2009;116(3):366–71.
18. Hughesdon PE. The structure of endometrial cysts of the ovary. J Obstet Gynaecol Br Emp. 1957;64(4):481–7.
19. Brosens I, Puttemans P. Endometriosis and the ovary. In: Kurjak A, editor. Ultrasound and the ovary. New York: Parthenon Pub. Group; 1994. p. 157–63.
20. Donnez J, Nisolle M, Gillerot S, Anaf V, Clerckx-Braun F, Casanas-Roux F. Ovarian endometrial cysts: the role of gonadotropin-releasing hormone agonist and/or drainage. Fertil Steril. 1994;62(1):63–6.
21. Athey PA, Diment DD. The spectrum of sonographic findings in endometriomas. J Ultrasound Med. 1989;8(9):487–91.
22. Kupfer MC, Schwimer SR, Lebovic J. Transvaginal sonographic appearance of endometriomata: spectrum of findings. J Ultrasound Med. 1992;11(4):129–33.
23. Patel MD, Feldstein VA, Chen DC, Lipson SD, Filly RA. Endometriomas: diagnostic performance of US. Radiology. 1999;210(3):739–45.
24. Mais V, Guerriero S, Ajossa S, Angiolucci M, Paoletti AM, Melis GB. The efficiency of transvaginal ultrasonography in the diagnosis of endometrioma. Fertil Steril. 1993;60(5):776–80.
25. Guerriero S, Mais V, Ajossa S, Paoletti AM, Angiolucci M, Labate F, Melis GB. The role of endovaginal ultrasound in differentiating endometriomas from other ovarian cyst. Clin Exp Obstet Gynecol. 1995;22(1):20–2.
26. Alcázar JL, Laparte C, Jurado M, López-García G. The role of transvaginal ultrasonography combined with color velocity imaging and pulsed Doppler in the diagnosis of endometrioma. Fertil Steril. 1997;67(3):487–91.
27. Asch E, Levine D. Variations in appearance of endometriomas. J Ultrasound Med. 2007;26:993–1002.
28. Brown DL, Dudiak KM, Laing FC. Adnexal masses: US characterization and reporting. Radiology. 2010;254(2):342–54.
29. Guerriero S, Ajossa S, Mais V, Risalvato A, Lai MP, Melis GB. The diagnosis of endometriomas using colour Doppler energy imaging. Hum Reprod. 1998;13:1691–5.
30. Alcázar JL. Transvaginal colour Doppler in patients with ovarian endometriomas and pelvic pain. Hum Reprod. 2001;16(12): 2672–5.
31. Aleem F, Pennisi J, Zeitoun K, Predanic M. The role of color Doppler in diagnosis of endometriomas. Ultrasound Obstet Gynecol. 1995;5(1):51–4.
32. Guerriero S, Alcazar JL, Pascual MA, Ajossa S, Gerada M, Bargellini R, Virgilio B, Melis GB. Diagnosis of the most frequent benign ovarian cysts: is ultrasonography accurate and reproducible? J Womens Health (Larchmt). 2009;18(4):519–27.
33. Kurjak A, Kupesic S. Scoring system for prediction of ovarian endometriosis based on transvaginal color and pulsed Doppler sonography. Fertil Steril. 1994;62(1):81–8.
34. Volpi E, De Grandis T, Zuccaro G, La Vista A, Sismondi P. Role of transvaginal sonography in the detection of endometriomata. J Clin Ultrasound. 1995;23(3):163–7.
35. Guerriero S, Ajossa S, Paoletti AM, Mais V, Angiolucci M, Melis GB. Tumor markers and transvaginal ultrasonography in the diagnosis of endometrioma. Obstet Gynecol. 1996;88(3):403–7.
36. Sokalska A, Timmerman D, Testa AC, Van Holsbeke C, Lissoni AA, Leone FP, Jurkovic D, Valentin L. Diagnostic accuracy of transvaginal ultrasound examination for assigning a specific diagnosis to adnexal masses. Ultrasound Obstet Gynecol. 2009; 34(4):462–70.
37. Edwards A, Clarke L, Piessens S, Graham E, Shekleton P. Acoustic streaming: a new technique for assessing adnexal cysts. Ultrasound Obstet Gynecol. 2003;22(1):74–8.
38. Van Holsbeke C, Zhang J, Van Belle V, Paladini D, Guerriero S, Czekierdowski A, Muggah H, Ombelet W, Jurkovic D, Testa AC, Valentin L, Van Huffel S, Bourne T, Timmerman D. Acoustic streaming cannot discriminate reliably between endometriomas and other types of adnexal lesion: a multicenter study of 633 adnexal masses. Ultrasound Obstet Gynecol. 2010;35(3):349–53.
39. Raine-Fenning N, Jayaprakasan K, Deb S. Three-dimensional ultrasonographic characteristics of endometriomata. Ultrasound Obstet Gynecol. 2008;31(6):718–24.
40. Guerriero S, Alcazar JL, Ajossa S, Pilloni M, Melis GB. Three-dimensional sonographic characteristics of deep endometriosis. J Ultrasound Med. 2009;28:1061–6.
41. Pascual MA, Guerriero S, Hereter L, Barri-Soldevila P, Ajossa S, Graupera B, Rodriguez I. Diagnosis of endometriosis of the recto-vaginal septum using introital three-dimensional ultrasonography. Fertil Steril. 2010;94(7):2761–5.
42. Guerriero S, Pilloni M, Alcazar JL, Sedda F, Ajossa S, Mais V, Melis V, Melis GB, Saba L. Tissue characterization in deep infiltrating endometriosis by using Mean Gray Value (MGV) analysis. Ultrasound Obstet Gynecol. 2013;41(4):459–64.
43. Alcázar JL, Iturra A, Sedda F, Aubá M, Ajossa S, Guerriero S, Jurado M. Three-dimensional volume off-line analysis as compared to real-time ultrasound for assessing adnexal masses. Eur J Obstet Gynecol Reprod Biol. 2012;161(1):92–5.
44. Alcázar JL, León M, Galván R, Guerriero S. Assessment of cyst content using mean gray value for discriminating endometrioma from other unilocular cysts in premenopausal women. Ultrasound Obstet Gynecol. 2010;35(2):228–32.
45. Jacobs I, Bast Jr RC. The CA 125 tumour-associated antigen: a review of the literature. Hum Reprod. 1989;4(1):1–12.
46. Pittaway DE, Fayez JA, Douglas JW. Serum CA-125 in the evaluation of benign adnexal cysts. Am J Obstet Gynecol. 1987; 157(6):1426–8.
47. Guerriero S, Ajossa S, Caffiero A, Mais V. Relationship between abnormally high levels of plasma CA 125 and resolution of acute pelvic pain in two women with endometrioma. Gynecol Obstet Invest. 1995;40(1):61–3.
48. Paoletti AM, Serra GG, Mais V, Ajossa S, Guerriero S, Orrù M, Melis GB. Involvement of ovarian factors magnified by pharmacological induction of multiple follicular development (MFD) in the increase in Ca125 occurring during the luteal phase and the first 12 weeks of induced pregnancies. J Assist Reprod Genet. 1995;12(4):263–8.
49. Koninckx PR, Riittinen L, Seppala M, Cornillie FJ. CA-125 and placental protein 14 concentrations in plasma and peritoneal fluid of women with deeply infiltrating pelvic endometriosis. Fertil Steril. 1992;57(3):523–30.
50. Alcázar JL, Guerriero S, Mínguez JÁ, Ajossa S, Paoletti AM, Ruiz-Zambrana A, Jurado M. Adding cancer antigen 125 screening to gray scale sonography for predicting specific diagnosis of benign adnexal masses in premenopausal women: is it worthwhile? J Ultrasound Med. 2011;30(10):1381–6.
51. Kobayashi H, Sumimoto K, Moniwa N, Imai M, Takakura K, Kuromaki T, Morioka E, Arisawa K, Terao T. Risk of developing ovarian cancer among women with ovarian endometrioma: a cohort study in Shizuoka, Japan. Int J Gynecol Cancer. 2007;17(1):37–43. PubMed PMID: 17291229.

52. Kobayashi H, Sumimoto K, Kitanaka T, Yamada Y, Sado T, Sakata M, Yoshida S, Kawaguchi R, Kanayama S, Shigetomi H, Haruta S, Tsuji Y, Ueda S, Terao T. Ovarian endometrioma – risks factors of ovarian cancer development. Eur J Obstet Gynecol Reprod Biol. 2008;138(2):187–93. Epub 2007 Dec 26.
53. Testa AC, Timmerman D, Van Holsbeke C, Zannoni GF, Fransis S, Moerman P, Vellone V, Mascilini F, Licameli A, Ludovisi M, Di Legge A, Scambia G, Ferrandina G. Ovarian cancer arising in endometrioid cysts: ultrasound findings. Ultrasound Obstet Gynecol. 2011;38(1):99–106.
54. Van Holsbeke C, Van Belle V, Leone FP, Guerriero S, Paladini D, Melis GB, Greggi S, Fischerova D, De Jonge E, Neven P, Bourne T, Valentin L, Van Huffel S, Timmerman D. Prospective external validation of the 'ovarian crescent sign' as a single ultrasound parameter to distinguish between benign and malignant adnexal pathology. Ultrasound Obstet Gynecol. 2010;36(1):81–7.
55. Barbieri M, Somigliana E, Oneda S, Ossola MW, Acaia B, Fedele L. Decidualized ovarian endometriosis in pregnancy: a challenging diagnostic entity. Hum Reprod. 2009;24(8):1818–24. Epub 2009 Apr 10.
56. Guerriero S, Ajossa S, Piras S, Parodo G, Melis GB. Serial ultrasonographic evaluation of a decidualized endometrioma in pregnancy. Ultrasound Obstet Gynecol. 2005;26:304–6.
57. Somigliana E, Berlanda N, Benaglia L, Viganò P, Vercellini P, Fedele L. Surgical excision of endometriomas and ovarian reserve: a systematic review on serum antimüllerian hormone level modifications. Fertil Steril. 2012;98(6):1531–8.
58. Raffi F, Metwally M, Amer S. The impact of excision of ovarian endometrioma on ovarian reserve: a systematic review and meta-analysis. J Clin Endocrinol Metab. 2012;97(9):3146–54.
59. Exacoustos C, Zupi E, Amadio A, Szabolcs B, De Vivo B, Marconi D, Elisabetta Romanini M, Arduini D. Laparoscopic removal of endometriomas: sonographic evaluation of residual functioning ovarian tissue. Am J Obstet Gynecol. 2004;191(1):68–72.
60. Exacoustos C, Zupi E, Amadio A, Amoroso C, Szabolcs B, Romanini ME, Arduini D. Recurrence of endometriomas after laparoscopic removal: sonographic and clinical follow-up and indication for second surgery. J Minim Invasive Gynecol. 2006;13(4):281–8.
61. Zanetta G, Lissoni A, Dalla Valle C, Trio D, Pittelli M, Rangoni G. Ultrasound-guided aspiration of endometriomas: possible applications and limitations. Fertil Steril. 1995;64(4):709–13.
62. Zhu W, Tan Z, Fu Z, Li X, Chen X, Zhou Y. Repeat transvaginal ultrasound-guided aspiration of ovarian endometrioma in infertile women with endometriosis. Am J Obstet Gynecol. 2011;204(1):61.e1–6.
63. Hsieh CL, Shiau CS, Lo LM, Hsieh TT, Chang MY. Effectiveness of ultrasound-guided aspiration and sclerotherapy with 95% ethanol for treatment of recurrent ovarian endometriomas. Fertil Steril. 2009;91(6):2709–13. Epub 2008 Jun 20.
64. Alcázar JL, Olartecoechea B, Guerriero S, Jurado M. Expectant management of adnexal masses in selected premenopausal women: a prospective observational study. Ultrasound Obstet Gynecol. 2013;41(5):582–8.
65. Guerriero S, Ajossa S, Lai MP, Mais V, Paoletti AM, Melis GB. Transvaginal ultrasonography in the diagnosis of pelvic adhesions. Hum Reprod. 1997;12(12):2649–53.
66. Guerriero S, Ajossa S, Gerada M, D'Aquila M, Piras B, Melis GB. "Tenderness guided" transvaginal ultrasonography: a new method for the detection of deep endometriosis in patients with chronic pelvic pain. Fertil Steril. 2007;88:1293–7.
67. Guerriero S, Ajossa S, Gerada M, Virgilio B, Angioni S, Melis GB. Diagnostic value of transvaginal 'tenderness-guided' ultrasonography for the prediction of location of deep endometriosis. Hum Reprod. 2008;23(11):2452–7. Epub 2008 Jul 29. PubMed PMID: 18664469.
68. Saba L, Guerriero S, Sulcis R, Pilloni M, Ajossa S, Melis G, Mallarini G. MRI and "tenderness guided" transvaginal ultrasonography in the diagnosis of recto-sigmoid endometriosis. J Magn Reson Imaging. 2012;35(2):352–60. doi:10.1002/jmri.22832. Epub 2011 Oct 27. PubMed PMID: 22034232.
69. Guerriero S, Piras B, Peddes C, Paladino E. Transvaginal sonography in diagnosis of vesicoperitoneal fistula due to deep infiltrating endometriosis as a cause of uroperitoneum. Ultrasound Obstet Gynecol. 2012;40(6):727–9. doi:10.1002/uog.11198. PubMed PMID: 22648704.
70. Guerriero S, Ajossa S, Garau N, Alcazar JL, Mais V, Melis GB. Diagnosis of pelvic adhesions in patients with endometrioma: the role of transvaginal ultrasonography. Fertil Steril. 2010;94(2):742–6. Epub 2009 Apr 14. PubMed PMID: 19368917.
71. Ghezzi F, Raio L, Cromi A, Duwe DG, Beretta P, Buttarelli M, Mueller MD. "Kissing ovaries": a sonographic sign of moderate to severe endometriosis. Fertil Steril. 2005;83(1):143–7.
72. Exacoustos C, Zupi E, Carusotti C, Rinaldo D, Marconi D, Lanzi G, Arduini D. Staging of pelvic endometriosis: role of sonographic appearance in determining extension of disease and modulating surgical approach. J Am Assoc Gynecol Laparosc. 2003;10(3):378–82.
73. Holland TK, Yazbek J, Cutner A, Saridogan E, Hoo WL, Jurkovic D. Value of transvaginal ultrasound in assessing severity of pelvic endometriosis. Ultrasound Obstet Gynecol. 2010;36(2):241–8.
74. Bazot M, Darai E. Value of transvaginal sonography in assessing severe pelvic endometriosis. Ultrasound Obstet Gynecol. 2010;36(2):134–5.
75. Reid S, Lu C, Casikar I, Reid G, Abbott J, Cario G, Chou D, Kowalski D, Cooper M, Condous G. Can we predict pouch of Douglas obliteration in women with suspected endometriosis using a new real-time dynamic transvaginal ultrasound technique: the "sliding sign". Ultrasound Obstet Gynecol. 2013;41(6):685–91.

Endometrioma: Computed Tomography and Magnetic Resonance Imaging

Luca Saba, Rosa Sulcis, Sara Spiga, Mario Piga, Jasjit S. Suri, Silvia Ajossa, and Stefano Guerriero

Abstract

Endometriosis is a benign, estrogen-dependent gynecological disease that affects 10–15 % of women of the reproductive age, and ovarian endometriosis may manifest as fibrotic implants on the ovarian surface and as peculiar retention cysts characterized by cyclic bleeding called endometriomas. CT and in particular MR are involved in the diagnostic process of endometrioma as second-level step because in a significant percentage of cases, the ultrasonography offers an excellent result. In particular the use of MR may be useful to exclude endometriosis in a woman with pelvic pain or infertility or considering endometrioma in the differential diagnosis of an adnexal mass. In this chapter we will present CT and MR findings of ovarian endometrioma by underlining the specific signs and the newer technological evolutions.

Keywords

Endometriosis • Endometrioma • Ultrasound • Computed tomography • Magnetic resonance • Imaging

Introduction

Endometriosis is a benign, estrogen-dependent gynecological disease that affects 10–15 % of women of the reproductive age; it is classically defined as the presence of functional endometrial epithelium and stroma outside the uterine cavity. It is well demonstrated in previous publication that ectopic endometrium responds to hormonal stimulation with various degrees of cyclic hemorrhage, resulting in typical symptoms and imaging features [1, 2]. Endometriosis can virtually affect any part of the body, but ovaries are one of the most common affected sites. Ovarian endometriosis may manifest as fibrotic implants on the ovarian surface and as peculiar retention cysts characterized by cyclic bleeding called endometriomas [3, 4].

Sometimes the terms *endometriosis* and *endometrioma* are used for the same conditions, but it is very important to remember, however, that endometriomas are only a part of the disease process, which also includes endometriotic implants and adhesions, which are extremely important features in the staging of disease, and normal results from an imaging procedure do not rule out the presence of disease [5].

L. Saba, MD (✉)
Department of Radiology, Azienda Ospedaliero Universitaria (A.O.U.), di Cagliari – Polo di Monserrato, s.s. 554, Monserrato (Cagliari) 09045, Italy

Department of Diagnostica per Immagini, University of Cagliari, Azienda Ospedaliera Universitaria di Cagliari, Monserrato, Italy
e-mail: lucasaba@tiscali.it

R. Sulcis • S. Spiga, MD • M. Piga, MD
Department of Radiology, Azienda Ospedaliero Universitaria (A.O.U.), di Cagliari – Polo di Monserrato, s.s. 554, Monserrato (Cagliari) 09045, Italy

J.S. Suri, MS, PhD, MBA, Fellow AIMBE
AtheroPoint LLC,
Roseville, CA, USA

Department of Biomedical Engineering,
Idaho State University (Affl.), Pocatello, ID, USA
e-mail: jsuri@comcast.net

S. Ajossa, MD • S. Guerriero, MD
Department of Gynecology, Azienda Ospedaliero Universitaria (A.O.U.), di Cagliari – Polo di Cagliari, Via Ospedale, Cagliari (Cagliari) 09045, Italy

L. Saba et al. (eds.), *Ovarian Neoplasm Imaging*,
DOI 10.1007/978-1-4614-8633-6_5,

Radiologists are often involved in the diagnostic process and work-up of this disease as second-level step (because in a significant percentage of cases, the ultrasonography offers an excellent result), specially in one of two scenarios: excluding endometriosis in a woman with pelvic pain or infertility or considering endometrioma in the differential diagnosis of an adnexal mass [3–6].

Endometrioma

Endometrioma, also known as "chocolate cysts," because of their characteristic content, represents an extremely important way of presentation of endometriosis; in fact the ovaries are one of the most common sites of endometriosis, and at least 20–40 % of affected women have some implants on one or both of their ovaries [3]. Endometriomas are probably the results of an intraperitoneal seeding of regurgitated cells, their subsequent collecting and implantation on ovarian surface, and their proliferative process, which lead to ovarian enlargement and the constitution of a peculiar ovarian cysts. They may completely replace normal ovarian tissue [6]. More than 90 % of endometrial cysts are formed by invagination of the ovarian cortex; the site of invagination is usually characterized by the retraction of the cortex, the presence of fibrosis, and islands of glandular endometriotic tissue and blood clots [34]. Endometrioma is characterized by a fibrous wall of variable thickness, lined by a thin endometrial-like mucosa consisting of a surface epithelium and highly vascularized stroma. Deposition of hemosiderin-laden macrophages in the cyst wall due to repeated hemorrhage is a pathologic feature of endometrioma [3, 5–7].

It also presents a peculiar content, characterized by a dense tar-like fluid (hence the name "chocolate cyst"), composed by a high concentrations of blood breakdown products accumulated over successive menstrual cycles. Large endometrial cysts may contain clots or thin septa and a hematocrit effect is occasionally observed [10]. Endometriomas may include also peripheral nodules (usually determined by blood clots) or present fluid levels due to recent bleeding [4].

Endometriomas are usually multiple, bilateral (>50 % of cases, but the preferential site for endometrioma is the left ovary because of its anatomical position), and multilocular, and they are frequently associated with inter-ovarian adhesions which determine the closing up of ovaries (this particular condition is called "kissing ovaries") and between ovaries and opposing pelvic structures, such as the peritoneum, fallopian tubes, and bowel [3, 8, 9].

Pathogenesis

The pathogenesis of endometriomas is still not clear. The most accredited etiopathogenetic theory is that retrograde passage of menstrual blood or shedding from endometriosis implants deposit on the ovary. The subsequent and progressive invagination of the ovarian cortex over these deposits leads to formation of the characteristic endometrioma. The bloody content of the cyst and its high concentrations of iron, presumably, are the results of a chronic bleeding within the ovary during the menses [3, 4, 7–11].

Symptoms

Endometriomas may be asymptomatic (approximately 33 % of patients affected) or may be associated with characteristic symptoms of endometriosis. It is important to remember that there is no correlation between the degree of symptoms and the degree of visible endometriosis. However, pain seems to be associated with the depth of tissue infiltration and the degree of peritoneal inflammation. The degree of pain seems also to be strictly correlated to the presence of intrapelvic/intra-abdominal adhesions [2, 6, 12–17]. Such symptoms may include, but not only, pelvic pain, history of progressively increasing pelvic pain and/or secondary dysmenorrhea (usually cyclic pain that accompanies bleeding at the time of menstruation), dyspareunia, and abdominal acute symptoms.

In case of rupture of an endometrioma, the symptoms the patient suffers may initially be characterized by peritoneal signs and symptoms, elevated white blood cell count, and low-grade fever, similar to patients with acute pelvic inflammatory disease or appendicitis [10].

Complication of Endometriomas

The presence of endometriomas sometimes can be associated with some complication that can occur in about 50 % of the cases. The most common complications of endometriomas include [2, 6, 18, 19]:

- *Adhesions* (between ovaries or between ovary and adjacent structures).
- *Reduced fertility*: 30–50 % of women (it may be caused by adhesions involving ovaries or fallopian tubes, abnormalities of the immune system or of endocrinal one, and peritoneal fluid factors).
- An increased risk of *miscarriage* or *giving birth prematurely*.
- *Acute abdomen*: even small endometriomas are vulnerable to rupture causing an emergency characterized by chemical peritonitis when massive fluid contents flow out of the cyst (rupture is more frequent during pregnancy because of cyst's enlargement).
- *Ovarian torsion*: uncommon, probably because of adhesions, large endometriomas may predispose the ovary to twist less often than other ovarian masses. The diagnosis of ovarian torsion may be established with MR findings of

an endometrioma in an enlarged poorly enhancing ovary with peripherally located follicles [13].

- An increased *risk of certain types of cancer*, particularly ovarian. Malignant transformation is a rare complication of endometriosis (<1 % of cases). Approximately 75 % of these tumors arise from endometriosis of the ovary. Other less common sites include the rectovaginal septum, rectum, and sigmoid colon. Endometrioid carcinoma is the most common histologic pattern followed by clear cell carcinoma [17, 19, 20].

Sometimes it is the presence of complication of endometriomas that starts the diagnostic process that allows to identify this pathology.

Imaging of Endometrioma: General Concepts

Imaging has progressively become an important tool for the diagnosis of ovarian endometrioma. Considering the increasing diagnosis of asymptomatic endometriomas in young women, an early diagnosis should make surgery less traumatic and function-preserving permitting to preserve the reproductive future of these patients [34]. There are several imaging modalities that allow to identify and characterize the endometriomas: ultrasound (US), computed tomography (CT), and magnetic resonance imaging (MRI) (Fig. 1). The value of the ultrasonography was described in the previous chapter, and it is important to underline that this technique is considered the first-level examination because of the very good sensitivity and specificity. However in some patients, the US is not sufficient and further exams are necessary. In the last years the evolution in the technology in the CT and MR field has been tremendous, and the diagnostic potentiality of MR technique, as we will see in the next paragraphs, is very high. However, the use of MR and CT should be carefully evaluated because of the cost and potential risks (in particular CT) of these techniques.

Computer-Assisted Tomography

As we previously described the computer-assisted tomography (CAT) is not considered the first-line approach for the examination and diagnosis of endometriomas, because the first line is the ultrasonography. Moreover, it is important to underline that the CT findings of this pathology are often unspecific and not diagnostic.

Nowadays the use of the CT for the detection of endometriomas is not correct and cannot be justified because of the issue related to the radiation dose and contrast material risk. For these reasons the identification of endometriomas using the CT is an occasional finding in patients that undergo CT of the pelvis.

The aspect of the endometrioma in the basal scan without the administration of contrast material is a solid (but sometimes it can be cystic or shows mixed form) mass characterized by and hyperdensity (HU values usually > 100). After the administration of contrast material, there is no contrast enhancement in the mass, but it is possible to identify a mild wall enhancement (Fig. 2).

The fact that endometriomas appear on CT scanning as solid, cystic, or mixed form may cause potential problems in differential diagnostic. *Buy et al*. [23] reported that the CT findings of a hyperdense focus inside an ovarian cyst are (in the basal scan) and can be considered as suggestive of endometriotic cysts. However, this is unspecific because other hemorrhagic lesions, such as hemorrhagic cysts, may also demonstrate this finding [6, 23, 43].

The appearance of endometriomas on CT may also overlap with pelvic inflammatory disease, as well as by benign or malignant ovarian tumors. For this reason CT scanning should not be relied on for the diagnosis [3, 4, 21–23, 43].

Contrariwise, CT may be useful in detecting complications of endometriosis in general, such as bowel obstruction or ureteral obstruction, which may determine hydronephrosis, or complication of endometriomas such as rupture which may determine a condition of acute abdomen [22, 23]. Considering the low specificity and elevated radiation dose and also the poor contrast resolution, the use of CT in the evaluation of endometriomas has been replaced by MRI [22–25].

Magnetic Resonance Imaging

MRI represents a noninvasive approach which, according to recent reports, is widely considered an excellent technique for diagnosis and evaluation of endometriosis. *Nishimura et al*. firstly reported in 1987 the usefulness of MR imaging in the diagnosis and staging of this important disease [26–28]. Thanks to its high space/contrast resolution and its large field of view, MR imaging allows an optimal pre-surgery mapping, an excellent tissue characterization, and a multiplanar evaluation of the pelvis without using ionizing radiation or iodinated contrast agents [6, 26–28].

Besides, MR imaging is recommended in presence of extensive pelvic adhesions (which represents a limitation to the laparoscopic investigation) and permits a panoramic assessment and a complete survey of the anterior and posterior compartments of the pelvis unlike ultrasound approach [27, 29]. Moreover, MR imaging presents a higher accuracy than TVUS in distinguishing benign from malignant ovarian masses, especially when the examination is completed with the use of contrast enhancement [7, 30–33].

MR Protocol

The MR examination is usually performed regardless of menstrual cycle phase; in fact, in several studies, it has

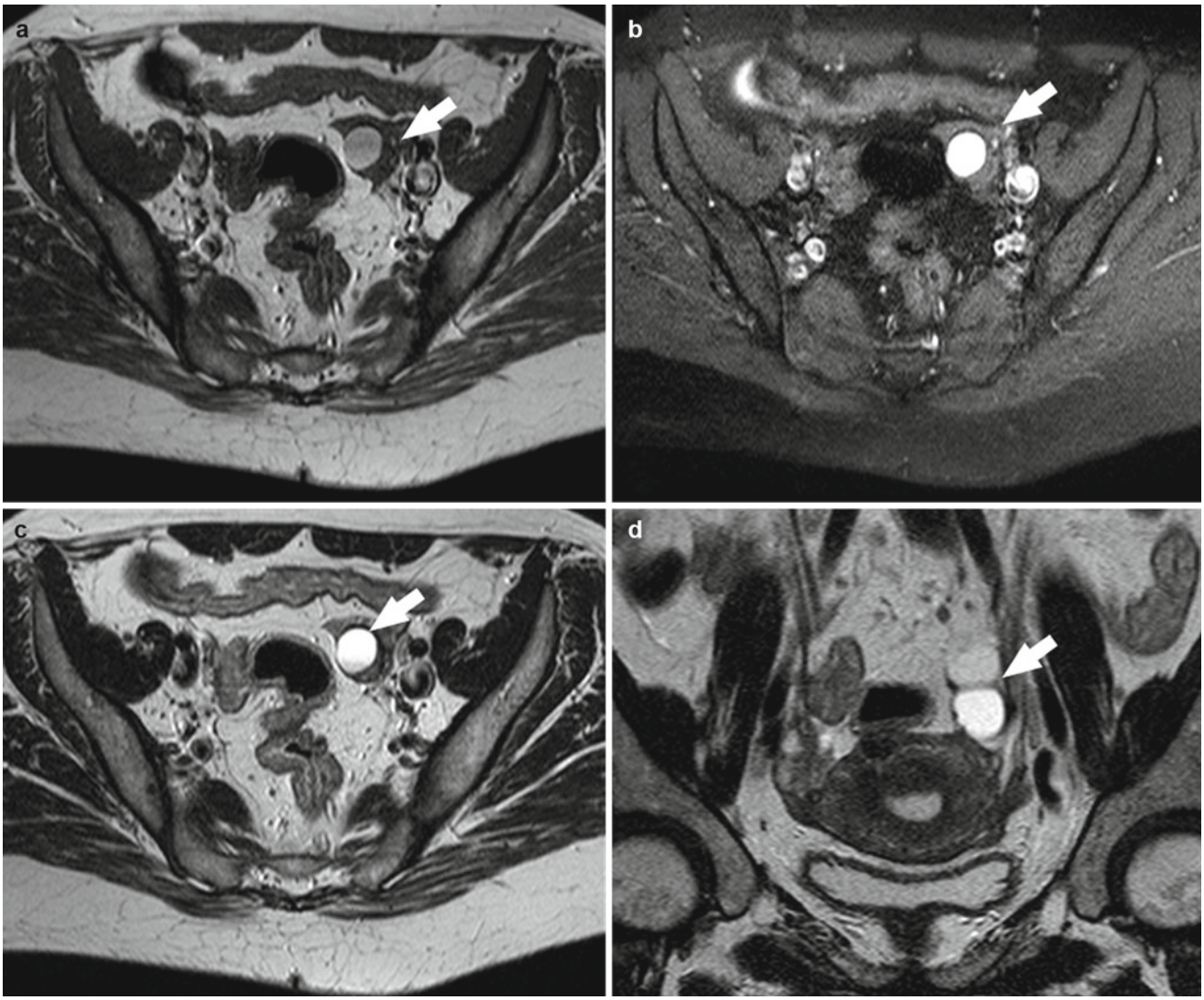

Fig. 1 A 31-year-old patient. Axial T1-weighted sequence (**a**), axial T2-weighted sequence (**b**), axial T1-weighted fat sat sequence (**c**), and coronal T2-weighted sequence (**d**) images show a 1.3 cm endometrioma (*white arrows*) characterized by the presence of hyper-signal in T1-weighted/T1-weighted fat sat/T2-weighted sequences

been reported that the MR signal of the nodules of endometriosis does not change according to the menses, and there is no evidence of a greater diagnostic accuracy in MR performed during the menstrual period [3, 35]. The patients are instructed to fast for 4/6 h before the onset of MR examination. Some reports recommend also a bowel preparation (consisting usually in the use of oral laxative the day before imaging and in a low-residue dietary regimen on the day before and the day of the MR examination) [3, 4]. A moderate repletion of the patient's bladder is recommended in order to determine a modification of the angle of uterine anteversion; in fact an empty or overfilled bladder may obliterate the adjacent recesses [3, 27, 36]. Antispasmodic drug (20 mg of scopolamine-N-butyl bromide/Buscopan) is usually intravenously administrated just before the beginning of MR examination, in order to reduce artifacts determined by bowel peristaltic movements [3, 36]. If available, MR examination should be performed using a *phased-array surface coil*, because it ensures a higher signal/noise ratio, improves spatial resolution, and enhances anatomic details, permitting a better characterization of soft tissue in the female pelvis.

A conventional MR protocol for evaluation of pelvic endometriosis usually includes three standard planes: axial, sagittal, and coronal T2- and T1-weighted pulse sequences before and after fat suppression (Table 1, Fig. 3).

Fat-suppressed T1-weighted sequences, in fact, are the most sensitive for the detection of bloody foci, whereas high-resolution T2-weighted sequences are used for the evaluation

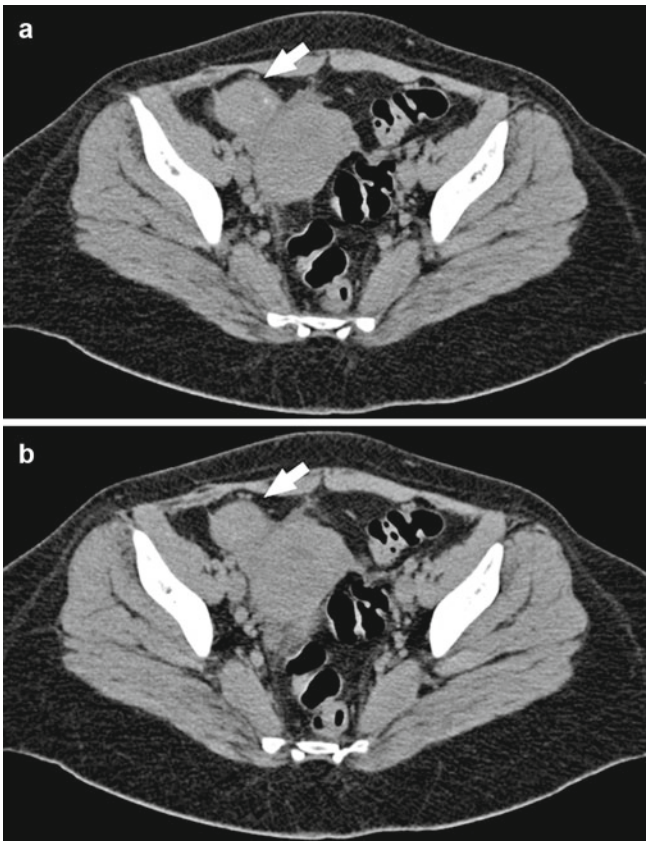

Fig. 2 A 29-year-old patient. Axial CT images (**a**, **b**) demonstrate a round mass that at the histopathological analysis was confirmed to be an endometrioma in the right adnexa

Table 1 Protocol for the MR imaging of endometriosis

Sequence	Plane
T2-W	Sag-Ax-Cor
T1-W	Ax
T1-W fat sat	Ax
T1-W enhanced	Ax
T1-W fat sat enhanced	Ax

Ax axial, *Sag* sagittal, *Cor* coronal

of fibrotic lesions [3, 36]. Moreover, fat-suppressed sequences are very helpful, especially in the detection of small lesions, because they narrow the dynamic signal range increasing differences in tissue signal and permitting to discriminate between endometrioma (characterized by an hemorrhagic content) and other adnexal masses such as dermoid cyst (characterized by a fatty content) and to better evaluate small implants [3, 36–39, 46] (Fig. 4).

The use of contrast-enhanced images (Gadolinium-DTPA) is usually reserved for a specific case, especially when there is a suspicion of malignant transformation (mural nodule in a hyperintense endometrioma) or in presence of suspicion of ureteral infiltration [3, 39–42].

Endometrioma: MR Findings

Although US represents the first-line approach and the main important method in the evaluation of endometrioma, MR imaging plays an important role in the diagnostic process, especially in presence of uncertain findings [3, 20, 32, 33]. The appearance of endometriomas on MR imaging is extremely variable and depends on the concentration of iron and protein in the fluid, products of blood degradation [7].

Most endometriomas have a coarse appearance of chocolate cysts, for the presence of highly concentrated blood products. On MR imaging, endometriomas (>1 cm) usually appear as cystic masses with very high and relatively homogeneous signal intensity on T1-weighted images ("light bulb-like brightness," similar to or greater than that of fat, which is attributed to the high concentration of paramagnetic hemoglobin in blood breakdown products) and intermediate-to-low-signal intensity on T2-weighted images [7, 10, 39, 44, 45]. The degree of T1 and T2 shortening in endometriomas is attributable to their high protein concentration and viscosity (Fig. 5).

Another common and very important feature of endometriomas is the "shading sign" which is characterized by the loss of signal within the lesion on T2-weighted images and is used to discriminate endometriomas from functional hemorrhagic cysts (Fig. 6). The precise mechanism of the shading sign is complex. Endometriotic cysts are highly viscous and have a high concentration of protein and iron from recurrent hemorrhage. All of these components may determine a shorten T2 and may contribute to signal intensity loss (or shading). In addition, intra-and extracellular methemoglobin markedly shorten the T1 of fluids. This results in hyperintensity on T1-weighted images and hypointensity on T2-weighted images [45–49].

Some endometriomas, however, are filled with watery fluid on gross cut sections and may not exhibit typical MRI findings [7]. *Togashi et al*. in their studies had reported that a "definitive" diagnosis of an endometrioma was made when a cyst was hyperintense on T1-weighted images and shading was observed on T2-weighted images [44, 49].

Another important feature is also represented by the frequent multiplicity of endometriotic cysts, because the cysts have a tendency to undergo repeated rupture due to recurrent cycles of internal hemorrhage (Fig. 7). Therefore, the presence of multiple T1 hyperintense cysts regardless of their signal intensity on T2-weighted images could be considered a diagnostic criteria permitting a reliable differentiation, with a high rate of accuracy (as demonstrated by Togashi et al. in 1991 that yielded an overall sensitivity, specificity, and accuracy of 90, 98, and 96 %, respectively), between endometriomas and other hemorrhagic lesions [7, 10, 46, 47, 49].

Considering that endometriomas are often bilateral (>50 % of cases), multilocular, and frequently associated with adhesions, another important diagnostic sign is

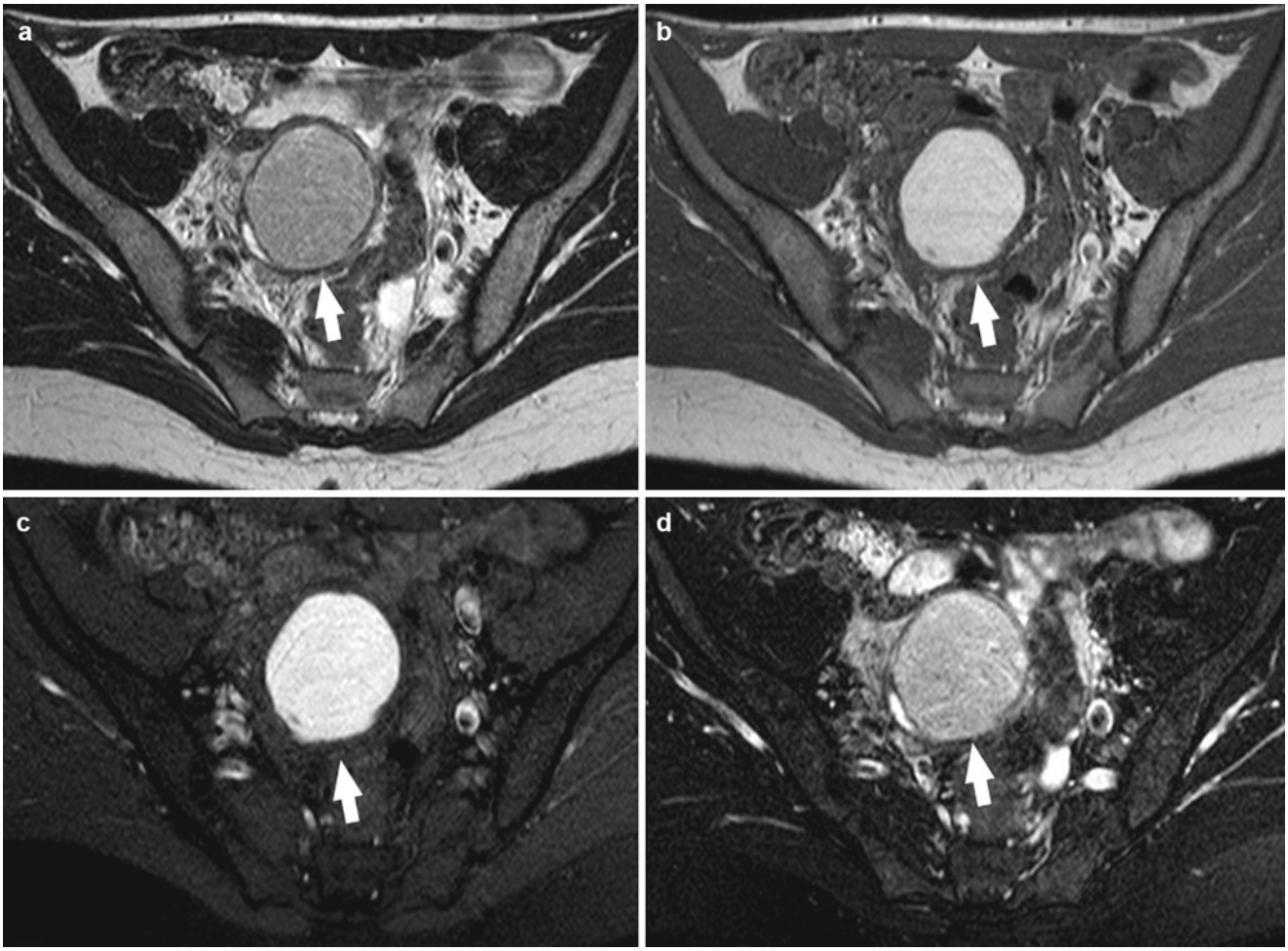

Fig. 3 A 23-year-old patient. Axial T2-weighted sequence (**a**), axial T1-weighted sequence (**b**), axial T1-weighted fat sat sequence (**c**), and axial T1-weighted fat sat sequence after administration of contrast material (**d**) images show a 3.5 cm endometrioma (*white arrows*) characterized by the presence of hyper-signal in T1-weighted/T1-weighted fat sat/T2-weighted sequences

"kissing ovaries" (Fig. 8) (characterized by the closing up of ovaries caused by inter-ovarian adhesions). Contrast material-enhanced MR imaging may show an intense contrast enhancement of the peripheral low-signal-intensity rim, which represents the thick fibrous wall of the endometrioma [10].

Large endometrial cysts may contain clots or thin septa. A hematocrit effect is occasionally observed (Fig. 9) [10], especially in endometriomas that does not exhibit typical MR features. It may be helpful in the visualization of hemosiderin deposition in the cyst wall. *Takeuchi et al*., in 2008, had reported the usefulness of *susceptibility-weighted MR*, which is an MR technique that maximizes sensitivity to susceptibility effects and has excellent sensitivity to blood products such as hemosiderin and deoxyhemoglobin combining magnitude and phase information from fully velocity-compensated gradient-echo sequences. The magnetic susceptibility effects generated by local inhomogeneity of the magnetic field caused by hemosiderin or deoxyhemoglobin are visualized as signal voids, increasing, in this way, the diagnostic accuracy of MR approach [7]. Therefore, we can consider the following as imaging criteria for the diagnosis of endometrioma:

- One or more cysts with hyperintensity on T1-weighted fat-suppressed images
- Shading sign on T2-weighted images
- Presence of adhesions
- Contrast enhancement of the peripheral low-signal-intensity rim of the thick fibrous capsule of the cyst

Using these criteria it has been demonstrated that MR imaging has a diagnostic accuracy of 91–96 %, a sensitivity of 90–92 %, and a specificity of 91–98 % [7, 10, 46, 47, 49, 61, 63].

In 1993, Outwater et al. [38] compared the MR imaging features of endometriomas and hemorrhagic cysts and concluded that endometriomas usually have higher T1 and lower T2 signal intensities than hemorrhagic cysts. Bilaterality and multifocality of adnexal lesions can help establish a diagnosis of endometrioma with even greater specificity than T1 signal hyperintensity alone.

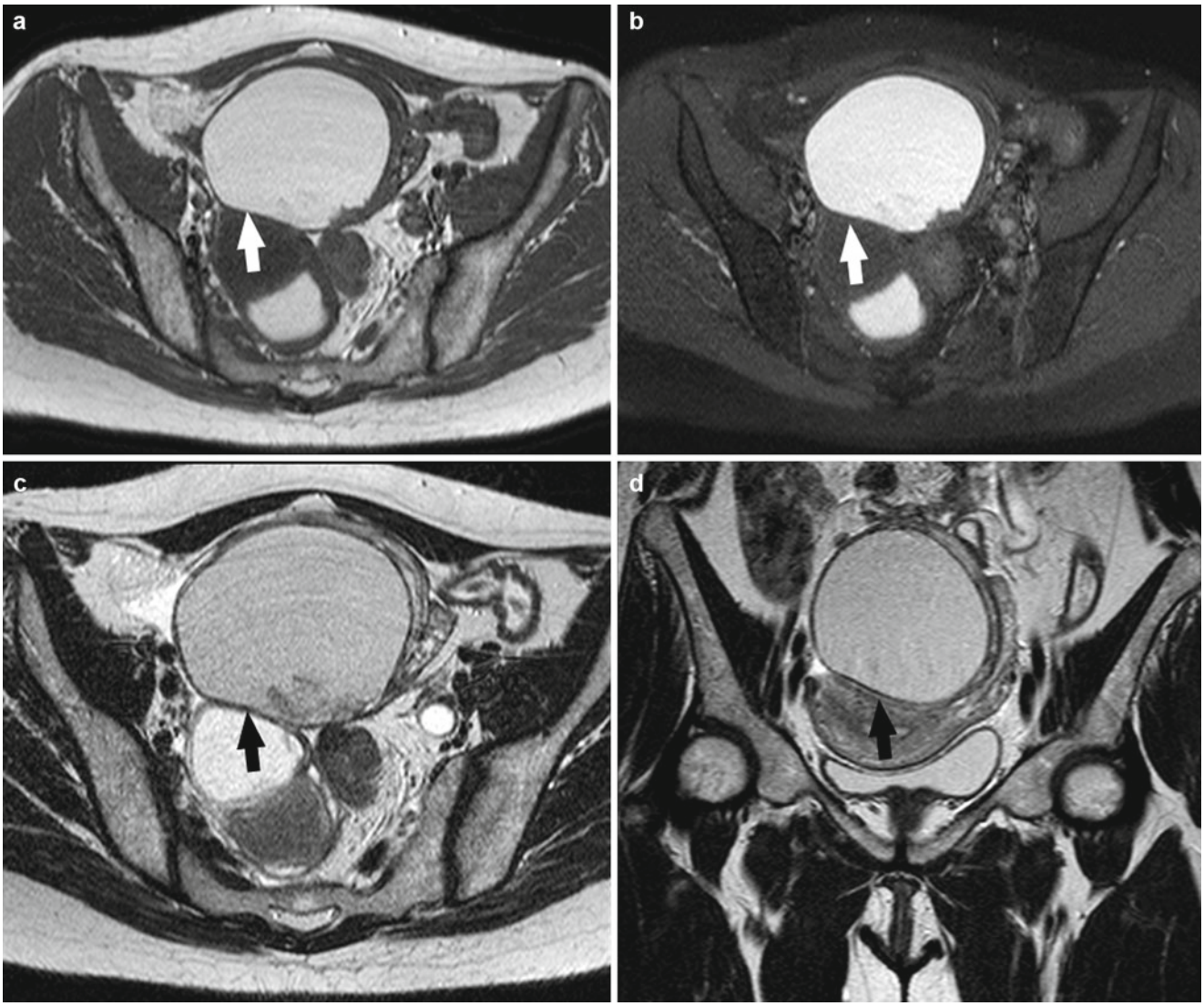

Fig. 4 A 25-year-old patient. Axial T1-weighted sequence (**a**), axial T1-weighted fat sat sequence (**b**), axial T2-weighted fat sat sequence (**c**), and coronal T2-weighted sequence (**d**) images show a 4.1 cm endometrioma (*white arrows* and *black arrows*) characterized by the presence of hyper-signal in T1-weighted/T1-weighted fat sat/T2-weighted sequences

In some centers it is used in the STIR sequence to exclude the presence of fat (and therefore the presence of teratoma), but low-signal intensity of adnexal masses on STIR MR images cannot be considered as specific for mature cystic teratoma and does not exclude endometrioma [71]. As previously demonstrated by *Krinsky et al*., the loss of T1 signal hyperintensity on STIR images is not a finding specific to fat because hemorrhagic ovarian cysts and endometriomas can have T1 relaxation times similar to that of fat (i.e., they can show "suppressed" signal intensity) and thus may mimic mature cystic teratomas at STIR imaging. Therefore, the use of an MR imaging system capable of chemically selective T1-weighted fat-suppressed imaging will help to prevent this pitfall.

It is possible to find also a rare condition of the so-called polypoid endometriosis of the ovary [76] that is characterized in the microscopic examination, by solid components with dilated endometrial glands with various amounts of endometrial stroma containing fibrous tissues. There are few papers describing this condition in the literature, and in each of these cases, there was a mass with cystic component containing polypoidal areas that were hyperintense on T2-weighted image and demonstrated homogeneous enhancement after administration of contrast material [69, 77, 78].

Diffusion-Weighted Imaging in MR

Recent technical advances in diffusion-weighted imaging (DWI) greatly enhanced the clinical value of magnetic resonance imaging (MRI) of the body. In fact DWI can provide

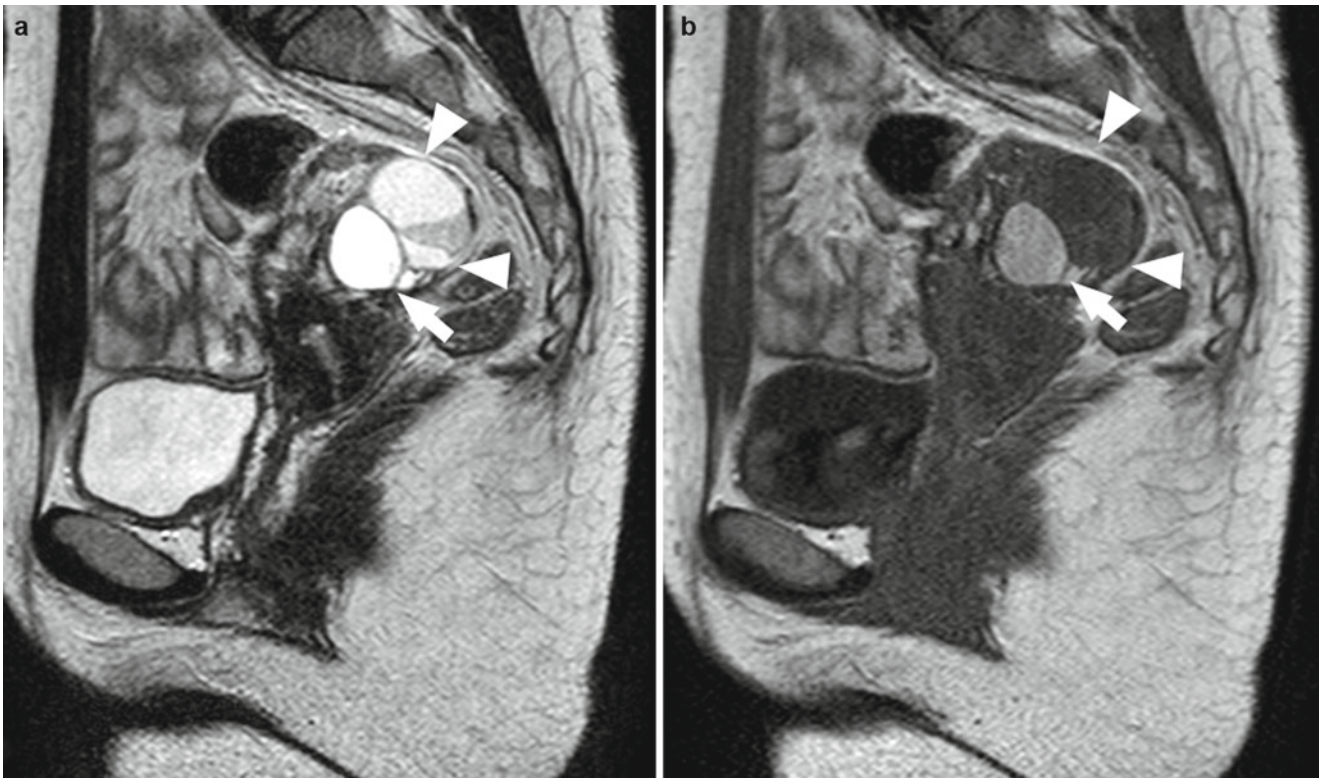

Fig. 5 A 21-year-old patient. Sagittal T2-weighted sequence (**a**) and sagittal T1-weighted sequence (**b**). In the left adnexa there are three visible formations: an endometrioma characterized by an high-signal intensity in both T1-weighted sequence and T2-weighted sequence (*white arrows*) and two cysts characterized by high signal in T2-weighted sequence and very low signal in T1-weighted sequence (*white arrowheads*)

excellent tissue contrast based on molecular diffusion [50–55]. Quantitative measurement of the apparent diffusion coefficient (ADC) may be valuable in distinguishing between malignant and benign lesions, and in the last years, it has been suggested to use the diffusion-weighted imaging with quantitative assessment of apparent diffusion coefficient (ADC) values into pelvic MR imaging protocols (Figs. 11 and 12).

Endometriomas usually have low ADC values in part because of the so-called "T2 blackout effects" [72]. On a diffusion-weighted image obtained with a low *b* value (which is a type of T2-weighted fat-suppressed image), an endometrioma exhibits low-signal intensity resembling the T2 shading. Thus, endometriomas have less signal intensity to lose on images obtained with higher *b* values than adnexal masses with higher T2 signal intensity do. Because the ADC value is based on the slope of the signal intensity loss between acquisitions at low *b* values and those at higher *b* values, endometriomas often have low ADC values. *Busard et al*. showed a significant correlation between the T2 signal intensity and the ADC value in a study evaluating both endometriomas and solid endometrial implants [73].

Previous publications demonstrated that restricted diffusion and low ADC values within an adnexal lesion does not have a high PPV (positive predictive value) or specificity for the diagnosis of malignancy because endometriomas demonstrate restricted diffusion but also benign hemorrhagic ovarian cysts solid endometrial implants as well as benign mature cystic teratomas also demonstrate restricted diffusion.

3 T MRI Imaging

In the last years, 3 T systems have been introduced in the clinical use [74, 75] and, compared with 1.5 T, the signal-to-noise ratio at 3 T has been increased and background suppression has been improved, which allows better categorization of variable components of endometriomas. The 3 T systems guarantee high spatial and contrast resolution, providing also an accurate information about endometriosis implants, with a good pre-surgery mapping of the lesions involving both bowels and bladder surface and recto-uterine ligaments. In a recently published paper in Radiology by *Hottat et al*., the sensitivity and specificity in detecting endometriomas using a 3 T system was 96 % and 80 %, respectively, and also a very high interobserver agreement was found. However, further investigations are necessary to define the role of this technology in the detection and characterization of endometrioma.

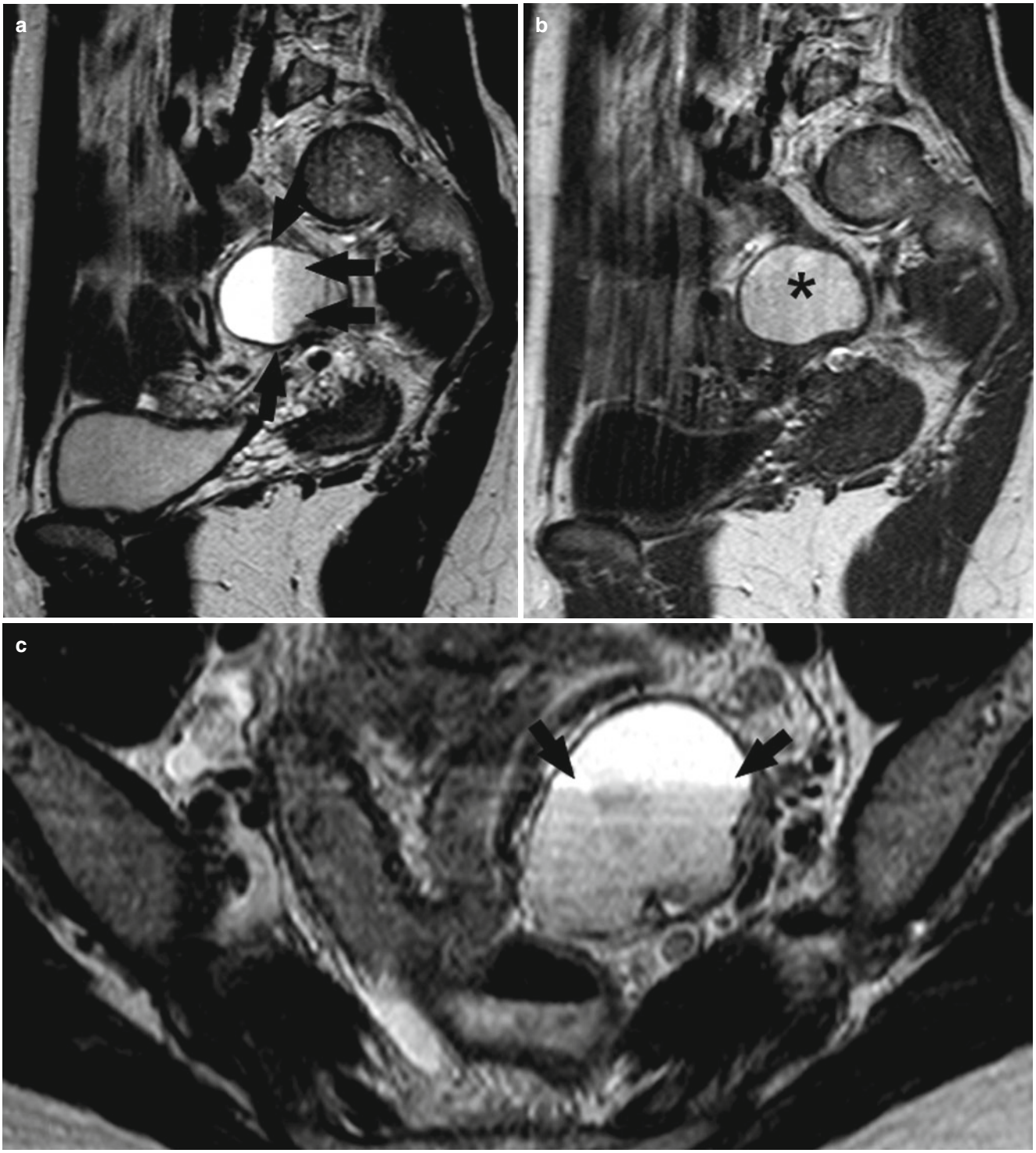

Fig. 6 A 36-year-old patient. Sagittal T2-weighted sequence (**a**), sagittal T1-weighted sequence (**b**), and axial T2-weighted sequence (**c**). In this patient with a 3.5 cm endometrioma in the left adnexa and in the T2-weighted sequences (**a**, **c**), the shading sign (*black arrows*) is visible where this effect is not visible in the T1-weighted sequence (**b**) (*black asterisk*)

Differential Diagnosis

MR findings of endometrioma may overlap with MR findings of other adnexal masses, in particular with other lesions that appear with high-signal intensity on T1-weighted images, such as dermoid cysts, hemorrhagic masses, mucinous cyst, and neoplasms. Thus, a differential diagnosis is necessary [6, 44, 49]:

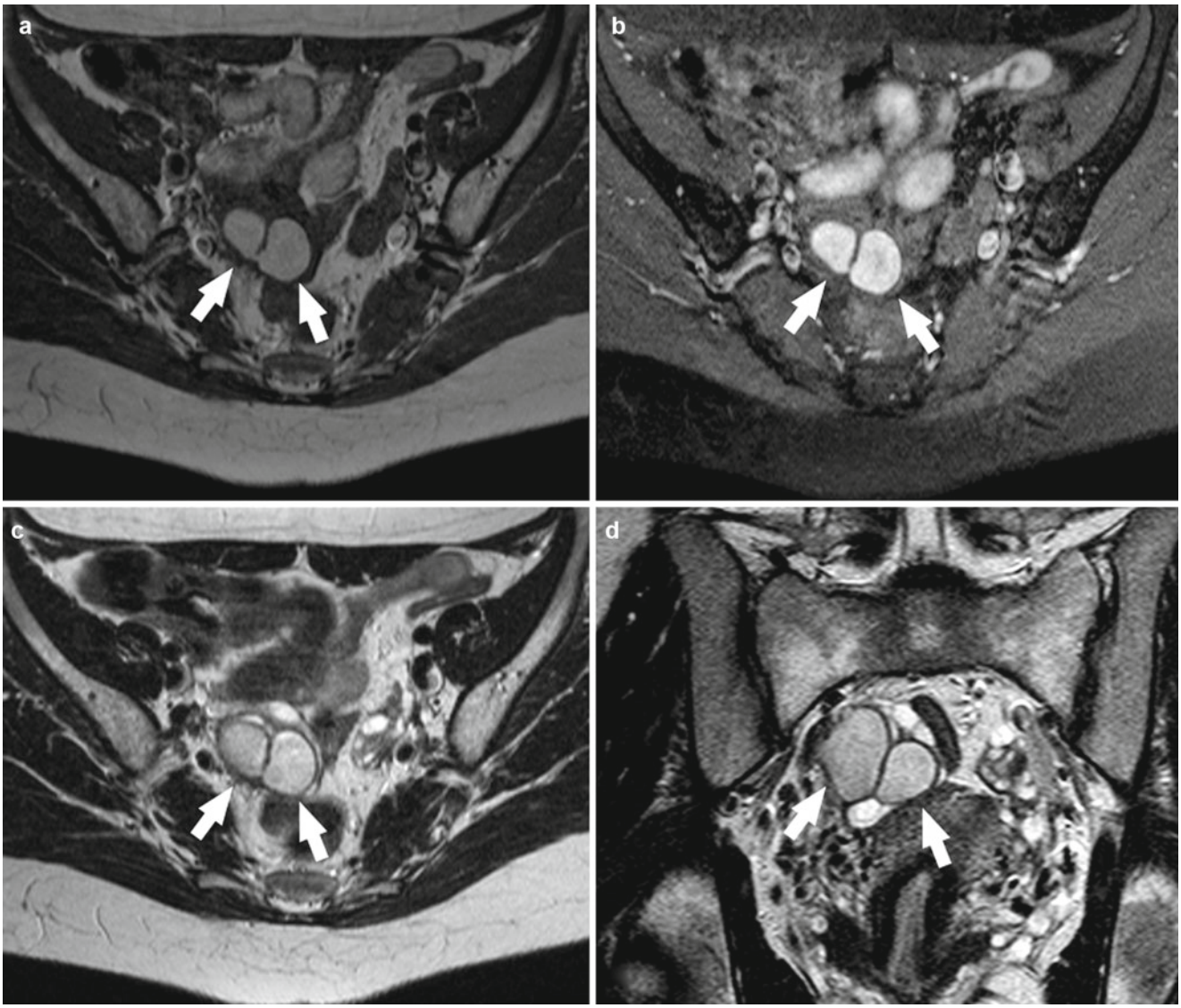

Fig. 7 A 19-year-old patient. Axial T1-weighted sequence (**a**), axial T1-weighted fat sat sequence (**b**), axial T2-weighted sequence (**c**), and coronal T2-weighted sequence (**d**) images show in the right adnexa the presence of 2 endometriomas repeated rupture due to recurrent cycles of internal hemorrhage (*white arrows*)

- *Dermoid cysts* may be differentiated from endometriomas thanks to fat-saturated T1-weighted sequences, in which the endometrioma's signal intensity does not decrease. This signal characteristic differentiates endometriomas from fatty adnexal masses, such as dermoids that show instead a chemical shift artifact and signal dropout [10, 44, 49] (Fig. 10).
- *Mucinous lesions* present a definitely lesser increased signal intensity on T1-weighted images than that of fat or blood [6].
- *Hemorrhagic cysts* (most commonly a corpus luteum cyst) represent the most difficult differential diagnosis, because of the similarity in MR imaging appearance to that of endometriomas. In fact hemorrhagic cysts remain bright on fat-saturated T1-weighted images. However, what better allows in the differential diagnosis is that, unlike endometriomas, hemorrhagic cysts are usually solitary, unilocular, and thin walled. They do not exhibit shading on T2-weighted image, since they do not repeatedly bleed. Without recurrent hemorrhage and concentration of contents, viscosity of the cyst remains lower, and shading is unlikely to be present. Endometriomas that are not bright on T1-weighted images may be difficult to distinguish from other adnexal masses [4, 7, 10]. In addition, hemorrhagic cyst will resolve with time, so it is helpful a follow-up examination rather with TVUS [4, 45, 64].
- *Multiple corpora lutea* represent another important differential diagnosis that must be considered in women who have undergone treatments for assisted conception; this condition may be seen after induced ovulation. The isolated

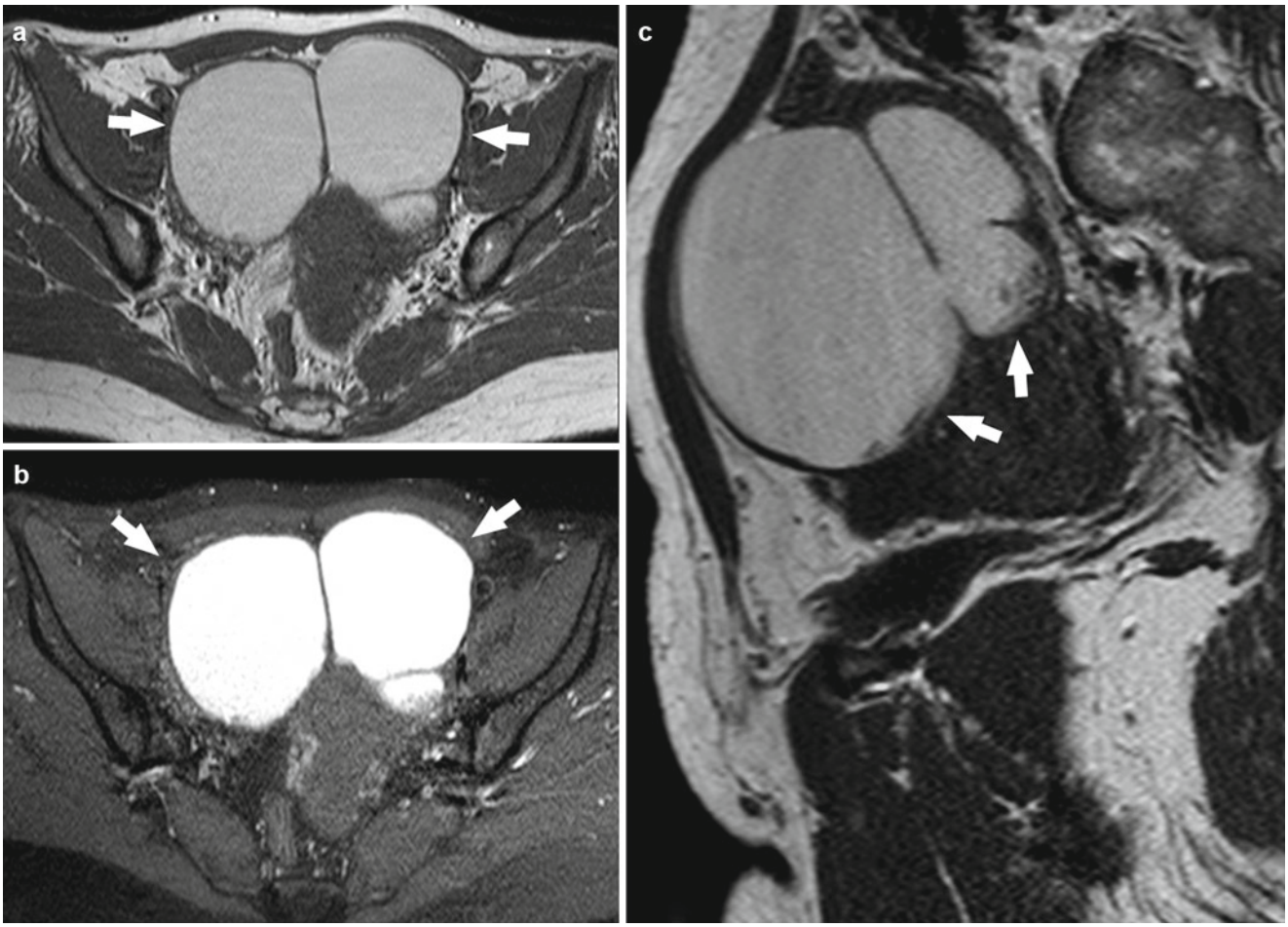

Fig. 8 A 25-year-old patient. Axial T1-weighted sequence (**a**), axial T1-weighted fat sat sequence (**b**), and sagittal T2-weighted sequence (**c**) images show in the right and left adnexa the presence of endometriomas that have the kissing ovaries configuration (*white arrows*)

appearance of each corpus luteum cyst in such cases is similar to that of endometrioma, but the patient's medical history including recent oocyte retrieval helps to the diagnosis [4].

- *Ovarian carcinoma*: Although malignant transformation is a rare complication of endometriosis (<1 % of cases), it is very important following and evaluation of the disease. Several studies have found an increased overall cancer incidence in women with endometriosis, and many retrospective and epidemiologic studies have reported an increased rate of endometriosis in women with ovarian cancer, especially endometrioid and clear cell histologies showing that endometriosis is correlated to an increased risk of developing ovarian cancer [8, 9]. Sampson et al., in 1925, first reported some cases of malignant tumors that were diagnosed in women with endometriosis [7–9]. The neoplastic degeneration of endometrioma is an uncommon complication, and considering that the overall frequency of endometrioma in the general population may range from 1 to 10 % and combining this data with the incidence of ovarian cancer in the general population (10 cases per 100,000 person per year), we can assert that most ovarian endometrioma do not develop ovarian cancer [8, 9, 56, 57, 59, 60, 62]. The histologic composition of cancer arising in endometrioma is different from that of other ovarian cancers, with a preponderance of clear cell (14.8 %) and endometrioid (66.7 %) carcinomas [7–9, 42]. These tumors clinically represent a distinct subtype of epithelial ovarian cancers. Endometriosis associated with ovarian cancer usually affects women who are 10–20 years younger than those affected by other subtypes of epithelial ovarian cancer, but fortunately, patients affected usually have an earlier stage and lower grade of disease and have a significantly better overall survival rate. Considering these features, an early detection is needful in order to improve the prognosis and preserve fertility [7–9]. However, it is unclear whether the increased survival is related to the younger age and/or the earlier diagnosis reported in women with endometriosis, inasmuch as typical symptoms of endometriosis might facilitate earlier diagnosis, whereas ovarian cancers are frequently asymptomatic until advanced stages [67, 68]. In 1925, Sampson first proposed the diagnostic criteria still in use to identify malignant tumors that arised from endometriosis:
- Clear evidence of endometriosis close to the tumor.

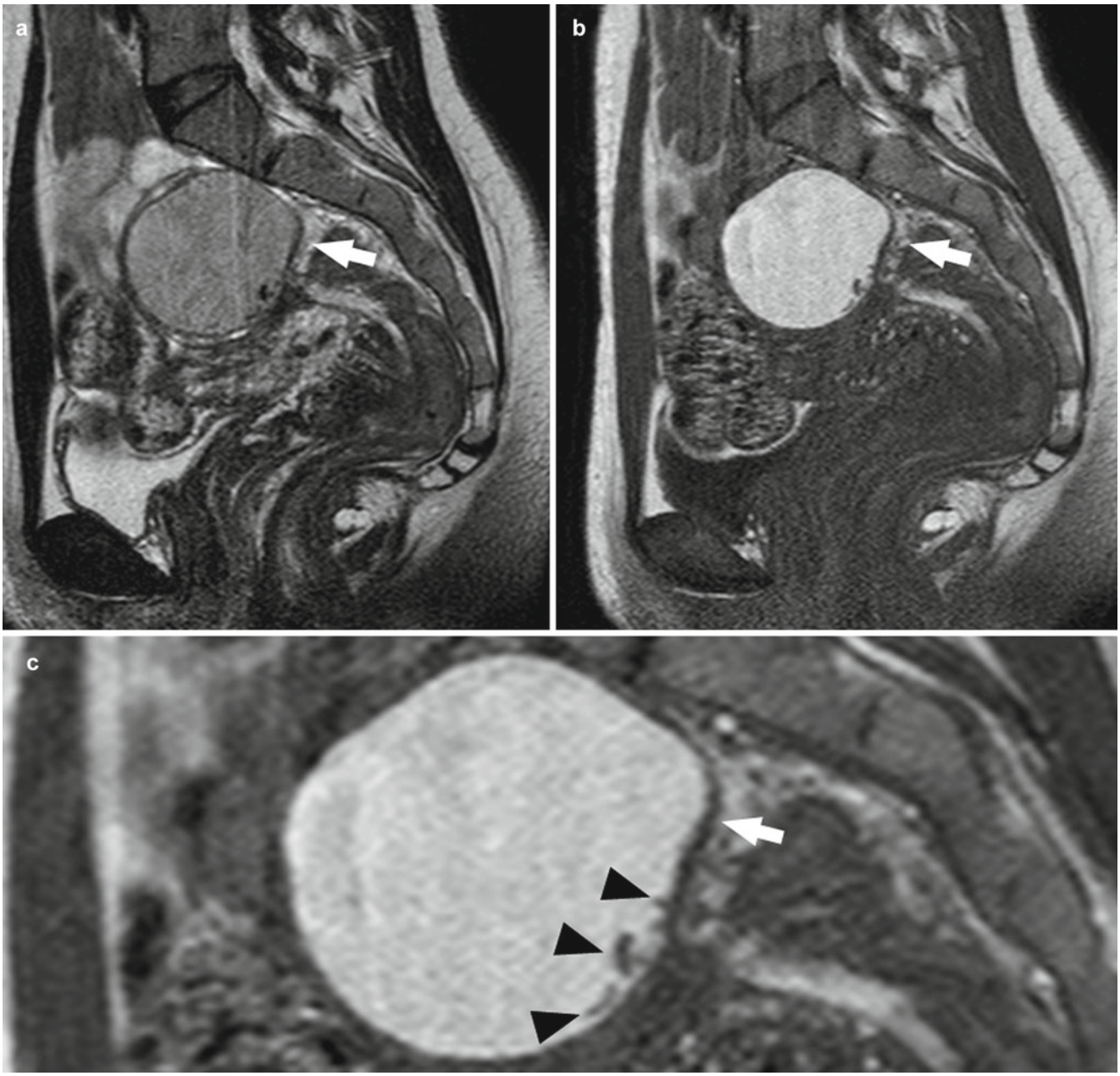

Fig. 9 A 28-year-old patient. Sagittal T2-weighted sequence (**a**), sagittal T1-weighted sequence (**b**), and sagittal T2-weighted sequence, zoom 200 % (**c**). In this patient with a 2.7 cm endometrioma (*white arrows*), some linear hypo-intense spot (*black arrowheads*) are present due to hemosiderin deposition in the cyst wall

- The carcinoma must be seen to arise in endometriosis and not to be invading it from some other sources.
- Presence of tissue resembling endometrial stroma surrounding characteristic glands.

Scott proposed in 1953 an additional histopathologic diagnostic criteria: the coexistence of endometriosis and tumor with an intervening transitional lesion (40 % of cases, transitional lesions are characterized by ectopic endometrium with mild/severe atypia interposed between endometrium without atypia and adenocarcinoma) [7–9, 65, 67].

Pathogenesis and Risk Factors for Malignant Transformation

Cancers that arise in ovarian or extraovarian endometriosis are a distinct disease category with a histologic profile different from that of the more common epithelial ovarian cancers and with a better prognosis. The pathogenesis of malignant transformation of endometriomas is still unclear; some clarified risk factors for ovarian cancer are nulliparity, late conception of firstborn, unopposed estrogen replacement therapy, and

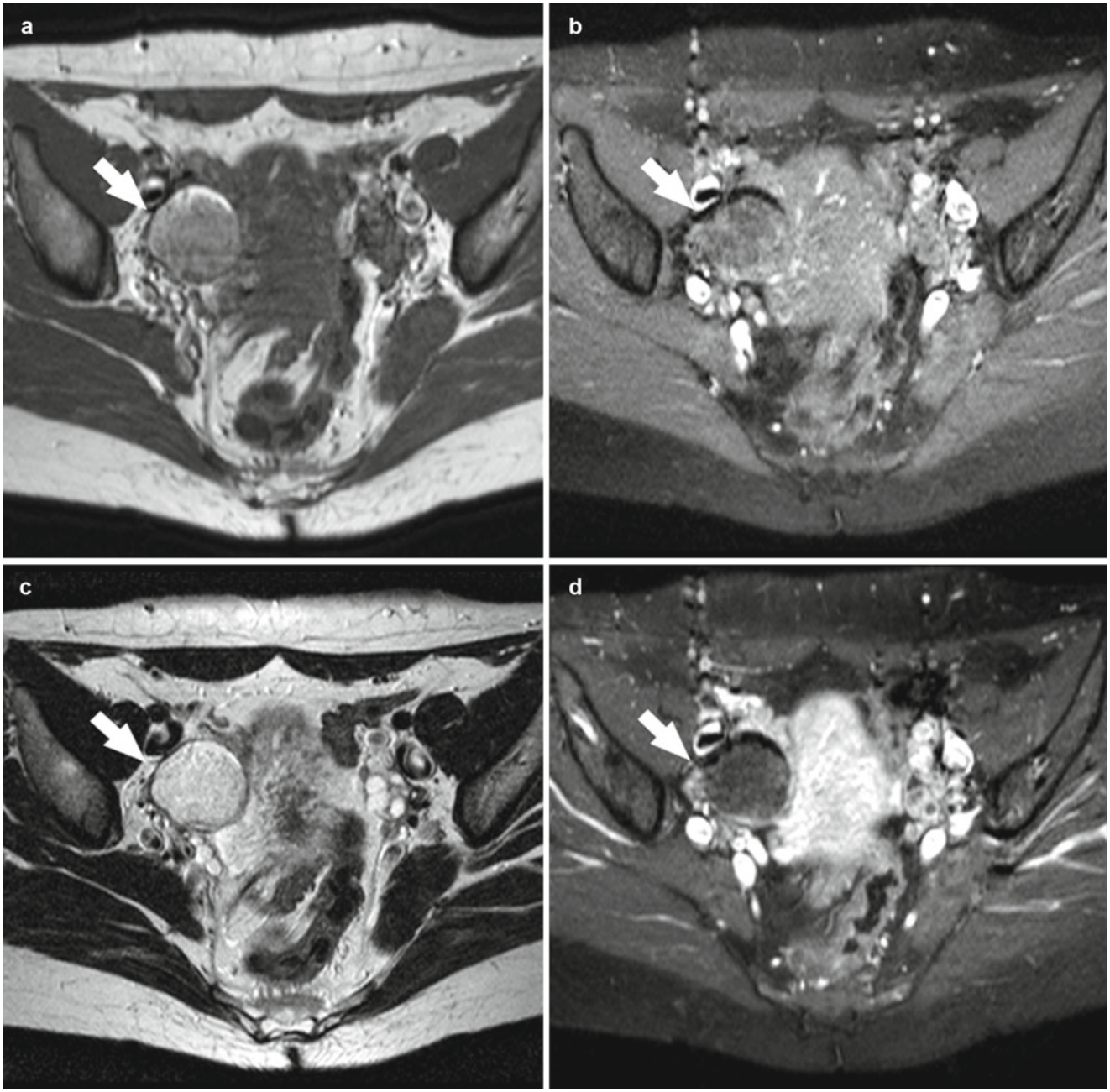

Fig. 10 A 33-year-old patient. Axial T1-weighted sequence (**a**), axial T1-weighted fat sat sequence (**b**), axial T2-weighted fat sat sequence (**c**), and axial T1-weighted fat sat sequence after contrast material (**d**) images show a 2.4 cm dermoid cyst (*white arrows*) characterized by the presence of moderate hyper-signal in T1-weighted and T2-weighted sequences and suppression in the T1-weighted fat sat sequence

family history. These risk factors suggest that estrogen may probably play a significant role; for this reason endometriosis should be treated and monitored closely in women of reproductive age [8, 9, 56, 57, 59, 60, 62]. Besides an advanced age, however, little is known about the risk factors of development of ovarian cancer among women with ovarian endometrioma. Furthermore, it has been established that the predisposition to develop an ovarian cancer is limited to endometrioid and clear cell carcinoma. Instead, oral contraceptive use, hysterectomy, and tubal ligation are considered to be major protective factors [7–9, 40, 58, 59].

Ness et al. in 2003 reported that the same pathophysiology that induces the development of endometriosis (such as immune alterations, estrogen excess, and steroid hormone interaction) may orchestrate the progression of endometriosis and its transformation to ovarian cancer [66]. The epithelial lining of cystic ovarian endometriosis, similarly to its eutopic uterine counterpart, may develop metaplastic,

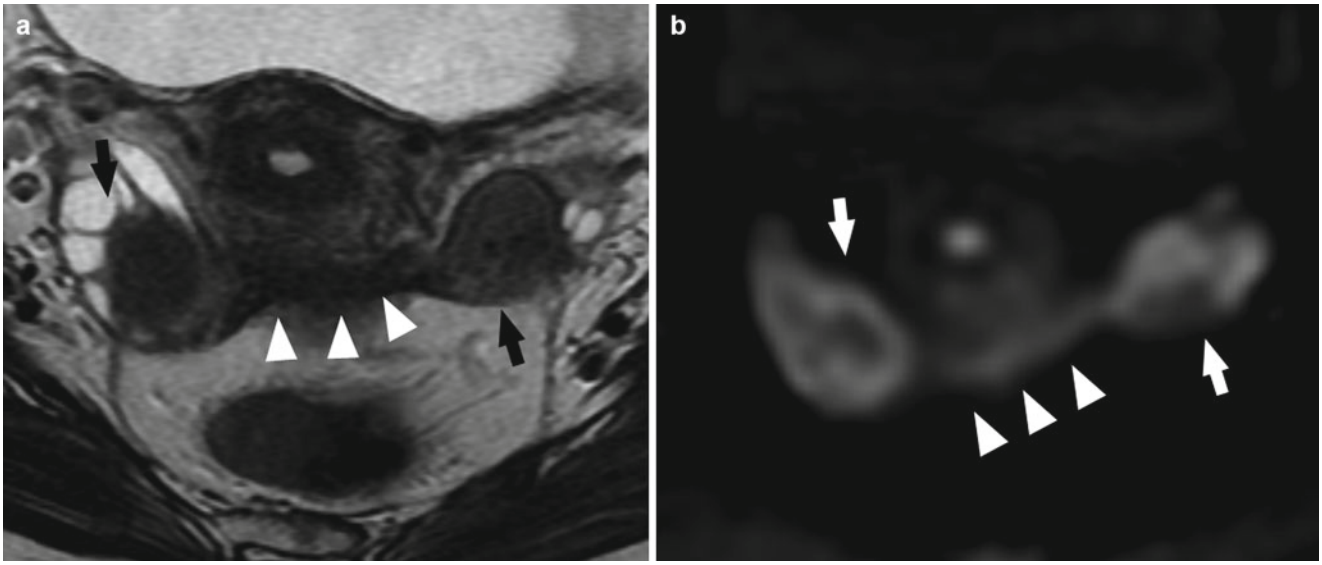

Fig. 11 A 29-year-old patient. Axial T2-weighted sequence (**a**) and axial DWI (*b* value = 1,000) (**b**). Bilateral endometrioma (*white* and *black arrows*) well demonstrated by the DWI; the presence of fibrosis involving the retrocervical region (*white arrowheads*) is also visible (Images courtesy of Carlo Nicola de Cecco MD – University of Rome la Sapienza – Polo Pontino)

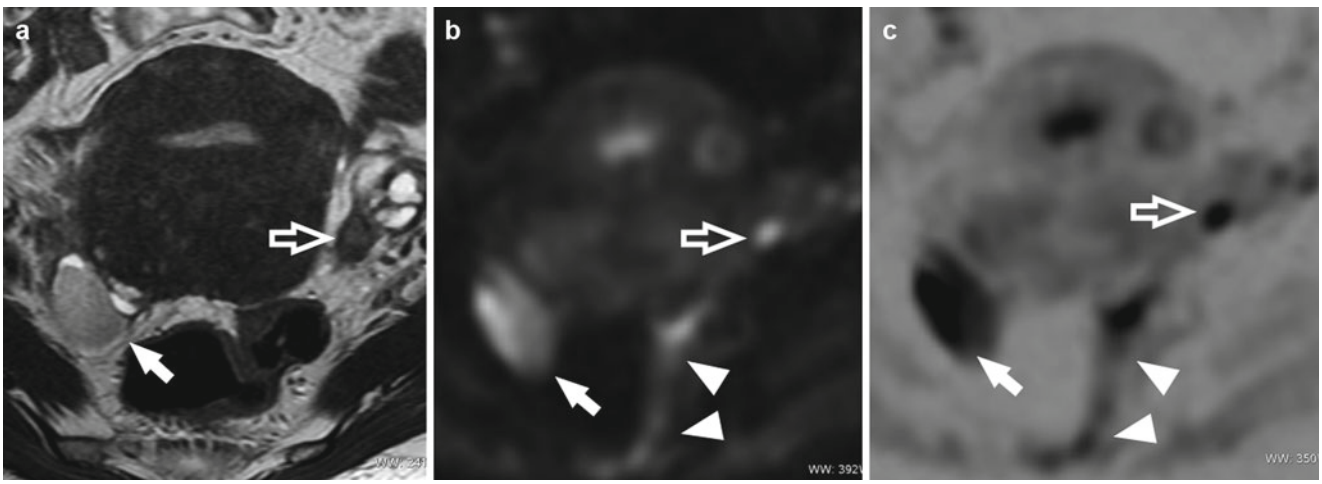

Fig. 12 A 24-year-old patient. Axial T2-weighted sequence (**a**), axial DWI (*b* value = 1,000) (**b**), and axial DWI (*b* value = 1,000) with inverted window (**c**). Endometrioma in the right adnexa (*white arrows*) well demonstrated by the DWI; there is also a visible nodule of endometriosis in the para-uterine region (*white open arrows*) and the presence of fibrosis involving the sigma (*white arrowheads*) (Images courtesy of Carlo Nicola de Cecco MD – University of Rome la Sapienza – Polo Pontino)

hyperplastic, or atypical changes, but the precise prevalence of these alterations in endometriosis and their significance in terms of risk of malignant transformation are not defined [67].

Prefumo et al., Fukunaga et al., and Ogawa et al. reported in their studies a significant increased presence of severe atypia in endometriomas associated with ovarian cancer, suggesting that carcinoma may arise from endometriosis through a multi-step process in which typical endometriosis may change into mild to severe atypia (with or without hyperplasia) and then into carcinoma [68, 69]. Kobayashi et al. in 2007 reported that the endometriotic tissue and its surroundings will be enriched in growth factors and cytokines causing a deleterious effect on the growth regulation of other cells [8, 9].

Recent studies have shown the possible biologic mechanisms involved in the malignant transformation process: inactivation of the phosphatase and tensin homologue deleted on chromosome 10 (*PTEN*) tumor suppressor gene is an early event in the development of ovarian endometrioid carcinoma and has established the role of *K-ras* and *PTEN* in the development of mouse models of endometriosis and

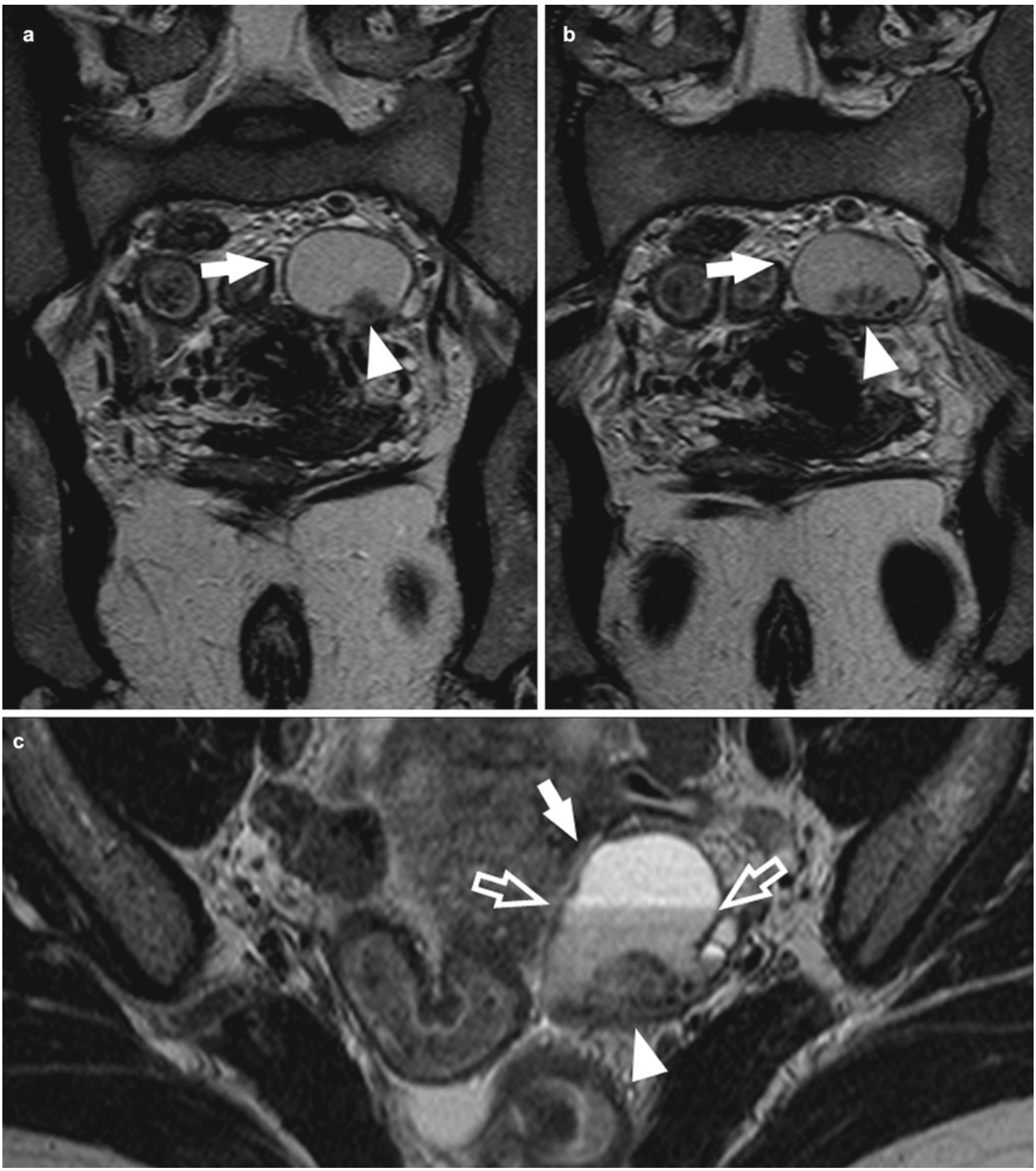

Fig. 13 A 20-year-old patient. Coronal T2-weighted sequences (**a**, **b**) and axial T2-weighted sequence (**c**). Endometrioma with malignant degeneration (proven by histology) in the left adnexa (*white arrows*) with the presence of mass (*white arrowheads*). In the axial image is the visible shading effect (*white open arrows*)

endometrioid ovarian cancer [8, 9, 66–70]. Kobayashi et al. in 2008 also conducted an important study providing several epidemiological and clinical data on development of ovarian cancer in women affected by ovarian endometrioma in Japan.

They reported that women in *postmenopausal age*, with endometriomas that were *9 cm* or greater in diameter, had the highest prevalence rate of ovarian cancer. They made a multivariate Cox proportional-hazards regression model, in

which they demonstrated that the risk of development of ovarian cancer highly increased with 9 cm or greater in diameter (HR, 5.51; 95 % CI, 2.09–9.22; $P=0.031$) and postmenopausal (HR, 3.21; 95 % CI, 1.79–4.69; $P=0.039$).

According to their results, the size of ovarian endometrioma and advancing age are significant independent predictors of development of ovarian cancer (in particular clear cell and endometrioid ovarian subtype), and the presence of endometriomas that are 9 cm or greater in diameter and the postmenopausal condition increases the risk of development of ovarian cancer.

They also suggested that an early aggressive therapy (including surgery) should be recommended, in this cluster of patients, in order to prevent the high risk of development of ovarian cancer.

MR Findings in Malignant Transformation of Endometrioma

Endometrioma has been reported to develop into malignant tumor in about 0.7–0.8 % of cases. An established MRI finding of endometrioma associated with malignant tumor is a cystic component with mass formation (Fig. 13) that shows gadolinium enhancement. In the past years some diagnostic criteria have been suggested to identify the malignant transformation of endometrioma:

- Presence of contrast enhancement of a mural nodule at fat-suppressed T1-weighted images [40]
- Lack of shading on T2-weighted images represents an important risk factor for malignancy, as reported in the study of Tanaka et al. in 2000 and 2010 (these features are amenable to the dilution of hemorrhagic contents by the nonhemorrhagic fluid secreted by malignant masses or to interval enlargement of the endometrial cyst) [40]
- A mural nodule diameter of more than 3 cm
- An interval increase in the size of the cyst

Ancillary findings suggestive of metastases, such as a large volume of ascites and peritoneal implants, are exceedingly rare in patients with malignant transformation of an endometrioma [7, 10, 40].

The typical morphologic appearance of an endometrioma associated with carcinoma is that of a unilateral large cystic mass containing hemorrhagic fluid and mural nodules. The mural nodules usually appear contrast enhanced on postcontrast T1-weighted images, and their signal intensity is low on T1-weighted images and variable on T2-weighted images (signal intensity on T2-weighted images and the shape of mural nodules are not related to the histologic subtype of the carcinoma). Usually, cystic components of the mass appear hyperintense on both T1- and T2-weighted images. The presence of shading sign on T2-weighted images within the mass is rarely observed [7, 10, 40].

It is important to consider that the hyperintense hemorrhagic fluid on T1-weighted images may mask the contrast enhancement of small mural nodules; for this reason it may be helpful to use *contrast-enhanced dynamic subtraction images* obtained with a gradient-echo sequence in order to evaluate the degree of enhancement of such nodules. The signal intensity of myometrium, or that of the small bowel wall (if the uterus is absent), is used as standard reference for the qualitative assessment of lesion signal intensity on diffusion-weighted images and apparent diffusion coefficient (ADC) maps. Masses that show relative signal hyperintensity on diffusion-weighted images and hypo/isointensity on ADC maps are considered to demonstrate restricted diffusion.

But several studies have demonstrated that restricted diffusion in ovarian cystic masses is not a specific criterion for malignancy; in fact it may also be seen in benign conditions such as decidual reaction of pregnancy or in polypoid endometriosis.

An abnormal increase in signal intensity at diffusion-weighted imaging is seen in almost half of endometriomas. But contrary to the restricted diffusion seen in the solid components of borderline or malignant tumors, the abnormal diffusion seen in benign endometriomas is usually seen within the interior cystic portions [7–10, 13, 40].

Lizuka et al. have also shown that the high concentration of iron in an ovarian cyst helps in differentiating endometriomas from serous cystadenocarcinomas, which do not contain a high concentration of iron [7–10, 13].

The radiological appearance of endometrioma associated with malignant tumor is solid components in the cystic lesion on enhanced MR imaging, and sometimes this appearance may be confused with that of polypoid endometriosis of the ovary. In this case the DWI analysis (and in particular the ADC map analysis) can be very important because an ADC map image of the solid component of the polypoid endometriosis of the ovary did not yield a low ADC value in the same way as those of malignant ovarian tumors. This fact can be explained because the rich extracellular component of endometrial tissue resulting from dilated endometrial glands may give a relatively high ADC value on an ADC map image, whereas the hypercellularity of the solid component of endometrioma associated with a malignant tumor may limit water motion to give a relatively low ADC value [76].

Pitfalls and Differential Diagnosis at MR Imaging

The presence of enhancing mural nodules within an endometrioma represents a sensitive (97 %) but not a specific (56 %) feature for the diagnosis of cancer arising from an endometrioma. Indeed, also benign entities can produce enhancing mural nodules, and a differential diagnosis is needful:

- Inflammation
- Polypoid endometriosis associated with exogenous hormone therapy (e.g., tamoxifen)
- Adjacent ovarian parenchyma (in such case an extracystic crescent-shaped lesion, which may contain follicles, is the characteristic finding)
- Intracystic blood clots (they may demonstrate abnormal signal intensity on diffusion-weighted images, but do not usually enhance after the administration of contrast material)
- Decidual reaction of pregnancy (in this case the nodules have high-signal intensity similar to that of normal endometrium on T2-weighted images; this findings, associated with the patient's medical history, helps distinguishing these nodules from the isointense nodules of malignancy; in addition they regress postpartum; thus a postpartum follow-up imaging should be performed)

Conclusion

In the detection and characterization of endometriomas, the MRI plays a fundamental role because of its high sensitivity and specificity that allow to identify this pathology and solve the differential diagnosis issues. The main limitation of this technique is the cost that remains to date very high. The CT should not be used for the detection and characterization of endometrioma because of the suboptimal sensitivity and specificity, risk induced by the radiation dose, and use of the contrast material.

References

1. Serdar E, Bulun MD. Mechanism of disease. Endometriosis. N Engl J Med. 2009;360:268–79.
2. Giudice LC, Kao LC. Endometriosis. Lancet. 2004;364:1789–99.
3. Saba L, Guerriero S, Sulcis R, Pilloni M, Ajossa S, Melis G, Mallarini G. MRI and "tenderness guided" transvaginal ultrasonography in the diagnosis of recto-sigmoid endometriosis. J Magn Reson Imaging. 2012;35(2):352–60. doi:10.1002/jmri.22832. Epub 2011 Oct 27. PubMed PMID: 22034232
4. Chamié LP, Blasbalg R, Pereira RM, Warmbrand G, Serafini PC. Findings of pelvic endometriosis at transvaginal US, MR imaging, and laparoscopy. Radiographics. 2011;31(4):E77–100.
5. Clement MD. Diseases of the peritoneum (including endometriosis). 5th ed. New York: Springer; 2002. p. 729–89.
6. Woodward PJ, Sohaey MD, Mezzetti TP, LDCR, USNR, MC. From the archives of the AFIP. Endometriosis : radiologic-pathologic correlation. Radiographics. 2001;21:193–216.
7. Takeuchi M, Matsuzaki K, Nishitani H. Susceptibility-weighted MRI of endometrioma: preliminary results. AJR Am J Roentgenol. 2008;191(5):1366–70. PubMed PMID:18941070.
8. Kobayashi H, Sumimoto K, Moniwa N, Imai M, Takakura K, Kuromaki T, Morioka E, Arisawa K, Terao T. Risk of developing ovarian cancer among women with ovarian endometrioma: a cohort study in Shizuoka, Japan. Int J Gynecol Cancer. 2007;17(1):37–43. PubMed PMID: 17291229.
9. Kobayashi H, Sumimoto K, Kitanaka T, Yamada Y, Sado T, Sakata M, Yoshida S, Kawaguchi R, Kanayama S, Shigetomi H, Haruta S, Tsuji Y, Ueda S, Terao T. Ovarian endometrioma – risks factors of ovarian cancer development. Eur J Obstet Gynecol Reprod Biol. 2008;138(2):187–93. Epub 2007 Dec 26. PubMed PMID: 18162283.
10. McDermott S, Oei TN, Iyer VR, Lee SI. MR imaging of malignancies arising in endometriomas and extraovarian endometriosis. Radiographics. 2012;32(3):845–63. PubMed PMID: 22582363.
11. Dohke M, Watanabe Y, Okumura A, Amoh Y, Hayashi T, Yoshizako T, Yasui M, Nakashita S, Nakanishi J, Dodo Y. Comprehensive MR imaging of acute gynecologic diseases. Radiographics. 2000;20(6):1551–66. Review. PubMed PMID:11112810.
12. Olive DL, Schwartz LB. Endometriosis. N Engl J Med. 1993;328(24):1759–69.
13. Gougoutas CA, Siegelman ES, Hunt J, Outwater EK. Pelvic endometriosis: various manifestations and MR imaging findings. AJR Am J Roentgenol. 2000;175(2):353–8.
14. Agarwal N, Subramanian A. Endometriosis – morphology, clinical presentations and molecular pathology. J Lab Physicians. 2010;2:1–9.
15. Schifrin BS, Erez S, Moore JG. Teen-age endometriosis. Am J Obstet Gynecol. 1973;116:973–80.
16. Gedgaudas-McClees RK. Gastrointestinal complications of gynecologic diseases. In: Textbook of gastrointestinal radiology. Philadelphia: Saunders; 1994. p. 2559–67.
17. Clement PB. Diseases of the peritoneum. In: Kurman RJ, editor. Blaustein's pathology of the female genital tract. 4th ed. New York: Springer; 1994. p. 660–80. 30.
18. Zondervan KT, Yudkin PL, Vessey MP, et al. Chronic pelvic pain in the community-symptoms, investigation, and diagnoses. Am J Obstet Gynecol. 2001;184(6):1149–55.
19. Crum CP. The female genital tract. In: Cortran RS, Kumar V, Collins T, editors. Robbins pathologic basis of disease. 6th ed. Philadelphia: Saunders; 1999. p. 1057–9. 13.
20. Guerriero S, Ajossa S, Paoletti AM, Mais V, Angiolucci M, Melis GB. Tumor markers and transvaginal ultrasonography in the diagnosis of endometrioma. Obstet Gynecol. 1996;88:403–7.
21. Guerriero S, Spiga S, Ajossa S, Peddes C, Perniciano M, Soggiu B, De Cecco CN, Laghi A, Melis GB, Saba L. Role of imaging in the management of endometriosis. Minerva Ginecol. 2013;65(2):143–66.
22. Duleba AJ. Diagnosis of endometriosis. Obstet Gynecol Clin North Am. 1997;24:331–46.
23. Buy JN, Ghossain MA, Mark AS, et al. Focal hyperdense areas in endometriomas: a characteristic finding on CT. AJR Am J Roentgenol. 1992;159(4):769–71. PubMed PMID: 1326887.
24. Biscaldi E, Ferrero S, Remorgida V, Rollandi GA. Bowel endometriosis: CT-enteroclysis. Abdom Imaging. 2007;32:441–50.
25. Jung SI, Kim YJ, Jeon HJ, Jeong KA. Deep infiltrating endometriosis: CT imaging evaluation. J Comput Assist Tomogr. 2010;34(3):338–42.
26. Hottat N, Larrousse C, Anaf V, et al. Endometriosis: contribution of 3.0 T pelvic MR imaging in preoperative assessment – initial results. Radiology. 2009;253:126–34.
27. Del Frate C, Girometti R, Pittino M, et al. Deep retroperitoneal pelvic endometriosis: MR imaging appearance with laparoscopic correlation. Radiographics. 2006;26:1705–18.
28. Zanardi R, Del Frate C, Zuiani C, Del Frate G, Bazzocchi M. Staging of pelvic endometriosis based on MRI findings versus laparoscopic classification according to the American Fertility Society. Abdom Imaging. 2003;28(5):733–42.
29. Carbognin G, Guarise A, Minelli L, et al. Pelvic endometriosis: US and MRI features. Abdom Imaging. 2004;29(609–618):52.
30. Kurtz AB, Tsimikas JV, Tempany CM, et al. Diagnosis and staging of ovarian cancer: comparative values of Doppler and conventional US, CT, and MR imaging correlated with surgery and

histopathologic analysis-report of Radiology Diagnostic Oncology Group. Radiology. 1999;212(1):19–27.
31. Umek WH, Morgan DM, Asthon-Miller JA, John OL. Quantitative analysis of uterosacral ligament origin and insertion by magnetic resonance imaging. Obstet Gynecol. 2004;103:447–57.
32. Saba L, Guerriero S, Sulcis R, Pilloni M, Ajossa S, Melis G, Mallarini G. Learning curve in the detection of ovarian and deep endometriosis by using magnetic resonance: comparison with surgical results. Eur J Radiol. 2011;79(2):237–44. Pubmed PMID:20171820.
33. Saba L, Guerriero S, Sulcis R, Ajossa S, Melis G, Mallarini G. Agreement and reproducibility in identification of endometriosis using magnetic resonance imaging. Acta Radiol. 2010;51(5):573–80. PubMed PMID:20380608.
34. Brosens I, Puttemans P, Campo R, Gordts S, Kinkel K. Diagnosis of endometriosis: pelvic endoscopy and imaging techniques. Best Pract Res Clin Obstet Gynaecol. 2004;18(2):285–303. Review. PubMed PMID: 15157643.
35. Kinkel K, Brosens J, Brosens I. Preoperative investigations. In: Sutton C, Jones KD, Adamson GD, editors. Modern management of endometriosis. Philadelphia: Informa Healthcare; 2005. p. 448–51.
36. Coutinho Jr A, Bittencourt LK, et al. MR imaging in deep pelvic endometriosis: a pictorial essay. Radiographics. 2011;31:549–67.
37. Sugimura K, Okizuka H, Imaoka I, et al. Pelvic endometriosis: detection and diagnosis with chemical shift MR imaging. Radiology. 1993;188:435–8.
38. Outwater E, Schiebler ML, Owen RS, Schnall MD. Characterization of hemorrhagic adnexal lesions with MR imaging: blinded reader study. Radiology. 1993;186(2):489–94.
39. Grasso RF, Di Giacomo V, Sedati P, et al. Diagnosis of deep infiltrating endometriosis: accuracy of magnetic resonance imaging and transvaginal 3D ultrasonography. Abdom Imaging. 2010; 35:716–25.
40. Tanaka YO, Yoshizako T, Nishida M, Yamaguchi M, Sugimura K, Itai Y. Ovarian carcinoma in patients with endometriosis: MR imaging findings. AJR Am J Roentgenol. 2000;175(5):1423–30. PubMed PMID: 11044056.
41. Wu TT, Coakley FV, Qayyum A, Yeh BM, Joe BN, Chen LM. Magnetic resonance imaging of ovarian cancer arising in endometriomas. J Comput Assist Tomogr. 2004;28:836–8.
42. Tanaka YO, et al. MRI of endometriotic cysts in association with ovarian carcinoma. AJR Am J Roentgenol. 2010;194:355–61.
43. Swart JE, Fishman EK. Gynecologic pathology on multidetector CT: a pictorial review. Emerg Radiol. 2008;15(6):383–9. Epub 2008 May 21. Review. PubMed PMID: 18493806.
44. Togashi K, Nishimura K, Kimura I, et al. Endometrial cysts: diagnosis with MR imaging. Radiology. 1991;180:73–8.
45. Siegelman ES, Outwater EK. Tissue characterization in the female pelvis by means of MR imaging. Radiology. 1999;212:5–18.
46. Outwater EK, Dunton CJ. Imaging of the ovary and adnexa: clinical issues and applications of MR imaging. Radiology. 1995;194: 1–18.
47. Arrive L, Hricak H, Martin MC. Pelvic endometriosis: MR imaging. Radiology. 1989;171:687–92.
48. Dooms GC, Hricak H, Tscholakoff D. Adnexal structures: MR imaging. Radiology. 1986;158:639–46.
49. Togashi K. Endometriosis. In: MRI of the female pelvis. Tokyo: Igaku-Shoin; 1993. p. 203–26.
50. Jung SE, Lee JM, Rha SE, Byun JY, Jung JI, Hahn ST. CT and MR imaging of ovarian tumors with emphasis on differential diagnosis. Radiographics. 2002;22(6):1305–25. Review. PubMed PMID: 12432104.
51. Chang WC, Meux MD, Yeh BM, Qayyum A, Joe BN, Chen LM, Coakley FV. CT and MRI of adnexal masses in patients with primary nonovarian malignancy. AJR Am J Roentgenol. 2006;186(4): 1039–45. PubMed PMID: 16554576.
52. Lalwani N, Prasad SR, Vikram R, Shanbhogue AK, Huettner PC, Fasih N. Histologic, molecular, and cytogenetic features of ovarian cancers: implications for diagnosis and treatment. Radiographics. 2011;31(3):625–46. Review. PubMed PMID: 21571648.
53. Mohaghegh P, Rockall AG. Imaging strategy for early ovarian cancer: characterization of adnexal masses with conventional and advanced imaging techniques. Radiographics. 2012;32(6):1751–73. doi:10.1148/rg.326125520. PubMed PMID: 23065168.
54. Takeuchi M, Matsuzaki K, Uehara H, Nishitani H. Malignant transformation of pelvic endometriosis: MR imaging findings and pathologic correlation. Radiographics. 2006;26(2):407–17. Review. PubMed PMID: 16549606.
55. Siegelman ES, Oliver ER. MR imaging of endometriosis: ten imaging pearls. Radiographics. 2012;32(6):1675–91. doi:10.1148/rg.326125518. PubMed PMID:23065164.
56. Spencer JA, Ghattamaneni S. MR imaging of the sonographically indeterminate adnexal mass. Radiology. 2010;256(3):677–94. Review. PubMed PMID: 20720065.
57. Iyer VR, Lee SI. MRI, CT, and PET/CT for ovarian cancer detection and adnexal lesion characterization. AJR Am J Roentgenol. 2010;194(2):311–21. Review. PubMed PMID: 20093590.
58. Nougaret S, Addley HC, Colombo PE, Fujii S, Al Sharif SS, Tirumani SH, Jardon K, Sala E, Reinhold C. Ovarian carcinomatosis: how the radiologist can help plan the surgical approach. Radiographics. 2012;32(6):1775–800. doi:10.1148/rg.326125511. PubMed PMID: 23065169.
59. Lee SI. Radiological reasoning: imaging characterization of bilateral adnexal masses. AJR Am J Roentgenol. 2006;187(3 Suppl):S460–6. PubMed PMID: 16928898.
60. Brinton LA, Sakoda LC, Sherman ME, Frederiksen K, Kjaer SK, Graubard BI, Olsen JH, Mellemkjaer L. Relationship of benign gynecologic diseases to subsequent risk of ovarian and uterine tumors. Cancer Epidemiol Biomarkers Prev. 2005;14(12):2929–35. PubMed PMID: 16365012.
61. Khashper A, Addley HC, Abourokbah N, Nougaret S, Sala E, Reinhold C. T2-hypointense adnexal lesions: an imaging algorithm. Radiographics. 2012;32(4):1047–64. PubMed PMID: 22786993.
62. Bennett GL, Slywotzky CM, Cantera M, Hecht EM. Unusual manifestations and complications of endometriosis – spectrum of imaging findings: self-assessment module. AJR Am J Roentgenol. 2010;194 (6 Suppl):S84–8. PubMed PMID: 20489123.
63. Kier R, Smith RC, McCarthy SM. Value of lipid- and water-suppression MR images in distinguishing between blood and lipid within ovarian masses. AJR Am J Roentgenol. 1992;158(2):321–5. PubMed PMID: 1729791.
64. Guerriero S, Mais V, Ajossa S, et al. The role of endovaginal ultrasound in differentiating endometriomas from other ovarian cysts. Clin Exp Obstet Gynecol. 1995;22(1):20–2.
65. SCOTT RB. Malignant changes in endometriosis. Obstet Gynecol. 1953;2(3):283–9. PubMed PMID: 13087921.
66. Ness RB. Endometriosis and ovarian cancer: thoughts on shared pathophysiology. Am J Obstet Gynecol. 2003;189(1):280–94. Review. PubMed PMID: 12861175.
67. Somigliana E, Vigano' P, Parazzini F, Stoppelli S, Giambattista E, Vercellini P. Association between endometriosis and cancer: a comprehensive review and a critical analysis of clinical and epidemiological evidence. Gynecol Oncol. 2006;101(2):331–41. Epub 2006 Feb 13. Review. PubMed PMID: 16473398.
68. Prefumo F, Todeschini F, Fulcheri E, Venturini PL. Epithelial abnormalities in cystic ovarian endometriosis. Gynecol Oncol. 2002;84(2):280–4. PubMed PMID: 11812087.
69. Fukunaga M, Nomura K, Ishikawa E, Ushigome S. Ovarian atypical endometriosis: its close association with malignant epithelial tumours. Histopathology. 1997;30(3):249–55. PubMed PMID: 9088954.
70. Ogawa S, Kaku T, Amada S, Kobayashi H, Hirakawa T, Ariyoshi K, Kamura T, Nakano H. Ovarian endometriosis associated with

ovarian carcinoma: a clinicopathological and immunohistochemical study. Gynecol Oncol. 2000;77(2):298–304. PubMed PMID: 10785482.
71. Siegelman ES, Oliver ER. MR imaging of endometriosis: ten imaging pearls. Radiographics. 2012;32(6):1675–91.
72. Namimoto T, Awai K, Nakaura T, Yanaga Y, Hirai T, Yamashita Y. Role of diffusion-weighted imaging in the diagnosis of gynecological diseases. Eur Radiol. 2009;19(3):745–60.
73. Busard MP, Mijatovic V, van Kuijk C, Pieters-van den Bos IC, Hompes PG, van Waesberghe JH. Magnetic resonance imaging in the evaluation of (deep infiltrating) endometriosis: the value of diffusion-weighted imaging. J Magn Reson Imaging. 2010;32(4): 1003–9.
74. Zhang H, Zhang GF, He ZY, Li ZY, Zhu M, Zhang GX. Evaluation of primary adnexal masses by 3T MRI: categorization with conventional MR imaging and diffusion-weighted imaging. J Ovarian Res. 2012;5(1):33.
75. Manganaro L, Fierro F, Tomei A, Irimia D, Lodise P, Sergi ME, Vinci V, Sollazzo P, Porpora MG, Delfini R, Vittori G, Marini M. Feasibility of 3.0T pelvic MR imaging in the evaluation of endometriosis. Eur J Radiol. 2012;81(6):1381–7.
76. Kozawa E, Inoue K, Iwasa N, Fujiwara K, Yasuda M, Tanaka J, Kimura F. MR imaging of polypoid endometriosis of the ovary. Magn Reson Med Sci. 2012;11(3):201–4.
77. Takeuchi M, Matsuzaki K, Furumoto H, Nishitani H. Case report: a case of polypoid endometriosis: MR pathological correlation. Br J Radiol. 2008;81:e118–9.
78. Ozaki K, Gabata T, Tanaka M, et al. Polypoid endometriosis: an uncommon and distinctive variant of endometriosis. Eur J Radiol Extra. 2008;65:97–100.

Part III

Benign Tumors

Epithelial Stromal Tumors: Serous and Mucinous (Clinical Setting and Ultrasound)

Maria Àngela Pascual

Abstract

Benign serous and mucinous tumors of the ovary are mostly cystic and are derived from the epithelium and stroma of the surface, often without evidence of hormonal activity or clinical manifestations, and are often discovered incidentally during the course of routine gynecological or abdominal scans performed for other reasons. They can occur at any age, and if there are clinical manifestations, they are usually due to size. They can be large and although less frequent can cause twisting, bleeding, or rupturing of the cyst. This is manifested by acute pain. Excellent definition provided by transvaginal ultrasound with color Doppler can allow a diagnosis of these types of cysts. Based on macroscopic descriptions provided by pathologists and the correlation of both the morphological sonographic findings as well as those derived from the vascularization of the cyst studied, the diagnosis can be made. The contribution of three-dimensional sonography allows diagnosis of these types of cysts based primarily on the fact that it allows for more of an anatomical view of the structure to be studied, both from a morphologic and a vascular point of view.

Keywords

Epithelial stromal tumor • Serous stromal tumor • Mucinous stromal tumor • Imaging • Ultrasound

Introduction

Mature ovaries measure from 2 to 4.5 cm in length by 0.5 to 1.5 cm in width. They can weigh between 5 and 10 g and are connected to the rest of the pelvis via the mesovarium.

Broadly, the ovary is composed of two main areas: cortical and medullary.

The cortical, or peripheral, area accounts for about one-quarter of the ovarian volume. In the stroma there are ovarian follicles in various stages of development. This cortical area is, essentially, the functional region of the ovary, where two types of phenomena play out: the hormonal secretion of progesterone and estrogen and ovulation.

The surface of the ovary is almost always coated by simple cuboidal epithelia, the only epithelial element of the gland.

The spinal cord is the central area, rich in blood and lymphatic vessels, immersed in low-density stroma, ensuring vascularization of the cortical layer. There aren't any follicles in the medullary zone.

The ovarian hilum is the zone where blood vessels penetrate into the gland. At the hilum level, the pelvic peritoneum replaces the inconsistent cuboidal epithelia of the ovarian lining.

Thus, the ovary contains several cell types:

- Epithelial tissue: cubic epithelial lining
- Connective tissue: ovarian stroma
- Germ cells: intrafollicular oocytes
- Follicular cells: cells of the theca and granulosa

M.À. Pascual, MD, PhD
Gynecologic Imaging Service, Department of Obstetrics, Gynecology and Reproduction, Instituto Universitario Dexeus, Granvia Carlos III, 71-75, Barcelona 08028, Spain
e-mail: marpas@dexeus.com

L. Saba et al. (eds.), *Ovarian Neoplasm Imaging*,
DOI 10.1007/978-1-4614-8633-6_6,

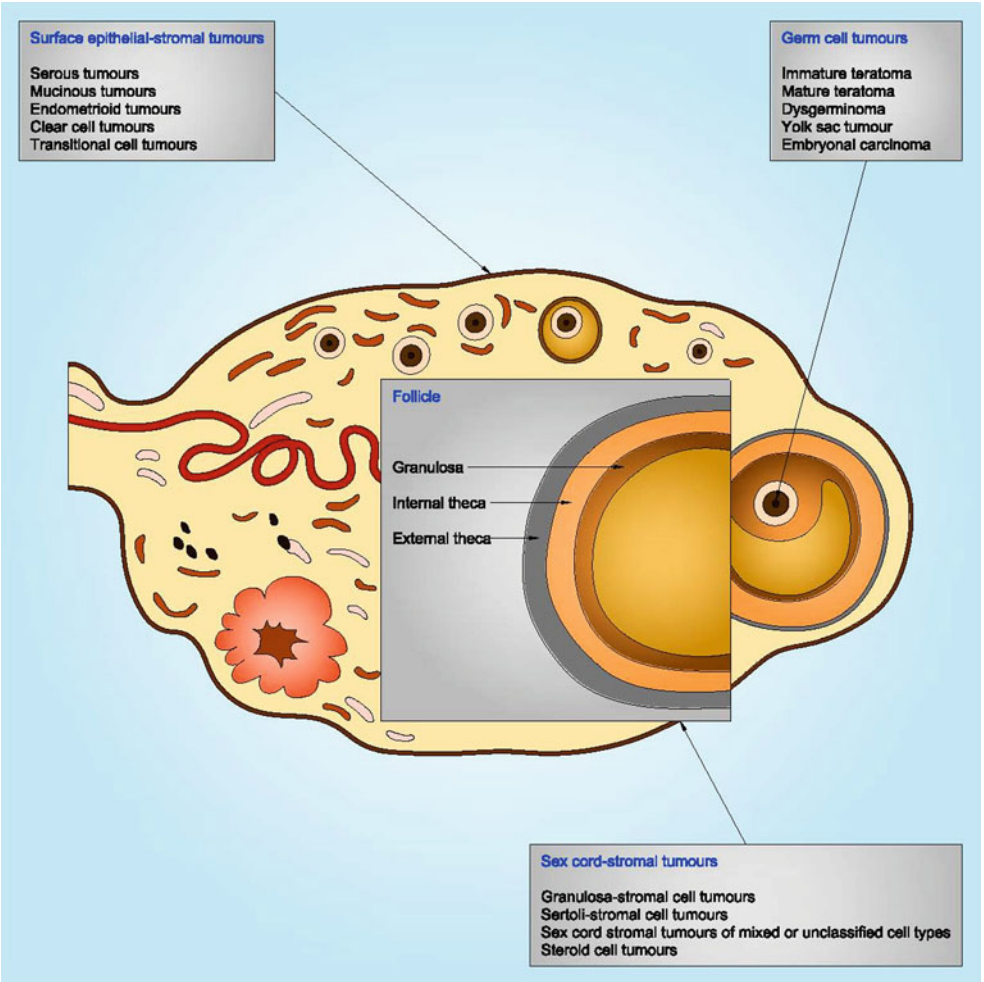

Fig. 1 Graphic representation of the ovary, which reflects the wide variety of cell types that compose it

The broad spectrum of histologic features associated with ovarian tumors reflects the diversity of cell types present in normal gonads (Fig. 1).

Neoplastic ovarian cysts are not the most frequent cause of increase in the size of the ovary. The presence of these lesions is usually indicated by menstrual irregularities (due to an imbalance between estrogen and progesterone) and by abdominal pain.

As opposed to benign tumors, neoplasms, in general, are asymptomatic until they acquire enough size to cause mechanical symptoms.

Nonneoplastic cysts are subdivided, at the hormonal level, into functional, when corresponding to an abnormal development of an ovarian follicle, and non-functional, also called organic cysts, that correspond to a proliferative syndrome of the ovarian parenchyma.

Epidemiology and Classification of Benign Ovarian Tumors

Benign ovarian lesions make up around 80 % of the tumors that affect the ovary, 10–15 % are primary malignant tumors of the ovary, and around 5 % are metastatic tumors.

Benign ovarian cysts, both serous and mucinous, can occur at any age.

Alcazar et al. [3], in a series of 1,980 patients, found that the serous cyst is more prevalent in menopausal women, while the mucinous cyst does not present a significant difference in prevalence between premenopausal and postmenopausal patients. In our experience, Pascual et al. [52], among a population of 13,177 postmenopausal patients, we observed the presence of benign ovarian lesions in 1.7 % of patients. Of these lesions, 51 % were simple and/or serous cysts and 1.8 % were mucinous cysts.

Over the course of 25 years, Grapsa et al. [28] observed 86 tumors in adolescent patients between 11 and 19 years of age, 26.7 % of which were epithelial tumors. Twenty-one of them were benign (14 serous cysts and 7 mucinous cysts); two others were borderline. They concluded that the most common cysts among tumors of epithelial origin were benign serous.

Of the three basic components that are involved in the morphogenic development of the gonad: coelomic epithelium, germ cells, and mesenchyme, the first is highly important because it is found in the majority tumors that originate in the ovary. In fact, 70–75 % of all ovarian tumors are of epithelial origin. Of these it is estimated that around 30 % are

Table 1 WHO histological classification of benign serous and mucinous tumors of the ovary

	ICD-O codes
Benign serous tumors	
Cystadenoma	8441/0
Papillary cystadenoma	8460/0
Surface papilloma	8461/0
Adenofibroma and cystadenofibroma	9014/0
Benign mucinous tumors	
Cystadenoma	8470/0
Adenofibroma and cystadenofibroma	9015/0
Mucinous cystic tumor with mural nodules	
Mucinous cystic tumor with pseudomyxoma peritonei	8480/3

serous, of which 60 % are benign, and 20–25 % are mucinous, of which 80 % are benign [10, 62].

Tumors derived from the coelomic epithelium, which retain their Müllerian differentiation potential, belong to the group of common epithelial tumors. If the potential retained by the coelomic structures is tubal, serous tumors will form; if they retain the ability to develop in the uterine direction, endometrioid or mucinous neoplasms will be developed.

The need to methodically sort ovarian tumors led them to establish their classification based primarily on histogenesis.

The current World Health Organization (WHO) classification [63] consists of the following varieties of benign tumors of epithelial origin (Table 1).

Clinical Findings

The majority of benign ovarian tumors are cystic derivatives of the epithelium and surface stroma. They are predominantly serous, mucinous, or mixed and are typically asymptomatic.

When these tumors are present but asymptomatic, the diagnosis is usually obtained through explorations stemming from another disease [56] or from a routine gynecological examination either by physical examination or ultrasonography (US).

Clinical manifestations are linked to the size of the cyst; the symptoms are often vague with generalized pelvic discomfort due to pressure on adjacent structures. They may present with abdominal pain of varying intensity and when the growth of the cyst is slow may be accompanied by a sensation of abdominal heaviness.

Larger tumors may be accompanied by an increase in abdominal girth. The extra pressure affects neighboring structures, such as the intestine and ureters, causing bowel and kidney obstructions. When the pressure of the tumor affects vascular structures, complications, such as varicose veins, hemorrhoids, and edema of the lower extremities, can occur due to inferior vena cava compression.

Nonspecific symptoms such as nausea and vomiting, fever, or vagal symptoms may also occur.

Benign ovarian cysts, like serous and mucinous cysts, may occur due to complications such as ovarian torsion, intracystic or intraperitoneal hemorrhage, or a ruptured cyst.

The twisting of the ovary is the most frequent of the aforementioned complications and can occur when there is a significant increase in volume caused by the cyst. Varras et al. [74], in a study of 92 patients with ovarian lesions that were examined for torsion, conclude that 89 % of torsion cases are associated with a benign ovarian tumor. Acute pain is the main symptom, although it may spontaneously recede when the torsion self-corrects. Houry and Abbott [38] also found the same association with ovarian torsion at an 89 % rate in a group of 87 patients and concluded that the diagnosis of ovarian torsion is often missed and ovarian salvage is rare. Characteristics of pain are variable and objective findings are uncommon in ovarian torsion. Prompt diagnosis and treatment through laparoscopy allows for conservative management [12]. Structural changes depend on the evolutionary stage of the process. When only return circulation is affected, marked congestion, edema, and extravasation of blood are observed. In more advanced stages, hemorrhagic necrosis occurs and urgent surgical treatment is needed.

Intracystic hemorrhage results from breakage of some of the vessel wall, without altering it. Intraperitoneal hemorrhage may be seen depending on the size of the affected blood vessel. Hemorrhage presents with intense abdominal pain and the patient can exhibit signs of shock. The condition may spontaneously disappear. Hemorrhagic ovarian cysts are also found in asymptomatic patients.

The rupturing of an ovarian cyst is not a frequent complication. The symptoms depend primarily on the type of tumor and its contents. In the case of a serous cyst, it may even be asymptomatic. The liquid content is drained out through the abdominal cavity, but compared to other ovarian cysts the fluid from the serous cyst is not normally irritating. The rupture of a mucinous cyst may be more serious, since the cells that drain into the abdominal cavity can become implanted in the peritoneum and cause pseudomyxoma peritonei [45], which is complicated to treat. Baratti et al. [7] and Terence et al. [64] obtained acceptable results with radical surgical treatment and intraperitoneal chemotherapy.

Benign ovarian cysts may be discovered in the course of a pregnancy, given that an ultrasound examination is part of routine prenatal care. All guidelines developed include assessment of the ovaries and the adnexa as a required component of a first-trimester examination and are considered clinically appropriate and technically feasible in standard second- and third-trimester examination.

The demonstration of an incidental ovarian or adnexal lesion may provide a morphological evaluation baseline to guide subsequent diagnostic and management strategies. In addition, this information may prove valuable if an acute clinical situation were to develop later on in the pregnancy.

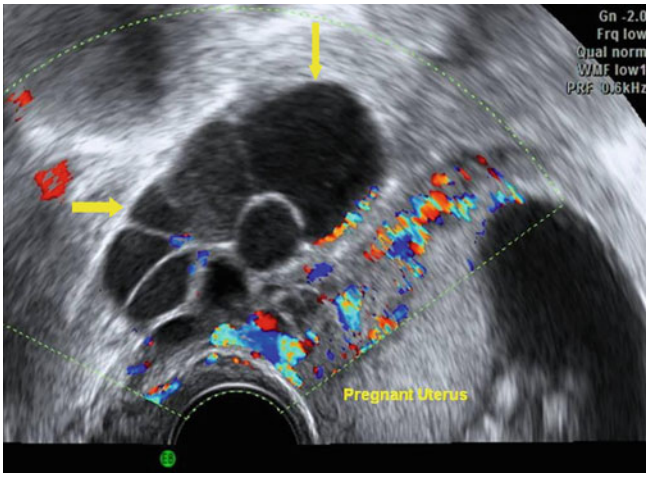

Fig. 2 Transvaginal US showing a pregnant uterus with a histologic benign mucinous cyst (*yellow arrows*) in the right adnexal. The image is from a 35-year-old patient with a history of contralateral tumor adnexectomy and ipsilateral cystectomy due to borderline mucinous ovarian tumors. Laparoscopy was performed at 13 weeks gestation due to the rapid growth of the cyst and history. Later, the patient was scheduled for a cesarean due to placenta previa, and a healthy female fetus was born

Frequently, the sonographic features of common adnexal lesions such as simple cysts, hemorrhagic cysts, mucinous cysts (Fig. 2), endometriomas, mature cystic teratomas, and ovarian conditions specific to pregnancy, such as ovarian hyperstimulation and large luteinized follicular cysts [47] may permit classification. This allows patients to be classified into conservative management protocols versus those that require further diagnostic and management decisions [26].

The goal of US evaluation is to identify those patients in whom conservative management is appropriate versus those who require more immediate intervention such as surgery. The risks of surgical intervention need to be balanced against the potential risks of nonintervention. These may include torsion, rupture, hemorrhage, or the rare spread of a malignant cancer. Atypical features or persistent large lesions should initiate a multidisciplinary team approach to optimize diagnostic and management strategy. Acute symptoms may precipitate emergency intervention at any point in the pregnancy.

Histologic Features

Many pelvic masses have a macroscopic appearance very similar to the image that can be obtained using transvaginal ultrasound in expert hands. Knowing the morphology and characteristics of ovarian tumors is of great help. Sutton et al. [62] reviews the anatomy, embryology, and physiology of the ovary and the different diagnostic modalities, concluding that it is essential to understand the microscopic image in order to make a good differential diagnosis of ovarian masses using US. Lil Valentin [68] confirms that the similarity of the ultrasonographic pattern and the microscopic findings is often very useful for the diagnosis. However, it may also result in false positives, for example, an adenofibroma, which is benign and contains papillary projections.

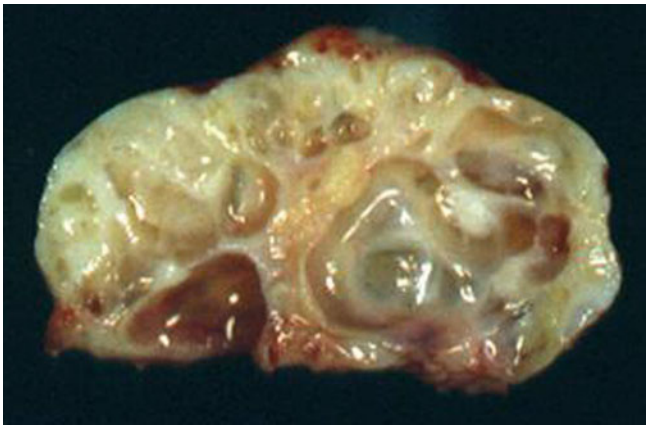

Fig. 3 Gross appearance of a mucinous cystadenoma with multiple septa delimitating cystic spaces filled with mucin

According to Grases [29], serous tumors are characterized by having an epithelial lining similar to that of the tubal mucosa or the ovarian surface epithelium, with a tendency to form buds and, less frequently, to coat the glandular spaces that are surrounded by fibrous stroma.

Four varieties are distinguished macroscopically, which serves as the basis for their classification. In the cystadenoma, the cavity is unilocular and the wall tends to be thin. When there are numerous buds that stand out in plain view, the term papillary cystadenoma is used. When the papillary proliferation is predominantly present on the outer surface, it qualifies as papilloma or papillomatosis of the surface. For those cases in which the epithelial lesion is part of a solid tumor with abundant fibrous stroma (cellular, edematous, or hyalinized), it is identified as serous adenofibroma, and if there is a combination of solid and cystic lesions, the term cystadenofibroma is used.

In mucinous tumors, the lining epithelium is cylindrical. When cells are mucous secreting and similar to those of the epithelium of the endocervical mucosa or the gastric pyloric mucosa, they are classified as endocervical mucinous cystadenoma. When the epithelium resembles the intestinal mucosa, it is classified as an intestinal mucinous cystadenoma.

Macroscopically, the majority of these tumors is multilocular and can occasionally achieve enormous volume. The external surface is smooth and upon cutting multiple cells of variable size and configuration can be seen, with a smooth, bright, and wavy inner lining (Fig. 3). They are filled with fairly thick mucinous material. Occasionally, there are only a few lobes and rarely a single cavity (Fig. 4).

Serous tumors, less frequently solid tumors, can be found with a predominance of the fibrous stroma and with a sparse mucinous epithelial component. This is the case

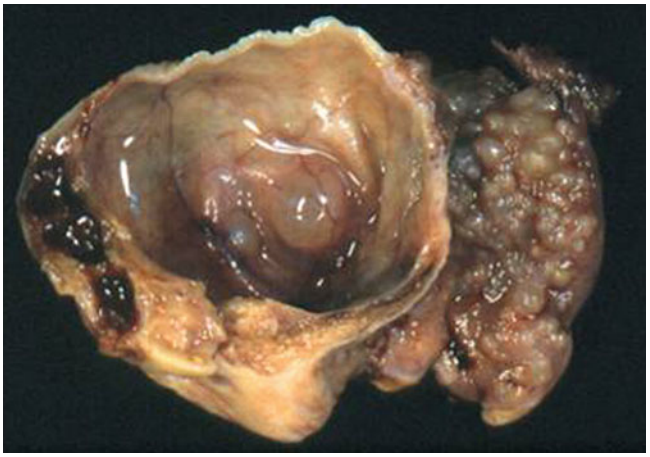

Fig. 4 Gross appearance of a mucinous cystadenoma with a focal thickening of the wall lining showing a whitish tissue

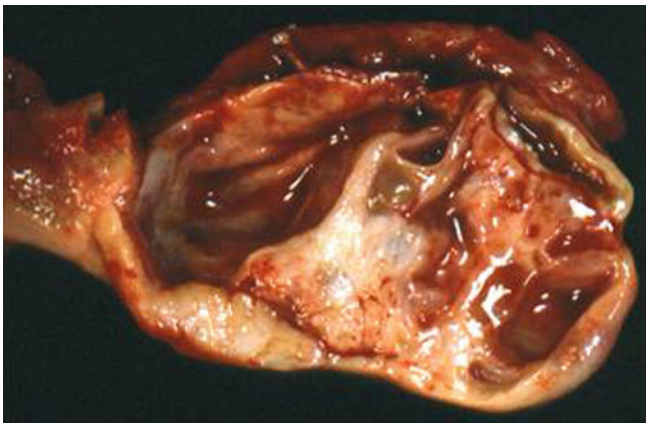

Fig. 5 Gross appearance of a benign mucinous cystadenofibroma with solid areas and mucin filled cystic spaces

with mucinous adenofibromas. When the solid component alternates with cysts lined by mucinous epithelium without atypia, the term mucinous cystadenofibroma is used (Fig. 5).

The mucinous cystadenoma can coexist with mature cystic teratoma or with other types of ovarian cysts, including those that are malignant.

Occasionally, various types of mural nodules are found in the walls of mucinous ovarian tumors. They include anaplastic carcinoma, carcinosarcoma and sarcoma-like nodules, mixed nodules, and leiomyomas [5].

Diagnostics

The possibility of obtaining an initial diagnosis of a suspected ovarian tumor is based on correct history, general clinical, and, in particular, gynecological examination. The physical examination provides information related to the increase in the size of the ovaries, their mobility, consistency, surface roughness, and whether it is unilateral or bilateral.

A finding of unilaterality, cystic consistency, mobility, and a regular surface point to a benign nature of the tumor. However, it is essential to confirm the suspected ovarian pathology, with US being the technique of choice before considering other more complex, and often unnecessary, technological approaches. Guerriero et al. [31], in a prospective study of 161 premenopausal patients, 83 of which had persistent adnexal mass, concluded, by comparing the results of transvaginal ultrasound and computed tomography (CT), that in premenopausal women, transvaginal ultrasonography remains a cost-effective method in the diagnosis of most cystic ovarian lesions.

Imaging Techniques

The ultrasound for the study of gynecological organs must be transvaginal and whenever possible, with color or power Doppler. Abdominal US with a full bladder is indicated in virgin patients and for completing ultrasound study carried out by transvaginal US in adnexal masses of considerable size.

The majority of tumors affecting the ovaries are benign, and despite the fact that ultrasound is considered the most effective method to predict the histological type, even today, in the absence of clinical symptoms, unnecessary interventions are still recommended instead of minimally invasive procedures or conservative management. An important objective is, therefore, recognizing the different subtypes of benign cysts to make an adequate therapeutic and clinical decision.

Significant advances in technology over the last decade, and improvements in knowledge and training, have allowed experienced ultrasound examiners to correctly classify the majority of growths and in some cases suggest the specific diagnosis through a subjective assessment of sonographic findings in grayscale and color Doppler [68].

Subjective sonographic characterization of benign ovarian cysts based on pattern recognition has been shown to be accurate [67], as well as reproducible [34].

Three-dimensional ultrasound (3D-US) is a technological advance that produces 3D images that give a more realistic reconstruction of anatomical structures in three dimensions. 3D-US enables a more detailed analysis of internal cyst walls, borders, and vascularization, while improving the diagnostic accuracy of US in the evaluation of adnexal masses. The Ultrasound Consensus Conference Statement of the Society of Radiologists [44] concludes that there are many areas for future research that will further our ability to appropriately diagnose and follow adnexal cysts. One of the recommendations is to refine the clinical importance of 3D-US and Doppler findings.

Regarding the management of ovarian and other adnexal cysts imaged sonographically in asymptomatic women, the recommendations of the Society of Radiologists in Ultrasound [44] are:

- For reproductive age and postmenopausal women with simple adnexal cysts larger than 7 cm, further imaging with magnetic resonance (MR) or surgical evaluation should be considered because the cysts may be difficult to assess completely with US.
- Multiple thin septations or solid nodules without detectable flow at Doppler US are features that we would specifically consider as indeterminate. These findings are suggestive of neoplasms, most often benign. Irregularities or tiny areas of focal thickening of the cyst wall may be difficult to distinguish from a small solid component and thus cannot determine malignancy. Cysts with either of these indeterminate features merit more attention than the previously described cysts with typical benign sonographic findings. In a woman of reproductive age, this entails a short-interval follow-up (6–12 weeks) with US or, occasionally, further examination with MR imaging. MR imaging may be particularly helpful to confirm the absence of MR contrast enhancement in sonographically solid-appearing areas that do not have demonstrable flow at Doppler US.

A short-interval follow-up of 6–12 weeks with US should be enough time for a physiologic cyst to resolve. However, it should be at a different phase of the menstrual cycle, ideally between the third and tenth day, so that development of a new cyst does not complicate interpretation.

The larger the cyst the more time it may take to resolve. If the lesion persists and continues to have indeterminate findings at US or MRI, surgery should be considered. Although size cannot be used to distinguish between benign and malignant cysts, once cyst size increases above 10 cm, the lesion has a 13 % chance of being malignant [25].

Benign Serous Tumors

Cystadenoma

Cystadenoma tumors are usually 1–10 cm in diameter (Fig. 6) but occasionally reach up to 30 cm or more (Tavassoli et al. [63]).

Ultrasonographic findings that define serous cystadenomas are described as unilocular or multilocular cysts, with liquid content and thin walls, and without solid or papillary images in their interior (Fig. 7). They show posterior acoustic enhancement and acoustic streaming. Edwards et al. [20] describe this phenomenon as a visualization of particle movement within the cyst, away from the transducer during color Doppler imaging, after the ultrasound probe had been

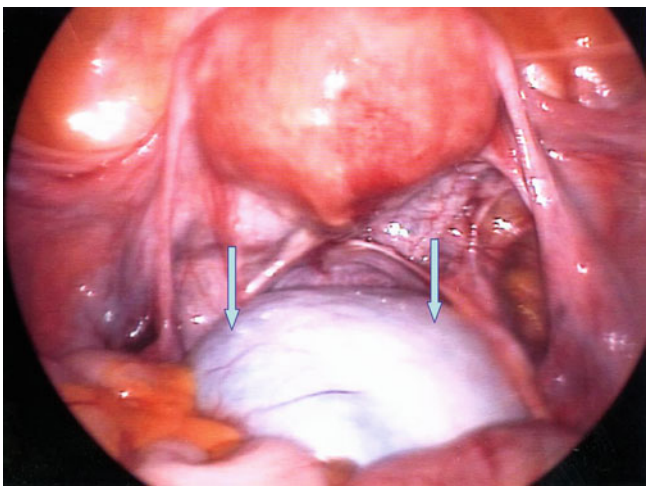

Fig. 6 Laparoscopy of a serous cyst (*arrows*)

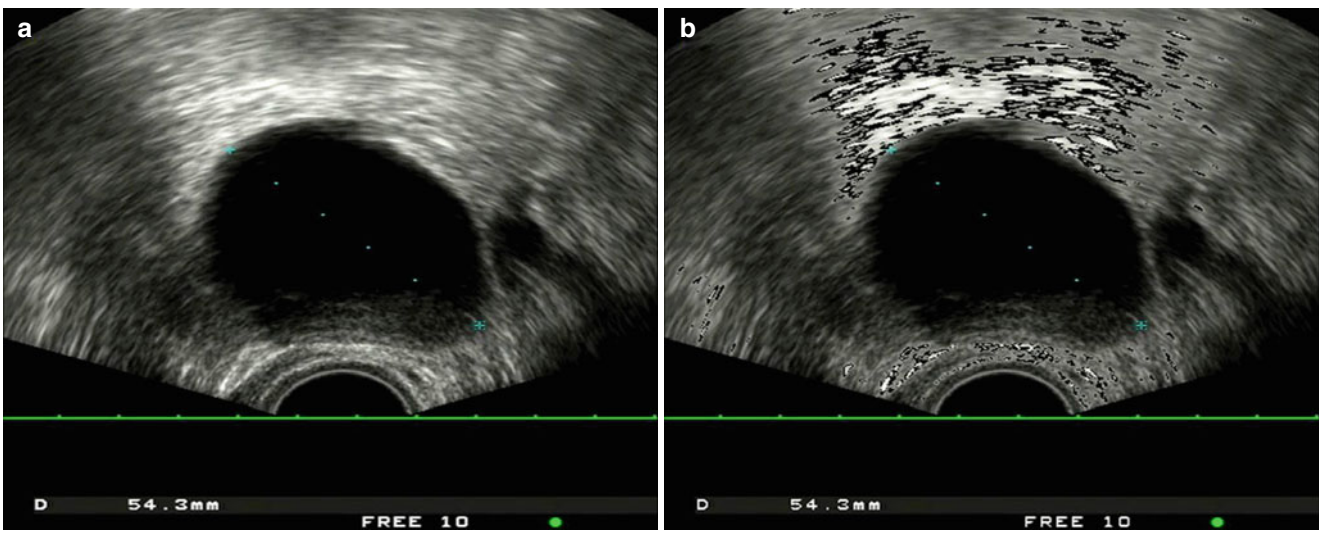

Fig. 7 (**a**) Transvaginal US shows a unilocular cyst, 54 mm in diameter, with fluid content and thin walls, and no solids or papillary images inside. We can observe posterior acoustic enhancement. In image (**b**), the prominent posterior acoustic enhancement has been brightened

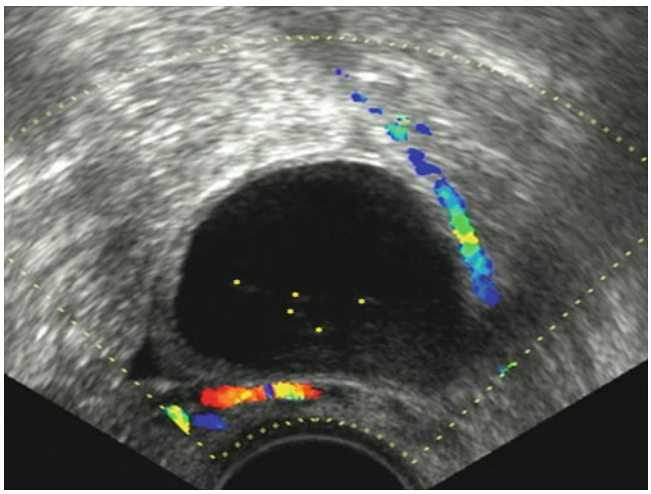

Fig. 8 Transvaginal US of a unilocular cyst with vascularization score of 1. Note that the vessels are outside the cystic structure. The phenomenon of acoustic streaming can be seen inside the cyst (*yellow asterisks*)

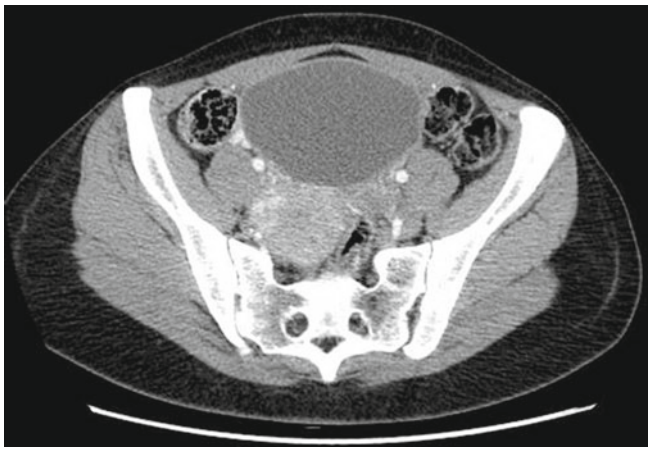

Fig. 9 Contrast-enhanced CT scan image shows a unilocular cyst with thin walls and water-density contents

held still for some time, and this finding was observed in 80 % of cystadenomas. Later, Van Holsbeke et al. [72] observed this phenomenon in 44 % of serous cysts by using data from 1,938 patients with an adnexal mass included in Phase 2 of the International Ovarian Tumor Analysis (IOTA) study.

The vascular features of cystadenoma according to the IOTA consensus [65] show a score of 1 (no blood flow found in the lesion) and sometimes a score of 2 (only minimal flow detected in the cyst wall or within the septa) (Fig. 8).

The differential diagnosis of cystadenoma must include both paraovarian and functional cysts. The diagnosis of paraovarian cysts can be made when the ipsilateral ovary is clearly visible. Uncertainty as to whether the mass is ovarian or extraovarian is likely to occur when the ipsilateral ovary is not seen and is probably more likely when the cyst is large. In premenopausal patients, ultrasonographic monitoring of functional cysts will determine their diagnosis [50]. When the cyst persists, it is likely to be a serous cyst.

Guerriero et al. [34] demonstrated that a serous cyst is not difficult to diagnose and it has good interobserver agreement (k 0.72–0.80) between experts and moderately experienced sonologists.

In a prospective study of over 300 patients, Alcázar et al. [2] concluded that for selected asymptomatic premenopausal women, the most sonographically benign ovarian cysts remain unchanged during long-term follow-up. In these cases the data support conservative management.

Valentin et al. [70], in a recent paper, found that the malignancy rate in surgically removed adnexal lesions, which were judged to be unilocular cysts at transvaginal scan, is around 1 %. Postmenopausal status, personal history of breast or ovarian cancer, and hemorrhagic cyst contents at scan increase the risk of malignancy. To avoid misclassifying adnexal lesions as unilocular cysts when scanned, it is important to scrutinize unilocular cysts for the presence of solid components.

Serous cysts at CT appear as well-defined, thin-walled cystic tumors. MRI shows simple fluid signal, hypointense on T1-wieghted sequences, and hyperintense on T2 (Figs. 9 and 10).

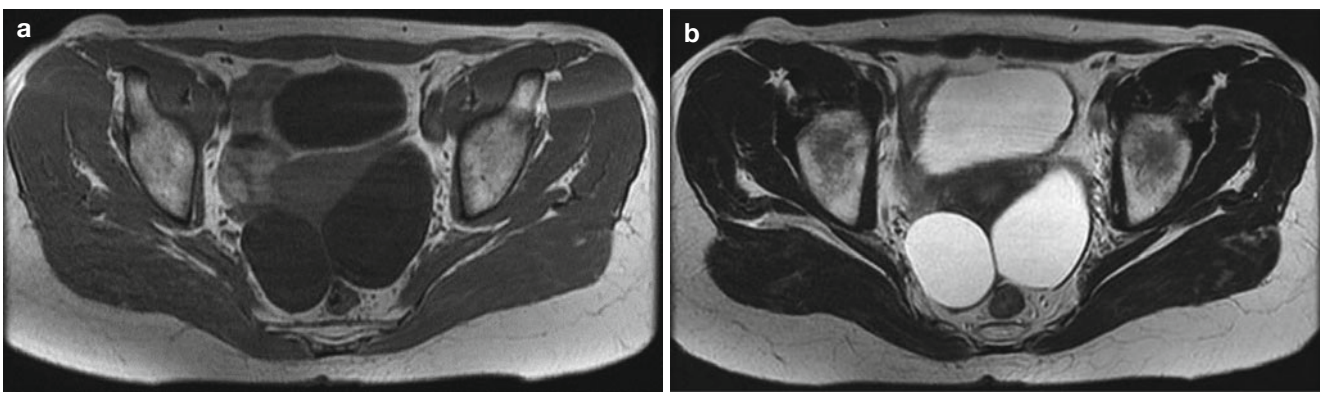

Fig. 10 Axial images show bilateral unilocular cysts with homogeneous hypointense signal on T1-weighted sequence (**a**) and hyperintense on T2 (**b**)

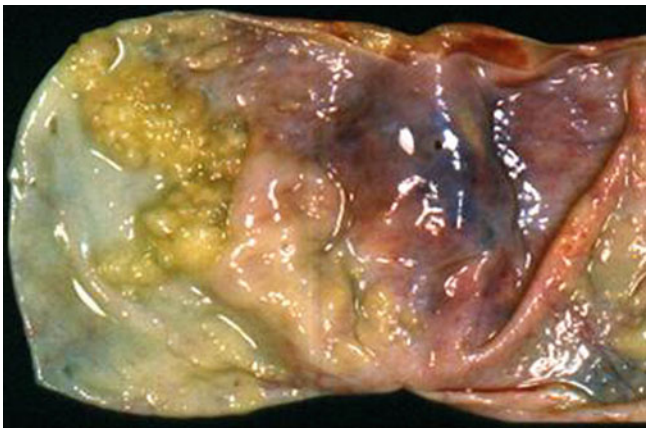

Fig. 11 Gross appearance of a serous papillary cystadenoma showing yellowish papillae in cystic formation with a smooth inner surface

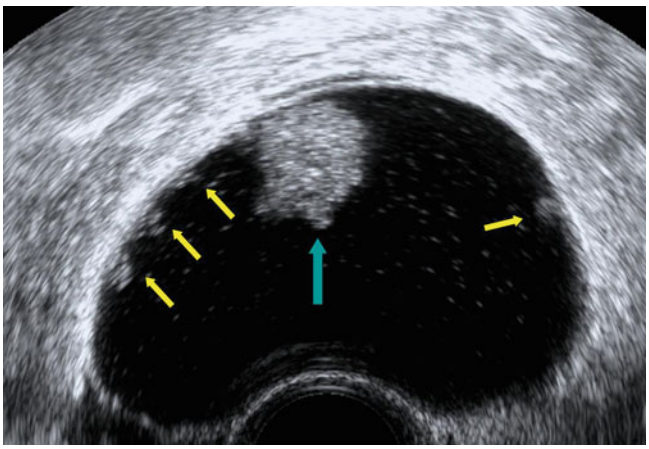

Fig. 12 Illustration of a unilocular cyst with a papillary projection with an irregular surface (*blue arrow*) and various small papillations (*yellow arrows*)

Papillary Cystadenoma

One variety of macroscopic serous cysts has projections in its external or internal wall, or both. When the papillations are present in the outer wall, as is the case with papillary surface, it is very difficult to detect with US (Fig. 11).

Thin-walled unilocular cysts with thin septa and papillary projections sonographically characterize benign papillary cystadenomas (Fig. 12).

These projections can be small, vascularized projections that arise from the internal wall of the cyst or from the septum.

The papillary projections are an important US finding in the morphological classification of ovarian masses. They are defined as any solid projection from the internal cyst wall into the cyst cavity, with a height of ≥3 mm. The surface of the papillary projections can be smooth or irregular [65]; it is important to assess their vascularization by color/power Doppler (Fig. 13).

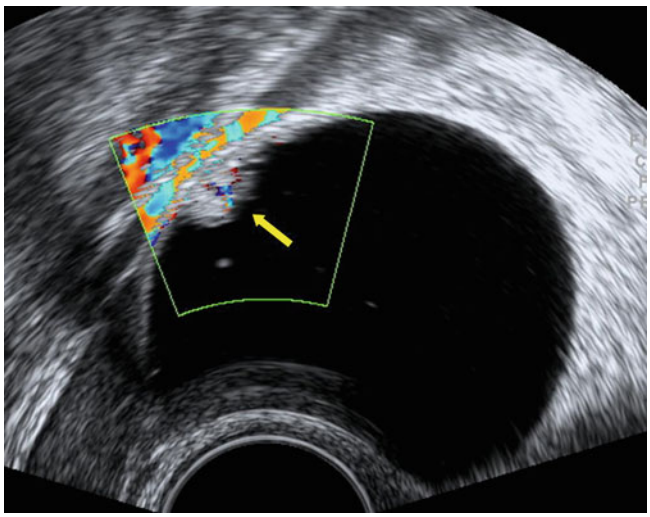

Fig. 13 A unilocular cyst with papillary projection (*yellow arrow*) with an irregular surface. Color Doppler detected minimal flow within the papillae (score 2)

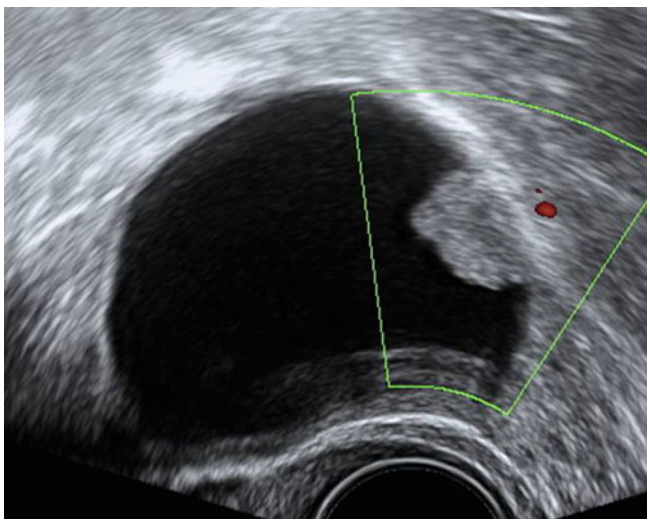

Fig. 14 A unilocular cyst with papillation in the inner wall. Power Doppler shows absence of flow within the papillation (score 1). At follow-up it disappeared and the ovary was normalized. Papillation image corresponds to a clot

On the other hand, some echogenic structures in the inner wall of the cyst may be confused with papillary projections. This is the main cause of false-positives of blood clots; although no color flow was detected in these false-positive cases, this is not sufficient to exclude papillary projections, because color flow may be absent in benign projections (Fig. 14).

A scoring system for masses containing papillary projections was suggested in order to characterize them. It was compared with the subjective evaluation of ultrasound images by an experienced examiner [67]. The results did not improve "pattern recognition" and concluded that the scoring

system was a relatively simple method that could be tested in less experienced hands. The idea was to see if its use would improve characterization of ovarian tumors by medical professionals who are not experts in gynecological ultrasonography [4].

Hassen et al. [36], using endovaginal ultrasound, evaluated the morphologic and color Doppler characteristics of papillary projections in benign epithelial stromal ovarian tumors and compared them with those that were borderline and malignant.

This study shows that using conventional ultrasound, topography, size, and morphologic findings correlate with macroscopic findings. The presence or absence of color flow can be used to characterize papillary projections. This demonstrated that benign epithelial tumors have fewer papillary projections than borderline or malignant masses. Furthermore, this study shows that a certain number of morphologic and Doppler findings can be highly suggestive of a diagnosis of benign, versus malignant, papillary projections. The same goes for borderline tumors even though an overlap exists. Large size, acute angle, irregular surface, and disseminated pattern are suggestive of malignancy, whereas absence of color flow in a papillary projection ≥10 mm is suggestive of benignity.

Valentin et al. [70], evaluating only unilocular cysts with papillary projections, found that the greater the number of and the larger the papillations, the higher the risk of malignancy. They concluded that unilocular cysts with papillary projections were more difficult to classify. One reason may be that benign papillary cysts are rare, and larger studies are needed so that more sonographic findings and clinical data can discriminate between borderline and invasive malignancy in unilocular cysts with papillations.

It is probable that in these types of difficult tumors, 3D-US can demonstrate its ability to show morphological structures such as papillary projections, their anatomical relationship with adjacent structures, and the details of their vascularization (Figs. 15 and 16).

Sladkevicius et al. [60] concluded that while using 3D power Doppler ultrasound to subjectively evaluate the morphology of the vessel tree (Fig. 17), as depicted by 3D power Doppler ultrasound, the clinician can discriminate between benign and malignant ovarian tumors. It adds little to grayscale ultrasound imaging in an ordinary population of tumors.

Although all patients with papillary cysts will likely undergo surgical removal, preoperative assessment of a tumor as benign, borderline, or malignant is fundamental, particularly in young women, in order to preserve fertility. This also helps the surgeon decide the type of surgery.

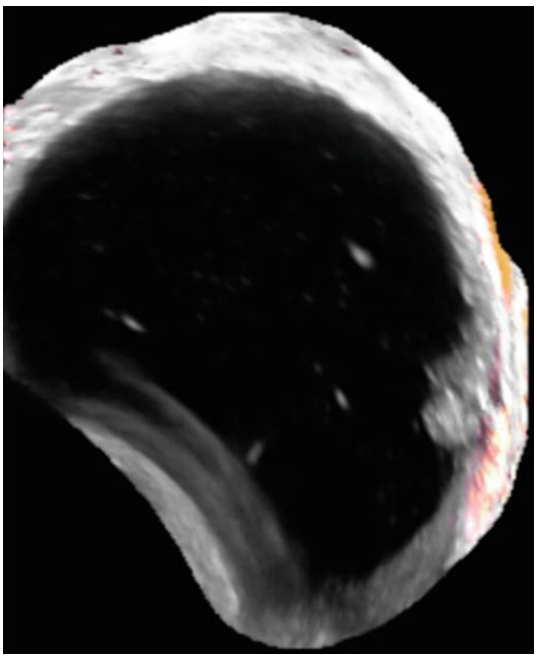

Fig. 15 Three-dimensional US, render mode shows detail of a papillary projection, without vascular flow signal, in the inner wall of a unilocular cyst

Adenofibroma and Cystadenofibroma

Adenofibroma and cystadenofibroma of the ovary are relatively rare benign tumors. Such tumors are characterized by their malignant sonographic appearance. Guerriero et al. [32], in a study of 572 histologically benign tumors, 10 cystadenofibromas of a total of 14 were diagnosed as malignant by US and color Doppler. In those cases in which the epithelial lesion was part of a solid tumor with abundant fibrous stroma (cellular, edematous, or intense hyalinization), it was identified as serous adenofibroma. If there was a combination of solid and cystic lesions, the term cystadenofibroma was used. The images show an example of adenofibroma (Figs. 18 and 19).

The cystadenofibroma has a low frequency, with a prevalence of around 5 %. Alcázar et al. [1], in a study of 23 ovarian cystadenofibromas, observed a predominantly cystic mass in all cases, with internal septa in 30.4 % (Fig. 20), and solid nodules or papillary projections in 56.5 %, of the cases (Fig. 21); 16 masses (69.6 %) showed an anechoic pattern (Fig. 22), while 7 masses (30.4 %) had echogenic content.

Vascularization is usually peripheral with scattered vessels, however, blood flow may be found in septa and solid nodules (Fig. 23). Alcázar et al. [1] found blood flow in 47.8 % of the cases.

Korbin et al. [40], in a study of 14 cases of paraovarian cysts, found serous cystadenofibroma located in 8 cases. US findings were predominantly cystic, and in 9 of 14 masses (64 %), one or more small (<1 cm) solid nodules were identified.

The differential diagnosis was with papillary cystadenoma (Fig. 24), borderline ovarian tumors (Figs. 25 and 26), and papillary serous carcinoma in the initial stages. Valentin

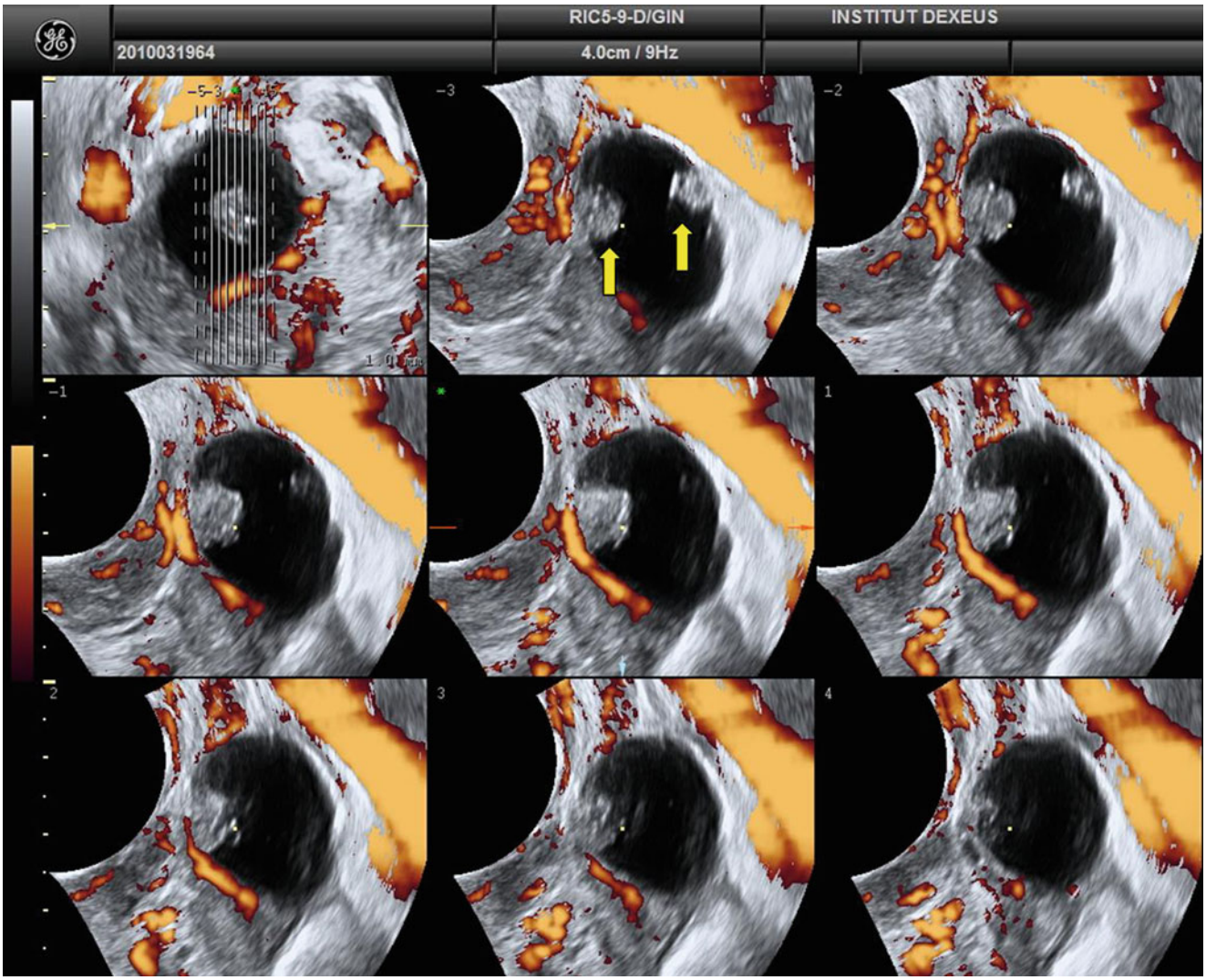

Fig. 16 Three-dimensional US, displayed in Tomographic Ultrasound Image (TUI mode), of a unilocular cyst with two papillary projections (*yellow arrows*). Multiple slices are shown in the 9 panels. The top left image is an axial view of the cyst, which is a reference image. The lines correspond to the views shown in the panels (*left to right*). The relationship between the papillary projections and the wall cyst is shown

et al. [69] included the adenofibromas and cystadenofibromas in the group of unclassifiable growths (benign/malignant), given that the ultrasonographic pattern included papillary projections, multilocular cysts with >10 locules, and masses with low-level echogenicity of cyst fluid. These US features are characteristic of borderline tumors [22, 51].

Using MRI in 13 cystadenofibromas, Outwater et al. [48] observed 12 multicystic masses with septa of very low signal intensity ranging from 2 to 20 mm, and one was predominantly solid fibrous tissue. Pathologic correlation with the specimen images showed that the low-signal intensity material was the subepithelial fibrous component of the cystadenofibromas. Fibrous components of ovarian fibromas and cystadenofibromas are demonstrable by MR as solid components representing fibrous tissue of very low signal intensity on T2-weighted images.

Benign Mucinous Tumors

Cystadenoma

The sonographic appearance of mucinous cystadenomas usually includes large (Fig. 27) unilateral uniloculated or multiloculated cysts (Figs. 28 and 29) with homogeneous low-level echogenic contents (Fig. 30). However, sometimes the different independent cavities of the cyst contain different types of mucin: endocervical-like (Müllerian) or the intestinal type [29]. The proportion of two types of mucin-producing cells may vary among different compartments in the same tumor. The difference in mucin types may explain the variable echogenicity in the tumor compartments as detected by sonography. Variable echogenicity in cyst compartments was described by Caspi et al. [10] as a more specific sign of a mucinous tumor (Fig. 31).

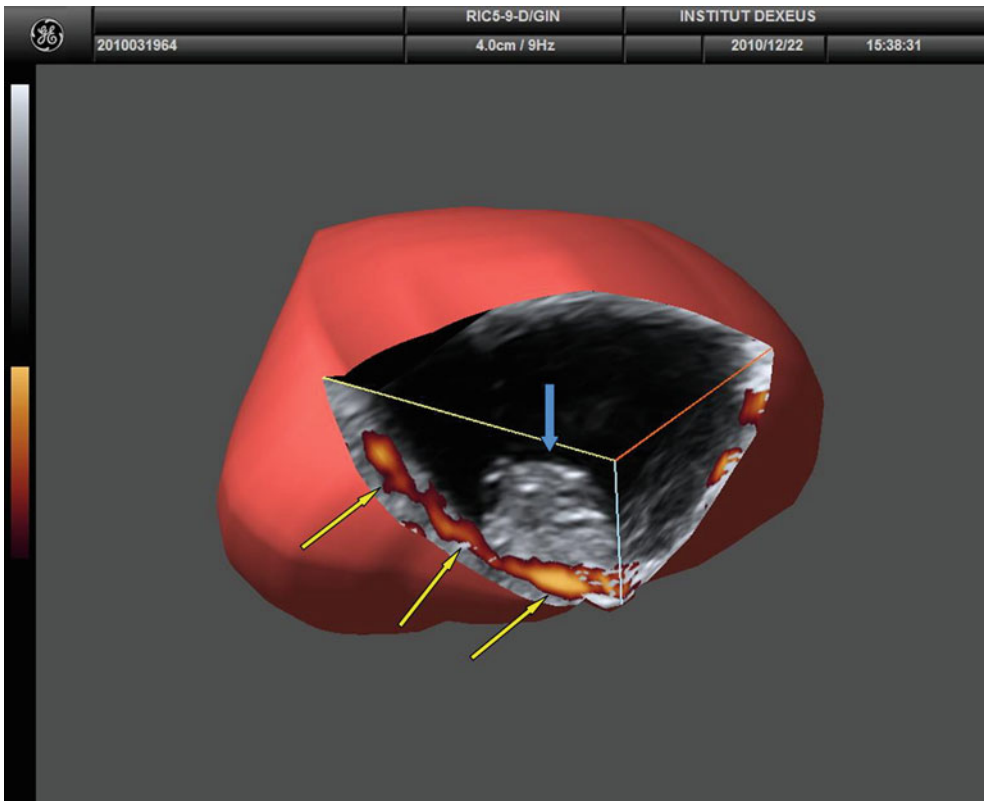

Fig. 17 3D-US, displayed in niche mode, shows an endocystic papillary projection (*blue arrow*) without vascular flow signal. Accurately observed that the blood vessels run through the cyst capsule without ramifications for papillation (*yellow arrows*)

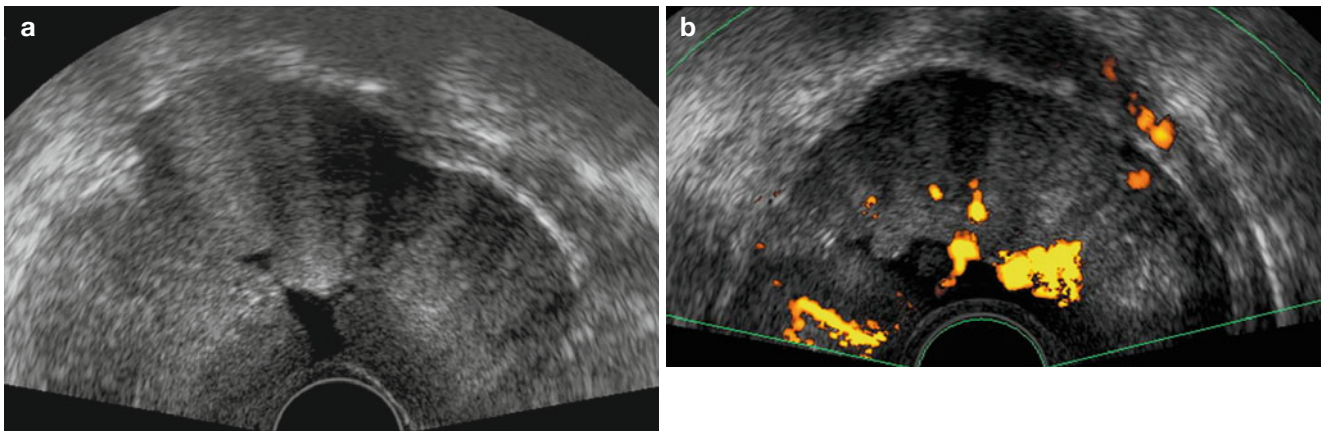

Fig. 18 (**a**) Transvaginal US shows a larger (about 90 mm) solid and heterogeneous mass suggestive of malignancy. (**b**) power Doppler shows moderate flow is present. Histology demonstrated that this corresponded to a benign adenofibroma

A rare presentation of mucinous cysts is described by Perlman et al. [54], which observed a multiloculated pelvic cystic mass that contained multiple compartments of various echotextures. A careful transvaginal sonographic assessment of the cyst revealed that one of the compartments contained echogenic material arranged in a pattern resembling onion skin shells.

Concentric echogenic layers are a well-known sonographic finding in other mucinous tumors. Degani et al. [16] were the first to describe this sign in a case of appendiceal mucocele, calling it the "onion skin" sign (Fig. 32).

The vascular features of benign mucinous cysts (Fig. 33), according to the IOTA consensus [65], tend to show a score of 2 (only minimal flow can be detected in the cyst wall or within the septae) and a score of 3 (moderate flow is present). A score of 4 (highly vascular) is rare.

Mucinous benign tumors can be difficult to differentiate from mucinous borderline tumors and cystadenocarcinomas. Color flow is of limited value when characterizing these tumors (Fig. 33). This difficulty also applies to CT and MRI techniques (Figs. 34 and 35).

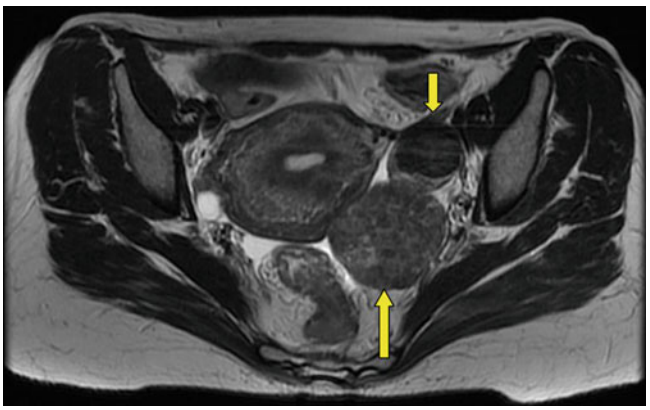

Fig. 19 Axial T2-weighted image shows solid bilobulated mass (*yellow arrows*) with a hypointense signal corresponding to the fibrous component

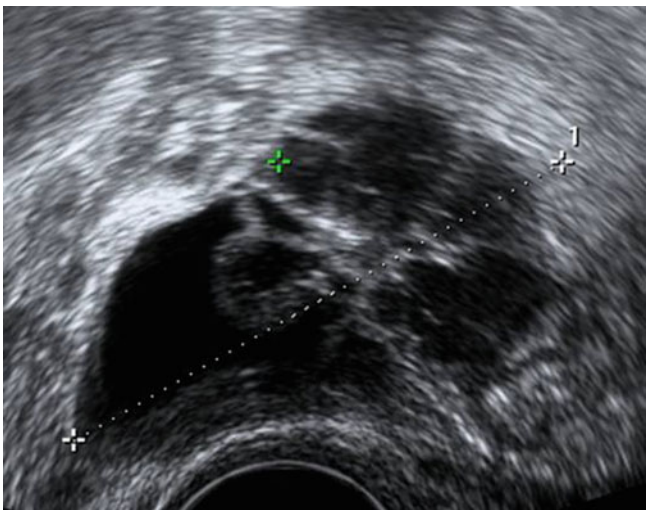

Fig. 20 Transvaginal US shows septations, but no nodularity was evident

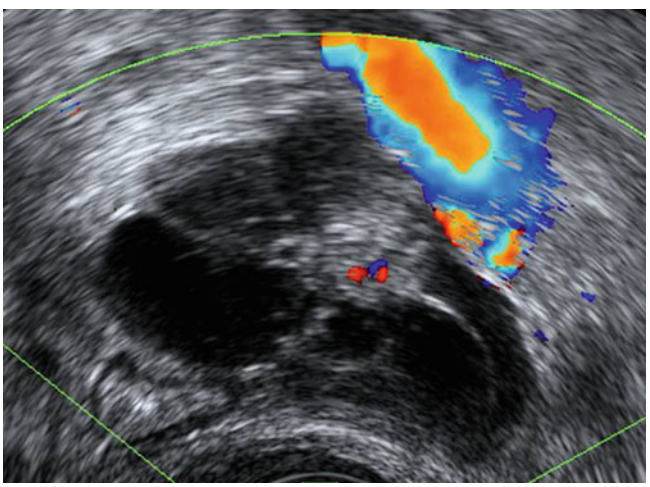

Fig. 21 A complex cystic mass contains evident blood flow within the solid nodule along with septations

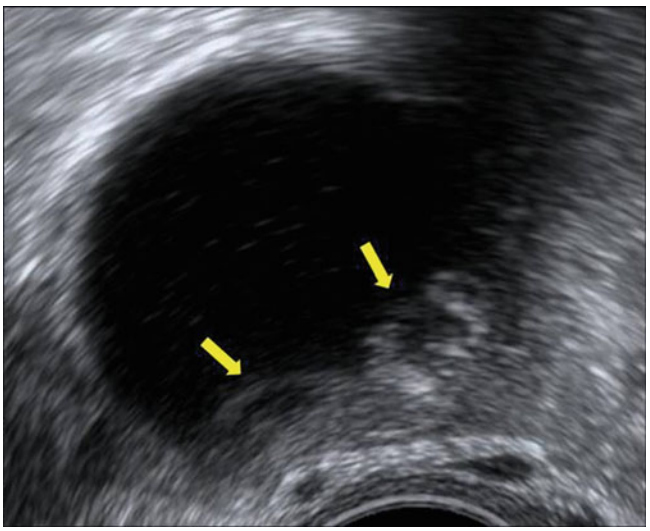

Fig. 22 Unilocular cyst with anechogenic cyst fluid and a few septations (*yellow arrows*)

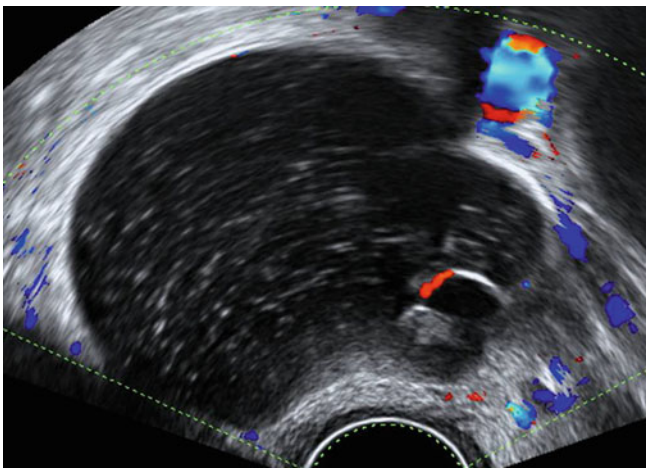

Fig. 23 A unilocular cyst with low-level echogenic contents and minimal blood flow (score 2) in the thin septa

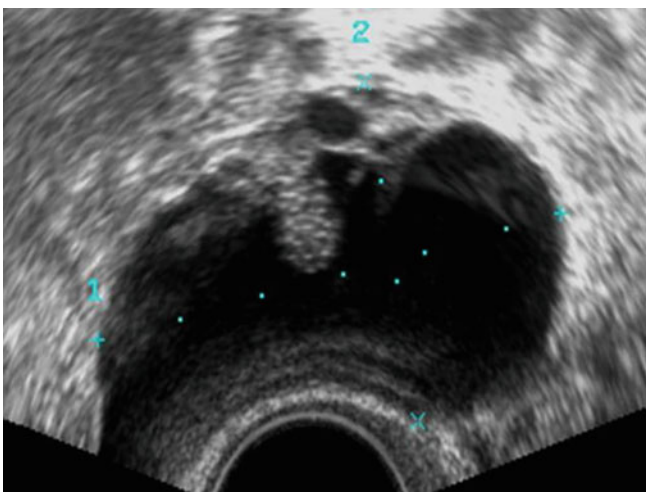

Fig. 24 A complex cyst with papillary projection. Histology corresponded to a benign papillary cystadenoma

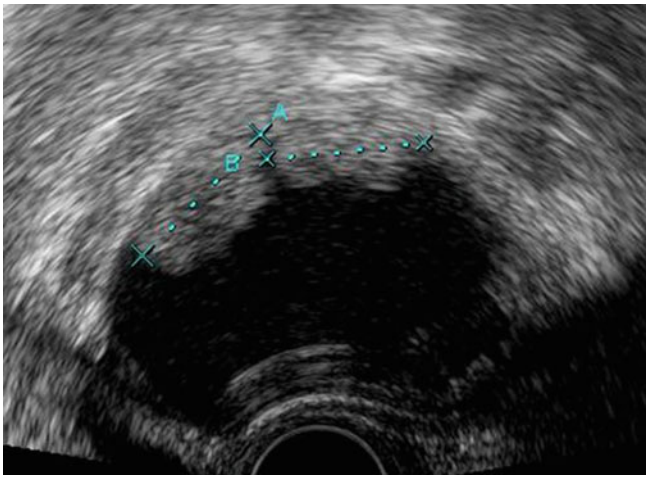

Fig. 25 A unilocular cyst with endocystic papillary projections, larger in the base (27 and 25 mm, respectively), with irregular surface; Histology corresponded to a serous borderline tumor

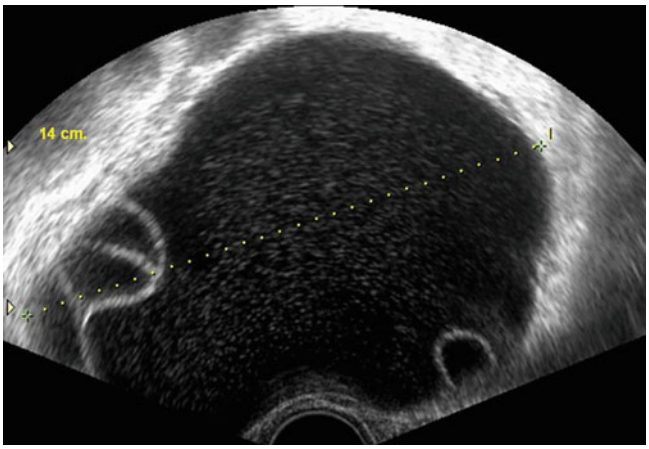

Fig. 27 Transvaginal US shows a larger cyst (140 mm), with smooth internal wall, thin septations, and homogeneous low-level echogenic contents

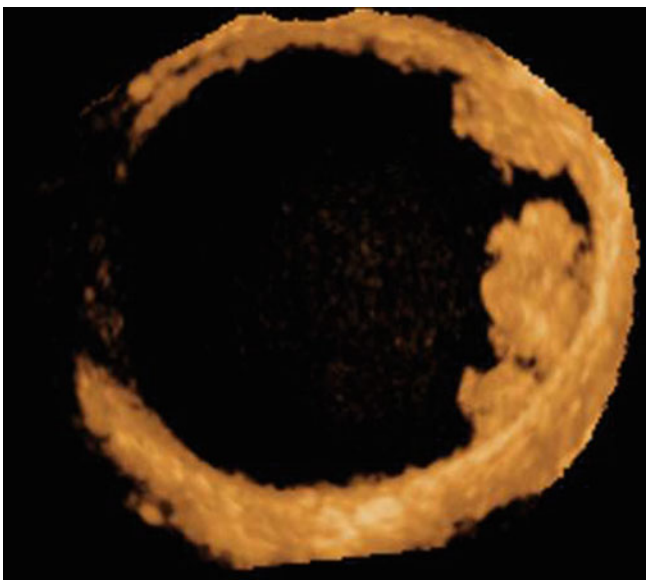

Fig. 26 Three-dimensional US, displayed in render mode, shows three papillary projections with irregular surface. Histology demonstrated that this corresponded to a serous borderline tumor

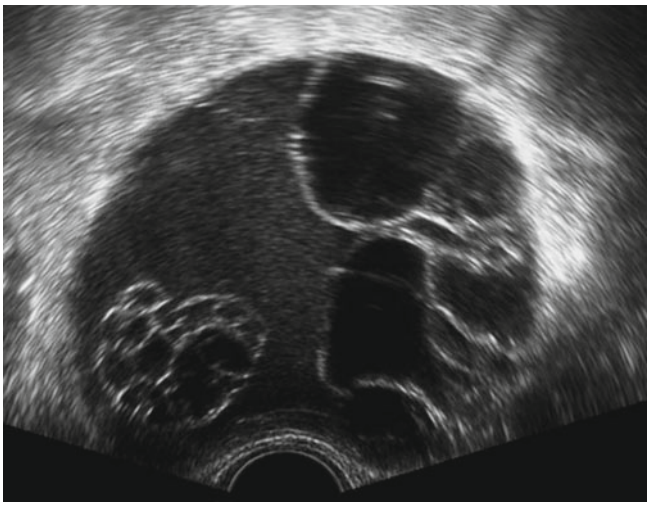

Fig. 28 Transvaginal US shows a multilocular, partly echogenic cyst with multiple septae

The differential diagnosis of a mucinous cyst should be considered on an endometrioma with a high fluid content and with peritoneal cysts [33].

Mucinous Cystic Tumor with Mural Nodules

Mucinous cystic tumors of the ovary, whether benign or malignant, may be associated with sarcoma-like mural nodules. Prat and Scully [57] first reported mucinous tumors of the ovary with "sarcoma-like nodules."

These nodules resemble gingival epulis or giant cell tumors of bone and are reactive rather than neoplastic.

Solid mural nodules within mucinous ovarian cysts are extremely rare. True sarcomatous nodules are usually larger than sarcoma-like mural nodules.

Benign mural nodules may appear sarcoma-like or have the features of a leiomyoma. These benign nodules are associated with favorable outcomes.

Different imaging techniques show a tumor that is usually large and multilocular, with a solid nodule in the internal wall.

Mucinous Cystic Tumor with Pseudomyxoma Peritonei

Preoperative knowledge of the mucinous nature of a tumor is of crucial importance because many of these tumors are

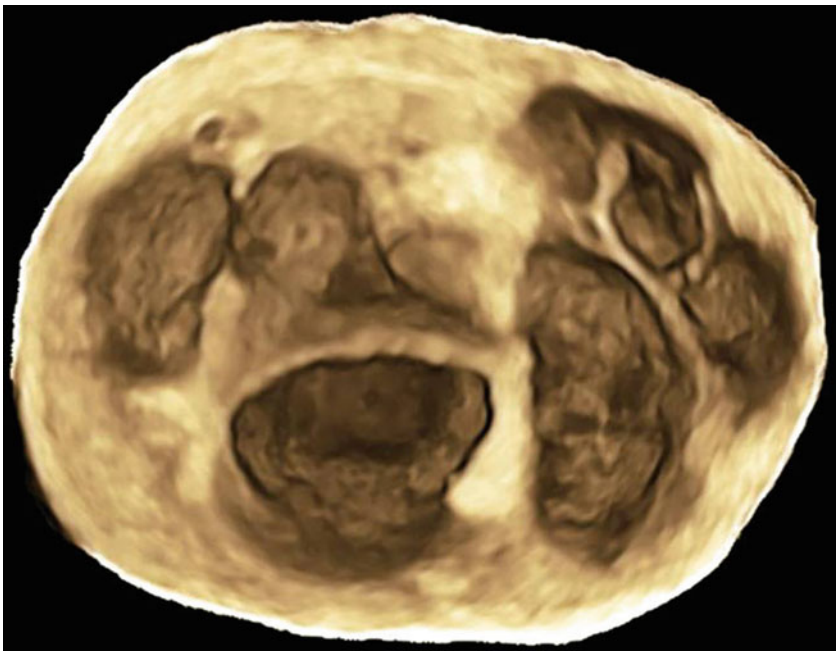

Fig. 29 Three-dimensional US, displayed in render mode, showing a multilocular cyst with thick and thin septae

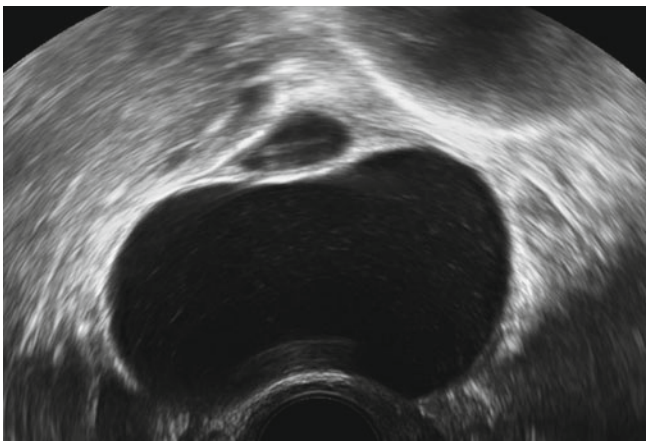

Fig. 30 Transvaginal US shows a large unilocular cyst, with smooth internal wall, and homogeneous low-level echogenic contents

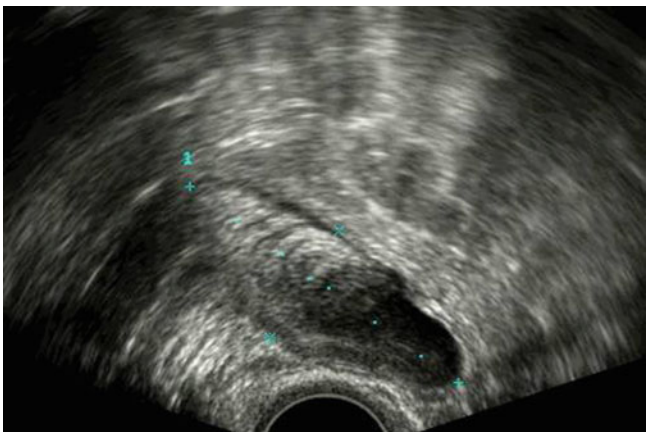

Fig. 32 Sagittal sonogram demonstrating contents arranged in "onion skin" thin concentric layers

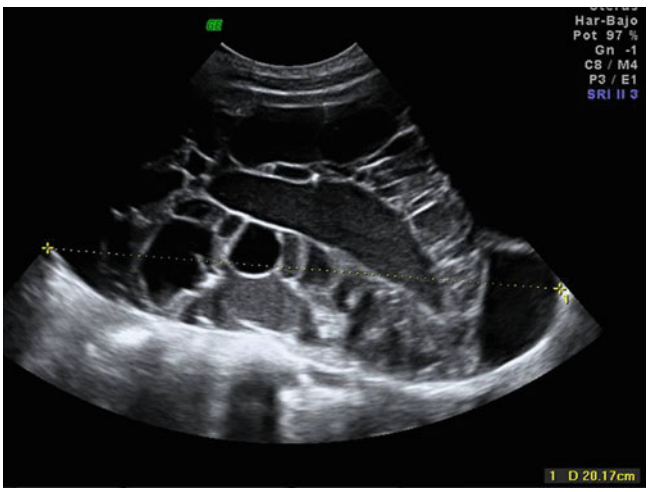

Fig. 31 Sonographic image of a benign mucinous cystadenoma showing variable echogenicity among different cavities

resected laparoscopically, and spillage may occur. Overflow should be prevented not only because of the potential spread of cells in malignant tumors but also because, in these particular tumors, spillage of mucin carries a serious risk of pseudomyxoma peritonei complication, albeit rare.

Pseudomyxoma peritonei follows the perforation of a mucinous appendiceal or ovarian neoplasm which leads to an intraperitoneal dissemination of mucinous implants that range in viscosity from purely liquid to a semisolid-like texture and that form on the peritoneal surfaces of the abdominal wall and visceral organs [58]. Though epithelial cells within the mucin implants can result in mucin production, they rarely invade and hence do not metastasize into the blood stream or lymphatics.

This mucinous material remains intra-abdominal and accumulates, eventually causing severe abdominal distension and anorexia from compression of the small bowel,

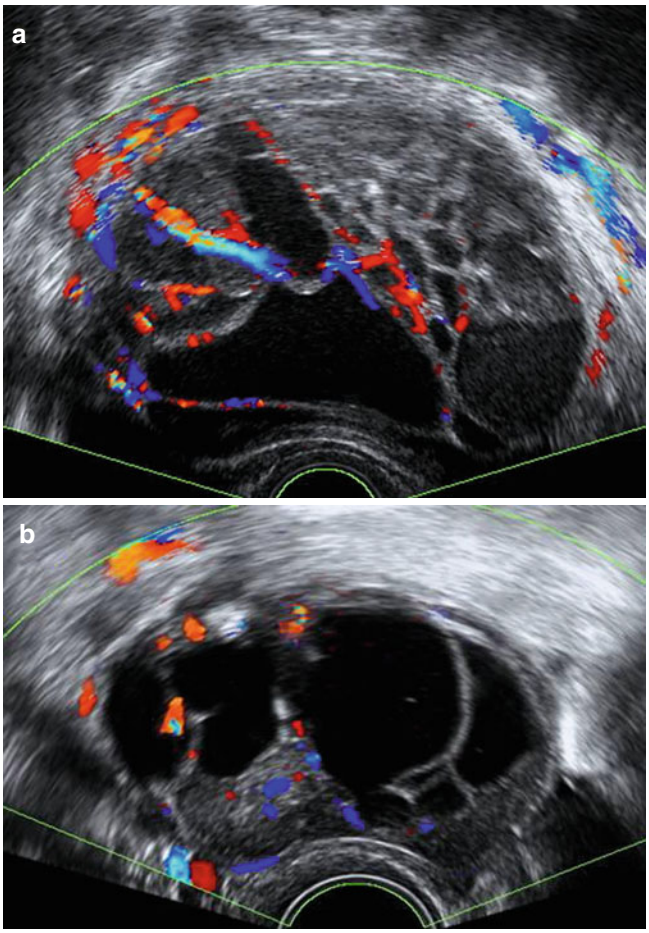

Fig. 33 Image (**a**) shows transvaginal US of a benign mucinous cystadenoma in a 55-year-old patient. The mass histology was 27 cm and 3,860 g. The morphologic pattern is complex with multiple septations, and a thickened and highly vascular pattern showing blood flow (score 4) within the septa. Image (**b**) shows a borderline mucinous tumor in a 35-year-old patient. Sonogram shows a multiloculated cystic structure containing echogenic material in some of the cavities. Moderate flow is present (score 3) within the septa and cyst walls

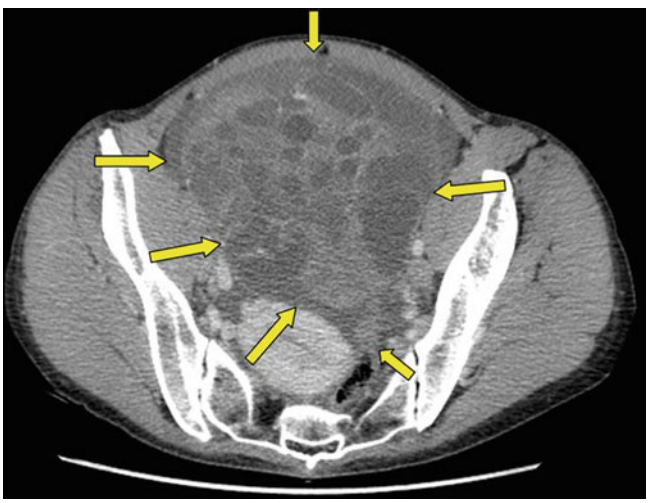

Fig. 34 Contrast-enhanced CT image shows multiloculated cystic lesion (*yellow arrows*) with different densities inside the locus

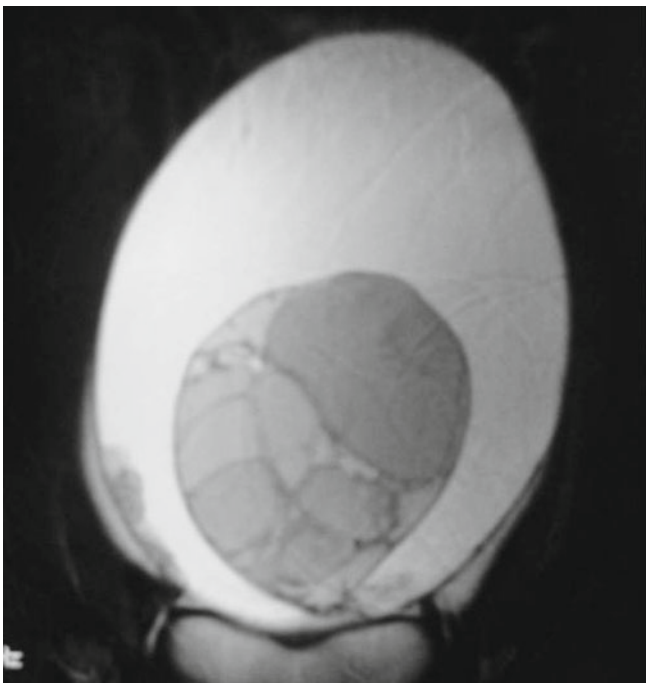

Fig. 35 Coronal fat-saturated T2-weighted image showing a cystic multiloculated lesion with different signal intensities and an intermediate signal corresponding to a mucinous component

which are the main causes of morbidity and mortality in untreated patients.

Tumor Markers

Tumor markers are important tools for screenings and follow-ups of patients with ovarian malignancies and have also been suggested to be valuable for early diagnosis. Although CA-125 is the most useful tumor marker, it does not sufficiently distinguish malignant from benign tumors when used alone. In addition CA-125 is very nonspecific, given that it may increase in other types of non-ovarian cancers, such as those of endometrial and gastrointestinal origin, and breast cancer. It is also elevated in benign processes such as endometriosis, pelvic inflammatory disease, cirrhosis, and gestation. Wakahara et al. [76] concluded that comparatively sonography is more effective in making a diagnosis than tumor markers (CA 125, CEA CA 19–9 and 72–4) prior to surgery on an adnexal mass.

Dikensoy et al. [18], in a study of 93 menopausal patients, noted that there were 77 patients with CA-125 values of less than 35 IU/ml, and they had histological findings that were benign. On the other hand, the remaining 16 patients with borderline tumor histology had CA-125 values between 35 and 50 IU/ml and had ultrasound results showing multilocular cysts greater than 13 cm in size.

Spinelli et al. [61], in a study of 120 adolescents with adnexal masses, found 100 % positivity of the tumor markers

in malignant tumors (5 cases) and 20.4 % positivity in benign ovarian cysts. Since their results were consistent with others published [59], he therefore concluded that the role of tumor markers was still controversial. This is the reason why, before considering radical treatment, we suggest caution in order to optimize future fertility.

Ultrasound-Guided Aspiration

An attractive possibility for increasing accuracy in diagnosing benign ovarian cysts, in particular serous cysts, is to aspirate the tumor in order to obtain material for cytological study.

The aspiration can be performed either by laparoscopy [11, 46] or sonographic control.

Pez et al. [55] concluded that an ovarian aspiration under sonographic control is a simple technique that avoids many laparoscopies, providing an early diagnosis so that any intervention may be done more quickly.

Montanari et al., in 1987 [46], observed a 53 % rate of recurrence in cysts that were aspirated percutaneously. Dargent and Desmettre [14] concluded that with selected patients, whether done vaginally, percutaneously, or via the urethra, the recurrence rate was equal to that obtained by laparoscopic puncture.

Granberg et al. [27] obtained results of aspirations in simple cysts under sonographic control, which were comparable to those obtained by laparoscopy by other authors [42], with a 70 % rate of no recurrence in the drained cysts.

De Crespigny et al. [15] published a new study of 109 aspirations in 88 patients with a 45 % rate of no recurrence.

In 1990 Forest and col. [24] obtained a 25.3 % rate of recurrence, and Troiano and Taylor [66] achieved good results in a study of 43 patients, which included pregnant women.

Recently, Koutlaki et al. [41], in 121 reproductive age and menopausal patients, have concluded that the aspiration of a benign cyst seems to increase success rates for any expected treatment. Previously, Duke et al. [19] had concluded that this technique was a good alternative for patients with high-surgical risk.

Nevertheless, the technique is controversial. There are authors who are against ovarian aspiration (laparoscopy or ultrasound), due to the danger presented by the spreading of cells, if the tumor is malignant [21, 30].

In our experience [49], we have not observed any cysts under sonographic control aspirated with a cytological result of malignant cells. Our results show a 53.6 % rate of nonrecurrence of benign cystic pathologies in general. If we exclude endometriotic cysts, the rate of nonrecurrence is 57.3 %; in other words, almost 2 of every 3 serous cysts are resolved with a puncture under sonographic control.

The main advantage of this technique is a reduction in surgical interventions. Consequently, the economic and social costs arising from surgical treatment of these pathologies are also reduced.

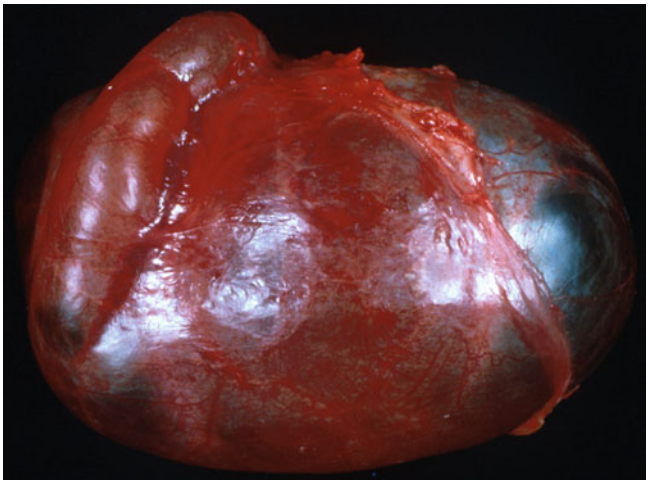

Fig. 36 Gross appearance of an infarcted ovary. Dilated vessels can be seen on the surface

However, if the cyst recurs, the value of reaspirating the cyst is doubtful, given that of patients that are aspirated more than once, 60 % end up in surgery [27].

In our experience just 15.7 % of patients eventually required surgery. The most frequent causes of intervention were due to an inability to drain the cyst; this is the case with diagnostic aspirations (7.6 %) and the recurrence of cysts previously under sonographic control.

Complications

Torsion

Ovarian torsion is caused by rotation of the ovary or adnexa with the vascular pedicle on its axis, resulting in arterial, venous, or lymphatic obstruction (Fig. 36).

The sonographic appearance of ovarian torsion varies according to the duration and degree of the torsion, whether it is complete or incomplete, and the presence or absence of an ovarian mass [23].

Helpful sonographic findings that have been described include the appearance of a cystic, complex mass, with or without pelvic fluid; thickening of the wall; and cystic hemorrhage. All of these are indirect signs of adnexal torsion. They may represent either the cause of torsion or its effects on the ovary, but not the torsion itself. Both the clinical symptoms of torsion, as well as these classic sonographic signs are relatively unspecific.

Van Voorhis et al. [73] and Desai et al. [17] described an enlarged ovary absent of, or with markedly diminished, ovarian blood flow on transvaginal and color Doppler sonography, as

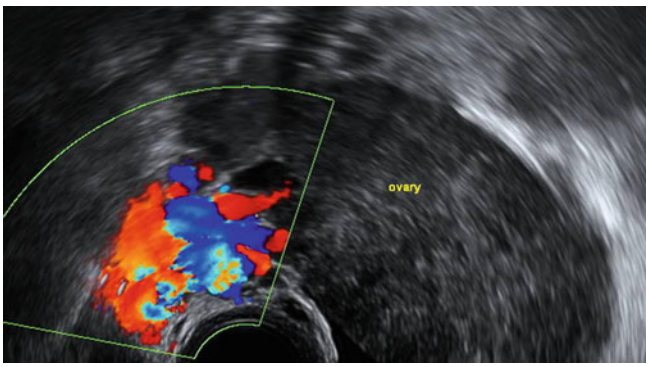

Fig. 37 This image shows an enlarged ovary without vascularization. It observes the vascular pedicle twisted on itself. The findings are highly suggestive of torsion. The patient immediately underwent a laparoscopy, releasing the torsion

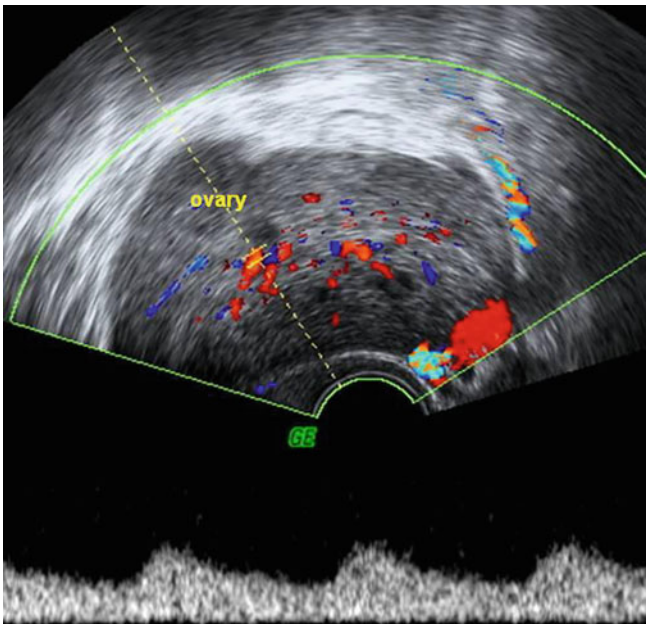

Fig. 38 Transvaginal US image shows an enlarged ovary, with edematous stroma, together with signs of twisted ovary. Presence of normal arterial flow can be seen

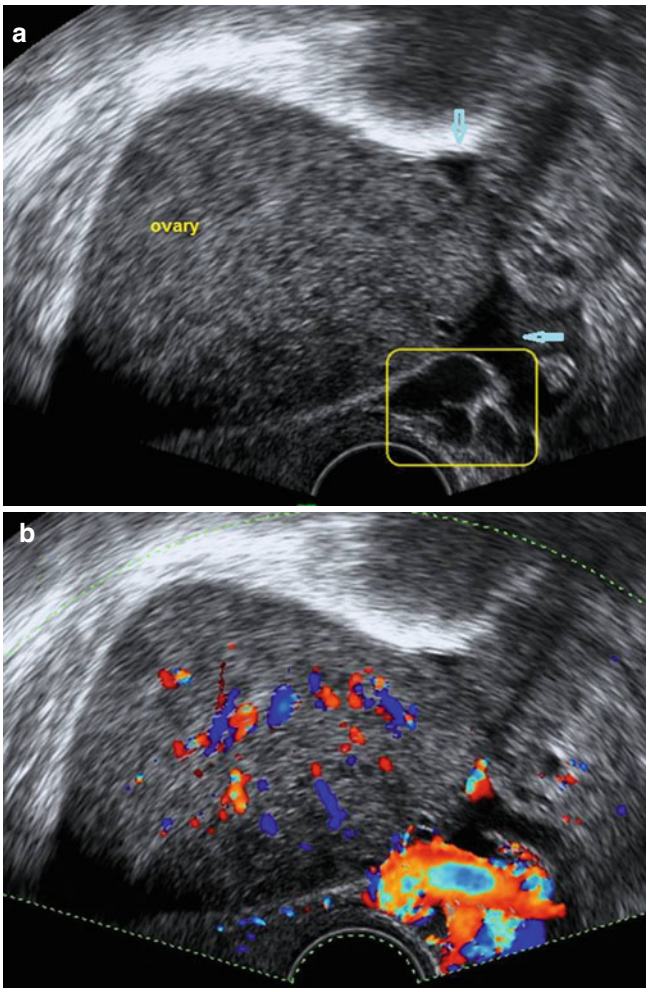

Fig. 39 Image (**a**) shows a transvaginal US with free fluid surrounding the ovary (*blue arrows*). It is a grayscale ultrasound image of a twisted ovarian ligament that resembles a spiral or whirlpool sign. Image (**b**) shows a color Doppler ultrasound image showing twisted vessels around the axis

a specific finding for the early diagnosis of ovarian torsion (Fig. 37).

Lee et al. [43] observed the presence of normal arterial flow, which suggested venous thrombosis without arterial occlusion, in addition to a dual blood supply to the ovary, as possible explanations for the occurrence (Fig. 38).

These different results indicated that, in partial or early torsion, both arterial and venous flow could be maintained with viable ovarian tissue.

Vijayaraghavan [75] described the whirlpool sign representing vessels wrapping around the central axis. Valsky et al. [71], in a study of 80 patients with suspected ovarian torsion, 22 included a search for the whirlpool sign. They concluded that the addition of the sonographic whirlpool sign, to the preoperative sonographic evaluation of patients with suspected torsion, appeared to improve the rate of true-positive diagnoses as confirmed by laparoscopy.

In order to find the whirlpool sign, it is necessary to focus the probe on the adnexal pedicle where the torsion is suspected.

The twisted pedicle should be evaluated in both grayscale and with color/power Doppler (Fig 39). The color Doppler view confirms that the whirlpool sign contains blood vessels.

During pregnancy the relatively rapid movement of the ovaries and fallopian tubes out of the pelvis during the mid-late first trimester, and the rapid return of these structures to their normal anatomical location after delivery, places the ovaries and ovarian masses at an increased risk of torsion [13]. Most cases occur in the first half of pregnancy and, followed by the puerperium, are far less common in the second half of pregnancy.

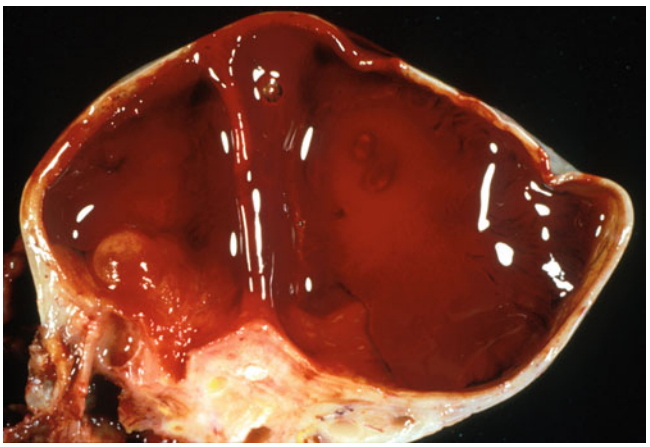

Fig. 40 Gross appearance of a bilobulated cyst with bloody fluid

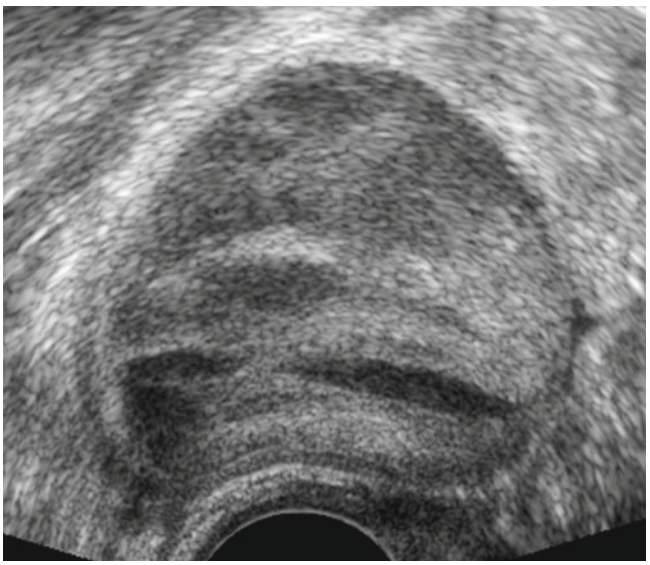

Fig. 41 A hemorrhagic cyst may occasionally appear solid, due to dense internal echoes and weak transmission. This may be seen in the subacute stage, when there is blood clot formation but the clot lysis has not yet begun

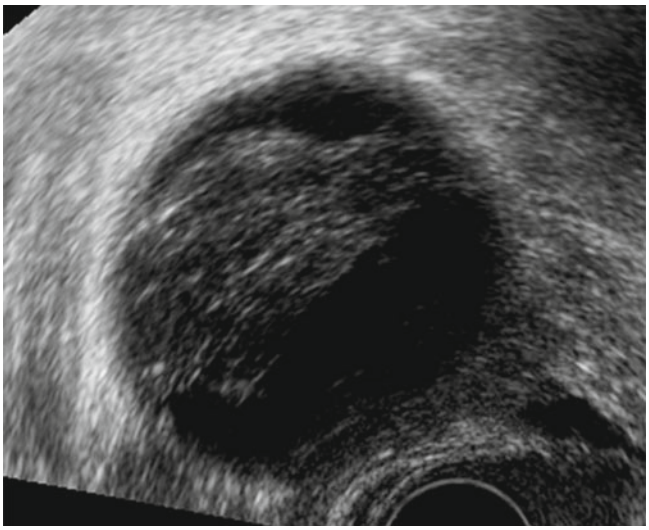

Fig. 42 A cystic mass is shown in the adnexal region with posterior acoustic enhancement. Within this mass, there are fine septations (fibrin strands), which have a reticular appearance. This pattern is common for a hemorrhagic cyst

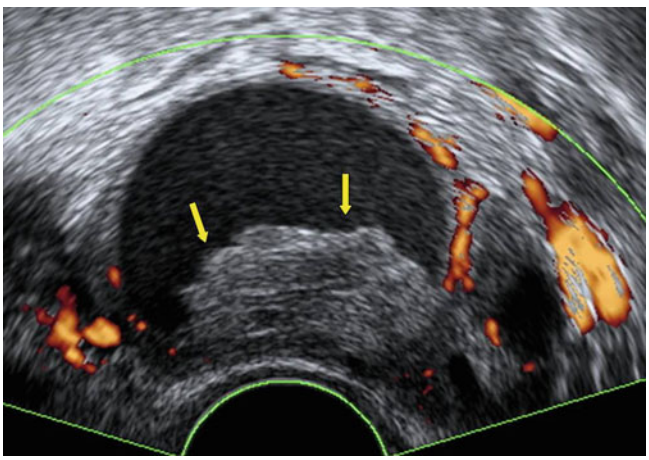

Fig. 43 Transvaginal US shows another common appearance of a hemorrhagic cyst, which is a retracting blood clot (*yellow arrows*). The clot may appear to be slightly homogeneous or may contain a reticular pattern due to fibrin strands. The remainder of the cystic mass appears anechoic. Occasionally, the retracting clot may simulate a papillary projection. Color and power Doppler sonography would fail to show blood flow in the clot

Hemorrhage

Most hemorrhagic ovarian cysts are nonneoplastic, and the few that are neoplastic are generally benign (Fig. 40). Hemorrhagic ovarian cysts are generally due to an expanding hemorrhage within a corpus luteum or other types of functional ovarian cysts [6].

Jain [39] described the hemorrhagic cyst ultrasound pattern with precision. The average cyst diameter was 3.0–3.5 cm (range, 2.5–8.5 cm). The cyst wall was thin (2 mm), well defined, and regular. Posterior-enhanced through-transmission is seen, signifying the basic cystic nature of the mass.

Hemorrhagic cysts tend to evolve slowly into various stages of acute hemorrhage, clot formation, and clot retraction, thus giving rise to changing sonographic appearances until they completely resolve. Normally, fresh blood is anechoic. In subacute stages when the clot forms, it becomes echogenic (Fig. 41). The echogenicity of hemorrhagic cysts diminishes when hemolysis of the cells begins. In the first 24 h after hemorrhage, the blood is echogenic. However, echogenicity then decreases after 2–4 days. Understanding this pathophysiologic process, it is easier to interpret sonographic appearances and can facilitate diagnosis of hemorrhagic cysts.

Patel et al. [53], in a study of 30 hemorrhagic cysts, found that fibrin strands (Fig. 42) and a retracting clot (Fig. 43) are vital observations that allow a degree of certainty in the diagnosis of hemorrhagic ovarian cysts. Approximately 90 % of

hemorrhagic ovarian cysts will exhibit at least one of these two features.

An acute onset of pain in the pelvis or lower abdomen, due to hemorrhagic cysts in women, closely mimics other gynecologic conditions such as ovarian torsion, ectopic pregnancy, and pelvic inflammatory disease. It can also mimic gastrointestinal disorders such as appendicitis, mesenteric adenitis, Crohn's disease, and other gastrointestinal conditions. Clinical correlation is crucial, because hemorrhagic cysts are unlikely in the presence of fever and leukocytosis. In summary, the definitive diagnosis of hemorrhagic cysts can be made in most cases with the use of transvaginal sonography, in light of an appropriate history, as well as characteristic sonographic findings.

To ensure resolution, the Ultrasound Consensus Conference Statement [44] recommends short-interval follow-up with US, for women in early postmenopause who have developed complex cysts that appear to be hemorrhagic. If the lesion does not change, then a hemorrhagic cyst is unlikely, and continued follow-up with US or MR imaging should then be considered. Since hemorrhagic cysts are not normally found in late postmenopausal women, any cyst with such an appearance should be considered neoplastic, and surgical evaluation should be considered.

Rupture

When a simple ovarian cyst ruptures, anechoic fluid is seen in the pelvis. However when a hemorrhagic cyst ruptures, echogenic fluid is seen in the pelvis. It might even result in massive hemoperitoneum. A ruptured hemorrhagic cyst with hemoperitoneum may have imaging features similar to those of hemoperitoneum resulting from other causes [37].

Echogenic blood may surround the uterus and adnexa. Moreover, sonographic findings of a ruptured hemorrhagic cyst can very closely mimic a ruptured ectopic pregnancy when a woman of childbearing age has acute pelvic pain and hemoperitoneum. This can become particularly challenging in the setting of positive pregnancy test results in a very early intrauterine pregnancy that is not visualized. The assertion that a positive β-human chorionic gonadotropin (β-hCG) finding indicates ectopic pregnancy and that a negative β-hCG finding suggests a ruptured hemorrhagic cyst becomes very limiting in such a situation [37].

Coincidental occurrence of a corpus luteal cyst rupture and an ectopic pregnancy has, in fact, been reported [35].

Complications from Aspiration

Complications during or after an ovarian aspiration have been observed, by some authors. Examples include bleeding (due to accidental puncture of an important vessel in the area), hematuria, or infections [8, 9].

However, in our experience, we have not observed such complications, either during or after the completion of the aspiration.

Acknowledgements Under the auspices of the Càtedra d' Investigació en Obstetrícia i Ginecologia de la Universitat Autònoma de Barcelona.

Histology images: Francisco Tresserra, MD, PhD. Department of Pathology

CT and MRI images: Belén Úbeda, MD, and Jean-Laurent Browne, MD of Gynecologic Imaging Service. Department of Obstetrics, Gynecology and Reproduction.

Instituto Universitario Dexeus. Barcelona (Spain)

Biography Mª Àngela Pascual graduated in Medicine and Surgery in 1981, obtaining a PhD degree in 1993 from the Universitat Autònoma de Barcelona. She is currently working in the Department of Obstetrics, Gynecology and Reproduction of Instituto Universitario Dexeus in Barcelona. She is a full member of the Spanish Society of Fertility (SEF), since 1989. She is also a member of the American Institute of Ultrasound in Medicine (AIUM) since 1990 and a Senior Member since 2000. In addition, she is a member of the Ultrasound Section Spanish Society of Gynecology and Obstetrics (SEGO) since 1991 and the International Society of Ultrasound in Obstetrics and Gynecology (ISUOG) since 1991. Her main research is in ultrasonographic diagnostics in the field of gynecology.

References

1. Alcázar JL, Errasti T, Minguez JA, et al. Sonographic features of ovarian cystadenofibromas. J Ultrasound Med. 2001;20:915–9.
2. Alcázar JL, Castillo G, Jurado M, et al. Is expectant management of sonographically benign adnexal cysts an option in selected asymptomatic premenopausal women? Hum Reprod. 2005;11:3231–4.
3. Alcazar JL, Guerriero S, Laparte C, et al. Diagnostic performance of transvaginal gray-scale ultrasound for specific diagnosis of

benign ovarian cysts in relation to menopausal status. Maturitas. 2011;68:182–8.
4. Ameye L, Valentin L, Testa AC, et al. A scoring system to differentiate malignant from benign masses in specific ultrasound-based subgroups of adnexal tumors. Ultrasound Obstet Gynecol. 2009;33:92–101.
5. Bagué S, Rodriguez M, Prat J. Sarcoma-like mural nodules in mucinous cystic tumors of the ovary revisited: a clinicopathologic analysis of 10 additional cases. Am J Surg Pathol. 2002;26:1467–76.
6. Baltarowich OH, Kurtz AB, Pasto ME, et al. The spectrum of sonographic findings in hemorrhagic ovarian cysts. AJR Am J Roentgenol. 1987;148:901–5.
7. Baratti D, Kusamura S, Nonaka D, et al. Pseudomyxoma peritonei: biological features are the dominant prognostic determinants after complete cytoreduction and hyperthermic intraperitoneal chemotherapy. Ann Surg. 2009;249:243–9.
8. Bessis R, Fonty B. Punction échoguidée des kystes de l'ovaire. Contracept Fertil Sex. 1987;15:535–42.
9. Broussin B. Les kystes ovariens -Confrontation écho-anatomique. Contracept Fertil Sex. 1991;19:223–30.
10. Caspi B, Hagay Z, Appelman Z. Variable echogenicity as a sonographic sign in the preoperative diagnosis of ovarian mucinous tumors. J Ultrasound Med. 2006;25:1583–5.
11. Chaparro J, Vera H, Cognat et al. Traitment coelioscopique des kystes de l'ovarie. Gynecologic. 1986;37:310–8.
12. Chapron C, Capella-Allouc S, Dubuisson JB. Treatment of adnexal torsion using operative laparoscopy. Hum Reprod. 1996;11:998–1003.
13. Chiang G, Levine D. Imaging of adnexal masses in pregnancy. J Ultrasound Med. 2004;23:805–19.
14. Dargent D, Desmettre O. Kystes de l'ovaire: punction échoguidée, coelioscopie ou laparotomie? Rev Fr Gynecol Obstet. 1988;83: 335–41.
15. De Crespigny LC, Robinson HP, Davoren RA, et al. The "simple" ovarian cyst; aspirate or operate? Br J Obstet Gynaecol. 1989;96: 1035–9.
16. Degani S, Shapiro I, Leibovitz Z, et al. Sonographic appearance of appendiceal mucocele. Ultrasound Obstet Gynecol. 2002;19:99–101.
17. Desai SK, Allahbadia GN, Dalal AK. Ovarian torsion: diagnosis by color Doppler ultrasonography. Obstet Gynecol. 1994;84:699–701.
18. Dikensoy E, Balat O, Ugur MG, et al. Serum CA-125 is a good predictor of benign disease in patients with postmenopausal ovarian cysts. Eur J Gynaecol Oncol. 2007;28:45–7.
19. Duke D, Colville J, Keeling A, et al. Transvaginal aspiration of ovarian cysts: long-term follow-up. Cardiovasc Intervent Radiol. 2006;29:401–5.
20. Edwards A, Clark L, Piessens S, et al. Acoustic streaming: a new technique for assessing adnexal cysts. Ultrasound Obstet Gynecol. 2003;22:74–8.
21. Einhorn N, Nilsson B, Sjóvall R. Factors influencing survival in carcinoma of the ovary. Cancer. 1985;55:2019–25.
22. Exacoustos C, Romanini ME, Rinaldo D, et al. Preoperative sonographic features of borderline ovarian tumors. Ultrasound Obstet Gynecol. 2005;25:50–9.
23. Fleischer AC, Stein SM, Cullinan JA, et al. Color Doppler sonography of adnexal torsion. J Ultrasound Med. 1995;14:523–8.
24. Forest AM, Bremond A, Leveque J, et al. Kyste de l'ovaire. J Gynecol Obstet Biol Reprod. 1990;19:829–36.
25. Ghezzi F, Cromi A, Bergamini V, et al. Should adnexal mass size influence surgical approach? A series of 186 laparoscopically managed large adnexal masses. BJOG. 2008;115:1020–7.
26. Glanc P, Salem S, Farine D. Adnexal masses in the pregnant patient: a diagnostic and management challenge. Ultrasound Q. 2008;24: 225–40.
27. Granberg S, Crona N, Enk L, et al. Ultrasound-guided puncture of cystic tumors in the lower pelvis of young women. J Clin Ultrasound. 1989;17:107–11.
28. Grapsa D, Kairi-Vassilatou E, Kleanthis C, et al. Epithelial ovarian tumors in adolescents: a retrospective pathologic study and a critical review of the literature. J Pediatr Adolesc Gynecol. 2011;6:386–8.
29. Grases PJ, editor. Ovario: transtornos benignos. Patología Ginecológica: Bases para el diagnóstico morfológico. Barcelona: Masson; 2003. p. 119–53.
30. Greer B, Rutledge F, Gallager S. Staging of restaging laparotomy in early-stage epithelial cancer of the ovary. Clin Obstet Gynecol. 1980;23:223–9.
31. Guerriero S, Mallarini G, Ajossa S, et al. Transvaginal ultrasound and computed tomography combined with clinical parameters and CA-125 determinations in the differential diagnosis of persistent ovarian cysts in premenopausal women. Ultrasound Obstet Gynecol. 1997;9:339–43.
32. Guerriero S, Alcazar JL, Coccia ME, et al. Complex pelvic mass as a target of evaluation of vessel distribution by color Doppler sonography for the diagnosis of adnexal malignancies: results of a multicenter European study. J Ultrasound Med. 2002;21:1105–11.
33. Guerriero S, Ajossa S, Mais V, et al. Role of transvaginal sonography in the diagnosis of peritoneal inclusion cysts. J Ultrasound Med. 2004;23:1193–200.
34. Guerriero S, Alcazar JL, Pascual MA, et al. Diagnosis of the most frequent benign ovarian cysts: is ultrasonography accurate and reproducible? J Womens Health. 2009;18:519–27.
35. Hallatt JG, Steele CH, Snyder M. Ruptured corpus luteum with hemoperitoneum: a study of 173 surgical cases. Am J Obstet Gynecol. 1984;149:5–9.
36. Hassen K, Ghossain MA, Rousset P, et al. Characterization of papillary projections in benign versus borderline and malignant ovarian masses on conventional and color Doppler ultrasound. AJR Am J Roentgenol. 2011;196:1444–9.
37. Hertzberg BS, Kliewer MA, Paulson EK, et al. Ovarian cyst rupture causing hemoperitoneum: imaging features and the potential for misdiagnosis. Abdom Imaging. 1999;24:304–8.
38. Houry D, Abbott JT. Ovarian torsion: a fifteen-year review. Ann Emerg Med. 2001;38:156–9.
39. Jain KA. Sonographic spectrum of hemorrhagic ovarian cysts. J Ultrasound Med. 2002;21:879–86.
40. Korbin FD, Douglas LB, William RW. Paraovarian cystoadenomas and cystoadenofibromas: sonographic characteristics in 14 cases. Radiology. 1998;208:459–62.
41. Koutlaki N, Niñas I, Dimitraki M, et al. Transvaginal aspiration of ovarian cysts: our experience over 121 cases. Minim Invasive Ther Allied Technol. 2011;20:155–9.
42. Larsen J, Pedersen O, Gregersen E. Ovarian cyst fenestration via the laparoscope. Acta Obstet Gynecol Scand. 1986;65:539–45.
43. Lee EJ, Kwon HC, Joo HJ, et al. Diagnosis of ovarian torsión with color Doppler sonography: depiction of twisted vascular pedicle. J Ultrasound Med. 1998;17:83–9.
44. Levine D, Brown DL, Andreotti RF, et al. Management of asymptomatic ovarian and other adnexal cysts imaged at US: Society of Radiologists in Ultrasound Consensus Conference Statement. Radiology. 2010;256:943–54.
45. Mariani L, Atlante M, Dionis B, et al. Pseudomyxoma peritonei: a case report. J Exp Clin Cancer Res. 2000;19:537–9.
46. Montanari L, Saviottic C, Zara C. Aspiration of ovarian cysts: laparoscopy or echography? Acta-Europ Fertil. 1987;18:45–9.
47. Mavromatidis G, Sotiriadis A, Dinas K, et al. Large luteinized follicular cyst of pregnancy. Ultrasound Obstet Gynecol. 2010;36:517–20.
48. Outwater EK, Siegelman ES, Talerman A, et al. Ovarian fibromas and cystadenofibromas: MRI features of the fibrous component. J Magn Reson Imaging. 1997;7:465–71.
49. Pascual MA. Valor de la Ecotomografía en la Propedéutica de los Quistes de Ovario. Doctoral thesis, Universidad Autonoma de Barcelona; 1993.

50. Pascual MA, Hereter L, Tresserra F, et al. Transvaginal sonographic appearance of functional ovarian cysts. Hum Reprod. 1997;12: 1246–9.
51. Pascual MA, Tresserra F, Grases PJ, et al. Borderline cystic tumors of the ovary: gray-scale and color Doppler sonographic findings. J Clin Ultrasound. 2002;30:76–82.
52. Pascual MA, Hereter L, Graupera B, et al. Prevalence of benign ovarian lesions in asymptomatic postmenopausal women. Ultrasound Obstet Gynecol. 2012;40S1:39. doi:10.1002/uog.11345.
53. Patel MD, Feldstein VA, Filly RA. The likelihood ratio of sonographic findings for the diagnosis of hemorrhagic ovarian cysts. J Ultrasound Med. 2005;24:607–14.
54. Perlman S, Hazan Y, Hagay Z, et al. "Onion skin" sign in an ovarian mucinous cyst. J Clin Ultrasound. 2012. doi:10.1002/jcu.21872.
55. Pez J, Henry-Suchet J, Mintz M, et al. Ponctions des kystes ovariens sous échoguidage. Contracept Fertil Sex. 1987;15:393–8.
56. Pickhardt PJ, Hanson ME. Incidental adnexal masses detected at low-dose unenhanced CT in asymptomatic women age 50 and older. Radiology. 2010;257:144–50.
57. Prat J, Scully RE. Ovarian mucinous tumors with sarcoma-like mural nodules. A report of seven cases. Cancer. 1979;44:1332–44.
58. Ronnett BM, Zahn CM, Kurman RJ, et al. Disseminated peritoneal adenomucinosis and peritonealmucinous carcinomatosis. A clinicopathologic analysis of 109 cases with emphasis on distinguishing pathologic features, site of origin, prognosis, and relationship to "pseudomyxoma peritonei". Am J Surg Pathol. 1995;19: 1390–408.
59. Ruttenstock EM, Saxena AK, Schwinger W, et al. Pediatric ovarian tumors - dilemmas in diagnosis and management. Eur J Pediatr Surg. 2010;20:116–20.
60. Sladkevicius P, Jokubkiene L, Valentin L. Contribution of morphological assessment of the vessel tree by three-dimensional ultrasound to a correct diagnosis of malignancy in ovarian masses. Ultrasound Obstet Gynecol. 2007;30:874–82.
61. Spinelli C, Pucci V, Buti I, et al. The role of tumor markers in the surgical approach of ovarian masses in pediatric age: a 10-year study and a literature review. Ann Surg Oncol. 2012;9:1766–73.
62. Sutton CL, McKinney CD, Jones JE, et al. Ovarian masses revisited: radiologic and pathologic correlation. Radiographics. 1992;12:853–77.
63. Tavassoli FA, Devilee P, editors. World Health Organization classification of tumours. Pathology and genetics of tumours of the breast and female genital organs. Lyon: IARC Press; 2003.
64. Terence C, Al-Mohaimeed K, Liauw W, et al. Pseudomyxoma peritonei: a need to establish evidence-based standard of care – is this the right trial? Ann Surg Oncol. 2009;16:2675–7.
65. Timmerman D, Valentin L, Bourne TH, et al. Terms, definitions and measurements to describe the sonographic features of adnexal tumors: a consensus opinion from the International Ovarian Tumor Analysis (IOTA) group. Ultrasound Obstet Gynecol. 2000;16:500–5.
66. Troiano RN, Taylor KJ. Sonographically guided therapeutic aspiration of benign-appearing ovarian cysts and endometriomas. AJR Am J Roentgenol. 1998;171:1601–5.
67. Valentin L. Pattern recognition of pelvic masses by gray-scale ultrasound imaging: the contribution of Doppler ultrasound. Ultrasound Obstet Gynecol. 1999;14:338–47.
68. Valentin L. Use of morphology to characterize and manage common adnexal masses. Best Pract Res Clin Obstet Gynaecol. 2004;18:71–89.
69. Valentin L, Ameye L, Jurkovic D, et al. Which extrauterine pelvic masses are difficult to correctly classify as benign or malignant on the basis of ultrasound findings and is there a way of making a correct diagnosis? Ultrasound Obstet Gynecol. 2006;27:438–44.
70. Valentin L, Ameye L, Savelli L, et al. Unilocular adnexal cysts with papillary projections but no other solid components: is there a diagnostic method that can reliably classify them as benign or malignant before surgery? Ultrasound Obstet Gynecol. 2012. doi:10.1002/uog.12294.
71. Valsky DV, Esh-Broder E, Cohen SM, et al. Added value of the gray-scale whirlpool sign in the diagnosis of adnexal torsion. Ultrasound Obstet Gynecol. 2010;36:630–4.
72. Van Holsbeke C, Zhang J, Van Belle V, et al. Acoustic streaming cannot discriminate reliably between endometriomas and other types of adnexal lesion: a multicenter study of 633 adnexal masses. Ultrasound Obstet Gynecol. 2010;35:349–53.
73. Van Voorhis BJ, Schwaiger J, Syrop CH, et al. Early diagnosis of ovarian torsion by color Doppler ultrasonography. Fertil Steril. 1992;58:215–7.
74. Varras M, Tsikini A, Polyzos D, et al. Uterine adnexal torsión: pathologic and gray-scale ultrasonographic findings. Clin Exp Obstet Gynecol. 2004;XXXI:34–8.
75. Vijayaraghavan SB. Sonographic whirlpool sign in ovarian torsion. J Ultrasound Med. 2004;23:1643–9.
76. Wakahara F, Kikkawa F, Nawa A, et al. Diagnostic efficacy of tumor markers, sonography, and intraoperative frozen section for ovarian tumors. Gynecol Obstet Invest. 2001;52:147–52.

Benign Surface Stromal Tumors of the Ovary: Computed Tomography and Magnetic Resonance

Takashi Koyama

Abstract

Serous cystadenomas are thin-walled cysts, and cystadenofibroma has a solid component of low intensity on T2-weighted MR images. Mucinous cystadenomas are multilocular cystic tumors of "stained glass" appearance. Brenner tumor is typically a solid mass of low intensity on T2-weighted MR images containing calcification on CT, but commonly associated with cyst formation of variable degree.

Keywords

Epithelial stromal tumor • Serous stromal tumor • Mucinous stromal tumor • Imaging • Computed tomography • Magnetic resonance

Generally, surface epithelial stromal tumors of the ovary are subdivided into five large categories based on epithelial differentiation: serous, mucinous, endometrioid, clear cell, and transitional. The overwhelming majority of benign tumors are cystadenoma of either serous or mucinous type. Benign tumor of transitional cell type is known as Brenner tumor. Although benign tumors of clear cell and endometrioid types are known to form adenofibromas, they are extremely rare tumors with only few reports in the literature [1–4].

Benign Serous Tumors

Benign serous tumors include cystadenomas, adenofibromas, and cystadenofibromas. These tumors are common and account for two-thirds of benign ovarian epithelial tumors [5]. Although serous cystadenomas can occur in any age, they show peak incidence in the fourth to sixth decade. They are bilateral in 12–23 % of cases [5]. Histologically, the epithelium lining the cyst is usually a single layer of flattened columnar cells, often combined with secretory cells and ciliated cells, as in the normal fallopian tube. The epithelial cell has a tendency to show fine papillary structures and may form small papillary projections arising from the inner surface. When the stroma of benign serous tumors becomes highly cellular and fibrous, and forms a solid component, the tumor is designated as adenofibroma or, if cystic, cystadenofibroma.

Serous cystadenomas commonly appear as unilocular thin-walled cysts filled with simple fluid (Fig. 1). Although multilocular form may occur, the number of the locules is usually limited (Fig. 2). On MR imaging, the content of the cyst typically exhibits signal pattern of water, low intensity on T1-weighted images, and bright intensity on T2-weighted images (Fig. 1). Occasionally, small papillary excrescences may be associated with the cyst, and they typically show low intensity reflecting fibrous core. When these papillary excrescences become prominent, serous tumor of borderline malignancy may be suspected.

Cystadenofibromas typically manifest as a complex cystic mass associated with solid components. On MR imaging, the solid component typically shows distinct low intensity on T2-weighted images, reflecting the fibrous stroma with

T. Koyama, MD, PhD
Department of Diagnostic Radiology,
Osaka Red Cross Hospital,
5-30 Fudegasaki-cho, Tennoji-ward,
Osaka 543-8555, Japan
e-mail: montpeti@kuhp.kyoto-u.ac.jp

L. Saba et al. (eds.), *Ovarian Neoplasm Imaging*,
DOI 10.1007/978-1-4614-8633-6_7,

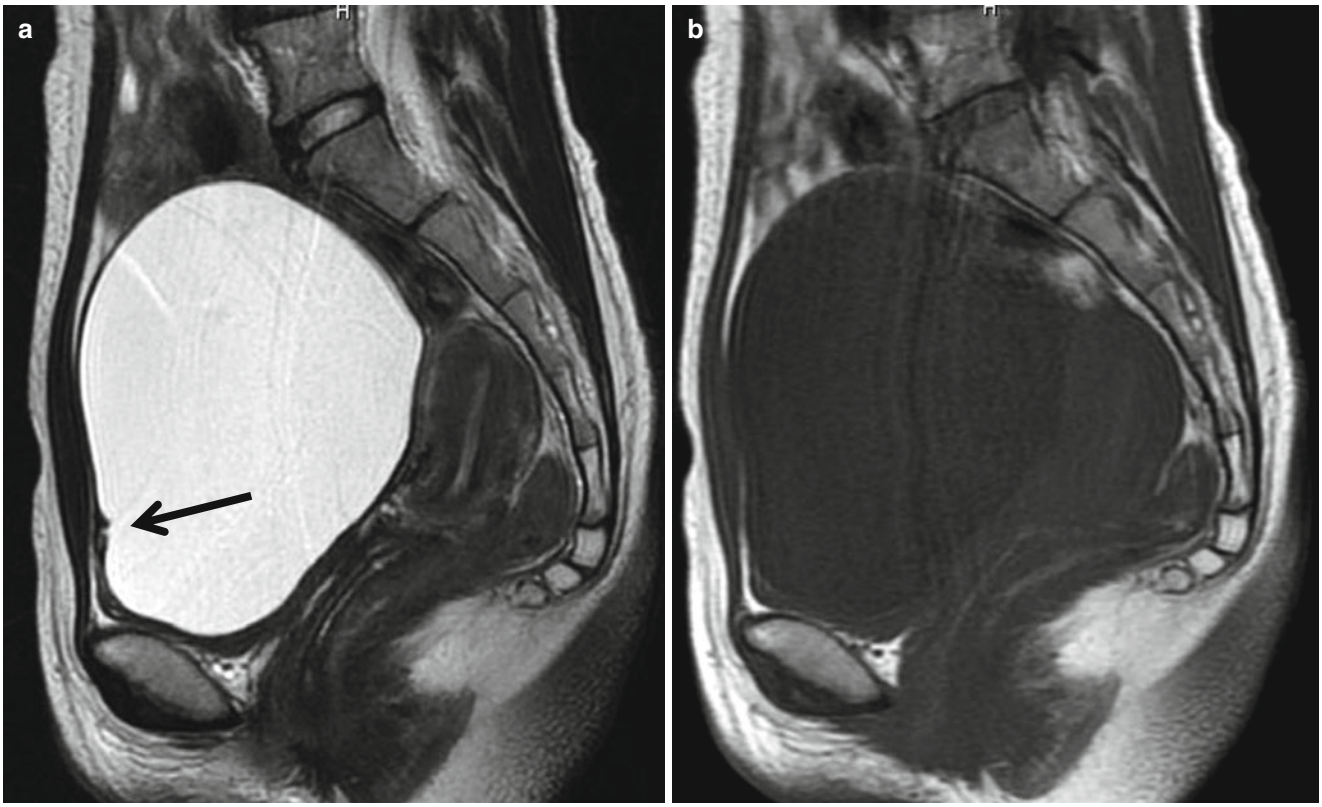

Fig. 1 Serous cystadenoma in a 26-year-old woman. (**a**) Sagittal T2-weigthed MR image shows a large unilocular cyst. There is a tiny papillary excrescence in the anterior wall of the cyst (*arrow*). (**b**) Sagittal T1-weighted MR image shows watery low intensity of the cyst content

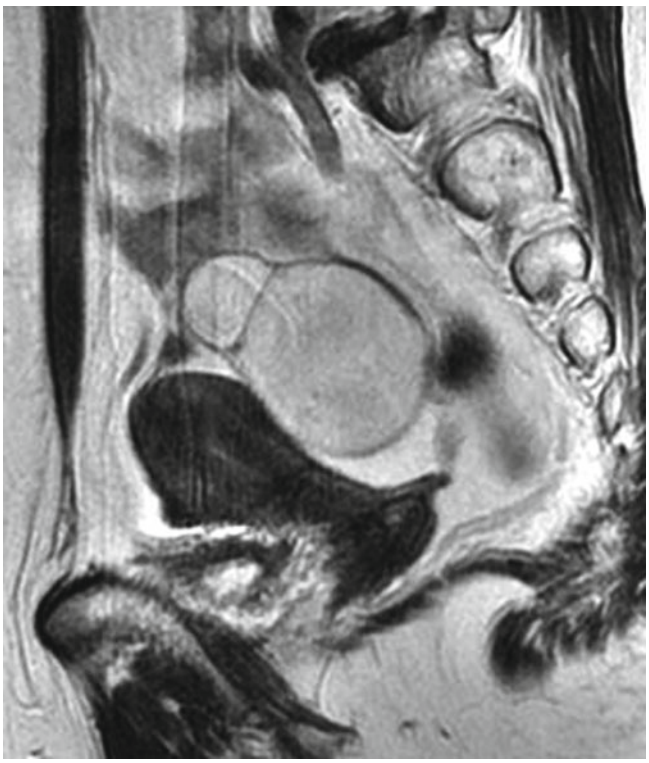

Fig. 2 Serous cystadenoma in a 59-year-old woman. Sagittal T2-weighted image shows bilocular cystic mass posterior to the uterus

dense collagen (Fig. 3) [6, 7]. The solid components may contain small or tiny cystic locules [8]. Although serous cystadenomas simulate malignant tumor because of solid components in the cystic mass, their distinct low intensity is an important MR finding for suggesting benignancy. The differential diagnosis of solid mass of low intensity associated with cyst formation includes Brenner tumor and fibrothecomas; both are virtually benign tumors.

Benign Mucinous Tumors

Mucinous cystadenomas comprise 13 % of benign ovarian epithelial neoplasms, and mean patient age is about 50 years [5]. In contrast to serous cystadenomas, they are bilateral in only 2–3 % of cases. Mucinous cystadenomas are typically multilocular cystic tumors in gross appearance and tend to larger than serous cystadenomas. The cysts usually contain thick, mucinous material, but occasionally contain watery liquid. The locules in mucinous cystadenomas are usually small and multiple. The epithelium in mucinous cystadenoma is characterized by a single layer of tall columnar cells with clear cytoplasm. Histologically, mucinous tumors are further subclassified into intestinal type and endocervical (müllerian) type, and the former comprises over 80 % of

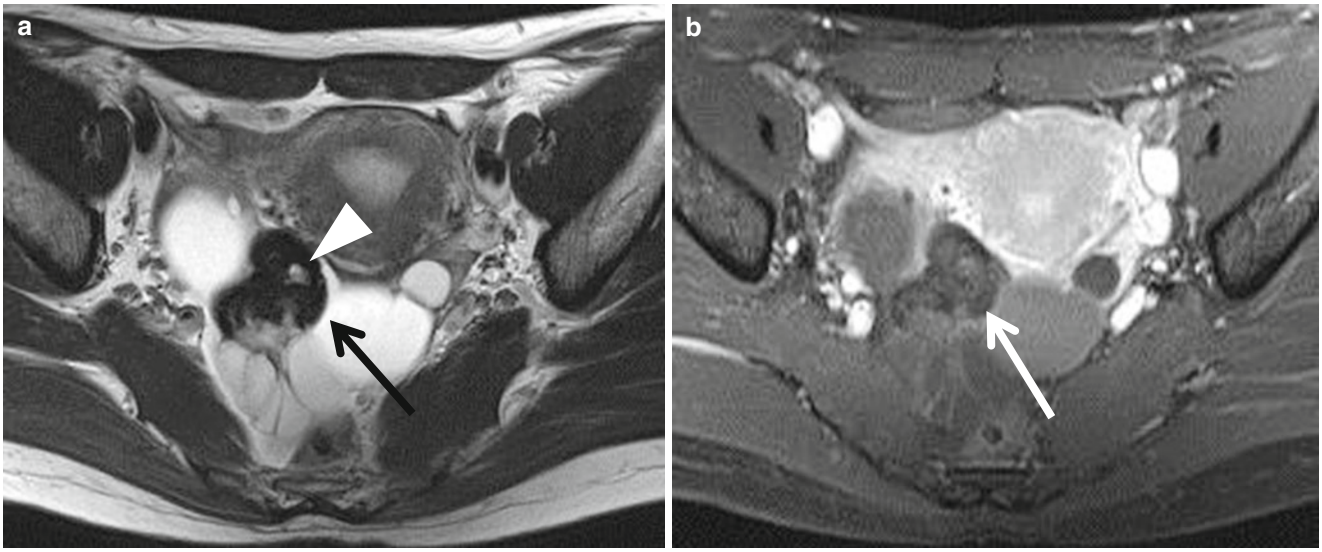

Fig. 3 Serous cystadenofibroma in a 48-year-old woman. (**a**) Axial T2-weighted MR image shows a complex cystic mass in the right adnexa. The mass contains an irregular-shaped solid component (*black arrow*) of distinct low intensity in its central portion, which also contains tiny cystic locule (*arrowhead*). (**b**) Post-contrast T1-weighted image shows poor enhancement in the solid component (*white arrow*)

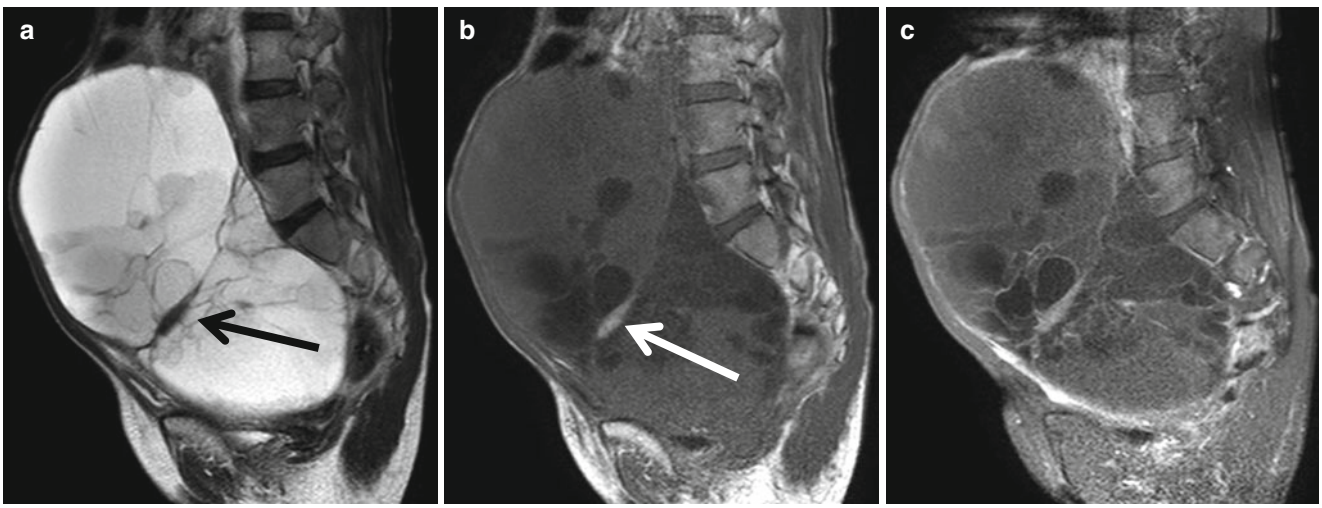

Fig. 4 Mucinous cystadenoma in a 60-year-old woman. (**a**) Sagittal T2-weighted image shows a large multilocular cystic mass. There is a focal area of distinct low intensity (*black arrow*), simulating the thickened septum. (**b**) T1-weighted image shows variable signal intensity in multiple locules. The area of low intensity on T2-weighted image exhibits high intensity (*white arrow*), suggesting densely viscose fluid. (**c**) Post-contrast T1-weighted image with fat suppression shows enhancement in the septi

mucinous cystadenomas. Up to 10 % of mucinous cystadenomas contain focal component of Brenner tumor.

On imaging studies, mucinous cystic tumor typically shows a characteristic multilocular appearance with varying signals in the locules ("stained glass appearance") on both T1- and T2-weighted images (Fig. 4) [7]. The locules containing watery fluid usually exhibit low signal on T1-weighted image and high signal on T2-weighted image, whereas those with thick mucinous fluid tend to show increased signal on T1-weighted images. The septi in the cysts exhibit low intensity on T2-weighted images and become enhanced when post-contrast T1-weighted is obtained. The differentiation of benign mucinous cystadenomas and borderline tumors is quite difficult and should depend on postoperative histologic findings. In general, the presence of a thick wall or septa may suggest borderline lesions, while the presence of solid components suggests carcinoma [9]. When the fluid in the locule is very viscose,

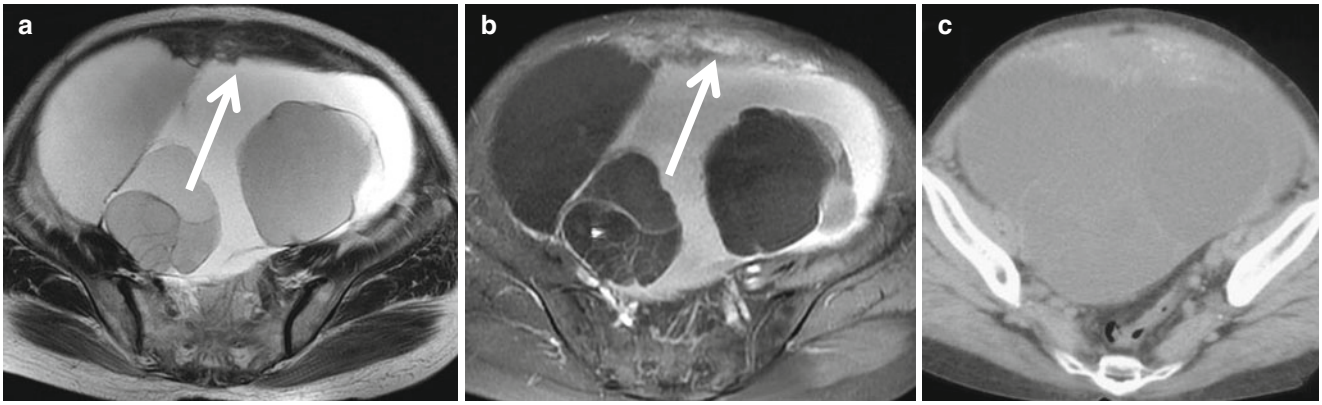

Fig. 5 Mucinous cystadenoma with focal component of Brenner tumor in a 67-year-old woman. (**a**) Axial T2-weighted image shows a predominantly cystic mass of multilocular cystic appearance. The mass is accompanied by a solid component of low intensity ventrally (*arrow*), which is a focal area of Brenner tumor. (**b**) Post-contrast T1-weighted image reveals stained glass appearance consisting of variable signal intensity in the multilocular cystic tumor, and heterogeneous enhancement in the solid component of Brenner tumor (*arrow*). (**c**) Unenhanced CT demonstrates fine calcifications in the solid component

the signal of the locule may be distinctively low on T2-weighted images, simulating thickened septi or solid mass. In such cases, lack of enhancement on post-contrast images in the area of increased intensity on unenhanced T1-weighted images will be of help for differentiating mucinous locule from solid mass. When mucinous cystadenoma is accompanied by focal component Brenner tumor, it shows distinct low intensity on T2-weighted images and enhanced on post-contrast study (Fig. 5). The presence of calcification on plain CT is also suggestive of Brenner tumor. When multilocular cystic tumors are observed in bilateral ovaries, metastatic ovarian tumors, especially from the colon and appendix, should be considered [10]. Metastatic tumors from mucin-producing carcinoma can show similar morphologic appearance to those of primary mucinous cystic tumor both grossly and microscopically. They commonly involve bilateral ovaries, whereas primary ovarian mucinous tumors are rarely bilateral.

Brenner (Benign Transitional) Tumors

Brenner tumors are uncommon surface epithelial tumors that account for about 2 % of ovarian neoplasms and commonly occur in postmenopausal women [11]. Histologically, Brenner tumor is characterized by varying numbers of rounded nests of transitional cells. Their cellular features are similar to Walthard nests, which are epithelial inclusions occasionally found in the hilar regions of the normal ovaries. In Brenner tumors, these nests of transitional nests are embedded in fibromatous stroma, which is composed of spindle cells with abundant collagen matrix and occasional hyalinization. The epithelial nests often become cystic. When cystic changes may become prominent, the epithelium lining the cyst may show metaplastic change from transitional cell to mucinous columnar epithelium. In approximately 30 % of cases, Brenner tumors are associated with components of mucinous cystadenomas [11]. These tumors show intimate admixture of both Brenner component and mucinous component and are designated as metaplastic Brenner tumor.

The gross appearance of Brenner tumor is typically a well-circumscribed solid tumor of small size. However, the tumor may be associated with variable proportion of cystic changes. Less commonly, the cystic components in Brenner tumor may become extensive and large, and they may show multilocular appearance. On MR imaging, the solid components in Brenner tumor typically exhibit distinct low intensity on T2-weighted images, reflecting fibrous stroma with collagen (Fig. 6) [12]. The areas of cystic changes within the tumor are depicted as areas of increased intensity on T2-weighted image (Fig. 7). When the cystic changes become extensive, the cystic components within the tumor may exhibit multilocular "stained glass" appearance containing locules of variable signal intensity on both T1- and T2-weighted images, as seen in mucinous cystadenomas described above (Fig. 8). On post-contrast T1-weighted images, the solid components usually show homogeneous enhancement [13]. The solid component typically contains extensive amorphous calcification on CT, which is one of the characteristic findings of Brenner tumors [13]. Although calcification may be also recognized in serous adenocarcinomas, the combination of calcifications demonstrated by CT and low intensity on T2-weighted images is suggestive of Brenner tumors.

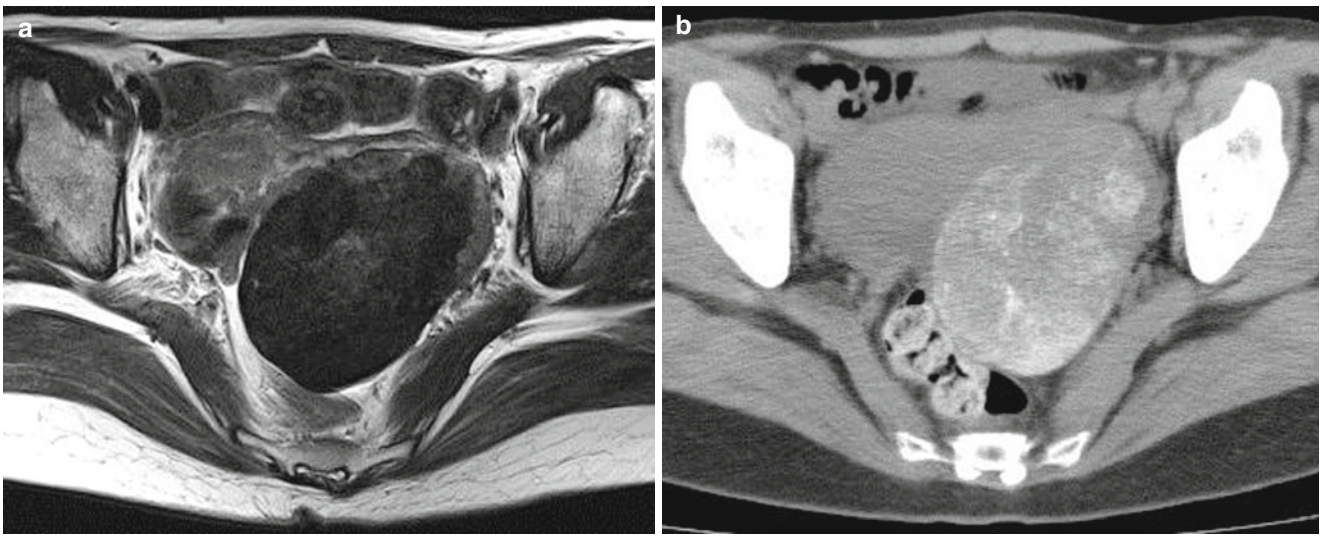

Fig. 6 Brenner tumor in a 61-year-old woman. (**a**) Axial T2-weighted MR image shows solid mass of distinct low intensity in the left adnexa. (**b**) Unenhanced CT shows extensive calcifications throughout the tumor

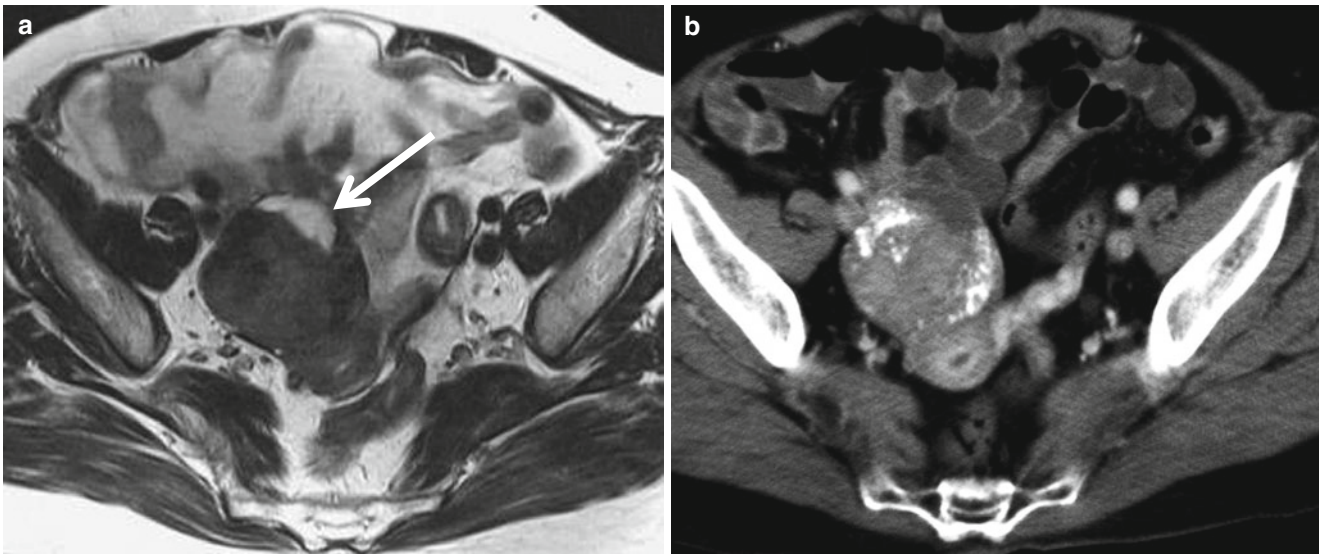

Fig. 7 Brenner tumor with cystic change in a 70-year-old woman. (**a**) Axial T2-weighted MR image shows a predominantly solid mass of distinct low intensity in the right adnexa. The lesion contains cystic components of high intensity ventrally (*arrow*). (**b**) Axial post-contrast computed tomography demonstrates numerous foci of amorphous calcification within the solid component of the tumor

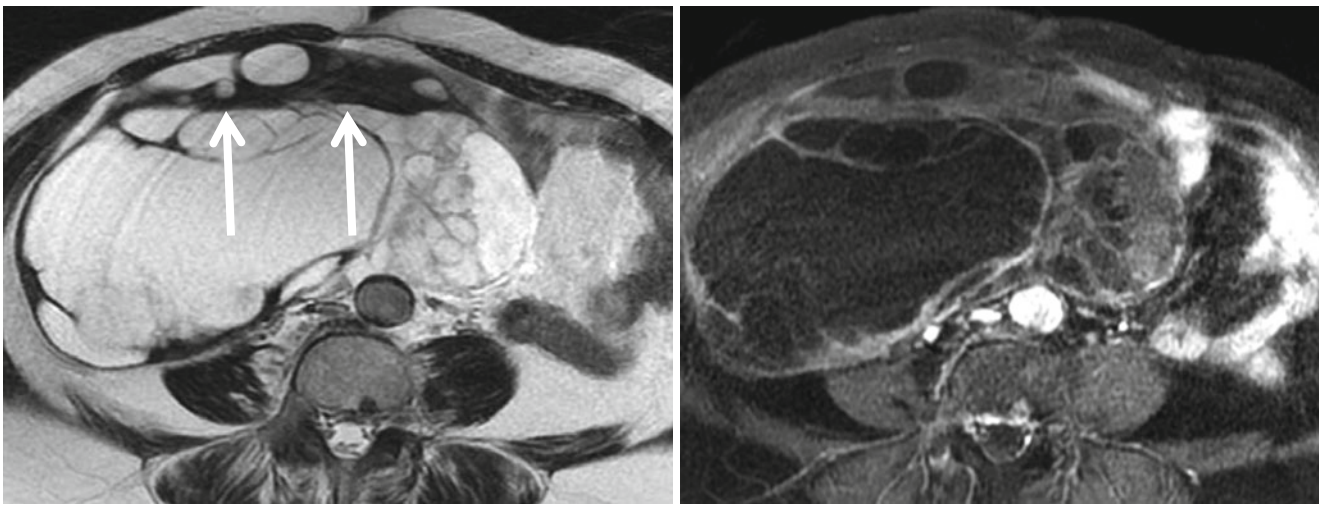

Fig. 8 Brenner tumor with mucinous cystic tumor in a 70-year-old woman. (**a**) Axial T2-weighted image shows a multilocular cystic mass, admixed with irregular-shaped solid component of distinct low intensity (*arrows*), which represents Brenner component. (**b**) Post-contrast T1-weighted image shows homogeneous enhancement in the solid component and septi in multicystic component, which represents mucinous cystic tumor of borderline malignancy

References

1. Zhao C, Wu LS, Barner R. Pathogenesis of ovarian clear cell adenofibroma, atypical proliferative (borderline) tumor, and carcinoma: clinicopathologic features of tumors with endometriosis or adenofibromatous components support two related pathways of tumor development. J Cancer Educ. 2011;2:94–106.
2. Chen R, Zhou H, Zhang Y. Ovarian benign clear cell adenofibroma in a patient with premature ovarian failure after 8-year hormone replacement therapy. Gynecol Endocrinol. 2013;29(3):216–8.
3. Pasaoglu O, et al. Benign clear cell adenofibroma of the ovary. A case report with literature review. Gynecol Obstet Invest. 2007;64(1):36–9.
4. Jain D, Siraj F, Aggarwal N. Endometrioid adenofibroma arising in an endometriotic cyst. J Obstet Gynaecol. 2011;31(4):352–4.
5. Seidman J, et al. Surface epithelial tumors of the ovary. In: Kurman R, Ellenson LH, Ronnett B, editors. Blaustein's pathology of the female genital tract. New York: Springer; 2011. p. 679–784.
6. Cho SM, et al. CT and MRI findings of cystadenofibromas of the ovary. Eur Radiol. 2004;14(5):798–804.
7. Pretorius ES, et al. Magnetic resonance imaging of the ovary. Top Magn Reson Imaging. 2001;12(2):131–46.
8. Takeuchi M, et al. Ovarian cystadenofibromas: characteristic magnetic resonance findings with pathologic correlation. J Comput Assist Tomogr. 2003;27(6):871–3.
9. Tamai K, et al. MR features of physiologic and benign conditions of the ovary. Eur Radiol. 2006;16(12):2700–11.
10. Koyama T, et al. Secondary ovarian tumors: spectrum of CT and MR features with pathologic correlation. Abdom Imaging. 2007;32(6):784–95.
11. Balasa RW, et al. The Brenner tumor: a clinicopathologic review. Obstet Gynecol. 1977;50(1):120–8.
12. Outwater EK, et al. Ovarian Brenner tumors: MR imaging characteristics. Magn Reson Imaging. 1998;16(10):1147–53.
13. Moon WJ, et al. Brenner tumor of the ovary: CT and MR findings. J Comput Assist Tomogr. 2000;24(1):72–6.

Ovarian Benign Sex Cord-Stromal Tumors: Clinical and Ultrasound Features

Juan José Hidalgo-Mora and Juan Luis Alcázar

Abstract

Ovarian sex cord-stromal tumors are a heterogeneous group of benign or malignant gynecological neoplasms that account for 5–10 % of all ovarian tumors, comprising 2 % of all primary malignant ovarian cancers. Their frequency is similar throughout the world and may appear in any age group, but they are more common in the fourth and fifth decades of life. The sex cord-stromal group includes tumors of mesenchymal (have been called mesenchymomas) and mesonephric origin. Some of these tumors, namely, fibromas and thecomas, have a fibrous appearance, and some appear to be derived from the granulosa cells or their testicular sex cord counterparts, the Leydig and Sertoli cells.

These tumors have been described at ultrasonography with several imaging findings and can be found as well-defined solid or multilocular cystic adnexal masses with centrally located, multiple, round or cleft-like cysts. In this chapter the ultrasonographic characteristics of the ovarian sex cord-stromal tumors will be described.

Keywords

Ovarian sex cord-stromal tumor • Granulosa-fibroma group • Sertoli-stromal cell tumor • Steroid cell tumor • Sclerosing stromal tumor • Imaging • Ultrasound

Introduction

Ovarian sex cord-stromal tumors are a heterogeneous group of benign or malignant gynecological neoplasms that account for 5–10 % of all ovarian tumors, comprising 2 % of all primary ovarian cancers [1, 2]. Their frequency is similar throughout the world and may appear in any age group, but they are more common in the fourth and fifth decades of life [3, 4].

J.J. Hidalgo-Mora
Department of Obstetrics and Gynecology,
Hospital Comarcal de Vinaroz, Castellón, Spain

J.L. Alcázar, MD, PhD (✉)
Department of Obstetrics and Gynecology,
Clinica Universidad de Navarra, University of Navarra,
Avenida Pio XII, 36, 31008 Pamplona, Spain
e-mail: jlalcazar@unav.es

The sex cord-stromal group includes tumors of mesenchymal (have been called mesenchymomas) and mesonephric origin. Some of these tumors, namely, fibromas and thecomas, have a fibrous appearance, and some appear to be derived from the granulosa cells or their testicular sex cord counterparts, the Leydig and Sertoli cells [5, 6]. They are usually composed of various combinations of elements, including the female-type cells (granulosa cells, theca cells, and their luteinized derivatives), male-type cells (Sertoli and Leydig cells), and fibroblasts of gonadal stromal origin as well as morphologically indifferent cells. Any of these cells may be present in varying degrees of differentiation [6, 7].

These tumors develop from the gonadal stroma, specifically from the dividing cell population that would normally give rise to cells surrounding the oocytes, including the cells that produce ovarian hormones [1]. Because of this production of sex steroid hormones, including estrogens and androgens, some of these tumors often are associated with

L. Saba et al. (eds.), *Ovarian Neoplasm Imaging*,
DOI 10.1007/978-1-4614-8633-6_8,

endocrine manifestations. This hormonal activity and the resultant symptoms, along with specific sonographic features of these tumors, allow that the majority of patients are diagnosed in early stages of the disease [8].

Ovarian sex cord-stromal tumors are divided into several histologic subtypes. The World Health Organization, within its classification of ovarian tumors, has classified them into different subtypes [5]:

1. Granulosa-stromal cell tumors: granulosa cell tumors, thecoma-fibroma group
2. Sertoli-stromal cell tumors, androblastomas: well-differentiated, Sertoli-Leydig cell tumor of intermediate differentiation, Sertoli-Leydig cell tumor poorly differentiated (sarcomatoid), retiform
3. Sex cord tumor with annular tubules
4. Gynandroblastoma
5. Unclassified
6. Steroid (lipid) cell tumors: stromal luteoma, Leydig cell tumor, unclassified

Thecomas and granulosa cell tumors are noted as estrogen-producing tumors. On the other hand, Sertoli-stromal cell tumors and steroid cell tumors are noted for their testosterone production. However, thecomas and granulosa cell tumors occasionally produce androgen and cause virilization, and the opposite can also occur [9].

The most common histotype is represented by granulosa cell tumors, which account for 70 % of all sex cord-stromal tumors. They are typically malignant (2–5 % of all cases of ovarian cancer), although in most cases of low-grade malignancy, with a favorable prognosis [8, 10].

Fibromas and thecomas together constitute about half of all stromal tumors and about 4–6 % of all ovarian neoplasms. They are usually benign, being malignant in less than 5 % of cases [3].

Sertoli-Leydig cell tumors account for less than 0.5 % of all ovarian tumors, being malignant less than 5 % of them [8]. Sex cord tumors with annular tubules, with features intermediate between those of Sertoli cell and granulosa cell tumors, are benign neoplasms with malignant behavior only in sporadic cases [11]. Gynandroblastomas are an extremely rare sexual cord-stromal tumor malignant in 100 % of cases [12].

Finally, steroid cell tumors account for approximately 0.1–0.2 % of all ovarian tumors. In adults 25 % of them are malignant, whereas there have been no reported malignant steroid cell tumors in young girls. Of these, stromal luteomas constitute 20 % and Leydig cell tumors 15–20 %, being generally benign. Steroid cell tumors not otherwise specified represent the remaining 60 % of the group [2, 13].

In this chapter we shall describe the histological, clinical, and sonographic features of benign ovarian sex cord-stromal tumors.

Granulosa-Fibroma Group

Fibromas, fibrothecomas, and thecomas are variants of a single entity of benign tumors. They account for 4–6 % of ovarian tumors and occur in both pre- and postmenopausal women [3, 14].

Pure fibromas consist of intersecting bundles of spindle cells that produce collagen, without theca cells or estrogenic effect, and have no epithelial component [5, 15]. When the predominant cells are round to oval, resembling theca cells, it is classified as ovarian thecoma and may be hormonally active and thus responsible for estrogenic manifestations. The term fibrothecoma is used, when a precise pathological distinction between these two forms is not possible [14, 16].

Tumors of this group are mostly benign, representing malignant thecomas and fibrosarcomas less than 1 % of the cases reported [17].

Fibromas

Ovarian fibromas are the most common solid tumor in the ovary and account for almost two-thirds of neoplasms of this group and approximately 4 % of all ovarian neoplasms [15, 18]. These tumors are more common during middle age and rare before age 30 years (90 % of patients are at least 30 years old). The mean age of the patients at the time of diagnosis is 48 years [5, 18].

Fibromas are usually unilateral (less than 5 % of cases are bilateral). They are often large, sometimes more than 10–15 cm in maximum diameter, with only one-third of them being smaller than 3 cm. Large tumors have a smooth or slightly irregular serosal surface and are solid. Small fibromas may be located within the ovary or may appear as polypoid nodules on the external surface of the ovary or as non-capsulated nodules in the ovary. The cut surface of a fibroma is white and slightly spiraled and may manifest areas of cystic degeneration. If these areas are large, they appear as cysts filled with protein-rich serous fluid and with ragged walls [6, 18].

Histologically, fibromas consist of cellular bundles and intersecting strips of hyaline-appearing collagen and fibrous tissue. The fibroblastic tumor cells have spindle-shaped nuclei with no signs of atypias. Dystrophic calcifications, focal necrosis, and hemorrhage are common. The normal adjacent ovarian tissue and the contralateral ovary may show signs of stromal hyperplasia. If fibromas exhibit aggregates of lipid-laden lutein-like cells, they are defined as luteinized thecomas or fibromas [17, 18]. When the tumors are composed of cells with closely packed nuclei with absent or minimal nuclear atypia and 1–3 mitoses/10 high-power fields, they are classified as cellular fibroma. When fibroblastic

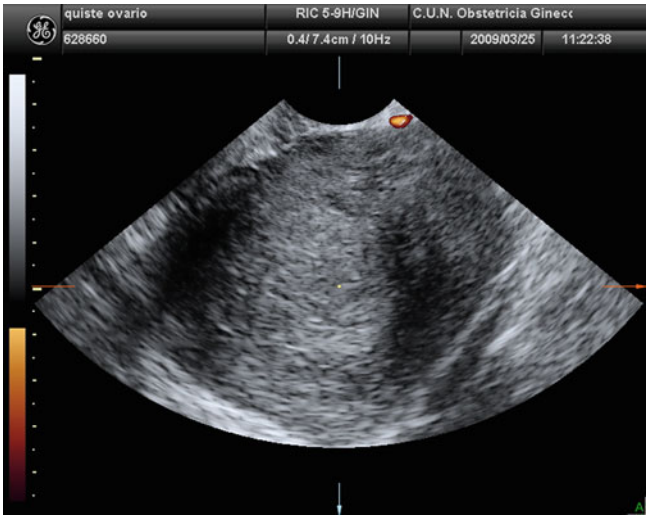

Fig. 1 Transvaginal ultrasound from an ovarian fibroma. A rounded, well-defined, purely solid adnexal mass is seen

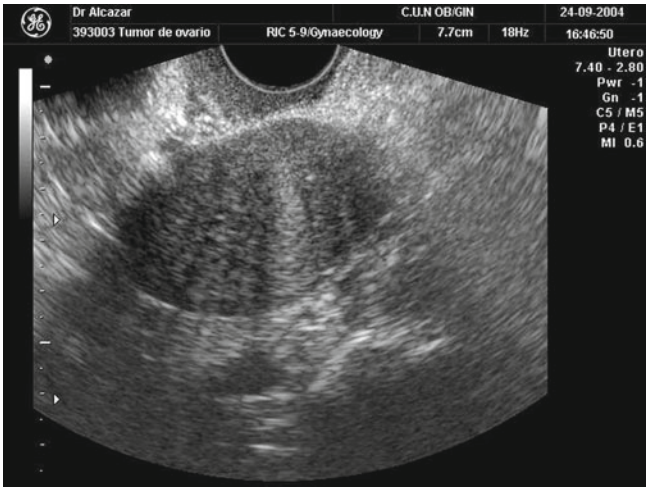

Fig. 2 Transvaginal ultrasound from an ovarian fibroma. As in the previous figure, a rounded, well-defined, purely solid adnexal mass is seen. However, in this case acoustic shadowing is more evident

tumors show moderate nuclear atypia and more than 3 mitoses/10 high-power fields, they often have a malignant course and are designated fibrosarcomas [16].

There are no specific clinical signs related to these tumors. They rarely are associated with hormone production, and women with these tumors are generally asymptomatic. Therefore, these masses are often an unexpected finding typically detected at palpation or ultrasound during routine gynecologic examination [15]. Nevertheless, these tumors may be associated with various clinical syndromes. The first is Meigs syndrome (ovarian fibroma, hydrothorax, and ascites), observed with 1–10 % of ovarian fibromas. The second association is Gorlin-Goltz syndrome or basal cell nevus syndrome (bilateral ovarian fibromas, multiple basal cell carcinomas of the skin, odontogenic keratocysts, and calcified dural folds), an autosomal dominant disorder that occurs generally in patients aged younger than 30 years. Finally, ovarian fibromas may also be associated with familiar polyposis such as Gardner and Richard syndrome and Peutz-Jeghers syndrome, also autosomal dominant disorders [17].

At ultrasound, a broad spectrum of ultrasound features may be seen, and in many cases the appearance of the tumor is nonspecific. In any case, fibromas most commonly manifest as round, oval, or lobulated solid, homogeneous hypoechoic masses with regular or irregular internal echogenicity and posterior acoustic shadowing, which at times may be striking [14, 15] (Figs. 1 and 2). The presence of stripy shadows is typical of benign fibromas, and it is possible that these stripy shadows can be explained by the cellular bundles and intersecting strips of hyaline-appearing collagen and fibrous tissue which are responsible for the "spiral pattern" seen on the cut surface of typical fibromas on macroscopic examination [18]. However, the ultrasound appearance is variable, and hyperechoic masses with increased through transmission may be seen [14, 15]. These tumors typically do not contain cystic areas, although in some cases have such structures in the periphery or inside the tumor [16, 18]. Variability in ultrasound morphology of fibromas might be explained by the varying degrees of cellularity, collagen content, and stromal edema that characterize these lesions. Hemorrhage, edema, and necrosis may explain the varying echogenicity of the fluid in the cystic spaces. Color Doppler findings are variable, but most fibromas manifest minimal to moderate vascularization [18] (Fig. 3). Hemorrhage is common, but calcification in ovarian fibromas is rare [16]. Ascites can be observed in 40 % of cases in where the tumor is larger than 10 cm [6].

It is important to make an accurate image diagnosis of ovarian fibromas because they often appear as nonspecific solid masses, thereby mimicking uterine fibroids or malignant neoplasms. There are some features to help differentiate ovarian fibromas from the more common uterine fibroid or ovarian malignancies. Firstly, when the ultrasound scan shows a solid pelvic mass next to but without a clear connection with the uterus, the diagnosis of a subserosal fibroid should be made with caution, and the possibility of an ovarian fibroma should be considered, unless a normal ovary can be clearly seen on the same side. Secondly, the vascular pattern on color flow Doppler assessment has been suggested to be useful in differentiating a uterine fibroid from an ovarian fibroma. A well-vascularized solid pelvic mass with high-speed flow is suggestive of a subserosal fibroid, while a less vascularized tumor with low-speed flow points towards the diagnosis of an ovarian fibroma. Thirdly, a primary ovarian

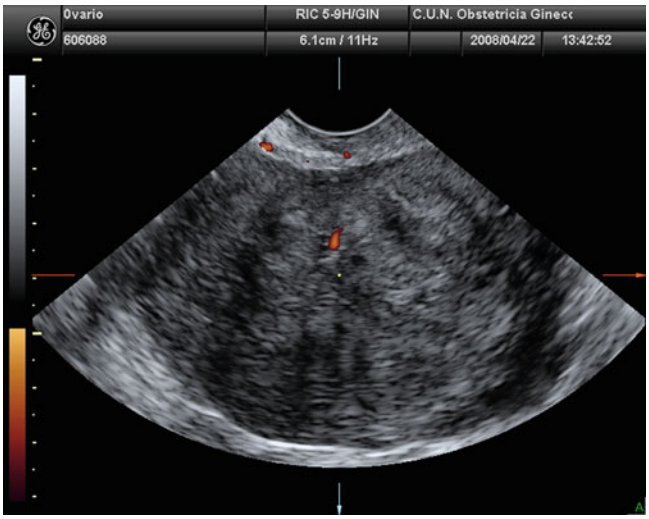

Fig. 3 Transvaginal ultrasound from an ovarian fibroma. With power Doppler examination scanty flow is detected

carcinoma is less likely to be a completely solid mass, while a secondary ovarian malignancy is typically a bilateral instead of a unilateral disease. Finally, supplementary computerized tomography and magnetic resonance imaging may help to improve the diagnostic accuracy. Most ovarian fibromas appear as a solid mass with delayed accumulation of contrast medium on computerized tomography scan and show marked T1 and T2 hypointensities on magnetic resonance imaging [15, 16].

Fibrothecomas

Fibrothecoma is the term commonly used to refer to a tumor with features that are intermediate between a fibroma and a thecoma.

Ovarian fibrothecomas are composed of an admixture of fibrous and thecomatous elements. Macroscopically these tumors are virtually indistinguishable from ovarian fibromas and often have a white whorled appearance closely resembling uterine leiomyomas. The tumor may be spherical or lobulated and is covered by intact ovarian mucosa. Edema and cystic degeneration are relatively common, especially in large fibrothecomas, whereas calcification and hemorrhage are rarely observed [18, 19].

Histologically, in comparison with fibromas, fibrothecomas show significant cellularity, a relatively large amount of collagen, and, in up to 50 % of cases, pronounced edema [18]. These tumors include spindle, oval, or round cells forming various amounts of collagen (cells that form fibromas) in addition to a smaller population of lipid-laden typical theca cells that can be present in small clusters [19, 20]. The presence of luteinized thecal cells would change the diagnosis to luteinized thecoma [18].

The clinical presentation of ovarian fibrothecomas is relatively nonspecific, and patients most commonly present with a pelvic mass, pelvic pain, and metrorrhagia [20]. The clinical examination generally finds a solid, mobile tumor with a regular surface and variable size. Rarely, fibrothecomas present with endocrine manifestations related to hormonally active tumors. In these cases, estrogenic or even some rare androgenic manifestations are reported [17]. Hormonal activity of these tumors depends upon the extent to which they resemble fibromas (lipid-poor, hormonally inert) or thecomas (lipid-containing, hormonally active) [21].

The sonographic appearance of ovarian fibrothecomas is usually nonspecific, showing a broad spectrum of sonographic features, which include especially echogenic and mixed echogenicity masses (Fig. 4). Hypoechoic masses have been also reported [17]. In large tumors areas of edema and cystic degeneration may be observed. Differential diagnosis of fibrothecomas includes pedunculated and intraligamentous leiomyomas and other solid ovarian masses such as Brenner tumors, granulosa cell tumors, and dysgerminomas. If extensive cystic degeneration is observed, the fibrothecoma can be easily mistaken for a malignant ovarian tumor [19, 20].

Thecomas

Ovarian thecoma is a rare solid fibromatous benign tumor of stromal cell origin, accounting for approximately 0.5–1 % of ovarian tumors [22]. Most thecomas are unilateral (bilateral in 3 % of cases), reach a size within 5–10 cm, and occur in pre- and postmenopausal women of 50–60 years of age (average age 59 years). Less than 10 % of the cases are encountered before the age of 30 years [6, 23].

Macroscopically, the appearance is typically that of firm or rubbery solid tissue, with a color ranging from white to yellowish due to the presence of accumulated lipids. Edema either focal or diffuse may be observed, with the presence of cyst formations being rare [6]. Histologically, they are solid tumors formed by stromal cells that resemble the theca cells that normally surround the ovarian follicles. Microscopic analysis reveals masses of round or ovoid cells, the nuclei of which have become rounded and the cytoplasm pale and vacuolated due to its large content of lipids. Hyaline bands frequently are observed interspersed with cells [6, 24].

These tumors usually exhibit estrogenic activity, and therefore, patients may show subsequent clinical manifestations, including postmenopausal uterine bleeding, endometrial hyperplasia, and endometrial cancer. It is estimated that 60 % of patients with this tumor present uterine bleeding, and more than 20 % have endometrial carcinoma. Because of their late age of onset, it is very unusual for sexual precocity to occur. Rarely, a thecoma causes virilization (11 % of

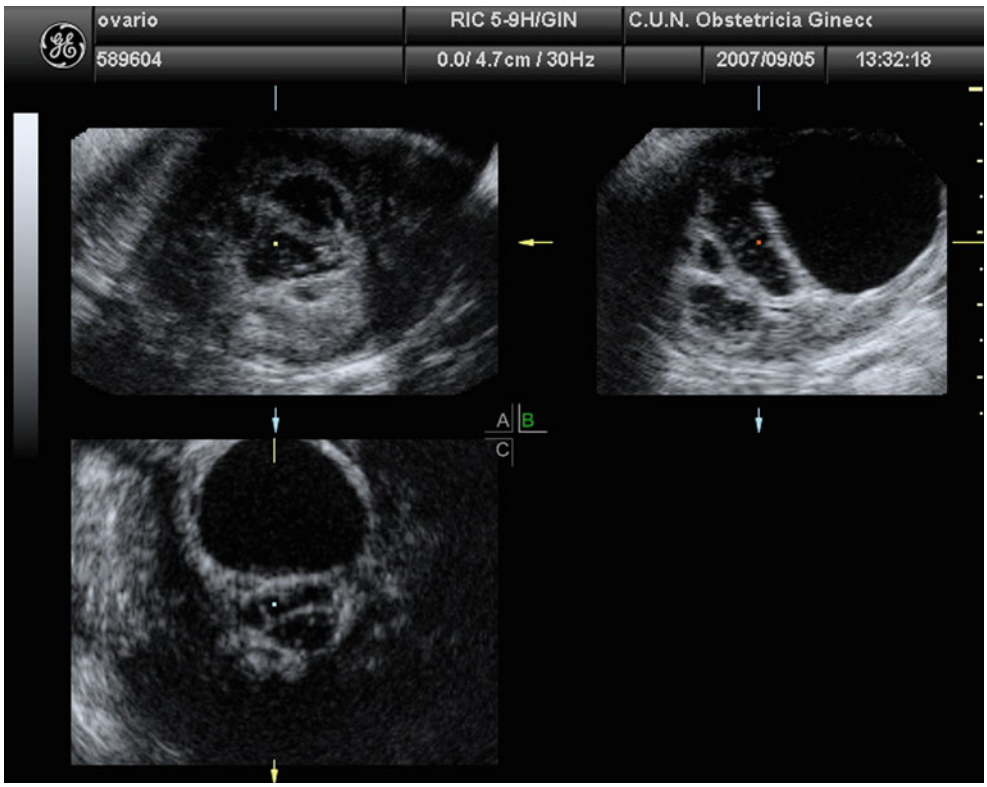

Fig. 4 Three-dimensional ultrasound from an ovarian fibrothecoma that depicts a multilocular adnexal mass with different echogenicity in locules

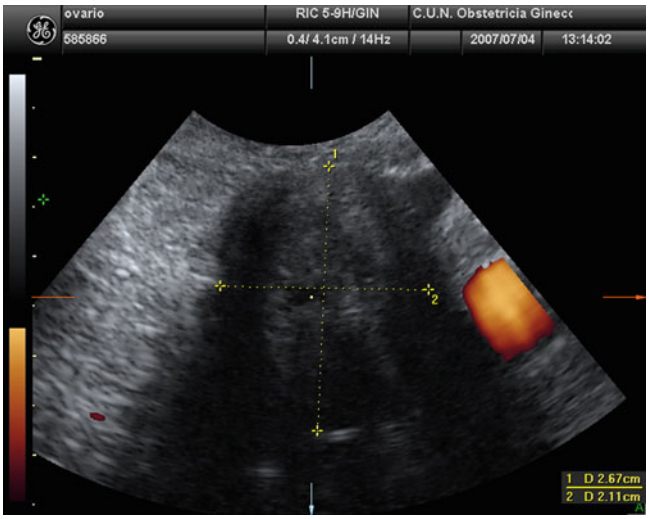

Fig. 5 Transvaginal ultrasound from an ovarian thecoma. The lesion is solid with significant acoustic shadowing. No vessels are detected with power Doppler examination

cases). Most thecomas are benign, and surgical excision is curative [5, 22].

At ultrasound, a thecoma may manifest as an echogenic mass with distal acoustic attenuation, a well-defined hypoechoic mass, or an anechoic lesion with through transmission (Fig. 5). Secondary features of hyperestrogenism, such as endometrial thickening, also may be seen on ultrasound images [22].

Granulosa Cell Tumors

Although granulosa cell tumors are considered as low potential tumors and not strictly as benign tumors, we shall consider the description of these tumors.

Granulosa cell tumors are rare sex cord ovarian tumors that are formed by cells believed to be derived from those that surround the germinal cells in the ovarian follicles. Two major forms of granulosa cell tumors are recognized: the *adult* form, which primarily occurs in middle-aged and older women, and the *juvenile* form, which typically occurs in children and younger women [10].

Most adult granulosa cell tumors are partially cystic, with multiple fluid-filled or blood-filled loci and solid areas. They represent approximately 95 % of all granulosa cell tumors. These tumors, the majority of which are unilateral, most often occur in postmenopausal women. Adult granulosa cell tumors are the ovarian tumor type most commonly associated with manifestations that are caused by the overproduction of female sex hormones (estrogenic manifestations). These manifestations include endometrial hyperplasia and endometrial cancer, which are present in 5–25 % of cases. Adult granulosa cell tumors are considered to be tumors of low-grade or low malignant potential. Ninety percent are stage I at diagnosis, with a reported 10-year survival rate of 86–96 %; the corresponding reported survival rate for patients with tumors found at more advanced stages is 26–49 %. Treatment is primarily surgical. Rupture of the

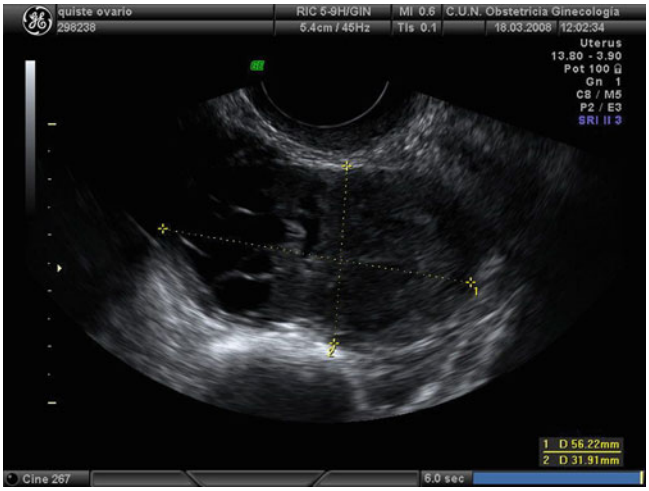

Fig. 6 Transvaginal ultrasound from a granulosa cell tumor. The lesion appears as a cystic-solid mass. Note that the cystic component is multiloculated with small locules

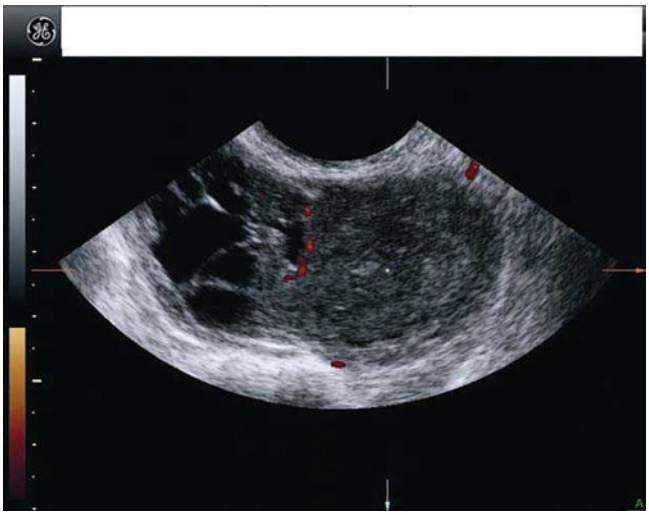

Fig. 7 The same lesion than in previous figure. Power Doppler ultrasound shows a moderate vascularization

tumor during surgery adversely affects prognosis. Recurrences can occur 30 years or more after removal. Juvenile granulosa cell tumors are grossly similar to those of the adult subtype. They account for only 5 % of all granulosa cell tumors. Most are unilateral, and approximately half occur before puberty. Because of their estrogenic hormone production, many of these tumors result in precocious sexual development. Most juvenile granulosa cell tumors are limited to the ovary at the time of diagnosis. Surgical excision is curative in most cases. Recurrences are rare and typically occur within 3 years.

On ultrasound scan these masses appear as multilocular solid (52 %) or purely solid (39 %) masses (Fig. 6). Vascularization usually is moderated (Fig. 7). Multilocular solid cysts typically contain large numbers of small locules. The echogenicity of the cyst content was most often mixed or low level. Papillary projections can be found in 17 % of the cases [25].

Sertoli-Stromal Cell Tumors

Ovarian Sertoli cell tumors and Sertoli-Leydig cell tumors are sometimes called Sertoli-stromal cell tumors, androblastomas, or arrhenoblastomas. They account for less than 1 % of all ovarian tumors and are most common in young patients. Approximately 75 % occur in women under the age of 30 years (mean age at diagnosis 25 years); less than 5 % are encountered in prepubertal girls and slightly over 10 % after the age of 45 years. Almost all cases present at stage I and may have androgenic, estrogenic, or progestagenic manifestations, but many have no endocrine manifestations at all. Prognosis is usually favorable, except for those poorly differentiated or with heterologous elements [6, 8, 26].

These tumors are composed of Sertoli cells, Leydig cells, and fibroblasts in varying proportions and varying degrees of differentiation [26].

Sertoli Cell Tumors

The mean age at diagnosis of Sertoli cell tumors is 30 years. They are lobulated, solid, yellow or brown tumors and rarely metastasize. These tumors may be large (mean diameter 9 cm) and are usually unilateral [5, 26].

Sertoli cell tumors are formed by cell proliferations that resemble the rete ovarii and rete testis, which characteristically are arranged in hollow or solid tubules dispersed within fibrous stroma containing no or only a few Leydig cells [5, 26]. The predominant microscopic pattern of ovarian Sertoli cell tumors is tubular, but other patterns, particularly cord-like and diffuse, are common [1].

These tumors usually do not exhibit hormonal activity, but they may produce estrogens that can induce precocious puberty, bleeding disturbances, and hyperplastic endometrium or, in rare cases, can be associated with androgenic effects and the development of virilization [5, 26]. Some of these tumors may also secrete renin, leading to refractory hypertension and hypokalemia [27].

At ultrasound, most Sertoli cell tumors are large solid tumors, confined to the ovary at presentation, and not associated with ascites or calcification (Fig. 8). When these tumors are small, they can be difficult to identify by ultrasound [26, 28].

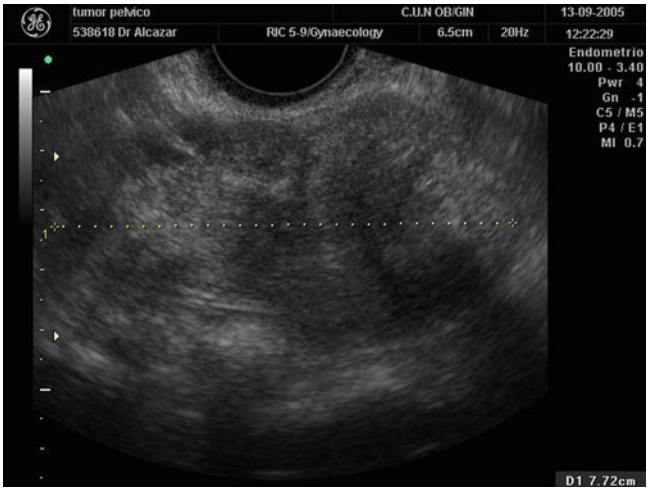

Fig. 8 Transvaginal ultrasound from a Sertoli cell tumor depicting a solid large tumor

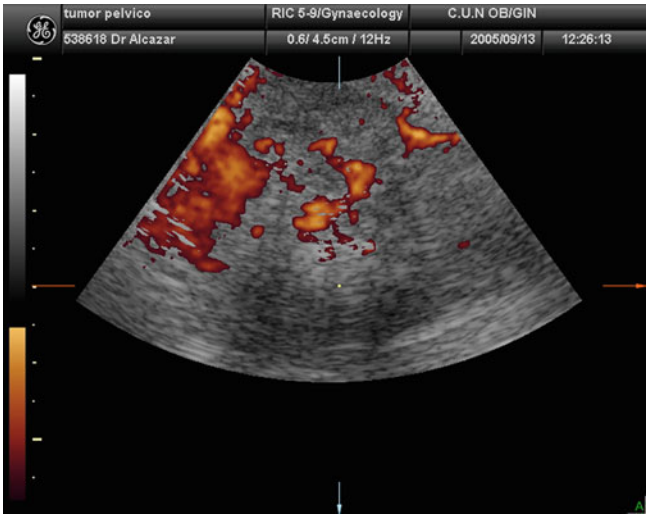

Fig. 9 Transvaginal ultrasound from a Sertoli-Leydig tumor. In this occasion the tumor is solid and vascularization is abundant

Sertoli-Leydig Cell Tumors

Sertoli-Leydig cell tumors account for less than 0.5 % of all ovarian tumors and are the most common virilizing tumor. However, only 30 % of these tumors are hormonally active [14].

Sertoli-Leydig cell tumors are formed by variable proportion of cells that resemble epithelial and stromal testicular cells. Most commonly they range in size from 5 to 15 cm. Most are unilateral (bilateral in less than 5 % of cases) and the mean age at diagnosis is in the mid-twenties. These tumors vary greatly in gross appearance and typically form a firm, solid, lobulated mass with a smooth external surface. However, although they usually show a structure of solid tumor, they may also be partially cystic, or completely cystic, and may or not have polypoid or vesicular structures in their interior [5, 22].

Histologically they are composed of a combination of Sertoli cells, Leydig cells, and fibroblasts [5, 22]. They may be well, moderately, or poorly differentiated, retiform, and mixed, although there is considerable overlap between the different subtypes. Well-differentiated tumors have a tubular pattern, usually without heterologous or retiform components. The single most common pattern of the tumors of intermediate differentiation is a striking nodular growth with large cellular blue nodules being intersected by a stroma that is often edematous [1]. Poorly differentiated tumors may be difficult to distinguish from pure sarcomas and present as differential features small diagnostic areas composed of clusters of dark blue Sertoli cells and some cells that are consistent with Leydig cells or their precursors [1]. Retiform Sertoli-Leydig cell tumors have a tubular pattern with elongated, often slit-like, branching tubules that may focally or extensively be cystically dilated and may contain large papillary projections into the tubules and cysts [1, 5, 26]. Mixed tumors do not differ significantly from otherwise subtypes of Sertoli-Leydig cell tumors, but some of them are predominantly cystic and on microscopic examination have heterologous elements of two basic types: endodermal elements, characterized by gastrointestinal-type epithelium, and mesenchymal elements, immature skeletal muscle or cartilage [1].

About half of Sertoli-Leydig cell tumors have no hormonal activity, and endocrine manifestations and symptoms may be pain or abdominal swelling. About a third of Sertoli-Leydig cell tumors show increased levels of testosterone, androstenedione, and other androgens and are associated with virilization, presenting symptoms as oligomenorrhea, amenorrhea, breast atrophy, hirsutism, acne, deepening of the voice, clitoris hypertrophy, or male pattern baldness. Occasionally Sertoli-Leydig cell tumors are hyperestrogenic, presenting symptoms such as menorrhagia/metrorrhagia or postmenopausal bleeding. Rupture or spread outside the ovary complicates some of these tumors but ascites is rare. After surgical removal of a virilizing Sertoli-Leydig cell tumor, menses usually resume within a month, some excessive hair may disappear, but a deepened voice and clitoromegaly tend not to regress [26].

At ultrasound, unlike pure Sertoli cell tumors, Sertoli-Leydig cell tumors may have more variable and heterogeneous morphology because they include both cystic and solid components. They may appear as unilateral solid or multilocular solid masses with purely solid areas mixed with areas of closely packed small cyst locules and may resemble mucinous cysts. These tumors usually contain no papillary projections, and color score information shows moderate or abundant vascularization (Fig. 9), with a low vascular resistive index. Bilateral occurrences are extremely rare (1.5 % of cases) [22, 26, 29]. Sertoli-Leydig cell tumors in patients

with virilization are often small and difficult to detect even with transvaginal ultrasound [9].

Sex Cord Tumor with Annular Tubules

Sex cord tumor with annular tubules is an unusual form of ovarian sex cord tumor with morphologic features of both granulose cell and Sertoli cell tumors. Although there is no consensus on whether the cells of these tumors are of granulosa or Sertoli type, there is some agreement that this tumor is composed of primitive cells of sex cord origin which have a potential to differentiate into either granulosa or Sertoli cells [30, 31].

Histologically the tumor demonstrates rounded epithelial nests containing eosinophilic hyaline bodies with two distinct architectural patterns. One pattern involves a continuous closed tubule with a central hyaline body. The other pattern is that of larger nests of continuous tubules rotating about multiple hyaline bodies [30].

These tumors may be feminizing, inducing isosexual precocity, menstrual irregularities, and postmenopausal bleeding in young girls, women of reproductive age, and postmenopausal women, respectively [11]. Of the patients diagnosed with this type of tumor, approximately one-third have Peutz-Jeghers syndrome, an autosomal dominant hereditary disorder characterized by mucocutaneous melanin deposits, hamartomatous polyps of the gastrointestinal tract, and an increased risk for cancer of gastrointestinal and nongastrointestinal sites [21, 30]. Both sporadic and Peutz-Jeghers syndrome associated sex cord tumor with annular tubules have since been reported in patients ranging in age from 4 to 76 years, with most being diagnosed in the third or fourth decade of life. When occurring in association with Peutz-Jeghers syndrome, they typically are bilateral, multifocal, small (size less than 3 cm), and benign, and may also cause abdominal and pelvic pain or tenderness [11].

At ultrasound, this tumor can appear as multiple and lobulated highly echogenic masses or tumorlets, some of which are confluent, within unilateral or bilateral enlarged ovaries [30].

Steroid (Lipid) Cell Tumors

Ovarian steroid cell tumors account for approximately 0.1–0.2 % of all ovarian tumors and affect patients from a wide range of ages but usually those in the fifth or sixth decade of life [3]. They are subcategorized as stromal luteomas, Leydig cell tumors, and steroid cell tumors not otherwise specified [13]. Because the cells of these tumors typically contain abundant intracellular lipid, they were initially also called *lipid* or *lipoid cell tumors*. However, these terms would be misleading for tumors in this group with little or no lipid content. The term *steroid cell tumors* recognizes the fact that a minority of them contain little or no stainable fat and refers to their clinical manifestations, unifying a group of tumors which secret steroid hormones [3].

These tumors originate from adrenal rest cells, ovarian stromal lutein cells, or Leydig cells. They are usually small (less than 3 cm); often yellow, reflecting their high lipid content; and typically unilateral and solid. These tumors are usually well circumscribed, occasionally lobulated, and rarely display a cystic composition [2].

Histology of steroid cell tumors usually shows a diffuse pattern of cell growth. Occasionally, nests or columns are also seen. The stroma is generally sparse, consisting of a delicate connective tissue containing a rich vascularity. The neoplastic cells are usually of two types. The predominant cell type is medium sized and polygonal, and it contains eosinophilic, slightly granular cytoplasm; the cell borders are distinct, showing a central nucleus with a single nucleolus. The second cell type is larger and has abundant vacuolated cytoplasm. The mitotic activity is variable. In these tumors, foci of necrosis and hemorrhage may be seen [2].

In most cases these tumors are virilizing, producing androgens, and typically present with hirsutism. Nevertheless, estrogen-producing tumors have also been reported [3].

Stromal Luteoma

Twenty percent of steroid cell tumors are stromal luteomas [13]. These tumors are usually unilateral small tumors confined to the ovarian stroma and are frequently associated with stromal hyperthecosis [2]. They are formed by cells that resemble adrenal gland cells [5].

Eighty percent of them occur in postmenopausal women with an average patient age of 55–60 years at the time of diagnosis and are associated with estrogenic manifestations in 60 % of cases, the most common of which is uterine bleeding. Also androgenic effects have been described in 12 % of cases [5, 13, 22].

At ultrasound, stromal luteomas appear as solid and well-circumscribed masses. They are rarely bilateral and usually do not exceed 3 cm in size [13].

Leydig Cell Tumor

Leydig cell tumors account for only 15–20 % of steroid cell tumors [13]. The majority of Leydig cell tumors occur in premenopausal and postmenopausal women (mean age 58 years) and are associated with hirsutism and virilization in 75 % of cases [26].

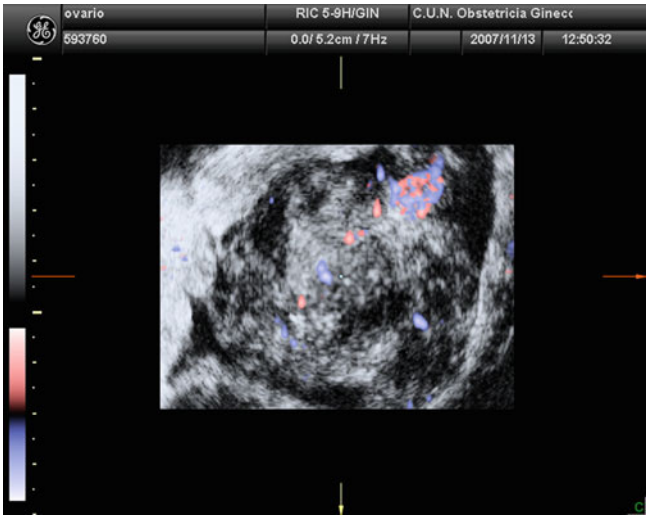

Fig. 10 Transvaginal ultrasound from a Leydig cell tumor. Ultrasound pattern is quite similar to the previous ones

Macroscopically, the neoplastic tissue exhibits a brown to yellow color. They are usually small tumors, with an average diameter of 2.4 cm; solid; and generally unilateral [26].

These tumors are composed of lutein cells, Leydig cells, and adrenocortical cells. Microscopic examination of them reveals a circumscribed mass of steroid cells with eosinophilic cytoplasm. To make the diagnosis of ovarian Leydig cell tumor, crystals of Reinke must be identified in the cytoplasm of the cells [22, 26].

The onset of androgenic symptoms is often slow, and the symptoms may have been present for many years by the time the diagnosis is made. Estrogenic manifestations, as endometrial hyperplasia, and even endometrial polyps or carcinoma, are rare [26].

At ultrasound, these tumors are small, solid, and well-circumscribed tumors confined within an ovary of almost normal size, with moderate or abundant vascularization [26] (Fig. 10).

Steroid Cell Tumors Not Otherwise Specified

Steroid cell tumors not otherwise specified account for 60 % of ovarian steroid cell tumors, and they are usually benign and unilateral. They occur at any age, even rather before puberty, but typically at a younger age (mean age 43 years) than other types of ovarian steroid tumors. They are typically solid, yellow, well circumscribed, and occasionally lobulated. These tumors are larger than the other steroid cell tumors, and the average size at diagnosis is approximately 8.5 cm [2, 13].

These tumors are composed of two similar-appearing polygonal cell types that differ only in their cytoplasmic appearance, eosinophilic versus vacuolated. They differ from Leydig cell tumors in that they lack crystals of Reinke in their cytoplasm [2, 32].

Steroid cell tumors not otherwise specified are most commonly associated with androgenic changes. Hirsutism and virilization are the most common symptoms, occurring in 55–75 % of patients. Furthermore, it is not unusual for these tumors to produce hormones other than testosterone. The excess of estrogen production can result in menorrhagia and postmenopausal bleeding. Even they may secrete adrenal cortex steroid hormones that can induce hypercortisolism (Cushing's syndrome) in 6–10 % of cases [5, 32]. In addition, patients can present pain, abdominal distention, and bloating. However, ascites and elevated CA-125 are infrequent [2, 33]. An additional 10–15 % of patients will be asymptomatic, with tumors detected incidentally during routine pelvic examination or at the time of hysterectomy or other surgical interventions [13].

By ultrasonography, ovarian steroid cell tumors not otherwise specified may be identified as solid ovarian tumors by careful assessment of the texture of the ovary using grayscale ultrasonography. Even when these tumors are small in size, an area of different echogenicity from that of the surrounding ovary can be observed. This area within the ovary will be well demarcated by the different echogenicity. If such an area of different echogenicity is detected, further sonographic evaluation using color Doppler flow or color power flow amplitude should follow helping to confirm the presence of the tumor. Doppler evaluation can show a high vascularity with low resistance to flow in the intratumoral blood vessels [32, 34].

Sex Cord-Stromal Tumors, Unclassified

Occasional tumors are encountered which clearly fall in the sex cord-stromal category but do not lend themselves to placement in the more specific categories, leading them to be termed sex cord-stromal tumor unclassified. The proportion of sex cord-stromal tumors assigned to this category varies between different studies, but may be about 10 % of total [1, 6].

A disproportionate number of tumors from pregnant patients are placed in this group. There is nothing unique about the general clinical profile of the unclassified sex cord-stromal tumors of the ovary, and the prognosis of individual cases has to be evaluated using basic principles according to their features [1]. Nevertheless, these tumors have usually a poorer differentiation, so that their degree of malignancy may be greater than that of other types of tumors in this group [6].

Other Sex Cord-Stromal Tumors: Sclerosing Stromal Tumor of Ovary

Sclerosing stromal tumor of the ovary is a rare benign tumor that is classified as a distinct entity in the sex cord-stromal tumors. This tumor differs clinically, radiologically, and histologically from other ovarian stromal tumors [35]. They account for 6 % of ovarian stromal tumors and usually occur in a younger age group. Whereas other types of stromal tumors are most common in the fifth and sixth decades, about 80 % of sclerosing stromal tumors of the ovary are encountered during the second and third decades (mean age 27.5 years) [36–38].

These tumors are fibrotic, unilateral, and well circumscribed, with a size ranging from 1.5 to 20 cm in diameter and have a variegated gray-white to yellow cut surface [3]. Microscopically, sclerosing stromal tumors of the ovary are characterized by some distinctive features: a pseudolobular growth pattern, in which cellular areas are separated by edematous and collagenous hypocellular areas; collagenous sclerosis within the cellular areas (hence the name of the tumor); prominent vascularity, with a hemangiopericytomatous pattern; and heterogeneity of the cell population, with two distinct cell populations of spindle and polygonal cells [36, 38].

Their most common presenting symptom is menstrual irregularities. Hormonal activity has been reported in a few cases, and ascites is rare. If it is hormonally active, it is usually androgenic and most frequently occurs during pregnancy [35, 37, 38].

These tumors have been described at ultrasonography as well-defined solid and multilocular cystic adnexal masses with centrally located, multiple, round, or cleft-like cysts. Color Doppler ultrasonography reveals prominent vascularity in the peripheral portion together with slight central vascularity in the intercystic spaces [35, 36, 39].

References

1. Young RH. Sex cord-stromal tumors of the ovary and testis: their similarities and differences with consideration of selected problems. Mod Pathol. 2005;18:S81–98.
2. Varras M, Vasilakaki T, Skafida E, Akrivis C. Clinical, ultrasonographic, computed tomography and histopathological manifestations of ovarian steroid cell tumour, not otherwise specified: our experience of a rare case with female virilisation and review of the literature. Gynecol Endocrinol. 2011;27:412–8.
3. Outwater EK, Wagner BJ, Mannion C, McLarney JK, Kim B. Sex cord-stromal and steroid cell tumors of the ovary. Radiographics. 1998;18:1523–46.
4. Thrall MM, Paley P, Pizer E, Garcia R, Goff BA. Patterns of spread and recurrence of sex cord-stromal tumors of the ovary. Gynecol Oncol. 2011;122:242–5.
5. Chen VW, Ruiz B, Killeen JL, Coté TR, Wu XC, Correa CN. Pathology and classification of ovarian tumors. Cancer. 2003;97(10 Suppl):2631–42.
6. Scully RE. Sex cord-stromal tumors. In: Hartmann WH, editor. Tumors of the ovary and maldeveloped gonads. Washington, D.C.: Armed Forces Institute of Pathology; 1979. p. 152–210.
7. Colombo N, Parma G, Zanagnolo V, Insinga A. Management of ovarian stromal cell tumors. J Clin Oncol. 2007;25:2944–51.
8. Zanagnolo V, Pasinetti B, Sartori E. Clinical review of 63 cases of sex cord stromal tumors. Eur J Gynaecol Oncol. 2004;25:431–8.
9. Tanaka YO, Saida TS, Minami R, Yagi T, Tsunoda H, Yoshikawa H, et al. MR findings of ovarian tumors with hormonal activity, with emphasis on tumors other than sex cord-stromal tumors. Eur J Radiol. 2007;62:317–27.
10. Geetha P, Nair K. Granulosa cell tumors of the ovary. Aust N Z J Obstet Gynaecol. 2010;50:216–20.
11. Lele SM, Sawh RN, Zaharopoulos P, Adesokan A, Smith M, Linhart JM, et al. Malignant ovarian sex cord tumor with annular tubules in a patient with Peutz-Jeghers syndrome: a case report. Mod Pathol. 2000;13:466–70.
12. Limaïem F, Lahmar A, Ben Fadhel C, Bouraoui S, M'zabi-Regaya S. Gynandroblastoma. Report of an unusual ovarian tumour and literature review. Pathologica. 2008;100:13–7.
13. Mok JE, Sohn WS. Surgical management of steroid cell tumors of the ovary. CME J Obstet Oncol. 2003;8:173–8.
14. Jung SE, Lee JM, Rha SE, Byun JY, Jung JI, Hahn ST. CT and MT imaging of ovarian tumors with emphasis on differential diagnosis. Radiographics. 2002;22:1305–25.
15. Jeong YY, Outwater EK, Kang HK. Imaging evaluation of ovarian masses. Radiographics. 2000;20:1445–70.
16. Leung SW, Yuen PM. Ovarian fibroma: a review on the clinical characteristics, diagnostic difficulties, and management options of 23 cases. Gynecol Obstet Invest. 2006;62:1–6.
17. Chechia A, Attia L, Temime RB, Makhlouf T, Koubaa A. Incidence, clinical analysis, and management of ovarian fibromas and fibrothecomas. Am J Obstet Gynecol. 2008;199:473.e1–4.
18. Paladini D, Testa A, Van Holsbeke C, Mancari R, Timmerman D, Valentin L. Imaging in gynecological disease (5): clinical and ultrasound characteristics in fibroma and fibrothecoma of the ovary. Ultrasound Obstet Gynecol. 2009;34:188–95.
19. Troiano RN, Lazzarini KM, Scoutt LM, Lange RC, Flynn SD, McCarthy S. Fibroma and fibrothecoma of the ovary: MR imaging findings. Radiology. 1997;204:795–8.
20. Son CE, Choi JS, Lee JH, Jeon SW, Hong JH, Bae JW. Laparoscopic surgical management and clinical characteristics of ovarian fibromas. JSLS. 2011;15:16–20.
21. Roth LM, Czernobilsky B. Perspectives on pure ovarian stromal neoplasms and tumor-like proliferations of the ovarian stroma. Am J Surg Pathol. 2011;35:e15–33.
22. Shanbhogue AK, Shanbhogue DK, Prasad SR, Surabhi VR, Fasih N, Menias CO. Clinical syndromes associated with ovarian neoplasms: a comprehensive review. Radiographics. 2010;30:903–19.
23. Lee MH, Moon YJ, Ha CW, Hoh JK. Ovarian thecoma with virilizing manifestations. Yonsei Med J. 2009;50:169–73.
24. Cronjé HS, Niemand I, Bam RH, Woodruff JD. Review of the granulosa-theca cell tumors from the Emil Novak ovarian tumor registry. Am J Obstet Gynecol. 1999;180:323–7.
25. Van Holsbeke C, Domali E, Holland TK, Achten R, Testa AC, Valentin L, Jurkovic D, Moerman P, Timmerman D. Imaging of gynecological disease (3): clinical and ultrasound characteristics of granulosa cell tumors of the ovary. Ultrasound Obstet Gynecol. 2008;31(4):450–6.
26. Demidov VN, Lipatenkova J, Vikhareva O, Van Holsbeke C, Timmerman D, Valentin L. Imaging on gynecological disease (2):

clinical and ultrasound characteristics of Sertoli cell tumors, Sertoli-Leydig cell tumors and Leydig cell tumors. Ultrasound Obstet Gynecol. 2008;31:85–91.
27. Oliva E, Alvarez T, Young RH. Sertoli cell tumors of the ovary: a clinicopathologic and immunohistochemical study of 54 cases. Am J Surg Pathol. 2005;29:143–56.
28. Outwater EK, Marchetto B, Wagner BJ. Virilizing tumors of the ovary: imaging features. Ultrasound Obstet Gynecol. 2000;15: 365–71.
29. Franzin CM, Kraft ML, Faundes D, Zeferino LC, Alvarenga M, Marussi EF. Detection of ovarian Sertoli-Leydig cell tumors exclusively by color Doppler sonography. J Ultrasound Med. 2006;25:1327–30.
30. Swanger RS, Brudnicki A. Ultrasound of ovarian sex-cord tumor with annular tubules. Pediatr Radiol. 2007;37:1270–1.
31. Ahn GH, Chi JG, Lee SK. Ovarian sex cord tumor with annular tubules. Cancer. 1986;57:1066–73.
32. Reedy MB, Richards WE, Ueland F, Uy K, Lee EY, Bryant C, et al. Ovarian steroid cell tumor, not otherwise specified: a case report and literature review. Gynecol Oncol. 1999;75:293–7.
33. Kim YT, Kim SW, Yoon BS, Kim SH, Kim JW, Cho NH. An ovarian steroid cell tumor causing virilization and massive ascites. Yonsei Med J. 2007;48:142–6.
34. Monteagudo A, Heller D, Husami N, Levine RU, McCaffrey R, Timor-Trisch IE. Ovarian steroid cell tumors: sonographic characteristics. Ultrasound Obstet Gynecol. 1997;10:282–8.
35. Lee MS, Cho HC, Lee Y-H, Hong SR. Ovarian sclerosing stromal tumors: gray scale and color Doppler sonographic findings. J Ultrasound Med. 2001;20:413–7.
36. Deval B, Rafii A, Darai E, Hugol D, Buy JN. Sclerosing stromal tumor of the ovary: color Doppler findings. Ultrasound Obstet Gynecol. 2003;22:531–4.
37. Kim JY, Jung KJ, Chung DS, Kim OD, Lee JH, Youn SK. Sclerosing stromal tumor of the ovary: MR-pathologic correlation in three cases. Korean J Radiol. 2003;4:194–9.
38. Peng HH, Chang TC, Hsueh S. Sclerosing stromal tumor of ovary. Chan Gung Med J. 2003;26:444–8.
39. Joja I, Okuno K, Tsunoda M, Takeda Y, Sugita K, Mizutani Y, et al. Sclerosing stromal tumor of the ovary: US, MR, and dynamic MR findings. J Comput Assist Tomogr. 2001;25:201–6.

Sex Cord-Stromal Tumors: Computed Tomography and Magnetic Resonance

Takashi Koyama

Abstract

Sex cord-stromal tumors are frequently accompanied by hormonal production and secondary hormonal manifestations, including endometrial hyperplasia and occasional development of endometrial carcinoma. Most of sex cord tumors are solid tumors of low to intermediate intensity on T2-weighted MR images, but granulosa cell tumors typically contain hemorrhagic cyst of high intensity on T1-weighted images.

Keywords

Ovarian sex cord-stromal tumor • Granulosa fibroma group • Sertoli-stromal cell tumor • Steroid cell tumor • Sclerosing stromal tumor • Imaging • Computed tomography • Magnetic resonance

Sex cord-stromal tumors account for approximately 8 % of all ovarian tumors and are a group of ovarian tumors which derive from two types of cells: sex cord cells and stromal cells. The cells derived from sex cord include granulosa cells in the normal ovary and Sertoli cells in the testis. On the other hand, stromal cells include fibroblasts, theca cells, and Leydig cells in the testis. Sex cord-stromal tumors are roughly subclassified into granulosa-stromal cell tumors and Sertoli-stromal tumors. Granulosa-stromal cell tumors further include granulosa cell tumors, fibromas and thecomas, and sclerosing stromal tumor. Sertoli-stromal tumors are represented by Sertoli-Leydig cell tumor. Other sex cord-stromal tumors include steroid cell tumors, gynandroblastomas, and sex cord-stromal tumors with annular tubules; however, these tumors are quite rare.

Clinically, many tumors in this category are characterized by the hormonal production from the tumor cells and the secondary endocrine manifestations. The estrogenic manifestation is commonly seen in patients with granulosa cell tumors. The patients typically present with vaginal bleeding from endometrial hyperplasia, due to prolonged exposure to estrogen produced by the tumor. Endometrial carcinomas may develop in 3–25 % of cases, and these tumors are almost always of the well-differentiated type [1–4]. On the other hand, the androgenic manifestations such as hirsutism or virilization are typically seen in patients with Sertoli-stromal tumors, but they are also seen in some patients with granulosa cell tumors and sclerosing stromal tumor. On the contrary, Sertoli-Leydig cell tumor can rarely be estrogenic.

The vast majority of sex cord-stromal tumors are confined within one ovary at presentation. Consequently, the prognosis is generally good. However, granulosa cell tumors and Sertoli-Leydig cell tumors have potential for malignant behavior, and these tumors are categorized in low-grade malignancy.

Granulosa Cell Tumors

Granulosa cell tumors (GCT) are the most common clinically estrogenic ovarian tumors. GCT is further subdivided into adult and juvenile types based on different

T. Koyama, MD, PhD
Department of Diagnostic Radiology, Osaka Red Cross Hospital,
5-30 Fudegasaki-cho, Tennoji-ward,
Osaka 543-8555, Japan
e-mail: montpeti@kuhp.kyoto-u.ac.jp

L. Saba et al. (eds.), *Ovarian Neoplasm Imaging*,
DOI 10.1007/978-1-4614-8633-6_9,

clinical and histopathologic features. Adult granulosa cell comprises about 95 % of cases and often occurs in postmenopausal than premenopausal women, with peak incidence between 50 and 55 years. Patients typically present with abnormal genital breeding because of secondary endometrial hyperplasia. On the other hand, juvenile GCT typically occurs in young girls causing precocious puberty and accounts for 10 % of precocious puberty in girls [5]. Juvenile GCT may be seen in patients with Maffucci syndrome and Ollier syndrome and should be considered a heading diagnosis for an ovarian mass in young patients with these conditions [5–8]. Rarely, androgenic manifestation can be seen in GCTs, and such tumors tend to be cystic with either unilocular or multilocular appearance [5, 9, 10]. Occasionally, patients may present with acute abdomen and hemoperitoneum due to the rupture of the cystic component of GCT [11].

Histologically, GCT reveals granulosa cells in a variety of patterns, including microfollicular, macrofollicular, insular, trabecular, sarcomatoid, and the moiré silk patterns. These patterns are commonly admixed and frequently accompanied by theca cells and fibroblasts. The small cavities seen in microfollicular pattern are called as Call-Exner bodies, which simulate the developing graafian follicle. The cells in adult GCT are characterized by the peculiar nuclear groove, which is often referred to as coffee-bean appearance. On the other hand, juvenile GCTs are distinguished from adult GCTs by their larger cells, hyperchromatic nuclei, and lack of the characteristic nuclear grooves seen in adult GCT.

Adult GCTs are typically large, unilateral, and solid masses with variable amount of cystic components (Figs. 1 and 2) or multilocular masses with thick, irregular septations and solid components (Fig. 3) [11, 12]. On MR imaging, the tumor consists of solid components of intermediate intensity and cysts of high intensity on T2-weighted images (Fig. 1). The characteristic finding on MR imaging is the presence of the cysts of high intensity on T1-weighted images, reflecting hemorrhage within the cysts (Fig. 1) [12]. On post-contrast T1-weighted images, the solid components in GCTs typically show marked enhancement same as uterine myometrium. Rarely, GCT may be totally solid (Fig. 4), and such tumors tend to be small in size. In patients with adult GCTs, the uterus is often enlarged and the endometrium is thickened, reflecting estrogenic effect caused by the tumor (Fig. 2). When the junctional zone is clearly observed in the myometrium of the postmenopausal women with ovarian tumor, estrogen production from the tumor may be suspected (Fig. 3). At the same time, the uterine endometrium should be carefully evaluated for associated endometrial carcinoma (Fig. 5). The gross appearance and the imaging appearance in juvenile type GCTs do not significantly differ from those in adult GCTs, despite their different clinical manifestations and histologic features (Fig. 6) [8, 13].

Thecoma/Fibroma

Fibromas and thecomas are virtually benign tumors commonly seen in pre- and postmenopausal women and are the most common sex cord-stromal tumor, constituting half of all sex cord-stromal tumors. These tumors constitute a spectrum of tumors, ranging from purely fibroblastic tumor to pure thecoma composed of lipid-rich theca cells, which is estrogenic. Thus, the tumors with intermingled pathology between fibroma and thecoma are often designated as fibrothecoma.

Thecoma and fibrothecoma are less commonly estrogenic than GCTs and occur in older patients, who commonly present with abnormal genital bleeding and associate with endometrial hyperplasia and carcinomas [14]. In contrast to thecomas and fibrothecomas, ovarian fibroma is not estrogenic. Ovarian fibromas and fibrothecomas may rarely be associated with ascites and pleural effusion, the condition known as Meigs syndrome (Fig. 7). Although this condition may lead to a mistaken impression of a malignant condition, this manifestation is dramatically resolved following the removal of the tumor [15, 16]. Ascites alone of a variable amount is commonly associated with ovarian fibromas [17, 18]. Ovarian fibroma is also a part of the hereditary basal cell nevus syndrome known as Gorlin syndrome, which is characterized by basal cell carcinomas, keratocysts of the jaw, and extensive calcification of the dura. Fibromas in this syndrome are commonly bilateral, multinodular, and calcified and occur in young women [19–21].

The gross appearance of these tumors is usually solid mass. Thecoma typically shows yellowish surface reflecting lipid content, whereas fibroma shows whitish surface reflecting collagenous matrix. The size of these tumors is usually less than 10 cm with an average of 6 cm [22]. However, they may become so large that they are mistaken as malignant tumors. Occasionally, cystic changes may be accompanied (Fig. 8). Rarely, these tumors may show extensive calcifications.

MR features of these tumors can vary according to the proportion of the fibrotic components. Thecomas with little or no fibrosis show intermediate to increased signal intensity on T2-weighted images (Fig. 9). As the fibrotic component becomes abundant, the tumor exhibits prominently decreased signal intensity on T2-weighted images [18, 23]. In large fibromas and fibrothecomas, the tumors tend to show heterogeneous appearance with capsule of distinctive low intensity, degenerative changes, and peripheral subcapsular cystic areas on T2-weighted images (Fig. 10) [24]. Post-contrast

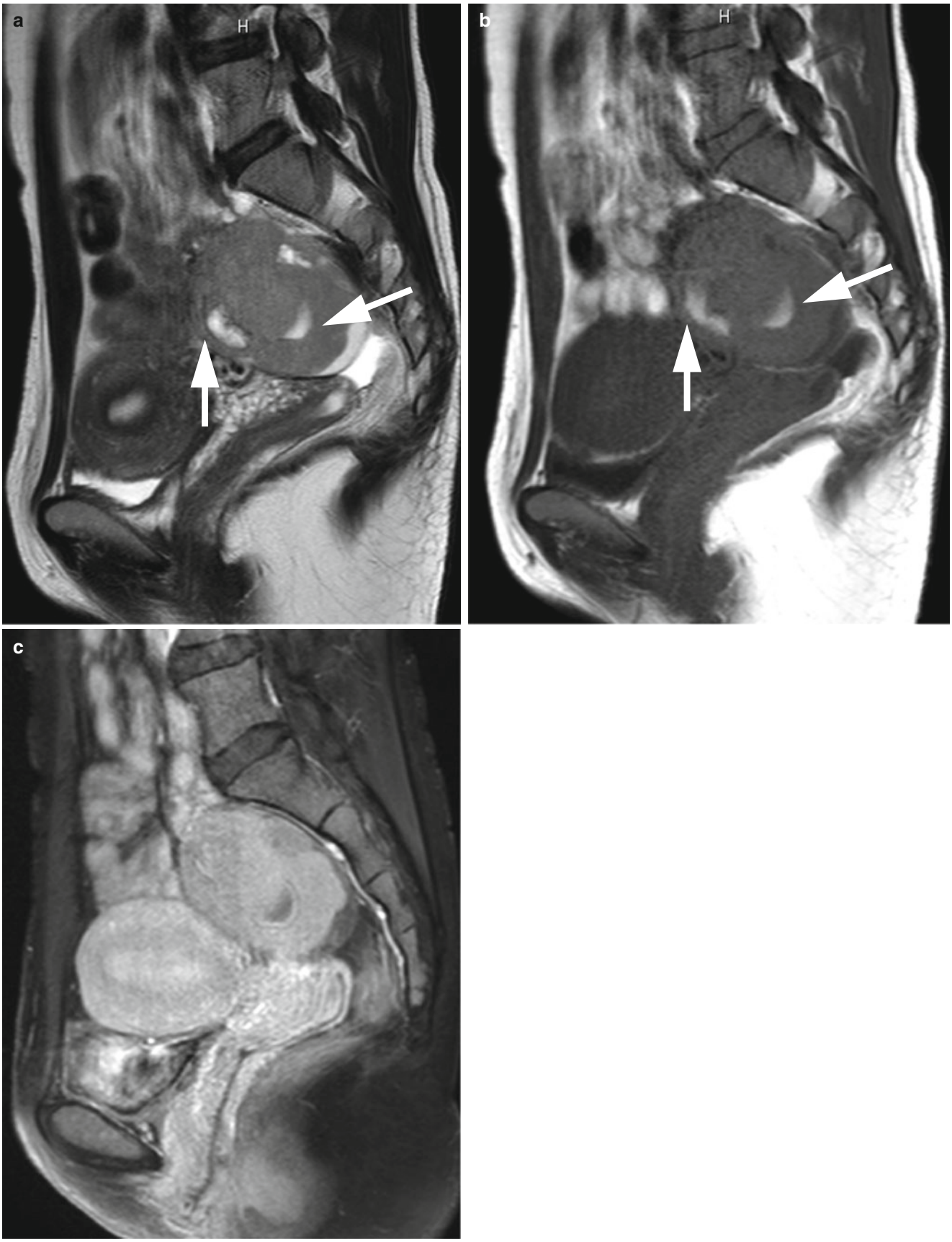

Fig. 1 Granulosa cell tumor in a 37-year-old woman. (**a**) Sagittal T2-weighted image demonstrates a solid tumor of intermediate intensity, containing irregular-shaped cystic components of bright intensity (*arrows*). (**b**) T1-weighted image demonstrates high intensity corresponding to the cystic foci (*arrows*). (**c**) Post-contrast T1-weighted image with fat suppression shows homogeneous enhancement within the solid component

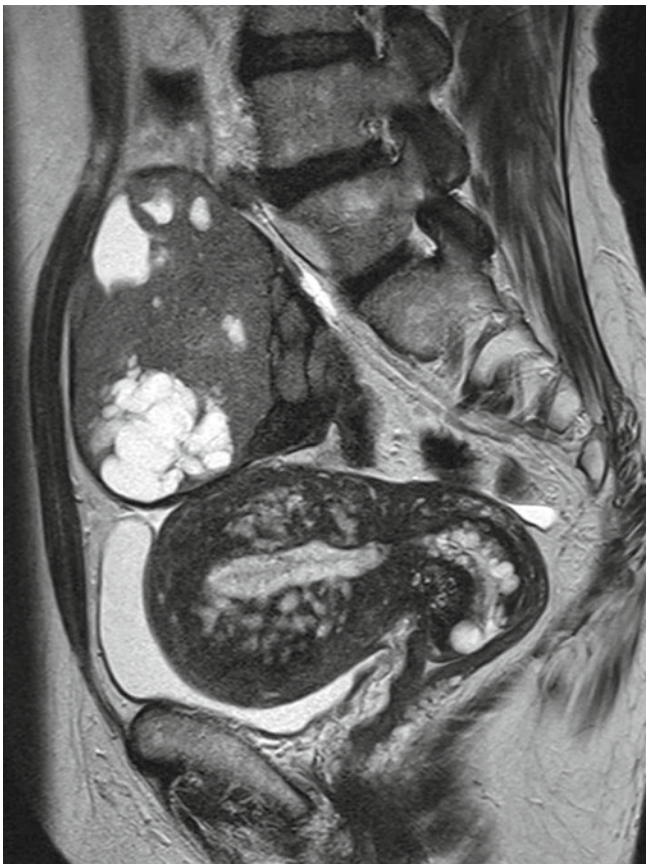

Fig. 2 Granulosa cell tumor in a 68-year-old woman. T2-weighted image demonstrates a predominantly solid tumor of intermediate intensity, containing multiple cystic foci of high intensity. The uterus is abnormally enlarged with thickened endometrium. The thickened myometrium contains numerous foci of high intensity same as the endometrium, reflecting the ectopic endometrium in adenomyosis, which is quite unusual for this age of the patient

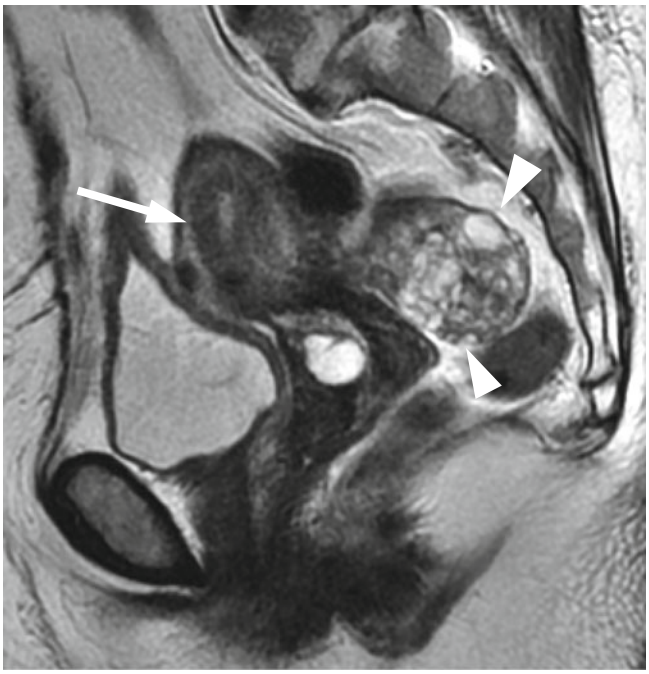

Fig. 3 Granulosa cell tumor in a 70-year-old woman. T2-weighted images reveal a multilocular cystic tumor (*arrowheads*), consisting of small locules of bright intensity and irregular septations. The uterus is enlarged for this age, and the junctional zone is clearly observed (*arrow*)

T1-weighted images usually show less enhancement in the tumor than the uterine myometrium and heterogeneous enhancement in cases of large tumors (Fig. 9).

Sclerosing Stromal Tumors

Sclerosing stromal tumor (SST) is a rare benign sex cord-stromal tumor, first described by Chalvardjian and Scully in 1973 [25]. SST occurs predominantly in young women in their second and third decades of life, with mean age of 27 years old [26]. Patients commonly present with menstrual irregularity. As well as other sex cord-stromal tumors, SST may show hormonal manifestation, which can be either estrogenic or androgenic [27–29]. Histologically, SST is characterized by cellular areas mainly composed of theca cells with increased vascularity, which are separated by

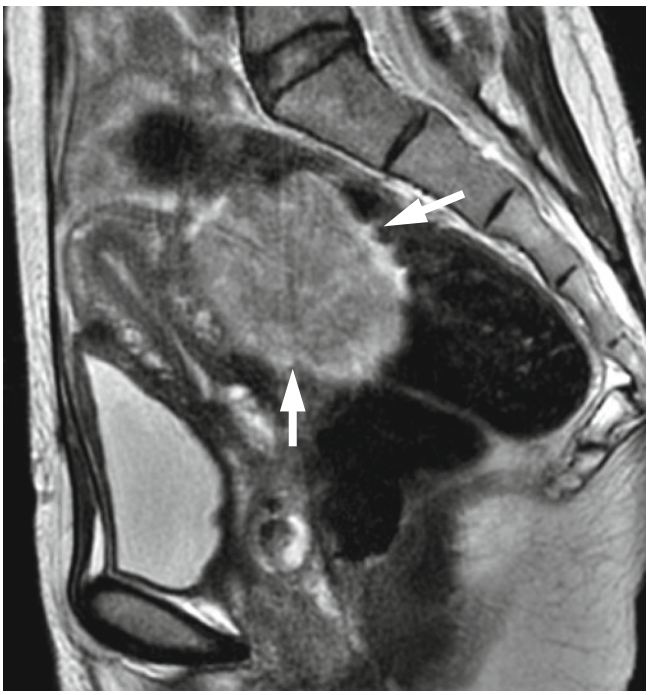

Fig. 4 Granulosa cell tumor in a 52-year-old woman. T2-weighted image shows an entirely solid mass (*arrows*) of homogeneously intermediate intensity

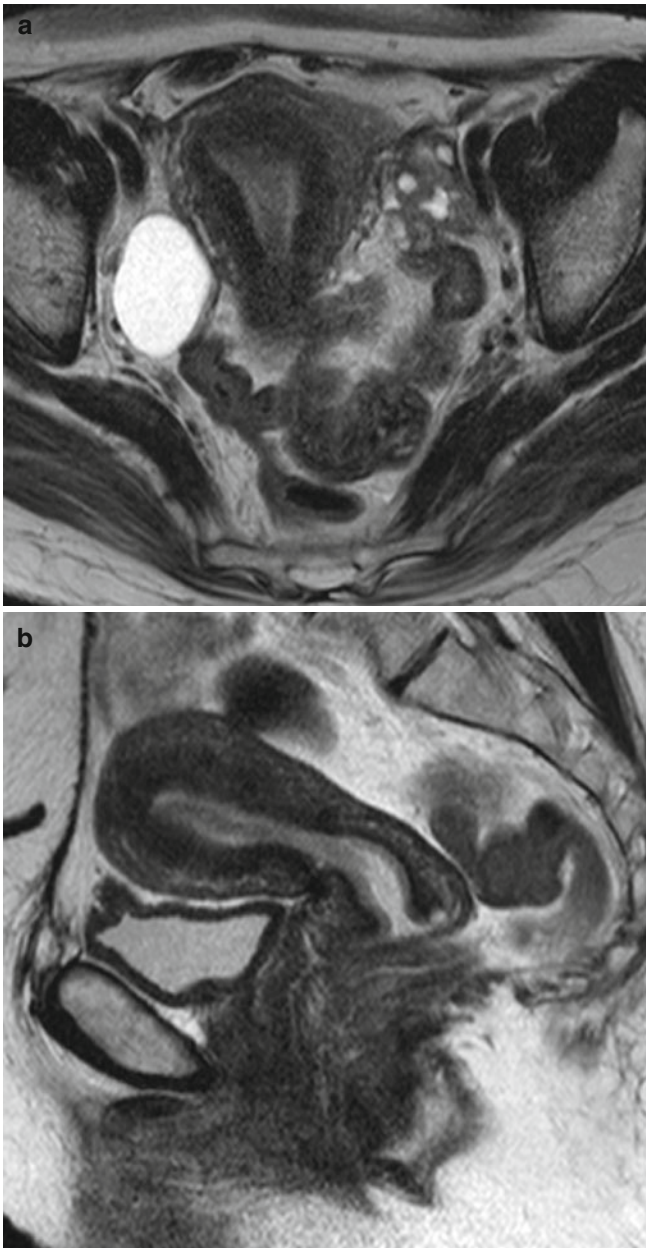

Fig. 5 Granulosa cell tumor and uterine endometrial adenocarcinoma in a 45-year-old woman. (**a**) Axial T2-weighted image reveals diffusely decreased signal intensity in the uterine endometrium, and a small solid mass of intermediate intensity, containing cystic foci of high intensity. There is a functional cyst in her right ovary. (**b**) Sagittal T2-weighted image shows a well-differentiated endometrial carcinoma of decreased intensity in the endometrial cavity

"sclerosing" hypocellular areas which consist of densely collagenous stroma. The sclerosing areas are often accompanied by edematous change.

On MR imaging, SST consists of heterogeneous solid components of low to high signal intensity on T2-weighted images (Fig. 11). The areas of low intensity are considered to represent microscopically cellular areas, whereas those of high intensity are considered to represent edematous area. On post-contrast T1-weighted images, the areas of decreased intensity on T2-weighted images are well enhanced, reflecting rich vascularity in the cellular areas. When dynamic contrast-enhanced imaging is obtained, the areas are known to show striking early enhancement [30–32].

Sertoli-Leydig Cell Tumors

Sertoli-Leydig cell tumor (SLCT) is the most common virilizing tumor, although it represents only 0.5 % of all ovarian tumors. This tumor belongs to a category of Sertoli-stromal cell tumors, which encompass a spectrum of tumors composed of Sertoli cells, Leydig cells, and fibroblasts in varying proportions. Other tumors within this group include pure Sertoli cell tumors and pure Leydig cell tumors, but they are extremely rare.

SLCT commonly affects young females, and approximately 75 % of the patients are less than 30 years old [33]. SLCT is the most common androgen-producing tumor, and virilization can be a clinical clue to suspect this tumor. However, SLCTs in patients with virilization tend to be small and may not be detected on ultrasonography or CT [34]. Meanwhile, two-thirds of all SLCTs are nonfunctioning and their clinical symptoms are nonspecific [33]. SLCT is stage I at the presentation in 92 % of cases and the majority of tumor behaves as benign [33, 35].

The gross appearance of SLCT is usually solid and lobulated mass, but the tumor may be accompanied by cyst formation (Fig. 12). The majority of SLCT is within 5–15 cm in diameter, though the size tends to be larger in poorly differentiated subtype [36]. Microscopically, SLCT is characterized by the biphasic proliferation of Sertoli cells and Leydig cells in varying degrees of differentiation [26, 37]. SLCTs are pathologically divided into four categories including well differentiated, intermediately differentiated, poorly differentiated, and retiform [38]. Poorly differentiated SLCT tends to contain areas of hemorrhage and necrosis more frequently compared to well-differentiated tumor [39]. The retiform pattern is occasionally associated with cyst formation [40].

The imaging feature in SLCT is usually predominantly solid tumor, occasionally accompanied by a variable proportion of cystic components (Fig. 12). In MR imaging, the solid portion of the tumor tends to show low intensity on T2-weighted image [8]. The low intensity in the solid components is considered to represent abundant stroma in the tumor. In a rare instance, the tumor can be totally cystic with multilocular appearance (Fig. 13) [41].

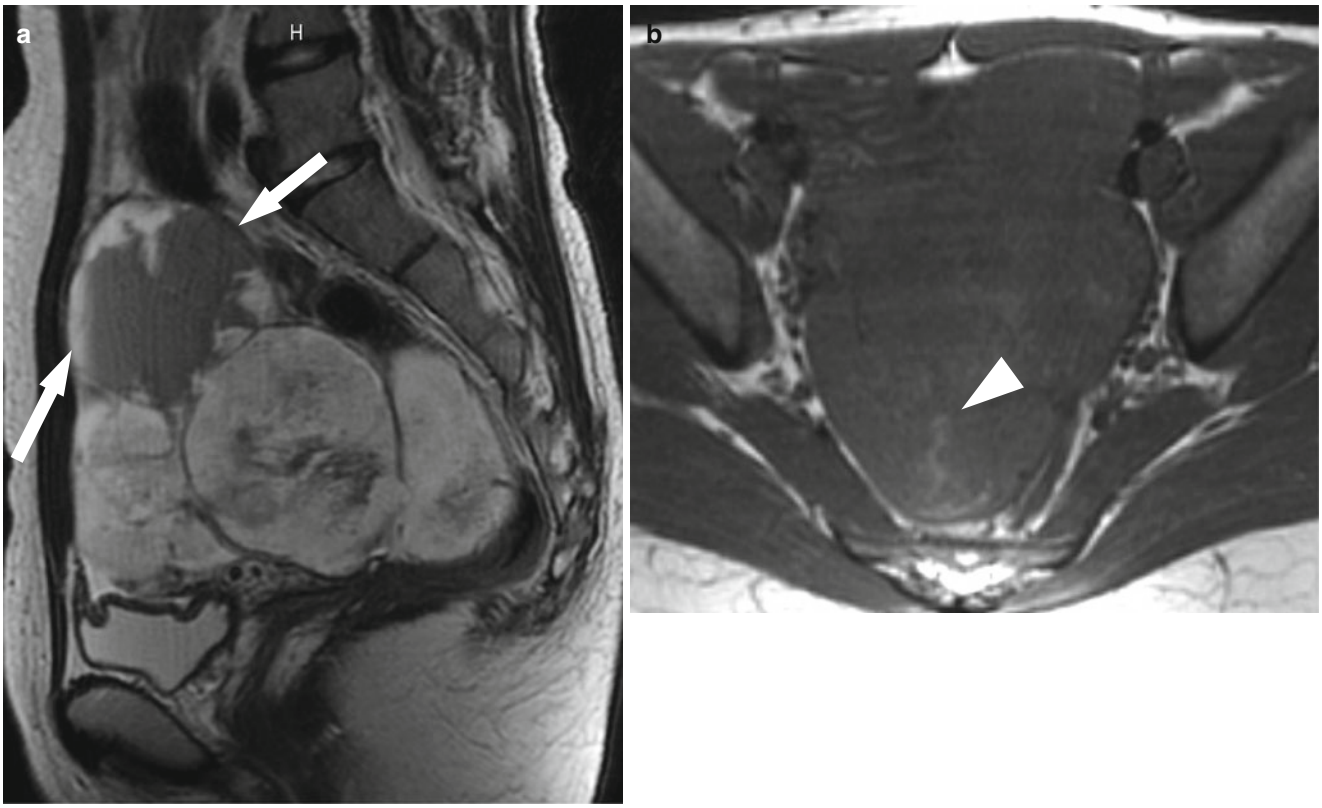

Fig. 6 Juvenile granulosa cell tumor in a 34-year-old woman. (**a**) Sagittal T2-weighted MR image shows a large lobulated pelvic mass, consisting of solid component of high intensity and cystic component caudally, containing a fluid-fluid level (*arrows*). (**b**) Axial T1-weighted image reveals a large lobulated mass of predominantly low intensity, containing areas of high intensity (*arrowheads*), representing hemorrhage within the tumor (Courtesy of Dr. Kazuhiro Yamamoto, Dept. of Radiology, Osaka Medical College)

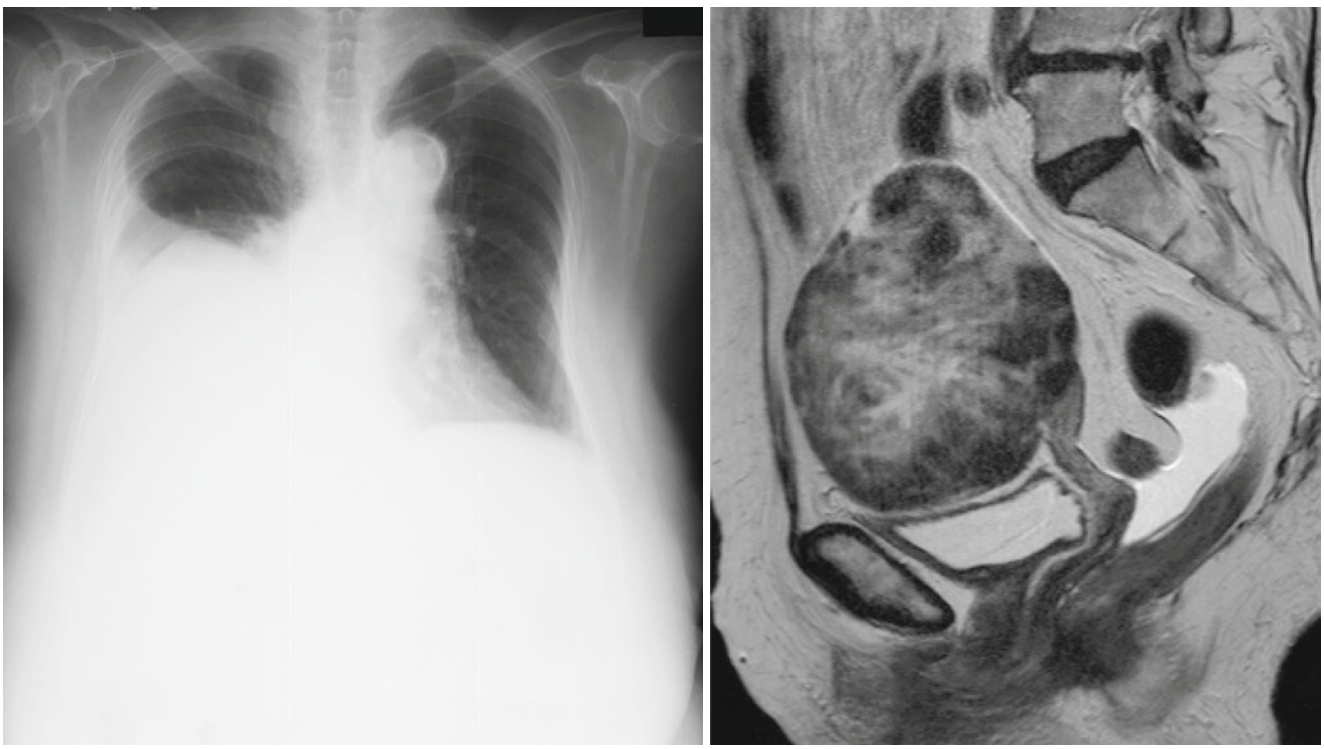

Fig. 7 Fibroma with Meigs syndrome in an 85-year-old woman. (**a**) Plain radiograph shows a large amount of pleural effusion in the right thorax. (**b**) Sagittal T2-weighted image shows a well-demarcated solid mass, containing peripheral areas of distinct low intensity and central areas of high intensity. There is a small amount of ascites in the cul-de-sac

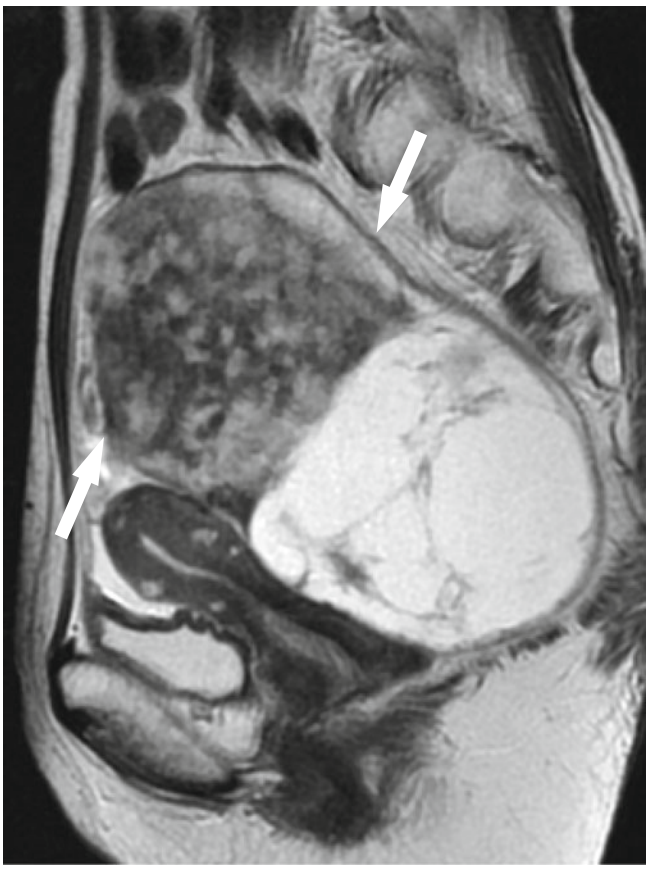

Fig. 8 Fibrothecoma with prominent cyst formation in a 61-year-old woman. Sagittal T2-weighted image shows a large ovarian tumor (*arrows*), consisting of a solid component of heterogeneous low intensity anteriorly and a cystic component of multilocular appearance posteriorly

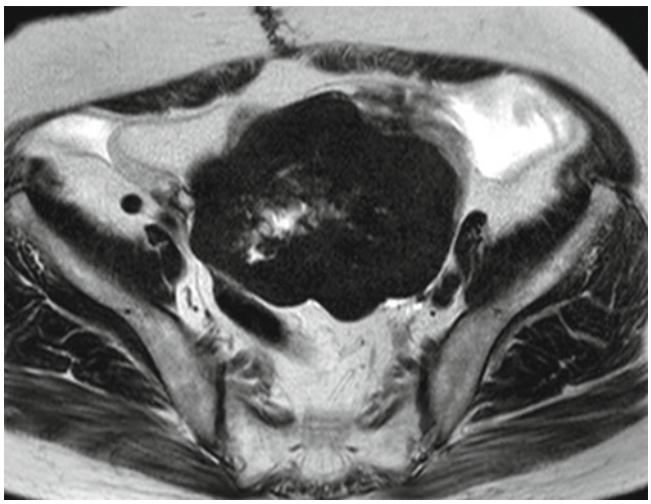

Fig. 10 Fibroma in a 77-year-old woman. Axial T2-weighted image shows a lobular mass of distinct low intensity and central area of increased intensity representing edematous degeneration

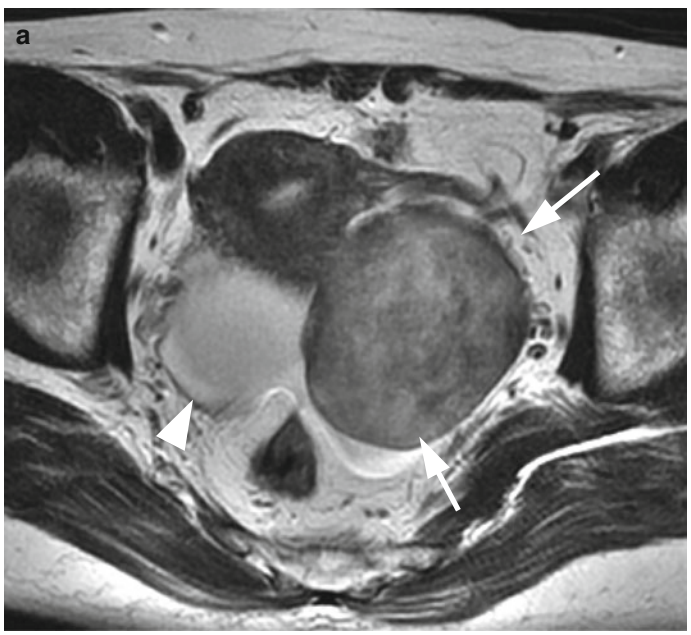

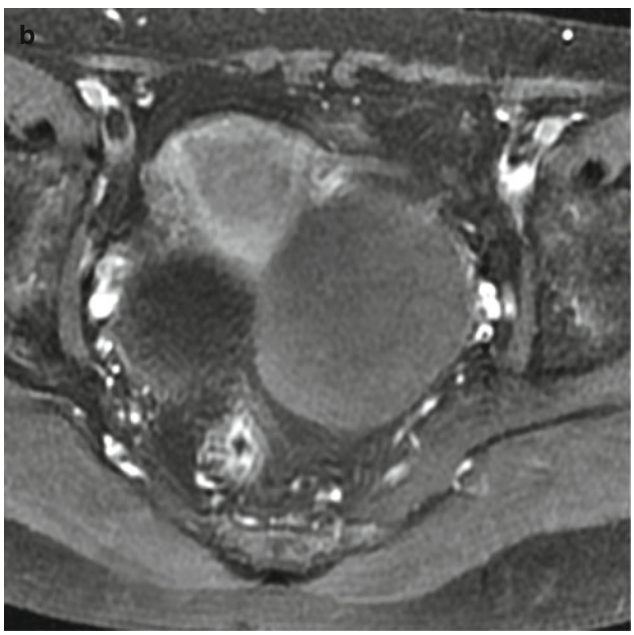

Fig. 9 Thecoma in a 59-year-old woman. (**a**) Axial T2-weighted images show a well-demarcated solid tumor of intermediate intensity in her left ovary (*arrows*). Note that the uterus is enlarged for this age of the patient, and the junctional zone (subendometrial band of low intensity) can be clearly identified. The right ovary has a simultaneous serous cystadenoma (*arrowhead*). (**b**) Post-contrast T1-weighted image with fat suppression shows less enhancement in the left ovarian tumor, compared to the uterine myometrium

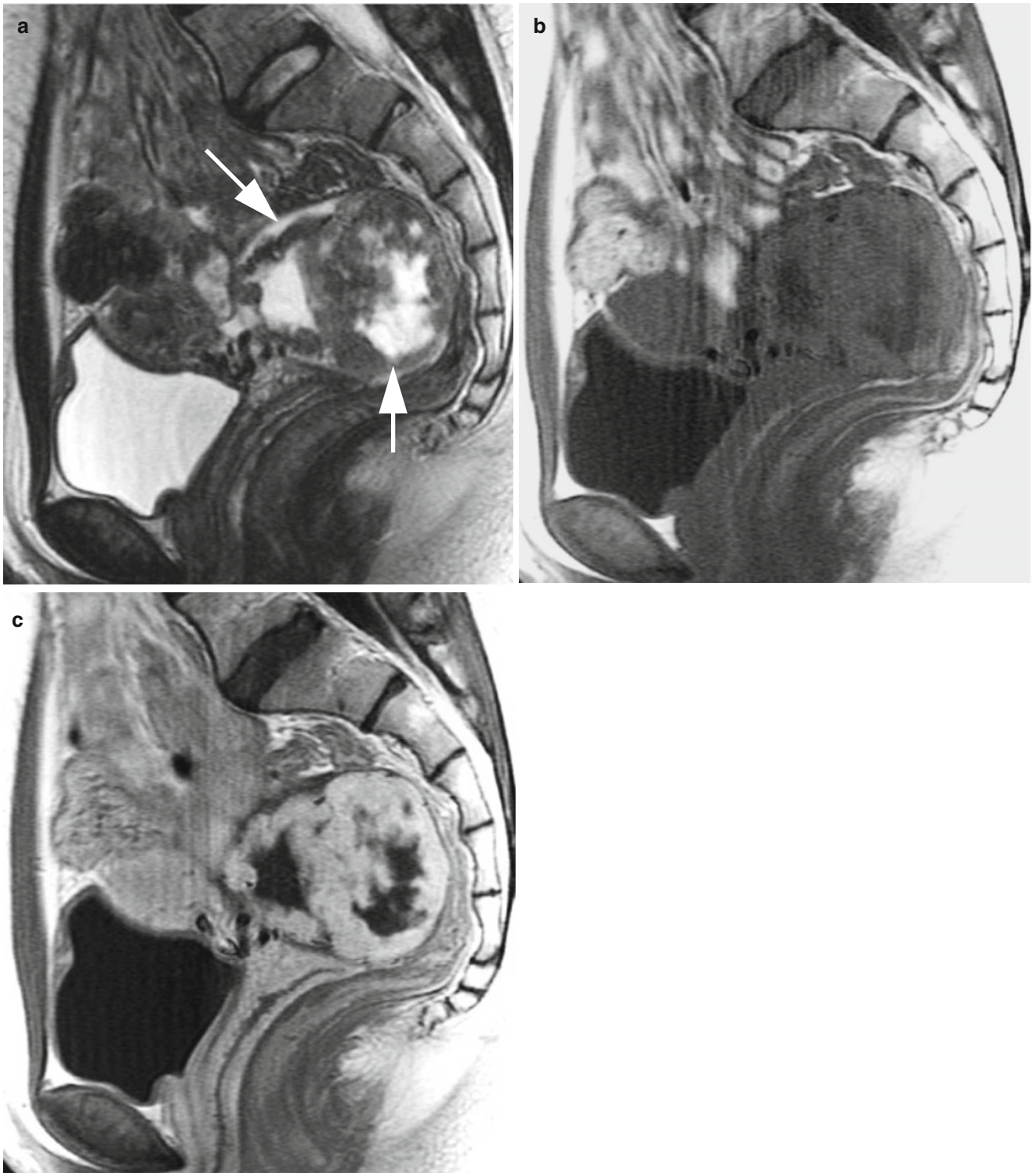

Fig. 11 Sclerosing stromal tumor in a 20-year-old woman. (**a**) Sagittal T2-weighted image shows a mass of heterogeneous low intensity (*arrows*), containing ill-defined central areas of high intensity. (**b**) T2-weighted image reveals the lesion consisting of high and low intensity. (**c**) Post-contrast T1-weighted image shows well enhancement in the areas corresponding to low intensity areas on T2-weighted image

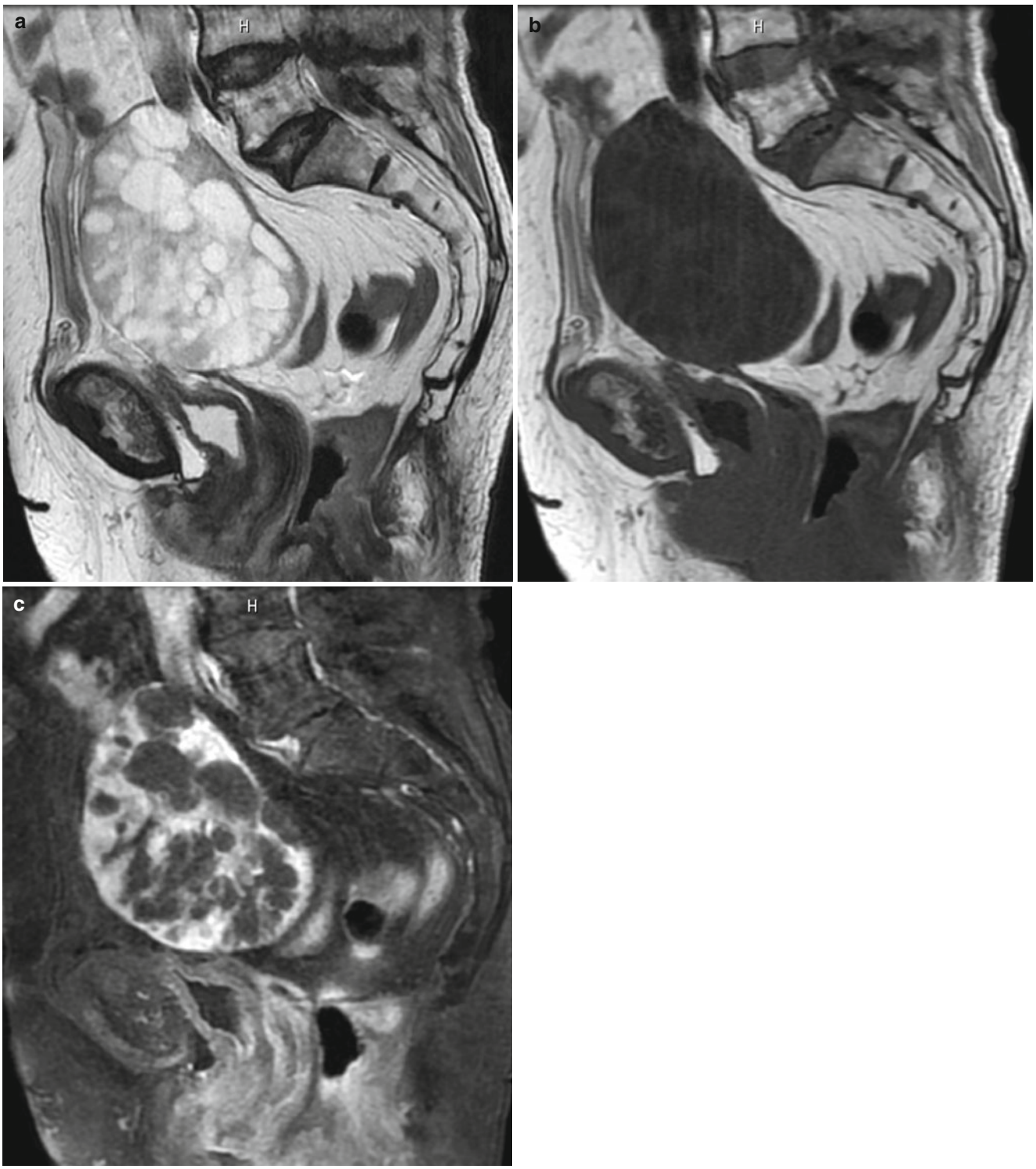

Fig. 12 Sertoli-Leydig cell tumor in an 86-year-old woman. (**a**) Sagittal T2-weighted image shows a solid mass of intermediate intensity, containing multiple cystic foci of bright intensity. (**b**) T1-weighted image shows decreased signal corresponding to the cystic components. (**c**) Contrast-enhanced T1-weighted images with fat suppression show marked enhancement in the solid components

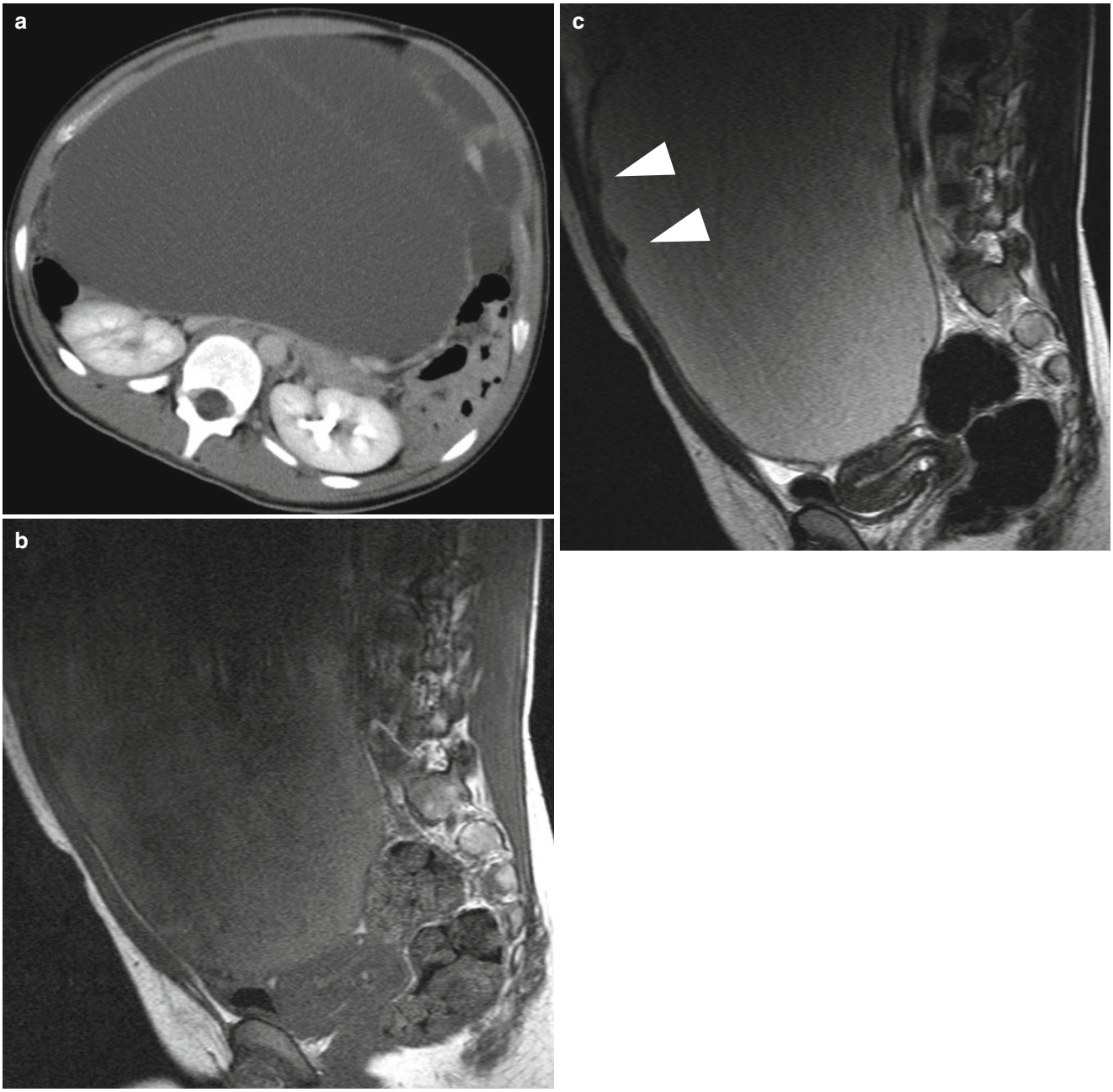

Fig. 13 Sertoli-Leydig cell tumor in a 14-year-old girl who presented with rapidly deteriorating abdominal fullness and anemia. (**a**) Contrast-enhanced CT at the level of the kidney shows a huge multilocular cystic tumor, containing irregularly thickened septi. (**b**) Sagittal T1-weighted image shows a cystic mass of increased intensity. (**c**) T2-weighted image shows cyst of high intensity and irregular-shaped mural nodules of decreased signal intensity in the anterior wall (*arrowheads*)

Acknowledgement I would like to acknowledge Dr. Kazuhiro Yamamoto, Dept. of Radiology, Osaka Medical College, for providing me a precious case of juvenile granulosa cell tumor; Dr. Ken Tamai, Kuzuha Diagnostic Imaging Clinic, for his great help in searching many cases; and Dr. Sayo Otani, Dr. Maya Honda, and Dr. Sonoko Oshima in Dept. of Diagnostic Radiology, Osaka Red Cross Hospital, for their kind advices for preparing the manuscript.

References

1. Malmstrom H, et al. Granulosa cell tumors of the ovary: prognostic factors and outcome. Gynecol Oncol. 1994;52(1):50–5.
2. Brown J, et al. Patterns of metastasis in sex cord-stromal tumors of the ovary: can routine staging lymphadenectomy be omitted? Gynecol Oncol. 2009;113(1):86–90.
3. Thrall MM, et al. Patterns of spread and recurrence of sex cord-stromal tumors of the ovary. Gynecol Oncol. 2011;122(2):242–5.
4. Stenwig JT, Hazekamp JT, Beecham JB. Granulosa cell tumors of the ovary. A clinicopathological study of 118 cases with long-term follow-up. Gynecol Oncol. 1979;7(2):136–52.
5. Fox H, Agrawal K, Langley FA. A clinicopathologic study of 92 cases of granulosa cell tumor of the ovary with special reference to the factors influencing prognosis. Cancer. 1975;35(1):231–41.
6. Tanaka Y, et al. Ovarian juvenile granulosa cell tumor associated with Maffucci's syndrome. Am J Clin Pathol. 1992;97(4):523–7.
7. Leyva-Carmona M, Vazquez-Lopez MA, Lendinez-Molinos F. Ovarian juvenile granulosa cell tumors in infants. J Pediatr Hematol Oncol. 2009;31(4):304–6.
8. Outwater EK, et al. Sex cord-stromal and steroid cell tumors of the ovary. Radiographics. 1998;18(6):1523–46.
9. Evans 3rd AT, et al. Clinicopathologic review of 118 granulosa and 82 theca cell tumors. Obstet Gynecol. 1980;55(2):231–8.
10. Fujimoto T, et al. Histopathological prognostic factors of adult granulosa cell tumors of the ovary. Acta Obstet Gynecol Scand. 2001;80(11):1069–74.
11. Young RH, Dickersin GR, Scully RE. Juvenile granulosa cell tumor of the ovary. A clinicopathological analysis of 125 cases. Am J Surg Pathol. 1984;8(8):575–96.
12. Morikawa K, et al. Granulosa cell tumor of the ovary: MR findings. J Comput Assist Tomogr. 1997;21(6):1001–4.
13. Kitamura Y, et al. MR imaging of juvenile granulosa cell tumour of the ovary: a case report. Pediatr Radiol. 2000;30(5):360.
14. Bjorkholm E, Silfversward C. Theca-cell tumors. Clinical features and prognosis. Acta Radiol Oncol. 1980;19(4):241–4.
15. Bierman SM, Reuter KL, Hunter RE. Meigs syndrome and ovarian fibroma: CT findings. J Comput Assist Tomogr. 1990;14(5):833–4.
16. Nemeth AJ, Patel SK. Meigs syndrome revisited. J Thorac Imaging. 2003;18(2):100–3.
17. Samanth KK, Black 3rd WC. Benign ovarian stromal tumors associated with free peritoneal fluid. Am J Obstet Gynecol. 1970;107(4):538–45.
18. Outwater EK, et al. Ovarian fibromas and cystadenofibromas: MRI features of the fibrous component. J Magn Reson Imaging. 1997;7(3):465–71.
19. Gorlin RJ. Nevoid basal-cell carcinoma syndrome. Medicine (Baltimore). 1987;66(2):98–113.
20. Clendenning WE, Block JB, Radde IG. Basal cell nevus syndrome. Arch Dermatol. 1964;90:38–53.
21. Seracchioli R, et al. Conservative treatment of recurrent ovarian fibromas in a young patient affected by Gorlin syndrome. Hum Reprod. 2001;16(6):1261–3.
22. Young RH, Scully RE. Sex-cord stromal tumor, steroid cell, and other ovarian tumors with endocrine, paraendocrine, and paraneoplastic manifestations. In: Kurman RJ, editor. Blaustein's pathology of the female genital tract. New York: Springer; 1994. p. 783–847.
23. Troiano RN, et al. Fibroma and fibrothecoma of the ovary: MR imaging findings. Radiology. 1997;204(3):795–8.
24. Shinagare AB, et al. MRI features of ovarian fibroma and fibrothecoma with histopathologic correlation. AJR Am J Roentgenol. 2012;198(3):W296–303.
25. Chalvardjian A, Scully RE. Sclerosing stromal tumors of the ovary. Cancer. 1973;31(3):664–70.
26. Young RH, Scully RE. Ovarian sex cord-stromal tumors. Problems in differential diagnosis. Pathol Annu. 1988;23 Pt 1:237–96.
27. Martinelli G, et al. Sclerosing stromal tumor of the ovary. A hormonal, histochemical and ultrastructural study. Virchows Arch A Pathol Anat Histopathol. 1983;402(2):155–61.
28. Duska LR, Flynn C, Goodman A. Masculinizing sclerosing stromal cell tumor in pregnancy: report of a case and review of the literature. Eur J Gynaecol Oncol. 1998;19(5):441–3.
29. Huang SC, et al. Ascites and elevated androgen level in a pregnant patient with an ovarian sclerosing stromal tumor. J Formos Med Assoc. 2003;102(2):124–6.
30. Ihara N, et al. Sclerosing stromal tumor of the ovary: MRI. J Comput Assist Tomogr. 1999;23(4):555–7.
31. Joja I, et al. Sclerosing stromal tumor of the ovary: US, MR, and dynamic MR findings. J Comput Assist Tomogr. 2001;25(2):201–6.
32. Matsubayashi R, et al. Sclerosing stromal tumor of the ovary: radiologic findings. Eur Radiol. 1999;9(7):1335–8.
33. Young RH, Scully RE. Ovarian Sertoli-Leydig cell tumors. A clinicopathological analysis of 207 cases. Am J Surg Pathol. 1985;9(8):543–69.
34. Yanushpolsky EH, Brown DL, Smith BL. Localization of small ovarian Sertoli-Leydig cell tumors by transvaginal sonography with color Doppler. Ultrasound Obstet Gynecol. 1995;5(2):133–5.
35. Roth LM, et al. Sertoli-Leydig cell tumors: a clinicopathologic study of 34 cases. Cancer. 1981;48(1):187–97.
36. Young RH, Scully RE. Sex cord-stromal, steroid cell, and other ovarian tumors with endocrine, paraendocrine, and paraneoplastic manifestations. In: Kurman RJ, editor. Blaustein's pathology of the female genital tract. 5th ed. Berlin/Heiderberg/New York: Springer; 2002. p. 905–66.
37. Gee DC, Russell P. The pathological assessment of ovarian neoplasms. IV: The sex cord-stromal tumours. Pathology. 1981;13(2):235–55.
38. Chen VW, et al. Pathology and classification of ovarian tumors. Cancer. 2003;97(10 Suppl):2631–42.
39. Prat J, Young RH, Scully RE. Ovarian Sertoli-Leydig cell tumors with heterologous elements. II. Cartilage and skeletal muscle: a clinicopathologic analysis of twelve cases. Cancer. 1982;50(11):2465–75.
40. Scully RE, Young RH, Clement PB. Tumors of the ovary, maldeveloped gonads, fallopian tube, and broad ligament. In: Rosai J, editor. Atlas of tumor pathology, fact 23, ser 3. AFIP (Armed Forces Institute of Pathology); Washington, D.C.:1996.
41. Fox H. Pathologic prognostic factors in early stage adult-type granulosa cell tumors of the ovary. Int J Gynecol Cancer. 2003;13(1):1–4.

Ovarian Teratomas: Clinical Setting and Ultrasound Findings

Tom Holland and Davor Jurkovic

Abstract

Teratomas belong to the group of ovarian tumours called germ cell tumours. Teratomas contain all three germinal layers: endoderm, mesoderm and ectoderm. They are mostly benign but can be malignant. The benign variety is the most common persistent tumours of the ovary and often contains dermal tissues giving rise to hair- and sebum-containing cysts, hence the common name for them: dermoid cysts.

Transvaginal ultrasonography has an established role in the evaluation of adnexal masses and provides an accurate assessment of ovarian morphology. It is also well known that dermoid cysts have distinct sonographic grayscale morphological features, which can be used to accurately diagnose dermoid cysts.

This chapter will cover the pathology and ultrasound appearance of the more common teratomas: mature cystic teratomas, immature teratomas and struma ovarii. The rare teratomas such as primary carcinoid and strumal carcinoid are so unusual as to be outside the scope of this chapter.

Keywords

Ovarian teratomas • Mature cystic teratoma • Immature teratoma • Imaging • Ultrasound

Introduction

Teratomas belong to the group of ovarian tumours called germ cell tumours. Teratomas contain all three germinal layers: endoderm, mesoderm and ectoderm. They are mostly benign but can be malignant. The benign variety is the most common persistent tumours of the ovary and often contains dermal tissues giving rise to hair- and sebum-containing cysts, hence the common name for them: dermoid cysts.

This chapter will cover the pathology and ultrasound appearance of the more common teratomas: mature cystic teratomas, immature teratomas and struma ovarii. The rare teratomas such as primary carcinoid and strumal carcinoid are so unusual as to be outside the scope of this chapter.

Mature Cystic Teratomas

Epidemiology

Mature cystic teratomas of the ovary are the most common persistent benign tumours of the ovary accounting for 44 % of all excised ovarian neoplasms [17] and 36 % of excised adnexal tumours in a population of pregnant women undergoing 11–14-week pregnancy scan [39]. They constitute 95 % of all excised germ cell tumours [11]. Prevalence in the general population is uncertain as many small mature cystic

T. Holland • D. Jurkovic (✉)
Department of Obstetrics and Gynaecology,
Gynaecology Diagnostic and Outpatient Treatment Unit,
University College Hospital, London, UK
e-mail: davor.jurkovic@uclh.nhs.uk

L. Saba et al. (eds.), *Ovarian Neoplasm Imaging*,
DOI 10.1007/978-1-4614-8633-6_10,

teratomas are likely to remain asymptomatic and therefore never diagnosed or excised.

Pathogenesis

Mature cystic teratomas are parthenogenic tumours [20] derived from postmyotic germ cells [36] and in theory can display practically all the mature tissues present in the adult, sometimes with an organoid character [11]. Commonly, the cysts are lined by epidermis, accompanied by its appendages, and contain usually one or more other adult-type tissues. The term 'dermoid cyst' is now in common usage for mature cystic teratomas but should strictly only be applied to cysts composed exclusively of skin (epidermal) and related structures. Very few mature teratomas have a solid macroscopic appearance and these are not within the scope of this chapter.

Clinical Presentation

These tumours can present at any age from newborns to the very elderly but most present in women of childbearing age [9, 21]. The traditional clinical presentation was either with pain, with or without torsion, or from the pressure effects of large cysts (Figs. 1 and 2). Cyst rupture is rare and can cause significant pain, and peritonitis and may result in widespread peritoneal granulomatosis [28] that can mimic carcinomatosis or tuberculosis. Many small mature cystic teratomas (MCTs) are asymptomatic, and the increasing availability of high-quality ultrasound scanning, especially in pregnancy, has led to more asymptomatic teratomas being detected [39]. Many are found at laparotomy or laparoscopy for an unrelated indication such as Caesarean section or tubal ligation.

Management and Prognosis

As these tumours are by definition benign, their prognosis is very good.

Traditional practice recommends removal on the grounds that this prevents torsion and malignant transformation. However, many small MCTs found incidentally on transvaginal ultrasound can be managed conservatively and if slow growing are unlikely to cause clinical symptoms [6, 7, 12]. Factors which increase the likelihood of women managed expectantly then choosing to have surgery include multiparity, young age, larger cysts, bilateral cysts and past history of ovarian cyst [12]. Larger symptomatic cysts may need excision by the open or laparoscopic route. If predominantly cystic, these cysts can usually be managed laparoscopically, but care needs to be taken to avoid spillage of the contents into the abdominal cavity as this can stimulate a peritonitic reaction [16]. The use of endoscopic retrieval bags can help to minimise this. As small asymptomatic cysts are being found with increasing frequency, these are increasingly being managed conservatively with success [6, 7] (Fig. 3).

Macroscopic Examination

MCT is bilateral in between 10 and 15 % of cases [1]. Multiple teratomas are seen in the ipsilateral ovary in less than 1 % of cases [10]. The tumours are round or ovoid and range in size from 1 to 30 cm, but most are within the 5–10 cm diameter range [25]. They have thick white capsules, which are usually free of adhesions. They are usually

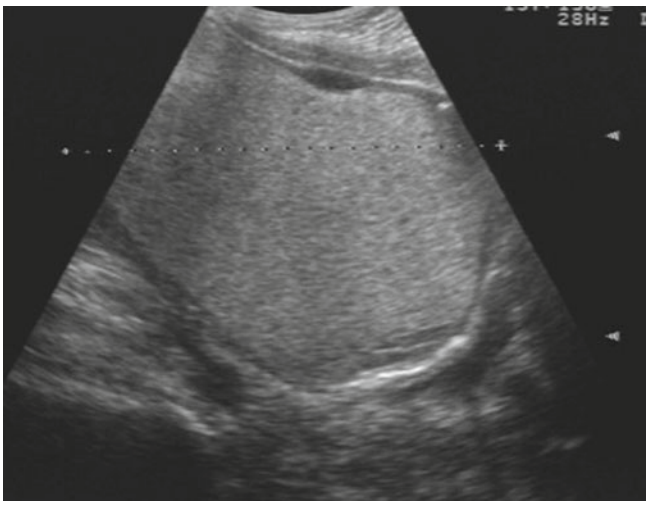

Fig. 1 A large cyst with predominantly hyperechoic contents

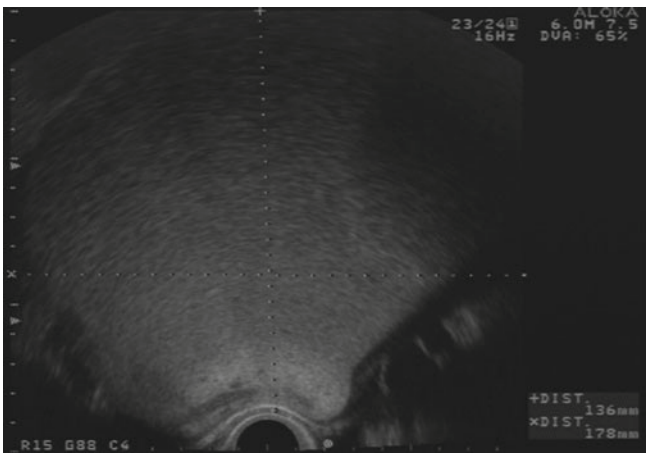

Fig. 2 A large cyst with predominantly hyperechoic contents

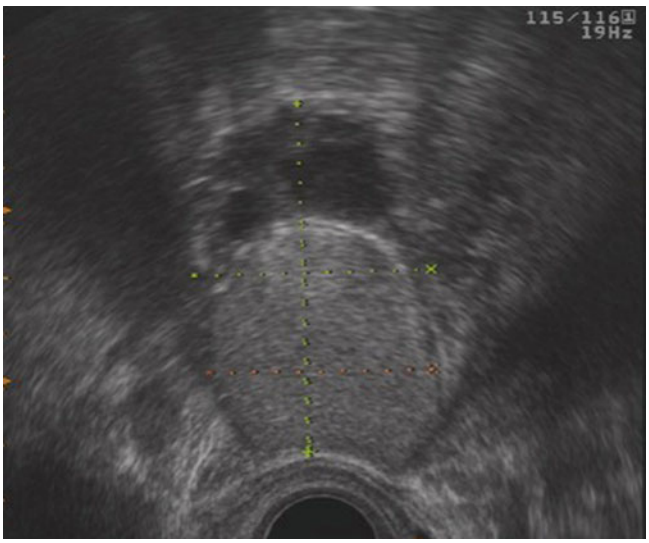

Fig. 3 A medium sized cyst with normal ovarian tissue

unilocular cysts filled with thick greasy sebaceous material and matted hair [25]. These sometimes round up to form sebum and hair balls (Figs. 4 and 5). The sebaceous contents have a fluid consistency above 35 °C which becomes doughy or solid at room temperature [11, 32]. Some cysts however are filled with predominantly mucoid or clear fluid. Most are unilocular, and between 5 and 10 % are multilocular. In 87 % of cases [11], a protuberance can be seen projecting into the cyst cavity called a dermoid protuberance (or Rokitansky tubercle/dermoid mamilla) [32]. The cyst lining is usually smooth like skin and the hair generally grows from this tubercle. Teeth are present in up to one third of cases. Other tissues commonly identified are cartilage, bone, brain and adipose tissue. Older lesions may exhibit marked dystrophic calcification [25]. Hemangiomas are unusual and give rise to highly vascular structures [11]. More organised structures such as intestine; skeletal parts, especially jaw bone; and eyes may be present [25] (Figs. 6 and 7).

Microscopy

Typically, the inner surface of the cyst is lined by epidermis which desquamates into the lumen [11]. Skin adnexal structures such as hair follicles and sebaceous and sweat glands are often present on the dermal papilla [25] and a large amount of mature tissues are usually found at and around this area [11]. Other ectodermal derivatives such as cerebrum, cerebellum, choroid plexus and retina may also be found [24]. The most common mesodermal derivatives are smooth or striated muscle, adipose tissue, bone, teeth and cartilage. Less common tissues are thyroid, peripheral nerve, respiratory and gastrointestinal epithelium, teeth and salivary gland [25].

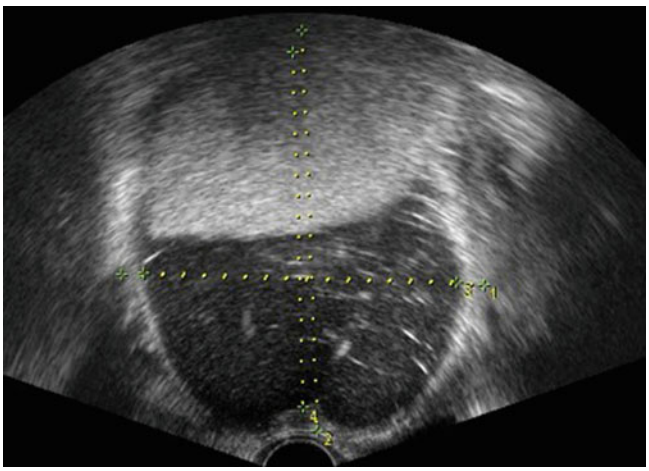

Fig. 4 Sebum, half low level echogenic fluid with "hair" flecks

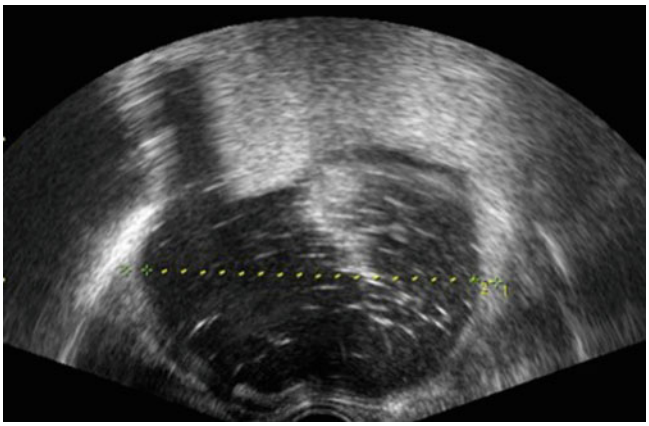

Fig. 5 Half sebum, half low level echogenic fluid with "hair" flecks

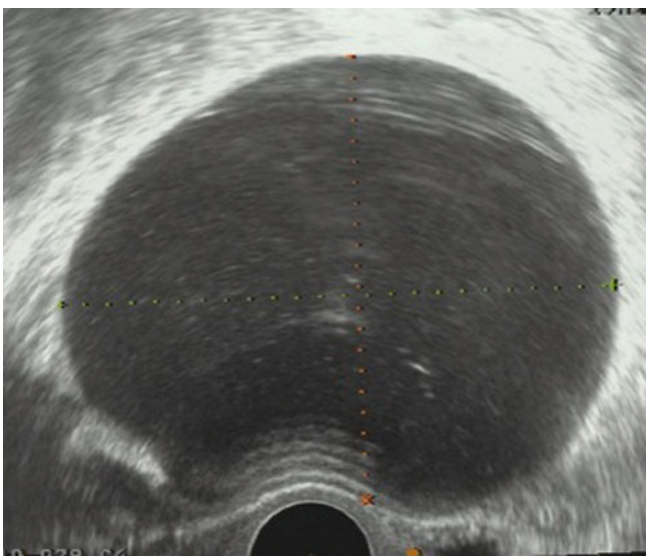

Fig. 6 Anechoic fluid with a few hair flecks but no sebum

Ultrasound Features of Mature Cystic Teratomas

Transvaginal ultrasonography has an established role in the evaluation of adnexal masses and provides an accurate assessment of ovarian morphology. It is also well known that dermoid cysts have distinct sonographic grayscale morphological features, which can be used to accurately diagnose dermoid cysts ('pattern recognition method') [14, 33–35] (Figs. 8 and 9).

Previous studies examining the ultrasound morphology of MCT have tried to analyse the appearance of the whole tumour. Laing et al. [18] in 1981 analysed 51 MCTs and found that '33 % of the cases demonstrated "typical" findings, i.e. "an echogenic focus with acoustic shadowing in a predominantly cystic mass", 23.5 % were predominantly solid, 20 % were almost entirely cystic, and 23.5 % were not visible' on ultrasound scan (Fig. 10). Bronshtein used an in vitro simulation with hair and oil in a glove and showed that this replicated the 'white ball' of dermoid very well. They also showed that hair in water can produce the same 'dot and dash' echo pattern seen in some dermoid cysts. Cohen [8] in 1993 and Caspi [5] in 1996 attempted to categorise the morphology of MCT into different groups based on the presence of acoustic shadowing and the amount of echogenic material within the cyst cavity. It is our opinion that this approach is rather complicated and that once individual features of hair or sebum are recognised, these alone are sufficient to make a diagnosis in the vast majority of MCT.

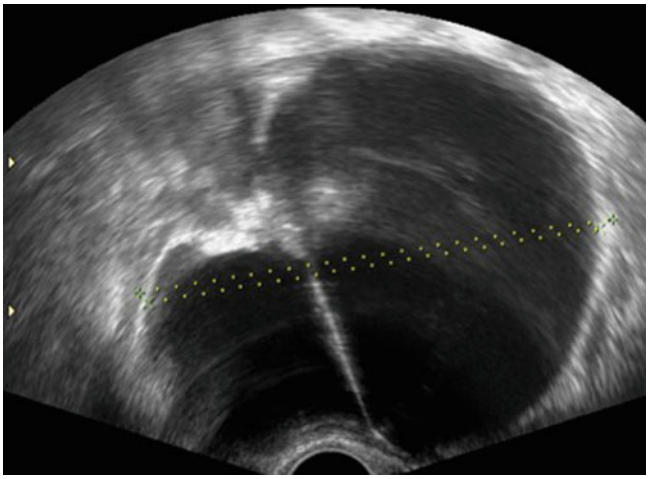

Fig. 7 Anechoic fluid with a single septum and hyperechoic tubercle

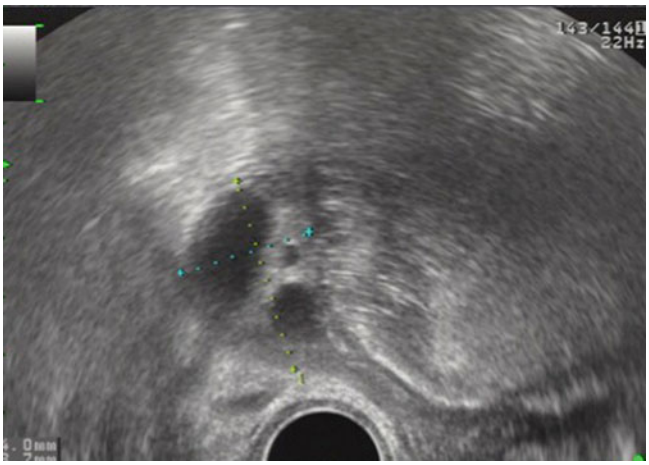

Fig. 8 Healthy ovarian tissue with follicles (The ovarian cresent sign)

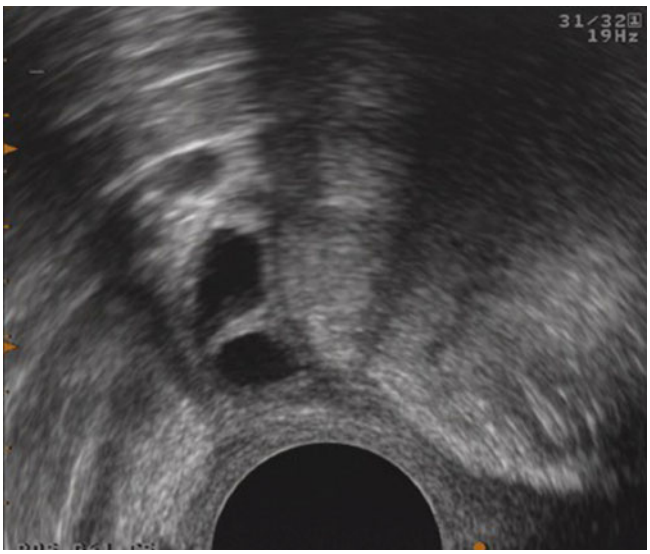

Fig. 9 Healthy ovarian tissue with follicles (The ovarian cresent sign)

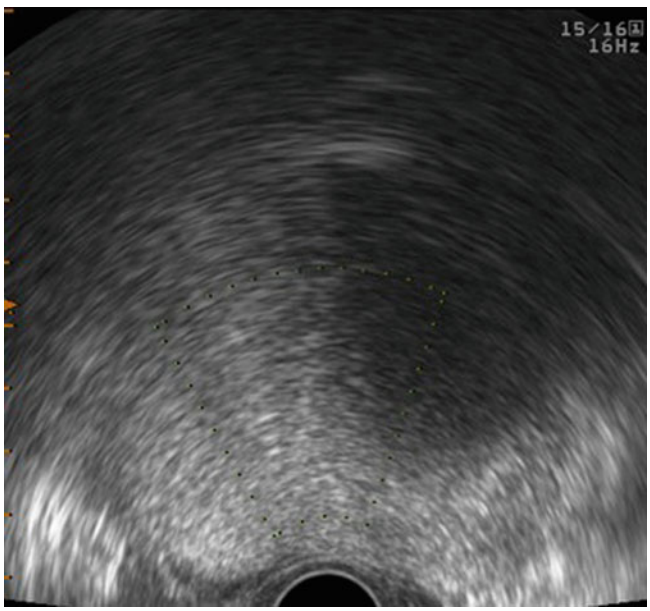

Fig. 10 Acoustic shadowing

Immature Teratomas

Immature teratomas, in common with the mature teratomas, contain tissues from the three germinal layers, but in contrast to mature teratomas, they contain immature or embryonal structures [31]. These tumours arise from postmitotic germ cells and contain immature (embryonal) structures as well as mature elements in most cases [13]. The additional presence of other malignant germ cell tumour elements places the tumour in the teratomas group, and these are excluded from this study. Pure immature teratomas are rare tumours which comprise <1 % of ovarian teratomas overall [15, 22, 31, 32, 37]. They represent 20 % of malignant germ cell tumours and approximately 1 % of malignant ovarian tumours [3] and account for up to 25 % of malignant ovarian tumours presenting in girls <17 years of age [4].

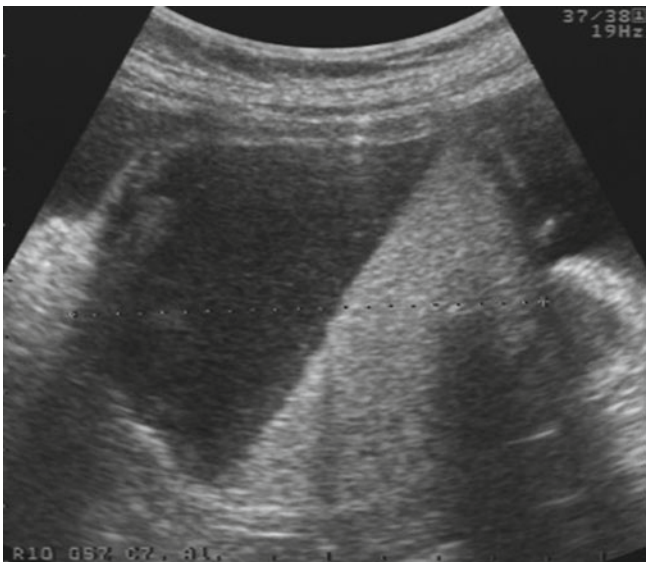

Fig. 11 Fluid level

Clinical Presentation

These tumours present between <1 and 58 years of age with median of 18–19.5 and a mean of 20.6 years [4, 19, 22, 23]. Most patients present with an abdominal mass (80 %), approximately half with pain and a quarter with bleeding irregularity (except in premenarchal patients) [22]. These tumours rarely present in pregnancy or as incidental findings in asymptomatic women. Raised α-fetoprotein levels may be present in 60 % of patients and raised β-HCG outside pregnancy may signal a mixed malignant germ cell tumour [15].

Prognosis and Management

The prognosis depends on grade of tumour in stage 1 and grade of metastasis in stage 2–4. Low-grade stage 1 tumours may be cured with excision alone and have a survival rate of 95 % if chemotherapy is used for recurrences [23]. Higher-grade and higher-stage tumours benefit from chemotherapy, and their survival rates have been reported as less than 82 %. Modern improved chemotherapy may offer improved survival rates. Management is with conservative fertility-sparing surgery for low-grade stage 1–2 tumours. In higher-grade stage 1 and 2 tumours and any grade stage 3 tumours, chemotherapy is recommended [25].

Macroscopic Features

These tumours are almost always unilateral unless they present with widespread disease [23], but in 5–10 % of patients, a contralateral mature cystic teratoma is present [23, 38]. Local spread is local peritoneal spread, spread to the omentum, etc., or via lymphatic spread to retroperitoneal, paraaortic, mesenteric and mediastinal nodes [23, 38]. ITs are large tumours presenting with a mean diameter of 16–20 cm and a range of 5–42 cm [23, 38] and a mean weight of 1,300 g (range 22–7, 150 g).

The tumours are predominantly solid although there are usually multiple small cysts of less than 1 cm in diameter present; however, occasional larger cysts may be present [25]. Some contain sebaceous material or hair, but most are degenerative in type and filled with clear mucoid or blood-stained fluid [25]. Solid areas with haemorrhage or necrosis are common and are important as these are more likely to contain the less well-differentiated tissues [4, 23, 25] (Fig. 11).

Microscopic Features

All three germinal layers are usually present, and the range of tissues includes all those that may be observed in mature cystic teratomas. The ectodermal and mesodermal components predominate, and it is in these areas that the immaturity is most clearly evident. The various tissues are admixed in a haphazard way, which contrasts with benign dermoid cysts, where the tissues are more organised. Neural tissue may be present and may mimic intracranial malignant tumours. Squamous epithelium may also be present and may show evidence of malignancy. Cartilage and bone may be present. Mesodermal elements show loose fibrous connective tissue which may resemble undifferentiated myxoid embryonic mesenchyme. Smooth—but not striated—muscle is quite common (Figs. 12 and 13).

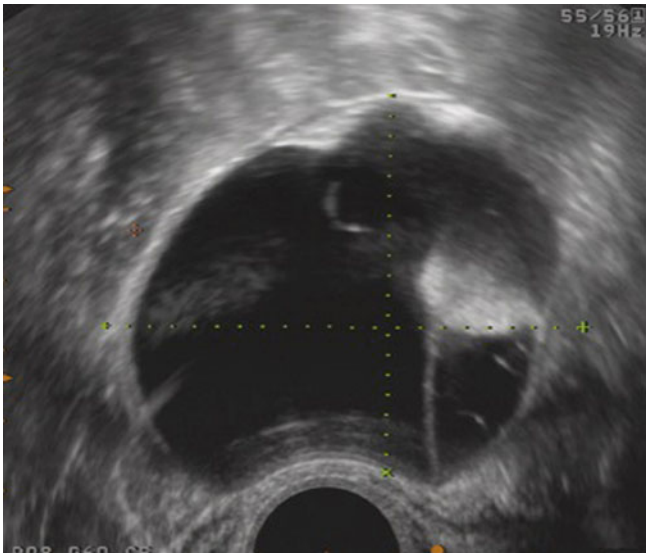

Fig. 12 White ball

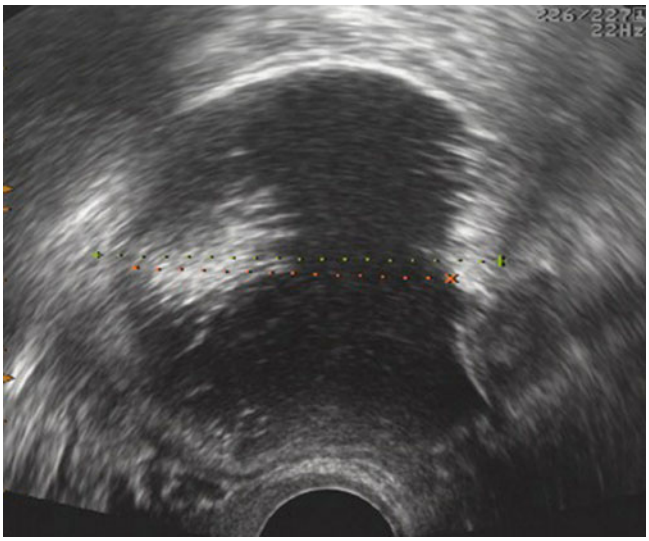

Fig. 13 White ball

Endodermal elements are less well represented than the above elements in most tumours. Tubules lined with non-specific columnar epithelium may be present, and the presence of bronchial or gastrointestinal epithelium may be rarely observed. About 70 % of ITs had evidence of necrosis or haemorrhage and almost all have mature elements [23].

Grading is important, as together with staging, this has a significant effect on prognosis and treatment. There are two grading systems in use. Robboy and Scully [26] proposed 4 grades (0–3) based on the relative amounts of immature and mature tissue, degree of differentiation and the mitotic activity within the immature components. The other system proposed by O'Connor and Norris [23] proposed low and high grades, corresponding to grade 1 and grades 2–3, respectively, in order to reduce intraobserver variability. Low-grade neoplasms contain less than one low-power field of immature neuroepithelium on any one microscopic section. In high-grade neoplasms, immature neuroepithelium is common and exceeds one low-power field of one or more microscopic sections.

Ultrasound Appearance

There have been no previous published descriptions of the preoperative ultrasound appearance of immature teratomas. Here, we present a few pictures of two cases we have seen which are in keeping with the previous macroscopic pathological descriptions of these tumours. Previous pathological descriptions have described the tumours as 'predominantly solid although there are usually multiple small cysts present of less than 1 cm in diameter, however occasional larger cysts may be present' [25]. These findings were found at ultrasound with all the tumours being predominantly solid or multilocular solid. 'Some contain sebaceous material or hair but most are degenerative in type and filled with clear mucoid or blood-stained fluid'. These findings were also found with the cystic areas containing fluids with differing echogenicities. In addition, hyperechoic flecks reminiscent of hair were seen throughout the solid areas (Figs. 14, 15, 16, and 17). When these morphological characteristics are present, a correct preoperative diagnosis may be possible.

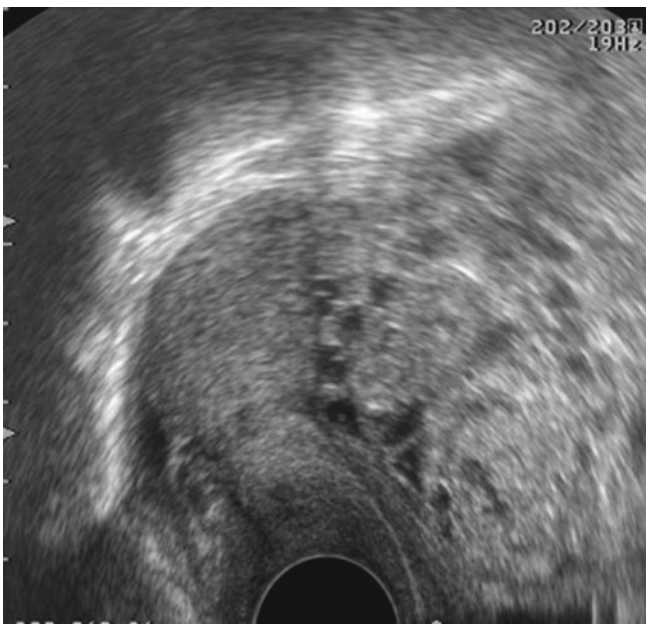

Fig. 14 Small uterus and tumour

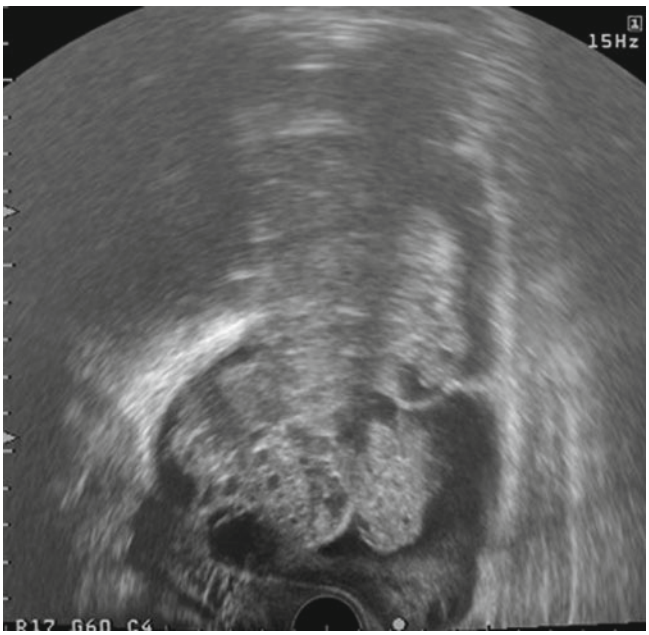

Fig. 15 Large irregular complex tumour

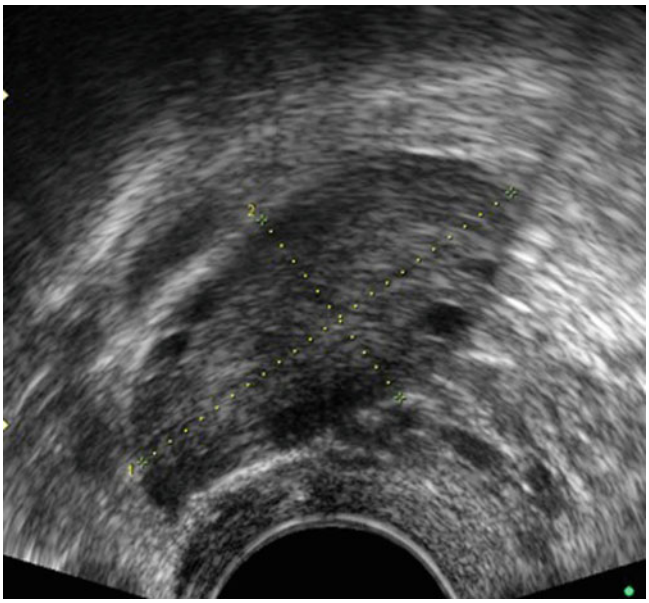

Fig. 16 Two years prior to presentation same ovary!

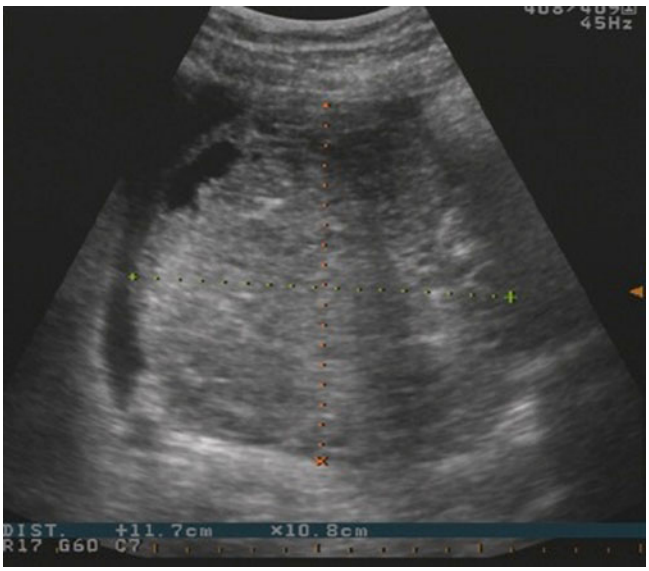

Fig. 17 Large irregular tumour with mixed echogenicity small cystic spaces.

Struma Ovarii

Background

Thyroid tissue can be found in up to 20 % of mature cystic teratomas on histopathological examination; however, macroscopically, it is only identified in 3 % of teratomas [29]. When ovarian teratomas are composed entirely or predominantly of thyroid tissue, they are called struma ovarii [32]. Keeping this definition, struma ovarii constitutes approximately 3 % of all ovarian teratomas and 2–4 % of all germ cell tumours of the ovary [2, 32]. It is thought that the thyroidal elements have overgrown the other tissues [29]. Malignant transformation is uncommon, only about 5 % of struma ovarii being malignant [2]. In many of the malignant cases, there is only a small focus of malignant tissue. Metastases are found in 5–6 % of patients with malignant struma ovarii [40]. Most patients with struma ovarii are in their reproductive years, but struma ovarii may be diagnosed at any age, even in children [32].

Microscopy

The thyroid tissue of struma ovarii is similar to the thyroid tissue consisting of colloid-containing follicles of various sizes lined by a single layer of follicular cells [25]. Occasionally, there is evidence of over- or underactivity [29, 32]. Other abnormal thyroidal histological appearances are sometimes present. The diagnosis of malignancy has previously been using the same criteria as thyroid tissue in the neck, but on long-term follow-up, even benign struma ovarii has been known to recur [27].

Macroscopy

Struma ovarii tumours are almost always unilateral, vary in size but usually measure less than 10 cm in diameter and may be associated with a mature cystic teratoma in the same

or contralateral ovary [25, 27]. The external wall of struma ovarii is usually smooth. Most cases of struma ovarii are solid tumours or cystic–solid tumours. The cystic spaces contain colloid or mucoid material. Occasionally, they are predominantly multilocular cystic. In most cystic cases of struma ovarii, there are solid protrusions into the cyst lumen. Macroscopic features which are likely to increase the risk of malignancy are the size of the strumal component, the presence and extent of adhesions, the presence of ascites and blood in the ascites [27].

Clinical Symptoms

Most cases of struma ovarii present in the reproductive years with a peak in the 40s [25]. Most patients are asymptomatic, but some patients complain of abdominal distension, pain, urinary or intestinal obstruction, infertility or hot flushes, the latter being explained by steroid hormone production [30]. Occasionally, patients present with ascites or with both ascites and pleural effusion (pseudo-Meigs' syndrome).

Prognosis

The incidence of malignancy in struma ovarii is rare and patients with benign struma ovarii are almost always cured by surgical removal of the tumour. If histological or clinical features of malignancy are present, the 10-year survival is 89 % and 25 years survival is 84 % [27]. If ascites and/or pleural effusion is present, they usually disappear after surgery.

Ultrasound Findings

The largest case series of the ultrasound features of struma ovarii (31 cases) showed that the size and sonographic appearance of benign pure struma ovarii are variable [30]. The majority of the tumours were large with a largest diameter ≥9.5 cm. Most cases of benign pure struma ovarii contained solid components, but cystic components were always present, and more than half of the masses were multilocular (>five cyst locules). The cyst fluid was almost always anechogenic or of low-level echogenicity. Almost half of the masses were perceived to have irregular internal cyst walls, and papillary projections were noted in 40 %. The colour content at Doppler examination varied, with most tumours (40 %) being moderately vascularised.

Pure struma ovarii had a significantly variable appearance, but the majority of the cystic tumours contain one or more well-circumscribed roundish solid areas with smooth contours, which the authors named 'struma pearls'. These were similar, but not identical, to the 'round white ball' seen in dermoid cysts. (Need to ask permission to use figures from the Savelli paper).

The size and sonographic appearance of impure struma ovarii were variable, but none of these tumours was associated with ascites or with fluid in the pouch of Douglas, and in all cases, no or only minimal vascularisation was detected on colour Doppler examination. Shadowing was present in 44 % [30].

Conclusions

Mature cystic teratomas have various appearances on ultrasound, which can be confusing for the less-experienced observers, but certain characteristics are very easily recognised and aid in the confidence diagnosis. Immature teratomas tend to be larger tumours, which present earlier and have a predominantly solid complex appearance. The appearance of these tumours is markedly different from the mature cystic teratomas. Struma ovarii has a very varied appearance and preoperative diagnosis is likely to cause difficulty.

Biography Mr Tom Holland is a senior trainee in obstetrics and gynaecology and is currently working in London, England. He is completing a Research Doctorate on the use of ultrasound and serum markers for the diagnosis of endometriosis. His research interests include ultrasound, ovarian tumours and endometriosis.

Davor Jurkovic is a Consultant Gynaecologist and Director of Gynaecology Diagnostic and Outpatient Treatment Unit at University College Hospital, London. He is an internationally recognised expert in gynaecological and early pregnancy ultrasound. He has published extensively on these topics and has edited five books. He has helped to develop and run the RCOG training programmes in gynaecological ultrasound, acute gynaecology and early pregnancy. He is also a founding member of the educational charity Focus on Gynaecology.

References

1. Ayhan A, Aksu T, Develioglu O, et al. Complications and bilaterality of mature ovarian teratomas (clinicopathological evaluation of 286 cases). Aust N Z J Obstet Gynaecol. 1991;31:83–5.
2. Ayhan A, Yanik F, Tuncer R, et al. Struma ovarii. Int J Gynaecol Obstet. 1993;42:143–6.
3. Berg J, Baylor S. The epidemiological pathology of ovarian cancer. Hum Pathol. 1973;4:537–47.
4. Breen JL, Neubecker RD. Ovarian malignancy in children, with special reference to the germ-cell tumors. Ann N Y Acad Sci. 1967;142:658–74.
5. Caspi B, Appelman Z, Rabinerson D, et al. Pathognomonic echo patterns of benign cystic teratomas of the ovary: classification, incidence and accuracy rate of sonographic diagnosis. Ultrasound Obstet Gynecol. 1996;7:275–9.
6. Caspi B, Appelman Z, Rabinerson D, et al. The growth pattern of ovarian dermoid cysts: a prospective study in premenopausal and postmenopausal women. Fertil Steril. 1997;68:501–5.
7. Caspi B, Levi R, Appelman Z, et al. Conservative management of ovarian cystic teratoma during pregnancy and labor. Am J Obstet Gynecol. 2000;182:503–5.
8. Cohen L, Sabbagha R. Echo patterns of benign cystic teratomas by transvaginal ultrasound. Ultrasound Obstet Gynecol. 1993;3:120–3.
9. Comerci JT, Licciardi F, Bergh PA, et al. Mature cystic teratoma: a clinicopathologic evaluation of 517 cases and review of the literature. Obstet Gynecol. 1994;84:22–8.
10. Damewood M, Rosenshein NB, Woodruff JD. Multiple benign cystic teratomas of the ovary. Report of two cases and review of the literature. Diagn Gynecol Obstet. 1982;4:243–5.
11. Fox H, Wells M. Germ cell tumours of the ovary. In: Obstetrical and gynaecological pathology. New York: Churchill Livingstone; 2002.
12. Hoo W, Yazbek J, Holland T, et al. Expectant management of ultrasonically diagnosed ovarian dermoid cysts: is it possible to predict the outcome? Ultrasound Obstet Gynecol. 2010;36:235–40.
13. Inoue M. Histogenetic analysis of ovarian germ cell tumours by DNA fingerprinting. Cancer Res. 1992;52:6823–6.
14. Jermy K, Luise C, Bourne T. The characterization of common ovarian cysts in premenopausal women. Ultrasound Obstet Gynecol. 2001;17:140–4.
15. Kawai M, Kano T, Furuhashi Y, et al. Immature teratoma of the ovary. Gynecol Oncol. 1991;40:133–7.
16. Kondo W, Bourdel N, Cotte B, et al. Does prevention of intraperitoneal spillage when removing a dermoid cyst prevent granulomatous peritonitis? BJOG. 2010;117:1027–30.
17. Koonings PP, Campbell K, Mishell DR, et al. Relative frequency of primary ovarian neoplasms: a 10-year review. Obstet Gynecol. 1989;74:921–6.
18. Laing FC, Van Dalsem VF, Marks WM, et al. Dermoid cysts of the ovary: their ultrasonographic appearances. Obstet Gynecol. 1981;57:99–104.
19. Li H, Hong W, Zhang R, et al. Retrospective analysis of 67 consecutive cases of pure ovarian immature teratoma. Chin Med J (Engl). 2002;115:1496–500.
20. Linder D, McCaw BK, Hecht F. Parthenogenic origin of benign ovarian teratomas. N Engl J Med. 1975;292:63–6.
21. Malkasian GD, Dockerty MB, Symmonds RE. Benign cystic teratomas. Obstet Gynecol. 1967;29:719–25.
22. Norris HJ, Zirkin HJ, Benson WL. Immature (malignant) teratoma of the ovary: a clinical and pathologic study of 58 cases. Cancer. 1976;37:2359–72.
23. O'Connor DM, Norris HJ. The influence of grade on the outcome of stage I ovarian immature (malignant) teratomas and the reproducibility of grading. Int J Gynecol Pathol. 1994;13:283–9.
24. Prat J. Pathology of the ovary. Philadelphia: W B Saunders Co.; 2004.
25. Robboy SJ, Anderson MC, Russell P. Pathology of the female reproductive tract. In: Robboy SJ, Anderson MC, Russell P, editors. 2nd edition. 2008 published by Churchill Livingstone. ISBN: 0443074771
26. Robboy SJ, Scully RE. Ovarian teratoma with glial implants on the peritoneum. An analysis of 12 cases. Hum Pathol. 1970;1:643–53.
27. Robboy SJ, Shaco-Levy R, Peng RY, et al. Malignant struma ovarii: an analysis of 88 cases, including 27 with extraovarian spread. Int J Gynecol Pathol. 2009;28:405–22.
28. Roman H, Accoceberry M, Bolandard F, et al. Laparoscopic management of a ruptured benign dermoid cyst during advanced pregnancy. J Minim Invasive Gynecol. 2005;12:377–8.
29. Roth LM, Talerman A. The enigma of struma ovarii. Pathology. 2007;39:139–46.
30. Savelli L, Testa AC, Timmerman D, et al. Imaging of gynecological disease (4): clinical and ultrasound characteristics of struma ovarii. Ultrasound Obstet Gynecol. 2008;32:210–9.

31. Talerman A. Chapter 18: Pathology of the ovaries in diagnosis and management of ovarian disorders. Albert Altchek, editor. Academic Press; 2003.
32. Talerman A. Chapter 20: Germ cell tumours of the ovary. In: Blaustein's pathology of the female genital tract. New York: Springer; 2002.
33. Valentin L. Prospective cross-validation of Doppler ultrasound examination and gray-scale ultrasound imaging for discrimination of benign and malignant pelvic masses. Ultrasound Obstet Gynecol. 1999;14:273–83.
34. Valentin L. Pattern recognition of pelvic masses by gray-scale ultrasound imaging: the contribution of Doppler ultrasound. Ultrasound Obstet Gynecol. 1999;14:338–47.
35. Valentin L. Use of morphology to characterize and manage common adnexal masses. Best Pract Res Clin Obstet Gynaecol. 2004;18:71–89.
36. Vortmeyer AO, Devouassoux-Shisheboran M, Li G, et al. Microdissection-based analysis of mature ovarian teratoma. Am J Pathol. 1999;154:987–91.
37. Wisniewski M, Deppisch LM. Solid teratomas of the ovary. Cancer. 1973;32:440–6.
38. Yanai-Inbar I, Scully RE. Relation of ovarian dermoid cysts and immature teratomas: an analysis of 350 cases of immature teratoma and 10 cases of dermoid cyst with microscopic foci of immature tissue. Int J Gynecol Pathol. 1987;6:203–12.
39. Yazbek J, Salim R, Woelfer B, et al. The value of ultrasound visualization of the ovaries during the routine 11–14 weeks nuchal translucency scan. Eur J Obstet Gynecol Reprod Biol. 2006;132:154–8.
40. Zakhem A, Aftimos G, Kreidy R, et al. Malignant struma ovarii: report of two cases and selected review of the literature. J Surg Oncol. 1990;43:61–5.

CT and MR of Benign Ovarian Germ Cell Tumours

Ingrid Millet, H. Perrochia, E. Pages-Bouic,
F. Curros-Doyon, G. Rathat, and P. Taourel

Abstract

Up to a quarter of ovarian masses originate from germ cells. Germ cell tumours occur at a higher frequency than epithelial tumours in Oriental and African populations. Mature cystic teratomas (MCTs), or the so-called dermoid cysts because of the overall predominance of skin elements, are not only the most common germ cell tumours but also the most common benign ovarian neoplasms in women under 45 years old. This chapter will cover CT and MR appearance of the more common teratomas: mature cystic teratomas; immature teratomas and struma ovarii.

Keywords

Ovarian teratomas • Mature cystic teratoma • Immature teratoma • Imaging • Computed tomography • Magnetic resonance

Mature Cystic Teratoma (MCT)

Epidemiology

Up to a quarter of ovarian masses originate from germ cells [1]. Germ cell tumours occur at a higher frequency than epithelial tumours in Oriental and African populations [2].

I. Millet, MD (✉) • E. Pages-Bouic • F. Curros-Doyon • P. Taourel
Department of Medical Imaging,
Centre Hospitalier Universitaire Lapeyronie,
191 avenue du Doyen Gaston Giraud,
Montpellier 34295, France
e-mail: i-millet@chu-montpellier.fr

H. Perrochia
Department of Pathology,
Centre Hospitalier Universitaire Lapeyronie,
191 avenue du Doyen Gaston Giraud,
Montpellier 34295, France

G. Rathat
Department of Gynaecologic Surgery,
Centre Hospitalier Universitaire Arnaud de Villeneuve,
191 avenue du Doyen Gaston Giraud,
Montpellier 34295, France

Mature cystic teratomas (MCTs), or the so-called dermoid cysts because of the overall predominance of skin elements, are not only the most common germ cell tumours but also the most common benign ovarian neoplasms in women under 45 years old. When MCTs were first described 300 years ago, people believed them to be small babies, and one of the greatest concerns at that time was whether they should be baptised [3]. They are part of a subclass of ovarian germ cell tumours that are believed to arise from primordial germ cells. In its pure form, mature cystic teratomas are always benign. Secondary development of malignancy is a rare but well-known phenomenon [4].

MCTs account for 20 % of all ovarian tumours in adults and 50 % of all ovarian tumours in children. Their reported incidence is 1.2–14.2 cases per 100,000 people per year [5, 6], with the incidence peaking between 20 and 40 years old [7]. They affect a younger age group (mean patient age, 30 years) than epithelial ovarian neoplasms [8].

MCTs are often asymptomatic at presentation, discovered incidentally at routine pelvic examination. When symptomatic, abdominal pain and fullness are the most common symptoms, related only to the weight of the mass

L. Saba et al. (eds.), *Ovarian Neoplasm Imaging*,
DOI 10.1007/978-1-4614-8633-6_11,

itself or to a complication. Growth of a teratoma during pregnancy is an uncommon condition but has already been reported [9].

Surgical excision by laparoscopy is the treatment of choice for MCT [10]. However, as MCTs are reported to grow slowly at an average rate of 1.8 mm per year, some investigators advocate nonsurgical management of smaller (<6 cm) tumours [11].

Histology

MCTs belong to a germ cell tumour group and are composed of well-differentiated tissues derived from three pluripotential germ cell layers: ectoderm (skin derivates and neural tissue), mesoderm (fat, bone, cartilage, muscle) and endoderm (gastrointestinal and bronchial epithelium, thyroid tissue) [12]. Most ovarian MCTs contain a variable amount of sebaceous material, hair and desquamated debris. A wide variety of rare histological tissues may be found, including renal, adrenal and prostatic tissues [13].

A large recent population-based study in England indicated that the observed age–incidence patterns suggested a common initiation of germ cell tumours in embryonic/fetal life, with variable rates of tumour progression as a result of subsequent events that may be site specific. The authors concluded that future genetic studies should consider germ cell tumours from all sites to gain greater insight into their aetiology [14].

In a gross pathologic examination, mature cystic teratomas typically appear like unilocular cystic tumours filled with sebaceous material, which is liquid at body temperature and semisolid at room temperature [15] (Fig. 1). They may also appear as multilocular masses with numerous septa and more rarely as solid masses (about 6 % of cases) [7]. Squamous epithelium lines the cyst wall, and hair follicles, skin glands, muscle and other tissues lie within the wall. There is usually a raised protuberance projecting into the cyst cavity known as the Rokitansky nodule and present in 92 % of MCTs. Most of the hair typically arises from this protuberance, and when bone or teeth are present, they also tend to be located within this nodule. Fat in the cystic lumen is present in 93 % or more of cases, reflecting the sebaceous material or less commonly adipose tissue. This is the most specific imaging finding indicative of MCT [16, 17]. Ectodermal tissue (skin derivatives and neural tissue) is invariably present. Mesodermal tissue (fat, bone, cartilage, muscle) is present in over 90 % of cases, with teeth seen in one-third and endodermal tissue (e.g. gastrointestinal and bronchial epithelium, thyroid tissue) seen in the majority of cases [18].

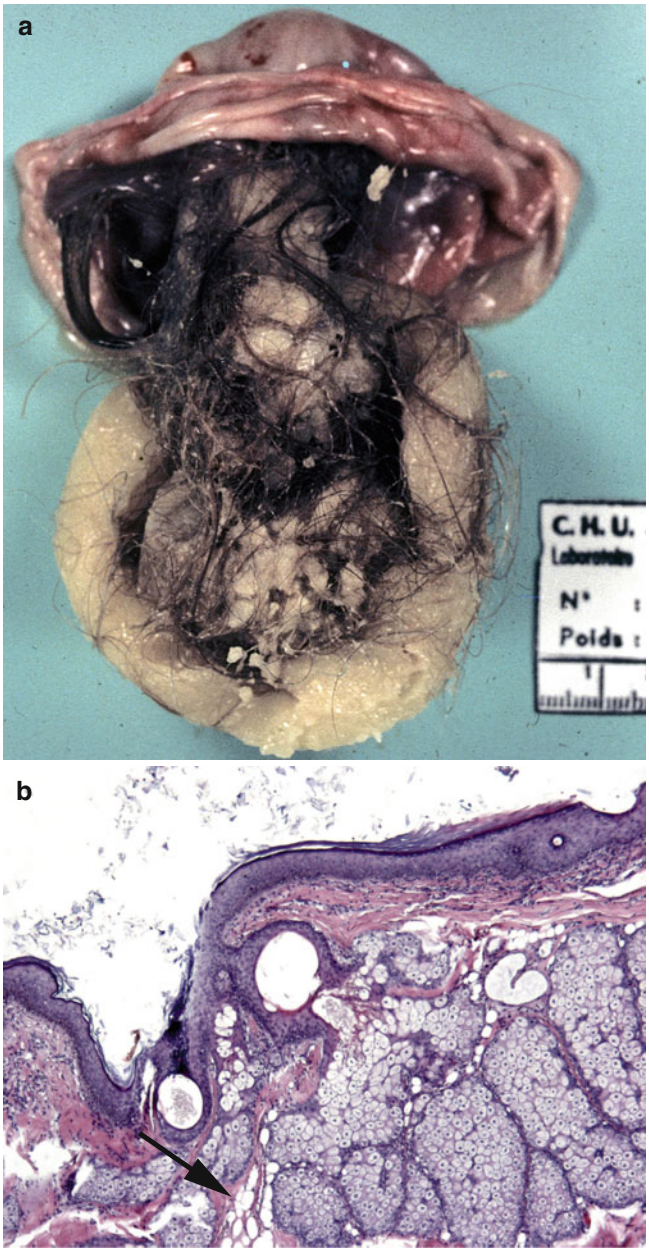

Fig. 1 Histology of a typical mature cystic ovarian teratoma. (**a**) Macroscopic findings show an unilocular cyst with typical content of sebaceous material and hairs. (**b**) Microscopic findings show a mature cystic teratoma lined by mature epidermis and subtended by connective tissue containing exuberant pilosebaceous follicles (*arrow*)

Typical Imaging Findings

Unlike US imaging for which MCT diagnosis could be difficult because of confusion with bowel or perforated appendicitis with appendicolith or ovarian carcinomas [19, 20], cross-sectional imaging (i.e. CT and MR) allows a relatively easy diagnosis because both of these modalities

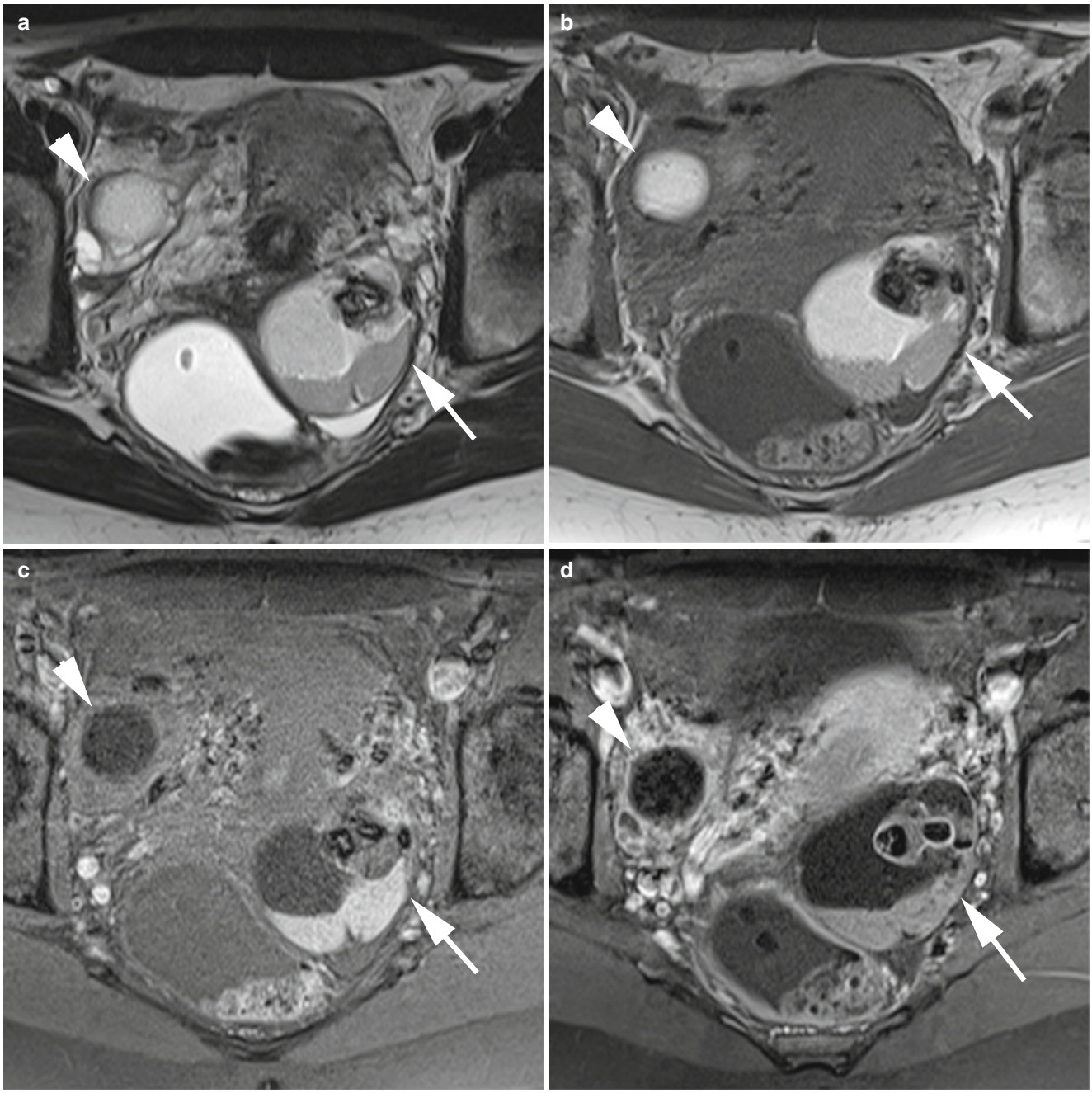

Fig. 2 MR of a bilateral ovarian teratoma in a 29-year-old woman. (**a**) Axial T2-weighted TSE, (**b**) axial T1-weighted GE, (**c**) axial fat-suppressed T1-weighted GE, (**d**) axial gadolinium-enhanced fat-suppressed T1-weighted GE. This patient was treated by bilateral cystectomy, and the final histological findings revealed a left cystic mature teratoma and a left monodermal teratoma. Note the typical appearance of the left one with a fat cystic component with hair level and the Rokitansky nodule with calcification and thin enhancement after contrast

are extremely sensitive with respect to the presence of fat and calcifications (teeth), which represent the most frequent diagnostic findings in MCTs [21].

Most cases present as an asymptomatic adnexal mass incidentally detected on routine pelvic examination. If abdominal pain is present, the imaging findings show evidence of a complication such as MCT torsion, or else rupture must be sought.

The bilateral MCT involvement rate in the literature is 8–15 % (Fig. 2), and the mean diameter is reported to be around 7 cm [7]. The surface of a benign MCT is always smooth. Most are unilocular cysts and contain a large amount

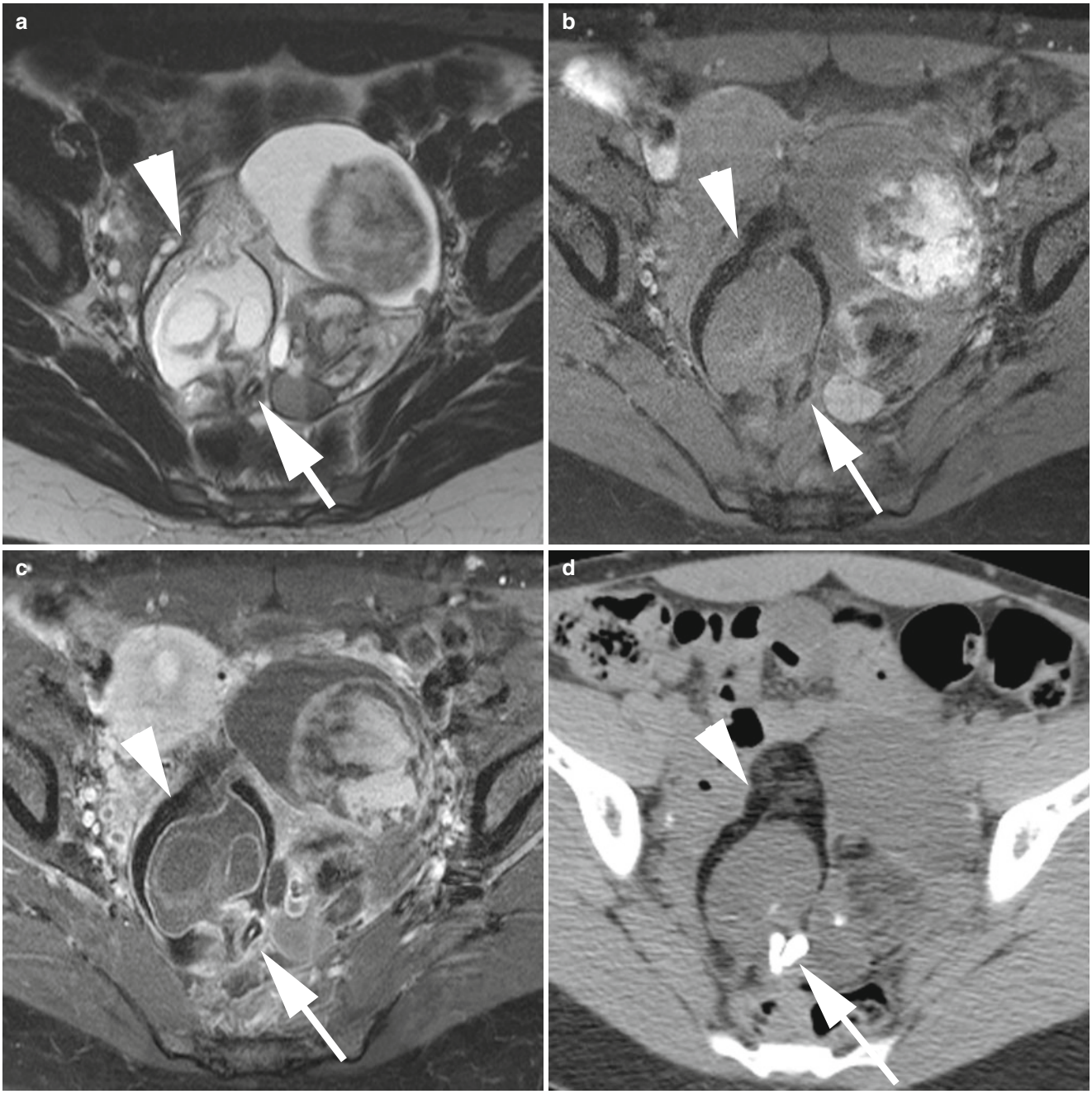

Fig. 3 Imaging of a complex ovarian mature teratoma. (**a**) Axial T2-weighted TSE, (**b**) axial fat-suppressed T1-weighted GE, (**c**) axial gadolinium-enhanced fat-suppressed T1-weighted GE, (**d**) axial unenhanced CT scan (image at the same level as MR). Note the complex multicystic mass with areas of fat components (*arrowheads*) and teeth (*arrows*). The septa and the wall were enhanced after contrast but without extension beyond the capsule. The final histological findings revealed a cystic mature teratoma without malignancy

of fat in the form of liquid sebum, which is of low density on CT, with a high signal on MR images. Exceptional cases of solid mature teratomas have been reported in imaging studies [22, 23]. Fluid may fill the dependent portion of the tumour, producing a fat/fluid interface with the overlying liquid sebum. Layering or floating debris or both can also be encountered at this fat/fluid interface. Calcifications are commonly noted, but their presence does not indicate ovarian teratomas, and therefore, it is necessary to focus on detecting intratumoural fat in order to confirm the diagnosis. A nodular or palm tree-like mural protrusion, known as a Rokitansky protuberance or dermoid plug, is common. There is only one plug, which is usually rounded and typically contains fat, calcium or hair and a minority of diverse other tissues. Although these protuberances may be partly solid, they never show transmural growth (Fig. 3). Recently, intracystic

Table 1 Cross-sectional imaging findings of mature cystic teratomas

	Imaging findings
Typical imaging	Unilocular
<45 years	Intracystic fat
<10 cm	Teeth/calcifications
	Fat/fluid level
	No enhanced Rokitansky protuberance
	Floating balls
Atypical imaging	Multilocular
	No fat in the cyst cavity
	Small amount of fat in the wall or the Rokitansky nodule
	Complex mass: raises the possibility of a collusive tumour, mixed germ cell or degenerescence
Suspicion of complication	Torsion: enlarged tubal mass, displacement of adnexa, deviation of uterus, pelvic fat infiltration, asymmetric smooth wall thickening
Symptomatic with pain or fever	Rupture: flattened shape or discontinuity of the wall, ascites, omental infiltration, fatty implants, dense adhesions
	Malignancy (see below)
	Infection: concomitant local or systemic infection, pelvic fat infiltration, thickened enhanced wall
Suspicion of malignancy	Highly enhanced Rokitansky nodules
>45 years	Solid portion with moderate or intense enhancement
>10 cm	Solid portion with transmural growth (outside the septa or the mass wall)
	Neighbouring organ invasion
	Disseminated metastasis

floating balls were reported to be pathognomonic of mature cystic teratomas [24, 25] and were generated by sebaceous debris with skin squamae and hair [26]. These spherical structures are approximately 1–3 cm in diameter, and there may be more than 100 [27]. However, these teratomas usually have fat in their walls or in the Rokitansky nodule.

The identification of teeth or a Rokitansky protuberance or a large fatty component is a diagnostic sign of a benign cystic ovarian teratoma (cf. Table 1).

CT Imaging

Only a few original studies have reported CT imaging findings of benign MCT series [28–30]. The largest study includes 41 proven histological lesions and was published in 1989 by Buy et al. [17].

At CT, fat attenuation within an unilocular or multilocular ovarian cyst is a diagnostic sign of mature cystic teratomas and was found to be present in 84–93 % [17, 29] of cases. Fat is easily depicted, especially if its proportion is large (Fig. 4), thus allowing density measurement (typically found to be −20 UH or less). Sometimes, only a careful in-depth evaluation will reveal a fat-containing lesion when the fat proportion is millimetric, particularly when located in the wall or the Rokitansky nodule. A fat–fluid level is reported in 12 % of cases and teeth and other calcifications (even in the cyst wall) in 56–84 % of cases. Tufts of hair were common and present in 65 % of cases [17]. If hair is mixed with sebum, the lesion may have a radiologic density greater than that of fat (water density up to +8 UH [29]). There have been some reports on the presence of spherical structures (single or multiple) floating at the fat–aqueous fluid interface, this is the so-called floating mass which appears to be hypodense [31], typical of MCT. CT showed a Rokitansky protuberance in 21/23 (91 %) cases in Guinet's series and in 35/43 (81 %) of cases in Buy's series. A Rokitansky protuberance is defined as a solid or partially solid rounded (or bridge) structure, clearly linked to the cyst wall, projecting inside the cyst, or as a flattened (possibly irregular) wall thickening containing dense structures (calcified structures) and\or areas of fatty tissue [29].

To date, the best suggestive patterns at CT include a fat-containing ovarian cyst and/or identification of a Rokitansky protuberance [29].

MR Imaging

At MR imaging, the sebaceous component of dermoid cysts has a very high signal intensity on T1-weighted images, similar to retroperitoneal fat. The signal intensity of the sebaceous component on T2-weighted images is variable, usually approximating that of fat (Fig. 5). Fat saturation techniques are essential in order to differentiate whether hyperintense areas in the tumours on T1-weighted images are due to haemorrhage, fat and/or fluid of high protein content. In MCT, fat is currently detected with spectral fat saturation, chemical shift imaging (in-opposed phase) or STIR (short T1 inversion recovery) sequences, with the first two being commonly used and chemical shift imaging being the most sensitive, especially to depict very small amounts of fat [32–34]. Intratumoural fat gives a high signal intensity on T1-weighted images and the signal drops on fat-saturated T1-weighted images. It is essential that images be obtained at the same level for each sequence in order to characterise each tissue component, and thus to be able to depict small amounts of fat. When used, chemical shift artefacts were encountered at the interface of fatty and non-fatty components. Fat may be seen in the cavity of the cyst or as a round mass floating at the water and fatty fluid interface, or only in the Rokitansky nodule. In addition, intracystic nondependent spheres of lipid material can occasionally be identified in an MCT, with a striking appearance [35].

Calcifications and teeth both give a low signal intensity on T1 and T2-weighted images. Some mobile globules (so-called floating balls) can be encountered as spherical structures with a centre having a relatively low signal

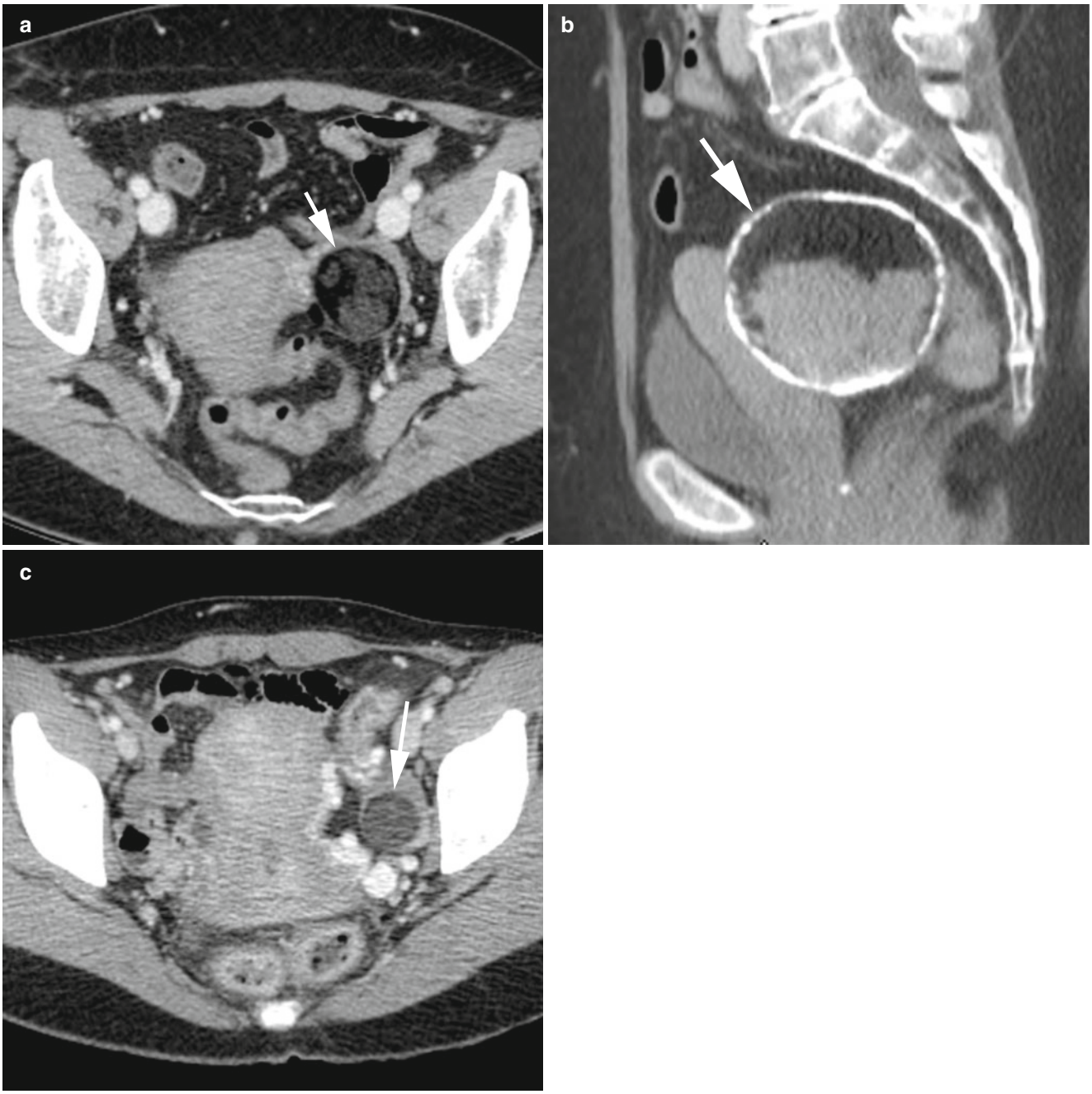

Fig. 4 CT of a left ovarian mature cystic teratoma (*arrows*) in three different women. (**a**–**c**) Axial contrast-enhanced CT scan (venous phase). Note the fatty component which is always predominant, easy to depict. Note also the thin calcifications in the wall of case "b", which are rare; calcifications are usually found in the form of teeth

intensity on T1-weighted MR images compared with the outer portion, corresponding to hair or softer components [25] (Fig. 6). In T2-weighted images, the outer portion of the spherical structures are hypointense and the centre relatively hyperintense. The specific gravity of spherules or globules is lower than that of the surrounding fluid, so they float and are mobile in the cyst [26]. It has been postulated that each spherule is formed by the aggregation of sebaceous matter around a nidus (a tiny focus of debris, desquamative material or fine hair shafts) and may be formed within a discrete mass because of the difference in physical and thermal properties of the material being deposed [21].

Recently, Nakayama et al. [36], showed that mature cystic teratomas tended to show significantly higher signal intensity on diffusion images and had areas of lower ADC (apparent diffusion coefficient) values than endometrial cysts and other benign and malignant neoplasms. This result was attributable to the keratinoid substance within the tumours (Fig. 7).

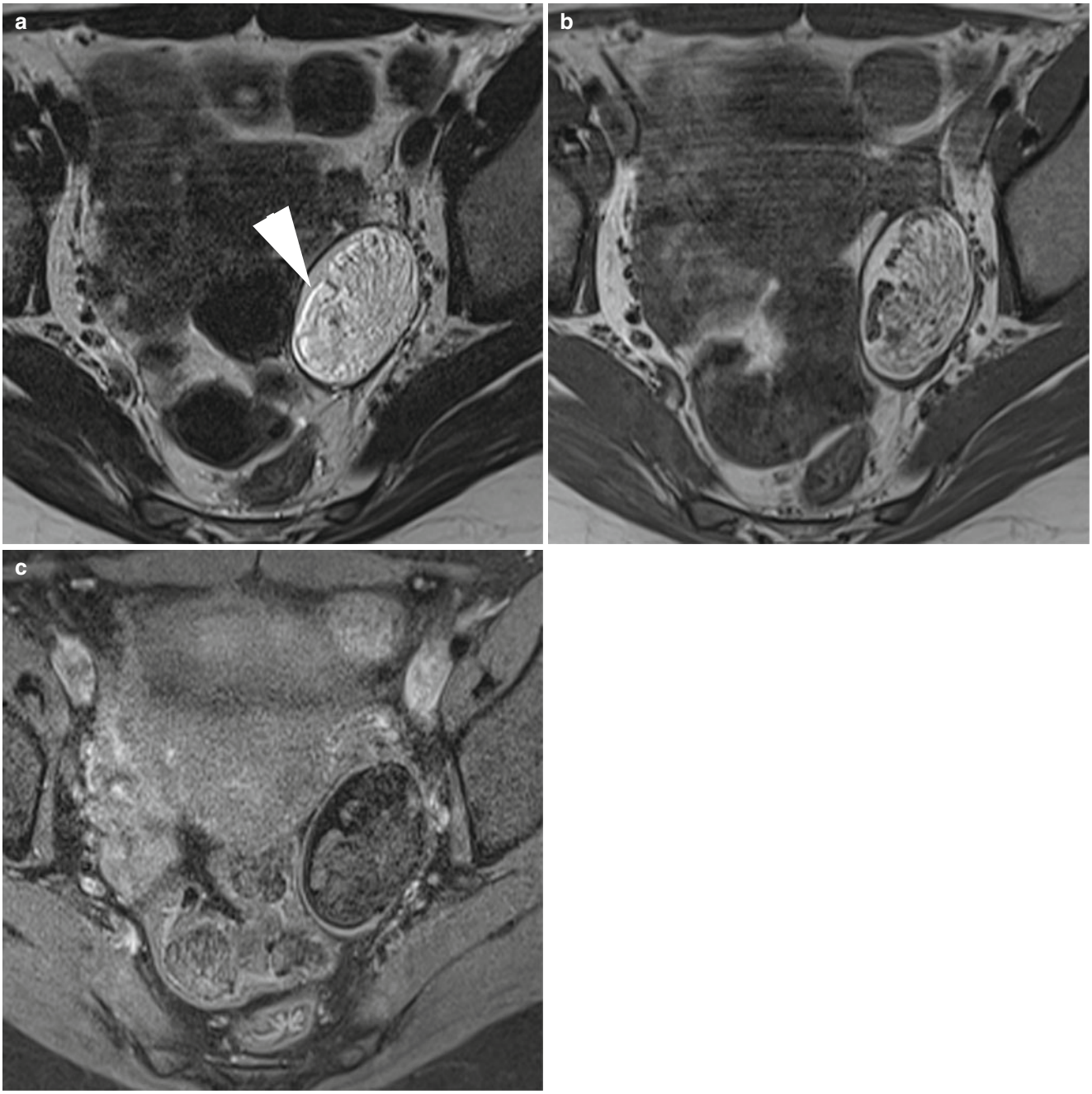

Fig. 5 MR of a typical left ovarian cystic mature teratoma. (**a**) Axial T2-weighted TSE, (**b**) axial T1-weighted GE, (**c**) axial fat-suppressed T1-weighted GE. Note the chemical artefact on the T2-weighted image (*arrowhead*) at the fatty–non-fatty interface

Atypical Aspect

Without Fat in the Cystic Cavity

A minor percentage (arising 15 % in a retrospective series of 78 of MCT in MRI [37]) of MCTs has only a small amount of fat or no visible fat in imaging studies. Small fat components must be carefully searched for in the cystic wall or in Rokitansky nodules [37] (Figs. 8 and 9). A fat-saturated MR imaging technique is advocated to improve diagnosis by showing small amounts of fat. A gradient echo technique with both in-phase and opposed-phase imaging seems better than the fat saturation method [21].

With a Pure fatty Component in the Cavity

These tumours are rare and may mimic other uncommon lipid-containing pelvic tumours (see section "Other lipid-containing pelvis tumours").

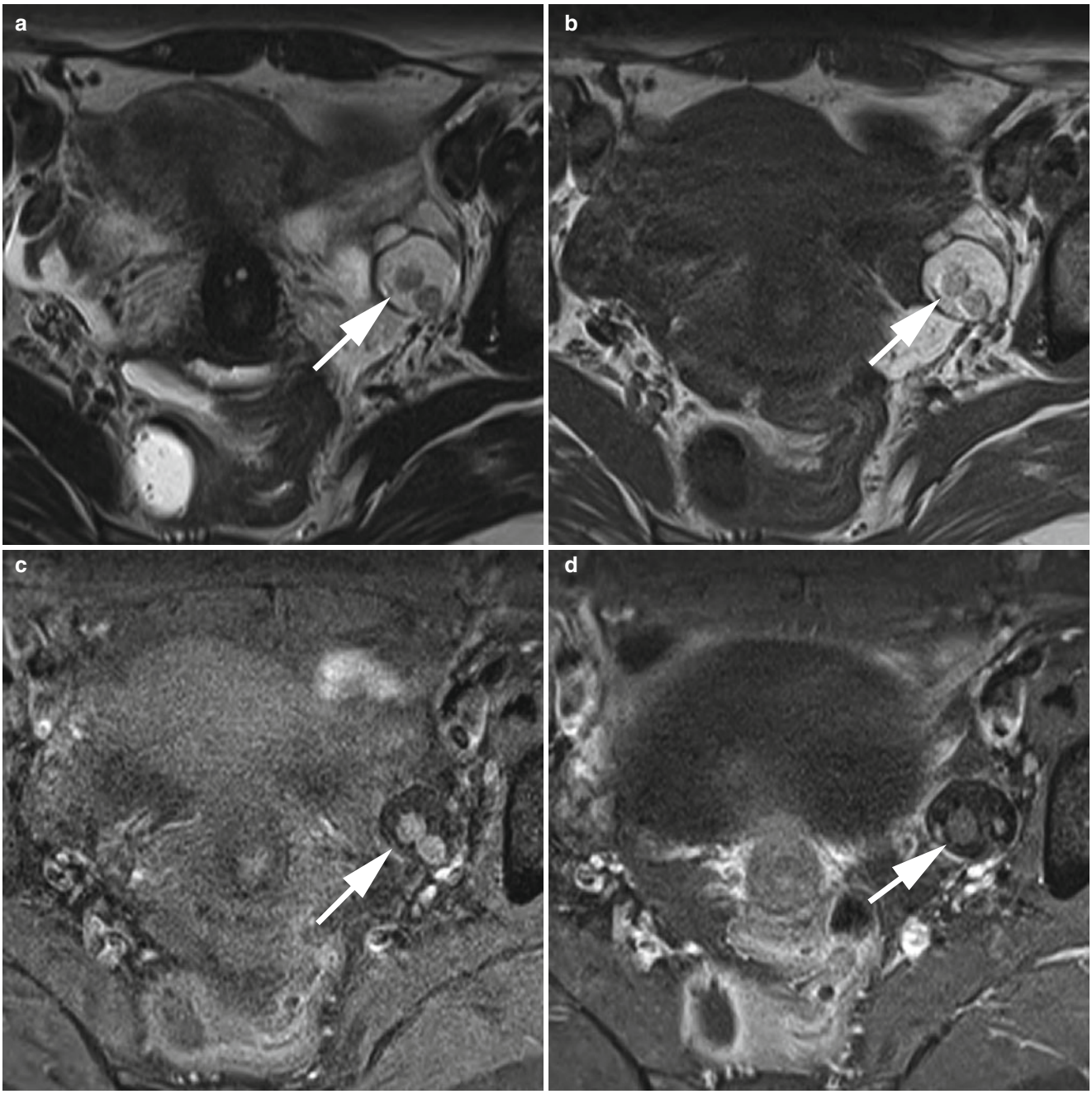

Fig. 6 Floating ball (*arrows*) in a left ovarian cystic teratoma in MRI. (**a**) Axial T2-weighted TSE, (**b**) axial T1-weighted GE, (**c**) axial fat-suppressed T1-weighted GE, (**d**) axial gadolinium-enhanced fat-suppressed T1-weighted GE

Only Solid

This is a very rare finding, and these tumours are indistinguishable from other ovarian tumours, particularly with malignancy.

Collision Tumours

Collision tumours are tumours in which the different neoplastic components remain histologically distinct and separated from each other by narrow stromata or their respective basal laminae. There are various hypotheses concerning the formation of collision tumours. According to the first hypothesis, coexistence of two primary tumours in the same tissue is due to a "chance accidental meeting". Secondly, it has been proposed that the presence of a first tumour alters the microenvironment and gives rise to the development of a second primary tumour or seeding of metastatic tumour cells. The third theory suggests that each primary tumour originates from a common stem cell.

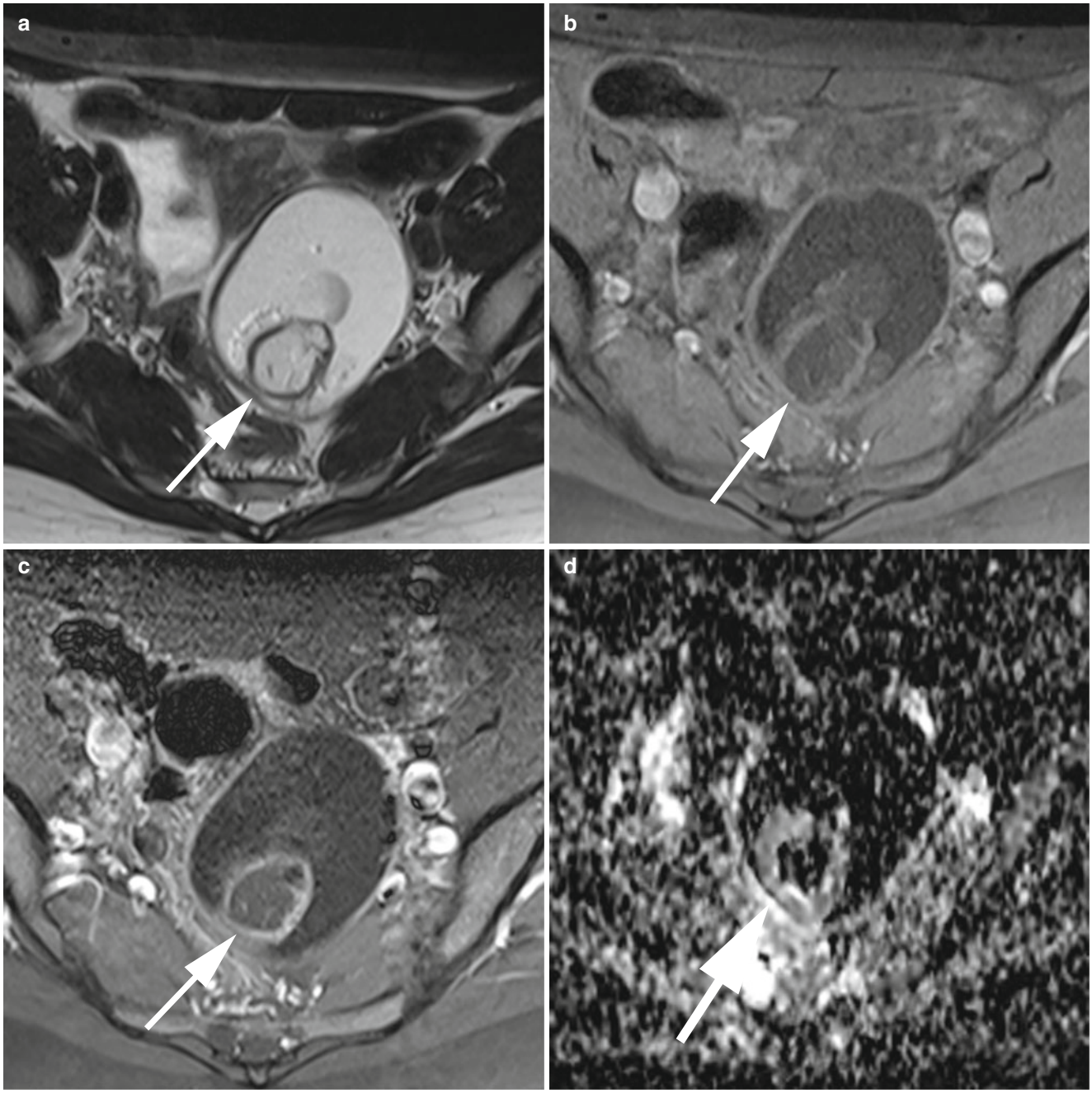

Fig. 7 MR of a typical ovarian cystic mature teratoma. (**a**) Axial T2-weighted TSE, (**b**) axial fat-suppressed T1-weighted GE, (**c**) axial gadolinium-enhanced fat-suppressed T1-weighted GE, (**d**) axial diffusion-weighted (ADC). This is a unilocular fat-containing cyst with a fatty Rokitansky protuberance (*arrows*). Note the very low ADC of the fatty component and the linear thin enhancement of the Rokitansky nodule wall

Concerning teratomas such an association had been reported with granulosa cell tumours [38], with serous cystadenocarcinomas [7, 39, 40] and more commonly with benign or malign mucinous tumours [41–43]. Mucinous tumours were found to coexist with 11.3 % of dermoid cysts, and dermoid cysts were found to coexist with 7.8 % of mucinous tumours [44]. Imaging studies of a collision tumour composed of a teratoma and a mucinous tumour show a typical multiloculated cystic mass with an internal loculi filled with pure fat (Fig. 10). The differential diagnosis was with mixed germ cell tumours, mixed epithelial tumours or malignant degeneration of cystic teratomas. Preoperative suggestion of a collision tumour is possible [41] and may lead the pathologist to perform an in-depth examination and take sections from suspicious areas, thus preventing underdiagnosis during intraoperative consultation for the tumour.

Mixed Germ Cell Tumours

A mixed tumour has intermixed varying histological components derived from a common stem cell. In the case of mixed germ cell tumours, virtually any combination of cell types can occur among embryonal carcinomas, dysgerminomas, teratomas and yolk sac tumours (endodermal sinus tumours). The imaging findings of mixed germ cell tumours are variable and reflect the diversity of this group of tumours. When a predominantly solid and heterogeneous ovarian tumour contains fatty areas or calcifications suggestive of a mature cystic teratoma or when a mature cystic teratoma contains an enhancing solid portion, a mixed germ cell tumour diagnosis should be considered.

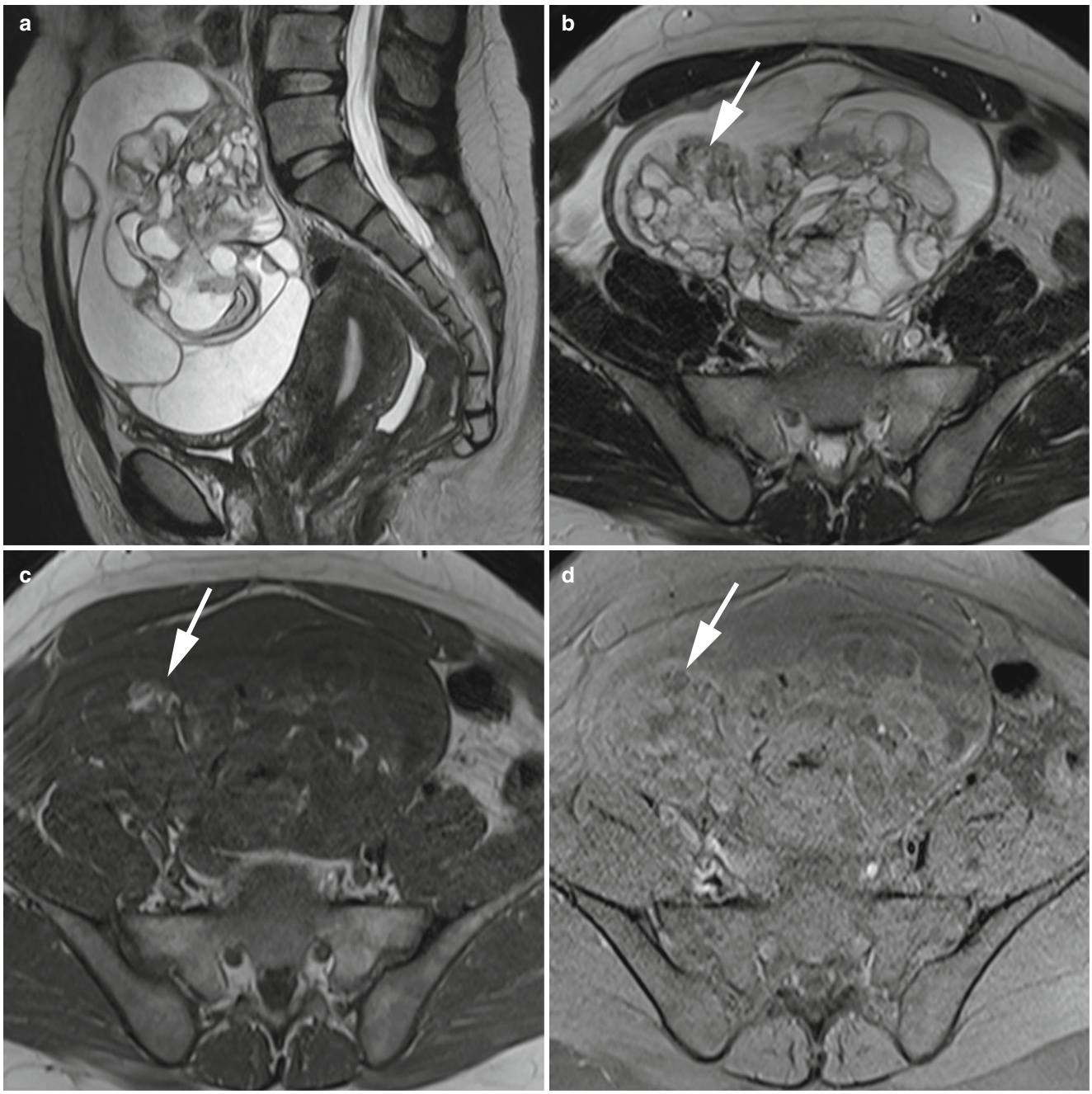

Fig. 8 MR of an atypical ovarian mature teratoma in a 19-year-old woman. (**a**) Sagittal T2-weighted TSE, (**b**) axial T2-weighted TSE, (**c**) axial T1-weighted GE, (**d**) axial fat-suppressed T1-weighted GE, (**e**) axial diffusion-weighted (b1000) (**f**) axial diffusion-weighted (ADC). Note the multicystic appearance of the mass, which corresponds to a multicystic Rokitansky nodule. Some of these loculi contain fat components (*arrows*) which appear with very low ADC values

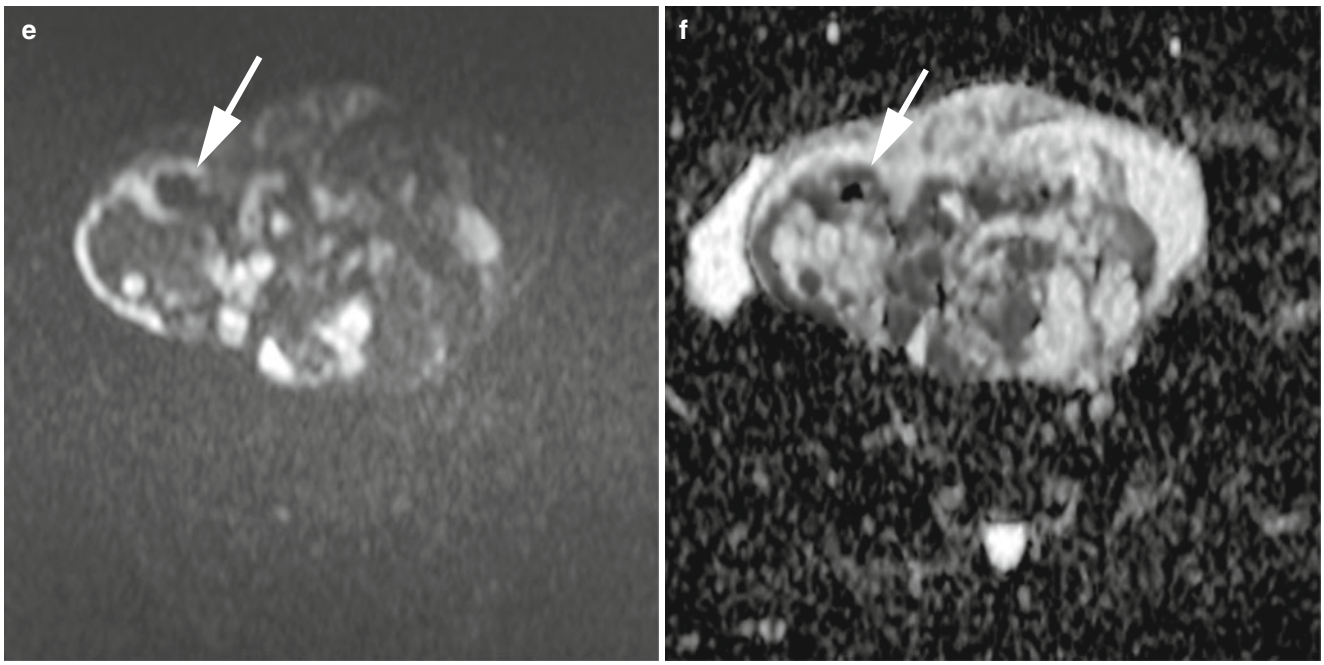

Fig. 8 (continued)

Elevated serum α-fetoprotein (yolk sac tumour) and human chorionic gonadotropin (dysgerminome) levels and younger age can help in the diagnosis of mixed germ cell tumours [45].

Growing Teratoma Syndrome

Growing teratoma syndrome (GTS) is a rare finding, defined as an enlarging mature teratoma that arises during or following chemotherapy for a malignant germ cell tumour, especially an immature teratoma [46]. These tumours can undergo tissue maturation and take on an appearance more typical of mature cystic teratomas, a phenomenon also known as retroconversion [47]. Selective elimination of malignant cells by chemotherapeutic agents or differentiation of malignant cells into mature teratoma components following exposure to chemotherapeutic agents may be the two possible mechanisms responsible for GTS development. As a result, this is often misinterpreted as a chemoresistant tumour or recurrence [48]. These retroconverted masses can remain stable for a long period of time. By definition, GTS must exhibit normalisation of previously elevated tumour markers (alpha-fetoprotein [AFP] or beta human chorionic gonadotropin [HCG]), tumour enlargement or the presence of a new tumour mass and only mature teratoma elements in the pathologic examination. The radiologic features include increased mass density with well-circumscribed margins, onset of internal calcification with fatty areas and cystic changes [49].

Complications

MCT complications include torsion (16 %), malignant degeneration (2 %), rupture (1–2 %) and infection (1 %) [50].

Torsion

Torsion is the most common complication associated with mature cystic teratomas. The torsion rate was reported at 3.2–16 % [8]. From another standpoint, about 30 % of ovarian torsions are due to mature cystic teratomas which, along with serous cystadenomas, represent the most common cause of ovarian torsion [51]. The classical clinical presentation includes sharp, localised right or left lower abdominal pain, tenderness, peritoneal findings and a pelvic mass. Gastrointestinal complaints with nausea and vomiting are encountered in approximately two-thirds of patients, whereas fever is an argument in favour of necrosis complicating ovary torsion.

The cross-sectional imaging diagnosis includes visualisation of a fat-containing adnexal mass in association with several signs of torsion, as listed below [52]:

- The presence of an enlarged solid tubal mass seen between the uterus and the ovarian mass (Fig. 11), which is the most specific imaging finding for adnexal torsion; it manifests as an amorphous or tubular mass-like structure or has a target-like appearance between the torsed teratoma and the uterus or a beaklike protrusion extending from the uterus and partially covering the ovarian teratoma [53].

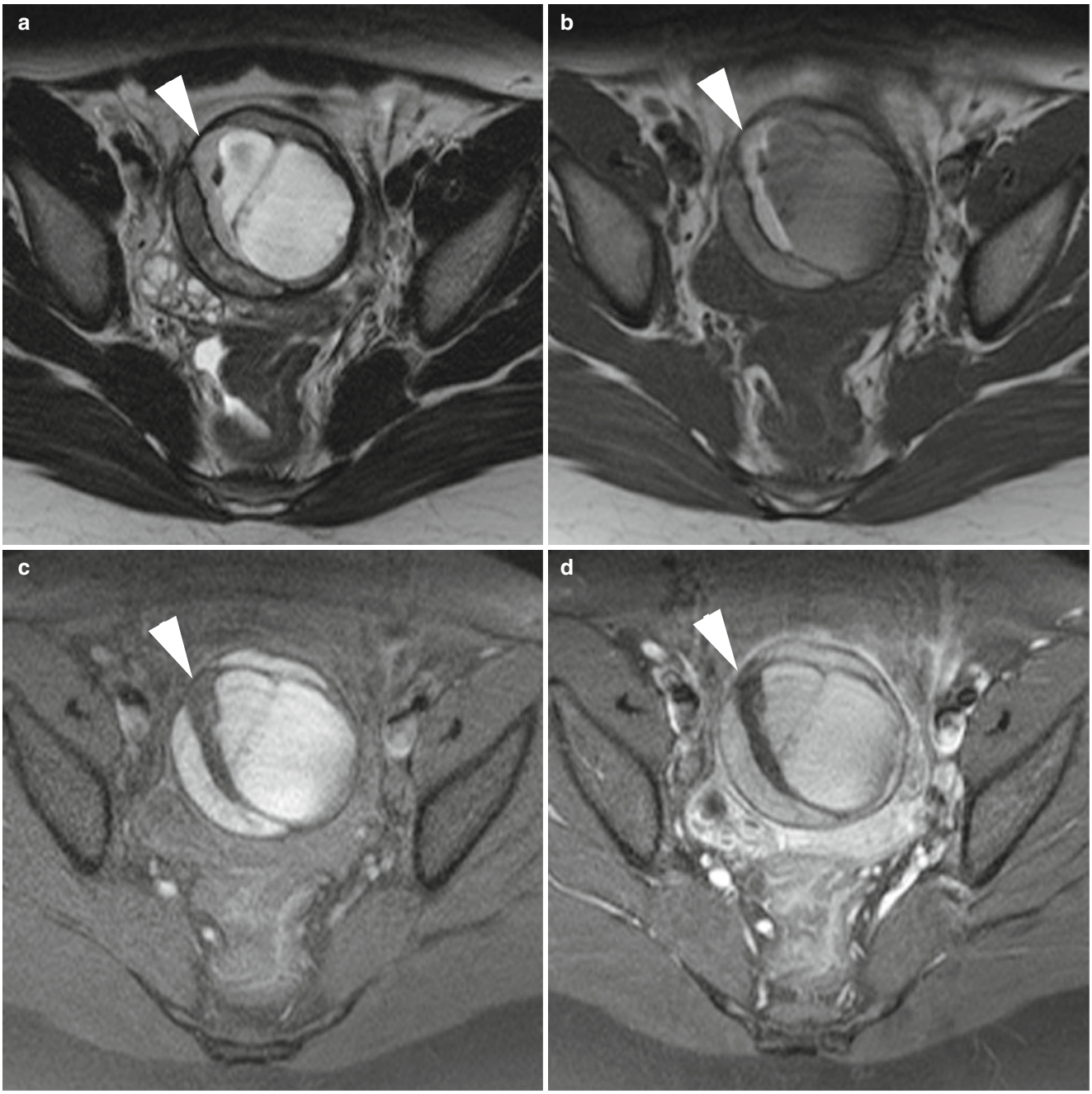

Fig. 9 MR of a left atypical ovarian mature cystic teratoma in a 12-year-old girl. (**a**) Axial T2-weighted TSE, (**b**) axial T1-weighted GE, (**c**) axial fat-suppressed T1-weighted GE, (**d**) axial gadolinium-enhanced fat-suppressed T1-weighted GE. Note the atypical fatty component which is crescent-shaped (*arrowheads*) inside a multilocular lesion. The histological findings revealed simple mature cystic teratomas without neither malignancy nor mixed tumours

- The identification of a smooth wall thickening without nodularity on the cystic mass, this thickening is more often eccentric and >1 cm [54] than concentric.
- The displacement of adnexa which may be on the contralateral side of the pelvis or on the midline in a far anterior position abutting the anteropelvic fascia or posterior in the pouch of Douglas (Fig. 12).
- The deviation of uterus and the pelvic space infiltration on the side of a twisted ovary.

Mature cystic teratomas affected by torsion are larger than average (mean diameter, 11 cm versus 6 cm); this enlargement could be the result of torsion rather than the cause of it. Torsion does not eradicate the fatty components.

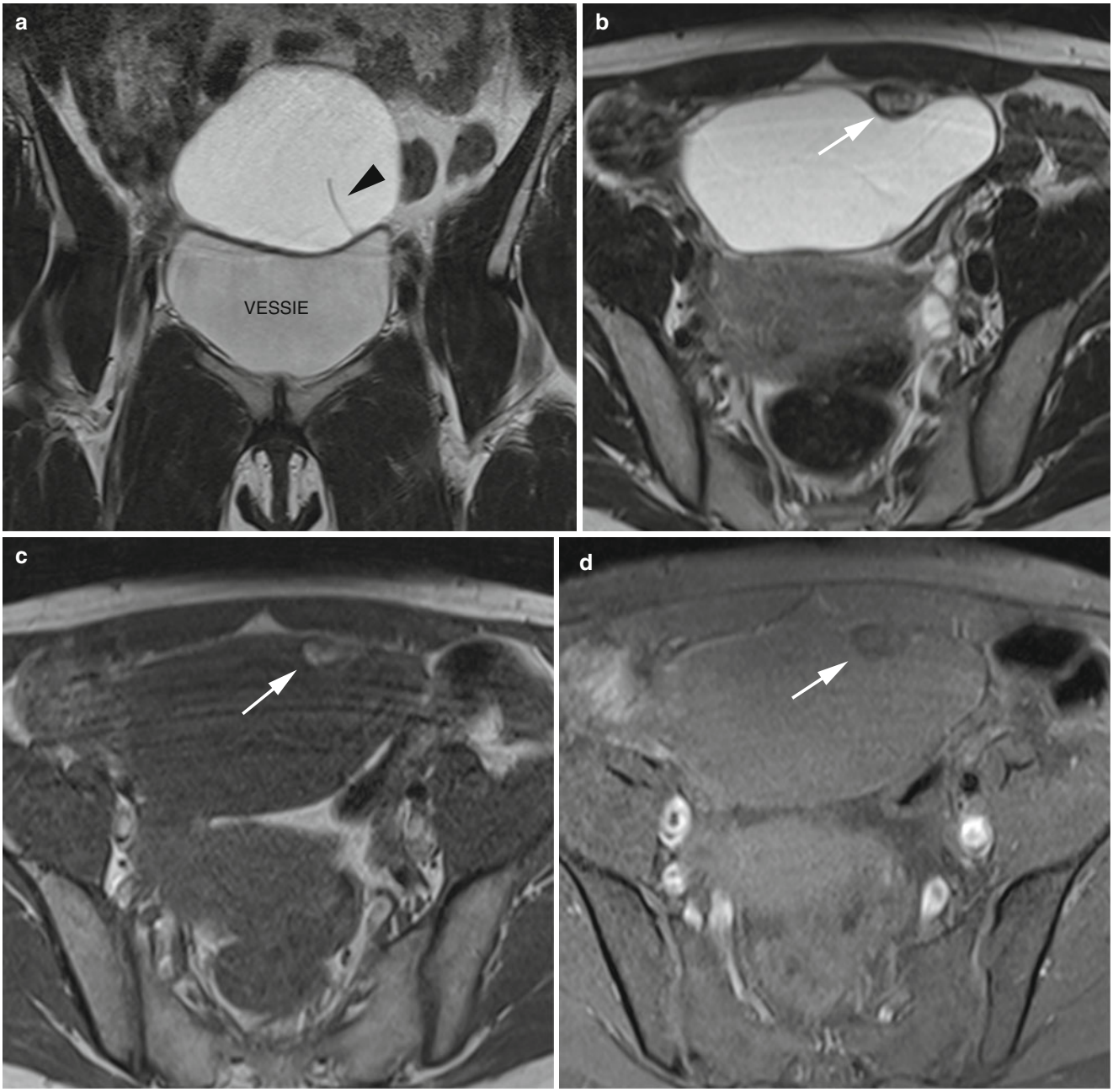

Fig. 10 MR of an ovarian collusive tumour in a 28-year-old woman. (**a**) Coronal T2-weighted turbo spin echo (TSE), (**b**) axial T2-weighted TSE, (**c**) axial T1-weighted gradient echo (GE), (**d**) axial fat-suppressed T1-weighted GE. The mass was predominantly cystic with thin septa (*arrowhead*). Note the small and unique loculi which contain fat components (*arrows*). The histological findings revealed an association of a mature teratoma and a mucinous cystadenoma

Degenerescence

Malignant transformation occurs in 0.17–2 % of cases [55] and may occur in any of the three germ cell layers, including the ectoderm, mesoderm and endoderm. The epithelial component of mature cystic teratomas commonly transforms into squamous cell carcinomas (more than 80 % of cases [56]) although other neoplasms, including adenocarcinomas [57], low-grade carcinoid tumours [58], neuroendodermal tumours, malignant melanomas [59], oligodendrogliomas [60], thyroid papillary carcinomas [61] and highly aggressive sarcomas [62, 63], have been reported. Most cases are discovered as incidental microscopic foci of squamous cell carcinomas in benign-appearing gross specimens of cystic teratomas.

Clinically, malignant transformation cannot be readily identified. Malignant transformation has been mainly found in women of over 50 years old, with high concentrations of squamous-cell-carcinoma antigen (SCC) and cancer antigen CA125 and with ovarian tumours more than 100 mm in size [4].

In imaging, the features reported in favour of malignancy are [30, 55]:

- A diameter larger than 10 cm
- The presence of an enhancing soft tissue mass component, especially contrast enhancement of the Rokitansky protuberance, which suggests the possibility of malignant transformation [56]
- An obtuse angle between the enhanced soft tissue mass and the inner cyst wall
- Areas of haemorrhage and necrosis
- An extracapsular tumour growth with extension into adjacent structures
- A disseminated metastasis

Direct invasion of adjacent tissue is common for squamous cell carcinomas arising in ovaries as well as in other parts of the body. Conversely, the most important mode of spreading in common epithelial ovarian carcinoma is dissemination by lymphatic spreading and peritoneal carcinomatosis. Consequently, an invasive growth pattern in an ovarian mass is an argument in favour of a degenerated mature cystic teratoma with squamous cell carcinoma.

Mori et al. reported that the combination of the patient's age (>40 years) and serum SCC antigen level (>2.5 ng/mL) was 77 % sensitive and 96 % specific for malignant transformation [64].

The malignant teratoma prognosis is good if the tumour is completely excised and does not extend beyond the capsule [65]. Hence, a surgical approach (laparotomy versus laparoscopy) should be chosen carefully and based on the results of clinical and imaging investigations as well as tumour marker profiles. Complete resection together with hysterectomy, bilateral salpingo-oophorectomy and lymphadenectomy for patients with advanced disease, followed by adjuvant chemotherapy with an alkylating drug, was associated with higher survival, whereas radiotherapy was not [4].

Rupture

There is a low rate of spontaneous rupture of mature cystic teratomas (1.2–3.8 %) because of the usually thick capsule. It causes leakage of the liquified sebaceous contents into the peritoneum and leads to either acute or chronic clinical presentations [66], and the latter is the most common.

- *Acute Chemic Peritonitis*

This is caused by the sudden rupture of tumour contents, which may occur spontaneously or more commonly in association with torsion, trauma, infection or labour [67]. On imaging, detection of a flattened shape or discontinuity of the tumour wall is a sign of a ruptured teratoma and can present with ascites and diffuse or focal omental infiltration.

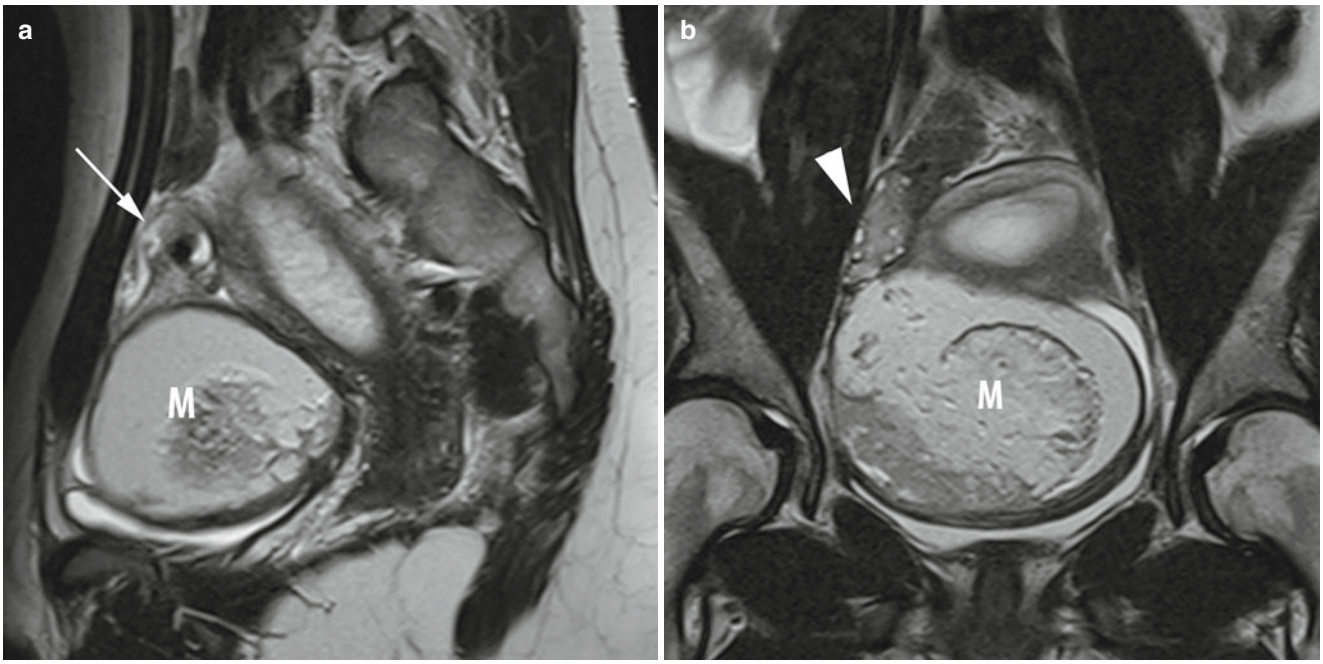

Fig. 11 MR of a left ovarian cystic teratoma torsion in a pregnant woman. (**a**–**c**) Respectively sagittal, coronal and axial T2-weighted TSE, (**d**) axial T1-weighted GE, (**e**) axial fat-suppressed T1-weighted GE. Note the normal right ovary (*arrowhead*), the spire of the torsed vascular pedicle (*arrow*) and the cystic teratoma (*M*). This patient was treated by total ovariectomy

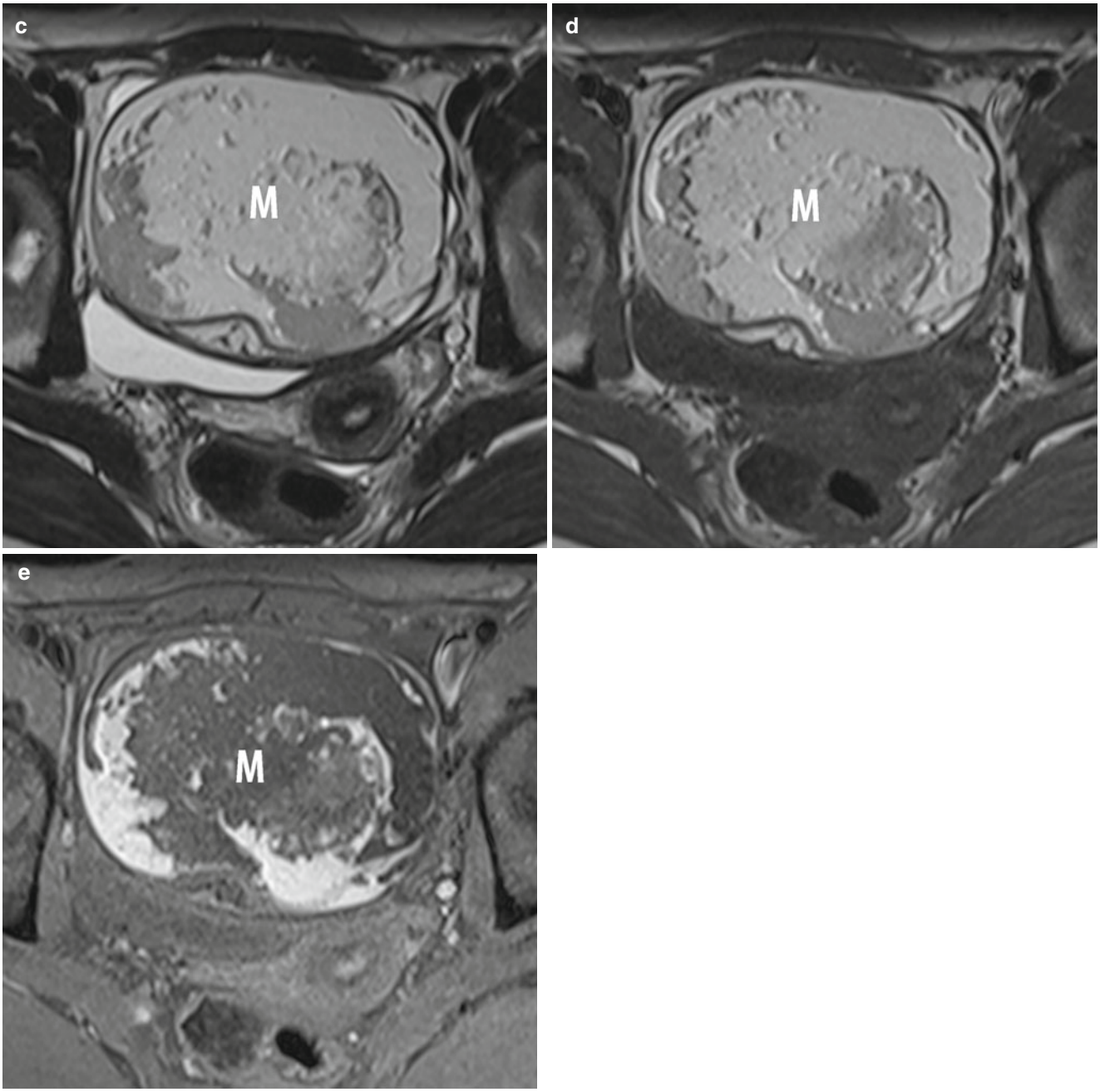

Fig. 11 (continued)

- *Chronic Granulomatous Peritonitis*

This results from a chronically leaking dermoid cyst, which can be characterised by multiple small white peritoneal implants, dense adhesions and variable ascites that simulate carcinomatosis or tuberculous peritonitis. Sometimes, fatty implants may be identified within the peritoneal cavity which are diagnostic signs in this case [68].

Furthermore, in addition to rupture into the peritoneal cavity, perforation into other intra-abdominal organs has been reported, including rupture into the bladder, small bowel, rectum, sigmoid colon, vagina and even through the abdominal wall.

Another entity has been described, which is referred to as a "parasitic ovarian dermoid tumour" that could occur when an ovarian dermoid tumour has undergone autoamputation (total or semi) and reimplantation on another abdominal site [69]. The most common is reported in the greater omentum (Fig. 13), but other sites have been described, such as within an indirect inguinal hernia sac [70] or within an extensive intra-abdominal parasitic form [71]. Autoamputation could be inaugural (the so-called parasitism) or secondary to torsion or surgical rupture. Another theory is that primary teratomas of the omentum originate from displaced germ

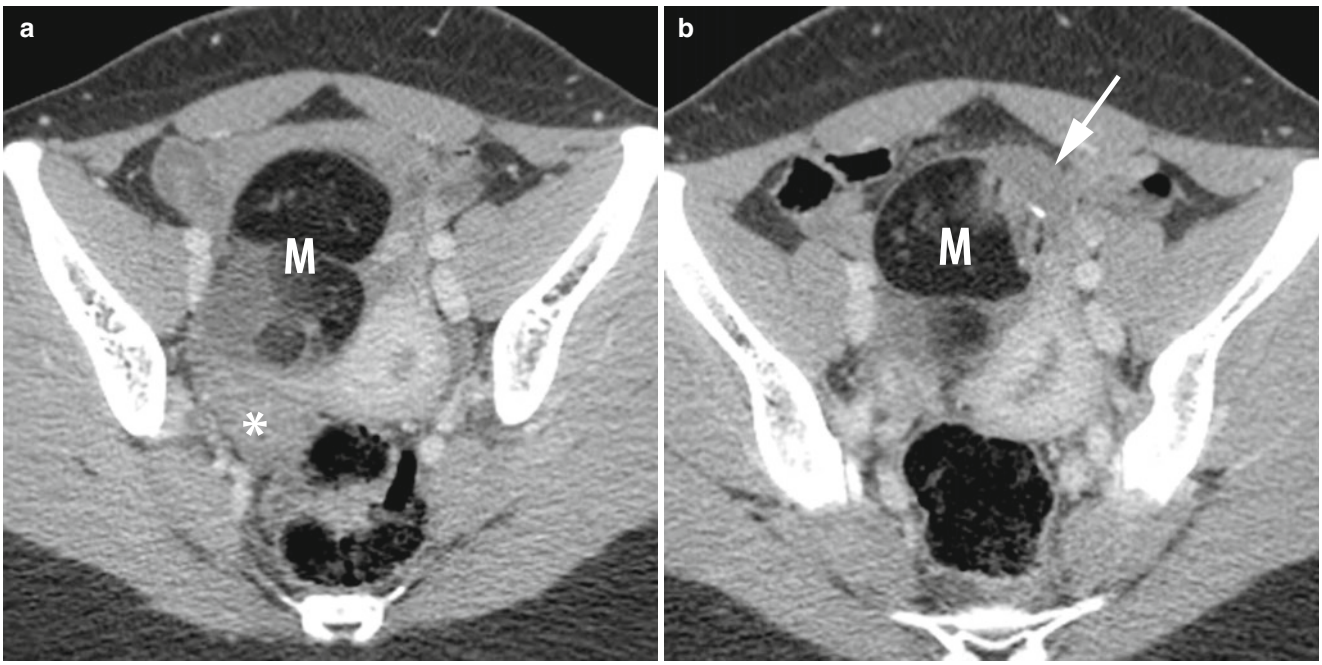

Fig. 12 CT of a left ovarian cystic teratoma torsion. (**a**, **b**) Axial contrast-enhanced CT scan (venous phase). Note the normal right ovary (*star*), the typical left ovarian cystic teratoma with a fat component (*M*), the uterine displacement on the twisted (i.e. left) ovary and the thickened tubal mass (*arrow*) between the uterus and the teratoma

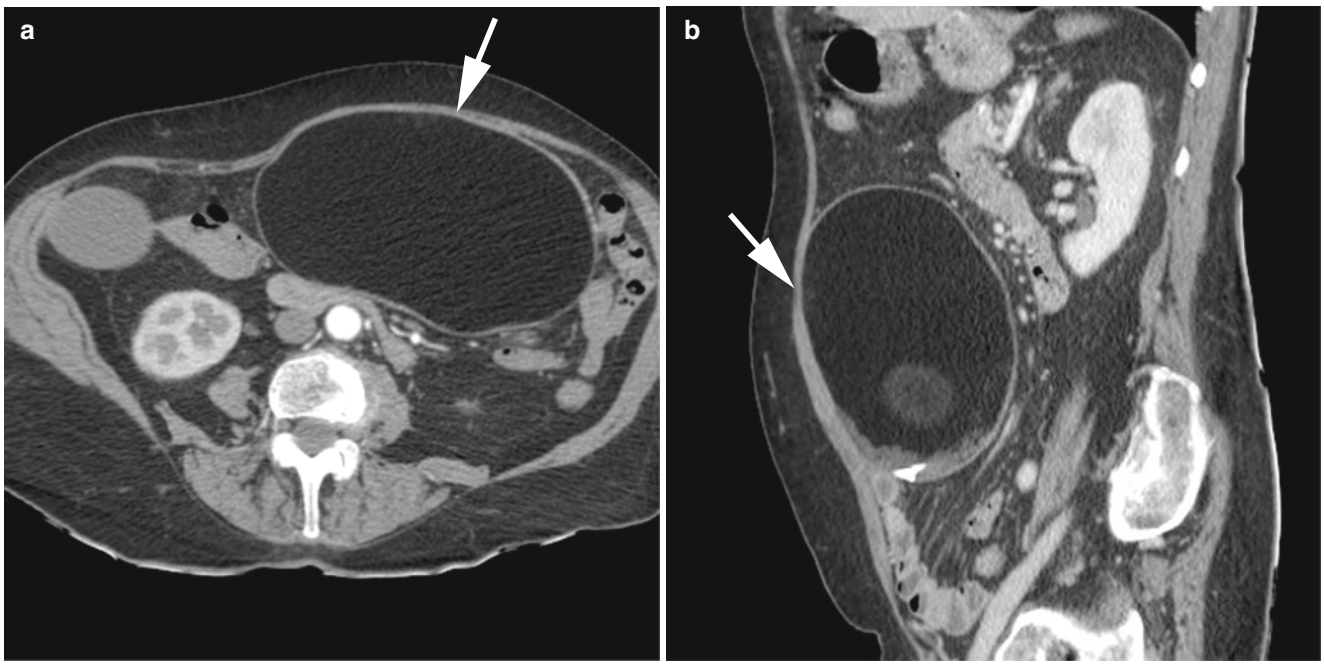

Fig. 13 CT of an omental dermoid cyst (*arrow*) in a 76-year-old woman. (**a**, **b**) Respectively axial and sagittal contrast-enhanced CT scan (venous phase)

cells. They could also develop in congenital omental supernumerary ovaries. At imaging, it appeared like an ovarian mature cystic teratoma with a fat component at an ectopic location.

Infection

This is a very uncommon complication, with less than ten cases reported in the literature. All were associated with a concomitant pathology or systemic infection, which leads to

subsequent infection of dermoid cysts. While infected dermoid cysts are rare, any concomitant intra-abdominal pathology should raise suspicion and prompt appropriate action by the gynaecologist to remove the dermoid cyst, avoid spilling cyst contents, obtain cultures and consider empirical broad-spectrum antibiotics [72]. At imaging, the dermoid cyst could appear as normal or show thickened walls or pericystic fat infiltration.

Differential Diagnosis

Other Lipid-Containing Pelvis Tumours [73]

Nonteratomatous Lipomatous Ovarian Tumours

- Ovarian Lipoleiomyoma [74, 75]

To the best of our knowledge, they are only four imaging cases reported in the English literature. These are large extrauterine fatty mass containing considerable amounts of nonlipomatous soft tissue. A mass with this appearance is more likely to be a pedunculated uterine fatty tumour, an ovarian lipoleiomyoma or a benign cystic ovarian teratoma that has undergone malignant transformation. The tumour is identified by the presence of mature adipose tissue intimately admixed with smooth muscle cells. If

- Ovarian Lipoma

Ovarian lipomas are a rare entity, with most being described as being of teratomatous origin. Only one case was well documented in the literature to our knowledge [76]. The microscopic pattern showed a proliferation of benign adipose tissue with focal areas of fibrovascular septa and no other tissue of different origin. They present a pure fatty appearance in imaging without other components.

Pedunculated Lipomatous Uterine Tumours

These are uncommon benign neoplasms, with an incidence ranging from 0.03 to 0.2 % [77], that occur most frequently in postmenopausal women. The histological spectrum includes pure lipomas and lipoleiomyomas. The MRI findings [78] are similar to a leiomyoma with a well-encapsulated uterine mass, containing variable amounts of fatty components. Sequences with fat-suppressed imaging are useful for the identification of a small fat component. Identification of a lipomatous pelvic mass that is of obvious uterine origin is virtually a diagnostic sign of a lipomatous uterine tumour. The diagnosis is harder if the mass is primarily exophytic or pedunculated. The contact angle between the mass and the uterus, the existence of a vascular pedicle or the content of the mass can allow us to differentiate ovarian from uterine mass because lipoleiomyomas do not have either Rokitansky nodules or fluid–fluid levels.

Benign Pelvic Lipomas [79]

Benign pelvic lipomas are uncommon retroperitoneal masses composed of mature lipocytes and minimal fibrous tissue. They are usually well-defined, homogeneous encapsulated masses that tend to produce mass effects rather than invade adjacent structures. On CT and MR, they are of homogeneous fat density except for a few thin low-density septa or fat necrosis.

Liposarcomas

They can be asymptomatic for a long period of time and commonly present in elderly patients (fifth to seventh decades of life). The presence of a predominantly solid soft tissue component or adjacent organ invasion should raise suspicion of liposarcoma. The liposarcoma imaging appearance varies depending on the tumour grade. Well-differentiated liposarcomas appear as well-defined, predominantly fat-containing lesions with minimal soft tissue attenuation (= lipogenic form, the least malignant potential), whereas poorly differentiated tumours appear as locally invasive, predominantly soft tissue masses with minimal fat (myxoid form) [79].

Other Malignant Ovarian Tumours, if Degenerated

Degenerated teratoma could mimic other malignant tumor as epithelial ones (see section "Degenerescence")

Endometriomas or Haemorrhagic Cysts

These do not have any fat component, and their haematic component can be easily differentiated from fat using MR fat saturation techniques. Signals within each loculus should be carefully sought.

Immature Teratomas

Immature teratomas differ from mature cystic teratomas by demonstrating clinically malignant behaviour; they are much less common (<1 % of ovarian teratomas), affect a younger age group (usually during the first two decades of life) and are histologically distinguished by the presence of immature or embryonic tissues [18]. They are typically larger (>14 cm) and have a prominent irregular solid component with cystic elements, coarse calcifications and small foci of fat compared to MCT. Haemorrhage is often present. The tumours frequently demonstrate perforation of the capsule, which is not always well defined. Tumour grading is based on the amount of immature tissue present.

Implications for Patient Care

Diagnosis of mature cystic teratomas must be easily done by MR or CT because of their characteristic intratumoural fat component. This is important considering the prevalence and

benignity of this condition. Indeed, surgery may frequently be postponed after clinical diagnosis, especially in young patients of reproductive age, or should be conservative in order to preserve fertility. In a randomised prospective study of 102 patients requiring surgical management of ovarian masses not suspected to be malignant, the laparoscopic approach offers significant advantages over conventional laparotomy in terms of reduced morbidity, hospital stay and recovery, without increasing the risk of spillage of the cyst contents [80].

Younger patients and bilateral or multiple dermoid cysts should be followed up closely because the recurrence risk was reported to be higher [10, 81].

Preoperative suggestion of a mixed or a degenerated tumour must be made if a teratoma has unusual imaging findings, such as large size, irregular border, strong contrast enhancement of dermoid plugs or evidence of extracapsular growth. Serum tumour markers could orient the diagnosis. Indeed, CA 125, CA 19–9, SCC and carcinoembryonic antigen (CEA) are commonly elevated, but high concentrations of tumour markers have been reported in patients with benign tumours [82, 83]. Therefore, the accuracy of intraoperative section analysis for histological confirmation is very important, especially in young women before proceeding with radical surgery.

Monodermal Teratoma

Monodermal teratomas are composed predominantly or solely of one tissue type.

Struma Ovarii

Struma ovarii (the so-called thyroid goitres) are rare ovarian tumours composed solely or predominantly of thyroid tissue having cystic portions filled with high proteinaceous gelatinous fluid of eosinophilic colloid, and their solid portions consisting of thyroid tissues and stroma containing abundant blood vessels and fibrous tissue. Pure struma ovarii with microscopic or macroscopic thyroid tissue account for 2.7–3 % of all ovarian teratomas [84]. If the mature thyroid tissue in this tumour is hyperfunctioning, symptoms and signs of hyperthyroidism may be present, but this is uncommon (reported in no more than 5 % of cases [85]). They affect women in perimenopausal aging [86].

CT findings were evaluated in a series of 13 pathologically proven cases, and they appeared most often as a smooth, marginated, multicystic mass with an intracystic high attenuation on precontrast scans (>90 HU) and no or moderate cyst wall enhancement [87]. It has been suggested that these high-density CT scan values are caused by thyroglobulin and thyroid hormones in follicular thyroids that could significantly attenuate the X-ray [87]. Shen et al. [88] found that the high-density cavities noted in CT scans were high signals in T1W1 and low signals in T2W1 and that the presence of extremely hypointense loculi on T2WI was a useful sign of this tumour (Fig. 14). It was reported that it may reflect gelatinous viscid material such as triiodothyronine, thyroxine, thyroglobulin, and thyroid hormones within the tumour [89]. Conversely, high intensities on both T1- and T2-weighted images were pathologically proved to be due to hemorrhagic products and viscous colloid components. Kim et al. [86] reported, in a retrospective study of 10 struma ovarii in MRI, the pattern of a unilateral complex mass of multiple cysts and some solid components with a multilobulated surface and thickened septa. The multiple cysts of struma ovarii may have variable size, shape, numbers (range 3–40) and signal intensities depending on the amount, density, or concentration of viscous proteinaceous fluid in thyroid follicles. Solid portions or septa were isointense relative to the adjacent muscles on T1-weighted images, iso- or hyperintense on T2-weighted images and intensely or moderately enhanced on postcontrast T1-weighted images. No fat was present in these lesions.

In a small number of cases, ascites and pleural effusion with elevated CA125 level may be found (the so-called pseudo-Meigs' syndrome) mimicking ovarian malignancy [90, 91]. In clinical practice, struma ovarii should be differentiated from mucous or serous ovarian cystadenomas; these latter showed low- rather than high-density cystic fluids, with protrusions of nodular soft tissues.

Most struma ovarii are benign and can be treated by surgical resection of the diseased ovary with or without excision of the ipsilateral fallopian tube. Malignancy is uncommon.

Carcinoid Tumours

These are uncommon, with a reported incidence of 0.1 % of all malignant ovarian tumours [92]; this is a neoplasm with low-grade malignant potential. They may be insular (islet tumours), trabecular, mucinous and strumal carcinoids, each characterised by fibrous stroma from serotonin produced by the tumour that separates nests of tumour cells. They are usually unilateral, frequently associated with an MCT, and occur in post- or perimenopausal women [93]. Clinical manifestations such as typical carcinoid syndrome (flushing and diarrhoea) or chronic constipation have been reported, but most of them are asymptomatic.

At imaging, they are commonly solid lesions that mimic an ovarian fibroma, or they present as a solid component of low intensity within a multilocular cystic mass that mimic

Brenner tumours with coexisting mucinous cystadenomas or mucinous cystadenofibromas. The hypointense component on T2-weighted images was reported to have a high signal on diffusion-weighted images with low apparent diffusion coefficient (ADC) [93], reflecting hypercellularity which would help to distinguish them from other benign fibrous tumours (fibromas, Brenner tumours, etc.) that exhibit low signal intensity on diffusion-weighted images. Moreover, they showed hypervascularity in contrast dynamic studies, suggesting functioning tumours and rarely observed in benign fibrous tumours [18]. Rarely, they could have hormonal activity with oestrogenic manifestations [94]. Although they are considered to have a malignancy potential, most of these tumours have a relatively benign clinical course, with metastases being uncommon. Surgical excision is curative.

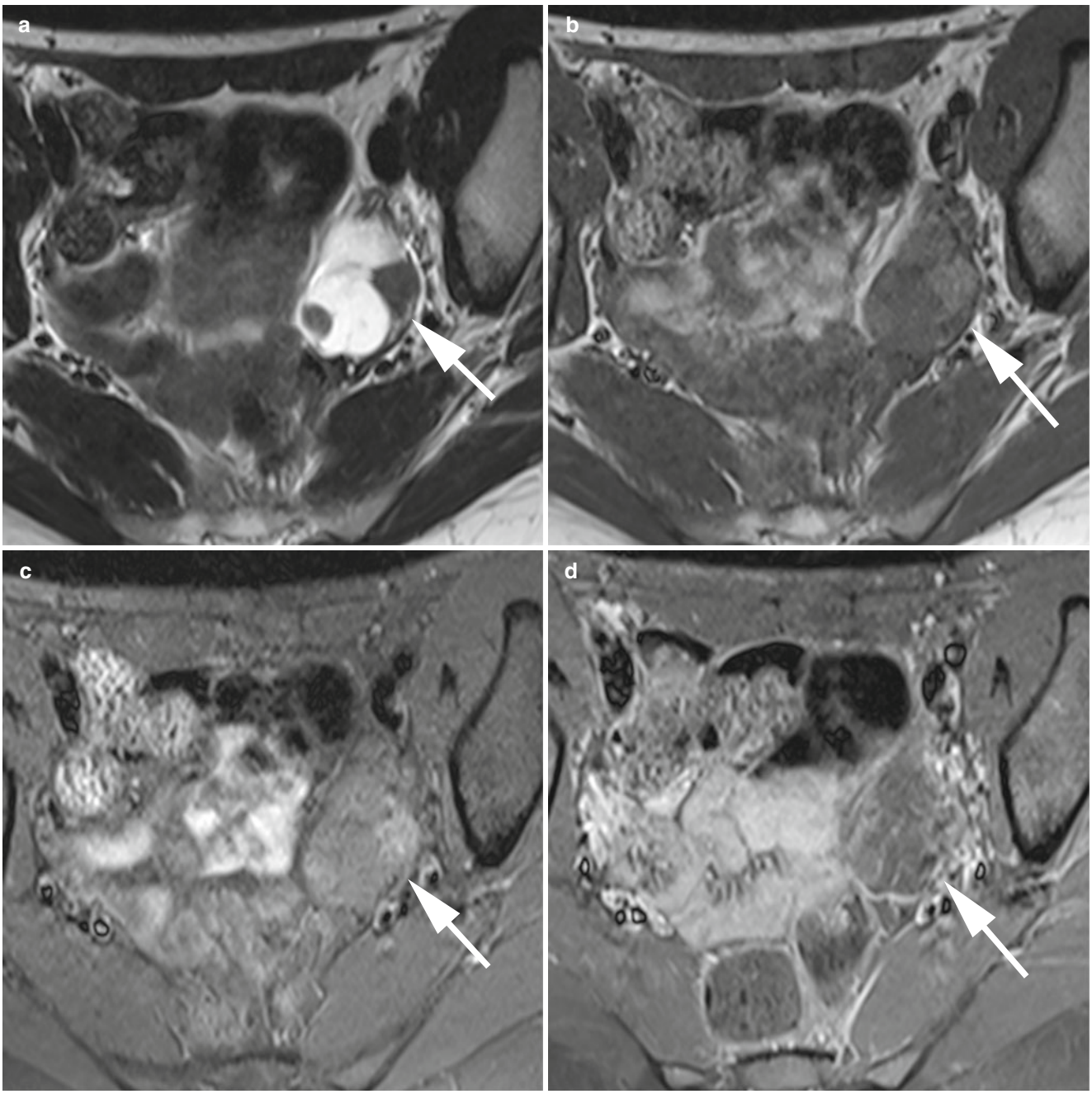

Fig. 14 MR of a left ovarian struma ovarii (*arrows*). (**a**) Axial T2-weighted TSE, (**b**) axial T1-weighted GE, (**c**) axial fat-suppressed T1-weighted GE, (**d**) axial gadolinium-enhanced fat-suppressed T1-weighted GE, (**e**) axial diffusion-weighted (ADC). Note the multiloculated mass with variable signals in each loculus, especially loculi with very low intensity on T2-weighted images and moderate high intensity on T1-weighted images, which is suggestive of this diagnosis. There is moderate enhancement of the wall and the septa after contrast

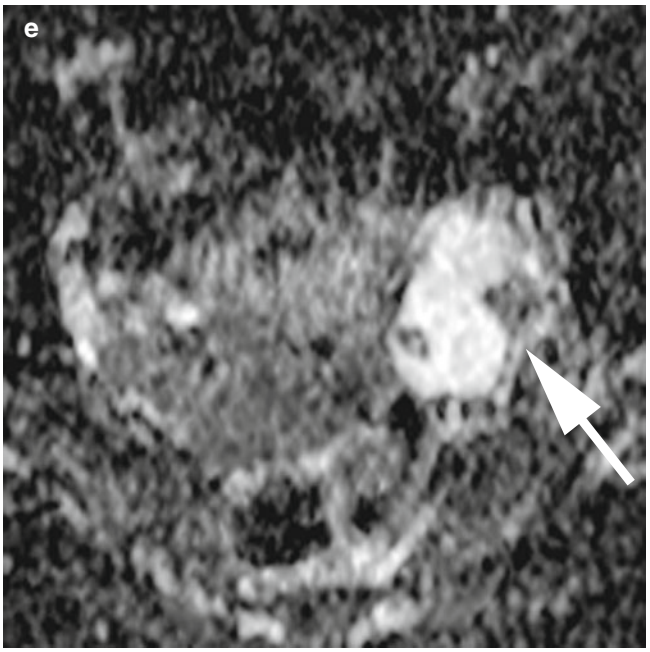

Fig. 14 (continued)

Neural Tumours

Monodermal teratomas with neuroectodermal differentiation can form benign, ependymoma-like tumours or primitive neuroectodermal tumours [95]. The latter are very aggressive tumours with a poor prognosis. They affect young women in their first or second decades. In imaging, the appearance varies from cystic (uni or multi [96]) to solid and is indistinguishable from other ovarian neoplasms.

References

1. Disaia P, Creasman W. Germ cell stromal and other ovarian tumours. Clinical gynaecological oncology. St Louis: Mosby; 1997. p. 351–71.
2. Sah SP, Uprety D, Rani S. Germ cell tumors of the ovary: a clinicopathologic study of 121 cases from Nepal. J Obstet Gynaecol Res. 2004;30(4):303–8.
3. Peterson WF. Malignant degeneration of benign cystic teratomas of the overy; a collective review of the literature. Obstet Gynecol Surv. 1957;12(6):793–830.
4. Hackethal A, Brueggmann D, Bohlmann MK, Franke FE, Tinneberg HR, Münstedt K. Squamous-cell carcinoma in mature cystic teratoma of the ovary: systematic review and analysis of published data. Lancet Oncol. 2008;9(12):1173–80.
5. Westhoff C, Pike M, Vessey M. Benign ovarian teratomas: a population-based case–control study. Br J Cancer. 1988;58(1):93–8.
6. Koonings PP, Campbell K, Mishell Jr DR, Grimes DA. Relative frequency of primary ovarian neoplasms: a 10-year review. Obstet Gynecol. 1989;74(6):921–6.
7. Ozgur T, Atik E, Silfeler DB, Toprak S. Mature cystic teratomas in our series with review of the literature and retrospective analysis. Arch Gynecol Obstet. 2011;285(4):1099–101.
8. Comerci Jr JT, Licciardi F, Bergh PA, Gregori C, Breen JL. Mature cystic teratoma: a clinicopathologic evaluation of 517 cases and review of the literature. Obstet Gynecol. 1994;84(1):22–8.
9. Altinbas SK, Yalvac S, Kandemir O, Altinbas NK, Karcaaltincaba D, Dede H, et al. An unusual growth of ovarian cystic teratoma with multiple floating balls during pregnancy: a case report. J Clin Ultrasound. 2010;38(6):325–7.
10. Song Y, Zhu L, Lang J. Recurrent mature ovarian teratomas: retrospective analysis of 20 cases. Zhonghua Yi Xue Za Zhi. 2007;87(17):1184–6.
11. Caspi B, Appelman Z, Rabinerson D, Zalel Y, Tulandi T, Shoham Z. The growth pattern of ovarian dermoid cysts: a prospective study in premenopausal and postmenopausal women. Fertil Steril. 1997; 68(3):501–5.
12. Bouic-Pagès E, Perrochia H, Mérigeaud S, Giacalone PY, Taourel P. MR imaging of primary ovarian tumors with pathologic correlation. J Radiol. 2009;90(7–8 Pt 1):787–802.
13. Las Heras F, Pritzker KP, Colgan TJ. Chordoma arising in a mature cystic teratoma of the ovary: a case report. Pathol Res Pract. 2007;203(6):467–71.
14. Arora RS, Alston RD, Eden TOB, Geraci M, Birch JM. Comparative incidence patterns and trends of gonadal and extragonadal germ cell tumors in England, 1979 to 2003. Cancer. 2012;118(17):4290–7.
15. Caruso PA, Marsh MR, Minkowitz S, Karten G. An intense clinicopathologic study of 305 teratomas of the ovary. Cancer. 1971;27(2):343–8.
16. Togashi K, Nishimura K, Itoh K, Fujisawa I, Sago T, Minami S, et al. Ovarian cystic teratomas: MR imaging. Radiology. 1987;162(3):669–73.
17. Buy JN, Ghossain MA, Moss AA, Bazot M, Doucet M, Hugol D, et al. Cystic teratoma of the ovary: CT detection. Radiology. 1989;171(3):697–701.
18. Outwater EK, Siegelman ES, Hunt JL. Ovarian teratomas: tumor types and imaging characteristics. Radiographics. 2001;21(2):475–90.
19. Hertzberg BS, Kliewer MA. Sonography of benign cystic teratoma of the ovary: pitfalls in diagnosis. AJR Am J Roentgenol. 1996;167(5):1127–33.
20. Patel MD, Feldstein VA, Lipson SD, Chen DC, Filly RA. Cystic teratomas of the ovary: diagnostic value of sonography. AJR Am J Roentgenol. 1998;171(4):1061–5.
21. Saba L, Guerriero S, Sulcis R, Virgilio B, Melis GB, Mallarini G. Mature and immature ovarian teratomas: CT, US and MR imaging characteristics. Eur J Radiol. 2009;72(3):454–63.
22. Kawakami S, Togashi K, Egawa H, Kimura I, Fukuoka M, Mori T, et al. Solid mature teratoma of the ovary: appearances at MR imaging. Comput Med Imaging Graph. 1994;18(3):203–7.
23. Nanda S, Kalra B, Arora B, Singh S. Massive mature solid teratoma of the ovary with gliomatosis peritonei. Aust N Z J Obstet Gynaecol. 1998;38(3):329–31.
24. Gürel H, Gürel SA. Ovarian cystic teratoma with a pathognomonic appearance of multiple floating balls: a case report and investigation of common characteristics of the cases in the literature. Fertil Steril [Internet]. 2008;90(5) [Cited 2012 Aug 22]. Available from: http://www.sciencedirect.com/science/article/pii/S0015028208000150
25. Kawamoto S, Sato K, Matsumoto H, Togo Y, Ueda Y, Tanaka J, et al. Multiple mobile spherules in mature cystic teratoma of the ovary. Am J Roentgenol. 2001;176(6):1455–7.
26. Otigbah C, Thompson MO, Lowe DG, Setchell M. Mobile globules in benign cystic teratoma of the ovary. BJOG. 2000;107(1):135–8.
27. Tongsong T, Wanapirak C, Khunamornpong S, Sukpan K. Numerous intracystic floating balls as a sonographic feature of benign cystic teratoma: report of 5 cases. J Ultrasound Med. 2006;25(12):1587–91.
28. Friedman AC, Pyatt RS, Hartman DS, Downey Jr EF, Olson WB. CT of benign cystic teratomas. AJR Am J Roentgenol. 1982;138(4): 659–65.

29. Guinet C, Ghossain MA, Buy JN, Malbec L, Hugol D, Truc JB, et al. Mature cystic teratomas of the ovary: CT and MR findings. Eur J Radiol. 1995;20(2):137–43.
30. Park SB, Cho K-S, Kim JK. CT findings of mature cystic teratoma with malignant transformation: comparison with mature cystic teratoma. Clin Imaging. 2011;35(4):294–300.
31. Rathod K, Kale H, Narlawar R, Hardikar J, Kulkarni V, Joseph J. Unusual "floating balls" appearance of an ovarian cystic teratoma: sonographic and CT findings. J Clin Ultrasound. 2001; 29(1):41–3.
32. Yamashita Y, Torashima M, Hatanaka Y, Harada M, Sakamoto Y, Takahashi M, et al. Value of phase-shift gradient-echo MR imaging in the differentiation of pelvic lesions with high signal intensity at T1-weighted imaging. Radiology. 1994;191(3):759–64.
33. Stevens SK, Hricak H, Campos Z. Teratomas versus cystic hemorrhagic adnexal lesions: differentiation with proton-selective fat-saturation MR imaging. Radiology. 1993;186(2):481–8.
34. Krinsky G, Rofsky NM, Weinreb JC. Nonspecificity of short inversion time inversion recovery (STIR) as a technique of fat suppression: pitfalls in image interpretation. AJR Am J Roentgenol. 1996;166(3):523–6.
35. Muramatsu Y, Moriyama N, Takayasu K, Nawano S, Yamada T. CT and MR imaging of cystic ovarian teratoma with intracystic fat balls. J Comput Assist Tomogr. 1991;15(3):528–9.
36. Nakayama T, Yoshimitsu K, Irie H, Aibe H, Tajima T, Nishie A, et al. Diffusion-weighted echo-planar MR imaging and ADC mapping in the differential diagnosis of ovarian cystic masses: usefulness of detecting keratinoid substances in mature cystic teratomas. J Magn Reson Imaging. 2005;22(2):271–8.
37. Yamashita Y, Hatanaka Y, Torashima M, Takahashi M, Miyazaki K, Okamura H. Mature cystic teratomas of the ovary without fat in the cystic cavity: MR features in 12 cases. Am J Roentgenol. 1994;163(3):613–6.
38. Dgani R, Rozenman D, Lifschitz-Mercer B. Granulosa cell tumor arising in an ovary with mature cystic teratoma. Int J Gynaecol Obstet. 1993;41(3):287–9.
39. Bige O, Demir A, Koyuncuoglu M, Secil M, Ulukus C, Saygili U. Collision tumor: serous cystadenocarcinoma and dermoid cyst in the same ovary. Arch Gynecol Obstet. 2008;279(5):767–70.
40. Kajo K, Macháleková K. Collision of invasive serous adenocarcinoma and mature cystic teratoma in the ovary. Letter to the editor. APMIS. 2007;115(6):769–71.
41. Kim SH, Kim YJ, Park BK, Cho JY, Kim BH, Byun JY. Collision tumors of the ovary associated with teratoma: clues to the correct preoperative diagnosis. J Comput Assist Tomogr. 1999;23(6):929–33.
42. Tang P, Soukkary S, Kahn E. Mature cystic teratoma of the ovary associated with complete colonic wall and mucinous cystadenoma. Ann Clin Lab Sci. 2003;33(4):465–70.
43. Hunter V, Barnhill D, Jadwin D, Crooks L. Ovarian mucinous cystadenocarcinoma of low malignant potential associated with a mature cystic teratoma. Gynecol Oncol. 1988;29(2):250–4.
44. Okada S, Ohaki Y, Ogura J, Ishihara M, Kawamura T, Kumazaki T. Computed tomography and magnetic resonance imaging findings in cases of dermoid cyst coexisting with surface epithelial tumors in the same ovary. J Comput Assist Tomogr. 2004;28(2):169–73.
45. Jung SE, Lee JM, Rha SE, Byun JY, Jung JI, Hahn ST. CT and MR imaging of ovarian tumors with emphasis on differential diagnosis. Radiographics. 2002;22(6):1305–25.
46. Logothetis CJ, Samuels ML, Trindade A, Johnson DE. The growing teratoma syndrome. Cancer. 1982;50(8):1629–35.
47. Moskovic E, Jobling T, Fisher C, Wiltshaw E, Parsons C. Retroconversion of immature teratoma of the ovary: CT appearances. Clin Radiol. 1991;43(6):402–8.
48. Kampan N, Irianta T, Djuana A, Pei Shan L, Hashim Omar M, Hatta Mohd Dali AZ. Growing teratoma syndrome: a rare case report and review of the literature. Case Rep Obstet Gynecol. 2012;2012:134032.
49. Sengar AR, Kulkarni JN. Growing teratoma syndrome in a post laparoscopic excision of ovarian immature teratoma. J Gynecol Oncol. 2010;21(2):129.
50. Lipson SA, Hricak H. MR imaging of the female pelvis. Radiol Clin North Am. 1996;34(6):1157–82.
51. Bouguizane S, Bibi H, Farhat Y, Dhifallah S, Darraji F, Hidar S, et al. Adnexal torsion: a report of 135 cases. J Gynecol Obstet Biol Reprod (Paris). 2003;32(6):535–40.
52. Taourel P, Curros DF, Millet I. CT of the acute abdomen. Gynecological emergencies. Springer-Verlag Berlin Heidelberg; 2011. p. 377–92.
53. Rha SE, Byun JY, Jung SE, Jung JI, Choi BG, Kim BS, et al. CT and MR imaging features of adnexal torsion. Radiographics. 2002;22(2):283–94.
54. Kim YH, Cho KS, Ha HK, Byun JY, Auh YH, Rhim HC, et al. CT features of torsion of benign cystic teratoma of the ovary. J Comput Assist Tomogr. 1999;23(6):923–8.
55. Park SB, Kim JK, Kim K-R, Cho K-S. Preoperative diagnosis of mature cystic teratoma with malignant transformation: analysis of imaging findings and clinical and laboratory data. Arch Gynecol Obstet. 2007;275(1):25–31.
56. Kido A, Togashi K, Konishi I, Kataoka ML, Koyama T, Ueda H, et al. Dermoid cysts of the ovary with malignant transformation: MR appearance. AJR Am J Roentgenol. 1999;172(2):445–9.
57. Yahata T, Kawasaki T, Serikawa T, Suzuki M, Tanaka K. Adenocarcinoma arising from respiratory ciliated epithelium in benign cystic teratoma of the ovary: a case report with analyzes of the CT, MRI, and pathological findings. J Obstet Gynaecol Res. 2008;34(3):408–12.
58. Guney N, Sayilgan T, Derin D, Ozcan D. Primary carcinoid tumor arising in a mature cystic teratoma of the ovary: a case report. Eur J Gynaecol Oncol. 2009;30(2):223–5.
59. O'Gorman T, Olaitan A. Primary malignant melanoma arising in an ovarian cystic teratoma. Eur J Gynaecol Oncol. 2009;30(1):88–9.
60. Opris I, Ducrotoy V, Bossut J, Lamy A, Sabourin J-C. Oligodendroglioma arising in an ovarian mature cystic teratoma. Int J Gynecol Pathol. 2009;28(4):367–71.
61. Tanaka H, Sakakura Y, Kobayashi T, Yoshida K, Asakura T, Taniguchi H. A case of thyroid-type papillary carcinoma derived from ovarian mature cystic teratoma, resected by laparoscopic surgery. Asian J Endosc Surg. 2011;4(2):86–9.
62. Yasunaga M, Saito T, Eto T, Okadome M, Ariyoshi K, Nishiyama K, et al. Dedifferentiated chondrosarcoma arising in a mature cystic teratoma of the ovary: a case report and review of the literature. Int J Gynecol Pathol. 2011;30(4):391–4.
63. Kefeli M, Kandemir B, Akpolat I, Yildirim A, Kokcu A. Rhabdomyosarcoma arising in a mature cystic teratoma with contralateral serous carcinoma: case report and review of the literature. Int J Gynecol Pathol. 2009;28(4):372–5.
64. Mori Y, Nishii H, Takabe K, Shinozaki H, Matsumoto N, Suzuki K, et al. Preoperative diagnosis of malignant transformation arising from mature cystic teratoma of the ovary. Gynecol Oncol. 2003;90(2):338–41.
65. Ulker V, Numanoglu C, Akbayir O, Akyol A, Tuncel A, Akca A, et al. Malignant transformation arising from mature cystic teratoma of the ovary: a report of six cases. J Obstet Gynaecol Res [Internet]. 2012 [Cited 2012 Aug 25]. Available from: http://onlinelibrary.wiley.com/doi/10.1111/j.1447-0756.2011.01797.x/full
66. Rha SE, Byun JY, Jung SE, Kim HL, Oh SN, Kim H, et al. Atypical CT and MRI manifestations of mature ovarian cystic teratomas. Am J Roentgenol. 2004;183(3):743–50.
67. Park SB, Kim JK, Kim K-R, Cho K-S. Imaging findings of complications and unusual manifestations of ovarian teratomas. Radiographics. 2008;28(4):969–83.
68. Fibus TF. Intraperitoneal rupture of a benign cystic ovarian teratoma: findings at CT and MR imaging. AJR Am J Roentgenol. 2000;174(1):261–2.

69. Ushakov FB, Meirow D, Prus D, Libson E, BenShushan A, Rojansky N. Parasitic ovarian dermoid tumor of the omentum-A review of the literature and report of two new cases. Eur J Obstet Gynecol Reprod Biol. 1998;81(1):77–82.
70. Shetty NS, Vallabhaneni S, Patil A, Babu MM, Baig A. Unreported location and presentation for a parasitic ovarian dermoid cyst in an indirect inguinal hernia. Hernia [Internet]. 2011 Sep 9 [Cited 2012 Aug 25]. Available from: http://www.ncbi.nlm.nih.gov/pubmed/21904862
71. Sinha R, Sundaram M, Lakhotia S. Multiple intraabdominal parasitic cystic teratomas. J Minim Invasive Gynecol. 2009;16(6):789–91.
72. Spencer RJ, Kurek KC, Laufer MR. Ovarian dermoid cyst superinfected with methicillin-sensitive Staphylococcus aureus leading to the misdiagnosis of appendicitis in an adolescent. J Pediatr Adolesc Gynecol. 2011;24(2):e25–8.
73. Dodd GD, Budzik Jr RF, et al. Lipomatous tumors of the pelvis in women: spectrum of imaging findings. Am J Roentgenol. 1990;155(2):317–22.
74. Ghosh B, McKeown B, Gumma A. Lipoleiomyoma. BMJ Case Rep [Internet]. 2011 [Cited 2012 Aug 15]. Available from: http://www.ncbi.nlm.nih.gov/pubmed/22679054
75. Dodd GD, Lancaster KT, Moulton JS, et al. Ovarian lipoleiomyoma: a fat-containing mass in the female pelvis. Am J Roentgenol. 1989;153(5):1007–8.
76. Zwiesler D, Lewis SR, Choo YC, Martens MG. A case report of an ovarian lipoma. South Med J. 2008;101(2):205–7.
77. Brandfass RT, Everts-Suarez EA. Lipomatous tumors of the uterus; a review of the world's literature with report of a case of true lipoma. Am J Obstet Gynecol. 1955;70(2):359–67.
78. Kitajima K, Kaji Y, Imanaka K, Sugihara R, Sugimura K. MRI findings of uterine lipoleiomyoma correlated with pathologic findings. Am J Roentgenol. 2007;189(2):W100–4.
79. Shanbhogue AK, Fasih N, Macdonald DB, Sheikh AM, Menias CO, Prasad SR. Uncommon primary pelvic retroperitoneal masses in adults: a pattern-based imaging approach. Radiographics. 2012;32(3):795–817.
80. Yuen PM, Yu KM, Yip SK, Lau WC, Rogers MS, Chang A. A randomized prospective study of laparoscopy and laparotomy in the management of benign ovarian masses. Am J Obstet Gynecol. 1997;177(1):109–14.
81. Anteby EY, Ron M, Revel A, Shimonovitz S, Ariel I, Hurwitz A. Germ cell tumors of the ovary arising after dermoid cyst resection: a long-term follow-up study. Obstet Gynecol. 1994;83(4):605–8.
82. Emin U, Tayfun G, Cantekin I, Ozlem UB, Umit B, Leyla M. Tumor markers in mature cystic teratomas of the ovary. Arch Gynecol Obstet. 2008;279(2):145–7.
83. Dede M, Gungor S, Yenen MC, Alanbay I, Duru NK, Haşimi A. CA19-9 may have clinical significance in mature cystic teratomas of the ovary. Int J Gynecol Cancer. 2006;16(1):189–93.
84. Talerman A. Germ cell tumors of the ovary. In: Kurman RJ, editor. Blaustein's pathology of the female genital tract. 3rd ed. New York: Springer; 1987. p. 687–721.
85. Grandet PJ, Remi MH. Struma ovarii with hyperthyroidism. Clin Nucl Med. 2000;25(10):763–5.
86. Kim JC, Kim SS, Park JY. MR findings of struma ovarii. Clin Imaging. 2000;24(1):28–33.
87. Jung SI, Kim YJ, Lee MW, Jeon HJ, Choi J-S, Moon MH. Struma ovarii: CT findings. Abdom Imaging. 2008;33(6):740–3.
88. Shen J, Xia X, Lin Y, Zhu W, Yuan J. Diagnosis of Struma ovarii with medical imaging. Abdom Imaging. 2011;36(5):627–31.
89. Joja I, Asakawa T, Mitsumori A, Nakagawa T, Hiraki Y, Kudo T, et al. Struma ovarii: appearance on MR images. Abdom Imaging. 1998;23(6):652–6.
90. Loizzi V, Cormio G, Resta L, Fattizzi N, Vicino M, Selvaggi L. Pseudo-Meigs syndrome and elevated CA125 associated with struma ovarii. Gynecol Oncol. 2005;97(1):282–4.
91. Rim SY, Kim SM, Choi HS. Struma ovarii showing clinical characteristics of ovarian malignancy. Int J Gynecol Cancer. 2005;15(6):1156–9.
92. Athavale RD, Davies-Humphreys JD, Cruickshank DJ. Primary carcinoid tumours of the ovary. J Obstet Gynaecol. 2004;24(1):99–101.
93. Takeuchi M, Matsuzaki K, Uehara H. Primary carcinoid tumor of the ovary: MR imaging characteristics with pathologic correlation. Magn Reson Med Sci. 2011;10(3):205–9.
94. Tanaka YO, Ide Y, Nishida M, Nishide K, Tsunoda H, Kajitani M, et al. Ovarian tumor with functioning stroma. Comput Med Imaging Graph. 2002;26(3):193–7.
95. Kleinman GM, Young RH, Scully RE. Primary neuroectodermal tumors of the ovary. A report of 25 cases. Am J Surg Pathol. 1993;17(8):764–78.
96. Sah SP, Verma K, Rani S. Neurogenic cyst of ovary: an unusual massive monodermal teratoma. J Obstet Gynaecol Res. 2001;27(1):21–5.

Part IV

Borderline and Malignant Tumor

Borderline Tumor (Serous/Mucinous/Endometrioid) (Clinical Setting and US)

Caterina Exacoustos

Abstract

Borderline ovarian tumors are epithelial tumors with a low growth rate and a low potential to invade or metastasize. These tumors have been studied with increased interest over the past decade. A pathologic definition was accepted by the International Federation of Gynecology and Obstetrics. They differ from malignant tumors because of the absence of stromal invasion in the former tumors, without regard to the features of any coexisting extraovarian disease.

Transvaginal sonography is the primary screening imaging technique in patients with ovarian masses. Borderline ovarian tumors are more difficult to diagnose correctly than benign and invasive malignant ovarian tumors.

Though various studies have described the morphological characteristics of borderline tumors, actually no ultrasound rule has up to now demonstrated the ability to discriminate, with high accuracy, a borderline tumor from a benign tumor or from an invasive tumor.

Keywords

Borderline tumors • Imaging • Ultrasound

Introduction

Borderline ovarian tumors (BOTs) or low malignant potential (LMP) are epithelial tumors with a low growth rate and a low potential to invade or metastasize. BOTs have been studied with increased interest over the past decade, but their clinical entity was initially reported by Taylor in 1929 [72]. A pathologic definition was accepted by the International Federation of Gynecology and Obstetrics (FIGO) in 1971 [36]. They differ from malignant tumors because of the absence of stromal invasion in the former tumors, without regard to the features of any coexisting extraovarian disease.

C. Exacoustos
Department of Obstetrics and Gynecology,
Università degli Studi di Roma "Tor Vergata",
Ospedale Generale S. Giovanni Calibita 'Fatebenefratelli',
Isola Tiberina 39, Rome 0186, Italy
e-mail: caterinaexacoustos@tiscali.it

BOTs constitute about 10–15 % of epithelial ovarian tumors; more than 96 % of which are either of serous or mucinous origin. Other rare types are endometrioid, clear cell, and transitional cell (Brenner) tumors. BOT can be associated with extraovarian disease, and they are staged the same way as ovarian cancer. However, extraovarian disease is defined as "implants" rather than metastasis. These implants are further subdivided into invasive and noninvasive one.

BOT can be either symptomatic or discovered incidentally during the course of investigations for other medical conditions. These tumors tend to occur in younger women and are often diagnosed in an earlier stage of the disease than invasive carcinomas. About 80 % of women with BOT present with stage I disease, contrary to their ovarian cancer counterparts. Women presenting with BOT are approximately 10–15 years younger than those with invasive epithelial ovarian cancer [1, 44].

The patients with early stage lesions have an excellent prognosis, while stage III lesions with peritoneal implants,

L. Saba et al. (eds.), *Ovarian Neoplasm Imaging*,
DOI 10.1007/978-1-4614-8633-6_12, © Springer Science+Business Media New York 2013

which are not uncommon, are correlated with a worse prognosis [8, 9, 26, 64]. Spread to lymph nodes is not uncommon, but it does not affect survival [2] and is very rare in stage I tumors (1 %) [8, 67, 71].

Because of the good prognosis associated with these tumors and the younger age of patients, fertility-sparing conservative treatments for BOT have been proposed. An endoscopic approach can be suggested for BOT with an accurate surgical staging. A preoperative identification of patients with ovarian lesions suspected of being BOT may be helpful in their management.

Different imaging techniques are available in the diagnostic workup of ovarian lesion; only few studies focused on BOT. Magnetic resonance imaging (MRI) and computerized tomography (CT) can characterize adnexal masses into benign and malignant in up to 93 % [3, 35, 70] and 89 % [80] of the cases, respectively. Bazot et al. [4] reported a sensitivity and specificity of MR imaging for the diagnosis of benign, borderline, and invasive tumors of 91.4 and 89.7 %, 45.5 and 96.1 %, and 91.7 and 88.7 %, respectively [4]. This study underlines the limitations of MR imaging for determining the borderline nature of ovarian tumors, with a sensibility of only 45.4 %. The sensitivity of combined positron emission tomography/computerized tomography (PET/CT) in detecting ovarian malignant tumors has been reported to range from 62 to 100 %, and the specificity has been reported to range from 85 to 100 % [10, 50, 57, 89]. Borderline ovarian tumors are not PET avid and hence are interpreted as "benign" tumors on PET [39, 57]. Ovarian masses that show complex features on MRI that are concerning for malignancy but appear as "benign" on PET are said to be characteristic of borderline ovarian tumors [57]. In particular, PET/CT seems to better enhance the ability to discriminate between malignant or borderline malignant tumors and benign than CT or MRI [50]. However, PET/CT is expensive and access is limited.

Transvaginal sonography (TVS) is actually the most used presurgical diagnostic test in the management of adnexal lesions. The differential diagnosis of adnexal masses still represents a challenge despite the tremendous efforts that have been made to improve the sonographically based diagnoses. This diagnosis is based on "pattern recognition," scoring systems, or mathematical models. Doppler techniques (color, power, pulsed) have also been proposed to distinguish benign from malignant lesions. Recently three-dimensional (3D) sonography has been introduced to overcome some limitations of conventional two-dimensional ultrasound.

It is well known that ultrasound is effective in differentiating benign from malignant ovarian tumors, and in most studies reporting sonographic features of ovarian tumors, BOT have been considered together with invasive malignant tumors [78, 84]. Only few studies [12, 21, 76, 90] have focused on the sonographic appearance of BOT. The assessment of sonographic features that distinguish BOT from both benign and malignant tumors makes it possible to treat them appropriately and in a more conservative way. This preoperative information is important, since neither serum tumor marker nor frozen section is particularly accurate in the diagnosis of borderline tumors [34, 40, 47].

Considering the increasing recommendation from the gynecologic oncologic community [20] to preserve fertility in young women undergoing surgery, considering the well-known low accuracy of serological tumor markers in discriminating benign and malignant ovarian tumors in premenopausal patients [84] and the limitations of MRI and PET/CT (costs and less availability), ultrasonography becomes the most important diagnostic tool for the surgeon to plan the appropriate treatment as well as to inform and counsel the patient about the surgery. Especially in case of small masses in young patients, the surgical decision to perform cystectomy instead of oophorectomy represents a clinical challenge. In these women, the suspicion of an invasive tumor would justify a complete removal of the ovary in order to avoid the high risk of spillage during cystectomy, which is related to a worsening of prognosis [54, 87]. On the contrary, recent data in literature [15, 44] prove that oophorectomy might be considered an overtreatment in young patients with borderline ovarian tumors.

Histological Aspects

Histological features that distinguish BOT from their benign counterparts are those of epithelial proliferation, varying degree of nuclear atypia, and absence of stromal invasion [63]. Except for the microinvasive variety, these tumors do not exhibit stromal invasion, and a serous or mucinous cystadenoma can be defined borderline, when the proportion of the abnormal proliferative foci constitutes at least 10 % of the tumor; otherwise, it is called serous or mucinous cystadenoma with focal atypia. However, this 10 % cutoff assumes careful gross examination and adequate directed sampling of the tumor [63].

A model has been proposed [14, 65, 66, 68, 69] for the development of ovarian carcinoma in which all histological types of surface epithelial tumors are divided into two categories—designated type I and type II—corresponding to 2 pathways of tumorigenesis.

Type I tumors include low-grade serous carcinoma, mucinous carcinoma, endometrioid carcinoma, malignant Brenner tumor, and clear cell carcinoma which develop in a stepwise fashion from well-recognized precursors, namely, "borderline" tumors. Benign precursors include cystadenomas/adenofibromas in the case of serous and mucinous tumors and endometriosis or endometriomas in

the case of endometrioid and clear cell tumors. Type I tumors are slow growing as evidenced by their large size and confinement to the ovary at diagnosis.

In contrast, type II tumors are high grade and usually have spread beyond the ovaries at presentation. Type II carcinomas include high-grade serous carcinoma ("moderately" and "poorly" differentiated), malignant mixed mesodermal tumors (carcinosarcomas), and undifferentiated carcinoma. These tumors are rarely associated with morphologically recognizable precursor lesions, and it has been proposed that they develop "de novo" from ovarian inclusion cysts.

This model explains the relationship of borderline tumors to invasive carcinoma and suggests that the majority of high-grade and low-grade carcinomas develop independently but, in rare cases, a high-grade serous carcinoma may arise from an atypical proliferative serous BOT. Therefore it is important to diagnose and treat early BOT, to follow-up the patients after surgical conservative treatment and to complete surgical ovarian removal after childbearing.

Sonographic Aspects

Transvaginal sonography is the primary screening imaging technique in patients with ovarian masses [78, 84, 85]. BOTs are more difficult to diagnose correctly than benign and invasive malignant ovarian tumors [90]. Valentin et al., studying which extrauterine pelvic masses are difficult to correctly classify on the basis of ultrasound findings, observed that BOTs are the most difficult to diagnose with only 47 % being correctly classified, 29 % being incorrectly classified, and 24 % being unclassifiable versus 90 % of non-borderline tumors being correctly classified, 3 % being incorrectly classified, and 8 % being unclassifiable ($p < 0.0001$) [82].

The low accuracy may be explained by variations in the morphological appearance of borderline ovarian tumors, which sometimes display features similar to benign or well-differentiated invasive ovarian malignancy [21, 22, 83].

It has been suggested that, using pattern recognition, it is possible to establish a correct preoperative diagnosis of borderline ovarian tumors with an accuracy not better than 69 % [21, 92].

Though various studies have described the morphological characteristics of borderline tumors [21, 25, 83, 92], actually no ultrasound rule has up to now demonstrated the ability to discriminate, with high accuracy, a borderline tumor from a benign tumor or from an invasive tumor [22, 75, 92].

To understand better sonographic features of BOT tumors, a histological differentiation may be useful.

Table 1 summarizes the most important histological features and prognostic factors of different BOT types and correlated them to ultrasound features.

Serous BOT (S-BOT)

Two distinct subtypes of S-BOT have been identified over the last few years, the typical pattern and the micropapillary/cribriform type [7, 61, 62]. The majority is of the typical subtype; in one population-based study, they constituted up to 74 % of all S-BOTs [27]. Micropapillary S-BOTs have higher frequencies of bilaterality (59–82 %), surface ovarian involvement (50–65 %), advanced stage at diagnosis (43–84 %), and stromal microinvasive foci and invasive implants (16–91 %) [7, 13, 17, 61, 62]. This is translated into higher recurrence rates and lower survival among treated patients with micropapillary S-BOT [1].

The diagnostic image that appears to correlate best with S-BOT is that of a cyst with internal papillae without other sign of complexity (such as solid pattern or thick septa) (Fig. 1). This sonographic finding is observed in 49–63 % of S-BOTs [12, 21, 25, 92]. Papillary projection seemed to be more typical in serous tumors; however unilocular cyst without any solid components was also observed. In fact there are studies [12, 18, 21, 25, 29, 52, 53, 92] which reported that up to 22.5 % of S-BOTs can exhibit sonographic features such as unilocular smooth sonolucent cysts without endophytic papillary growth. Gotlieb [29] reported 13 % and Emoto [18] 17 % of BOT with a sonographic appearance of unilocular cysts while Osmers [52] demonstrated that malignancy occurred in 0.8 % of unilocular smooth-walled cysts, of which 0.5 % were BOTs. These findings were in agreement with the study of Yazbek et al. [92] that showed a low sensitivity of ultrasound pattern-recognition method for the diagnosis of borderline ovarian tumors, with 11 % (4/35) of them presenting as simple cysts that could not be differentiated from benign cyst [92]. Similar findings have been reported by others [21, 25].

It seems however that the risk of finding a malignant or borderline tissue in a simple ovarian cyst declines with decreasing tumor size and decreasing age. It could happen that TVS evaluation of the cyst wall did not observe small papillae which further will be described among the histological features [21, 25]. This could be due to the fact that the TVS examination of large cysts could be less accurate because the distal cyst wall is too far away or is not well seen on the screen. On the other hand, the sonographic transabdominal evaluation of large cysts is not able to identify small papillae because of technical features (probe of lower frequency, thick abdominal wall, etc.). Therefore, large unilocular cysts should be managed with more caution than smaller ones (< 5 cm).

A cyst with internal papillae is the typical ultrasound image that appears to correlate with S-BOT [12, 21, 25, 92]. When the sonographic appearance of papillae is combined with the presence of internal vascularization (Figs. 2 and 3), a high specificity but a low sensitivity is observed; therefore,

Table 1 The most important histological features and prognostic factors of different BOT types and correlation to ultrasound features

Type of BOT	Precursor	Progression to	Histology, characteristic features, and subtypes	Ultrasound	Prognosis
Serous	Serous cystadenoma or adenofibroma	Invasive low-grade serous carcinoma May follow dualistic oncogenic pathway Invasive or noninvasive implants may occur Presence of invasive implants is a poor prognostic factor	Typical subtype (90 %) Micropapillary subtype (10 %) is closely associated with invasive implants	Unilocular cyst Fluid content Papillary projections Papillae with internal vascularization Papilla size >10 mm Irregular surface of the papilla	70 % of cases are stage I; survival is almost 100 % 30 % of cases are advanced stages; survival is 95.3 % if implants are noninvasive and 66 % if implants are invasive
Mucinous	Intestinal subtype: mucinous cystadenoma	Intraepithelial carcinoma then to invasive mucinous carcinoma	Intestinal subtype (90 %) Is unilateral Is multicystic with smooth capsule Is associated with pseudomyxoma peritonei	Multilocular cystic lesions More than 10 locules Fluid or dense fluid content Honeycomb nodule	82 % of cases are stage I; 5-year survival is up to 99–100 % 18 % of cases are advanced stages; mortality may reach up to 50 % depending on stage
	Endocervical Müllerian subtype: endometriotic cysts?	Intraepithelial carcinoma then to invasive mucinous carcinoma	Endocervical subtype (10 %) Is bilateral in 20–30 % Is exophytic Is loculate Mimics serous tumors	Unilocular cyst or few septation Fluid-dense content Papillary projections Papillae with internal vascularization	Stage I; 5-year survival is up to 99–100 % Mortality may reach up to 50 % depending on stage
Endometrioid	Endometriosis, endometrioid adenofibroma	Intraepithelial carcinoma then to low-grade invasive endometrioid carcinoma		Unilocular cyst Fluid-dense content Papillary projections Papillae with internal vascularization	Benign course with high survival rates
Clear cell	Endometriosis, clear cell adenofibroma Brenner tumor	Intraepithelial carcinoma then to invasive clear cell carcinoma		Multilocular solid lesion Papillary projections Papillae and solid tissue with internal vascularization	Benign course with high survival rates
Brenner	Benign Brenner	Malignant Brenner?		Solid or multiloculate solid Moderate to abundant vascularization	Benign course with high survival rates

the power or color Doppler examination of BOT seemed to have quantitative characteristics similar to those of malignant tumors and qualitative characteristics more similar to those of benign tumors. Earlier reports suggested that PI [93] or RI [32] might represent independent parameters allowing the differentiation of benign from malignant tumors. More recent evidences from the analysis of larger populations suggest that neither PI nor RI is sufficient, if taken singly.

Hassen evaluates recently also different sonographic features of the papillae in order to distinguish between benign, malignant, and BOTs. The mean size of the papillary projections was 9.6, 15.7, and 35.3 mm in benign, borderline, and malignant tumors, respectively ($p=0.0007$). An acute angle was present in 68 % of benign tumors and an obtuse angle in 40 % of borderline and 89 % of malignant tumors ($p=0.0001$). The surface was regular in 77 % of benign tumors and irregular in 50 % of borderline and 88 % of malignant tumors ($p=0.0000$). Calcifications were present only in benign tumors (18 %). For papillary projections ≥10 mm, color flow was present in all malignant, in 86 % of borderline (Fig. 2), and absent in all benign tumors (Fig. 3) [31].

Also Fagotti et al. [22] recently reported that unilocular solid ovarian lesions with a largest solid component >14 mm, presence of papillation flow, and the combination of the two parameters provided a sensitivity (100 %) superior than that of subjective evaluation and a specificity (61 %, 59 %, 75 %, respectively) lower than that of subjective evaluation (92 %) [22].

It has been shown that papillary projections in benign tumors have a loose stromal fibromatous core, whereas malignant tumors have intricate papillary projections with a central fibrovascular core [43]. Because of the presence or absence of angiogenesis, size and number of vessels are substantially more common in malignant than in borderline or benign tumors [31]. Several studies showed that the

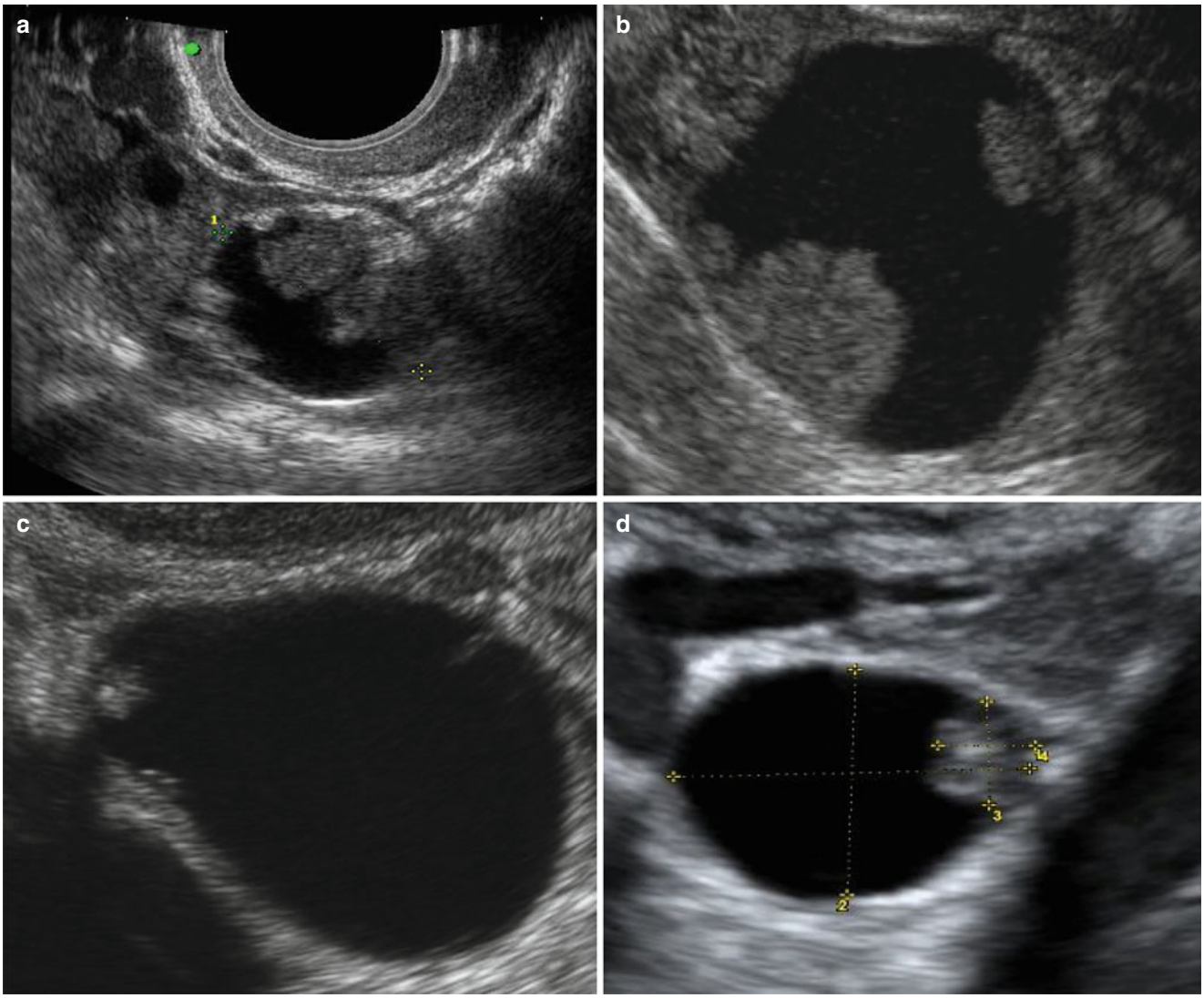

Fig. 1 Ultrasound images of unilocular cysts with papillary projections: (**a**, **b**) Serous BOT. (**c**) Benign cystadenofibroma. (**d**) Benign serous cyst

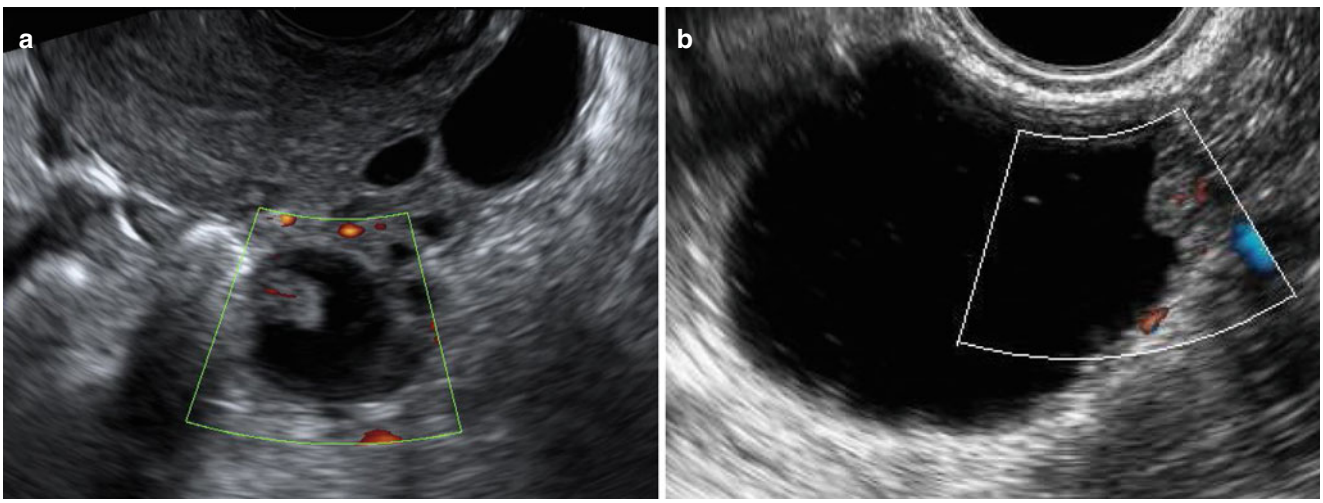

Fig. 2 Ultrasound images of unilocular cysts with vascularized papillae: (**a**, **b**) Benign serous cystadenoma. (**c**, **d**) Serous BOT (note the papillae of large volume)

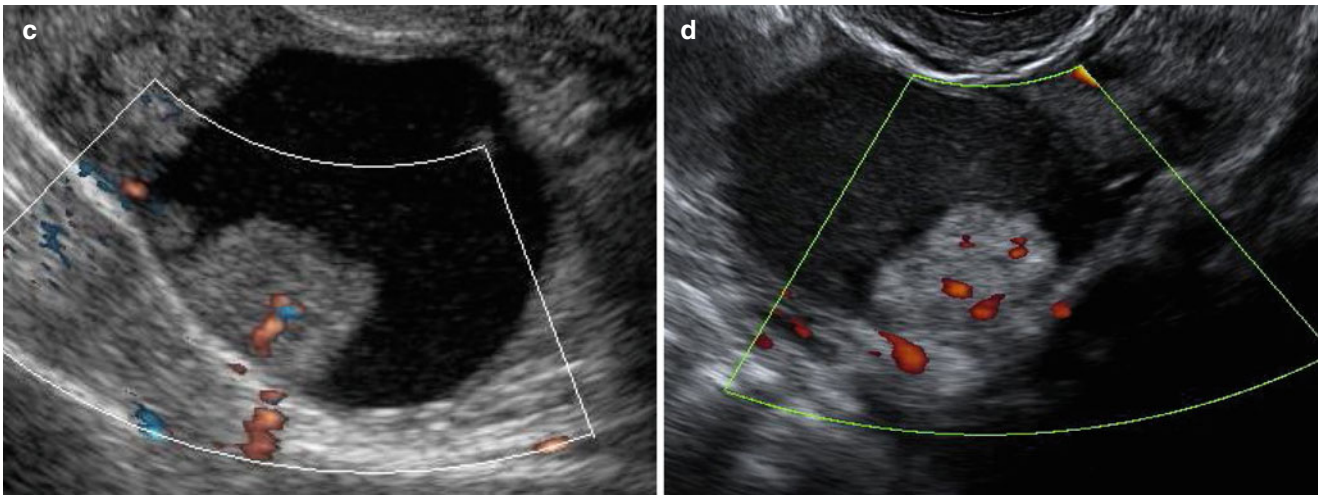

Fig. 2 (continued)

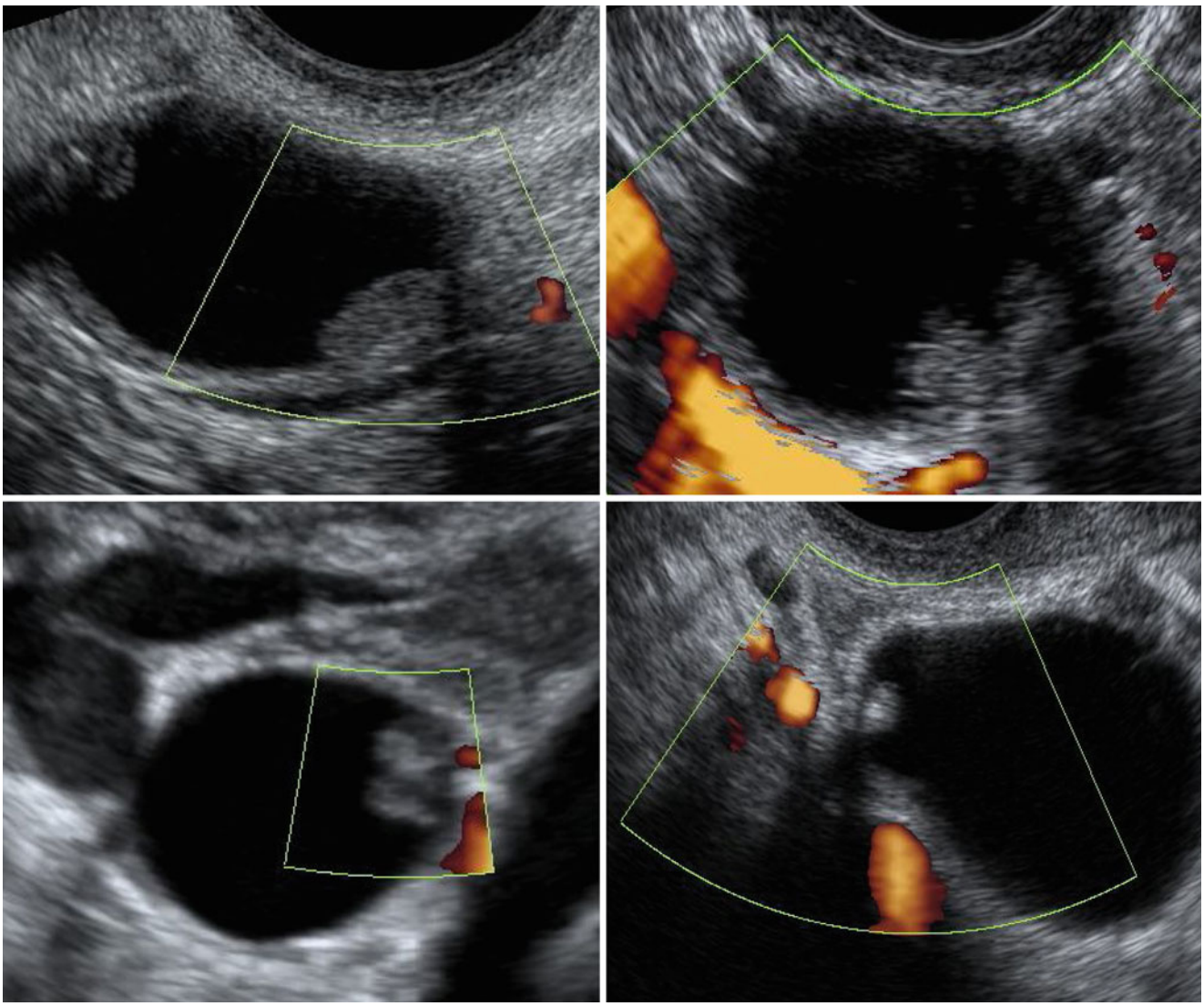

Fig. 3 Benign serous cystadenoma: ultrasound images of unilocular cysts with not vascularized papillae

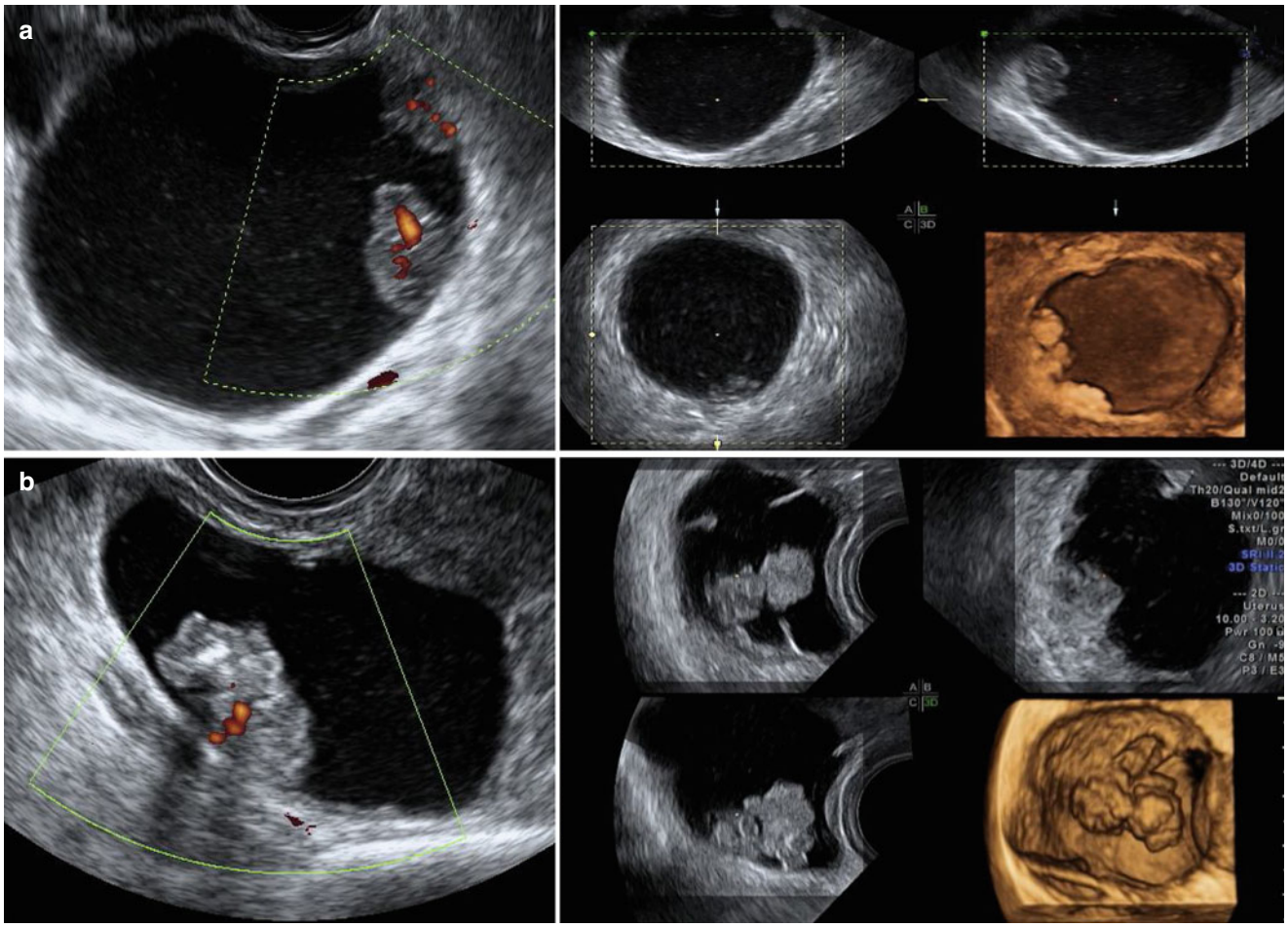

Fig. 4 Ultrasound imaging of vascularized papillary in two different ovarian lesions: (**a**) Serous BOT. (**b**) Serous cystadenocarcinoma grade 1 (note the similarity of the papillary to the power Doppler features and the irregular surface at the 3D rendering)

absence of color flow in papillary projections <10 mm is associated to benign papillary projections (Fig. 3). Conversely, in cases of malignant and BOT, color flow was present in the papillary projection [21, 22, 76] and the size of the papillae was ≥10 mm [22, 31]. Absence of color flow in a papillary projection <10 mm is suggestive of benignity. A certain number of morphologic and Doppler findings can highly suggest the diagnosis of benign versus malignant papillary projection, although an overlap exists, especially with serous BOT (Fig. 4).

Mucinous BOT (M-BOT)

M-BOT can exhibit features of intraepithelial carcinoma as well as microinvasion, but both features are difficult to diagnose definitively; however, tumors showing these features still behave in a benign way [38].

Mucinous borderline tumors which are the most common histological type of ovarian borderline tumors appear to show a better prognosis than mucinous carcinoma. Sherman et al. analyzed a large number of M-BOTs and reported that survival rates for women with both stage I and II borderline tumors and carcinomas were excellent, but survival was clearly decreased for women with borderline tumors associated with extraovarian disease [64]. Most cases of pseudomyxoma peritonei are associated with mucinous tumors of the appendix rather than spread from ovarian tumor [24, 42, 56, 58]. Furthermore, mucinous borderline tumor is further resistant to anticancer drugs compared with mucinous carcinoma, and neoadjuvant chemotherapy is not available as a weapon to improve the prognosis. Therefore, complete resection of mucinous borderline tumor is very important to achieve a good prognosis in patients with advanced mucinous borderline tumors [42].

Borderline tumors of the mucinous variety fall into one of the two types:

- The gastrointestinal type which constitute the majority of the M-BOT
- The endocervical (also called Mullerian or seromucinous) type

The vast majority of the gastrointestinal type of M-BOTs are stage I and have a benign course.

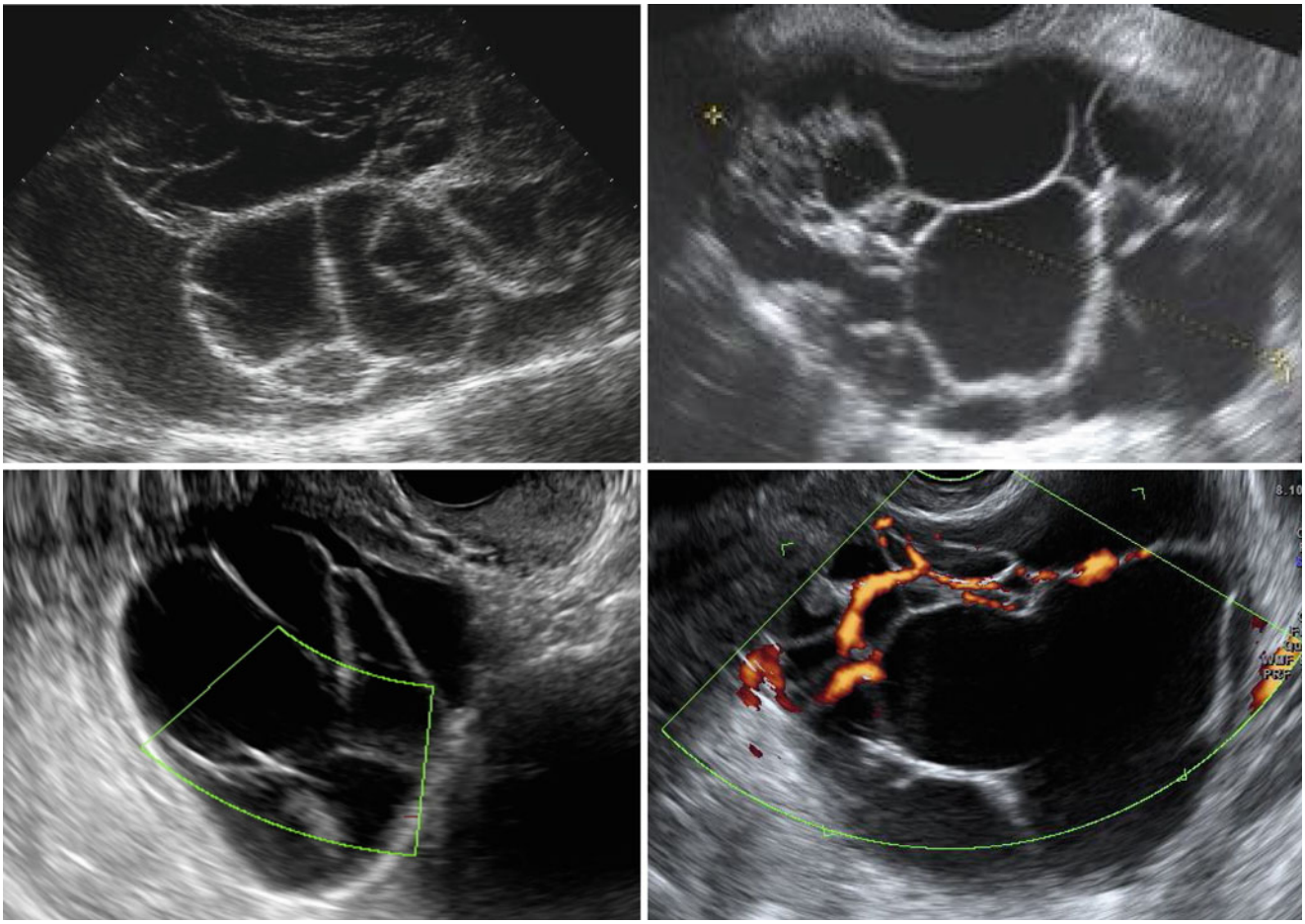

Fig. 5 Mucinous BOT of intestinal type: multilocular lesions with the more than ten locules

In contrast with the gastrointestinal type of M-BOT, the endocervical type is much less common, frequently bilateral, and displays both endocervical type mucinous and serous elements including micropapillary features. Interestingly, endometriosis is found in association with up to 40 % of endocervical type of M-BOT [60].

Different sonographic features has been observed between M-BOT of intestinal and endocervical type.

Gastrointestinal (GI)-type M-BOT

The sonographic characteristics of intestinal-type M-BOTs were in agreement with the histological descriptions of these unilateral, large, multicystic tumor with a smooth capsule. GI-type M-BOTs are generally characterized by a larger diameter and a multilocular aspect, with hyperechoic tissue connecting the multiple locules and no clear definition of solid tissue or papillary projection (Fig. 5). A multilocular nodule ("honeycomb nodule") was defined as a predominantly solid nodule with cystic areas arising from the inner cyst wall [92] (Fig. 6). The presence of a honeycomb nodule and thick echogenic fluid content is indicative of a GI-type M-BOT. Although slightly more than half of the GI-type BOTs had a honeycomb nodule, this nodule was also present in a case of benign mucinous cystadenoma. On the other hand, all GI-type BOTs had thick fluid noted within the cyst, which makes this finding a highly sensitive marker for this subtype of mucinous BOT. Thick fluid content was however also a characteristic of the majority of ovarian endometriomas, a few serous–endocervical-type BOTs and some epithelial malignant ovarian tumors.

Finally, the typical pattern of mucinous GI-type BOT is a multilocular cyst with a high number of locules (Fig. 7). Using the International Ovarian Tumor Analysis (IOTA) classification, these tumors should indeed be described as multilocular cysts, specifying the presence of more than 10 locules or the presence of the honeycomb nodule, which represent a subgroup of multilocular cysts. This distinction is important, as many benign and invasive tumors are classified as multilocular cysts. Nearly two-thirds of benign cystadenomas appeared as multilocular cysts and, without performing a more detailed analysis, they could be wrongly classified as GI-type BOT [92].

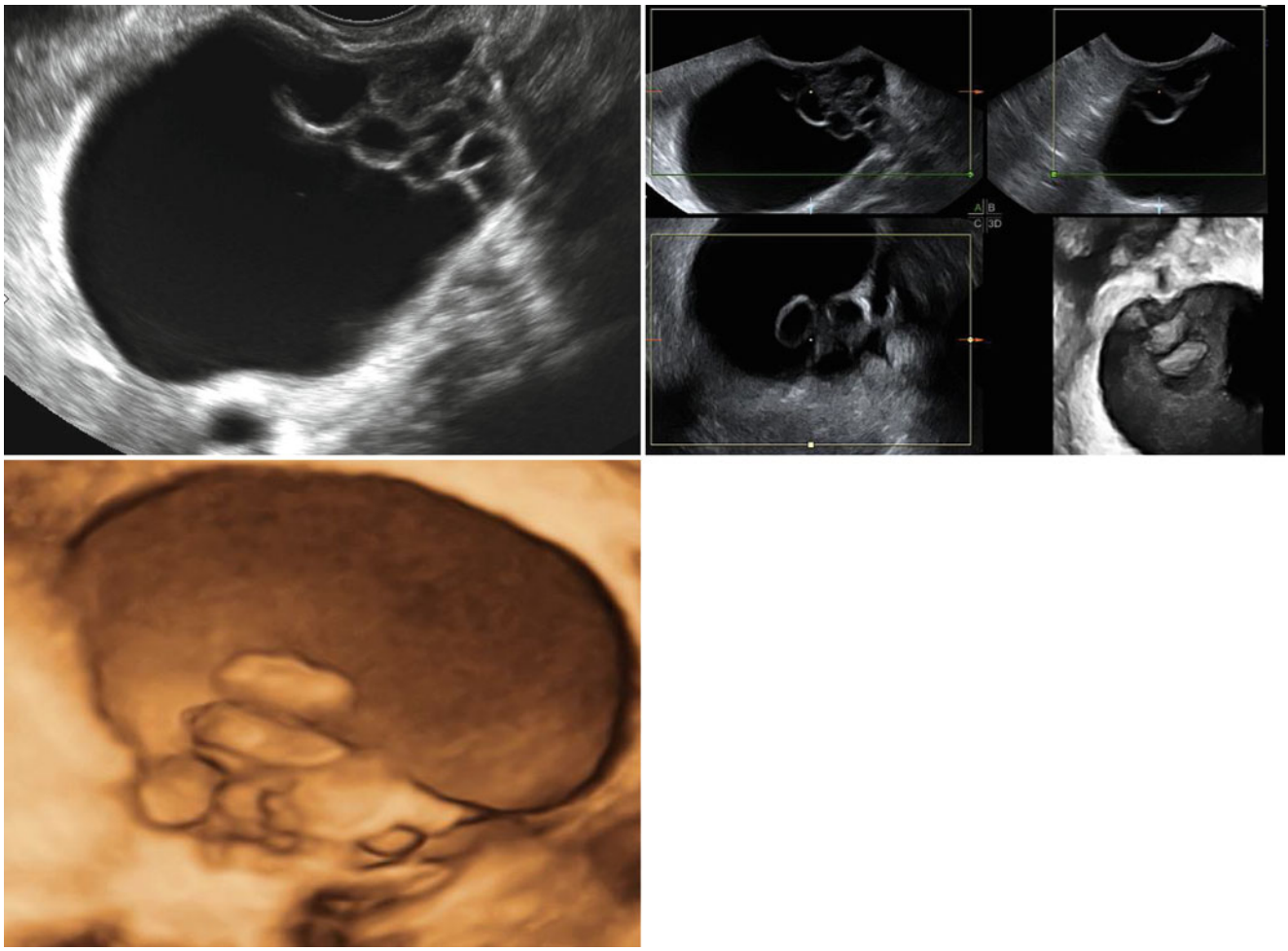

Fig. 6 Mucinous gastrointestinal-type borderline ovarian tumor. A "honeycomb nodule" is seen in the cyst cavity

Endocervical-Type M-BOT

Endocervical-type M-BOTs have similar sonographic features to S-BOT: unilocular solid cyst, with vascularized papillae and rare presence of few septations.

Compared with the GI-type M-BOTs, these tumors are characterized by a smaller maximum diameter, fewer locules (they were usually unilocular solid lesions), a higher number of papillary excrescences within the lesions, and a higher rate of vessels inside the papillations (Fig. 8).

Table 2 shows some important definitions of M-BOT as well as histological and ultrasound features of both mucinous BOT, respectively.

Other Types of BOT: Endometrioid, Clear Cell, and Brenner types

Clear cell borderline ovarian tumors have low malignant potential and are characterized by the presence of clear or hobnail cells set in a dense fibrous stroma with absence of stromal invasion. Borderline Brenner tumors are ovarian transitional cell tumors with atypical or malignant features of the epithelium but lacking stromal invasion [1, 44].

These tumors do not show characteristic imaging features and may resemble other borderline ovarian tumors as well as early-stage or low-grade ovarian carcinomas (Fig. 9).

Endometriosis and endometrioid adenofibromas serve as precursors of endometrioid borderline ovarian tumors. Endometrioid borderline ovarian tumors have the potential to progress to low-grade invasive carcinoma. Although clear cell borderline ovarian tumors have been associated with endometriosis and adenofibromas, a stepwise molecular pathway for the progression of endometriosis or adenofibroma to clear carcinoma has not yet been identified [44].

Testa et al. [76] described an endometrioid borderline tumor that developed in an endometrioid cyst that appeared as a unilocular solid ovarian lesion (largest diameter of mass,

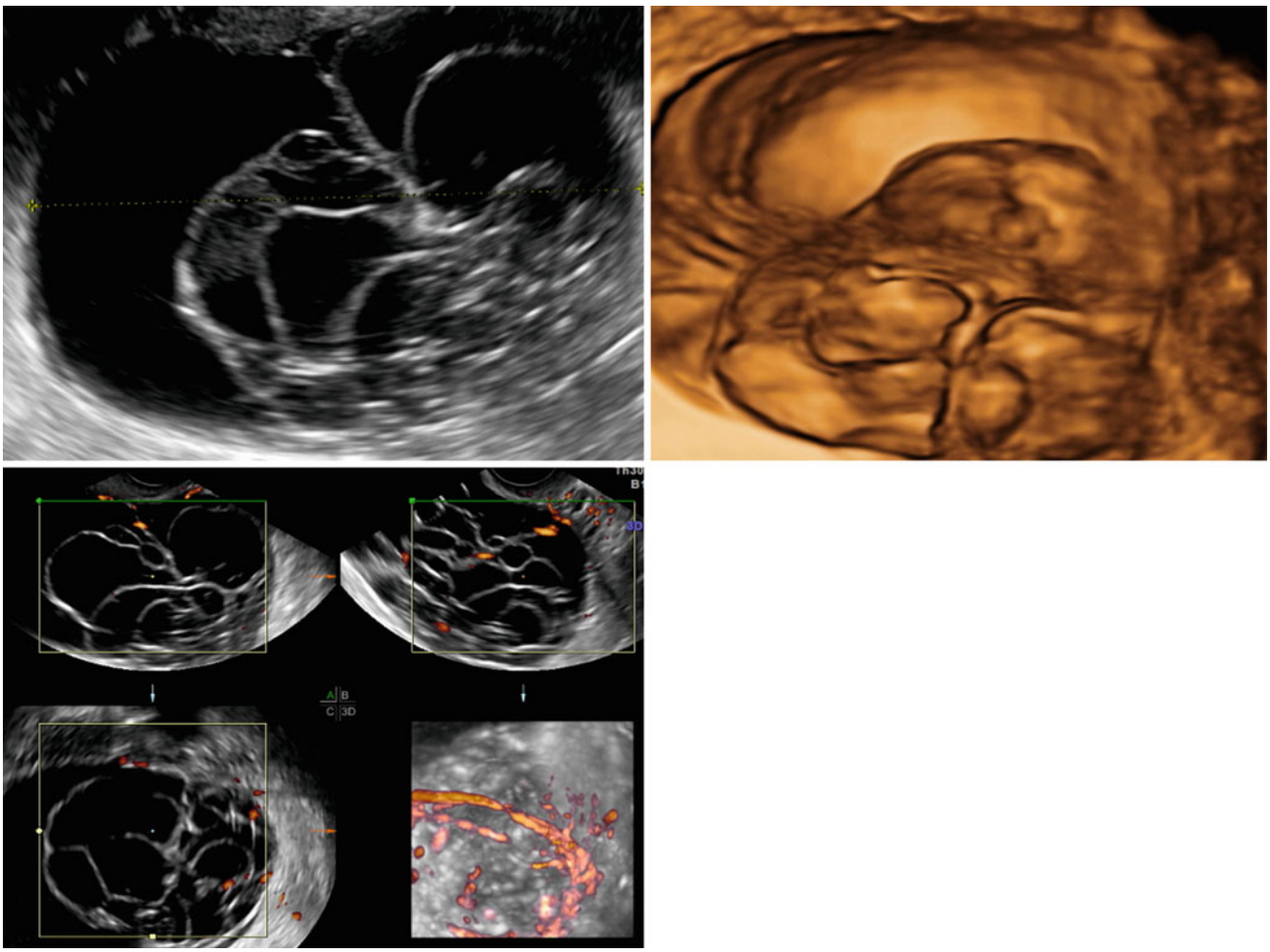

Fig. 7 Mucinous BOT gastrointestinal type: 2D and 3D rendering and the power Doppler view

46 mm) with a papillary projection (height = 29 mm), which was highly vascularized at power Doppler examination, similar to the typical features of S-BOT or endocervical M-BOT [76].

Borderline tumors and carcinomas arising from endometrioid cysts show a vascularized solid component at ultrasound examination (Fig. 10). Testa findings suggest that benign endometrioid cysts and malignancies and BOT arising from endometriosis might not represent a specifically difficult category of ovarian masses for assessment by an expert ultrasound examiner compared with the general population of ovarian masses. This seems not to be valid for ovarian cyst during pregnancy where the differentiation between BOT and decidualized endometriotic cyst could be difficult. Ultrasound examiners should always take into account the phenomenon of decidualization, which is one of the most important sources of incorrect diagnosis, while examining pregnant women.

Sonographic Differential Diagnosis

S-BOT Versus M-BOT

Serous BOT are smaller than mucinous types; they are multilocular in 30 % of cases and present with solid parts or papillary pattern in the majority of cases (78 %). Mucinous BOTs are multilocular in 50 % of cases and present with solid parts or papillary pattern in only 40 % of cases [29]. One study showed that intestinal-type M-BOTs have a different ultrasonography appearance when compared with S-BOT and endocervical-type M-BOT [25].

S-BOTs and endocervical-type M-BOTs have similar sonographic features. They are characterized by a higher rate of unilocular solid lesions, a higher number of papillary excrescences, and a lower percentage of multilocular lesions. Compared with the intestinal-type M-BOTs, these tumors were characterized by a smaller maximum diameter, fewer

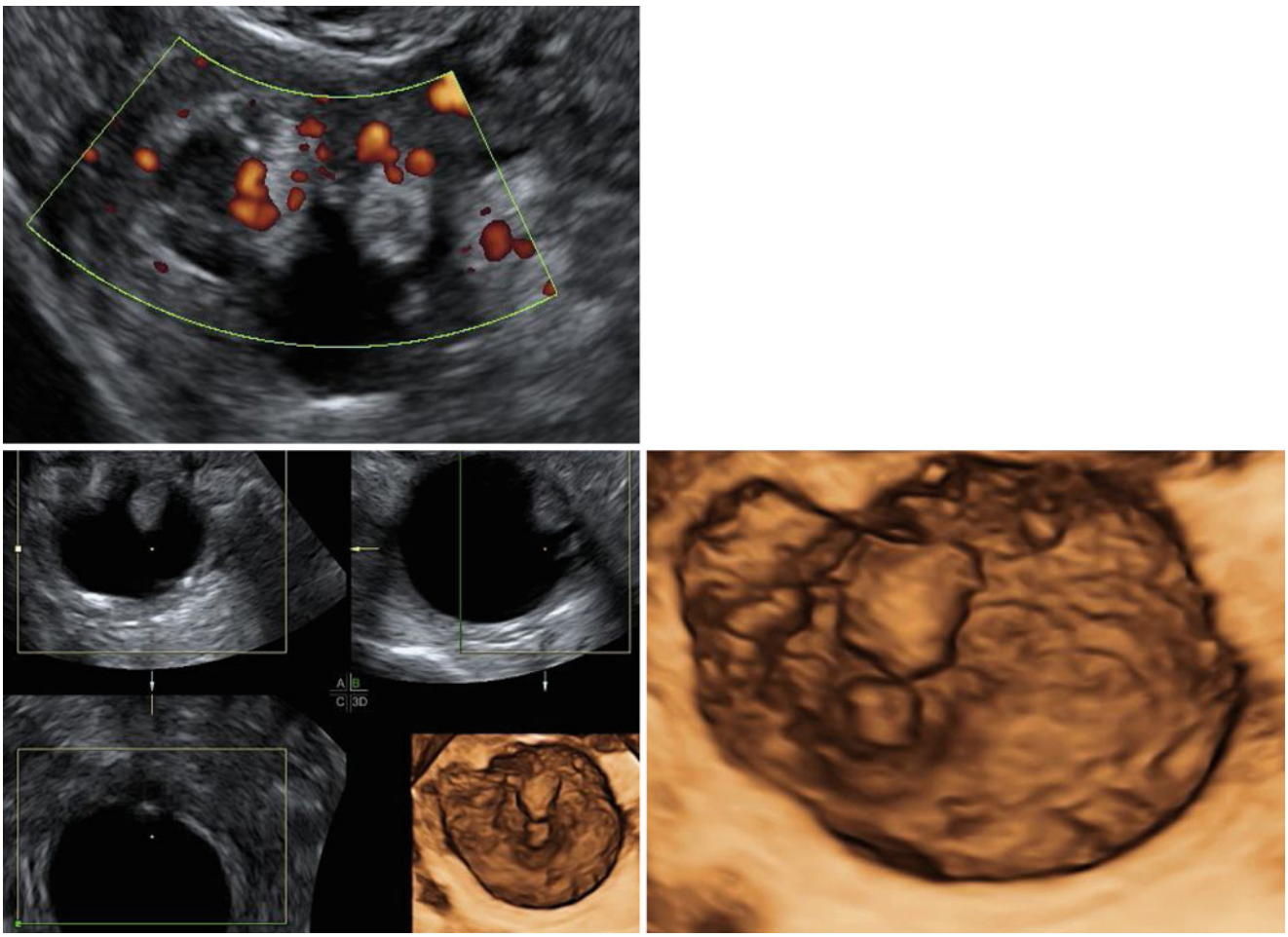

Fig. 8 Mucinous BOT endocervical type: ultrasound image of a multilocular solid cysts (one septum) and papillary projections

Table 2 Mucinous BOT: histological and ultrasound characteristics of different subtypes

Mucinous BOT	Gastrointestinal type	Endocervical type
Frequency	Common	Rare
Localization	Unilateral	Bilateral
Histology features		
Macroscopic	Multicystic, smooth capsule	Exophytic
Microscopic	Proliferative, mucinous epithelium, villoglandular or intraglandular pattern of growth, varying nuclear atypia	Usually combination serous and endocervical-type epithelium with mixed cell types
Ultrasound features	Multilocular >10 locules Honey comb nodule	Cyst with papillary projections Vascularized solid component

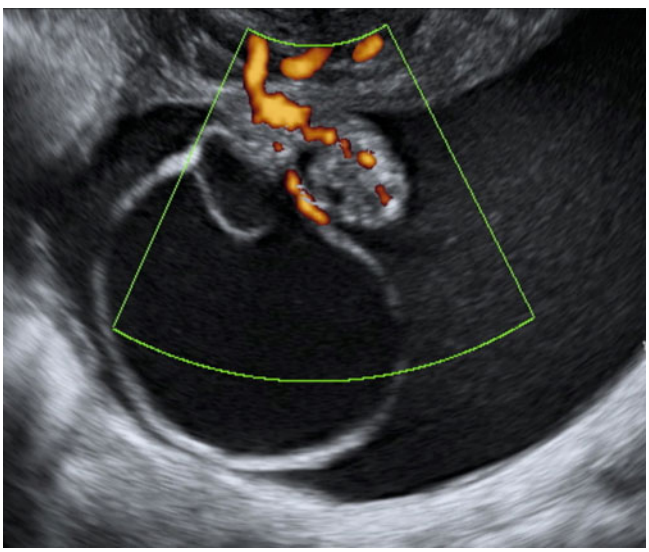

Fig. 9 Ultrasound and power Doppler image of a clear cells borderline ovarian tumor

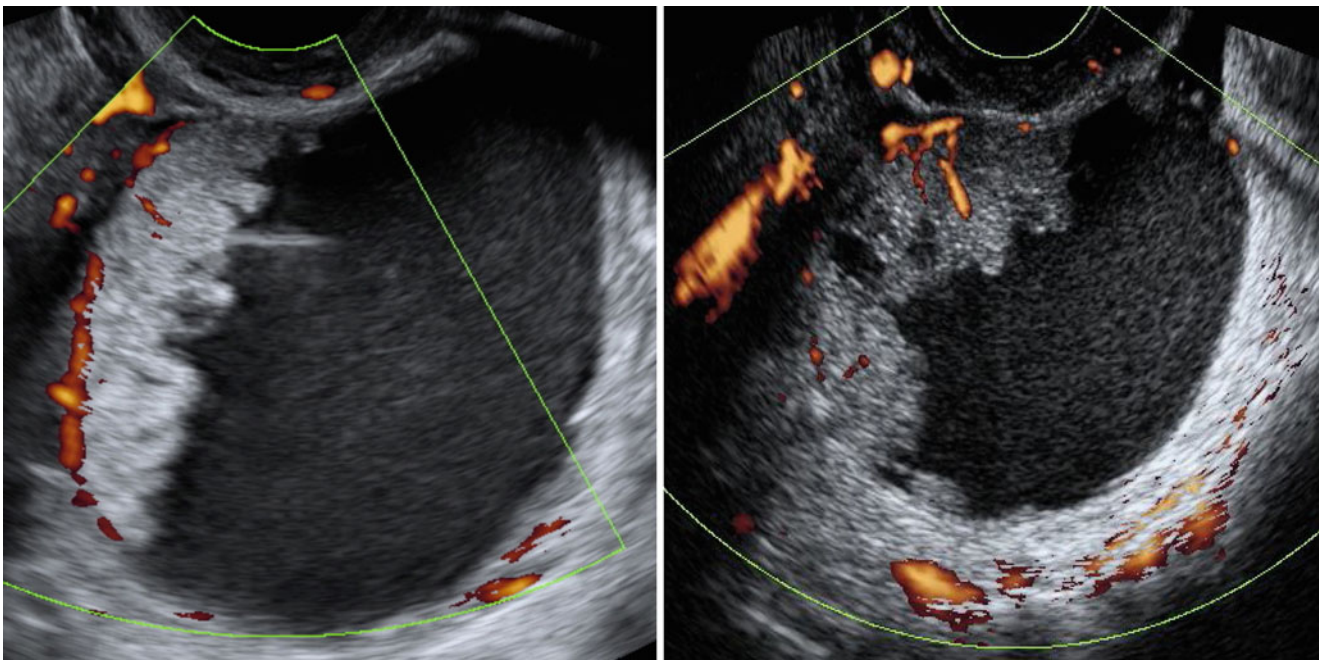

Fig. 10 Ultrasound and power Doppler image of two cases of endometrioid borderline tumor

locules, a higher number of papillary excrescences within the lesions, and a higher rate of vessels inside the papillations. This is in agreement with data from the pathology literature that report that endocervical-type M-BOTs resemble S-BOTs architecturally.

In comparison with other S-BOTs, intestinal-type M-BOTs were characterized by a larger diameter and a multilocular aspect, with hyperechoic tissue connecting the multiple locules and no clear definition of solid tissue or papillary projection.

A multilocular nodule (honeycomb nodule), which is a predominantly solid nodule with cystic areas arising from the inner cystic wall, is a highly specific feature of gastrointestinal-type BOT, but its sensitivity is low because it is absent in nearly half of these tumors [92]. No significant difference is observed in the detection of the intratumoral blood flow between different histopathologic types [18].

Gotlieb et al. [29] reported a comparison of serum CA125 level between serous and mucinous borderline tumors, and serous borderline tumors were associated more frequently with elevated CA125 levels than mucinous borderline tumors [29]. Several studies reported for M-BOT higher sensitivity of CA19-9 and CA72-4 than that of CA125 [29, 47], although these markers are less useful to distinguish malignant tumors from whole ovarian tumors than CA125. Some studies [19, 42] reported that CA19-9 was more frequently elevated than CA125 in patients with mucinous borderline tumors. Kikkawa showed recently that CA72-4 is the most useful tumor marker to distinguish borderline tumor and cancer from benign tumor among four clinically available tumor markers; CA125 was the lowest in mucinous tumor. These findings suggested that measurement of CA72-4 and Ca 19–9 is useful when multilocular cysts were observed by TVS [42].

BOT Versus Benign or Malignant Ovarian Lesions

As is well known, ultrasound has a high accuracy in differentiating benign and malignant ovarian tumors and is actually one of the most important presurgical diagnostic tests in the management of adnexal lesions.

The accuracy in differentiating malignant from benign ovarian lesions ranged depending on the methods used (scores, logistic regressions, pattern recognition). In most of the studies evaluating sonographic accuracy in diagnosing ovarian lesions' histology, malignant and borderline tumors were considered together as invasive tumors. Only few studies [12, 21, 25, 92] distinguish BOT from both benign and malignant tumors when evaluating diagnostic accuracy of TVS. Some authors have reported BOT to have a preoperative appearance similar to that of benign cysts. In particular, experienced ultrasonographers perform better when differentiating invasive from noninvasive (benign and borderline) ovarian tumors than when discriminating malignant (borderline and invasive) from benign masses, mainly owing to a tendency to misclassify BOT as benign lesions [90]. TVS seems to be more accurate in discriminating between invasive (malignant) and noninvasive (benign and borderline) tumors. In particular, the combination of the largest diameter and the vascularization of the solid component was shown to provide higher sensitivity and

lower specificity than subjective evaluation in recognizing invasive tumors (100 % vs. 60 %; 75 % vs. 92 %). Yazbek and colleagues demonstrated that the absence of normal healthy tissue (namely, "ovarian crescent sign") is able to identify all invasive tumors and differentiating them better from borderline and benign lesions [33, 91]. These parameters however failed to reach the same predictive performance when tested prospectively in a multicenter study (sensitivity 94 % vs. 100 % and specificity 40 % vs. 76 %) [86].

Recently Van Claster [85] compared guidelines from the Royal College of Obstetricians and Gynaecologists (RCOG) based on the Risk of Malignancy Index (RMI) with a protocol based on logistic regression model LR2 developed by the International Ovarian Tumour Analysis (IOTA) group in diagnosing ovarian mass [77]. The IOTA protocol classified more borderline tumors as high risk than the RCOG protocol. This implies that with the IOTA protocol more women with borderline tumors would be managed in gynecological oncology centers, and even though there may be more conservative fertility-sparing treatment options in these women, decisions about such treatments are likely to be better handled by subspecialist gynecological oncologists [85].

The problem that arises from all the sonographic studies on BOT is not only the inability to differentiate benign tumors from BOT but especially the inaccuracy in distinguishing BOT from malignancy. It seems that BOTs do not have a pathognomonic or typical sonographic pattern. In fact, the presence of papillae can also be found in benign serous tumors, and if internal vascularization of the papillae is considered, it is very difficult to distinguish BOT from invasive malignant tumors. It has also been noted that there is little difference between BOT and well-differentiated invasive malignant tumors [59, 62]. Tumors that are of higher grading or are undifferentiated are associated with greatrìer amount of solid tisusses with irregular structure, whereas low-grade malignant tumors preserve the structural characteristics of the original histological type [59, 62]. Therefore, differentiation between BOT and invasive malignant tumors seems not to be stage dependent but is probably grade dependent. In other words, it seems to be very difficult to distinguish a well-differentiated serous ovarian carcinoma from a serous BOT, since both can appear at ultrasound as a cyst with vascularized papillae. A grade 3 serous carcinoma, however, generally presents a sonographically more complex structure with a large amount of solid tissue. On the other hand, papillae can also be observed in benign cystadenomas or cystadenofibromas, and in these cases perhaps, the vascularization inside the papilla could suggest BOT or malignancy, even though avascular papilla is not always associated with benign tumors and vice versa [21]. In order to differentiate BOT from malignant and benign ovarian tumors by better analyzing vascular quantification and surface of the papilla, the use of intravenous injection of contrast medium and three-dimensional ultrasound has been proposed.

Contrast Media

It has been suggested that intravenous injection of contrast medium might increase the ability to discriminate benign tumors, BOT, and invasive ovarian cancers [46, 51, 73–75] based on the capacity of the contrast agent to perfuse microvessels in the solid tissue and analyzing the quantity, quality, and the dynamic pattern of the perfusion (time–intensity curve, wash-in and washout time) of the intravascular contrast media. It has been shown that the signal enhancement from intravenous injection of the contrast agent is quicker, stronger, and of longer duration in malignant tumors than in benign cysts. Utrasound distribution of contrast media (SonoVue) in the microcirculation of unilocular and multilocular ovarian masses with papillary projections was used to investigate whether the qualitative evaluation of the passage of the contrast agent can improve the performance of sonography in distinguishing benign from malignant masses with papillary projections (Fig. 11). Testa [74] found that qualitative evaluation of blood circulation in papillary projections using ultrasound contrast evaluation does not improve the discrimination of benign from borderline/malignant ovarian masses with papillary projections. Furthermore, it was reported that rising time was highest in BOT and low in benign and invasive ovarian tumors [46]. A recent multicenter international study observed that quantitative contrast sonographic parameters (peak contrast, signal intensity, and area under the contrast signal intensity curve) in invasive malignant tumors were significantly higher than those in borderline and benign tumors, while those for the benign and borderline tumors were similar [75]. Findings on ultrasound differed between benign and malignant tumors, but there was a substantial overlap in contrast findings between BOT and benign tumors. Unfortunately, these contrast variables cannot be routinely used in clinical practice, which instead calls for objective, noninvasive, and simple parameters.

Three-Dimensional TVS

3D ultrasound allows a more detailed assessment of intracystic structure and elimination of internal echoes mimicking solid tissue, such as clots, debris, and fatty and mucinous plugs. Especially in cyst suspected to be borderline, 3D TVS with rendering improves the visualization of the surface of internal capsule wall and excrescences, and the addition of 3D power Doppler seems to be very helpful (Fig. 12). 3D TVS rendering of the internal aspect of cystic masses can yield high detail of internal papillae previously identified on 2D TVS. This ruling out excrescences inside the cyst seems to be useful in the

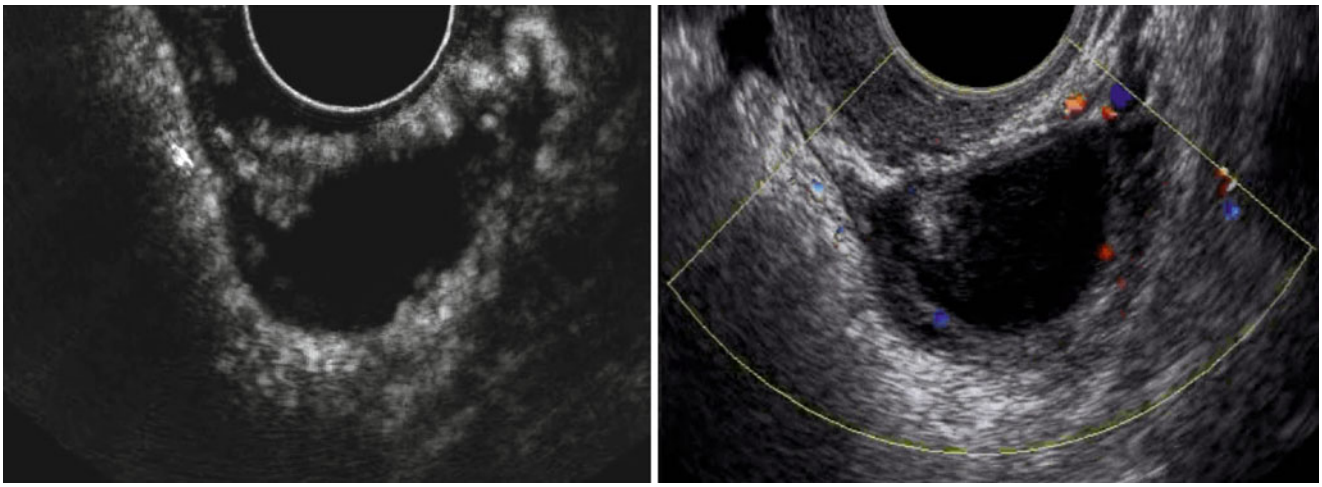

Fig. 11 Cysts with papilla: 2D and color Doppler view and image during intravenous contrast agent injection (note the hyperechoic contrast media in the microvessels of the papilla)

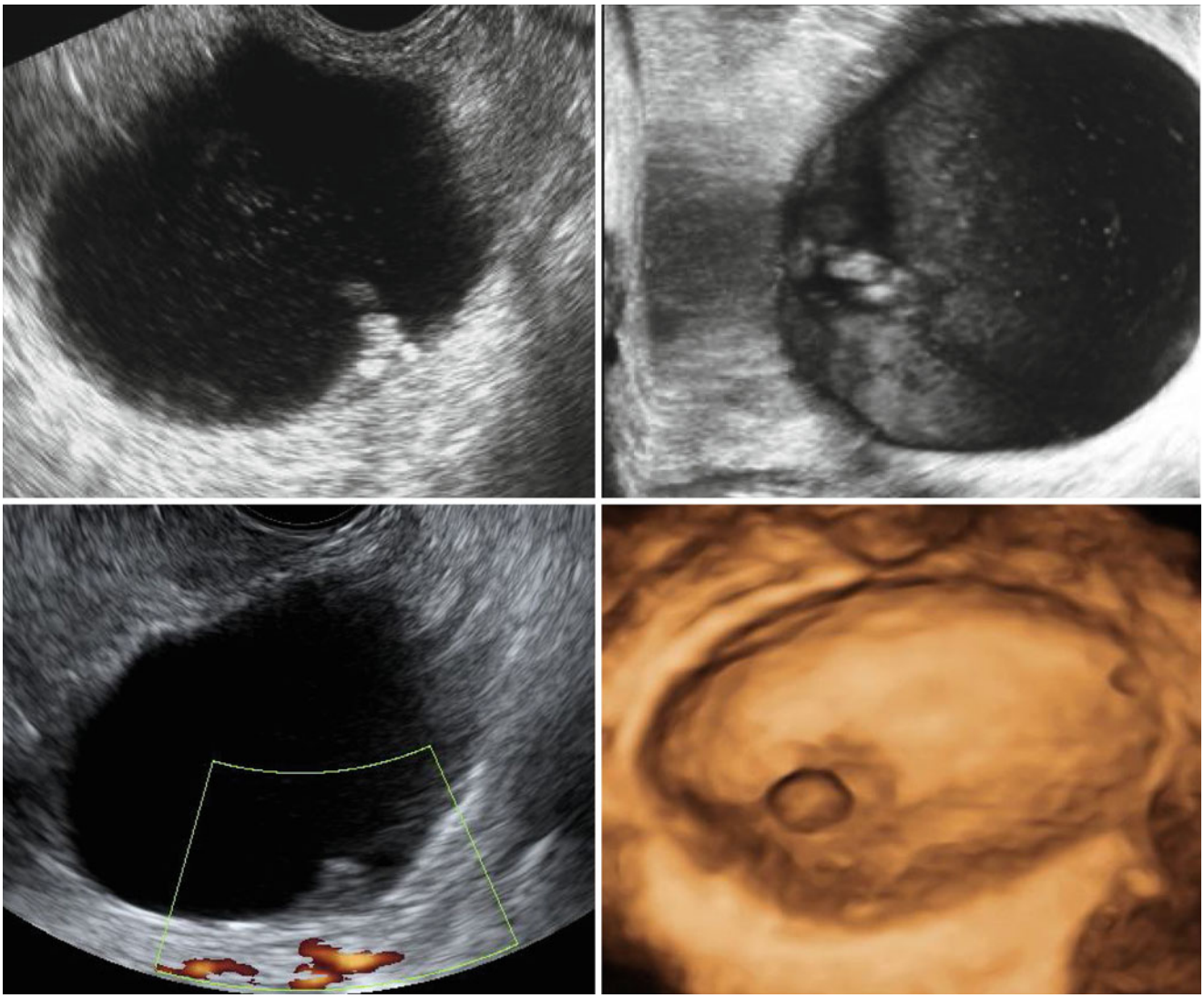

Fig. 12 3D rendering of benign serous cystadenoma (note the smooth surface of the papilla)

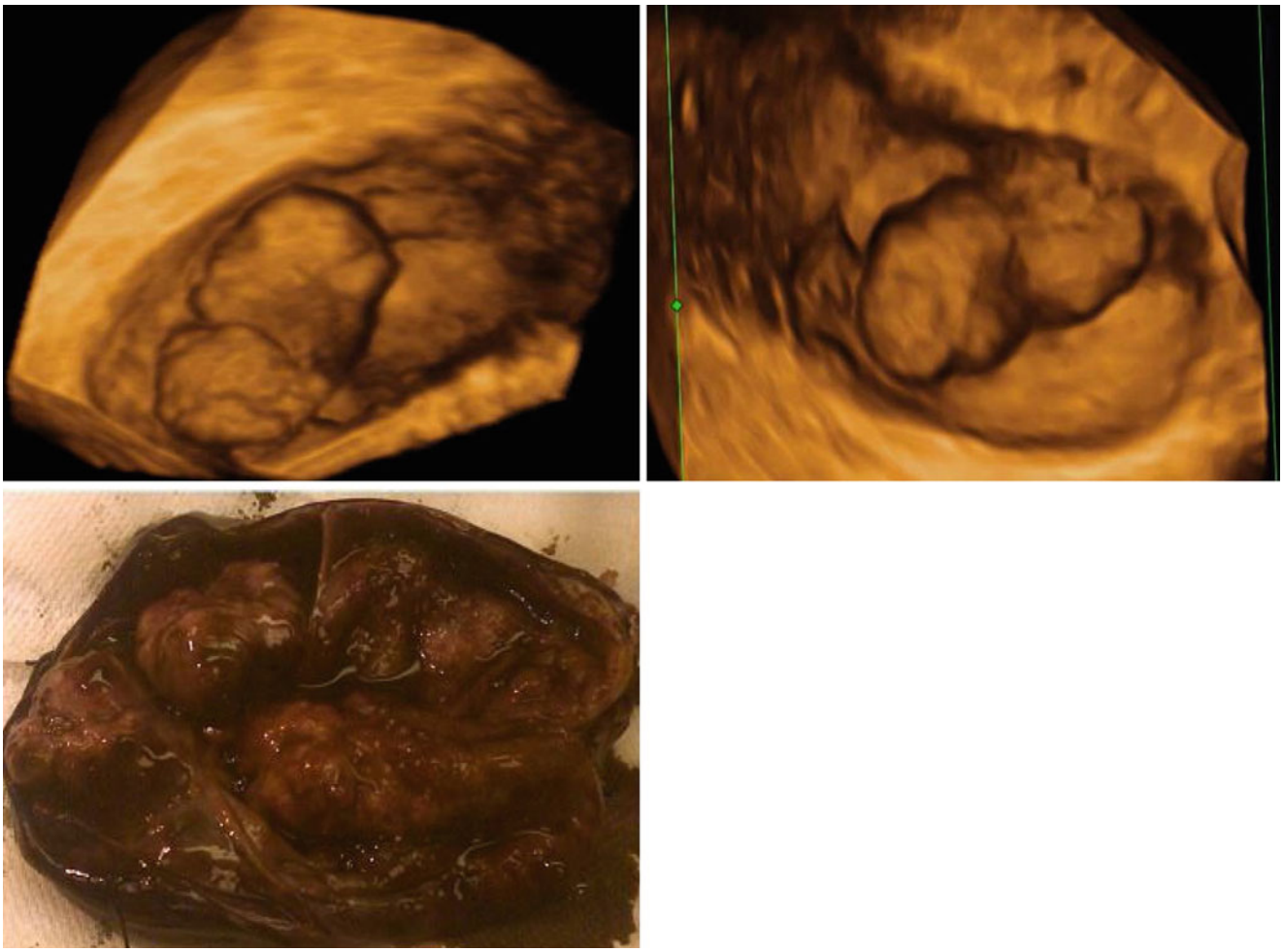

Fig. 13 3D rendering of a serous BOT (note irregular surface of the papillae, very similar of the macroscopic view of the tumor)

identification of BOT, having the papillae of BOT a more irregular surface (Figs. 4, 13 and 14). Combining 3D morphology and 3D power vascular pattern analysis and vascular indexes calculations (VI vascular index, flow index, FI, VFI) could be performed on papillary projections and honeycomb nodule (Figs. 15 and 16).

3D flow index with the best diagnostic performance is VI in a sample and seems to be superior to that of the subjective color content of the tumor. Using 3D power Doppler ultrasound, the color content of the tumor scan can be determined objectively, even though the selection of the most vascularized area (i.e., selection of the papillae sample site) is necessarily subjective. The objective 3D power Doppler method confirms those previously obtained using subjective estimation of the color content of the tumor scan during 2D color/power Doppler scanning, namely, that malignant adnexal tumors appear to be more richly vascularized than benign adnexal tumors [37].

To date the efficiency of 3D TVS and PD imaging in identifying BOT has yet to be determined.

Follow-Up After Surgery

Published series have shown recurrence rates of approximately 10–30 % among women treated with such conservative surgery [16, 28, 49], with the vast majority of recurrences occurring as a second borderline tumor [23, 94]. Recurrence rate for patients who underwent a primary pelvic clearance was lower (1.6 %) compared to fertility-sparing conservative surgery (3.3 %) [88]. It appears that surgical resection is the main stay of treatment, surgical staging being important to identify invasive extraovarian implants that portend an adverse prognosis. Patients treated by cystectomy were three times more likely to recur than those treated by oophorectomy [5, 30, 71].

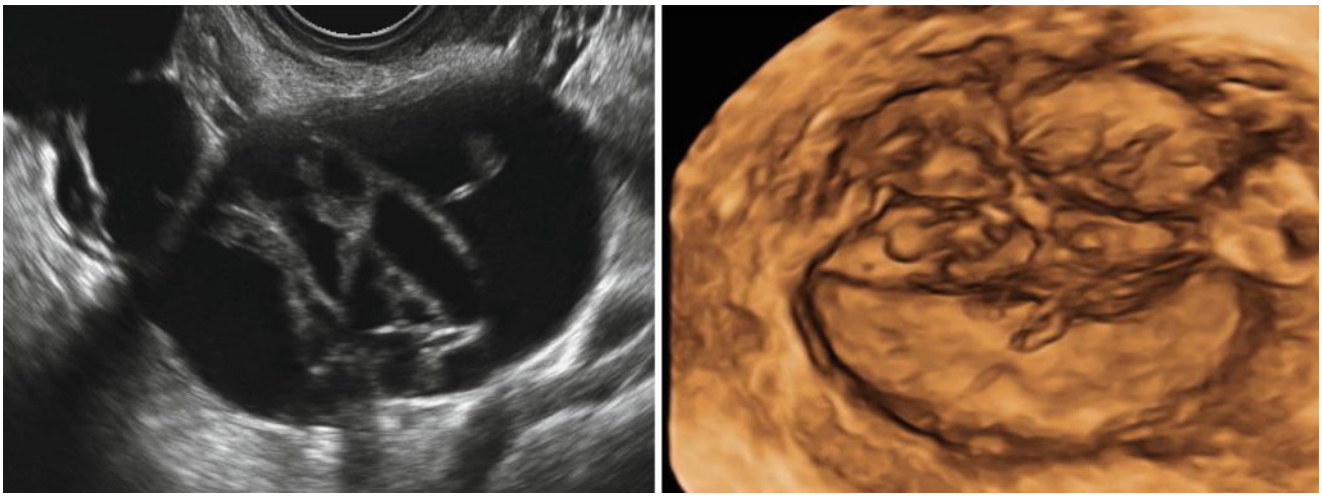

Fig. 14 3D rendering of mucinous BOT of gastrointestinal type

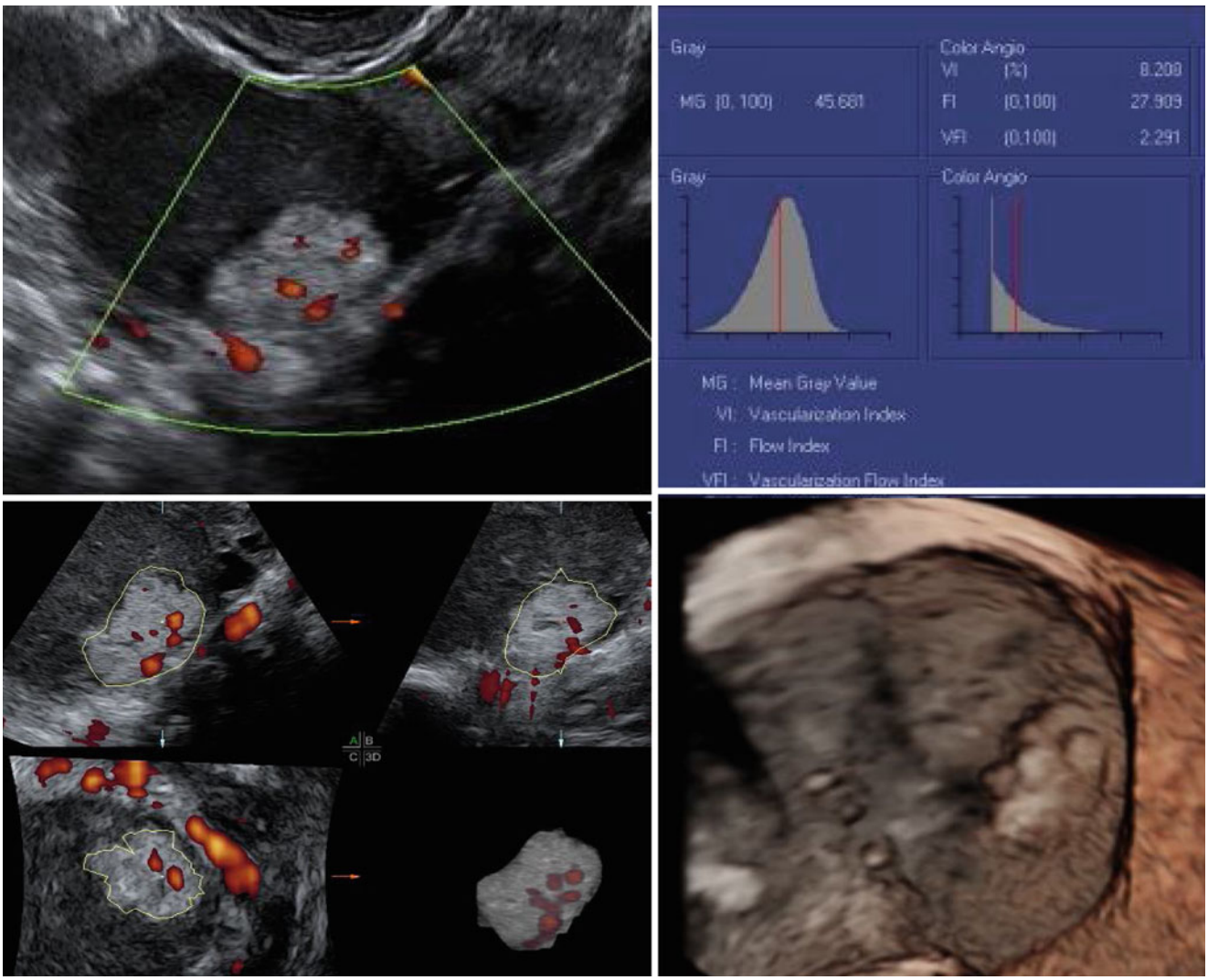

Fig. 15 3D evaluation of a serous BOT: surface rendering and calculation of vascular index of the papillary volume manually delineated

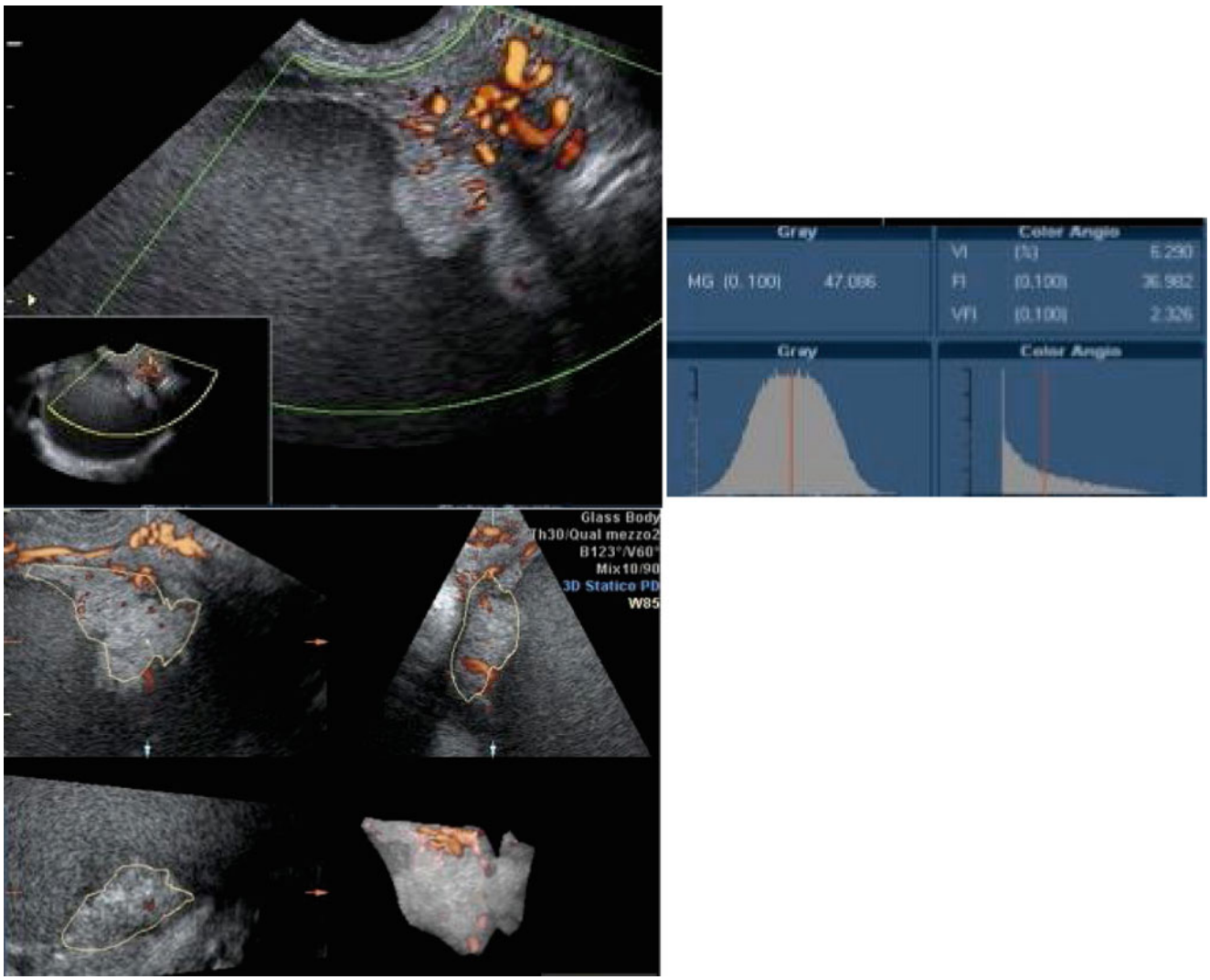

Fig. 16 3D evaluation of a serous BOT: surface rendering and calculation of vascular index of the papillary volume manually delineated

Rarely, the disease can reoccur as a malignant tumor which can result in progressive and fatal disease [11]. The term "malignant transformation" has been used to refer to this phenomenon although the exact pathogenesis in these cases is controversial. The concern over recurrent and possible malignant future disease had led to earlier recommendations that women initially treated with fertility-sparing surgery undergo additional surgery to remove remaining ovarian tissue once child-bearing is completed. Although previous studies have found prognosis for these patients to be excellent and the long-term risk of malignant disease to be low, meaningful conclusions have often been limited by small study size and relatively short follow-up intervals.

Ovarian serous borderline tumors with noninvasive implants have been considered relatively indolent tumors with a 5-year survival rate of 95 %; however, the reported recurrence rate for this type of tumor has been variable, ranging from 8 to 32 % [11, 41, 45, 55]. The wide range of these results may be related to differences in the length of follow-up obtained in the various studies.

Silva in 2006 found that the recurrence rate of 5 years was 10 %; however, if the follow-up was extended to 10 years, 29 % of patients developed recurrences; at 15 years, 39 % of patients had developed recurrences; and after 15 years, 44 % of patients had recurrences. On the basis of these findings, it seems that patients should be followed for a minimum of 10 years [67].

Because the most frequent tumor found in the recurrence is low-grade serous carcinoma and as this is a low-grade neoplasm, there is no rapid progression of the disease and most patients died of disease after 15 years of follow-up [67]. Patients with serous borderline tumor with noninvasive implants should have a minimum follow-up of 10 years to evaluate for recurrences and a follow-up of 20 years to evaluate for survival.

Studies with long follow-up periods are crucial in understanding the behavior of these tumors.

A high proportion (30 %) of patients with a serous borderline tumor and peritoneal implants develop recurrences most commonly in the form of low-grade serous carcinoma [6, 48, 79]. Nevertheless, some of these recurrences can be in the form of invasive disease, requiring early diagnosis.

Very few studies have specified the mode of diagnosis of recurrences and few ultrasound studies have been dedicated to this subject in the case of advanced-stage borderline tumors. Uzan in 2011 demonstrates that ultrasound is the most relevant follow-up procedure in the follow-up of patients treated surgically for BOT [81]. Also the blood CA 125 test is of particular interest for detecting invasive recurrent disease.

Ultrasound studies with long follow-up periods are crucial in understanding the behavior of these tumors, the sonographic appearance of recurrence in correlation to the primary BOT type and the accuracy in recurrence detection.

Conclusions

The main concern for BOT remains that they must not be managed with overly aggressive therapy, and therefore, a very accurate presurgical diagnosis is desirable.

Ideally an ultrasound examination should differentiate accurately between benign, borderline, and invasive malignant ovarian tumors. In current practice, most ultrasonographers classify adnexal tumors as benign or malignant, and only a few experts would attempt to make a preoperative diagnosis of a borderline ovarian tumor.

The diagnostic performance with regard to discrimination between benign, borderline, and invasive malignant ovarian tumors when using pattern recognition depends on the confidence with which the operator has reached the diagnosis. Borderline ovarian tumors are the main source of diagnostic uncertainty also using logistic regression systems or score classifications. The presence of morphological features typical of benign, borderline, or primary invasive tumors increased the level of diagnostic confidence of the experts. However, a number of adnexal tumors exhibit complex or unusual morphological features, which has a detrimental effect on diagnostic certainty. The imaging findings may be indistinguishable from those of early well-differentiated invasive ovarian carcinomas (stage 1, grade 1).

An accurate sonographic examination of an ovarian lesion can suggest BOT on the basis of the presence of papillae or multiple septa. However, neither papillae nor septa constitute highly sensitive sonographic markers. This means that conservative surgery for a suspected BOT, the actual sonographic diagnosis not being able to exclude totally invasive malignancy, has to be associated with frozen section and greater care than normal should be taken not to rupture the cyst capsule.

Number, size, morphology, and Doppler findings of the papilla can highly suggest the diagnosis of benign versus malignant papillary projection, although an overlap exists, especially with borderline tumors. Absence of color flow in a papillary projection is suggestive of benignity. S-BOTs and endocervical-type M-BOTs have similar sonographic features, compared with the intestinal-type M-BOTs; these tumors were characterized by a smaller maximum diameter, fewer locules (they were usually unilocular-solid lesions), a higher number of papillary excrescences within the lesions, and a higher rate of vessels inside the papillations. Gastrointestinal-type M-BOTs were characterized by a larger diameter and a multilocular aspect, with hyperechoic tissue connecting the multiple locules and no clear definition of solid tissue or papillary projection. These findings will help the surgeon decide the type of surgery and the surgical approach.

References

1. Ahmed ASM, Lawton FG. Borderline ovarian tumours: current concepts and management. Rev Gynaecol Pract. 2005;5:139–51.
2. Andersen ES, Knudsen A, Rix P, et al. Risk of malignancy index in the preoperative evaluation of patients with adnexal masses. Gynecol Oncol. 2003;90:109–12.
3. Bazot M, Darai E, Nassar-Slaba J, et al. Value of magnetic resonance imaging for the diagnosis of ovarian tumors: a review. J Comput Assist Tomogr. 2008;32:712–23.
4. Bazot M, Nassar-Slaba J, Thomassin-Naggara I, et al. MR imaging compared with intraoperative frozen-section examination for the diagnosis of adnexal tumors; correlation with final histology. Eur Radiol. 2006;16:2687–99.
5. Boran N, Cil AP, Tulunay G, et al. Fertility and recurrence results of conservative surgery for borderline ovarian tumors. Gynecol Oncol. 2005;97:845–51.
6. Borgfeldt C, Iosif C, Masback A. Fertility-sparing surgery and outcome in fertile women with ovarian borderline tumors and epithelial invasive ovarian cancer. Eur J Obstet Gynecol Reprod Biol. 2007;134:110–4.
7. Burks RT, Sherman ME, Kurman RJ. Micropapillary serous carcinoma of the ovary. A distinctive low-grade carcinoma related to serous borderline tumors. Am J Surg Pathol. 1996;20:1319–30.
8. Cadron I, Amant F, Van Grop T, et al. The management of borderline tumours of the ovary. Curr Opin Oncol. 2006;18:488–93.
9. Cadron I, Leunen K, Van Gorp T, et al. Management of borderline ovarian neoplasms. J Clin Oncol. 2007;25:2928–37.
10. Castellucci P, Perrone AM, Picchio M, et al. Diagnostic accuracy of 18F-FDG PET/CT in characterizing ovarian lesions and staging ovarian cancer: correlation with transvaginal ultrasonography, computed tomography, and histology. Nucl Med Commun. 2007;28:589–95.
11. Crispens MA, Bodurka D, Deavers M, et al. Response and survival in patients with progressive or recurrent serous ovarian tumors of low malignant potential. ACOG. 2002;99:3–10.
12. Darai E, Teboul J, Walker F, et al. Epithelial ovarian carcinoma of low malignant potential. Eur J Obstet Gynecol Reprod Biol. 1996;66:141–5.

13. Deavers MT, Gershenson DM, Tortolero-Luna G, et al. Micropapillary and cribriform patterns in ovarian serous tumors of low malignant potential: a study of 99 advanced stage cases. Am J Surg Pathol. 2002;26:1129–41.
14. Dehari R, Robert J, Kurman RJ, et al. The development of high-grade serous carcinoma from atypical proliferative (borderline) serous tumors and low-grade micropapillary serous carcinoma a morphologic and molecular genetic analysis. Am J Surg Pathol. 2007;31:1007–12.
15. Desfeux P, Bats AS, Bensaid C, et al. Impact of the surgical route on staging and outcome of early borderline ovarian tumors. Gynecol Obstet Fertil. 2007;35:193–8.
16. Donnez J, Munschke A, Berliere M, et al. Safety of conservative management and fertility outcome in women with borderline tumors of the ovary. Fertil Steril. 2003;79:1216–21.
17. Eichhorn JH, Bell DA, Young RH, et al. Ovarian serous borderline tumors with micropapillary and cribriform patterns: a study of 40 cases and comparison with 44 cases without these patterns. Am J Surg Pathol. 1999;23:397–409.
18. Emoto M, Udo T, Obama H, et al. The blood flow characteristics in borderline ovarian tumors based on both color Doppler ultrasound and histopathologic analyses. Gynecol Oncol. 1998;70:351–7.
19. Engelen MJ, de Bruijn HW, Hollema H, et al. Serum CA 125, carcinoembryonic antigen, and CA 19–9 as tumor markers in borderline ovarian tumors. Gynecol Oncol. 2000;78:16–20.
20. Eskander RN, Randall LM, Berman ML, et al. Fertility preserving options in patients with gynecologic malignancies. Am J Obstet Gynecol. 2011;205:103–10.
21. Exacoustos C, Romanini ME, Rinaldo D, et al. Preoperative sonographic features of borderline ovarian tumors. Ultrasound Obstet Gynecol. 2005;25:50–9.
22. Fagotti A, Ludovisi M, De Blasis I, et al. The sonographic prediction of invasive carcinoma in unilocular-solid ovarian cysts in premenopausal patients: a pilot study. Hum Reprod. 2012;27:2676–83.
23. Fauvet R, Poncelet C, Boccara J, et al. Fertility after conservative treatment for borderline ovarian tumors: a French multicenter study. Fertil Steril. 2005;83:284–90.
24. Ferreira CR, Carvalho JP, Soares FA, et al. Mucinous ovarian tumors associated with pseudomyxoma peritonei of adenomucinosis type: immunohistochemical evidence that they are secondary tumors. Int J Gynecol Cancer. 2008;18:59–65.
25. Fruscella E, Testa AC, Ferrandina G, et al. Ultrasound features of different histopathologic subtypes of borderline ovarian tumors. Ultrasound Obstet Gynecol. 2005;26:644–50.
26. Gershenson DM. Clinical management potential tumors of low malignancy. Best Pract Res Clin Obstet Gynaecol. 2002;16:513–27.
27. Gilks CB, Alkushi A, Yue JJ, et al. Advanced-stage serous borderline tumors of the ovary: a clinicopathologic study of 49 cases. Int J Gynecol Pathol. 2003;22:29–36.
28. Gotlieb WH, Flikker S, Davidson B, et al. Borderline tumors of the ovary: fertility treatment, conservative management, and pregnancy outcome. Cancer. 1998;82:141–6.
29. Gotlieb WH, Soriano D, Achiron R, et al. CA 125 measurement and ultrasonography in borderline tumors of the ovary. Am J Obstet Gynecol. 2000;183:541–6.
30. Ha JE, Jueng IC, Lee YS, et al. Clinical analysis of borderline ovarian tumors. Eur J Gynaecol Oncol. 2011;22:69–72.
31. Hassen K, Ghossain MA, Rousset P, Sciot C, et al. Characterization of papillary projections in benign versus borderline and malignant ovarian masses on conventional and color Doppler ultrasound. AJR Am J Roentgenol. 2011;196:1444–9.
32. Hata K, Hata T, Manabe A, et al. Ovarian tumors of low malignant potential: transvaginal Doppler ultrasound features. Gynecol Oncol. 1992;45:259–64.
33. Hillaby K, Aslam N, Salim R, et al. The value of detection of normal ovarian tissue (the 'ovarian crescent sign') in the differential diagnosis of adnexal masses. Ultrasound Obstet Gynecol. 2004;23:63–7.
34. Houck K, Nikrui N, Duska L, et al. Borderline tumors of the ovary: correlation of frozen and permanent histopathologic diagnosis. Obstet Gynecol. 2000;95(6):839–43.
35. Hricak H, Chen M, Coakley FV, et al. Complex adnexal masses: detection and characterization with MR imaging – multivariate analysis. Radiology. 2000;214:39–46.
36. International Federation of Gynecology and Obstetrics. Classification and staging of malignant tumors in the female pelvis. Acta Obstet Gynecol Scand. 1971;50:1–7.
37. Jokubkiene L, Sladkevicius P, Valentin L. Does three-dimensional power Doppler ultrasound help in discrimination between benign and malignant ovarian masses? Ultrasound Obstet Gynecol. 2007;29:215–25.
38. Jones MB. Borderline ovarian tumors: current concepts for prognostic factors and clinical management. Clin Obstet Gynecol. 2006;49:517–25.
39. Jung DC, Choi HJ, Ju W, et al. Discordant MRI/FDG-PET imaging for the diagnosis of borderline ovarian tumors. Int J Gynecol Cancer. 2008;18:637–41.
40. Kayikcioglu F, Pata O, Cengiz S, et al. Accuracy of frozen section diagnosis in borderline ovarian malignancy. Gynecol Obstet Invest. 2000;49:187–9.
41. Kennedy AW, Hart WR. Ovarian papillary serous tumors of low malignant potential (serous borderline tumors): a long term follow-up study, including patients with microinvasion, lymph node metastasis, and transformation to invasive serous carcinoma. Cancer. 1996;78:278–86.
42. Kikkawa F, Nawa A, Kajiyama H, et al. Clinical characteristics and prognosis of mucinous tumors of the ovary. Gynecol Oncol. 2006;103:171–5.
43. Krigman H, Bentley R, Robboy SJ. Pathology of epithelial ovarian tumors. Clin Obstet Gynecol. 1994;37:475–91.
44. Lalwani N, Shanbhogue AK, Vikram R, et al. Current update on borderline ovarian neoplasms. AJR Am J Roentgenol. 2010;194:330–6.
45. Leake JF, Currie JL, Rosenshein NB, et al. Long-term follow-up of serous ovarian tumors of low malignant potential. Gynecol Oncol. 1992;47:150–8.
46. Marret H, Sauget S, Giraudeau B, et al. Contrast-enhanced sonography helps in discrimination of benign from malignant adnexal masses. J Ultrasound Med. 2004;23:1629–39.
47. Milojkovic M, Hrgovic Z, Hrgovic I, et al. Significance of CA 125 serum level in discrimination between benign and malignant masses in the pelvis. Arch Gynecol Obstet. 2004;269:176–80.
48. Morice P. Borderline tumours of the ovary and fertility. Eur J Cancer. 2006;42:149–58.
49. Morice P, Camatte S, El Hassan J, et al. Clinical outcomes and fertility after conservative treatment of ovarian borderline tumors. Fertil Steril. 2001;75:92–6.
50. Nam EJ, Yun MJ, Oh YT, et al. Diagnosis and staging of primary ovarian cancer: correlation between PET/CT, Doppler US, and CT or MRI. Gynecol Oncol. 2010;116:389–94.
51. Orden MR, Jurvelin JS, Kirkinen PP. Kinetics of a US contrast agent in benign and malignant adnexal tumors. Radiology. 2003;226:405–10.
52. Osmers RGW, Osmers M, von Maydell B, et al. Preoperative evaluation of ovarian tumors in premenopause by transvaginosonography. Am J Obstet Gynecol. 1996;175:428–34.
53. Osmers RGW, Osmers M, von Maydell B, et al. Evaluation of ovarian tumors in postmenopausal women by transvaginal sonography. Eur J Obstet Gynecol Reprod Biol. 1998;77:81–8.

54. Paulsen T, Kærn J, Tropé C. Improved 5-year disease-free survival for FIGO stage I epithelial ovarian cancer patients without tumor rupture during surgery. Gynecol Oncol. 2011;122:83–8.
55. Prat J, De Nictolis M. Serous borderline tumors of the ovary. A long-term follow-up study of 137 cases, including 18 with a micropapillary pattern and 20 with microinvasion. Am J Surg Pathol. 2002;26:1111–28.
56. Prayson RA, Hart WR, Petras RE. Pseudomyxoma peritonei. A clinicopathologic study of 19 cases with emphasis on site of origin and nature of associated ovarian tumors. Am J Surg Pathol. 1994;18:591–603.
57. Risum S, Hogdall C, Loft A, et al. The diagnostic value of PET/CT for primary ovarian cancer—a prospective study. Gynecol Oncol. 2007;105:145–9.
58. Ronnett BM, Kurman RJ, Zahn CM, et al. Pseudomyxoma peritonei in women: a clinicopathologic analysis of 30 cases with emphasis on site of origin, prognosis, and relationship to ovarian mucinous tumors of low malignant potential. Hum Pathol. 1995;26: 509–24.
59. Russel P. Surface epithelial-stromal tumors of the ovary. In: Ed Kurman RJ, editor. Blaunstein's pathology of the female genital tract. 4th ed. New York/Berlin/Heidelberg: Springer; 1994. p. 705–82.
60. Rutgers JL, Scully RE. Ovarian mixed-epithelial papillary cystadenomas of borderline malignancy of mullerian type. A clinicopathologic analysis. Cancer. 1988;61:546–54.
61. Seidman JD, Kurman RJ. Subclassification of serous borderline tumors of the ovary into benign and malignant types. A clinicopathologic study of 65 advanced stage cases. Am J Surg Pathol. 1996;20:1331–45.
62. Seidman JD, Kurman RJ. Ovarian serous borderline tumors: a critical review of the literature with emphasis on prognostic indicators. Hum Pathol. 2000;31:539–57.
63. Seidman JD, Soslow RA, Vang R, et al. Borderline ovarian tumors: diverse contemporary viewpoints on terminology and diagnostic criteria with illustrative images. Hum Pathol. 2004;35:918–33.
64. Sherman ME, Mink PJ, Curtis R, et al. Survival among women with borderline ovarian tumors and ovarian carcinoma. A population-based analysis. Cancer. 2004;100:1045–52.
65. Shih I-M, Kurman RJ. Ovarian tumorigenesis-a proposed model based on morphological and molecular genetic analysis. Am J Pathol. 2004;164:1511–8.
66. Shih I-M, Kurman RJ. Molecular pathogenesis of ovarian borderline tumors: new insights and old challenges. Clin Cancer Res. 2005;11:7273–9.
67. Silva EG, Gershenson DM, Malpica A, et al. The recurrence and the overall survival rates of ovarian serous borderline neoplasms with noninvasive implants is time dependent. Am J Surg Pathol. 2006;30:1367–71.
68. Singer G, Kurman RJ, Chang H-W, et al. Diverse tumorigenic pathways in ovarian serous carcinoma. Am J Pathol. 2002;160: 1223–8.
69. Smith Sehdev AE, Sehdev PS, Kurman RJ. Noninvasive and invasive micropapillary (low-grade) serous carcinoma of the ovary: a clinicopathologic analysis of 135 cases. Am J Surg Pathol. 2003;27:725–36.
70. Sohaib SA, Sahdev A, Van Trappen P, Jacobs IJ, Reznek RH. Characterization of adnexal mass lesions on MR imaging. AJR Am J Roentgenol. 2003;180:1297–304.
71. Suh-Burgmann E. Long-term outcomes following conservative surgery for borderline tumor of the ovary: a large population-based study. Gynecol Oncol. 2006;103:841–7.
72. Taylor Jr HC. Malignant and semimalignant tumors of the ovary. Surg Gynecol Obstet. 1929;48:702–12.
73. Testa AC, Ferrandina G, Fruscella E, et al. The use of contrasted transvaginal sonography in the diagnosis of gynecologic diseases: a pre liminary study. J Ultrasound Med. 2005;24:1267–78.
74. Testa AC, Timmerman D, Exacoustos C, et al. The role of CnTI-SonoVue in the diagnosis of ovarian masses with papillary projections: a preliminary study. Ultrasound Obstet Gynecol. 2007;29:512–6.
75. Testa AC, Timmerman D, Van Belle V, et al. Intravenous contrast ultrasound examination using contrast-tuned imaging (CnTI) and the contrast medium SonoVue for discrimination between benign and malignant adnexal masses with solid components. Ultrasound Obstet Gynecol. 2009;34:699–710.
76. Testa AC, Timmerman D, Van Holsbeke C, et al. Ovarian cancer arising in endometrioid cysts: ultrasound findings. Ultrasound Obstet Gynecol. 2011;38:99–106.
77. Timmerman D, Testa A, Bourne T, et al. Logistic regression model to distinguish between the benign and malignant adnexal mass before surgery: a multicenter study by the International Ovarian Tumor Analysis Group. J Clin Oncol. 2005;23:8794–801.
78. Timmerman D, Van Calster B, Testa AC, et al. Ovarian cancer prediction in adnexal masses using ultrasound based logistic regression models: a temporal and external validation study by the IOTA group. Ultrasound Obstet Gynecol. 2010;36:226–34.
79. Tinelli R, Tinelli A, Tinelli FG, et al. Conservative surgery for borderline ovarian tumors: a review. Gynecol Oncol. 2006;100: 185–91.
80. Tsili AC, Tsampoulas C, Charisiadi A, et al. Adnexal masses: accuracy of detection and differentiation with multidetector computed tomography. Gynecol Oncol. 2008;110:22–31.
81. Uzan C, Kane A, Rey A, et al. How to follow up advanced-stage borderline tumours? Mode of diagnosis of recurrence in a large series stage II–III serous borderline tumours of the ovary. Ann Oncol. 2011;22:631–5.
82. Valentin L, Ameye L, Jurkovic D, et al. Which extrauterine pelvic masses are difficult to correctly classify as benign or malignant on the basis of ultrasound findings and is there a way of making a correct diagnosis? Ultrasound Obstet Gynecol. 2006;27:438–44.
83. Valentin L, Ameye L, Testa A, et al. Ultrasound characteristics of different types of adnexal malignancies. Gynecol Oncol. 2006;102: 41–8.
84. Valentin L, Jurkovic D, Van Calster B, et al. Adding a single CA 125 measurement to ultrasound imaging performed by an experienced examiner does not improve preoperative discrimination between benign and malignant adnexal masses. Ultrasound Obstet Gynecol. 2009;34:345–54.
85. Van Calster B, Timmerman D, Valentin L, et al. Triaging women with ovarian masses for surgery: observational diagnostic study to compare RCOG guidelines with an International Ovarian Tumour Analysis (IOTA) group protocol. BJOG. 2012;119:662–71.
86. Van Holsbeke C, Van Belle V, Leone FP, et al. Prospective external validation of the 'ovarian crescent sign' as a single ultrasound parameter to distinguish between benign and malignant adnexal pathology. Ultrasound Obstet Gynecol. 2010;36:81–7.
87. Vergote I, De Brabanter J, Fyles A, et al. Prognostic importance of degree of differentiation and cyst rupture in stage I invasive epithelial ovarian carcinoma. Lancet. 2001;357:176–82.
88. Wong HF, Low JJ, Chua Y, et al. Ovarian tumors of borderline malignancy: a review of 247 patients from 1991 to 2004. Int J Gynecol Cancer. 2007;17:342–9.
89. Yamamoto Y, Oguri H, Yamada R, et al. Preoperative evaluation of pelvic masses with combined (18)F-fluorodeoxyglucose positron emission tomography and computed tomography. Int J Gynaecol Obstet. 2008;102:124–7.
90. Yazbek J, Ameye L, Timmerman D, et al. Use of ultrasound pattern recognition by expert operators to identify borderline ovarian tumors: a study of diagnostic performance and interobserver agreement. Ultrasound Obstet Gynecol. 2010;35:84–8.
91. Yazbek J, Aslam N, Tailor A, et al. A comparative study of the risk of malignancy index and the ovarian crescent sign for the diagnosis of invasive ovarian cancer. Ultrasound Obstet Gynecol. 2006;28:320–4.

92. Yazbek J, Raju KS, Ben-Nagi J, et al. Accuracy of ultrasound subjective 'pattern recognition' for the diagnosis of borderline ovarian tumors. Ultrasound Obstet Gynecol. 2007;29:489–95.
93. Zanetta G, Lissoni A, Cha S, et al. Pre-operative morphological and colour Doppler features of borderline ovarian tumours. Br J Obstet Gynaecol. 1995;102:990–6.
94. Zanetta G, Rota S, Chiari S, et al. Behavior of borderline tumors with particular interest to persistence, recurrence, and progression to invasive carcinoma: a prospective study. J Clin Oncol. 2001; 19:2658–64.

Computed Tomographic and Magnetic Resonance Imaging of Borderline and Serous Tumors

Eito Kozawa

Abstract

Ovarian tumors arise from the surface epithelium, mesothelium, germ cells, or gonadal stroma. Surface epithelial ovarian tumors include serous, mucinous, endometrioid, transitional cell, and mixed tumors and clear cell carcinomas and may be benign, borderline, or malignant. In general, benign tumors are primarily cystic, and malignant tumors demonstrate more solid tissue elements and thicker septa. This chapter exhibits magnetic resonance (MR) and computed tomographic (CT) features of borderline and serous tumors, which commonly include papillary projections, psammomatous calcifications, and appearance resembling sea anemone or black sponge as well as other focal attributes. Knowledge of these features of ovarian tumors could assist specific diagnosis or substantially narrow differential diagnosis.

Keywords

Borderline tumors • Serous tumors • Imaging • Computed tomography • Magnetic resonance

CT and MR Imaging of Borderline Tumor

General Considerations for Borderline Ovarian Tumor

In 1929, Taylor used the term semimalignant tumor to introduce the concept of borderline ovarian tumor [1], but this concept was not immediately accepted. In 1971, the histological classification of the International Federation of Gynecology and Obstetrics (FIGO) described a tumor with low malignant potential, proliferating epithelial cells, and nuclear abnormalities but no infiltrative destructive growth as a cystadenoma [2]. In 1973, the World Health Organization (WHO) added the synonym carcinoma of low malignant potential to their classification of ovarian tumors to describe tumors of borderline malignancy [3], and in 2003, they used the terms borderline tumor and atypical proliferative tumor to indicate noninvasive neoplasms with nuclear abnormalities and mitotic activity intermediate between benign and malignant tumors of similar cell type [4]. Borderline ovarian tumors are also termed tumor or cystadenoma of borderline malignancy, tumor of low malignant potential, and atypical proliferative tumor and comprise tumors of every surface epithelial cell type–serous, mucinous, endometrioid, clear, transitional, and mixed. However, serous borderline tumor and mucinous borderline tumor of intestinal type are most common. In a case review, Link and colleagues identified 50 % of ovarian borderline tumors as serous, 46 % as mucinous, and 4 % as mixed, endometrioid, clear cell, or transitional cell [5].

E. Kozawa
Department of Imaging Diagnosis,
Saitama Medical University, International Medical Center,
1397-1, Yamane, Hidaka-shi, Saitama 350-1298, Japan
e-mail: 8kozawa@saitama-med.ac.jp

L. Saba et al. (eds.), *Ovarian Neoplasm Imaging*,
DOI 10.1007/978-1-4614-8633-6_13,

Borderline ovarian tumors are a distinct histological and clinical entity diagnosed in 15–20 % of patients who present with ovarian epithelial neoplasms [6] and are common in younger women, with mean age (40–50 years) at presentation approximately 10 years earlier than with invasive ovarian carcinomas [7, 8]. Clinically, borderline ovarian tumors are often benign and have an excellent prognosis [4, 9]. Abdominal pain, increasing abdominal girth or distension, and abdominal masses are the most frequent initial manifestations, but Webb and colleague reported 16 % of patients as asymptomatic at diagnosis [10].

Serous Borderline Ovarian Tumor

General Considerations for Serous Borderline Ovarian Tumor

Serous type is the most common histological subtype of borderline ovarian tumors. This tumor is seen bilaterally in 25–50 % of serous histological type cases [9] and most commonly appears during the fourth and fifth decades of life, with average patient age of 46 years [11, 12]. Although these tumors are slow-growing neoplasms, about a third are associated with peritoneal implants and about 20–30 % involve the regional lymph node, with implants and node involvement usually coexisting [13, 14]. Psammoma calcifications are concentric lamellated calcified structures seen in primary and metastatic lesions and enlarged lymph nodes of thyroid or ovarian carcinoma [15] and in epithelial ovarian tumors, especially serous borderline ovarian tumors [16].

Imaging Appearances of Serous Borderline Ovarian Tumor

Typically, serous epithelial neoplasms are primarily cystic and may be either uni- or multilocular with malignant varieties demonstrating varying proportions of solid components [8]. CT or ultrasonogaphic (US) appearance are generally inadequate for determining serous or mucinous cell type [8]. The features of benign serous cystadenoma that most suggest benign cystic neoplasm include unilocularity of cysts, thin walls, minimal septations, and absence of solid components on CT and MR images (Fig. 1a–c). Serous borderline tumors show more proliferation of solid components than do serous cystadenomas, and these may metastasize throughout the peritoneum but are not true malignancies. The solid components proliferating in epithelial tumors show papillary projections. On T_2-weighted images, large projections include a core of fibrous tissue with low signal intensity and proliferating neoplasmic epithelia with very high signal intensity (Fig. 2a), and small projections show intermediate signal intensity. Large and small papillary projections show high signal intensity on contrast-enhanced study (Fig. 2b). Multiple papillary projections, often observed most clearly after contrast enhancement, strongly suggest borderline or malignant tumors, especially serous borderline malignant tumors [17, 18].

The signal intensity of the contents of serous cystic lesions varies but is usually low to intermediate on T_1-weighted MR images and high on T_2-weighted images. At CT, psammomatous calcifications can show these tumors or their implants to have very high attenuation [17]. On MR images, serous borderline ovarian tumors appear as unilocular cysts with papillary projections within the cyst wall (Fig. 3a, b), minimally separate cysts with septa that demonstrate frond-like papillary projections within the cysts that involve both the wall and septa (Fig. 4a, b), or markedly septate lesions with plaque-like excrescences (Fig. 5a–c) [16]. Approximately one-third of these tumors are bilateral. The papillary projections of the solid components commonly show moderate enhancement during contrast-enhanced CT or dynamic MR imaging. Subtraction 3-dimensional (3D) enhanced T_1-weighted images are especially useful when intracystic fluid shows high signal intensity on T_1-weighted image (Fig. 5c) [19].

Differential Diagnosis of Serous Borderline Ovarian Tumor

Serous borderline tumors often present as complex adnexal masses. Serous cystadenoma or mucinous cystadenoma may be a probable differential diagnosis. Neither of these has a solid component, and subtraction 3D enhanced T_1-weighted images are useful to rule out debris or thrombus. Because serous borderline ovarian tumors appear benign clinically, their differentiation from early invasive malignant ovarian tumor is important.

Both serous borderline and stage I invasive malignant ovarian tumors are usually multiloculated with significant solid elements that include smooth round nodules, plaque-like thickening, and papillary projections. Septation thickness and nodule size are greater in malignant tumors, and papillary projections are more frequent in serous borderline tumors.

The imaging findings of serous borderline ovarian tumors are indistinguishable from those of other borderline ovarian tumors, such as mucinous, endometrioid, clear cell, transitional

Focus Points

Serous borderline tumor should be considered when an ovarian cystic tumor with papillary projections is seen in younger patients.

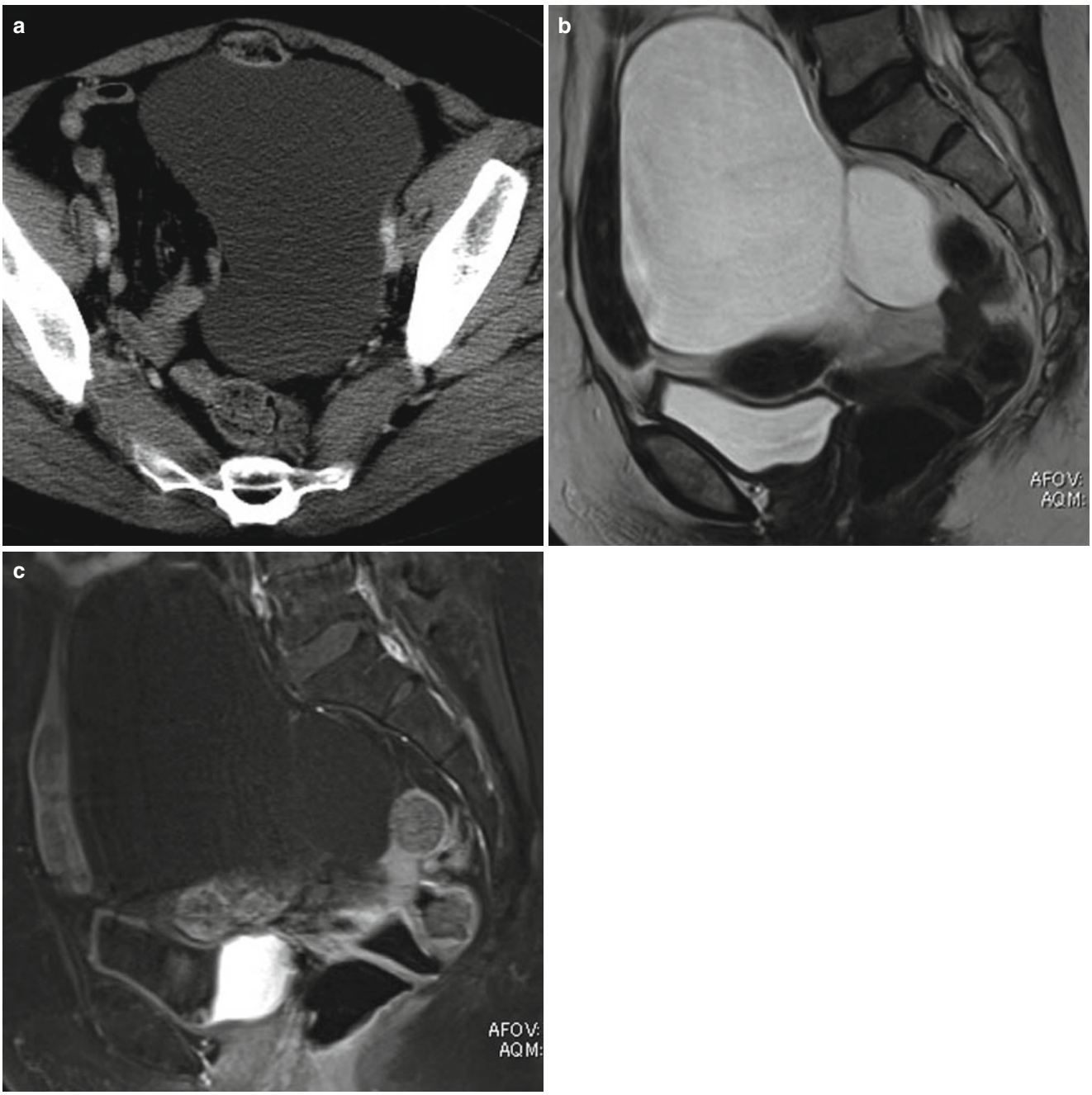

Fig. 1 (**a**) A 49-year-old woman with benign serous cystadenoma. Contrast-enhanced computed tomographic scan shows a unilocular cystic mass in the pelvic space. There are no solid components. (**b**) Sagittal T_2-weighted magnetic resonance (MR) image shows a large cystic mass with a septation in the pelvic space. (**c**) Sagittal fat-saturated contrast-enhanced T_1-weighted MR image shows a large cystic mass with a septation and no solid component in the pelvic space

cell, and mixed-type tumors, except for the serous surface papillary borderline tumor, which is described immediately following. However, serous borderline ovarian tumor may be the more probable diagnosis when MR imaging shows the ovary as unilocular or with minimally separate cystic lesions with the signal intensity of water and containing multiple papillary projections.

Serous Surface Papillary Borderline Tumor

General Considerations for Serous Surface Papillary Borderline Tumor

Serous benign tumors include cystadenomas, adenofibromas, cystadenofibromas, and surface papillomas. Serous surface papillomas are benign tumors that grow exophytically

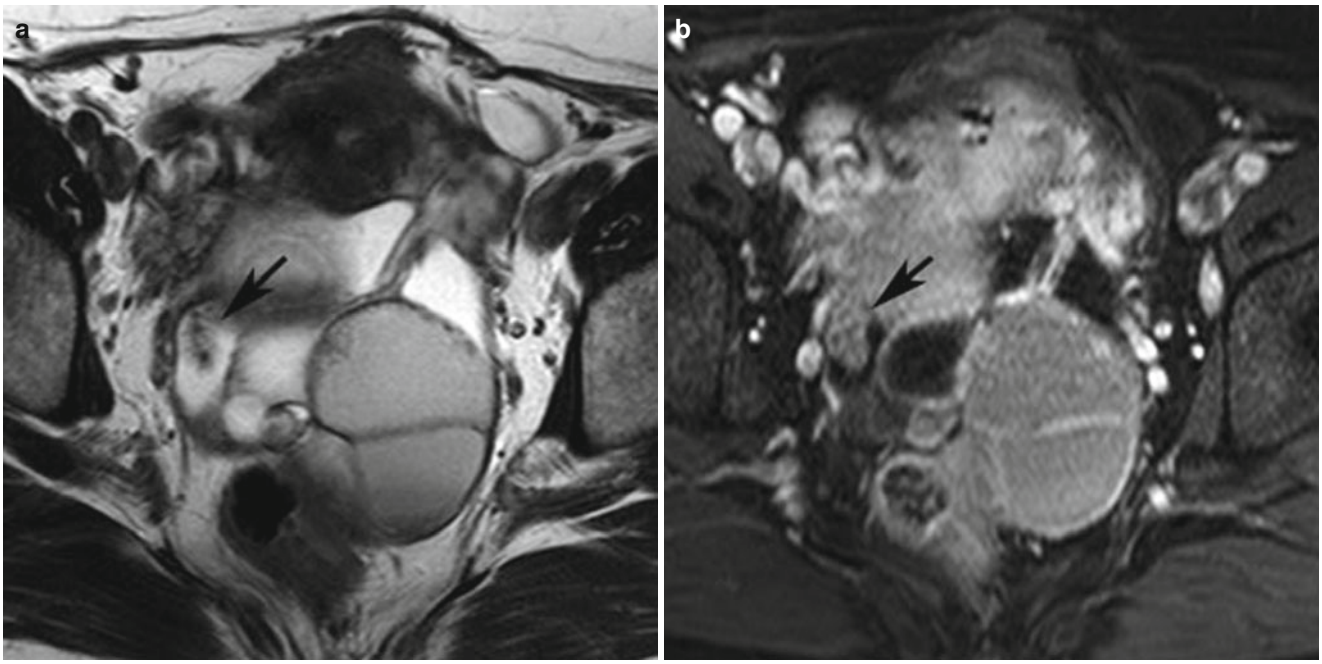

Fig. 2 (**a**) A 52-year-old woman with serous borderline tumor. Axial T_2-weighted magnetic resonance (MR) image shows a complex cystic mass with multiple septa. Large papillary projection shows high signal intensity with low signal intensity cores (*black arrow*). (**b**) Axial fat-saturated contrast-enhanced T_1-weighted MR image shows a large complex cystic mass with multiple septa. Large papillary projection shows high signal intensity with slightly low signal intensity cores (*black arrow*)

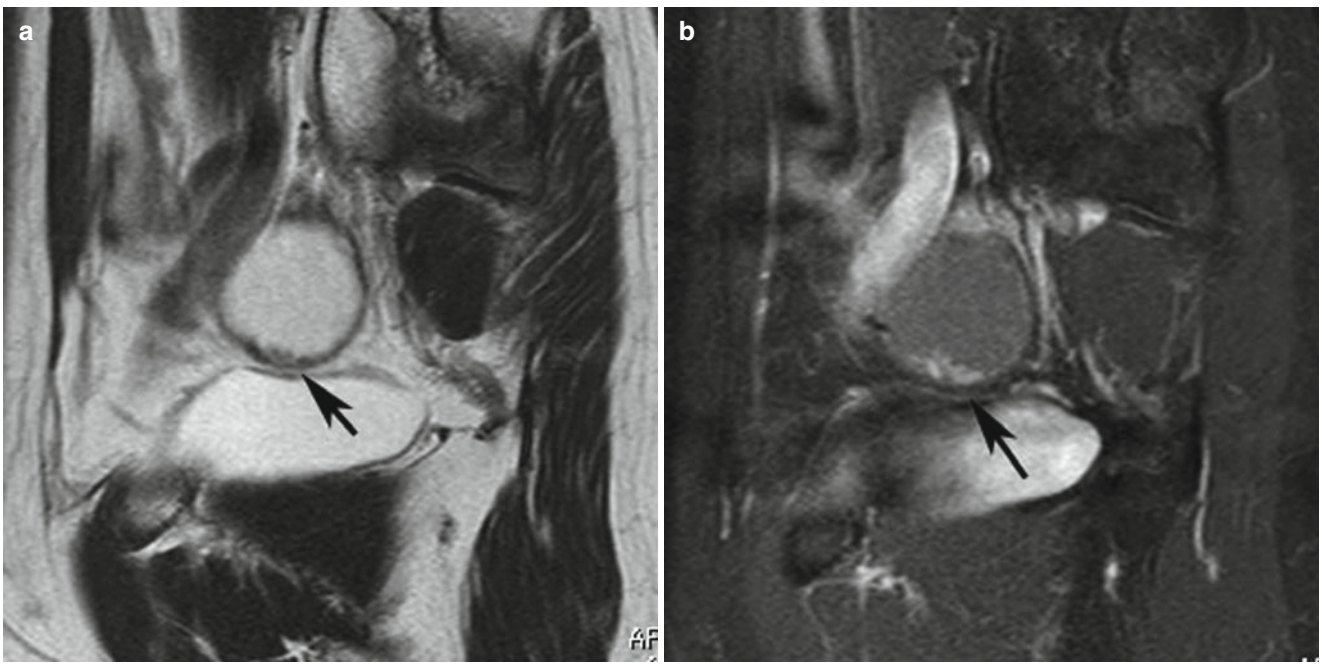

Fig. 3 (**a**) A 52-year-old woman with serous borderline tumor. Sagittal T_2-weighted magnetic resonance (MR) image shows unilocular cystic ovarian lesion superior to the bladder. Intracystic papillary-like projections showing multiple areas of low intensity extend from the cystic wall (*black arrow*). (**b**) Sagittal fat-saturated contrast-enhanced T_1-weighted MR image following gadolinium administration shows unilocular cystic ovarian lesion superior to the bladder. Intracystic papillary-like projections showing multiple areas of high signal intensity extend from the cystic wall (*black arrow*)

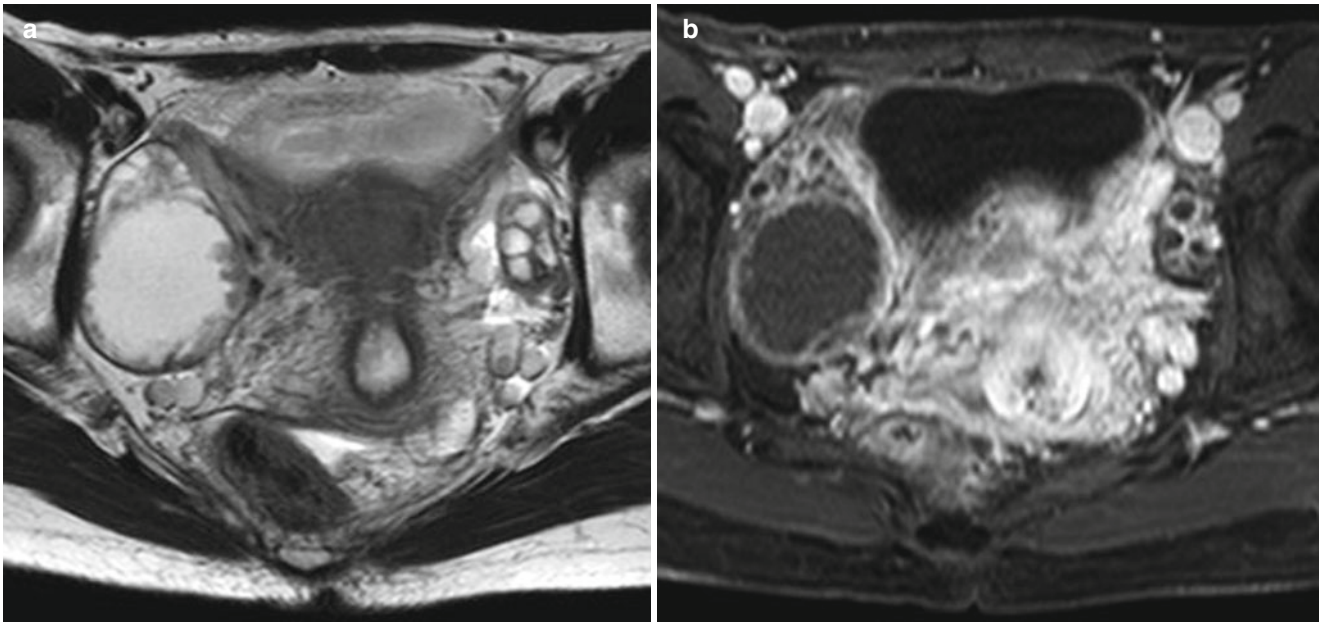

Fig. 4 (**a**) A 44-year-old woman with serous borderline tumor. Axial T_2-weighted magnetic resonance (MR) image shows a solitary cystic lesion with several septa with intracystic papillary projections showing multiple small areas of slight low intensity in both the wall and septa in the right adnexal region. (**b**) Axial fat-saturated contrast-enhanced T_1-weighted MR image shows a solitary cystic lesion with several septa with intracystic papillary projections showing multiple small areas of slight high signal intensity in both the wall and septa in the right adnexal region

on the ovarian surface. Such tumors that demonstrate little or no involvement of the serous borderline tumor are termed serous surface papillary borderline tumor [20] and generally manifest as an entirely solid mass without necrosis or hemorrhage or as a solid mass with cyst [20, 21]. Serous surface papillary borderline tumor may be a precursor of low-grade serous surface papillary carcinoma in the adenoma–carcinoma sequence because the two entities can coexist [8].

Imaging Appearances of Serous Surface Papillary Borderline Tumor

On CT, serous surface papillary borderline tumors demonstrate varying proportions of solid components on the ovarian cystic surface (Fig. 6a). The CT findings are similar to the malignant ovarian tumor with peritoneal dissemination. The limited soft-tissue contrast of the CT did not permit visualization of the normal ovaries inside the masses, but the good soft-tissue contrast of MRI allowed our observation of the characteristic ovarian features of this tumor. On MR imaging, a T_2-weighted image showed papillary architecture with high signal intensity and a hypointense branch-like structure on the surface of the normal ovary, findings resembling a sea anemone that suggest serous surface papillary borderline tumor (Fig. 6b) [20, 21]. Histologically, this papillary architecture correlates with epithelial multilayering, and the branching structure is a thick fibrous stalk [20]. After gadolinium administration, the papillary architecture on the T_2-weighted image showed strong high signal intensity, and the low signal intensity of the branch-like structure was weakly enhanced.

Differential Diagnosis of Serous Surface Papillary Borderline Tumor

On diagnostic MRI and CT, ovarian tumors with a rich solid component are considered malignant. However, serous surface papillary borderline tumors have many solid components and so resemble malignant ovarian tumors, and they sometimes show multiple solid components with cystic lesion that may mimic peritoneal dissemination and malignant ovarian tumor (Fig. 7a–c). Accurate diagnosis requires evaluation of images of different direction and detection of the high signal intensity of papillary architecture and low intensity of branch-like structures on the ovarian surface that resemble sea anemone-like masses on T_2-weighted images (Fig. 7b, c).

Focus Points

Serous surface papillary borderline tumor should be considered when an ovarian solid mass shows papillary architecture with high signal intensity and branch-like structures on the surface of the ovary with low intensity on T_2-weighted image.

Mucinous Borderline Ovarian Tumor

General Considerations for Mucinous Borderline Ovarian Tumor

Mucinous borderline ovarian tumors account for approximately 10 % of mucinous ovarian tumors and 30–50 % of

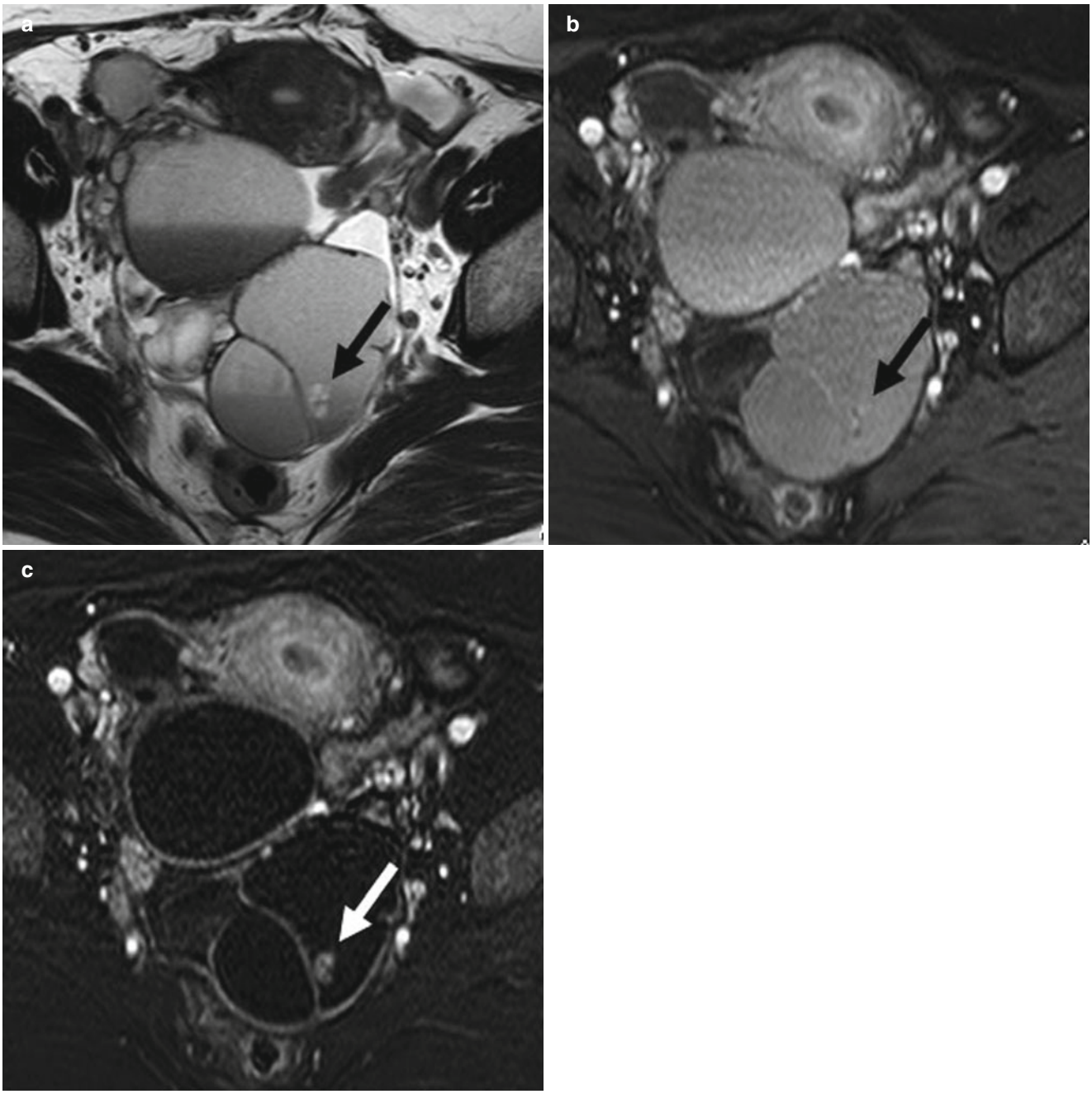

Fig. 5 (**a**) A 65-year-old woman with serous borderline tumor. Axial T_2-weighted magnetic resonance (MR) image shows a large complex cystic mass with multiple septa. Irregular plaque-like soft tissue shows high signal intensity (*black arrow*). (**b**) Axial fat-saturated contrast-enhanced T_1-weighted MR image shows a large complex cystic mass with multiple septa. Irregular plaque-like soft tissue is present but unclear (*black arrow*). (**c**) Axial 3-dimensional (3D) fat-saturated T_1-weighted MR subtraction image shows a large complex cystic mass with multiple septa. Irregular plaque-like soft tissue displays strong contrast enhancement (*white arrow*)

ovarian epithelial borderline tumors [19]. They are classified as either intestinal or endocervical type [19], which show very different pathologic and imaging features.

Intestinal Type Mucinous Borderline Tumor

Intestinal type mucinous ovarian borderline tumors represent about 90 % of mucinous borderline tumors. Mean age of patients is 45–50 years [22]. The average size of these tumors is about 20 cm, and they are usually unilateral, occurring bilaterally in only about 5 % of cases. The tumors are rarely associated with ipsilateral ovarian endometriosis [22] and are reported to coexist with pseudomyxoma peritonei in up to 17 % of cases [19].

Imaging Appearances of Intestinal Type Mucinous Borderline Tumor

On CT and MR imaging, intestinal type mucinous borderline ovarian tumor may be twice the size of serous borderline ovarian tumors and manifest as either uni- or

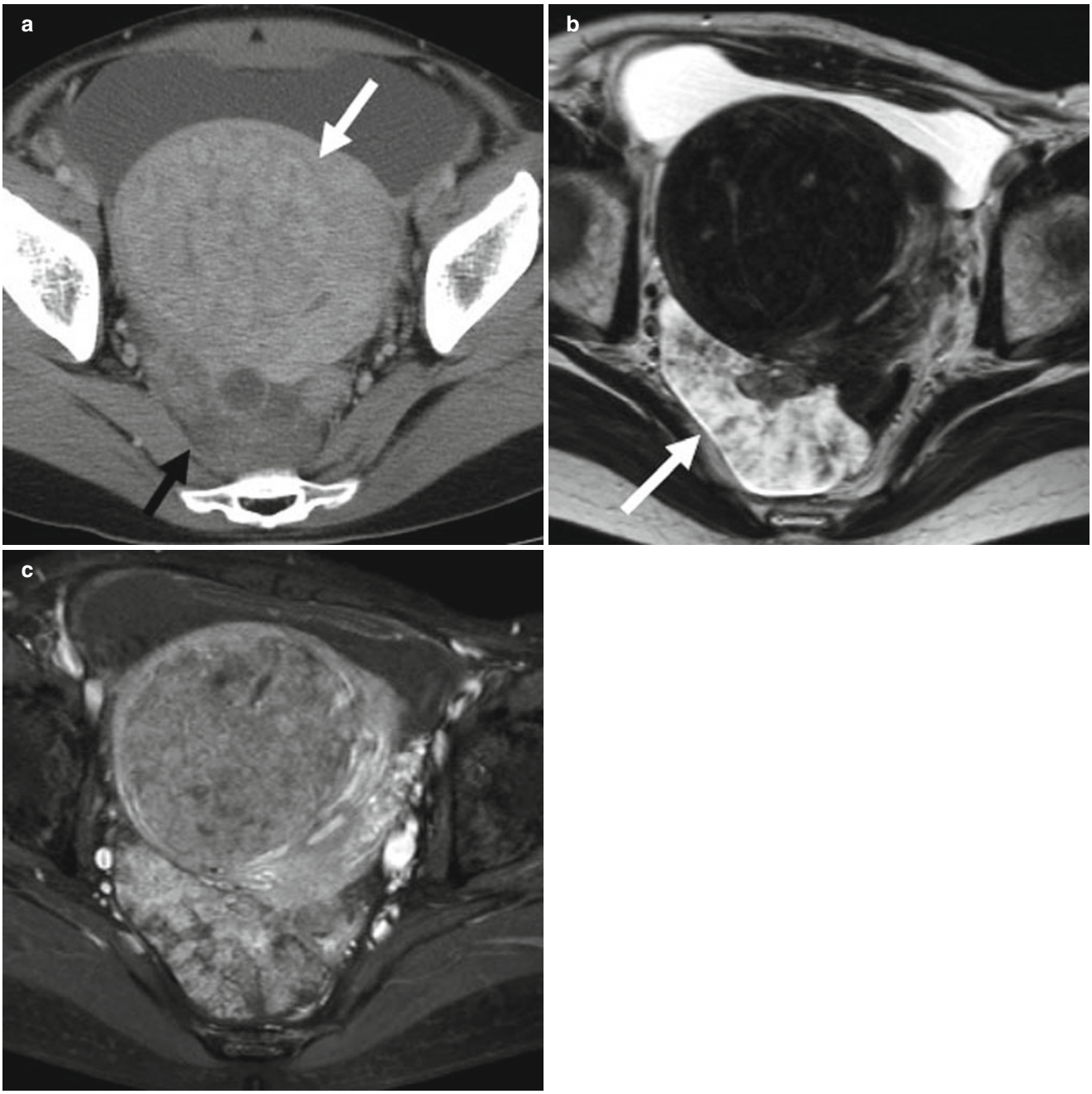

Fig. 6 (**a**) A 41-year-old woman with serous surface papillary borderline tumor. Contrast-enhanced computed tomography (CT) shows a heterogeneous enhanced mass posterior to the uterus (*black arrow*). *White arrow* is uterine leiomyoma. (**b**) Axial T_2-weighted image shows an entirely solid lobulated mass with hyperintense papillary architecture on the surface and hypointense branch-like structure within it (*white arrow*). (**c**) Axial fat-saturated T_1-weighted image shows an entirely solid lobulated mass; the papillary architecture shows high signal intensity after administration of gadolinium diethylenetriaminepentaacetic acid (DTPA)

multilocular cystic masses (Fig. 8a–c) [16], though a unilocular cystic mass is usually a serous borderline tumor. Mucinous borderline ovarian tumors commonly appear as multilocular cystic masses with numerous septa and contain fluids of different signal intensities on T_1- or T_2-weighted MR images (Fig. 9a–c) [8]. The variable signal intensities of the loculi and daughter cysts on both T_1- and T_2-weighted images is described as having a "stained-glass" appearance. These variable signal intensities depend on the viscosity of the materials present, such as mucin, blood products, or debris, and these findings suggest mucinous cystic tumor [23–25].

Diagnosis of serous ovarian tumors on CT requires the detection of psammomatous calcifications. Mucinous cystic ovarian tumors that contain mucinous borderline tumors can also contain calcifications, but they differ from psammomatous calcifications and appear as curved lines in the cystic wall of ovarian tumors (Fig. 10a, b) [26].

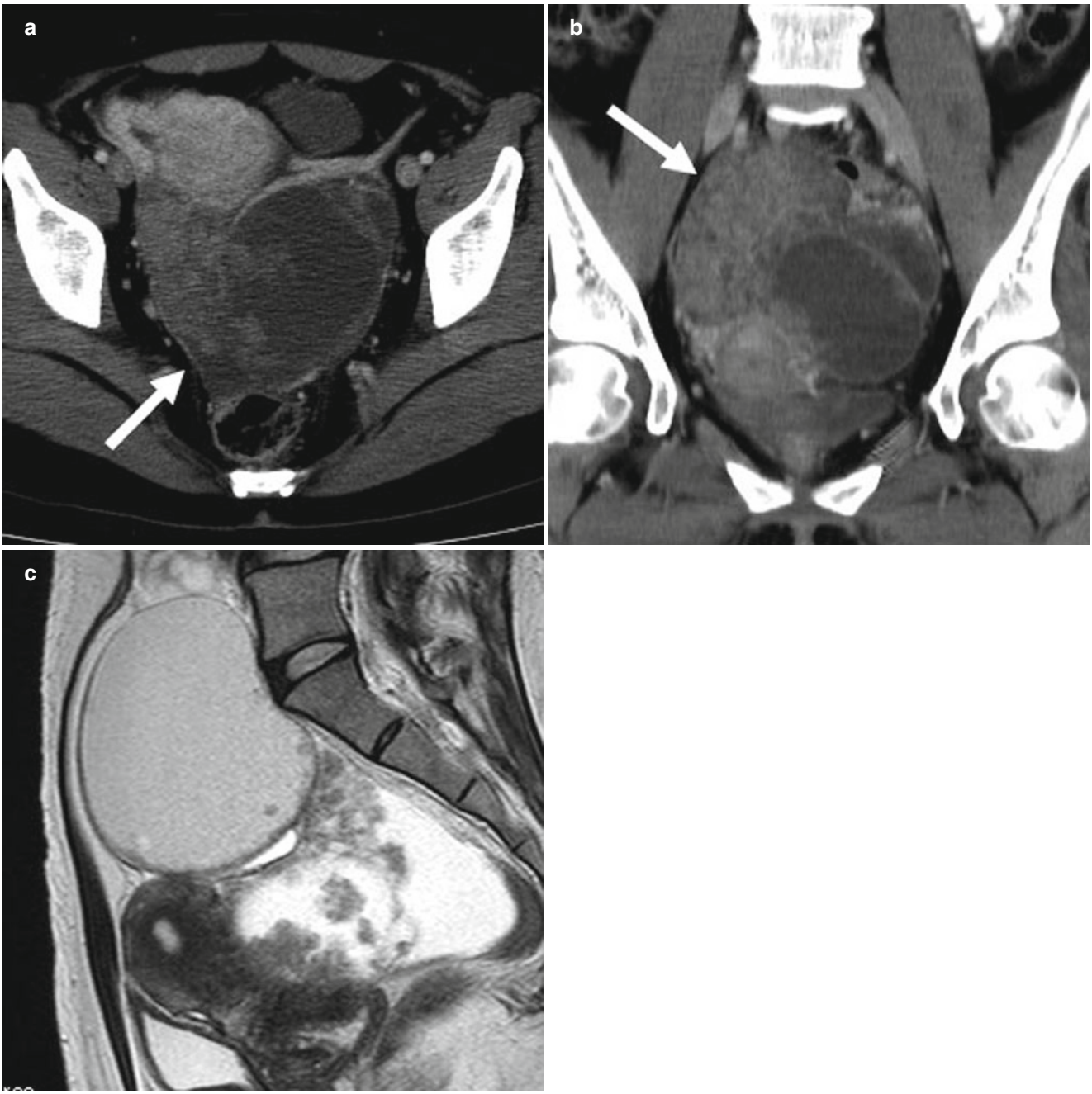

Fig. 7 (**a**) A 37-year-old woman with serous surface papillary borderline tumor. Contrast-enhanced axial computed tomography (CT) shows a cystic and solid mass (*arrow*) posterior to the uterus in the pelvis. The axial CT image is similar to that of peritoneal dissemination posterior to the uterus. (**b**) Contrast-enhanced coronal CT shows cystic masses superior-right lateral to solid components (*arrow*) in the pelvis. (**c**) Sagittal T_2-weighted image shows that hyperintense papillary architecture on the surface and hypointense branch-like structure within the mass on the surface of cystic lesion

Differential Diagnosis of Intestinal Type Mucinous Borderline Tumor

The MR findings of intestinal type mucinous borderline tumors herein identified resemble those reported for mucinous cystadenoma and mucinous carcinoma. Mucinous cystadenoma consists of a few solid components and mucinous carcinoma of many solid components that show strong contrast enhancement [8]. MR imaging findings of a solid component in the tumor generally suggest primary malignant ovarian epithelial tumor. Furthermore, mucinous cystadenocarcinomas or mucinous borderline ovarian tumors tend to show numerous fine loculi in larger numbers than in mucinous cystadenoma. Some mucinous borderline ovarian tumors appear as multilocular cystic masses with large solid

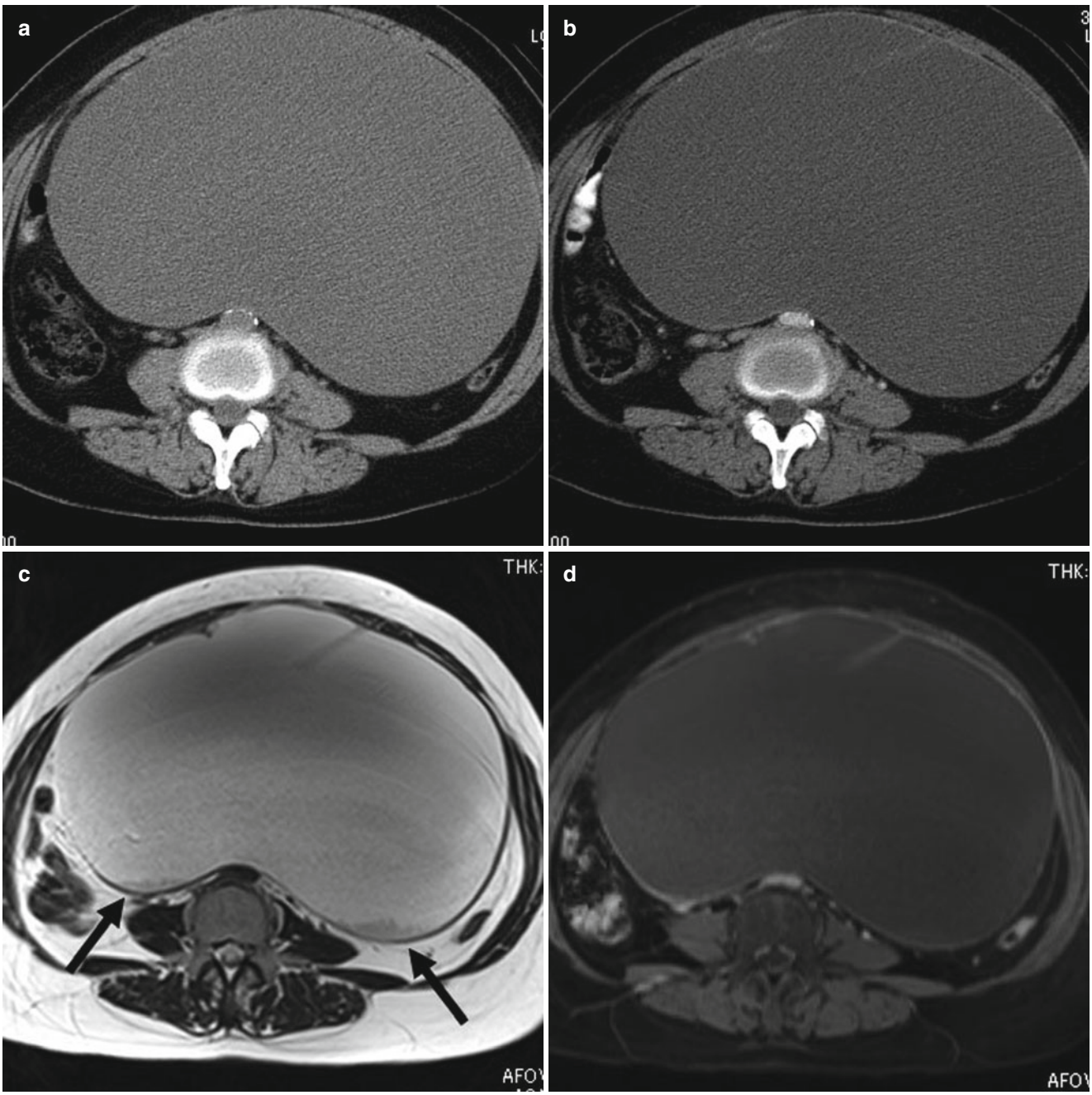

Fig. 8 (**a**) A 59-year-old woman with mucinous borderline tumor of intestinal type. Axial plain computed tomographic (CT) image shows large cystic mass and homogeneous density. (**b**) Axial contrast-enhanced CT image shows large cystic mass with thick septa and wall. (**c**) Axial T_2-weighted magnetic resonance (MR) image shows a large cystic lesion with thick septa and globules of intermediate signal in the dorsal aspect (*black arrows*). (**d**) Axial fat-saturated contrast-enhanced T_1-weighted MR image shows a large cystic lesion with thick septa. The globules in the (c) do not demonstrate contrast enhancement

components that result from the accumulation of small cystic components that contain mucinous fluid (Fig. 11a–d) [27]. MR findings overlap considerably between intestinal type mucinous borderline tumor and mucinous adenocarcinoma.

Differentiating borderline mucinous tumor and ovarian metastasis from gastrointestinal tumor can be difficult. Ovarian metastasis sometimes demonstrates a stained-glass pattern on T_1- and T_2-weighted images, and the solid components are small in size. When both ovaries demonstrate multilocular cystic masses and mucinous tumor is suspected, gastrointestinal study or evaluation of tumor marker is necessary [28].

The imaging findings of mucinous borderline ovarian tumor are indistinguishable from other borderline ovarian tumors, such as serous, endometrioid, clear cell, and transitional cell

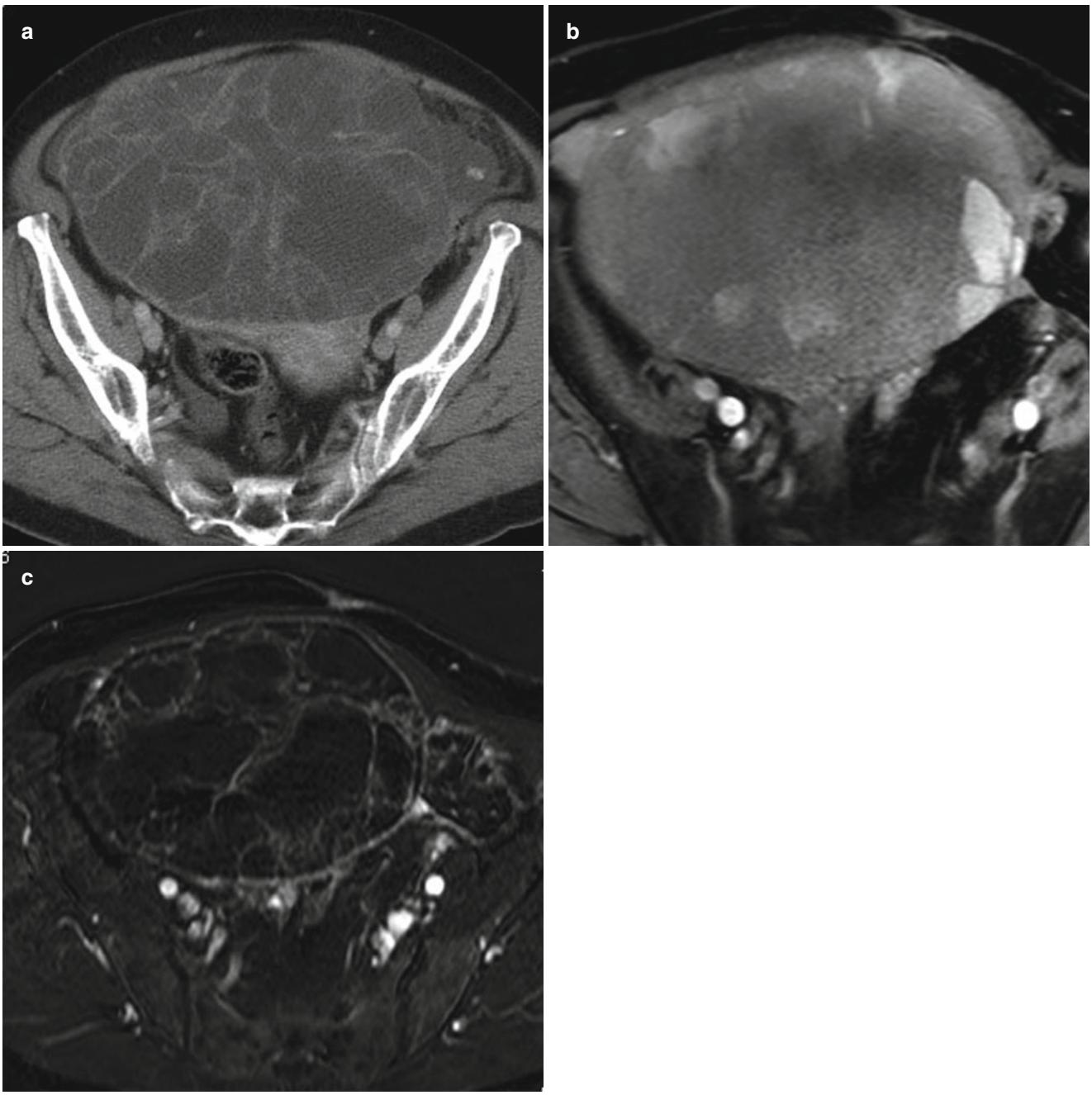

Fig. 9 (**a**) A 76-year-old woman with mucinous borderline tumor of intestinal type. Contrast-enhanced computed tomographic (CT) scan shows a large multilocular cystic mass with smooth contour, honeycomb appearance, and heterogeneous attenuation in the locules. Some septa are thickened. (**b**) Axial fat-saturated contrast-enhanced T_1-weighted magnetic resonance (MR) image shows a large multilocular mass with heterogeneous high signal intensity but with variable signal intensity in the locules. Some septa are thickened. (**c**) Axial 3-dimensional (3D) fat-saturated contrast-enhanced T_1-weighted MR subtraction image shows a large multilocular mass and several small solid components

tumors, except for the serous surface papillary borderline tumor. However, MR spectroscopy has recently been reported useful for differentiating mucinous and nonmucinous tumors. Takeuchi and colleagues showed a peak of N-acetylmucinous compounds of 2 ppm in mucinous tumors on MR spectroscopy [29]. The peaks of these compounds on MR spectroscopy could help distinguish mucinous and nonmucinous tumors for more reliable diagnosis of borderline tumors.

Focus Points

On MR imaging, mucinous borderline ovarian tumors commonly appear as multilocular cystic masses with numerous septa and contain fluids of different signal intensities, but they can contain a large solid component that results from the accumulation of small cystic components that contain mucinous fluid.

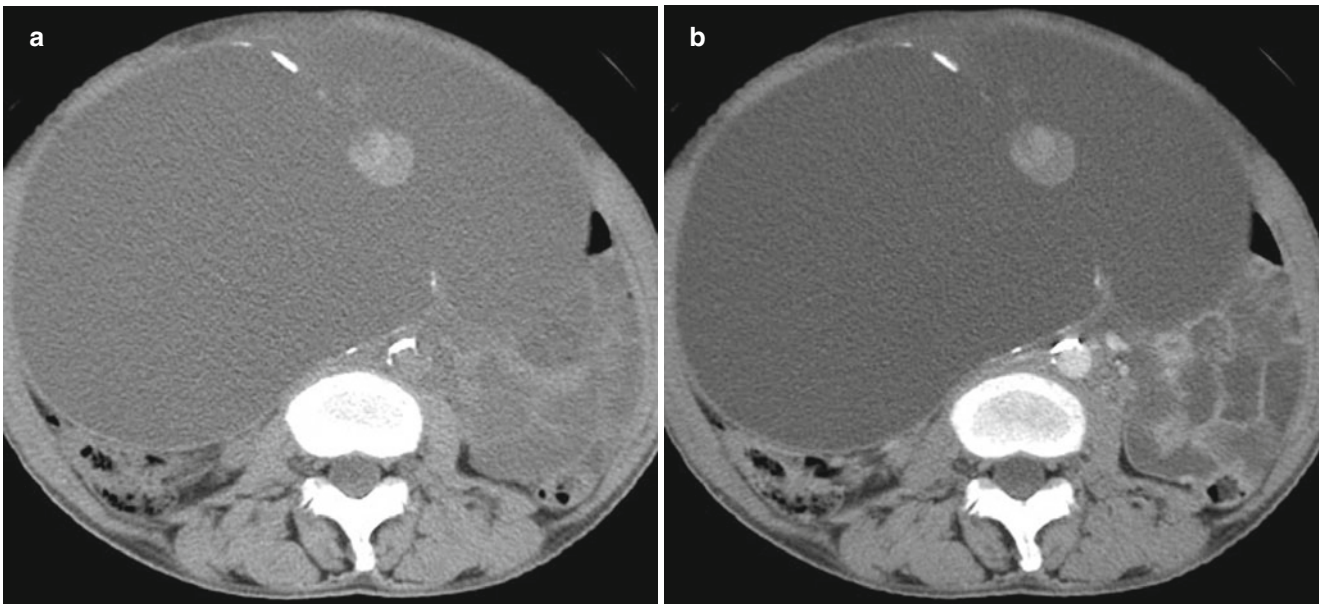

Fig. 10 (**a**) A 61-year-old woman with mucinous borderline tumor of intestinal type. Non-contrast axial computed tomographic (CT) scan shows a linear curve-shaped calcification in the cyst wall and septum. A mucinous component is seen along the septum. (**b**) Contrast contrast-enhanced CT scan shows linear curve-shaped calcification in the cyst wall and septum. A mucinous component along the septum shows no enhancement

Müllerian Type Mucinous Borderline Tumor

General Considerations for Müllerian Mucinous Borderline Tumor

Rutgers and Scully described müllerian type mucinous borderline tumor in 1988 [30]. These tumors manifest at a younger age than intestinal type tumors. The average tumor diameter is 9 cm, and about 70 % are unilocular or have only a few locules. Most tumors show grossly visible intracystic papillae. Approximately 30 % are bilateral at diagnosis. The tumors coexist with ovarian or pelvic endometriosis in 20–30 % of cases as do several types of malignant ovarian tumors that arise from endometriotic cysts [30]; few other borderline tumors coexist with endometriosis. Müllerian mucinous borderline ovarian tumors do not coexist with pseudomyxoma peritone. The tumors somewhat mimic serous borderline ovarian tumors and are also termed "seromucinous borderline ovarian tumors." These tumors may be associated with abdominal or pelvic implants, which may be invasive.

Imaging Findings of Müllerian Mucinous Borderline Tumor

Clues to müllerian mucinous borderline ovarian tumors may be bilaterality and association with endometriosis. The tumors are typically uni- or paucilocular cystic masses with mural nodules (Fig. 12a–d). The fluid component shows high intensity on both T_1- and T_2-weighted images, and the mural nodule shows prominent high intensity on T_2-weighted images (Fig. 12b, c) [30] that reflects stromal edema. The fluid component may show high signal intensity on both T_2- and T_1-weighted image that results from intraluminal mucinous material.

Differential Diagnosis of Müllerian Mucinous Borderline Tumor

MR findings of the müllerian mucinous borderline tumors identified herein resemble those reported for malignant tumors associated with endometrial cyst, such as clear cell or endometrioid carcinomas. These malignant tumors that arise from endometriotic cysts are frequently present as cystic masses filled with fluid of high signal intensity and nodular solid components [28]. However, differentiation of müllerian mucinous borderline tumors and malignant tumors associated with endometrial cyst is important because the prognosis of patients with the müllerian type is much better. Though definitive diagnosis may be difficult, T_2-weighted image findings of prominently high signal intensity of mural nodules mingled with a layer of higher signal intensity around the nodules may suggest a more probable diagnosis of Müllerian mucinous borderline tumor (Fig. 13a–c) [31].

Focus Points

Mucinous borderline ovarian tumor of endocervical type appears as a few locular cystic masses with a solid component of high signal intensity on T_2-weighted image; mingling of these findings with a layer of higher signal intensity around the solid component may increase the likelihood of this diagnosis.

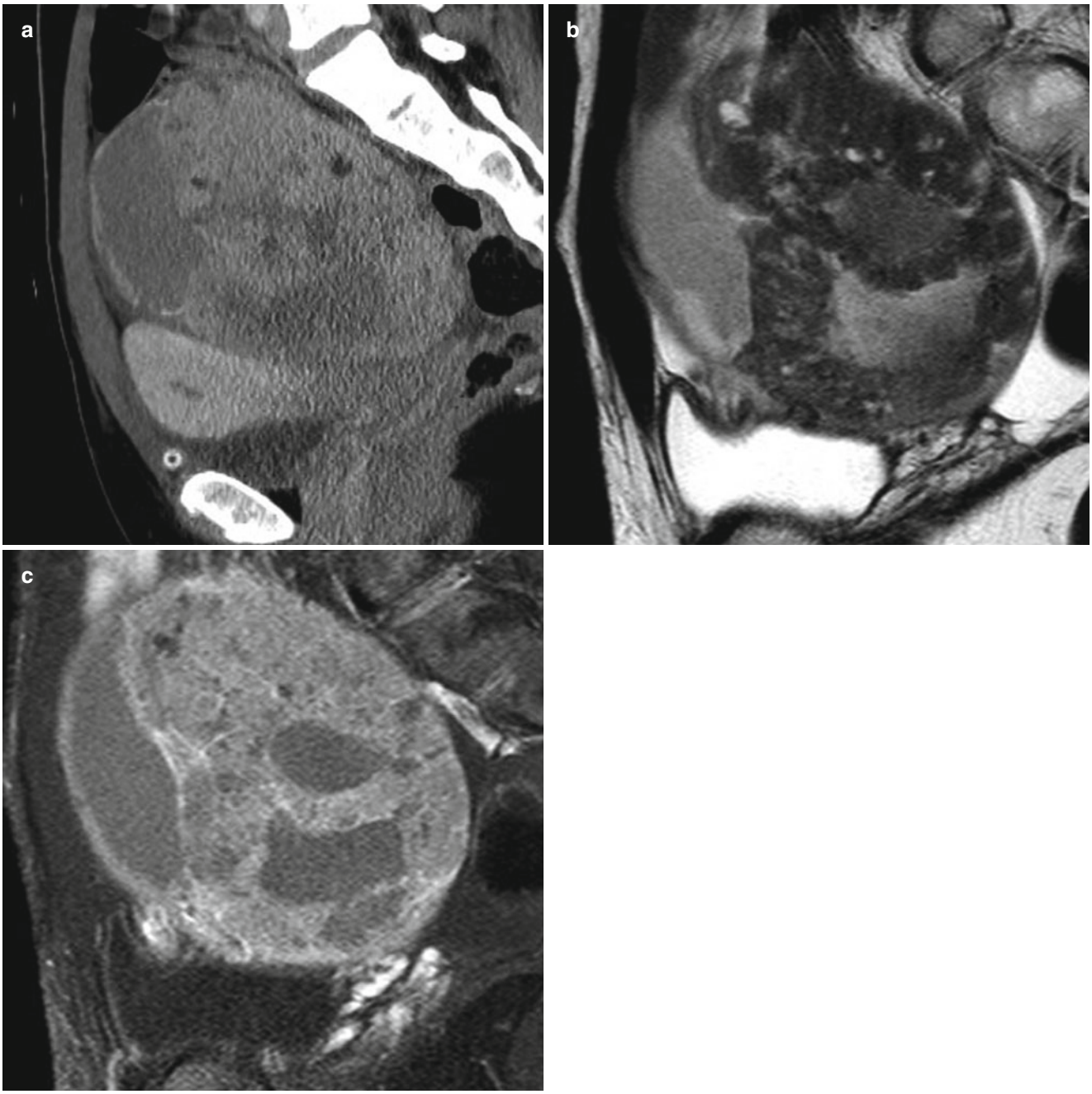

Fig. 11 (**a**) A 39-year-old woman with mucinous borderline tumor of intestinal type. Reconstruction image of contrast-enhanced computed tomographic (CT) scan shows a large solid mass with cystic parts in the pelvic space. (**b**) Sagittal T_2-weighted magnetic resonance (MR) image shows the solid component of the mass with cystic parts. The signal of the solid component was slightly hypointense and contained markedly small areas of hyperintensity. (**c**) Sagittal fat-saturated contrast-enhanced T_1-weighted MR image shows heterogeneous enhancement of the tumor in the solid component

Other Ovarian Borderline Tumors

General Considerations for other Ovarian Borderline Tumors

Uncommon subtypes represent 3–4 % of all borderline ovarian tumors [32] and include endometrioid, clear cell, transitional cell, and mixed-type tumors. The mean ages for these other tumors range between 45 and 65 years [32]. Nonserous and nonmucinous borderline ovarian tumors do not show characteristic imaging features and may resemble serous or mucinous borderline ovarian tumors as well as early-stage ovarian carcinomas (Fig. 14a–d). The other ovarian borderline tumors also run a benign course after tumor removal, with recurrences or metastasis exceptionally rare.

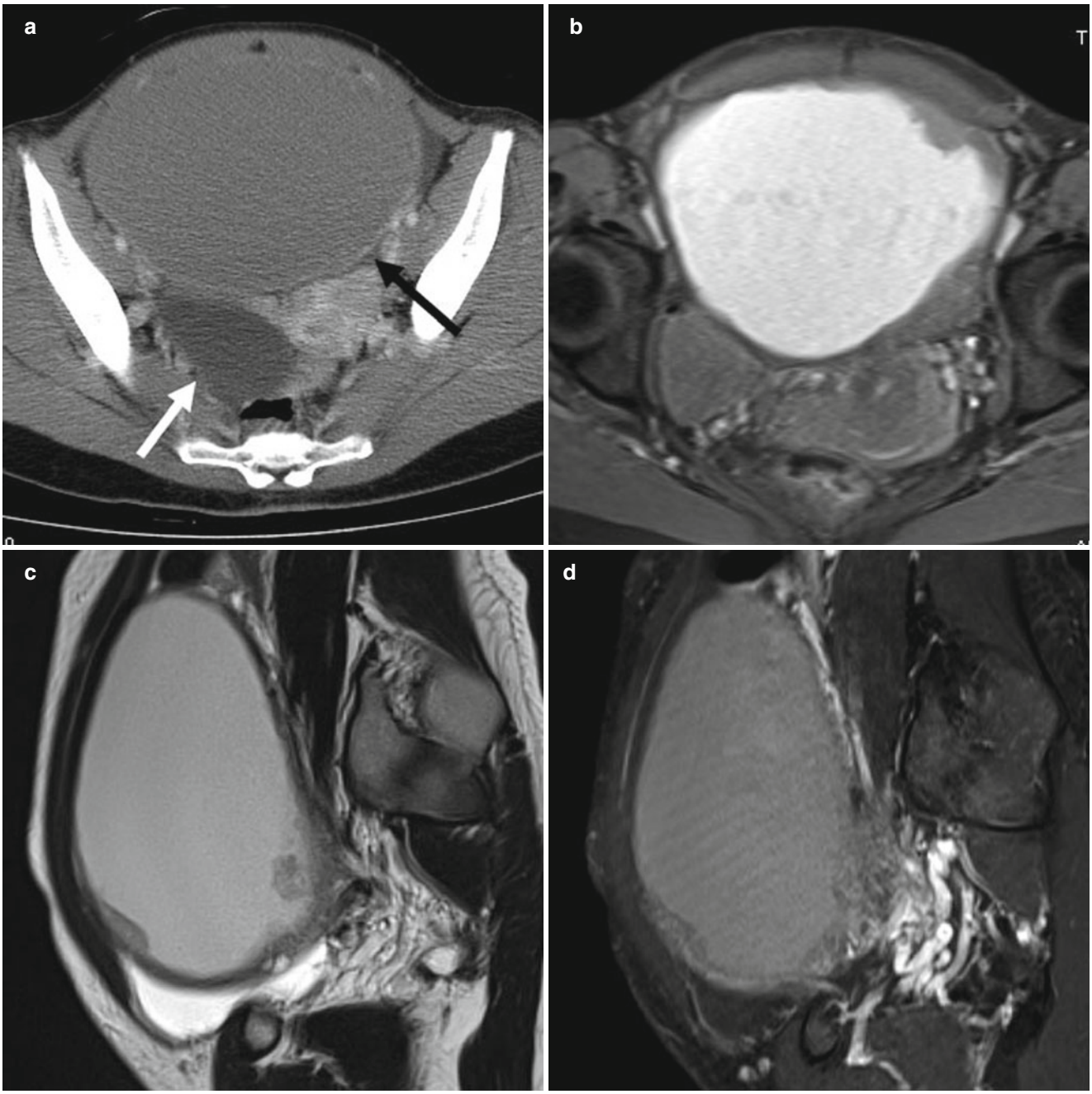

Fig. 12 (**a**) A 34-year-old woman with mucinous borderline tumor of endocervical type. Contrast-enhanced axial computed tomographic (CT) scan shows a large cystic mass anterior to the uterus in the pelvic space (*black arrow*). A solid part in the cystic lesion is unclear. Normal functional cyst is seen in the right adnexal region (*white arrow*). (**b**) Axial fat-saturated T_1-weighted image shows a large cystic mass anterior to the uterus in the pelvic space. A solid part in the cystic lesion is seen in the left frontal region. The fluid shows high signal intensity that reflects hemorrhage. (**c**) Sagittal T_2-weighted image shows a large cystic mass anterior to the uterus in the pelvic space. Solid parts in the cystic lesion are seen as areas of high signal intensity along the cystic wall, and thickening of the cystic wall appears with low signal intensity. These changes may reflect changes from endometriosis. (**d**) Sagittal fat-saturated contrast-enhanced T_1-weighted image shows a large cystic mass anterior to the uterus in the pelvic space. A solid part in the cystic lesion is seen in the left frontal region and shows high signal intensity

Differential Diagnosis of other Ovarian Borderline Tumors

Nonserous and nonmucinous borderline ovarian tumors resemble serous or mucinous borderline ovarian tumors as well as early-stage ovarian carcinomas, and it is difficult to differentiate nonserous and nonmucinous tumors from other borderline tumors. However, Thomassin-Naggara and colleagues recently showed that the early enhancement patterns of ovarian epithelial tumors on dynamic contrast-enhanced MR images could help distinguish

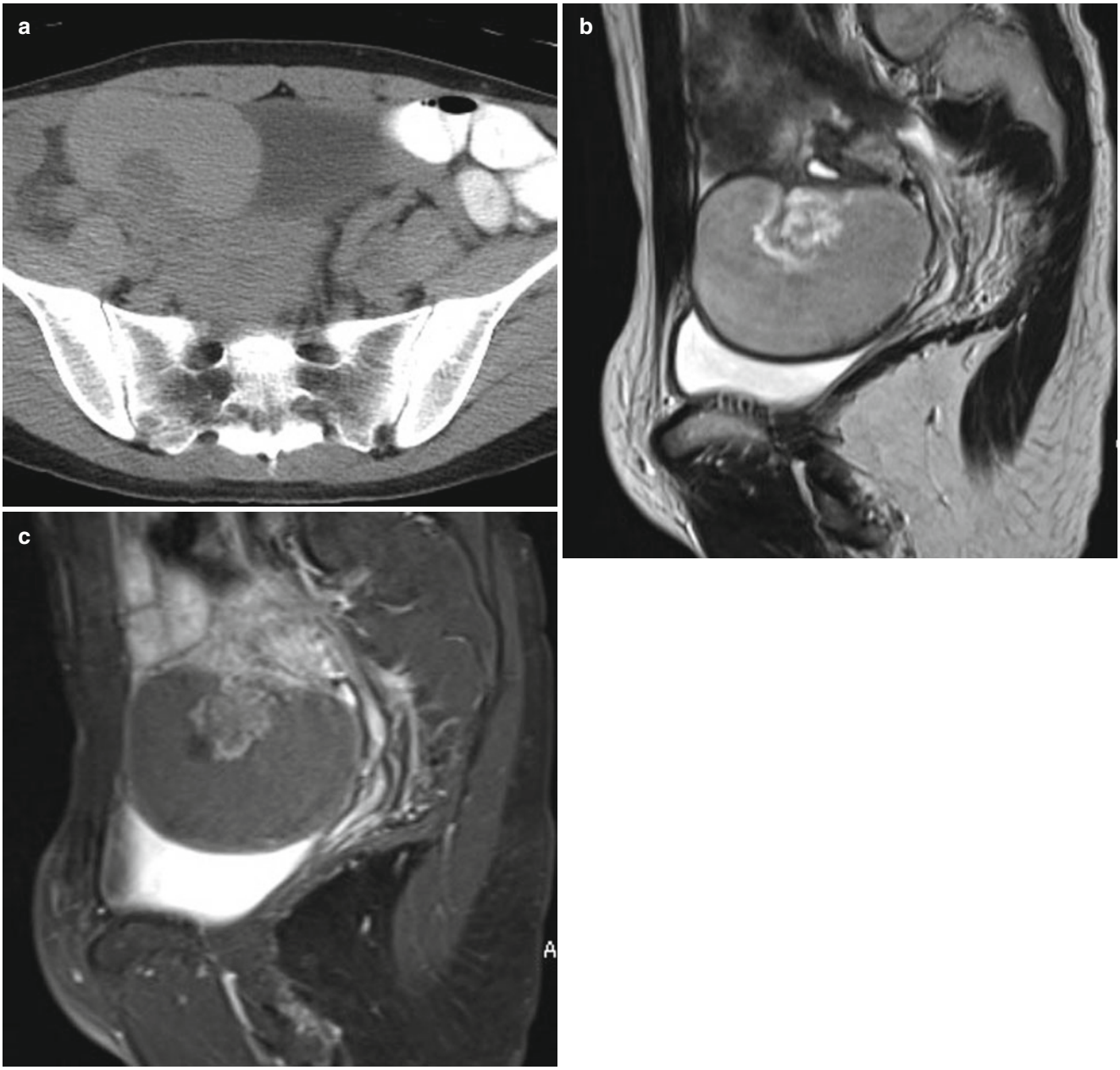

Fig. 13 (**a**) A 23-year-old woman with mucinous borderline tumor of endocervical type. Axial plain computed tomographic (CT) scan shows cystic mass with solid component in the right adnexal region. (**b**) Sagittal T_2-weighted image shows a large cystic mass superior to the bladder in the pelvic space. A solid part mingles with a layer of higher signal intensity around the solid component along the cystic wall in the superior region. (**c**) Sagittal fat-saturated contrast-enhanced T_1-weighted image shows a large cystic mass anterior to the uterus in the pelvic space. A solid part in the cystic lesion shows heterogeneous high signal intensity

among benign, borderline, and invasive tumors and were found to correlate with tumoral angiogenic status when maximal slope of perfusion parameters were employed [33]. Maximal slope of dynamic contrast study could be helpful to distinguish among benign, borderline, and malignant ovarian epithelial tumors [33].

CT and MR Imaging of Serous Tumors

General Considerations for Serous Tumors

The WHO histological classification separates ovarian neoplasms into surface epithelial–stromal, sex cord–stromal, and

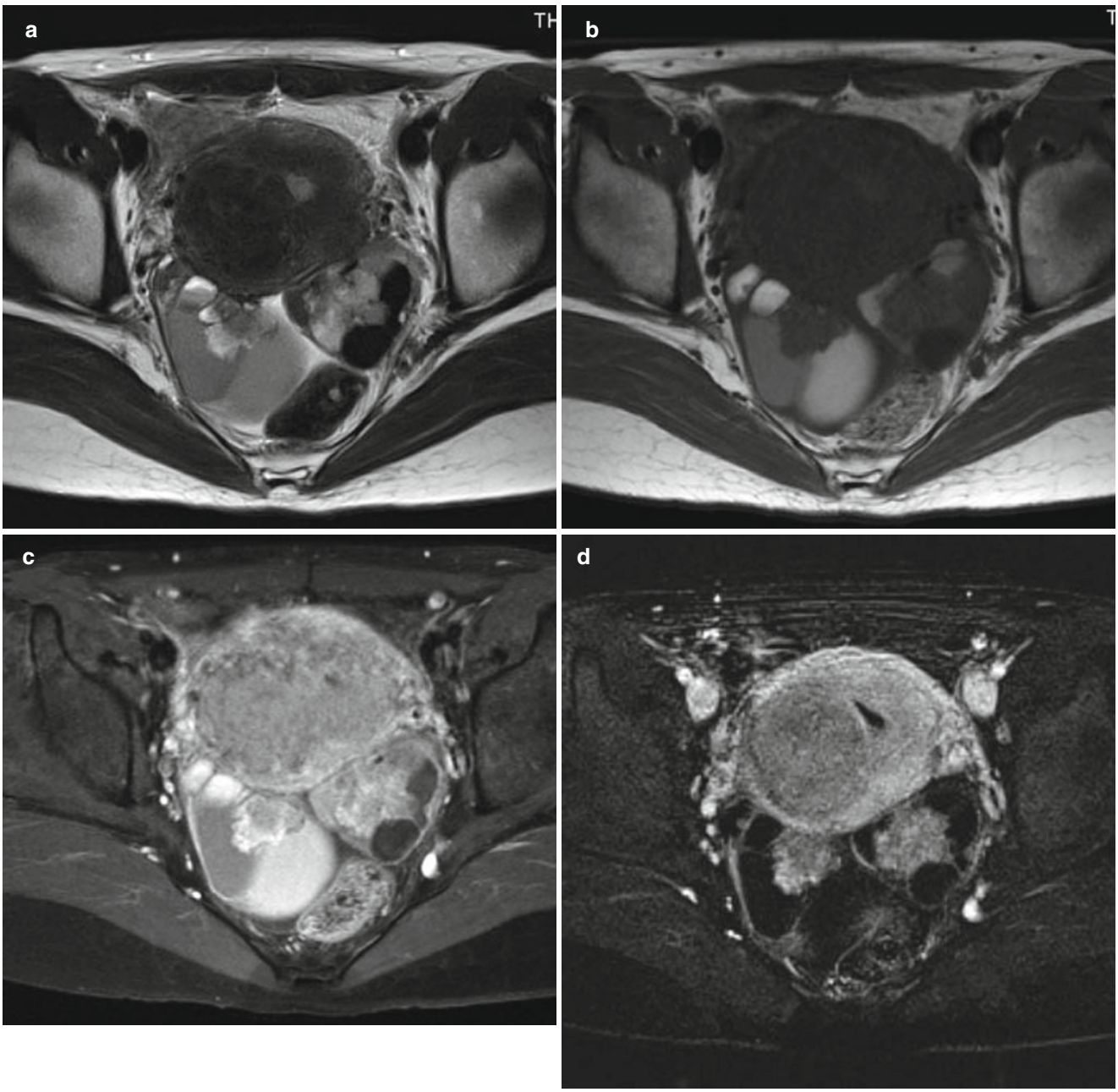

Fig. 14 (**a**) A 32-year-old woman with endometrioid borderline tumor. Axial T_2-weighted magnetic resonance (MR) image shows a large complex cystic mass with multiple septa. The variable signal intensities of the loculi demonstrate the so-called "stained-glass" appearance. (**b**) Axial T_1-weighted MR image shows a large complex cystic mass with multiple septa. The variable signal intensities of the loculi demonstrate the so-called "stained-glass" appearance. (**c**) Axial 3-dimensional (3D) fat-saturated contrast-enhanced T_1-weighted MR image shows a large complex cystic mass with multiple septa. The loculi show variable signal intensities, but the solid components are unclear. (**d**) Axial 3D fat-saturated T_1-weighted subtraction MR image shows a large complex cystic mass with multiple septa. Irregularly marginated solid components are seen along the cystic wall

germ cell tumors according to the most probable tissue of origin [1]. Surface epithelial–stromal tumors comprise serous, mucinous, endometrioid, clear cell, and Brenner tumors; serous tumors are the most common type of epithelial neoplasm [7].

Serous tumors are surface epithelial–stromal tumors and are categorized by their malignant potential and clinical behavior into serous benign tumor, serous borderline tumor, and serous carcinoma. Serous tumors include serous cystadenoma,

serous cystadenofibroma, cystadenoma of borderline malignancy, or malignant cystadenocarcinoma. Serous tumors represent about 30 % of all ovarian neoplasms, about 60–65 % of benign tumors, about 10 % of borderline malignancies, and about 25–30 % of malignant tumors [22]. Serous cystadenocarcinomas account for approximately 40 % of all cancers of the ovary and are the most common malignant ovarian tumor.

Benign Serous Tumors

Benign serous tumors are most commonly found in women of reproductive age, between 20 and 50 years. Patients generally demonstrate no symptoms, but the tumors sometimes cause pelvic pain or discomfort [34]. These tumors usually showing about 1–3 cm are incidentally found, and the size is usually within 15 cm [22, 34]. About 10–20 % are bilateral [22]. According to the WHO histological classification, serous benign tumors include serous cystadenomas, adenofibromas, cystadenofibromas, and surface papillomas [1].

Serous Cystadenoma

General Considerations for Serous Cystadenoma

Benign serous tumors are commonly encountered as serous cystadenomas of benign epithelial–stromal tumors. Benign ovarian tumors are most commonly caused by mature teratoma, followed by serous cystadenoma [22]. Serous cystadenomas of the ovary appear as thin-walled cysts that contain serous fluid, and the tumors are lined by a single layer of epithelium [22]. From 12 to 20 % of these tumors are bilateral. Histologically, psammoma bodies are present in the stroma in 15 % [33]. More aggressive tumors are termed borderline serous cystadenoma and serous cystadenocarcinoma.

Imaging Appearances of Serous Cystadenoma

On CT images, serous cystadenomas appear as one or more well-defined cysts with thin regular wall or septum that contain fluid of homogeneous low density and usually show no endo- or exocystic vegetation [34] (Fig. 15a). Contrast-enhanced CT images do not show a solid component (Fig. 15b). CT findings generally show a uni- (Fig. 15a, b) rather than multilocular (Fig. 16a) mass. Tumors that show a multilocular mass usually demonstrate thin separations (Fig. 16b, c), and papillary projections and nodular vegetations occasionally appear as small nodular projections (Fig. 17a, b), features specific to epithelial ovarian neoplasms. Like ovarian cancer, cystadenoma may display papillary projections, but it does so less frequently (9 % of cases) than malignant tumors [35], and such projections are small in the serous cystadenoma. Accordingly, contrast administration (if possible, subtraction MR image) can facilitate differentiation from intracystic clot or debris. The size of the cysts can be quite large (Fig. 18a–c), and as with other serous tumors, psammomatous calcification can be a feature.

Differential Diagnosis of Serous Cystadenoma

On CT images, serous cystadenoma may be differentiated as a uni- or multilocular cystic mass with homogeneous CT attenuation and thin regular wall or septum. A unilocular cystic ovarian lesion may be differentiated by its cystic positions, such as ovarian functional cysts, paraovarian cysts, and paraovarian cystadenoma. Usually, paraovarian cysts and paraovarian cystadenomas keep at a small distance of normal ovary and do not have beak sign. However, compression of the ovary by large cystic lesions makes it difficult to differentiate ovarian serous cystadenoma from paraovarian cysts and paraovarian cystadenomas. Ovarian cysts are usually no larger than 5 cm. The differential diagnosis for multilocular cystic lesion includes ovarian mucinous cystadenoma. On CT image, differentiation between serous and mucinous cystadenoma is difficult because attenuation of the serous and mucinous fluids is equivocal. Furthermore, on MR images, differentiation between serous and mucinous tumor is sometimes difficult because hemorrhage in the cystic component of serous cystadenomas manifests as high signal intensity on T_1-weighted MR image due to varying amounts of blood in the lesion and mucinous fluid in the cystic component of mucinous cystadenoma manifests as high signal intensity on T_1-weighted MR image due to gelatinous material or fluid of various viscosities in the lesion.

Focus Points

Serous cystadenomas generally show homogeneous low signal intensity on T_1-weighted image and high signal intensity on T_2-weighted image, but variable concentrations of blood in the tumor can lead to varying signal intensity.

Serous Cystadenofibroma

General Considerations for Cystadenofibroma

The 2003 WHO histological classification designates ovarian cystadenofibromas as surface epithelial–stromal tumors. Histologically, the ovarian tumors known as adenofibroma and cystadenofibroma are characterized by a prominent fibrous tissue component in addition to their epithelial elements [22]. Whereas adenofibromas of the ovary are tumors with neoplastic glandular elements and a predominant benign stroma, cystadenofibromas are partially or entirely cystic [22]. These tumors are classified according to epithelial cell type as serous, endometrioid, mucinous, clear cell, or mixed

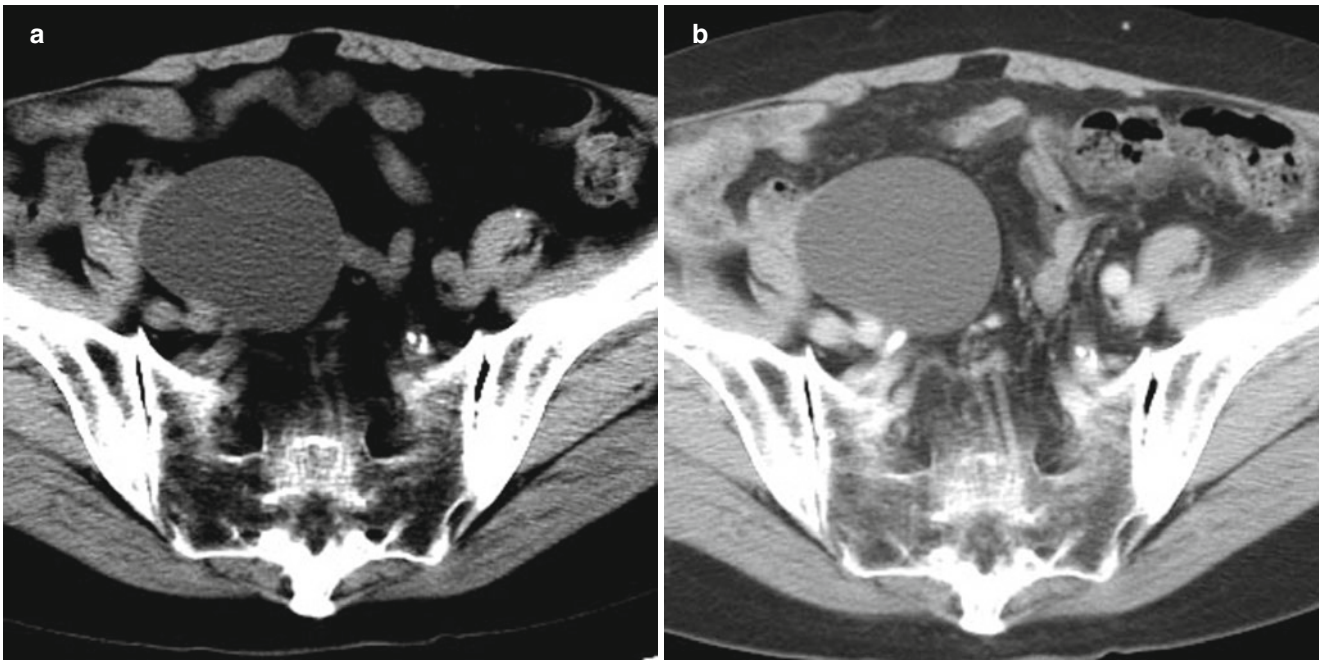

Fig. 15 (**a**) A 49-year-old woman with benign serous cystadenoma. Axial plain computed tomographic (CT) scan shows a unilocular cystic mass in the right lower quadrant. The wall of the mass shows no evidence of excrescence within. (**b**) Axial contrast-enhanced CT scan shows a unilocular cystic mass in the right lower quadrant. The wall of the mass shows no evidence of excrescence within

[1]. Serous adenofibroma and serous cystadenofibroma sometimes represent malignant change [36].

Cystadenofibromas account for only 1.2 % of all benign ovarian tumors and are most commonly seen in women of reproductive age with a range of age 15–65 years [37, 38]. Slieva and colleagues report that adenofibroma and cystadenofibroma are more common among patients with breast cancer and thyroid disorders [39]. Gross findings in a study of Cho and colleagues reported half of ovarian cystadenofibromas as purely cystic and the other half as complex cystic with one or more solid components [40].

Imaging Appearances of Cystadenofibroma

Although CT can be used to image serous cystadenofibromas, its role in the diagnostic evaluation of these neoplasms is minimal. The CT findings of serous cystadenofibroma are similar to those of other malignant ovarian neoplasms that demonstrate a cystic mass with an enhancing solid portion as the prominent and nonspecific findings. CT images reflect gross findings and show a uni- or multilocular cystic mass with solid nodules that enhance following contrast administration (Fig. 19a, b).

MR images from the Cho and colleagues study showed half of ovarian cystadenofibromas as purely cystic and the other half as complex cystic with one or more solid components [40]. Based on imaging criteria, cystadenofibromas may mimic malignancy by appearing as multilocular cystic masses with solid components or irregular thick septae. MR images are the most valuable modality in distinguishing cystadenofibroma from malignant neoplasm, and accurate diagnosis can avoid excess surgery. MR images can show apparently pure cystic lesion or complex cystic lesions with solid lesions and allow accurate evaluation of solid lesions with regard to the presence of rims, plaques, or nodules that demonstrate low signal intensity on T_2-weighted images and gadolinium-contrast images (Fig. 20a, b).

On T_2-weighted images, serous cystadenofibromas can be recognized by the foci of low signal intensity that correspond to intratumoral regions of dense fibrous tissue [41]. MR findings of diffuse or partial thickening of the cystic wall with T_2 dark signal intensity in multilocular cystic masses suggest ovarian serous adenofibroma. Small or tiny cystic locules within the solid component are considered characteristic findings of cystadenofibroma and correspond to a black spongelike appearance on T_2-weighted image (Fig. 21a, b).

Differential Diagnosis of Cystadenofibroma

On MR imaging, serous cystadenofibromas appear as numerous cystic components with low signal intensity or a thick low signal component on T_2-weighted image [37, 38, 40]. On contrast-enhanced CT study, serous cystadenofibroma and malignant ovarian neoplasm may display similar findings. MR findings of a solid portion of low signal intensity on T_2-weighted image suggest fibrous tissue. If there is a black spongelike appearance in the solid component, the black

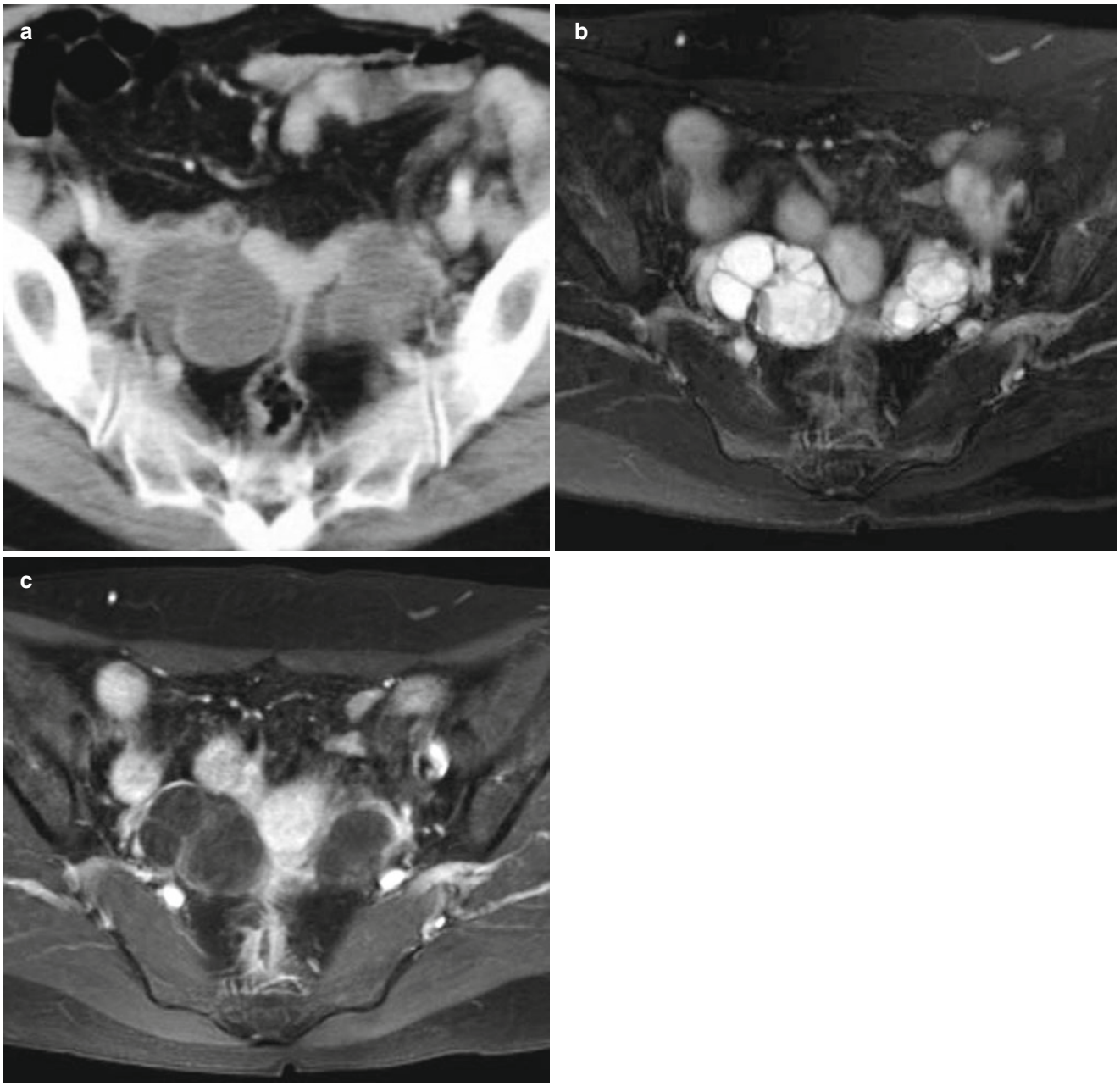

Fig. 16 (**a**) A 65-year-old woman with benign serous cystadenoma. Axial contrast-enhanced computed tomographic (CT) scan shows a multilocular cystic mass in the bilateral lower quadrant. The wall of the mass shows no evidence of excrescence within. (**b**) Axial fat-saturated T_2-weighted magnetic resonance (MR) image shows a multilocular cystic mass in the bilateral lower quadrant (*arrows*). The loculi show homogeneous high signal intensity. (**c**) Axial fat-saturated contrast-enhanced T_1-weighted MR image shows a multilocular cystic mass in the bilateral lower quadrant. The loculi show homogeneous high signal intensity

spongelike appearance tends to be fewer than malignant ovarian neoplasm (Fig. 21a, b). Serous cystadenofibrocarcinoma or borderline cystadenofibroma is invariably missed on imaging. An ovarian mass with fibrous component may resemble serous cystadenofibroma, especially fibroma, fibrothecoma, and Brenner tumor with cystic degeneration when these tumors do not have a black spongelike appearance. Metastatic ovarian tumors may also have fibrous tissues that show low signal intensity on T_2-weighted image, but these tumors usually involve both ovaries and demonstrate strongly enhancing solid portions.

Focus Points

Serous cystadenofibroma appears as numerous cystic components with low signal intensity or as a thick component of low signal on T_2-weighted image.

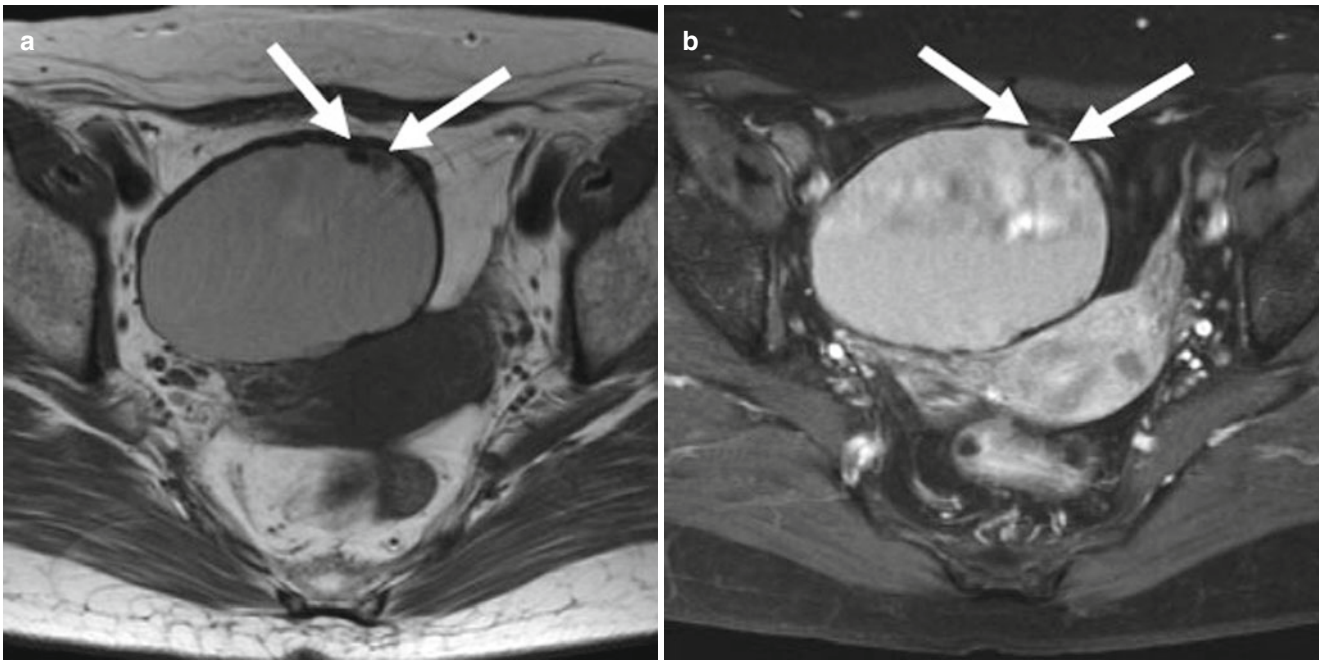

Fig. 17 (**a**) A 57-year-old woman with benign serous cystadenoma. Axial T_2-weighted magnetic resonance (MR) image shows a unilocular cystic mass in the pelvic space right anterior to the uterus with two small nodules of low signal intensity along the cystic wall (*white arrows*). (**b**) Axial fat-saturated contrast-enhanced T_1-weighted MR image shows a unilocular cystic mass in the pelvic space right anterior to the uterus with two small nodules (papillary projections) of slightly high signal intensity along the cystic wall (*white arrows*)

Ovarian Serous Carcinoma

General Considerations for Ovarian Serous Carcinoma

Ovarian serous carcinomas represent about 85 % of malignant neoplasms of the ovary, and serous cystadenocarcinoma is the most common malignant epithelial tumor cell type [34]. Ovarian serous carcinoma is histologically divided into low and high grades [34], which display different epidemiology, pathogenesis, and clinical course [34]; about 97 % are high grade, and about 3 % are low grade. Low-grade serous carcinoma is synonymous with invasive micropapillary serous carcinoma (MPSC). High-grade serous carcinoma arises de novo from the ovarian surface epithelium from an unknown precursor lesion and progresses rapidly. However, low-grade serous tumors develop in a stepwise fashion from known precursor lesions and display a less rapid aggressive pattern of spread [34].

High-grade serous carcinoma is the most common ovarian cancer and represents about 63 % of ovarian carcinomas [34]. These tumors most often occur in the sixth and seventh decade and most frequently present with symptoms of abdominal pain and distension due to ascites and bulky abdominal tumor. Two-thirds of advanced-stage cases involve both ovaries, and nearly all advanced-stage ovarian carcinomas involve peritoneal surfaces.

Low-grade serous carcinoma is a rare ovarian cancer, accounting for only about 4 % of ovarian carcinomas. The tumor shows a worse progression than serous borderline tumors. The mean age of patients is 45 years, and the most common presentation is an asymptomatic pelvic mass; 89 % of these tumors are bilateral, and 94 % are advanced stage [34].

Imaging Findings of Ovarian Serous Carcinoma

Typically, epithelial tumors, such as serous, mucinous, clear cell, and endometrioid types, are primarily cystic, may be either uni- or multilocular, and demonstrate varying proportions of solid components when malignant . Malignant epithelial tumors are commonly encountered as ovarian serous and mucinous carcinomas. Because epithelial malignant tumors tend to be cystic and solid components on morphologic examination in many cases, their cell types cannot be differentiated on the basis of MR or CT appearance. However, CT or MR imaging can show some features of ovarian serous carcinoma and distant invasion.

On CT, advanced ovarian serous carcinoma typically appears as cysts with thick walls, septations, and solid components (Fig. 22a, b). After contrast administration, malignant lesions tend to have more solid components than benign lesions. Subordinate CT findings of pelvic organ or sidewall invasion, peritoneal implants, lymph adenopathy, and ascites increase the likelihood of malignancy (Fig. 23a–d). Psammomatous calcifications are a common finding in serous adenocarcinomas, seen at histological analysis in up to 30 % of malignant serous tumors (Fig. 24a, b) [40] and detected

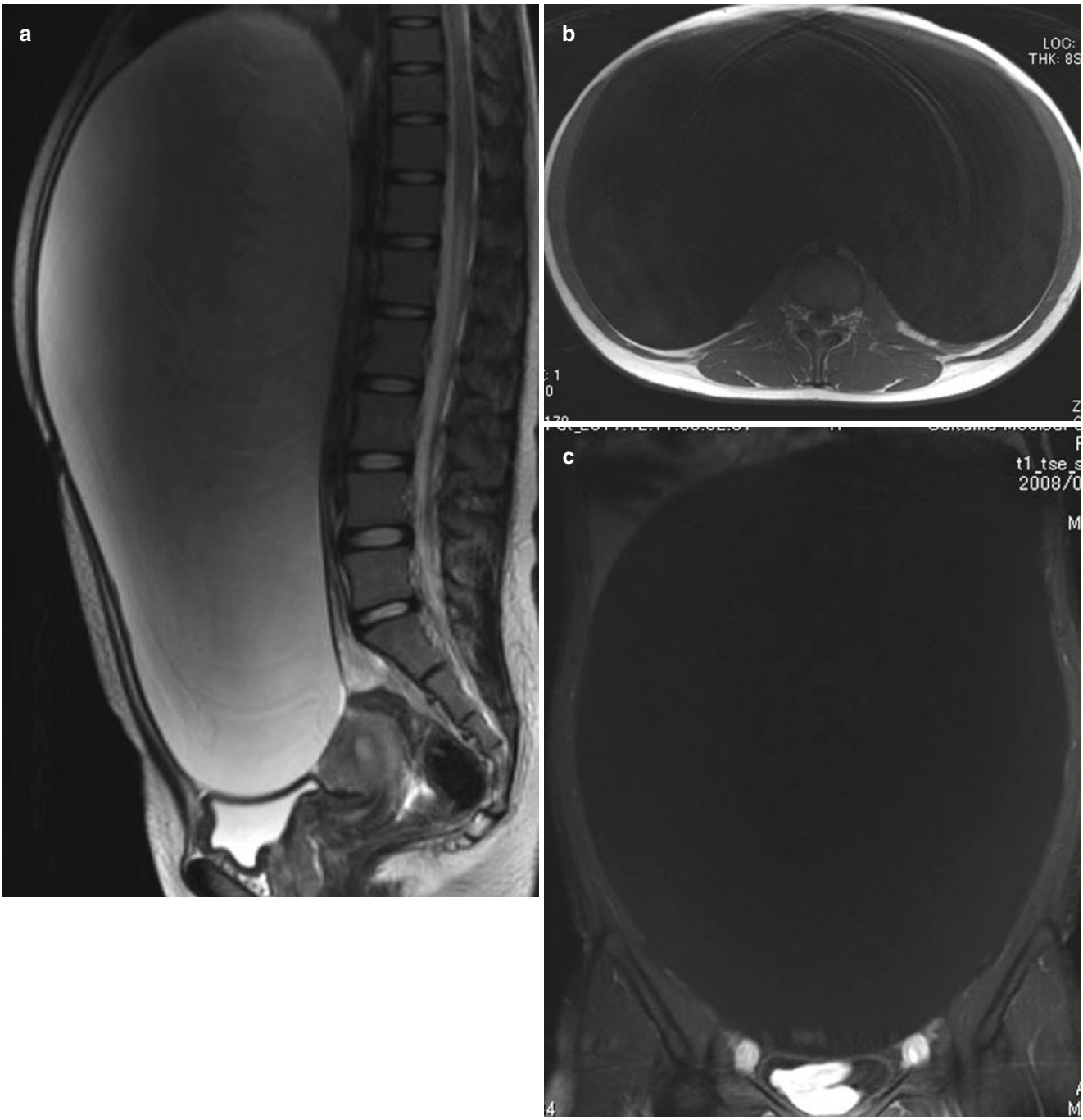

Fig. 18 (**a**) An 18-year-old woman with benign serous cystadenoma. Sagittal T_2-weighted magnetic resonance (MR) image shows a giant unilocular cystic mass in the pelvic space and abdomen. The cystic mass has no solid component and shows homogeneous high signal intensity. (**b**) Axial T_1-weighted MR image shows a giant unilocular cystic mass with homogeneous low signal intensity. (**c**) Coronal fat-saturated contrast-enhanced T_1-weighted MR image shows a giant unilocular cystic mass in the pelvic space and abdomen with no solid component and homogeneous low signal intensity

with CT in approximately 12 % of malignant serous tumors [42]. However, psammomatous calcifications are also seen in benign serous, serous borderline, and other tumors [26].

Malignant epithelial tumors demonstrate no characteristic signal intensity pattern on MR imaging. Typically, MR imaging demonstrates serous carcinoma as a cystic mass with solid or papillary components. Gadolinium enhancement aids accurate characterization of some adnexal lesions and is especially useful for delineating necrosis, solid components, papillary projections, peritoneal implants, and omental disease. Serous carcinomas are predominantly cystic masses with solid components (Fig. 25a–c) but sometimes demonstrate a

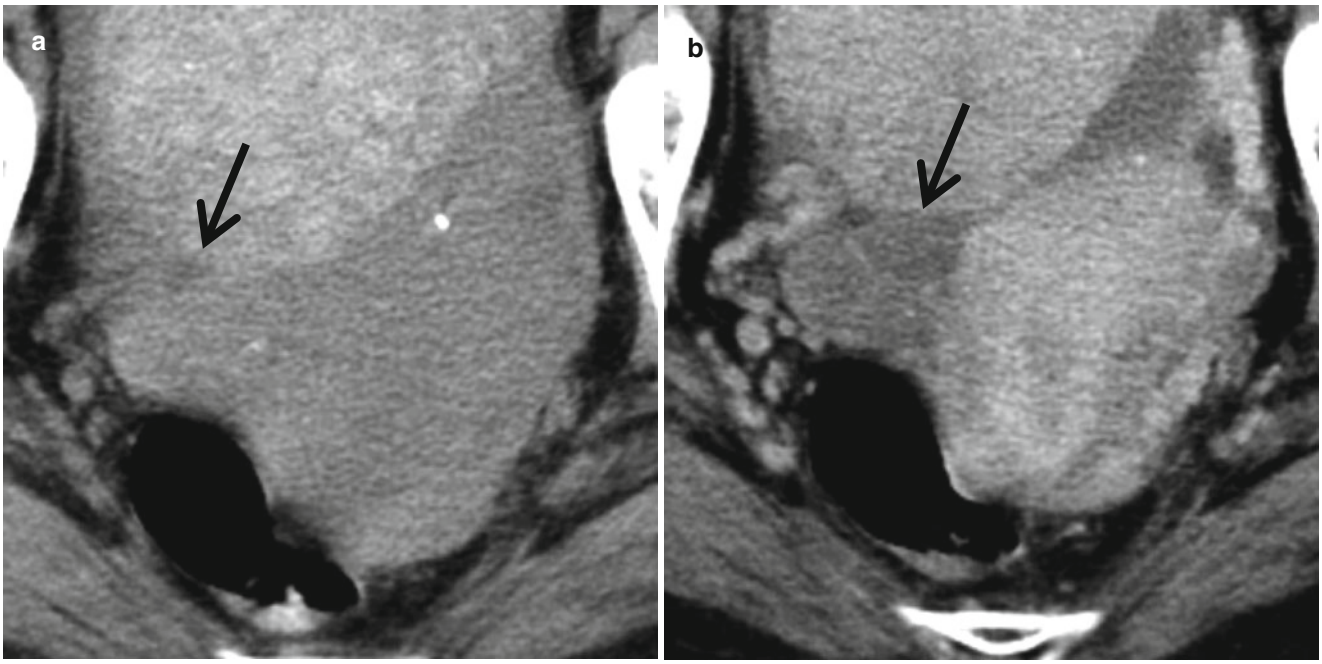

Fig. 19 (**a**) A 57-year-old woman with serous adenofibroma. Axial plain computed tomographic (CT) scan shows a complex heterogeneous mass in the right adnexal region (*black arrow*). (**b**) Axial contrast-enhanced CT scan shows a complex solid and cystic mass in the right adnexal region. There are several smoothly thickened septa. These solid components are slightly enhanced (*black arrow*)

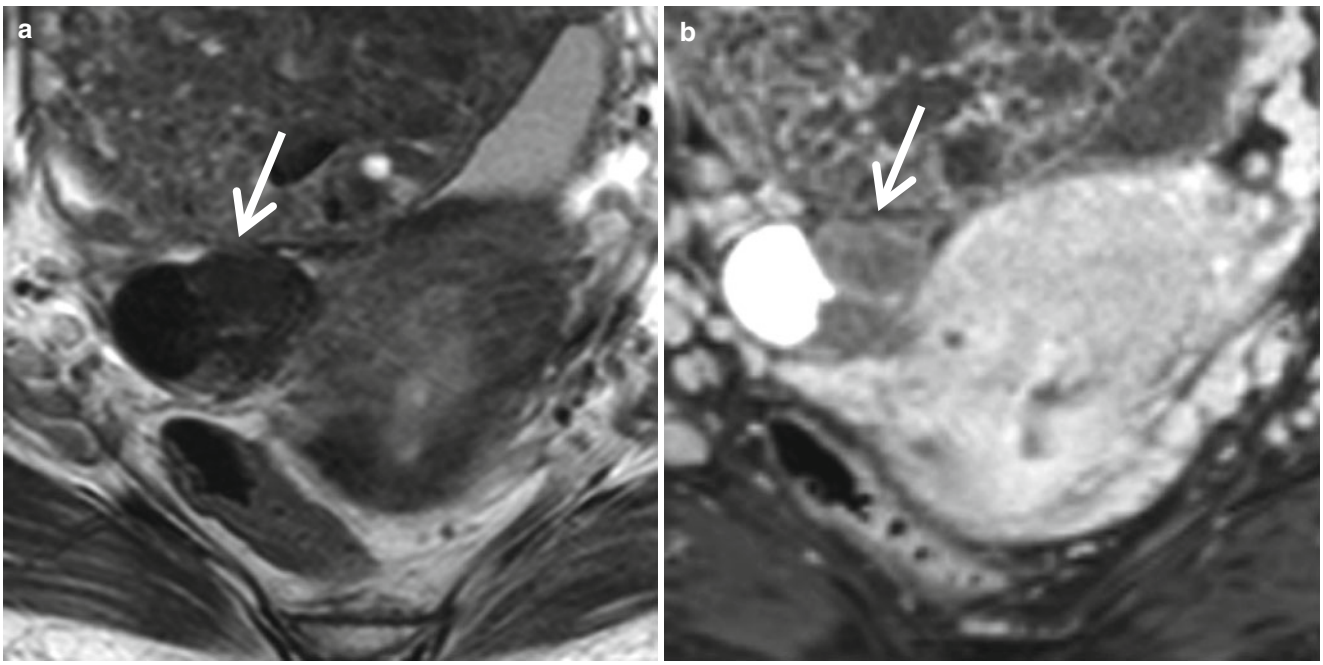

Fig. 20 (**a**) A 57-year-old woman with serous adenofibroma. Axial T_2-weighted image shows a complex solid and cystic mass in the right adnexal region. The mass has multiple septa and solid portions. Solid portions show low signal intensity compared to myometrium (*white arrow*). (**b**) Axial fat-saturated contrast-enhanced T_1-weighted image shows a complex solid and cystic mass in the right adnexal region. The mass has enhancing multiple septa and solid portions. Solid portions show slight high signal intensity (*white arrow*)

solid mass. In the evaluation of cystic ovarian masses, the presence of papillary projections is highly specific for malignant epithelial ovarian neoplasms containing serous carcinoma. Serous carcinoma can often show intraperitoneal dissemination and lymph node metastasis, and CT is useful as a staging tool. Recently, diffusion-weighted imaging has been shown useful for evaluating intraperitoneal dissemination and lymph node metastasis (Fig. 26a–c).

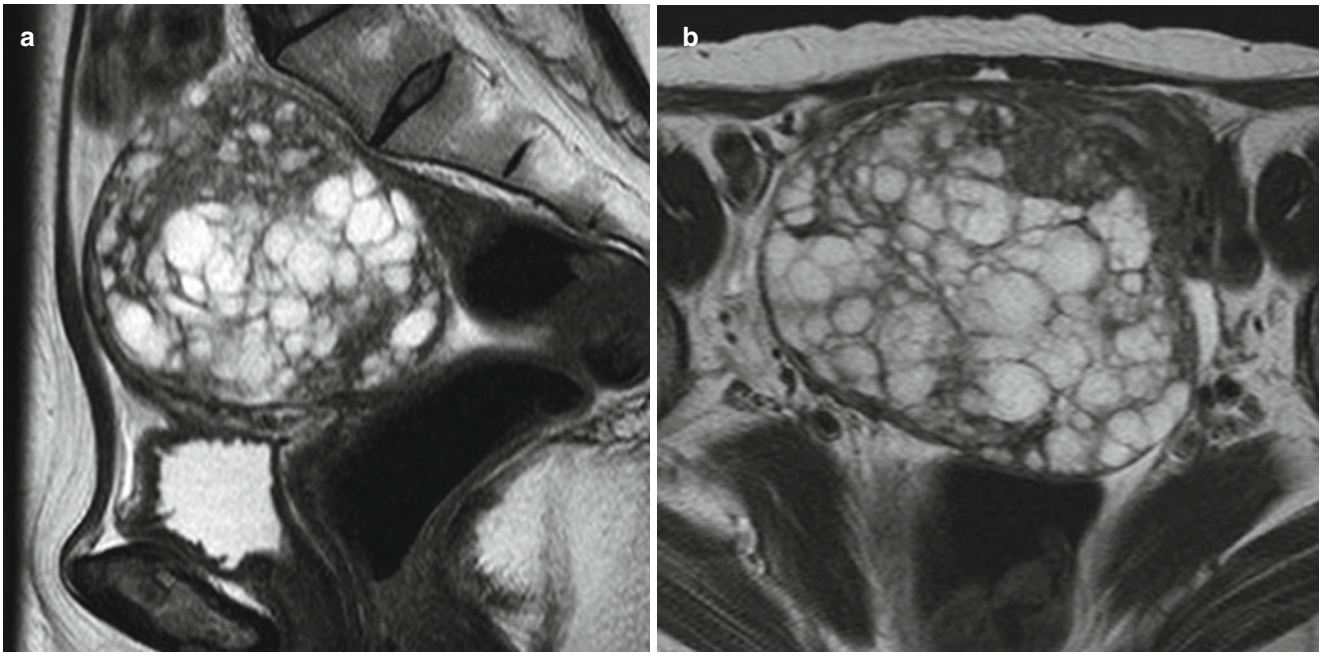

Fig. 21 (**a**) A 67-year-old woman with cystadenofibroma. Sagittal T_2-weighted image shows a multilocular cystic mass with solid components of very low intensity containing tiny cysts of very high intensity. (**b**) Axial T_2-weighted image shows a multilocular cystic mass with solid components of very low intensity containing tiny cysts of very high intensity. The portion of tiny cysts of high intensity resembles black sponge

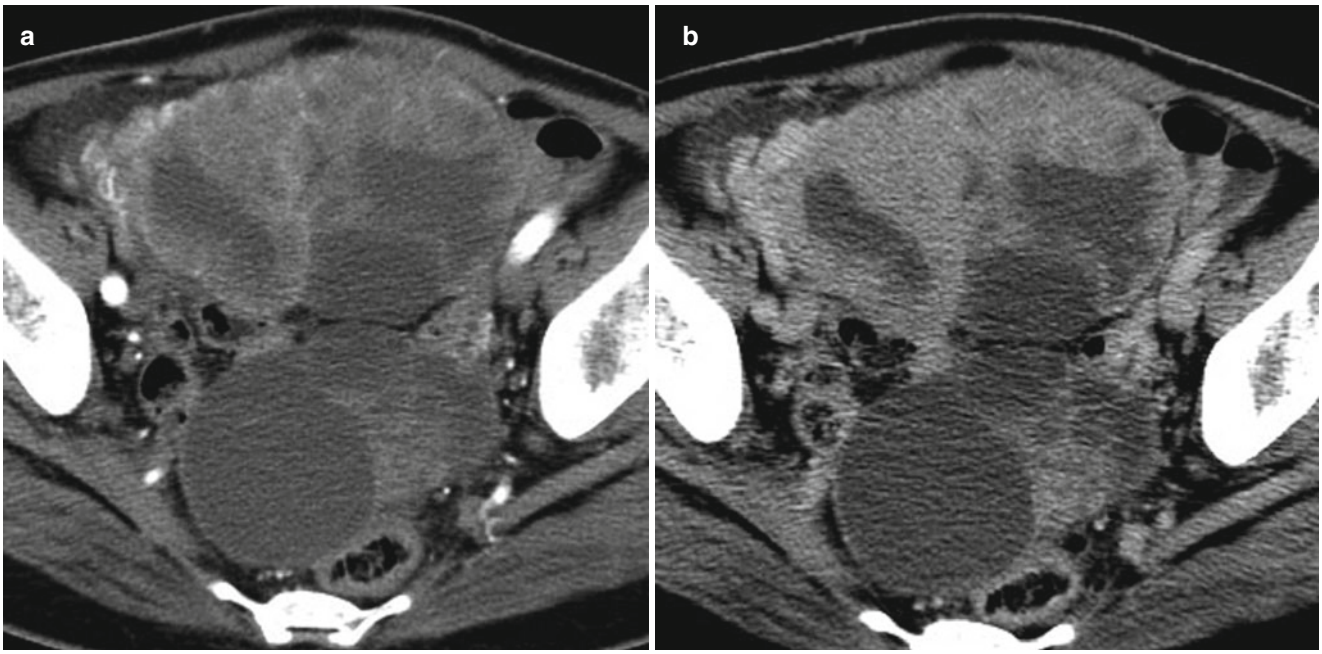

Fig. 22 (**a**) A 67-year-old woman with serous cystadenocarcinoma. Axial contrast-enhanced computed tomography (CT) of the arterial phase shows cystic and solid mass at the dorsal aspect and at the ventral aspect in the pelvic space. (**b**) Axial contrast-enhanced CT of the venous phase shows cystic and solid mass at the dorsal aspect and at the ventral aspect in the pelvic space

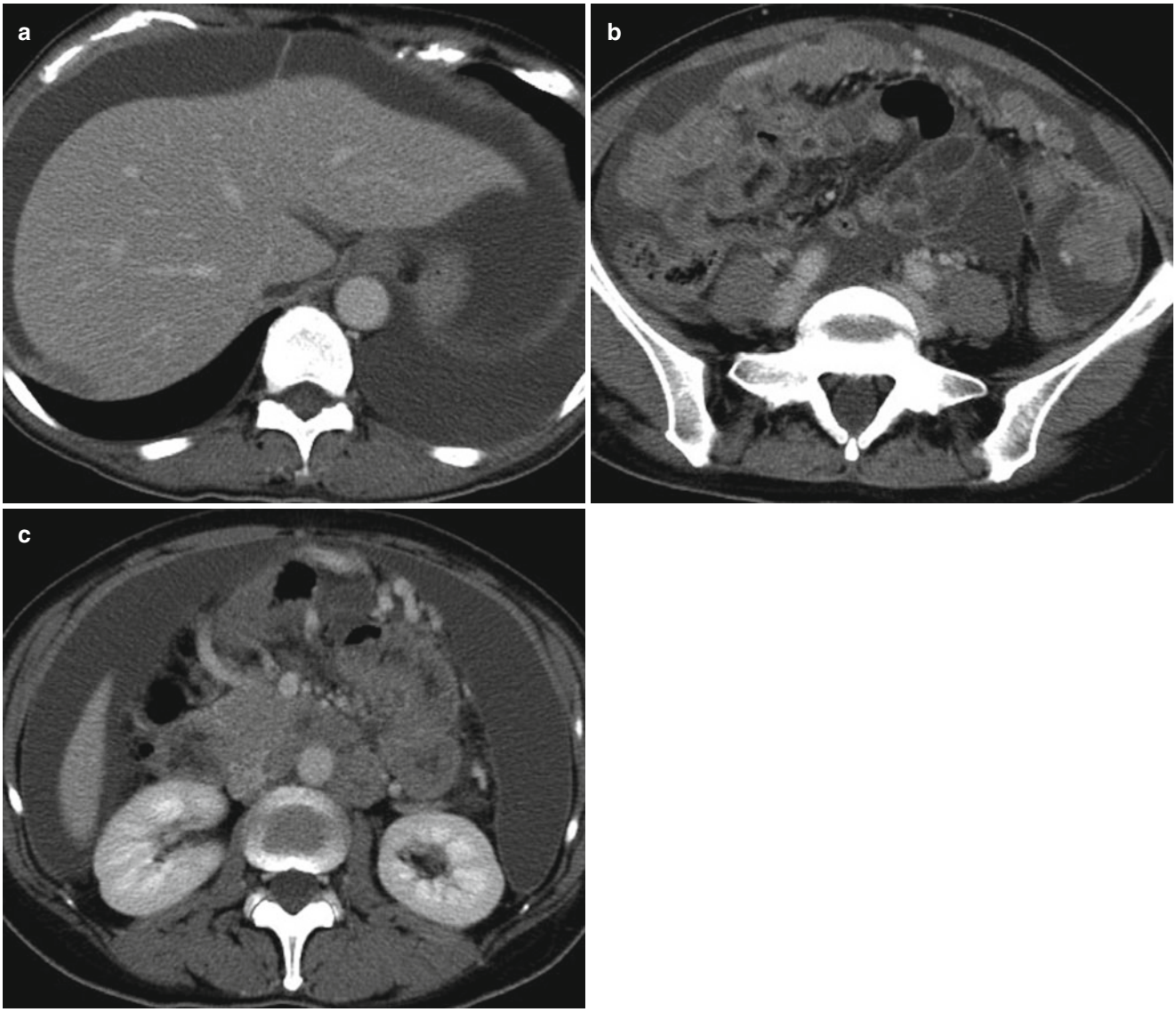

Fig. 23 (**a**) A 48-year-old woman with serous cystadenocarcinoma. Axial contrast-enhanced computed tomography (CT) shows multiple subcapsular liver implants, ascites, and left pleural effusion. (**b**) Axial contrast-enhanced CT scan shows multiple peritoneal implants in the omentum. (**c**) Axial contrast-enhanced CT scan shows enlarged lymph nodes around the abdominal aorta and ascites

Differential Diagnosis of Ovarian Serous Carcinoma

The typical MR imaging appearance of serous carcinoma is a cystic mass with solid or papillary component. However, papillary projections also occur in serous borderline tumor and serous cystadenoma, with a higher proportion in serous borderline tumors.

Differentiation of serous from mucinous carcinoma may be difficult because serous carcinoma can show various signal intensities on MR imaging and cystic mass with solid component. Because the incidence of bilateral ovarian mass, peritoneal dissemination, and papillary projections is low in mucinous carcinoma, these findings may be key to diagnosing serous carcinoma.

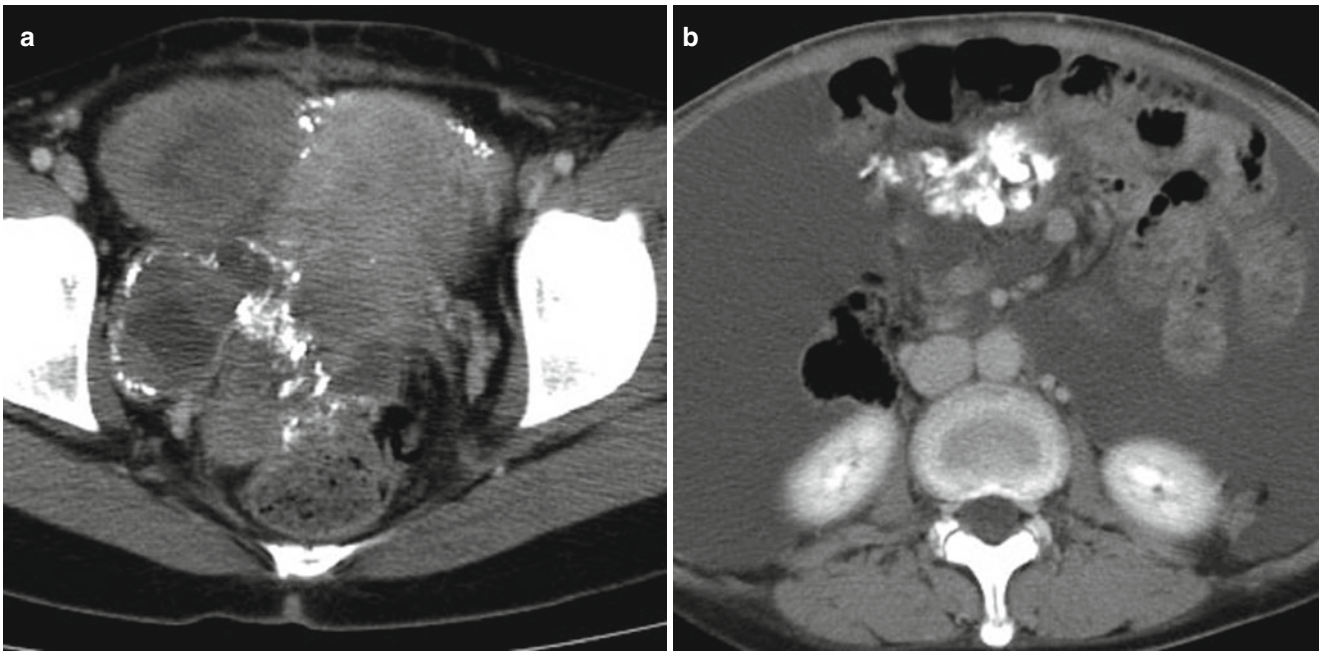

Fig. 24 (**a**) A 60-year-old woman with papillary serous adenocarcinoma. Axial contrast-enhanced computed tomographic (CT) scan shows bilateral complex solid and cystic adnexal tumors. The tumors have multiple calcifications that show that some of the calcifications demonstrate psammoma. (**b**) Axial contrast-enhanced CT scan shows large calcifications in the omentum and massive ascites

Because serous carcinoma often involves both ovaries, ovarian metastasis is one of the most important differential diagnoses. The MR imaging appearance of bilateral serous carcinoma and bilateral ovarian metastases is similar. Furthermore, gastric cancer or colon cancer metastases can show peritoneal dissemination with psammomatous calcifications. Clues to diagnosis may be knowledge of clinical information and exclusion of the existence of the primary cancer.

Focus Points

Serous carcinoma is the most probable diagnosis when a cystic mass with solid component or papillary projections is present bilaterally and shows peritoneal dissemination containing psammomatous calcifications.

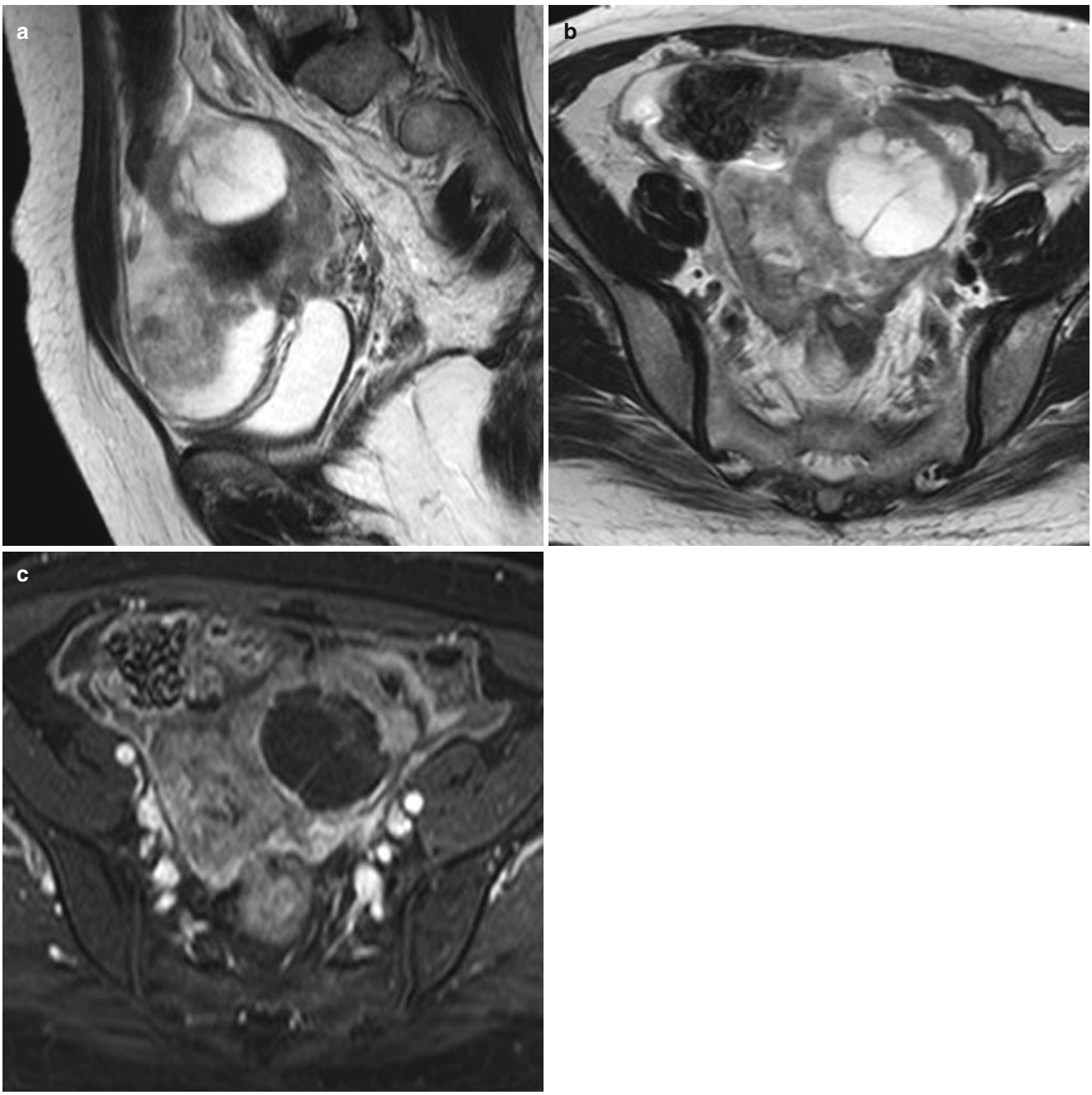

Fig. 25 (**a**) A 64-year-old woman with serous surface papillary carcinoma. Sagittal T_2-weighted image shows a relatively hypointense lobulated solid mass with cystic mass. (**b**) Axial T_2-weighted image shows a relatively hypointense lobulated solid mass with cystic mass and no internal branching. (**c**) Axial fat-saturated contrast-enhanced T_1-weighted image shows a relatively hyperintense lobulated solid mass with cystic mass

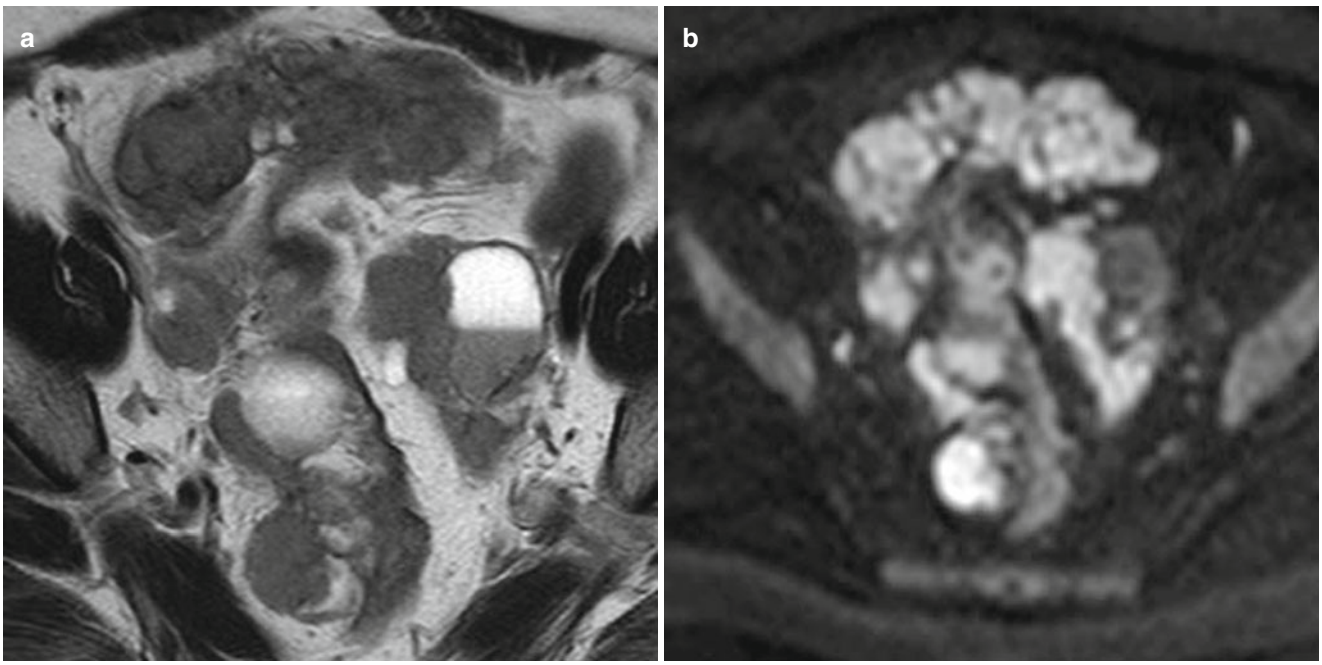

Fig. 26 (**a**) A 61-year-old woman with serous adenocarcinoma. Axial T2-weighted image demonstrates an ill-defined large mesenteric mass in the dorsal aspect. Solid and cystic mass lesions are seen in the bilateral adnexal region. (**b**) Axial diffusion-weighted image demonstrates a relatively large mesenteric mass showing high signal intensity in the dorsal aspect. Mass lesions with high signal intensity are seen in the bilateral adnexal region

References

1. Taylor Jr HC. Malignant and semi-malignant tumors of the ovary. Surg Gynecol Obstet. 1929;48:204–30.
2. The General Assembly of FIGO. International Federation of Gynecology and Obstetrics. Classification and staging of malignant tumours in the female pelvis. Acta Obstet Gynecol Scand. 1971;50:1–7.
3. Serov SF, Scully RE, Sobin LH, International Histologic Classification of Tumours. No. 9. Histological typing of ovarian tumours. Geneva: World Health Organization; 1973.
4. Lee KR, Scully RE. Mucinous tumors of the ovary: a clinicopathologic study of 196 borderline tumors (of intestinal type) and carcinomas, including an evaluation of 11 cases with 'pseudomyxoma peritonei'. Am J Surg Pathol. 2000;24:1447–64.
5. Link Jr CJ, Reed E, Sarosy G, et al. Borderline ovarian tumours. Am J Med. 1996;101:217–25.
6. Acs G. Serous and mucinous borderline (low malignant potential) tumors of the ovary. Am J Clin Pathol. 2005;123:S13–57.
7. Gotlieb WH, Chetrit A, Menczer J, et al. Demographic and genetic characteristics of patients with borderline ovarian tumors as compared to early stage invasive ovarian cancer. Gynecol Oncol. 2005;97:780–3.
8. Bent CL, Sahdev A, Rockall AG, et al. MRI appearances of borderline ovarian tumours. Clin Radiol. 2009;64:430–8.
9. Tinelli R, Tinelli A, Tinelli FG, et al. Conservative surgery for borderline ovarian tumours: a review. Gynecol Oncol. 2006;100:185–91.
10. Webb PM, Purdie DM, Grover S, et al. Symptoms and diagnosis of borderline, early and advanced epithelial ovarian cancer. Gynecol Oncol. 2004;92(1):232–9.
11. Koonings PP, Campbell K, Mishell Jr DR, et al. Relative frequency of primary ovarian neoplasms: a 10-year review. Obstet Gynecol. 1989;74:921–6.
12. Scully RE. Ovary. In: Henson DE, Albores-Saavedra J, editors. The pathology of incipient neoplasia. Philadelphia: Saunders; 1986. p. 279–93.
13. Seidman JD, Kurman RJ. Ovarian serous borderline tumors: a critical review of the literature with emphasis on prognostic indicators. Hum Pathol. 2000;31:539–57.
14. McKenney JK, Balzer BL, Longacre TA. Patterns of stromal invasion in ovarian serous tumors of low malignant potential (borderline tumors): a reevaluation of the concept of stromal microinvasion. Am J Surg Pathol. 2006;30:1209–21.
15. Fausett MB, Zahn CM, Kendall BS, et al. The significance of psammoma bodies that are found incidentally during endometrial biopsy. Am J Obstet Gynecol. 2002;186:180–3.
16. Trimble CL, Trimble EL. Management of epithelial ovarian tumors of low malignant potential. Gynecol Oncol. 1994;55:52–61.
17. Ghossain MA, Buy JN, Ligneres C, et al. Epithelial tumors of the ovary: comparison of MR and CT findings. Radiology. 1991;181:863–70.
18. Krigman H, Bentley R, Robboy SJ. Pathology of epithelial ovarian tumors. Clin Obstet Gynecol. 1994;37:475–91.
19. Geza A. Serous and mucinous borderline (low malignant potential) tumors of the ovary. Am J Clin Pathol. 2005;123:13–57.
20. Tanaka YO, Okada S, Satoh T, et al. Ovarian serous surface papillary borderline tumors form sea anemone-like masses. J Magn Reson Imaging. 2011;33(3):633–40.
21. Kim SH, Yang DM, Kim SH. Borderline serous surface papillary tumor of the ovary: MRI characteristics. AJR Am J Roentgenol. 2005;184:1898–900.
22. Reichert RA. Chapter 7: Endometrial carcinoma. In: Reichert RA, editor. Diagnostic gynecologic and obstetric pathology. Philadelphia: Lippincott Williams & Wilkins; 2012.
23. Wagner BJ, Buck JL. From the archives of the AFIP: ovarian epithelial neoplasm's: radiologic–pathologic correlation. Radiographics. 1994;14:1351–74.

24. Gner BJ, Buck JL, Seidman JD, McCabe KM. Ovarian epithelial neoplasms: radiologic-pathologic correlation. Radiographics. 1994;14:1351–74.
25. Hart WR, Norris HJ. Borderline and malignant mucinous tumors of the ovary. Histologic criteria and clinical behavior. Cancer. 1973;31:1031–45.
26. Okada S, Ohaki Y, Inoue K, et al. Calcifications in mucinous and serous cystic ovarian tumors. J Nippon Med Sch. 2005;72:29–33.
27. Okamoto Y, Tanaka YO, Tsunoda H. Malignant or borderline mucinous cystic neoplasms have a larger number of loculi than mucinous cystadenoma: a retrospective study with MR. J Magn Reson Imaging. 2007;26:94–9.
28. Tanaka YO, Yoshizako T, Nishida M, et al. Ovarian carcinoma in patients with endometriosis: MR imaging findings. AJR Am J Roentgenol. 2000;175:1423–30.
29. Takeuchi M, Matsuzaki K, Harada M. Preliminary observations and clinical value of N-acetyl resonances in ovarian tumours using in-vivo proton MR spectroscopy at 3T. Eur Radiol. 2011;21: 2640–6.
30. Rutgers JL, Scully RE. Ovarian müllerian mucinous papillary cystadenomas of borderline malignancy. A clinicopathologic analysis. Cancer. 1988;61:340–8.
31. Kataoka M, Togashi K, Koyama T, et al. MR imaging of müllerian mucinous borderline tumors arising from endometriotic cysts. J Comput Assist Tomogr. 2002;26:532–7.
32. Lalwani N, Shanbhogue AK, Vikram R, et al. Current update on borderline ovarian neoplasms. AJR Am J Roentgenol. 2010;194: 330–6.
33. Thomassin-Naggara I, Bazot M, Daraï E, et al. Epithelial ovarian tumors: value of dynamic contrast-enhanced MR imaging and correlation with tumor angiogenesis. Radiology. 2008;248:148–59.
34. Seidman JD, Cho KR. Chapter 14: Surface epithelial tumors of the ovary. In: Kurman RJ, Ellenson LH, Ronnnet BM, editors. Blaustein's pathology of the female genital tract. 6th ed. New York: Springer; 2011.
35. Kim KA, Park CM, Lee JH, et al. Benign ovarian tumors with solid and cystic components that mimic malignancy. AJR Am J Roentgenol. 2004;182:1259–65.
36. Compton HL, Finck FM. Serous adenofibroma and cystadenofibroma of the ovary. Obstet Gynecol. 1970;36:636–45.
37. Outwater EK, Siegelman ES, Talerman A, et al. Ovarian fibromas and cystadenofibromas: MRI features of the fibrous component. J Magn Reson Imaging. 1997;7:465–71.
38. Takeuchi M, Matsuzaki K, Kusaka M, et al. Ovarian cystadenofibromas: characteristic magnetic resonance findings with pathologic correlation. J Comput Assist Tomogr. 2003;27:871–3.
39. Cho SM, Byun JY, Rha SE, et al. CT and MRI findings of cystadenofibromas of the ovary. Eur Radiol. 2004;14:798–804.
40. Kawamoto S, Urban BA, Fishman EK. CT of epithelial ovarian tumors. Radiographics. 1999;19:85–102.
41. Jung SE, Lee JM, Rha SE, et al. CT and MR imaging of ovarian tumors with emphasis on differential diagnosis. Radiographics. 2002;22:1305–25.
42. Mitchell DG, Hill MC, Hill S, Zaloudek C. Serous carcinoma of the ovary: CT identification of metastatic calcified implants. Radiology. 1986;158:649–52.

Malignant Ovarian Tumors (Serous/Mucinous/Endometrioid/Clear Cell Carcinoma): Clinical Setting and Ultrasound Appearance

Juan Luis Alcázar and Jesús Utrilla-Layna

Abstract

Epithelial ovarian cancer remains as the most deadly gynecological malignancy and it is the seventh leading cause of cancer in women in developed countries. Worldwide more than 200,000 new cases are diagnosed annually, resulting in more than 140,000 deaths. Histologically, ovarian malignancies are classified in two broad groups: epithelial and non-epithelial ovarian cancer. Epithelial ovarian cancers are subclassified based on hystotype, with serous, endometrioid, clear cell, and mucinous carcinomas accounting for 96 % of all cases. In this chapter we shall review the origin, clinical setting, and ultrasound appearance of serous, endometrioid, and mucinous carcinomas.

Keywords

Serous carcinoma • Mucinous carcinoma • Endometrioid carcinoma • Clear cell • Imaging • Ultrasound

Introduction

Epithelial ovarian cancer remains as the most deadly gynecological malignancy and it is the seventh leading cause of cancer in women in developed countries. Worldwide more than 200,000 new cases are diagnosed annually, resulting in more than 140,000 deaths [1].

Histologically, ovarian malignancies are classified in two broad groups: epithelial and non-epithelial ovarian cancer [2]. Epithelial ovarian cancers account more than 90 % of all ovarian malignancies [2].

J.L. Alcázar, MD, PhD (✉)
Department of Obstetrics and Gynecology,
Clínica Universidad de Navarra, University of Navarra,
Avenida Pio XII, 36, 31008 Pamplona, Spain
e-mail: jlalcazar@unav.es

J. Utrilla-Layna, MD
Department of Obstetrics and Gynecology,
Clínica Universidad de Navarra, Pamplona, Spain

Epithelial ovarian cancers are subclassified based on hystotype, with serous, endometrioid, clear cell, and mucinous carcinomas accounting for 96 % of all cases [3].

In this chapter we shall review the origin, clinical setting, and ultrasound appearance of serous, endometrioid, and mucinous carcinomas.

Origin of Epithelial Ovarian Cancer

Currently, recent morphologic, immunohistochemical, and molecular genetic studies have led to a new theory for the pathogenesis and origin of epithelial ovarian cancer (EOC): the dualistic model of EOC carcinogenesis [4].

According to this model, EOCs are divided into two categories: type I and type II.

EOC type I include low-grade serous, low-grade endometrioid, clear cell, and mucinous carcinomas, as well as transitional cell cancers. These tumors are usually indolent and slow-growing tumors. Generally they are diagnosed at early stage and they are characterized by some specific mutations. They account about 25 % of ECOs.

L. Saba et al. (eds.), *Ovarian Neoplasm Imaging*,
DOI 10.1007/978-1-4614-8633-6_14, © Springer Science+Business Media New York 2013

Table 1 Genetic alterations in EOC

HGSC	p53 (95 %), BRCA (50 %)
LGSC	KRAS (70 %), BRAF (68 %), HER-2 (9 %)
Clear cell	ARID1 A (50 %), PIK 3CA (50 %), PTEN (20 %)
Endometrioid	ARID1 A (36 %), PTEN (20 %), CTNNBI (38–50 %)
Mucinous	KRAS (75–85 %), HER-2 (15–20 %)

Type II EOCs compromise high-grade serous, high-grade endometrioid carcinosarcomas and undifferentiated carcinomas. Generally, these tumors are aggressive, present in advanced stage, and harbor different mutations than EOC type I. They account about 75 % of ECOs.

Serous Ovarian Cancer

Ovarian serous carcinoma is the most frequent EOC (60 % of all cases). As stated above serous EOCs are divided into low-grade (LGSC) and high-grade (HGSC) carcinomas.

About 10 % of serous EOCs are diagnosed at stage I, 8 % at stage II, 55 % at stage III, and 27 % at stage IV [5].

HGSCs constitute 90 % of all serous EOCs, whereas LGSCs account for 10 % of serous EOCs.

Current evidence suggests that HGSC actually arise from the epithelium from the fimbriated end of the fallopian tube [4]. These lesions implant on the ovary surface resembling a primary ovarian origin at gross examination. HGSC are characterized by p53 mutations (more than 95 % of the cases) and BRCA1 and BRCA2 mutations (about 80 % of the cases) (Table 1).

Most BRCA-related ovarian cancers (60–100 %) are HGSCs. Mutations of BRCA1 and BRCA 2 are found in 40–50 % of sporadic HGSCs.

They are genetically unstable. These features confer a high aggressiveness and high cellular proliferation.

In contrast to HGSC, LGSC EOCs rarely contain p53 mutations but they are characterized by KRAS, BRAF, and HER-2 mutations (Table 1) and they are much more genetically stable. There is evidence that LGSC EOCs develop in a stepwise fashion from a benign epithelium from ovarian or tubal origin to borderline tumor, ending in an invasive cancer [4].

Endometrioid and Clear Cell Carcinomas

Endometrioid and clear cell carcinomas constitute about 15–20 % of all EOCs.

The most frequent genetic mutations of these EOCs are shown in Table 1.

Endometrioid carcinomas are also subclassified into low-grade endometrioid carcinoma (LGEC) and high-grade endometrioid carcinoma (HGEC); morphologic studies and more recently molecular studies have shown that both, endometrioid and clear cell carcinomas, arise from endometriosis [4].

Mucinous Carcinomas

Mucinous carcinomas account for less than 5 % of all EOCs.

The most frequent mutations are KRAS and HER-2 (Table 1).

Current evidence support that these cancers develop also in a stepwise fashion from a benign epithelium to a borderline lesion, leading to an invasive carcinoma [4].

The origin of mucinous carcinomas is rather intriguing, because unlike serous, endometrioid, and clear cell carcinomas, they do not show a müllerian phenotype. It seems that mucinous tumors could have the same histogenesis than transitional cell tumors, arising from microscopic transitional cell nets at the tuboperitoneal junction [4].

Histologically, there are two variants: intestinal type and endocervical type, the former being the most frequent one.

Clinical Setting

Current knowledge about EOC carcinogenesis and pathogenesis highlights the heterogeneity of this disease.

From the clinical point of view, there are some differences in clinical presentation of EOC depending on the hystotype.

High-Grade Serous Carcinomas

Mean patient age at diagnosis is 55.5 years old, or even earlier in BRCA-related carcinomas [6].

Up to 85 % of these patients present intra-abdominal spread of the disease at diagnosis. Extra-abdominal disease at presentation, such as liver, lung, or brain metastases, is not common at diagnosis (2–3 %). For this reason symptoms related to intra-abdominal spread such as abdominal swelling, bloating, constipation, or dyspepsia are common in these women.

Some studies have shown that the most of these women referred symptoms suggestive for EOC several months before diagnosis [7]. Thus, paying attention to those symptoms could lead to an earlier diagnosis or the so-called minimal volume disease diagnosis [8].

Low-Grade Serous Carcinomas

Mean patient age at diagnosis is 62.6 year old, being younger (40 year) in borderline serous tumors [6].

Most of these tumors present at early stage although a small proportion could present with intraperitoneal or visceral metastases.

These tumors generally are slow growing and do have an indolent course, so a significant proportion of women are asymptomatic at diagnosis.

Endometrioid Carcinomas

These tumors usually appear in the fifth and sixth decades of life [6].

Association with endometriosis is frequent and past history of complaints related to endometriosis such as pelvic pain and infertility is common.

About 30 % of these tumors are diagnosed at stage I.

Clear Cell Carcinomas

Patient's mean age at presentation is 57 years old [6]. Association with endometriosis is also common.

These tumors generally manifest as large unilateral adnexal masses with nonspecific symptoms.

About 50 % of these carcinomas are diagnosed at stage I.

Mucinous Carcinomas

Mucinous carcinomas are usually diagnosed during the fourth to fifth decades of life. Only 20 % are invasive carcinomas whereas 80 % are borderline tumors at diagnosis.

Most of the tumors present as large unilateral adnexal masses.

About 80 % of mucinous carcinomas are diagnosed at stage I.

Ultrasound Features of Epithelial Ovarian Cancer

In spite of the significant amount of published studies addressing the role of ultrasound for predicting ovarian malignancy in adnexal or pelvic tumors, there is a paucity of studies describing the specific features of epithelial ovarian cancers [9–14].

Ultrasound in High-Grade Serous Cancer

It could be considered that the "typical" sonographic features of HGSC are the presence of cystic–solid or solid irregular adnexal masses [6] (Figs. 1 and 2). Bilaterally it is frequently found out (60–84 %).

The content of the cystic portion generally is anechoic.

The presence of ascites (Fig. 3) and abdominal metastases is also a common finding in most of the cases (Figs. 4 and 5).

Color or power Doppler ultrasound generally shows moderation or abundance within solid components (Figs. 6 and 7).

Septations may be present (Fig. 8). The size of the lesion may vary significantly but is not rarely found out as small adnexal lesions (Fig. 9).

Ultrasound in Low-Grade Serous Cancer

Low-grade serous cancers appear as large cystic adnexal masses with septation and solid components (Figs. 10 and 11). The cyst's content also is anechoic in most cases.

Bilaterally it is found in 60–75 % of cases, and abdominal carcinomatosis and ascites can also be found out in advanced-stage cases.

Small lesions and solid lesions are not common in this type of EOC.

With color or power Doppler ultrasound, the tumor generally exhibits a moderate or abundant amount of flow.

In cases of borderline tumor, the mass typically appears as a cystic mass with large vascularized papillary projections (Figs. 12 and 13).

Ultrasound in Endometrioid and Clear Cell Carcinomas

Endometrioid and clear cell ovarian cancers usually appear as unilateral (65–72 % of cases) cystic masses with solid components (Figs. 14 and 15). Cyst's content generally is low level – resembling that of endometriotic cysts (Fig. 16) – and tumor size may vary. Septations are a frequent finding.

Like serous carcinomas, color or power Doppler examination will show a significant amount of blood flow within the tumor (Fig. 17).

Mucinous Carcinomas

Mucinous carcinoma usually appears as significantly large (>10 cm) unilateral adnexal masses. Their typical finding is the multilocularity (>10 locules) (Fig. 18). Solid components may be present (Fig. 19) or not.

Content of the cystic area may be different from one locule to another (Fig. 20) and blood flow is usually seen within septations (Fig. 21).

Since most of these tumors are early-stage cancers, ascites or carcinomatosis is not a frequent finding.

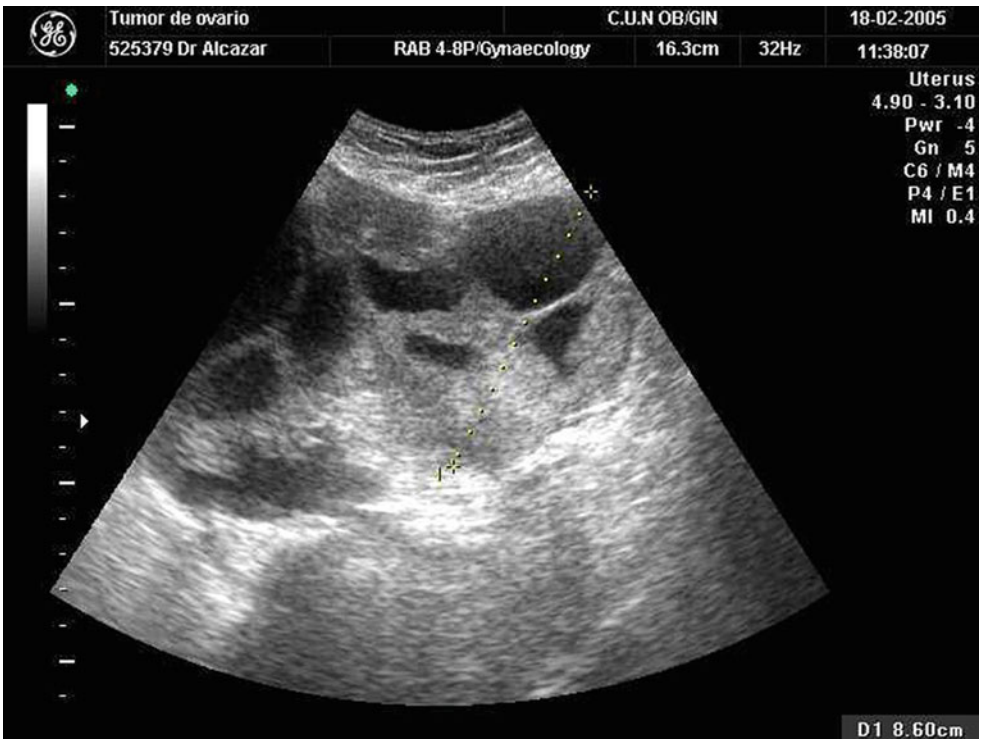

Fig. 1 Transvaginal sonogram of an HGSC showed as a large irregular cystic–solid adnexal mass

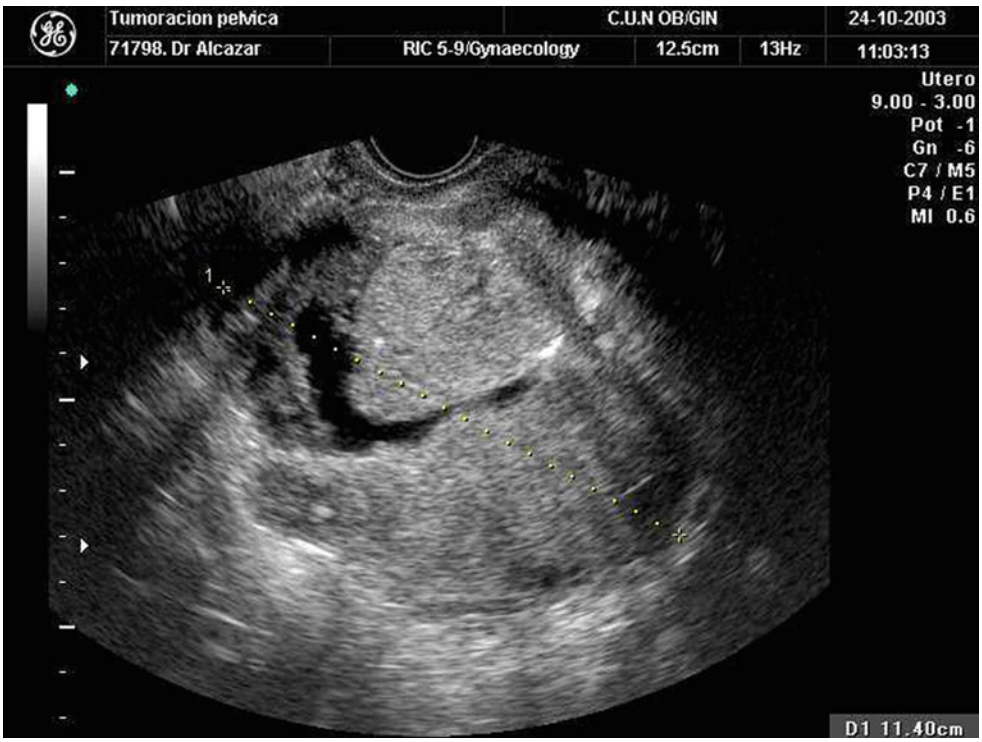

Fig. 2 Transvaginal sonogram of an HGSC showed as an irregular solid adnexal mass

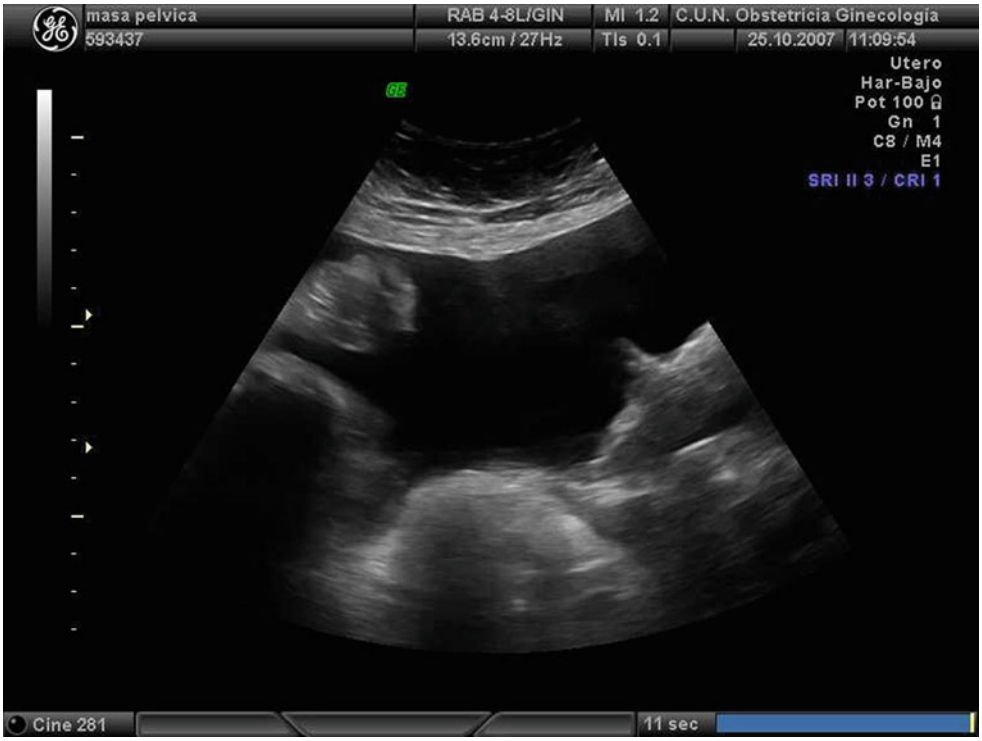

Fig. 3 Transabdominal ultrasound showing a significant amount of ascites in a patient with stage IIIc high-grade ovarian serous ovarian cancer

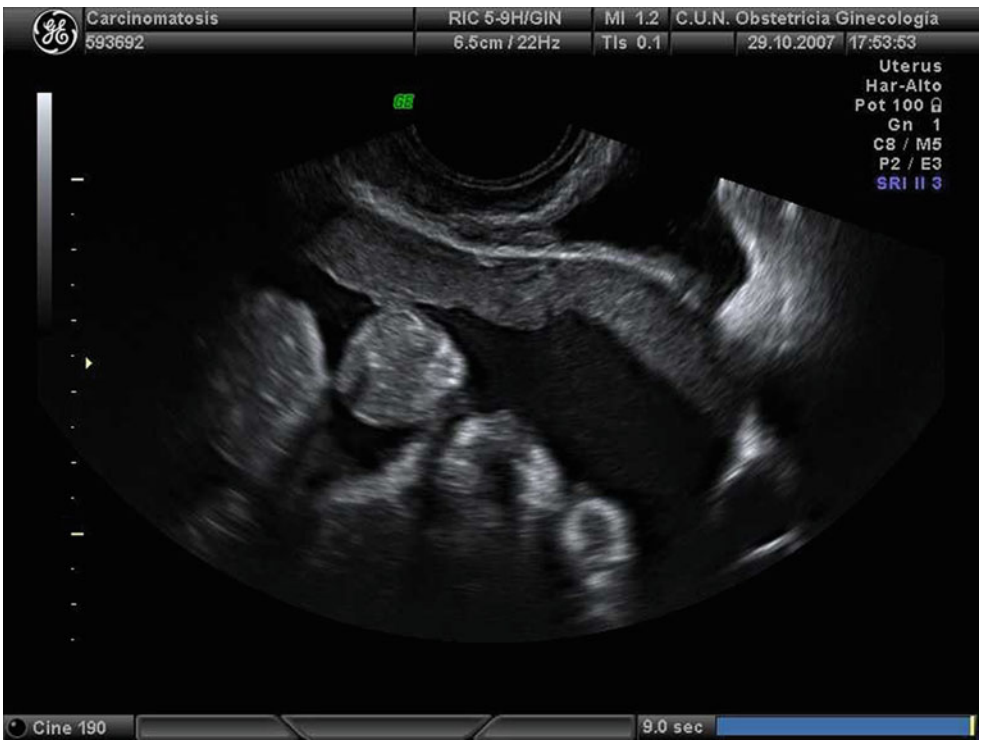

Fig. 4 Transvaginal ultrasound showing carcinomatosis involving the peritoneum of the bladder

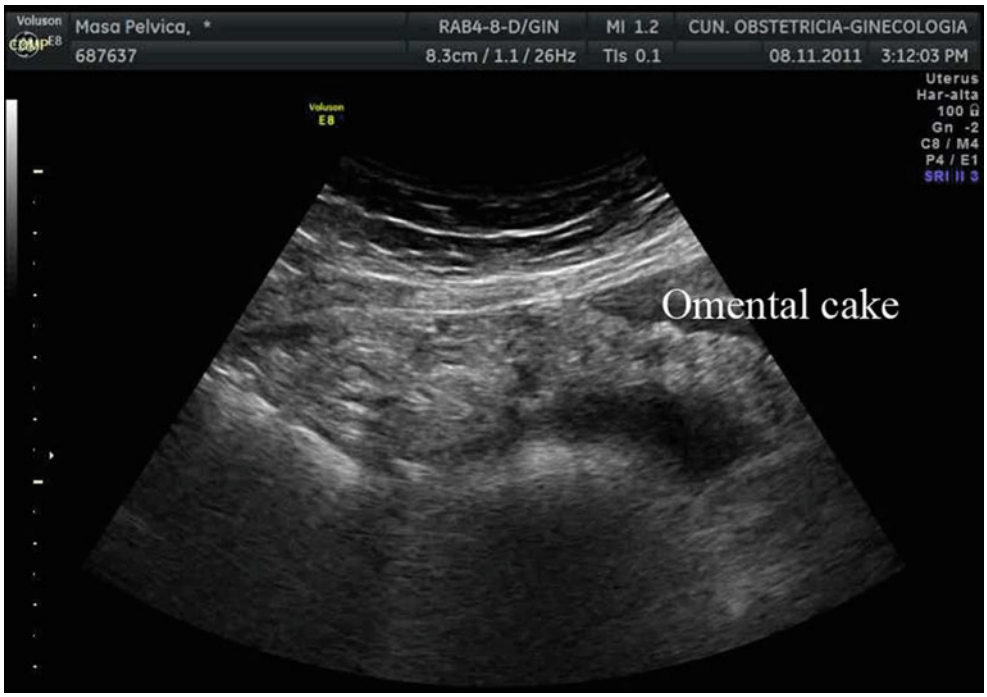

Fig. 5 Transabdominal ultrasound showing omentum involvement in a woman with intra-abdominal spread for ovarian cancer

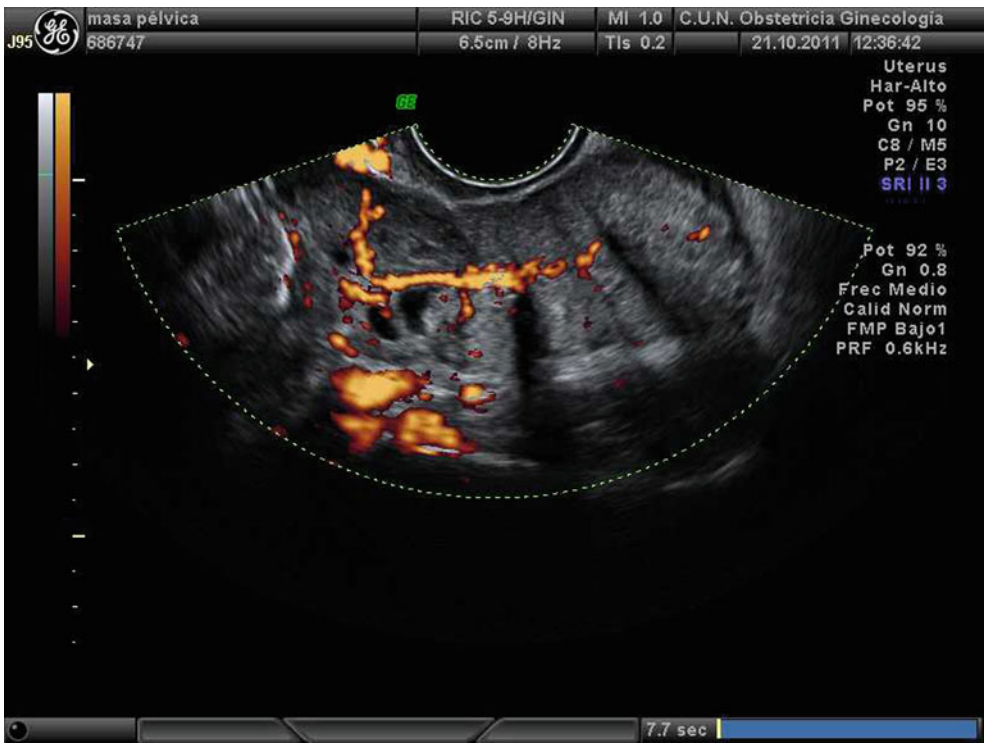

Fig. 6 Transvaginal ultrasound showing an irregular solid mass with abundant vascularization

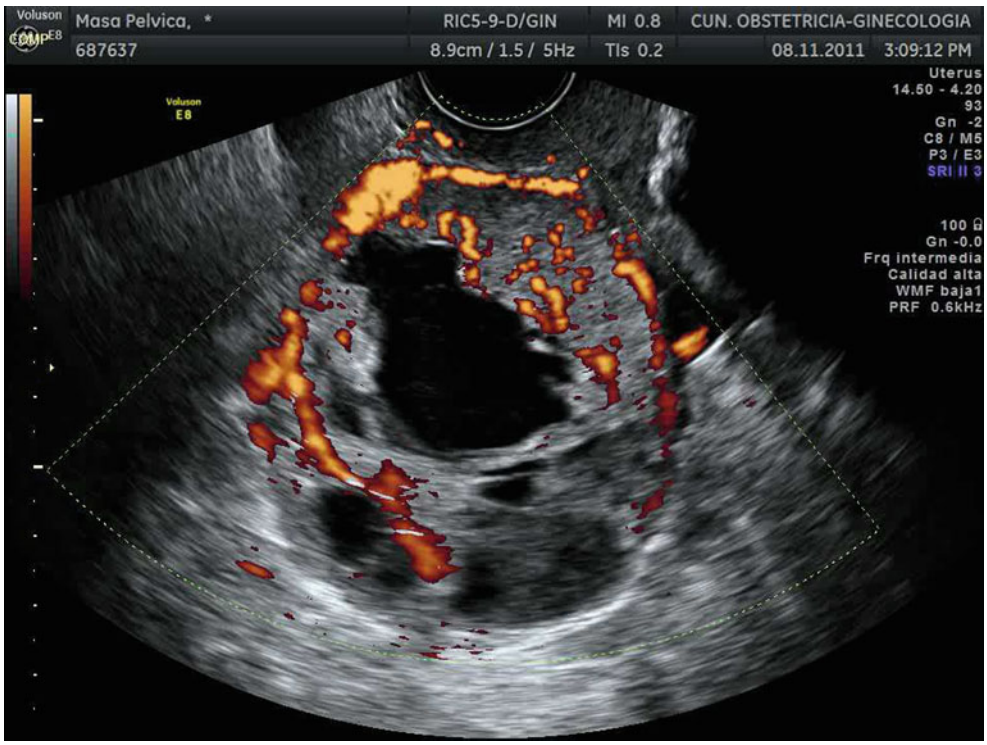

Fig. 7 Transvaginal ultrasound showing a cystic–solid mass with abundant vascularization within the solid portions of the tumor

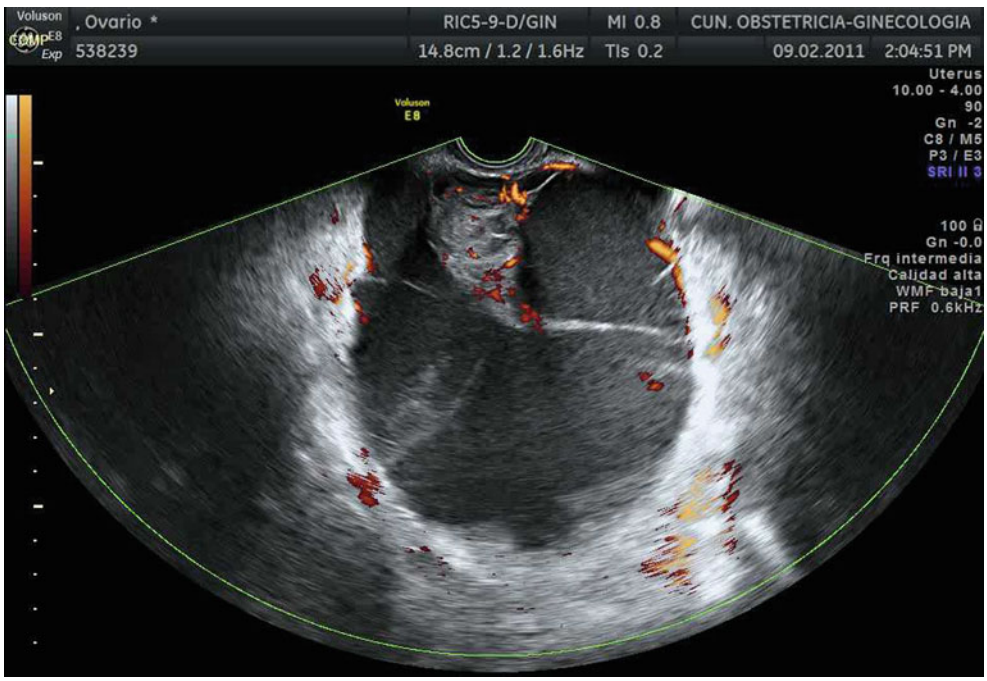

Fig. 8 Transvaginal ultrasound showing a predominantly cystic mass with a solid area and septations. Histology revealed an HGSC stage II

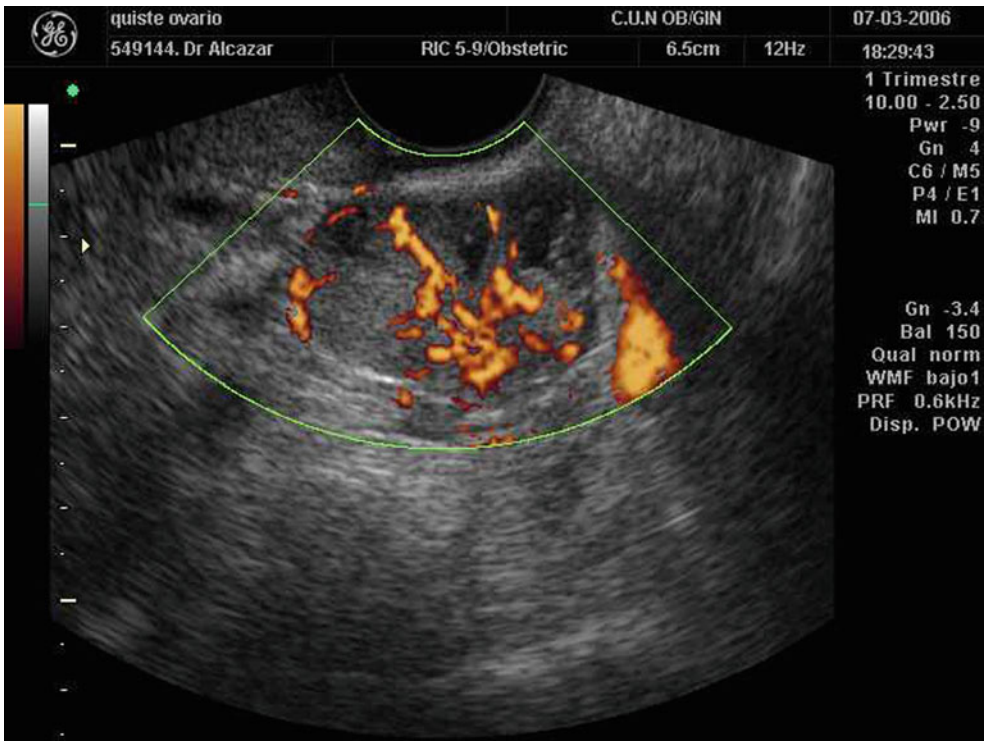

Fig. 9 Transvaginal ultrasound showing a small, highly vascularized, solid mass that corresponded to HGSC stage III

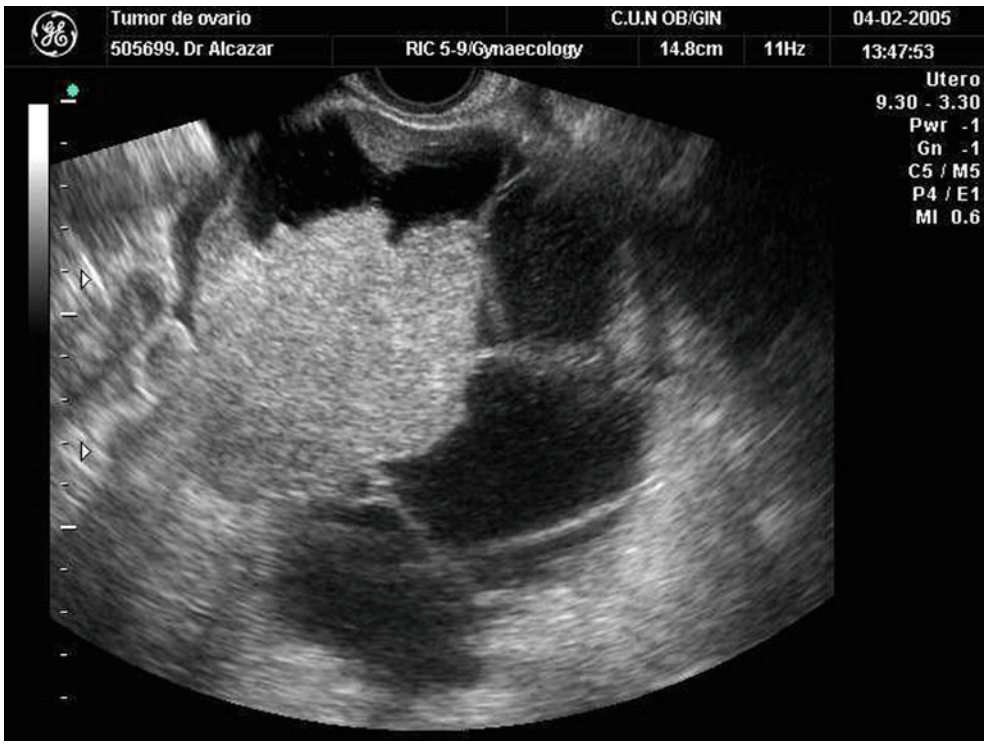

Fig. 10 Transvaginal ultrasound showing a multilocular cystic–solid mass. Histology confirmed an LGSC stage II

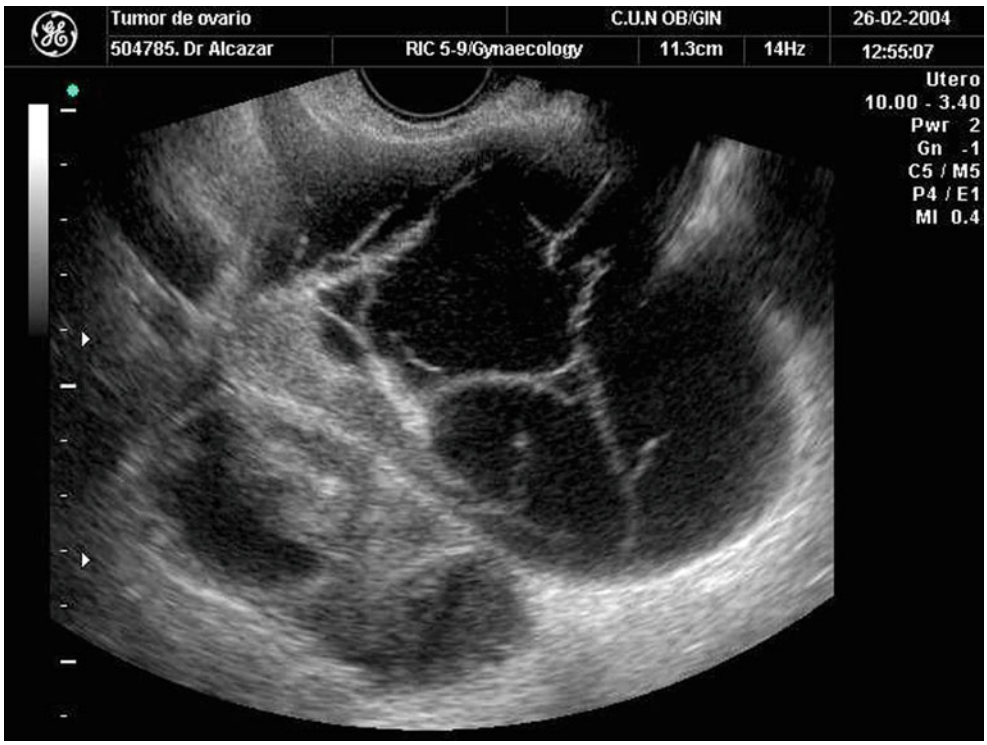

Fig. 11 Transvaginal ultrasound showing a multilocular solid mass. Histology revealed an LGSC, stage III

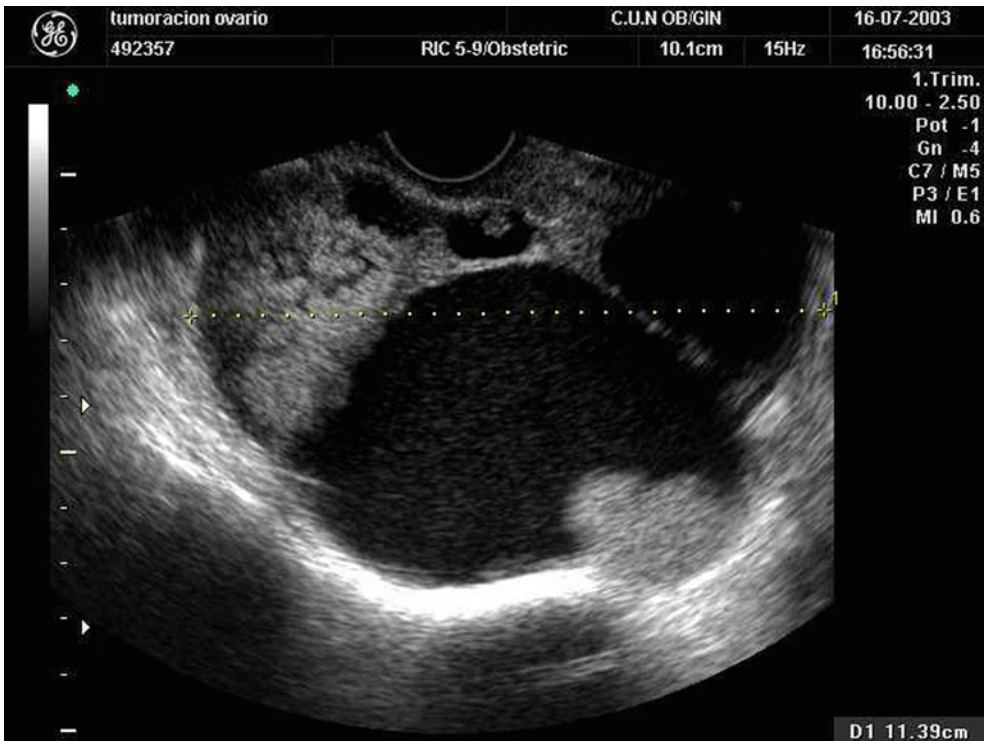

Fig. 12 Transvaginal ultrasound showing a regular cystic mass with solid components and septations. Histology confirmed a stage I borderline serous tumor

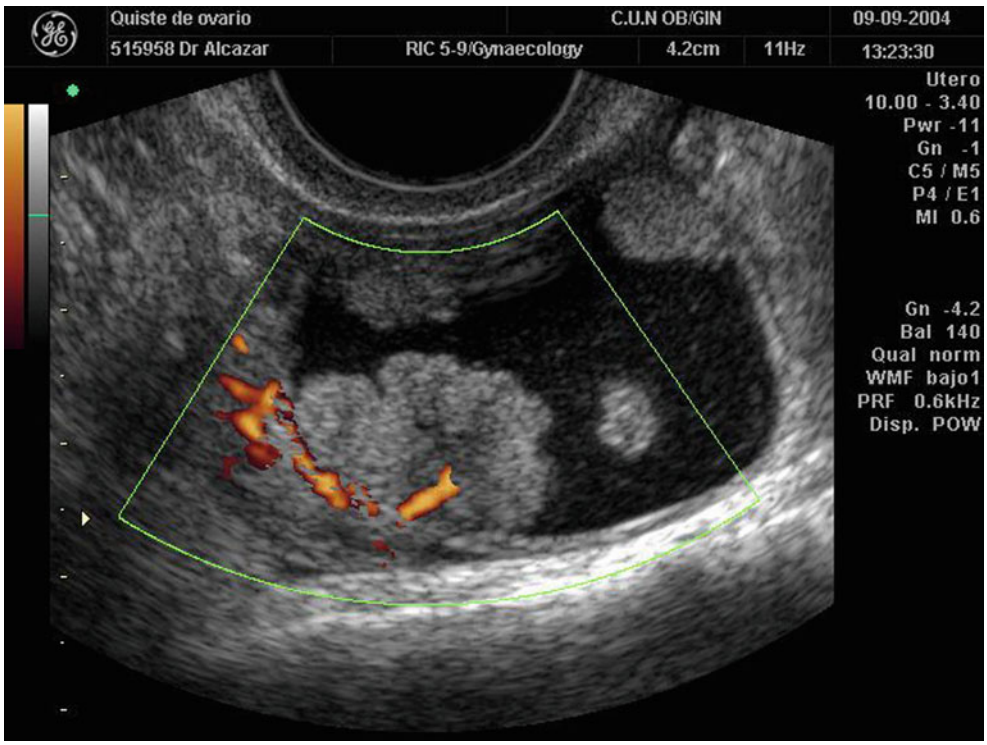

Fig. 13 Transvaginal ultrasound showing a regular cystic mass with thick papillary projections from a borderline serous tumor

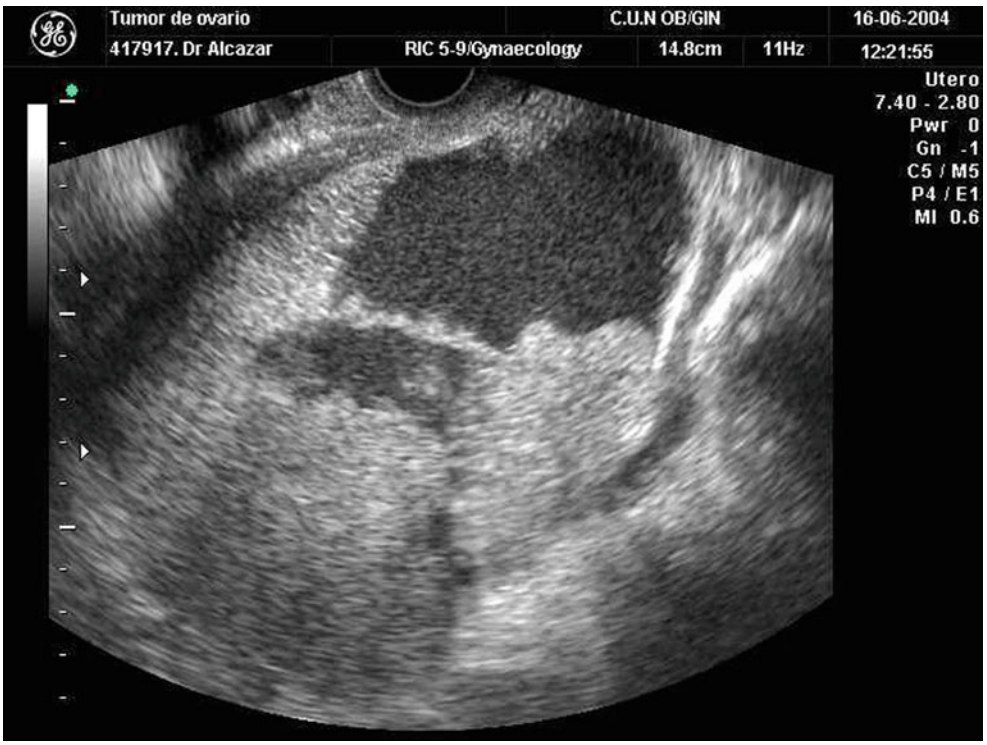

Fig. 14 Transvaginal ultrasound showing an irregular cystic–solid mass that corresponds to a clear cell ovarian carcinoma

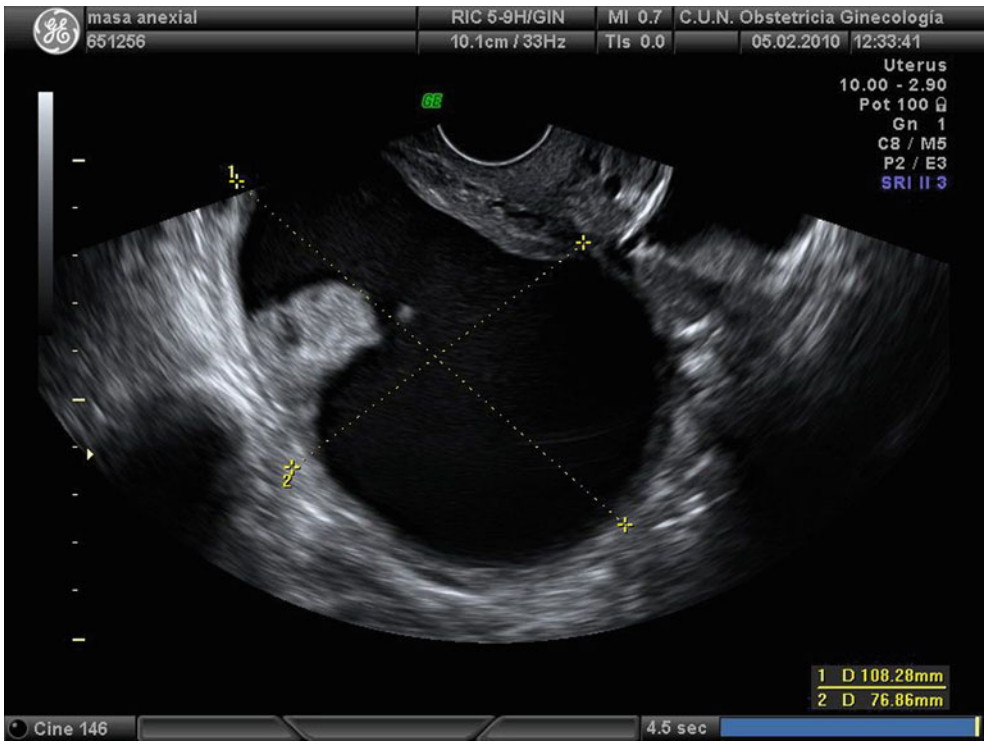

Fig. 15 Another cystic mass with a thick papillary projection. It corresponded to a stage I endometrioid carcinoma

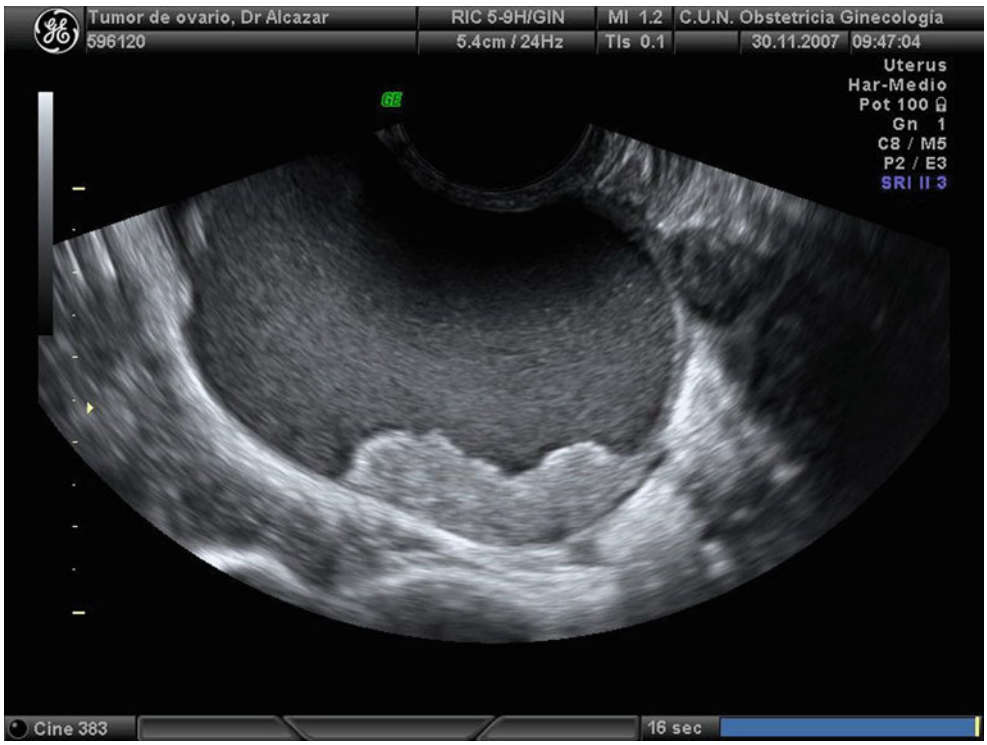

Fig. 16 Unilocular cystic mass with a focal wall irregularity. Cyst's content is homogeneous low level. Histology revealed a stage I endometrioid carcinoma

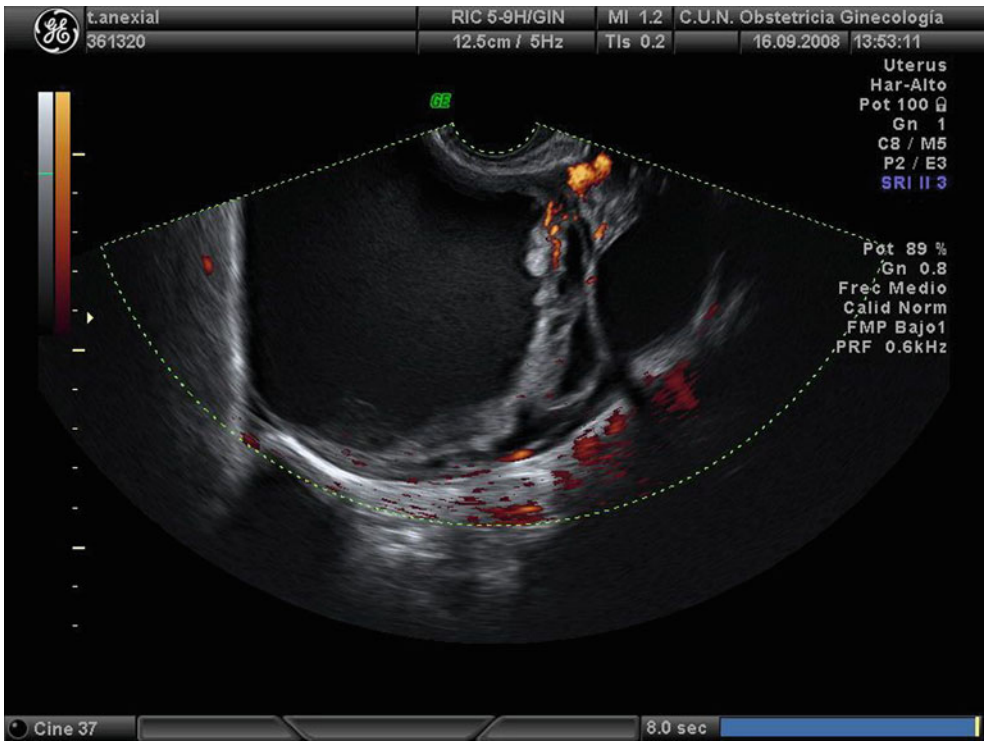

Fig. 17 Transvaginal ultrasound from an endometrioid ovarian carcinoma showing moderate vascularization at power Doppler examination

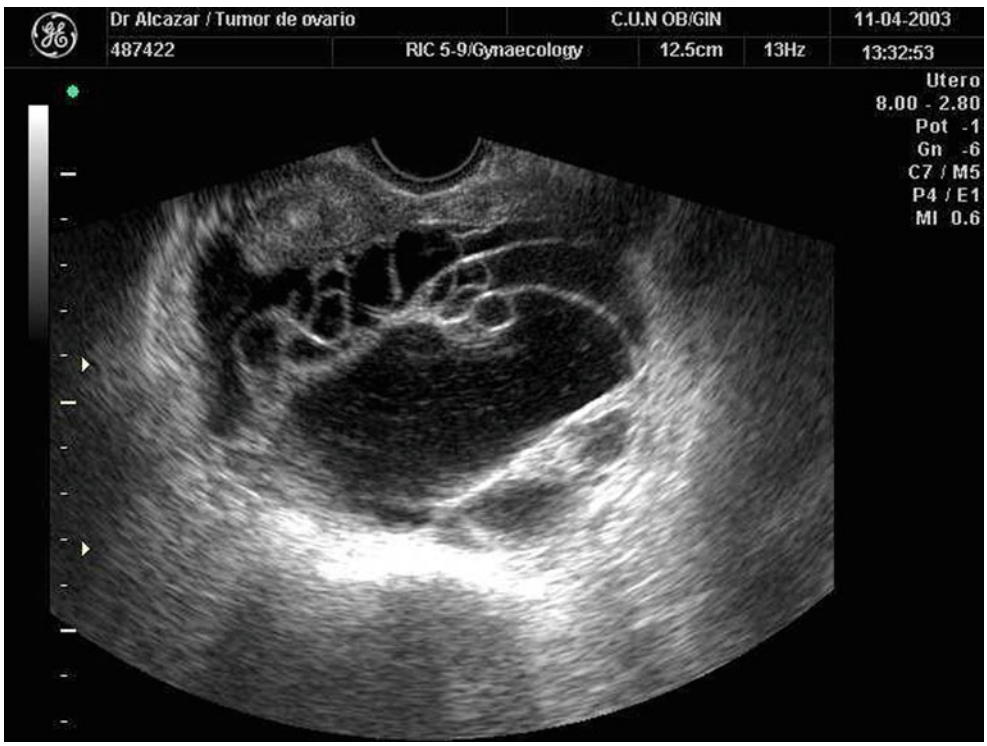

Fig. 18 Multilocular cystic mass with more than 10 locules, characteristic for mucinous carcinoma

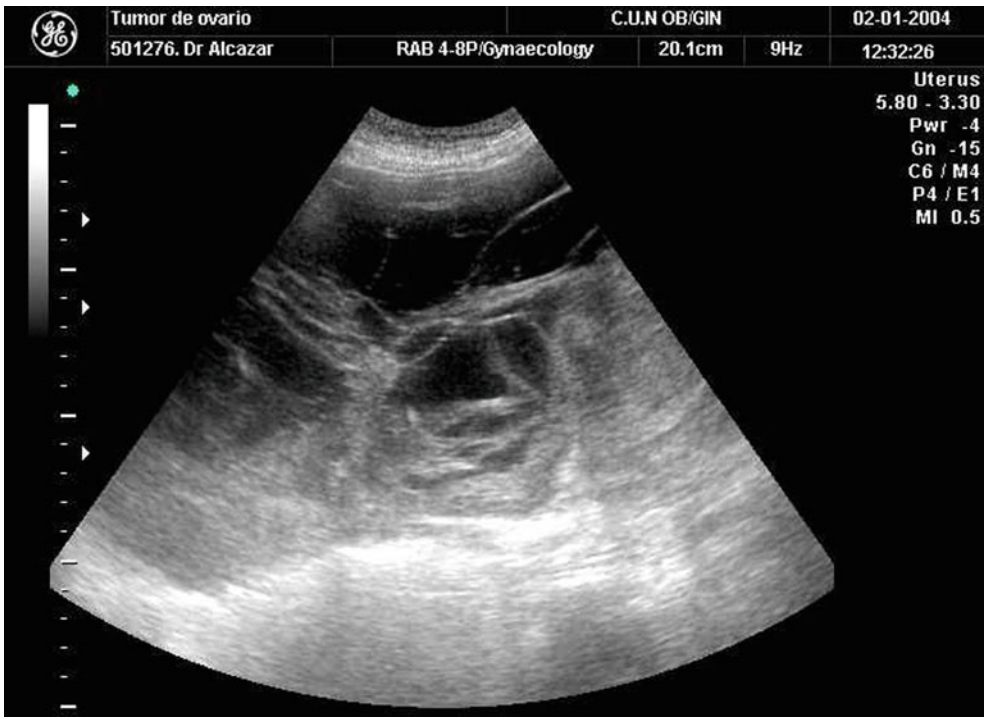

Fig. 19 Similar image than previous figure corresponding to a mucinous carcinoma. In this case solid components are present

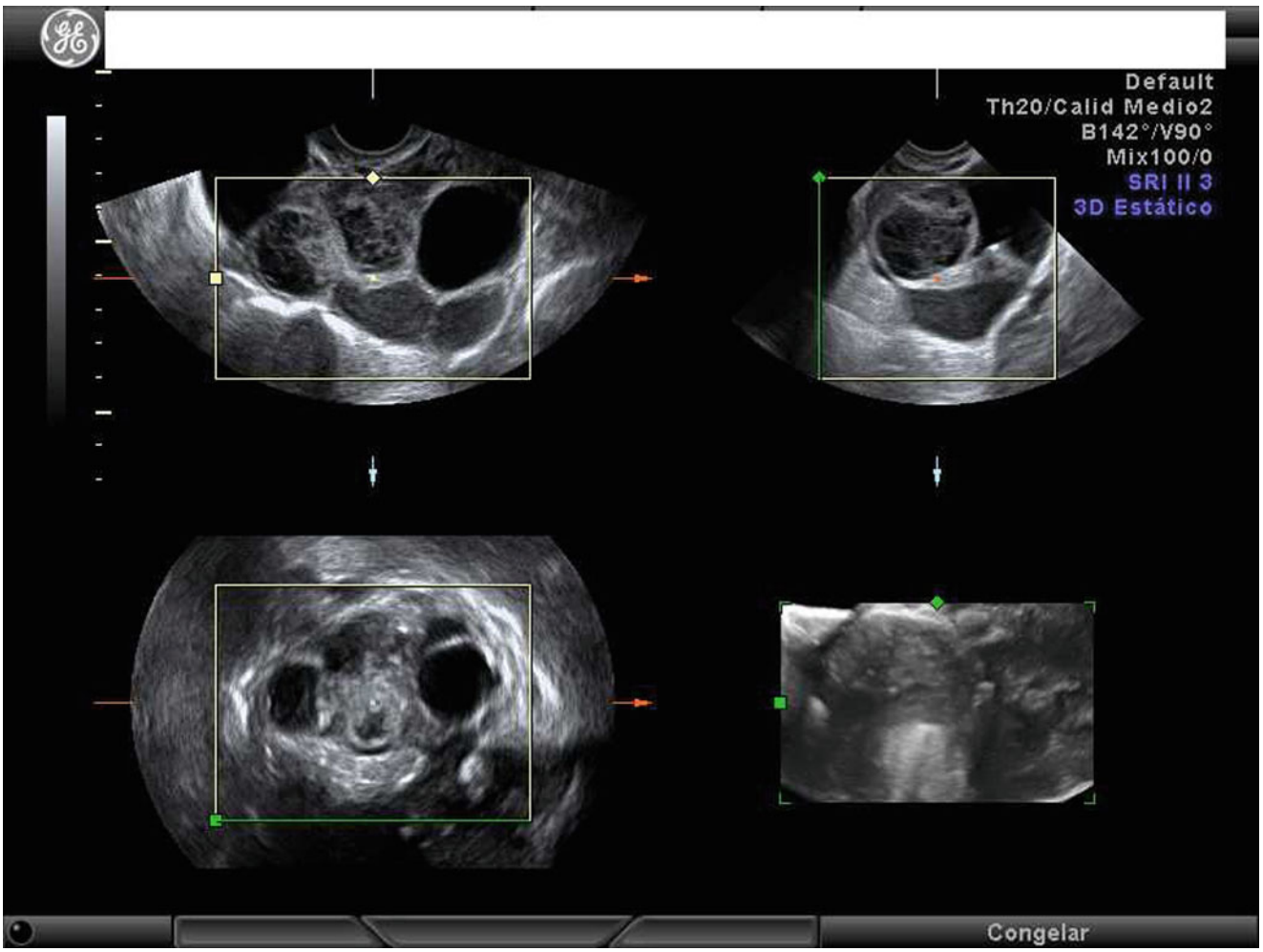

Fig. 20 Three-dimensional ultrasound from a mucinous carcinoma showing a multilocular mass. Note different content is different locules

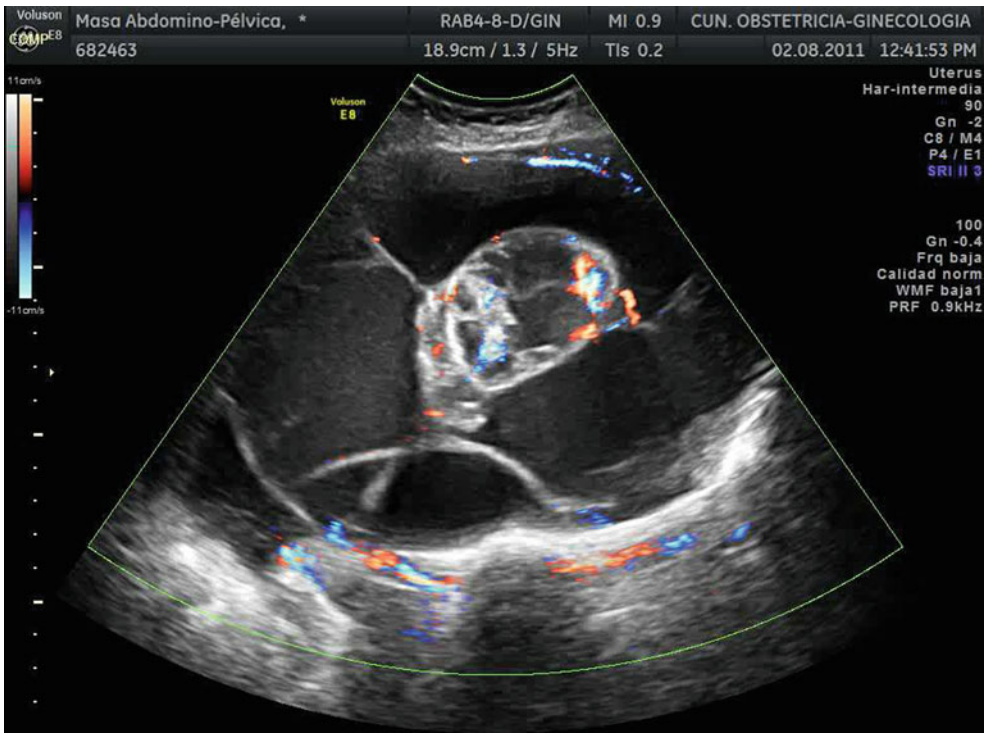

Fig. 21 Multilocular cystic mass with more than 10 locules, characteristic for mucinous carcinoma. Note blood flow within septations

References

1. Jemal A, Bray F, Center MM, Ferlay J, Ward E, Forman D. Global cancer statistics. CA Cancer J Clin. 2011;61:69–90.
2. Chen VW, Ruiz B, Killeen JL, Coté TR, Wu XC, Correa CN. Pathology and classification of ovarian tumors. Cancer. 2003;97:2631–42.
3. Chan A, Gilks B, Kwon J, Tinker AV. New insights into the pathogenesis of ovarian carcinoma: time to rethink ovarian cancer screening. Obstet Gynecol. 2012;120:935–40.
4. Kurman RJ. Molecular pathogenesis and extraovarian origin of epithelial ovarian cancer – shifting the paradigm. Human Pathol. 2011;42:918–31.
5. Plaxe SC. Epidemiology of low-grade serous ovarian cancer. Am J Obstet Gynecol. 2008;198:459.e1–8.
6. Lalwani N, Prasad SR, Vikram R, Shanbhogue AK, Huettner PC, Fasih N. Histologic, molecular, and cytogenetic features of ovarian cancers: implications for diagnosis and treatment. Radiographics. 2011;31:625–46.
7. Golf B. Symptoms associated with ovarian cancer. Clin Obstet Gynecol. 2012;55:36–42.
8. Kurman RJ, Visvanathan K, Roden R, Wu TC, Shih IM. Early detection and treatment of ovarian cancer: shifting from early stage to minimal volume of disease based on a new model of carcinogenesis. Am J Obstet Gynecol. 2008;198:351–6.
9. Brown DL, Zou KH, Tempany CM, Frates MC, Silverman SG, McNeil BJ, Kurtz AB. Primary versus secondary ovarian malignancy: imaging findings of adnexal masses in the Radiology Diagnostic Oncology Group Study. Radiology. 2001;219:213–8.
10. Alcázar JL, Galán MJ, Ceamanos C, García-Manero M. Transvaginal gray scale and color Doppler sonography in primary ovarian cancer and metastatic tumors to the ovary. J Ultrasound Med. 2003;22:243–7.
11. Valentin L, Ameye L, Testa A, Lécuru F, Bernard JP, Paladini D, Van Huffel S, Timmerman D. Ultrasound characteristics of different types of adnexal malignancies. Gynecol Oncol. 2006;102:41–8.
12. Antila R, Jalkanen J, Heikinheimo O. Comparison of secondary and primary ovarian malignancies reveals differences in their pre- and perioperative characteristics. Gynecol Oncol. 2006;101:97–101.
13. Van Calster B, Valentin L, Van Holsbeke C, Testa AC, Bourne T, Van Huffel S, Timmerman D. Polytomous diagnosis of ovarian tumors as benign, borderline, primary invasive or metastatic: development and validation of standard and kernel-based risk prediction models. BMC Med Res Methodol. 2010;10:96.
14. Alcázar JL, Guerriero S, Pascual MÁ, Ajossa S, Olartecoechea B, Hereter L. Clinical and sonographic features of uncommon primary ovarian malignancies. J Clin Ultrasound. 2012;40:323–9.

CT and MR Imaging of Ovarian Adenocarcinoma (Serous/Mucinous/Endometrioid)

Marc Bazot, Isabelle Thomassin-Naggara, and Emile Daraï

Abstract

MR imaging (MRI) and multidetector computed tomography (MCT) play a major role for characterization of suspicious adnexal masses and staging of advanced-stage ovarian tumors. The most frequent ovarian cancers are mainly represented by serous, mucinous, and endometrioid epithelial-stromal ovarian tumors. Each histologic subtype has characteristics allowing their preoperative presumable diagnosis on MRI and MCT.

Keywords

Ovarian cancer • Epithelial-stromal ovarian tumors • Magnetic resonance imaging • Computed tomography

Introduction

Surface epithelial-stromal tumors of the ovaries account for about two-third of ovarian tumors and nearly 90 % of ovarian cancers [1]. The most frequent epithelial ovarian cancers are subtyped as serous, endometrioid, and mucinous. These ovarian tumors are classified by FIGO classification that distinguishes early- (stages I–II) and advanced-stage diseases (stages III–IV). Tumor spread is variable according to histologic subtypes. Most serous ovarian carcinomas are diagnosed at advanced stage with peritoneal carcinomatosis in nearly 75 % of cases. In contrast, mucinous and endometrioid ovarian carcinomas are commonly confined in pelvic cavity at the time of diagnosis.

In presence of a woman with an adnexal mass, the main challenge for the gynecologist is to assess the likelihood of malignancy. After physical examination, ultrasonography is the first-line imaging technique for the diagnosis of adnexal mass. Based on clinical and sonographic criteria, adnexal masses can be divided into different categories: firstly, a benign adnexal mass; secondly, a suspicious adnexal mass without clear evidence of metastatic spread (potential early-stage disease); and finally, an ovarian cancer with evidence of peritoneal dissemination (advanced-stage disease). Ultrasonography has limitations for the characterization of complex or indeterminate (suspicious) adnexal masses and for the staging of advanced ovarian cancers. Hence, several studies have reported the value of multidetector computed tomography and MR imaging for preoperative assessment of ovarian tumors [2–19]. Moreover, morphological and functional MR imaging has been proved to be the best technique for characterization of complex adnexal masses [10–16, 20]. In contrast, multidetector CT is the most simple and reproducible technique for staging and follow-up of patients with advanced-stage diseases.

M. Bazot, MD (✉) • I. Thomassin-Naggara, MD, PhD
Department of Radiology,
Hopitaux Universitaires Est-Parisiens, Hôpital Tenon, APHP,
58 Avenue Gambetta, 75020 Paris, France
e-mail: marc.bazot@tnn.aphp.fr

E. Daraï, MD, PhD
Department of Gynecology,
Hopitaux Universitaires Est-Parisiens, Hôpital Tenon, APHP,
58 Avenue Gambetta, 75020 Paris, France

L. Saba et al. (eds.), *Ovarian Neoplasm Imaging*,
DOI 10.1007/978-1-4614-8633-6_15,

The aim of this chapter is threefold:

1. To recall general features according to serous, mucinous, and endometrioid subtypes
2. To review the role of MR imaging and multidetector CT for characterization of suspicious adnexal masses without extrapelvic extension suggestive of serous, mucinous, and endometrioid ovarian adenocarcinomas
3. To review the role of multidetector CT and MR imaging for staging of advanced-stage serous, mucinous, and endometrioid ovarian adenocarcinomas

General Features

Serous Ovarian Tumors

Serous ovarian tumors account for about 30 % of all ovarian neoplasms; of these, approximately 60 % are benign, 10 % borderline, and 30 % carcinomatous [1]. Serous ovarian carcinomas account for approximately 40–50 % of ovarian cancers [21]. They are bilateral in about 57.5 % of cases (one-third at stage I) and are widely disseminated in 80–85 % of cases at the time of diagnosis [22]. Serous carcinoma is exceedingly rare in the first two decades but there is a progressively increasing rise in age-specific incidence subsequently, with an average age of 56 years [1]. Recent literature has suggested a dual pathway of ovarian serous carcinogenesis, with most serous carcinomas falling into one of two categories, low grade and high grade [23]. These are considered to represent two distinct tumor types with a different underlying pathogenesis and associated with different molecular events, clinical behavior, and prognosis [23]. In this setting, low-grade serous carcinoma is thought to evolve in many instances from a preexisting serous borderline tumor and cystadenoma [23]. Moreover, recent studies have suggested that ovarian cancers are subsequent to tubal abnormalities mainly represented by the presence of serous tubal intraepithelial carcinoma (STIC) with a cascade of genetic alterations mainly concerning p53 gene [24].

Macroscopically, serous carcinomas range from predominantly cystic papillary tumors to entirely solid masses, often having papillary surfaces [1]. Focal or diffuse calcific deposits suggest the serous nature of the tumor. The serum level of CA 125 is elevated in over 80 % of cases of serous carcinoma [1]. But CA 125 can be normal in up to 50 % of stage I ovarian cancer.

Mucinous Ovarian Tumors

Mucinous ovarian tumors account for about 12–15 % of all ovarian tumors; of these, approximately 75 % are benign, 10 % borderline, and 15 % carcinomatous [1]. Mucinous ovarian carcinomas represent 5–10 % of malignant primary ovarian neoplasms, being bilateral in 7 % of cases [22]. Mucinous carcinomas occur in women in the fourth to sixth decades, with an average age of 54 years [1]. Mucinous carcinomas tend to remain confined to the ovary and pelvis for a longer time than serous carcinomas, with abdominal spread encountered in operation in less than 20 % of cases [1]. The distinction between mucinous carcinoma and metastatic adenocarcinomas of intestinal origin is sometimes difficult. The exclusion of a primary site in the gastrointestinal tract or pancreas whose metastatic spread might mimic primary ovarian cancer is required. Mucinous ovarian tumors develop in association with dermoid cysts in 3–5 % or Brenner tumors.

Macroscopically, mucinous neoplasms tend to be the largest of all ovarian tumors (15–30 cm in diameter). Malignant mucinous ovarian tumors exhibit more often multiple loculi, which typically have thick irregular wall and often contain papillae and solid areas. Mucinous tumors unlike serous or endometrioid tumors often vary in their degree of differentiation from one area to another, and benign, borderline, and invasive patterns may coexist within the same specimen. Malignant component may be diffused within a mucinous tumor or involve only a small portion of it. In this setting, optimal sampling is required to detect malignancy (i.e., borderline and/or invasive) within a mucinous tumor. CA 125 is elevated in 35–67 % mucinous carcinoma; CEA and CA 19–9 are above normal in 88 and 83 %, respectively [1].

Endometrioid Ovarian Tumors

Endometrioid ovarian tumors account for about 2–4 % of all ovarian tumors [1]. These tumors are almost always malignant, being borderline or frankly invasive in nearly 20 and 80 % of cases, respectively [21]. Endometrioid carcinomas are the second most frequently encountered malignant ovarian epithelial tumors, accounting for 10–20 % of ovarian carcinomas [21]. They occur in postmenopausal women, with an average age of 56 years [1]. Endometrioid carcinomas are confined to the ovaries and adjacent pelvic structures in most patients, and in such instances only 13 % are bilateral (overall: 26.8 %) [21, 22]. CA 125 is elevated in 80 % endometrioid carcinomas.

Macroscopically, no gross features distinguish endometrioid carcinomas from other surface epithelial-stromal tumors [1]. Interestingly, up to 31 % of the tumors are associated with endometriosis in the same ovary or elsewhere in the pelvis [25]. Another association of endometrioid carcinoma of the ovary is with carcinoma of the endometrium, present in nearly 15–20 % of cases [1].

Suspicious Adnexal Tumors ("Local Disease")

Preoperative characterization of adnexal masses, and especially their benign or malignant nature, is a key determinant of surgical strategy. Preoperative differentiation between invasive and borderline ovarian tumors is also crucial for the

surgeon. In a presence of suspicious adnexal mass on ultrasonography, a recent meta-analysis has demonstrated that MRI performs better than CT and color Doppler ultrasonography for optimal characterization [6]. In this setting, a lot of studies have reported the high accuracy of MR imaging for distinguishing malignant from benign tumors ranging from 83 to 93 % [5, 10, 11]. Recent MR studies have demonstrated that the addition of diffusion- and perfusion-weighted MR sequences to conventional MRI protocol improved the preoperative characterization of complex adnexal masses, especially epithelial ovarian tumors [12–16].

All epithelial ovarian tumors (i.e., benign, borderline, and invasive) are mainly cystic. The presence of solid, nonfatty, nonfibrous tissue is the most powerful predictor of malignancy [5, 10–12, 26, 27]. Solid tissue is represented by vegetation, solid area, and thickened irregular septa [12]. Among these criteria, the presence of vegetations in a cystic mass is the sole criterion pathognomonic of epithelial ovarian tumors [28]. At histopathological examination, vegetations are present in 20, 62, and 92 % of benign, borderline, and malignant cystic masses, respectively [29]. Serous papillary projections are papillary in shape, protruding internally and/or externally. Malignant epithelial tumors demonstrate greater, more numerous papillary projections than benign masses [29].

Different MRI and CT features may suggest the specific histologic subtypes of epithelial, especially non advanced-stage serous, mucinous, and endometrioid ovarian tumors.

MR Imaging and Multidetector CT

Serous Subtype

Less than 20 % of serous cystadenocarcinomas are diagnosed at early-stage ovarian tumors. At MR imaging, serous cystadenocarcinoma is suggested when an ovarian mass of variable size has an irregular solid mass, with an intermediate signal on T2-weighted images, associated or not with numerous endocystic or exophytic vegetations (Fig. 1) [12]. The utility of MRI dynamic contrast enhancement (DCE) for distinguishing invasive, borderline, and benign epithelial ovarian tumors has been recently demonstrated [12, 13, 15, 30, 31]. Hence, the MR diagnosis of malignancy is reinforced when an early uptake of contrast medium by a solid mass or vegetations is noted during the arterial phase of dynamic MR imaging [12, 13, 15, 30, 31]. In a recent study, Thomassin-Naggara et al. suggested that curve type 3 appeared specific for invasive ovarian tumors whereas curve type 1 was never observed in such tumors (Fig. 2) [15]. In contrast to DCE MRI, diffusion-weighted (DW) MR imaging seems less useful than DCE MRI to assess malignant ovarian tumors [14, 32]. In this setting, Thomassin-Naggara et al. suggested that only the combination of intermediate signal intensity on T2-weighted MRI sequence and a high signal intensity on DWI of solid mass was statistically significant for distinguishing invasive from noninvasive ovarian tumors [14].

Several studies underlined the limitation of all these criteria (i.e., solid mass and vegetations) to distinguish invasive stage IA–B from borderline or benign ovarian tumors [33]. Different comments could be provided according to these potential limitations. Firstly, with the exception of benign cystadenofibromas (and Brenner tumors), almost all benign serous ovarian tumors are predominantly cystic or cystic papillary without solid area [25]. In addition, the solid component of cystadenofibroma (and Brenner tumor) is almost always hypointense on T2-weighted MR imaging, this criterion being a well-known finding predictive of benignity [34, 35]. Secondly, a lot of MR studies have shown vegetations in 38–48 % and 61–67 % of invasive and borderline ovarian tumors (BOT), respectively [3, 12]. In a recent study using multivariate analysis, Bazot et al. suggested that the presence of vegetations displaying intermediate signal on T2-weighted MRI and curve type 2 on DCE MRI sequence was highly suggestive of serous BOT (Fig. 3) [36]. A particular form of serous BOT (i.e., serous surface papillary borderline ovarian tumors) (SSPBT) was recently underlined [36–38]. Serous surface papillary tumor of the ovary displays a surface proliferative pattern and shows papillary excrescences on its surface [1]. SSPBT is therefore usually an entirely solid mass that generally lacks areas of necrosis or hemorrhage [25]. During differential diagnosis, ovarian tumors with a rich solid component are considered malignant based on cross-sectional imaging findings [12, 25]. SSPBT may therefore be diagnosed as a highly malignant ovarian tumor by MRI [25]. However, Tanaka et al. recently reported six cases showing a papillary architecture and internal branching (PA&IB) pattern with frond-like projections on T2WI correlated at histopathology with epithelial multilayering, forming papillae with a thick fibrous stalk (Fig. 4) [25]. This PA&IB pattern appears as a characteristic MR imaging feature of SSPBT that cannot be obtained using CT alone [25]. Another striking finding is visualization of normal ovaries in the mass or masses (if bilateral), most clearly on T2-weighted MR images [37]. In contrast, serous ovarian carcinomas with exophytic vegetations have always associated solid masses.

Few studies have specifically evaluated the value of CT for the differentiation of ovarian cancer subtypes [39, 40]. Calcification is the most frequent finding suggestive of serous ovarian carcinoma. However, this criterion is not specific, being present in many benign ovarian tumors such as mature teratoma, fibroma, or Brenner tumor. The presence of calcifications (psammoma bodies) is variable in ovarian carcinoma histopathological studies (14.3–30 %) [1, 41]. CT compared to histology has a low sensitivity to detect calcification within ovarian tumors (4.7–8 %) but provides an overview of the abdominal and pelvic cavity. In this setting, Burkill et al. reported that calcifications tend to occur most commonly in serous cystadenocarcinomas of lower grade [42].

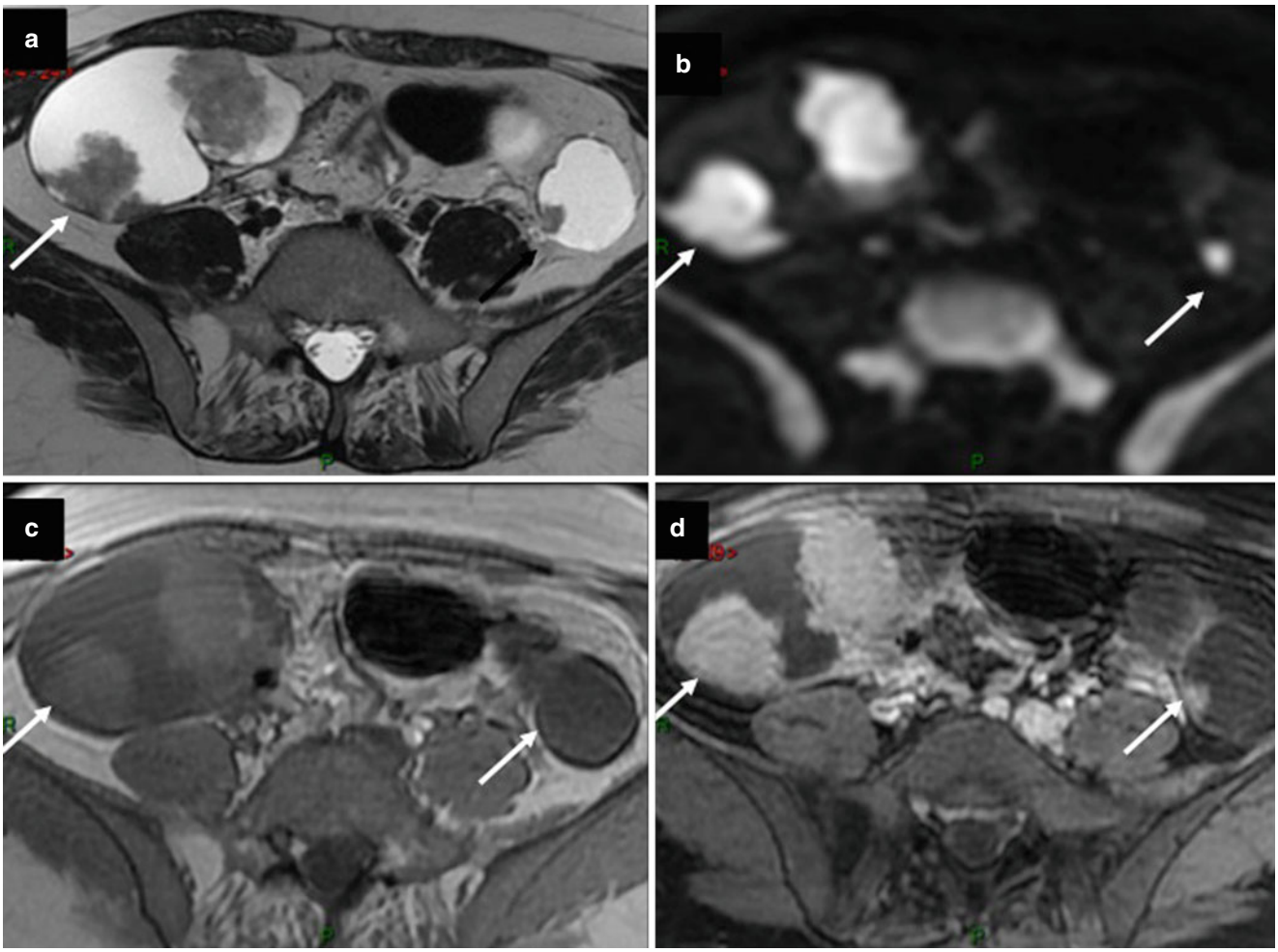

Fig. 1 Images in a 35-year-old woman with bilateral low-grade serous carcinoma developed on serous borderline tumors, Figo IC (*large white arrows*). (**a**) Transverse T2-weighted MR image shows bilateral complex adnexal tumors with right cystic and solid irregular components and left endocystic nodule with intermediate signal intensity (*arrows*), (**b**) transverse DW MR image obtained at $b = 1{,}000$ s/mm^2 shows the presence of high signal intensity in solid components (*arrows*), (**c**) transverse T1-weighted MR image obtained without fat suppression, (**d**) transverse fat-suppressed T1-weighted MR image shows enhancement in the solid components of both tumors (*arrows*). Note that the combination of intermediate signal intensity on T2-weighted MRI sequence and high signal intensity on DWI of solid components was significant for distinguishing invasive from noninvasive ovarian tumors

Mucinous Subtype

More than 80 % of mucinous cystadenocarcinomas tend to remain confined to the ovary and pelvis (early stage) at the time of diagnosis [1]. Mucinous malignant ovarian tumors are unilateral, generally cystic, and often very large and tend to be multiloculated [43]. They often have variable signal intensity in the loculi, owing to proteinaceous or mucinous contents and hemorrhage [27]. It must be reemphasized that mucinous tumors, unlike serous tumors, often vary in their degree of differentiation from one area to another at histopathological examination [1]. Hence, benign, borderline, and invasive patterns may coexist within the same specimen [1]. In our experience, the presence of solid mass with intermediate intensity on T2-weighted MR sequence in a large multiloculated lesion is the best predictive criterion of malignancy among mucinous ovarian tumors. MR imaging is the best technique to depict such solid tissue. The presence of high signal intensity within solid mass on DWI is low predictive of malignancy [14]. However, the presence of curve type 2 or 3 on DCE MR sequence in solid mass reinforces the diagnosis of malignancy (Fig. 5). The combination of all these findings is valuable, allowing distinction of mucinous cystadenocarcinoma from other large multiloculated cystic ovarian tumors. In this setting, different epithelial and nonepithelial ovarian tumors should be ruled out to avoid misinterpretations [12]. The most frequent ovarian lesions that may resemble to ovarian cystadenocarcinoma are cystadenofibroma, struma ovarii, granulosa tumors, ovarian metastases, and collision tumors. Some important features are important to recall allowing potential differential diagnosis.

Benign cystadenofibroma may present as a multiloculated cystic mass with irregular thickened septa with heterogeneous

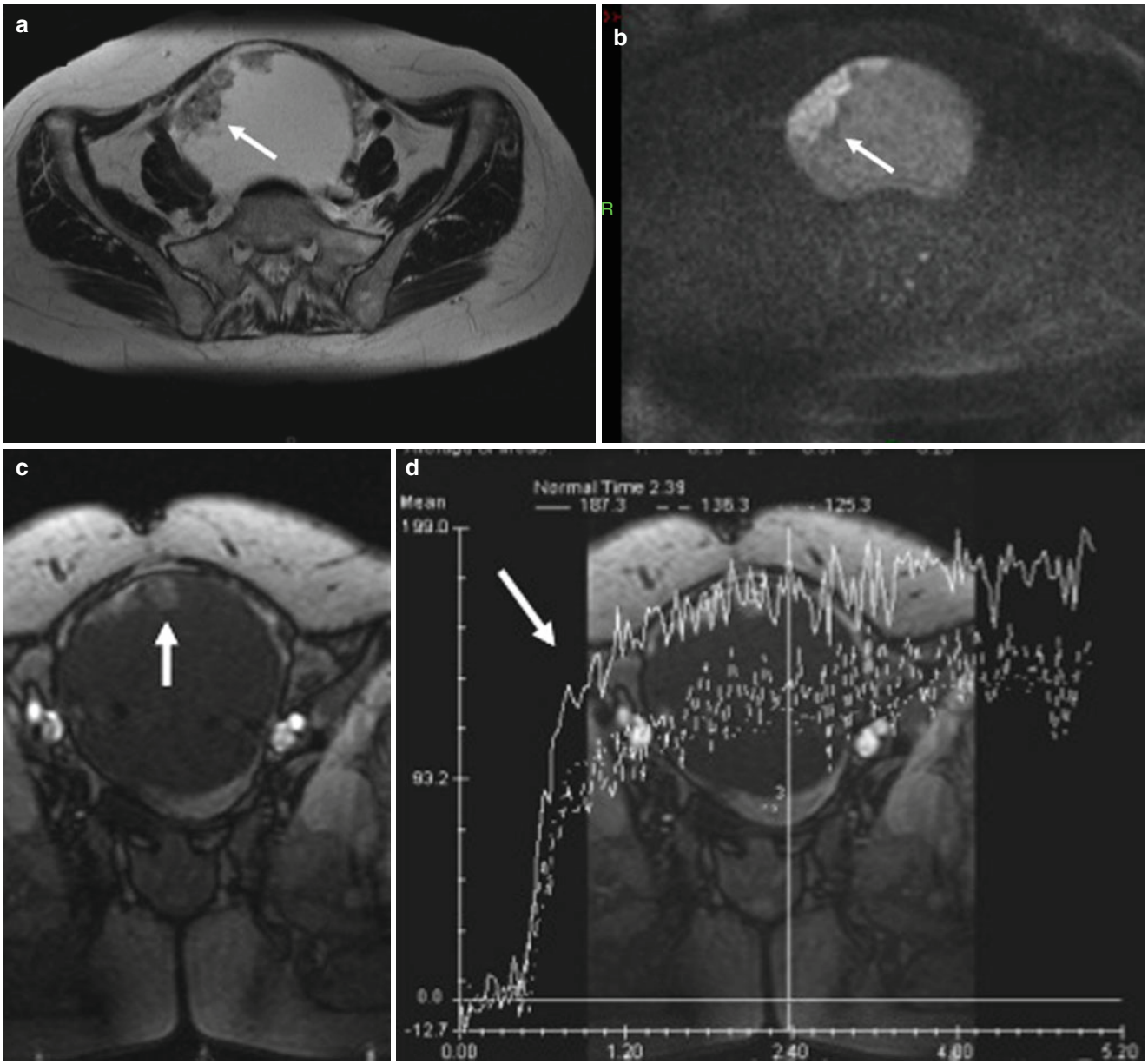

Fig. 2 Images in a 70-year-old woman with left low-grade serous carcinoma, Figo IC. (**a**) Transverse T2-weighted MR image shows multiple endocystic vegetations displaying intermediate signal intensity (*arrow*), (**b**) transverse DW MR image obtained at $b = 1{,}000$ s/mm^2 shows the presence of high signal intensity in endocystic vegetations (*arrow*), (**c**) coronal T1-weighted DCE MR image obtained without fat suppression shows uptake of contrast medium in vegetations, (**d**) coronal T1-weighted DCE MR image obtained without fat suppression shows a curve type 3 in endocystic vegetations (*arrow*). Note that the combination of vegetations with intermediate signal intensity on T2-weighted MRI sequence, high signal intensity on DWI, and curve type 3 was pathognomonic of serous cystadenocarcinoma

signal intensity on T1- or T2-weighted MR images or with a regular solid mass exhibiting low signal intensity on T2-weighted MR images with slight delayed uptake of contrast medium on postcontrast T1-weighted images. In addition to low signal intensity on T2-weighted, the presence of a curve type 1 on DCE MR sequence within solid tissue is a valuable tool for the diagnosis of cystadenofibroma (Fig. 6).

Struma ovarii is suggested when a multiloculated cystic mass comprised loculi or small cysts showing low signal intensity on T1-weighted images and very low signal intensity on T2-weighted images [44] (Fig. 7). The presence of early significant enhancement on DCE MR imaging may mimic malignancy [44]. However, half of struma ovarii are mixed with dermoid cyst [45]. Thanks to the high capability of MRI or CT to perform the diagnosis of dermoid cyst, this could represent a potential clue for differential diagnosis.

Granulosa cell tumors show a spectrum of imaging manifestations due to various histologic appearances and various

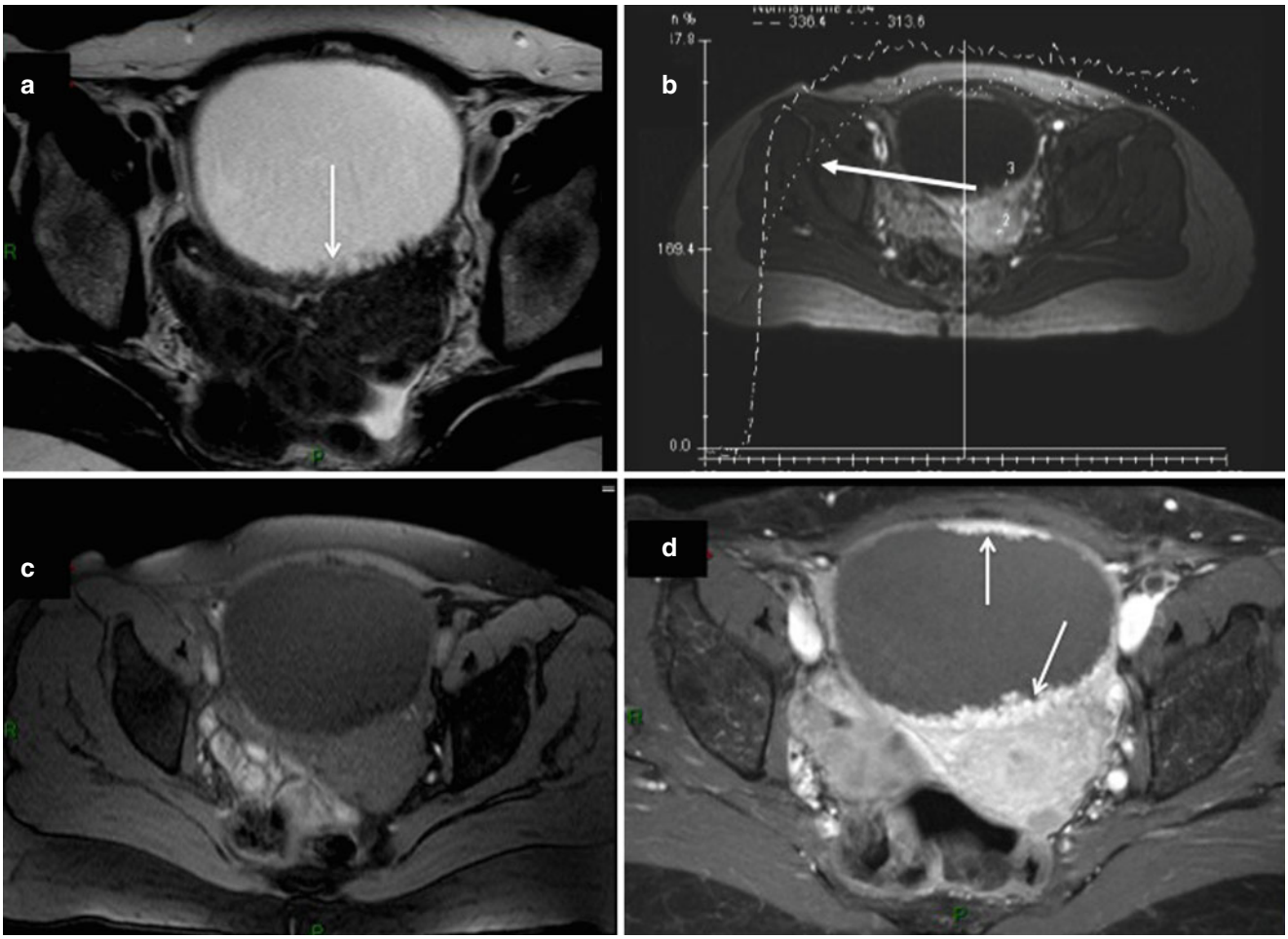

Fig. 3 Images in a 63-year-old woman with serous borderline ovarian tumor. (**a**) Transverse T2-weighted MR image shows left unilocular cystic tumor containing multiple irregular endocystic vegetations with intermediate signal intensity (*arrows*), (**b**) transverse dynamic contrast-enhanced (DCE) MR image shows curve type 2 within endocystic vegetations, (**c**) transverse T1-weighted MR image obtained without fat suppression, (**d**) transverse fat-suppressed T1-weighted MR image shows enhancement in anterior and posterior endocystic vegetations (*arrows*). Note that the combination of the presence of vegetations displaying intermediate signal on T2-weighted MRI without associated solid masses and curve type 2 on DCE MRI sequence was highly suggestive of serous BOT

arrangements of tumor cells. They have frequently the appearance of multiloculated cystic lesions resembling to mucinous cystadenocarcinoma [46]. These multiple cystic spaces are filled with watery fluid or hemorrhage. Similarly to mucinous cystadenocarcinoma, granulosa cell tumor is confined to the ovary at the time of diagnosis and is usually unilateral (90 %). Granulosa cell tumors of the ovary represent the most common clinically estrogenic ovarian tumor. In this setting, they are frequently associated with endometrial hyperplasia, polyps, and carcinoma (3–25 % of cases). All these features are depicted using MR imaging representing a useful tool to differentiate granulosa from malignant mucinous ovarian tumor (Fig. 8). Some unusual presentations can be confusable when rupture and hemoperitoneum occur. In all circumstances, dosage of estradiol and inhibin A should be proposed to reinforce the preoperative diagnosis of granulosa cell tumor.

Metastatic tumors of the ovary, especially Krukenberg tumors, usually originate in the gastrointestinal tract. Differentiation between metastatic and primary ovarian carcinoma is of great importance with respect to treatment and prognosis. Imaging findings in metastatic lesions are nonspecific, consisting of predominantly solid components, mixed, or multiloculated cystic mass. However, Krukenberg tumor demonstrates some distinctive findings, including bilateral complex masses with hypointense solid components (dense stromal reaction) and internal hyperintensity (mucin) on T1- and T2-weighted MR images, respectively [47] (Fig. 9). In addition, the visualization of primary gastrointestinal tract, especially on multidetector CT, is sometimes possible.

The possibility of collision tumor has to be suggested in a presence of unusual ovarian tumor presentation on imaging analysis. Collision tumor represents the coexistence of two adjacent but histologically distinct tumors with no histologic

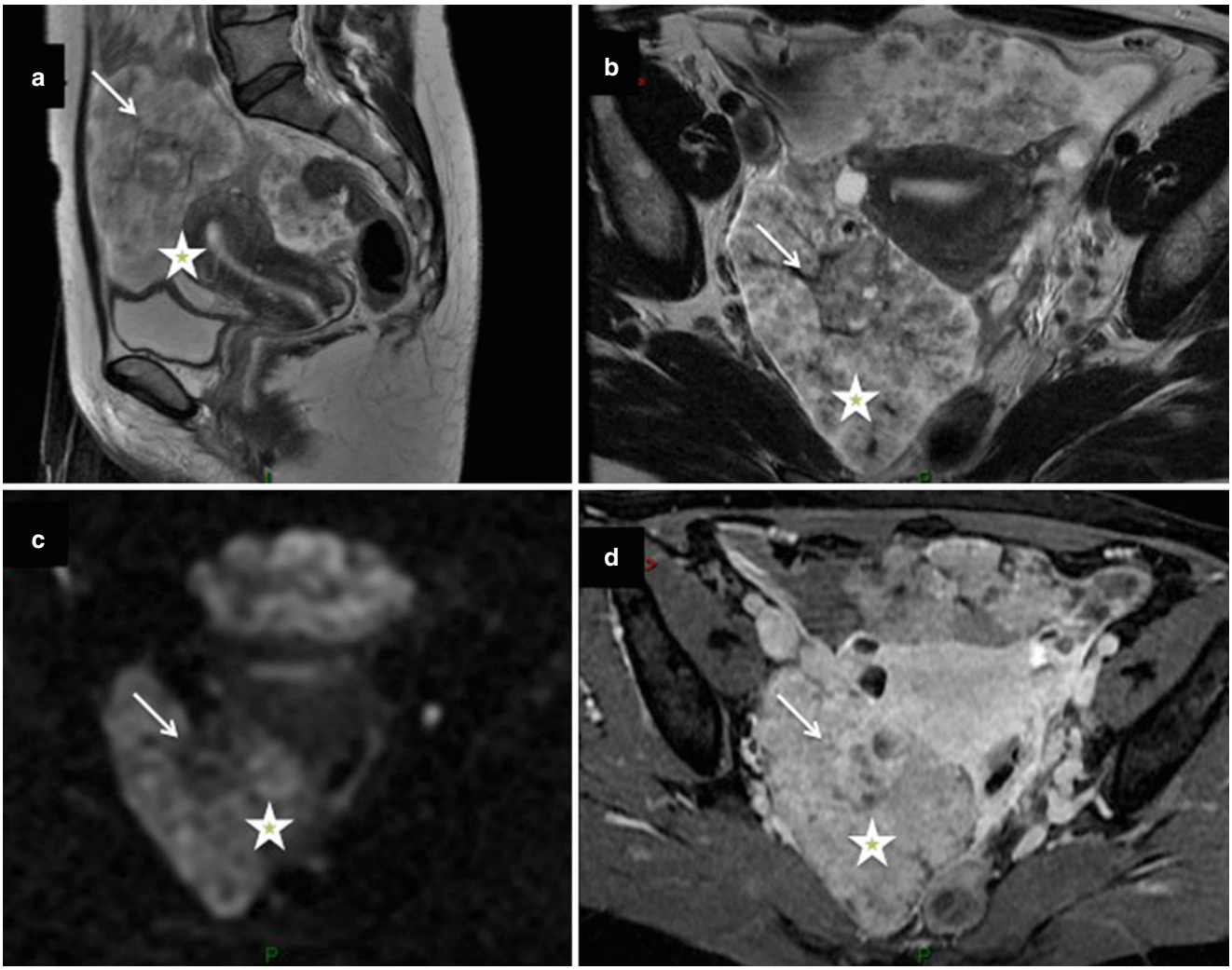

Fig. 4 Images in a 42-year-old woman with bilateral serous surface papillary borderline tumors. (**a**) Sagittal and (**b**) transverse T2-weighted MR images show bilateral, entirely solid ovarian tumors showing a papillary architecture and internal branching pattern with frond-like projections with intermediate signal intensity (*asterisks*), (**c**) transverse DW MR image obtained at $b = 1{,}000$ s/mm^2 shows the presence of high signal intensity in solid components (*arrows*), (**d**) transverse fat-suppressed T1-weighted MR image shows enhancement in the exophytic vegetations of both tumors (*asterisk*). Note the visualization of normal ovary in the right mass, most clearly on T2-weighted MR images (*arrows*)

admixture at the interface. Even so rare, ovarian collision tumors are most commonly composed of mucinous ovarian tumors and teratoma or Brenner tumors. MRI or CT images of a collision tumor composed of a mucinous tumor (potentially malignant) and a teratoma show a typical multiloculated cystic mass with internal loculi filled with pure fat. Mucinous cystadenocarcinoma can be more difficult to differentiate from collision tumor composed of mucinous and Brenner tumors. In this setting, the presence of solid mass with intermediate signal intensity on T2-weighted, high signal intensity on DWI, and a curve type 2 or 3 on DCE favors the diagnosis of mucinous cystadenocarcinoma. In contrast, Brenner tumor displays very low signal intensity on T2-weighted MR sequence with mild homogeneous enhancement on postcontrast CT and MRI (Fig. 10) [48, 49].

In addition, Moon et al. demonstrated that amorphous calcification in a solid mass was a characteristic finding of Brenner tumor of the ovary on CT and MRI [49]. However, mucinous cystic ovarian tumors sometimes also contain calcifications. In a recent study, Okada et al. retrospectively investigated the radiological and histopathological evidence of calcifications in 44 cases of ovarian mucinous cystic tumors (22 benign, 13 borderline, and 9 cancers) in which a non-contrast CT scan was performed. Calcifications were noted in 34.1 % of mucinous cystic tumors on CT scans and 56.8 % in histopathological studies, and they were found in two locations, intramural and intracystic, according to the histopathological findings. Intramural calcifications were frequent in benign tumors, and intra-cystic calcifications were frequent in proliferating tumors.

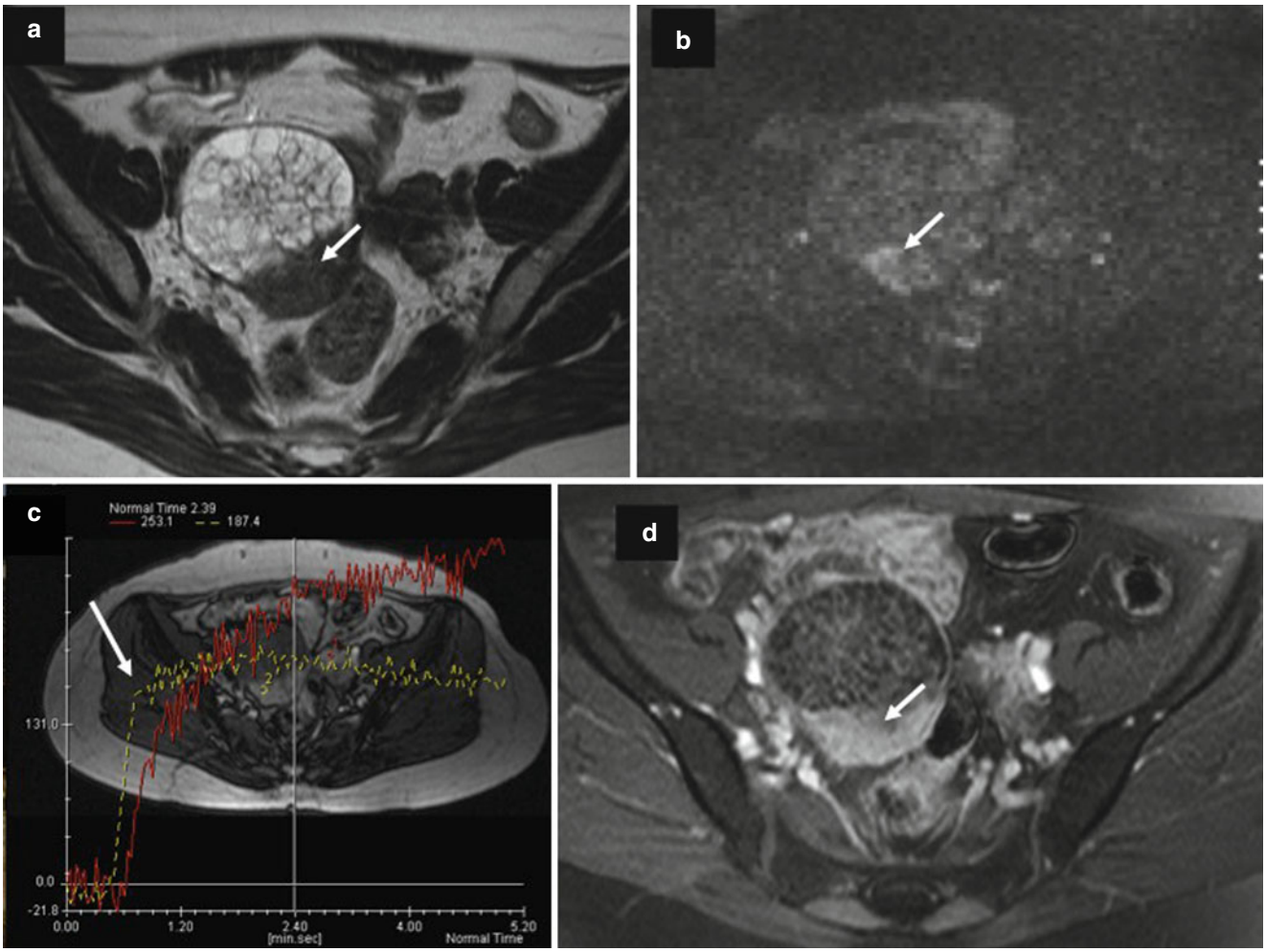

Fig. 5 Images in a 64-year-old woman with mucinous cystadenocarcinoma. (**a**) Transverse T2-weighted MR image shows a multiloculated cystic ovarian tumor with multiple irregular septa and posterior solid mass with heterogeneous intermediate signal intensity (*arrow*), (**b**) transverse DW MR image obtained at $b = 1{,}000$ s/mm^2 shows the presence of high signal intensity in solid mass (*arrow*), (**c**) transversal T1-weighted DCE MR image obtained without fat suppression shows a curve type 3 in solid mass related to carcinomatous component (*arrow*), (**d**) transversal T1-weighted postcontrast MR image shows enhancement of irregular septa and solid mass (*arrow*)

Endometrioid Subtype

Endometrioid cystadenocarcinomas are almost always confined to the ovary and pelvis at the time of diagnosis [1]. Imaging findings are nonspecific and include a large, complex cystic mass with solid components. However, their association with endometriosis or endometrial disease has been previously underlined (see supra). In this setting, MR imaging represents the best imaging technique to visualize associated endometriotic lesions or endometrial thickening.

The exact prevalence of malignant tumors arising from endometriotic cysts of the ovary is unknown but is estimated of approximately 0.7 % [50]. In a recent study, Tanaka et al. confirmed that the most common histologic subtype in malignant tumors developed on pelvic endometriosis was endometrioid adenocarcinoma [50]. In this study, these authors revealed that malignant tumors associated with endometriotic cysts tended to appear in older patients (>45 years old), with larger endometriotic cysts (>10 cm) and with endometriotic cysts without shading on MRI [50]. The use of gadolinium is usually not required to differentiate blood clots (hypointense on T2 weighted) and mural nodules (intermediate on T2 weighted). However, the presence of mural nodules larger than 3 cm in maximum diameter was a strong indicator of coexisting malignancy in their study [50]. In this setting, DCE MR sequence followed by postcontrast MR imaging should be performed because enhanced mural nodules are an important finding to assess malignancy (Fig. 11). However, some exceptions, such as decidualization or endometrial polyp, should be noted to avoid potential false-positive cases of malignancy [50].

When the ovary and the uterus corpus are both involved by endometrioid carcinomas, the question arises whether both cancers are primary or one is metastatic from the other [51]. At histologic examination, three different possibilities are discussed. First, a direct myometrial invasion from serosal surface by ovarian tumor favors the diagnosis of ovarian primary and corpus metastasis. Second, if the endometrial

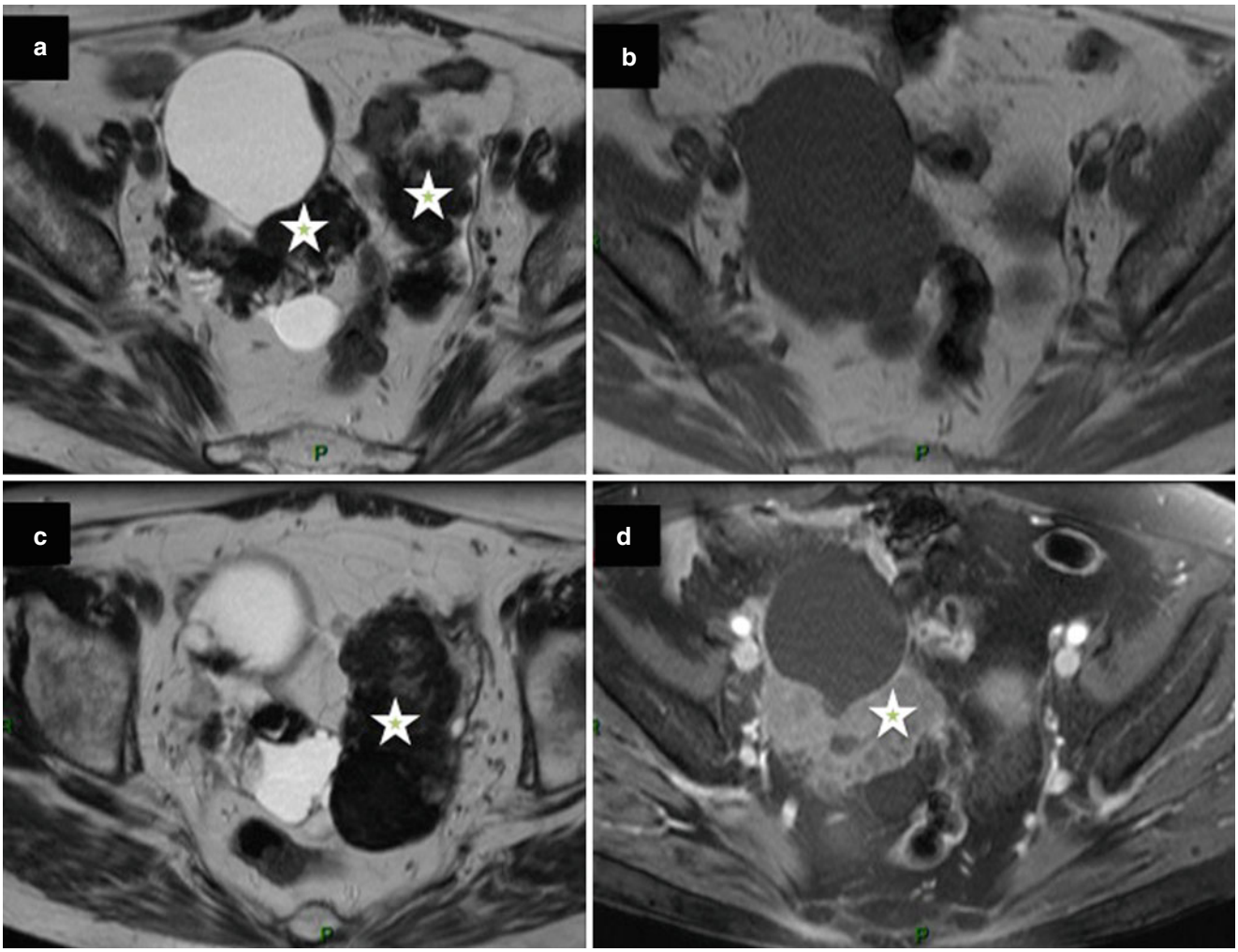

Fig. 6 Images in a 67-year-old woman with bilateral cystadenofibroma. (**a**, **c**) Transverse T2-weighted MR images show bilateral mixed ovarian tumors with cystic components and solid regular components with low signal intensity (*asterisk*), (**b**) transverse T1-weighted MR image obtained without fat suppression, (**d**) transverse fat-suppressed T1-weighted MR image shows enhancement in the solid components of both tumors (*asterisk*)

carcinoma is small and limited to the endometrium or with limited myometrial invasion, and if there is a central located ovarian, sometimes arising on a background of endometriosis, the tumors are probably independent primaries [51]. Finally, if the endometrial carcinoma extends deeply into the myometrium, it is usually reasonable to conclude that the ovarian involvement is secondary [51]. These distinctions are important to consider because of the implications for treatment. In this setting, MR imaging may be a valuable tool for such differentiation, providing useful information for preoperative planning (Fig. 12).

Advanced-Stage Disease

Several studies have suggested that MRI and CT perform equally to perform staging of advanced-stage cancer [52–54]. In clinical practice, the availability of CT makes it the investigation of choice for planning surgery in women believed to have advanced-stage ovarian cancer.

Computed Tomography and MR Imaging

Serous (and Endometrioid) Cystadenocarcinomas

Multidetector CT (MCT) is the first-line technique examination for staging ovarian cancer, especially serous carcinomas, given its widespread availability and general use. However, CT remains inferior to surgical staging in detection of tiny peritoneal, omental, mesenteric, and diaphragmatic nodules [18]. Hence, laparoscopy remains the gold standard to predict resectability. Despite its limitations, MCT should be always performed providing major informations for the surgeon to discuss surgical and other therapeutic options with the patient (i.e., biopsy and neoadjuvant

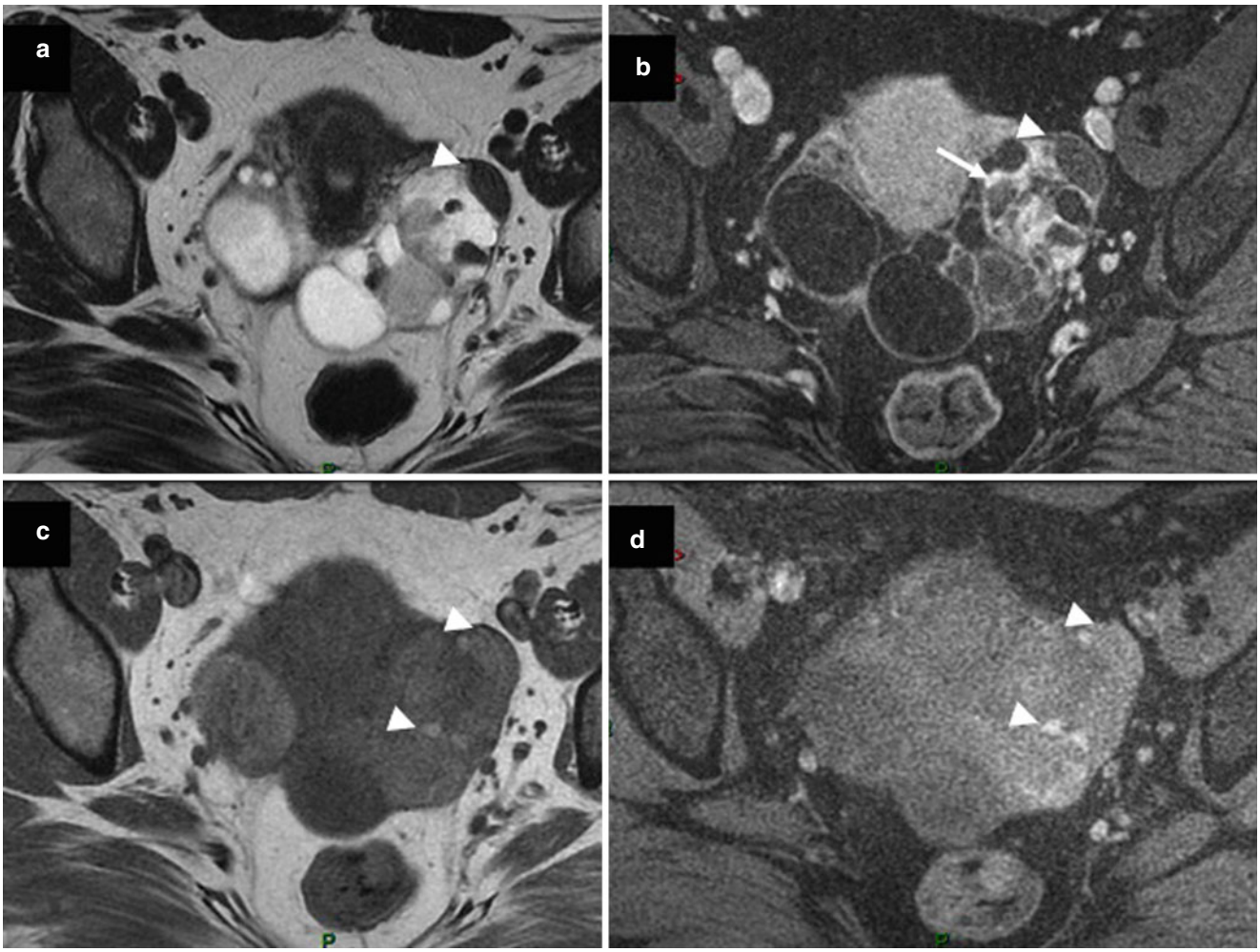

Fig. 7 Images in a 53-year-old woman with bilateral struma ovarii. (**a**) Transverse T2-weighted MR image shows a left multiloculated cystic mass with loculi or small cysts showing very low signal intensity (*arrowhead*), (**b**) transverse fat-suppressed T1-weighted MR image after gadolinium injection shows strong delayed enhancement in the solid components of the left ovarian tumor (*arrow*), (**c**, **d**) transverse T1-weighted MR image obtained without and with fat suppression shows left multiloculated cystic mass comprised of loculi or small cysts with low to intermediate signal intensity (*arrowheads*)

chemotherapy). In the presence of bulky peritoneal tumor, CT predicts when cytoreductive surgery is likely to be incomplete by defining sites of unresectable tumor [18] (Fig. 13). Multidetector CT indicates when the oncologist surgeon has to perform extensive surgery as a clear relation has been demonstrated between the extent of surgical procedures and perioperative complications and mortality (e.g., rectosigmoid colon, small bowel, or spleen).

The diverse morphological patterns of peritoneal carcinomatosis of ovarian carcinomas reflect the different anatomic and physiologic pathways of the spread of disease. Peritoneal spread of ovarian cancer occurs by intraperitoneal dissemination and by direct extension along ligaments and peritoneal reflections. Direct extension results in tumor invasion of the tubes, uterus, bladder, rectosigmoid colon, and pelvic sidewall. Intraperitoneal dissemination occurs when cancer cells slough off the ovarian epithelium and, following the flow of intraperitoneal fluid, deposit in peritoneal sites depending on the net effects of gravity, respiratory motion, peristaltic activity, and lymphatic resorption [55]. In accordance with different surgical classifications (i.e., Sugarbaker, Eisenkopp), a systematic analysis of the different potential metastatic locations should be always performed using MCT [56] (i.e., Douglas pouch, lateral paravesical recesses, pelvic organs, right and left paracolic gutters, omentum, mesentery, right and left diaphragms, hepatic and splenic capsules, lesser peritoneal sac, gallbladder fossa, hepatorenal, gastrosplenic and pancreaticosplenic ligaments, and pelvic and retroperitoneal lymph nodes) (Fig. 14). In clinical practice, the three most frequent locations of peritoneal carcinomatosis detected by CT are Douglas pouch, omentum, and right subdiaphragmatic space [57]. A diffuse pattern of disease is commonly encountered in the omentum, where replacement of normal fat by tumor may range from subtle micronodular infiltration to

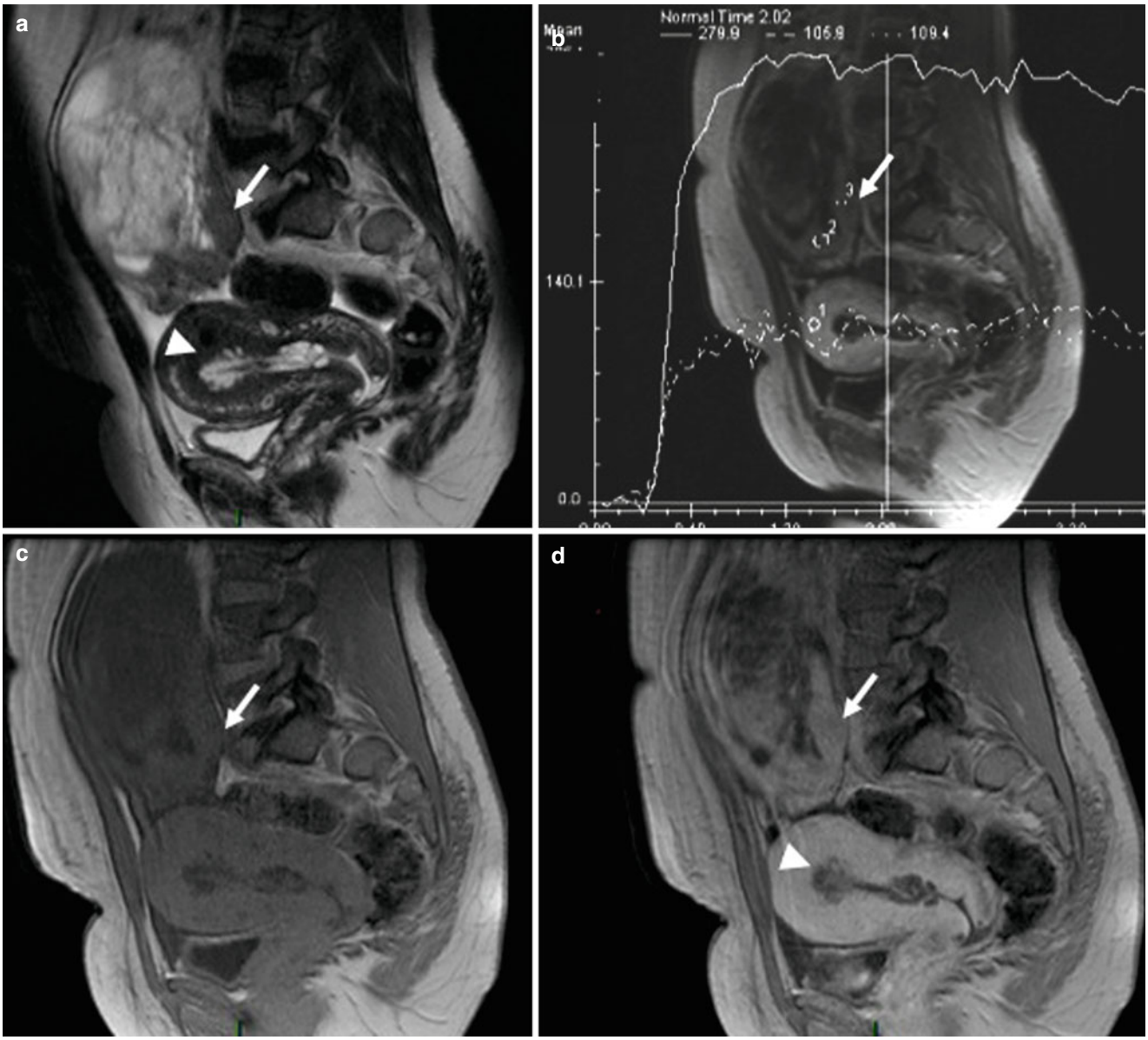

Fig. 8 Images in a 63-year-old woman with granulosa tumor. (**a**) Sagittal T2-weighted MR image shows multiloculated cystic lesions with multiple cystic spaces and posterior solid mass displaying intermediate signal intensity (*arrow*); adenomyosis and endometrial thickening are also present (*arrowhead*). (**b**) Sagittal dynamic contrast-enhanced (DCE) MR image shows curve type 2 within solid mass. (**c**) Sagittal fat-suppressed T1-weighted MR image without fat suppression. (**d**) Sagittal T1-weighted MR image without fat suppression shows enhancement in the posterior solid mass (*arrow*). Adenomyosis and endometrial thickening are also visualized (*arrowhead*)

solid "omental cake." Early infiltration of the perivascular and perilymphatic spaces in the small bowel mesentery increases their attenuation and produces linear striations [55]. Infiltration of the mesentery also sometimes manifests with a pleated pattern produced by stiffening of the connective tissue, with resultant tethering and crowding of the mesenteric vessels [55]. Focal disease can take the form of discrete nodules with a diameter of 5–20 mm, bulky intraperitoneal masses, or plaques along peritoneal fissures and ligaments [55]. In many patients, however, MCT is unable to demonstrate peritoneal metastases because of their small size. The presence of calcifications improves the sensitivity of CT in diagnosing metastases from ovarian carcinoma (Fig. 15) [41, 42, 58]. Hence, serous cystadenocarcinoma contains histologic calcification in approximately 30 % of cases.

Whatever the value of MCT, the distinction between serous ovarian carcinoma and primitive peritoneal cancer is usually difficult. In a recent study, Choi et al. compared the clinicopathological characteristics of 20 advanced primary serous ovarian carcinomas with ovaries of normal size and 7 primary peritoneal carcinomas (PPCs). There were few significantly different features between the two groups. The

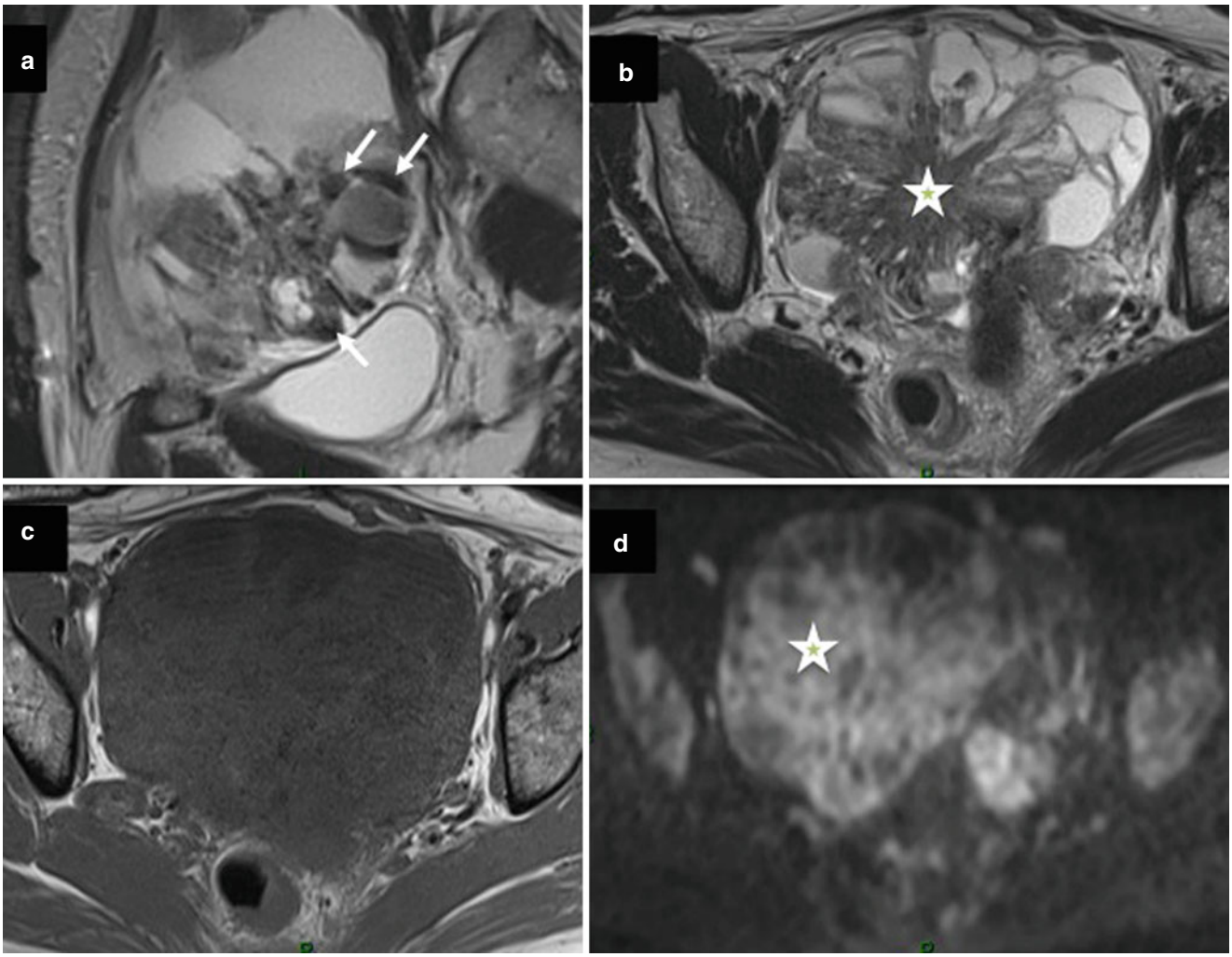

Fig. 9 Images in a 52-year-old woman with sigmoid colon cancer and bilateral ovarian metastases. (**a**) Sagittal T2-weighted MR image shows a multiloculated cystic lesion and solid component with low signal intensity (*arrow*), (**b**) transversal T2-weighted MR image shows a multiloculated cystic lesion with large solid mass displaying intermediate signal intensity (*asterisk*), (**c**) transversal T1-weighted MR image without fat suppression, (**d**) transversal diffusion-weighted MR image shows diffuse high signal intensity in solid component (*asterisk*)

patients with ovarian carcinoma tended to have less severe omental involvement [59]. Preoperative distinction between serous ovarian cancer and primitive peritoneal cancer may not be as important, in which surgical debulking is the standard of care for both diseases.

Some very unusual presentation of ovarian cystadenocarcinoma can be present. Hence, serous psammocarcinoma, a rare variant of ovarian serous carcinoma, is characterized histologically by the presence of a large quantity of psammoma bodies. In this case, computed tomography scans showed extensively calcified pelvic and peritoneal masses. At CT, diffuse psammomatous calcifications may cause these tumors to have very high attenuation and could be a radiological marker of ovarian psammocarcinoma [60] (Fig. 16).

Several studies using conventional MRI sequences (i.e., T2, T1) have suggested that MR imaging is equally accurate than CT in the detection of extension of disease [52–54]. MR imaging is currently limited by availability, duration of examination, lack of widespread reader experience, and expense. However, recent development of functional MR imaging (i.e., perfusion and diffusion) have reinforced the potential value of MRI for the evaluation of advanced-stage ovarian cancer. In this setting, the combined interpretation of conventional MR images with diffusion-weighted images has been shown to increase accuracy in the staging of ovarian cancer by allowing the detection of more sites of involvement [61, 62] (Fig. 17).

Although Vergote et al. suggested that neoadjuvant chemotherapy followed by interval debulking surgery was a valuable treatment option for patients with bulky stage IIIC or IV ovarian carcinoma [63], primary debulking surgery before initiation of chemotherapy remains the standard of care for patients with advanced stages of ovarian cancer [64]. Indeed, complete resection is obtained in up to 70–80 %

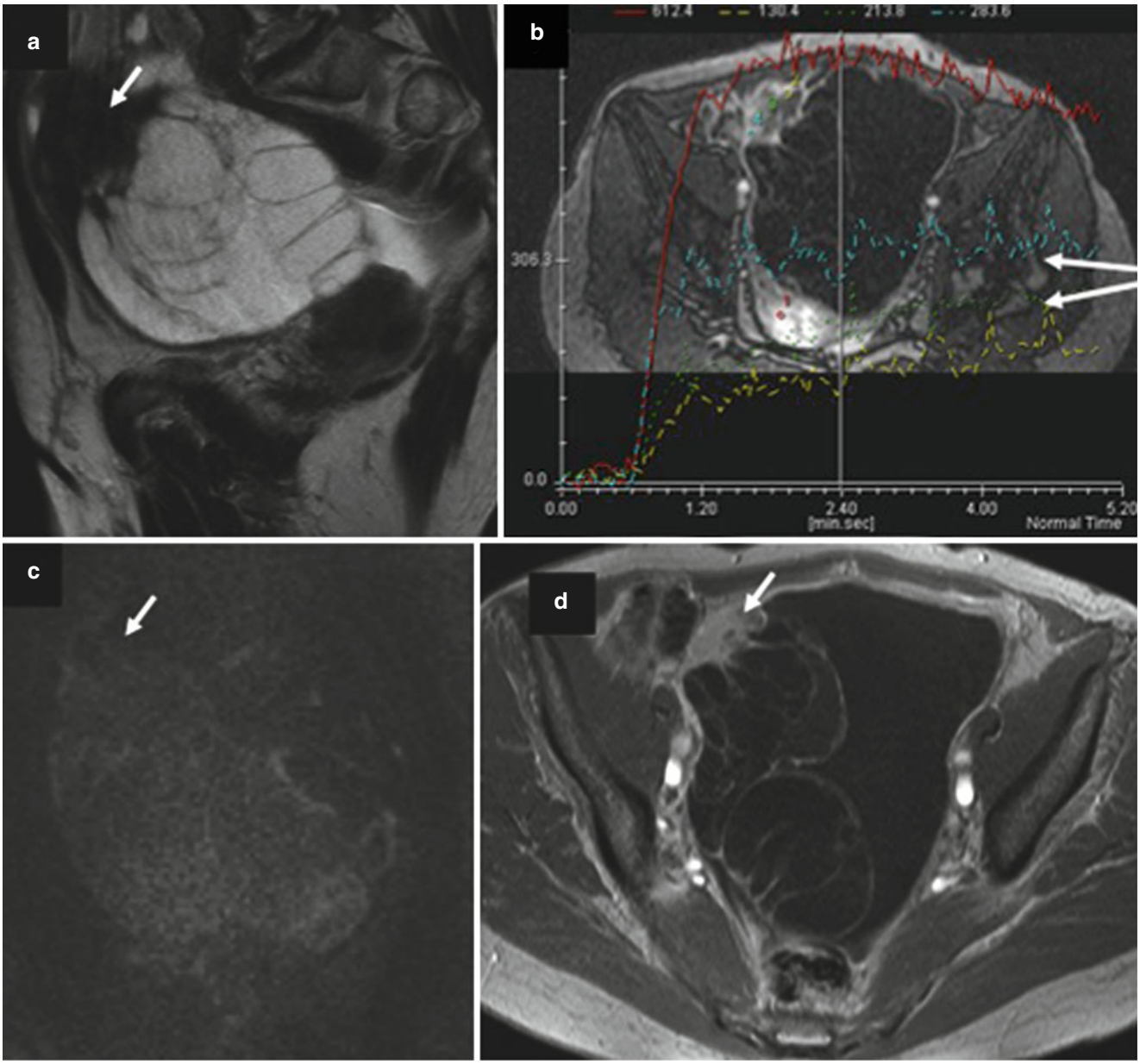

Fig. 10 Images in a 68-year-old woman with mucinous borderline ovarian tumor associated with Brenner tumor. (**a**) Sagittal T2-weighted MR image shows a multiloculated cystic lesion with upper solid irregular mass displaying low signal intensity (*arrow*), (**b**) transversal dynamic contrast-enhanced (DCE) MR image shows curves type 2 within solid mass (*arrow*). (**c**) Sagittal diffusion-weighted MR image shows the absence of high signal intensity in solid mass (*arrow*), (**d**) transversal fat-suppressed T1-weighted MR image with fat suppression shows enhancement of irregular septa and solid mass (*arrow*)

of patients with an increased disease-free survival compared to neoadjuvant chemotherapy [64, 65]. Finally, 20–30 % of patients are initially unresectable. In this setting, Sala et al. using multiparametric MR imaging suggested that assessment of response to neoadjuvant chemotherapy could be performed [66]. In this study, 19/22 (86 %) women with advanced-stage disease had high-grade serous carcinomas. Their results demonstrated significant differences in baseline ADCs among primary ovarian lesions, omental cake, and peritoneal deposits, with peritoneal deposits showing the lowest ADCs and VSFs [66].

Finally, lymph node size at CT or MR imaging has suboptimal sensitivity (30 %) for the detection of nodal disease in advanced-stage ovarian cancers [20]. Preoperative lymph node characterization may not be as important in cases of advanced-stage ovarian cancer; indeed, in case of complete intraperitoneal resection of ovarian cancer, comprehensive surgery includes systematic pelvic and para-aortic lymphadenectomy [55].

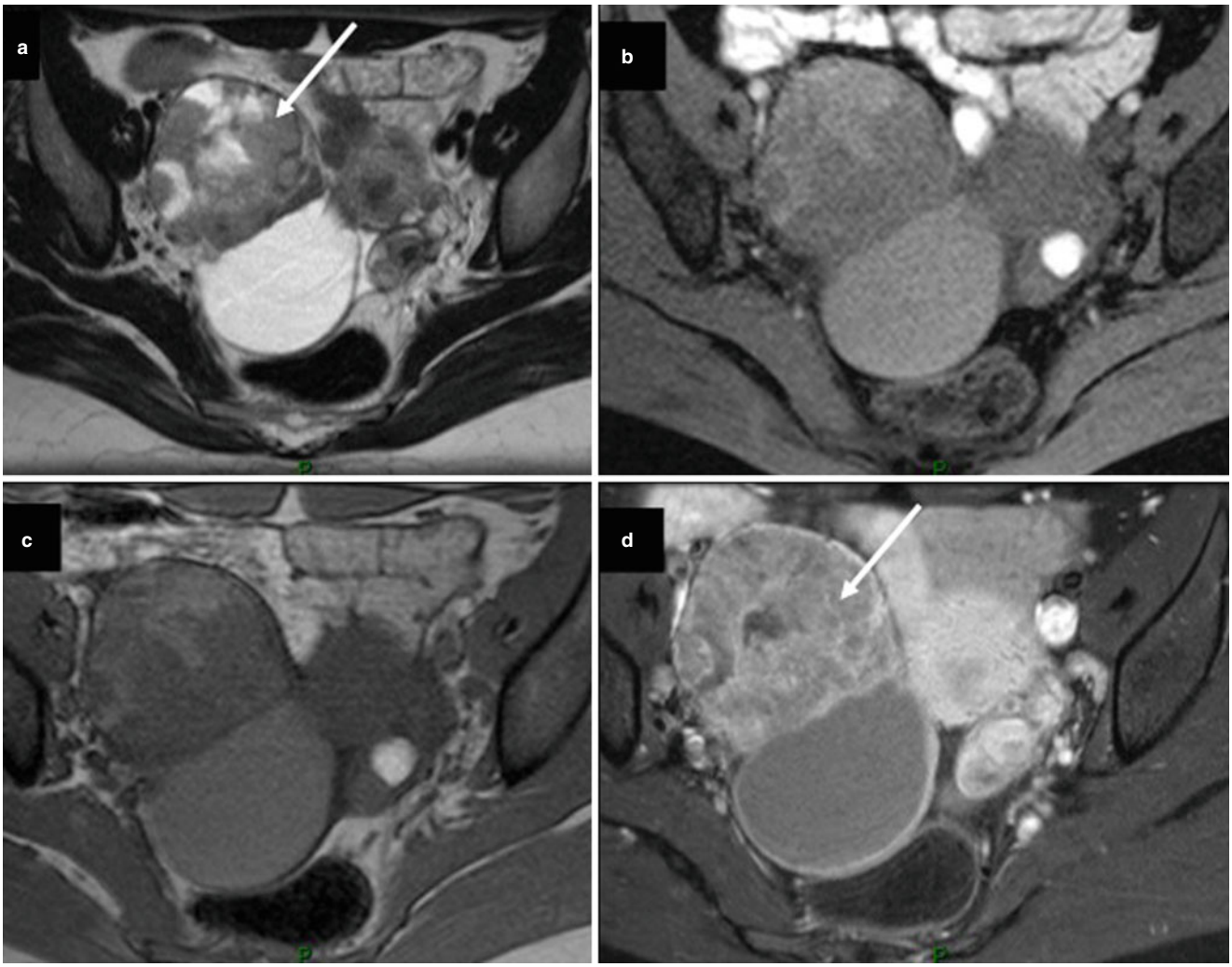

Fig. 11 Images in a 31-year-old woman with endometrioid cystadenocarcinoma grade 1 FIGO stage IA associated with endometrial cyst. (**a**) Transversal T2-weighted MR image shows a solid-cystic right ovarian tumor. Solid portion displays heterogeneous intermediate signal intensity (*arrow*). (**b**) Transversal T1-weighted MR image with fat suppression shows cystic component displaying intermediate signal intensity, (**c**) transversal T1-weighted MR image without fat suppression shows cystic component displaying intermediate signal intensity, (**d**) transversal fat-suppressed T1-weighted MR image with fat suppression shows heterogeneous enhancement of solid component (*arrow*). Note the presence of contralateral small endometrial cyst displaying high signal intensity on T1-weighted MR images and shading on T2-weighted MR image

Mucinous Cystadenocarcinomas

Pseudomyxoma peritonei is another potential form of peritoneal spread and is by far the most common extraovarian manifestation of mucinous tumors. Pseudomyxoma peritonei is now clearly recognized to be subsequent to gastrointestinal tumor. Histologic examination discloses large pools of mucin surrounded by or associated with well-differentiated mucinous epithelial of intestinal type.

It is important to be aware that current thinking about the origin of pseudomyxoma peritonei has changed. It is now recognized that in the vast majority of cases, the primary tumor is actually from the appendix with metastases to the ovary, rather than being a primary ovarian tumor [67]. In every case of pseudomyxoma peritonei, the appendix should be thoroughly examined and special tissue testing done to differentiate pseudomyxoma peritonei of gastrointestinal origin from ovarian origin. Pseudomyxoma peritonei should be distinguished from localized collections of acellular mucin surrounding a ruptured mucinous ovarian tumor or an appendiceal mucocele (clement).

Several studies have reported the aspect of pseudomyxoma peritonei on CT or MR imaging. Computed tomography is the most widely used technique in diagnosing and determining the extent of pseudomyxoma peritonei [68]. Mucinous peritoneal implants generally have low attenuation on CT scans and do not calcify [67]. Mucinous ascites is generally heterogeneous and of fat density with attenuation values greater than those of water [69]. The amorphous,

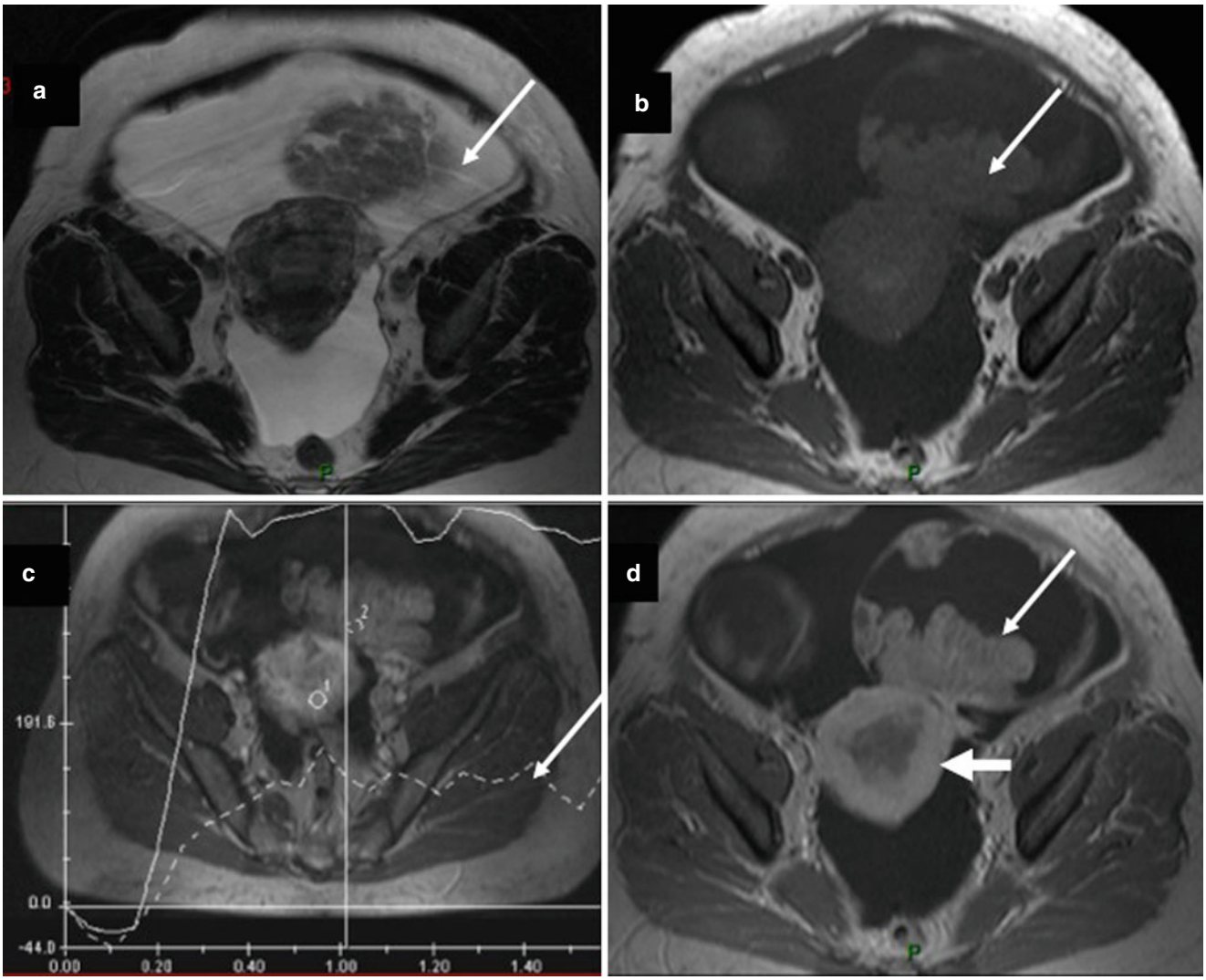

Fig. 12 Images in a 59-year-old woman with bilateral endometrioid ovarian cystadenocarcinoma associated with endometrioid endometrial cystadenocarcinoma. (**a**) Transversal T2-weighted MR image shows a solid-cystic right ovarian tumor. Solid portion displays heterogeneous intermediate signal intensity (*arrow*). (**b**) Transversal T1-weighted MR image without fat suppression, (**c**) transversal DCE MR imaging shows a curve type 2 in right irregular solid mass, (**d**) transversal fat-suppressed T1-weighted MR image with fat suppression shows heterogeneous enhancement of solid component (*arrow*). Note endometrial irregular thickening related to endometrial carcinoma (*large arrow*)

mucoid material insinuates itself around and in between the mesenteric reflections, bowel, and solid organs. The low attenuation and diffuse nature of this process may be confused with ascites. Unlike simple ascites, however, pseudomyxoma peritonei has mass effect and causes scalloping along the liver capsule and abdominal organs. Scalloping refers to extrinsic pressure on the liver or splenic margins by adjacent peritoneal implants without parenchymal metastases. Due to mass effect, bowel loops are displaced centrally and posteriorly, rather than free floating, and subtle septations may be noted [70]. Curvilinear calcifications (though infrequent) and omental thickening, if found, may reinforce the diagnosis of pseudomyxoma peritonei [68].

The role of MR imaging in patients with pseudomyxoma peritonei is still being investigated. Based on a limited number of patients reported in the medical literature, MR imaging may prove more helpful than CT in assessing the rare visceral invasion by the mucinous tumor [71]. In a recent study, Siegelman et al. suggested that some MR characteristics of pseudomyxoma peritonei could be highlighted [35]. Hence, mucin displays low to intermediate and high signal intensity on T1- and T2-weighted MR imaging, respectively. In addition, a peripheral enhancement with or without lacelike can be present [35]. In three cases of pseudomyxoma peritonei analyzed by MR imaging findings, Buy et al. suggested that both implants and mucoid ascites displayed a low signal intensity on T1-weighted

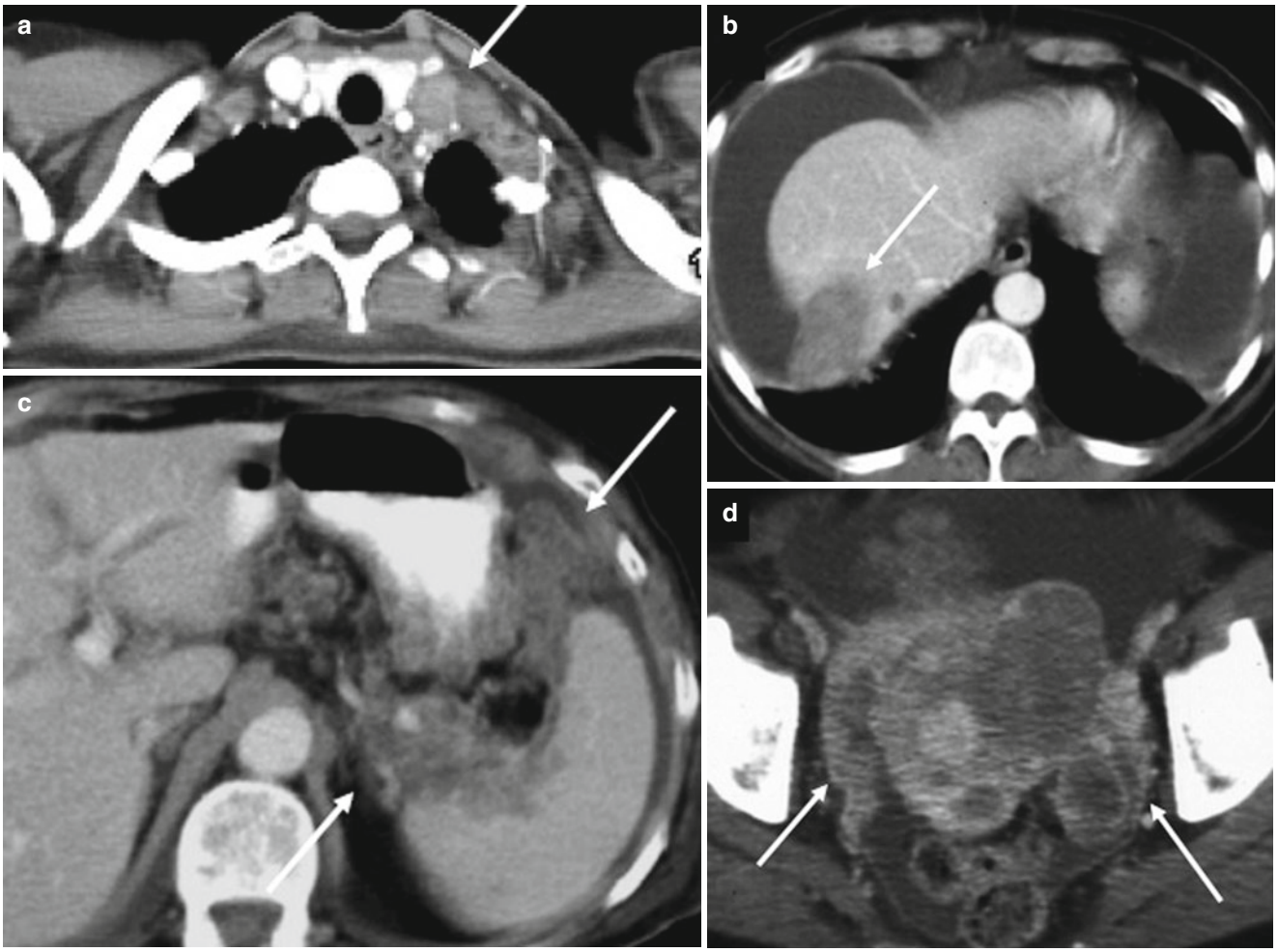

Fig. 13 Multidetector computed tomography (MCT) images in a 72-year-old woman with advanced serous ovarian carcinoma FIGO stage IV. (**a**) MCT image passing through pulmonary apex shows left supraclavicular lymph node metastasis (*arrow*). (**b**) MCT image passing through the liver shows liver capsule metastasis (*arrow*), (**c**) MCT image shows gastrosplenic and pancreaticosplenic ligament carcinomatosis (*arrow*), (**d**) MCT image passing through the pelvis shows frozen pelvis (*arrow*)

images close to that of muscle tissue. On T2-weighted images, there was general hyperintensity of signals, which was more pronounced in mucoid ascites than in implants and which approached signal intensities of water [71].

In conclusion, serous, mucinous, and endometrioid ovarian cancers have suggestive histopathological features that can be used when performing MRI and MCT for characterization and staging.

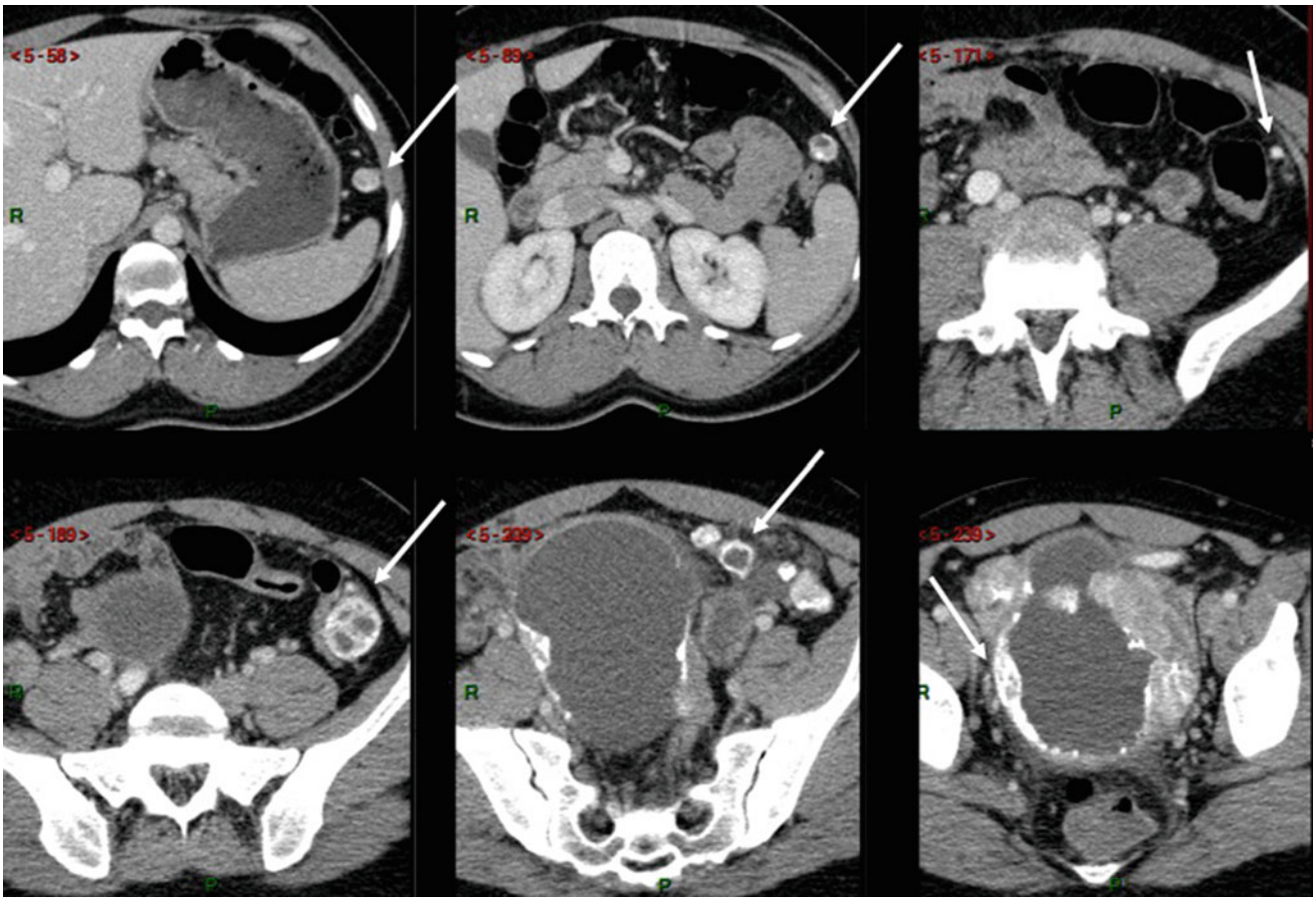

Fig. 14 Multidetector computed tomography (MCT) images in a 27-year-old woman with advanced serous ovarian carcinoma FIGO stage IIIC show calcific deposits within ovarian cancer and in multiple peritoneal metastases (*arrows*)

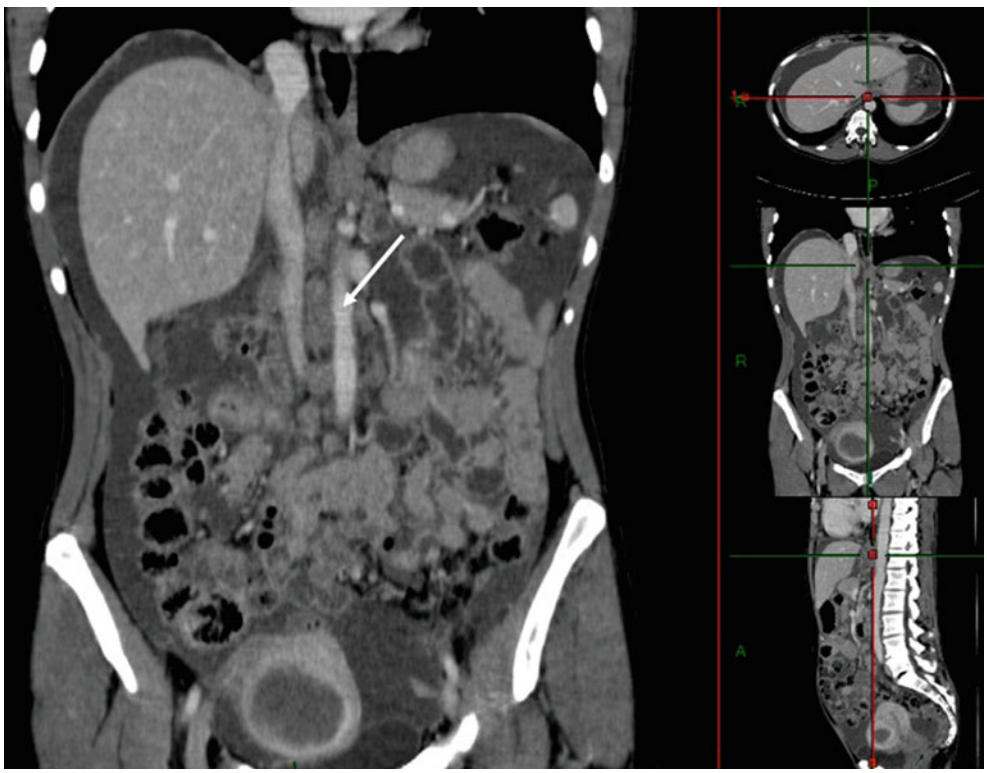

Fig. 15 Multidetector computed tomography (MCT) image in a 68-year-old woman with advanced serous ovarian carcinoma FIGO stage IIIC shows several retroperitoneal lymph nodes (*arrow*)

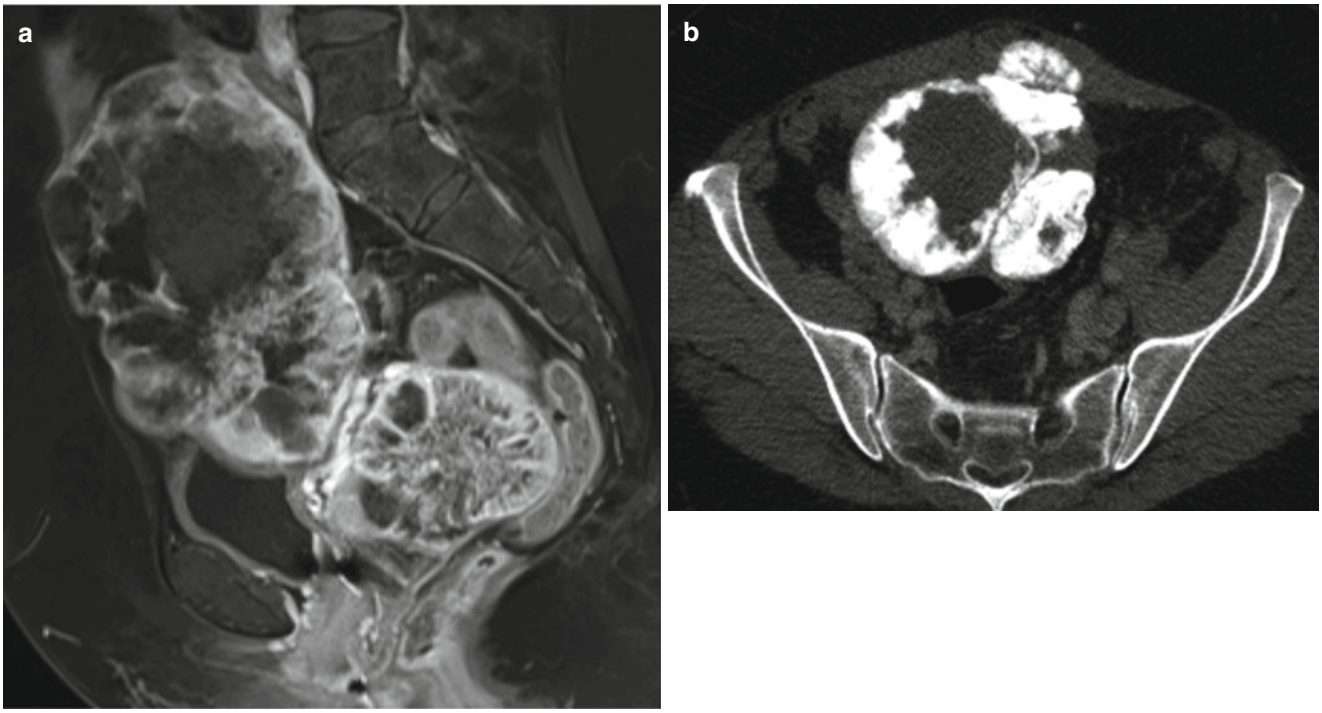

Fig. 16 Images in a 69-year-old woman with bilateral ovarian psammocarcinoma. (**a**) Postcontrast sagittal T1-weigthed MR image with fat suppression shows bilateral solid-cystic malignant ovarian tumors, (**b**) MCT image shows diffuse calcifications within right ovarian tumor highly suggestive of psammocarcinoma

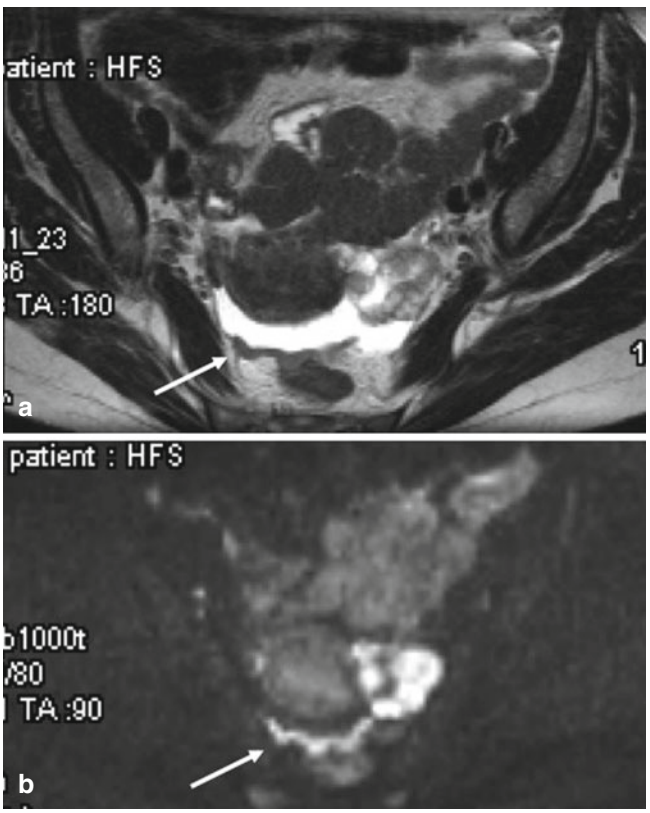

Fig. 17 Images in a 60-year-old woman with serous ovarian cystadenocarcinoma FIGO stage IIIC. (**a**) Transversal T2-weigthed MR image shows ovarian tumor associated with peritoneal thickening (*arrow*), (**b**) transversal DW MR image at the same level shows high signal intensity of peritoneal carcinomatosis (*arrow*)

References

1. Scully E, Young J, Clement PB. Surface epithelial-stromal tumors. In: Rosai J, editor. Tumors of the ovary and maldeveloped gonads, fallopian tube, and broad ligament. Washington, D.C.: Armed Forces Institute of Pathology; 1998. p. 53–168.
2. Buy JN, Ghossain MA, Sciot C, Bazot M, Guinet C, Prevot S, et al. Epithelial tumors of the ovary: CT findings and correlation with US. Radiology. 1991;178:811–8.
3. Ghossain MA, Buy JN, Ligneres C, Bazot M, Hassen K, Malbec L, et al. Epithelial tumors of the ovary: comparison of MR and CT findings. Radiology. 1991;181:863–70.
4. Forstner R, Hricak H, Occhipinti KA, Powell CB, Frankel SD, Stern JL. Ovarian cancer: staging with CT and MR imaging. Radiology. 1995;197:619–26.
5. Hricak H, Chen M, Coakley FV, Kinkel K, Yu KK, Sica G, et al. Complex adnexal masses: detection and characterization with MR imaging– multivariate analysis. Radiology. 2000;214:39–46.
6. Kinkel K, Lu Y, Mehdizade A, Pelte MF, Hricak H. Indeterminate ovarian mass at US: incremental value of second imaging test for characterization – meta-analysis and Bayesian analysis. Radiology. 2005;236:85–94.
7. Qayyum A, Coakley FV, Westphalen AC, Hricak H, Okuno WT, Powell B. Role of CT and MR imaging in predicting optimal cytoreduction of newly diagnosed primary epithelial ovarian cancer. Gynecol Oncol. 2005;96:301–6.
8. Sala E, DeSouza N, Lee SI, Atri M, Hricak H. Ovarian cancer: the role of functional imaging as an end point in clinical trials. Int J Gynecol Cancer. 2010;20:971–8.
9. Stevens SK, Hricak H, Stern JL. Ovarian lesions: detection and characterization with gadolinium- enhanced MR imaging at 1.5 T. Radiology. 1991;181:481–8.
10. Sohaib SA, Sahdev A, Van Trappen P, Jacobs IJ, Reznek RH. Characterization of adnexal mass lesions on MR imaging. AJR Am J Roentgenol. 2003;180:1297–304.

11. Bazot M, Darai E, Nassar-Slaba J, Lafont C, Thomassin-Naggara I. Value of magnetic resonance imaging for the diagnosis of ovarian tumors: a review. J Comput Assist Tomogr. 2008;32:712–23.
12. Bazot M, Nassar-Slaba J, Thomassin-Naggara I, Cortez A, Uzan S, Darai E. MR imaging compared with intraoperative frozen-section examination for the diagnosis of adnexal tumors; correlation with final histology. Eur Radiol. 2006;16:2687–99.
13. Thomassin-Naggara I, Bazot M, Darai E, Callard P, Thomassin J, Cuenod CA. Epithelial ovarian tumors: value of dynamic contrast-enhanced MR imaging and correlation with tumor angiogenesis. Radiology. 2008;248:148–59.
14. Thomassin-Naggara I, Darai E, Cuenod CA, Fournier L, Toussaint I, Marsault C, et al. Contribution of diffusion-weighted MR imaging for predicting benignity of complex adnexal masses. Eur Radiol. 2009;19:1544–52.
15. Thomassin-Naggara I, Darai E, Cuenod CA, Rouzier R, Callard P, Bazot M. Dynamic contrast-enhanced magnetic resonance imaging: a useful tool for characterizing ovarian epithelial tumors. J Magn Reson Imaging. 2008;28:111–20.
16. Thomassin-Naggara I, Toussaint I, Perrot N, Rouzier R, Cuenod CA, Bazot M, et al. Characterization of complex adnexal masses: value of adding perfusion- and diffusion-weighted MR imaging to conventional MR imaging. Radiology. 2011;258:793–803.
17. Forstner R, Sala E, Kinkel K, Spencer JA. ESUR guidelines: ovarian cancer staging and follow-up. Eur Radiol. 2010;20:2773–80.
18. Spencer JA. A multidisciplinary approach to ovarian cancer at diagnosis. Br J Radiol. 2005;78 Spec No 2:S94–102.
19. Spencer JA, Forstner R, Cunha TM, Kinkel K. ESUR guidelines for MR imaging of the sonographically indeterminate adnexal mass: an algorithmic approach. Eur Radiol. 2011;20:25–35.
20. Van Vierzen PB, Massuger LF, Ruys SH, Barentsz JO. Borderline ovarian malignancy: ultrasound and fast dynamic MR findings. Eur J Radiol. 1998;28:136–42.
21. Russell P. Surface epithelial-stromal tumors of the ovary. In: Kurman R, editor. Blaustein's pathology of the female genital tract. New York: Springer; 1995. p. 705–82.
22. Boger-Megiddo I, Weiss NS. Histologic subtypes and laterality of primary epithelial ovarian tumors. Gynecol Oncol. 2005;97: 80–3.
23. Boyd C, McCluggage WG. Low-grade ovarian serous neoplasms (low-grade serous carcinoma and serous borderline tumor) associated with high-grade serous carcinoma or undifferentiated carcinoma: report of a series of cases of an unusual phenomenon. Am J Surg Pathol. 2012;36:368–75.
24. Kurman RJ, McConnell TG. Characterization and comparison of precursors of ovarian and endometrial carcinoma: parts I and II. Int J Surg Pathol. 2010;18:181S–9.
25. Lee KR, Russel P, Tavassoli FA. Tumours of the ovary and peritoneum. In: Tavassoli FA, Devilee P, editors. WHO classification: tumors of the breast and female genital organs. Lyon: IARC Press; 2003. p. 113–202.
26. Brown DL, Doubilet PM, Miller FH, Frates MC, Laing FC, DiSalvo DN, et al. Benign and malignant ovarian masses: selection of the most discriminating gray-scale and Doppler sonographic features. Radiology. 1998;208:103–10.
27. Jeong YY, Outwater EK, Kang HK. Imaging evaluation of ovarian masses. Radiographics. 2000;20:1445–70.
28. Outwater EK, Huang AB, Dunton CJ, Talerman A, Capuzzi DM. Papillary projections in ovarian neoplasms: appearance on MRI. J Magn Reson Imaging. 1997;7:689–95.
29. Granberg S, Wikland M, Jansson I. Macroscopic characterization of ovarian tumors and the relation to the histological diagnosis: criteria to be used for ultrasound evaluation. Gynecol Oncol. 1989;35:139–44.
30. Thomassin-Naggara I, Cuenod CA, Darai E, Marsault C, Bazot M. Dynamic contrast-enhanced MR imaging of ovarian neoplasms: current status and future perspectives. Magn Reson Imaging Clin N Am. 2008;16:661–72, ix.
31. Thomassin-Naggara I, Balvay D, Aubert E, Darai E, Rouzier R, Cuenod CA, et al. Quantitative dynamic contrast-enhanced MR imaging analysis of complex adnexal masses: a preliminary study. Eur Radiol. 2012;22:738–45.
32. Roussel A, Thomassin-Naggara I, Darai E, Marsault C, Bazot M. Value of diffusion-weighted imaging in the evaluation of adnexal tumors. J Radiol. 2009;90:589–96.
33. deSouza NM, O'Neill R, McIndoe GA, Dina R, Soutter WP. Borderline tumors of the ovary: CT and MRI features and tumor markers in differentiation from stage I disease. AJR Am J Roentgenol. 2005;184:999–1003.
34. Bazot M, Lafont C, Roussel A, Jarboui L, Nassar-Slaba J, Thomassin-Naggara I. Soft tissue characterization of the female pelvis with MRI. J Radiol. 2010;91:453–64.
35. Siegelman ES, Outwater EK. Tissue characterization in the female pelvis by means of MR imaging. Radiology. 1999;212:5–18.
36. Bazot M, Haouy D, Darai E, Cortez A, Dechoux-Vodovar S, Thomassin-Naggara I. Is MRI a useful tool to distinguish between serous and mucinous borderline ovarian tumours? Clin Radiol. 2013;1:47–54.
37. Kim SH, Yang DM. Borderline serous surface papillary tumor of the ovary: MRI characteristics. AJR Am J Roentgenol. 2005; 184:1898–900.
38. Tanaka YO, Okada S, Satoh T, Matsumoto K, Oki A, Nishida M, et al. Ovarian serous surface papillary borderline tumors form sea anemone-like masses. J Magn Reson Imaging. 2011;33:643–40.
39. Wagner BJ, Buck JL, Seidman JD, McCabe KM. From the archives of the AFIP. Ovarian epithelial neoplasms: radiologic- pathologic correlation. Radiographics. 1994;14:1351–74. quiz 75–6.
40. Kawamoto S, Urban BA, Fishman EK. CT of epithelial ovarian tumors. Radiographics. 1999;19 Spec No:S85–102; quiz S263-4.
41. Okada S, Ohaki Y, Inoue K, Kawamura T, Hayashi T, Kato T, et al. Calcifications in mucinous and serous cystic ovarian tumors. J Nippon Med Sch. 2005;72:29–33.
42. Burkill GJ, Allen SD, A'Hern RP, Gore ME, King DM. Significance of tumour calcification in ovarian carcinoma. Br J Radiol. 2009; 82:640–4.
43. Okamoto Y, Tanaka YO, Tsunoda H, Yoshikawa H, Minami M. Malignant or borderline mucinous cystic neoplasms have a larger number of loculi than mucinous cystadenoma: a retrospective study with MR. J Magn Reson Imaging. 2007;26:94–9.
44. Matsuki M, Kaji Y, Matsuo M, Kobashi Y. Struma ovarii: MRI findings. Br J Radiol. 2000;73:87–90.
45. Scully RE, Young RH, Clement PB. Germ cell tumors. In: Rosai J, editor. Tumors of the ovary and maldeveloped gonads, fallopian tube, and broad ligament. Washington, D.C.: Armed Forces Institute of Pathology; 1998. p. 226–99.
46. Jung SE, Rha SE, Lee JM, Park SY, Oh SN, Cho KS, et al. CT and MRI findings of sex cord-stromal tumor of the ovary. AJR Am J Roentgenol. 2005;185:207–15.
47. Jung SE, Lee JM, Rha SE, Byun JY, Jung JI, Hahn ST. CT and MR imaging of ovarian tumors with emphasis on differential diagnosis. Radiographics. 2002;22:1305–25.
48. Outwater EK, Siegelman ES, Kim B, Chiowanich P, Blasbalg R, Kilger A. Ovarian Brenner tumors: MR imaging characteristics. Magn Reson Imaging. 1998;16:1147–53.
49. Moon WJ, Koh BH, Kim SK, Kim YS, Rhim HC, Cho OK, et al. Brenner tumor of the ovary: CT and MR findings. J Comput Assist Tomogr. 2000;24:72–6.
50. Tanaka YO, Yoshizako T, Nishida M, Yamaguchi M, Sugimura K, Itai Y. Ovarian carcinoma in patients with endometriosis: MR imaging findings. AJR Am J Roentgenol. 2000;175:1423–30.
51. Young RH, Scully RE. Metastatic tumors of the ovary. In: Kurman R, editor. Blaustein's pathology of the female genital tract. New York: Springer; 1995. p. 939–74.
52. Kurtz AB, Tsimikas JV, Tempany CM, Hamper UM, Arger PH, Bree RL, et al. Diagnosis and staging of ovarian cancer: comparative values of Doppler and conventional US, CT, and MR imaging

correlated with surgery and histopathologic analysis – report of the Radiology Diagnostic Oncology Group. Radiology. 1999; 212:19–27.
53. Brown DL, Zou KH, Tempany CM, Frates MC, Silverman SG, McNeil BJ, et al. Primary versus secondary ovarian malignancy: imaging findings of adnexal masses in the Radiology Diagnostic Oncology Group Study. Radiology. 2001;219:213–8.
54. Tempany CM, Zou KH, Silverman SG, Brown DL, Kurtz AB, McNeil BJ. Staging of advanced ovarian cancer: comparison of imaging modalities – report from the Radiological Diagnostic Oncology Group. Radiology. 2000;215:761–7.
55. Kyriazi S, Collins DJ, Morgan VA, Giles SL, deSouza NM. Diffusion-weighted imaging of peritoneal disease for noninvasive staging of advanced ovarian cancer. Radiographics. 2010; 30:1269–85.
56. Dromain C, Leboulleux S, Auperin A, Goere D, Malka D, Lumbroso J, et al. Staging of peritoneal carcinomatosis: enhanced CT vs. PET/CT. Abdom Imaging. 2008;33:87–93.
57. Buy JN, Moss AA, Ghossain MA, Sciot C, Malbec L, Vadrot D, et al. Peritoneal implants from ovarian tumors: CT findings. Radiology. 1988;169:691–4.
58. Mitchell DG, Hill MC, Hill S, Zaloudek C. Serous carcinoma of the ovary: CT identification of metastatic calcified implants. Radiology. 1986;158:649–52.
59. Choi CH, Kim TJ, Kim WY, Ahn GH, Lee JW, Kim BG, et al. Papillary serous carcinoma in ovaries of normal size: a clinicopathologic study of 20 cases and comparison with extraovarian peritoneal papillary serous carcinoma. Gynecol Oncol. 2007;105:762–8.
60. Hiromura T, Tanaka YO, Nishioka T, Tomita K. Serous psammocarcinoma of the ovary: CT and MR findings. J Comput Assist Tomogr. 2007;31:490–2.
61. Fujii S, Matsusue E, Kanasaki Y, Kanamori Y, Nakanishi J, Sugihara S, et al. Detection of peritoneal dissemination in gynecological malignancy: evaluation by diffusion-weighted MR imaging. Eur Radiol. 2008;18:18–23.
62. Low RN, Sebrechts CP, Barone RM, Muller W. Diffusion-weighted MRI of peritoneal tumors: comparison with conventional MRI and surgical and histopathologic findings – a feasibility study. AJR Am J Roentgenol. 2009;193:461–70.
63. Vergote I, Trope CG, Amant F, Kristensen GB, Ehlen T, Johnson N, et al. Neoadjuvant chemotherapy or primary surgery in stage IIIC or IV ovarian cancer. N Engl J Med. 2010;363:943–53.
64. Chi DS, Liao JB, Leon LF, Venkatraman ES, Hensley ML, Bhaskaran D, et al. Identification of prognostic factors in advanced epithelial ovarian carcinoma. Gynecol Oncol. 2001;82:532–7.
65. Chereau E, Ballester M, Selle F, Cortez A, Darai E, Rouzier R. Comparison of peritoneal carcinomatosis scoring methods in predicting resectability and prognosis in advanced ovarian cancer. Am J Obstet Gynecol. 2010;202:178.e1–10.
66. Sala E, Kataoka MY, Priest AN, Gill AB, McLean MA, Joubert I, et al. Advanced ovarian cancer: multiparametric MR imaging demonstrates response- and metastasis-specific effects. Radiology. 2012;263:149–59.
67. Woodward PJ, Hosseinzadeh K, Saenger JS. From the archives of the AFIP: radiologic staging of ovarian carcinoma with pathologic correlation. Radiographics. 2004;24:225–46.
68. Walensky RP, Venbrux AC, Prescott CA, Osterman Jr FA. Pseudomyxoma peritonei. AJR Am J Roentgenol. 1996;167:471–4.
69. Seshul MB, Coulam CM. Pseudomyxoma peritonei: computed tomography and sonography. AJR Am J Roentgenol. 1981;136:803–6.
70. Yeh HC, Shafir MK, Slater G, Meyer RJ, Cohen BA, Geller SA. Ultrasonography and computed tomography in pseudomyxoma peritonei. Radiology. 1984;153:507–10.
71. Buy JN, Malbec L, Ghossain MA, Guinet C, Ecoiffier J. Magnetic resonance imaging of pseudomyxoma peritonei. Eur J Radiol. 1989;9:115–8.

Rare Malignant Tumor (Clear Cell Adenocarcinoma, Transitional Cell Carcinoma, Malignant Brenner Tumor) (Clinical Setting and US)

Testa Antonia Carla, Ludovisi Manuela, De Blasis Ilaria, Giansiracusa Carmelo, and Mascilini Floriana

Abstract

Clear cell carcinomas and transitional cell tumors represent rare histotypes of epithelial ovarian tumors. Two clinicopathologic types of malignant transitional cell tumor have been described: malignant Brenner tumor, in which a benign or atypical proliferative (borderline) Brenner component is identified within or contiguous with the tumor, and transitional cells carcinoma (TCC), in which no benign or borderline Brenner is identified.

Keywords

Brenner tumor • Transitional carcinoma • Clear cell • Imaging • Ultrasound

More than 90 % of ovarian malignancies are derived from the surface epithelium, mainly of serous or mucinous type [1]. Clear cell carcinomas and transitional cell tumors represent rare histotypes of epithelial ovarian tumors.

Clear Cell Tumors

Pathology and Clinical Setting

The vast majority of clear cell neoplasms of the ovaries are carcinomas and comprise 8.5 % of ovarian carcinomas. Clear cell adenofibromas and atypical proliferative (borderline) clear cell neoplasms are extremely rare. The mullerian nature of clear cell tumors of the ovary, previously thought to be of mesonephric origin, is endorsed by close association with endometriosis, their frequent admixture with endometrioid carcinoma, the occurrence of identical tumors in the endometrium, and their origin in vaginal adenosis in DES-exposed women [2]. Among all cell types of ovarian carcinoma, clear cell carcinoma holds the strongest association with endometriosis.

The mean age of patients with clear cell carcinoma is 50–53 years. Symptoms usually relate to a pelvic or abdominal mass. Clear cell carcinoma is the most common epithelial ovarian neoplasm to be associated with vascular thrombotic events and paraneoplastic hypercalcemia [3, 4].

About 35–60 % of clear cell carcinomas present in FIGO stage I and 9–22 % in stage II [5–7]. Several recent studies have shown that stage I clear cell carcinoma is more likely to be stage IC as compared to the other cell type. The reason for this is not clear, but it seems to be correlated with a higher risk of tumor rupture [2].

There are conflicting data on the behavior of clear cell carcinoma. Historically, clear cells carcinomas have foreboded a very poor outcome. Nevertheless, this has not been confirmed in many recent studies where large series have been analyzed [8, 9]. Similar to all ovarian carcinomas, FIGO stage I cell carcinoma has a 90 % or better 5-year survival. Evidence that clear cell histology in advanced stage is an adverse prognostic factor is rather more convincing [8, 10]. The treatment is similar to that of other epithelial cell types of ovarian carcinoma.

T.A. Carla (✉) • L. Manuela
D.B. Ilaria • G. Carmelo • M. Floriana
Department of Gynecology,
Catholic University of Sacred Heart,
Largo A. Gemelli 8, Rome 00168, Italy

L. Saba et al. (eds.), *Ovarian Neoplasm Imaging*,
DOI 10.1007/978-1-4614-8633-6_16,

Macroscopy

The size of clear cell carcinomas ranges up to 30 cm with a mean of about 13–15 cm [2]. Although they may be solid, more commonly the cut surface reveal a thick-walled unilocular cyst with multiple yellow-beige fleshy nodules protruding into the lumen or a multilocular mass with loculles containing watery or mucinous fluid. Most tumor arise in endometriosis and display features of an endometriotic cyst which typically contains chocolate-brown fluid, and thickened polypoid or nodular area in the wall, or a larger solid area reflecting the focus of malignant transformation [2].

Ultrasound

In the literature, sonographic characteristics of clear cell carcinomas are usually described together with the other more common "epithelial malignant tumors," and a separate analysis of this type of malignancy has not usually reported. In Valentin's paper [11], for instance, 11 cases with clear cells carcinomas were included, but no detailed assessment was made in this subgroup of cancers.

Only recently, a paper by Alcazar et al. [1] reported the ultrasound features of 16 cases of clear cell carcinomas.

According to the morphology at grayscale evaluation, 13 (81 %) of 16 tumors were unilocular/multilocular-solid, one (6 %) tumor was unilocular, and two (13 %) were solid. Median size was 231 ml (range 9–2,432). All tumors but one were vascularized at color Doppler, with moderate and rich vascularization in 13 (81 %) cases.

In a study aimed at comparing the sonographic patterns of borderline tumors and primary ovarian cancers arising in endometrioid cysts versus sonographic features of benign endometriotic cysts, six cases of clear cell carcinoma arising in endometriotic cysts have been collected (five cases were FIGO stage I and one case FIGO stage II disease). All cases were characterized by the presence of solid tissue, vascularized at color Doppler examination [12].

Ultrasound images of clear cell carcinoma are shown in Figs. 1, 2, and 3.

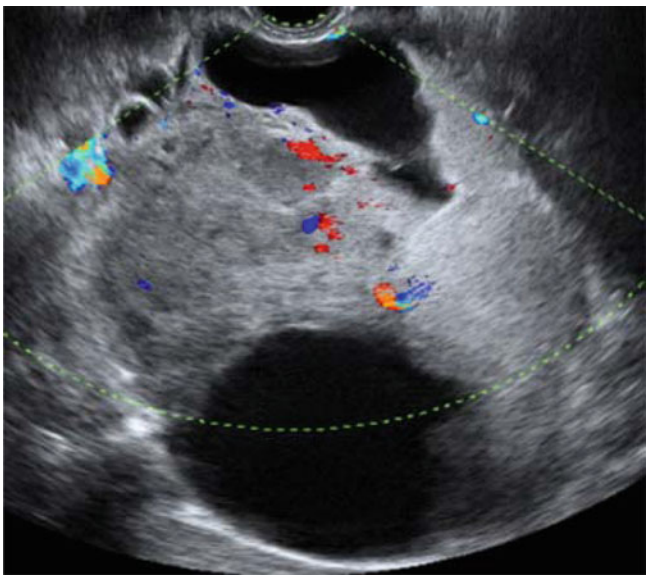

Fig. 1 Ultrasound image of a clear cell carcinoma in a 74-year-old woman showing a multilocular-solid mass with minimal vascularization at color Doppler examination

Transitional Cells Tumors

Pathology and Clinical Setting

Transitional cells tumors comprise 10 % of ovarian epithelial tumors. The transitional epithelial cell type, characterized by a relatively uniform population of stratified cells with ovoid nuclei displaying nuclear grooves, is named because of its resemblance to urothelium [2].

Two clinicopathologic types of malignant transitional cell tumor have been described: malignant Brenner tumor, in which a benign or atypical proliferative (borderline) Brenner component is identified within or contiguous with the tumor, and transitional cells carcinomas (TCC), in which no benign or borderline Brenner is identified [13].

The histologic patterns of TCC are often mixed with other types of carcinoma, most often serous. Approximately 10 % of ovarian carcinomas containing the TCC pattern are said to be pure. More than 50 % of the tumor should display the pattern of TCC for a diagnosis of TCC. In addition to not having a benign Brenner tumor component, TCC lacks the prominent stromal calcification [14–16].

Since TCC of the ovary has marked morphological similarities to TCC of the bladder and it behaves more aggressive than malignant Brenner tumors, Austin and Norris [14] concluded that ovarian TCC arises directly from the pluripotent surface epithelium of the ovary and from cells with urothelial potential, rather than from a benign or proliferative Brenner tumor precursor.

Eichhorn and Young provided a detailed description of ovarian TCC [17], which typically displays undulating, diffuse, insular, and trabecular growth patterns. The tumor cell nuclei are oblong or round, often exhibiting nucleoli with longitudinal patterns. The cytoplasm is often pale and granular and is rarely clear or eosinophilic.

Malignant Brenner tumors occur at a mean age of 63 years, while TCCs present at a mean age of 56 years.

Almost all Brenner tumors are asymptomatic and discovered by chance, for example, at the time of imaging for an unrelated indication or at surgery [13, 17–22]. Among patients

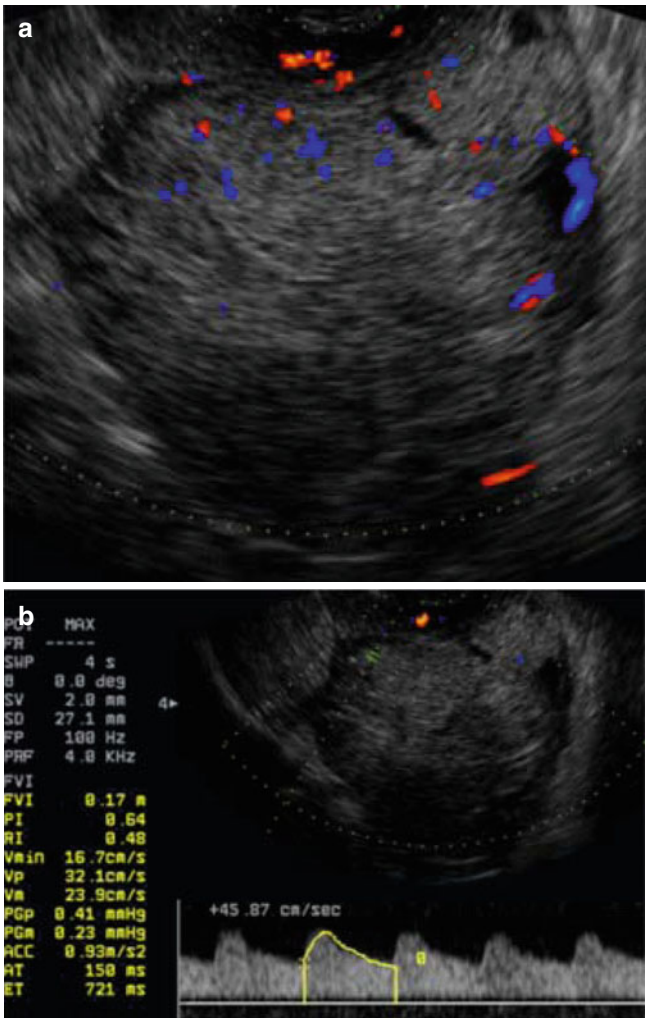

Fig. 2 Ultrasound image of a clear cell carcinoma in a 63-year-old woman showing a solid mass moderately vascularized at color Doppler examination (**a**) with high velocities (Peak Systolic Velocity = 32 cm/s) (**b**)

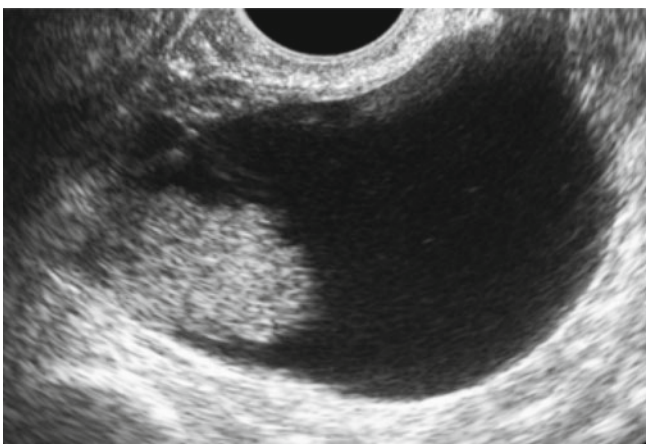

Fig. 3 Ultrasound image of a clear cell carcinoma in a 48-year-old woman showing a unilocular-solid mass. The internal cyst wall is irregular with a large protruding solid component

who are symptomatic, vaginal bleeding (explained by estrogenic activity) [13, 19, 23–25], pelvic pain, or the presence of a palpable pelvic mass are frequently reported [24, 25]. Patients may also present with urinary retention [15], ascites [1], or Meigs' syndrome [2]. The common presenting symptoms of TCC of the ovary are abdominal pain, abdominal swelling or distension, and weight loss. Occasionally, the patient may present with uterine bleeding, back pain, and bowel or urinary symptoms. However, the clinical presentation is not discernible from other types of ovarian carcinoma [14, 17].

CA125 is clinically useful as a serum marker of advanced stages, tumor progression, and recurrence, although early stages may be CA125-negative.

The stage distribution of malignant Brenner tumor is as follows: stage I, 64 %; stage II, 12 %; stage III, 18 %; and stage IV, 6 %. In contrast, 53 % of TCCs present in advanced stage [2].

Ovarian TCC is clinically different from malignant Brenner tumor.

TCC presents in advanced stages, while most malignant Brenner tumors present in stage I. TCC is a variant of high-grade serous carcinoma and thus is a type II tumor. In contrast, malignant Brenner tumor has features of a type I tumor [2].

Because of the rarity of malignant Brenner tumors, there is little information on the prognosis and long-term survival of women with borderline or malignant Brenner tumors [26].

Given that malignant Brenner tumors are rare, we find scant information on the prognosis and long-term survival of women with borderline or malignant Brenner tumors [26].

Progression of malignant Brenner tumors is associated with metastases within the abdominal cavity [19]. Metastases are also seen in the pleura, lungs, kidneys, liver, urinary bladder, and skeleton [27]. Long-term disease-free survival is extremely rare, although well-differentiated tumors appear to have a better prognosis [25]. Roth described 14 patients with a borderline tumor: during a follow-up time of 6 months to 10 years, 13 patients remained disease-free, and the 14th patient died of acute leukemia shortly after diagnosis [25].

TCC is more chemosensitive than serous carcinoma. Patients with TCC had better prognosis compared to patients with all other types of ovarian carcinomas following standardized chemotherapy [27], even if limited data of survival are available. The estimated 5-year survival following surgery for patients with TCC was 37 %, whereas for patients who received chemotherapy, survival was at 41 % [15, 16].

Macroscopy

The mean size of Brenner tumors is 14 cm (ranging up to 25 cm) and the mean size of TCCs is 10 cm [17].

In the malignant Brenner tumor, the benign Brenner component can be distinguished as a solid fibrous nodule within

a cyst wall. At times a malignant Brenner tumor can also be completely solid.

The gross appearance of TCC is similar to high-grade serous carcinoma, typically solid and cystic. The cysts may exhibit polypoid friable mural nodules, and the cyst fluid is watery or mucinous. Hemorrhage and necrosis may be remarkable.

In addition, malignant Brenner tumors, like their benign counterparts, often have marked stromal calcification that is usually speculated, in contrast to TCCs in which calcification is less common and more often psammomatous.

Ultrasound

A few papers in the literature deal with sonographic characteristics of malignant transitional cell tumors.

The large prospective multicenter study collecting sonographic characteristics of ovarian tumors (International Ovarian Tumor analysis (IOTA) protocol) grouped these tumors in the subgroup of "rare malignancies," but a separate analysis of the different types was not performed.

There is only one recent publication describing 15 cases of transitional cells carcinoma. In all cases solid component was observed, 9 (60 %) of the 15 tumors being solid and 9 (40 %) being unilocular or multilocular-solid. Thirteen (87 %) cases were richly vascularized at color Doppler examination. Median size was 180 ml (range 6–1,766) [1].

As highlighted by the authors, no statistically significant differences between various types of malignant rare tumors were observed in terms of tumor size, morphology, and amount of vascularization.

As far as malignant Brenner tumors are concerned, clinical and sonographic characteristics were analyzed by Dierickx and colleagues in a recent multicenter study [26]. In a large series of 29 Brenner tumors they found 2 borderline and 3 invasively malignant Brenner tumors.

Whereas most benign Brenner tumors (17/24, 71 %) contained solid components and manifested no or minimal blood flow at Doppler examination (19/24, 79 %), 3 out of 5 (60 %) borderline and invasively malignant Brenner tumors contained solid components and 3 out of 5 (60 %) manifested moderate or high flow at color Doppler examination.

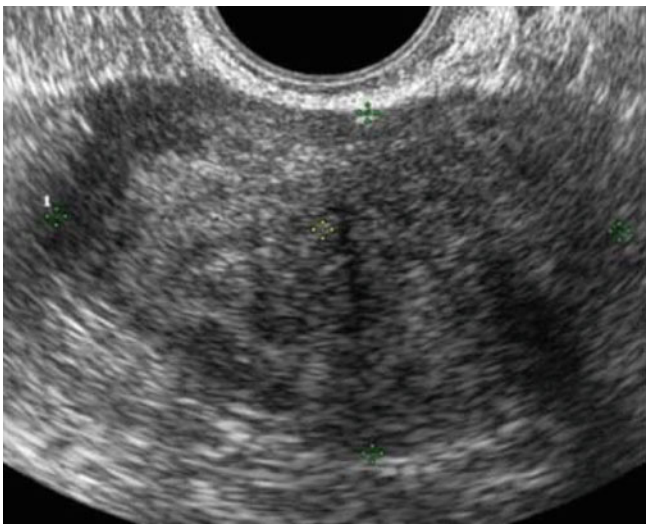

Fig. 4 Ultrasound image of a 5 cm purely solid benign Brenner tumor in a 60-year-old woman

Papillations were present in one of the two borderline tumors, and irregular internal cyst walls were noted in three (60 %) of the five malignancies. Information about calcifications was available for four malignant Brenner tumors and in three of these (75 %) calcifications were present.

In their paper, Diericks and colleagues failed to identify specific ultrasound features for Brenner tumors, and the number of borderline and invasively malignant Brenner tumors was too small to draw a conclusion and be able to describe possible typical ultrasound features of malignant Brenner tumors [26].

Ultrasound findings compatible with calcifications did seem to be common in Brenner tumors, and there were described in almost all malignant ones. However, the information on presence/absence of calcifications was collected retrospectively and it could have been biased; thus, it ought to be interpreted with caution.

Another publication by Hata et al. reports the ultrasound features of one borderline Brenner tumor. This borderline Brenner tumor was described as a 14 cm multilocular-solid tumor with papillations arising from its septae [28].

Ultrasound images of benign and borderline Brenner tumor are shown in Figs. 4 and 5.

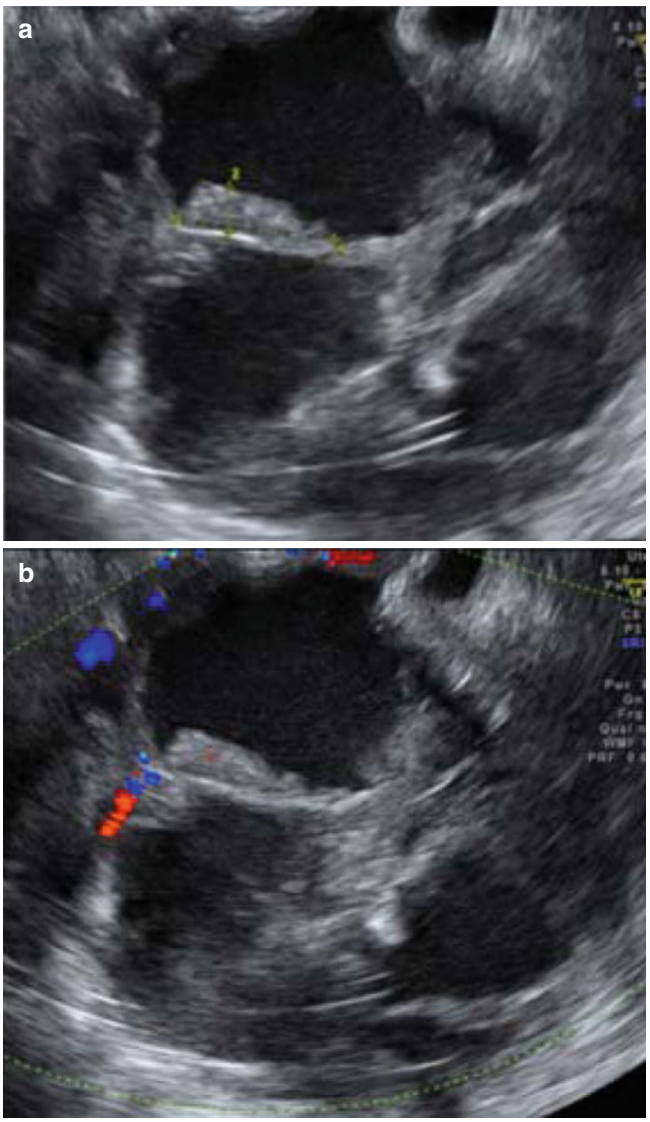

Fig. 5 Ultrasound images of a 16 cm multilocular-solid borderline Brenner tumor in a 60-year-old woman. The internal cyst wall and the septa are irregular because of multiple papillary projections (**a**) with minimal detectable blood flow at color Doppler examination (**b**)

References

1. Alcázar JL, Guerriero S, Pascual MÁ, Ajossa S, Olartecoechea B, Hereter L. Clinical and sonographic features of uncommon primary ovarian malignancies. J Clin Ultrasound. 2012;40:323–9.
2. Kurman RJ. Blaustein's pathology of the female genital tract. 6th ed. New York: Springer; 2011.
3. Pather S, Quinn MA. Clear cell cancer of the ovary-is it chemosensitive? Int J Gynecol Cancer. 2004;15:432–7.
4. Tan DSP, Kaye S. Ovarian clear cell adenocarcinoma: a continuing enigma. J Clin Pathol. 2007;60:355–60.
5. Chung HH, Hwang SY, Jung KW, Won YJ, Shin HR, Kim JW, Lee HP, Gynecologic Oncology Committee of Korean Society of Obstetrics and Gynecology. Ovarian cancer incidence and survival in Korea: 1993–2002. Int J Gynecol Cancer. 2007;17:595–600.
6. Mizuno M, Kikkawa F, Shibata K, Kajiyama H, Suzuki T, Ino K, Kawai M, Mizutani S. Long-term prognosis of stage I ovarian carcinoma. Prognostic importance of intraoperative rupture. Oncology. 2003;65:29–36.
7. Seidman JD, Yemelyanova AV, Khedmati F, Bidus MA, Dainty L, Boice CR, Cosin JA. Prognostic factors for stage I ovarian carcinoma. Int J Gynecol Pathol. 2010;29:1–7.
8. Chan JK, Teoh D, Hu JM, Shin JY, Osann K, Kapp DS. Do clear cell ovarian carcinomas have poorer prognosis compared to other epithelial cell types? A study of 1411 clear cell ovarian cancers. Gynecol Oncol. 2008;109:370–6.
9. Timmers PJ, Zwinderman AH, Teodorovic I, Vergote I, Trimbos JB. Clear cell carcinoma compared to serous carcinoma in early ovarian cancer: same prognosis in a large randomized trial. Int J Gynecol Cancer. 2009;19:88–93.
10. Chan JK, Tian C, Monk BJ, Herzog T, Kapp DS, Bell J, Young RC, Gynecologic Oncology Group. Prognostic factors for high-risk early-stage epithelial ovarian cancer: a Gynecologic Oncology Group study. Cancer. 2008;112:2202–10.
11. Van Holsbeke C, Van Belle V, Leone FP, Guerriero S, Paladini D, Melis GB, Greggi S, Fischerova D, De Jonge E, Neven P, Bourne T, Valentin L, Van Huffel S, Timmerman D. Prospective external validation of the 'ovarian crescent sign' as a single ultrasound parameter to distinguish between benign and malignant adnexal pathology. Ultrasound Obstet Gynecol. 2010;36:81–7.
12. Testa AC, Timmerman D, Van Holsbeke C, Zannoni GF, Fransis S, Moerman P, Vellone V, Mascilini F, Licameli A, Ludovisi M, Di Legge A, Scambia G, Ferrandina G. Ovarian cancer arising in endometrioid cysts: ultrasound findings. Ultrasound Obstet Gynecol. 2011;38:99–106.
13. Jorgensen EO, Dockerty MB, Wilson RB, Welch JS. Clinicopathologic study of 53 cases of Brenner's tumors of the ovary. Am J Obstet Gynecol. 1970;108:122–7.
14. Austin R, Norris H. Malignant Brenner tumor and transitional cell carcinoma of the ovary: a comparison. Int J Gynecol Pathol. 1987;6:29–39.
15. Tazi E, Lalya I, Tazi M, Ahellal Y, M'rabti H, Errihani H. Transitional cell carcinoma of the ovary: a rare case and review of literature. World J Surg Oncol. 2010;8:98–101.
16. Lin C, Liu F, Ho E. Transitional cell carcinoma of the ovary. Taiwan J Obstet Gynecol. 2006;45:268–71.
17. Eichhorn J, Young R. Transitional cell carcinoma of the ovary: a morphologic study of 100 cases with emphasis on differential diagnosis. Am J Surg Pathol. 2004;28:453–63.
18. Green GE, Mortele KJ, Glickman JN, Benson CB. Brenner tumors of the ovary: sonographic and computed tomographic imaging features. J Ultrasound Med. 2006;25:1245–51.
19. Balasa RW, Adcock LL, Prem KA, Dehner LP. The Brenner tumor: a clinicopathologic review. Obstet Gynecol. 1977;50:120–8.
20. Silverberg SG. Brenner tumor of the ovary: a clinicopathologic study of 60 tumors in 54 women. Cancer. 1971;28:588–96.
21. Ehrlich CE, Roth LM. The Brenner tumor. A clinicopathologic study of 57 cases. Cancer. 1971;27:332–42.
22. Fox H, Agrawal K, Langley FA. The Brenner tumour of the ovary: a clinicopathologic study of 54 cases. J Obstet Gynaecol Br Commonw. 1972;79:661–5.

23. Hermanns B, Faridi A, Rath W, Füzesi L, Schröder W. Differential diagnosis, prognostic factors, and clinical treatment of proliferative Brenner tumor of the ovary. Ultrastruct Pathol. 2000;24:191–6.
24. Yoonessi M, Abell MR. Brenner tumors of the ovary. Obstet Gynecol. 1979;54:90–6.
25. Roth LM, Czernobilsky B. Ovarian Brenner tumors. II. Malignant. Cancer. 1985;56:592–601.
26. Dierickx I, Valentin L, Van Holsbeke C, Jacomen G, Lissoni AA, Licameli A, Testa A, Bourne T, Timmerman D. Imaging in gynecological disease (7): clinical and ultrasound features of Brenner tumors of the ovary. Ultrasound Obstet Gynecol. 2012;40(6):706–13.
27. Kommoss F, Kommoss S, Schmidt D, Trunk M, Pfisterer J, du Bois A. Survival benefit for patients with advanced-stage transitional cell carcinomas vs. other subtypes of ovarian carcinoma after chemotherapy with platinum and paclitaxel. Gynecol Oncol. 2005;97:195–9.
28. Hata K, Hata T, Senoh D, Kitao M. Doppler ultrasound in a patient with ovarian Brenner tumor of low malignant potential: comparison with gray-scale ultrasound, magnetic resonance imaging and tumor marker suggesting malignancy. Gynecol Obstet Invest. 1997;43:135–8.

Rare Ovarian Tumors: Computed Tomography and Magnetic Resonance

Takashi Koyama, Takashi Ikeuchi, and Kaori Togashi

Abstract

Clear cell carcinoma is typically a cystic mass containing multiple mural nodules. The cyst content typically shows high intensity on both T1- and T2-weighted images. Malignant Brenner tumor is typically a large multilocular cystic mass containing papillary projections and solid elements. Carcinosarcoma is typically a large heterogeneous mass, containing hemorrhage and necrosis.

Keywords

Brenner tumor • Transitional carcinoma • Clear cell • Imaging • Computed tomography • Magnetic resonance

This chapter deals with rare ovarian epithelial tumors, including clear cell tumors, malignant transitional cell tumors, and mixed müllerian tumors.

Clear Cell Tumors

Clear cell tumors of the ovary are histologically characterized by the cells with clear cytoplasms. These cells may show hobnail appearance that bulge into the lumen, known as "hobnail cells." The vast majority of clear cell neoplasms are carcinoma, whereas clear cell adenofibroma and atypical proliferative clear cell tumors, which has also been called as clear cell adenofibroma of borderline malignancy, are extremely rare.

T. Koyama, MD, PhD (✉)
Department of Diagnostic Radiology,
Osaka Red Cross Hospital, 5-30 Fudegasaki-cho,
Tennoji-Ward, Osaka-City,
Osaka 543-8555, Japan
e-mail: montpeti@kuhp.kyoto-u.ac.jp

T. Ikeuchi, MD
Department of Radiology, Shiga Medical Center for Adults,
5-4-30 Moriyama, Moriyama-City,
Shiga 524-8524, Japan

K. Togashi, MD, PhD
Department of Diagnostic Radiology,
Graduate School of Medicine, Kyoto University,
54 Kawahara-cho, Shogoin, Sakyo-Ward,
Kyoto 606-8507, Japan

Clear Cell Carcinomas

Clear cell carcinomas (CCCs) comprise 8.5 % of ovarian carcinomas in Western countries, whereas their incidence in Japan is estimated as at least 20 %. CCCs in Japan are the second common epithelial ovarian carcinoma following serous adenocarcinomas, and their incidence is still in increase, though the reasons for their high and increasing incidence remain unclear. CCC usually occurs in patients in the fifth to seventh decades, with median age of 54 years.

CCC has several clinical characteristics different from other types of epithelial ovarian carcinomas. CCCs are the most common ovarian epithelial tumor to be associated with paraneoplastic thrombophlebitis known as Trousseau syndrome and paraneoplastic hypercalcemia (Fig. 1) [1, 2]. A thromboembolic event, including deep venous thrombosis

L. Saba et al. (eds.), *Ovarian Neoplasm Imaging*,
DOI 10.1007/978-1-4614-8633-6_17,

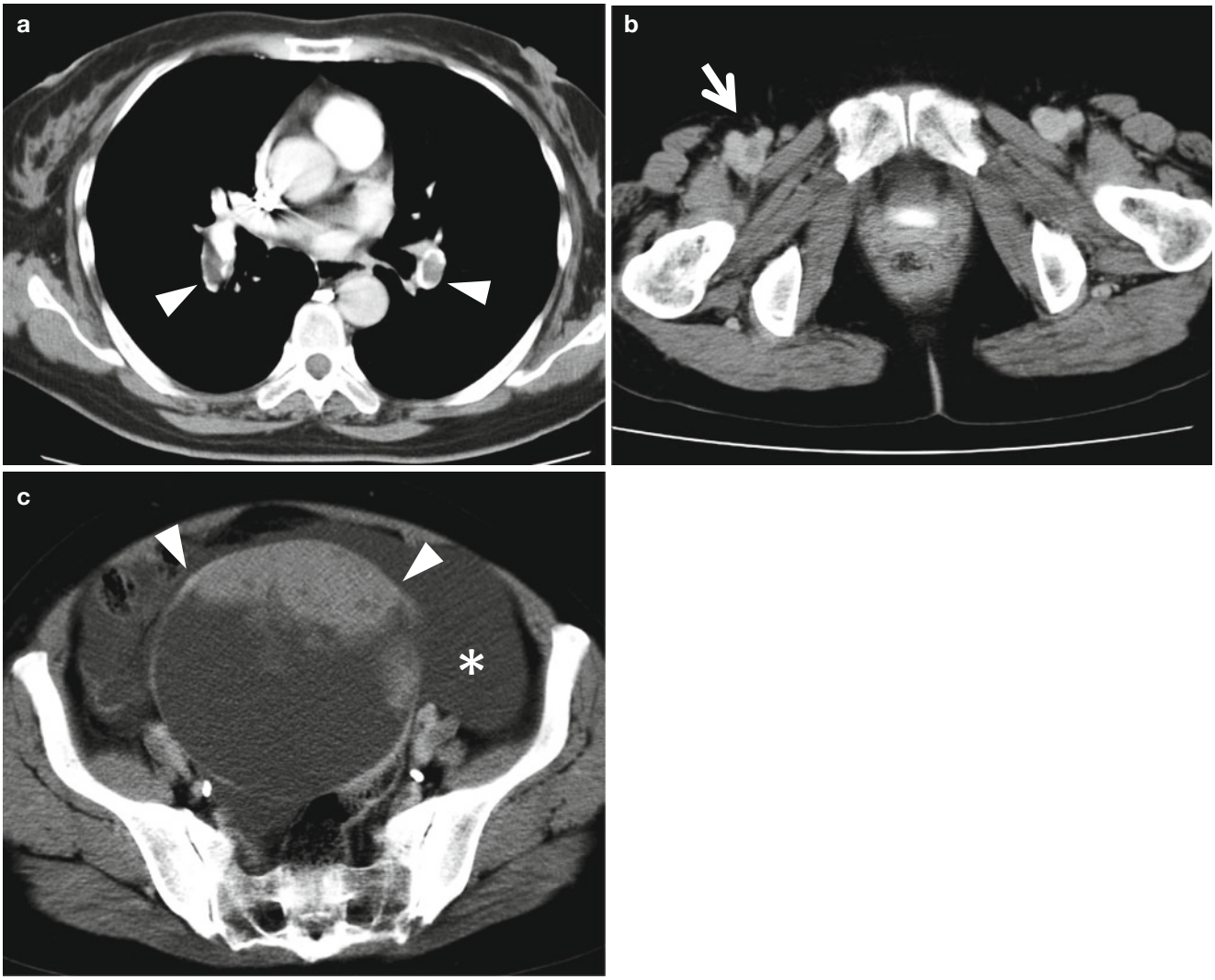

Fig. 1 Clear cell carcinoma with paraneoplastic migratory thrombophlebitis in a 40-year-old woman who presented with sudden respiratory distress by pulmonary embolism. (**a**) Contrast-enhanced CT of the thorax shows pulmonary embolisms in the bilateral pulmonary (*arrowheads*). (**b**) CT at the inguinal level shows a venous thrombus in her right femoral vein (*arrow*). (**c**) CT of the pelvis demonstrates a well-demarcated cystic mass containing irregular-shaped solid components ventrally (*arrowheads*). Ascites (*asterisk*) is present in her left pelvic cavity

or pulmonary embolisms, has been observed in 27.3 % of patients with CCC, while it is seen in 6.8 % of patients with other epithelial ovarian cancers [3]. The patients with Trousseau syndrome may also have noninfectious endocarditis and subsequent arterial embolisms in a variety of organs, including brain and kidney. Another clinical characteristic of CCC is that this tumor has the strongest relationship with endometriosis among all cell types of ovarian carcinomas [4]. CCCs usually arise from preexisting endometrial cysts [5]. Endometriotic implants are commonly seen in the vanity of the tumor or elsewhere in the pelvic cavity.

CCCs usually present as a large cystic mass, and they rarely occur in bilateral. CCC tends to present in early FIGO stages, with 35–60 % in stage I disease and 9–22 % in stage II. However, stage I CCC is more likely to be stage IC, probably because of higher risk of tumor rupture [6]. Their tendency of early clinical stage at presentation is explained by that CCC usually arises from preexisting endometriomas. However, clear cell carcinoma in early stages had a poorer outcome or a tendency toward poor outcome compared with other ovarian carcinomas [7, 8].

The gross appearances of CCC are characterized by multiple mural nodules within a thick-walled unilocular cyst, which represent endometriomas (Fig. 2) [4]. On MR imaging, the content of the cysts typically shows high intensity

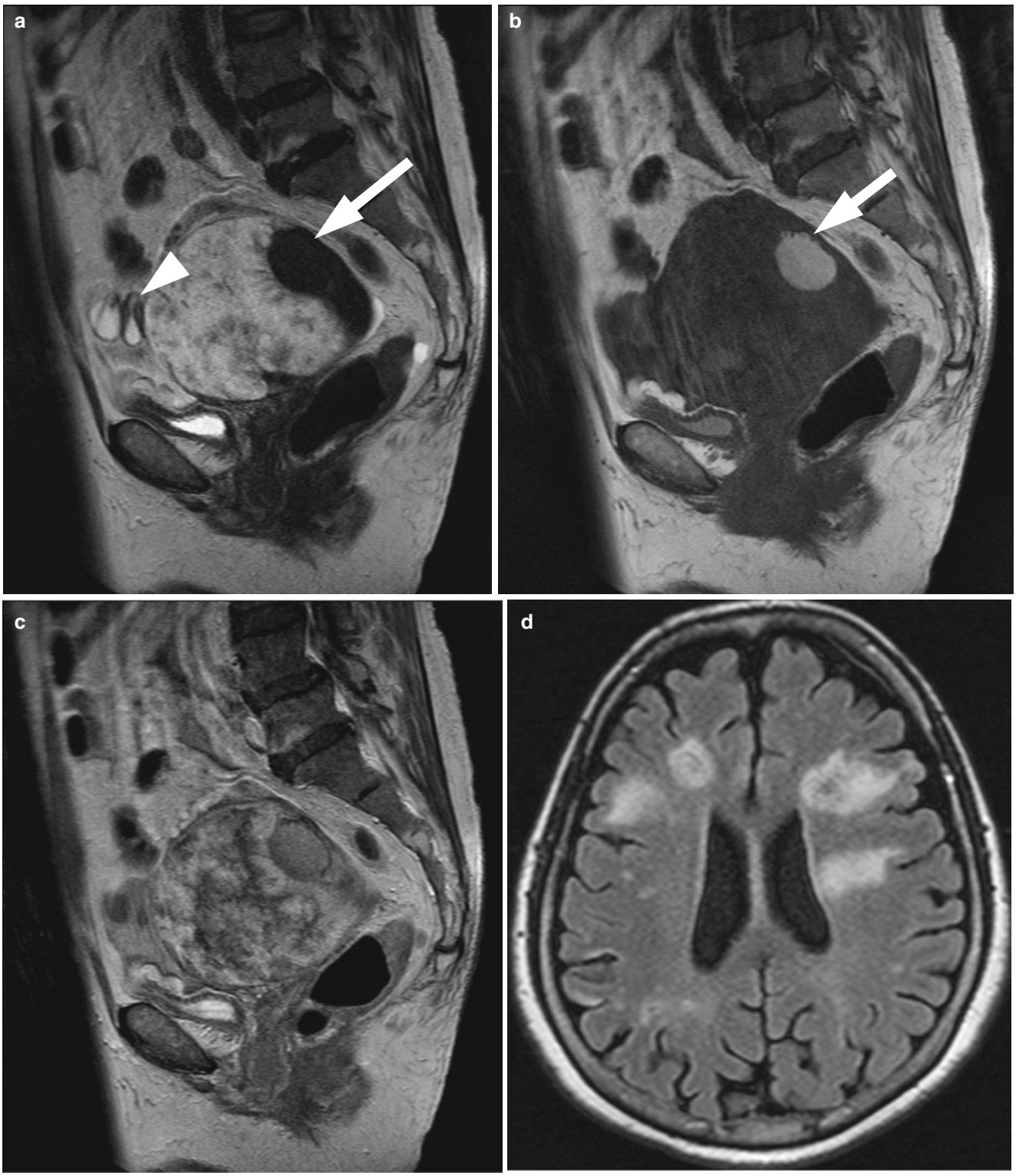

Fig. 2 Clear cell carcinoma in a 64-year-old woman who presented with multifocal acute cerebral infarction. (**a**) Sagittal T2-weighted image demonstrates an irregular-shaped tumor of high intensity (*arrowheads*) and endometrioma of distinct low intensity (*arrow*). (**b**) T1-weighted image shows predominantly low intensity in the tumor and high intensity in the endometrioma (*arrow*). (**c**) Contrast-enhanced T1-weigthed image shows heterogeneous enhancement in the tumor. (**d**) Fluid attenuated inversion recovery (FLAIR) image shows multiple foci of high intensity, representing acute embolitic infarctions

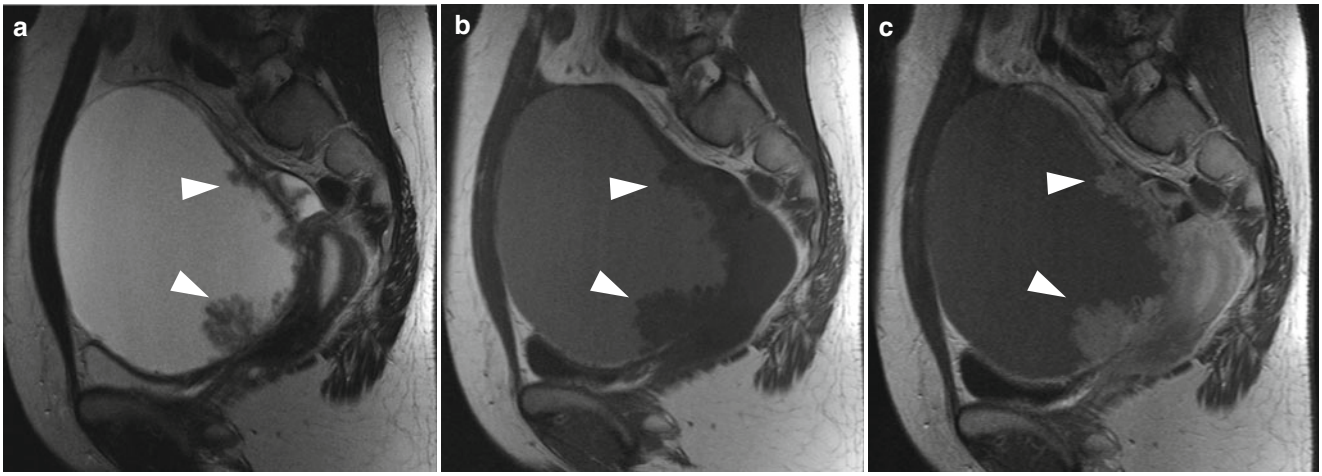

Fig. 3 Clear cell carcinoma in a 57-year-old woman. (**a**) Sagittal T2-weighted image shows a large unilocular cyst, associated with multiple papillary projections of intermediate intensity (*arrowheads*). (**b**) T1-weighted image shows increased signal intensity in the cyst content and mural nodules of low intensity. (**c**) Post-contrast T1-weighted image shows enhancement in the papillary projections (*arrowheads*)

on T1-weighted images, as usually seen in endometriomas. However, the signal intensity on T2-weighted images is usually high, rather than low intensity commonly seen in endometriomas [9]. The neoplastic nodule in CCC can show variable size, ranging from tiny nodule to large mass that is about to fulfill the entire cystic cavity. On MR imaging, they usually show low intensity on T1-weigthed images, but variably low to high intensity on T2-weighted images (Fig. 3). Post-contrast image reveals enhancement in the nodules. The confirmation of enhancement on post-contrast image is important for differentiating neoplastic mural nodules from coagulated clots, which are commonly seen in endometriomas but never enhanced. Imaging features in CCCs described above are also seen as endometrioid adenocarcinomas, which can also arise from endometrioma. However, the presence of simultaneous thromboembolitic events, including thrombophlebitis, pulmonary embolisms, and infarctions of many organs, may suggest the diagnosis of CCC (Figs. 1 and 3).

Clear Cell Adenofibromas/Clear Cell Adenofibromas of Borderline Malignancy

Clear cell adenofibromas (CCAs) of borderline malignancy is also called as atypical proliferative clear cell tumor [4]. The gross appearance of these tumor is characterized by microcystic structures of honeycomb appearance, embedded within firm rubbery stroma [4]. Histology of these tumors shows tubular glands lined by a layer of hobnail cells. In CCA of borderline malignancy, the glands are more crowded, and the cells display nuclear atypia. These tumors are considered to be precursors of CCCs, and clear cell carcinoma may accompany these tumors. As like CCCs, these tumors may associate with endometrioma. Although imaging findings of CCAs have not been documented, our experience case of CCA appeared as multilocular cystic mass containing numerous fine septi (Figs. 4 and 5). The areas with abundant fibrous stromas in CCA were demonstrated as solid component of low intensity on T2-weighted images (Fig. 4).

Malignant Transitional Cell Tumor

Transitional cell tumors comprise approximately 10 % of ovarian epithelial tumors, and nearly all of these are benign Brenner tumors. Borderline Brenner tumor and malignant transitional cell tumor are very uncommon. Borderline Brenner tumor is also called as atypical proliferative Brenner tumor, proliferating Brenner tumor or Brenner tumor of low malignant potential [4]. Malignant transitional cell tumors are further subdivided into malignant Brenner tumor and transitional cell carcinoma (TCC). These tumors are characterized by the histologic stromal invasion by transitional tumor cells, while this finding is absent in borderline tumor.

Malignant Brenner tumor is pathologically defined by the presence of benign Brenner components within the tumor, while transitional cell carcinoma does not contain these components. Recent reports on immunohistochemical and genetic studies have shown that Brenner tumor has true urothelial differentiation, while TCC is a variant of high-grade serous carcinoma [10, 11]. This recognition is also supported by the observation that high-grade serous adenocarcinomas frequently have focal areas that display features like of TCC [4].

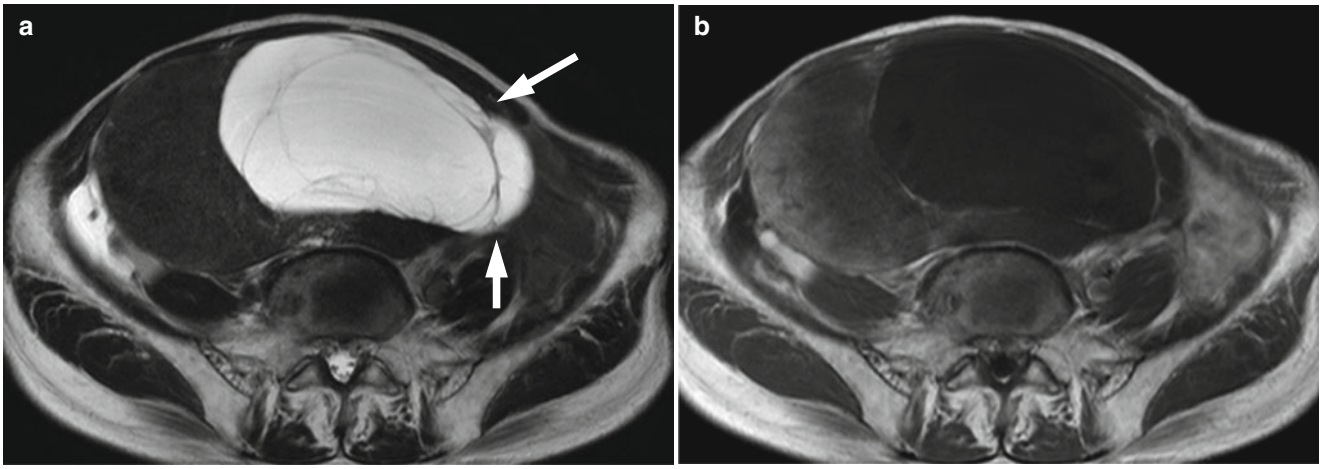

Fig. 4 Clear cell adenofibroma in an 89-year-old woman. (**a**) Axial T2-weighted image shows a large solid mass containing a cystic component of multilocular appearance (*arrows*) with fine septi. (**b**) Post-contrast T1-weighted image shows week enhancement in the periphery of the solid component

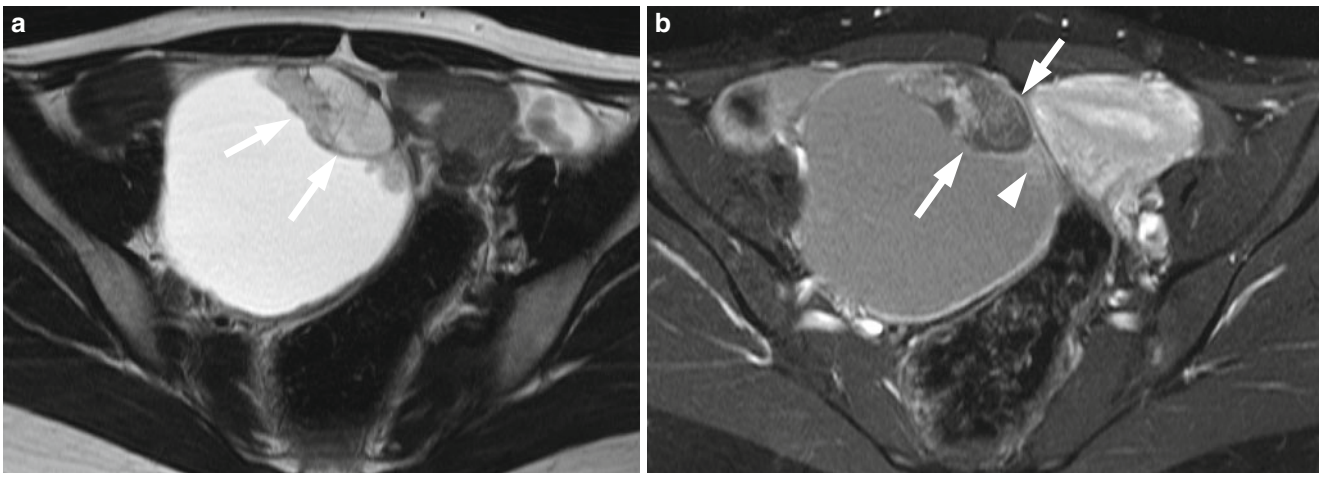

Fig. 5 Clear cell borderline cystadenofibroma in endometrioma in a 32-year-old woman. (**a**) Axial T2-weighted image shows complex mural nodules of heterogeneous intermediate intensity (*arrows*). (**b**) Post-contrast-enhanced T1-weighted image reveals microcystic structure within mural nodules with numerous fine septi (*arrows*). The papillary projections (*arrowhead*) beside the microcystic lesion are enhanced. These projections correspond to clear cell carcinomas arising from clear cell adenofibroma

Both borderline and malignant Brenner tumors are usually larger than their benign counterparts and tend to be multilocular cystic in appearance (Figs. 6 and 7). The tumors typically contain multiple papillary projections and irregular-shaped solid components (Fig. 7) [12]. Meanwhile, the gross appearance of TCC is similar to high-grade serous carcinomas and typically is an irregular-shaped solid mass. On T2-weighted images of MR imaging, the signal intensity of solid components have been reported to be higher in malignant transitional cell tumors compared with those in benign and borderline Brenner tumors [13].

Mixed Müllerian Tumor of the Ovary

Mixed müllerian tumor (MMT) is histologically characterized by the presence of both epithelial and mesenchymal elements. The mesenchymal cells exhibit varying degree of proliferation and are often sarcomatous. MMTs with benign epithelial components are designated as adenosarcoma, while those with malignant epithelial components are carcinosarcoma. Although MMTs are more commonly encountered in the uterus, MMTs are quite rare in the ovaries [14, 15]. The imaging features of ovarian MMT have not been well documented.

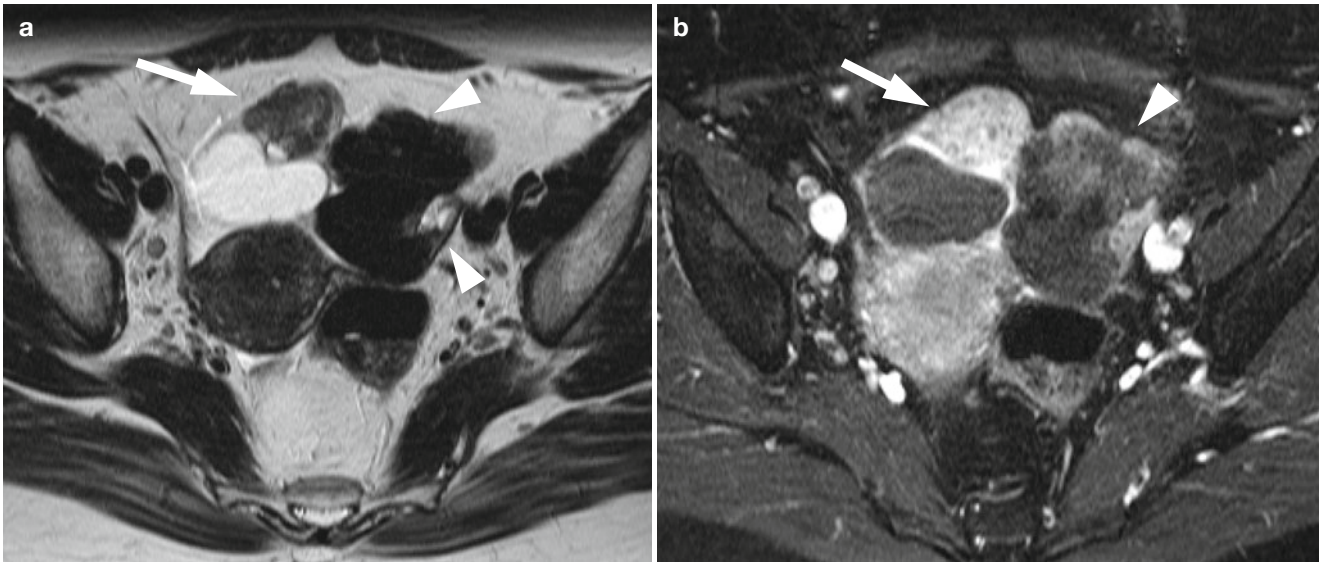

Fig. 6 Borderline Brenner tumor in the right ovary and benign Brenner tumor in the left ovary. (**a**) Axial T2-weighted image shows bilateral ovarian tumors. Right ovarian tumor is composed of a cystic component dorsally and a solid component (*arrow*), which exhibits heterogeneously intermediate intensity. Left ovarian tumor is a lobulated solid mass of distinct low intensity (*arrowheads*). (**b**) Post-contrast T1-weighted image with fat suppression demonstrates marked but heterogeneous enhancement in the solid component (*arrow*) of the right ovarian mass and poor enhancement in the left ovarian mass (*arrowhead*)

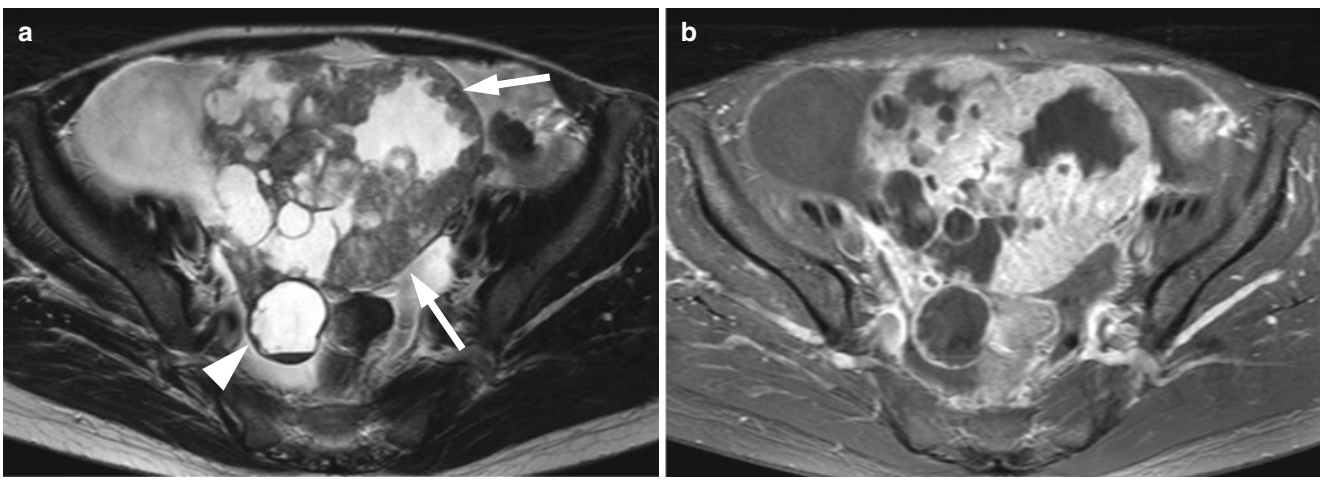

Fig. 7 Malignant Brenner tumor. (**a**) Axial T2-weighted image shows a complex multilocular cystic mass containing numerous papillary projections and irregular-shaped solid components (*arrows*). There is another cystic mass with a fluid-fluid level in her right ovary (*arrowhead*). (**b**) Post-contrast T1-weighted image shows marked enhancement in the papillary projections and solid components in the heterogeneous tumor. The peritoneal surface is thickened and enhanced, representing carcinomatous peritonitis

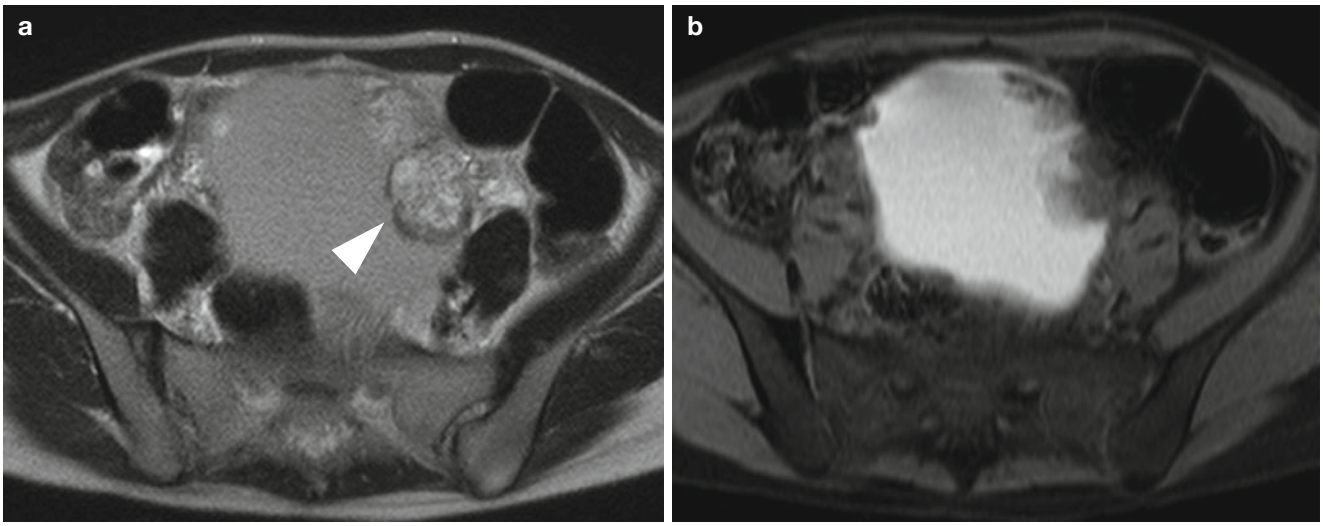

Fig. 8 Adenosarcoma arising from endometrioma in a 32-year-old woman. (**a**) T2-weighted image shows mural nodules of heterogeneous high intensity (*arrowhead*), covered by clots of decreased intensity. (**b**) T1-weighted images shows cyst content of high intensity and mural nodules of low intensity

Adenosarcoma

Adenosarcoma usually occurs in both pre- and postmenopausal women, with mean age of 54 years old [16]. About 65 % of patients present in FIGO stage I. The microscopic feature in adenosarcoma is periglandular stromal condensation and increased mitotic index in these hypercellular areas. Histologically, one-fourth of tumors are considered as high grade, while the rests are low grade. The 5-year disease-free survival is 45 % for low grade and 25 % for high grade [16]. The overall 5-year survival is about 65 %. The gross appearance of adenosarcoma is predominantly solid mass with some cystic areas, but 10 % of tumors are predominantly cystic [16]. Adenosarcomas are known to arise from preexisting endometrial cyst [17]. In our experienced case, adenosarcoma presented as mural nodule arising in endometrioma on MR imaging (Fig. 8) [18]. The nodule shows heterogeneously low intensity on T2-weighted images. In another experienced cases of adenosarcoma, a lobulated soft tissue mass almost fulfilled the cystic cavity. The mass exhibit high intensity on T2-weigthed images and reticular pattern of enhancement on post-contrast images (Fig. 9).

Carcinosarcoma

Carcinosarcoma is a highly aggressive tumor and convey poor prognosis with median survival of approximately 8 months [19]. Patients with carcinosarcomas are usually elderly women with mean age of 64–66 years, which is higher than that of other ovarian carcinomas [20]. The microscopic feature is characterized by the admixture of malignant epithelial and stromal elements. The epithelial elements is commonly serous or endometrioid carcinoma. The stromal elements are usually composed of spindle-shaped cells with marked nuclear atypia and mitosis and commonly associated with heterologous components of most commonly chondrosarcoma, osteosarcoma, and rhabdomyosarcoma. Recent immunohistochemical and genetic studies suggest that ovarian carcinosarcoma is a

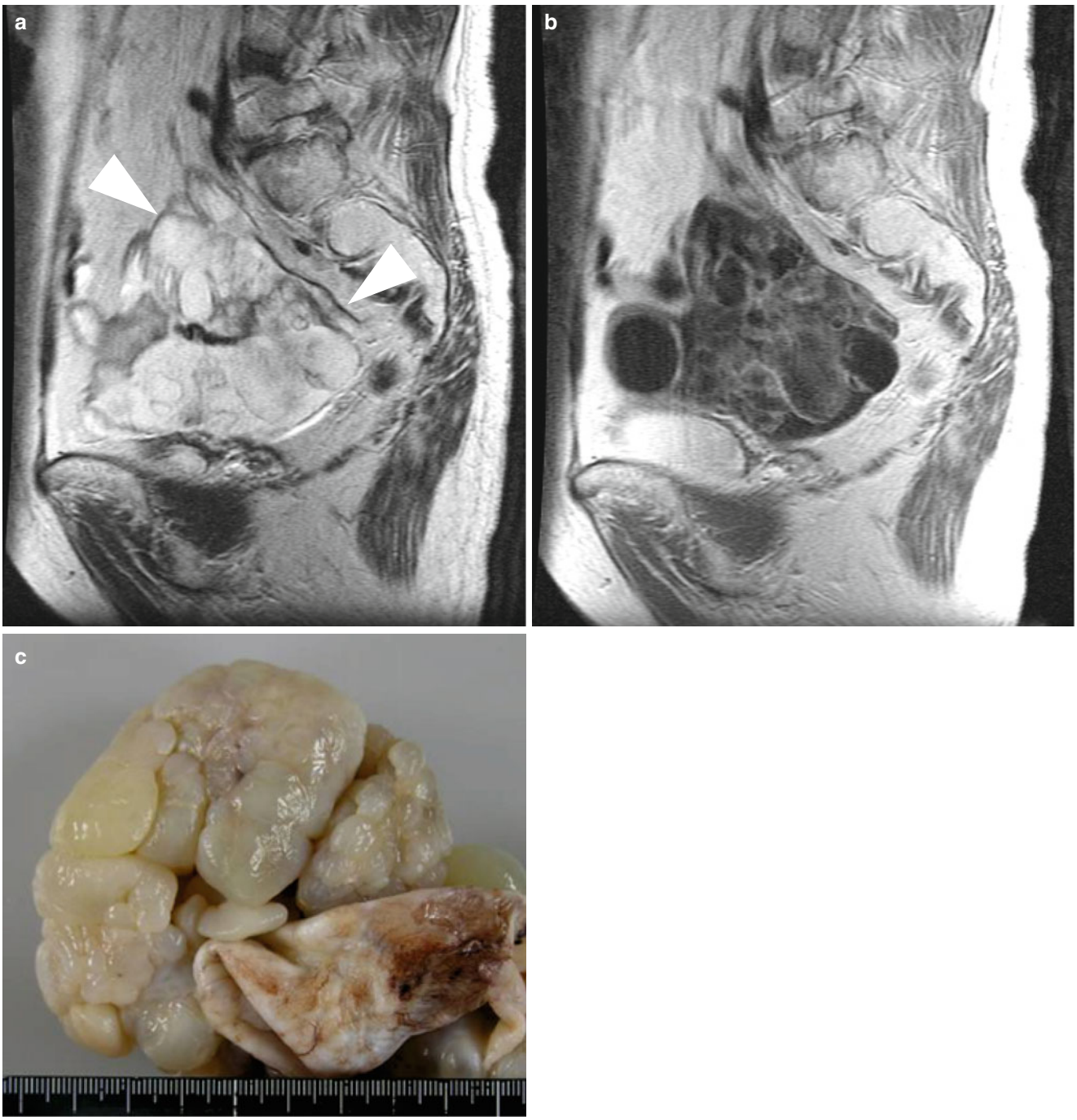

Fig. 9 Adenosarcoma of the ovary in a 69-year-old woman. (**a**) T2-weighted image shows a well-demarcated cystic lesion (*arrowheads*), containing complex lobular mass. (**b**) Post-contrast T1-weighted image shows reticular enhancement in the tumor. (**c**) Gross picture of the tumor shows a lobulated soft tissue within the cyst

kind of metaplastic carcinoma [21, 22]. These tumors are usually large, and gross appearance is characterized by the presence of hemorrhage and necrosis, as well as their counterpart in the uterus. On MR imaging, ovarian carcinosarcoma is depicted as a large heterogeneous mass containing area of hemorrhagic necrosis (Fig. 10), which show increased signal on T1-weighted image and decreased intensity on T2-weighted images. The tumor is heterogeneously enhanced on post-contrast T1-weighted image because of extensive necrosis within the tumor. As like adenosarcomas, carcinosarcomas may arise from pre-existing endometrioma [23].

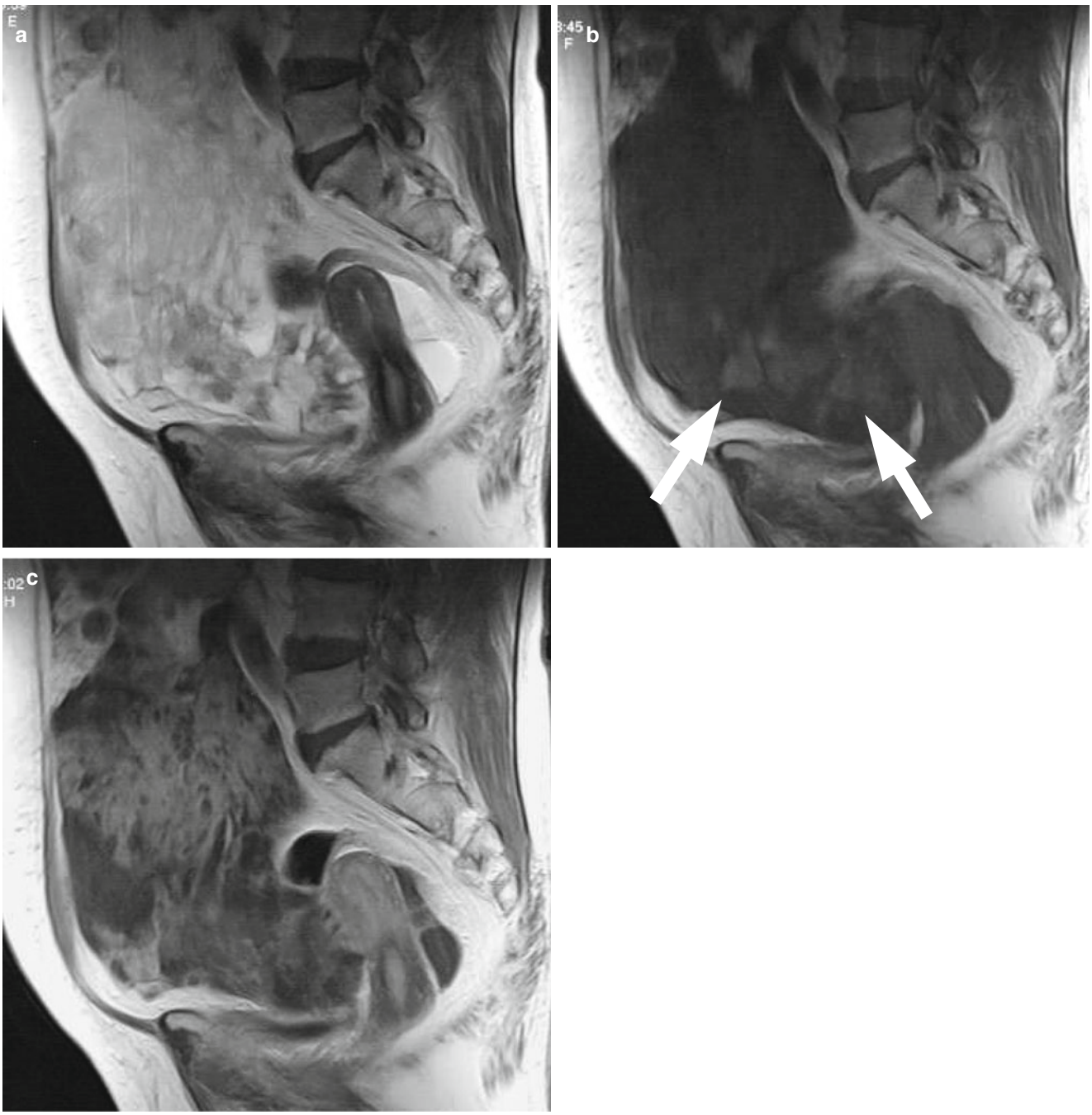

Fig. 10 Carcinosarcoma in a 66-year-old woman. (**a**) Sagittal T2-weighted image shows a huge mass of heterogeneous high intensity anterior to the uterus. (**b**) T1-weighted images reveals foci of increased intensity (*arrows*), representing hemorrhage within the tumor. (**c**) Post-contrast T1-weigthed image shows heterogeneous enhancement within the tumor due to multifocal unenhanced area, reflecting hemorrhage and necrosis

References

1. Pather S, Quinn MA. Clear-cell cancer of the ovary-is it chemosensitive? Int J Gynecol Cancer. 2005;15(3):432–7.
2. Tan DS, Kaye S. Ovarian clear cell adenocarcinoma: a continuing enigma. J Clin Pathol. 2007;60(4):355–60.
3. Matsuura Y, et al. Thromboembolic complications in patients with clear cell carcinoma of the ovary. Gynecol Oncol. 2007;104(2):406–10.
4. Seidman J, et al. Surface epithelial tumors of the ovary. In: Kurman R, Ellenson LH, Ronnett B, editors. Blaustein's pathology of the female genital tract. New York: Springer; 2011. p. 679–784.
5. Kobayashi H, et al. Risk of carcinoma in women with ovarian endometrioma. Front Biosci (Elite Ed). 2011;3:529–39.
6. Mizuno M, et al. Long-term prognosis of stage I ovarian carcinoma. Prognostic importance of intraoperative rupture. Oncology. 2003; 65(1):29–36.
7. Jenison EL, et al. Clear cell adenocarcinoma of the ovary: a clinical analysis and comparison with serous carcinoma. Gynecol Oncol. 1989;32(1):65–71.
8. Kennedy AW, et al. Ovarian clear cell adenocarcinoma. Gynecol Oncol. 1989;32(3):342–9.
9. Tanaka YO, et al. Ovarian carcinoma in patients with endometriosis: MR imaging findings. AJR Am J Roentgenol. 2000;175(5):1423–30.
10. Ordonez NG. Transitional cell carcinomas of the ovary and bladder are immunophenotypically different. Histopathology. 2000;36(5): 433–8.
11. Riedel I, et al. Brenner tumors but not transitional cell carcinomas of the ovary show urothelial differentiation: immunohistochemical staining of urothelial markers, including cytokeratins and uroplakins. Virchows Arch. 2001;438(2):181–91.
12. Takahama J, et al. Borderline Brenner tumor of the ovary: MRI findings. Abdom Imaging. 2004;29(4):528–30.
13. Oh SN, et al. Transitional cell tumor of the ovary: computed tomographic and magnetic resonance imaging features with pathological correlation. J Comput Assist Tomogr. 2009;33(1):106–12.
14. Gallardo A, Prat J. Mullerian adenosarcoma: a clinicopathologic and immunohistochemical study of 55 cases challenging the existence of adenofibroma. Am J Surg Pathol. 2009;33(2):278–88.
15. Sreenan JJ, Hart WR. Carcinosarcomas of the female genital tract. A pathologic study of 29 metastatic tumors: further evidence for the dominant role of the epithelial component and the conversion theory of histogenesis. Am J Surg Pathol. 1995;19(6):666–74.
16. Eichhorn JH, et al. Mesodermal (mullerian) adenosarcoma of the ovary: a clinicopathologic analysis of 40 cases and a review of the literature. Am J Surg Pathol. 2002;26(10):1243–58.
17. Chen ZW, Saad RS. Ovarian adenosarcoma arising from benign cystadenoma and associated intraoperative consultation pitfalls. Int J Gynecol Pathol. 2010;29(5):415–8.
18. Shintaku M, Mise Y. Mullerian adenosarcoma with a neuroectodermal component associated with an endometriotic cyst of the ovary: a case report. Pathol Int. 2012;62(4):271–5.
19. Chang J, et al. Carcinosarcoma of the ovary: incidence, prognosis, treatment and survival of patients. Ann Oncol. 1995;6(8):755–8.
20. Mano MS, et al. Current management of ovarian carcinosarcoma. Int J Gynecol Cancer. 2007;17(2):316–24.
21. Jin Z, et al. Carcinosarcomas (malignant mullerian mixed tumors) of the uterus and ovary: a genetic study with special reference to histogenesis. Int J Gynecol Pathol. 2003;22(4):368–73.
22. Matias-Guiu X, et al. Clonality analysis in synchronous or metachronous tumors of the female genital tract. Int J Gynecol Pathol. 2002;21(3):205–11.
23. Marchevsky AM, Kaneko M. Bilateral ovarian endometriosis associated with carcinosarcoma of the right ovary and endometrioid carcinoma of the left ovary. Am J Clin Pathol. 1978;70(4): 709–12.

Sex Cord-Stromal Tumors: Clinical Setting and Ultrasound Findings

Caroline Van Holsbeke and Dirk Timmerman

Abstract

Ovarian sex cord-stromal tumors (SCST) are tumors that arise from the non-germ cells and non-epithelial cells that surround the oocytes, including the cells that produce ovarian hormones. These tumors show proteiform ultrasonographic patterns and usually they appear as solid tumor with color score 3–4.

Keywords

Ovarian sex cord-stromal tumors • Granulosa cell tumor • Theca cell tumor • Sertoli cell tumor • Leydig cell tumor • Imaging • Ultrasound

Introduction

Ovarian sex cord-stromal tumors (SCST) are tumors that arise from the non-germ cells and non-epithelial cells that surround the oocytes, including the cells that produce ovarian hormones [1], i.e., the granulosa cells, theca cells, Sertoli cells, Leydig cells, and fibroblasts (Fig. 1). Therefore, the SCST display areas of gonadal stromal differentiation, such as granulosa, theca, Sertoli, or Leydig differentiation.

Most consist of ovarian cell types, but testicular (Sertoli cell) and mixed ovarian and testicular (gynandroblastoma) cell types can occur.

Epidemiology

Sex cord-stromal ovarian neoplasms are rare, and the incidence is estimated around 0.2 per 100,000 women [1].

C.V. Holsbeke (✉)
Department of Obstetrics and Gynecology,
Ziekenhuis Oost-Limburg, Genk, Belgium

Department of Obstetrics and Gynecology,
University Hospitals Leuven, Leuven, Belgium
e-mail: caroline.van.holsbeke@skynet.be

D. Timmerman
Department of Obstetrics and Gynecology,
University Hospitals Leuven, Leuven, Belgium

They are a mix of benign and malignant neoplasms but comprise only 1.2 % of the ovarian cancers, most of them (1 % out of the 1.2 %) being granulosa cell tumors.

In comparison with epithelial ovarian cancer, malignant sex cord-stromal tumors are rare, are found in younger patients, are diagnosed at an earlier stage, and may produce estrogens or androgens. These sex steroid hormones not only result in particular symptoms but may also function as tumor markers and will help in the diagnosis [2, 3]. Sex cord-stromal neoplasms have no known association with the BRCA germline mutations or a genetic predisposition to breast cancer.

In this chapter we will describe the most important and relevant sex cord-stromal tumors. Most clinicopathological information was found in Blaustein's pathology [4] and in the pictorial essays that were published by the IOTA group [5, 6]. The sonographic features are described following the IOTA (International Ovarian Tumor Analysis) terms and definitions [7].

Granulosa Cell Tumors

Epidemiology

The granulosa cell tumor (GCT) is a rare tumor that accounts for 1–3 % of all ovarian tumors, but is the most common sex

L. Saba et al. (eds.), *Ovarian Neoplasm Imaging*,
DOI 10.1007/978-1-4614-8633-6_18,

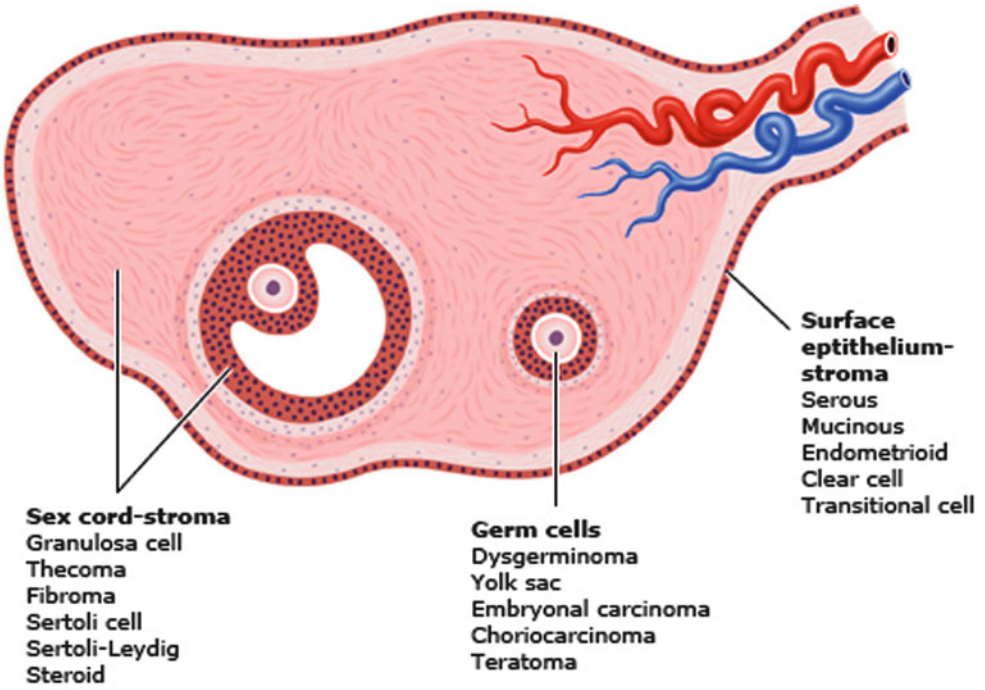

Fig. 1 Origin of all different types of ovarian tumors

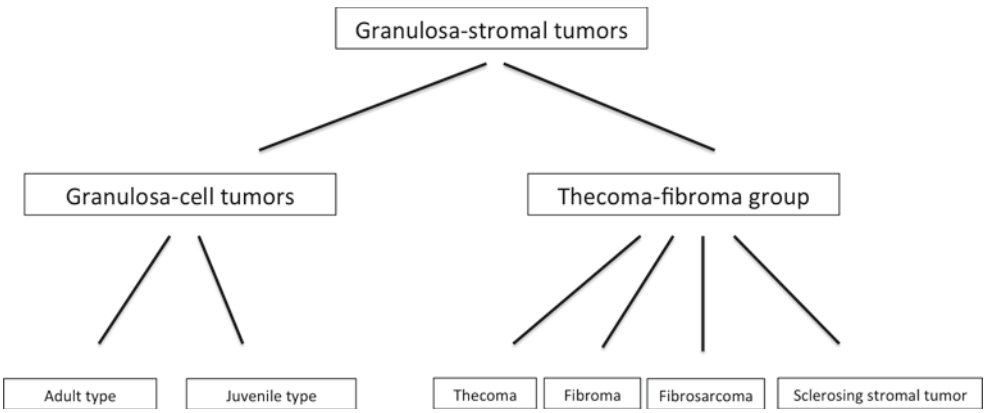

Fig. 2 Classification of the granulosa-stromal tumors

cord-stromal tumor (70 %) and the most common (80 %) hormone-producing ovarian tumor [8–11].

The incidence is 0.5–1.5/100,000 women per year [12]. One-third of granulosa cell tumors occur in premenopausal women, more than 50 % in postmenopausal women and 5 % in the prepubertal period [11]. It is widely thought that granulosa cell tumors develop as a result of stimulation of the granulosa cells but the stimulus is unknown. Radiation therapy, damage to the ova and granulosa cells, increased release of gonadotropins during fertility treatment, and the use of tamoxifen (due to the estrogenic activity caused by the estrogenic metabolites) have all been proposed to be potential causal factors, but there is no real evidence to support any of these hypotheses [13]. There are two types of GCTs, the adult type and the juvenile type (Fig. 2). The juvenile type comprises only 5 % of granulosa cell tumors [11, 14]. The differences between both types are merely histopathological (Table 1).

Clinical Symptoms

A hyperestrogenic state due to the hormone production inside the tumor is often seen in patients with a granulosa cell tumor and results in clinical symptoms that facilitate the diagnosis [15]. Children usually present with isosexual precocious puberty or occasionally galactorrhea [11, 16]. Estrogen-related symptoms in adolescents or adults are bleeding disorders and breast enlargement. Depending on the diagnostic criteria, 24–80 % of the patients with a GCT have endometrial pathology [17]; 20–65 % of the endometrial pathology being endometrial hyperplasia and up to 10 % being endometrial cancer [18, 19].

Other clinical symptoms are abdominal distension and pain. This might be related to the fact that granulosa cell tumors tend to be large and that they may rupture spontaneously resulting in a painful hematoperitoneum or a hemorrhagic component inside the tumor.

Table 1 Comparison between the adult and juvenile type granulosa cell tumor

	Adult GCT	Juvenile GCT
Incidence	1–3 % of all ovarian tumors 95 % of all GCTs	5 % of all GCTs
Benign or malignant	Malignant	Malignant
Prognosis	Low malignant potential ≥75 % stage I Late recurrence 10 years survival: 60–90 % Survival is related to stage and size	
Recurrence	25 %	5 %
Age	Postmenopausal > premenopausal 50–55 years	97 % < 30 years
Typical features	Macroscopic Large, lobulated, gray or yellow, solid, and cystic components, hemorrhagic areas Microscopic Pale nuclei, grooved (coffee bean), Call-Exner bodies, no luteinization, low mitotic activity	Macroscopic Same presentation as adult type Microscopic Dark nuclei, no grooves, Call-Exner bodies are very rare, often luteinization, high mitotic activity
Typical symptoms	Estrogenic symptoms: bleeding disorders, endometrial pathology (hyperplasia, adenoca (<5 %))	Estrogenic symptoms: irregular cycle and bleeding disorders, isosexual pseudoprecocity in children

Most granulosa cell tumors are slow-growing lesions that progressively fill the pelvis or abdomen. Overall, 75 % of the granulosa cell tumors are diagnosed in stage I, 20 % in stage II, 8 % in stage III, and 6 % in stage IV [18, 20].

Macroscopic Appearance

GCT's are typically rather large, commonly encapsulated tumors with a smooth or lobulated surface. The tumor has a gray- to yellow-sectioned surface and is composed of solid and cystic areas in variable proportions. Especially in the large tumors, hemorrhagic areas are often found. Totally cystic lesions comprise a minority [17].

Microscopic Appearance

Two major subtypes are recognized, an adult and a juvenile type. The differences between them are mostly the age that they arise and the histopathological findings. The most important differences are described in Table 1.

Prognosis

The natural course of the GCT is that of a slow-growing tumor with a local spread that recurs rather seldom or very late, sometimes even as late as after 37 years [17, 18, 20, 21]. Therefore, it seems more appropriate to call a granulosa cell tumor a "tumor with a low malignant potential." There is a recurrence rate of up to 25 % and most authors report an average time to recurrence that varies between 5 and 10 years. Recurrences are usually intraperitoneal. For stage I disease, the 5-year survival rate is more than 90 %, but for the more advanced stages, the 5-year survival rate varies between 0 and 22 %.

Despite their more aggressive histological appearance, only about 5 % of juvenile GCTs recur or metastasize. Their prognosis mainly depends on tumor stage. It is excellent for stage I tumors but poor at stage II to IV.

Sonographic Characteristics

The largest study describing the sonographic characteristics of GCT's was performed by the IOTA group [6]. Twenty-three patients with a GCT were included in four international centers that all participated in the International Ovarian Tumor Analysis (IOTA) studies. The patients were all scanned using 2D color Doppler and grayscale imaging by experienced ultrasound examiners following the standardized examination technique, terms, and definitions recommended by the IOTA group for examination of adnexal masses [7]. At the end of the scan, the ultrasound examiner suggested a diagnosis of a benign or malignant mass on the basis of his or her subjective evaluation of the ultrasound findings, i.e., pattern recognition or subjective assessment. Eighteen (78 %) of the GCTs were of the adult type, 3 GCTs (13 %) were of the juvenile type, and in 2 (9 %) cases the tumor type was not defined by the pathologist. For patients with a primary GCT, all but one were stage I tumors, one patient was diagnosed with a stage IIb tumor, and three patients had a recurrence of a GCT.

The ultrasound characteristics of the granulosa cell tumors are presented in Table 2. All but one tumor contained solid

Table 2 Overview of grayscale and color Doppler findings in 23 granulosa cell tumors included in the IOTA studies

Locularity	Unilocular	0/23 (0 %)
	Unilocular solid	1/23 (4.3 %)
	Multilocular	1/23 (4.3 %)
	Multilocular solid	12/23 (52 %)
	Solid	9/23 (39 %)
Number of locules[a]	≥5	13/13 (100 %)
	≥10	10/13 (77 %)
Presence of papillarities		4/23 (17 %)
Largest diameter of lesion	Median: 102 mm	Range: 37–242
	0–50 mm	1 (4.3 %)
	51–80 mm	6 (26 %)
	81–100 mm	4 (17 %)
	>100 mm	12 (52 %)
Echogenicity cyst content[b]	Anechoic	2/16 (12.5 %)
	Ground glass	0/16 (0 %)
	Low level	7/16 (44 %)
	Hemorrhagic	1/16 (6 %)
	Mixed	6/16 (38 %)
Color score	1: No flow	0/23 (0 %)
	2: Minimal flow	2/23 (9 %)
	3: Moderate flow	13/23 (57 %)
	4: Highly vascularized	8/23 (35 %)
	≥ 3	21/23 (91 %)
Ascites		5/23 (22 %)

[a]Only multilocular or multilocular-solid masses can be considered
[b]Only masses with a cystic component can be considered

components. Twelve were multilocular solid (52 %), 9 were purely solid (39 %), one was unilocular solid (4.3 %), and one was multilocular (4.3 %). Of the 13 multilocular/multilocular-solid masses, all 13 masses contained 5 locules or more and 10 out of 13 (77 %) contained 10 locules or more. The echogenicity of the cyst content was usually low level (7/16, 44 %) or mixed (6/16, 38 %). Papillary projections were found in only four patients (17 %). GCTs are large tumors. The median largest diameter was 102 mm (range 37–242). Only one mass was smaller than 50 mm, and more than 50 % of the masses were larger than 100 mm. Ascites was found in five cases (22 %).

Most granulosa cell tumors manifested moderate (color score 3) to high color (color score 4) content at color or power Doppler examination (color score 3 in 13/23, 57 %; color score 4 in 8/23, 35 %). GCT's often contain hemorrhagic components.

After pattern recognition, two typical patterns were described: the first pattern was a solid mass with heterogeneous echogenicity of the solid tissue as can be seen in necrotic tissue. An example of this pattern is demonstrated in Figs. 3 and 4a, b. The second pattern is a multilocular-solid mass containing a considerable amount of solid tissue around relatively small locules but with no papillary projections. It typically has a "Swiss cheese" appearance due to the large number of small locules with a variable thickness of solid tissue around the cystic areas (Figs. 5, 6, 7, and 8). But GCTs

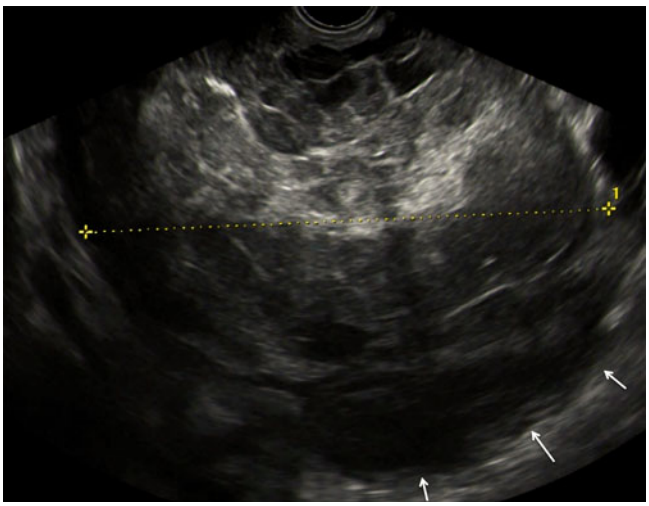

Fig. 3 Large purely solid GCT with an irregular external wall (*arrows*). The mixed echogenicity of the solid tissue suggests necrosis

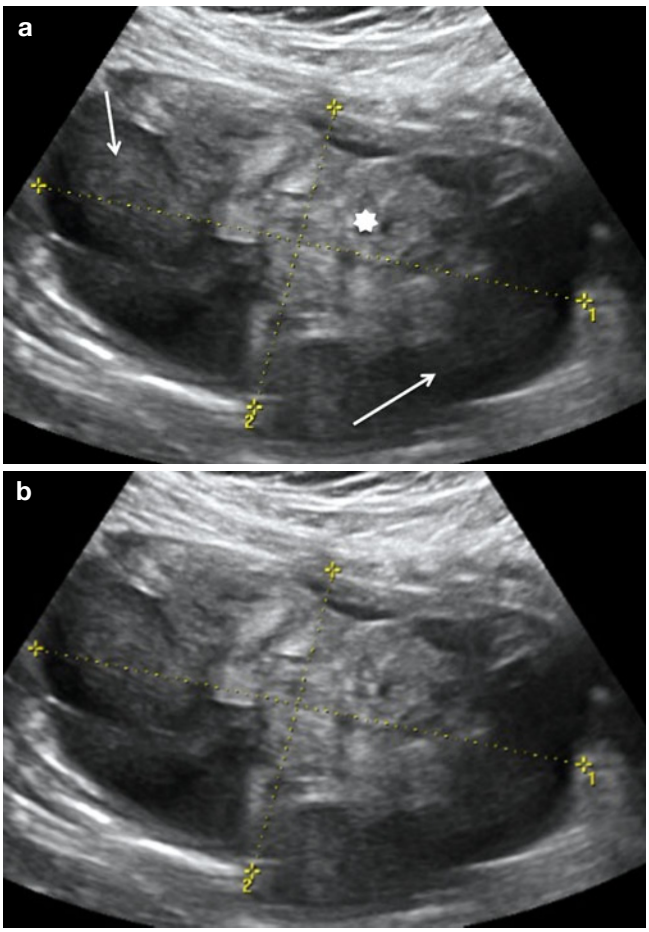

Fig. 4 (**a**, **b**) The echogenicity of this mass is in homogenous and gives the impression that large cystic components surrounding the solid tissue (★) are hemorrhagic (*arrows*). This GCT demonstrates the typical necrotic type

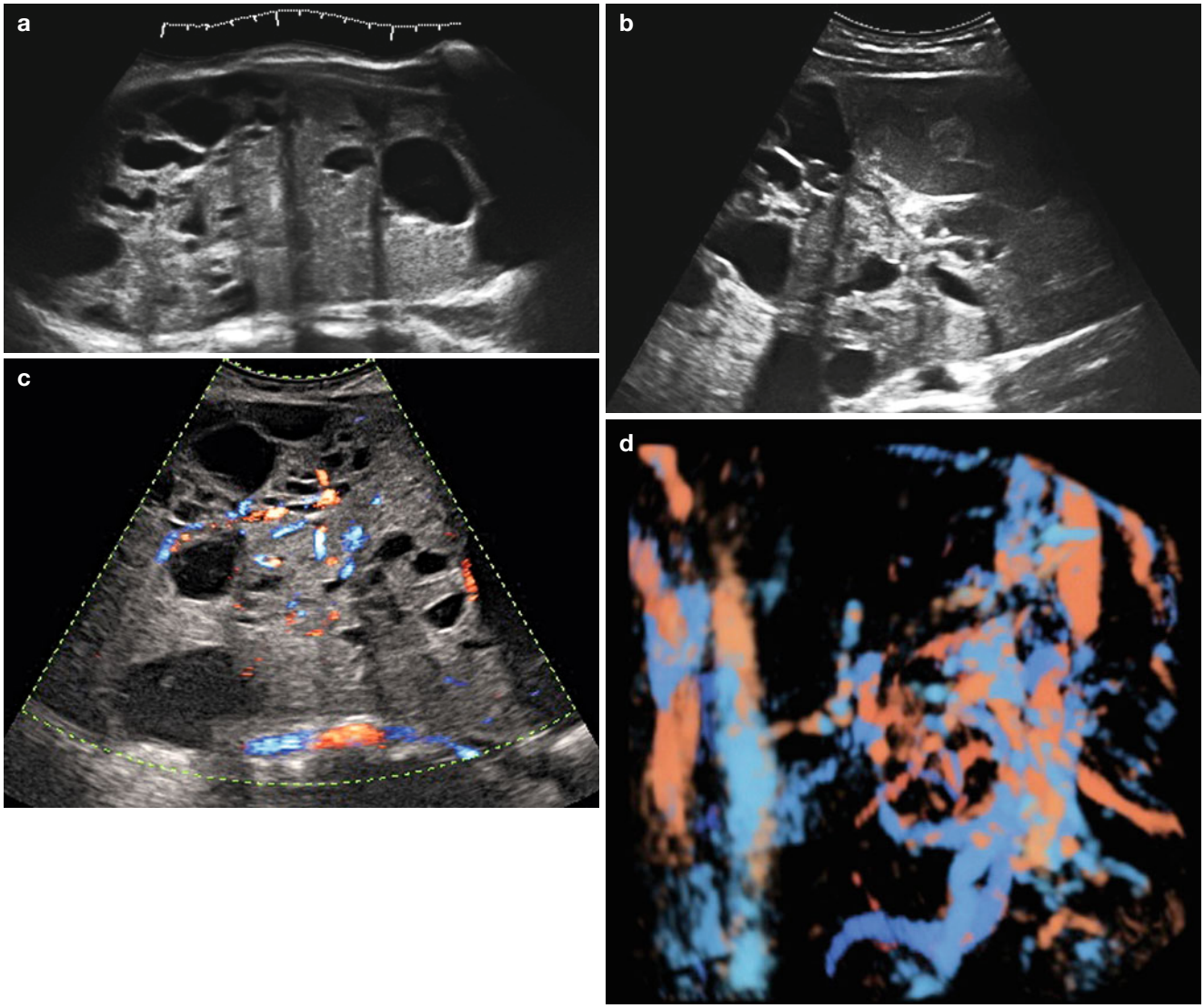

Fig. 5 (**a**–**d**) Grayscale (**a**, **b**) and color Doppler (**c**, **d**) images of a very large (174×127×206 mm) stage Ia granulosa cell tumor in a 26-year-old patient (coincidental finding during investigation for arterial hypertension). The whole of the tumor can only be measured using the extended view modus (**a**). Figure (**d**) is a rendered 3D HD flow Doppler image demonstrating the vascular tree of the tumor

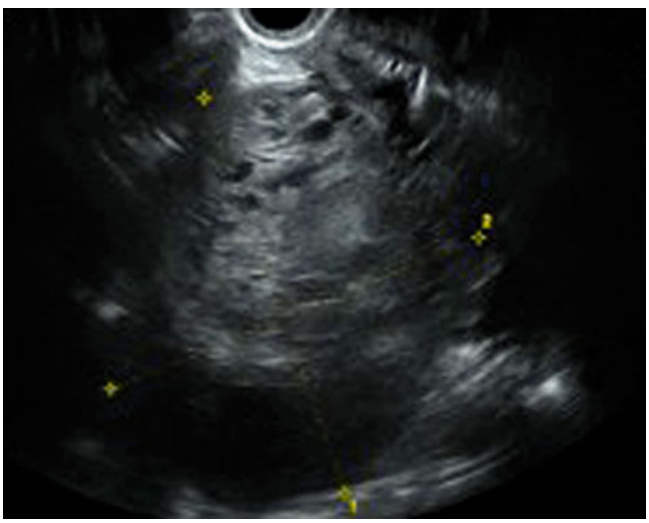

Fig. 6 Grayscale image of a large (209×81×181 mm) solid ovarian mass with a color score of 2 in a 49-year-old patient with a stage Ic GCT. The small cystic components give the typical Swiss cheese appearance

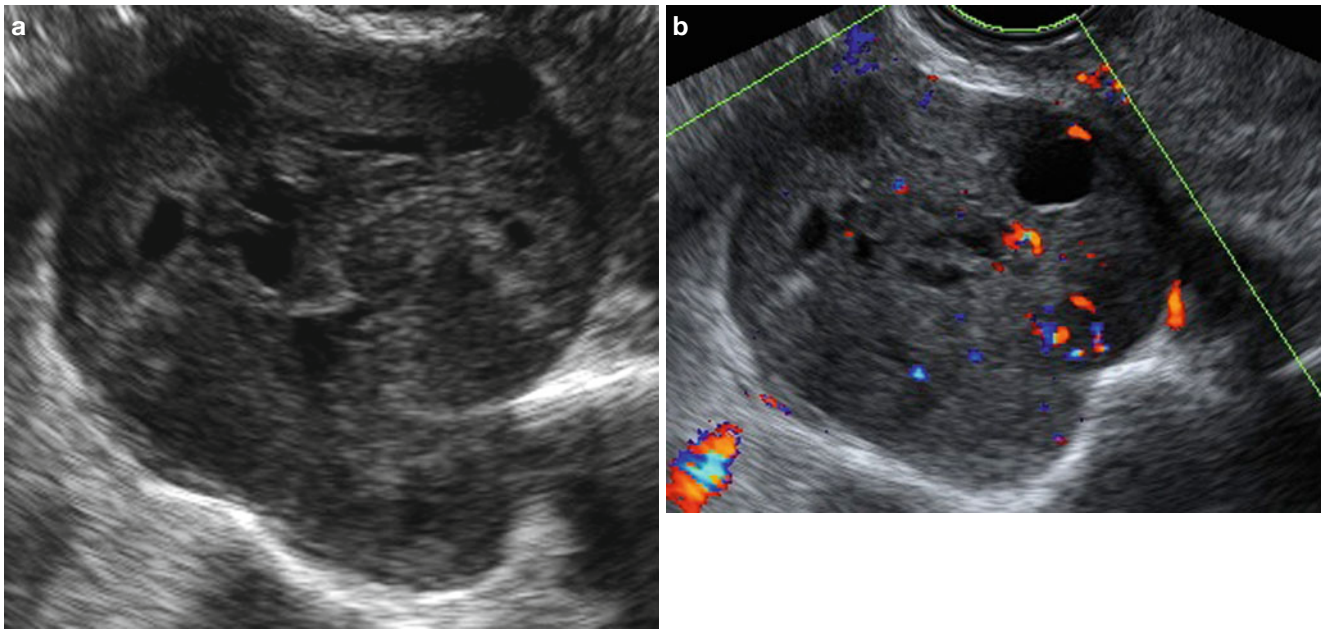

Fig. 7 (**a**, **b**) Grayscale (**a**) and color Doppler (**b**) image of coincidental finding of a solid mass (42×42×44 mm) with a small (<20 %) amount of cystic components in a 48-year-old patient. Images demonstrate the swiss cheese type GCT. The color score was 3

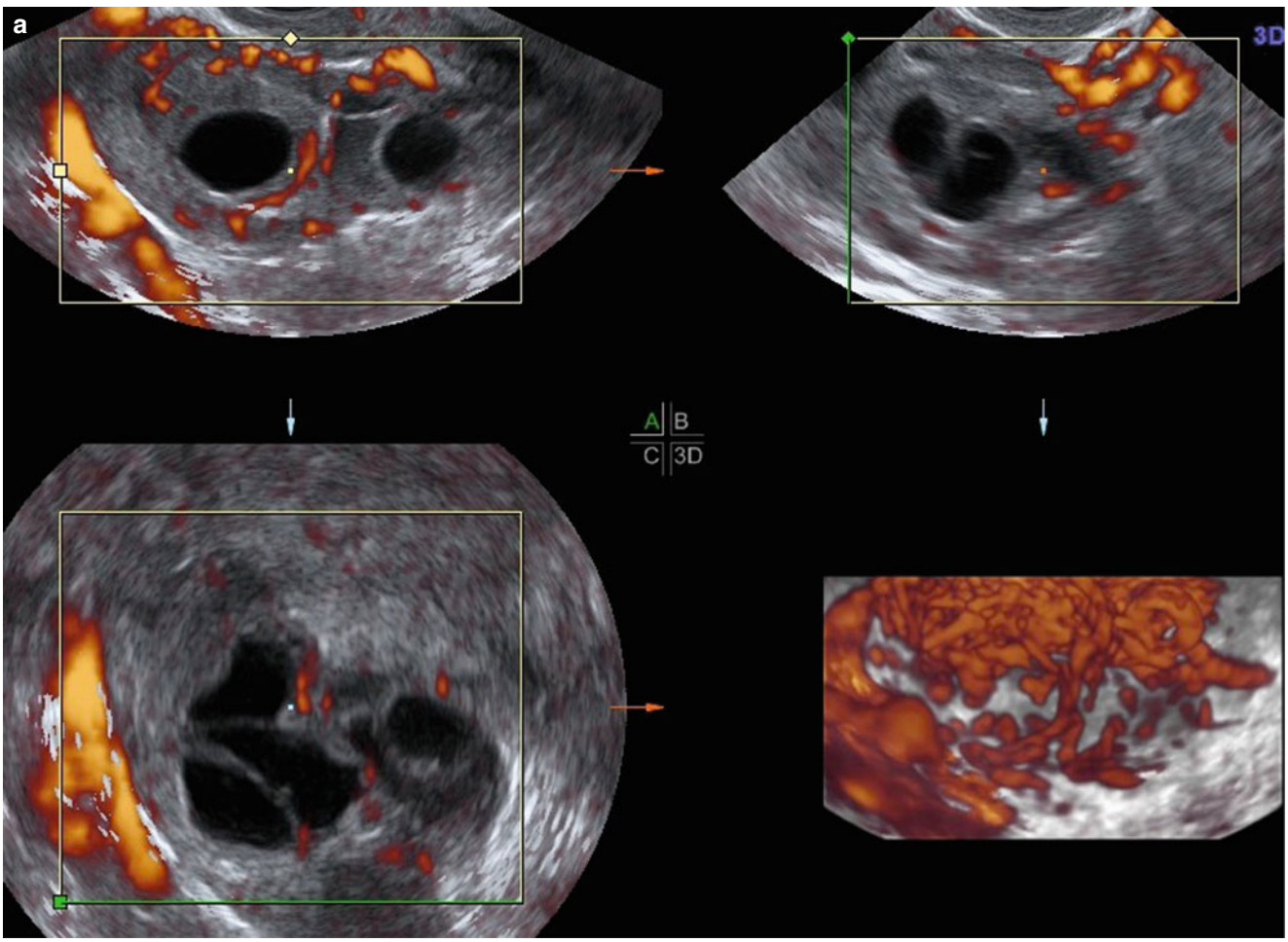

Fig. 8 (**a**, **b**) A 50-year-old patient who came for menorrhagia and incidentally was diagnosed with a stage I GCT. TVS demonstrated beside adenomyosis and a regular endometrium, a multilocular-solid lesion with papillary projections in the right ovary (52×31×43 mm). The echogenicity of the cyst fluid was anechoic or hemorrhagic depending on the cyst locule. The color score was 4

Fig. 8 (continued)

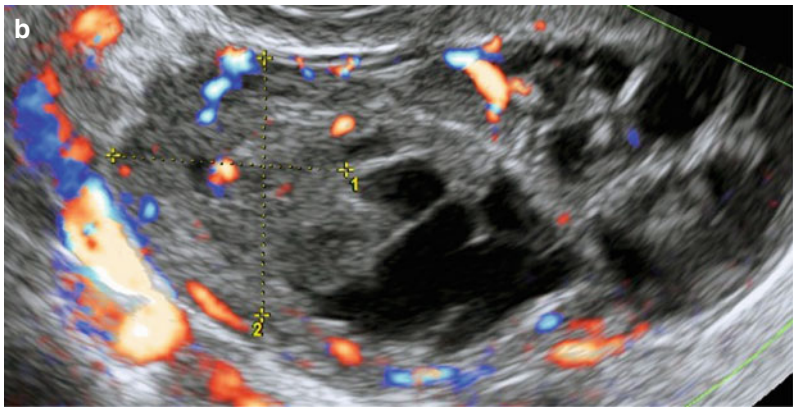

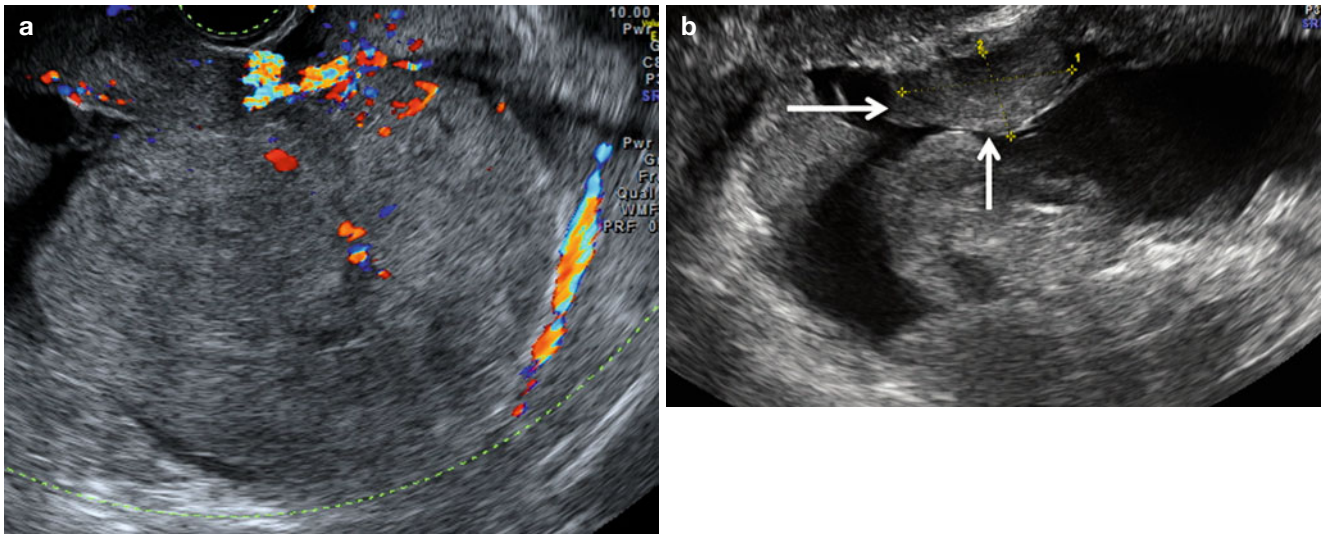

Fig. 9 (**a**, **b**) Solid ovarian mass and a metastatic peritoneal lesion (*arrows*) in the pouch of Douglas in a patient with an adult granulosa cell tumor stage IIIc. Pattern recognition could not assign the necrotic type neither the Swiss cheese type

cannot always be assigned to either one of the groups as demonstrated in Fig. 9a, b.

In the IOTA series, only three juvenile granulosa cell tumors were included, making the group too small to make a meaningful comparison between ultrasound findings of the juvenile and the adult type. All three juvenile cases contained a considerable amount of solid tissue. One mass was unilocular solid, the other two were multilocular solid (Figs. 10, 11, and 12). They were found in two children of 3 and 8 years old and in one woman of 31 years old. There was no pattern recognized in the two GCT's of the juvenile type presenting as a multilocular-solid mass with very large locules (Figs. 10 and 11) and as a unilocular-solid mass (Fig. 12).

Sertoli-Stromal Cell Tumors

The Sertoli-stromal cell tumors are divided in the Sertoli cell tumors and the Sertoli-Leydig cell tumors (Fig. 13).

Sertoli Cell Tumors

Epidemiology

Ovarian Sertoli cell tumors account for 4 % of the Sertoli-stromal cell tumors.

Clinical Symptoms

Most tumors are nonfunctional, look clinically benign, and do not cause specific symptoms. The tumors typically occur in young females, sometimes children. If the tumor is hormonally active, it can cause precocious puberty, bleeding disturbances, and hyperplastic endometrium. Occasionally patients have Peutz-Jeghers syndrome.

Macroscopic Appearance

The tumors are generally large, lobulated, solid, yellow, or brown masses.

Microscopic Appearance

Most of them show a uniform tubular pattern.

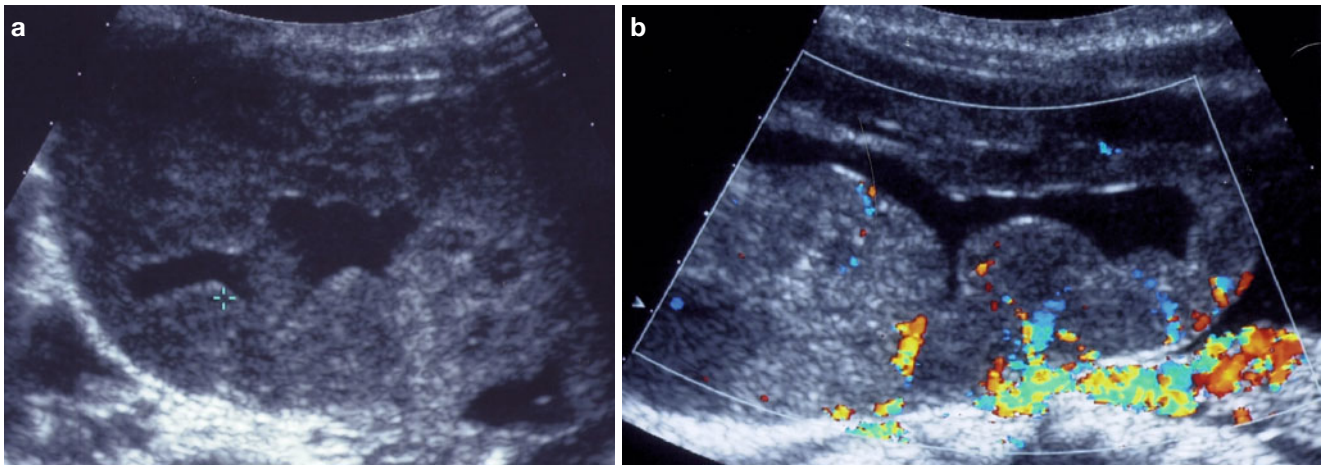

Fig. 10 (**a**, **b**) Atypical image of a unilocular-solid stage Ic granulosa cell tumor of the juvenile type in a 3-year-old girl with isosexual pseudoprecocity. The mass contains solid papillary projections protruding from the cyst wall and shows abundant vascularization. This was the only unilocular-solid mass in the IOTA series (Image reproduced from Van Holsbeke et al. [6])

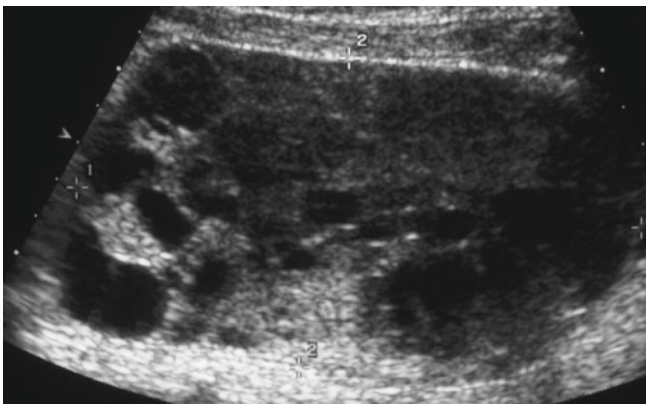

Fig. 11 Grayscale image of a multilocular-solid mass (185×150×85 mm) with more than 10 locules, anechogenic echogenicity of the cystic components, and a color score of 3. Histopathologic diagnosis was a stage Ia juvenile GCT in a 31-year-old patient (Image reproduced from Van Holsbeke et al. [6])

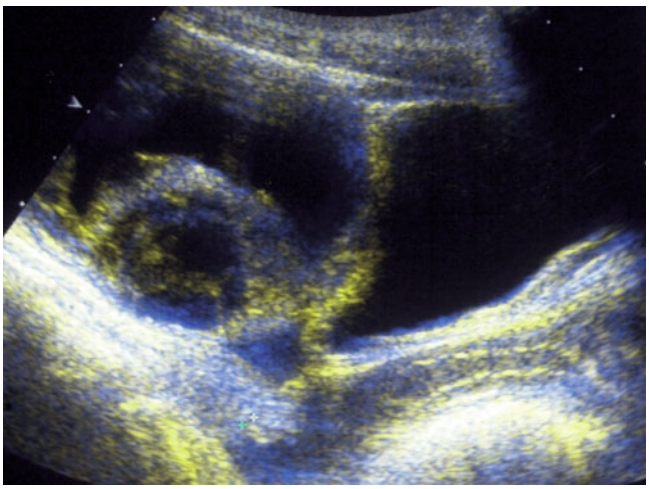

Fig. 12 Grayscale image of a multilocular-solid mass (73×67×58 mm) with eight locules, anechogenic echogenicity of the cyst content, and a color score of 4 (stage Ia juvenile GCT in an 8-year-old patient)

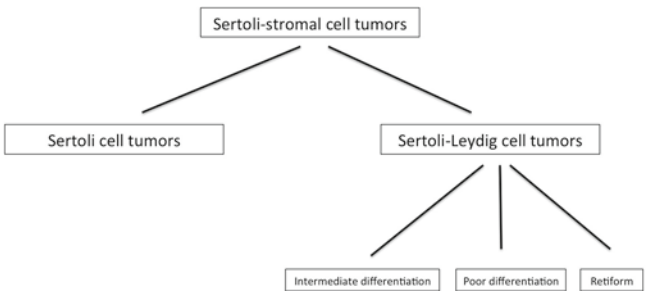

Fig. 13 Classification of the Sertoli-stromal cell tumors

Prognosis

Most tumors are stage I and have an excellent prognosis [4, 22].

Sonographic Characteristics

The Sertoli cell tumors are mostly larger, purely solid tumors with a color score of 3 or 4.

Because it is a very rare tumor, the IOTA study group identified only two Sertoli tumors of which the pictures are presented in Fig. 14 [5]. Other examples can be found in Figs. 15 and 16.

Sertoli-Leydig Cell Tumors

Epidemiology

The Sertoli-Leydig cell tumors account for less than 0.2 % of all the ovarian cancers. Although they can occur in all age groups, the highest incidence is found during the reproductive years.

Clinical Symptoms

Half of the patients present with symptoms caused by virilization, i.e., oligomenorrhea, amenorrhea, breast

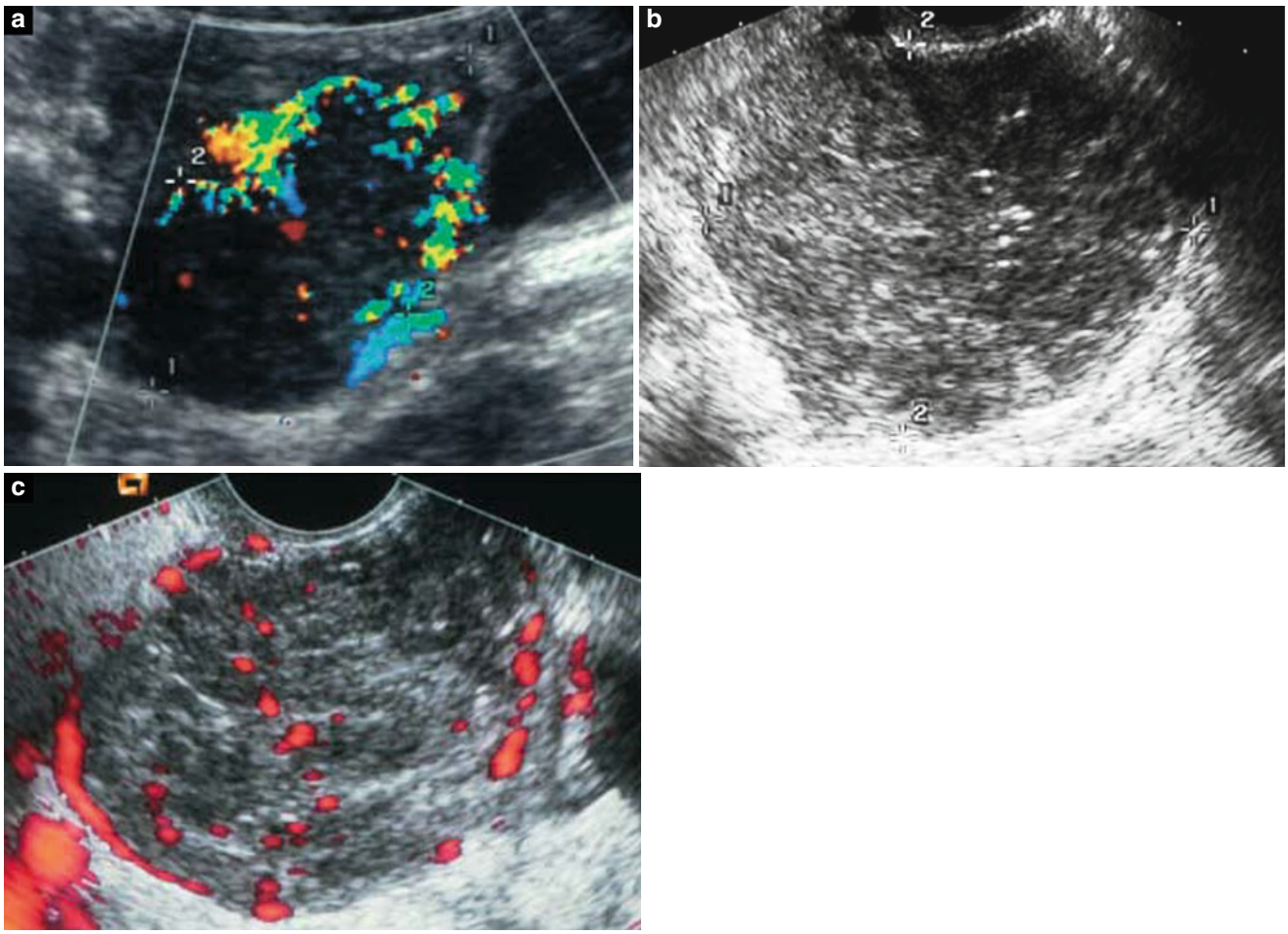

Fig. 14 Ultrasound images showing a 4-cm solid highly vascularized Sertoli cell tumor in a 4-year-old girl with pubertas precox (**a**) and a 7-cm solid moderately vascularized Sertoli cell tumor in a 59-year-old asymptomatic woman (**b**, **c**) (Image reproduced from Demidov et al. [5])

atrophy, hirsutism, acne, deepening of voice, clitoris hypertrophy, or balding. Serum levels of testosterone, androstenedione, and other androgens may be increased. A minority has estrogenic manifestations causing menometrorrhagia or postmenopausal bleeding. Half of them have no endocrine manifestations; in these cases presenting symptoms may be pain or abdominal swelling. Sometimes the tumors rupture or spread outside the ovary. This is more common in the poorly differentiated tumors. Ascites is rare [4].

Macroscopic Appearance

In most cases the tumor is unilateral and rather large with an average diameter of 10 cm. The masses are firm, lobulated yellow or tan masses with a smooth external surface.

Microscopic Appearance

On microscopy there are three categories: the intermediate differentiated type, the poor differentiated type, and the retiform type.

Prognosis

Most of the Sertoli-Leydig cell tumors are diagnosed at stage I. Survival depends on the degree of differentiation but is quite good for stage I. Tumors that present at a higher stage have a poor prognosis. Sertoli-Leydig cell tumors typically reappear within 1 year, and almost 95 % recur within 5 years. Recurrent tumors are usually confined to the pelvis or abdomen.

Sonographic Characteristics

The 15 Sertoli-Leydig cell tumors that were found in the IOTA group were either small- (3–4 cm) or medium-sized (6–7 cm) solid tumors or multilocular-solid tumors of any size (3–18 cm) with purely solid areas mixed with areas of innumerable closely packed small-cyst locules [23] (Fig. 17). Other examples can be found in Figs. 17, 18, 19, and 20.

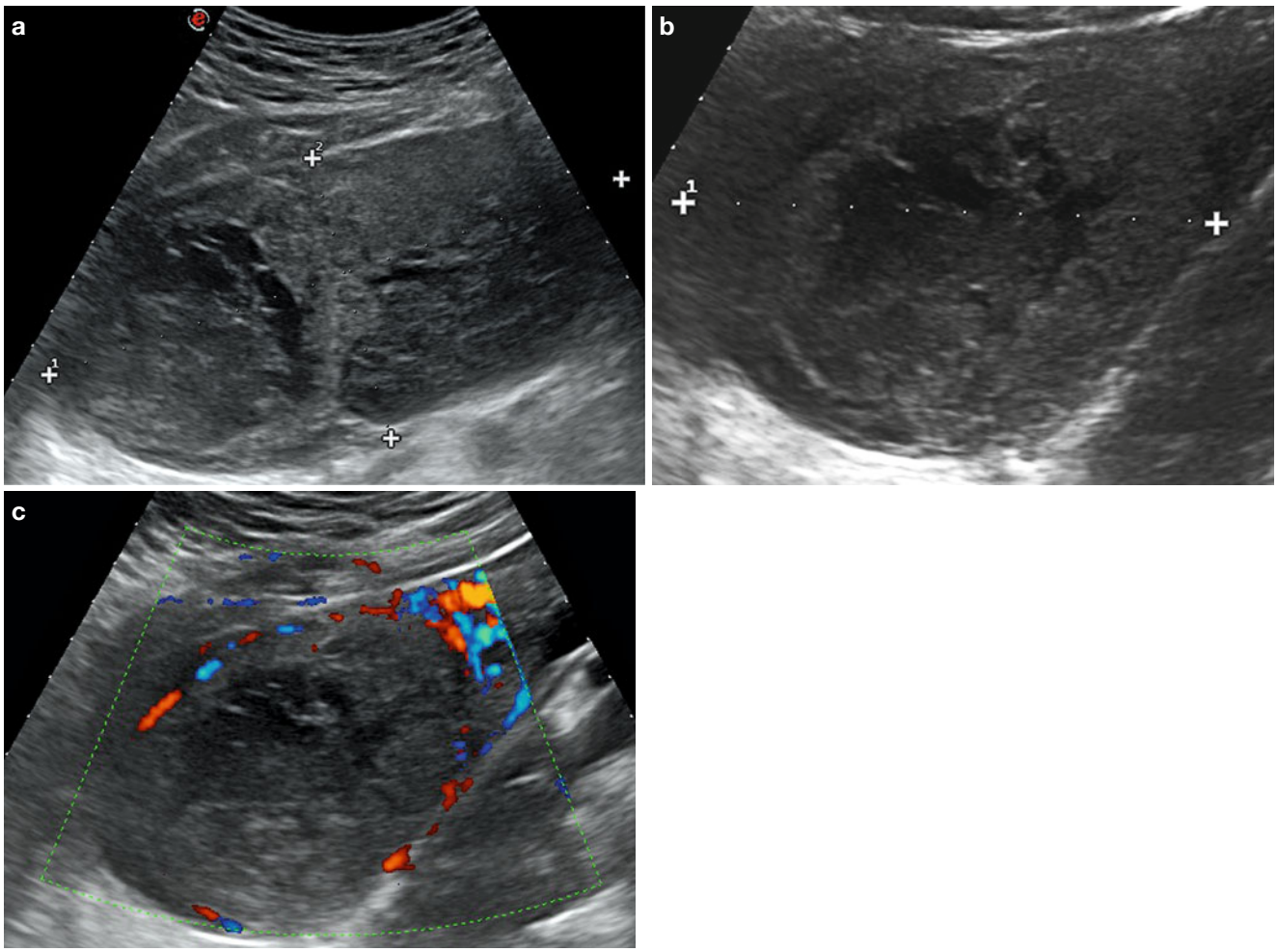

Fig. 15 (**a**–**c**) Stage Ic Sertoli cell tumor in a 17-year-old patient: large (150×94×73 mm) solid mass with more than 80 % solid tissue, necrotic areas, and a color score of 3

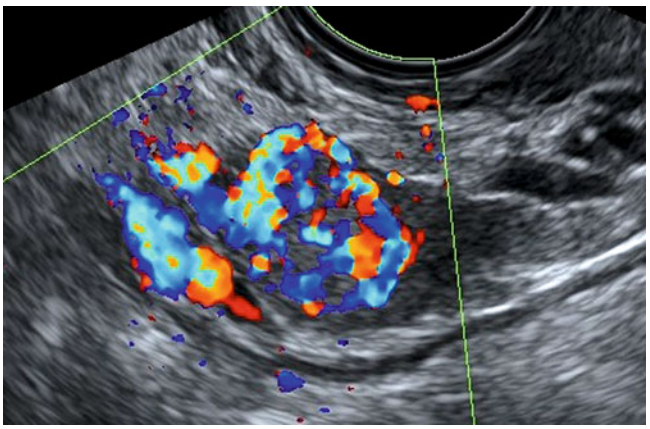

Fig. 16 A 50-year-old patient who came for investigation of postmenopausal bleeding. TVS demonstrated two endometrial polyps and a small (28×16×27 mm) solid lesion in the left ovary with very strong vascularization. Histology demonstrated that it was a stage Ia Sertoli cell tumor

Steroid Cell Tumors

The group of the steroid cell tumors is divided in the stromal luteoma (25 %) and the Leydig cell tumor (75 %). They account for only 0.1 % of all ovarian tumors and are benign lesions. The characteristics of both tumor types can be found in Table 3.

Leydig Cell Tumors

Epidemiology

For many years these tumors were called lipid cell or lipoid cell tumor. Later on the term, steroid cell tumors were introduced since 25 % of the tumors contained no or only a little amount of lipid. They account for 0.1 % of the ovarian masses. Leydig cell tumors are hilus cell tumors or Leydig cell tumors of the non-hilar type (Fig. 21), the latter being extremely rare [4].

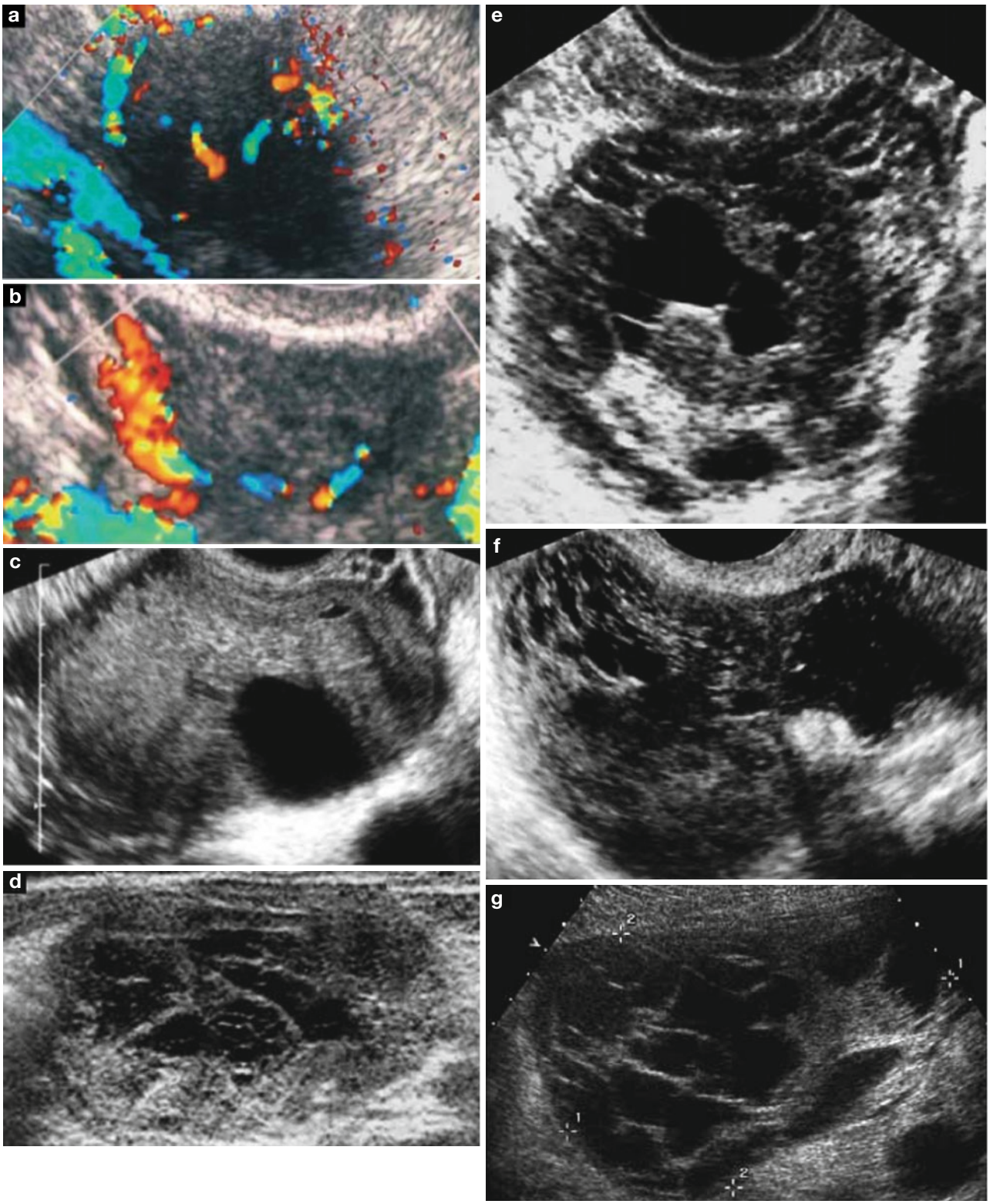

Fig. 17 Sertoli-Leydig cell tumors were either moderately or abundantly vascularized purely solid tumors (**a**–**c**) or multilocular-solid tumors (**d**–**g**) with areas of innumerable closely packed small-cyst locules mixed with solid areas. Ultrasound images showing a 4-cm abundantly vascularized solid Sertoli-Leydig cell tumor in a 60-year-old woman with hirsutism (**a**), a 3-cm abundantly vascularized solid. Sertoli-Leydig cell tumor in a 61-year-old woman with bleeding during hormone replacement therapy (**b**), a 7-cm solid Sertoli-Leydig cell tumor in a 29-year-old woman with oligomenorrhea and hirsutism (this woman had bilateral tumors, the 6-cm tumor on the contralateral side having virtually identical ultrasound morphology) (**c**), a 5-cm multilocular-solid Sertoli-Leydig cell tumor in a 37-year-old woman with increased cycle length (**d**), a 6-cm multilocular-solid Sertoli-Leydig cell tumor in a 36-year-old woman with amenorrhea for 2 years (**e**), a 7-cm multilocular-solid Sertoli-Leydig cell tumor in a 25-year-old woman with oligomenorrhea (**f**), and a 13-cm moderately vascularized multilocular-solid Sertoli-Leydig cell tumor of low differentiation in a 33-year-old woman with bleeding disturbance and pain (the pain was probably explained by tumor rupture) (**g**) (Image reproduced from Demidov et al. [5])

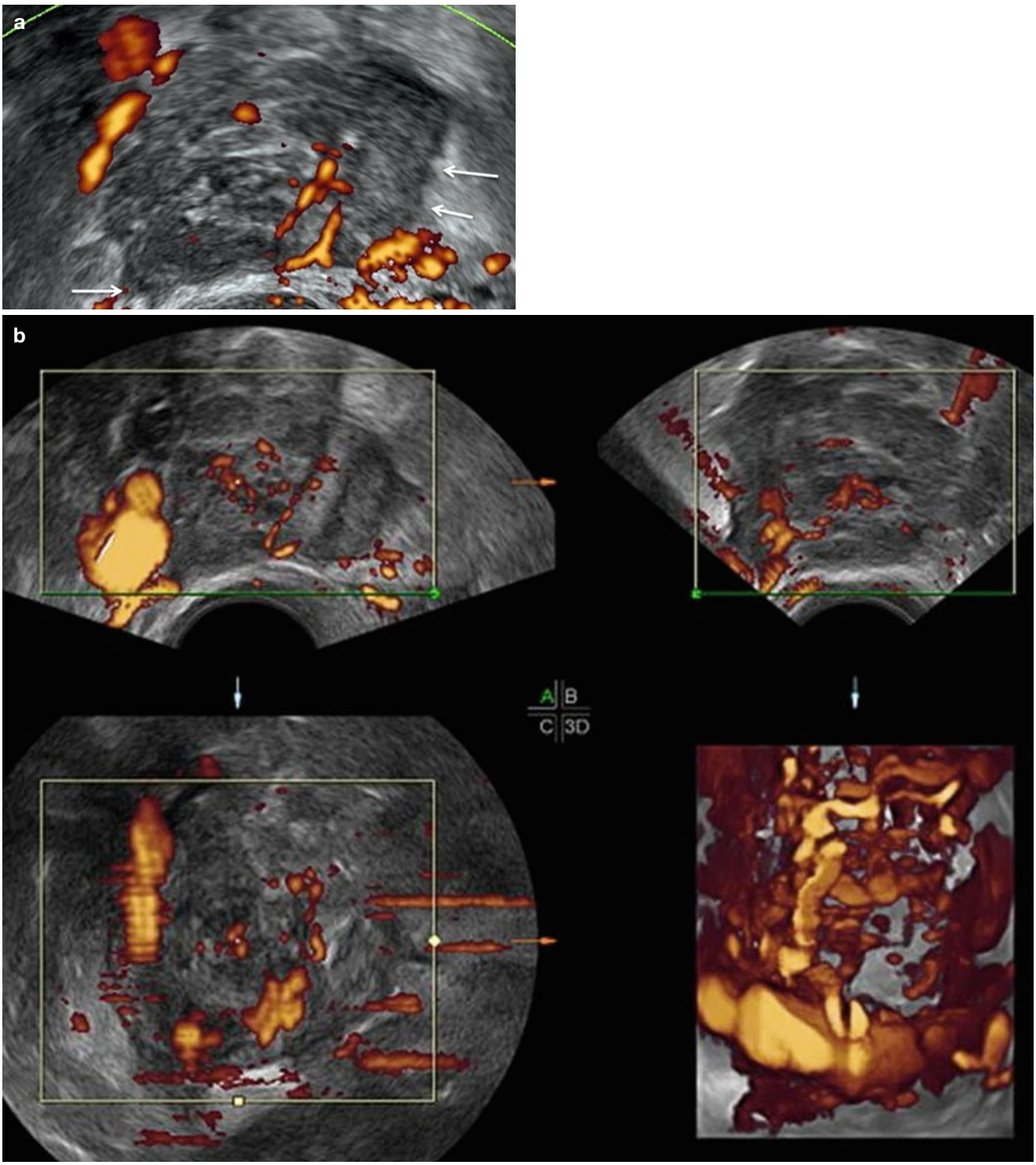

Fig. 18 (**a**, **b**) 2D and 3D color Doppler images of a stage I Sertoli-Leydig cell tumor in a 51-year-old woman. The mass was a purely solid lesion with a color score of 4 and irregular borders (*arrows*)

Clinical Symptoms

Leydig cell tumors of the hilar type are associated with hirsutism and virilization in 75 % of cases. Estrogenic manifestations are rare. The onset of androgenic symptoms is often slow, and the symptoms, which tend to be milder than those associated with Sertoli-Leydig cell tumors, may have been present for many years when the diagnosis is made.

Macroscopic Appearance

Leydig cell tumors may resemble mucinous cysts on gross examination; they are small (mean diameter 2.4 cm), solid, brown to yellow tumors, and usually are unilateral.

Microscopic Appearance

Microscopic examination of hilus cell tumors reveals a circumscribed mass of steroid cells with eosinophilic cytoplasm. For a diagnosis of ovarian Leydig cell tumor to be made, crystals of Reinke must be identified in the cytoplasm of the neoplastic cells.

Prognosis

Leydig cell tumors are almost always benign and have a good prognosis.

Sonographic Characteristics

Using pattern recognition, the five Leydig cell tumors that were included in the IOTA pictorial essay [23] were small solid tumors (largest diameter of 1–3 cm) with a color score of 3 or 4 (Fig. 22).

Stromal Luteoma

A stromal luteoma is very rare benign tumor and only a few cases have been described.

Most tumors occur in postmenopausal women that present with bleeding disorders but in some cases virilizing signs may be observed as well. The tumor is surrounded by ovarian stroma and entirely composed of luteinized cells devoid of crystals of Reinke. Hyperthecosis of ovarian stroma is often observed [23].

Due to its rare incidence we could not find any representative ultrasound image.

Sex Cord Tumor with Annular Tubules (SCTAT)

These tumors are very rare and vary clinically and pathologically depending on the fact whether the patient has Peutz-Jeghers syndrome or not. In Peutz-Jeghers syndrome patients, both ovaries demonstrate several lesions of this type of tumor that all tend to be small and are mostly

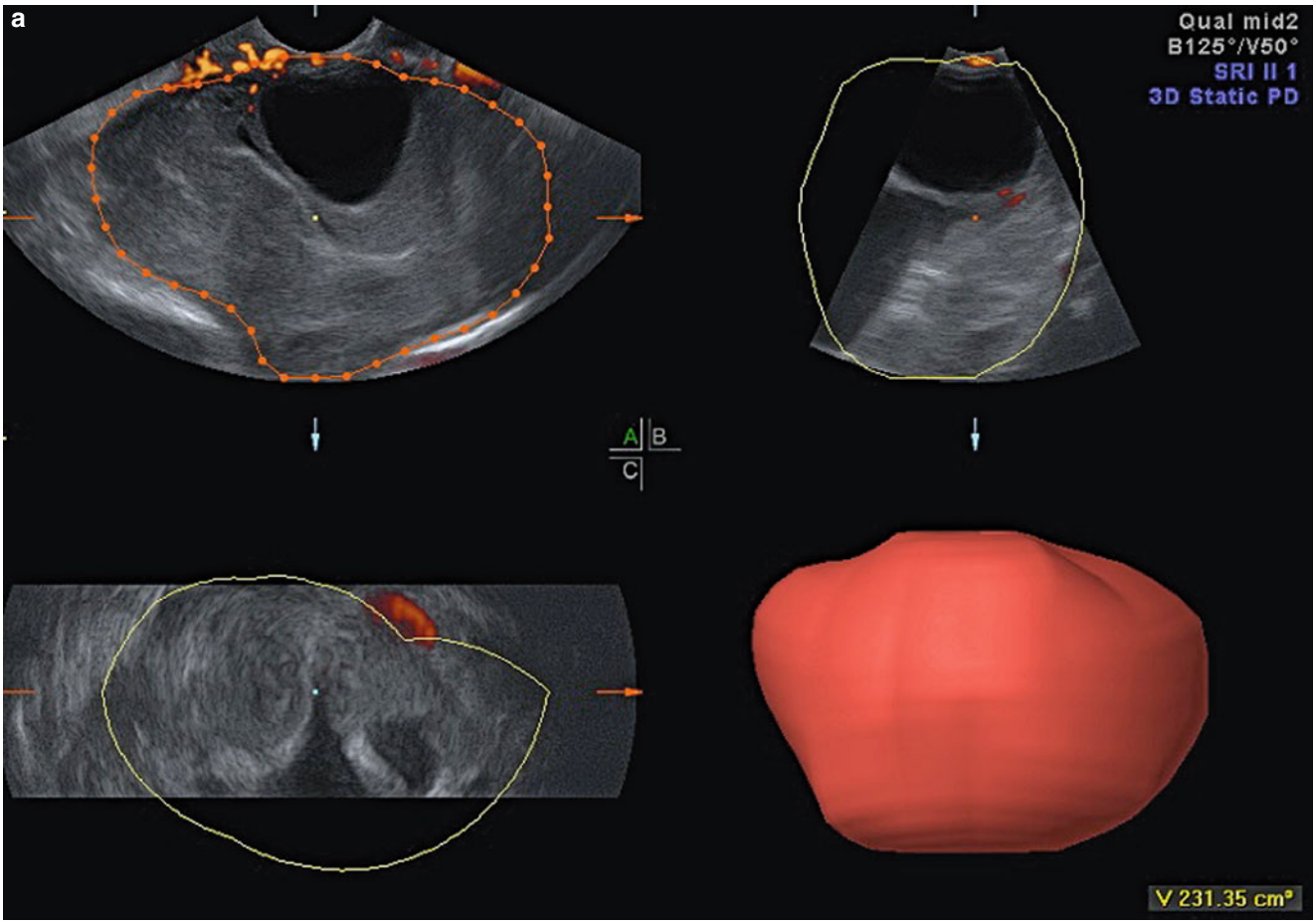

Fig. 19 (**a**, **b**) Multilocular-solid mass (125 × 113 × 94 mm) with more than 10 locules and a color score of 3 in a 39-year-old patient with a Sertoli-Leydig cell tumor

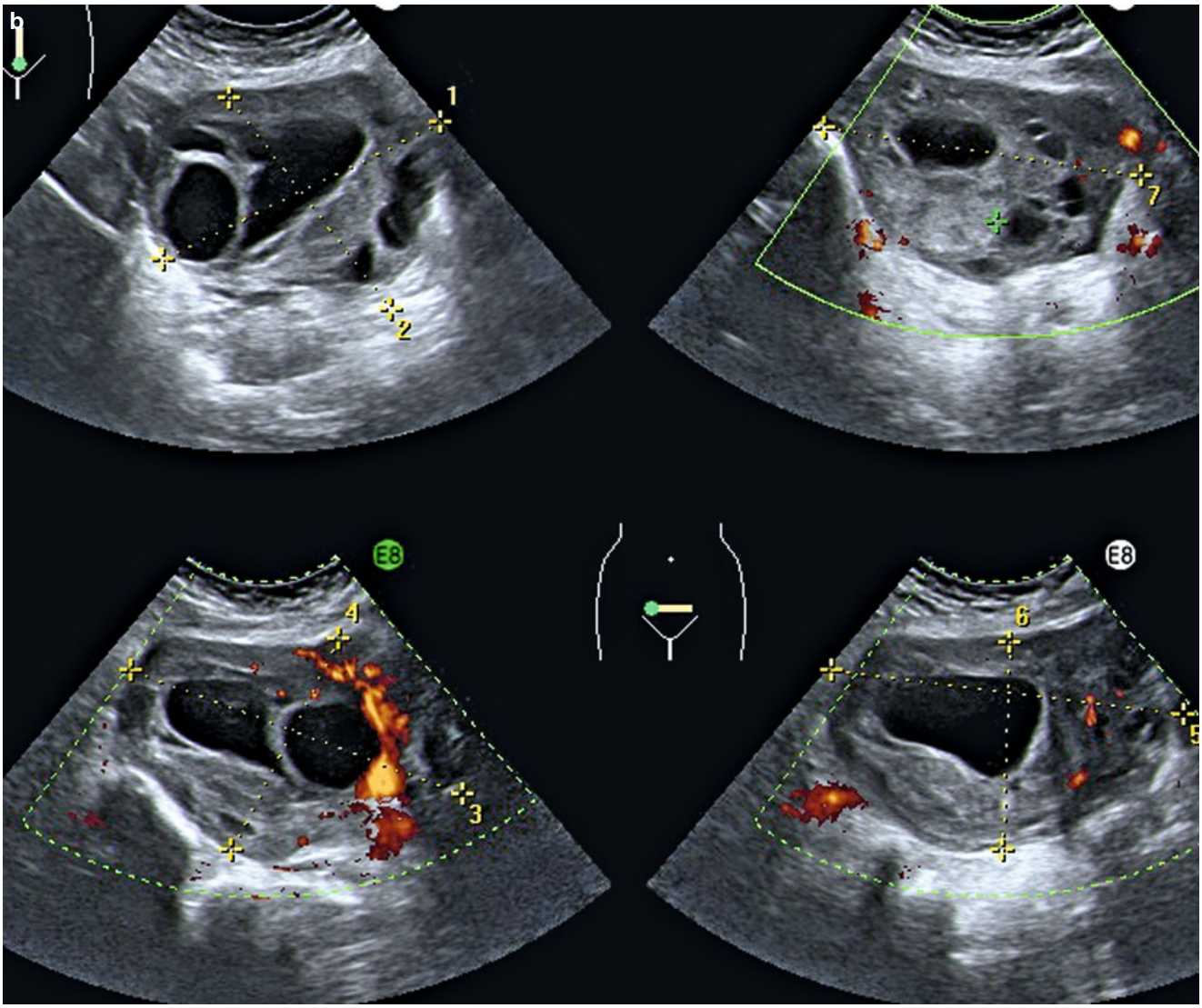

Fig. 19 (continued)

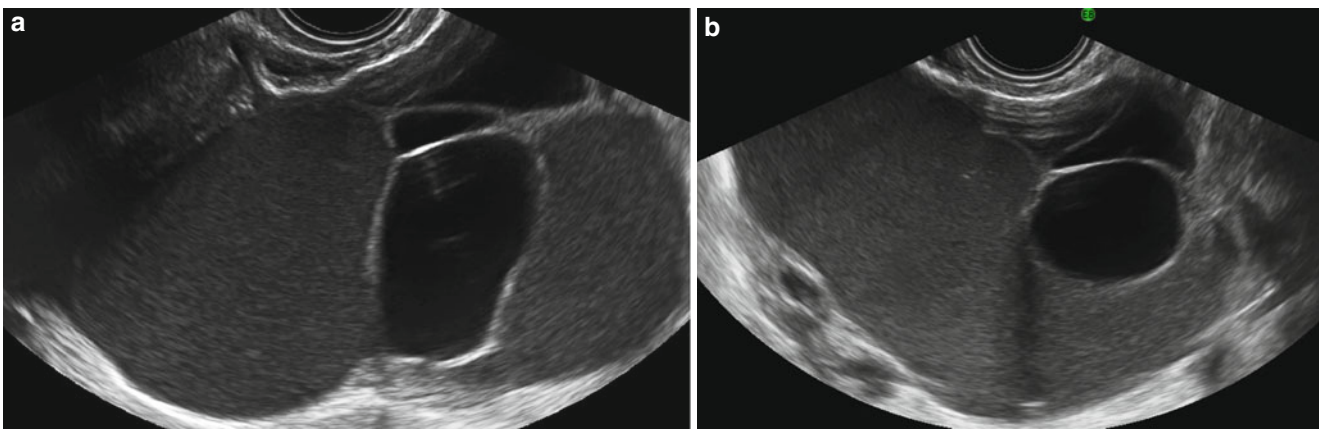

Fig. 20 Sertoli-Leydig cell tumor in a 61-year-old patient that presented as a Multilocular-solid mass (92×65×59 mm) with 5 locules with ground glass echogenicity and a color score of 2

Table 3 Characteristics of stromal luteoma and leydig cell tumor

	Stromal luteoma	Leydig cell tumor
Incidence	0.1 % of all ovarian tumors 25 % of steroid cell tumors	75 % of steroid cell tumors
Age	80 % postmenopausal Average age is 58 years	Average age is 43 years
Benign or malignant	Benign	Benign
Symptoms	60 % estrogenic symptoms (bleeding disorders)	Virilization 83 % in the hilar type 33 M in the non-hilar type
Typical features	Macroscopic Small (3 cm) Unilateral Solid Gray-white, yellow or brown-red	Macroscopic Large (8.4 cm)
	Microscopic Arises from the ovarian stroma much more often than from adrenal rest cells or Leydig cells	Microscopic
	Stromal hyperthecosis (same or contralateral ovary) 90 %	Stromal hyperthecosis 23–67 %

incidental findings when the ovary is removed for other reasons. In case the patient has no Peutz-Jeghers syndrome, the tumors are unilateral, large palpable masses that can transform to a GCT. Forty percent have estrogenic secretion that causes symptoms that are related to endometrial changes. Twenty percent of the tumors are malignant, but the prognosis is quite good and recurrences are late (Fig. 23a–c) [4].

Gynandroblastoma

Gynandroblastoma is an extremely rare tumor, and the diagnosis should be restricted to tumors that contain significant components of the Sertoli-Leydig cell tumor as well as the granulosa cell tumor, and the minor component should be at least 10 % of one of either types. The gynandroblastoma is malignant but due to its very low incidence, the malignant potential is unknown. Due to its rare incidence we could not find any representative ultrasound image.

Acknowledgements I would like to thank my friends and colleagues from the IOTA group for helping me to find new interesting images, especially Luca Savelli, Antonia C. Testa, Artur Czekierdowski, Stefano Guerriero, Jeroen Kaijser, and Dirk Timmerman.

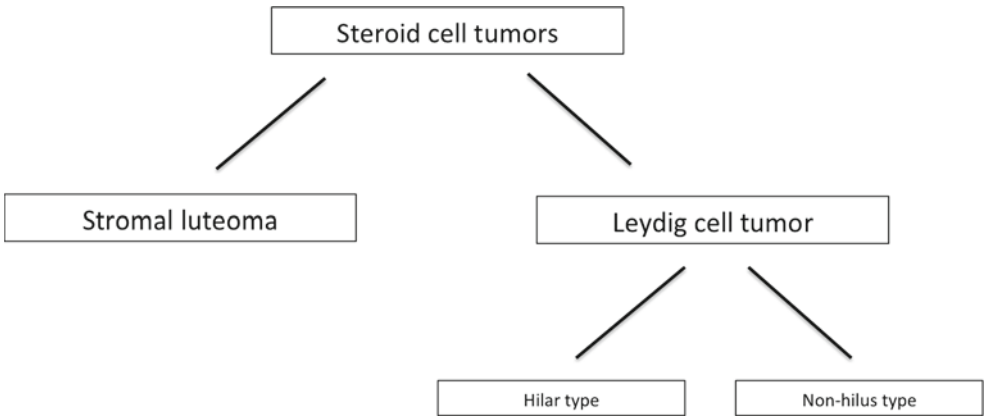

Fig. 21 Classification of the steroid cell tumors

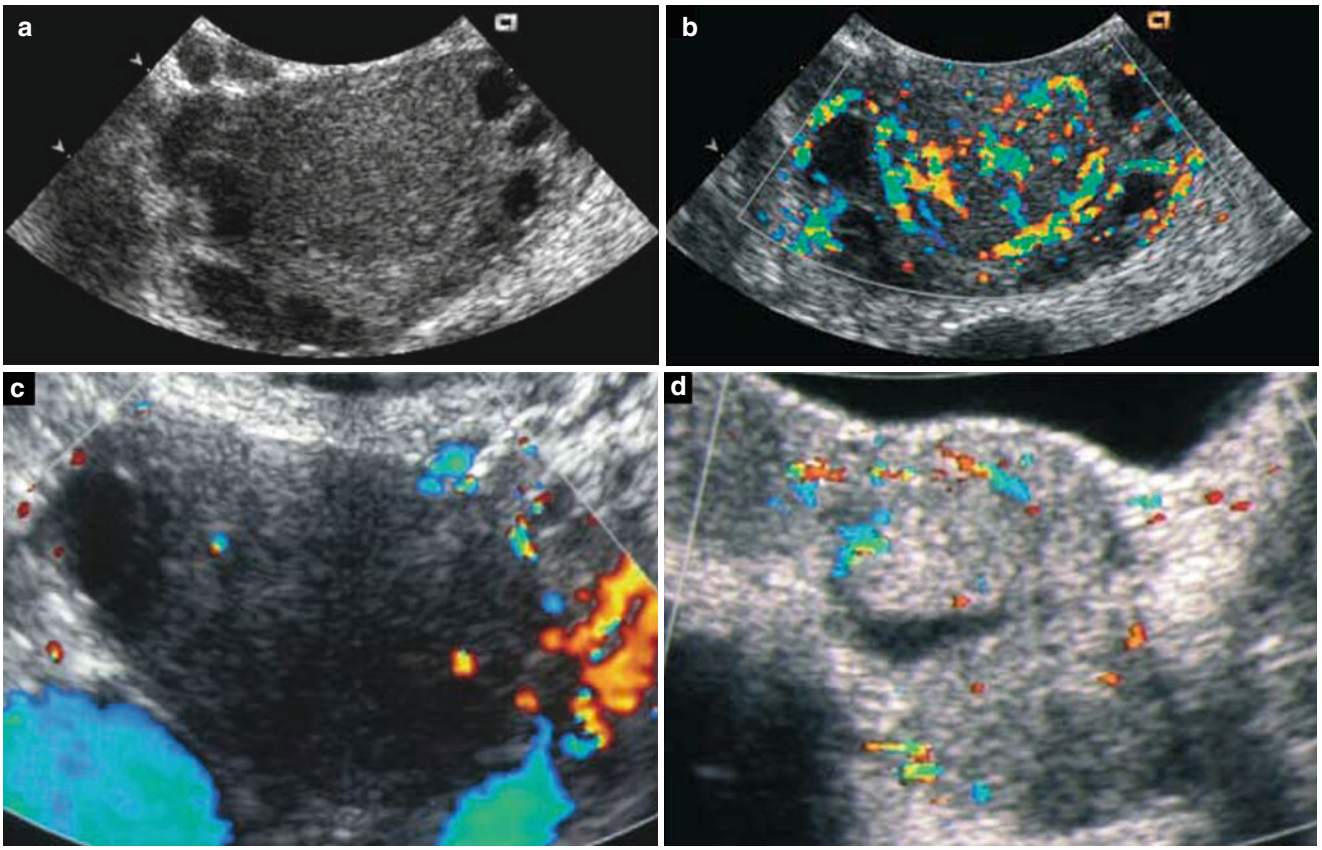

Fig. 22 Ultrasound images of Leydig cell tumors. Most were small solid tumors confined within an ovary of almost normal size. A 2-cm solid Leydig cell tumor, well circumscribed, and abundantly vascularized, in a 38-year-old woman with amenorrhea for 1 year (**a**, **b**), a 3-cm moderately vascularized solid Leydig cell tumor in a 23-year-old woman with an irregular cycle and hirsutism (**c**), and a 7-cm moderately vascularized solid Leydig cell tumor in a 20-year-old woman with an irregular menstrual cycle (**d**) (Image reproduced from Demidov et al. [5])

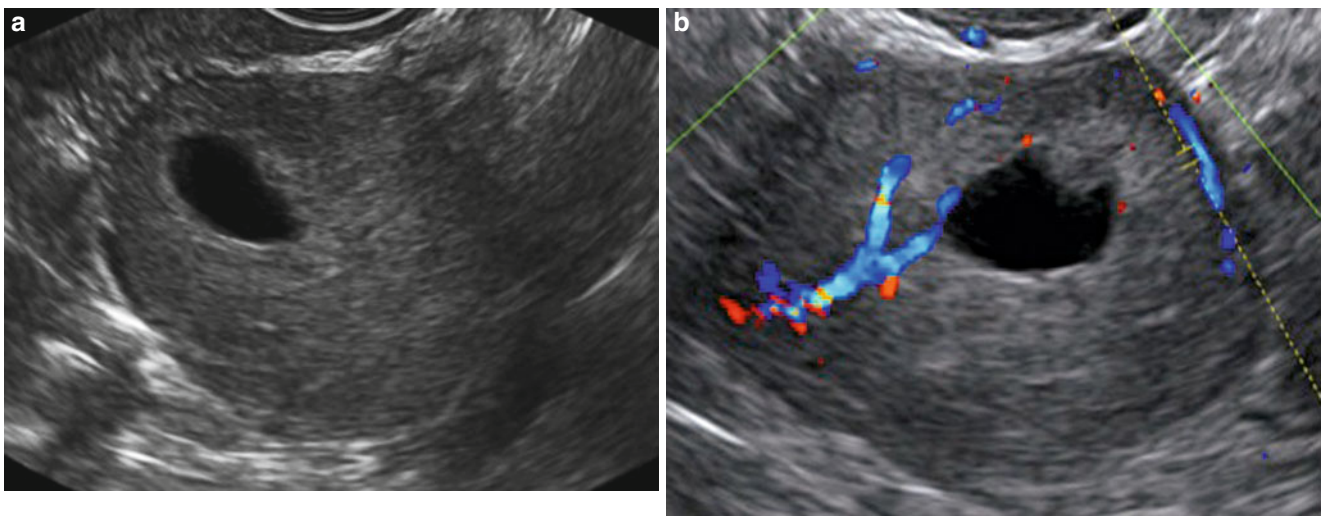

Fig. 23 (**a**–**c**) Grayscale (**a**) and color Doppler (**b**) image of a solid mass with one small central cystic component and a color score of 3 in an asymptomatic 25-year-old patient. Figure (**c**) is a grayscale rendered volume of the mass. That proved to be a sctat on final histology

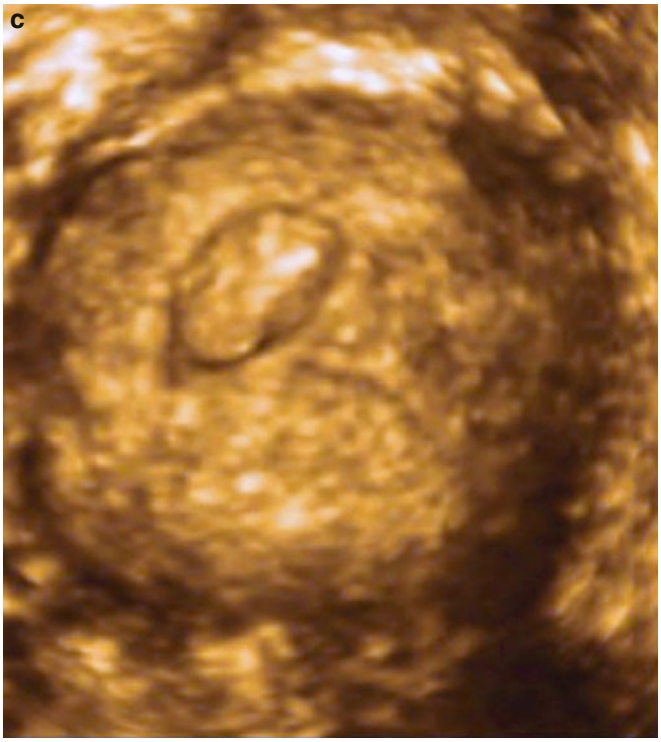

Fig. 23 (continued)

References

1. Quirk JT, Natarajan N. Ovarian cancer incidence in the United States, 1992–1999. Gynecol Oncol. 2005;97:519–23.
2. Varras M, Vasilakaki T, Skafida E, Akrivis C. Clinical, ultrasonographic, computed tomography and histopathological manifestations of ovarian steroid cell tumour, not otherwise specified: our experience of a rare case with female virilization and review of the literature. Gynecol Endocrinol. 2011;27:412–8.
3. Busquets M, Gonzalez-Bosquet E, Muchart J, Rovira C, Laïlla JM. Granulosa cell tumor and endometrial cancer: a case report and review of the literature. Eur J Gynaecol Oncol. 2010;31:575–8.
4. Kurman RJ, Ellenson LH, Ronnett BM, editors. Blaustein's pathology of the female genital tract. 6th ed. New York: Springer; 2011.
5. Demidov V, Lipatenkova J, Vokhareva O, Van Holsbeke C, Timmerman D, Valentin L. Imaging of gynecological disease (2): clinical and ultrasound characteristics of Sertoli cell tumors, Sertoli–Leydig cell tumors and Leydig cell tumors. Ultrasound Obstet Gynecol. 2008;31:85–91.
6. Van Holsbeke C, Domali E, Holland TK, Achten R, Testa AC, Valentin L, Jurkovic D, Moerman P, Timmerman D. Imaging of gynecological disease (3): clinical and ultrasound characteristics of granulosa cell tumors of the ovary. Ultrasound Obstet Gynecol. 2008;31:450–6.
7. Timmerman D, Valentin L, Bourne TH, et al. Terms, definitions and measurements to describe the ultrasonographic features of adnexal tumors: a consensus opinion from the international ovarian tumor analysis (IOTA) group. Ultrasound Obstet Gynecol. 2000;16:500–5.
8. Scully RE. Tumors of the ovary and mal developed gonads. Atlas of tumorpathology, series 2 fascicles 16. Washington, D.C.: Armed Forces Institute of Pathology; 1979. p. 152–73.
9. Zaloudek C. The ovary. In: Gompel C, Silverberg SG, editors. Pathology in gynecology and obstetrics. 4th ed. Philadelphia: Lippincott; 1994. p. 313–413.
10. Cohen DJ. Ovary and adnexa. In: Thurmond AS, Jones MK, Cohen DJ, editors. Gynecologic, obstetric and breast radiology. Cambridge, MA: Blackwell Science; 1996. p. 255–322.
11. Young RH, Dickersin GR, Scully RE. Juvenile granulosa cell tumor of the ovary: a clinicopathological analysis of 125 cases. Am J Surg Pathol. 1984;8:575–96.
12. Malmström H, Hogberg T, Risberg B, et al. Granulosa cell tumors of the ovary: prognostic factors and outcome. Gynecol Oncol. 1994;52:50–5.
13. Willemsen W, Kruitwagen R, Bastiaans B, Hanselaar T, Rolland R. Ovarian stimulation and granulosa-cell tumour. Lancet. 1993;341:986–8.
14. Scully RE. Juvenile granulosa cell tumor. Pediatr Pathol. 1988;8:423–7.
15. Novak E, Kutchmeshgi J, Mupas R, Woodruff J. Feminizing gonadal stromal tumors. Analysis of granulosa-theca cell tumors of ovarian tumor registry. Obstet Gynecol. 1971;38:701–13.
16. Vassal G, Flamant F, Cailland JM, et al. Juvenile granulosa cell tumor of the ovary in children : a clinical study of 15 cases. J Clin Oncol. 1988;6:990–5.
17. Fox H, Agrawal K, Langley FA. A clinicopathological study of 92 cases of granulosa cell tumor of the ovary with special reference to the factors influencing prognosis. Cancer. 1975;35:231–41.
18. Evans AT, Gaffey TA, Malkasian GD, et al. Clinicopathological review of 118 granulosa and 82 theca cell tumors. Obstet Gynecol. 1980;55:231–8.
19. Savage P, Constenla D, Fisher C, Shepherd JH, Barton DP, Blake P, et al. Granulosa cell tumors of the ovary: demographics, survival and the management of advanced disease. Clin Oncol. 1998;10:242–5.
20. Björkholm E, Silfversward C. Prognostic factors in granulosa cell tumors. Gynecol Oncol. 1981;11:261–74.
21. Ohel G, Kaneti H, Schenker JG. Granulosa cell tumors in Israel: a study of 172 cases. Gynecol Oncol. 1983;15:278–86.
22. Oliva E, Alvarez T, Young RH. Sertoli cell tumors of the ovary: a clinicopathologic and immunohistochemical study of 54 cases. Am J Surg Pathol. 2005;29:143–56.
23. Hayes M, Scully R. Stromal luteoma of the ovary: a clinicopathological analysis of 25 cases. Int J Gynecol Pathol. 1987;6:313–21.

Malignant Sex Cord-Stromal Tumor: Computed Tomography and Magnetic Resonance

Takashi Koyama

Abstract

Although majority of sex cord-stromal tumor is benign, some granulosa cell tumor and Sertoli-Leydig tumors show malignant behavior. Stage is the most important prognostic factor. The recurrent sex cord-stromal tumors are usually peritoneal seeding or retroperitoneal nodule, occasionally containing intratumoral hemorrhage.

Keywords

Ovarian sex cord-stromal tumor • Granulosa cells tumor • Theca cells tumor • Sertoli cells tumor • Leydig cells tumor • Imaging • Computed tomography • Magnetic resonance imaging

Although the majority of sex cord-stromal tumors are benign, both granulosa cell tumors (GCT) of and Sertoli-Leydig cell tumors (SLCT) have potential for malignant behavior. They recur in 20 % of patients 10 years after the original diagnosis. The metastasis or recurrence usually occurs late, even as much as 20–30 years following the primary diagnosis [1, 2]. There, these tumors are considered as low-grade malignancy. However, in pediatric ages, both GCT and SLCT account for 10 % of malignant ovarian tumors [3].

The staging system for sex cord-stromal tumor is generally adopted from that used for epithelial ovarian cancer, as originally defined by the International Federation of Obstetrics and Gynecology (FIGO). In GCT, patients generally present with stage I disease (78–91 %), whereas the remainder has advanced disease with variable involvement of the pelvis, intra-abdominal organs, and peritoneum. Rarely, patients can present with metastatic disease involving the liver, lung, or bone.

In GCTs, the stage is the most important prognostic factor [4–6]. Most of studies have shown a greater than 90 % 5-year survival rate in patients with stage I GCT. This contrasts with the 55–75 % 5-year survival rate for patients with stage II tumors and the 22–50 % survival rate for stage III/IV. As a prognostic factor, the age of the patients at the presentation is controversial. Some reports show favorable prognosis with age less than 40 years [1], whereas others conclude that age greater than 40 years is more favorable [7]. Tumors greater than 10 cm in diameter have been shown to associate with an increased risk of death, independent of stage [1, 7, 8].

Although a number of histologic features have also been evaluated for the prognostic significance, in granulose cell tumors, the histologic feature does not enable an accurate prediction of clinical behavior [6, 9]. In a recent study which evaluated several histopathologic variables including stage, *p53* status, histologic pattern, mitotic index, and lymphovascular space invasion, only mitotic and lymphovascular space invasion were independent prognostic factors [10]. Thereafter, the preoperative imaging findings predictive of malignant GCT include large tumors size and the presence of extraovarian lesions such a peritoneal implants (Fig. 1). Otherwise, the imaging feature of malignant GCT may not significantly differ from those ordinary GCT, that is, solid masses with variable amount of cystic components, containing hemorrhagic fluid [11, 12]. The simultaneous presence of the enlarged uterus with thickened endometrium is a clue to suspect estrogen production from GCT (Fig. 1).

T. Koyama, MD, PhD
Department of Diagnostic Radiology, Osaka Red Cross Hospital,
5-30 Fudegasaki-cho, Tennoji-Ward, Osaka-City,
Osaka 543-8555, Japan
e-mail: montpeti@kuhp.kyoto-u.ac.jp

L. Saba et al. (eds.), *Ovarian Neoplasm Imaging*,
DOI 10.1007/978-1-4614-8633-6_19,

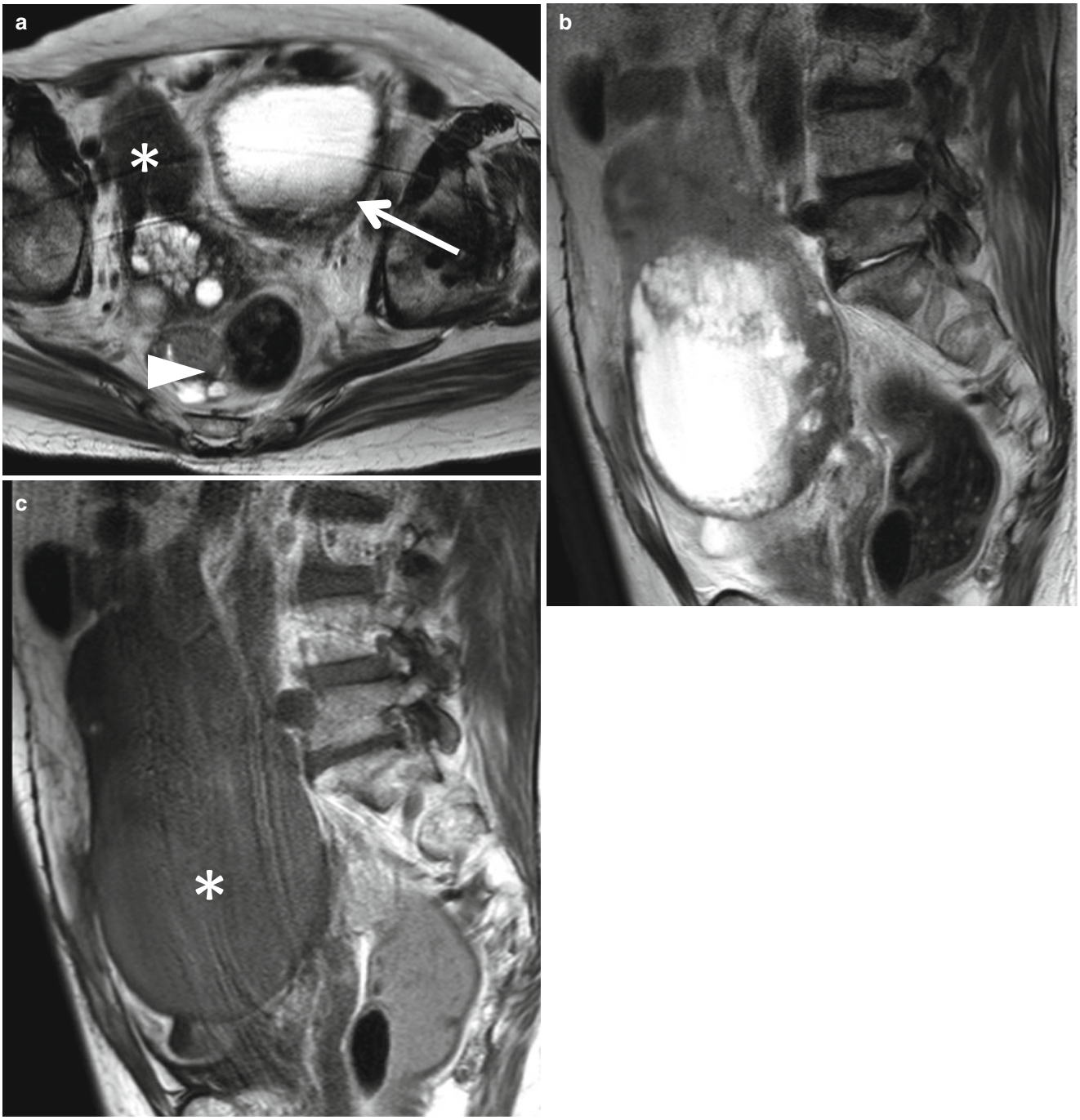

Fig. 1 Granulosa cell tumor with peritoneal dissemination in an 80-year-old woman. (**a**) Axial T2-weighted images shows a cystic mass (*arrow*) containing a fluid-fluid level, reflecting intratumoral hemorrhage. There is a peritoneal implant in a cul-de-sac (*arrowhead*). The uterus (*asterisk*) is markedly enlarged for this age of the patient, and the cervix contains aggregated Nabothian cysts. (**b**) Sagittal T2-weighted image shows a large mass containing an irregular-shaped cyst of high intensity. (**c**) Sagittal T-weighted image also shows increased intensity in the cyst (*asterisk*), suggestive of hemorrhagic nature of the fluid

In SLCTs, the most important prognostic factors in these tumors are their stage and degree of differentiation [13]. Although all well-differentiated SLCTs behave as benign, 11 % of tumors with intermediate differentiation, 59 % of tumors with poor differentiation are malignant [13–15]. Poorly differentiated SLCTs tend to contain areas of hemorrhage and necrosis more frequently, compared to well-differentiated tumor [16].

The recurrent sex cord-stromal tumors are usually peritoneal seeding as nodules or infiltrative masses on the peritoneal

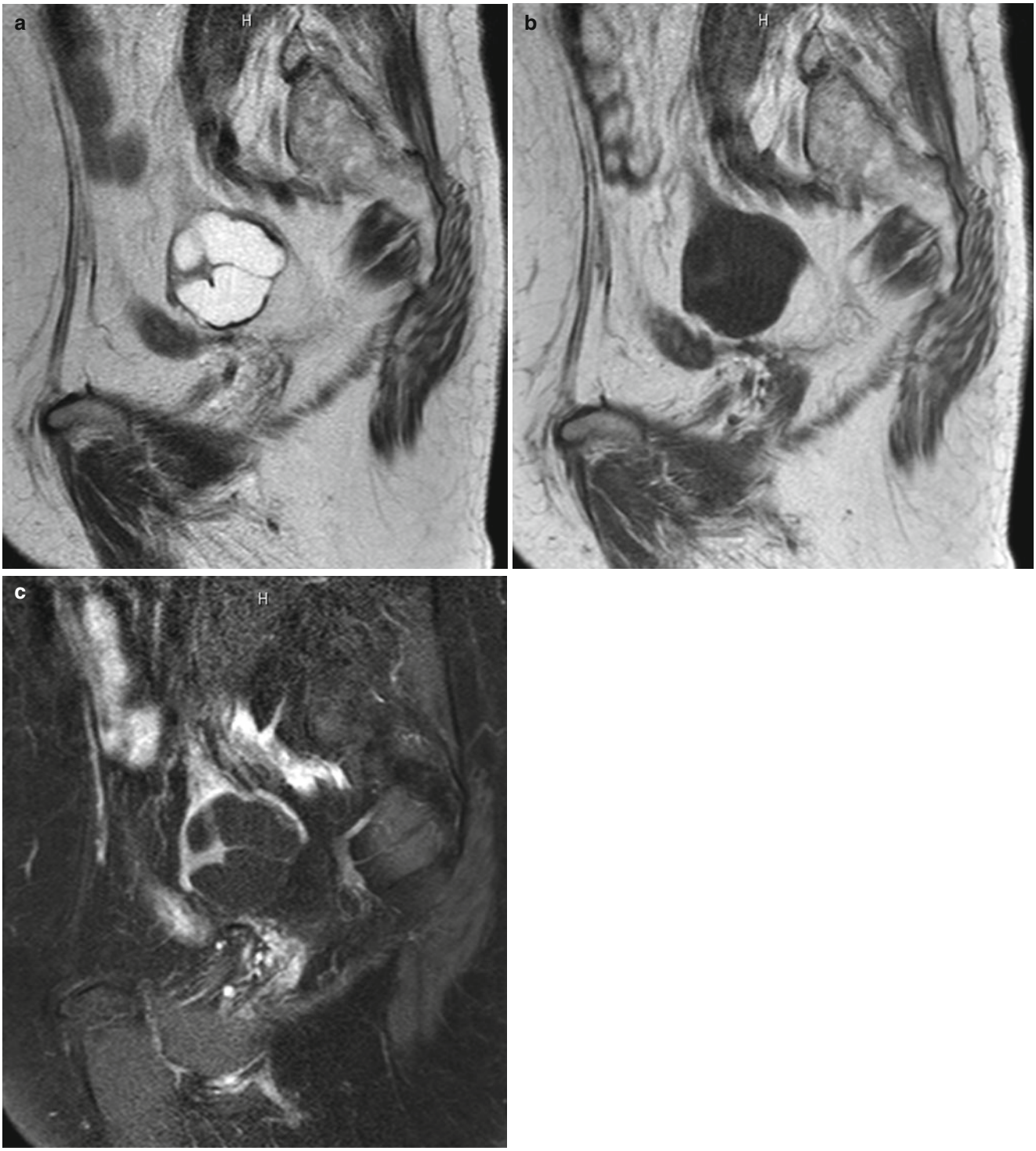

Fig. 2 Recurrent granulosa cell tumor in a 79-year-old woman. The patient has a past history of unilateral salpingo-oohorectomy and hysterectomy for granulosa cell tumor of the contralateral ovary in approximately 30 years ago. (**a**) Sagittal T2-weighted image shows a predominantly cystic mass in the left ovary. (**b**) T1-weighted image shows low intensity of the cyst content. (**c**) Post-contrast T1-weighted images with fat suppression shows enhancement in the septi and wall of the cystic mass

surface, most commonly in the pelvic cavity or around the liver or undersurface of diaphragm (Fig. 2). Occasionally, recurrent tumor may also be encountered in the retroperitoneum (Fig. 3). The tumors may show variable imaging appearances from thin-walled cystic masses to solid masses (Fig. 2) [17]. The cystic mass may be accompanied

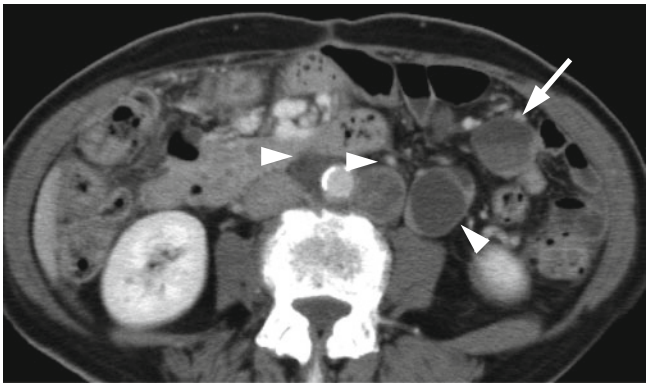

Fig. 3 Recurrent granulosa cell tumor in a 70-year-old woman. She had history of granulosa cell tumor in 8 years before. Contrast-enhanced CT demonstrates multiple nodes of low intensity in the para-aortic region and retroperitoneum (*arrowheads*). There is another well-demarcated cystic mass in the mesenterium (*arrow*), which contains a fluid-fluid level suggestive of intratumoral hemorrhage

by a fluid-fluid level, reflecting intratumoral hemorrhage (Fig. 3). Although nodal involvement at the time of primary surgery is extremely low, nodal involvement at the time of recurrence has been documented in 5 % of cases [18]. However, different from nodal metastases in ovarian carcinomas, the number of nodal involvement is usually limited. In cases of recurrent GCTs, omental or mesenteric infiltration and a large amount of ascites is quite unusual, unlike more common ovarian carcinomas of epithelial type [17].

Acknowledgement I would like to acknowledge Prof. M. Kataoka in Dept. of Diagnostic Radiology, Kyoto University, for her great help to find CT images and clinical information of patients with recurrent granulosa cell tumor.

References

1. Stenwig JT, Hazekamp JT, Beecham JB. Granulosa cell tumors of the ovary. A clinicopathological study of 118 cases with long-term follow-up. Gynecol Oncol. 1979;7(2):136–52.
2. Gershenson DM, et al. Treatment of poor-prognosis sex cord-stromal tumors of the ovary with the combination of bleomycin, etoposide, and cisplatin. Obstet Gynecol. 1996;87(4):527–31.
3. Surratt JT, Siegel MJ. Imaging of pediatric ovarian masses. Radiographics. 1991;11(4):533–48.
4. Schumer ST, Cannistra SA. Granulosa cell tumor of the ovary. J Clin Oncol. 2003;21(6):1180–9.
5. Malmstrom H, et al. Granulosa cell tumors of the ovary: prognostic factors and outcome. Gynecol Oncol. 1994;52(1):50–5.
6. Miller BE, et al. Prognostic factors in adult granulosa cell tumor of the ovary. Cancer. 1997;79(10):1951–5.
7. Fox H, Agrawal K, Langley FA. A clinicopathologic study of 92 cases of granulosa cell tumor of the ovary with special reference to the factors influencing prognosis. Cancer. 1975;35(1):231–41.
8. Evans 3rd AT, et al. Clinicopathologic review of 118 granulosa and 82 theca cell tumors. Obstet Gynecol. 1980;55(2):231–8.
9. Costa MJ, et al. Immunohistochemical phenotype of ovarian granulosa cell tumors: absence of epithelial membrane antigen has diagnostic value. Hum Pathol. 1994;25(1):60–6.
10. Fujimoto T, et al. Histopathological prognostic factors of adult granulosa cell tumors of the ovary. Acta Obstet Gynecol Scand. 2001;80(11):1069–74.
11. Morikawa K, et al. Granulosa cell tumor of the ovary: MR findings. J Comput Assist Tomogr. 1997;21(6):1001–4.
12. Outwater EK, et al. Sex cord-stromal and steroid cell tumors of the ovary. Radiographics. 1998;18(6):1523–46.
13. Young RH, Scully RE. Ovarian Sertoli-Leydig cell tumors. A clinicopathological analysis of 207 cases. Am J Surg Pathol. 1985;9(8):543–69.
14. Roth LM, et al. Sertoli-Leydig cell tumors: a clinicopathologic study of 34 cases. Cancer. 1981;48(1):187–97.
15. Zaloudek C, Norris HJ. Sertoli-Leydig tumors of the ovary. A clinicopathologic study of 64 intermediate and poorly differentiated neoplasms. Am J Surg Pathol. 1984;8(6):405–18.
16. Prat J, Young RH, Scully RE. Ovarian Sertoli-Leydig cell tumors with heterologous elements. II. Cartilage and skeletal muscle: a clinicopathologic analysis of twelve cases. Cancer. 1982;50(11):2465–75.
17. Rha SE, et al. Recurrent ovarian granulosa cell tumors: clinical and imaging features. Abdom Imaging. 2008;33(1):119–25.
18. Brown J, et al. Patterns of metastasis in sex cord-stromal tumors of the ovary: can routine staging lymphadenectomy be omitted? Gynecol Oncol. 2009;113(1):86–90.

Malignant Germ Cell: Stromal Tumors (Clinical Setting and US)

Dorella Franchi, Ailyn Vidal Urbinati, and Vanna Zanagnolo

Abstract

Malignant ovarian germ cell tumors (MOGCTs) and sex cord-stromal tumors belong to the nonepithelial malignancies of the ovary that are the second largest group of the malignant ovarian neoplasms (of the ovary), with an incidence of 10 % of all ovarian cancers. MOGCTs are rare neoplasms that affect girls and young women and have, with adequate therapy, excellent prognosis at all stages of disease. Young-aged sex cord-stromal tumor patients as the majority of MOGCTs subjects retain their reproductive function. This chapter outlines the most common clinical presentations and summarizes the most frequent ultrasonographic features that are helpful in the appropriate diagnosis of these tumors therefore allowing their correct management.

Keywords

Malignant ovarian germ cell • Choriocarcinoma • Embryonal carcinoma • Imaging • Ultrasound

Introduction

Germ cell and sex cord-stromal tumors belong to the nonepithelial malignancies of the ovary that are the second largest group of the malignant neoplasms of the ovary, with an incidence of 10 % of all ovarian cancers [1]. We can classify them from the cell of origin: germ cell tumors derive from primitive germ cells of the embryonic gonad, and may undergo germinomatous or embryonic differentiation, and the sex cord-stromal tumors derive from the sex cords and the ovarian stromal cells or mesenchyme.

Germ Cell Malignant Tumors

Germ cell tumors (GCTs) consist of a broad spectrum of tumor types histogenetically derived from the primordial germ cells of the ovary and that account for 2–3 % of all ovarian malignancies [2]. In women, ovarian germ cell tumor account for 20–25 % of all ovarian neoplasm, but only 3–5 % of these are malignant [3]. They predominantly affect women between the second and third decades of life, but they do sometimes occur in infants and older women. In children and adolescents, GCTs account for over 60 % of ovarian neoplasms, of which one-third are malignant [4].

In the USA the age-adjusted incidence is 0.41 per 100,000 women, which is 40 times less common than epithelial tumors. Though if we look at the gynecological tumors in women aged 25 or younger, the MOGCTs become the most common histology (35 % of cases) [3].

D. Franchi, MD (✉) • A.V. Urbinati, MD
V. Zanagnolo, MD
Preventive Gynecology Unit,
Gynecological Oncology Division,
European Institute of Oncology,
Via Ripamonti 435, 20141 Milan, Italy
e-mail: dorella.franchi@ieo.it;
ailyn.vidalurbinati@ieo.it;
vanna.zanagnolo@ieo.it

L. Saba et al. (eds.), *Ovarian Neoplasm Imaging*,
DOI 10.1007/978-1-4614-8633-6_20,

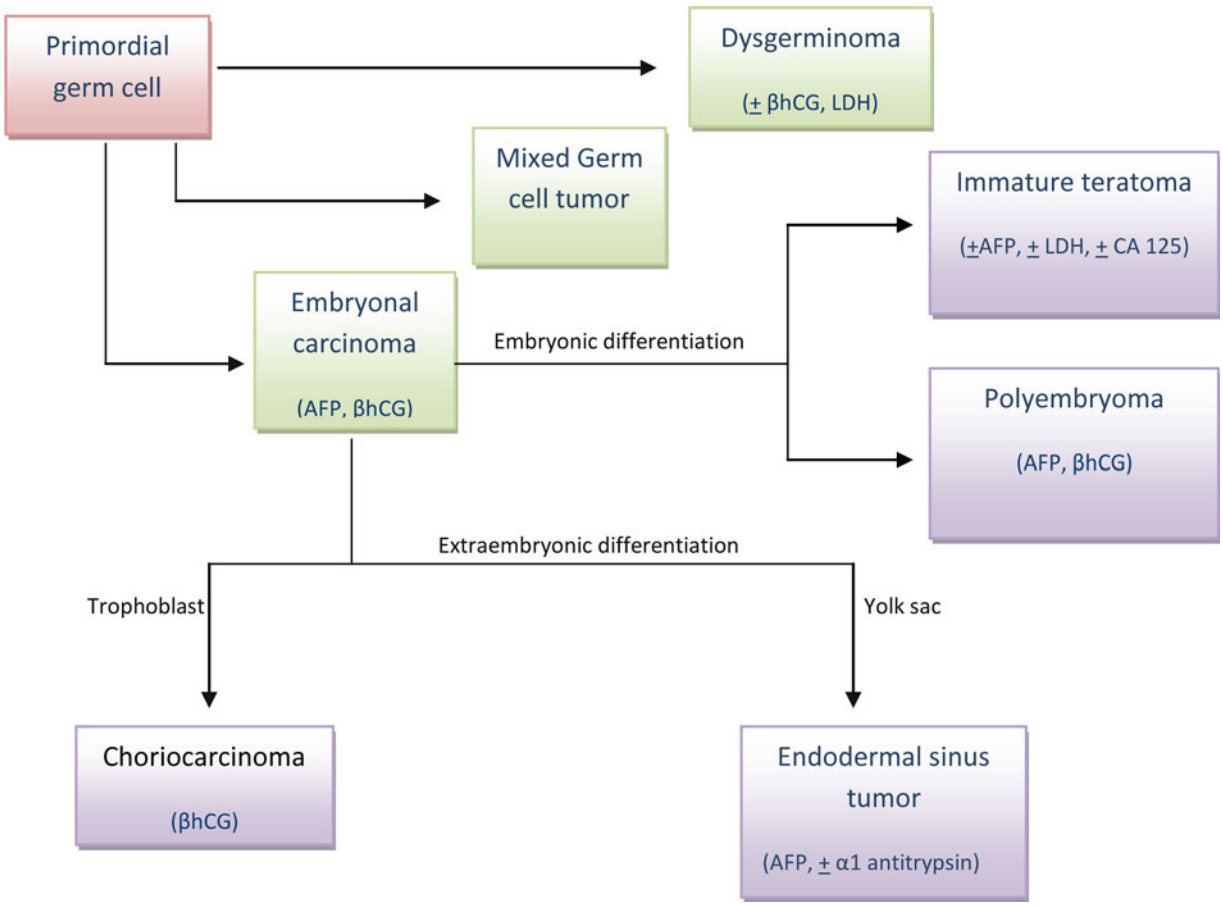

Fig. 1 Relationship between examples of pure malignant germ cell tumors and their secreted marker substances (Data derived from Rice [48] and John Hopkins Pathology, 2001)

The majority of germ cell tumors arise in the gonad from the undifferentiated germ cells. However, this kind of tumors can arise in extragonadal sites such as mediastinum or retroperitoneum, due to the embryonic migration of the germ cells from the caudal part of yolk sacs to the dorsal mesentery prior to their incorporation into the sex cords of the developing gonads [1].

Cure rate of MOGCTs is high, with clinical stage and elevated tumor markers as independent poor prognostic factors [5]. The management of patients with ovarian germ cell tumors has largely been extrapolated from the experience of treating the more common testicular germ cell tumors [1], helping in the selection of patients who might require more intensive therapeutic strategies. A multimodal therapy with fertility-sparing surgery and platinum-based chemotherapy, if required, is the most frequent approach to these patients with a very good response rate regardless the stage of the disease.

MOGCTs tend to be quite large and rapidly growing malignancies [6, 7]. The most common symptom is abdominal pain associated with palpable pelvic–abdominal mass occurring in 85 % of the patients [3].

Approximately 60–70 % of cases are diagnosed as FIGO stage I or II. Bilateral ovarian involvement is uncommon, except in the case of dysgerminomas [8].

Tumor markers play an important role for the diagnosis and follow-up of MOGCTs to confirm complete remission or to suggest recurrence [3] (Fig. 1).

Dysgerminoma

Epidemiology

Dysgerminoma is the most common malignant germ cell tumor, accounting for approximately 30–40 % of all malignant neoplasms of germ cell origin [1]; however, it represents only 1–2 % of all ovarian cancers [4, 9]. Seventy-five percent of dysgerminomas occur between the ages of 10 and 30 years and 5 % occur before the age of 10 (years) and rarely after age 50 [1, 9]. After cistoadenoma, it represents the second most frequent tumor diagnosed during pregnancy, accounting for 20–30 % of ovarian neoplasms during gestation [1, 4].

According to a survey conducted in the USA and comprising 1,262 cases of malignant ovarian germ cell tumors registered from 1973 to 2002, the age-adjusted incidence rate of ovarian dysgerminoma was 0.109 per 100.000 women-years [9].

Approximately 5 % of dysgerminomas are diagnosed in phenotypic females with abnormal gonads [1], such as 46XY (bilateral streak gonads), 46X0/46XY (unilateral streak gonad, contralateral testis), and Morris syndrome (46XY, testicular feminization). Therefore, when this tumor is diagnosed in premenarchal patients, the karyotype should be determined.

Approximately 65 % of dysgerminomas are diagnosed at stage I (confined to one or both ovaries). Dysgerminoma is the only germ cell malignancy with a 10–15 % rate of bilaterality, whereas the other germ cell tumors are rarely bilateral [1, 4]. The most common tumor spreading pathway (of the tumor) is through the lymphatic system, particularly to the higher para-aortic nodes, occurring in 25 % of the patients.

Up to 95 % of patients with ovarian dysgerminoma have an elevated serum level of lactic dehydrogenase (LDH) at presentation, with the level varying with the size and stage of the tumor [10, 11]. Determination of this marker may also be useful in detecting tumor recurrence and in monitoring response to therapy. When the neoplasm contains syncytiotrophoblastic giant cells (5 % of cases) [12], it may produce β-human chorionic gonadotropin (βhCG) [3, 9]. Serum levels of CA 125 and placental-like alkaline phosphatase (PLAP) can be elevated in some cases, but CA 125 is an unreliable marker in premenopausal women and PLAP is much more useful as a histochemical marker than as a serum one [3].

Macroscopy

Ovarian dysgerminomas most frequently are solid, well-encapsulated tumors with size ranging from barely visible nodules to masses that virtually fill the entire abdomen and have an average diameter of 15 cm. On cutting surface it appears to consist of different lobules often soft and fleshy, and with a yellow to white to gray to pink appearance. Areas of coagulative necrosis and hemorrhage typically associated with cystic changes may be observed [13, 14].

Microscopy

Histologically identical to seminoma of the testis, ovarian dysgerminomas are composed of a monotonous population of rounded cells resembling primordial germ cells in a predominantly diffuse or insular arrangement. The cells are polygonal, with distinct cell membranes with abundant eosinophilic to clear glycogen-rich cytoplasm. The nuclei are large, central, and rounded, and they contain one or a few prominent nucleoli. Mitoses are often numerous. The nests of tumor cells are separate by fibrous septa frequently infiltrated by T lymphocytes [13]. A scattered multinuclear cells positive for βhCG can be observed, confirming their identity as syncytiotrophoblastic giant cells [12].

Clinical Symptoms

Clinically, ovarian dysgerminomas may be incidentally detected in women with no gynecological symptoms. These tumors grow rapidly; therefore, the most common symptoms are abdominal distension and the presence of a pelvic or abdominal mass felt by the patient herself. Often they can be characterized by the onset of acute pelvic pain caused by the distention of the ovarian capsule, hemorrhage, necrosis, and torsion [15].

When the syncytiotrophoblastic giant cells are present, menstrual and endocrine abnormalities may be observed due to high levels of βhCG resembling pregnancy [12], and extremely rarely precocious puberty can occur due to the presence of yolk sac tumor elements in a mixed tumor with AFP secretion [16].

Prognosis

Clinical characteristics that differentiate dysgerminoma from the other MOGCTs are as follows: (a) it is more likely diagnosed as stage IA, (b) bilateral involvement is more common (10–15 %), (c) retroperitoneal spread is more frequent than intraperitoneal dissemination, and (d) it is radiosensitive [3]. Due to these features, ovarian dysgerminomas have a good prognosis: in patients with initial stage IA disease, unilateral oophorectomy alone results in a 5-year disease-free survival rate greater than 95 % [1].

Lymph node metastasis was reported in the 28 % of dysgerminomas in the Kumar et al. series [17]. Lymph node involvement was an independent predictor of poor survival at multivariate analysis with 95.7 % 5-year survival rate for negative node patients as opposed to 82.8 % for patients with positive nodes [1].

In MITO-9 series, relapse rate was 10.2 and 77 % of these recurrences occurred within 24 months from diagnosis; the 2-year recurrence-free survival was 91.3 %, and the 5-year overall survival (OS) was 97.9 % [18].

Gordon et al. reported a 95 % 5-year overall survival rate in patients with stage IA pure dysgerminoma treated by unilateral adnexectomy alone. Survival in these patients was not affected by tumor size [19].

Historically risk factors associated with a higher recurrence rate are lesion diameter larger than 10–15 cm, age younger than 20 years, and a microscopic pattern picturing numerous mitosis, anaplasia, and medullary pattern [1].

Ninety to 100 % cure rates have been reported in advanced-stage disease with the use of bleomycin–etoposide–cisplatin (BEP) or etoposide–carboplatin (EC) combination regimen therapy [1].

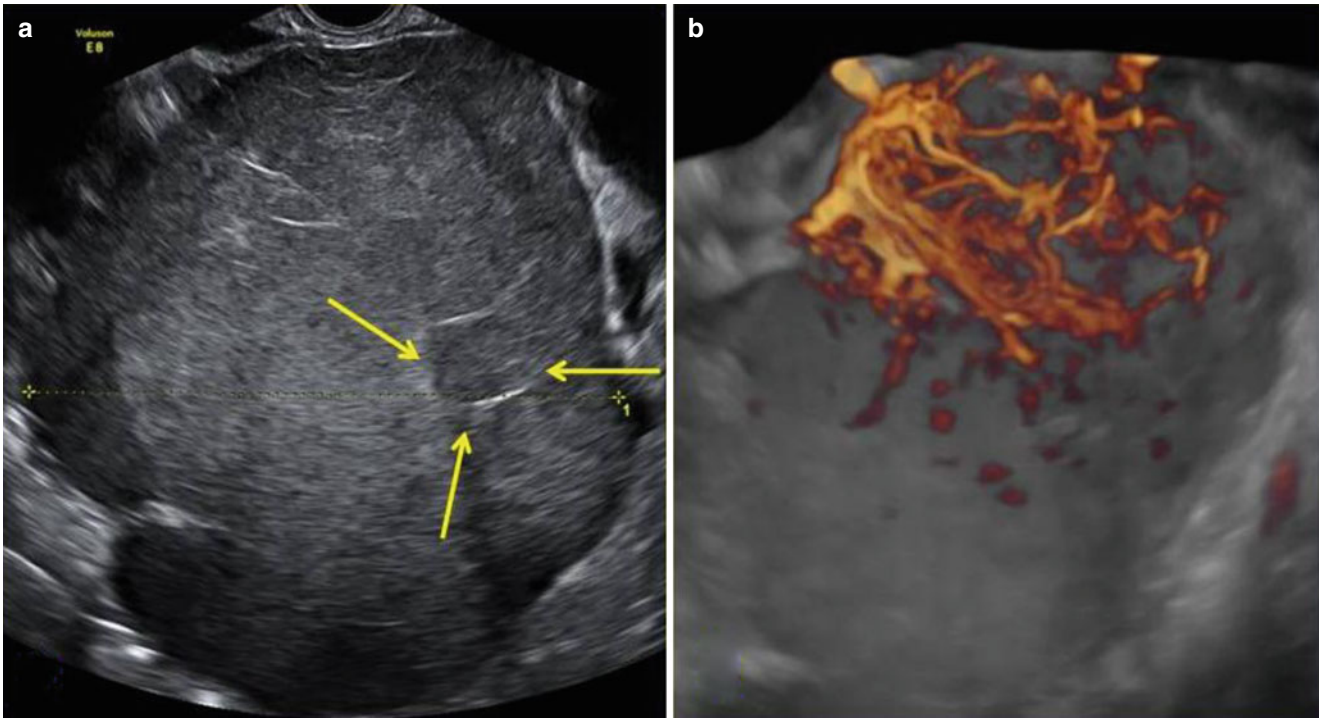

Fig. 2 (**a**) A large (14 cm) solid ovarian dysgerminoma stage IA with a multilobulated appearance (a lobule is shown between the *arrows*) and smooth well-defined lobulated contour in a 24-year-old patient. The internal echogenicity is rather irregular. (**b**) Three-dimensional power Doppler image showing densely packed tortuous vessels with irregular branching and caliber changes in an ovarian dysgerminoma

Ultrasound Characteristics

The most common ultrasound features of dysgerminoma are large pure solid adnexal tumor divided into different lobules, with irregular internal echogenicity, smooth lobulated contours, and well-defined borders [4, 9]. Less typical appearance is that of a solid tumor with cystic areas, some of them with irregular internal cystic borders and even papillary projections [9]. In the Guerriero et al. series, half of the patients had free fluid in the pouch of Douglas (common and unspecific ultrasound finding in women of fertile age) and only one presented with ascites [9].

Power Doppler ultrasound images show vascularized tumor with a color scores moderate or abundant. Three-dimensional power Doppler ultrasound volumes revealed densely packed vessels, irregular branching, caliber changes, and tortuosity of tumor vessels in the three dysgerminomas evaluated in Guerriero et al. series [9] (Figs. 2 and 3).

In three reported cases Kim et al. showed prominent arterial flow within the fibrovascular septa of the tumor. The resistive index values ranged between 0.44 and 0.70 (mean 0.59), and the pulsatility index values ranged between 0.60 and 1.32 (mean 0.98) [20].

There are not specific features to distinguish the ultrasound patterns of dysgerminomas from those of other solid malignant ovarian tumors such as solid metastases or lymphoma, but the ultrasound findings of a large, solid, lobulated adnexal mass with irregular internal echogenicity and highly vascularized at color or power Doppler ultrasound in a 20–30-year-old woman should raise the suspicion of ovarian dysgerminoma [9].

Immature Teratomas

Immature teratomas contain tissue elements that resemble those of the embryo. They vary considerably in size and are usually round or oval with mixed content composed of hair and fatty material surrounded by a firm capsule [14]. Immature teratoma elements may occur in combination with other germ cell tumors as mixed germ cell tumors [1].

Epidemiology

Pure immature teratoma accounts for fewer than 1 % of all ovarian malignancies; however, it is the second most common germ cell tumor. In women younger than 20 years, this neoplasm represents 10–20 % of all ovarian malignancies and 30 % of the deaths from ovarian cancer in this age group. Approximately 50 % of pure immature teratomas occur in female patients between the ages of 10 and 20 years; on the contrary, it is extremely rare in postmenopausal women [1, 15].

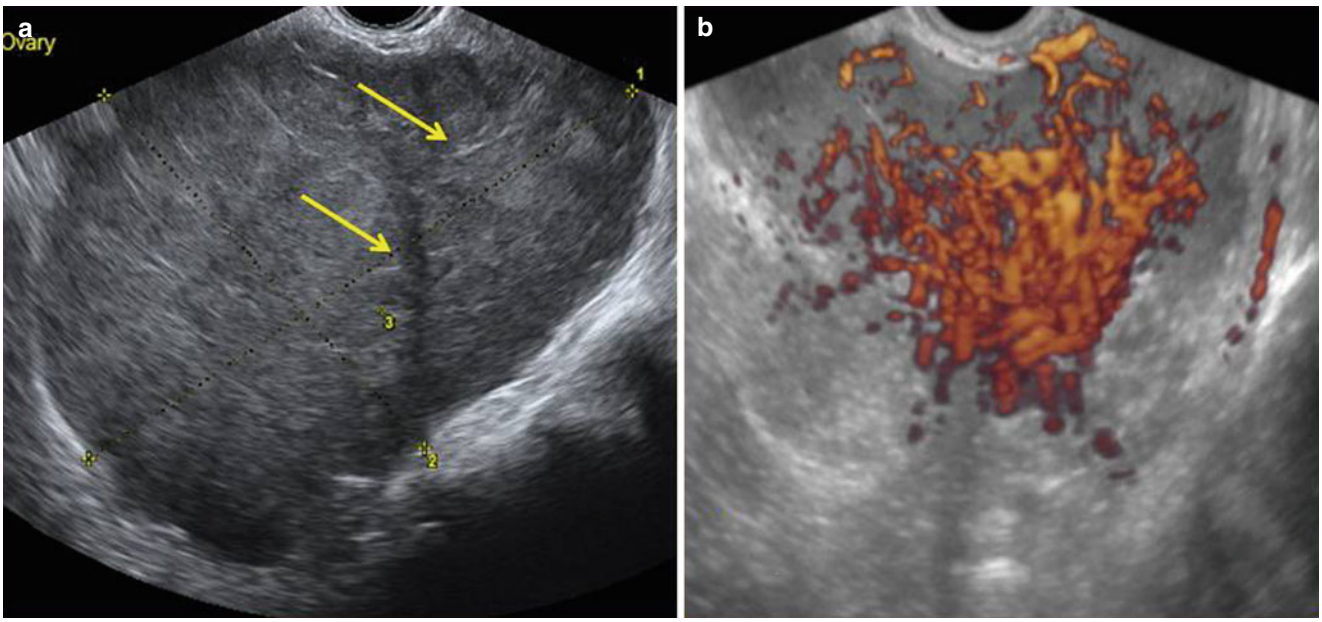

Fig. 3 (**a**) Grayscale ultrasound images of an 11 cm ovarian dysgerminoma stage IIIC in a 27-year-old patient with a less-evident multilobulated appearance with well-defined lobulated but smooth contours. Lobules are separated by fine connective tissue (*arrows*). (**b**) Three-dimensional power Doppler image showing densely packed tortuous vessels with irregular branching and caliber changes in the same ovarian dysgerminoma

Survival rate is related to histology grade that depends on the proportion of immature neuroepithelium tissues (in histological sections). Grade 1 has a survival of at least 95 %, whereas grades 2 and 3 appear to have a lower overall survival (approximately 85 %) [1, 15].

Immature ovarian teratomas are associated with gliomatosis peritonei, a favorable prognostic finding if composed of completely mature tissues, with the seemingly unexpected recent discovery, using molecular methods, that these glial "implants" are not tumor derived but represent teratoma-induced metaplasia of submesothelial cells [21].

Immature teratomas can be associated with mature cystic teratomas. Ipsilateral typical mature cystic teratomas are present in 26 % of cases of immature teratoma, whereas 10 % of the patients present with an immature teratoma in the contralateral ovary [22].

Malignant transformation of a mature teratoma is a rare event and the squamous cell carcinoma is the most frequent histological type in this case, but adenocarcinomas, primarily melanomas and carcinoids, may also occur. The risk reported in the literature is between 0.5 and 2 % of teratomas, usually in postmenopausal women [1].

Microscopy

Immature teratoma is composed of immature tissue differentiating toward cartilage, glands, bone, muscle, nerve, and others [14].

In contrast to the other forms of malignant ovarian germ cell tumor, immature ovarian teratoma usually shows relatively minor cytogenetic abnormalities that increase as the grade of the immaturity worsens [21].

The most common monodermal teratoma (composed predominantly or solely of one tissue type) is the struma ovarii, a rare ovarian tumor composed entirely or predominantly of thyroid tissues. It constitutes approximatively 3 % of all ovarian teratomas, 2 % of all germ cell tumors, and 0.5 % of all ovarian tumors. The malignant transformations occur only in about 5 % of all struma ovarii [21, 23]. Histologically it can be described as mature thyroid tissue consisting of colloid-containing follicles of different size lined by a single layer of follicular cells [23].

Macroscopy

Immature teratomas are typically large (14–25 cm) and have a smooth external surface. On section, they are solid or predominantly solid, cystic areas can be present as well and usually filled with serous or mucinous fluid or sometimes with fatty sebaceous material. The solid areas within immature teratomas, which are usually composed predominantly of neural tissue, are typically soft, fleshy, and gray to pink and may be focally hemorrhagic or necrotic. Mature components such as hair, fatty tissue, cartilage, bone, and calcification are usually present [22].

Immature teratomas grow rapidly and frequently infiltrate the capsule; that therefore is not always well defined [14, 22].

Clinical Symptoms

Immature teratoma is often discovered incidentally during a physical or ultrasound examination of the female pelvis.

Given the large size, patients with immature teratoma can present with the onset of acute pelvic pain due to either rupture or torsion of the ovarian mass. Some patients complain of abdominal distension, pain, urinary or bowel symptoms, and infertility. Rarely patients can experience sexual pseudoprecocity due to the production of steroid hormones [1].

Tumor markers are usually negative unless a mixed germ cell tumor is present [1], such as in the case of the presence of yolk sac tumor within immature teratomas that is the source of AFP in affected patients [22].

Prognosis

The most important prognostic feature is the grade of the lesions. Patients with stage IA grade 1 tumors have an excellent prognosis, and adjuvant therapy is not required. In case of stage IA grade 2 or 3, adjuvant chemotherapy is commonly recommended. Combination platinum-based chemotherapy is the treatment of choice (BEP regimen) [1, 15].

For patients with all stages, pure immature teratomas' 5-year survival rate is 70–80 %, and it is 90–95 % for patients with surgical stage I lesions. The presence of residual disease at the end of primary surgery has been reported to significantly lower 5-year survival rate from 94 to 50 % [1].

Ultrasound Characteristics

The ultrasound appearance of immature teratoma is nonspecific, and it is very difficult to differentiate them from the benign counterparts.

Three ultrasound patterns most commonly occur in mature teratoma. The most common setting is a cystic lesion with a densely echogenic tubercle (Rokitansky nodule) projecting into the cyst lumen; the second one is a diffusely or partially echogenic mass with the echogenic area usually demonstrating sound attenuation owing to sebaceous material and hair within the cyst cavity; and the third one consists of multiple thin, echogenic bands due to the presence of hair in the cyst cavity [22].

There are different echogenicities depending on the characteristics of the material filling the dermoid cyst: pure sebum may be hypoechoic or anechoic; fluid–fluid levels result from sebum floating above aqueous fluid, which appears more echogenic than the sebum layer; dermoid plug is echogenic, with shadowing due to adipose tissue or calcifications within the plug or to hair arising from it. Diffuse echogenicity in these tumors is caused by hair mixed with the cyst fluid [22].

The immature teratomas typically are large masses with heterogeneous, partially solid lesions. Scattered calcifications are usually presents. Ultrasonographically, these features can appear as heterogeneous internal signal intensity with punctate high signal intensity or echogenic mass with sound attenuation or heterogeneous mass containing echogenic reflectors representing hair [22] (Fig. 4).

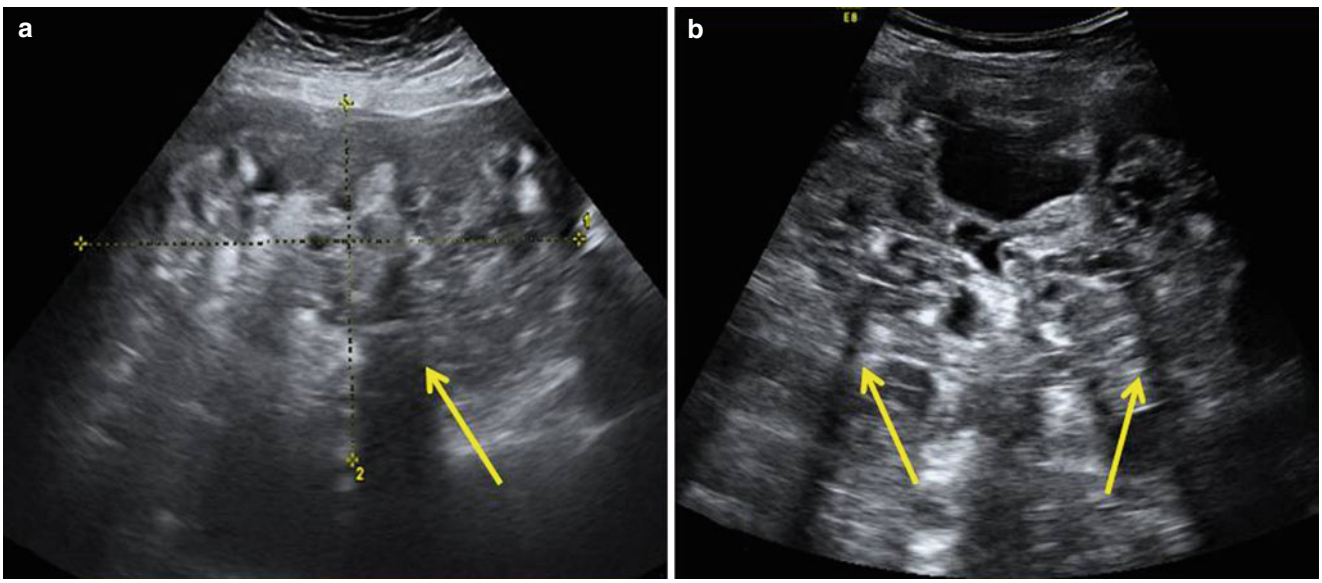

Fig. 4 Large prominent solid pure ovarian immature teratomas in a 50-year-old patient with a 24 cm mass (**a**) and in a 12-year-old girl with a 28 cm mass (**b**) with a heterogeneous appearance and cystic elements. The internal echogenicity is rather irregular; echogenic sebaceous material and scattered calcifications determining cone shadows (*arrows*) are present; contours are undefined

Endodermal Sinus Tumor

It is also called yolk sac carcinoma since it derives from a multipotential embryonal carcinoma by selection and dedifferentiation toward primitive yolk sacs structures; it is the third most frequent malignant germ cell tumor of the ovary [1, 14]. It usually occurs in the second decade of life with a median age of 18 years. Approximately one-third of the patients are premenarchal at the time of initial presentation [1, 24].

Endodermal sinus tumor often is characterized by extremely rapid growth and extensive intra-abdominal spreading sometimes characterized by poor prognosis [24]. The tumor appears to involve a single ovary, but it grows rapidly and aggressively [14]. Abdominal or pelvic pain is the most frequent presenting symptoms (75 % of cases), whereas an asymptomatic pelvic mass is documented only in 10 % of patients [1].

The tumor is frequently encapsulated, rounded, oval, or globular. On section, they are solid and frequently present with cystic areas [4]. Extensive areas of hemorrhage and necrosis are common. A honeycomb appearance due to many small cysts may indicate the presence of a polyvesicular-vitelline component. The histological feature is a glomerulus-like structure composed of a central blood vessel surrounded by germ cells within a space similarly lined by germ cells (Schiller–Duval body). Similar structures are observed in the yolk sac of the rat placenta, but in the tumor, loose meshwork of communicating spaces lined by primitive tumor cells with clear or vacuolated cytoplasm is observed. Conspicuous intracellular and extracellular hyaline droplets are present in all neoplasms [14, 24]. The tumor is rich in AFP and α1 antitrypsin. The serum levels of these markers, particularly AFP, are useful in the diagnosis and monitoring of a patient's response to treatment. It may rarely produce detectable serum levels of α1 antitrypsin [1].

The standard treatment of this tumor consists of surgical exploration, unilateral salpingo-oophorectomy, resection of any gross metastases if feasible, followed by adjuvant cisplatin-based combination chemotherapy, such as BEP, that is considered the standard of care. Most patients have early stage disease: 71 % stage I, 6 % stage II, and 23 % stage III. Nowadays, cure rate approaches 100 % for early stage disease and at least 75 % for more advanced stages [1, 15].

Ultrasonographically, endodermal sinus tumors range from entirely solid to predominantly cystic patterns, but heterogeneous appearance consisting of a mixture of solid and cyst features has been reported. The cystic component might be due to cystic degeneration or necrosis [24].

It has been reported that this tumor shows an intense vascularization with vessels with low blood flow resistance detected at the color Doppler flow velocity measurement [24] (Fig. 5).

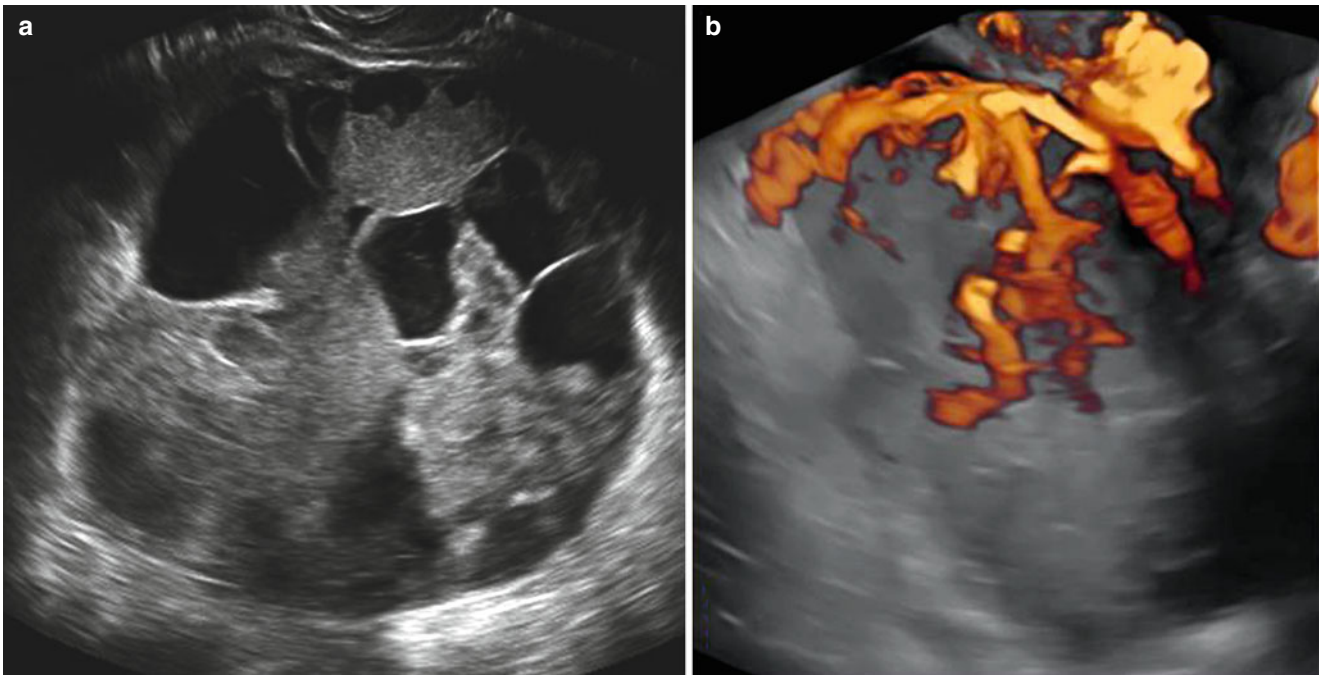

Fig. 5 (**a**) Grayscale ultrasound images of a large (19 cm) stage IIB endodermal sinus tumor in a 19-year-old patient with a preeminent solid round-shaped mass with cystic areas representing necrosis. (**b**) Three-dimensional power Doppler image showing intense vascularization, tortuous vessels with irregular branching, and caliber changes in the endodermal sinus tumor

Rare Germ Cell Tumors of the Ovary

Embryonal Carcinoma

Embryonal carcinoma of the ovary is an extremely rare tumor characterized by large primitive cells resembling those of the embryonic germ disk and growing in solid, papillary, and glandular patterns [1]. It is rarely diagnosed as a pure form, and most commonly it occurs as a component of a germ cell tumor [25]. Patients are very young, ranging in age from 4 to 28 years with a mean age at diagnosis of 14 years [15]. Patients may present with precocious pseudopuberty or with abnormal uterine bleeding since embryonal cell carcinoma may produce estrogen [25]. Moreover, these lesions frequently secrete AFP and hCG that are useful markers to follow the response to subsequent therapies [26].

The most common symptoms described in the literature are abdominal *or* pelvic mass, abdominal pain, fever, and marked weight loss. Signs of abnormal hormonal production can occur such as precocious puberty manifested by bilateral breast development, vaginal bleeding, and growth of hair on the vulva in prepubertal girls and amenorrhea, irregular vaginal bleeding, infertility, and mild hirsutism in postmenarchal woman [27].

The primary lesions tend to be large, and approximately two-thirds of them are confined to one ovary at the time of presentation [1]. In Kurman et al. series, the greatest tumor diameter ranged from 10 to 25 cm, the median being 17 cm [27]. At surgery spread to the peritoneum is observed in 40 % of the cases, sometimes accompanied by parenchymal involvement of pelvic or intra-abdominal viscera [25].

Macroscopically the tumors had smooth, glistening external surfaces with a yellow to gray tissue on transection, solid for the most part, but cystic spaces containing mucoid material are frequently observed as well [27].

Microscopically, the embryonal carcinomas present solid proliferation of cells and isolated clusters of syncytiotrophoblast. The cells of this tumor, like those of dysgerminoma, tend to form sheets but are easily distinguished from dysgerminoma by their larger size, more hyperchromatic nuclei, and tendency to form a glandular pattern. The stroma of embryonal carcinoma is either loose with foci of hemorrhage and necrosis or more collagenous. The overall microscopic appearance of embryonal carcinoma suggests a uniphasic overgrowth by cytotrophoblast with scattered, isolated syncytiotrophoblast cells [27].

Women with embryonal carcinomas and other germ cell tumors should be usually treated with conservative surgery followed by BEP regimen chemotherapy. While there are some data to suggest that the presence of embryonal carcinoma in mixed tumors is associated with a higher relapse rate following conservative treatment than that of other germ cell tumors, those neoplasms appear to respond to chemotherapy as their counterparts in males and the other ovarian germ cell tumors do [25]. Surveillance for recurrence should be intensive in the first 2 years, with a more relaxed schedule thereafter. Ongoing surveillance for second malignancies and chemotherapy-related toxicity should be included in the follow-up of these patients [25].

Choriocarcinoma of the Ovary

Non-gestational choriocarcinoma of the ovary can be pure or mixed with other germ cell tumors. Pure type is less frequent than mixed type and the diagnosis of non-gestational choriocarcinoma of the ovary is very difficult in the reproductive period [28]. A primary germ cell origin may be difficult to prove purely on a histological basis except in those cases that develop in premenarchal or virginal patients [29]. The majority of patients with this cancer are younger than 20 years [1]. The distinction between gestational versus non-gestational choriocarcinoma is important because a non-gestational choriocarcinoma carries a worse prognosis than the gestational type [19, 30]. Another poor prognostic factor is the presence of metastases to other organs (parenchyma) at the time of initial diagnosis [1].

Similarly to other ovarian neoplasms, the presenting symptoms of non-gestational choriocarcinoma are nonspecific [19] such as abdominal pain, irregular bleeding, precocious puberty, and positive pregnancy test without pregnancy because of the markedly elevated tumor-associated HCG levels [19]. The presence of HCG can be useful in monitoring the patient's response to treatment [1].

On gross examination, the pure choriocarcinoma is typically solid, hemorrhagic, and friable.

Histologically, non-gestational pure choriocarcinoma of the ovary presents the same appearance as the gestational choriocarcinoma metastatic to the ovaries [28].

There are only a few limited reports on the use of chemotherapy for these non-gestational choriocarcinomas, but complete responses have been reported to the MAC regimen (methotrexate, actinomycin D, and cyclophosphamide) used in the same manner as described for gestational trophoblastic disease [28]. These tumors are so rare that definitive data are not available, but other chemotherapy regimens such as BEP or cisplatin, vincristine, methotrexate, bleomycin, actinomycin D, cyclophosphamide, and etoposide (POMB-ACE) have shown a positive impact on survival (Fig. 6).

Polyembryoma

Polyembryomas are extremely rare germ cell tumors [1]. Since the original description, only 14 ovarian polyembryomas have been reported in the English literature during the last four decades [31]. This tumor is composed of "embryoid bodies" and replies the structure of early embryonic differentiation (i.e., the three somatic layers: endoderm, mesoderm, and ectoderm) [1].

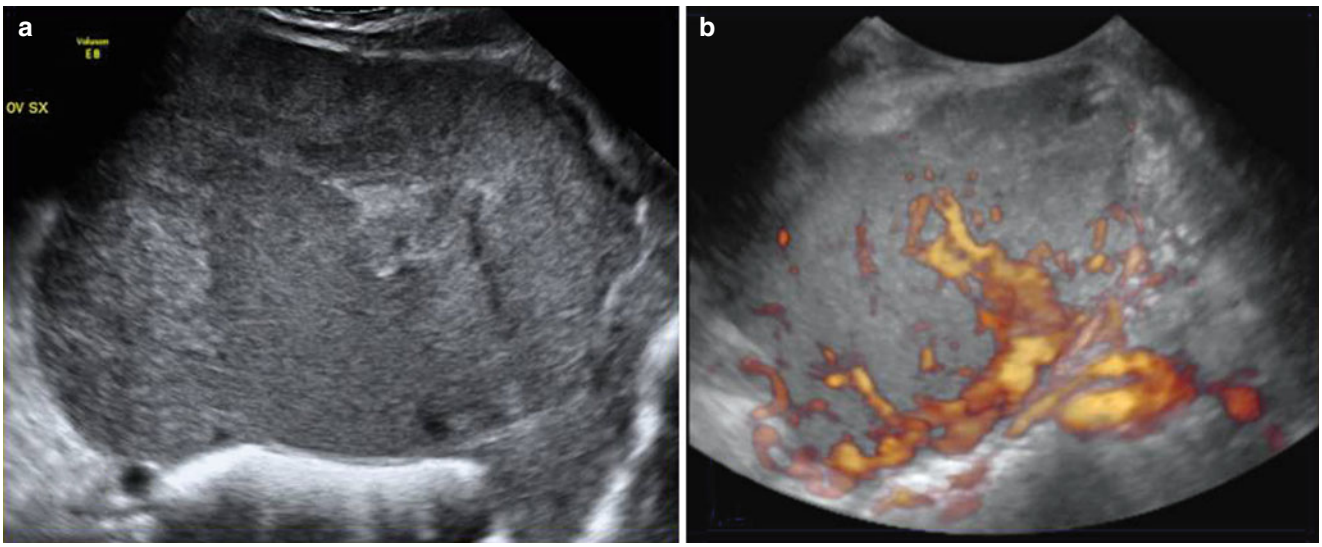

Fig. 6 (**a**) Grayscale ultrasound images of a large (14 cm) stage IA mixed germ cell tumor consisting of choriocarcinoma, embryonal carcinoma, and a majority amount of clear cell carcinoma with a solid appearance and inhomogeneous echotexture due to hemorrhage and necrosis. Margins are rather regular and well defined. (**b**) Three-dimensional power Doppler image showing intense vascularization, tortuous vessels with irregular branching

The age of the patients ranged from 3 to 44 years; the average age was 24.5 years [31]. Immature teratoma and yolk sac tumor were the two most common additional components identified in the reported cases of polyembryoma [31]; therefore, signs of pseudopuberty and high levels of AFP and HCG are usually observed [1].

Polyembryoma is usually diagnosed at an early stage (79 % in stage I) [31]. In Jondle et al. review of 14 patients, six died of disease within 1 and 12 months postoperatively prior to 1980, and only one had received chemotherapy. On the contrary, of the six patients who were followed up after 1980, five underwent chemotherapy and were alive with no evidence of disease 12–106 months postoperatively [31].

Sex Cord-Stromal Tumors

Sex cord-stromal tumors account for approximately 5–8 % of all ovarian malignancies [1, 8, 30]; approximately 50 % of these tumors are fibromas [4].

Sex cord-stromal tumors of the ovary derive from the sex cords of the embryonic gonad and the ovarian stroma or mesenchyme. The tumors usually are composed of various combination of elements, including the female cells (granulosa cells, theca cells, and their luteinized derivatives), male cells (Sertoli and Leydig cells), and fibroblast of gonadal stromal origin as well as morphologically indifferent cells [1, 32] (Table 1).

Table 1 Classification of malignant germ cell stromal tumor

Granulosa-stromal cell tumors
Granulosa
Adult type
Juvenile type
Tumors in the thecoma–fibroma group
Thecoma
Fibroma–fibrosarcoma
Sclerosing stromal tumor
Androblastomas, Sertoli–Leydig cell tumors
Sertoli
Leydig
Sertoli–Leydig
Well differentiated
Intermediate differentiation
Poorly differentiated
With heterologous elements
Retiform
Mixed
Gynandroblastoma
Unclassified

Modified and reprinted from Colombo et al. [32], with permission

Granulosa-Stromal Cell Tumor

Granulosa-stromal cell tumors include granulosa cell tumor (GCT), thecomas, and fibromas. The GCTs are a low-grade malignancy. As the name implies, GCT is derived from granulosa cell, a hormonally active component of the ovarian

stroma that is responsible for estradiol production. Thecomas and fibromas are benign but rarely may have morphologic features of malignancy and then may be referred to as fibrosarcomas [1].

Granulosa Cell Tumor

Epidemiology

GCTs account for approximately 70 % of malignant sex cord-stromal tumors and represent 3–5 % of all ovarian neoplasms [32]. The estimated incidence in the USA is 0.99/100.000, whereas the reported incidence in other developed countries varies from 0.4 to 1.7 patient cases per 100.000 women [33]. It is the most common hormone-producing ovarian tumor [34]. One-third of GCTs occur in premenopausal women, more than 50 % in postmenopausal subjects, and 5 % in the prepubertal period [34]. They are bilateral in only 2 % of patients [1].

There are two types of GCT, the adult and the juvenile types. The juvenile GCTs represent approximately 5 % of all granulosa cell neoplasms [32]. The differences between the two types are merely histopathological [35]. However, since the clinical and pathological characteristics of the tumors occurring after the menopause are different from those occurring in children and younger patients, the adult and juvenile granulosa cell types are considered separately:

1. Adult type
   The adult type accounts for 95 % of all GCTs with a median age at diagnosis between 50 and 54 years in most series [33]. The highest incidence is in the immediate postmenopausal age group, women aged 51–60 years [15].
2. Juvenile type
   The GCT is only 5–7 % of childhood ovarian neoplasms [34]. Approximately 90 % of juvenile GCTs occur in prepubertal girls [34]. In Young et. al's series of 125 cases, 44 % of the tumors occurred before age 10 years, and only 3 % after the third decade of life [34]. As the adult type the bilaterality and an extraovarian spread are infrequently observed. Almost all tumors are diagnosed at stage I [32].

Microscopy

GCTs are defined as tumors composed for at least 10 % of granulosa cells, often in a fibrothecomatous stroma [35].

The histological diagnosis can be facilitated by staining for GCTs markers such as inhibin, CD99, and MIS. To this purpose antibodies against inhibin, though not specific, appear to be the most useful [1]:

1. Adult type
   The adult type is a predominantly solid cellular tumor with an almost exclusive population of granulosa cells or more often, with an additional component of theca cells, fibroblast, or both [32]. Granulosa cells, the hallmark of GCTs, have a round or ovoid nucleus with a longitudinal groove ("coffee bean nuclei") and scant cytoplasm [35].
   Adult-type GCTs may display a variety of growth patterns: microfollicular, macrofollicular, insular, or trabecular [32]. The microfollicular is the most typical pattern characterized by the presence of the rosette-like structure (Call–Exner bodies), which contains eosinophilic material and pyknotic nuclei, observed in 30–60 % of cases [32–35].
   The mitotic activity is low [35].
2. Juvenile type
   The juvenile type is predominantly solid cellular tumor with a nodular or diffuse growth pattern with scattered macrofollicles [32, 35]. The tumor has distinct histopathologic features: hyperchromatic granulosa cells with round nuclei, abundant eosinophilic and/or vacuolated cytoplasm (indicating luteinization), and absent nuclear grooves [32, 35]. Moreover Call–Exner bodies are not a feature of juvenile-type GCTs [35].
   The mitotic activity is high [32].

Macroscopy

GCTs are typically rather large, commonly encapsulated tumors with a smooth or lobulated surface. The tumor has a gray or yellow cut surface, due to lipids content, and may present predominantly a solid component and cystic areas in variable proportions [14, 32, 35]. Completely cystic lesions are rare. Hemorrhagic areas are often seen in larger tumors, but necrosis is uncommon [35].

Clinical Symptoms

Hormone production is frequent, with predominance of estrogen, and it results in clinical symptoms that may facilitate the diagnosis [32, 35]. Postmenopausal bleeding is a common presenting symptom and is caused by prolonged exposure of the endometrium to tumor-produced estradiol, resulting in endometrial hyperplasia or endometrial adenocarcinoma [32–35]. Depending on the diagnostic criteria, 24–80 % of patients with a GCT present with endometrial abnormalities: 20–65 % are diagnosed with endometrial hyperplasia and up to 10 % with endometrial cancer that usually is a well-differentiated endometrioid adenocarcinoma [33, 35].

In premenopausal women, estrogen-related symptoms like menstrual irregularity, menorrhagia, or even secondary amenorrhea can occur [32–35]. However, infertility, virilizing features, or hirsutism is rare [33].

When GCT develops in premenarchal girls, isosexual precocious pseudopuberty, breast enlargement, or occasionally galactorrhea can be observed [33, 35].

Other clinical symptoms are abdominal distension and pain [32–35]. This might be related to the fact that GCTs tend to be large measuring up to 40 cm in diameter, with an average of approximately 12 cm, and hemorrhagic [32–35]. More acute onset of pelvic pain may be the result of ovarian torsion, or spontaneous rupture, resulting in a painful hematoperitoneum [33, 35]. Most GCTs are slow-growing lesions that progressively fill the pelvis or abdomen [35]. Ascites is less common in these tumors than in stage I or II or in more advanced epithelial ovarian cancer stages (22 % vs. 31 % and 61 %, respectively) [35].

Inhibin is secreted by granulose cell tumors and it is a useful marker to monitor response to treatment or to detect disease recurrence. An elevated serum inhibin level in a premenopausal woman presenting with amenorrhea and infertility is suggestive of a GCT [1, 35].

Mullerian inhibitory substance (MIS), which is also produced by granulose cells, is emerging as a potential marker for these tumors, but the laboratory test is not clinically available except for research purpose [1].

Prognosis

GCTs are slow-growing tumors with local spread that seldom or very late recur, sometimes as long as 37 years later [35].

The prognosis of granulosa cell tumor of the ovary depends on disease surgical stage at the time of diagnosis [1]. Overall, 75 % of the GCTs are diagnosed as stage I, 20 % as stage II, 8 % as stage III, and 6 % as stage IV [35]. In one report of 37 women with stage I disease, survival rates at 5, 10, and 20 years were 94, 82, and 62 %, respectively. The survival rates for stages II to IV at 5 and 10 years were 55 and 34 %, respectively [33].

In adult-type tumors, cellular atypia, mitotic rate, and absence of Call–Exner bodies are the only significant pathological predictors of early recurrence [1]. The presence of residual disease at the end of primary surgery was found to be the most important predictor of progression-free survival, and DNA ploidy was another independent prognostic factor [1].

In the juvenile type of GCTs, approximately 90 % are diagnosed as stage I and have a favorable prognosis. This type of tumor seems to behave less aggressively than the adult type [1, 32].

The treatment of GCTs depends on the age of the patient and the extent of disease. Fertility-sparing surgery with unilateral salpingo-oophorectomy and staging seems to be reasonable in patients wishing to preserve their fertility in the absence of extraovarian spread. An endometrial curettage must be performed to rule out concomitant endometrial abnormality [1, 30]. In postmenopausal women and in patients with advanced-stage disease or with bilateral ovarian involvement, abdominal hysterectomy and bilateral salpingo-oophorectomy should be performed with a careful surgical staging [32].

There are no data to support any kind of postoperative adjuvant treatment for patients with stage I GCTs, given the indolent nature of these neoplasms and the overall good prognosis [32].

Due to the rarity of these tumors, well-designed randomized studies assessing the role of adjuvant therapy for patients with stages II to IV disease are not feasible [1]. However, platinum-based regimens such as BEP seem to be clearly active [33].

Ultrasound Characteristics

The sonographic and CT findings of adult ovarian granulosa cell tumor vary widely, ranging from solid masses to tumors with variable degrees of hemorrhagic or fibrotic changes to multilocular cystic lesions to completely cystic tumors [36]. Most of the masses are solid; a minority are partially or totally cystic [4, 35].

Ko et al. described the sonographic characteristics of 13 GCTs [36]; they found that 46 % were multilocular solid with a small solid component, 15 % were multilocular solid with a thickened solid component, 8 % were cystic, and 31 % were solid [36]. Hong and co-workers described nine GCTs cases, 89 % as complex multicystic masses and one as a huge cyst with a thin septum [37].

The ultrasound findings using a standardized examination technique, terms, and definitions recommended by the IOTA (International Ovarian Tumor Analysis) group are listed in the literature in only one article. Van Holsbeke et al. described the sonographic characteristics of 23 GCTs. All but one tumor contained solid components. Twelve (52 %) were multilocular solid, nine (39 %) were purely solid, one (4 %) was unilocular solid, and one was multilocular (4 %). All 13 multilocular/multilocular-solid masses contained five locules or more and 10/13 (77 %) contained 10 or more locules. The echogenicity of the cyst content was usually low level (7/16, 44 %) or mixed (6/16, 38 %). Papillary projections were found in only four patients (17 %). The GCTs were large, with a median largest diameter of 102 (range, 37–242) mm. Only one mass was smaller than 50 mm and more than 50 % were larger than 100 mm. Most GCTs presented moderate to high color content at color or power Doppler examination (color score 3 in 13/23, 57 %; color score 4 in 8/23, 35 %) [35].

Using pattern recognition Van Holsbeke et al. identified two typical patterns. The first was a solid mass with heterogeneous echogenicity of the solid tissue as, for example, in necrotic tissue. The second pattern was a multilocular-solid mass containing a considerable amount of solid tissue around relatively small locules, but with no papillary projections. It

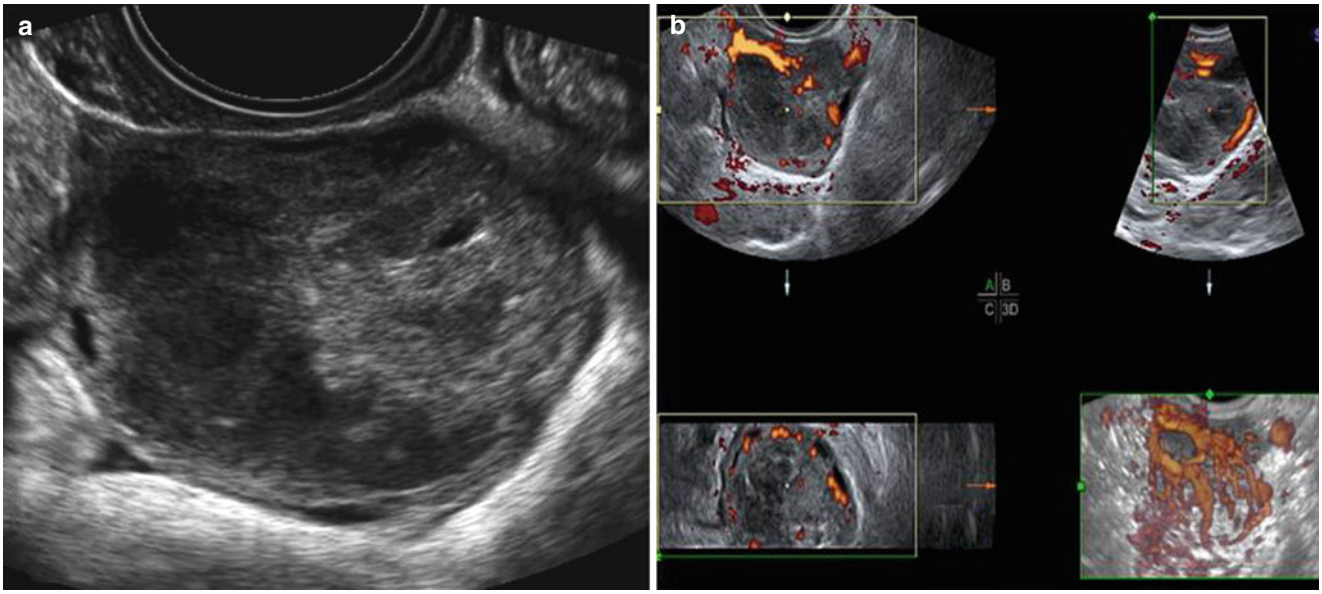

Fig. 7 (**a**) Grayscale ultrasound images of a small (3 cm) granulosa cell tumor adult type stage IA in a 34-year-old woman with a solid appearance, heterogeneous echogenicity, and smooth surface. (**b**) Three-dimensional power Doppler image showing intense vascularization, tortuous vessels with irregular branching

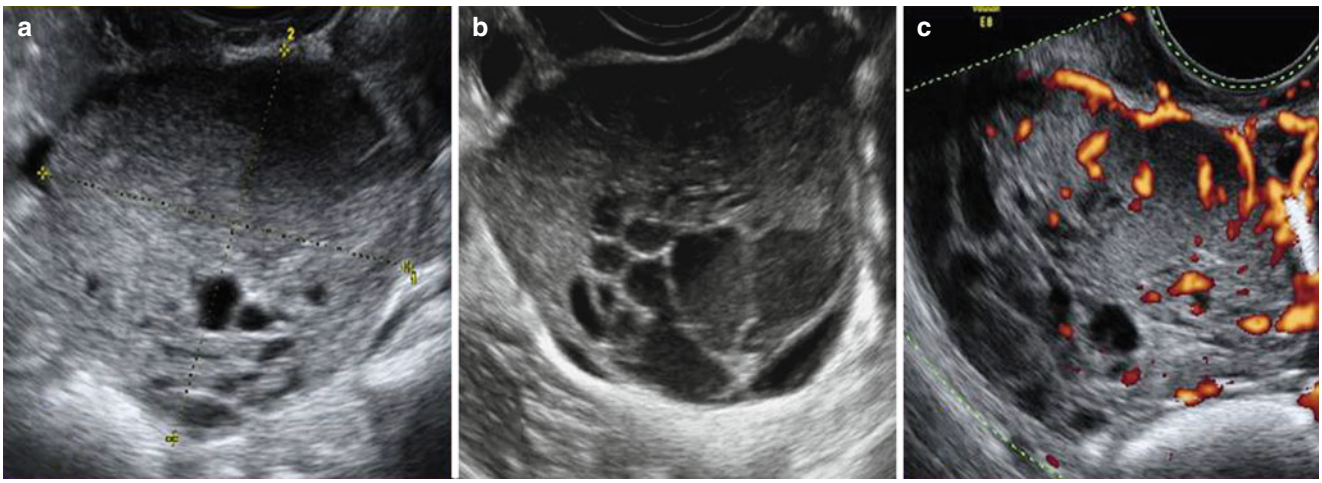

Fig. 8 (**a**, **b**) Grayscale ultrasound images of a small (4 cm) granulosa cell tumor adult type stage IC in a 36-year-old woman with a predominant solid appearance, inhomogeneous echotexture and multiple small locules (Swiss cheese aspect), and smooth surface. (**c**) Two-dimensional power Doppler image showing intense vascularization

typically had a "Swiss cheese" appearance owned to the large number of small locules with a variable thickness of solid tissue around the cystic areas [35]. No specific pattern was recognized in two GCTs of the juvenile type [35] (Figs. 7, 8, 9, and 10).

Ovarian Fibrosarcomas

Primary ovarian sarcomas represent a heterogeneous group comprising <3 % of all ovarian tumors [38]. Fibrosarcoma, on the other hand, is an unusual type of ovarian sarcomas and

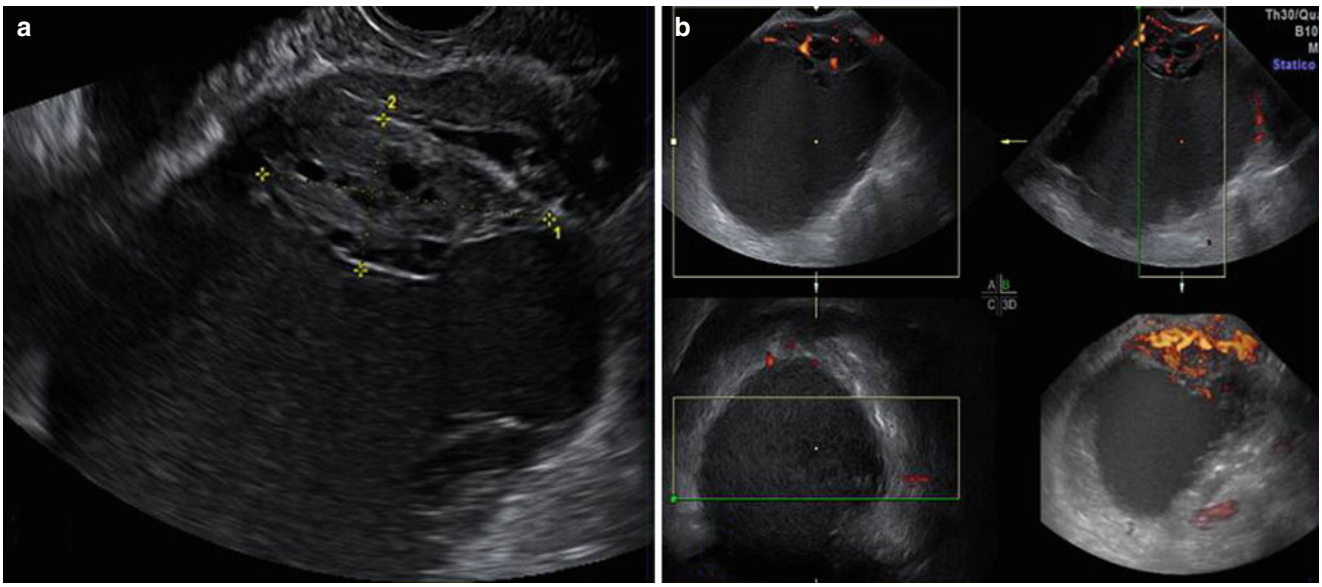

Fig. 9 (**a**) Grayscale ultrasound images of a granulosa cell tumor adult type stage IA in a 53-year-old woman with a multilocular-solid appearance containing a considerable amount of solid tissue around multiple small locules, but with no papillary projections. (**b**) Three-dimensional power Doppler image showing intense vascularization of the solid tissue

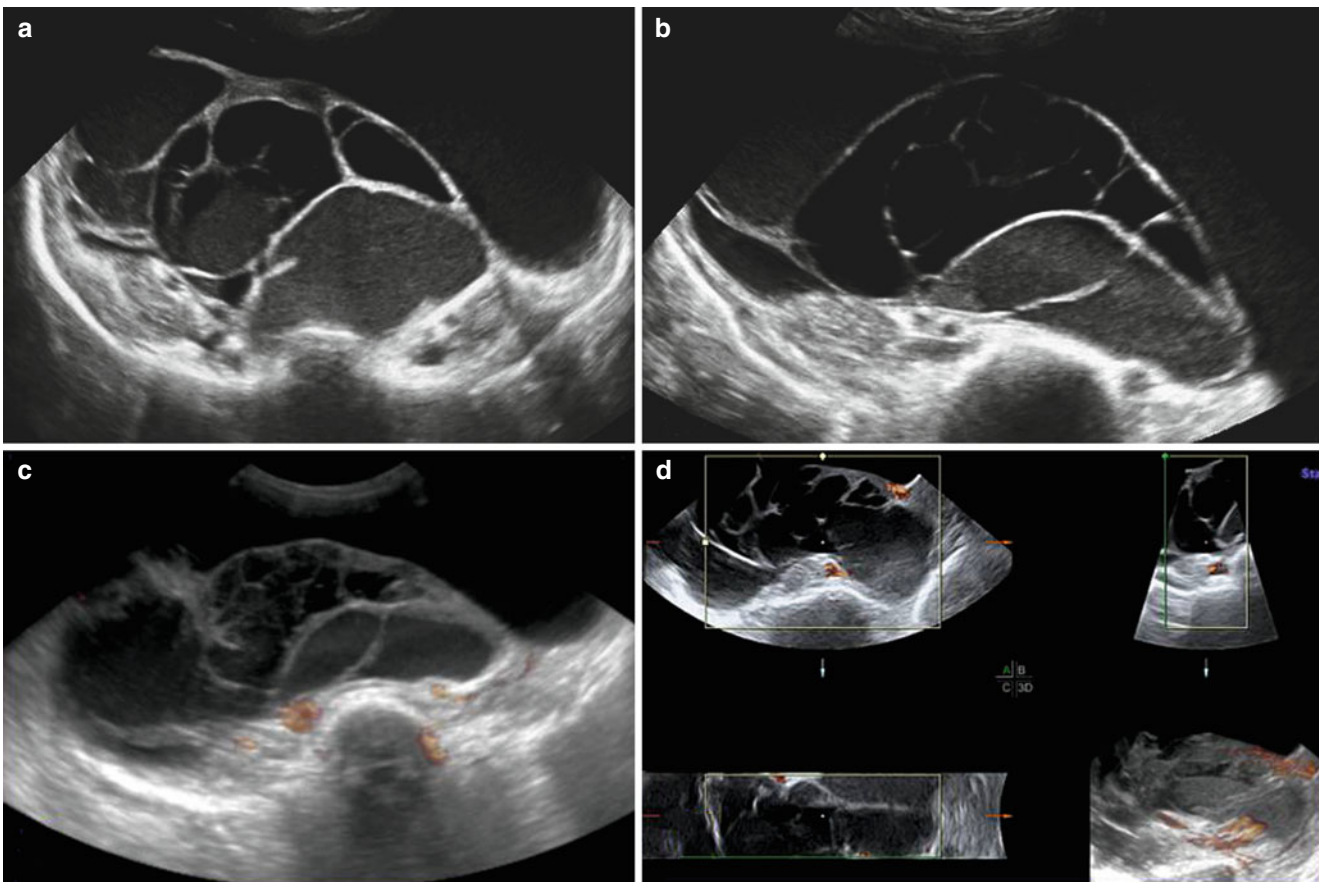

Fig. 10 (**a**, **b**) Grayscale ultrasound images of an atypical large (27 cm) granulosa cell tumor adult type stage IA in a 51-year-old woman with a multilocular appearance (more than 10 large locules) without any amount of solid tissue or papillary projection. (**c**, **d**) Three-dimensional power Doppler image showing moderate vascularization of septa

is an exceedingly rare tumor [1]. Most lesions are heterologous, and 80 % occur in postmenopausal women. These lesions are biologically aggressive, and the majority of patients present with evidence of metastases [1].

As increased cellularity and mitotic activity is present in both, to distinguish between cellular fibromas and fibrosarcomas is often very challenging [38]. Although Prat and Scully reported that the classification of benign cellular fibroma and malignant fibrosarcoma based on mitotic activity was more useful than the one based on the degree of nuclear atypia [39], to differentiate cellular fibroma from fibrosarcoma on the basis of the histological findings alone tends to be difficult in some cases because of the challenge of an accurate mitotic count. An important component of histopathological criteria for the diagnosis of fibrosarcoma is a mitotic count of ≥4 mitotic figures per 10 HPF [39], but a wide heterogeneity in clinical and pathomorphological features prevails in the ovarian fibrosarcomas reported in literature [40].

The immunohistochemical staining for Ki-67 antigen was employed to assess the proliferative activity. The Ki-67 labeling index has been related to prognosis for soft tissue sarcomas. However, Ki-67 antibody is effective only on frozen sections. Recently, MIB-1 antibody has been developed against a recombinant part of Ki-67 antigen, which can also react in formalin-fixed, paraffin-embedded tissue specimens [41]. The proliferative index (% of cells in S + G2 + M phase) in soft tissue fibrosarcoma is significantly higher than that observed in either nodular fasciitis or abdominal fibromatosis. Tsuji et al. described both the MIB-1 LI and the proliferative index in fibrosarcomas being higher than those in cellular fibromas, therefore can be considered useful additional parameters to distinguish between cellular fibromas and fibrosarcomas of the ovary [41].

A study published by Irving et al. noted that cases of ovarian fibromatous tumor showing very high mitotic count, but blunt nuclei, do not usually exhibit an aggressive course of disease and should be diagnosed as "mitotically active cellular fibromas" instead of fibrosarcomas [42].

The treatment of ovarian fibrosarcomas consists of cytoreductive surgery and postoperative platinum-containing combination chemotherapy. First-line cisplatin and ifosfamide or carboplatin and paclitaxel regimen have been associated with improved survival rate [1].

Ultrasound Characteristics

The sonographic features of ovary fibrosarcomas are solid masses, with heterogeneous echogenicity, irregular surface, and unilaterality. In particular, the presence of heterogeneous echogenicity, possibly related to necrosis and hemorrhage, could be helpful in the discrimination of ovarian fibrosarcomas from benign ovarian fibromatous tumors [42].

Doppler waveform analysis of intratumoral artery was described in only one case, with a very low intratumoral resistance and pulsatility index [43].

Sertoli–Leydig Cell Tumors

Epidemiology

Ovarian Sertoli cell tumors, Sertoli–Leydig cell tumors, and Leydig cell tumors are rare. Together they account for less than 1 % of all ovarian tumors [44]. They present most frequently in the third and fourth decades, with 75 % of the lesions observed in women younger than 40 years [1], whereas Leydig cell tumors are more common in slightly older patients, occurring at an average age of 58 years [44]. The tumors are most frequently low-grade malignancies, although occasionally a poorly differentiated variety may behave more aggressively [1].

Microscopy

Four subgroups are described: Sertoli cell tumor, Sertoli cell tumor with lipid storage (folliculome lipidique of Lecene), Leydig cell tumor, and combined Sertoli–Leydig cell tumor [45].

The ovarian Sertoli cell tumors and Sertoli–Leydig cell tumors consist of Sertoli cells, Leydig cells, fibroblasts, or all of these cells in varying proportions and varying degrees of differentiation [44].

Sertoli cell tumors are characterized by hollow or solid tubules dispersed within fibrous stroma containing no or only a few Leydig cells. Most are benign [44].

Sertoli–Leydig cell tumors may be well, moderately, or poorly differentiated. The well-differentiated tumors exhibit tubules composed of Sertoli cells or Leydig cells interspersed with stroma. The intermediate forms show only outlines of immature tubules and large eosinophilic Leydig cells. The poorly differentiated tumors have a sarcomatous pattern with a disorderly disposition of epithelial cell cords [14]. Approximately 20 % of Sertoli–Leydig cell tumors contain heterologous elements, such as gastric type or intestinal-type epithelium [44].

Leydig cell tumors are hilus or non-hilar types, the latter being extremely rare. Microscopic examination of hilus cell tumors reveals a circumscribed mass of steroid cells with eosinophilic cytoplasm [44]. Frequently, Reinke's crystals (lipofuscin pigment and rod-shaped crystal-like structures

3–20 μm in diameter) are found in the cytoplasm of the neoplastic cells [44].

Macroscopy

Sertoli cell tumors are lobulated, solid, yellow, or brown tumors. They may be large (mean diameter, 9 cm) and are usually unilateral [44].

The Sertoli–Leydig tumors were usually described as being well-circumscribed with a glistening, smooth outer surface. On cut surface they were solid, partly cystic, or totally cystic, with larger tumors being more likely to show cystic changes. The cysts sometimes contained clear yellow fluid and occasionally were blood stained. The solid areas of the tumor were firm, fleshy, or soft and varied in color from gray to yellow with areas of hemorrhage and necrosis [45]. They may be minute to huge, but most commonly they range in size from 5 to 15 cm. Almost all Sertoli–Leydig cell tumors are unilateral [44]. In the Roth et al. series, the median size of well-differentiated tumors was 6 cm, 7.5 cm for those tumors of intermediate differentiation, and 13.5 cm for poorly differentiated neoplasms [45].

Leydig cell tumors (hilus tumors) are small (mean diameter, 2.4 cm), solid, brown to yellow tumors. They are usually unilateral [44].

Clinical Symptoms

The tumors typically produce androgens, and clinical virilization is noted in 70–85 % of patients [1]. The incidence of virilization seems to increase as tumor differentiation decreases [45]. In the Roth et al. series, defeminization and/or virilization was noted in 77 % of patients with poorly differentiated tumors, in 73 % of patients with neoplasms of intermediate type, and in 25 % of patients with well-differentiated tumors [45].

Measurement of plasma androgens may reveal elevated testosterone and androstenedione levels, with normal or slightly elevated dehydroepiandrosterone sulfate [1].

Occasionally Sertoli–Leydig cell tumors may have estrogenic manifestations, such as menorrhagia/metrorrhagia or postmenopausal bleeding. Some are complicated by rupture or spread outside the ovary, more commonly in association with poorly differentiated tumors. However, ascites is rare [44].

Prognosis

Five-year survival rate is 70–90 %, and recurrences thereafter are uncommon [1]. Most important prognostic factors are stage of disease and differentiation. Most Sertoli–Leydig cell tumors are diagnosed at stage 1, and for this stage survival depends on the degree of differentiation. Tumors that present at higher stages have a poorer prognosis. When Sertoli–Leydig cell tumors recur, they typically do so within 1 year and almost 95 % relapse within 5 years. Recurrent tumors are usually confined to the pelvis or abdomen [44].

Because these tumors are rarely bilateral, the usual treatment is unilateral salpingo-oophorectomy and macroscopic evaluation of the contralateral ovary in patients who are in their reproductive age. In postmenopausal women, hysterectomy and bilateral salpingo-oophorectomy are appropriate [1].

Ultrasound Characteristics

The ultrasound features described in literature are based on a few published series. Monteagudo et al. described a solid, slightly hyperechogenic intraovarian Leydig cell tumor with a diameter of about 1 cm. They reported similar ultrasound findings in three cases of steroid cell tumor, two of the latter being associated with virilization. The tumors seem to be well vascularized [46]. Outwater et al. described the imaging of seven Sertoli–Leydig cell tumors, two Leydig cell tumors, and two steroid cell tumors. It is not reported how many of these tumors had been examined by ultrasound imaging. Steroid cell tumors were solid, whereas the Sertoli–Leydig cell tumors were more variable in their morphology, with some estimated to contain less than 50 % solid tissue by the imaging method used [47].

The ultrasound findings using a standardized examination technique, terms, and definitions recommended by the IOTA group are cited in the literature in only one article. Demidov et.al. described the sonographic characteristics of 22 patients; 15 had Sertoli–Leydig cell tumors, two had Sertoli cell tumors, and five had Leydig cell tumors. Twenty-two (96 %) of 23 tumors (one woman had bilateral tumors) contained a solid component; 16 (70 %) were purely solid. Pattern recognition showed that the Leydig cell tumors were small solid tumors (four of five had a largest diameter of 1–3 cm), and the two Sertoli cell tumors were somewhat larger solid tumors (4 and 7 cm); the Sertoli–Leydig cell tumors were either small-sized (3–4 cm) or medium-sized (6–7 cm) solid tumors or multilocular-solid tumors of any size (3–18 cm) with purely solid areas mixed with areas of innumerable closely packed small cyst locules [44]. The color score information was available for nine patients in this series: four patients with Sertoli–Leydig cell tumors, three with Leydig cell tumors, and two with Sertoli cell tumors. Eight tumors were moderately or abundantly vascularized, whereas one poorly differentiated Sertoli–Leydig cell tumor was poorly vascularized [44] (Figs. 11 and 12).

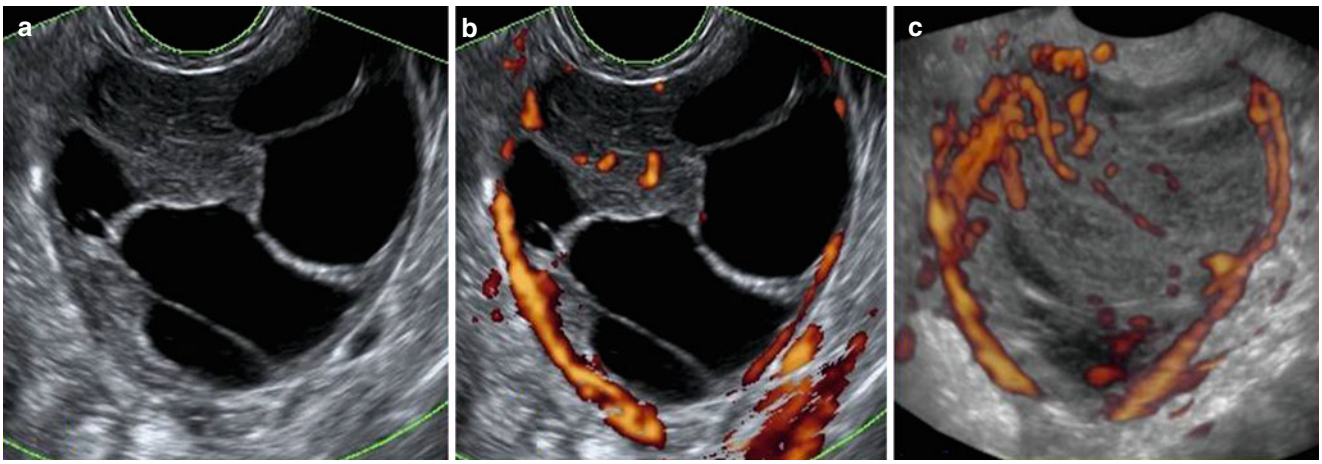

Fig. 11 (**a**) Grayscale ultrasound images of a 6 cm Sertoli–Leydig ovarian tumor stage IC in a 13-year-old girl with oligomenorrhea. The mass has a multilocular-solid appearance containing a considerable amount of solid tissue and multiple locules (<10 locules), but with no papillary projections. (**b**, **c**) Two- and three-dimensional power Doppler image showing intense vascularization of the capsula and of the solid tissue

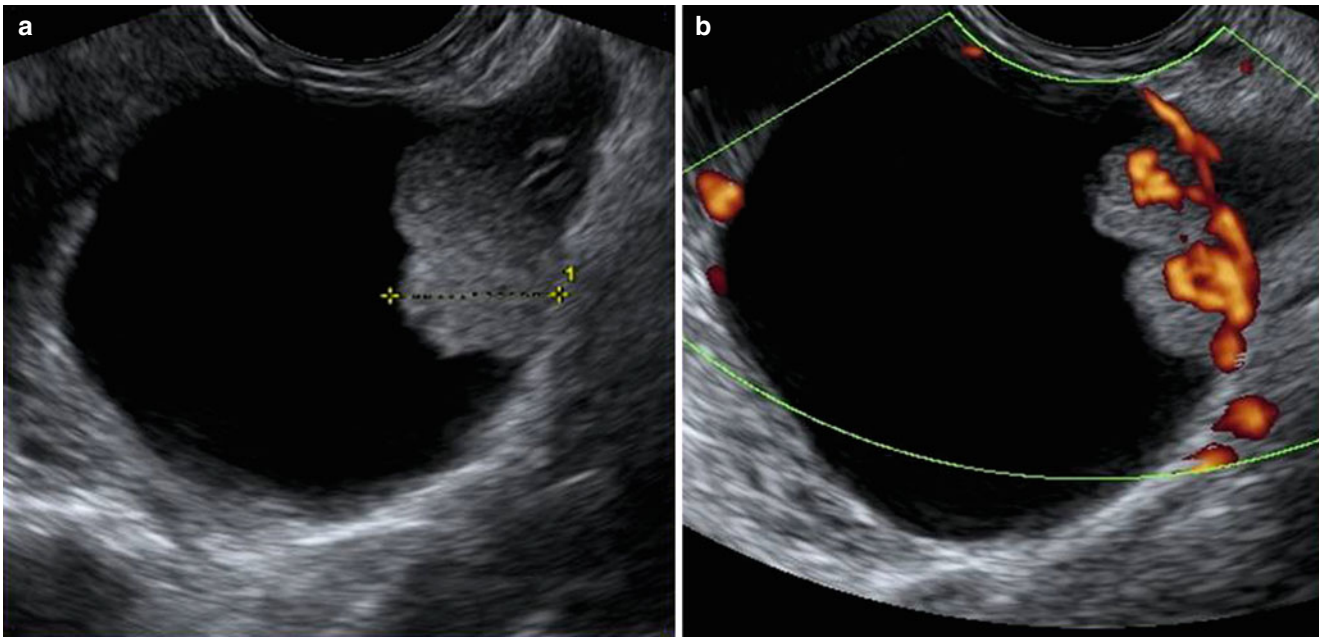

Fig. 12 (**a**) Grayscale ultrasound images of an atypical 5 cm Sertoli–Leydig stage IC in a 19-year-old woman with a multilocular-solid appearance containing a modest amount of solid tissue and multiple locules (2 locules). (**b**) Two-dimensional power Doppler image showing intense vascularization of the solid tissue

Biography Dorella Franchi received her MD degree at the University of Milan, Italy, and her specialty training at San Gerardo Hospital in Monza, Italy (obstetrics and gynecology), and at the European Institute of Oncology, Milan (gynecologic oncology). Currently, she is a Senior Deputy Director at the Preventive Gynecology Unit of the Gynecologic Oncology Division at the European Institute of Oncology. She is a member of the Italian Society of Ultrasound in Obstetrics and Gynecology (SIEOG) and a member of the International Society of Ultrasound in Obstetrics and Gynecology (ISUOG) and of the European Society of Gynecologic Oncology (ESGO).

References

1. Berek JS, Friedlander M, Hacker NF. Germ cell and other nonepithelial ovarian cancer. In: Berek JS, Hacker NF, editors. Gynecologic oncology. 5th ed. Philadelphia: Lippincott Williams & Wilkins; 2010.
2. Quirk JT, Natarajan N, Mettlin CJ. Age-specific ovarian cancer incidence rate patterns in the United States. Gynecol Oncol. 2005;99(1):248–50.
3. Pectasides D, Pectasides E, Kassanos D. Germ cell tumors of the ovary. Cancer Treat Rev. 2008;34:427–41.
4. Dill-Macky MJ, Atri M. Ovarian ultrasound. In: Callen PW, editor. Ultrasonography in obstetrics and gynecology. 4th ed. Philadelphia: W.B. Saunders; 2000.
5. Murugaesu N, Schmidt P, Dancey G, et al. Malignant ovarian germ cell tumors: identification of novel prognostic markers and long – term outcome after multimodality treatment. J Clin Oncol. 2006; 24:4862–6.
6. Kurman RJ, Norris HJ. Malignant germ cell tumors of the ovary. Hum Pathol. 1977;8(5):551–64.
7. Gershenson DM, Del Junco G, Copeland LJ, et al. Mixed germ cell tumors of the ovary. Obstet Gynecol. 1984;64(2):200–6.
8. Gershenson DM. Management of early ovarian cancer: germ cell and sex cord-stromal tumors. Gynecol Oncol. 1994;55:S62–72.
9. Guerriero S, Testa AC, Timmerman D, et al. Imaging of gynecological disease (6): clinical and ultrasound characteristics of ovarian dysgerminoma. Ultrasound Obstet Gynecol. 2011;37: 596–602.
10. Pressley RH, Muntz HG, Falkenberry S, Rice LW. Serum lactic dehydrogenase as a tumor marker in dysgerminoma. Gynecol Oncol. 1992;44:281–3.
11. Schwartz PE, Morris JM. Serum lactic dehydrogenase: a tumor marker for dysgerminoma. Obstet Gynecol. 1988;72:511–5.
12. Lazebnik N, Balog A, Bennett S, et al. Ovarian dysgerminoma a challenging clinical and sonographic diagnosis. J Ultrasound Med. 2009;28:1409–15.
13. Prat J. Germ cell tumors. In: Prat J, editor. Pathology of the ovary. 1st ed. Philadelphia: Saunders; 2004.
14. Crum CP. The female genital tract. In: Cotran RS, Kumar V, Robbins SL, editors. Robbins pathologic basis of disease. 6th ed. Philadelphia: WB Sanders; 1999.
15. DardiK R, Duska L, Bristoe R. Ovarian cancer. In: Bankowski BJ, Hearne AE, Lambrou NC, Fox HE, Wallach EE, editors. The Johns Hopkins manual of gynecology and obstetrics. 2nd ed. Philadelphia: Lippincott Williams & Wilkins; 2002.
16. Eun-Seop S, Jung-Pil L, Jae-Ho H, et al. Dysgerminoma of the ovary with precocious puberty: a case report. Gynecol Endocrinol. 2007;23(1):34–7.
17. Kumar S, Shah JP, Bryant CS, et al. The prevalence and prognostic impact of lymph node metastases in malignant germ cell tumors of the ovary. Gynecol Oncol. 2008;110:125–32.
18. Mangili G, Sigismondi C, Gadducci A, et al. Outcome and risk factors for recurrences in malignant ovarian germ cell tumors. A MITO-9 retrospective study. Int J Gynecol Cancer. 2011;21: 1414–21.
19. Gordon A, Lipton D, Woodruff JD. Dysgerminoma: a review of 158 cases from the Emil Novak ovarian tumor registry. Obstet Gynecol. 1981;58:497–504.
20. Kim HS, Kang BS. Ovarian dysgerminoma: color Doppler ultrasonographic findings and comparison with CT and MR imaging findings. J Ultrasound Med. 1995;14:843–8.
21. Ulbright TM. Germ cell tumors of the gonads: a selective review emphasizing problems in differential diagnosis, newly appreciated, and controversial issues. Mod Pathol. 2005;18:S61–79.
22. Outwater EK, Siegelman ES, Hunt JL. Ovarian teratomas: tumor types and imaging characteristics. Radiographics. 2001;21: 475–90.
23. Savelli L, Testa AC, Timmerman D, et al. Imaging of gynaecological disease (4): clinical and ultrasound characteristics of struma ovarii. Ultrasound Obstet Gynecol. 2008;32:210–9.
24. Hung JH, Shen SH, Hung J, et al. Ultrasound and magnetic resonance images of endodermal sinus tumor. J Chin Med Assoc. 2007;70(11):514–8.
25. Hogg R, Friedlander M. Management of embryonal carcinoma of the ovary. CME J Gynecol Oncol. 2002;7:234–7.
26. Kawai M, Kano T, Kikkawa F, et al. Seven tumor markers in benign and malignant germ cell tumors of the ovary. Gynecol Oncol. 1992;45:248–53.
27. Kurman RJ, Norris HJ. Embryonal carcinoma of the ovary. A clinicopathologic entity distinct from endodermal sinus tumor

resembling embryonal carcinoma of the adult testis. Cancer. 1976;38:2420–33.
28. Simşek T, Trak B, Tunç M, et al. Primary pure choriocarcinoma of the ovary in reproductive ages: a case report. Eur J Gynaecol Oncol. 1998;19(3):284–6.
29. Axe SR, Klein VR, Woodruff JD. Choriocarcinoma of the ovary. Obstet Gynecol. 1985;66(1):111–4.
30. Corakçi A, Ozeren S, Ozkan S. Pure nongestational choriocarcinoma of ovary. Arch Gynecol Obstet. 2005;271:176–7.
31. Jondle DM, Shahin MS, Sorosky J, et al. Ovarian mixed germ cell tumor with predominance of polyembryoma: a case report with literature review. Int J Gynecol Pathol. 2002;21(1):78–81.
32. Colombo N, Parma G, Zanagnolo V, et al. Management of ovarian stromal cell tumors. J Clin Oncol. 2007;25:2944–51.
33. Schumer ST, Cannistra SA. Granulosa cell tumor of the ovary. J Clin Oncol. 2003;21:1180–9.
34. Young RH, Dickersin GR, Scully RE. Juvenile granulosa cell tumor of the ovary: a clinicopathological analysis of 125 cases. Am J Surg Pathol. 1984;8:575–96.
35. Van Holsbeke C, Domali E, Holland TK, et al. Imaging of gynecological disease (3): clinical and ultrasound characteristics of granulosa cell tumors of the ovary. Ultrasound Obstet Gynecol. 2008;31: 450–6.
36. Ko SF, Wan YL, Ng SH, et al. Adult ovarian granulosa cell tumors: spectrum of sonographic and CT findings with pathologic correlation. AJR Am J Roentgenol. 1999;172:1227–33.
37. Hong BK, Jeng CJ, Huang SH, et al. Sonographic and clinical findings of granulosa cell tumor. Chin Med J. 1996;57:214–8.
38. Shakfeh SM, Woodruff JD. Primary ovarian sarcomas: report of 46 cases and review of the literature. Obstet Gynecol Surv. 1987; 42:331–49.
39. Prat J, Scully RE. Cellular fibromas and fibrosarcomas of the ovary: a comparative clinicopathologic analysis of seventeen cases. Cancer. 1981;47:2663–70.
40. Testa AC, Gaurilcikas A, Licameli A. Sonographic features of primary ovarian fibrosarcoma: a report of two cases. Ultrasound Obstet Gynecol. 2009;33:112–5.
41. Tsuji T, Kawauchi S, Utsunomiya T, et al. Fibrosarcoma versus cellular fibroma of the ovary: a comparative study of their proliferative activity and chromosome aberrations using MIB-1 immunostaging, DNA flow cytometry, and fluorescence in situ hybridization. Am J Surg Pathol. 1997;21(1):52–9.
42. Irving JA, Alkushi A, Young RH, et al. Cellular fibromas of the ovary: a study of 75 cases including 40 mitotically active tumors emphasizing their distinction from fibrosarcoma. Am J Surg Pathol. 2006;30:929–38.
43. Kaya H, Sezik M, Ozkaya O, et al. Color Doppler ultrasound in ovarian fibrosarcoma. Gynecol Oncol. 2004;94:229–31.
44. Demidov VN, Lipatenkova J, Vikhareva O, et al. Imaging of gynecological disease (2): clinical and ultrasound characteristics of Sertoli cell tumors, Sertoli – Leydig cell tumors and Leydig cell tumors. Ultrasound Obstet Gynecol. 2008;31:85–91.
45. Roth LM, Anderson MC, Govan AD, et al. Sertoli-Leydig cell tumors: a clinicopathologic study of 34 cases. Cancer. 1981;48: 187–2197.
46. Monteagudo A, Heller D, Husami N, et al. Ovarian steroid cell tumors: sonographic characteristics. Ultrasound Obstet Gynecol. 1997;10:282–8.
47. Outwater EK, Marchetto B, Wagner BJ. Virilizing tumors of the ovary: imaging features. Ultrasound Obstet Gynecol. 2000;15: 365–71.
48. Rice LW. The ovary. In: Ryan KJ, Berkowitz RS, Barbieri RL, Duanif A, eds. Kistner's Gynecology & Women's Health, 7th ed. St Louis: Mosby Inc. 1999:166–90.

CT and MR Imaging of Malignant Germinal and Stromal Ovarian Tumours

Corinne Balleyguier, Wassef Khaled, Sandra Canale, Laura Ciolovan, Elise Zareski, Pierre Duvillard, Laurence Brugières, and Philippe Morice

Abstract

Malignant germ cell tumours are less common than epithelial ovarian tumours, accounting for less than 2–3 % of all ovarian cancers in Western countries. They usually occur in younger women with a peak incidence before 20 years.

Malignant stromal tumours are developed on stromal tissue of the ovary and are frequently associated with hormonal secretion. In this group, malignant lesions are most represented by adult or juvenile granulosa cell tumours, Sertoli-Leydig tumours and fibrosarcoma.

Imaging and in particular CT and MR may help to characterise and to stage preoperatively these rare tumours, and besides common malignant features, it might be useful to detect some specific features to better assess these lesions.

Keywords

Malignant ovarian germ cell • Choriocarcinoma • Embryonal carcinoma • Imaging • Computed tomography • Magnetic resonance imaging

Malignant germ cell tumours are less common than epithelial ovarian tumours, accounting for less than 2–3 % of all ovarian cancers in Western countries. They usually occur in younger women with a peak incidence before 20 years. Increasing incidence of these neoplasms is noticed in black and Asian societies representing up to 15 % of ovarian cancers. Recognising these tumours is challenging because it is possible to treat them in a curative way while preserving fertility [1]. This group of neoplasms includes two different types of tumours: nonseminomatous germ cell tumours including immature teratoma, endodermal sinus tumour, embryonal carcinoma and choriocarcinoma and in the other group dysgerminoma.

Malignant stromal tumours are developed on stromal tissue of the ovary and are frequently associated with hormonal secretion. In this group, malignant lesions are most represented by adult or juvenile granulosa cell tumours, Sertoli-Leydig tumours and fibrosarcoma.

Imaging may help to characterise and to stage preoperatively these rare tumours, and besides common malignant

C. Balleyguier (✉) • W. Khaled • S. Canale
L. Ciolovan • E. Zareski
Radiology Department, Institut Gustave Roussy,
114 rue Edouard Vaillant, 94805 Villejuif, France
e-mail: corinne.balleyguier@igr.fr

P. Duvillard
Biopathology Department, Institut Gustave Roussy,
Villejuif, France
e-mail: pierre.duvillard@igr.fr

L. Brugières
Pediatry Department, Institut Gustave Roussy,
Villejuif, France
e-mail: laurence.brugieres@igr.fr

P. Morice
Surgery Department, Institut Gustave Roussy,
Villejuif, France
e-mail: philippe.morice@igr.fr

L. Saba et al. (eds.), *Ovarian Neoplasm Imaging*,
DOI 10.1007/978-1-4614-8633-6_21,

features, it might be useful to detect some specific features to better assess these lesions.

Malignant Germ Cell Tumours

Immature Teratoma

Immature teratomas of the ovary constitute the third most common primitive germ cell tumour representing 1 % of all teratomas and containing immature tissue from all three germ cell layers. They are much less common than their benign counterpart, mature cystic teratomas (dermoid cystic) approximately accounting for 15 % of germ cell tumours. It is important to differentiate malignant transformation of mature cystic teratomas rising to carcinomas or sarcomas from immature teratomas because these one usually do not arise from pre-existing mature teratomas. It affects young patients (first two decades of life). Immature teratomas tend to be larger (14–25 cm) than mature teratomas (7 cm) [1]. These tumours may be solid or cystic with a prominent solid part. This component may display (a) multiple foci of fat in contrast to the more uniform appearance of liquid sebum in mature cystic teratomas [2], (b) calcifications that are often coarse and ill-defined and (c) concomitant haemorrhage [3] (Fig. 1). Identification of these solid parts before surgery may be helpful although it is common to see multiple small solid parts, known as Rokitansky nodule [4] in mature cystic teratomas. The cystic areas in immature teratomas are usually filled with serous, mucinous fluid or with fatty content, showing variable signal on MR sequences [3] (Fig. 2). Some authors have suggested that solid part had irregular inner margins with a size larger than 5 cm, and the base formed an obtuse angle with the cyst wall [5]. Immature tumours show a significant contrast agent uptake in CT and MR scans. No correlation has been noticed between the tumour grade and the amount of solid tissue [4].

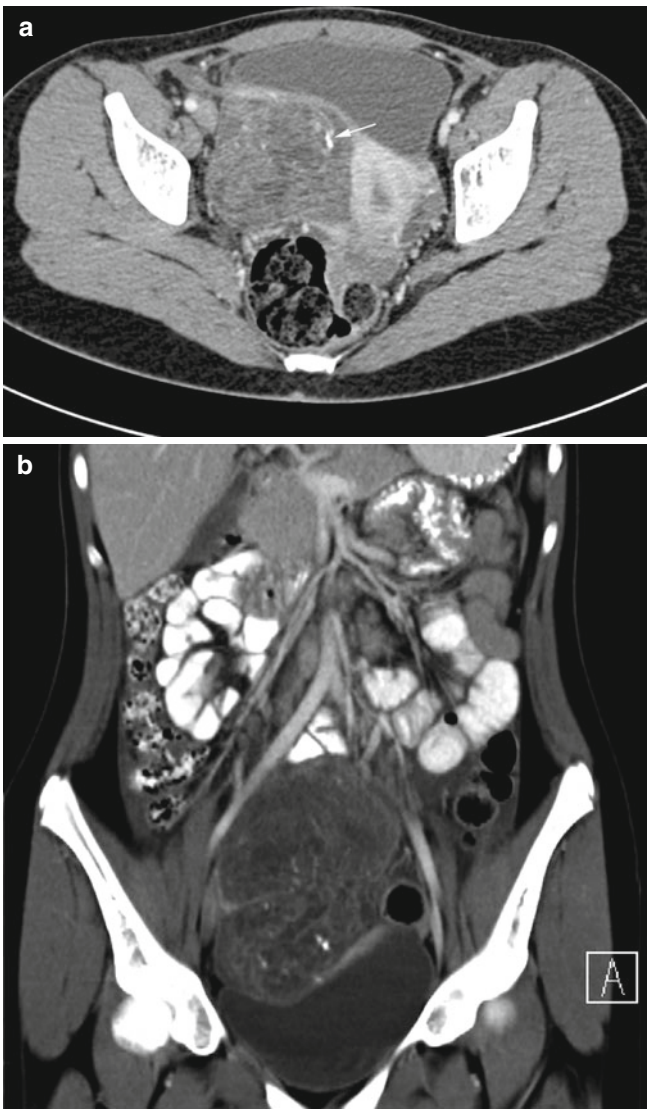

Fig. 1 Immature teratoma. A 16-year-old girl. CT with iodium injection (**a**) and coronal reconstruction (**b**). A right pelvic mass was detected on abdominal pain on ultrasound and CT. A right heterogeneous multicystic mass is seen on the right side of the pelvis, with uterus displacement. Calcifications are seen in the mass (*arrow*) and may suggest the diagnosis of immature teratoma

Malignant Transformation of Mature Teratomas

Histologic findings are usually completely different, and mature teratomas usually transform in squamous cell carcinomas (80–85 %) rising from the squamous cell lining of the wall cyst; the rest are carcinoid tumours or adenocarcinomas [6]. These tumours have a large size (>10 cm) and display high concentrations of squamous cell carcinoma antigen and CA-125 that are considered as markers for malignant transformation [6].

The gross appearance of malignant transformation of mature teratoma is similar to benign mature cystic teratomas with a more solid component [3]. Imaging must focus on Rokitansky nodule which is along with the cyst wall and the common site for degeneration. It has the appearance of the underlying mature teratoma. CT and MR findings consist of a fat-containing tumour with an enhancing, irregularly marginated, solid component with or without direct invasion of close organs [1]. Enhanced CT scan shows a single plug with cauliflower appearance and an irregular border forming an obtuse angle with the inner wall of the cyst [7]. Moreover, mature teratomas have a smooth surface, whereas transformed mature teratomas may have septa and a capsule [3].

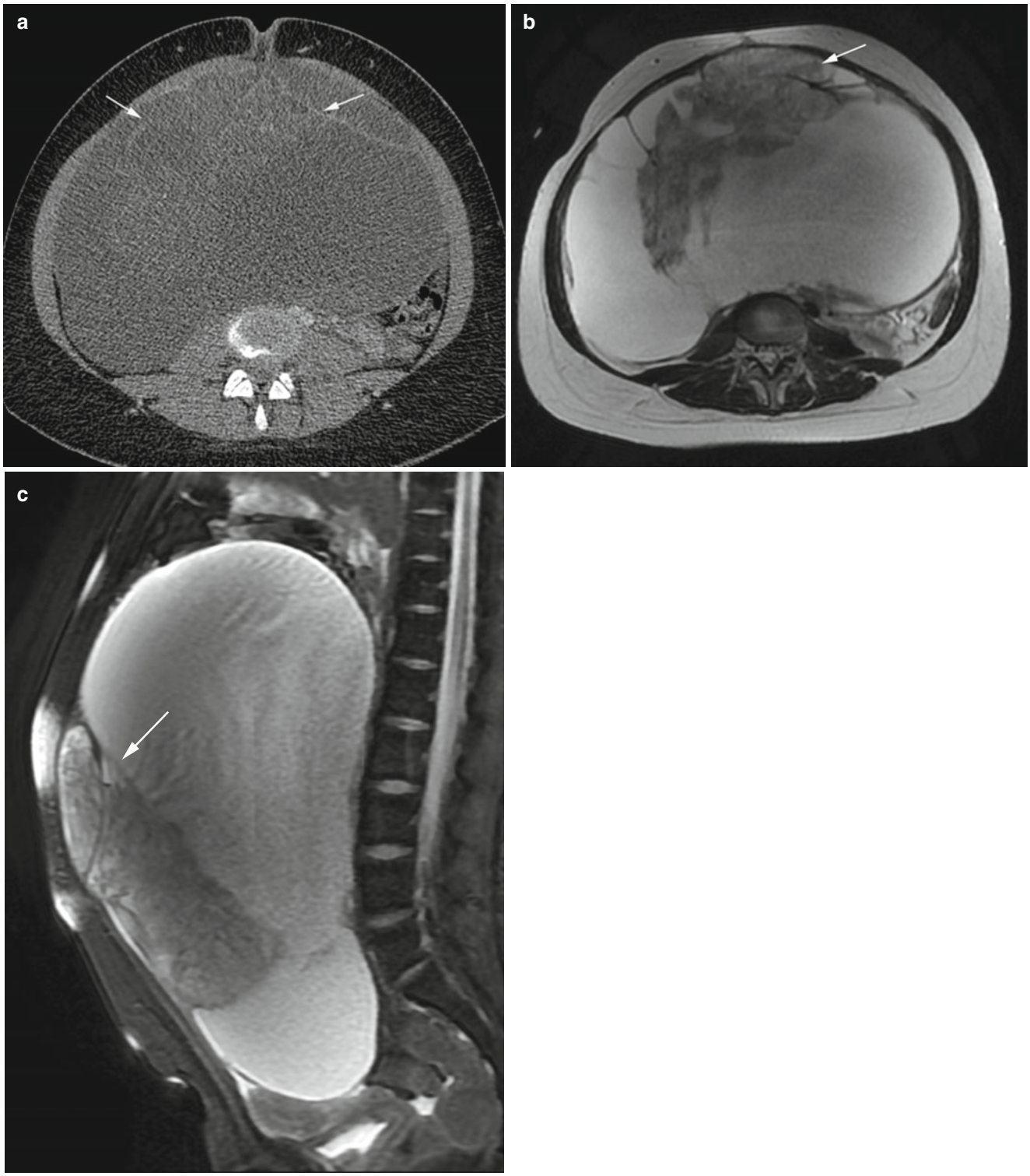

Fig. 2 Immature teratoma. A 24-year-old woman. CT with iodium injection (**a**), MRI (axial T2w, **b**) and sagittal T2w with fat suppression (**c**) 18 cm abdominal and pelvic mass discovered on abdominal pain and distension of the abdomen. CT shows a cystic mass with heterogeneous loculated thick wall (*arrows*, **a**). MRI depicts more clearly a heterogeneous solid content within the cystic mass (*arrows*) in the anterior part of the mass. In this immature teratoma, no fatty tissue or calcifications were seen on imaging or pathology

Besides, mature teratomas never show a transmural growth and contrast enhancement after injection [3]. In fact, it has been suggested that the contrast enhancement of the Rokitansky nodule is an early indicator of malignant transformation [8]. This difficult identification is important because changes of a mature teratoma usually display a bad prognosis.

Growing Teratoma

Growing teratoma syndrome (GTS) is defined as enlarging masses of mature teratoma following chemotherapy for malignant nonseminomatous germ cell tumours [9]. Tumour masses in GTS grow at the initial site of tumour with extension to more distant sites including the retroperitoneum, peritoneal cavity, liver, and lymph nodes. Follow-up imaging of patients with GTS is essential: MR imaging and CT are the most useful imaging examinations. Well-circumscribed masses with fat or punctuate calcifications and /or cystic areas may be seen on CT [9] (Fig. 3). MR imaging sequences using T1-weighted fat saturation sequences are recommended to detect fatty tissue within the masses (Fig. 3a). The classical appearance are similar to those of a dermoid cyst [9]. Nevertheless, some of the features on CT and MR can overlap with imaging findings of immature teratomas with the presence of cystic, fatty and calcified elements [10] (Fig. 3). However, immature teratomas are typically larger, less well defined with a prominent solid component and associated with foci of haemorrhage [1].

Complete surgical resection of recurrent masses in GTS is recommended when feasible [9].

Endodermal Sinus Tumour: Yolk Sac Ovarian Tumour

Yolk sac tumours of the ovary or endodermal sinus tumours are highly malignant germ cell tumours. They are most commonly encountered in women in the second and third decades and are rare in women over 40 years [11]. These lesions are rare, occurring in less 1 % of malignant ovarian tumours, 20 % of malignant germinal tumours. Rarely asymptomatic, it spreads outside of the pelvis in 50 % of cases (metastases in 40 % of cases) [12]. Few radiological descriptions are published in the literature. Imaging findings of yolk sac tumours vary from entirely solid to predominantly cystic [13]. But most often these tumours are heterogeneous associating mixed solid and cystic features [11] (Fig. 4). In the study of Yamaoka et al. [11], four lesions identified on MRI exhibited areas of haemorrhage on T1-weighted sequences. Another characteristic is high vascularisation (Fig. 5). In this study, all four tumours were associated with high signal voids, indicating rich vascular supply. On post-contrast CT or MR imaging, these areas are highly enhanced defining the "bright dot sign", because of dilated vessels. Moreover, solid parts may strongly enhance, in a more prominent way than the uterine myometrium. Stromal oedema is often seen on microscopic analysis and might be detected with high-signal intensity on T2-weighted images with prominent enhancement on post-contrast images (Fig. 6). Striking enhancement is also commonly seen on yolk sac ovarian tumours [11]. Striking enhancement may be also seen on sclerosing stromal tumour, which is one of differential diagnosis. Nevertheless, the rim of hypointensity on T2-weighted sequences with pseudolobulated lesions, such as low-intense nodules closed to high-intense stroma on T2-weighted images, may help to differentiate sclerosing stromal tumours from yolk sac tumours [14]. These tumours grow rapidly and have a poor prognosis [15]. Finally, yolk sac tumours are usually associated with an elevated serum level of α-fetoprotein. Ascites and hydronephrosis must be carefully examined.

Endodermal sinus tumour may be associated with teratoma in 15 % of cases [11]: in this case, coarse calcifications or fatty tissue contrast with high vascularity due to the yolk sac tumour component (Fig. 6).

Primary Ovarian Choriocarcinoma

Ovarian choriocarcinoma accounts for less than 1 % of ovarian tumours and the mean age of presentation is 15 years [16]. This tumour is generally associated with other germ cell tumours. Gestational ovarian choriocarcinoma can be metastatic (associated with intrauterine pregnancy) or primary (associated with ectopic ovarian pregnancy). The essential diagnostic criteria for non-gestational choriocarcinoma need exclusion of coexisting disease in the uterine cavity, molar pregnancy and intrauterine pregnancy [17].

Suggestive findings include a large, unilateral, hypervascular adnexal mass with multiple cystic cavities located in the peripheral part of the ovary and presence of haemorrhage associated with high β-hCG level "empty" uterus [17] (Fig. 7). MR may confirm the presence of haemorrhage with hyperintense foci on T1-weighted sequences [18]. Haemorrhagic content and necrotic changes are mostly located in the central part of the tumour (Fig. 7). CT can also show some calcifications within an ovarian heterogeneous mass [18].

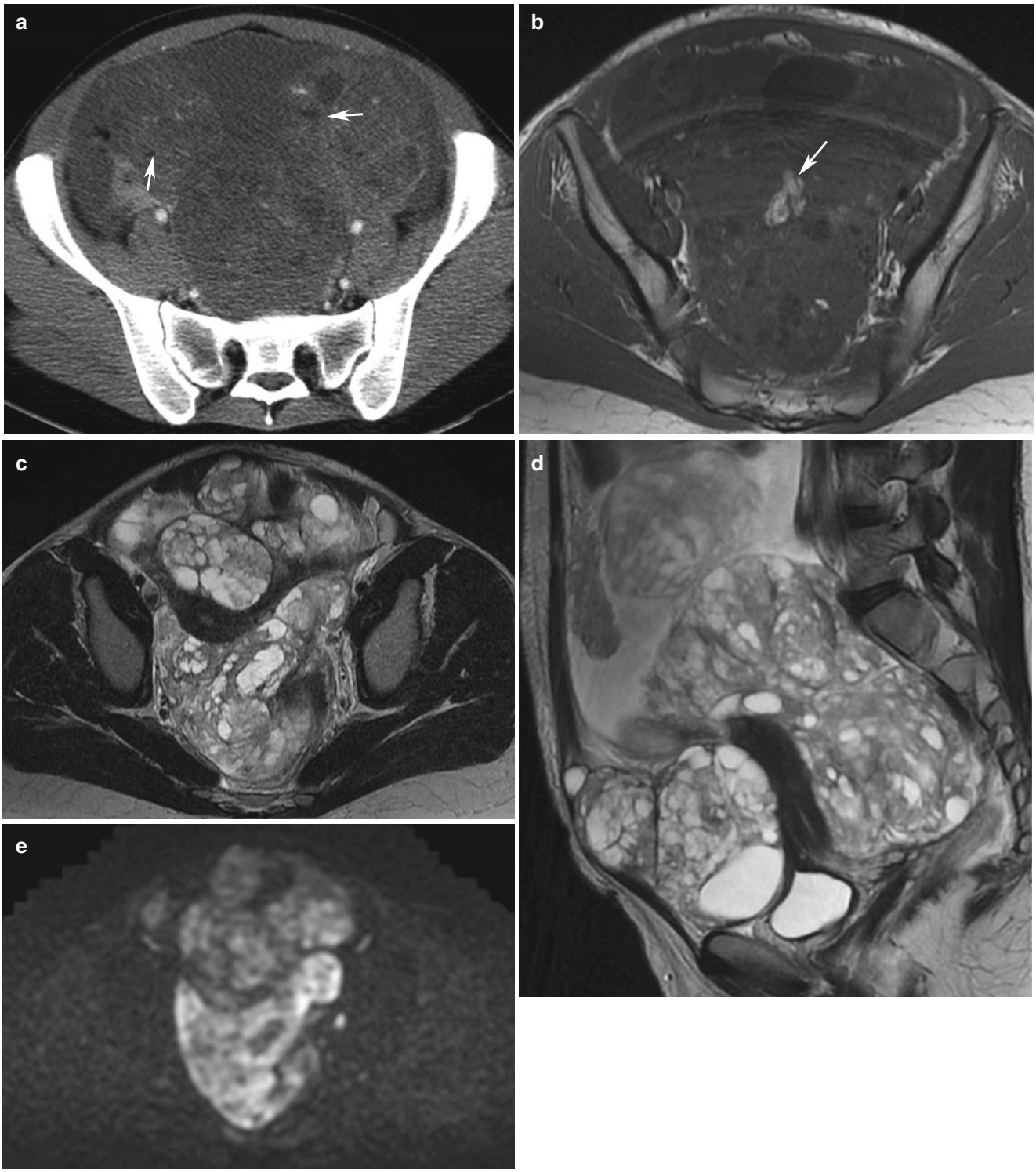

Fig. 3 Growing teratoma in a 22-year-old woman, treated previously with surgery and chemotherapy for an immature teratoma. CT with injection (**a**), MRI (axial T1w, **b**); axial T2, (**c**); sagittal T2, (**d**); b1000 DWI, (**e**); axial T1w with gadolinium chelates injection and fat suppression, (**f**). A large solid-cystic heterogeneous pelvic (**a**, **c**) and abdominal mass (**d**) appeared shortly after chemotherapy treatment for an immature teratoma. Fatty tissue is seen within the mass (**a** and **b**, *arrow*) Histology with complete surgical excision revealed mature teratoma, corresponding to a growing teratoma. This lesion is hyperintense on DWI (**e**) and enhances heterogeneously after injection (**f**). No recurrence occurred after complete surgical excision

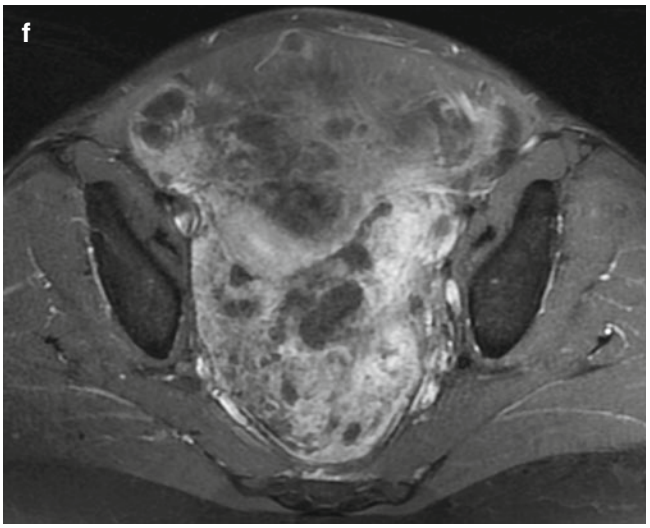

Fig. 3 (continued)

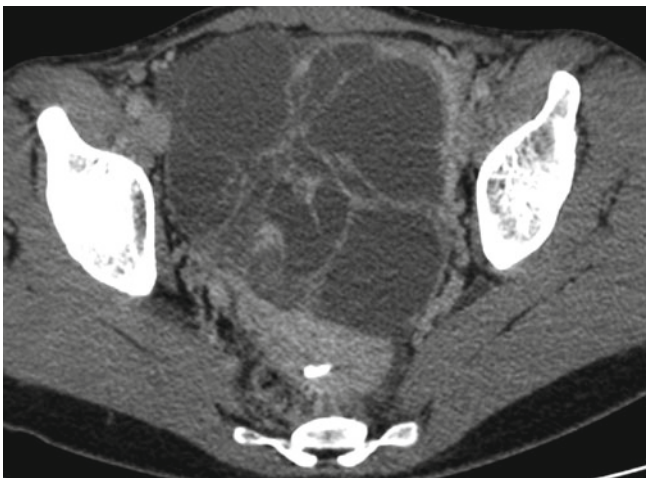

Fig. 4 Yolk sac ovarian tumour in a 44-year-old woman. CT with iodium injection. A left heterogeneous cystic mass is seen with thick septations in the left part of the uterus, developed in left ovary. Suspicious features include thick wall, thick septations and large size

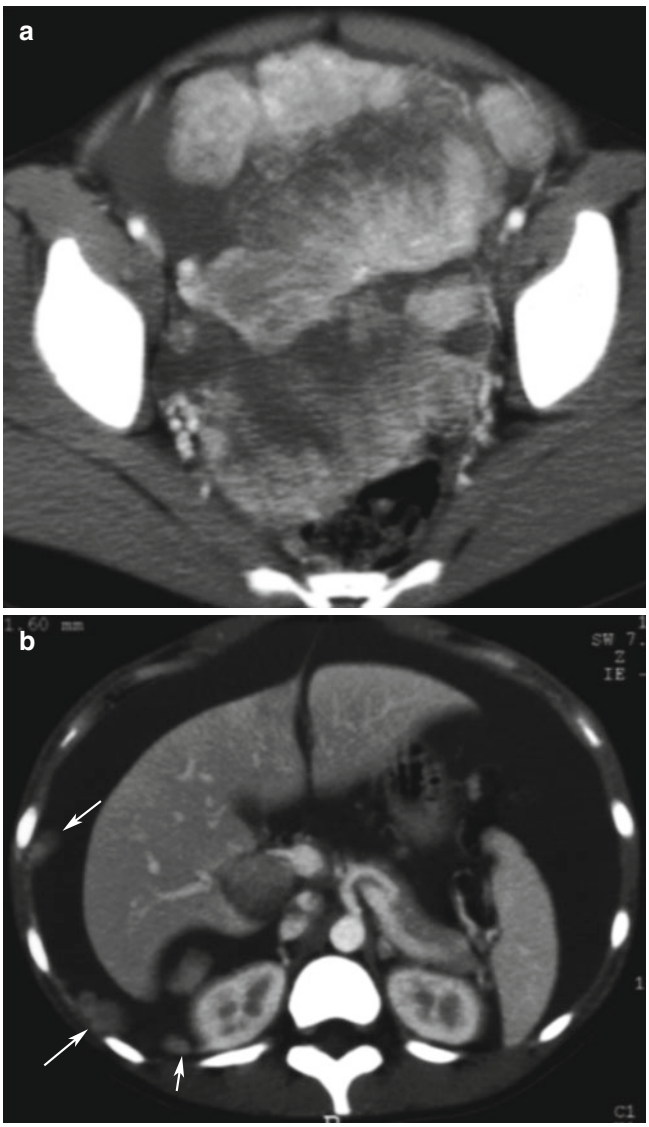

Fig. 5 Yolk sac tumour in a 13-year-old girl. CT with iodium injection (**a**, pelvis: **b**, abdomen). A 15 cm heterogeneous solid mass is located in the pelvis. High vascularisation is clearly seen on injected images (**a**). Malignant features include high vascularisation, ascites and peritoneal implants (**b**, *arrows*)

Embryonal Carcinoma

This malignant germ cell tumour is the ovarian counterpart of the embryonal carcinoma of the testis, even if it is less frequent. No study has described imaging features of this rare tumour: it is usually a heterogeneous mass with necrotic and haemorrhagic parts.

Malignant Mixed Germ Cell Tumour

Eight per cent of the ovarian malignant germ cell tumours are mixed as compared to 40 % of the testicular tumour [19]. Imaging findings show a solid heterogeneous mass varying according to different histological components.

Seminomatous Germ Cell Tumours: Dysgerminoma

Dysgerminoma is the ovarian counterpart of the seminoma in the testis. It is the most common malignant germ cell tumour occurring during the second and third decades of life [20]. Dysgerminoma are usually not associated with endocrine hormone secretion. Nevertheless, in 5 % of cases

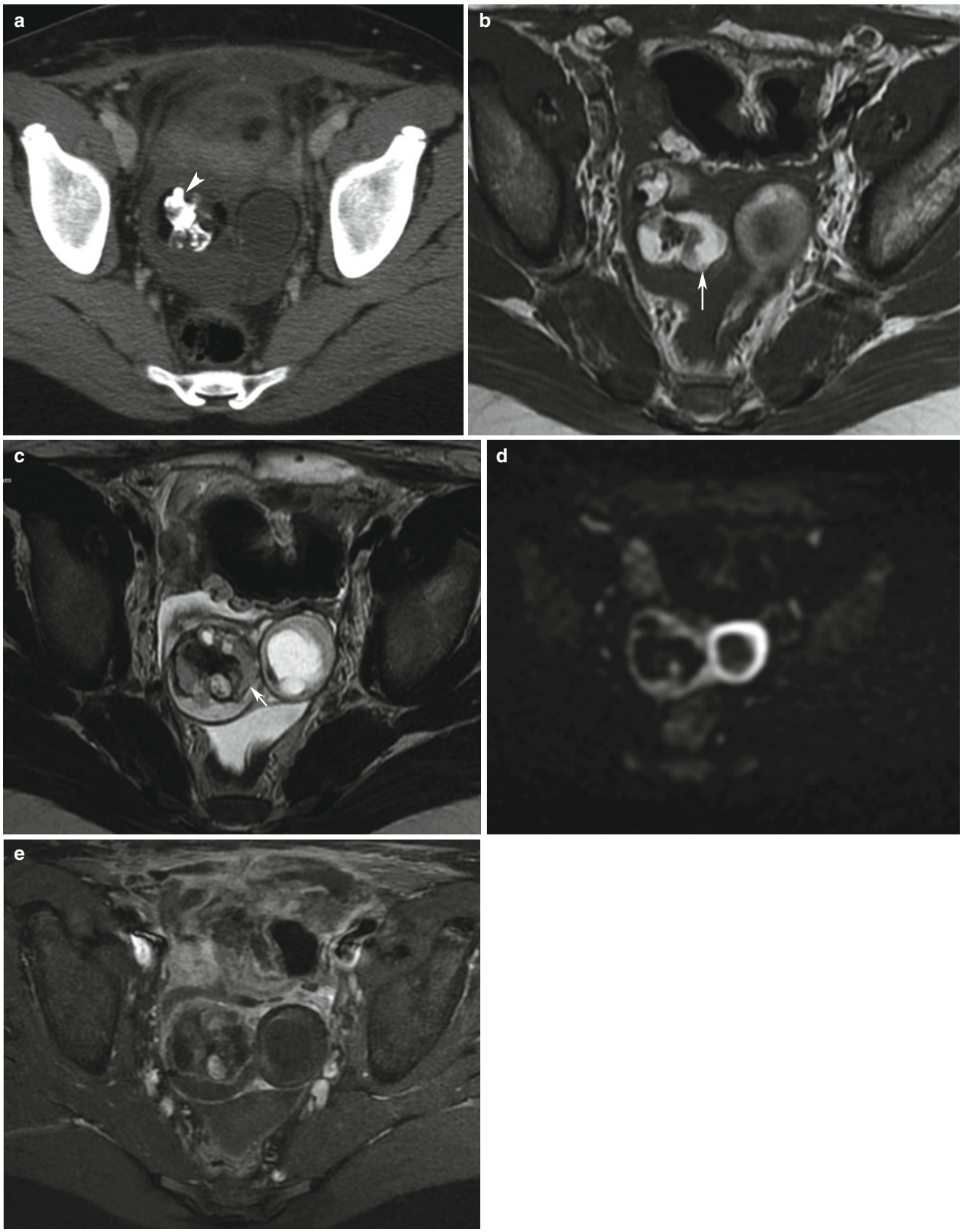

Fig. 6 Right yolk sac ovarian tumour (YST) associated with a mature teratoma in a 13-year-old girl. CT with injection (**a**), MRI (axial T1w, **b**: axial T2w, **c**; **d**, DWI b1000; **e**, axial T1 with Fat suppression and injection). A heterogeneous complex mass is seen in the right ovary. Mature teratoma might be associated to yolk sac tumour. Fat (*arrows*) and calcifications (*arrowhead*) are more likely suggestive of a teratoma. Pathology revealed a YST mixed within the teratoma. DWI depicts a hyperintense tumour with high cellularity (**d**)

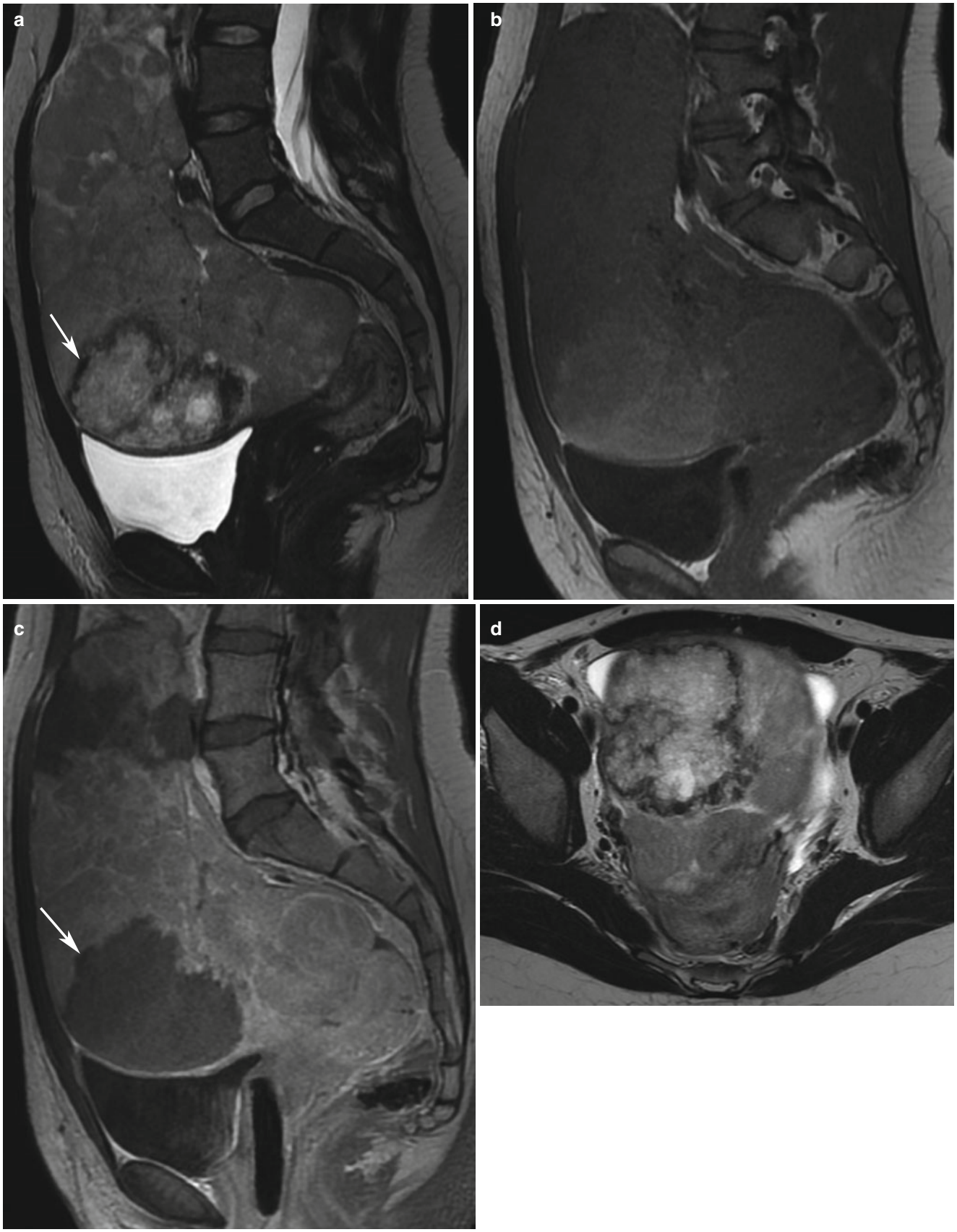

Fig. 7 Ovarian choriocarcinoma in a 23-year-old woman. MRI (sag T2w, **a**; sag T1w, **b**; sag T1w with injection, **c**; axial T2w, **d**). Uterus is posteriorly displaced by a huge solid, heterogeneous ovarian mass. Central necrosis with oedema (*arrows*) might suggest the diagnosis of choriocarcinoma, with a high level of **β**-hCG and a non-gravid uterus (**a**)

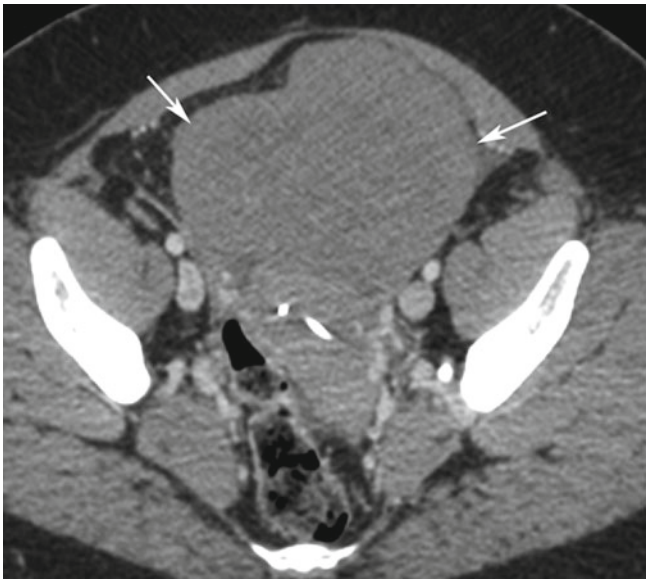

Fig. 8 Dysgerminoma in a 38-year-old woman. CT with injection. A solid homogenous lobulated mass is suggestive of a dysgerminoma (*arrows*). No fat or calcifications were depicted within the mass. Patient was treated surgically with three cycles of adjuvant chemotherapy

elevation of serum HCG levels are encountered. Even if diagnosis of a choriocarcinoma or embryonal carcinoma component will not be diagnosed by imaging, it is important to identify these components because it usually worsens the prognosis [21]. Dysgerminomas are usually large solid masses with a smooth lobulated external surface (Fig. 8). Ultrasound is the first imaging method to be done: dysgerminomas display inhomogeneous solid masses divided into lobules, with irregular hypoechoic lines, which may harbour a branching pattern. At Doppler examination, dysgerminomas have a prominent vascular pattern with branching off multiple vessels from a main feeding artery. The core of the tumour consisting in a highly vascularised tree contrasts with a highly vascularised ring at the periphery. Masses are well defined without any evidence of neighbour-organ invasion [22]. Some authors [23] showed prominent arterial flow with low arterial resistive index. Thus, every adnexal solid mass in a 20-year-old woman, with a lobule-like pattern, and signs of malignancy should raise the possibility of a dysgerminoma. The most common findings include multilobulated solid masses with fibrovascular septa [15] (Fig. 9). Because of fibrous contents, the septa appear as hypointense lines at MRI on T2-weighted sequences (Fig. 9a, b) [20]. On T1-weighted images, the lobules have the same signal intensity as the fibrovascular septa, so they can be overlooked (Fig. 9c). As there is usually important vascular component, fibrovascular septa exhibit intense enhancement after gadolinium-chelate injection and on contrast-enhanced CT. Some tumours also can show high-signal intensity areas corresponding to necrosis and haemorrhage [15]. Speckled calcifications are unusual and different from teratoma-related coarse calcifications and can be seen on CT. Their presence suggests a dysgerminoma rising from a pre-existing gonadoblastoma [19].

Malignant Stromal Tumours of the Ovary

Granulosa Cell Tumours

Granulosa cell tumour of the ovary is the most common malignant sex cord-stromal tumour as well as the most common oestrogen-producing ovarian tumour [15]. Thus, granulosa cell tumours represent only 2–3 % of malignant ovarian tumours. They grow slowly with common late recurrences 20–30 years after the initial diagnosis. Two histological subtypes are defined: juvenile subtype and adult subtype which is more common (95 %) and occurs in postmenopausal women.

Imaging findings in adult ovarian granulosa cell tumours are variable and range from solid masses to tumours with haemorrhagic or fibrous changes to multilocular cystic lesions or completely cystic lesions [15]. Thus, granulosa cell tumours are most commonly seen as complex cystic masses and are usually unilateral at the time of diagnosis [24] (Fig. 10). Solid granulosa cell tumours are uncommon. In case of solid appearance, granulosa cell tumours may be widely heterogeneous due to coexistence of haemorrhage, intratumoural bleeding or infarcts [25]. They usually don't have papillary projections and are more often located to the ovary without peritoneal seeding [15]. Estrogenic effects on the uterus may create a uterine enlargement or endometrial thickening.

Sertoli-Leydig Tumours

Sertoli stromal tumours account for less than 1 % of ovarian tumours, predominant in women under 30 years [24]. Sertoli-Leydig cell tumours are usually benign but may metastasise or recur after excision (in 20 % of cases) [24]. Sertoli-Leydig tumours are known as the most common androgen-producing tumour; two-thirds of Sertoli-Leydig cell tumours are non-functional with non-specific clinical findings [26]. Tumour size varies from 5 to 15 cm. Imaging findings show unilateral solid masses, sometimes containing cysts. Signal intensity on T2-weighted images depends on their fibrous content, but most tumours demonstrate predominantly low signal intensity with scattered areas of high signal intensity [24]. The low signal intensity in the solid components represents abundant stroma in the tumour.

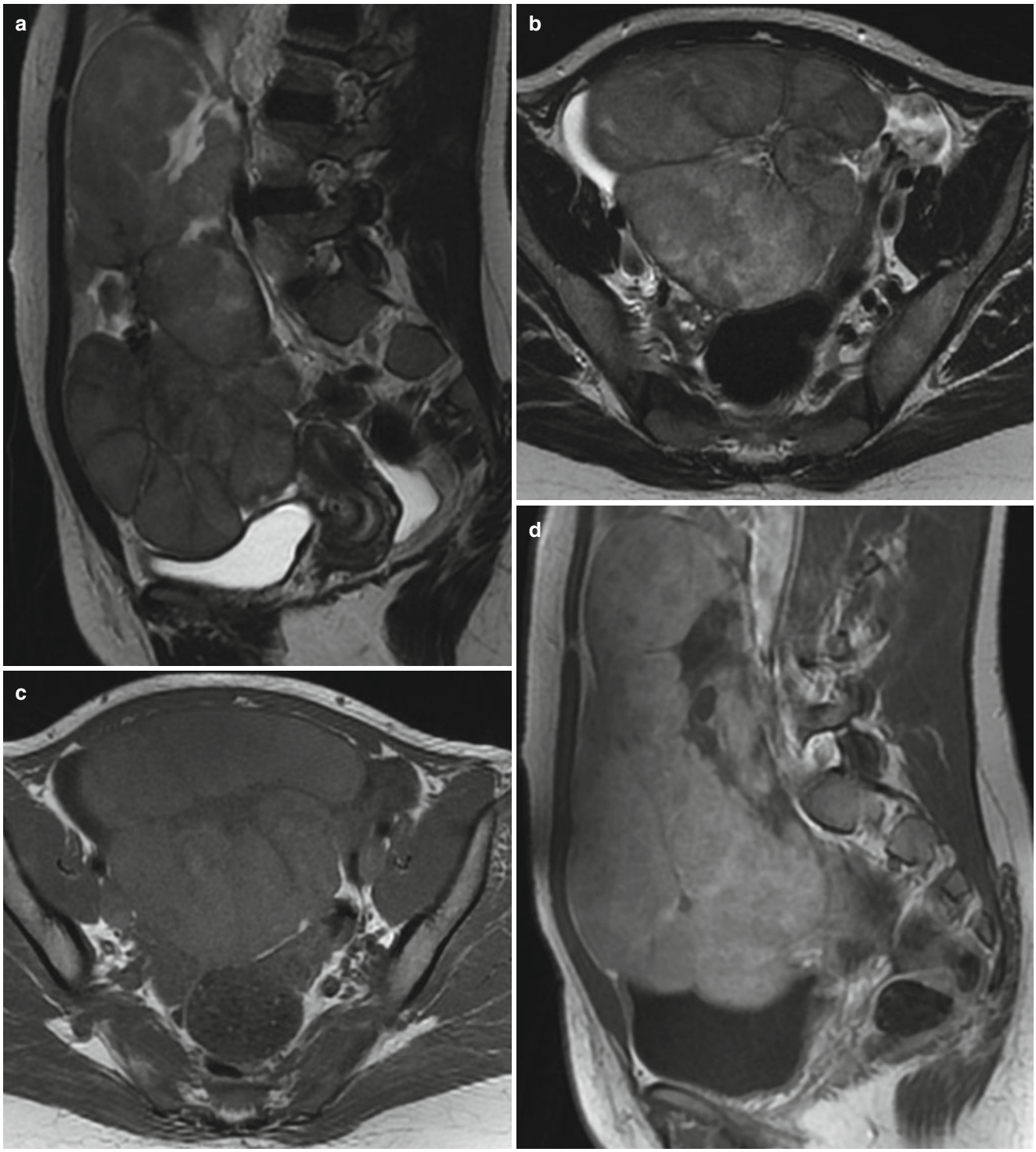

Fig. 9 Dysgerminoma in a 22-year-old woman. MRI (**a**, sag T2w; **b**, axial T2w; axial T1w, **c**; sagittal T1w+injection, **d**). An 18 cm solid lobulated mass is located in the pelvis. Extrauterine origin is clearly seen on figure (a) with an acute margin with the uterus. Fibrous septa seen on T2w images (**a**, **b**) delineate solid lobules, which is suggestive of a dysgerminoma

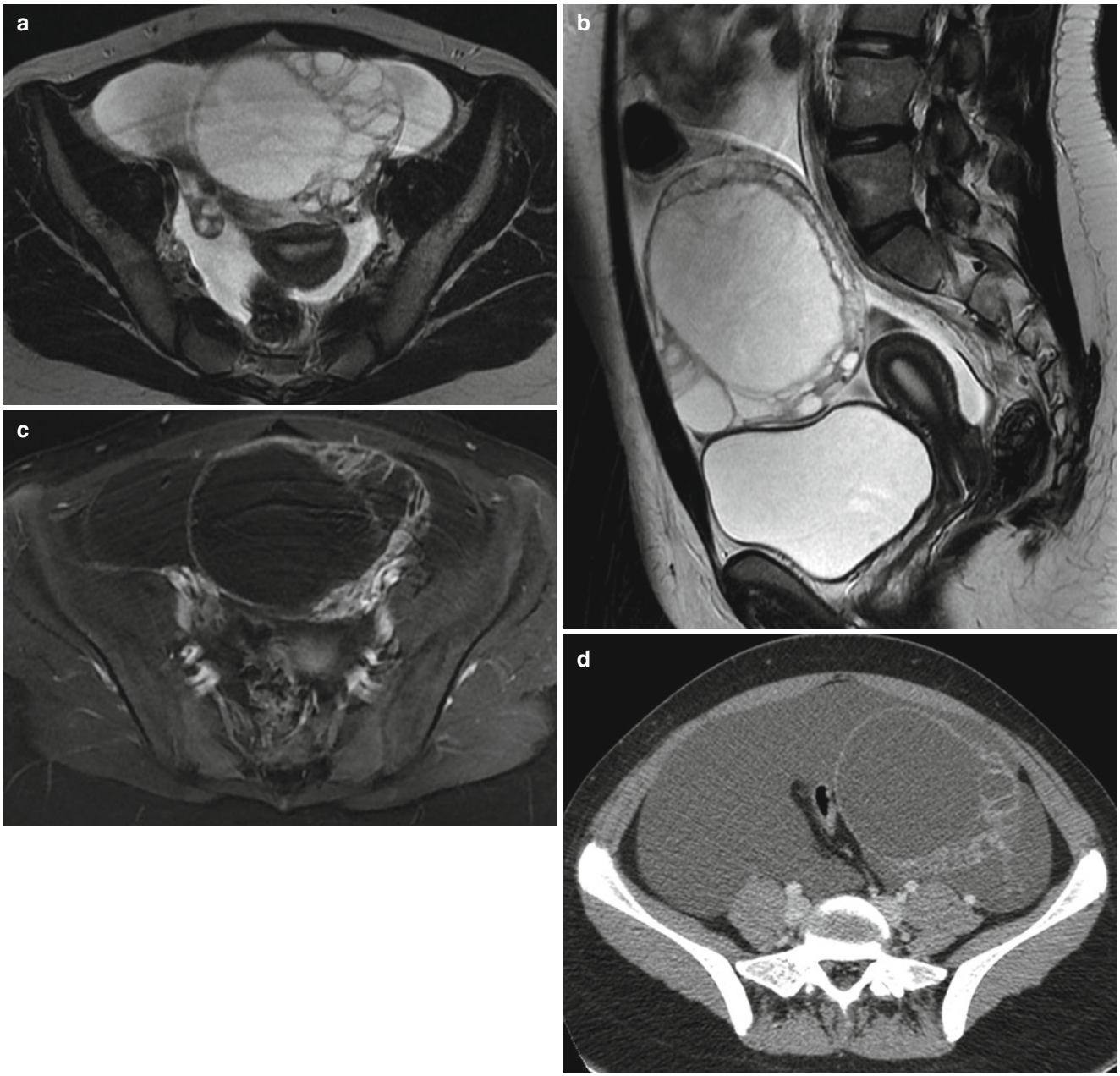

Fig. 10 Left juvenile granulosa cell tumour in a 15-year-old girl. MRI (**a**, axial T2w; **b**, sag T2w; **c**, axial T1+FS and injection; **d**, CT with injection). Juvenile granulosa cell tumours are most often cystic with multiple loculations (**a**). No solid component has been detected. Right ovary was normal. Ascites was present in this patient

Poorly differentiated Sertoli-Leydig cell tumours which are most commonly malignant tend to contain areas of haemorrhage and necrosis easily seen on MR images as hyperintense (Fig. 11) and haemorrhagic areas [26]. Thin-walled cysts are exceptional.

Fibrosarcoma

Ovarian fibrosarcoma is a very rare malignant stromal tumour developing in the ovary. It is often very difficult to differentiate clinically and histologically from cellular

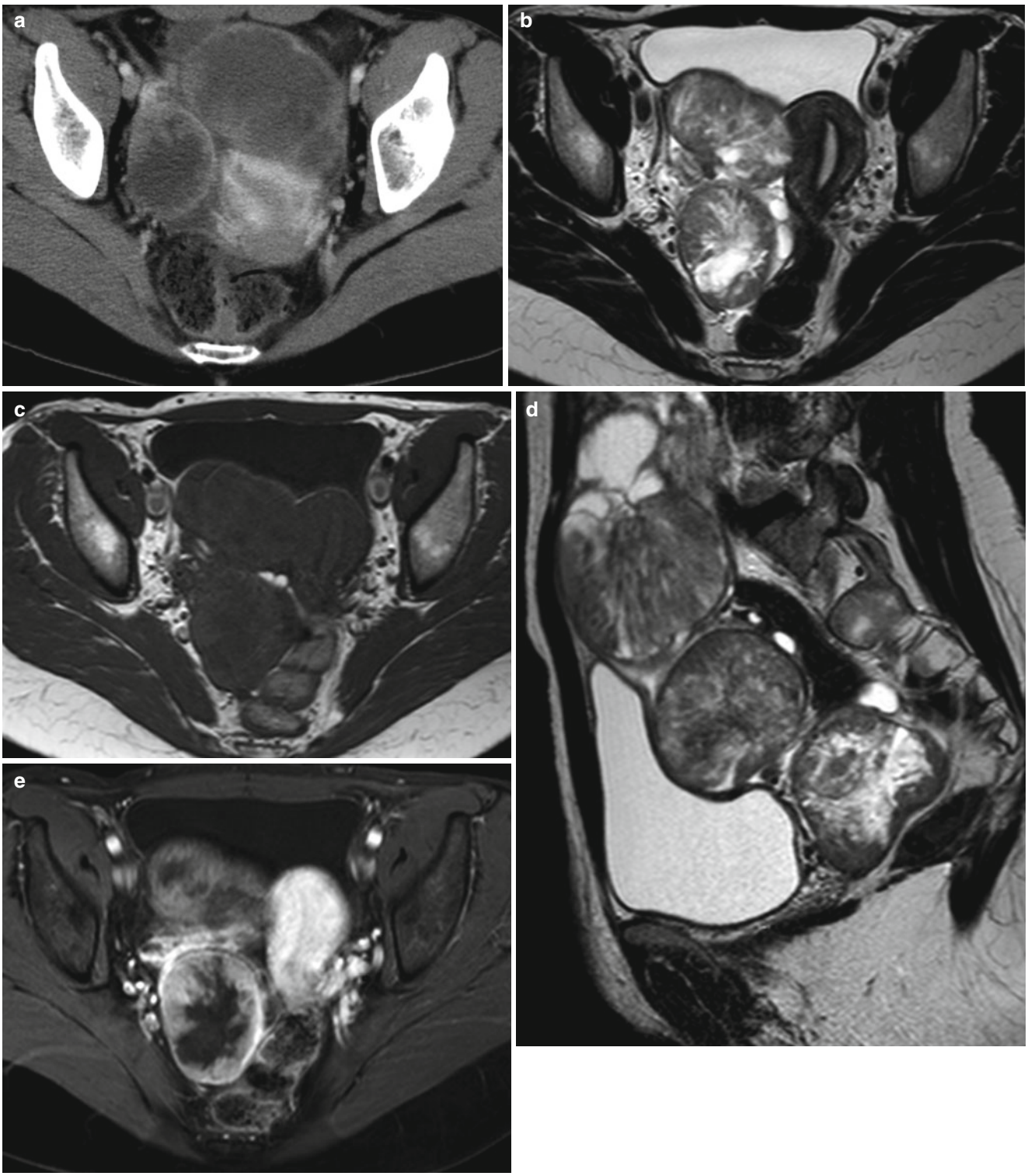

Fig. 11 Malignant Sertoli-Leydig ovarian tumour in a 36-year-old woman. CT + injection (**a**); MRI (axial T2w, **b**; axial T1w, **c**; sag T2w, **d**; axial T1w + FS, **e**). Lobulated right ovarian mass is solid, heterogeneous and hyperintense on T2w without central uptake (**a**, with necrotic content (**d**, **e**). In this case, pathology revealed a malignant Sertoli-Leydig ovarian mass; this tumour was non-secreting

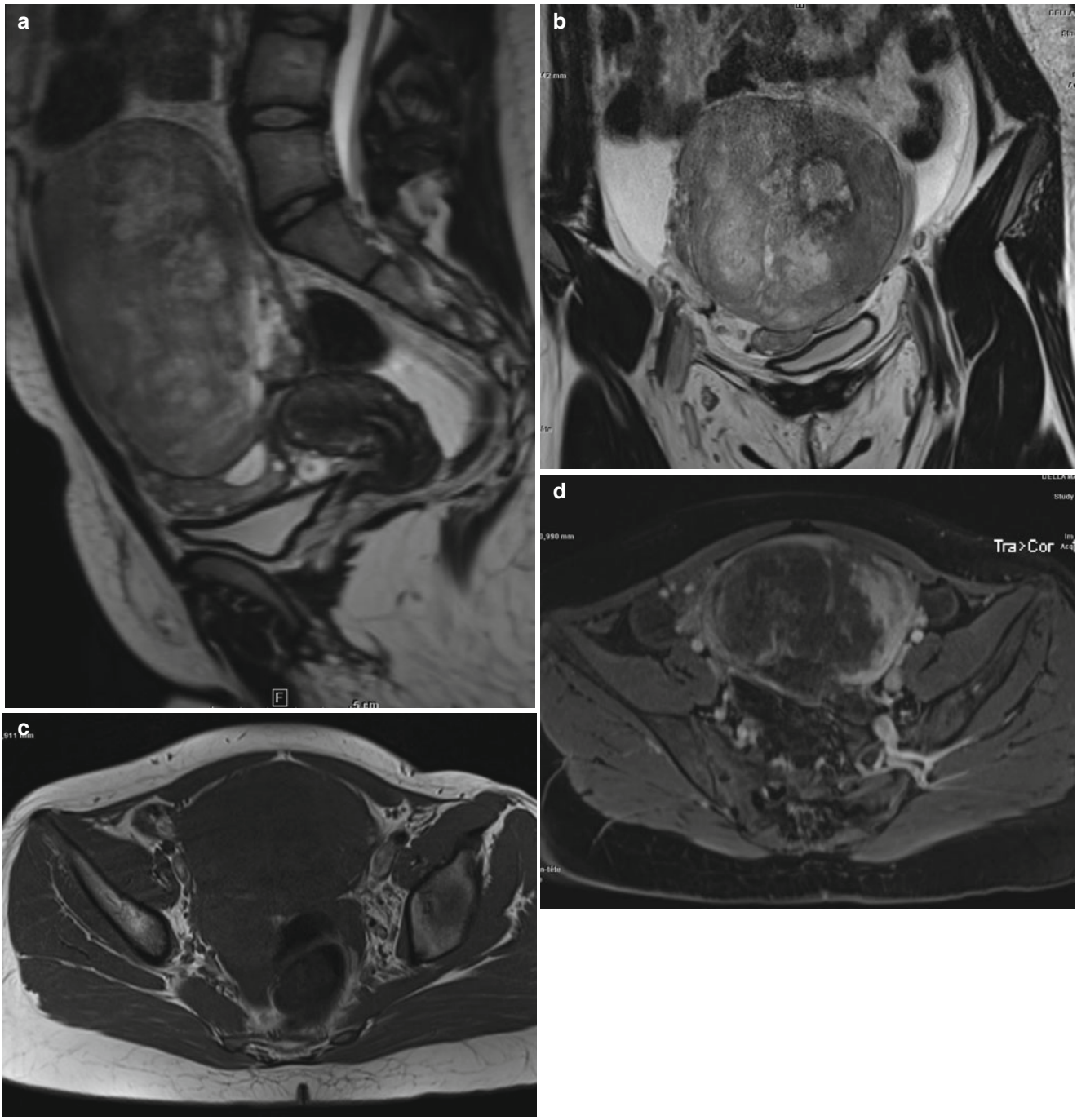

Fig. 12 Ovarian fibrosarcoma in a 15-year-old girl. MRI (**a**, sagittal T2w; coronal T2w, **b**; **c**, axial T1w; **d**, axial T1w+FS and injection). A large heterogeneous solid ovarian mass with hyperintense areas and heterogeneous peripheral enhancement is developed in left ovary. Right ovary is normal. Pathology revealed a fibrosarcoma. No specific feature is seen on these images; nevertheless heterogeneous enhancement with intense vascularisation in a solid mass is suggestive of malignancy

ovarian fibroma [27]. Mitotic activity is the most important findings to differentiate a fibrosarcoma from a cellular ovarian fibroma in comparison with nuclear grading and cellular pleomorphism [27]. Prat and Scully suggested that tumours containing 1–3 mitosis per 10 high-power fields should be considered as cellular fibroma, as tumours containing more than 4 mitotic figures per 10 high-power fields should be diagnosed as fibrosarcoma [28]. Imaging features are rarely described in the literature; some large solid ovarian masses with irregular internal calcifications, haemorrhage and necrosis have been described [27] (Fig. 12). Ascites and lymph node enlargement must also be systematically verified.

Table 1 Summary of main imaging features of malignant germ cell and stromal ovarian tumours

		Malignant teratoma				
Germ cell tumour	Dysgerminoma	Immature teratoma	Malignant transformation of mature teratomas	Yolk sac tumour	Choriocarcinoma	Embryonal Carcinoma
Frequency (%)						
All ovarian tumours	2			<1	Rare	Rare
Malignant germ cell tumours	50	20		20	Rare	<5
Histology			*Squamous cell carcinoma* (80–85 %) Adenocarcinoma Carcinoid tumours			
Biology	LDH		SCC/CA-125	AFP	HCG	
Radiology	Solid mass	Foci of fat	"Mature teratoma" like	Stromal oedema (high T2 signal)		
	Smooth lobulated external surface	Solid part	Transmural growth	Peripheral cystic cavities		
		Irregular margins		Metastatic dissemination		
		Obtuse angle with the cyst wall				
		>5 cm				
Vascularisation	Fibrovascular septa	Yes	Yes	Yes, solid part-striking enhancement Signal voids/ Bright dot sign (dilated vessels)		
Calcifications	Speckled (rising from gonadoblastoma)	Coarse, ill-defined	"Mature teratoma" like	Yes, possible		
Haemorrhage	Haemorrhagic and necrotic component	Yes		Yes, central haemorrhagic and necrotic component	Haemorrhagic and necrotic component	

The overall prognosis is poor. Metastases are common and recurrences usually occur within 2 years.

Conclusion

Even if malignant germ cell and stroma ovarian tumours are rare, some suggestive imaging features might be detected on CT or MRI. Most commonly malignant features are non-specific and include haemorrhage, calcifications or necrosis. A summary of main imaging features is detailed in Table 1.

Biography Dr Corinne Balleyguier radiologist at Institut Gustave Roussy, Villejuif, France. IGR is one of the biggest cancer center in Europe. Specialized in Women Imaging, Breast and gynecologic Imaging. Section editor on Woman Imaging for European Journal of Radiology since 2010. Chairwoman of Uro-Gynecological Imaging of ECR 2010. Involved in breast Imaging committee for ECR 2012–2013. Member of ESUR gynecological subcommittee since 2008. Member of scientific committee EUSOBI, since 2012.

References

1. Outwater EK, Siegelman ES, Hunt JL. Ovarian teratomas: tumor types and imaging characteristics. Radiographics. 2001;21(2): 475–90.
2. Choudhary S, Fasih N, Mc Innes M, Marginean C. Imaging of ovarian teratomas: appearances and complications. J Med Imaging Radiat Oncol. 2009;53(5):480–8.
3. Saba L, Guerriero S, Sulcis R, Virgilio B, Melis G, Mallarini G. Mature and immature ovarian teratomas: CT, US and MR imaging characteristics. Eur J Radiol. 2009;72(3):454–63.
4. Yamaoka T, Togashi K, Koyama T, Fujiwara T, Higuchi T, Iwasa Y, et al. Immature teratoma of the ovary: correlation of MR imaging and pathologic findings. Eur Radiol. 2003;13(2):313–9.
5. Bazot M, Cortez A, Sananes S, Boudghene F, Uzan S, Bigot JM. Imaging of dermoid cysts with foci of immature tissue. J Comput Assist Tomogr. 1999;23(5):703–6.
6. Hackethal A, Brueggmann D, Bohlmann MK, Franke FE, Tinneberg HR, Munstedt K. Squamous-cell carcinoma in mature cystic teratoma of the ovary: systematic review and analysis of published data. Lancet Oncol. 2008;9(12):1173–80.
7. Buy JN, Ghossain MA, Moss AA, Bazot M, Doucet M, Hugol D, et al. Cystic teratoma of the ovary: CT detection. Radiology. 1989;171(3):697–701.
8. Kido A, Togashi K, Konishi I, Kataoka ML, Koyama T, Ueda H, et al. Dermoid cysts of the ovary with malignant transformation: MR appearance. AJR Am J Roentgenol. 1999;172(2):445–9.
9. Nimkin K, Gupta P, McCauley R, Gilchrist BF, Lessin MS. The growing teratoma syndrome. Pediatr Radiol. 2004;34(3):259–62.
10. Itani Y, Kawa M, Toyoda S, Yamagami K, Hiraoka K. Growing teratoma syndrome after chemotherapy for a mixed germ cell tumor of the ovary. J Obstet Gynaecol Res. 2002;28(3):166–71.
11. Yamaoka T, Togashi K, Koyama T, Ueda H, Nakai A, Fujii S, et al. Yolk sac tumor of the ovary: radiologic-pathologic correlation in four cases. J Comput Assist Tomogr. 2000;24(4):605–9.
12. Choi HJ, Moon MH, Kim SH, Cho JY, Jung DC, Hong SR. Yolk sac tumor of the ovary: CT findings. Abdom Imaging. 2008;33(6): 736–9.
13. Levitin A, Haller KD, Cohen HL, Zinn DL, O'Connor MT. Endodermal sinus tumor of the ovary: imaging evaluation. AJR Am J Roentgenol. 1996;167(3):791–3.
14. Matsubayashi R, Matsuo Y, Doi J, Kudo S, Matsuguchi K, Sugimori H. Sclerosing stromal tumor of the ovary: radiologic findings. Eur Radiol. 1999;9(7):1335–8.
15. Jung SE, Lee JM, Rha SE, Byun JY, Jung JI, Hahn ST. CT and MR imaging of ovarian tumours with emphasis on differential diagnosis. Radiographics. 2002;22(6):1305–25.
16. Moniaga NC, Randall LM. Malignant mixed ovarian germ cell tumor with embryonal component. J Pediatr Adolesc Gynecol. 2011;24(1):e1–3.
17. Lalwani N, Shanbhogue AK, Bhargava P, Vikram R, Prasad SR. Rare, miscellaneous primary ovarian neoplasms: spectrum of cross-sectional imaging. Curr Probl Diagn Radiol. 2012;41(2): 73–80.
18. Bazot M, Cortez A, Sananes S, Buy JN. Imaging of pure primary ovarian choriocarcinoma. AJR Am J Roentgenol. 2004;182(6): 1603–4.
19. Brammer 3rd HM, Buck JL, Hayes WS, Sheth S, Tavassoli FA. From the archives of the AFIP. Malignant germ cell tumours of the ovary: radiologic-pathologic correlation. Radiographics. 1990; 10(4):715–24.
20. Tanaka YO, Kurosaki Y, Nishida M, Michishita N, Kuramoto K, Itai Y, et al. Ovarian dysgerminoma: MR and CT appearance. J Comput Assist Tomogr. 1994;18(3):443–8.
21. Lazebnik N, Balog A, Bennett S, Redline R, Liu J. Ovarian dysgerminoma: a challenging clinical and sonographic diagnosis. J Ultrasound Med. 2009;28(10):1409–15.
22. Guerriero S, Testa AC, Timmerman D, Van Holsbeke C, Ajossa S, Fischerova D, et al. Imaging of gynecological disease (6): clinical and ultrasound characteristics of ovarian dysgerminoma. Ultrasound Obstet Gynecol. 2011;37(5):596–602.
23. Kim SH, Kang SB. Ovarian dysgerminoma: color Doppler ultrasonographic findings and comparison with CT and MR imaging findings. J Ultrasound Med. 1995;14(11):843–8.

24. Shanbhogue AK, Shanbhogue DK, Prasad SR, Surabhi VR, Fasih N, Menias CO. Clinical syndromes associated with ovarian neoplasms: a comprehensive review. Radiographics. 2010;30(4):903–19.
25. Jung SE, Rha SE, Lee JM, Park SY, Oh SN, Cho KS, et al. CT and MRI findings of sex cord-stromal tumor of the ovary. AJR Am J Roentgenol. 2005;185(1):207–15.
26. Azuma A, Koyama T, Mikami Y, Tamai K, Fujimoto K, Morisawa N, et al. A case of Sertoli-Leydig cell tumor of the ovary with a multilocular cystic appearance on CT and MR imaging. Pediatr Radiol. 2008;38(8):898–901.
27. Choi WJ, Ha MT, Shin JK, Lee JH. Primary ovarian fibrosarcoma with long-term survival: a report of two cases. J Obstet Gynaecol Res. 2006;32(5):524–8.
28. Prat J, Scully RE. Cellular fibromas and fibrosarcomas of the ovary: a comparative clinicopathologic analysis of seventeen cases. Cancer. 1981;47(11):2663–70.

Metastatic Ovarian Tumors (Clinical Setting and US)

Daniela Fischerova

Abstract

Ovarian neoplasms of metastatic origin account for up to 20 % of all cases of ovarian malignant tumors and present a special challenge to accurate diagnosis with regard to their nature and origin. This chapter outlines the basic guidelines for a multifaceted approach to their diagnosis and summarizes extensive ultrasound observation into general principles that are helpful in correctly assessing the metastatic nature of these tumors as well as in finding the possible primary site. Using these combined methods, the diagnostic accuracy could reach 90 %.

Keywords

Metastatic neoplasm • Krukenberg tumor • Imaging • Ultrasound

Introduction

Ovarian tumors of metastatic origin account for 5–20 % [1] of all ovarian neoplasms. As a group, their special importance lies in the adverse consequences their misdiagnosis may have for the patient. The age distribution of patients with ovarian metastases correlates to a great extent with that of those with corresponding primary tumors. However, the higher frequency of ovarian metastases of the most common types (intestinal, gastric, breast) in young women may suggest that their richly vascularized ovaries are more receptive to hematogenous metastases than those of older patients. In addition, ovarian surface defects caused by ovulation may provide a point of entry for cancer cells present in the peritoneal cavity.

D. Fischerova, MD, PhD
Division of Gynecological Oncology Centre,
Department of Obstetrics and Gynecology,
First Faculty of Medicine and General University Hospital,
Charles University in Prague,
Apolinarska 18, 120 00 Prague, Czech Republic
e-mail: daniela.fischerova@seznam.cz

Metastatic tumors spreading to the ovary may be divided according to the type of spread and origin of the primary tumor. Their spread may occur by direct local extension (per continuitatem) or from distant extragenital sites (true metastatic tumors). Direct spread is an important pathway for carcinomas of the fallopian tube and uterus, mesotheliomas, bladder and colon carcinomas, and retroperitoneal sarcomas (Fig. 1).

Spread from distant sites occurs mainly via blood and lymph vessels and/or through transcoelomic dissemination with surface implantation (Fig. 2). The fallopian tube presents yet another route for possible metastatic spread from a carcinoma of the uterine corpus or cervix or the fallopian tube itself onto the ovarian surface (Fig. 2). Three main categories are suggested for the classification of site-specific tumors: (1) spread from extragenital sites, (2) spread from other sites in the genital tract, and (3) involvement by peritoneal tumors.

A metastasis to the ovary must be strongly considered if the distribution of disease or tumor sonomorphology is atypical for primary ovarian cancer. In such cases, a minimally invasive biopsy should be performed prior to primary cytoreductive surgery for ovarian malignancy. The optimal technique to achieve an adequate histological sample in one

L. Saba et al. (eds.), *Ovarian Neoplasm Imaging*,
DOI 10.1007/978-1-4614-8633-6_22,

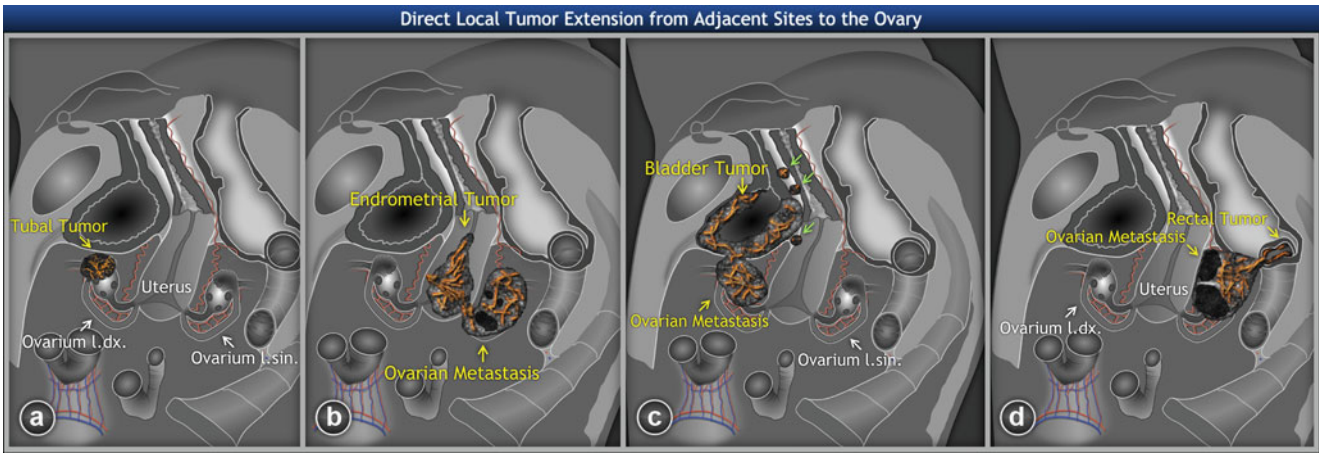

Fig. 1 Direct local tumor extension from adjacent sites (the fallopian tube, uterus, urinary bladder, colon) to the ovaries. *Green arrows* indicate infiltrated visceral lymph nodes surrounding the primary tumor

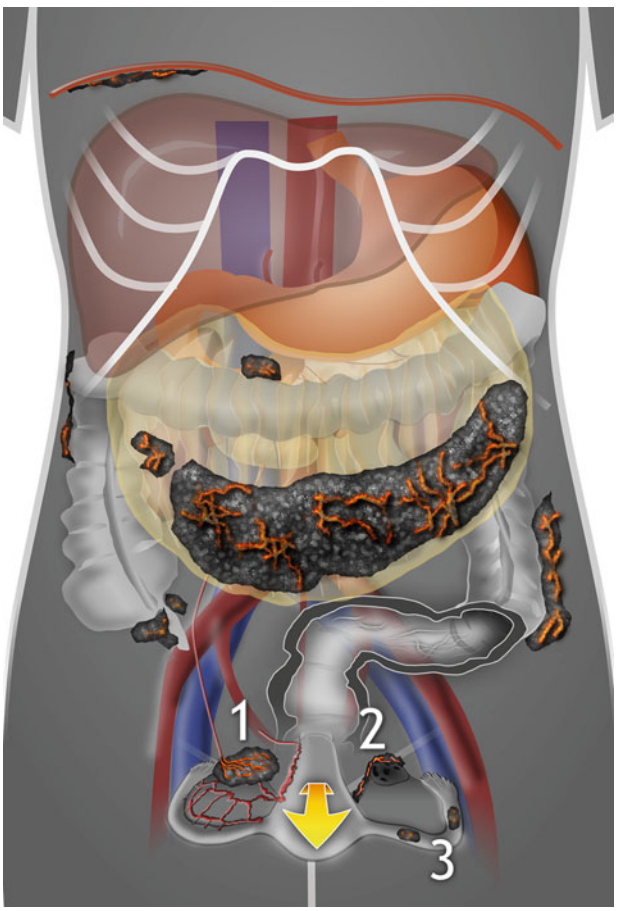

Fig. 2 Routes of tumor spread from distant extragenital sites. *1* Hematogenous and lymphatic spread, *2* generalized peritoneal spread of extraovarian primary tumor with ovarian surface implantation (visceral carcinomatosis); in this type of spread, foci of metastatic carcinoma located on the ovarian surface or superficially within the ovarian cortex are encountered, *3* spread of genital tract carcinomas (endocervical, endometrial, or tubal tumors) through the lumen of the fallopian tube onto the ovarian surface. Findings of highly perfused solid bilateral tumor, or tumor on the surface of the ovary without significant involvement of the underlying parenchyma, are suggestive of metastatic origin

setting is ultrasound-guided tru-cut biopsy [2, 3]. As with other bioptic techniques, this procedure should be avoided in cases of severe thrombocytopenia and other serious coagulative disorders, when the tumor is in a risky location or when the tumor capsule remains intact with no sign of spread. If all requirements can be met and the histological sample is obtained, it should be then subjected to thorough examination by an experienced pathologist using additional sections, special stains, and immunohistochemistry with the goal to pinpoint the origin of the primary tumor. Needless to say, this is of importance not only regarding the possible difference in treatment but also regarding the location of the primary tumor that in such cases is often not yet known. If the ovarian tumor is confirmed as metastatic and its histological origin ascertained, then the subsequent search for an extraovarian primary tumor could be sufficiently targeted, thus avoiding unnecessary laparotomies and allowing for timely initiation of an appropriate treatment. In some cases, the primary intra-abdominal tumor is discovered on ultrasound together with the metastatic ovarian tumor, or ovarian tumor suspect of metastatic nature is found during a patient follow-up after treatment for a non-ovarian tumor. In such situations, it is of benefit to compare the primary tumor histotype with an ovarian biopsy to exclude eventual concurrent primary ovarian neoplasm.

General Principles

Among the general principles that aid the sonographer in arriving at correct diagnosis of a metastatic tumor are (1) thorough clinical history aimed at the existence of concurrent or prior tumor in another organ, (2) awareness of the frequency with which the suspected primary tumor metastasizes and of its routes of spread, (3) targeted questioning about clinical symptoms attributable to primary origin of

neoplasia, (4) evaluation of blood tests and tumor markers if available, (5) systematic performance of transvaginal and transabdominal ultrasound, and (6) knowledge of sonomorphologic and Doppler patterns of the most common ovarian metastatic tumors, e.g., (A) the presence of ovarian bilateral lesions, (B) the findings of multiple tumor nodules (nests) within the ovary or (C) tumor on the surface of the ovary without significant involvement of the underlying parenchyma, (D) absence of a purely unilocular or multilocular ovarian tumor pattern, and (E) high color score in solid portion of ovarian masses on Doppler. However, many exceptions exist; for example, serous and undifferentiated primary ovarian carcinomas are commonly bilateral and may present with multinodular appearance involving ovarian parenchyma and/or with ovarian surface location.

Accurate diagnosis of the nature and origin of ovarian metastatic tumors is only possible if detailed transvaginal ultrasound is combined with transabdominal scan. Such a systematically performed ultrasound examination allows the detection of primary extraovarian tumor and/or concurrent disseminated disease (i.e., liver parenchymal metastases, visceral lymph nodes surrounding the primary tumor, carcinomatosis incl. omental infiltration, and ascites) [4]. The gray-scale ultrasound is combined with color or power Doppler evaluation of vessel density and their architecture. The diagnosis is usually made based on two-dimensional (2D) scan. Any additional value of three-dimensional ultrasound in diagnosing this population of tumors has yet to be ascertained. A subjective semiquantitative assessment of the amount of detectable blood flow within the tumor is made by using a color score (1, no color; 2, minimal color; 3, moderate amount of color; 4, abundant color density detected in the tumor) [5]. Using subjective color Doppler score [5], these masses are usually highly vascularized and, in a study by Guerriero et al. [6], 50–82 % of them presented with color score 4 (abundant perfusion). The dynamic 2D color or power Doppler also enables visualization of newly formed vessels entering the tumor from surrounding structures. Testa et al. observed that cases of metastases to the ovaries are characterized by a main peripheral vessel which penetrates into the central part of the ovarian mass with a tree-shaped morphology [7]. In addition, in metastatic ovarian masses presenting with multinodular appearance, we typically observe ring-shaped vessels around the nodules that may highlight their presence (Fischerova D. 2012, unpublished data).

Currently, there are no known tumor markers for specific types of cancer; however, general serum tumor markers are often elevated in disseminated disease and are being used clinically for monitoring the course of disease and relapse detection. Therefore, the evaluation of one or more tumor markers may contribute to the diagnosis of metastatic ovarian tumor and the detection of its primary source. Most serum tumor markers are tumor antigens (carcinoembryonic antigen [CEA], CA 19–9, CA 72–4, CA 15–3, CA 27.29, CA-125). Elevated CEA levels are found in a variety of cancers including colonic, pancreatobiliary, gastric, lung, breast, endocervical, and ovarian [8, 9]. They are, however, also often detected in noncancerous conditions that include cirrhosis, inflammatory bowel disease, chronic lung disease, and pancreatitis. Normal CEA level in an adult nonsmoker is <2.5 ng/mL and in a smoker <5.0 ng/mL. CA 19–9 (normal level <37 U/mL) is usually greatly elevated in advanced pancreatic carcinoma (in 71–93 % cases) and in about 65 % cases of bile duct cancer [9]. Elevated levels are also seen in 21–42 % cases of gastric cancer, 20–40 % cases of colon cancer, and in nonmalignant conditions such as chronic pancreatitis, cirrhosis, and acute cholangitis [10] as well as in cases of noncancerous bile duct obstruction. CA 72–4 is elevated in 40 % cases of gastrointestinal and 50 % cases of ovarian cancer [11]. CA 15–3 and CA 27.29 can detect advanced breast cancer and its recurrence after primary treatment [12, 13]. The normal range of CA 15–3 and CA 27.29 is <31 U/mL and <40 U/mL, respectively. In squamous cell cervical cancer, the serum concentrations of squamous cell carcinoma antigen (SCC) have been found to correlate with tumor stage, tumor size, residual tumor after treatment, recurrent or progressive disease, and patient survival [14]. Its normal level is <2.5 ng/mL. The serum CA-125 (cutoff value 35 U/mL) is elevated in nonmucinous ovarian carcinoma but also in endometrial, pancreatobiliary, lung, breast, and colon cancer and in noncancerous conditions including endometriosis, pelvic inflammatory disease, uterine myomas, and cirrhosis [9, 15]. The serum CA-125 level may be also elevated in secondary ovarian neoplasms contributing to potential confusion with primary ovarian neoplasia. Recent study by Calster et al. presented likelihood reference tables to interpret preoperative serum CA-125 results in patients with different ovarian pathologies [16]. In metastatic ovarian tumors, the median concentration of serum CA-125 in all population and in premenopausal and postmenopausal patients reached 99, 80, and 132 U/mL, respectively. Metastatic tumors were associated with CA-125 levels similar to stage I primary invasive tumors but with lower levels than higher stage primary invasive tumors (median: 229 U/mL for stage II, 401 U/mL for stage III, and 725 U/mL for stage IV) and higher stage borderline tumors (median: 165 U/mL for stage II and 327 U/mL for stage III–IV). Other useful tumor markers are chromogranin A (CgA) associated with neuroendocrine tumors and beta2-microglobulin (B2M) and lactate dehydrogenase (LDH) associated with lymphomas. A urine marker—bladder tumor antigen (BTA)—is frequently detected in cases of urothelial cancer. In addition, excessive production of estrogens, androgens, or progesterone does not exclude a metastatic tumor that may have a functioning stroma [17].

This combined diagnostic approach (knowledge of patient history and clinical symptoms, blood tests, and systematically performed ultrasound examination) enables the diagnosis of extraovarian metastatic tumors with sensitivity of 84.8 %, specificity of 92 %, positive and negative predictive value of 82.3 and 93.3 %, respectively, and accuracy of 89.9 % [2].

In many cases, when ultrasound examination is highly suggestive of extraovarian primary origin, a minimally invasive biopsy (optimally, an ultrasound-guided tru-cut biopsy) of ovary or other metastatic lesion (omentum, peritoneum, lymph nodes) is performed. If a transabdominal scan or other complementary imaging techniques reveal the potential site of primary tumor (stomach, pancreas, bile duct, colon, etc.), then endoscopy or endosonography permitting the biopsy of primary tumor is added. Once a diagnosis of metastatic disease is established, the patient is referred to a multidisciplinary team for appropriate staging and optimal oncological treatment.

Site-Specific Tumors

The establishment of specific (pathognomonic) ultrasound features that could be reliably used for differential diagnosis between primary and metastatic ovarian neoplasms presents a great challenge. Very few studies were performed with the aim to identify possible specific ultrasound characteristics of metastatic ovarian malignancies [6, 7, 18–21]. So far, none of the features initially promising in terms of assisting in diagnosis (e.g., the presence of lead vessel, necrosis, papillary projection specifically described in intestinal metastases to the ovary, mobility or elasticity of tumor, tumor heterogeneity) were prospectively validated. In addition, data revealing the tumor laterality might be compromised as in some cases the laterality of ovarian metastasis was diagnosed on ultrasound first and only suspect ovarian tumors were verified by tru-cut biopsy [21] or, in other studies, the sectioning of ovaries necessary for the detection of microscopic foci was not performed in sufficient detail. Moreover, in many studies the ultrasound-evaluated morphology of ovarian metastases was associated only with the original site of primary tumor and not with its histotype, not taking into account that many tumor histotypes with quite different gross appearance may derive from a single organ. For example, ovarian metastases from the appendix may be derived from at least three histological tumor types: (1) intestinal type or mucinous carcinoma presenting within the ovary as multilocular-solid masses, (2) signet ring cell carcinoma (Krukenberg tumor) manifesting in the ovary as a solid mass with a lead vessel, and (3) low-grade mucinous tumors resembling a primary ovarian mucinous intestinal borderline tumor. This implies that, in order to aid in the diagnostic process, the association of ultrasound morphology should be made primarily with the tumor histotype and only secondarily with the presumed site of its origin.

However, useful guidelines may still be derived from multiple observations that could be of help to an experienced sonographer in the process of diagnosing a secondary ovarian neoplasm as well as in identifying its original source. In general, ovarian metastases from signet ring cell tumors

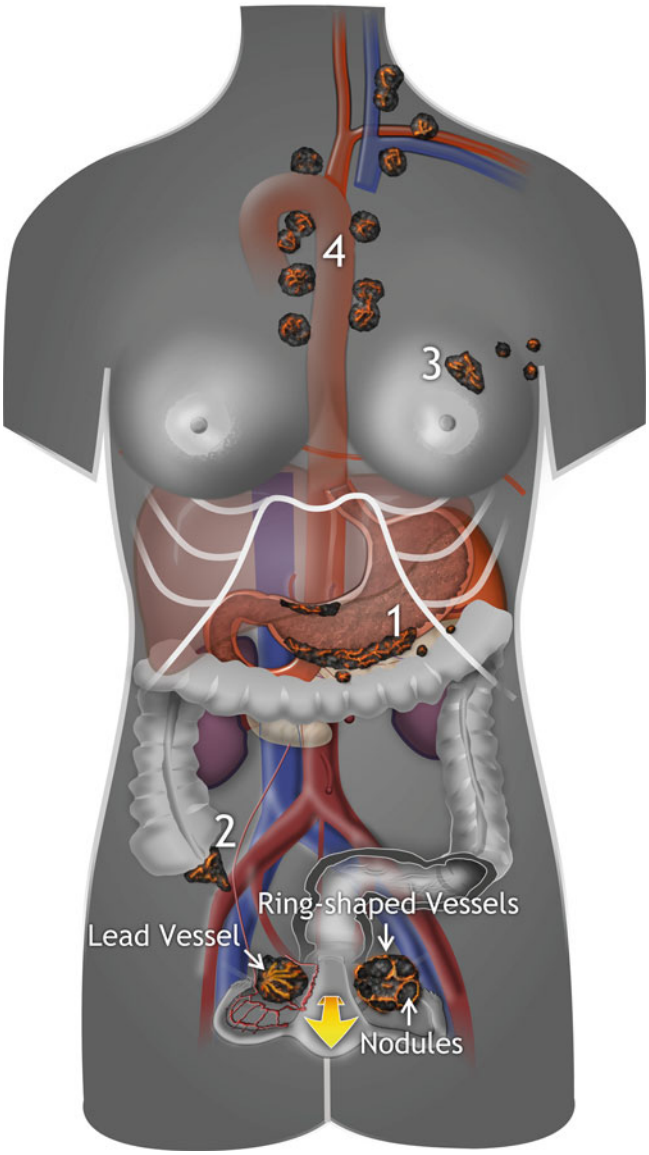

Fig. 3 Examples of primary origin of solid ovarian metastases. *1* Signet ring cell carcinoma (Krukenberg tumor) of gastric pylorus with multiple infiltrated visceral lymph nodes, *2* neuroendocrine tumor of the appendix, *3* breast carcinoma with multiple infiltrated axillary lymph nodes, *4* mediastinal lymphoma. Of note, the presence of multiple tumor nodules with ring-shaped vessel arrangement within the left ovary, and the lead vessel penetrating the right ovary with a tree-shaped architecture, is a finding typical for ovarian metastasis. These metastatic lesions are frequently accompanied by peritoneal involvement and ascites

(Krukenberg tumors) usually derive from the stomach and rarely from large intestine, appendix, and breast; neuroendocrine tumors (e.g., of small intestine, appendix, colon, stomach, pancreas, or lung), breast carcinoma, and secondary ovarian lymphoma are typically bilateral solid lesions (Fig. 3), whereas ovarian metastases derived from colorectal or pancreatobiliary adenocarcinoma show multilocular-solid morphology (Fig. 4). Metastatic tumors tend to appear

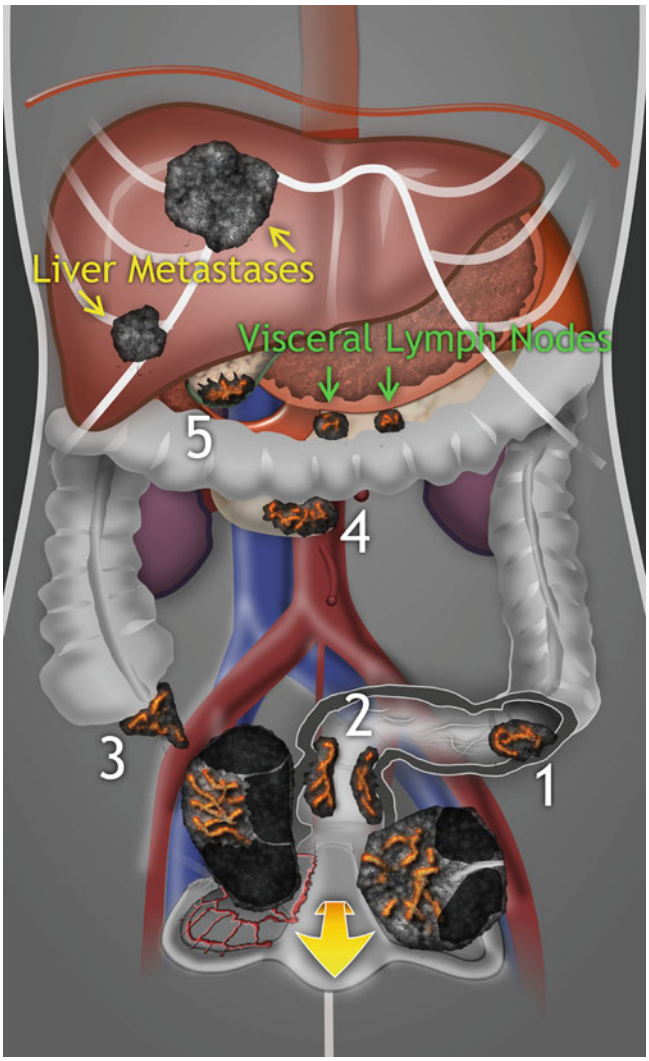

Fig. 4 Examples of origin of multilocular-solid ovarian metastases. Adenocarcinoma of sigmoid colon (*1*), rectum (*2*), appendix (*3*), pancreas (*4*), and biliary tract (*5*), often accompanied by parenchymal liver metastases and infiltrated visceral lymph nodes adjacent to the primary tumor. Of note, the ovarian metastases often have multilocular-solid appearance even when there is absence of cysts in the primary neoplasm

moderately or highly vascularized [6]. However, the sonomorphology and perfusion of ovarian metastases may change during the course of treatment.

In addition, a combination of detailed tumor sonomorphology with vessel tree arrangement visualized on Doppler may play a role in distinguishing primary and metastatic ovarian tumors of solid appearance. According to our observation, the presence of multiple hypoechogenic nodules located within the ovary (like tumor "nests") together with ring-shaped vessel arrangement detected on Doppler is often found in solid metastatic ovarian tumors commonly originating from signet ring cell carcinomas or breast cancer and other metastatic carcinomas. The multiple nodules within the ovarian tissue are due to embolic tumor spread, which is commonly accompanied by prominent intravascular tumor nests in the ovarian hilum, mesovarium, and mesosalpinx [22]. Moreover, Testa et al. described in more than 50 % of solid tumors the presence of lead vessel entering the tumor and penetrating the central part of the ovarian mass with a tree-shaped morphology [7].

Differential diagnosis between primary and metastatic ovarian tumors of multilocular-solid appearance in cases when biopsy proves mucinous histotype is often challenging. Using a simple rule suggested by Seidman at al. [23] and modified by Yemelyanova et al. [24] that classifies all bilateral mucinous carcinomas of any size and all unilateral mucinous carcinomas <13 cm as metastatic and unilateral mucinous carcinomas ≥13 cm as primary ovarian tumors, 82 % of ovarian metastases and 98 % of primary ovarian tumors can be correctly classified. Unfortunately, there are many exceptions to this algorithm, especially in cases of colorectal and endocervical carcinomas. Furthermore, the findings of implants on the surface of the ovary and/or multinodular ovarian tumors with mucinous features merit more serious consideration due to the possibility of being metastatic. Similarly, the distribution of disease may be helpful in distinction of primary and metastatic mucinous tumors involving the ovaries. For example, the presence of hepatic metastases and/or extensive peritoneal dissemination is an unusual pattern of spread for a primary ovarian mucinous cancer.

The characteristics of most common extraovarian metastatic tumors involving the ovaries are presented below.

Spread from Extragenital Sites

Carcinoma of the Stomach

Metastatic Tumor with Signet Ring Cells (Krukenberg Tumor)

Krukenberg tumor is characterized by the presence of mucin-filled signet ring cells accounting for at least 10 % of its mass. The source of metastatic Krukenberg tumor in the ovary is in a great majority of reported cases of gastric carcinoma. Carcinomas of the large intestine, appendix, and breast are the next most common primary sites; the gallbladder, biliary tract, pancreas, cervix, and urinary tract are rare sources of these tumors [25]. The average age of patients with Krukenberg tumor is about 45 years [26]. The age distribution is related to higher frequency of signet ring cell carcinomas in younger women and to the greater vascularity of the ovary in premenopausal women. A history of prior carcinoma of the stomach or another organ is present in 20–30 % of the cases, and disease-free interval is usually 6 months or less [27]. Almost all patients die within a year of the diagnosis of ovarian metastasis [28].

Diagnosis

Almost 90 % of patients with Krukenberg tumor have symptoms related to ovarian involvement. The gastrointestinal symptoms are frequently vague with weight loss, epigastric discomfort, nausea, vomiting, loss of appetite, fatigue, and early satiety. Miscellaneous symptoms are related to the spread to other sites such as lungs or bone. Tumor markers CEA and CA 19–9 are elevated in 40–50 % of patients with disseminated disease, and monitoring of these markers may be beneficial in the detection of recurrence [14].

On transvaginal scan, the Krukenberg tumor typically appears as a rounded or reniform richly vascularized solid mass (Fig. 5). Occasionally, these tumors contain cysts filled with anechogenic (watery) or hypoechogenic (mucinous) fluid separated by solid tissue (Fig. 6). Both ovaries are involved in 80 % or more of cases [29]. In differential diagnosis the Krukenberg tumor may resemble any primary solid ovarian tumor, e.g., ovarian fibroma or dysgerminoma. However, unlike the Krukenberg tumor, both these tumors are usually unilateral and of larger size. Fibromas also usually present with stripy shadows and minimal vascularity, while dysgerminomas differ from Krukenberg tumors in age distribution as they are mostly found in young women 20–30 years of age [30, 31]. Another distinguishing feature could be the finding of pelvic and abdominal peritoneal implants characteristic for Krukenberg tumor.

On transabdominal scan, the primary source of ovarian Krukenberg tumor is usually found in the pylorus. The sonographic appearance of advanced scirrhous gastric tumor is described in Figs. 5 and 6. Figure 12 (paragraph tumor of the appendix) shows the presence of pelvic and abdominal peritoneal implants of Krukenberg tumor originating in the appendix.

Metastatic Intestinal-Type Adenocarcinoma of the Stomach

These tumors resemble metastatic colon cancer rather than the typical Krukenberg tumor, and their characteristics are described in the paragraph “Intestinal carcinoma.”

In differential diagnosis, an advanced high-grade primary ovarian cancer may sometimes closely simulate metastatic tumors with signet ring cells or intestinal type adenocarcinoma of the stomach involving the ovaries, as documented in Fig. 7. Therefore, the diagnosis of metastatic ovarian tumor and its likely primary source should be always histologically verified (e.g., by tru-cut biopsy of the ovarian tumor and upper endoscopy of stomach).

Intestinal Carcinoma

Most metastatic ovarian tumors of intestinal origin come from the large intestine, with occasional exceptions of small intestine derivation [25]. It was thought that approximately 6 % of women with intestinal cancer have ovarian metastases at some point during the course of their disease [32], but further sectioning of removed ovaries into 2 mm slices increased this frequency to 10 % [33]. Metastases from large intestine to the ovary are seen relatively more frequently in women under 50 years [34]. Predominantly (in 50–75 % cases), the ovarian metastatic disease develops metachronously (following treatment for local-regional colorectal cancer) rather than synchronously and is mainly associated with advanced local tumor extent [25, 35]. In a study by Lash et al., 68 % cases of metastatic colorectal cancers were stage Dukes C [36]. The disease-free interval (time between primary tumor diagnosis and formation of metastatic lesion) is about 3 years [25].

Diagnosis

Clinical symptoms are dependent on the local and/or distant extent of disease. These symptoms include diarrhea/constipation, bloating, cramps, blood in stool, weight loss, iron-deficiency anemia, weakness and fatigue, and symptoms associated with pelvic mass. Relevant tumor markers include carcinoembryonic antigen (CEA) and CA 19–9.

Ovarian metastases from the colon are frequently bilateral (60 % of cases) [28] and may appear on ultrasound as multilocular-solid tumors with intracystic fluid of low-level echogenicity corresponding to mucin. In comparison to Krukenberg tumors or breast carcinoma, the colonic metastases involving ovaries are usually significantly larger [6], with a median of largest dimension being 11 cm (Fig. 8) [36].

In contrast to primary endometrioid and mucinous ovarian carcinoma, the typical features of metastatic colon cancer involving ovaries are the presence of necrosis in the solid portion, intracystic papillary projections with regular surface, and the presence of parenchymal metastases (Fig. 9) [21].

Because more than two-thirds of large intestine tumors are in the rectum or sigmoid colon, the occult intestinal tumors may be sometimes detected together with ovarian metastases by transvaginal scan (Fig. 10). On ultrasound, colon cancer appears as highly perfused hypoechogenic thickening of one layer or of the whole intestinal wall, with eventual narrowing of the lumen and/or with extraluminal spread (visceral lymph nodes, peritoneal carcinomatosis and ascites, liver metastases). Dilation of intestinal loops with compromised peristalsis proximal to tumor site might be observed.

Similarly to gastric tumors, differential diagnosis is difficult here as in some cases neither a gross examination nor any imaging technique could distinguish between a primary colon cancer extending into the ovary and an advanced

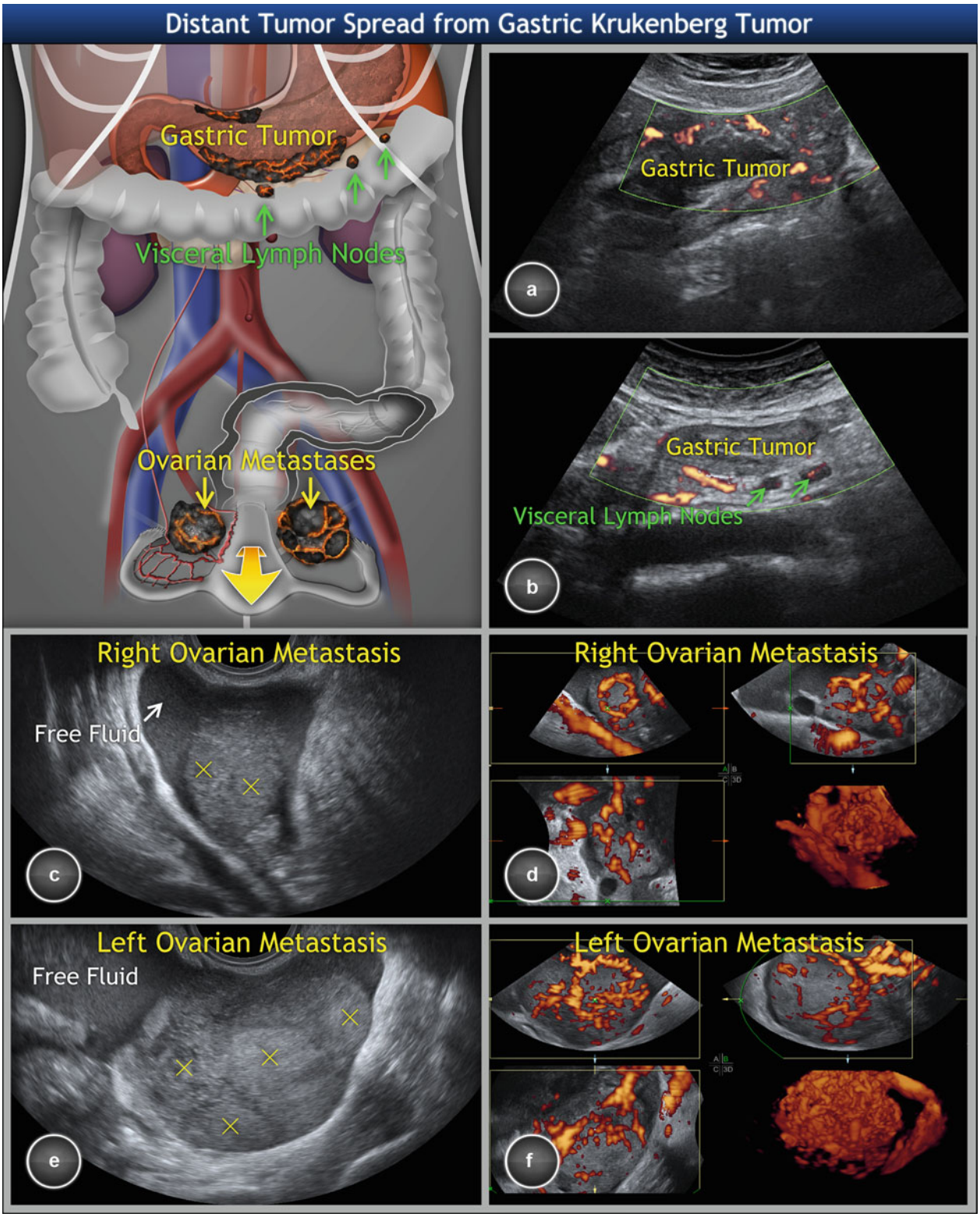

Fig. 5 Metastatic signet ring cell cancer of stomach involving ovaries (Krukenberg tumor). (**a**) Scirrhous gastric tumor of the greater and lesser curvature of stomach with a rich density of tumor vessels, hypoechogenic wall thickness of more than 5 mm, interrupted layering of the wall, and (**b**) infiltrated visceral lymph nodes (enlarged, homogeneous, well-circumscribed rounded structures) in the connective tissue surrounding the stomach. (**c**) Gray-scale and (**d**) three-dimensional power Doppler of a right ovarian metastasis enclosed in free fluid. (**e**, **f**) Similar finding in the left ovarian metastasis. Of note, the transvaginal scan of ovaries shows bilateral solid highly perfused tumors of 6 cm average diameter, with multiple nodules within the tumors (marked with *yellow crosses*) and demarcated with ring-shaped vessels suggesting metastatic nature. Three-dimensional power Doppler depicts dense, branching, and tortuous vessels with caliber changes and color splashes. Concurrent transabdominal scan revealed primary origin of tumor spread

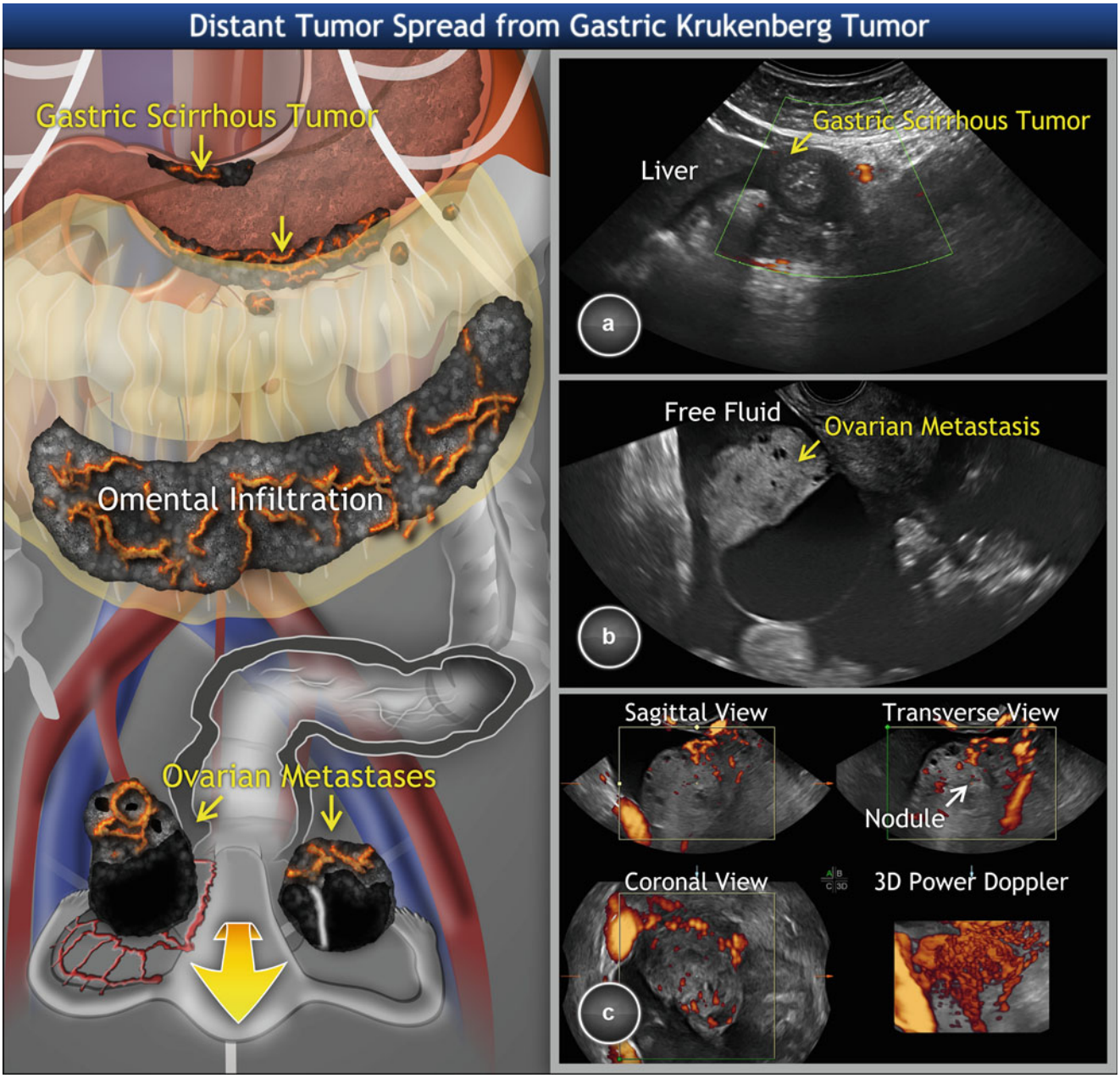

Fig. 6 Metastatic signet ring cell cancer of stomach involving ovaries (Krukenberg tumor). (**a**) Scirrhous gastric tumor of pylorus with a rich density of tumor vessels (circumscribed widening of the wall with loss of normal wall stratification, luminal narrowing). (**b**) Gray-scale and (**c**) three-dimensional power Doppler of a right ovarian unilocular-solid metastasis (size: 5 cm) enclosed in free fluid. The large thin-walled cyst contains fluid of low-level echogenicity. Doppler imaging reveals ring-shaped vessel arrangement around the tumor nodule in solid portion of mass (marked with *arrow*). The left ovarian tumor visible on schema has two thin-walled cysts separated by relatively small amount of solid tissue. The concurrent transabdominal scan revealed primary origin of tumor spread

ovarian cancer infiltrating the colon (Fig. 11). However, this problem may also arise on microscopic examination. The tumors presenting the highest challenge to accurate diagnosis are primary ovarian endometrioid and mucinous adenocarcinomas. Many intestinal metastases to the ovary are misinterpreted as primary ovarian adenocarcinomas on pathologic examination, even when there is known intestinal cancer [37]. In addition to microscopic evaluation, immunohistochemistry can be helpful in distinguishing a typical metastatic carcinoma of large intestine (CK7-/CK20+, CEA+, and CA-125-, estrogen receptor negativity) from a primary endometrioid adenocarcinoma (with opposite immunoprofile), but not from a primary ovarian mucinous tumor.

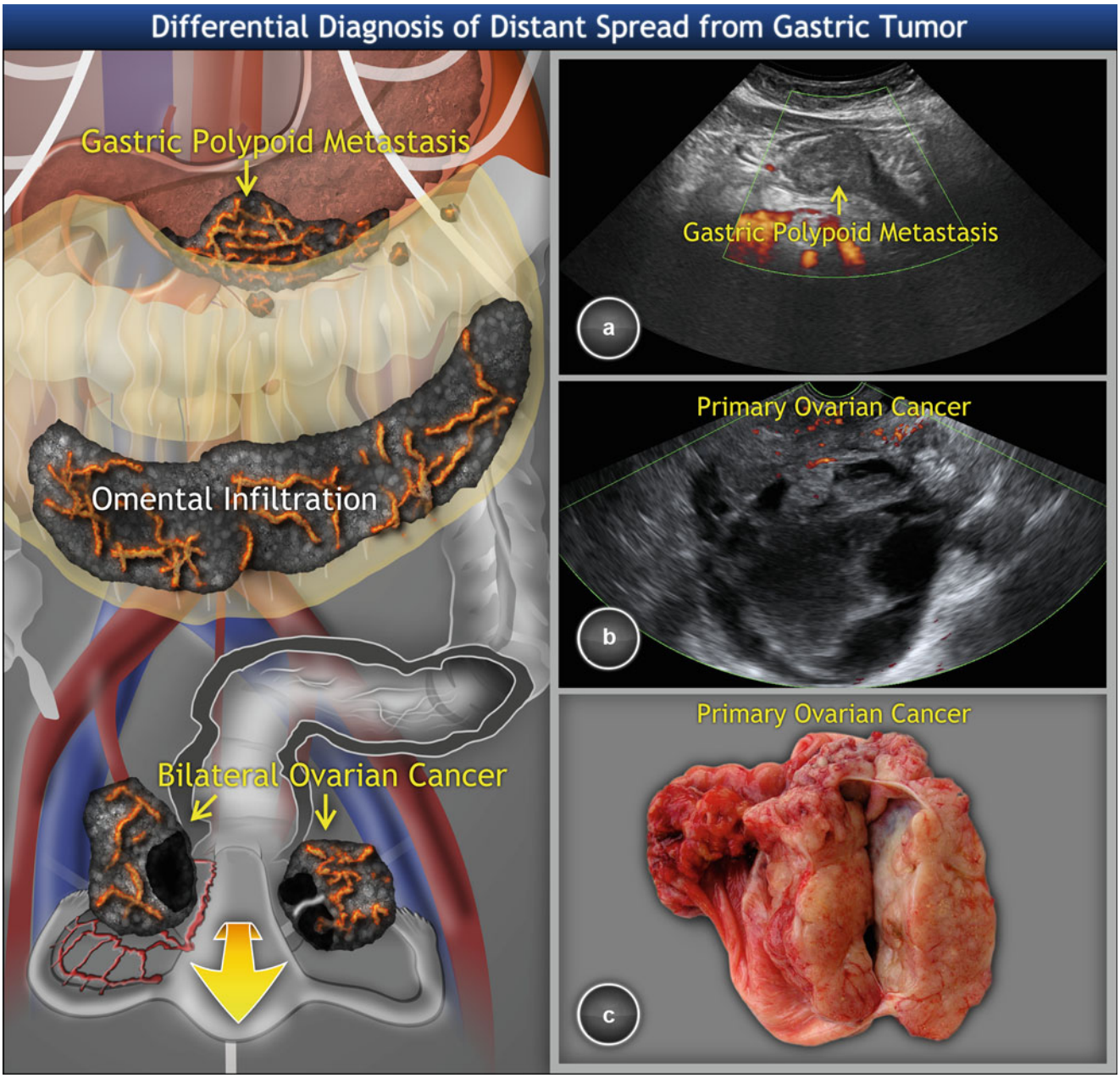

Fig. 7 Metastatic high-grade ovarian cancer involving stomach and disseminating on peritoneal surfaces. (**a**) Hypoechogenic polypoid tumor in gastric antrum on transabdominal scan. (**b**) Multilocular-solid ovarian cancer with intracystic fluid of low-level echogenicity and perfused solid component on transvaginal scan. (**c**) Sectioned tumor showing a mostly smooth-walled cyst surrounded by solid tumor tissue

Tumors of the Appendix

Ovarian involvement is most common in cases of low-grade mucinous tumors of the appendix that often have the gross features of a so-called mucocele. Ovarian spread may be also seen in cases of appendiceal invasive adenocarcinomas of the usual intestinal type and typical mucinous type, carcinomas with neuroendocrine differentiation, signet ring cell carcinomas, and others. The ultrasound features of appendiceal intestinal type and mucinous carcinomas and of signet ring cell carcinomas resemble those of similar types arising from the colon and stomach and were already discussed above (Fig. 12).

Low-Grade Appendiceal Mucinous Neoplasms

In many cases, ovarian involvement is the first evidence of an appendiceal neoplasm. The association with pseudomyxoma peritonei generally facilitates the recognition of these ovarian tumors as metastatic. For many years, pseudomyxoma

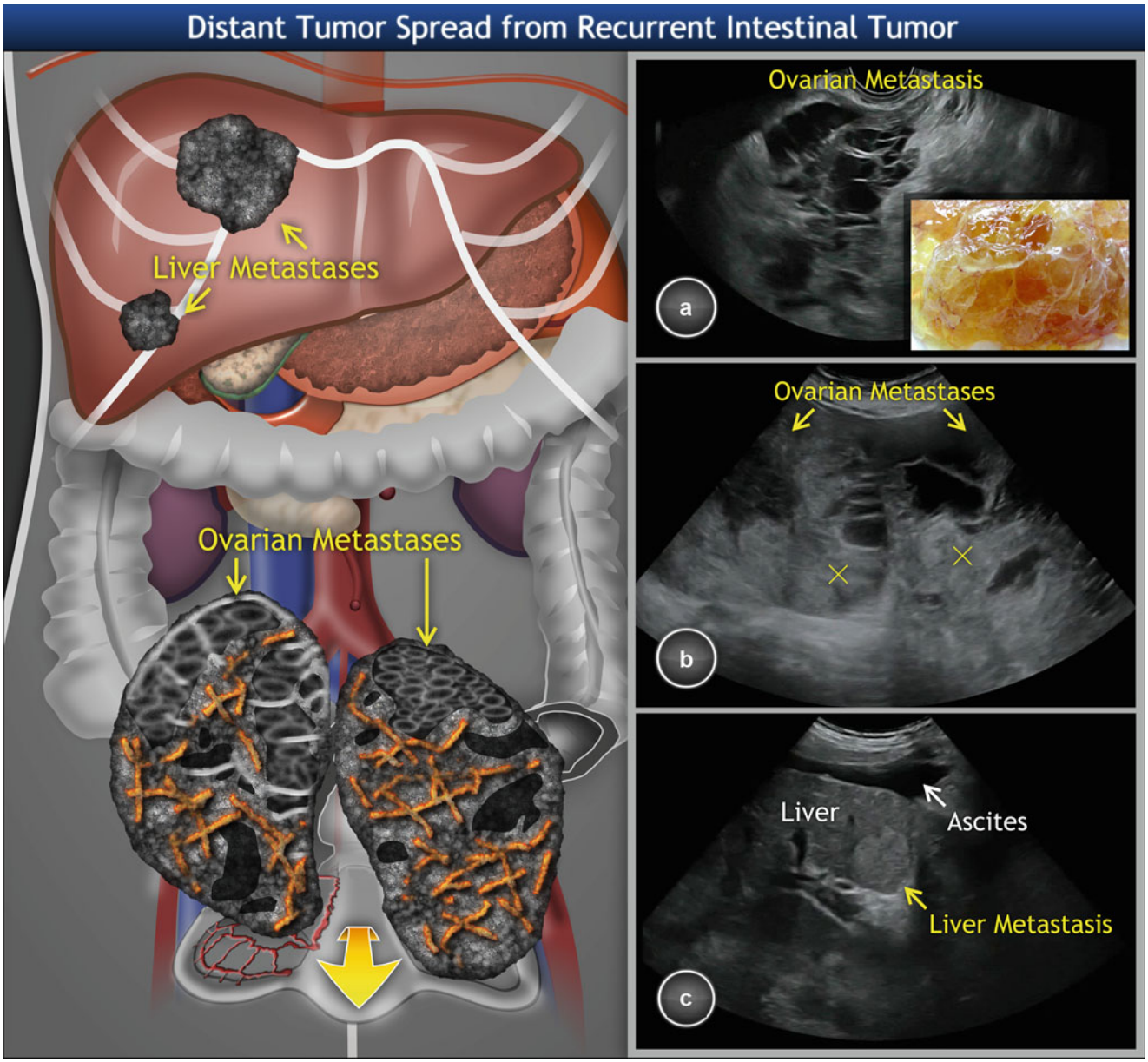

Fig. 8 Recurrent intestinal carcinoma involving the ovaries. (**a**) Transvaginal scan showing large ovarian multilocular-solid tumor with many small cysts. The tumor fills the whole pelvis. Sectioning reveals yellow tissue composed of multiple thin-walled cysts filled with mucinous fluid (detail). (**b**) Transabdominal scan depicts large bilateral ovarian tumors of multilocular-solid appearance. The solid component of locular tumors is heterogeneous (marked with *crosses*). (**c**) Furthermore, transabdominal scan reveals multiple hyperechogenic liver metastases and ascites resulting from a recurrent colorectal primary tumor

peritonei (i.e., the presence of mucinous ascites or mucoid nodules adherent to peritoneal surfaces) was thought to result from ovarian borderline tumors, but it has been recently revealed that virtually all ovarian tumors associated with pseudomyxoma peritonei represent metastases from ruptured primary low-grade mucinous (adenomatous) tumors of the appendix [38]. The rare exception to the gastrointestinal origin of pseudomyxoma peritonei is the occurrence of mucinous tumors arising in ovarian mature cystic teratomas [39, 40].

Diagnosis

The patients are usually middle aged or elderly and typically present with symptoms ascribable to adnexal mass. Other symptoms related to mucocele include pain in the right lower abdominal quadrant, palpable abdominal mass, weight

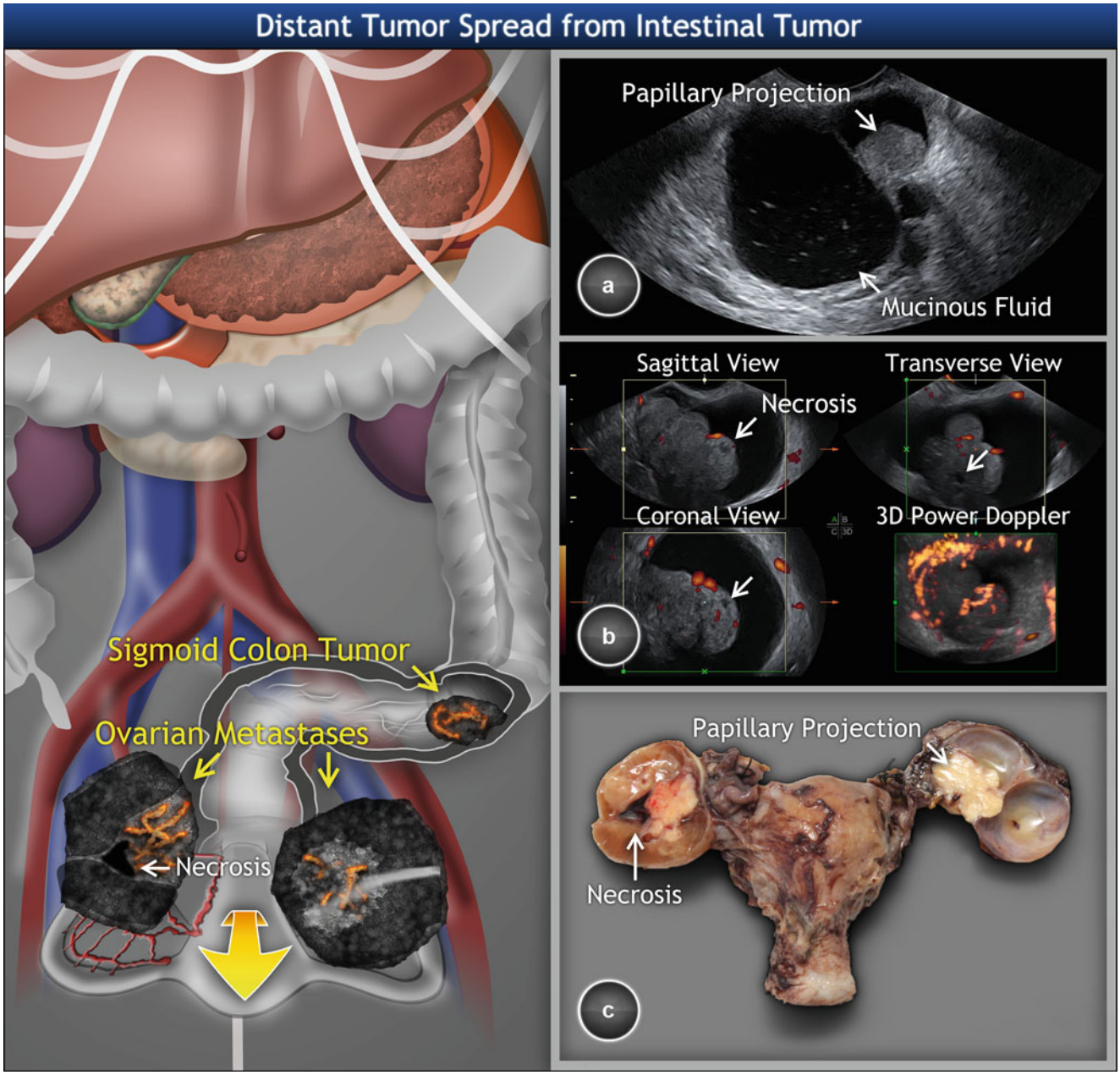

Fig. 9 Sonomorphologic and Doppler pattern of metastatic intestinal tumor involving the ovaries. Colorectal cancer metastasizes to the ovaries in the form of bilateral multilocular-solid large tumors. The intracystic fluid has low-level echogenicity with multiple small echogenic spots (**a**). The hyperechogenic papillary projection of regular surface is growing from thin hyperechogenic septa as presenting on transvaginal scan of right ovarian metastasis. (**b**) Three-dimensional power Doppler of the contralateral ovary demonstrating the presence of solid papillary projection with regular surface and tree-shaped vessels entering the papillary projections. The necroses (marked with *arrows*) present as avascular areas of mixed echogenicity with blurred borders. (**c**) Sectioned surface of tumors showing mucoid intracystic fluid consistent with primary neoplasm

loss, nausea, vomiting, change in bowel habits, anemia, etc. Preoperative CEA and CA19.9 levels are increased in 75 and 58 %, respectively, of patients with pseudomyxoma peritonei [41]. Ultrasound imaging typically shows bilateral ovarian involvement, on average about 16 cm in diameter (Fig. 13) [25].

The ovarian lesions are multilocular or—less often—multilocular-solid tumors with hypoechogenic intracystic fluid (jellylike mucoid material). It needs to be emphasized that ovarian metastases of this primary tumor often don't have a solid component, which is in contrast with two recently published studies reporting no ovarian metastatic tumors without

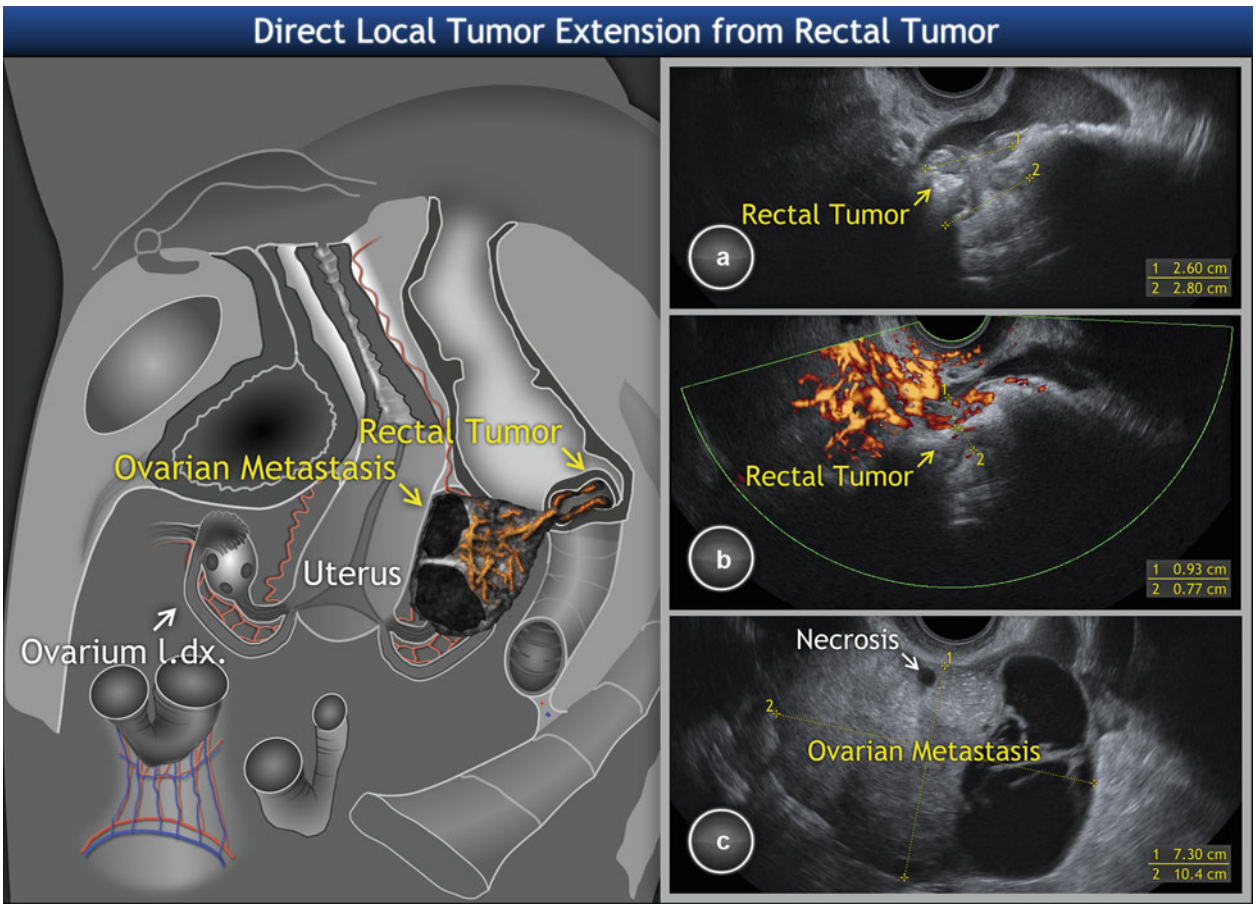

Fig. 10 Unilateral ovarian metastasis from synchronous primary rectal cancer. Transvaginal scan revealing cancerous narrowing of rectal lumen on (**a**) gray-scale and (**b**) power Doppler examination. The unilateral ovarian metastatic involvement shows the presence of hypoechogenic necrosis in a solid tissue and intracystic fluid of low-level echogenicity (**c**). Of note, the tree-shaped architecture of the multiple feeding vessels entering the ovarian tumor

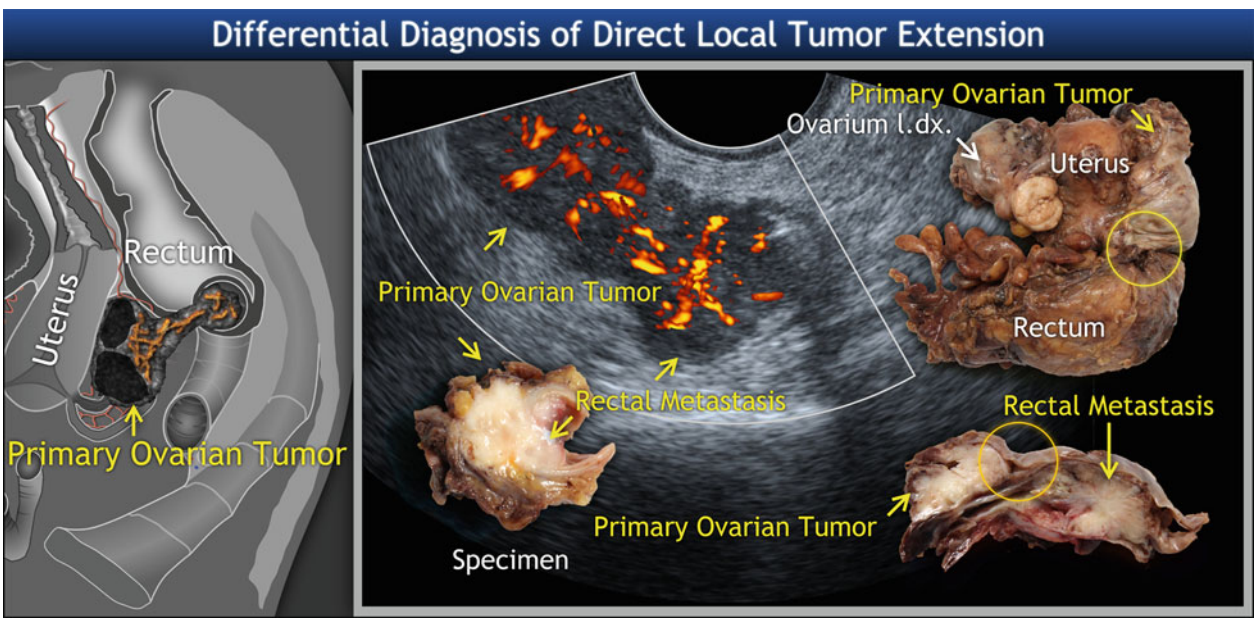

Fig. 11 Metastatic high-grade ovarian cancer protruding into the rectal lumen. Schema and ultrasound image of solid component of ovarian tumors penetrating the rectal wall and growing into the rectal lumen in a polypoid manner, with tree-shaped vessels spreading into the rectal tumor. Biopsy revealed high-grade serous adenocarcinoma originating from ovary. The *yellow circle* shows the contact of left ovary with rectum on uncut and sectioned specimen

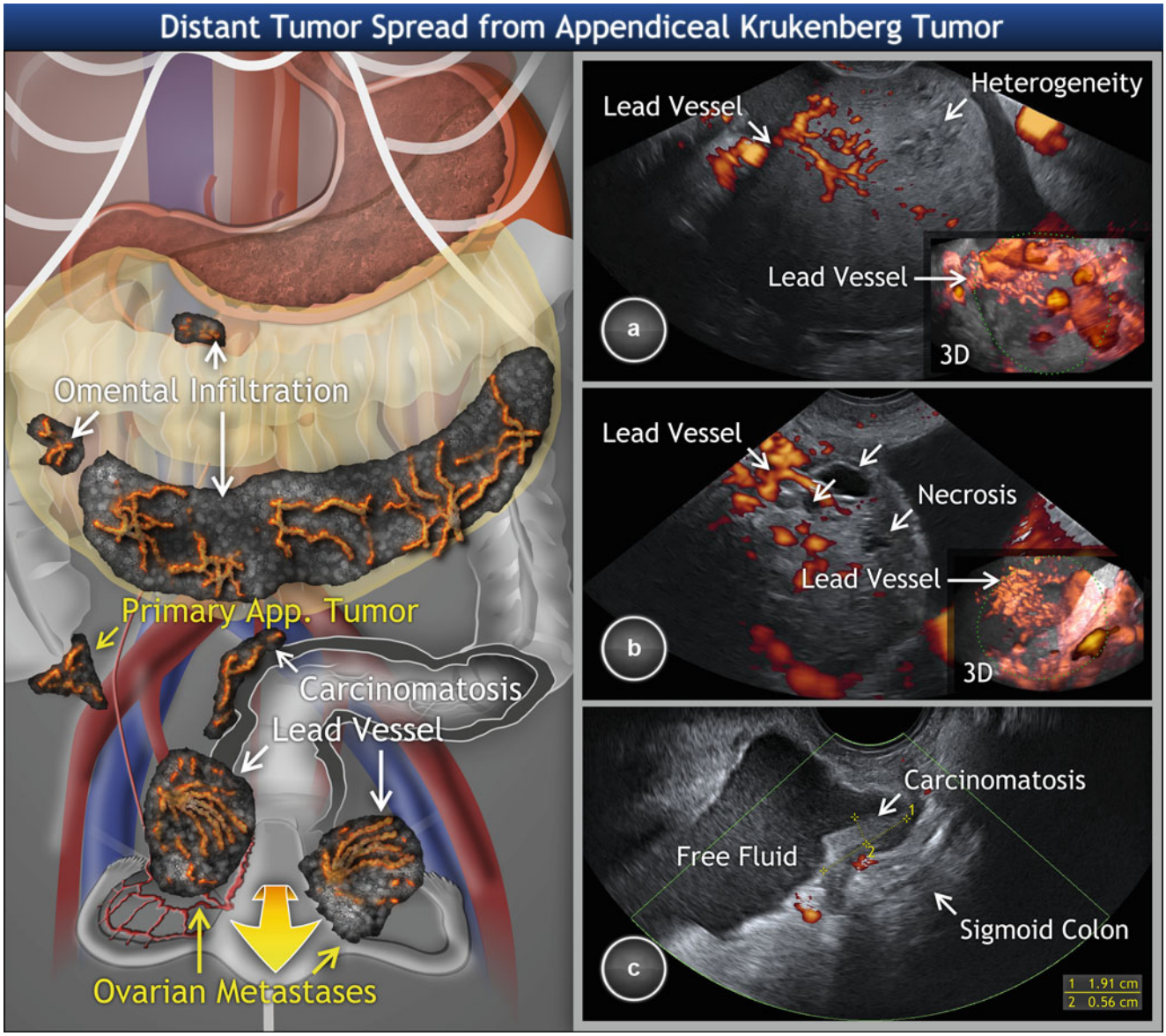

Fig. 12 Metastatic signet ring cell cancer of appendix involving ovaries (Krukenberg tumor). Transvaginal scan showing (**a**) right and (**b**) left solid Krukenberg tumor originating in appendix with a typical lead vessel on 2D and 3D ultrasound (detail). Both tumors present with necrosis (*arrows*) and heterogeneous structure. (**c**) Krukenberg tumor is accompanied by visceral carcinomatosis (peritoneal implants) on sigmoid colon and free fluid in the pelvis

a solid component. These studies, however, did not have a case of this histological entity included in the analyzed group [6, 21]. According to our observation, the pseudomyxoma peritonei presents on ultrasound as an intraperitoneal fluid of low echogenicity that contains immobile echogenic strips of organized mucin often adhering to intra-abdominal surfaces and/or arranged in layers. In the right upper quadrant, the transabdominal scan can detect a dilated tubular structure filled with fluid of low-level echogenicity or even a large multilocular tumor corresponding to appendiceal mucocele. In some cases the appendix is embedded in adhesions in the right iliac fossa. Regarding differential diagnosis, these ovarian metastases may mimic the ultrasound characteristics of mucinous ovarian cystadenomas or mucinous borderline tumors of intestinal type; those, however, are usually unilateral in contrast to ovarian metastases [42].

Neuroendocrine Tumors (NETs)

Neuroendocrine tumors originate mostly in the small intestine [43, 44] and only rarely in the appendix, colon, stomach, pancreas, or lung [25, 45, 46]. Neuroendocrine tumors with obvious evidence of malignant behavior, such as vascular invasion, gross local invasion, or metastases, are usually poorly differentiated neuroendocrine carcinomas.

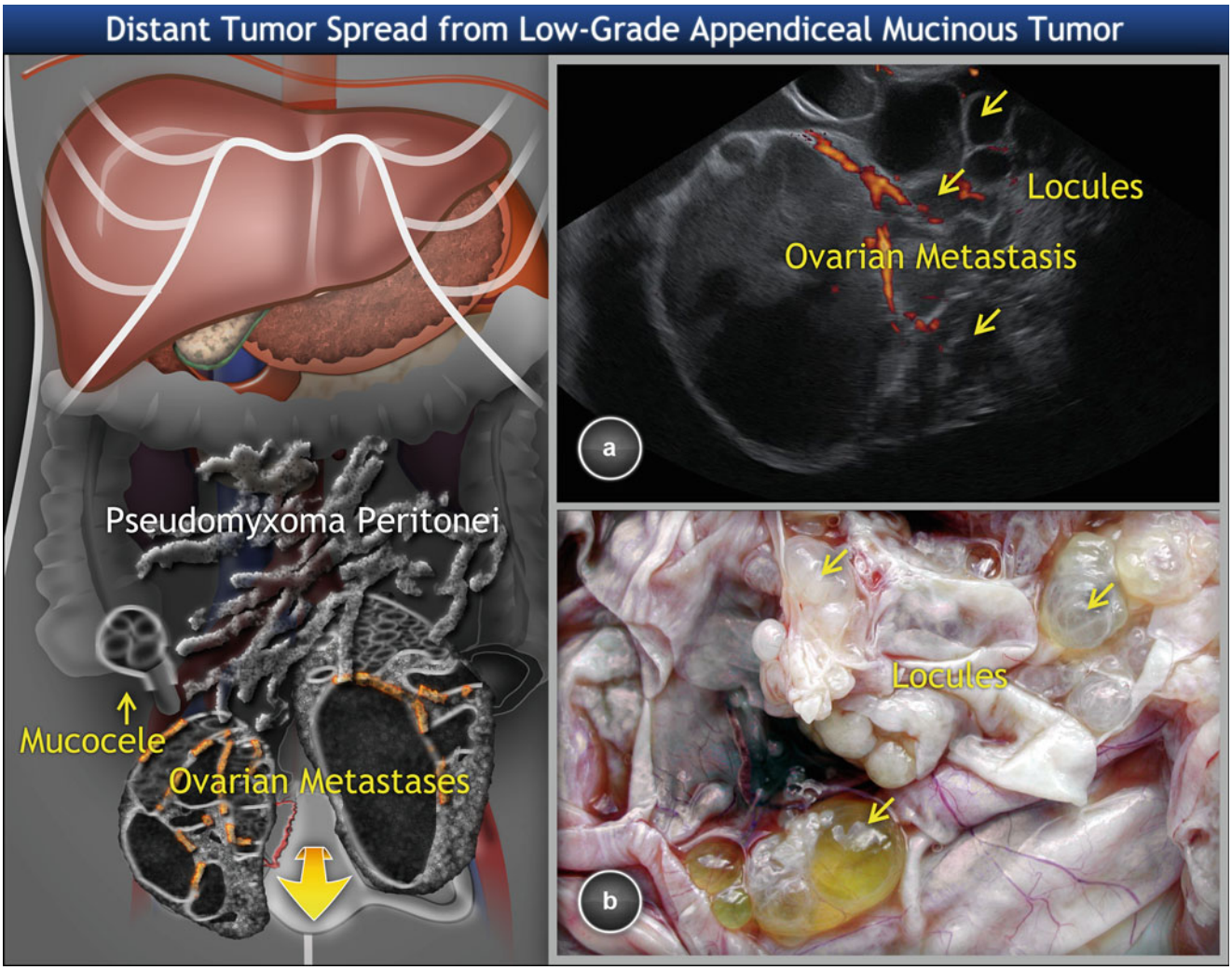

Fig. 13 Metastatic low-grade appendiceal mucinous tumor involving both ovaries. (**a**) Transvaginal scan showing multilocular ovarian mass with intracystic fluid of low-level echogenicity. Hyperechogenic septa are highly vascularized. (**b**) Sectioned surface of ovarian metastasis originating from low-grade appendiceal mucinous neoplasm with mucoid locules. Of note, schema showing gelatinous ascites containing echogenic strips arranged in layers and appendiceal multilocular mucocele

Diagnosis

In a study of Robboy et al., the median age of patients with NETs metastasizing to the ovary was 57 years [43]. Some of them had clinical symptoms consistent with intestinal or ovarian involvement and/or manifestation of carcinoid syndrome. Chromogranin A is a sensitive and specific marker of NETs and can be detected in serum and immunohistochemically [9]. The measurement of 5-hydroxyindole acetic acid in the urine is also useful in determination of metastatic origin of the ovarian tumor. On ultrasound, most of these tumors are bilateral, most often of only modest size and predominantly solid with smooth surface. According to our observation, their appearance on ultrasound resembles that of ovarian fibroma lacking acoustic strips (Fig. 14), while sometimes the tumors contain multiple cysts simulating a cystadenofibroma.

Tumors of the Pancreas

Spread of pancreatic carcinoma to the ovary is more common than previously thought [47]. The pancreatic tumors are usually typical ductal adenocarcinomas and only rarely mucinous cystadenocarcinomas [25]. The patients are usually middle age or elderly. Ovarian spread is often part of disseminated disease with visceral lymphadenopathy, parenchymal liver metastases, and peritoneal involvement including omental infiltration accompanied by ascites.

Diagnosis

Symptoms that may indicate pancreatic cancer as a primary source include abdominal pain, nausea, weight loss, and jaundice in addition to symptoms related to the ovarian masses. Serum CA 19–9 may be elevated along with other findings suggestive of primary pancreatic cancer [10].

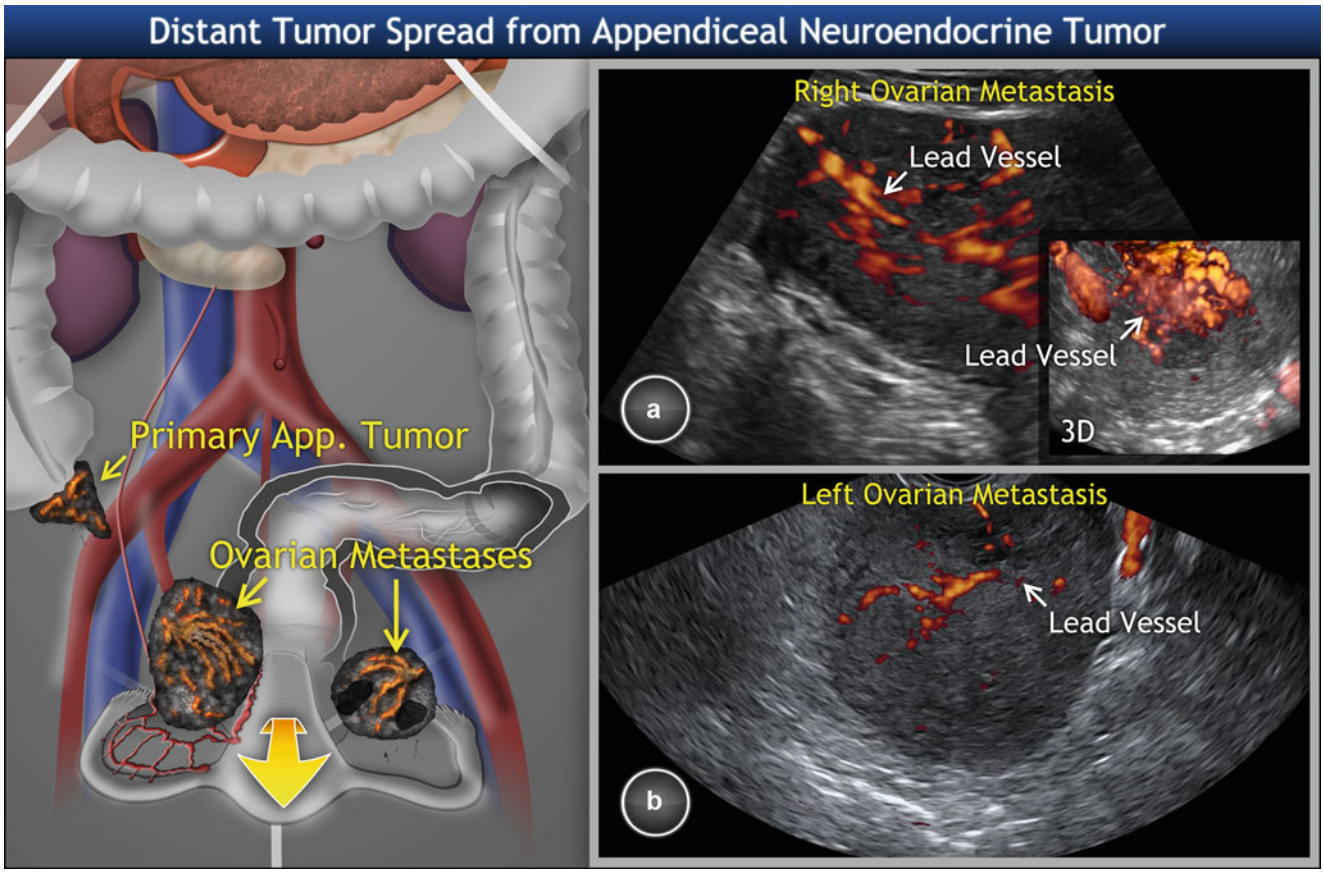

Fig. 14 Metastatic appendiceal neuroendocrine tumor involving ovaries. Transvaginal scan of right and left ovarian metastasis showing solid tumor mass with sporadic small hypoechogenic cysts (**a**, **b**). Detail of three-dimensional power Doppler ultrasound (3DPD) in image (a) shows the lead vessel architecture on 3D power Doppler ultrasound

On ultrasound, the ovarian metastases typically present as bilateral multilocular-solid tumors (Fig. 15). Sometimes, however, the ovarian involvement may be unilateral (Fig. 16), mimicking a primary ovarian tumor.

In differential diagnosis, the spread of pancreatic carcinoma to the ovary may be misdiagnosed as primary mucinous carcinoma and even mucinous borderline tumor. In contrast to primary mucinous tumors, which are typically larger, unilateral, and confined to the ovary without surface involvement, the metastatic lesions in the ovaries are usually smaller (<10 cm), bilateral, and involve the surface and superficial cortex [48]. The frequent presence of intra-abdominal spread is also consistent with secondary involvement of the ovary in cases of bilateral mucinous carcinoma. On microscopic evaluation, the so-called maturation phenomenon can be sometimes observed, referring to the propensity of some metastatic cancers—particularly mucinous ones—to differentiate and present with a borderline-like or even cystadenoma-like appearance [49].

The most frequent signs of pancreatic carcinoma on transabdominal scan are the presence of a hypoechogenic pancreatic tumor of low or moderate vascularity with necrotic avascular anechogenic areas, tumor invasion into splenic vessels, dilation of pancreatic duct, liver metastases, infiltrated visceral lymph nodes, carcinomatosis, and ascites.

Tumors of the Gallbladder and Extrahepatic Bile Ducts

Diagnosis

In a recently published and largest so far study of these tumors, the mean age of patients was 59 years [50]. Almost half the patients presented with gynecologic symptoms, and the remaining ones had typical painless obstructive biliary symptoms, which include pale stools, dark urine, and jaundice [51]. Elevated concentrations of serum CA 19–9 and CEA are often reported in bile duct cancer [9]. The overall ultrasound characteristics are similar to other cases of metastatic adenocarcinomas from various abdominal sites, including pancreas, with no unique features being evident other than the possibility of clinical determination of the primary site due to presence of biliary symptoms. The tumors are bilateral, usually multilocular solid [21] with mean size of 9.4 cm [50].

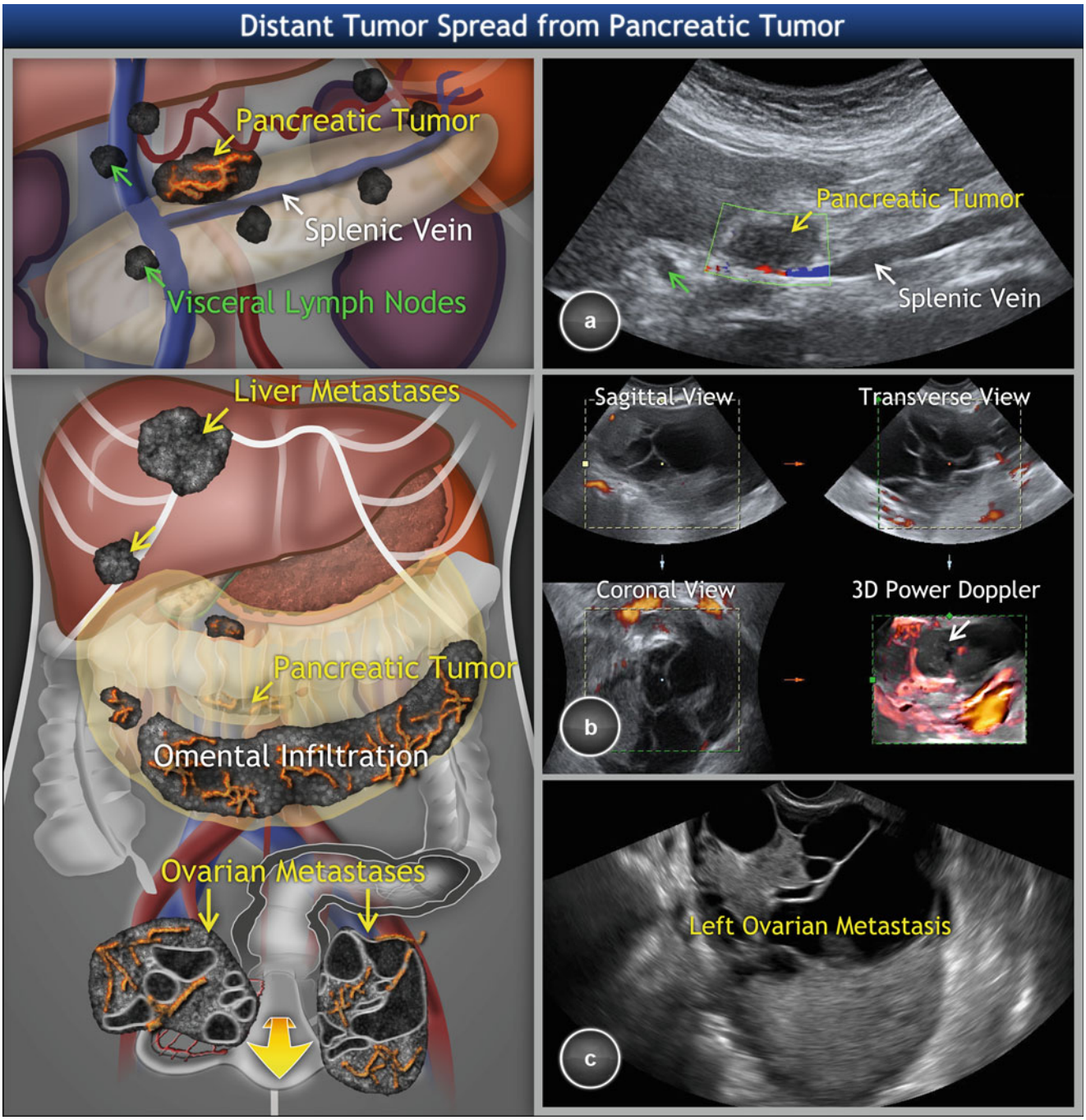

Fig. 15 Metastatic pancreatic adenocarcinoma involving both ovaries. (**a**) Hypoechogenic pancreatic carcinoma infiltrating the head of the pancreas with multiple small rounded hypoechogenic infiltrated visceral lymph nodes (marked with *green arrows*). The tumor compresses the splenic vessels. (**b**) Three-dimensional power Doppler of right ovarian metastasis showing ring-shaped vessel arrangement around the tumor nodule (*arrow*). (**c**) Gray scale of left ovarian metastasis showing a multilocular-solid tumor with low-level echogenicity of intracystic fluid

In many cases the primary gallbladder cancer is already in advanced stage, with the tumor penetrating and obscuring the gallbladder and growing into liver parenchyma. Concurrent liver metastases and thrombosis of ductus cysticus and vena portae are often present as well as infiltration of portal visceral lymph nodes. On ultrasound, the cholangiocarcinoma presents as a hypoechogenic tumor with irregular borders accompanied by a dilation of bile duct.

Breast Carcinoma

Ovarian involvement is seen on autopsy in about 10 % of cases of breast cancer. In a large series by Gagnon et al.,

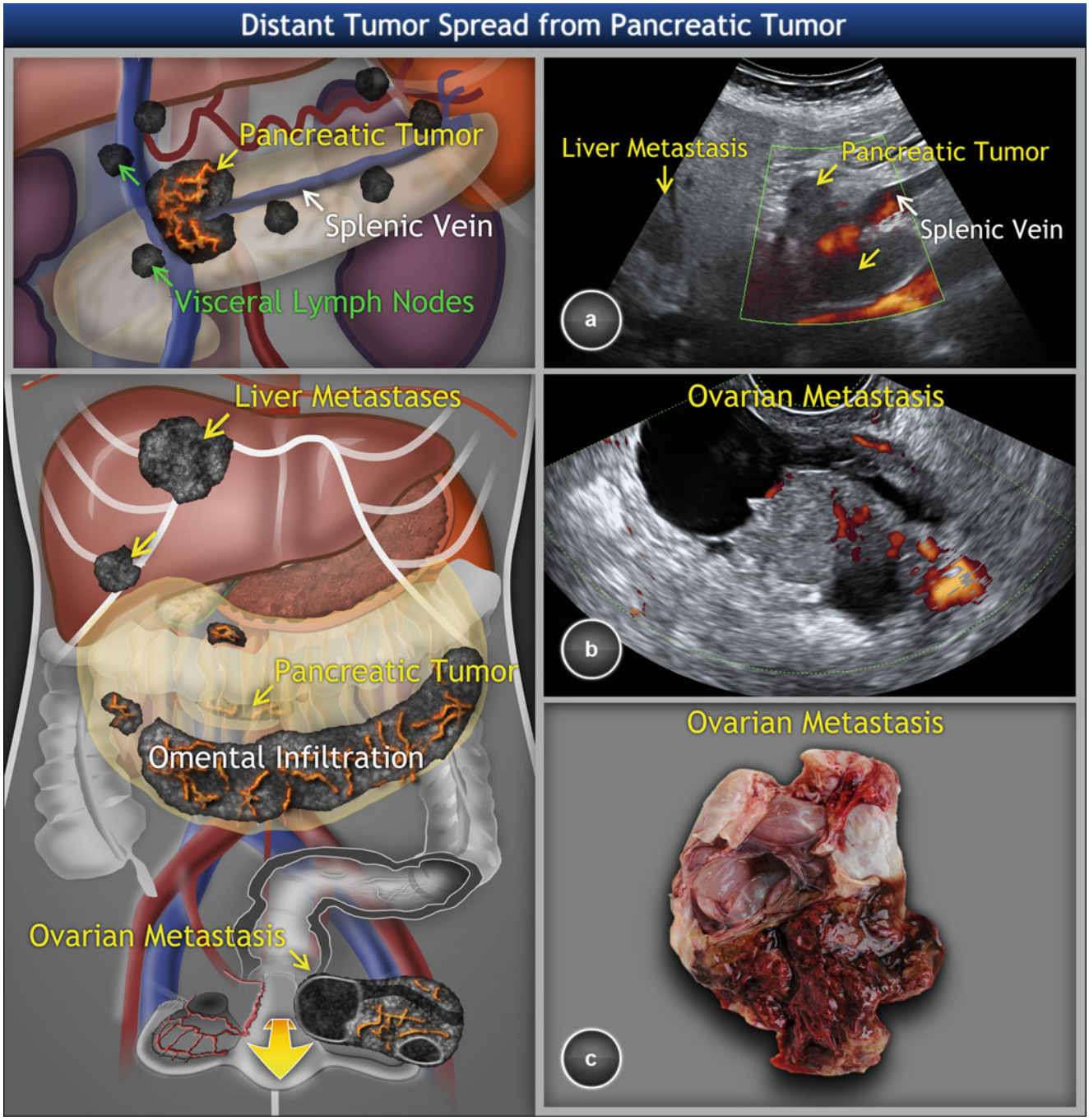

Fig. 16 Metastatic pancreatic adenocarcinoma involving one ovary. (**a**) Large hypoechogenic tumor in the head of pancreas (marked with *arrows*) infiltrating the splenic vessels with concurrent multiple hypoechogenic liver metastases. (**b**) Unilateral multilocular-solid metastasis of the left ovary with moderate vascularity of solid tissue and intracystic fluid of low-level echogenicity. (**c**) The sectioned specimen shows smooth inner wall of cysts

breast carcinoma accounted for almost 40 % of all metastases to the ovary, being slightly more common than metastases from the gastrointestinal tract [52]. In this series the mean age of patients was 48.6 years. Median interval between the diagnosis of breast carcinoma and that of ovarian metastases was 11.5 months, and it correlated with the initial stage of breast disease. Median survival after the diagnosis of ovarian metastases was 16 months [52]. Only rarely is the ovarian metastasis evident before breast cancer is detected [52, 53]. Lobular carcinomas, including those with signet ring cell type, spread to the ovary more frequently than those of ductal type [54].

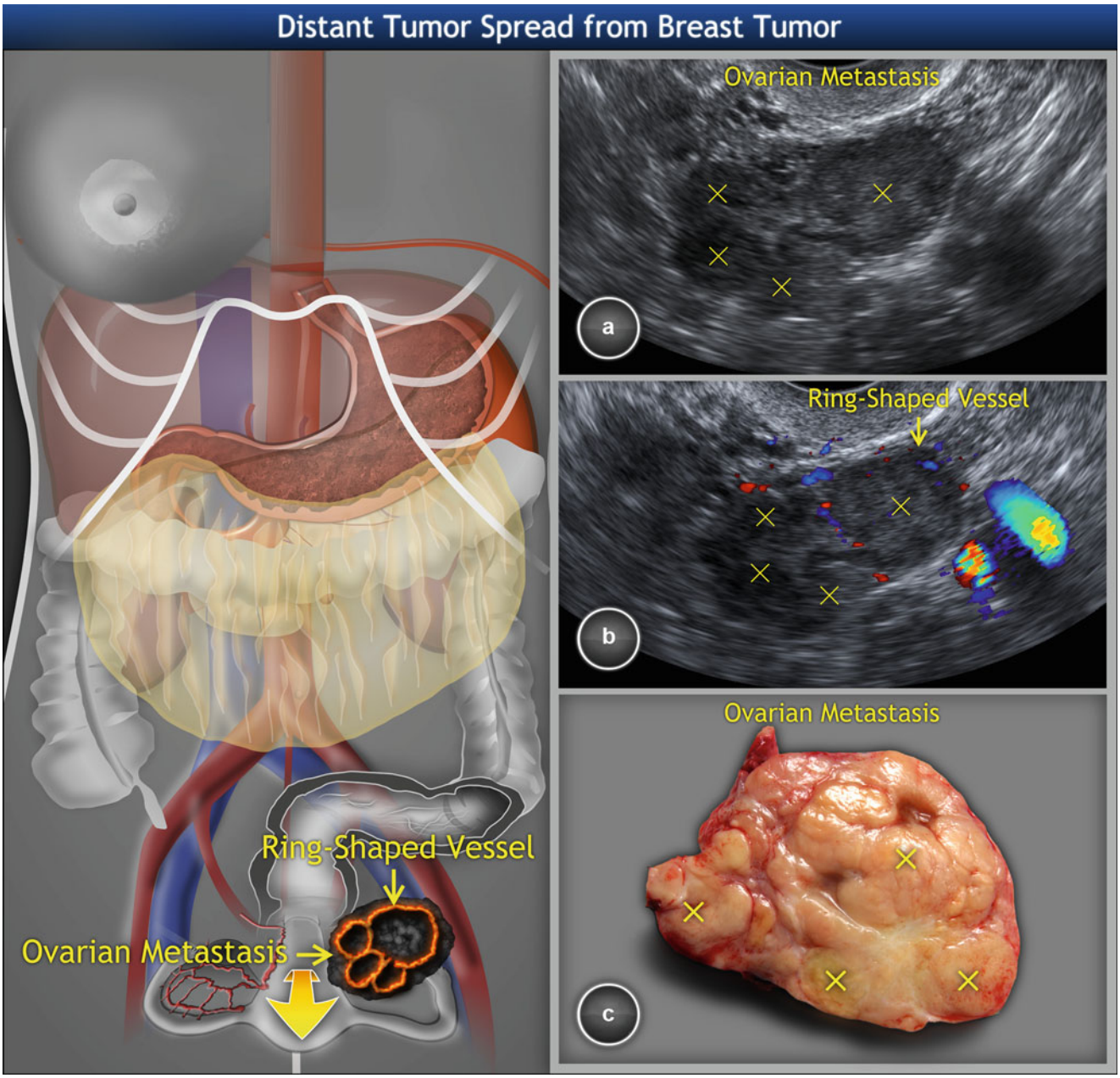

Fig. 17 Recurrent breast cancer involving left ovary. (**a**) Transvaginal scan of ovary with multiple superficial and parenchymatous tumor nodules (marked with *cross*). (**b**) Color Doppler showing ring-shaped vessel tree around the nodule (marked with *cross*). (**c**) Sectioned surface of tumor showing the corresponding multiple solid nodules within normal ovarian stroma (marked with *crosses*). The maximal diameter of tumor was less than 4 cm

Diagnosis

Ovarian involvement is often only a microscopic finding in therapeutic oophorectomy specimens, producing no signs or symptoms. However, isolated ovarian metastases are only sporadically encountered. More often, the ovarian metastases of breast cancer are accompanied by other foci of abdominal spread (liver metastases, carcinomatosis, ascites) causing the related symptoms. Elevated levels of CA 15–3 and CA 27.29 can predict recurrence of breast cancer [13].

The metastases are bilateral in approximately two-thirds of all cases detected at autopsy and surgery [21, 52]. However, the ovarian metastases are usually small, and in the series of 64 ovarian metastases of breast carcinoma, the ovaries were grossly normal in 27 (46 %) cases, and in 18 (31 %) cases the metastases were less than 1 mm in diameter [52]. Metastatic tumors spreading from the breast more often envelop preexisting normal ovarian structures (in contrast to primary ovarian tumors) and, according to our observation, typically contain nodules of various sizes located in the ovarian parenchyma (Fig. 17).

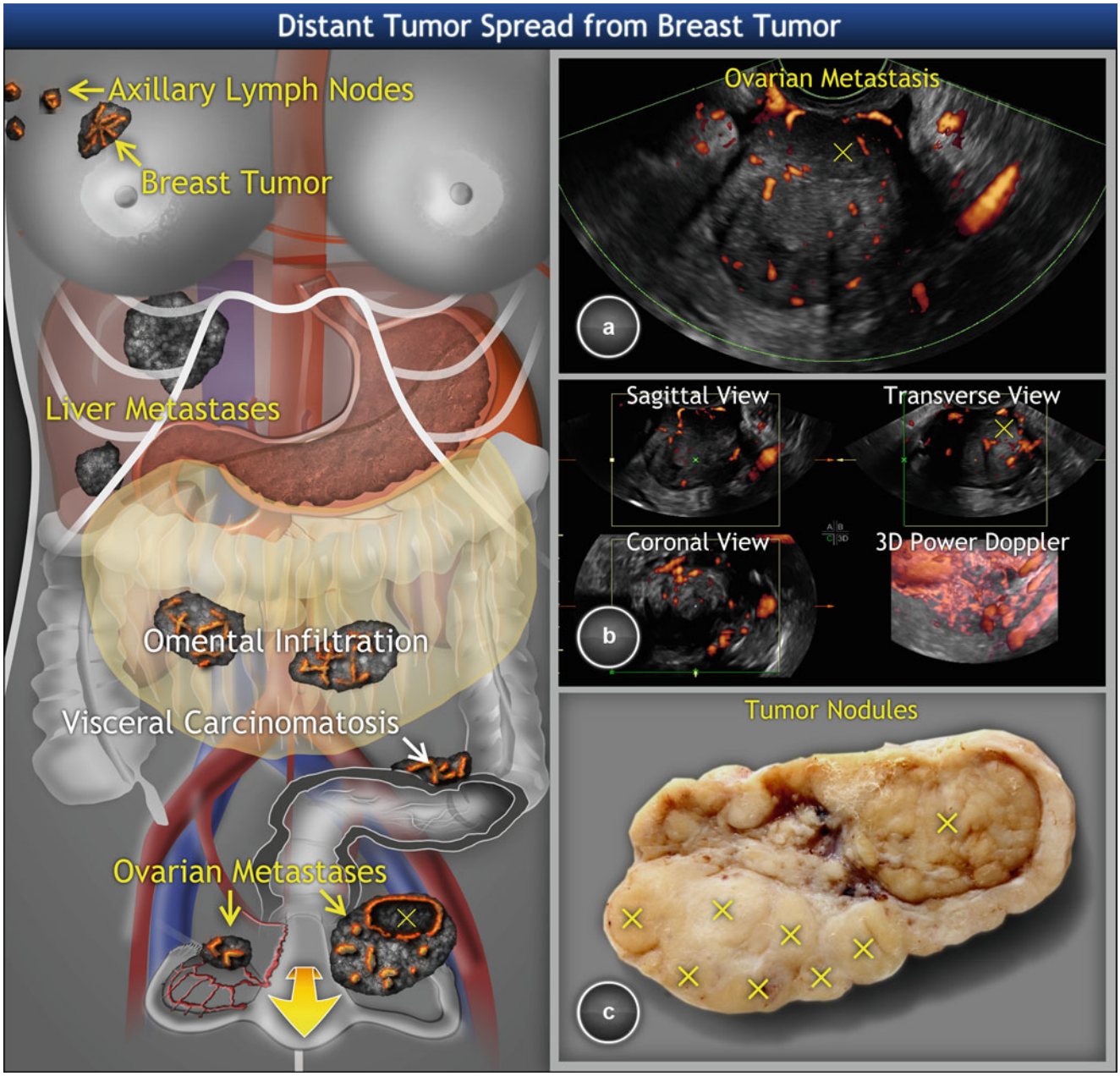

Fig. 18 Progredient breast cancer involving both ovaries. (**a**). Transvaginal scan of left ovarian metastasis with a nonhomogeneous solid component with solid hypoechogenic nodules (one nodule marked with cross). (**b**) 3DPD presenting the rich vascularity of left ovarian tumor and tumor nodule (marked with *cross*) bordered by ring-shaped vessels. (**c**) Specimen of left ovarian metastasis showing multinodularity within solid tumor of smooth surface (marked with *crosses*), with maximal diameter less than 4 cm. The right ovary was not enlarged, but was unusually richly vascularized in a postmenopausal woman, suggesting the presence of contralateral metastatic involvement (schema)

When the organ is wholly replaced by tumor, it is manifested as a solid, smooth-surfaced mass (Fig. 18). In a recent study presented by Guerriero et al., the breast cancer metastases were found in 20 of 116 metastatic ovarian masses. These metastatic tumors were significantly more frequently solid in comparison to stomach, colorectal, and uterine cancer metastases (95.0 % vs. 60.8 %, 46.8 % and 70.6 %, respectively; $P<0.05$) and tended to appear moderately or highly vascularized [6]. Based on our experience in differential diagnostics between primary and metastatic ovarian neoplasms, the most helpful tools in arriving at a correct diagnosis of metastatic origin of the ovarian lesion are the awareness of the patient's clinical history of advanced lobular breast cancer and familiarity with ultrasound findings,

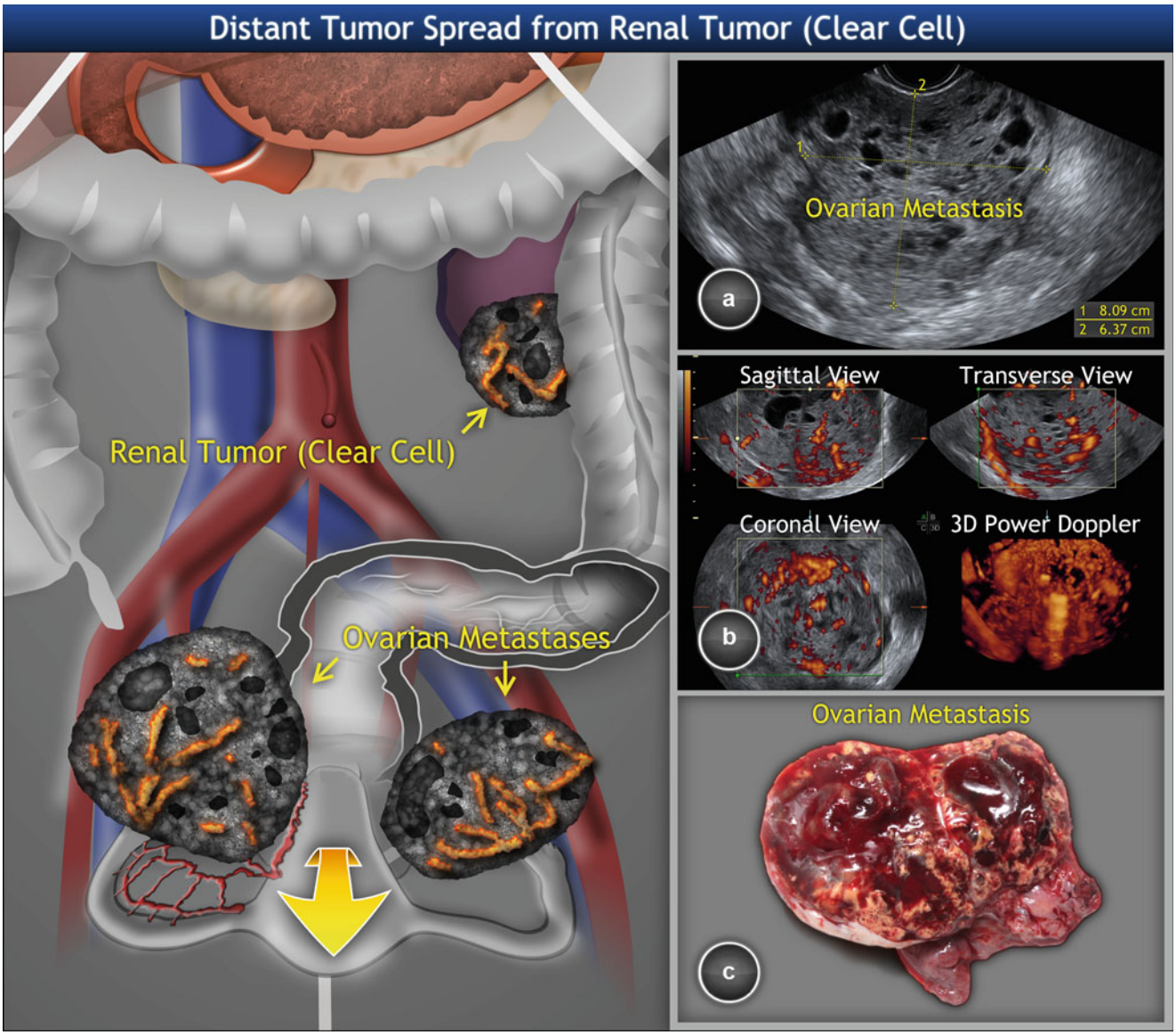

Fig. 19 Metastatic clear cell renal carcinoma involving both ovaries. (**a**) Ultrasound finding of right ovarian metastasis of solid structure with multiple small irregular cysts filled with hypoechogenic (hemorrhagic) intracystic fluid. (**b**) Three-dimensional power Doppler ultrasound of ovarian metastasis showing tumor structure and vessel tree. (**c**) Sectioned specimen of right ovarian metastasis from primary renal carcinoma. Of note, the patient presented with bilateral ovarian masses 20 years after right nephrectomy for clear cell renal carcinoma. Transabdominal scan reveals renal contralateral tumor (schema). The newly diagnosed renal tumor was rounded, of 4 cm in diameter. Ultrasound finding was suggestive of ovarian metastases originating from the previous or new renal cancer

typical for this condition: non-enlarged or slightly enlarged ovary/ies showing multiple solid nodules with ring-shaped vessel arrangement around the nodules and/or solid ovarian tumor with a smooth surface and high vascularity as well as occasional peritoneal involvement, ascites, and liver metastases.

Renal Tumors

Renal cell carcinoma rarely spreads to the ovary. If, however, the ovarian metastases are discovered first, this metastatic carcinoma may be misdiagnosed as primary ovarian clear cell carcinoma.

Diagnosis

The most common symptoms related to clear cell renal cancer are anemia, hepatic dysfunction, gross hematuria, hypoalbuminemia, flank pain, malaise, paraneoplastic hypercalcemia, and anorexia. Symptoms of ovarian metastases reflect the presence of pelvic or abdominal mass. There is no known specific serum tumor marker.

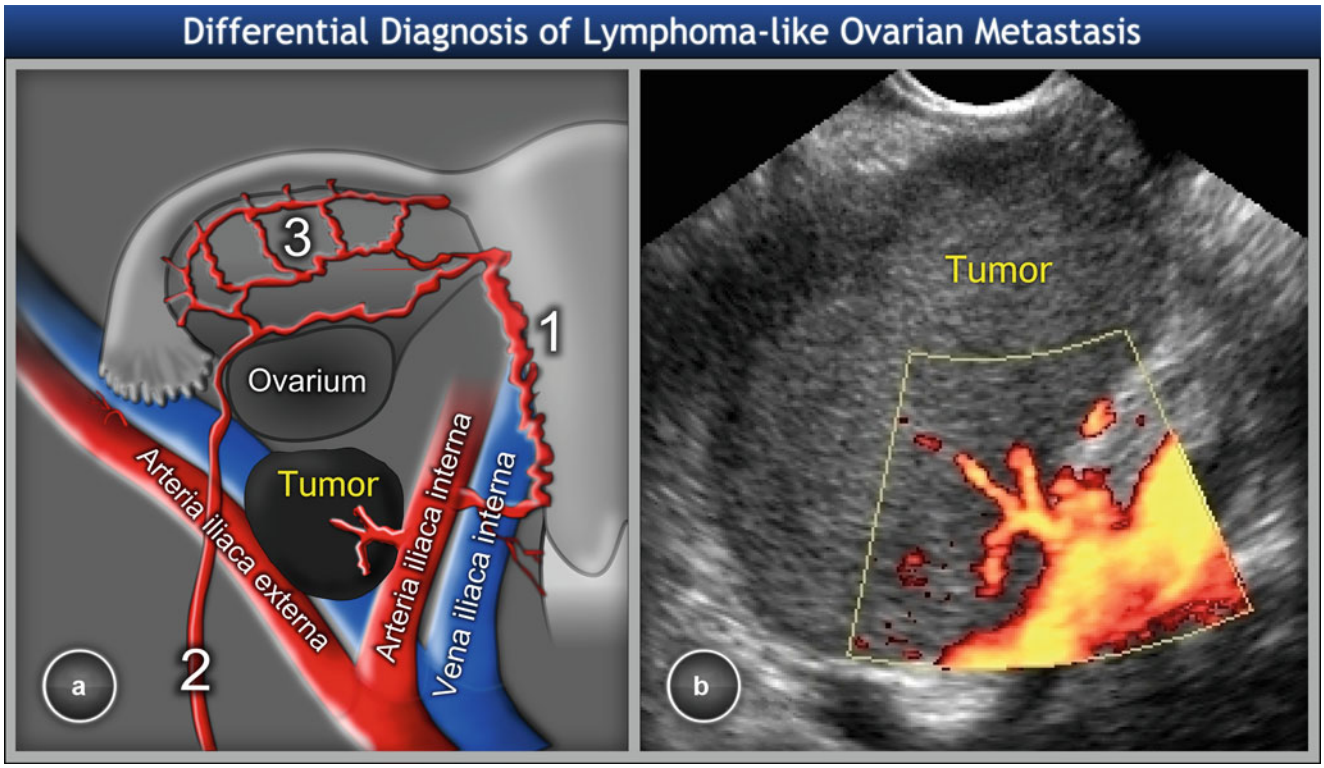

Fig. 20 Retroperitoneal lymphoma. Schema (**a**) and ultrasound image (**b**) of solid homogeneous tumor with a tree-shaped vessel radiating from right iliac artery and entering the tumor

The majority of those ovarian tumors are unilateral, often large, with the greatest dimension being 12.5 cm on average [25]. On ultrasound, solid tumor/s containing few small irregular locules or multilocular-solid tumors are usually depicted (Fig. 19). The cysts are filled with fluid of low-level or mixed echogenicity (hemorrhagic content). If the ovarian metastasis is discovered prior to its renal source, then subjective tumor pattern recognition on ultrasound may lead to misdiagnosis of primary ovarian clear cell carcinoma (also typically presenting as unilateral mass with a mean size about 13–15 cm [55]) or as granulosa cell tumor [56].

On transabdominal scan, the primary clear cell renal cancer presents in about one-third of patients as homogeneous iso- or hyperechogenic lesion with rich vascularity. In the presence of hemorrhage or necrosis, the tumor becomes heterogeneous with avascular areas of necrosis and hemorrhage. The pathognomonic marker of malignancy is the presence of thrombosis in renal vein or inferior vena cava.

Lymphoma

Among patients with disseminated lymphoma and lymphoid leukemias, the ovary is a relatively common site of involvement, although it may be asymptomatic [57, 58]. Any type of lymphoma may spread to the ovary, but mediastinal large B-cell lymphoma has a distinct tendency to involve the ovary [57]. The ovaries are usually not the only site of relapse—the involvement of peritoneum, omentum, fallopian tubes, lymph nodes, and central nervous system is frequent.

Diagnosis

The clinical complaints associated with lymphoma usually include fatigue, weight loss, fever, or nonspecific symptoms related to the presence of mass. Lymphoma may be associated with high serum levels of lactate dehydrogenase (LDH) and beta2-microglobulin (B2M).

The bilateral ovarian lesions are found in 80 %. On ultrasound the external surface of ovarian lymphoma is usually intact and the mass is solid and hypoechogenic in the majority of cases. In differential diagnosis the retroperitoneal lymphoma may be misinterpreted as an ovarian solid tumor, especially if the scan is performed by a less experienced examiner (Fig. 20).

Spread from Other Sites in the Genital Tract

Tubal Carcinoma

Recent studies have shown that a great number of high-grade carcinomas of the ovary (so-called Type II category)

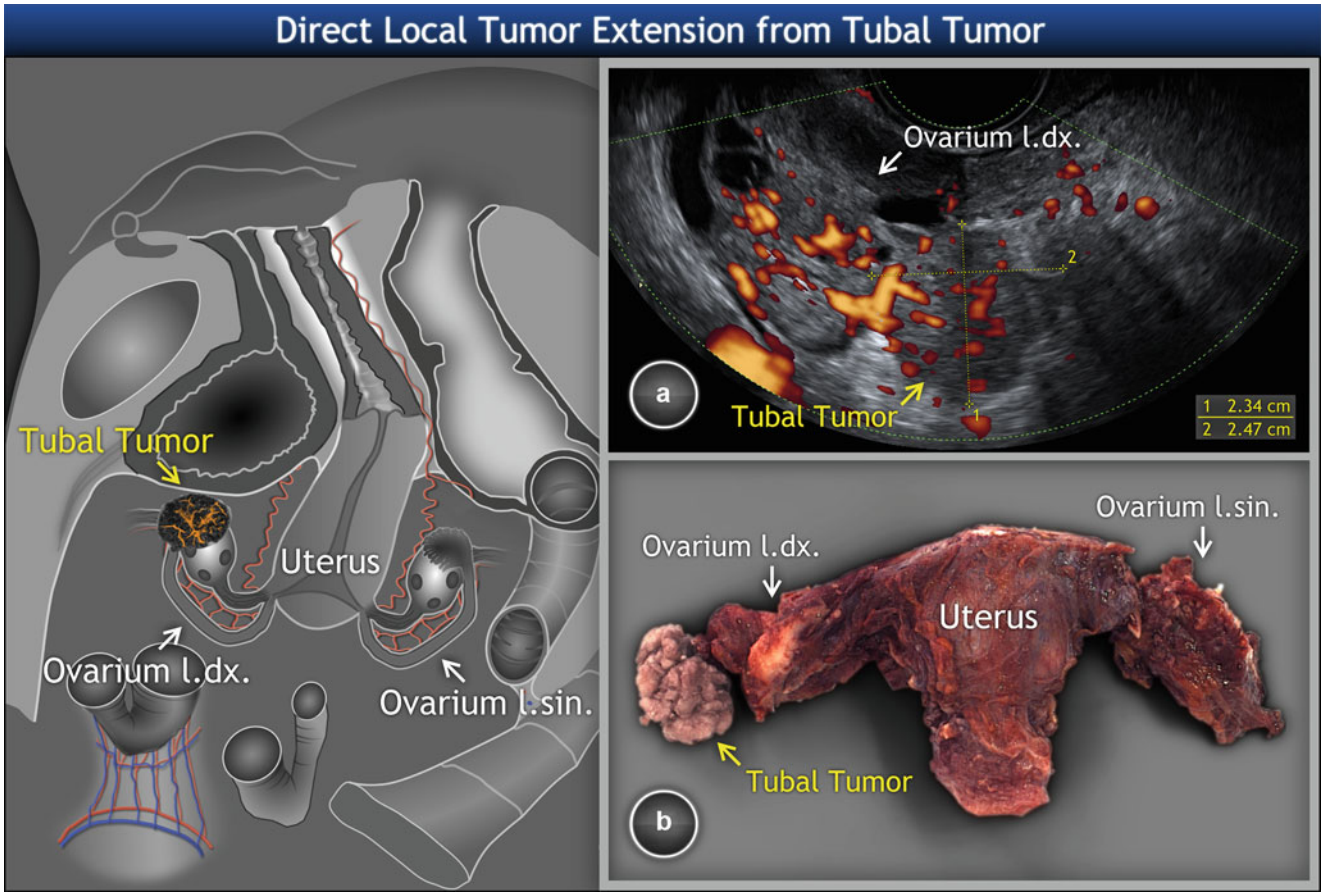

Fig. 21 Direct local extension from tubal cancer. (**a**)Transvaginal scan of highly perfused solid tumor originating from tubal fimbriae and infiltrating the adjacent right ovary. (**b**) Specimen of right tubal cancer

represent the spread of fallopian tube cancers, especially those of the fimbria (Fig. 21) [59]. Their sonographic appearance is therefore not different from primary high-grade ovarian cancers [4, 19]. At the time of diagnosis, most Type II tumors are already widely disseminated throughout the peritoneum.

Uterine Carcinoma

Endometrial Carcinoma

Ovarian involvement in cases of confirmed endometrial carcinoma has been reported in 34–40 % of autopsies and in 5–15 % of hysterectomy and bilateral salpingo-oophorectomy specimens [25]. Conversely, in approximately one-third of cases with established diagnosis of endometrioid carcinoma of the ovary, a primary uterine endometrial carcinoma is also found [25].

Diagnosis

Symptoms are related to the presence of endometrial cancer as the ovarian metastases are usually of small size. In a study conducted by Guerriero et al., the median volume of metastases from stomach, breast, lymphatic system, and uterus was significantly smaller than that of metastases deriving from colon, rectum, or biliary tract (65 mL vs. 234 mL) [6]. Advanced endometrial cancer may be accompanied by elevated serum CA-125.

On ultrasound, ovarian metastases originating from endometrial tumor present as either solid hyperechogenic tumors (consistent with the echogenicity of endometrial tumor), or unilocular-solid, or multilocular-solid tumors. Their solid portion is highly vascularized and the intracystic fluid is of low-level or ground glass echogenicity (Fig. 22). Ovarian metastases from endometrial cancer are more likely to be unilateral, with only 14–21 % reported as bilateral [28, 60]. The ultrasound appearance of uterine cancer is described elsewhere [61].

In cases of synchronous occurrence of uterine endometrial and ovarian endometrioid cancer, the following features (summarized in Table 1) should be considered in order to correctly establish the site of origin:

A primary endometrial tumor with secondary ovarian involvement is characterized by a deep myometrial penetra-

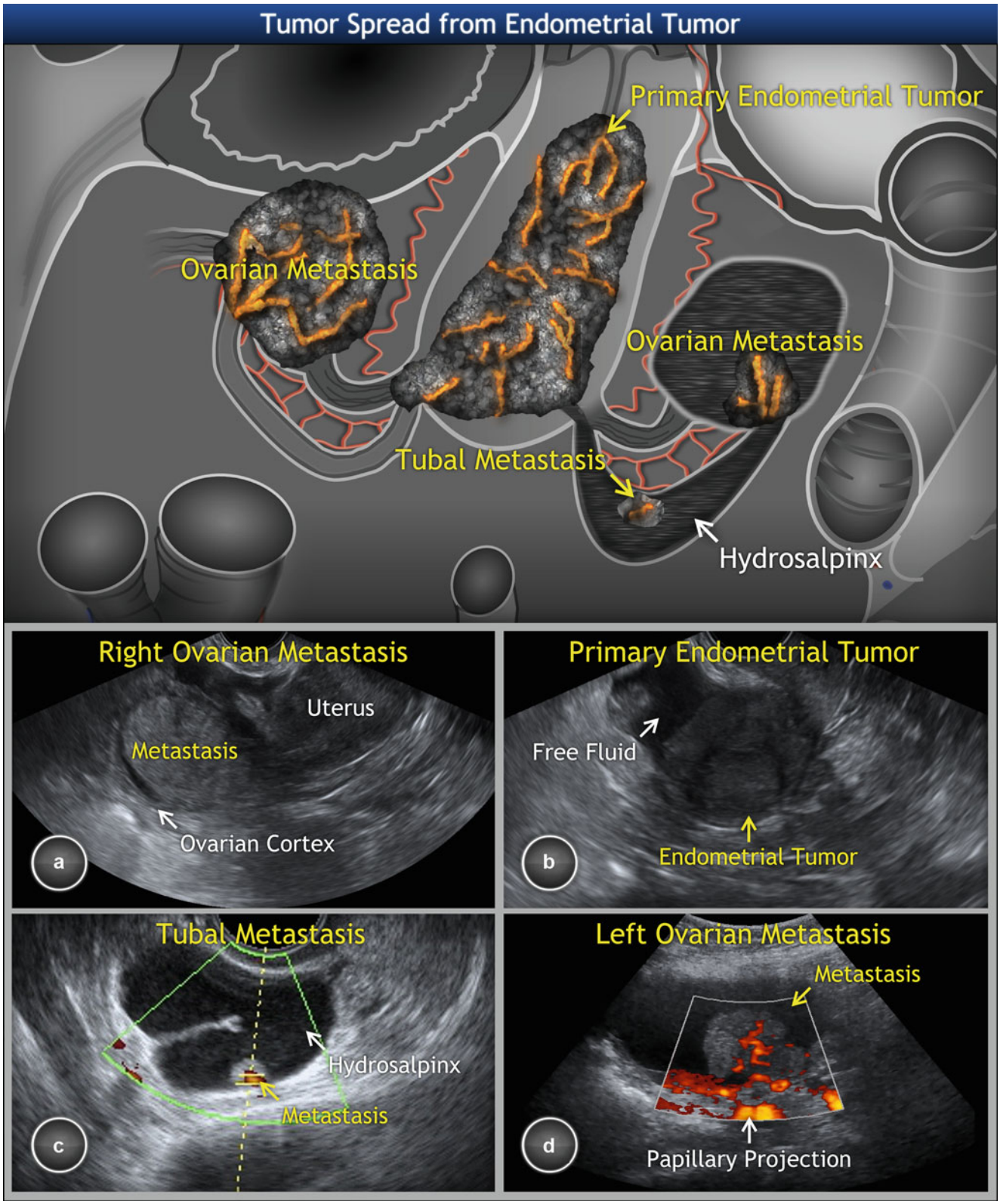

Fig. 22 Primary endometrial cancer involving both ovaries. (**a**) Transvaginal scan of right ovarian metastasis presenting as a solid mass within the right ovary. (**b**) Endometrial tumor deeply infiltrating the myometrium. (**c**) Tumor implant in a dilated left fallopian tube. (**d**) Left ovarian mass with unilocular-solid appearance and regular surface with papillary-solid projection; a tree-shaped vessel entering the papillary projection. Of note, fluid of ground glass echogenicity in left fallopian tube and in ovarian locule suggests hemorrhagic content

Table 1 Criteria for differential diagnostics of concomitant ovarian and endometrial carcinomas

Variables	Primary Uterine Endometrial Tumor and Ovarian Metastasis	Primary Ovarian Tumor and Endometrial Metastasis	Primary Ovarian and Primary Endometrial Tumor	Endometrial Metastasis and Ovarian Metastasis
Schema	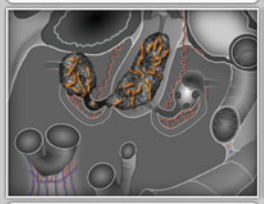	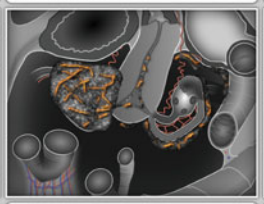	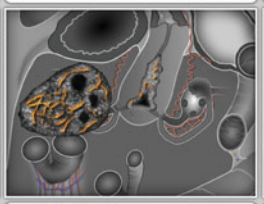	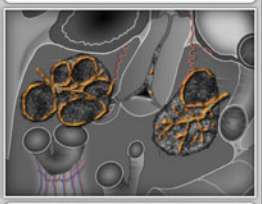
Deep myometrial invasion	Yes (from endometrium into deep myometrium)	Yes (from serosa)	No (superficial involvement)	No (endometrial stroma involvement)
Lymphatic or blood vessel invasion in uterine corpus, ovary, or both	Yes	Yes	No	Yes
Atypical hyperplasia of endometrium	Yes	No	Yes	No
Tumor involvement outside of uterus	Within fallopian tube, ovarian surface	Within ovary and sometimes in fallopian tube, on peritoneum	Within ovary	Bilateral ovarian involvement incl. ovarian surface
Presence of ovarian endometriosis	No	Yes	Yes	No
Histotype in endometrial and ovarian tumor	Uniform and consistent with primary endometrial tumor	Uniform and consistent with primary ovarian tumor	Uniform or dissimilar	Inconsistent with or unusual for either organ

Modified from Lerwill and Young [25]

tion with lymphatic and vascular invasion and tumor implants in the lumen of the fallopian tube, and/or on the ovarian surface, and within uterine corpus lymphatics or in blood vessels (Fig. 22) [60, 62]. In some cases the uterine endometrial cancer extends directly into the ovary as presented in Fig. 23.

A primary ovarian endometrioid cancer with uterine involvement would be a likely diagnosis if the ovarian tumor arises on a background of endometriosis and grossly infiltrates the ovary; the corpus carcinoma shows no signs of atypical hyperplasia, the myometrium is infiltrated from perimetrium, and the tumor is present within the scope of ovarian lymphatic and blood vessels.

The presence of independent primary tumors in the ovary and the uterus should be considered if these arise on a background of atypical hyperplasia in the uterus and endometriosis in the ovary; such tumors are limited to their original organ (absence of myometrial invasion or only superficial myometrial spread; no spread outside the ovary), and lymphatic and/or hematogenous spread is absent.

Both the uterus and the ovary may be involved by an extragenital primary tumor presenting with common features of metastatic disease: bilateral ovarian involvement, ovarian parenchymatous multinodularity, and tumor on the ovarian surface and in endometrial stroma showing a histotype atypical for both the ovary and the uterus (Fig. 24).

Some recent studies suggest that immunohistochemistry and DNA flow cytometry may be of value in the distinction between metastatic and independent tumors [63, 64]. In some cases, however, despite the employment of the above guidelines and a multidisciplinary approach, the correct diagnosis of the origin of concomitant uterine corpus and ovarian carcinomas may prove impossible.

Cervical Carcinoma

Ovarian spread of cervical carcinoma is more common in cases of adenocarcinoma (28, 6 %, 22/77 patients) than in

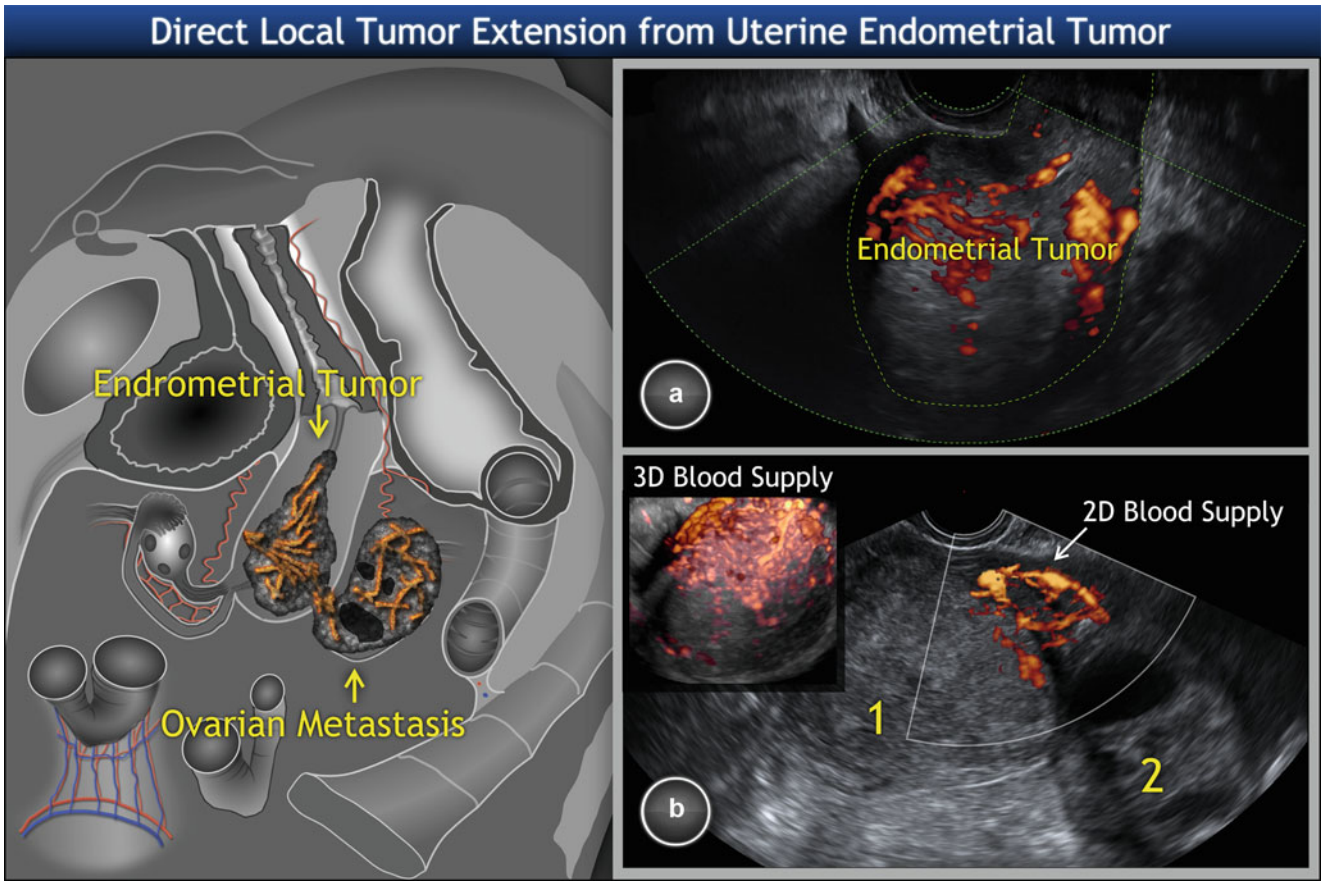

Fig. 23 Direct local extension from primary uterine (endometrial) tumor in the left ovary. (**a**) Ultrasound finding of locally advanced high-grade endometrial cancer of mixed echogenicity; higher color score and multiple focally entering vessels in an endometrial tumor deeply infiltrating the myometrium. (**b**) Endometrial tumor locally infiltrating the left ovary through the left uterine cornu. The multiple tumor vessels entering the ovary are presented on 2D and 3D images (*1* uterine endometrial tumor, *2* left ovarian metastasis of predominantly solid appearance with few hypoechogenic locules)

cases of squamous cell carcinoma (17 %, 104/597 patients) [65]. The presence of metastases is dependent on the stage of disease and presence of lymphatic and blood vessel invasion and is more common when the cervical carcinoma has already invaded the uterine corpus which increases the probability of transtubal spread to the ovarian surface.

Diagnosis

In a series conducted by Young et al., most patients presented with clinical manifestations of ovarian involvement; other symptoms were related to cervical cancer (i.e., abnormal vaginal bleeding, heavy discharge, pain during urination). SCC is the marker of choice in squamous cell cervical cancer, while CEA and CA-125 have been demonstrated of possible utility in patients with cervical adenocarcinoma [14].

Ovarian metastases originating from endocervical or mucinous adenocarcinomas are bilateral in only about one-third of all cases and are often larger than 10 cm [25]. According to our observation, these ovarian metastases mimic the sonomorphologic features of unilocular-solid or multilocular-solid tumors or are sometimes similar to mucinous borderline tumors. In a study involving 12 cases of ovarian metastases with cervical cancer histotype other than pure adenocarcinoma, the mean age of patients was 43 years; the tumors were bilateral in 6/12 patients (50 %), and extensive extracervical spread was often found. The cervical tumors were grossly evident in 10 patients and presented as solid (4/10 patients), solid and cystic (3/10 patients), or cystic (3/10 patients) [66]. The sonographic appearance of primary cervical cancer is described in a recent review [4].

Involvement by Peritoneal Tumors

Ovarian tissue may be involved by a primary peritoneal tumor originating from pelvic peritoneum and manifesting with diffuse peritoneal spread. There is an absence of obvious primary site, and the ovaries are grossly normal or minimally involved [67]. Most reported cases are of primary peritoneal serous papillary carcinoma.

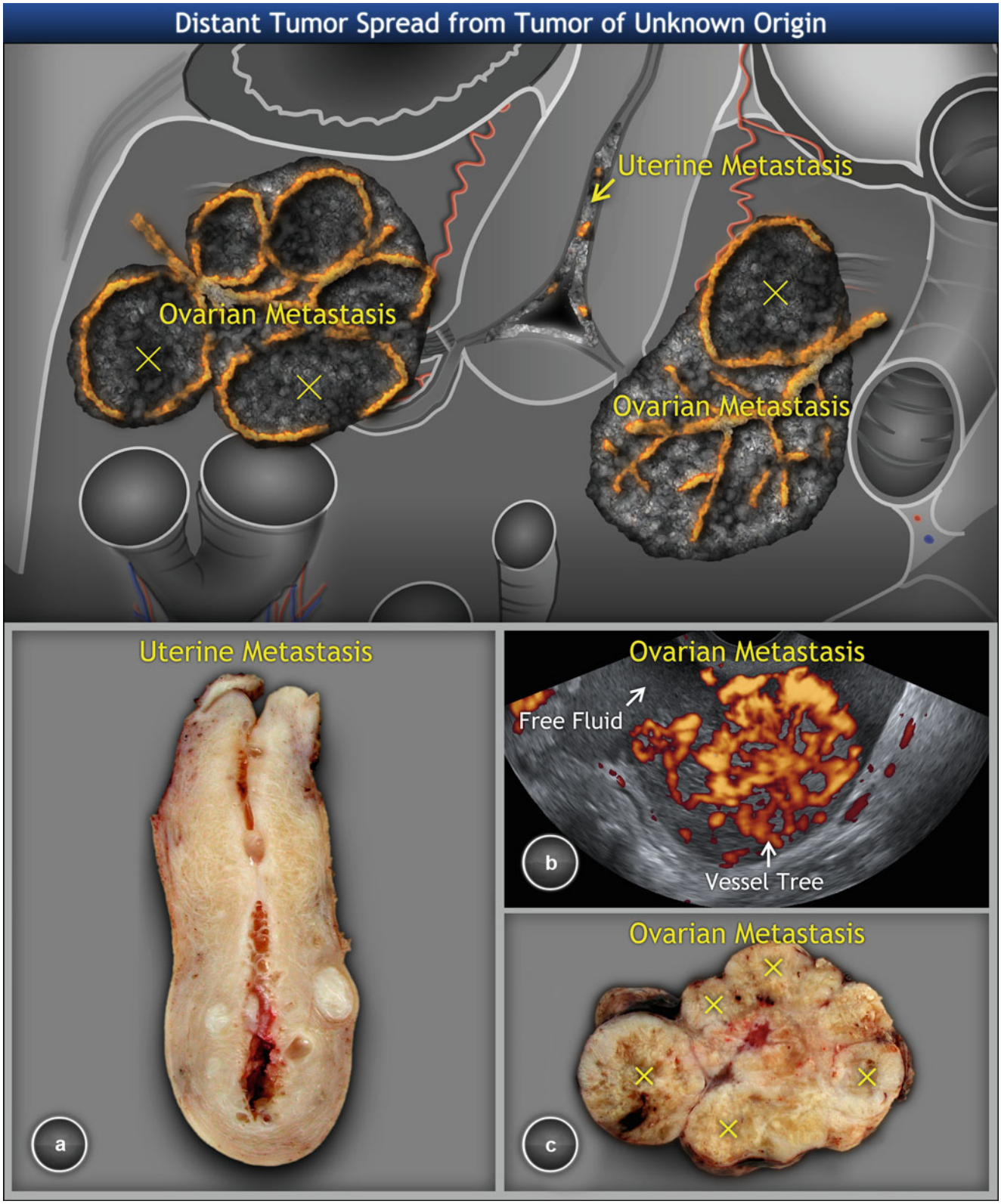

Fig. 24 Neuroendocrine tumor (NET) of unknown origin infiltrating ovaries and endometrial stroma. Sectioned specimen of uterus (**a**) with endometrial stroma involved by NET. (**b**) Power Doppler of left solid ovarian metastasis showing tumor vessel radiating in the center of ovary. (**c**) Sectioned specimen of the right ovarian metastasis shows multinodularity (marked with *crosses*) similar to that on schema

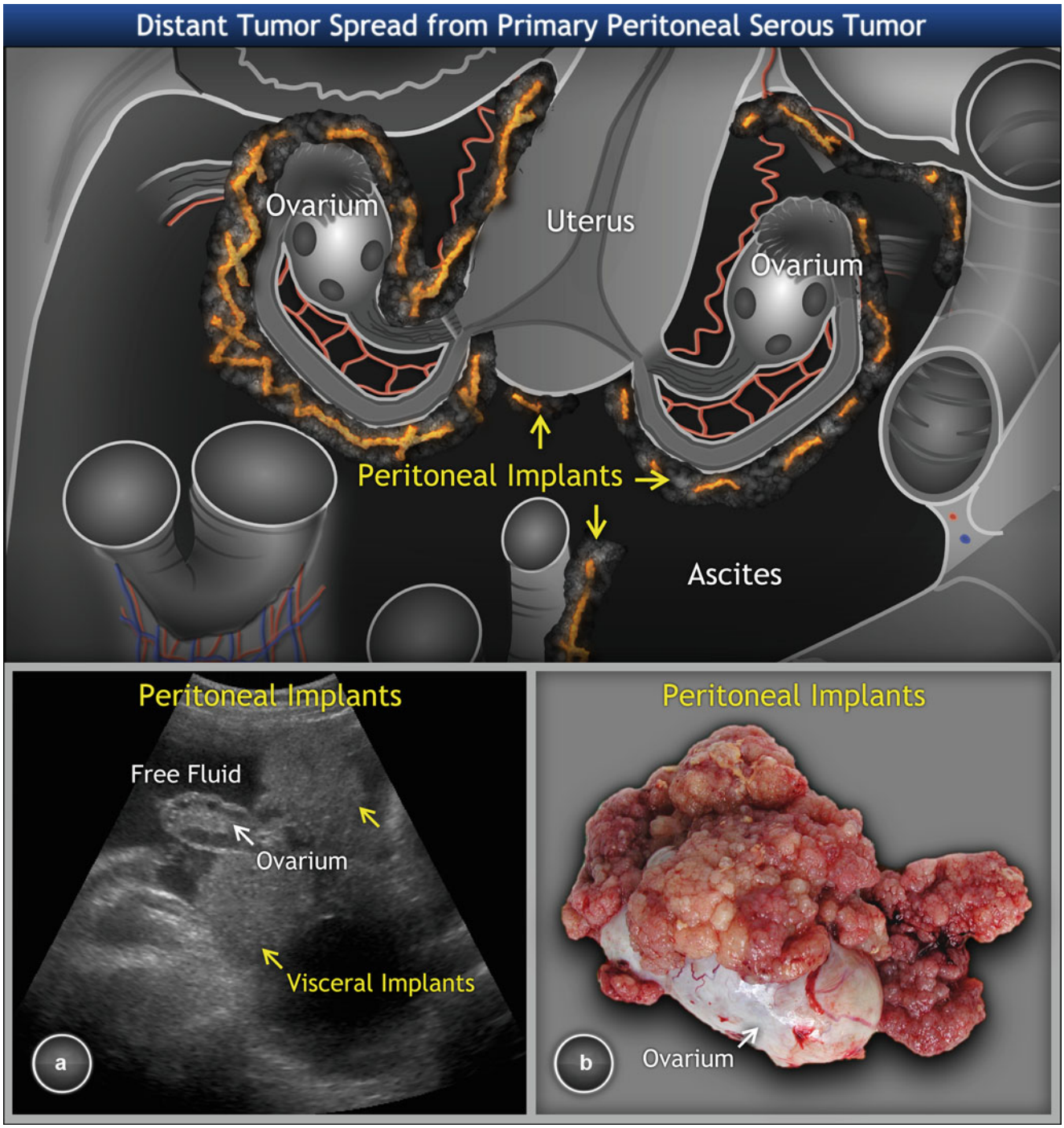

Fig. 25 Primary peritoneal serous tumor with ovarian implants. (**a**) Ultrasound finding of normal ovary surrounded by papillary serous tumor forming diffuse carcinomatosis involving the ovarian surface (visceral carcinomatosis). (**b**) Specimen of left ovary showing peritoneal spread onto the ovarian surface

Diagnosis

Peritoneal serous papillary carcinoma manifests with signs and symptoms similar to those of advanced ovarian carcinoma. The level of serum CA-125 corresponds to stages III–IV ovarian carcinoma [16].

Ovarian involvement often presents as small surface implants with retention of normal size and shape of the ovary (Fig. 25). Criteria for their distinguishing from primary ovarian serous carcinomas with peritoneal spread have been proposed by the Gynecologic Oncology Group and are as

follows: (1) both ovaries are either normal in size or enlarged by a benign process; (2) the bulk of the tumor is in the peritoneum, and the extent of tumor involvement at one or more extraovarian sites is greater than on the surface of either ovary; (3) microscopic examination of ovaries reveals no evidence of the tumor, which is confined to the surface epithelium with no sign of cortical invasion, or the tumor involves the ovarian surface and the underlying cortical stroma in an area less than 5 mm in diameter, or there is a tumor of less than 5 mm in diameter within the ovarian substance, with or without surface involvement; and (4) the histologic and cytologic characteristics of the tumor are predominantly serous and similar or identical to those of ovarian serous papillary adenocarcinoma of any grade [67].

The differential diagnosis includes metastatic serous carcinoma from an occult primary tubal or uterine serous carcinoma, or a malignant mesothelioma, or peritoneal carcinomatosis associated with an unknown primary tumor.

Conclusion

Secondary ovarian tumors present a special challenge to diagnosis within the scope of ovarian neoplasms, with the need for specific investigative and therapeutical approaches and especially adverse consequences in case of misdiagnosis as they often represent a first sign of a so far obscure primary tumor. Since these tumors are in many cases first discovered on ultrasound, basic features of their sonographic appearance and differential diagnostics should be known to an experienced examiner to arise the suspicion of extraovarian origin and to lead to the employment of further investigative methods (histological verification, detailed clinical history with the aim for possible occult tumor, targeted search for primary malignancy, etc.) in order to secure appropriate treatment in a timely manner.

Acknowledgement Thanks to Adam Preisler from the Faculty of Architecture, Czech Technical University in Prague for providing the illustrations. This work was supported by the Internal Grant Agency of the Ministry of Health, the Czech Republic (grant NT13070), and by Charles University in Prague (UNCE 204024 and PRVOUK-P27/LF1/1).

Biography Daniela Fischerova received her MD and PhD degrees at Charles University in Prague and her specialty training at Klinikum Kaufbeuren, Germany (Clinical Oncology), and at the Charles University (Obstetrics and Gynecology and Gynecologic Oncology). Currently, she is a senior consultant of the Gynecological Cancer Center at the General University Hospital of Charles University. She serves as a vice-president of the Czech Society of Ultrasound in Obstetrics and Gynecology and is a member of the scientific committee of International Society of Ultrasound in Obstetrics and Gynecology (ISUOG) and of a study group at the Arbeitsgemeinschaft für Gynäkologische Onkologie (AGO).

References

1. Young RH, Scully RE. Metastatic tumors in the ovary: a problem-oriented approach and review of the recent literature. Semin Diagn Pathol. 1991;8:250–76.
2. Fischerova D, Cibula D, Dundr P, et al. Ultrasound-guided tru-cut biopsy in the management of advanced abdomino-pelvic tumors. Int J Gynecol Cancer. 2008;18:833–7.
3. Zikan M, Fischerova D, Pinkavova I, et al. Ultrasound-guided tru-cut biopsy of abdominal and pelvic tumors in gynecology. Ultrasound Obstet Gynecol. 2010;36:767–72.
4. Fischerova D. Ultrasound scanning of the pelvis and abdomen for staging of gynecological tumors: a review. Ultrasound Obstet Gynecol. 2011;38:246–66.
5. Timmerman D, Valentin L, Bourne TH, et al. Terms, definitions and measurements to describe the sonographic features of adnexal tumors: a consensus opinion from the International Ovarian Tumor Analysis (IOTA) Group. Ultrasound Obstet Gynecol. 2000;16:500–5.
6. Guerriero S, Alcazar JL, Pascual MA, et al. Preoperative diagnosis of metastatic ovarian cancer is related to origin of primary tumor. Ultrasound Obstet Gynecol. 2012;39:581–6.
7. Testa AC, Mancari R, Di Legge A, et al. The 'lead vessel': a vascular ultrasound feature of metastasis in the ovaries. Ultrasound Obstet Gynecol. 2008;31:218–21.
8. Locker GY, Hamilton S, Harris J, et al. ASCO 2006 update of recommendations for the use of tumor markers in gastrointestinal cancer. J Clin Oncol. 2006;24:5313–27.
9. Malaguarnera G, Giordano M, Paladina I, et al. Markers of bile duct tumors. World J Gastrointest Oncol. 2011;3:49–59.
10. Steinberg W. The clinical utility of the CA 19–9 tumor-associated antigen. Am J Gastroenterol. 1990;85:350–5.
11. Guadagni F, Roselli M, Cosimelli M, et al. CA 72–4 serum marker – a new tool in the management of carcinoma patients. Cancer Invest. 1995;13:227–38.
12. Keshaviah A, Dellapasqua S, Rotmensz N, et al. CA15-3 and alkaline phosphatase as predictors for breast cancer recurrence: a combined analysis of seven International Breast Cancer Study Group trials. Ann Oncol. 2007;18:701–8.
13. Harris L, Fritsche H, Mennel R, et al. American Society of Clinical Oncology 2007 update of recommendations for the use of tumor markers in breast cancer. J Clin Oncol. 2007;25:5287–312.
14. Laboratory Medicine Practice Guidelines. 2010. Use of tumor markers in liver, bladder, cervical, and gastric cancers. www.aacc.org
15. Chaube A, Tewari M, Singh U, et al. CA 125: a potential tumor marker for gallbladder cancer. J Surg Oncol. 2006;93:665–9.
16. Van Calster B, Valentin L, Van Holsbeke C, et al. A novel approach to predict the likelihood of specific ovarian tumor pathology based on serum CA-125: a multicenter observational study. Cancer Epidemiol Biomarkers Prev. 2011;20:2420–8.
17. Scully RE, Richardson GS. Luteinization of the stroma of metastatic cancer involving the ovary and its endocrine significance. Cancer. 1961;14:827–40.
18. Testa AC, Ferrandina G, Timmerman D, et al. Imaging in gynecological disease (1): ultrasound features of metastases in the ovaries differ depending on the origin of the primary tumor. Ultrasound Obstet Gynecol. 2007;29:505–11.
19. Valentin L, Ameye L, Testa A, et al. Ultrasound characteristics of different types of adnexal malignancies. Gynecol Oncol. 2006;102:41–8.
20. Alcazar JL, Galan MJ, Ceamanos C, et al. Transvaginal gray scale and color Doppler sonography in primary ovarian cancer and metastatic tumors to the ovary. J Ultrasound Med. 2003;22:243–7.
21. Zikan M, Fischerova D, Pinkavova I, et al. Ultrasonographic appearance of metastatic non-gynecological pelvic tumors. Ultrasound Obstet Gynecol. 2012;39:215–25.
22. Prat J, Morice P. Secondary tumours of the ovary. In: Tavassoli FA, Devilee P, editors. Pathology and genetics of tumours of the breast and female genital organs. Lyon: IARC Press; 2003.
23. Seidman JD, Kurman RJ, Ronnett BM. Primary and metastatic mucinous adenocarcinomas in the ovaries: incidence in routine practice with a new approach to improve intraoperative diagnosis. Am J Surg Pathol. 2003;27:985–93.
24. Yemelyanova AV, Vang R, Judson K, et al. Distinction of primary and metastatic mucinous tumors involving the ovary: analysis of size and laterality data by primary site with reevaluation of an algorithm for tumor classification. Am J Surg Pathol. 2008;32:128–38.
25. Lerwill MF, Young RH. Metastatic tumors of the ovary. In: Kurman RJ, Ellenson LH, Ronnett BM, editors. Blaustein's pathology of the female genital tract. 6th ed. New York: Springer Science + Business Medica; 2011. p. 929–97.
26. Tso PL, Bringaze WL, Dauterive AH, et al. Gastric carcinoma in the young. Cancer. 1987;59:1362–5.
27. Hale RW. Krukenberg tumor of the ovaries. A review of 81 records. Obstet Gynecol. 1968;32:221–5.
28. Demopoulos RI, Touger L, Dubin N. Secondary ovarian carcinoma: a clinical and pathological evaluation. Int J Gynecol Pathol. 1987;6:166–75.
29. Savey L, Lasser P, Castaigne D, et al. Krukenberg tumors. Analysis of a series of 28 cases. J Chir (Paris). 1996;133:427–31.
30. Paladini D, Testa A, Van Holsbeke C, et al. Imaging in gynecological disease (5): clinical and ultrasound characteristics in fibroma and fibrothecoma of the ovary. Ultrasound Obstet Gynecol. 2009;34:188–95.
31. Guerriero S, Testa AC, Timmerman D, et al. Imaging of gynecological disease (6): clinical and ultrasound characteristics of ovarian dysgerminoma. Ultrasound Obstet Gynecol. 2011;37:596–602.
32. Birnkrant A, Sampson J, Sugarbaker PH. Ovarian metastasis from colorectal cancer. Dis Colon Rectum. 1986;29:767–71.
33. Graffner HO, Alm PO, Oscarson JE. Prophylactic oophorectomy in colorectal carcinoma. Am J Surg. 1983;146:233–5.
34. Judson K, McCormick C, Vang R, et al. Women with undiagnosed colorectal adenocarcinomas presenting with ovarian metastases: clinicopathologic features and comparison with women having known colorectal adenocarcinomas and ovarian involvement. Int J Gynecol Pathol. 2008;27:182–90.
35. Colon cancer. In: National Comprehensive Cancer Network Clinical Practice Guidelines in Oncology (NCCN Guidelines). Version 3.2012. www.nccn.org
36. Lash RH, Hart WR. Intestinal adenocarcinomas metastatic to the ovaries. A clinicopathologic evaluation of 22 cases. Am J Surg Pathol. 1987;11:114–21.
37. Ulbright TM, Goheen MP, Roth LM, et al. The differentiation of carcinomas of teratomatous origin from embryonal carcinoma. A light and electron microscopic study. Cancer. 1986; 57:257–63.
38. Ronnett BM, Kajdacsy-Balla A, Gilks CB, et al. Mucinous borderline ovarian tumors: points of general agreement and persistent controversies regarding nomenclature, diagnostic criteria, and behavior. Hum Pathol. 2004;35:949–60.
39. McKenney JK, Soslow RA, Longacre TA. Ovarian mature teratomas with mucinous epithelial neoplasms: morphologic heterogeneity and association with pseudomyxoma peritonei. Am J Surg Pathol. 2008;32:645–55.
40. Ronnett BM, Seidman JD. Mucinous tumors arising in ovarian mature cystic teratomas: relationship to the clinical syndrome of pseudomyxoma peritonei. Am J Surg Pathol. 2003;27:650–7.
41. van Ruth S, Hart AA, Bonfrer JM, et al. Prognostic value of baseline and serial carcinoembryonic antigen and carbohydrate antigen 19.9 measurements in patients with pseudomyxoma peritonei treated with cytoreduction and hyperthermic intraperitoneal chemotherapy. Ann Surg Oncol. 2002;9:961–7.

42. Fruscella E, Testa AC, Ferrandina G, et al. Ultrasound features of different histopathological subtypes of borderline ovarian tumors. Ultrasound Obstet Gynecol. 2005;26:644–50.
43. Robboy SJ, Scully RE, Norris HJ. Carcinoid metastatic to the ovary. A clinicopathologic analysis of 35 cases. Cancer. 1974;33:798–811.
44. Strosberg J, Nasir A, Cragun J, et al. Metastatic carcinoid tumor to the ovary: a clinicopathologic analysis of seventeen cases. Gynecol Oncol. 2007;106:65–8.
45. Ulbright TM, Roth LM, Stehman FB. Secondary ovarian neoplasia. A clinicopathologic study of 35 cases. Cancer. 1984;53:1164–74.
46. Brown BL, Scharifker DA, Gordon R, et al. Bronchial carcinoid tumor with ovarian metastasis: a light microscopic and ultrastructural study. Cancer. 1980;46:543–6.
47. Riopel MA, Ronnett BM, Kurman RJ. Evaluation of diagnostic criteria and behavior of ovarian intestinal-type mucinous tumors: atypical proliferative (borderline) tumors and intraepithelial, microinvasive, invasive, and metastatic carcinomas. Am J Surg Pathol. 1999;23:617–35.
48. Seidman JD, Soslow RA, Vang R, et al. Borderline ovarian tumors: diverse contemporary viewpoints on terminology and diagnostic criteria with illustrative images. Hum Pathol. 2004;35:918–33.
49. Young RH, Scully RE. Differential diagnosis of ovarian tumors based primarily on their patterns and cell types. Semin Diagn Pathol. 2001;18:161–235.
50. Khunamornpong S, Lerwill MF, Siriaunkgul S, et al. Carcinoma of extrahepatic bile ducts and gallbladder metastatic to the ovary: a report of 16 cases. Int J Gynecol Pathol. 2008;27:366–79.
51. Khan SA, Davidson BR, Goldin R, et al. Guidelines for the diagnosis and treatment of cholangiocarcinoma: consensus document. Gut. 2002;51 Suppl 6:VI1–9.
52. Gagnon Y, Tetu B. Ovarian metastases of breast carcinoma. A clinicopathologic study of 59 cases. Cancer. 1989;64:892–8.
53. Young RH, Carey RW, Robboy SJ. Breast carcinoma masquerading as primary ovarian neoplasm. Cancer. 1981;48:210–2.
54. Harris M, Howell A, Chrissohou M, et al. A comparison of the metastatic pattern of infiltrating lobular carcinoma and infiltrating duct carcinoma of the breast. Br J Cancer. 1984;50:23–30.
55. Seidman JD, Cho KR, Ronnett BM, et al. Surface epithelial tumors of the ovary. In: Kurman RJ, Ellenson LH, Ronnett BM, editors. Blaustein's pathology of the female genital tract. 6th ed. New York: Springer Science + Business Medica; 2011.
56. Van Holsbeke C, Domali E, Holland TK, et al. Imaging of gynecological disease (3): clinical and ultrasound characteristics of granulosa cell tumors of the ovary. Ultrasound Obstet Gynecol. 2008; 31:450–6.
57. Ferry JA. Hematologic neoplasm and selected tumor-like lesions involving the female reproductive organs. In: Kurman RJ, Ellenson LH, Ronnett BM, editors. Blaustein's pathology of the female genital tract. 6th ed. New York: Springer Science + Business Medica; 2011.
58. Barcos M, Lane W, Gomez GA, et al. An autopsy study of 1206 acute and chronic leukemias (1958 to 1982). Cancer. 1987;60:827–37.
59. Kurman RJ, Shih Ie M. The origin and pathogenesis of epithelial ovarian cancer: a proposed unifying theory. Am J Surg Pathol. 2010;34:433–43.
60. Takeshima N, Hirai Y, Yano K, et al. Ovarian metastasis in endometrial carcinoma. Gynecol Oncol. 1998;70:183–7.
61. Epstein E, Van Holsbeke C, Mascilini F, et al. Gray-scale and color Doppler ultrasound characteristics of endometrial cancer in relation to stage, grade and tumor size. Ultrasound Obstet Gynecol. 2011;38:586–93.
62. Ulbright TM, Roth LM. Metastatic and independent cancers of the endometrium and ovary: a clinicopathologic study of 34 cases. Hum Pathol. 1985;16:28–34.
63. Prat J, Matias-Guiu X, Barreto J. Simultaneous carcinoma involving the endometrium and the ovary. A clinicopathologic, immunohistochemical, and DNA flow cytometric study of 18 cases. Cancer. 1991;68:2455–9.
64. Halperin R, Zehavi S, Hadas E, et al. Simultaneous carcinoma of the endometrium and ovary vs endometrial carcinoma with ovarian metastases: a clinical and immunohistochemical determination. Int J Gynecol Cancer. 2003;13:32–7.
65. Tabata M, Ichinoe K, Sakuragi N, et al. Incidence of ovarian metastasis in patients with cancer of the uterine cervix. Gynecol Oncol. 1987;28:255–61.
66. Young RH, Gersell DJ, Roth LM, et al. Ovarian metastases from cervical carcinomas other than pure adenocarcinomas. A report of 12 cases. Cancer. 1993;71:407–18.
67. Bloss JD, Liao SY, Buller RE, et al. Extraovarian peritoneal serous papillary carcinoma: a case–control retrospective comparison to papillary adenocarcinoma of the ovary. Gynecol Oncol. 1993;50: 347–51.

Metastatic Tumours of the Ovaries: Computed Tomography and Magnetic Resonance

Stavroula Kyriazi, Jennifer C. Wakefield, and Nandita M. deSouza

Abstract

The ovaries constitute common sites for metastatic spread, and the distinction between a primary or secondary tumour is critical for appropriate patient management, especially when ovarian involvement is the initial manifestation of disease. Familiarisation with the typical imaging features according to the site of origin may assist in recognising the metastatic aetiology of these tumours.

Keywords

Metastatic neoplasm • Krukenberg tumour • Imaging • Computed tomography • Magnetic resonance

Introduction

Metastatic tumours are thought to account for 15–28 % of ovarian malignancies in the Western world [1–4], their frequency reflecting geographic variations in the incidence of certain types of cancer, as exemplified by the increased incidence of gastric cancer in the Japanese population [5]. They generally carry a dismal prognosis, with a median survival time of 7–20 months [2, 6, 7]. The primary nongenital sites which can metastasise to the ovaries include colon, stomach, breast, pancreas, lung, gallbladder, small intestine, kidneys and liver, as well as lymphoma, melanoma, sarcoma and carcinoid [5, 8, 9]. The precise incidence of ovarian metastases is difficult to determine due to factors relating to the biological diversity of the primary disease. A metastatic origin is generally presumed on the basis of a history of known malignancy and a resemblance of the ovarian lesion to the extra-ovarian tumour. However, several pitfalls may exist within this simple scenario. First, prior cancer history is only present in 20–38 % of cases [10–12]. Second, metastases, even when concurrent, may demonstrate different macro- and microscopic features from the primary tumour; the typical discrepancies include the frequently cystic appearance of metastases originating from a non-cystic primary and the presence of "follicle-like spaces" which resemble primary granulosa cell tumours [13]. The distinction between primary and metastatic ovarian neoplasms is of critical importance, since surgical cytoreduction constitutes the treatment of choice in the first group but is of disputed value in the second [7, 11, 14, 15]. Preoperative differentiation acquires even greater importance given the fact that in approximately 32–38 % of patients with synchronous metastases from the digestive system the prevalent clinical symptomatology arises from the ovarian lesions, leading to their detection earlier than the extra-ovarian primary [12, 16, 17]. Furthermore, in 17–44 % of patients the primary extragenital site is discovered either concomitantly or subsequently to diagnostic laparotomy for the ovarian mass [12, 18].

This chapter reviews the biologic diversity of secondary tumours to the ovary and describes their appearances on cross-sectional imaging (CT and MRI), with special focus

S. Kyriazi, MD (✉)
Department of CT/MRI, Athens Medical Centre, Distomou 5-7, Athens 15125, Greece
e-mail: stavroula.kyriazi@icr.ac.uk

J.C. Wakefield, FRCR • N.M. deSouza, BSc, MBBS, MRCP, MD, FRCP
Cancer Research UK and EPSRC Cancer Imaging Centre, Institute of Cancer Research and the Royal Marsden NHS Foundation Trust, Sutton, Downs Road, Surrey SM2 5PT, UK

L. Saba et al. (eds.), *Ovarian Neoplasm Imaging*,
DOI 10.1007/978-1-4614-8633-6_23, © Springer Science+Business Media New York 2013

on mucinous (including Krukenberg type), non-mucinous and endometrioid histological subtypes.

Demographics, Clinical Presentation and Prognosis

The majority of ovarian metastases originate in the gastrointestinal tract, with colorectal, gastric and appendiceal sites being the most frequent primary sources [19–23]. In a Scandinavian series of 255 patients with microscopically confirmed nongenital metastatic disease to the ovaries, 57.6 % had a primary gastrointestinal tumour, of whom 29.4 % had colorectal, 16.1 % gastric and 3.1 % appendiceal cancer, followed by pancreatic and small intestine (2.7 % each), gallbladder (1.7 %), oesophageal (0.8 %) and hepatocellular cancer (0.4 %) [23]. Among the 35 % of patients with a non-gastrointestinal tract malignancy, the vast proportion (29.4 %) had breast cancer, followed by lung (2.0 %), melanoma (1.6 %), kidney (0.8 %), lymphoma (0.8 %) and thyroid cancer (0.4 %). Tumours of an unknown primary origin have been reported in 7.5–16.9 % of cases [21, 23]. Genital tract metastases, mainly from carcinoma of the endometrium, account for 2.9–8 % of concomitant ovarian masses [24, 25]. Rarer primary sites include cervical carcinoma (mainly adenocarcinoma vs. squamous) [26–29], transitional cell carcinoma of the renal pelvis/ureter [30, 31], sarcomas [32], gastrointestinal stromal tumours (GIST) [33], malignant mesothelioma [34] and desmoplastic round cell tumours [35].

Women with ovarian nongenital tract metastases tend overall to be of a younger age than those with primary ovarian cancer (median age 46–53 years vs. 63 years, respectively) [11, 21–23, 36]. The origin of primary disease appears to determine different age distributions for the presence of metastatic disease. In the Scandinavian series, the median age of women with metastases from gastrointestinal primaries was 63 years compared to 50 years for their non-GI tract counterparts (predominantly arising from breast cancer) and did not differ considerably from the age of primary ovarian cancer diagnosis [23]. However, when studied in isolation, premenopausal women with gastrointestinal cancers have a three- to fivefold higher propensity to develop metastases to the ovaries compared with their postmenopausal counterparts [1, 37, 38]. Age and reproductive status as risk factors for ovarian involvement seem to be more pronounced in gastric cancer, possibly due to the interacting effect of histological variants. The signet-ring cell subtype of gastric adenocarcinoma has an increased incidence in younger patients compared to the intestinal subtype [39] with an approximately 4-fold propensity for ovarian spread [13], accounting, therefore, for the younger age predilection of gastric-associated metastatic disease to the ovaries. Moreover, women who present with ovarian metastases in the absence of a history of a known colorectal primary appear to be significantly younger than those with a precedent or concomitant (at the time of surgical exploration) diagnosis of colorectal cancer (median age, 47 vs. 61 years, respectively; $p=0.002$) [40]. Furthermore, bilateral involvement, both gross and microscopic, has been reported as significantly higher in the group with the undiagnosed primary (75 % vs. 32 %; $p=0.005$), suggesting the increased susceptibility of younger patients to metastatic seeding to the ovaries [40].

Overall ovarian metastases precede the diagnosis of the primary tumour in approximately 38–41 % of cases [12, 23, 41]. However, the type of primary malignancy appears to influence the sequence of clinical diagnosis, as in 41 % and 56 % of metastases from colorectal and gastric cancer, respectively, the diagnosis was made concomitantly or subsequently to surgical exploration of an abdominal or pelvic mass, in contrast to 12 % for breast and 87 % for appendiceal cancer [23]. A metachronous appearance has been documented in approximately 45–62 % of ovarian metastases from nongenital cancers, with a median time to clinical diagnosis of metastatic disease of 11.5 months for breast, 13.5 months for colorectal and 15.5 months for gastric cancer [22, 41, 42].

Clinical presentation of disease is frequently dominated by non-specific symptoms, such as abdominopelvic pain, distension, mass and nausea/vomiting, which have been reported with a frequency of 61–64 %, 22–46 %, 12–50 % and 21–46 %, respectively [11, 16, 43]. Rectal bleeding and change in bowel habits associated with a colorectal primary may be the presenting complaint in 14 % and 13–21 %, respectively [43, 44]. Vaginal bleeding has been reported in 4–9 % of patients with ovarian metastases, rising to 37 % in the subset with an endometrial primary [43, 45, 46]. Ovarian metastases, together with mucinous and endometrioid primary tumours, are the types mostly associated with hormonal production secondary to luteinisation of the stroma ("ovarian tumour with functioning stroma") [47–49]. Endocrine abnormalities usually involve androgen secretion, although progesterone and estrogens may be also produced [47, 50]. Approximately 10 % of patients remain asymptomatic, especially in the presence of an appendiceal or intestinal primary [11].

The prognosis for women with ovarian metastases is dismal, as overall 5-year survival has been reported 7.2–36 % compared to 40.8 % for women with primary ovarian cancer (epithelial and non-epithelial FIGO stages I–IV), with a median survival time of 42 months [2, 22, 23]. A relative better prognosis is associated with metastases from breast cancer, which carry a 5-year survival rate of 26–44 % in contrast to 8–12 % and 1–5.4 % for colorectal and gastric cancer, respectively [22, 23, 51]. Favourable prognostic factors include an unknown primary (adjusted hazard ratio for death, 0.30; 95 % CI, 0.16–0.59), a non-GI primary (HR, 0.61; 95 % CI, 0.43–0.86) and diagnosis of primary disease before surgery (HR, 0.78; 95 % CI, 0.57–1.05) [23]. An exception to the overall poor prognosis lies in metastatic spread from uterine malignancy, which carries a cumulative 5-year survival rate of 84–86 % [25, 46]. Moreover, patients with pseudomyxoma peritonei and ovarian metastases from mucinous appendiceal carcinoma, treated

with cytoreductive surgery and intraperitoneal chemotherapy, attain 5-year survival rates of 52–96 % [52].

Metastatic Pathway

Dissemination of non-gynaecological malignancy to the ovaries is haematogenous, lymphatic, transperitoneal or by direct extension [53, 54]. The first two routes require an aggressive histology for vascular invasion. However, the majority of ovarian secondary deposits occur in the absence of haematogenous metastatic disease in the lungs and liver, indicating the importance of the transperitoneal route. Transcoelomic spread may even occur in low-grade tumours, such as mucinous appendiceal or diffuse gastric carcinoma, which can mechanically dissect through the bowel wall and exfoliate tumour cells into the peritoneal cavity [54]. In premenopausal patients, the functioning ovary offers a hospitable environment for the adhesion of free tumour emboli, as follicular rupture incites a local inflammatory/haemorrhagic reaction coupled with a morphological rearrangement of the ovarian surface, which promotes tumour cell entrapment [55]. Increased vascularity of the ovarian stroma in the peri- and post-ovulatory phase further promotes the implantation and growth of tumour cells. In postmenopausal women haematogenous spread associated with a more invasive tumour histology is postulated, especially in the presence of hormonal dependency and multisystem metastatic disease [54]. Moreover, the accumulation of "milky spots", which are mesenchymal conglomerates with a prominent lymphatic component, in the perigonadal fat, combined with the higher concentration of free intraperitoneal tumour cells in gravity-dependent regions of the pelvis, facilitates their adherence on ovarian surface, even in the absence of functional hyperaemia [54]. Direct infiltration is the mechanism of spread in only 12–16 % of colorectal primaries, supported by the finding that the anatomic location of the primary tumour does not impact the incidence and laterality of ovarian metastases [56]. However, the incidence of ovarian metastases appears to correlate with the stage of the colorectal primary (31.8–40 % in Dukes' stage B and 60–68.2 % in Dukes' stage C), indicating a transmural/transperitoneal mechanism of tumour extension [56, 57]. Peritoneal seeding and haematogenous/lymphogenous dissemination have been reported in 93.7–95 % and 39.7–40 % of cases, respectively [56, 58].

General Imaging Features

Bilaterality

Bilaterality has been reported in 59–75 % of ovarian metastases on imaging studies and should potentially alert to the possibility of metastatic adnexal disease [41, 59–61]. In a surgical series of 154 women with nongenital cancers metastatic to the ovaries, bilateral involvement was confirmed in 57 % of patients [11]. An exception are metastases from endometrial cancer, which have been reported as unilateral in 79–86 % of cases [62]. However, bilaterality does not constitute a reliable discriminator for the origin of an ovarian lesion, since primary undifferentiated and serous ovarian adenocarcinoma have been reported as bilateral in up to 58 % of cases, whereas mucinous and endometrioid subtypes in 21 and 27 %, respectively [63].

Size

Metastatic tumours have been generally reported to be smaller than primary ones. In a series of 114 patients with primary and secondary adnexal masses, median size of metastases was 64 mm (95 % CI, 62–89 mm) compared to 105 mm (95 % CI, 104–143 mm) for primary cancers ($p=0.0002$) [36]. However, metastatic lesions, size may depend on the organ of origin, as cancer of the breast, stomach and uterus and lymphoma have been associated with significantly smaller metastases than gastrointestinal tract malignancies [36, 64].

Multilocularity

In a multimodality imaging study of 110 malignant ovarian masses the feature of multilocularity was found in 74 % of primary and 36 % of metastatic tumours on MRI ($p=0.01$) and was ascribed an 81 % positive predictive value and 61 % negative predictive value for a primary origin [65]. However, multilocularity demonstrated with CT was not significantly different between the two groups (51 % vs. 50 %; $p=0.99$), indicating the suboptimal capacity of the modality to delineate septa [65].

Composition

The appearance of metastatic lesions regarding a cystic or solid composition is variable. In a study of 34 ovarian metastases from non-gynaecological primary tumours, 13 (38 %) were predominantly cystic, 13 (38 %) were mixed cystic/solid and 8 (24 %) were predominantly solid [41]. In a series of 38 females with ovarian metastases and a control group of 76 patients with primary epithelial cancers, 50 % of metastatic and 10 % of primary tumours were solid ($p<0.005$), whereas 17 % of metastatic and 55 % of primary tumours were mixed ($p<0.001$) [36]. In a sonographic study of 67 patients with surgically confirmed secondary deposits to the ovaries, a solid appearance was found in 93 % of tumours derived from gastric, breast, uterine and lymphoma primaries in contrast to 18 % of tumours from colorectal, appendiceal and biliary primaries ($p<0.0001$) [64]. The latter group

was associated with multilocular or complex solid/multilocular metastases in 95 % [64].

MR Signal Intensity

Signal heterogeneity in both T1- and T2- weighted sequences has been documented in 33–81 % of ovarian metastases, regardless of their solid or cystic composition [61]. The presence of various amounts of T2-hypointense and T1-isointense (with reference to the myometrium) solid components in approximately 57 % of lesions has been histologically correlated to dense stromal fibrotic reaction [61]. Well-defined cystic components tend to exhibit homogeneously increased T2 signal intensity, consistent with serous fluid, or occasionally T1-hyperintensity, indicative of proteinaceous content or products of haemoglobin degradation. Ill-defined cysts display raised T2 signal heterogeneity, pathologically corresponding to a mixture of mucinous, serous and hemorrhagic elements. In a series of 86 primary and 10 secondary ovarian lesions, 33 % of primary tumours were characterised as highly proteinaceous or hemorrhagic and 24 % as of clear fluid content, whereas 60 % of metastases were designated as soft tissue ($p=0.02$); however, the reliability of this feature is hampered by the small number of metastases [65].

Vascularity

Moderate to strong contrast enhancement has been reported in the solid components of ovarian metastases and to a lesser degree in areas of mucinous or oedematous composition [61]. However, quantitative Doppler ultrasonography studies have not demonstrated any consistent differences in the haemodynamic behaviour of primary and metastatic tumours. A study of 36 primary and 6 secondary tumours documented a greater lowest resistive index (RI) in the cyst wall of metastases (0.77 vs. 0.54, $p=0.01$) but no difference in the pulsatility index (PI) [65]. In another study of adnexal masses in women with breast cancer, 54 % of malignant lesions had an abnormal PI compared to 40 % of benign, but the difference did not reach statistical significance [66]. No significant differences were seen in lowest RI, PI and maximal peak systolic velocity in a larger study of 143 patients with primary and metastatic lesions, implying similar angiogenic processes in the two groups [67].

Peritoneal Seeding

Peritoneal seeding on preoperative imaging has been reported in 44 % of metastases from colorectal tumours and in 60 % of primary ovarian cancer, but the difference was not statistically significant ($p=0.33$) [68]. In a study of 24 patients with ovarian metastases from extragenital primaries, 13 (54 %) had evidence of peritoneal dissemination with or without other visceral deposits or retroperitoneal lymphadenopathy and 11 (46 %) had macroscopically detectable disease limited to the adnexa [41]. Laparotomy findings in 116 patients report a 45 % incidence of peritoneal carcinomatosis in secondary tumours compared to 28 % in primary, although the difference was similarly nonsignificant [36]. The sensitivity of MRI in identifying coexistent peritoneal carcinomatosis has been reported as 82 % [61].

Krukenberg Tumours

The classic definition of Krukenberg tumours according to the World Health Organisation comprises the presence of mucin-producing neoplastic signet-ring cells and diffuse sarcomatoid proliferation of the ovarian stroma [69]. Krukenberg tumours represent approximately 1–2 % of all adnexal and 10–40 % of metastatic tumours [3, 10]. They were first described in 1896 by Friedrich Krukenberg (1871–1946), a German gynaecologist and pathologist, as a type of fibrosarcomatous tumour with an epithelial component [70]. Their metastatic origin from gastrointestinal adenocarcinomas was established 6 years later by Schlagenhaufer [71]. However, the term is often liberally albeit inaccurately used to denote all metastatic adnexal tumours from adenocarcinomas or gastrointestinal primaries.

The most common primary tumour associated with Krukenberg metastases in approximately 76 % of cases is gastric adenocarcinoma of signet-ring cell type (infiltrative or diffuse) [72]. Other primary sites include colon/rectum (11 %), appendix (5 %), breast (4 %) and gallbladder/biliary tract (3 %), while rare causes include pancreas, small intestine and urinary bladder [31, 72, 73]. In a series of 120 histologically proven Krukenberg tumours, the primary site of 62 (52 %) could not be identified [72].

Histologically the hallmark of Krukenberg tumours is a greater than 10 % epithelial component of mucin laden signet-ring cells, which characteristically are individually disposed. This classic type must be occasionally differentiated from primary mucinous adenocarcinoma and mucinous carcinoid tumour, either primary or metastatic (mainly from the appendix) [74]. However, primary mucinous tumours tend to be unilateral and display a more complex papillary epithelial growth pattern [75], whereas immunohistochemical identification of chromogranin and synaptophysin favours the diagnosis of a mucinous carcinoid tumour [1]. In the "tubular" variant of Krukenberg lesions, the arrangement of signet-ring cells follows a tubular pattern, which may warrant differentiation from a Sertoli-Leydig tumour, especially in the presence of luteinisation of the stroma and hormonal

secretion [8]. Nevertheless, Sertoli-Leydig tumours typically demonstrate less nuclear atypia [74] and stain positive to inhibin and negative to cytokeratins 7 and 20, as opposed to Krukenberg tumours [76, 77]. The mesenchymal component of Krukenberg tumours consists of ovarian fibrous stroma with varying degrees of oedema. A prominent desmoplastic reaction is occasionally encountered and may obscure the signet-ring cell pattern, requiring discrimination from a sclerosing stromal tumour, in which case negative mucin stains are helpful [8].

Krukenberg tumours constitute the type most frequently associated with stromal luteinisation and endocrine manifestations, especially in the setting of a pregnant patient experiencing virilisation. Among non-endocrine ovarian lesions with an androgenic stroma approximately 30 % are Krukenberg tumours, particularly those of gastric origin [13, 50]. Due to clinicopathological similarities, this feature may lead to an erroneous diagnosis of a Sertoli-Leydig sex cord-stromal tumour, especially if the Krukenberg tumour has a tubular microscopic pattern, and less frequently of a luteinised thecoma or a sclerosing stromal tumour [13].

The typical CT and MRI features, accounting for 67–86 % of Krukenberg tumours, are bilateral, lobulated and predominantly solid ovarian lesions with cystic components, the extent of which increases with overall lesion size due to haemorrhage and necrosis [59, 61]. Size is variable (range of diameter, 4–30 cm; mean diameter, 8–16 cm) and not helpful in discriminating from primary ovarian tumours, but predominantly solid masses tend to be smaller than cystic, indicating that cystic degeneration may be instigated by tumour growth [59, 61]. In a study of 32 Krukenberg tumours, 69 % were solid masses with intratumoural cysts, compared to 6 % of primary ovarian lesions ($p=0.001$), while only 12 % of Krukenberg tumours were predominantly cystic, compared to 63 % of primary ovarian lesions ($p=0.004$) [59]. Preservation of ovarian contour is a typical imaging finding [78]. Surface adhesions and peritoneal implants are generally uncommon, seen in approximately 15 % of cases [59]. Solid components are typically iso- and hypointense on T1- and T2-weighted images, respectively, ill-defined and randomly located in the periphery or central portion of the mass (Figs. 1 and 2) [78]. On diffusion-weighted imaging (DWI), the solid components typically demonstrate restricted diffusion, in keeping with increased cellularity or dense fibrosis, whereas myxoid areas have intermediate diffusion, indicative of raised viscosity (Fig. 2). On haemodynamic studies, the enhancement pattern tends to be heterogeneous, with areas of early and intense contrast uptake, which is sustained in the delayed interstitial phase (Figs. 1 and 3). T2-hypointensity of the solid elements has been correlated to the presence of dense collagenous stroma [61]; a similar appearance may occur in primary sex cord-stromal tumours, such as thecomas, fibrothecomas and sclerosing stromal tumours, as well as in primary undifferentiated carcinomas, although bilaterality favours a diagnosis of Krukenberg tumour [78, 79]. T2-weighted hyperintensity in the solid portions may stem from the production of mucin [79] or reflect the presence of oedema within connective tissue [80]. The presence of well-demarcated intratumoural cysts, surrounded by a hypointense rim of 3–5 mm in thickness, has been reported in 69 % of Krukenberg tumours [59] (Fig. 4). Strong contrast enhancement of their wall has been observed in 64 % of the cysts and has been pathologically correlated with compact tumour cell organisation surrounded by loose pericystic stroma [59]. Fibrous adhesions or peritoneal implants are not regularly seen [78].

Metastatic Mucinous Adenocarcinomas (Non-Krukenberg Type)

The majority of mucinous ovarian adenocarcinomas are metastatic; in a series of 52 mucinous ovarian tumours, 40 (77 %) were secondary deposits, originating in descending order of frequency from the gastrointestinal tract (35 %), pancreas (15 %), uterine cervix (10 %), breast (6 %) and endometrium (4 %), while in 7 % the primary site could not be identified [81]. Bilateral distribution and tumour size <10 cm were strongly associated with metastases (respective frequencies 77–94 % and 87–95 %), inasmuch as the criterion of a unilateral lesion larger than >10 cm could predict a primary tumour with 84–90 % accuracy [81, 82]. In a retrospective study of 194 mucinous tumours, performance of the algorithm was optimised at a size cut-off value of 13 cm, with correct classification of 98 % of primary tumours and 82 % of metastases (87 % overall accuracy) [83].

Mucinous metastases mainly originate from the uterine cervix (particularly adenocarcinomas) [28, 29, 84, 85], colon [86], pancreas [87, 88], gallbladder [73, 89] and appendix [90] and need to be differentiated from primary mucinous tumours of the ovaries. The most pertinent morphological and clinical criteria include localisation of mucin (intra- vs. extracellular), laterality and size of the lesion, presence of peritoneal dissemination and metastatic growth pattern (defined by ovarian surface involvement, lymphovascular invasion and desmoplastic response) [91]. For example, predominantly extracellular distribution of mucin, designating a colloid subtype of tumour, with concomitant peritoneal disease, defines pseudomyxoma peritonei, which most frequently arises from appendiceal low-grade or colloid mucinous carcinomas [92]. The term pseudomyxoma ovarii is used to describe extracellular mucin in tumour confined to the ovary and is frequently associated with ovarian mature teratomas [93]. Unilateral cystic carcinomas with predominantly intracellular deposition of mucin (greater than 50 % in

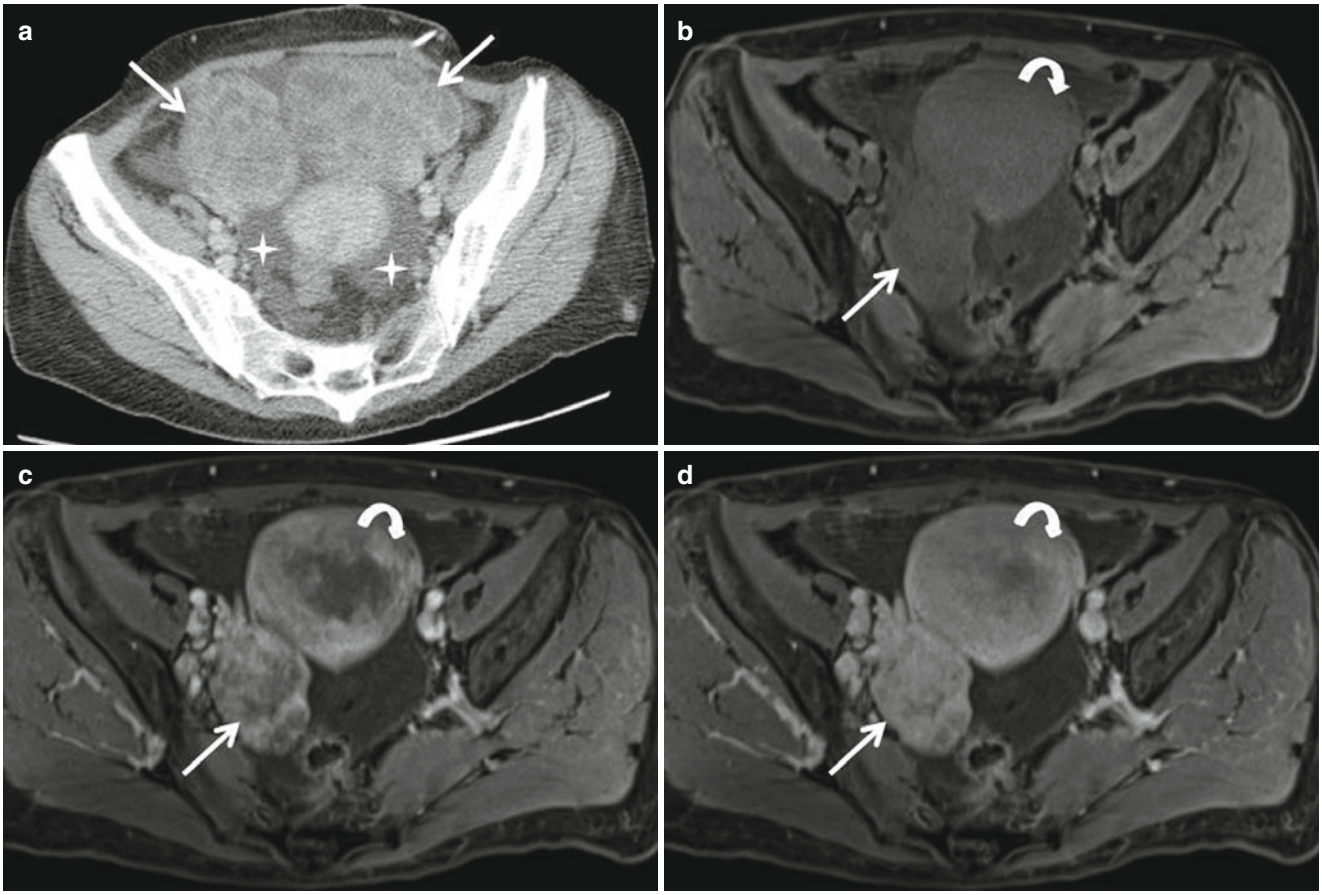

Fig. 1 Synchronous Krukenberg tumours of the ovaries in a 60-year-old woman who presented with abdominal distension. (**a**) Axial contrast-enhanced CT image demonstrates bilateral, bosselated, predominantly solid ovarian masses (*arrows*) with multiple minor cystic components and a heterogeneous enhancement pattern. A small amount of ascites is present (*asterisks*). Axial T1-weighted Volumetric Interpolated Breath-hold Examination (VIBE) images with fat-saturation pre- (**b**), 30 s (**c**) and 180 s (**d**) post-gadolinium injection demonstrate avid early heterogeneous enhancement of the right adnexal tumour, which persists in the delayed phase (*arrows*). The uterus is also seen (*curved arrows*)

at least 90 % of tumour cells) are the hallmark of primary mucinous tumours. Invasive mucinous carcinomas are distinguished from their low-grade counterparts by the presence of focal stromal invasion greater than 5 mm or an expansile growth pattern with lack of intervening stroma. Presence of peritoneal spread directs to a high probability of a metastatic origin of cystic tumours with intracellular mucin. In a histopathological study of 43 metastatic and 25 stage I primary mucinous tumours, morphological features indicating a metastatic vs. primary origin were bilaterality (75 % vs. 0 %, $p<0.0001$), microscopic surface involvement (79 % vs. 0 %, $p<0.0001$), an infiltrative invasive pattern (usually with desmoplastic stroma) (91 % vs. 16 %, $p<0.0001$), nodular growth pattern (42 % vs. 0 %, $p=0.0003$) and hilar involvement (31 % vs. 4 %, $p=0.0105$) [94]. Findings associated with primary tumours were size > 10 cm (88 % vs. 48 %, $p=0.007$), a smooth surface (80 % vs. 38 %, $p=0.005$), expansile invasive pattern (usually with no intervening stroma) (88 % vs. 18 %, $p<0.0001$), microscopic cysts < 2 mm (84 % vs. 40 %, $p=0.002$) and benign- or borderline-appearing regions (57–76 % vs. 30–36 %, $p \leq 0.045$). Macroscopic features which were not found discriminatory were a predominantly cystic or solid gross appearance and presence of focal papillary, necrotic or hemorrhagic areas [94].

On CT and MRI mucinous metastases from colorectal cancer typically manifest as unilocular or multilocular, predominantly cystic masses with various degrees of attenuation/signal intensity of the cystic components, reflecting the concentration of mucin and the extent of necrosis [68, 80]. Typically contrast enhancement is demonstrated by the internal septations and solid components [80]. In a study of 52 ovarian masses, smooth oval contours were reported in 92 % of metastases from colorectal cancer compared to 45 % of primary adnexal malignancies and were ascribed an odds ratio of 24.3 for the prediction of a metastatic aetiology [68]. Furthermore, a predominantly cystic appearance was documented in 86 % of metastases in contrast to 36 %

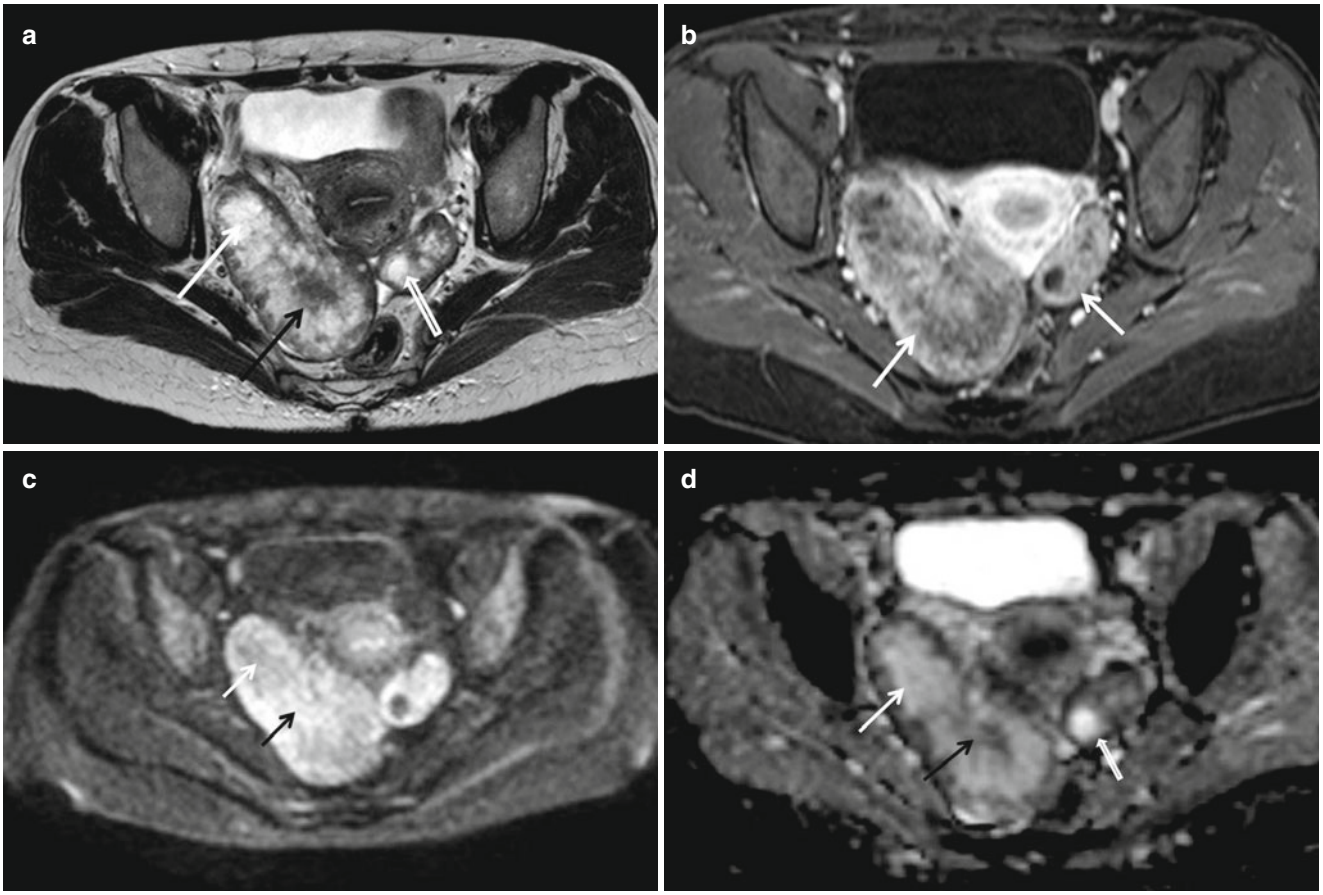

Fig. 2 Synchronous Krukenberg tumours of the ovaries in a 42-year-old woman with no prior history of malignancy, who presented with vaginal bleeding. Upper GI endoscopy, performed after imaging suggested the probability of ovarian metastases, diagnosed primary gastric cancer (diffuse adenocarcinoma with signet-ring cells). (**a**) Axial T2-weighted fast spin echo (FSE) MR image shows bilateral heterogeneous, predominantly solid adnexal masses, surrounding by a thin hypointense capsule, with areas of hyperintensity (*white arrow*), attributed to mucin/oedema, and scattered diffuse or linear relatively hypointense components (*black arrow*), representing fibrosis. A more well-defined intratumoural cyst is noted (*open arrow*). (**b**) Gadolinium-enhanced axial T1-weighted spin echo image with fat suppression demonstrates dense enhancement of the capsule and solid components of the lesions (*arrows*). (**c**) High *b*-value (1,000 smm^{-2}) axial diffusion-weighted image (DWI) shows increased signal intensity of the solid components (*black arrow*) and intermediate of the mucinous components (*white arrow*). (**d**) Corresponding mono-exponential apparent diffusion coefficient (ADC) map from *b*-values of 0, 100, 250, 500 and 1,000 smm^{-2} confirms restricted diffusion of the solid components (*black arrow*) and intermediate diffusion of the mucinous areas (*white arrow*). The intratumoural cyst shows free diffusion (*open arrow*)

of primary tumours ($p=0.005$) [68] (Fig. 5). This finding contrasts the predominantly solid composition of Krukenberg tumours originating principally from gastric cancers [59, 61]. In this study other imaging features such as bilaterality, size, degree of enhancement of cyst walls and solid portions, volume of ascites and presence of peritoneal implants were not discriminatory between metastatic and primary tumours [68].

Immunochemistry may be helpful in discriminating a primary ovarian mucinous tumour from metastatic colorectal adenocarcinoma. Positive staining for cytokeratins 7 and 20 (CK7+/CK20+) has been reported in 68–74 % of primary ovarian mucinous tumours, whereas the most common immunoprofile in lower intestinal tract tumours is CK7-/CK20+ (69–79 %) [95, 96]. In tumours with concomitant expression of CK7 and CK20, the pattern of immunostaining may be discriminatory; diffuse CK7 positivity, as defined by involvement of >50 % of tumour cells, with a focal or patchy (<50 % of tumour cells) CK20 distribution is frequently observed in primary ovarian tumours, whereas colorectal and appendiceal tumours typically display patchy CK7 and diffuse CK20 distribution [95, 96]. Loss of expression of Dpc4 tumour suppression gene has been reported of value in distinguishing metastatic pancreatic cancers from primary ovarian tumours, which often share the same pattern of CK7/CK20 positivity [88, 96]. The usefulness of other markers, such as the nuclear transcription factor CDX2 [97–102] and mucin core proteins MUC5AC and MUC2 [96, 103, 104], is limited by considerable overlap between primary and metastatic tumours.

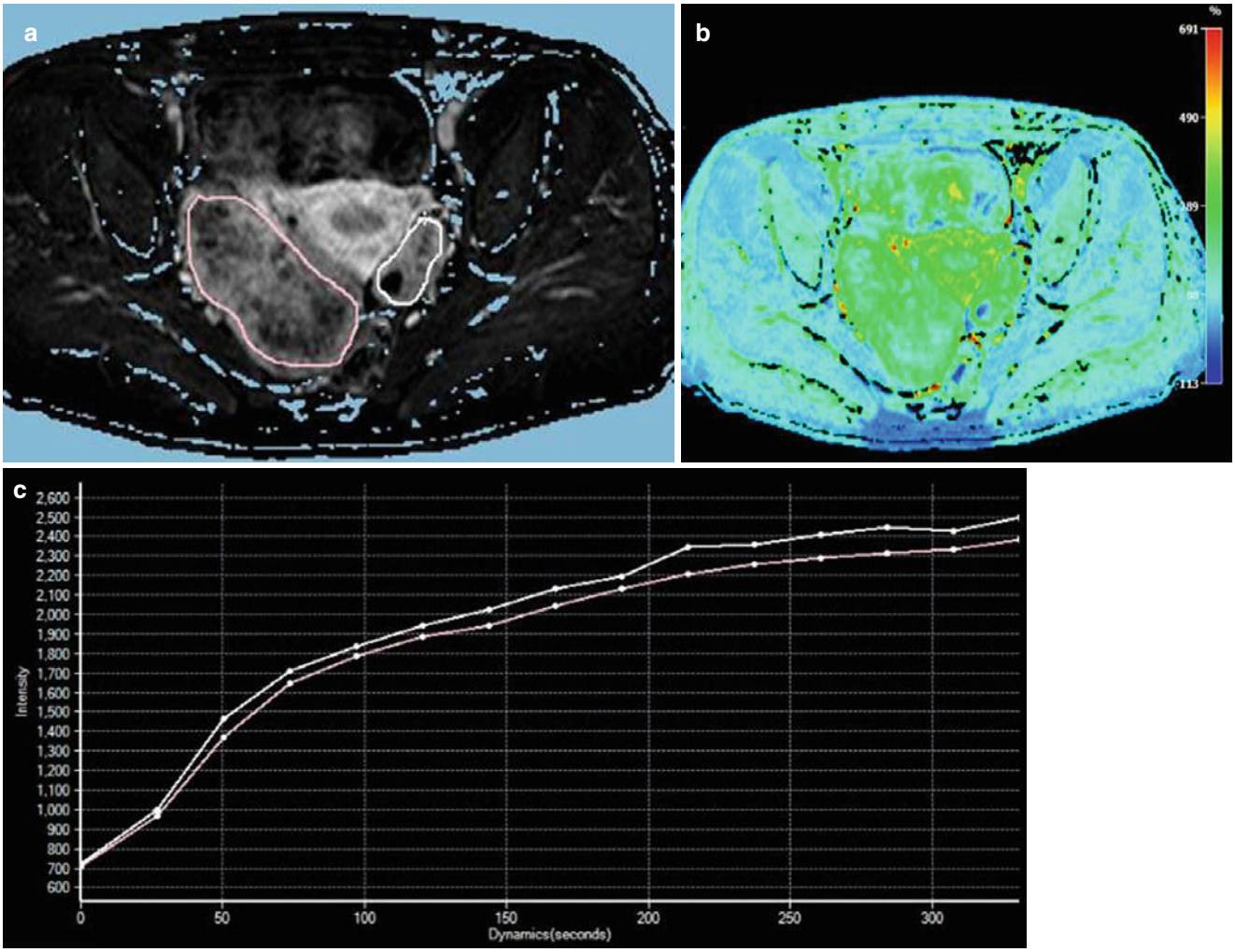

Fig. 3 Perfusion MR study of Krukenberg tumours of the ovaries in a 42-year-old woman with primary gastric adenocarcinoma (same patient as in Fig. 2). (**a**) Axial T1-weighted High Resolution Isotropic Volume Excitation (THRIVE) image with fat suppression after bolus administration of gadolinium chelate at a dose of 0.2 ml/kg body weight shows manually delineated regions of interest (ROI) encompassing the entire lesion area. Images were obtained sequentially at approximately 25 s for 5 min. (**b**) Colour-coded map of relative enhancement demonstrates moderate enhancement in the solid portions of both tumours. (**c**) Graph shows the signal intensity-time curve, characterised by early onset, high amplitude and delayed persistence of enhancement, indicative of an aggressive tumour behaviour

Metastatic Endometrial Adenocarcinomas

Synchronous endometrial and ovarian carcinomas occur in approximately 9–12 % of patients with ovarian and 5 % of patients with endometrial carcinoma [25, 46, 105]. The designation of a dual primary versus metastases may be challenging, since 68–93 % of tumours detected concurrently in the endometrium and ovary are of endometrioid type, with or without squamous differentiation [25, 106, 107]. However, the similar histology may result from metastatic disease or reflect a common tumourigenic process independently affecting multiple tissues of common embryologic descent [108]. The distinction is critical, since standard treatment of endometrial carcinoma with metastatic adnexal involvement (stage IIIA) comprises surgery and adjuvant chemo- and/or radiotherapy, whereas independent stage I uterine and ovarian endometrioid carcinomas have a better overall prognosis and do not routinely require adjuvant treatment [25, 107, 109, 110]. In clinical stage I and II endometrial cancer, the incidence of ovarian metastases has been reported as 5–8 % [62, 111, 112].

Ulbright and Roth developed "empirical" pathological criteria for the characterisation of primary endometrial cancer with ovarian metastases, which comprise a micronodular ovarian pattern (major criterion) or two or more of the following: small (<5 cm) size of ovaries, bilateral involvement, deep myometrial invasion, vascular invasion and tubal lumen involvement (minor criteria) [113]. Scully et al. proposed a more extensive list of clinicopathological features to delineate metastatic disease, which additionally include the

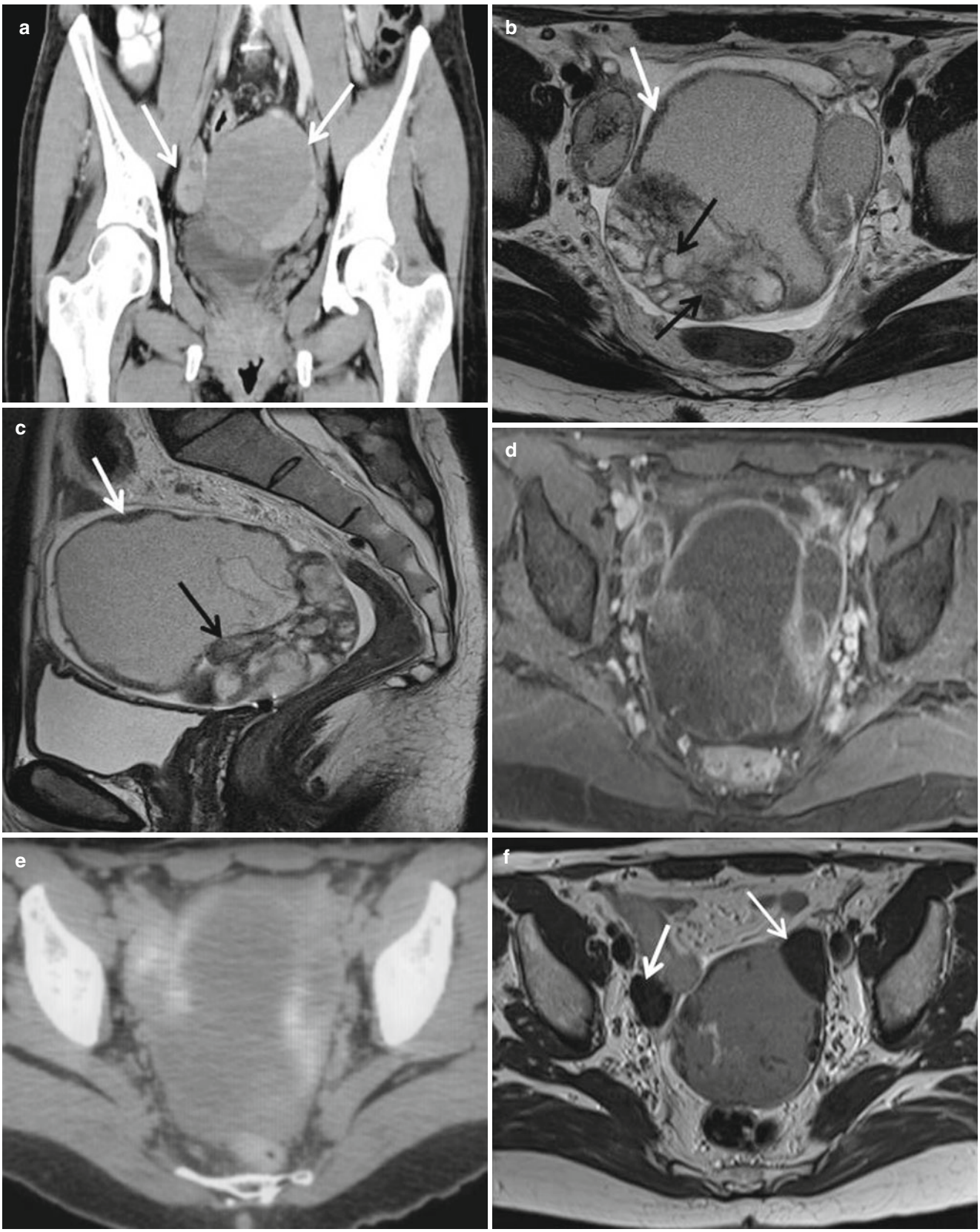

Fig. 4 Synchronous Krukenberg tumours from a moderately differentiated adenocarcinoma of the proximal rectum in a 48-year-old woman. (**a**) Coronal contrast-enhanced CT image demonstrates bilateral complex adnexal masses (*arrows*). On axial (**b**) and sagittal (**c**) T2-weighted FSE images, the bulky left ovarian tumour has dominant well-defined cystic components of varying mucin concentration surrounded by a thin hypointense rim (*white arrows*). In the more solid posterior portion of the tumour, abundant nodular and linear/branching hypointense septa are seen (*black arrows*). (**d**) Axial T1-weighted VIBE fat-saturated image demonstrates irregular and nodular enhancement of septa and rim. (**e**) Fused axial FDG-PET image shows low to moderate, predominantly peripheral metabolic activity. (**f**) Post-chemotherapy axial T2-weighted FSE image demonstrates reduction in size of the adnexal masses and development of new T2-hypointense areas (*arrows*), possibly due to a fibrotic response

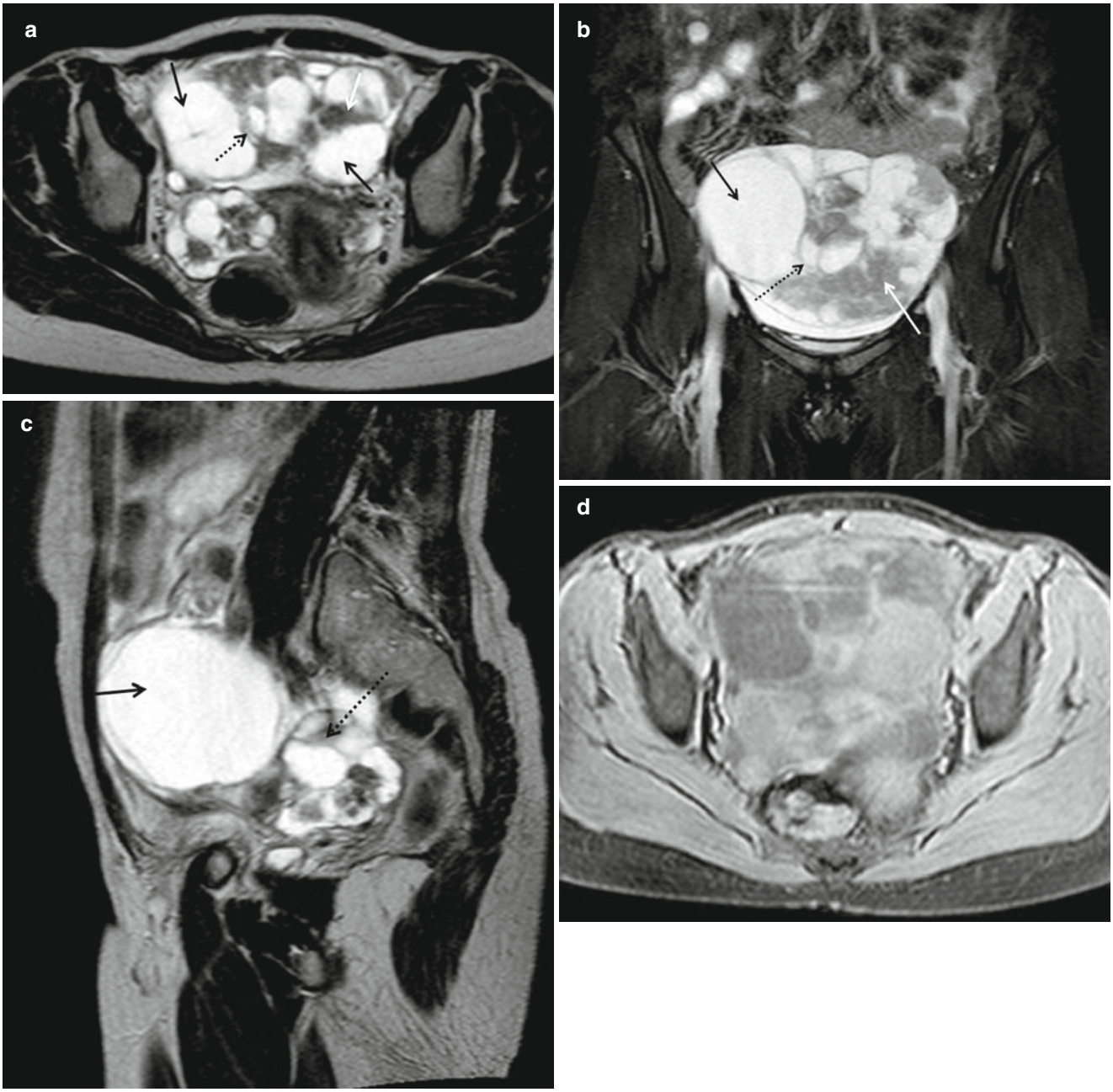

Fig. 5 Metachronous metastatic mucinous adnexal tumours in a 48-year-old woman with a history of primary colorectal adenocarcinoma (Dukes' stage B) resected 18 months previously, who presented with abdominal distention. Axial (**a**), coronal (**b**) and sagittal (**c**) T2-weighted FSE images demonstrate bilateral multiloculated, predominantly cystic (*black arrows*) complex adnexal masses, with smooth borders and various conglomerates of solid mural nodules (*white arrows*) and thick septa (*dotted arrows*). (**d**) Axial gadolinium-enhanced T1-weighted image shows heterogeneous enhancement of the solid components. The imaging features are indistinguishable from a primary mucinous cystadenocarcinoma

presence of atypical endometrial hyperplasia, absence of ovarian endometriosis, typical spread pattern of endometrial cancer, hilar location, vascular space invasion and surface implants in the ovarian site and similar molecular genetic and karyotypic abnormalities in both tumours [114]. Nevertheless, these criteria have not been independently validated. Furthermore, in a study of 74 cases with simultaneously detected endometrial and ovarian carcinomas, only 8 % of ovarian tumours exhibited a micronodular configuration and only 19 % had a less than 5 cm diameter [25].

Bilateral involvement was established in only 13.6 % of patients with surgically proven ovarian metastases from clinical stage I endometrial carcinoma [62].

Assessment of the histological subtype and grade of synchronous ovarian and endometrial tumours is important in establishing the correct diagnosis. Independent primaries are most probably represented by low-grade endometrioid adenocarcinomas, notably in the presence of atypical endometrial hyperplasia or ovarian endometriosis [9, 115]. High histological grade of the endometrial tumour and bilateral ovarian malignancy, characteristically with surface involvement and a micronodular pattern, suggest a uterine primary with adnexal metastases. Contrary to previous belief, depth of myometrial invasion and presence of lymphovascular invasion (LVI) have not been substantiated as reliable discriminators, since 36–100 % of genetically proven metastatic tumours demonstrate less than 50 % of myometrial invasion and lack of LVI, implying a transtubal pathway of disease dissemination [115, 116]. Location of the uterine tumour on the periphery of the myometrium with relative sparing of the endometrium favours the diagnosis of an ovarian primary with uterine infiltration [9]. A serous histology of synchronous endometrial and ovarian tumours poses similar diagnostic considerations, since uterine serous carcinoma demonstrates a marked tendency for extrauterine spread, mainly to the ovaries and peritoneum, even when the tumour is confined to an endometrial polyp without myometrial invasion, and conversely ovarian serous carcinoma may metastasise to the uterus [9]. In problematic cases immunohistochemistry may be helpful, as 95–97 % of ovarian serous carcinomas display positive reactivity to Wilms' tumour susceptibility gene 1 (WT1) (68 % with a moderate to strong positivity in >50 % of tumour cells), whereas 80–100 % of uterine serous carcinomas are negative [117, 118]. Furthermore, molecular profiling has been pursued with DNA flow cytometry, loss of chromosomal heterozygosity, microsatellite instability and analyses of alterations in *PTEN* and β-catenin, in order to determine the mono- or polyclonality of concomitant endometrial and ovarian tumours [109, 115, 116, 119–122].

On imaging, metastases from uterine cancer tend to be bilateral complex masses of smaller size and higher vascularity than their nongenital counterparts [64]. A solid composition has been reported in 85 % and a mixed multilocular/solid in 15 % of metastases [64]. Occasionally the synchronous primary endometrial tumour may be depicted on cross-sectional imaging and thus raise suspicion for the metastatic nature of the ovarian lesions (Figs. 6 and 7). However, endometrial thickening is present in 20–35 % of primary endometrioid ovarian carcinoma, which, nevertheless, appears as a large unilateral mass in 75 % of cases [123] (Fig. 8).

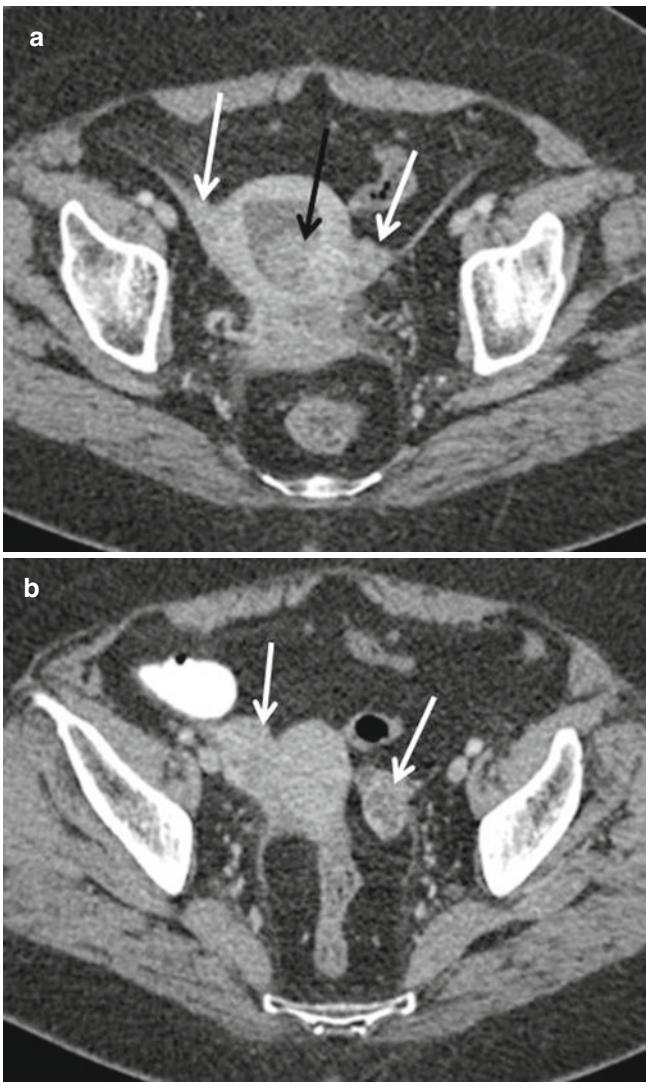

Fig. 6 Adnexal tumours in a 61-year-old patient with synchronous endometrial cancer. Axial contrast-enhanced CT images (**a**, **b**) demonstrate bilateral, small, complex ovarian lesions with heterogeneous enhancement (*white arrows*). A lobulated, enhancing solid tumour is depicted within the endometrial cavity (*black arrow* in **a**). A grade 3 endometrioid endometrial cancer was diagnosed on histology. High-grade endometrial tumour with bilateral small ovarian lesions is highly suggestive of secondary ovarian deposits

Metastases from Breast Primary

Breast origin accounts for 31–38 % of ovarian metastases [19, 42]. In patients with breast cancer, the estimated lifetime risk for developing ovarian cancer is approximately twofold, increasing to threefold for women younger than 40 years and to sevenfold in the presence of a family history of breast or ovarian cancer [124]. In a 15-year follow-up study of 644 patients with stage I and II breast cancer, 55 (9 %) were diagnosed with a subsequent nonmammary malignancy, among whom the most frequent primary type (20 %) was ovarian

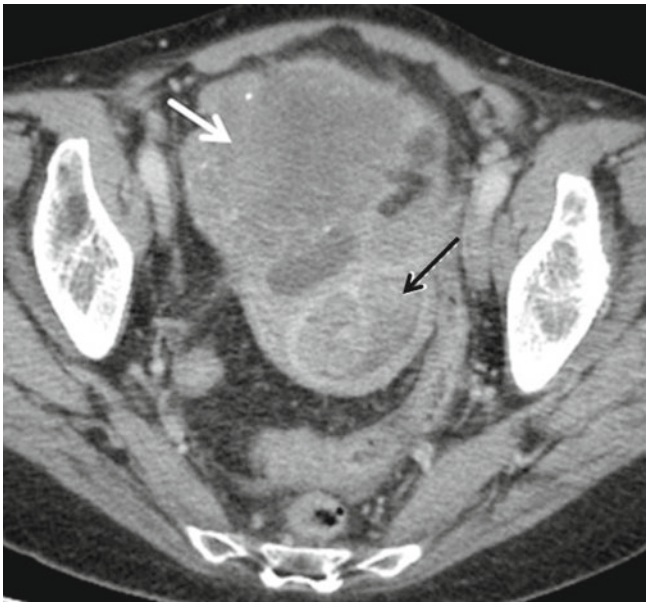

Fig. 7 Adnexal tumour in a 71-year-old patient with concomitant endometrial cancer. Axial contrast-enhanced CT image demonstrates a bulky, heterogeneously enhancing, partly cystic/necrotic complex right ovarian mass (*white arrow*) with minimal foci of calcification and a solid tumour expanding the endometrial cavity (*black arrow*). Histology revealed a grade 3 endometrioid adenocarcinoma of endometrium. In the context of endometrial cancer, the complex adnexal mass is likely to be a metastatic deposit in the right ovary

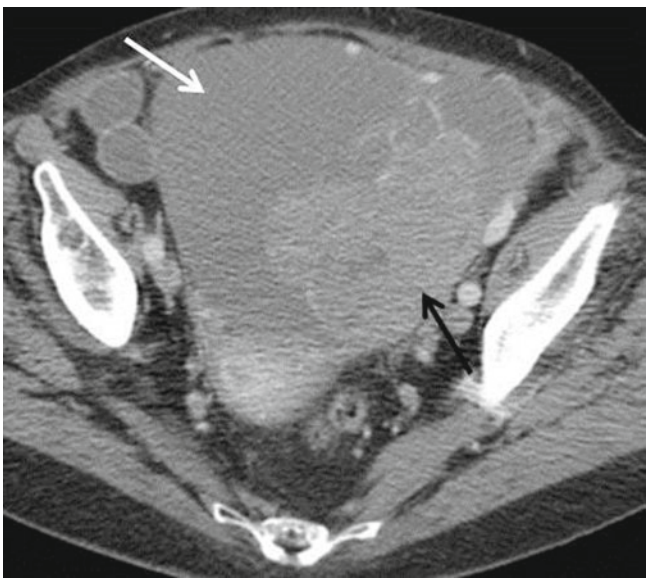

Fig. 8 Primary endometrioid adenocarcinoma of the ovary in an 80-year-old woman who presented with vaginal bleeding. Axial contrast-enhanced CT image demonstrates a unilateral left, bulky, complex adnexal mass with a dominant cystic portion (*white arrow*) and a large, solid, lobulated mural component arising from its lateral wall (*black arrow*). Histology revealed a primary grade 2 endometrioid ovarian adenocarcinoma. The large size and unilaterality of the lesion would be uncommon for metastases, but otherwise the imaging features are non-specific

[125]. The frequent association between breast and ovarian cancer has been ascribed to genetic predisposition; mutations in BRCA1 and BRCA2 genes, which mediate the homologous recombination DNA repair pathway, have been found in 5–15 % of ovarian [126] and in 2–6 % of breast malignancies [127]. For breast cancer the average cumulative lifetime risk in BRCA1- and BRCA2-mutation carriers has been reported as 54–65 % and 23–45 %, respectively [128, 129], whereas for ovarian cancer the corresponding estimates are 39–50 % and 11–27 % [128, 130, 131]. Among women with a history of breast cancer of any stage who develop an adnexal lesion, 18–50 % have a malignant diagnosis; in this subset of patients, 27–51 % of lesions have been reported of metastatic rather than of primary origin [66, 132, 133]. The prevalence of ovarian metastases critically depends on primary disease stage, as in patients with clinical stage IV breast cancer 58–68 % of all discovered adnexal masses represent metastases, in contrast to 0 % in patients with stage I disease [66, 134]. Typically the diagnosis of the primary mammary tumour precedes metastatic manifestations in 97–98 % of cases, with a median interval related to clinical stage, ranging between 0 months for stage IV and 24 months for stage II [2, 42]. By the time of diagnosis of ovarian involvement, most patients (73 %) have overt extra-ovarian metastatic disease [42].

The infiltrating lobular type of breast cancer is more likely to metastasise to the ovary; in an autopsy series of 92 metastatic breast cancers, 36 % of ovarian metastases originated from a lobular histology compared to 2.6 % from ductal ($p<0.002$) [135]. However, due to the highest incidence of the infiltrating ductal subtype among breast cancers [8], 55–73 % of breast-derived ovarian metastases are from ductal histology [136, 137]. In contrast to metastases from other organs, the diagnosis of breast cancer typically (86–97 %) precedes that of the ovarian mass with an overall median time of 11–97 months [2, 42, 138].

Typically ovarian metastases from breast cancer feature small (<5 cm) tumour size and bilaterality (85 and 64 %, respectively) [42]. On imaging they mostly manifest as solid tumours with a multinodular pattern and a minor cystic component [80] (Figs. 9 and 10). Normal gross appearances have been reported in 46 % of involved ovaries with 31 % having only microscopic (<1 mm) tumour foci [42], thus highlighting the difficulty of detection on imaging. The majority (97 %) of macroscopically enlarged tumours display a diffusely solid or multinodular pattern, whereas a predominantly cystic appearance or necrosis involving >10 % of tumour have been reported in only 3 and 10 % of cases, respectively [42].

The microscopic histopathological features of metastases with a predominantly glandular or papillary pattern may be evocative of primary epithelial tumours [139]. Immunostaining against oestrogen and progesterone receptors (ER and PR) is commonly positive for both primary and metastatic

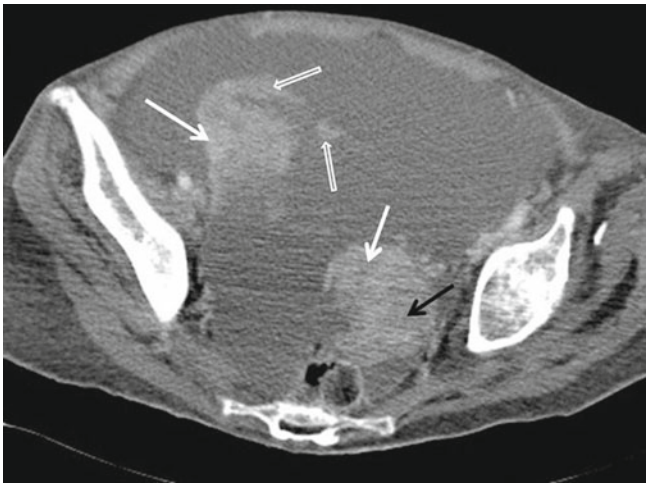

Fig. 9 Metachronous metastatic adnexal tumours in a 51-year-old woman with a 13-month history of mastectomy for stage IIIA infiltrating ductal carcinoma of the breast. The patient presented with abdominal distension and had local recurrence in the anterior thoracic wall. Axial contrast-enhanced CT demonstrates bilateral complex ovarian masses, with a prevailing solid component with avid enhancement (*white arrows*) and a minor cystic component (*black arrow*). The ill-defined shape of the lesions is atypical for breast metastases. There is marked ascites and scattered peritoneal nodularity (*open arrows*), suggestive of peritoneal dissemination

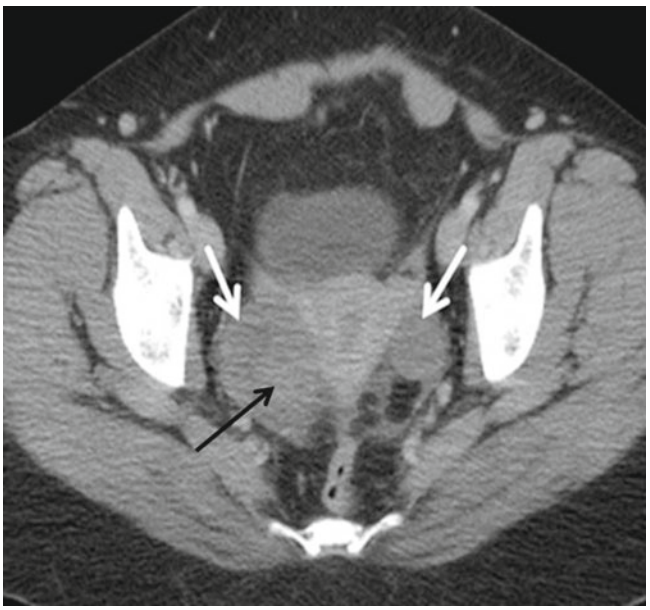

Fig. 10 Metachronous ovarian metastases in a 39-year-old woman with history of grade II invasive ductal breast carcinoma. Interval time from primary to metastatic diagnosis was 65 months. Axial contrast-enhanced CT image demonstrates relatively small (<5 cm) bilateral complex solid/cystic adnexal masses (*white arrows*) with preservation of the ovarian contour and moderate enhancement of the solid components (*black arrow*). The patient also had pulmonary and osseous secondary deposits

tumours. Nevertheless, intense and diffuse reactivity towards WT1 and carcinoembryonic antigen 125 (CA125) is displayed in 76–78 % and 78–90 % of primary ovarian cancers, respectively, compared to 0–3 % and 12–40 % of metastases from breast cancer, thus highlighting the potential of immunohistochemical panels for correct diagnosis [140, 141].

Lymphoma

Ovarian lymphoma is most commonly encountered in the presence of systemic disease rather than as a primary tumour and is almost exclusively of the non-Hodgkin type (particularly diffuse large B cell and follicular lymphoma) [142]. On CT the lesions are typically of large size (mean diameter 7.6–12 cm), bilateral in approximately 60 % of cases, well-defined and homogeneously hypodense, lacking calcification and displaying mild to moderate contrast enhancement [64, 142, 143] (Fig. 11). Areas of necrosis and haemorrhage are rare despite the frequent large dimensions of lesions. On MRI lesions demonstrate homogeneously low T1 and intermediate to high T2 signal intensity, which is typically lower than ovarian carcinoma [142, 143]. Another reported feature is preservation of ovarian shape and presence of T2-hyperintense septa with marked contrast enhancement [144]. Concomitant imaging findings, such as widespread lymphadenopathy, hepatosplenomegaly and bone marrow involvement, may aid towards the diagnosis of a haematological malignancy.

Malignant Melanoma

Most ovarian melanomas arise from a cutaneous or rarely choroidal tumour, although primary melanomas have been reported associated with teratomas [145, 146]. A definite history of prior melanoma is available in over 60 % of cases, but the interval between primary diagnosis and ovarian metastasis may be long, ranging from 15 to 228 months (mean 77.7 months) [146]. Extensive extra-ovarian metastatic disease is present in approximately 50–90 % at the time of presentation. Macroscopic melanin pigmentation, indicating the diagnosis, is present in only 22–35 % of tumours and often only focally [145–147]. Moreover, a similar brown colourisation may be produced by the lipochrome pigment of a steroid cell tumour, whereas amelanotic melanoma may be mistaken for a lipid-poor steroid cell tumour [8]. Average tumour size is approximately 10 cm (range 4.5–23 cm) and unilaterality is reported in 60–82 % [146, 148]. A minor or dominant cystic component is found in approximately 80–90 % of tumours [146] (Fig. 12). Imaging features are non-specific but when adequately present, melanin can be detected by its increased T1 signal intensity; differentiation from teratomas and endometriomas may be aided by the peripheral location of melanin-induced T1-hyperintensity in contrast to centrally located sebaceous/fatty and hemorrhagic components, respectively [149].

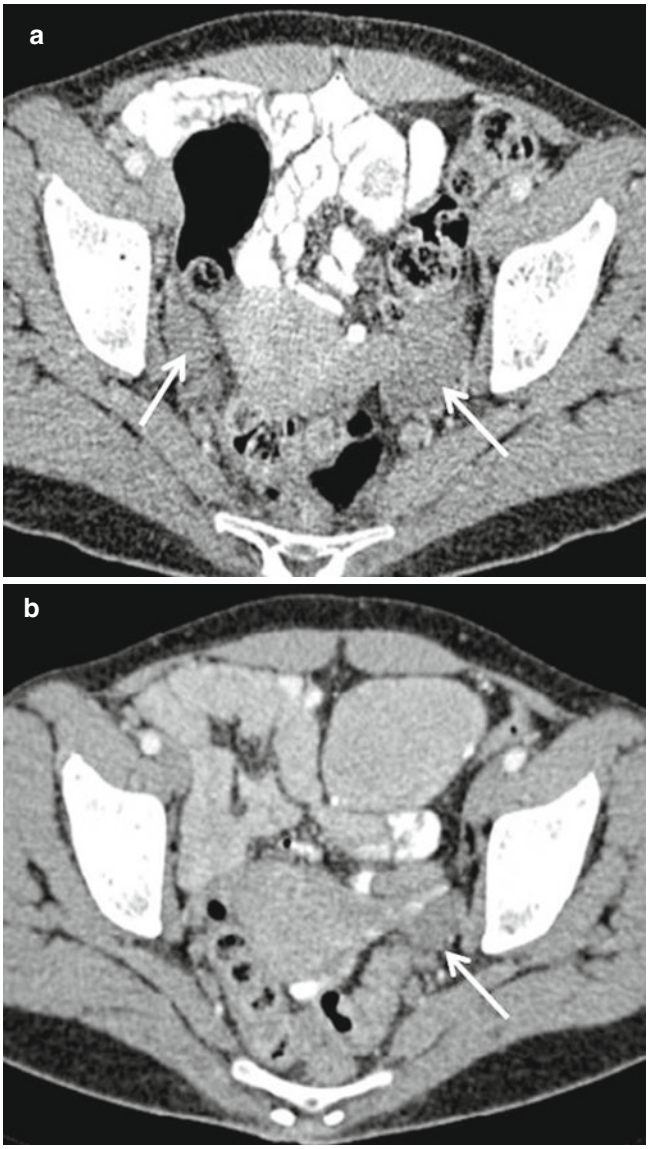

Fig. 11 Adnexal metastases in a 63-year-old patient with a history of diffuse large B cell non-Hodgkin lymphoma. Axial contrast-enhanced CT image (**a**) demonstrates bilateral, homogeneously hypodense, minimally enhancing ovarian lesions with smooth margins and preserved ovarian contour (*arrows*). A post-treatment contrast-enhanced CT image (**b**) demonstrates resolution of the right-sided tumour and a significant reduction in size of the left (*arrow*)

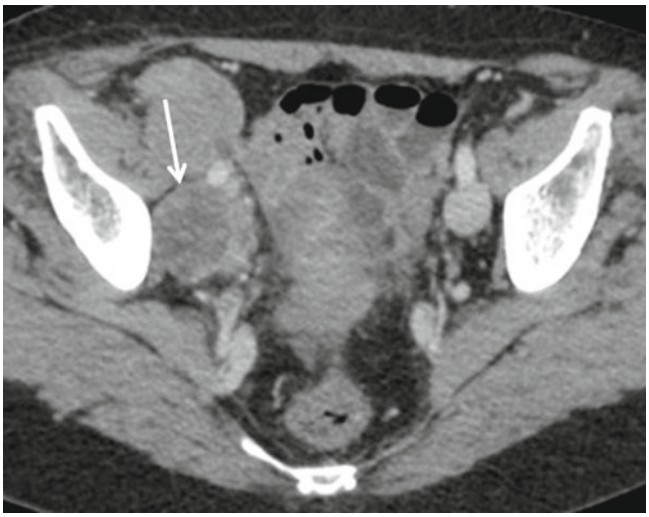

Fig. 12 Biopsy-proven adnexal metastasis in a 39-year-old patient with a history of cutaneous malignant melanoma excised 16 months previously. Axial contrast-enhanced CT image shows non-specific features of a unilateral, predominantly cystic right ovarian lesion (*arrow*), with sparse solid enhancing components

Conclusion

The ovaries are metastatic hosts to a multitude of primary tumours. The extensive overlap of imaging properties between primary and secondary ovarian tumours precludes a reliable distinction on the basis of CT/MRI-derived criteria. However, in conjunction with the clinical history, recognition of certain typical patterns of ovarian metastases depending on primary disease may facilitate the diagnosis. The principal imaging features and diagnostic considerations according to main metastatic tumour types are summarised in Table 1. A high suspicion index for secondary ovarian involvement is warranted in the setting of a known primary malignancy, especially of gastrointestinal, haematologic and melanoma origin. In approximately 40–50 % of cases, mainly of gastric and colorectal cancer, in which the discovery of adnexal disease precedes the primary diagnosis, features such as bilaterality, a predominantly solid appearance and lack of multilocularity may alert the radiologist to the possibility of a Krukenberg tumour, so that further diagnostic workup be pursued. A prevalent cystic appearance, combined with bilateral involvement and relatively small tumour size, may be indicative of metastatic mucinous tumour, particularly of gastrointestinal source. Bilaterality and small tumour size in a patient with a history of advanced breast cancer raise suspicion for metastases. In synchronous endometrial and ovarian tumours distinction on imaging is increasingly challenging, although bilaterality and solid composition may suggest a metastatic relationship.

Table 1 Imaging features and diagnostic considerations according to metastatic tumour types

Metastatic tumour type	Imaging feature				
	Laterality	Size	Composition	MR signal intensity	Diagnostic considerations
Krukenberg	67–86 % bilateral [59, 61]	Variable (mean diameter 8–16 cm), non-discriminatory [59, 61]	69 % solid with intratumoural cysts [59, 61]	T2-hypointensity in solid components due to collagen/ fibrosis	Needs to be distinguished from other T2-hypointense tumours (fibroma, fibrothecoma), usually unilateral
Mucinous (non-Krukenberg)	77–94 % bilateral [81, 82, 94]	87–95 % <10 cm [81, 82]	Uni- or multilocular cysts 86 % [68]	Various signal intensity of cystic components reflecting mucin concentration and necrosis	Combined criteria of unilaterality and size < 13 cm 87 % accuracy in discrimination from primary mucinous tumour [83]
Endometrioid	Empirical criterion of bilaterality, may be infrequent [62]	Empirical criterion of size < 5 cm, may be infrequent [25]	85 % solid [64] Empirical criterion of micronodular configuration, may be infrequent [25]	Non-specific	Frequent synchronous primary endometrioid ovarian tumour, 75 % unilateral [123]
Breast	64 % bilateral [42]	85 % <5 cm [42]	Solid multinodular tumours with minor cystic component [80]	Non-specific	46 % of involved ovaries have normal macroscopic appearance [42]
Lymphoma	60 % bilateral [142]	Variable but may be large (mean diameter 7.6–12 cm) [64, 142]	Solid with mild to moderate contrast enhancement [142, 143]	Homogeneously low T1 and intermediate T2 [142, 143]	Coexisting extensive lymphadenopathy
Melanoma	60–82 % unilateral [146, 148]	Variable (range 4.5–23 cm) [146]	80–90 % cystic component [146]	T1-hyperintensity when adequate melanin content	Needs to be distinguished from endometriomas and teratomas

Biography Dr Stavroula Kyriazi completed her radiology training in Athens, Greece, in 2008 and obtained her MD (Research) from the University of London in 2012 after a 2-year clinical fellowship at the Institute of Cancer Research in partnership with the Royal Marsden Hospital. Her research focused on developing imaging biomarkers for assessing treatment response in ovarian cancer. She is currently a Consultant Radiologist in Iatriko Hospital, Athens, with a special interest in gynaecological imaging.

Dr Jennifer Wakefield is a clinical research fellow in diagnostic imaging at The Royal Marsden NHS Foundation Trust and The Institute of Cancer Research, where she is currently studying for a Doctor of Medicine (Research). She completed her medical training at Nottingham Medical School in 2006 and undertook her general clinical radiology training at Imperial College NHS Trust in 2008. Her research is primarily focused on advances in diffusion-weighted magnetic resonance imaging in ovarian cancer.

Nandita M. deSouza (BSc, MBBS, MRCP, MD, FRCP) is professor in Translational Imaging and co-director of the MRI Unit, Institute of Cancer Research, UK. Her main interests are in magnetic resonance imaging of cancer, using MRI to understand biology, improve staging and monitor treatment response. Nandita holds a Cancer Research UK centre grant in imaging and several project and studentship grants. She has written >100 peer-reviewed articles and several book chapters and is editor of a multi-author book on Endocavitary MRI of the pelvis.

References

1. Yakushiji M, Tazaki T, Nishimura H, Kato T. Krukenberg tumors of the ovary: a clinicopathologic analysis of 112 cases. Nihon Sanka Fujinka Gakkai Zasshi. 1987;39(3):479–85.
2. Demopoulos RI, Touger L, Dubin N. Secondary ovarian carcinoma: a clinical and pathological evaluation. Int J Gynecol Pathol. 1987;6(2):166–75.
3. de Waal YR, Thomas CM, Oei AL, Sweep FC, Massuger LF. Secondary ovarian malignancies: frequency, origin, and characteristics. Int J Gynecol Cancer. 2009;19(7):1160–5.
4. Webb MJ, Decker DG, Mussey E. Cancer metastatic to the ovary: factors influencing survival. Obstet Gynecol. 1975;45(4):391–6.
5. Yada-Hashimoto N, Yamamoto T, Kamiura S, Seino H, Ohira H, Sawai K, et al. Metastatic ovarian tumors: a review of 64 cases. Gynecol Oncol. 2003;89(2):314–7.
6. Savey L, Lasser P, Castaigne D, Michel G, Bognel C, Colau JC. Krukenberg tumors. Analysis of a series of 28 cases. J Chir (Paris). 1996;133(9–10):427–31.
7. Kim HK, Heo DS, Bang YJ, Kim NK. Prognostic factors of Krukenberg's tumor. Gynecol Oncol. 2001;82(1):105–9.
8. Young RH. From Krukenberg to today: the ever present problems posed by metastatic tumors in the ovary. Part II. Adv Anat Pathol. 2007;14(3):149–77.
9. McCluggage WG, Wilkinson N. Metastatic neoplasms involving the ovary: a review with an emphasis on morphological and immunohistochemical features. Histopathology. 2005;47(3):231–47.
10. Holtz F, Hart WR. Krukenberg tumors of the ovary: a clinicopathologic analysis of 27 cases. Cancer. 1982;50(11):2438–47.
11. Ayhan A, Guvenal T, Salman MC, Ozyuncu O, Sakinci M, Basaran M. The role of cytoreductive surgery in nongenital cancers metastatic to the ovaries. Gynecol Oncol. 2005;98(2):235–41.
12. Petru E, Pickel H, Heydarfadai M, Lahousen M, Haas J, Schaider H, et al. Nongenital cancers metastatic to the ovary. Gynecol Oncol. 1992;44(1):83–6.
13. Young RH. From krukenberg to today: the ever present problems posed by metastatic tumors in the ovary: part I. Historical perspective, general principles, mucinous tumors including the krukenberg tumor. Adv Anat Pathol. 2006;13(5):205–27.
14. Cheong JH, Hyung WJ, Chen J, Kim J, Choi SH, Noh SH. Surgical management and outcome of metachronous Krukenberg tumors from gastric cancer. J Surg Oncol. 2004;87(1):39–45.
15. Munzone E, Botteri E, Esposito A, Sciandivasci A, Franchi D, Pruneri G, et al. Outcome and clinical-biological characteristics of patients with advanced breast cancer undergoing removal of ovarian/pelvic metastases. Ann Oncol. 2012;23(11):2884–90.
16. Miller BE, Pittman B, Wan JY, Fleming M. Colon cancer with metastasis to the ovary at time of initial diagnosis. Gynecol Oncol. 1997;66(3):368–71.
17. Lewis MR, Deavers MT, Silva EG, Malpica A. Ovarian involvement by metastatic colorectal adenocarcinoma: still a diagnostic challenge. Am J Surg Pathol. 2006;30(2):177–84.
18. Yazigi R, Sandstad J. Ovarian involvement in extragenital cancer. Gynecol Oncol. 1989;34(1):84–7.
19. Mazur MT, Hsueh S, Gersell DJ. Metastases to the female genital tract. Analysis of 325 cases. Cancer. 1984;53(9):1978–84.
20. Taylor AE, Nicolson VM, Cunningham D. Ovarian metastases from primary gastrointestinal malignancies: the Royal Marsden Hospital experience and implications for adjuvant treatment. Br J Cancer. 1995;71(1):92–6.
21. Moore RG, Chung M, Granai CO, Gajewski W, Steinhoff MM. Incidence of metastasis to the ovaries from nongenital tract primary tumors. Gynecol Oncol. 2004;93(1):87–91.
22. Kim WY, Kim TJ, Kim SE, Lee JW, Lee JH, Kim BG, et al. The role of cytoreductive surgery for non-genital tract metastatic tumors to the ovaries. Eur J Obstet Gynecol Reprod Biol. 2010;149(1):97–101.
23. Skirnisdottir I, Garmo H, Holmberg L. Non-genital tract metastases to the ovaries presented as ovarian tumors in Sweden 1990–2003: occurrence, origin and survival compared to ovarian cancer. Gynecol Oncol. 2007;105(1):166–71.
24. Walsh C, Holschneider C, Hoang Y, Tieu K, Karlan B, Cass I. Coexisting ovarian malignancy in young women with endometrial cancer. Obstet Gynecol. 2005;106(4):693–9.
25. Zaino R, Whitney C, Brady MF, DeGeest K, Burger RA, Buller RE. Simultaneously detected endometrial and ovarian carcinomas – a prospective clinicopathologic study of 74 cases: a gynecologic oncology group study. Gynecol Oncol. 2001;83(2):355–62.
26. Young RH, Gersell DJ, Roth LM, Scully RE. Ovarian metastases from cervical carcinomas other than pure adenocarcinomas. A report of 12 cases. Cancer. 1993;71(2):407–18.
27. Elishaev E, Gilks CB, Miller D, Srodon M, Kurman RJ, Ronnett BM. Synchronous and metachronous endocervical and ovarian neoplasms: evidence supporting interpretation of the ovarian neoplasms as metastatic endocervical adenocarcinomas simulating primary ovarian surface epithelial neoplasms. Am J Surg Pathol. 2005;29(3):281–94.
28. Tabata M, Ichinoe K, Sakuragi N, Shiina Y, Yamaguchi T, Mabuchi Y. Incidence of ovarian metastasis in patients with cancer of the uterine cervix. Gynecol Oncol. 1987;28(3):255–61.
29. Nakanishi T, Wakai K, Ishikawa H, Nawa A, Suzuki Y, Nakamura S, et al. A comparison of ovarian metastasis between squamous cell carcinoma and adenocarcinoma of the uterine cervix. Gynecol Oncol. 2001;82(3):504–9.
30. Young RH, Scully RE. Urothelial and ovarian carcinomas of identical cell types: problems in interpretation. A report of three cases and review of the literature. Int J Gynecol Pathol. 1988;7(3):197–211.
31. Irving JA, Vasques DR, McGuinness TB, Young RH. Krukenberg tumor of renal pelvic origin: report of a case with selected comments on ovarian tumors metastatic from the urinary tract. Int J Gynecol Pathol. 2006;25(2):147–50.
32. Young RH, Scully RE. Sarcomas metastatic to the ovary: a report of 21 cases. Int J Gynecol Pathol. 1990;9(3):231–52.
33. Irving JA, Lerwill MF, Young RH. Gastrointestinal stromal tumors metastatic to the ovary: a report of five cases. Am J Surg Pathol. 2005;29(7):920–6.
34. Clement PB, Young RH, Scully RE. Malignant mesotheliomas presenting as ovarian masses. A report of nine cases, including two primary ovarian mesotheliomas. Am J Surg Pathol. 1996; 20(9):1067–80.
35. Zaloudek C, Miller TR, Stern JL. Desmoplastic small cell tumor of the ovary: a unique polyphenotypic tumor with an unfavorable prognosis. Int J Gynecol Pathol. 1995;14(3):260–5.
36. Antila R, Jalkanen J, Heikinheimo O. Comparison of secondary and primary ovarian malignancies reveals differences in their pre- and perioperative characteristics. Gynecol Oncol. 2006;101(1):97–101.
37. MacKeigan JM, Ferguson JA. Prophylactic oophorectomy and colorectal cancer in premenopausal patients. Dis Colon Rectum. 1979;22(6):401–5.
38. Birnkrant A, Sampson J, Sugarbaker PH. Ovarian metastasis from colorectal cancer. Dis Colon Rectum. 1986;29(11):767–71.
39. Tso PL, Bringaze III WL, Dauterive AH, Correa P, Cohn Jr I. Gastric carcinoma in the young. Cancer. 1987;59(7):1362–5.
40. Judson K, McCormick C, Vang R, Yemelyanova AV, Wu LS, Bristow RE, et al. Women with undiagnosed colorectal adenocarcinomas presenting with ovarian metastases: clinicopathologic features and comparison with women having known colorectal adenocarcinomas and ovarian involvement. Int J Gynecol Pathol. 2008;27(2):182–90.
41. Megibow AJ, Hulnick DH, Bosniak MA, Balthazar EJ. Ovarian metastases: computed tomographic appearances. Radiology. 1985;156(1):161–4.
42. Gagnon Y, Tetu B. Ovarian metastases of breast carcinoma. A clinicopathologic study of 59 cases. Cancer. 1989;64(4):892–8.

43. Wright JD, Powell MA, Mutch DG, Rader JS, Gibb RK, Huettner PC, et al. Synchronous ovarian metastases at the time of laparotomy for colon cancer. Gynecol Oncol. 2004;92(3):851–5.
44. Qiu L, Yang T, Shan XH, Hu MB, Li Y. Metastatic factors for Krukenberg tumor: a clinical study on 102 cases. Med Oncol. 2011;28(4):1514–9.
45. Ayhan A, Guvenal T, Coskun F, Basaran M, Salman MC. Survival and prognostic factors in patients with synchronous ovarian and endometrial cancers and endometrial cancers metastatic to the ovaries. Eur J Gynaecol Oncol. 2003;24(2):171–4.
46. Lim YK, Padma R, Foo L, Chia YN, Yam P, Chia J, et al. Survival outcome of women with synchronous cancers of endometrium and ovary: a 10 year retrospective cohort study. J Gynecol Oncol. 2011;22(4):239–43.
47. Scully RE, Richardson GS. Luteinization of the stroma of metastatic cancer involving the ovary and its endocrine significance. Cancer. 1961;14:827–40.
48. Jolles CJ, Beeson JH, Abbott T. Progesterone production in adenocarcinoma of the colon metastatic to the ovaries. Obstet Gynecol. 1985;65(6):853–7.
49. Rome RM, Fortune DW, Quinn MA, Brown JB. Functioning ovarian tumors in postmenopausal women. Obstet Gynecol. 1981;57(6):705–10.
50. Tanaka YO, Ide Y, Nishida M, Nishide K, Tsunoda H, Kajitani M, et al. Ovarian tumor with functioning stroma. Comput Med Imaging Graph. 2002;26(3):193–7.
51. Abu-Rustum NR, Aghajanian CA, Venkatraman ES, Feroz F, Barakat RR. Metastatic breast carcinoma to the abdomen and pelvis. Gynecol Oncol. 1997;66(1):41–4.
52. Yan TD, Black D, Savady R, Sugarbaker PH. A systematic review on the efficacy of cytoreductive surgery and perioperative intraperitoneal chemotherapy for pseudomyxoma peritonei. Ann Surg Oncol. 2007;14(2):484–92.
53. Hirono M, Taniyama K, Matsuki K, Nakagami K, Niimoto M, Hattori T. Clinico-pathological studies on ovarian metastasis from gastric cancer. Jpn J Surg. 1983;13(1):25–31.
54. Sugarbaker PH, Averbach AM. Krukenberg syndrome as a natural manifestation of tumor cell entrapment. In: Sugarbaker PH, editor. Peritoneal carcinomatosis: principles of management. Massachusetts: Kluwer Academic Publishers; 1996.
55. Sternberg WH. Nonfunctioning ovarian neoplasms. In: Grady HF, Smith DE, editors. The ovary. Baltimore: Williams and Wilkins; 1963.
56. Herrera LO, Ledesma EJ, Natarajan N, Lopez GE, Tsukada Y, Mittelman A. Metachronous ovarian metastases from adenocarcinoma of the colon and rectum. Surg Gynecol Obstet. 1982; 154(4):531–3.
57. Lash RH, Hart WR. Intestinal adenocarcinomas metastatic to the ovaries. A clinicopathologic evaluation of 22 cases. Am J Surg Pathol. 1987;11(2):114–21.
58. Morrow M, Enker WE. Late ovarian metastases in carcinoma of the colon and rectum. Arch Surg. 1984;119(12):1385–8.
59. Kim SH, Kim WH, Park KJ, Lee JK, Kim JS. CT and MR findings of Krukenberg tumors: comparison with primary ovarian tumors. J Comput Assist Tomogr. 1996;20(3):393–8.
60. Kuhlman JE, Hruban RH, Fishman EK. Krukenberg tumors: CT features and growth characteristics. South Med J. 1989;82(10):1215–9.
61. Ha HK, Baek SY, Kim SH, Kim HH, Chung EC, Yeon KM. Krukenberg's tumor of the ovary: MR imaging features. AJR Am J Roentgenol. 1995;164(6):1435–9.
62. Takeshima N, Hirai Y, Yano K, Tanaka N, Yamauchi K, Hasumi K. Ovarian metastasis in endometrial carcinoma. Gynecol Oncol. 1998;70(2):183–7.
63. Boger-Megiddo I, Weiss NS. Histologic subtypes and laterality of primary epithelial ovarian tumors. Gynecol Oncol. 2005;97(1):80–3.
64. Testa AC, Ferrandina G, Timmerman D, Savelli L, Ludovisi M, Van HC, et al. Imaging in gynecological disease (1): ultrasound features of metastases in the ovaries differ depending on the origin of the primary tumor. Ultrasound Obstet Gynecol. 2007;29(5):505–11.
65. Brown DL, Zou KH, Tempany CM, Frates MC, Silverman SG, McNeil BJ, et al. Primary versus secondary ovarian malignancy: imaging findings of adnexal masses in the Radiology Diagnostic Oncology Group Study. Radiology. 2001;219(1):213–8.
66. Hann LE, Lui DM, Shi W, Bach AM, Selland DL, Castiel M. Adnexal masses in women with breast cancer: US findings with clinical and histopathologic correlation. Radiology. 2000; 216(1):242–7.
67. Alcazar JL, Galan MJ, Ceamanos C, Garcia-Manero M. Transvaginal gray scale and color Doppler sonography in primary ovarian cancer and metastatic tumors to the ovary. J Ultrasound Med. 2003;22(3):243–7.
68. Choi HJ, Lee JH, Seo SS, Lee S, Kim SK, Kim JY, et al. Computed tomography findings of ovarian metastases from colon cancer: comparison with primary malignant ovarian tumors. J Comput Assist Tomogr. 2005;29(1):69–73.
69. Serov SF, Scully RE. Histologic typing of ovarian tumours. Geneva: World Health Organization; 1973.
70. Krukenberg FE. Uber Das Fibrosarcoma ovarii mucocellulare (carcinomatodes). Arch Gynaekol. 1896;50:287–321.
71. Schlagenhaufer F. Ueber das metastatische ovarial-carcinom nach Krebs des Magens, Darmes, und anderer Bauchorgane. Monatsschr Geburtsh Gynaekol. 1902;15:485.
72. Kiyokawa T, Young RH, Scully RE. Krukenberg tumors of the ovary: a clinicopathologic analysis of 120 cases with emphasis on their variable pathologic manifestations. Am J Surg Pathol. 2006;30(3):277–99.
73. Young RH, Scully RE. Ovarian metastases from carcinoma of the gallbladder and extrahepatic bile ducts simulating primary tumors of the ovary. A report of six cases. Int J Gynecol Pathol. 1990;9(1):60–72.
74. Al-Agha OM, Nicastri AD. An in-depth look at Krukenberg tumor: an overview. Arch Pathol Lab Med. 2006;130(11):1725–30.
75. Lee KR, Scully RE. Mucinous tumors of the ovary: a clinicopathologic study of 196 borderline tumors (of intestinal type) and carcinomas, including an evaluation of 11 cases with 'pseudomyxoma peritonei'. Am J Surg Pathol. 2000;24(11):1447–64.
76. Wong PC, Ferenczy A, Fan LD, McCaughey E. Krukenberg tumors of the ovary. Ultrastructural, histochemical and immunohistochemical studies of 15 cases. Cancer. 1986;57(4):751–60.
77. Park SY, Kim HS, Hong EK, Kim WH. Expression of cytokeratins 7 and 20 in primary carcinomas of the stomach and colorectum and their value in the differential diagnosis of metastatic carcinomas to the ovary. Hum Pathol. 2002;33(11):1078–85.
78. Castro-Aragon I. Krukenberg tumor. In: Hricak H, editor. Diagnostic imaging: gynecology. 1 ed. Amirsys; Salt Lake City, Utah. 2007. p. 7:150–2.
79. Jung SE, Lee JM, Rha SE, Byun JY, Jung JI, Hahn ST. CT and MR imaging of ovarian tumors with emphasis on differential diagnosis. Radiographics. 2002;22(6):1305–25.
80. Koyama T, Mikami Y, Saga T, Tamai K, Togashi K. Secondary ovarian tumors: spectrum of CT and MR features with pathologic correlation. Abdom Imaging. 2007;32(6):784–95.
81. Seidman JD, Kurman RJ, Ronnett BM. Primary and metastatic mucinous adenocarcinomas in the ovaries: incidence in routine practice with a new approach to improve intraoperative diagnosis. Am J Surg Pathol. 2003;27(7):985–93.
82. Khunamornpong S, Suprasert P, Pojchamarnwiputh S, Na CW, Settakorn J, Siriaunkgul S. Primary and metastatic mucinous adenocarcinomas of the ovary: evaluation of the diagnostic approach using tumor size and laterality. Gynecol Oncol. 2006;101(1): 152–7.
83. Yemelyanova AV, Vang R, Judson K, Wu LS, Ronnett BM. Distinction of primary and metastatic mucinous tumors involving the ovary: analysis of size and laterality data by primary site with

reevaluation of an algorithm for tumor classification. Am J Surg Pathol. 2008;32(1):128–38.
84. Young RH, Scully RE. Mucinous ovarian tumors associated with mucinous adenocarcinomas of the cervix. A clinicopathological analysis of 16 cases. Int J Gynecol Pathol. 1988;7(2):99–111.
85. Shimada M, Kigawa J, Nishimura R, Yamaguchi S, Kuzuya K, Nakanishi T, et al. Ovarian metastasis in carcinoma of the uterine cervix. Gynecol Oncol. 2006;101(2):234–7.
86. Dionigi A, Facco C, Tibiletti MG, Bernasconi B, Riva C, Capella C. Ovarian metastases from colorectal carcinoma. Clinicopathologic profile, immunophenotype, and karyotype analysis. Am J Clin Pathol. 2000;114(1):111–22.
87. Young RH, Hart WR. Metastases from carcinomas of the pancreas simulating primary mucinous tumors of the ovary. A report of seven cases. Am J Surg Pathol. 1989;13(9):748–56.
88. Meriden Z, Yemelyanova AV, Vang R, Ronnett BM. Ovarian metastases of pancreaticobiliary tract adenocarcinomas: analysis of 35 cases, with emphasis on the ability of metastases to simulate primary ovarian mucinous tumors. Am J Surg Pathol. 2011;35(2):276–88.
89. Ayhan A, Guney I, Saygan-Karamursel B, Taskiran C. Ovarian metastasis of primary biliary and gallbladder carcinomas. Eur J Gynaecol Oncol. 2001;22(5):377–8.
90. Ronnett BM, Kurman RJ, Shmookler BM, Sugarbaker PH, Young RH. The morphologic spectrum of ovarian metastases of appendiceal adenocarcinomas: a clinicopathologic and immunohistochemical analysis of tumors often misinterpreted as primary ovarian tumors or metastatic tumors from other gastrointestinal sites. Am J Surg Pathol. 1997;21(10):1144–55.
91. Kelemen LE, Kobel M. Mucinous carcinomas of the ovary and colorectum: different organ, same dilemma. Lancet Oncol. 2011;12(11):1071–80.
92. Ronnett BM, Kurman RJ, Zahn CM, Shmookler BM, Jablonski KA, Kass ME, et al. Pseudomyxoma peritonei in women: a clinicopathologic analysis of 30 cases with emphasis on site of origin, prognosis, and relationship to ovarian mucinous tumors of low malignant potential. Hum Pathol. 1995;26(5):509–24.
93. McKenney JK, Soslow RA, Longacre TA. Ovarian mature teratomas with mucinous epithelial neoplasms: morphologic heterogeneity and association with pseudomyxoma peritonei. Am J Surg Pathol. 2008;32(5):645–55.
94. Lee KR, Young RH. The distinction between primary and metastatic mucinous carcinomas of the ovary: gross and histologic findings in 50 cases. Am J Surg Pathol. 2003;27(3):281–92.
95. Vang R, Gown AM, Barry TS, Wheeler DT, Yemelyanova A, Seidman JD, et al. Cytokeratins 7 and 20 in primary and secondary mucinous tumors of the ovary: analysis of coordinate immunohistochemical expression profiles and staining distribution in 179 cases. Am J Surg Pathol. 2006;30(9):1130–9.
96. Ji H, Isacson C, Seidman JD, Kurman RJ, Ronnett BM. Cytokeratins 7 and 20, Dpc4, and MUC5AC in the distinction of metastatic mucinous carcinomas in the ovary from primary ovarian mucinous tumors: Dpc4 assists in identifying metastatic pancreatic carcinomas. Int J Gynecol Pathol. 2002;21(4):391–400.
97. Vang R, Gown AM, Wu LS, Barry TS, Wheeler DT, Yemelyanova A, et al. Immunohistochemical expression of CDX2 in primary ovarian mucinous tumors and metastatic mucinous carcinomas involving the ovary: comparison with CK20 and correlation with coordinate expression of CK7. Mod Pathol. 2006;19(11):1421–8.
98. Werling RW, Yaziji H, Bacchi CE, Gown AM. CDX2, a highly sensitive and specific marker of adenocarcinomas of intestinal origin: an immunohistochemical survey of 476 primary and metastatic carcinomas. Am J Surg Pathol. 2003;27(3):303–10.
99. Fraggetta F, Pelosi G, Cafici A, Scollo P, Nuciforo P, Viale G. CDX2 immunoreactivity in primary and metastatic ovarian mucinous tumours. Virchows Arch. 2003;443(6):782–6.
100. Groisman GM, Meir A, Sabo E. The value of Cdx2 immunostaining in differentiating primary ovarian carcinomas from colonic carcinomas metastatic to the ovaries. Int J Gynecol Pathol. 2004;23(1):52–7.
101. Logani S, Oliva E, Arnell PM, Amin MB, Young RH. Use of novel immunohistochemical markers expressed in colonic adenocarcinoma to distinguish primary ovarian tumors from metastatic colorectal carcinoma. Mod Pathol. 2005;18(1):19–25.
102. Pinto PB, Derchain SF, Andrade LA. Metastatic mucinous carcinomas in the ovary: a practical approach to diagnosis related to gross aspects and to immunohistochemical evaluation. Int J Gynecol Pathol. 2012;31(4):313–8.
103. Shin JH, Bae JH, Lee A, Jung CK, Yim HW, Park JS, et al. CK7, CK20, CDX2 and MUC2 Immunohistochemical staining used to distinguish metastatic colorectal carcinoma involving ovary from primary ovarian mucinous adenocarcinoma. Jpn J Clin Oncol. 2010;40(3):208–13.
104. Fujii S, Kakite S, Nishihara K, Kanasaki Y, Harada T, Kigawa J, et al. Diagnostic accuracy of diffusion-weighted imaging in differentiating benign from malignant ovarian lesions. J Magn Reson Imaging. 2008;28(5):1149–56.
105. Kline RC, Wharton JT, Atkinson EN, Burke TW, Gershenson DM, Edwards CL. Endometrioid carcinoma of the ovary: retrospective review of 145 cases. Gynecol Oncol. 1990;39(3):337–46.
106. Brinkmann D, Ryan A, Ayhan A, McCluggage WG, Feakins R, Santibanez-Koref MF, et al. A molecular genetic and statistical approach for the diagnosis of dual-site cancers. J Natl Cancer Inst. 2004;96(19):1441–6.
107. Soliman PT, Slomovitz BM, Broaddus RR, Sun CC, Oh JC, Eifel PJ, et al. Synchronous primary cancers of the endometrium and ovary: a single institution review of 84 cases. Gynecol Oncol. 2004;94(2):456–62.
108. Eisner RF, Nieberg RK, Berek JS. Synchronous primary neoplasms of the female reproductive tract. Gynecol Oncol. 1989;33(3):335–9.
109. Guirguis A, Elishaev E, Oh SH, Tseng GC, Zorn K, DeLoia JA. Use of gene expression profiles to stage concurrent endometrioid tumors of the endometrium and ovary. Gynecol Oncol. 2008;108(2):370–6.
110. Eifel P, Hendrickson M, Ross J, Ballon S, Martinez A, Kempson R. Simultaneous presentation of carcinoma involving the ovary and the uterine corpus. Cancer. 1982;50(1):163–70.
111. Burrell MO, Franklin III EW, Powell JL. Endometrial cancer: evaluation of spread and follow-up one hundred eighty-nine patients with Stage I or Stage II disease. Am J Obstet Gynecol. 1982;144(2):181–5.
112. Creasman WT, Morrow CP, Bundy BN, Homesley HD, Graham JE, Heller PB. Surgical pathologic spread patterns of endometrial cancer. A Gynecologic Oncology Group Study. Cancer. 1987; 60(8 Suppl):2035–41.
113. Ulbright TM, Roth LM. Metastatic and independent cancers of the endometrium and ovary: a clinicopathologic study of 34 cases. Hum Pathol. 1985;16(1):28–34. Ref Type: Music Score.
114. Scully RE, Young RH, Clement PB. Tumors of the ovary, maldeveloped gonads, fallopian tube, and broad ligament. Atlas of tumor pathology. Bethesda: American Forces Institute of Pathology; 1999.
115. Irving JA, Catasus L, Gallardo A, Bussaglia E, Romero M, Matias-Guiu X, et al. Synchronous endometrioid carcinomas of the uterine corpus and ovary: alterations in the beta-catenin (CTNNB1) pathway are associated with independent primary tumors and favorable prognosis. Hum Pathol. 2005;36(6):605–19.
116. Fujii H, Matsumoto T, Yoshida M, Furugen Y, Takagaki T, Iwabuchi K, et al. Genetics of synchronous uterine and ovarian endometrioid carcinoma: combined analyses of loss of heterozygosity, PTEN mutation, and microsatellite instability. Hum Pathol. 2002;33(4):421–8.
117. Goldstein NS, Uzieblo A. WT1 immunoreactivity in uterine papillary serous carcinomas is different from ovarian serous carcinomas. Am J Clin Pathol. 2002;117(4):541–5.

118. Al-Hussaini M, Stockman A, Foster H, McCluggage WG. WT-1 assists in distinguishing ovarian from uterine serous carcinoma and in distinguishing between serous and endometrioid ovarian carcinoma. Histopathology. 2004;44(2):109–15.
119. Fujita M, Enomoto T, Wada H, Inoue M, Okudaira Y, Shroyer KR. Application of clonal analysis. Differential diagnosis for synchronous primary ovarian and endometrial cancers and metastatic cancer. Am J Clin Pathol. 1996;105(3):350–9.
120. Moreno-Bueno G, Gamallo C, Perez-Gallego L, de Mora JC, Suarez A, Palacios J. Beta-Catenin expression pattern, beta-catenin gene mutations, and microsatellite instability in endometrioid ovarian carcinomas and synchronous endometrial carcinomas. Diagn Mol Pathol. 2001;10(2):116–22.
121. Catasus L, Bussaglia E, Rodrguez I, Gallardo A, Pons C, Irving JA, et al. Molecular genetic alterations in endometrioid carcinomas of the ovary: similar frequency of beta-catenin abnormalities but lower rate of microsatellite instability and PTEN alterations than in uterine endometrioid carcinomas. Hum Pathol. 2004;35(11):1360–8.
122. Halperin R, Zehavi S, Hadas E, Habler L, Bukovsky I, Schneider D. Simultaneous carcinoma of the endometrium and ovary vs endometrial carcinoma with ovarian metastases: a clinical and immunohistochemical determination. Int J Gynecol Cancer. 2003;13(1):32–7.
123. Wagner BJ, Buck JL, Seidman JD, McCabe KM. From the archives of the AFIP. Ovarian epithelial neoplasms: radiologic-pathologic correlation. Radiographics. 1994;14(6):1351–74.
124. Bergfeldt K, Rydh B, Granath F, Gronberg H, Thalib L, Adami HO, et al. Risk of ovarian cancer in breast-cancer patients with a family history of breast or ovarian cancer: a population-based cohort study. Lancet. 2002;360(9337):891–4.
125. Rosen PP, Groshen S, Kinne DW, Hellman S. Nonmammary malignant neoplasms in patients with stage I (T1N0M0) and stage II (T1N1M0) breast carcinoma. A long-term follow-up study. Am J Clin Oncol. 1989;12(5):369–74.
126. Ramus SJ, Gayther SA. The contribution of BRCA1 and BRCA2 to ovarian cancer. Mol Oncol. 2009;3(2):138–50.
127. Malone KE, Daling JR, Doody DR, Hsu L, Bernstein L, Coates RJ, et al. Prevalence and predictors of BRCA1 and BRCA2 mutations in a population-based study of breast cancer in white and black American women ages 35 to 64 years. Cancer Res. 2006; 66(16):8297–308.
128. Antoniou A, Pharoah PD, Narod S, Risch HA, Eyfjord JE, Hopper JL, et al. Average risks of breast and ovarian cancer associated with BRCA1 or BRCA2 mutations detected in case Series unselected for family history: a combined analysis of 22 studies. Am J Hum Genet. 2003;72(5):1117–30.
129. King MC, Marks JH, Mandell JB. Breast and ovarian cancer risks due to inherited mutations in BRCA1 and BRCA2. Science. 2003;302(5645):643–6.
130. Brose MS, Rebbeck TR, Calzone KA, Stopfer JE, Nathanson KL, Weber BL. Cancer risk estimates for BRCA1 mutation carriers identified in a risk evaluation program. J Natl Cancer Inst. 2002;94(18):1365–72.
131. Ford D, Easton DF, Stratton M, Narod S, Goldgar D, Devilee P, et al. Genetic heterogeneity and penetrance analysis of the BRCA1 and BRCA2 genes in breast cancer families. The Breast Cancer Linkage Consortium. Am J Hum Genet. 1998;62(3):676–89.
132. Curtin JP, Barakat RR, Hoskins WJ. Ovarian disease in women with breast cancer. Obstet Gynecol. 1994;84(3):449–52.
133. Juretzka MM, Crawford CL, Lee C, Wilton A, Schuman S, Chi DS, et al. Laparoscopic findings during adnexal surgery in women with a history of nongynecologic malignancy. Gynecol Oncol. 2006;101(2):327–30.
134. Quan ML, Fey J, Eitan R, Abu-Rustum NR, Barakat RR, Borgen PI, et al. Role of laparoscopy in the evaluation of the adnexa in patients with stage IV breast cancer. Gynecol Oncol. 2004;92(1):327–30.
135. Harris M, Howell A, Chrissohou M, Swindell RI, Hudson M, Sellwood RA. A comparison of the metastatic pattern of infiltrating lobular carcinoma and infiltrating duct carcinoma of the breast. Br J Cancer. 1984;50(1):23–30.
136. Bigorie V, Morice P, Duvillard P, Antoine M, Cortez A, Flejou JF, et al. Ovarian metastases from breast cancer: report of 29 cases. Cancer. 2010;116(4):799–804.
137. Eitan R, Gemignani ML, Venkatraman ES, Barakat RR, Abu-Rustum NR. Breast cancer metastatic to abdomen and pelvis: role of surgical resection. Gynecol Oncol. 2003;90(2):397–401.
138. Metcalfe KA, Lynch HT, Ghadirian P, Tung N, Olivotto IA, Foulkes WD, et al. The risk of ovarian cancer after breast cancer in BRCA1 and BRCA2 carriers. Gynecol Oncol. 2005;96(1):222–6.
139. Young RH, Scully RE. Metastatic tumors in the ovary: a problem-oriented approach and review of the recent literature. Semin Diagn Pathol. 1991;8(4):250–76.
140. Tornos C, Soslow R, Chen S, Akram M, Hummer AJ, Abu-Rustum N, et al. Expression of WT1, CA 125, and GCDFP-15 as useful markers in the differential diagnosis of primary ovarian carcinomas versus metastatic breast cancer to the ovary. Am J Surg Pathol. 2005;29(11):1482–9.
141. Moritani S, Ichihara S, Hasegawa M, Endo T, Oiwa M, Yoshikawa K, et al. Serous papillary adenocarcinoma of the female genital organs and invasive micropapillary carcinoma of the breast. Are WT1, CA125, and GCDFP-15 useful in differential diagnosis? Hum Pathol. 2008;39(5):666–71.
142. Ferrozzi F, Tognini G, Bova D, Zuccoli G. Non-Hodgkin lymphomas of the ovaries: MR findings. J Comput Assist Tomogr. 2000;24(3):416–20.
143. Akin O. Lymphoma, ovary. In: Hricak H, editor. Diagnostic imaging: gynecology. 1 ed. Amirsys; Salt Lake City, Utah. 2007. p. 7:92–4.
144. Mitsumori A, Joja I, Hiraki Y. MR appearance of non-Hodgkin's lymphoma of the ovary. AJR Am J Roentgenol. 1999; 173(1):245.
145. Young RH, Scully RE. Malignant melanoma metastatic to the ovary. A clinicopathologic analysis of 20 cases. Am J Surg Pathol. 1991;15(9):849–60.
146. Gupta D, Deavers MT, Silva EG, Malpica A. Malignant melanoma involving the ovary: a clinicopathologic and immunohistochemical study of 23 cases. Am J Surg Pathol. 2004;28(6):771–80.
147. McCluggage WG, Bissonnette JP, Young RH. Primary malignant melanoma of the ovary: a report of 9 definite or probable cases with emphasis on their morphologic diversity and mimicry of other primary and secondary ovarian neoplasms. Int J Gynecol Pathol. 2006;25(4):321–9.
148. Fitzgibbons PL, Martin SE, Simmons TJ. Malignant melanoma metastatic to the ovary. Am J Surg Pathol. 1987;11(12):959–64.
149. Moselhi M, Spencer J, Lane G. Malignant melanoma metastatic to the ovary: presentation and radiological characteristics. Gynecol Oncol. 1998;69(2):165–8.

Part V

New Prospectives

Three-Dimensional Ultrasound in Adnexal Masses

Juan Luis Alcázar, Begoña Olartecoechea, and María Aubá

Abstract

Two-dimensional ultrasound is commonly used in gynecological practice, and it could be considered as the first-line imaging technique for diagnosing adnexal pathology. Three-dimensional ultrasound allows the acquisition of the so-called 3D volumes. Once the 3D volume is acquired, it can be digitally stored and transferred via DICOM to a personal computer for further assessment with dedicated software. An important ability of 3DUS is volume calculation even in irregularly shaped structures. In this chapter, the potentialities and the state of the art of the three-dimensional ultrasound will be reviewed.

Keywords

Ultrasound • Three-dimensional ultrasound • Ovarian neoplasm • Sensitivity • Specificity • Diagnostic confidence

Introduction

Two-dimensional ultrasound (2DUS) is commonly used in gynecological practice, and it could be considered as the first-line imaging technique for diagnosing adnexal pathology [1].

In the last 15 years, three-dimensional ultrasound (3DUS) has become available for clinical use.

Three-dimensional ultrasound allows the acquisition of the so-called 3D volumes [2, 3]. Once the 3D volume is acquired, it can be digitally stored and transferred via DICOM to a personal computer for further assessment with dedicated software. The 3D volume can be manipulated in several ways. Probably the most used and useful display is multiplanar display, which simultaneously shows three orthogonal planes (axial, longitudinal, and coronal) allowing navigation through these three planes (Fig. 1). Other displays for 3DUS are tomographic ultrasound imaging (TUI) that presents images like MRI does (Fig. 2), surface rendering that shows surfaces (Fig. 3) or allows a three-dimensional reconstruction of vessels (Fig. 4), the "omni-view" mode that shows the one perpendicular plane over other making simpler the imaging (Fig. 5), and the "inversion" mode that shows as "opaque" what is a fluid-filled structure giving a more precise idea of the shape the cystic cavity (Fig. 6). Another important ability of 3DUS is volume calculation even in irregularly shaped structures.

The addition of power Doppler to 3DUS allows the assessment of organ/tissue vascularity. By using 3D power Doppler angiography (3D-PDA), it is possible to reconstruct the vascular tree within a given structure, organ, or tissue. This reconstructed vascular tree can be subjectively analyzed [4].

On the other hand, using dedicated software three-dimensional power Doppler-derived indices can be calculated from the tissue or organ [5]. These indices were named vascularization index (VI), flow index (FI), and vascularization-flow index (VFI). These indexes are based and related to the total and relative amount of power Doppler information within the tissue. The vascularization index is expressed as percentage and measures the ratio between the

J.L. Alcázar, MD, PhD (✉) • B. Olartecoechea, MD
M. Aubá, MD
Department of Obstetrics and Gynecology,
Clínica Universidad de Navarra, University of Navarra,
Avenida Pio XII, 36, 31008 Pamplona, Spain
e-mail: jlalcazar@unav.es

L. Saba et al. (eds.), *Ovarian Neoplasm Imaging*,
DOI 10.1007/978-1-4614-8633-6_24,

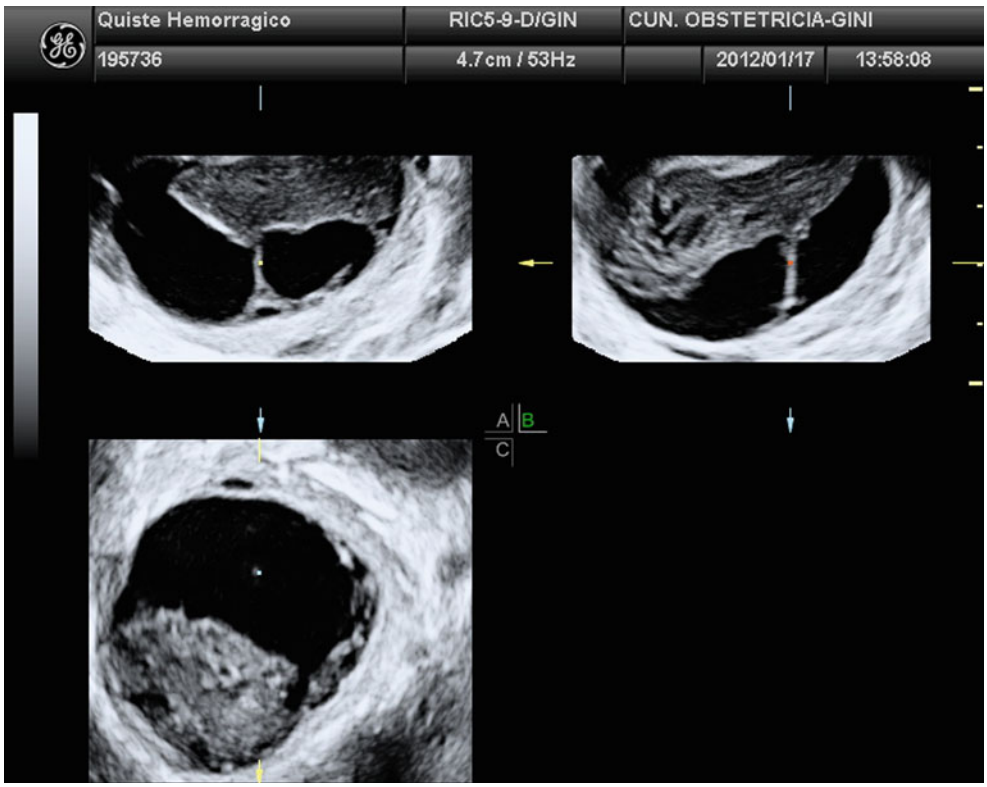

Fig. 1 Three-dimensional ultrasound from a hemorrhagic cyst that shows the lesion in the three orthogonal planes. The examiner may navigate through any of them having a precise idea of the ultrasound features of the lesion

number of color voxels and total number of voxels. The flow index (FI) is unitless and is the average color value of all color voxels. VI is thought to reflect the amount of vessels, whereas FI is thought to reflect the intensity of flow within those vessels at the time of 3D sweep. VFI is just a mathematical relationship between VI and FI, and it is thought to represent both blood flow and vascularization.

Finally, analysis can be done off-line and not in real time, which avoids the need for immediate reporting.

Gray-Scale Three-Dimensional Ultrasound

The first to report on the use of 3DUS for assessing adnexal masses were Bonilla-Musoles et al. [6]. They reported a series of 76 women in whom a single examiner performed both 3DUS and 2DUS, only five women had ovarian cancer. They found that using surface rendering 3DUS was able to show papillary projections in the inner surface of the mass that were missed at 2DUS in 7 % of the cases. 3DUS was more sensitive than 2DUS (100 % versus 80 %) with similar specificity (100 % versus 99 %).

Hata et al. reported a series of 20 women (7 malignant tumors) in whom the different examiners performed both 3DUS and 2DUS [7]. They found that 3DUS was more specific than 2DUS (92.3 % versus 38.4 %) with identical sensitivity (100 %). However, this series was small and the prevalence of malignancy was high.

Alcázar et al. reported a series of 41 women diagnosed as having complex adnexal masses on 2DUS [8]. Two different examiners performed 3DUS and 2DUS. The prevalence of ovarian malignancy was high (48 %). In this study 3DUS showed better than 2DUS for predicting ovarian malignancy in terms of sensitivity (100 % versus 90 %) and specificity (78 % versus 61 %), but these differences did not reach statistical significance. However, 3DUS reinforced examiner's diagnostic impression. This same group reported a second series with similar results to the previous one [9].

Laban et al. in a series of 50 masses – 33 % malignant tumors – found that 3DUS had a higher sensitivity (90 % versus 81 %) and specificity (84 % versus 79 %) than 2DUS [10].

The main shortcomings of all these studies are that series are small and the prevalence of malignancy is high.

Some studies have assessed the reproducibility of 3DUS when performed by different observers. Alcázar et al. [9] found that both intra-observer agreement was good and interobserver agreement were good. Pascual et al. [11] and Sladkevicius et al. [12] reached similar conclusions. This is a relevant factor when using this technique in clinical setting.

Thus, it can be concluded that 3DUS seems to have better diagnostic performance than 2DUS for predicting malignancy in adnexal masses, but further better designed studies are needed to draw definitive conclusions.

Two studies have focused on the use of 3DUS for diagnosing some specific types of lesions.

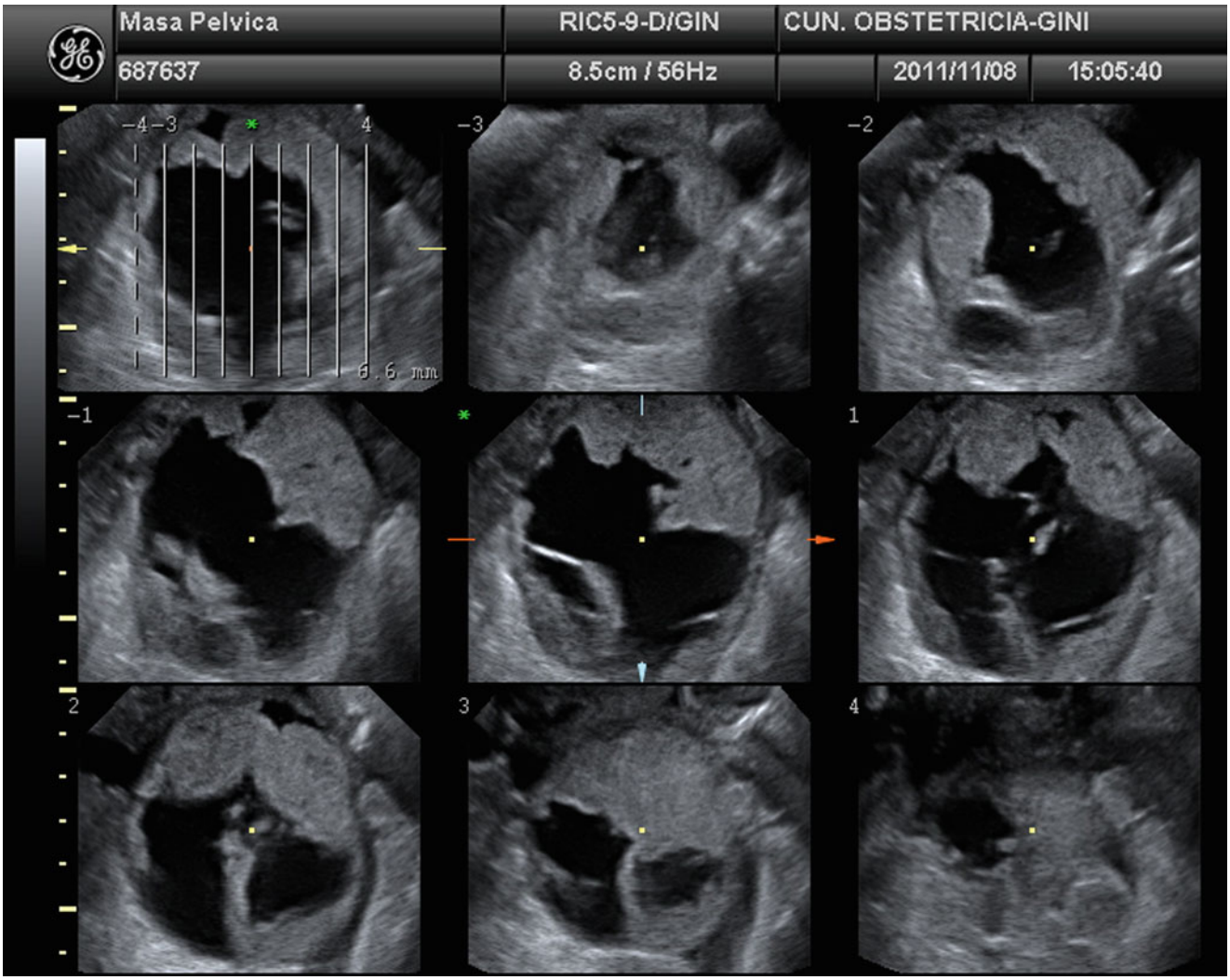

Fig. 2 Tomographic ultrasound imaging (TUI) displays the lesion in several parallel planes in an identical fashion that CT scan and magnetic resonance do. The examiner may have an impression of the lesion features by one click. Images from the three orthogonal planes can be interchangeably displayed

Timor-Tirtsch et al. showed that the use of inverted mode could be useful for diagnosing hydrosalpinx [13].

Alcázar et al. showed that the objective analysis of cyst content by calculating the so-called *mean gray value* could improve the performance of 2DUS for the diagnosis of ovarian endometrioma [14].

Three-Dimensional Power Doppler Ultrasound

As stated above, the use of 3D-PDA allows the assessment of the tumoral vascular network analyzing the presence of microaneurysms, arteriovenous shunts, abnormal vessels branching, tortuosity, and vessel caliber changes, all of them considered as suspicious for malignancy (Figs. 7 and 8) or the quantitative analysis of tumor vascularization by calculating the so-called 3D power Doppler indices (Fig. 9).

Cohen et al. aimed to determine if 3D-PDA could improve the specificity of 2DUS morphological ultrasound in a series of 71 complex adnexal masses [15]. They did not use 2D conventional color Doppler or 2D power Doppler. In their approach, they combined 2D and 3D morphological features with 3D-PDA evaluation of blood flow tumor location, considering a tumor as malignant in the presence of complex morphological pattern and central (in papillary projections and/or septations) blood flow location. They concluded that the addition of 3D-PDA improved the specificity of 2DUS (75 % versus 54 %), without decreasing the sensitivity (100 % both techniques). However, similar results can be achieved also by using a simpler technique such as 2D power Doppler as demonstrated by Alcázar et al. [16].

The first to use 3D-PDA for discriminating benign from malignant adnexal masses using the analysis of the tumoral vascular tree architecture were Kurjak et al. They applied an own designed scoring system that included 3DUS tumor vascular tree features and 2DUS morphological features. The criteria for 3D-PDA malignancy were the presence of chaotic vessel arrangement and complex branching pattern. In two different series they found that this 3D-PDA-/2DUS-based scoring system showed better performance than 2DUS alone [17, 18]. Kupesic et al. showed that contrast enhanced 3D-PDA could improve further the diagnostic performance [19].

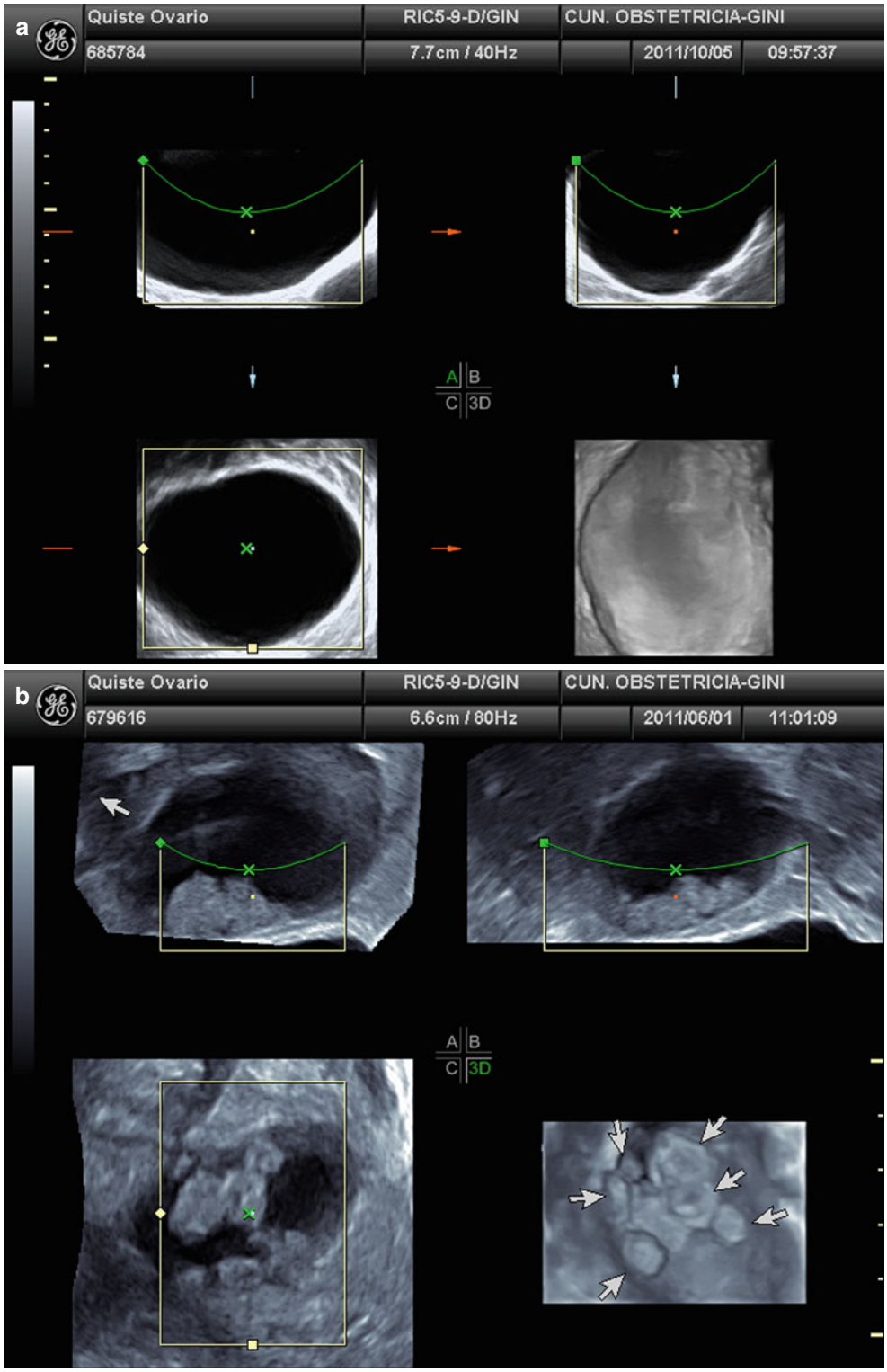

Fig. 3 Surface rendering from the internal wall of two different ovarian cysts. In one case a smooth cyst's wall is clearly seen (**a**). In the other case the surface of cyst wall irregularities is shown (**b**) and better depicted than by two-dimensional ultrasound (**c**)

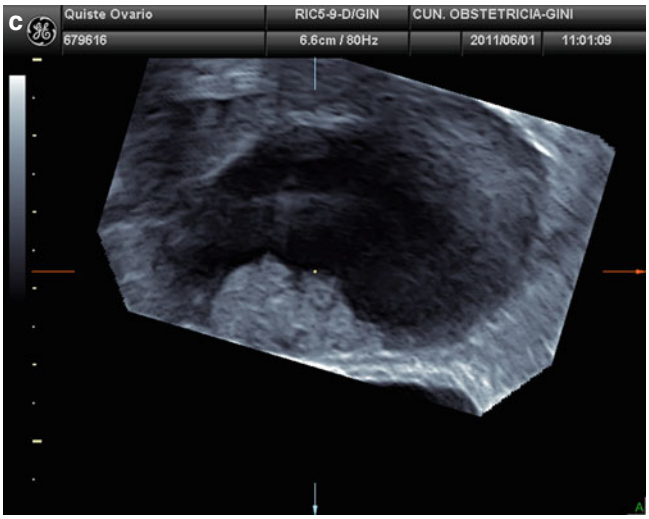

Fig. 3 (continued)

Chase et al. analyzed vascular architecture by 3D-PDA in a series of 66 women diagnosed as having an adnexal mass [20]. Their criterion for malignancy suspicion was the presence of chaotic vessel pattern. They also concluded that 3D-ultrasound examination of vascular architecture was discriminatory for distinguishing benign ovarian masses from malignancy. Chaotic vascular architecture correlated with malignancy in this group of high-risk patients.

However, some subsequent studies have challenged these results.

Laban et al. used the criteria proposed by Kurjak in a series on 50 selected patients with complex adnexal masses [10]. They reported that 3D-PDA was not superior to 2D power Doppler.

Sladkevicius et al. assessed the role of 3D tumoral vascular tree architecture in a series of 131 women with adnexal masses [21]. They analyzed separately several vascular features such as density, branching, tortuosity, vessel caliber change, and the presence of color splashes. They found that these parameters were reproducible between observers but added little valuable information to that obtained by 2DUS for predicting malignancy.

Alcázar et al. analyzed the role of vascular tree assessment by 3D-PDA in a series of 39 selected women with vascularized complex masses [22]. Criteria for malignancy were the presence of at least two of the following: irregular branching (>3 branches and close to 90° angulation branching), vessel caliber narrowing, microaneurysms, and vascular lakes. Their results showed that assessment of vascular tree was moderately reproducible between examiners with different expertise, and its diagnostic performance was moderate.

Dai et al. also assessed the role of vascular tree in a series of 36 women with complex ovarian masses [23]. Masses with the presence of penetrating vessels within papillary projections, solid areas or central areas of a solid tumor, or

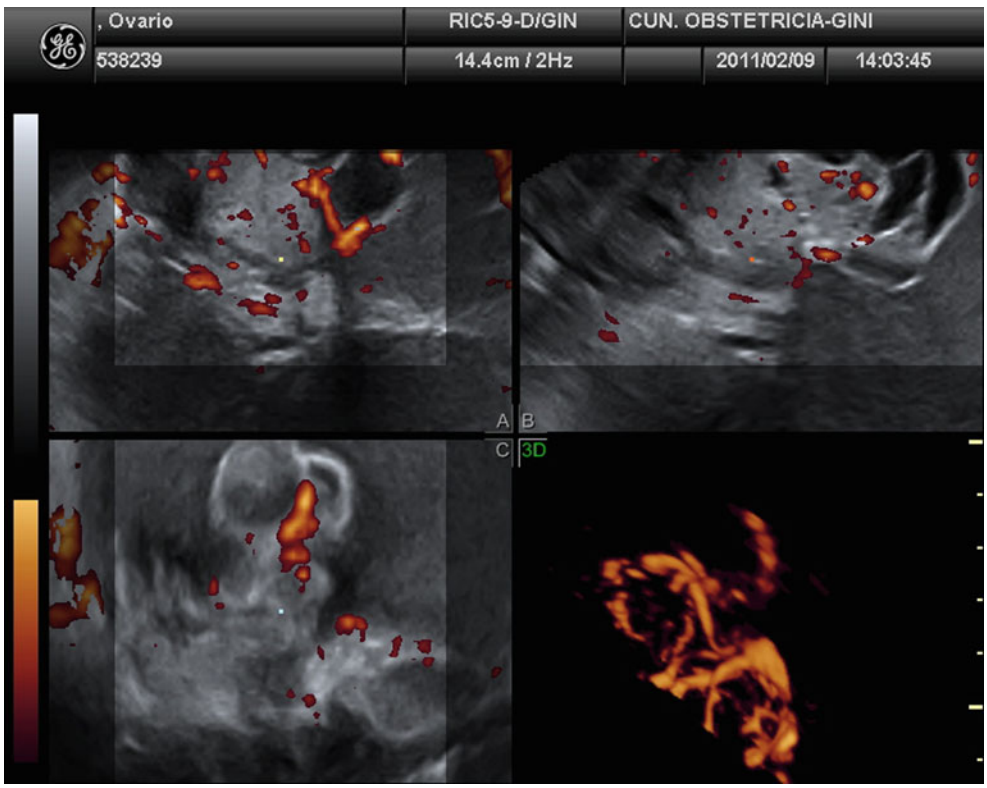

Fig. 4 Three-dimensional reconstruction of the vascular tree from an ovarian tumor depicted by power Doppler ultrasound

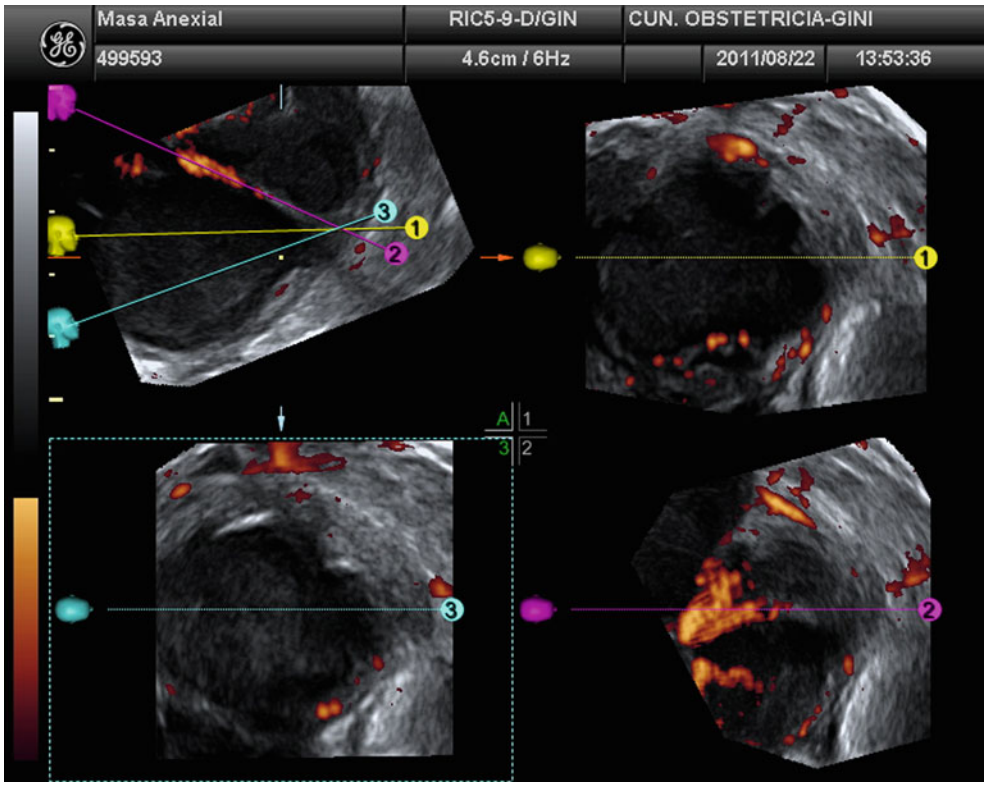

Fig. 5 Omni-view display of an adnexal mass. In this display mode three perpendicular views to the mass's longitudinal plane are seen. One of them (violet) passes through the vascularized septum

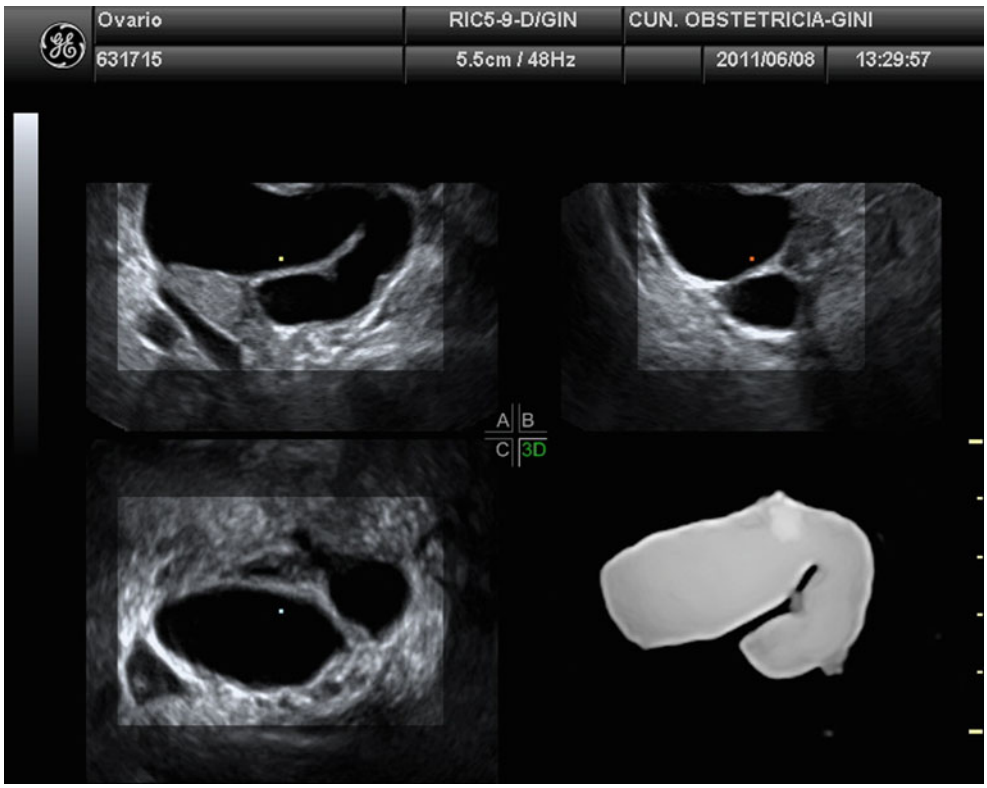

Fig. 6 Inversion mode from a hydrosalpinx. The sausage-like form is clearly depicted using this display mode

flow within septations were graded as malignant. They found that 3D-PDA had poorer diagnostic performance than 2DUS.

Mansour et al. evaluated 400 women with adnexal masses by 3D-PDA [24]. The pattern of vascularity of masses was interpreted as avascular, parallel, or chaotic, being chaotic pattern

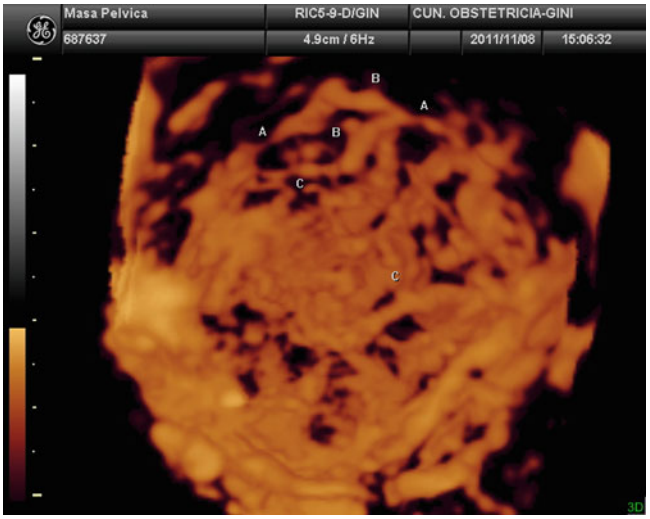

Fig. 7 Three-dimensional reconstruction of the vascular tree from an ovarian tumor depicted by power Doppler ultrasound. Abnormal features such as changes in caliber (**a**), microaneurysms (**b**), and irregular branching (**c**) are shown

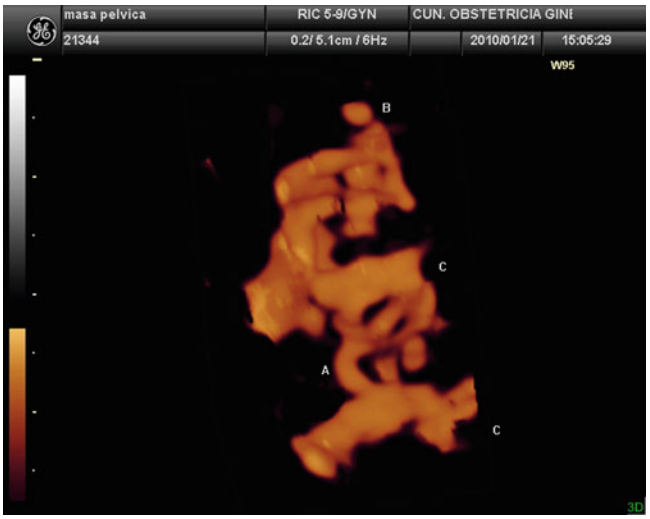

Fig. 8 Another three-dimensional reconstruction of the vascular tree from an ovarian tumor depicted by power Doppler ultrasound. Abnormal features such as microaneurysms (**b**) and irregular branching (**a**, **c**) are shown

suggestive of malignancy. They found that adding 3D-PDA information to the risk of malignancy index described by Jacobs [25] improved the diagnostic performance of this index.

The objective quantification of tumor vascularity using dedicated software was first proposed by Alcázar et al. [26]. In their report they proposed the off-line assessment of 3D-PD vascular indices within the most suspicious vascularized area from the tumor. The rationale for this proposal is based on two facts: First, ovarian malignant tumors are known to show a higher microvessel density as compared with benign ones in immunohistochemical studies and there is a correlation with Doppler ultrasound mapping. Second, it is thought that 3D-PD vascular indices reflect tissue vascularization. In a selected series of 69 vascularized solid and cystic-solid masses, which are the most difficult to characterize by conventional 2DUS. They found that all 3D-PD vascular indexes, namely, VI, FI, and VFI, were significantly higher in ovarian cancer as compared with benign tumors.

Almost simultaneously, Testa et al. reported similar findings using different software in a series of 24 women with solid ovarian masses [27].

After these pioneering reports, Geomini et al. reported data from a series of 181 women with adnexal masses using the method proposed by Alcázar [28]. This group included any kind of mass diagnosed at transvaginal ultrasound and performed the vascular assessment from the whole tumor. They found that FI, but not VI and VFI, was significantly higher in ovarian cancer.

Jokubkiene et al. proposed a different approach based on the use of a virtual 5-cc spherical sampling from the most vascularized area from the tumor [29]. They found that 3D-PDA vascular indices from the spherical sample were higher in ovarian cancers as compared with benign tumors, but they concluded that this information has little value as compared with gray-scale analysis performed by an experienced examiner. Probably this could be explained by the fact that 3D analysis was performed in nonselected adnexal masses, where many cases could be easily classified based on morphological appearance and there was no need for 3D ultrasound. Kudla et al. proposed using a 1-cc spherical sampling and also found that 3D-PDA indices were significantly higher in malignant tumors [30].

Only one study has not shown differences in 3D-PD indices between benign and malignant ovarian tumors. This study was reported by Ohel et al. [31]. However, the series was too small and the methods used were not fully explained.

Alcázar and Prka compared manual and spherical sampling and concluded that both methods are comparable and spherical sampling is faster to perform but 5-cc spherical sampling cannot be used in some small tumors [32].

Regarding the reproducibility of this method, Alcázar et al. showed that manual sampling was reproducible between observers with different expertise [33]. Spherical sampling is also reproducible [29, 32]. Furthermore, the size of the sphere does not affect reproducibility [34].

Some reports have shown that the use of 3D-PDA vascular indices could be useful to improve the specificity of conventional gray-scale and 2D power Doppler ultrasound in selected cystic-solid or solid adnexal masses.

Alcázar and Rodriguez evaluated 143 vascularized solid or cystic-solid adnexal masses (113 masses were malignant and 39 were benign) [35]. In this study the manual sampling method was used. Taking into account that based on morphological and two-dimensional power Doppler findings all

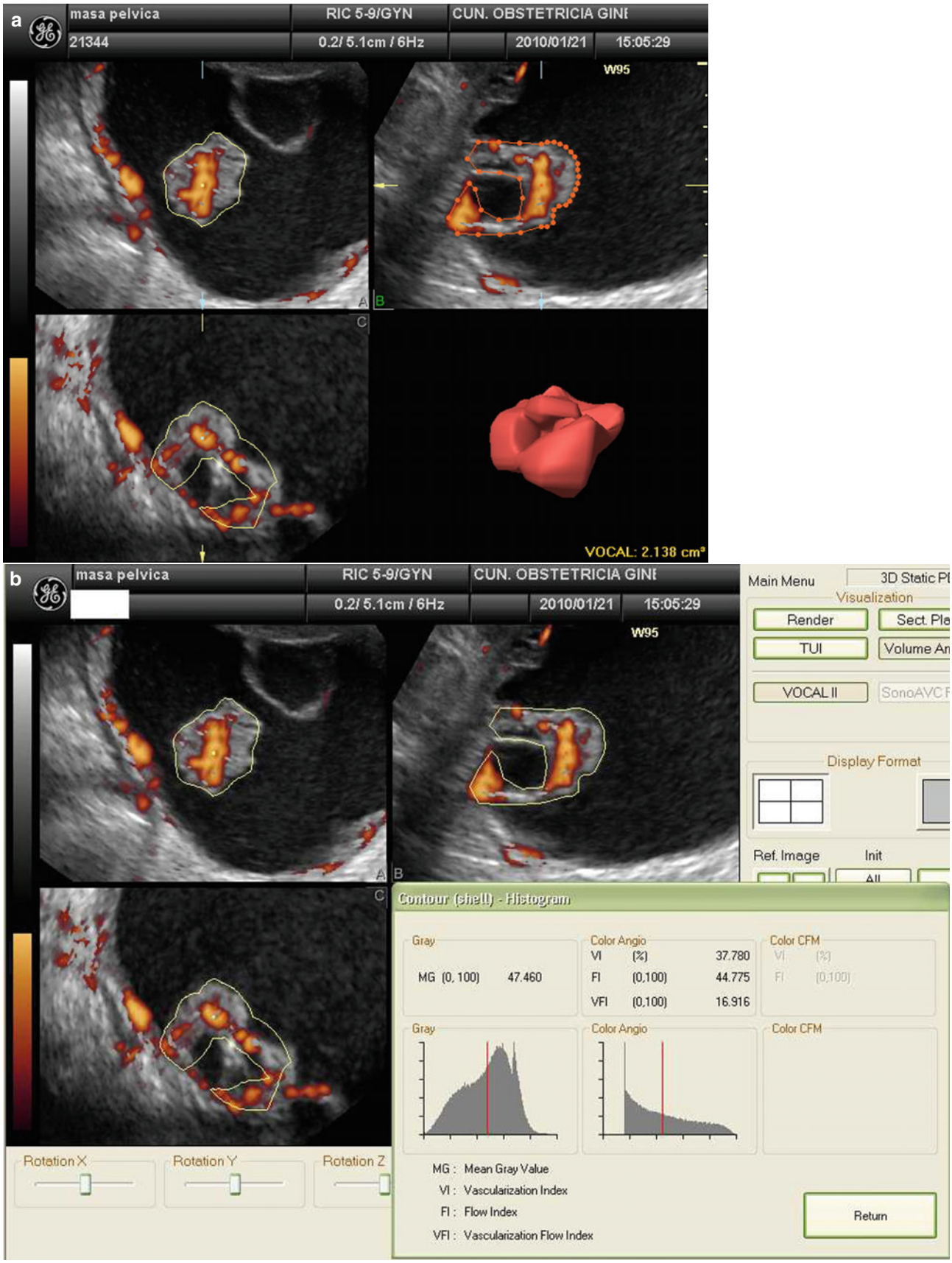

Fig. 9 Quantitative vascular assessment of a papillary projection using three-dimensional power Doppler ultrasound. (**a**) Manual sampling of the papillary projection (volume: 2.144 cc). (**b**) 3D vascular derived indices from the lesion using manual sampling. (**c**) Spherical sampling (1-cc) from the same lesion. (**d**) 3D vascular derived indices from the lesion using spherical sampling. Note that vascular indices differ from one method to another because the volume sampled is different

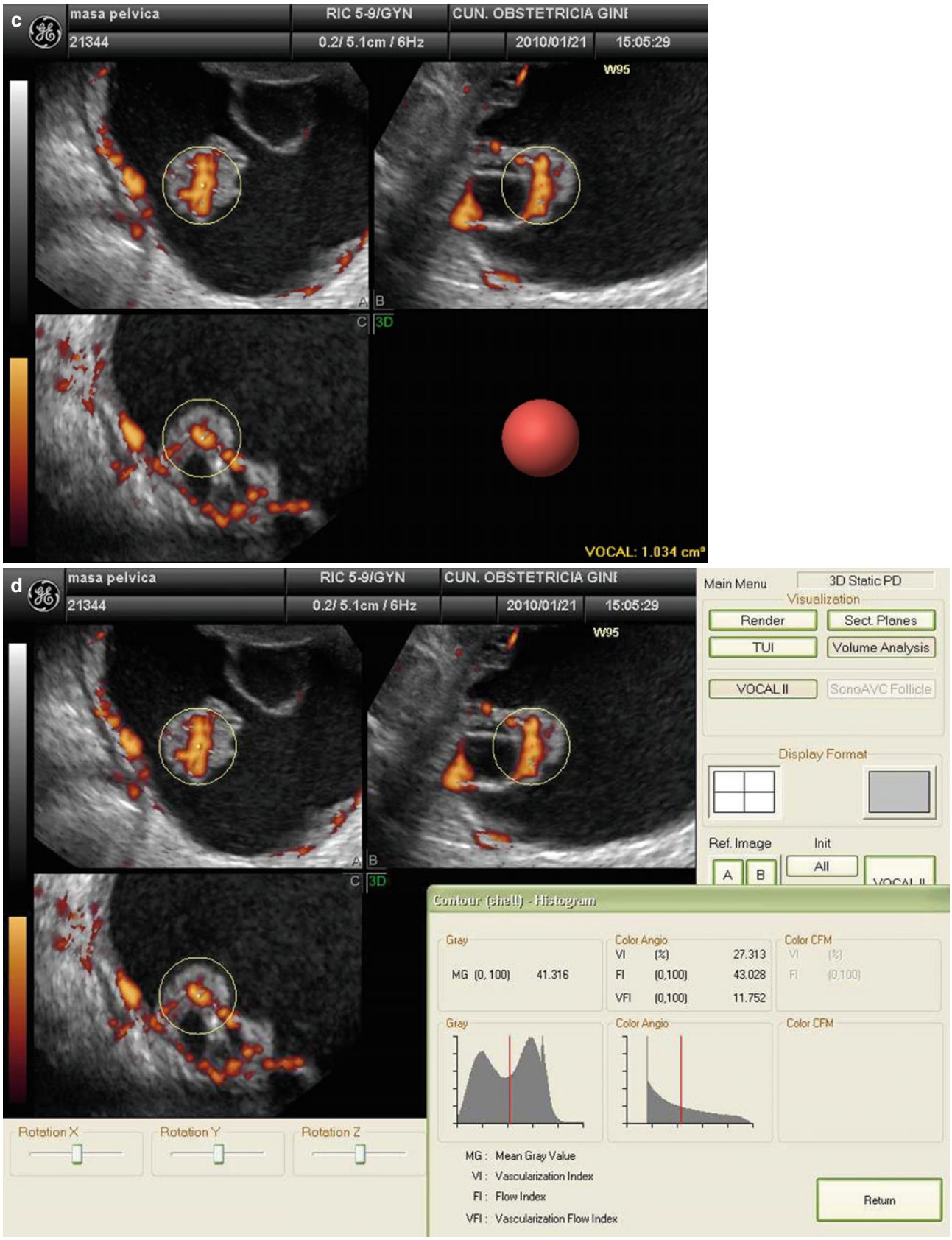

Fig. 9 (continued)

histologically benign tumors would be considered as questionable, they found that specificity could be improved by a 33 % without decreasing significantly sensitivity.

Kudla and Alcázar have shown that using a spherical sampling instead of the manual sampling could render an improvement of 77 % in specificity in selected vascularized solid or cystic-solid adnexal masses [36]. This study comprised 138 masses (only 26 benign tumors). Using 3D power Doppler 1-cc spherical sampling from the most vascularized area of the tumor subjectively determined by the examiner, 20 out of 26 benign tumors were correctly classified as benign. Sensitivity was 91 %.

However, Guerriero et al. found that this 3D-PDA was not useful for triaging patients with complex adnexal masses [37].

However, it should be borne in mind that the actual significance of these indices is not fully understood, there are some important technical limitations for this technique and standardization is lacking [38–41]. Thus, its potential use in clinical practice is debated [42, 43].

Finally, a recent study by Alcázar and colleagues has shown that remote off-line assessment of stored 3D volumes of adnexal masses may be feasible, showing a good agreement with real-time ultrasound and having a similar diagnostic performance [44].

References

1. Mettler L. The cystic adnexal mass: patient selection, surgical techniques and long-term follow-up. Curr Opin Obstet Gynecol. 2001; 13:389–97.
2. Alcázar JL. Three-dimensional ultrasound in gynecology: current status and future perspectives. Curr Women's Health Rev. 2005;1:1–14.
3. Bega G, Lev-Toaff AS, O'Kane P, Becker Jr E, Kurtz AB. Three-dimensional ultrasonography in gynecology: technical aspects and clinical applications. J Ultrasound Med. 2003;22:1249–69.
4. Alcázar JL. Three-dimensional ultrasound in gynecological practice. Rep Med Imaging. 2012;5:1–13.
5. Pairleitner H, Steiner H, Hasenoehrl G, Staudach A. Three dimensional power Doppler sonography: imaging and quantifying blood flow and vascularization. Ultrasound Obstet Gynecol. 1999;14:139–43.
6. Bonilla-Musoles F, Raga F, Osborne NG. Three-dimensional ultrasound evaluation of ovarian masses. Gynecol Oncol. 1995;59: 129–35.
7. Hata T, Yanagihara T, Hayashi K, Yamashiro C, Ohnishi Y, Akiyama M, Manabe A, Miyazaki K. Three-dimensional ultrasonographic evaluation of ovarian tumours: a preliminary study. Hum Reprod. 1999;14:858–61.
8. Alcázar JL, Galán MJ, García-Manero M, Guerriero S. Three-dimensional ultrasound morphologic assessment in complex adnexal masses a preliminary experience. J Ultrasound Med. 2003; 22:249–54.
9. Alcázar JL, García-Manero M, Galván R. Three-dimensional sonographic morphologic assessment of adnexal masses: a reproducibility study. J Ultrasound Med. 2007;26:1007–11.
10. Laban M, Metawee H, Elyan A, Kamal M, Kamel M, Mansour G. Three-dimensional ultrasound and three-dimensional power Doppler in the assessment of ovarian tumors. Int J Gynaecol Obstet. 2007;99:201–5.
11. Pascual MA, Graupera B, Hereter L, Rotili A, Rodriguez I, Alcázar JL. Intra- and interobserver variability of 2D and 3D transvaginal sonography in the diagnosis of benign versus malignant adnexal masses. J Clin Ultrasound. 2011;39:316–21.
12. Sladkevicius P, Valentin L. Intra- and inter-observer agreement when describing adnexal masses using the International Ovarian Tumour Analysis (IOTA) terms and definitions: a study on three-dimensional (3D) ultrasound volumes. Ultrasound Obstet Gynecol. 2013;41(3):318–27. doi:10.1002/uog.12289.
13. Timor-Tritsch IE, Monteagudo A, Tsymbal T. Three-dimensional ultrasound inversion rendering technique facilitates the diagnosis of hydrosalpinx. J Clin Ultrasound. 2010;38: 372–6.
14. Alcázar JL, León M, Galván R, Guerriero S. Assessment of cyst content using mean gray value for discriminating endometrioma from other unilocular cysts in premenopausal women. Ultrasound Obstet Gynecol. 2010;35:228–32.
15. Cohen LS, Escobar PF, Scharm C, Glimco B, Fishman DA. Three-dimensional ultrasound power Doppler improves the diagnostic accuracy for ovarian cancer prediction. Gynecol Oncol. 2001; 82:40–8.
16. Alcázar JL, Castillo G. Comparison of 2-dimensional and 3-dimensional power-Doppler imaging in complex adnexal masses for the prediction of ovarian cancer. Am J Obstet Gynecol. 2005;192:807–12.
17. Kurjak A, Kupesic S, Anic T, Kosuta D. Three-dimensional ultrasound and power Doppler improve the diagnosis of ovarian lesions. Gynecol Oncol. 2000;76:28–32.
18. Kurjak A, Kupesic S, Sparac V, Bekavac I. Preoperative evaluation of pelvic tumors by Doppler and three-dimensional sonography. J Ultrasound Med. 2001;20:829–40.
19. Kupesic S, Kurjak A. Contrast-enhanced three-dimensional power Doppler sonography for differentiation of adnexal masses. Obstet Gynecol. 2000;96:452–8.
20. Chase DM, Crade M, Basu T, Saffari B, Berman ML. Preoperative diagnosis of ovarian malignancy: preliminary results of the use of 3-dimensional vascular ultrasound. Int J Gynecol Cancer. 2009; 19:354–60.
21. Sladkevicius P, Jokubkiene L, Valentin L. Contribution of morphological assessment of the vessel tree by three-dimensional ultrasound to a correct diagnosis of malignancy in ovarian masses. Ultrasound Obstet Gynecol. 2007;30:874–82.
22. Alcázar JL, Cabrera C, Galván R, Guerriero S. Three-dimensional power Doppler vascular network assessment of adnexal masses: intraobserver and interobserver agreement analysis. J Ultrasound Med. 2008;27:997–1001.
23. Dai SY, Hata K, Inubashiri E, Kanenishi K, Shiota A, Ohno M, Yamamoto Y, Nishiyama Y, Ohkawa M, Hata T. Does three-dimensional power Doppler ultrasound improve the diagnostic accuracy for the prediction of adnexal malignancy? J Obstet Gynaecol Res. 2008;34:364–70.
24. Mansour GM, El-Lamie IK, El-Sayed HM, Ibrahim AM, Laban M, Abou-Louz SK, Abd Allah MY, El-Mahallawi MN, El-Lamie KI, Gad-Allah M. Adnexal mass vascularity assessed by 3-dimensional power Doppler: does it add to the risk of malignancy index in prediction of ovarian malignancy?: four hundred-case study. Int J Gynecol Cancer. 2009;19:867–72.
25. Jacobs I, Oram D, Fairbanks J, Turner J, Frost C, Grudzinskas JG. A risk of malignancy index incorporating CA 125, ultrasound and menopausal status for the accurate preoperative diagnosis of ovarian cancer. Br J Obstet Gynaecol. 1990;97:922–9.
26. Alcázar JL, Merce LT, Garcia MM. Three-dimensional power Doppler vascular sampling: a new method for predicting ovarian cancer in vascularized complex adnexal masses. J Ultrasound Med. 2005;24:689–96.
27. Testa AC, Ajossa S, Ferrandina G, Fruscella E, Ludovisi M, Malaggese M, Scambia G, Melis GB, Guerriero S. Does quantitative

analysis of three-dimensional power Doppler angiography have a role in the diagnosis of malignant pelvic solid tumors? A preliminary study. Ultrasound Obstet Gynecol. 2005;26:67–72.
28. Geomini PM, Kluivers KB, Moret E, Bremer GL, Kruitwagen RF, Mol BW. Evaluation of adnexal masses with three-dimensional ultrasonography. Obstet Gynecol. 2006;108:1167–75.
29. Jokubkiene L, Sladkevicius P, Valentin L. Does three-dimensional power Doppler ultrasound help in discrimination between benign and malignant ovarian masses? Ultrasound Obstet Gynecol. 2007;29:215–25.
30. Kudla MJ, Timor-Tritsch IE, Hope JM, Monteagudo A, Popiolek D, Monda S, Lee CJ, Arslan AA. Spherical tissue sampling in 3-dimensional power Doppler angiography: a new approach for evaluation of ovarian tumors. J Ultrasound Med. 2008;27:425–33.
31. Ohel I, Sheiner E, Aricha-Tamir B, Piura B, Meirovitz M, Silberstein T, Hershkovitz R. Three-dimensional power Doppler ultrasound in ovarian cancer and its correlation with histology. Arch Gynecol Obstet. 2010;281:919–25.
32. Alcázar JL, Prka M. Evaluation of two different methods for vascular sampling by three-dimensional power Doppler angiography in solid and cystic-solid adnexal masses. Ultrasound Obstet Gynecol. 2009;33:349–54.
33. Alcázar JL, Rodriguez D, Royo P, Galván R, Ajossa S, Guerriero S. Intraobserver and interobserver reproducibility of 3-dimensional power Doppler vascular indices in assessment of solid and cystic-solid adnexal masses. J Ultrasound Med. 2008;27:1–6.
34. Kudla M, Alcázar JL. Does the size of three-dimensional power Doppler spherical sampling affect the interobserver reproducibility of measurements of vascular indices in adnexal masses? Ultrasound Obstet Gynecol. 2009;34:732–4.
35. Alcázar JL, Rodriguez D. Three-dimensional power Doppler vascular sonographic sampling for predicting ovarian cancer in cystic-solid and solid vascularized masses. J Ultrasound Med. 2009;28:275–81.
36. Kudla MJ, Alcázar JL. Does sphere volume affect the performance of three-dimensional power Doppler virtual vascular sampling for predicting malignancy in vascularized solid or cystic-solid adnexal masses? Ultrasound Obstet Gynecol. 2010;35:602–8.
37. Guerriero S, Ajossa S, Piras S, Gerada M, Floris S, Garau N, Minerba L, Paoletti AM, Melis GB. Three-dimensional quantification of tumor vascularity as a tertiary test after B-mode and power Doppler evaluation for detection of ovarian cancer. J Ultrasound Med. 2007;26:1271–8.
38. Alcázar JL. Three-dimensional power Doppler derived vascular indices: what are we measuring and how are we doing it? Ultrasound Obstet Gynecol. 2008;32:485–7.
39. Raine-Fenning NJ, Nordin NM, Ramnarine KV, Campbell BK, Clewes JS, Perkins A, Johnson IR. Evaluation of the effect of machine settings on quantitative three-dimensional power Doppler angiography: an in-vitro flow phantom experiment. Ultrasound Obstet Gynecol. 2008;32:551–9.
40. Raine-Fenning NJ, Nordin NM, Ramnarine KV, Campbell BK, Clewes JS, Perkins A, Johnson IR. Determining the relationship between three-dimensional power Doppler data and true blood flow characteristics: an in-vitro flow phantom experiment. Ultrasound Obstet Gynecol. 2008;32:540–50.
41. Martins WP, Raine-Fenning NJ, Ferriani RA, Nastri CO. Quantitative three-dimensional power Doppler angiography: a flow-free phantom experiment to evaluate the relationship between color gain, depth and signal artifact. Ultrasound Obstet Gynecol. 2010;35:361–8.
42. Welsh A. The questionable value of VOCAL indices of perfusion. Ultrasound Obstet Gynecol. 2010;36:126–7.
43. Martins WP. Three-dimensional power Doppler: validity and reliability. Ultrasound Obstet Gynecol. 2010;36:530–3.
44. Alcázar JL, Iturra A, Sedda F, Aubá M, Ajossa S, Guerriero S, Jurado M. Three-dimensional volume off-line analysis as compared to real-time ultrasound for assessing adnexal masses. Eur J Obstet Gynecol Reprod Biol. 2012;161:92–5.

Ovarian Tumor Characterization Using 3D Ultrasound

U. Rajendra Acharya, M. Muthu Rama Krishnan, Luca Saba, Filippo Molinari, Stefano Guerriero, and Jasjit S. Suri

Abstract

Among gynecological malignancies, ovarian cancer is the most frequent cause of death. Preoperative determination of whether a tumor is benign or malignant has often been found to be difficult. Because of such inconclusive findings from ultrasound images and other tests, many patients with benign conditions have been offered unnecessary surgeries thereby increasing patient anxiety and healthcare cost. The key objective of our work is to develop an adjunct computer-aided diagnostic (CAD) technique that uses ultrasound images of the ovary and image mining algorithms to accurately classify benign and malignant ovarian tumor images. In this algorithm, we extract texture features based on Local Binary Patterns (LBP) and Laws Texture Energy (LTE) and use them to build and train a support vector machine (SVM) classifier. Our technique was validated using 1,000 benign and 1,000 malignant images, and we obtained a high accuracy of 99.9 % using a SVM classifier with a radial basis function (RBF) kernel. The high accuracy can be attributed to the determination of the novel combination of the 16 texture-based features that quantify the subtle changes in the images belonging to both classes. The proposed algorithm has the following characteristics: cost-effectiveness, complete automation, easy deployment, and good end-user comprehensibility. We have also developed a novel integrated index, *Ovarian Cancer Index* (*OCI*), which is a combination of the texture features, to present the physicians with a more transparent adjunct technique for ovarian tumor classification.

Keywords

Ovarian cancer • Local Binary Pattern • Laws Texture Energy • Classification • Support vector machine • Computer-aided diagnosis • Ovarian Cancer Index

U.R. Acharya, PhD, DEng
Department of Electronics and Computer Engineering, Ngee Ann Polytechnic, Singapore, Singapore

Department of Biomedical Engineering, Faculty of Engineering, University of Malaya, Kuala Lumpur, Malaysia

M.M.R. Krishnan, PhD
Department of Electronics and Computer Engineering, Ngee Ann Polytechnic, Singapore, Singapore

L. Saba, MD
Department of Radiology, Azienda Ospedaliero Universitaria di Cagliari, Cagliari, Italy

F. Molinari, PhD
Biolab, Department of Electronics and Telecommunications, Politecnico di Torino, Torino, Italy

S. Guerriero, MD
Department of Obstetrics and Gynecology, University of Cagliari, Ospedale San Giovanni di Dio, Via Ospedale 46, Cagliari 09124, Italy

J.S. Suri, PhD, MBA, Fellow AIMBE (✉)
Department of Biomedical Engineering, CTO, Global Biomedical Technologies, Roseville, CA, USA

Department of Biomedical Engineering, Idaho State University (Aff.), Pocatello, ID, USA
e-mail: jsuri@comcast.net

L. Saba et al. (eds.), *Ovarian Neoplasm Imaging*,
DOI 10.1007/978-1-4614-8633-6_25,

Abbreviations

CA125	Cancer antigen 125
CAD	Computer-aided diagnosis
DICOM	Digital Imaging and Communications in Medicine
FN	False-negatives
FP	False-positives
LBP	Local Binary Pattern
LTE	Laws Texture Energy
MS	Mass spectrometry
OCI	Ovarian Cancer Index
PPV	Positive predictive value
RBF	Radial basis function
SD	Standard deviation
SVM	Support vector machine
TEM	Texture energy measurements
TN	True-negatives
TP	True-positives

Introduction

Ovarian cancer is the cancer that forms in the tissues of the ovaries. The ovaries are located such that there is little interference to the other structures surrounding them. This is probably the reason why there are no symptoms during the initial stage of cancer. In most cases, only when there is significant ovarian enlargement or metastases, symptoms begin to appear, and it will be too late to achieve a good prognosis at this stage. Unlike for other types of cancers, there are no tests suitable for mass screening as so far no screening tests have demonstrated great promise in detecting this disease at its earliest stages. Therefore, inevitably, most of the ovarian cancers are detected only at the advanced stages. In 2011, in the United States, it is estimated that 21,990 new cases will be diagnosed and 15,460 women would die of ovarian cancer [1].

Sonography and the determination of the levels of a tumor marker called CA125 are currently the most commonly used techniques for evaluating this disease. In the case of sonography, wherein the diagnosis is based on manually imaging and analyzing ultrasound images obtained from pelvic masses, the accuracy of the diagnosis relies heavily on the experience and skill of the ultrasonographers and the interpreting radiologists. The other most common method is the cancer antigen 125 (CA125) test. Serum CA125 has been found to be elevated only in 50 % of stage 1 cancers [2]. Moreover, CA125 can also be raised in other malignancies (uterine and pancreatic) and in many benign conditions such as fibroids, endometriosis, pelvic inflammatory disease, and benign ovarian cysts [3]. Menon et al. [4] examined women with elevated CA125 levels and found that the ultrasound parameters give varying sensitivity to diagnosing cancer ranging from 84 to l00 %, with a specificity of 97 %, but only a positive predictive value (PPV) of 37.2 %. Other modalities such as computerized tomography, magnetic resonance imaging, and radioimmunoscintigraphy are limited by cost, device availability, and radiation exposure.

Owing to the limitations of the available diagnostic modalities, on the screening front, several large studies and clinical trials are still currently underway to determine if screening healthy women with sonography and the tumor marker CA125 or a combination of tumor markers or using multimodal screening techniques are accurate and cost-effective [5]. On the diagnostic front, preoperative determination of whether an ovarian tumor is malignant or benign, especially when the tumor has both solid and cystic components, has been mostly found to be difficult [6]. At times, surgical procedures such as bilateral oophorectomy with or without hysterectomy have been offered to patients with benign ovarian tumor because of the inconclusive preoperative diagnosis. Hence, there is a need to develop one of the following devices: (a) a stand-alone modality or a multimodality protocol that has the capability to screen the presence of ovarian cancer at its earliest stages; or (b) an adjunct tool/technique that can provide accurate second opinions on the primary diagnosis.

In this work, we have attempted to develop one such adjunct computer-aided diagnostic (CAD) technique. Since ultrasound is the most widely used and available low-cost modality in all countries, we chose it as our base image acquisition device and attempted to evaluate the acquired images using data mining techniques. CAD techniques generally have the following steps: (a) image acquisition, (b) pre-processing, (c) feature extraction, (d) feature selection, (e) classifier development, and (f) classifier validation. Features are values that adequately quantify the subtle changes in the acquired images. In the area of ovarian disease management, CAD techniques have been used for automatic follicle segmentation in order to better understand ovarian follicle dynamics [7, 8]. It has also been employed for Polycystic Ovary Syndrome detection [9], ovarian cyst classification [10], and ovarian ultrasound image retrieval [11]. There are very few studies in the application of CAD for ovarian cancer detection. A literature review on these techniques (presented in brief in the discussion section of this paper) indicates that there is a need for CAD algorithms that use the ultrasound images and less number of significant image features to predict benign and malignant tumors with high accuracy. Therefore, in this work, we have (a) proposed a novel image mining CAD technique using texture features for the classification of benign and malignant ovarian tumors from ultrasound images and (b) developed a novel integrated index formulated as a combination of the texture

features to present the physicians a more transparent adjunct technique for ovarian tumor classification. Thus the proposed technique has the following characteristics: zero radiation usage, complete automation, and good end-user comprehensibility. Our proposed technique is not tuned towards detecting the cancer at its earliest stages. However, by indicating if the primary diagnosis of whether the tumor is benign or malignant is correct, our technique allows the surgeon to make a more confident call with respect to the subsequent treatment protocol. This reduces the need for, and cost and patient anxiety associated with unwanted biopsies.

Data

Twenty women, age ranging from 29 to 74 years (mean ± SD = 49.5 ± 13.48), were recruited for this study. Out of the 20 patients, 11 (55 %) women were premenopausal and 9 (45 %) were postmenopausal. Briefly, first B-mode ultrasonography was performed to characterize the morphology of the adnexal masses, which were classified as one of the following: unilocular, multilocular, unilocular – solid, multilocular – solid or solid. After B-mode evaluation was performed, 2D power Doppler was used to assess tumor vascularization. Power Doppler settings were set to achieve maximum sensitivity for detecting low-velocity flow without noise (frequency, 5 MHz; power Doppler gain, 0.8; dynamic range, 20–40 dB; edge, 1; persistence, 2; color map, 5; gate, 2; filter, L1; PRF, 0.6 kHz).

All the women were evaluated prior to surgery by 3D transvaginal ultrasonography using a Voluson-I (GE Medical Systems) by one of the authors (blinded for peer review) according to a predefined scanning protocol. The 3D volume of the suspicious areas, e.g., thick papillary projections, or solid areas was obtained, or in the case of mostly solid tumors, the whole tumor was imaged, if possible. Once a 3D volume was obtained, it was stored on a hard disk (*Sonoview*™, GE Medical Systems). Volume acquisition time ranged from 2 to 6 s depending on the size of the volume box. In cases in which a given adnexal mass had more than one volume stored because it contained more than one solid area, we used only the first of the stored volumes for further analysis in this study. Among the 20 patients, 10 had malignancy in their ovaries and 10 had benign conditions. We chose the middle 100 images from each volume from each subject. Thus, the evaluated database consisted of 1,000 benign images and 1,000 malignant images. In this study, we adopted an automated procedure for the extraction of the region of interest (ROI) containing the suspicious area of the tumor. First, we automatically cropped the ultrasound image by using the vertical and horizontal gradients to detect the boundaries of the black frame border surrounding the ultrasound image [12]. Then, from the frames, we cropped only the area containing the ultrasound data. Subsequently, with the help of the gynecologist and radiologist, we delineated a squared ROI starting from the cropped image. We enclosed in the ROI the suspicious portion of the image. We decided to take a 256 × 256 central ROI, since the lesion was always central in all the images in our dataset, and we observed that 256 × 256 was good to enclose the suspicious region. Figure 1 shows typical ultrasound images of benign and malignant classes.

Methods

Figure 2 depicts the general block diagram of the proposed CAD technique for ovarian cancer detection. The dataset is split into a training set and a test set. The training set images are used to develop the classifiers. The classifiers are evaluated using the test set to simulate a real-time diagnosis scenario. In Fig. 2, steps involved in the off-line training procedure are shown in the blocks outside the shaded rectangular box, and the blocks inside the shaded box indicate the steps in the online real-time system. In the off-line training system, texture features based on Local Binary Patterns (LBP) and Laws Texture Energy (LTE) are extracted from the images in the training database. Only highly discriminative features are selected. These features and the ground truth of whether the training images are benign or malignant are used to train the support vector machine (SVM) classifier. The outputs of this off-line training system are the SVM classifier parameters that are tuned to accurately predict the class labels (benign or malignant) given the input significant features. To test this built classifier, we extract the significant features from the test set images and apply the SVM classifier parameters on them to determine the class. The classifier performance is evaluated using performance measures such as sensitivity, specificity, accuracy, and PPV.

In the remainder of this section, we describe the LBP and LTE texture features, the SVM classifier, and the feature selection test (*t*-test) used in this work.

Feature Extraction

Local Binary Pattern (*LBP*): LBP [13] was initially proposed as an efficient texture operator which processes the image pixels by thresholding the 3 × 3 neighborhood and by representing the resultant label as a binary number. The histogram of these labels was used as a texture descriptor. Subsequently, the LBP operator was extended to neighborhoods of various sizes [14]. LBP has been successfully applied to a wide range of different applications from texture segmentation [15] to

face recognition [16]. The LBP feature vector is determined using the following steps:

(a) Consider a circular neighborhood around a pixel. P points are chosen on the circumference of the circle with radius R such that they are all equidistant from the center pixel. Let g_c be the gray level intensity value of the center pixel. Let g_p, $p=0, \ldots, P-1$, be the gray level intensity values of the P points. Figure 3 depicts circularly symmetric neighbor sets for different values of P and R.

(b) These P points are converted into a circular bitstream of 0's and 1's according to whether the intensity of the pixel is less than or greater than the intensity of the center pixel. For example, the value of the LBP code of the center pixel (x_c, y_c) with intensity g_c is calculated using the following equation.

$$\mathrm{LBP}_{P,R}^{\mathrm{orig}} = \sum_{p=0}^{P-1} s\left(g_p - g_c\right) \tag{1}$$

where

$$s(x) = \begin{cases} 1, & x \geq 0 \\ 0, & x < 0 \end{cases}$$

In their subsequent study, in order to reduce the length of the feature vector, Ojala et al. [14] introduced the concept of uniformity. This concept is based on the fact that some binary patterns occur more commonly than others. Each pixel is classified as uniform or nonuniform and uniform pixels are used for further computation of the texture descriptor. These uniform fundamental patterns have a uniform circular structure that contains very few spatial transitions U (number of spatial bitwise 0/1 transitions). Generally, an LBP is called uniform if the binary pattern contains at most two bitwise transitions from 0 to 1 or vice versa when the bit pattern is traversed circularly. Some examples of uniform patterns are: 00000000 (0 transitions), 01110000 (2 transitions), and 11001111 (2 transitions). Thus, a rotation invariant measure called $\mathrm{LBP}_{P,R}$

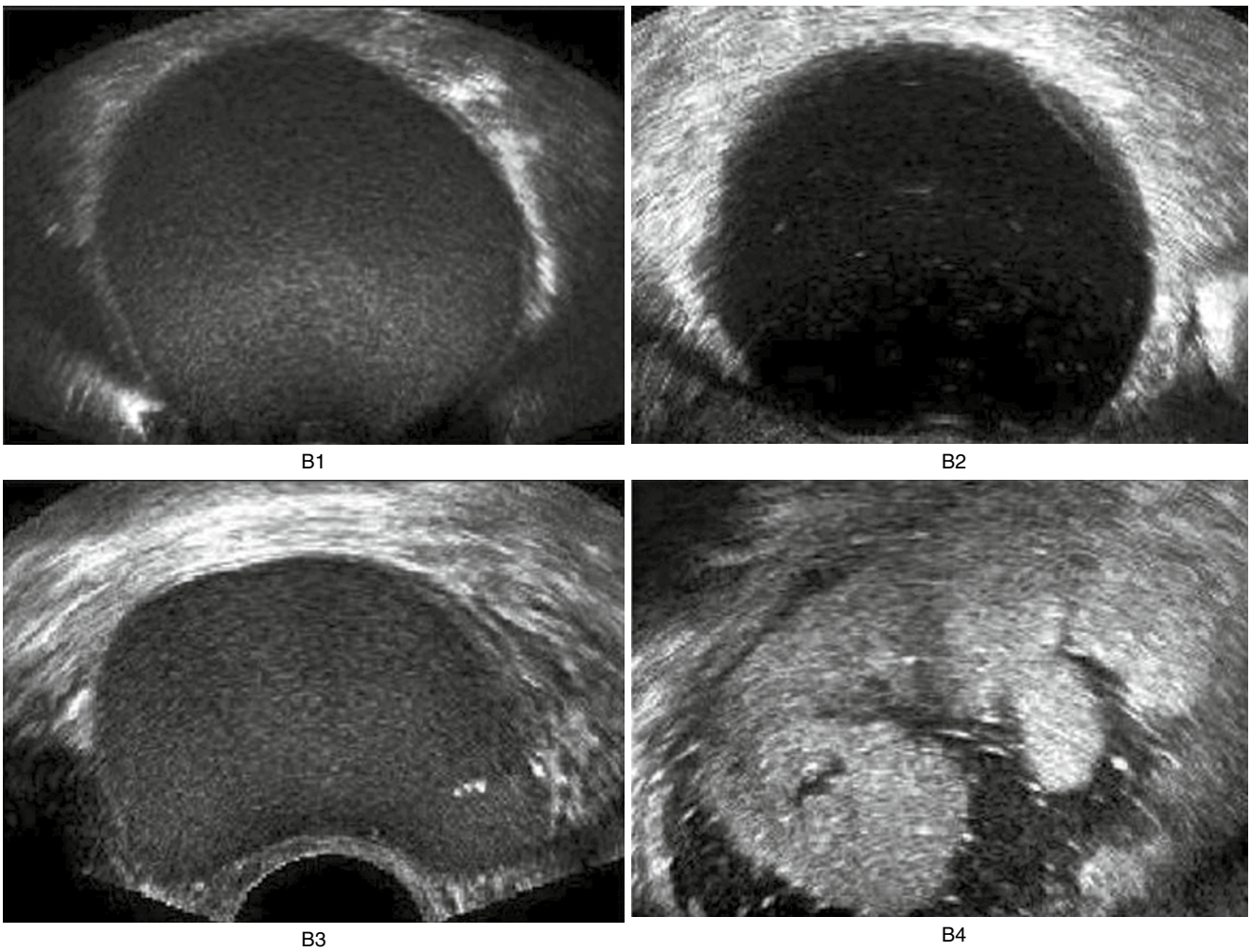

Fig. 1 Ultrasound images of the ovary: (*B1–B4*) benign conditions (*M1–M4*) malignant tumor

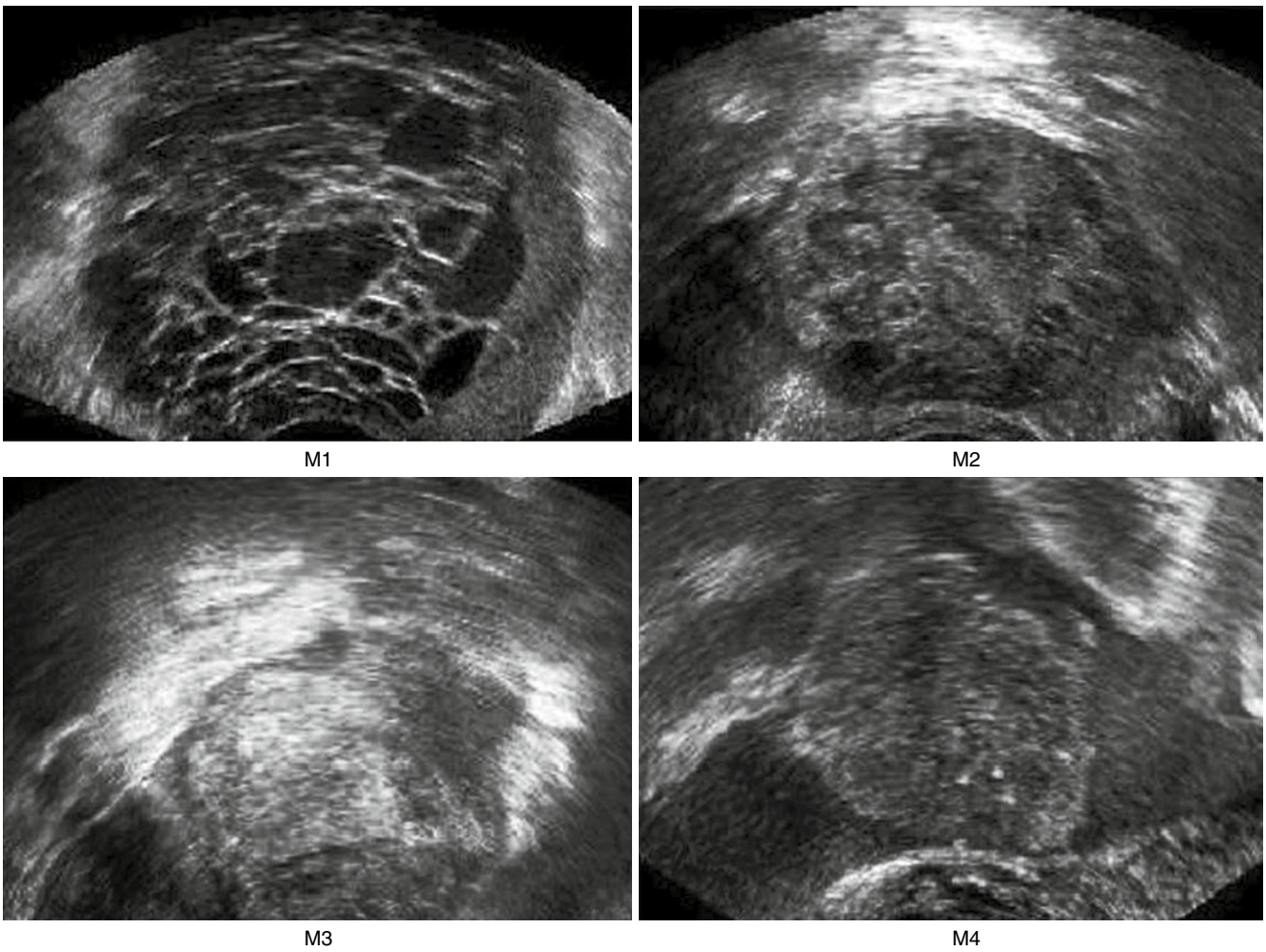

Fig. 1 (continued)

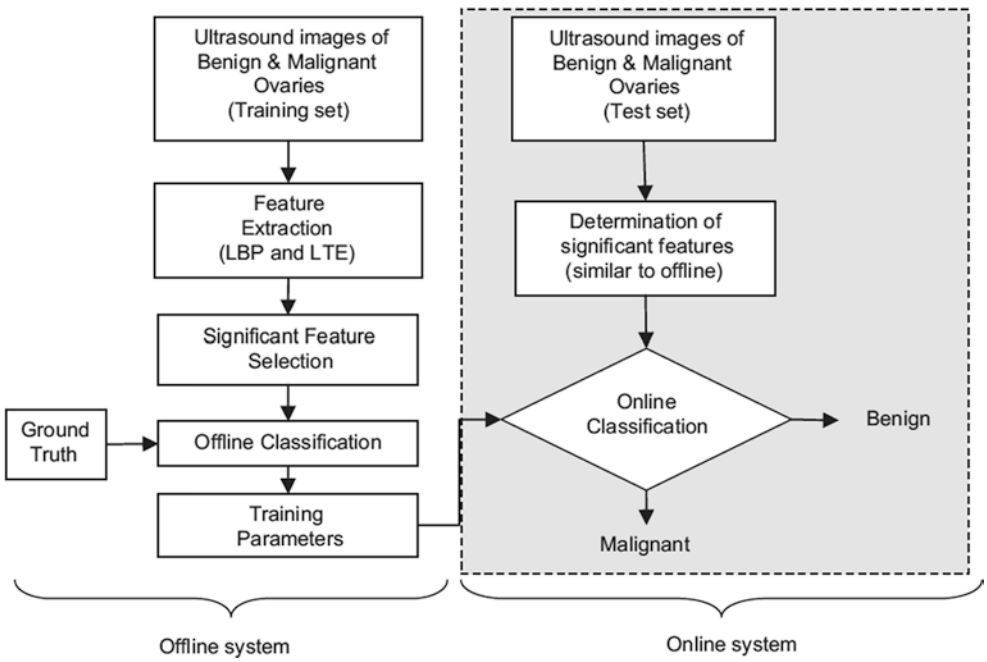

Fig. 2 Block diagram of the proposed system for ovarian cancer detection; the blocks outside the *dotted shaded rectangular box* represent the flow of off-line training system, and the blocks within the *dotted box* represent the online real-time system

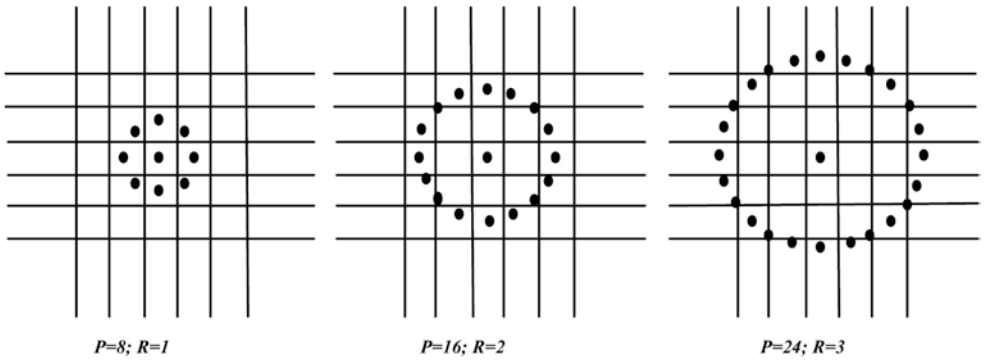

Fig. 3 Circularly symmetric neighbor sets for different P and R. The center pixel denotes g_c and the surrounding pixels depict g_p, $p=0,\ldots, P-1$; *left*: $P=8$, $R=1$, *middle*: $P=16$; $R=2$; *right*: $P=24$, $R=3$

using the uniformity measure $U \leq 2$ *is* calculated based on the number of transitions in the neighborhood pattern (Eq. 2).

$$\mathrm{LBP}_{P,R}(x) = \begin{cases} \sum_{p=0}^{P-1} s(g_p - g_c) & \text{if} \quad U(x) \leq 2 \\ P+1 & \text{otherwise} \end{cases} \tag{2}$$

where

$$s(x) = \begin{cases} 1, & x \geq 0 \\ 0, & x < 0 \end{cases}$$

Multi-scale analysis of the image using LBP is done by choosing circles with various radii around the center pixels and then constructing separate LBP image for each scale. In our work, energy and entropy of the LBP image, constructed over different scales ($R=1$, 2, and 3 with the corresponding pixel count P being 8, 16, and 24, respectively, see Fig. 3), were used as feature descriptors. Thus, there were in all six LBP-based features. For example, LBP entropy obtained using $R=1$ and $P=8$ is denoted as $LBP_{18}Ent$ and LBP energy obtained using $R=1$ and $P=8$ is denoted as $LBP_{18}Ene$.

Laws Texture Energy (*LTE*): Laws empirically determined that several masks of appropriate sizes were useful for discriminating between different kinds of texture [17]. The method is based on applying such masks to the image and then estimating the energy within the pass region of filters [17]. The texture energy measures are obtained by using three 1D vectors: L3, E3, and S3 that describe the following features: level, edge, and spot, respectively. L3 = [1, 2, 1], E3 = [−1, 0, 1], S3 = [−1, 2, −1]. By convolving any vertical 1D vector with a horizontal one, nine 2D masks of size 3 × 3, namely, L3L3, L3E3, L3S3, E3E3, E3L3, E3S3, S3S3, S3L3, and S3E3, are generated. For example,

$$\underset{\text{L3}}{\begin{pmatrix} 1 \\ 2 \\ 1 \end{pmatrix}} \times \underset{\text{E3}}{\begin{pmatrix} -1 & 0 & 1 \end{pmatrix}} = \underset{\text{L3E3}}{\begin{pmatrix} -1 & 0 & 1 \\ -2 & 0 & 2 \\ -1 & 0 & 1 \end{pmatrix}} \tag{3}$$

All these masks, except L3L3, have zero mean. We used these eight zero-sum masks numbered 1–8. To extract texture information from an image $I(i, j)$, the image is first convolved with each 2D mask. For example, if we used E3E3 to filter the image $I(i, j)$, the result was a texture image $\mathrm{TI}_{\mathrm{E3E3}}$ as shown below.

$$\mathrm{TI}_{\mathrm{E3E3}} = I(i, j) \times \mathrm{E3E3} \tag{4}$$

To make the resultant images contrast independent, the texture image $\mathrm{TI}_{\mathrm{L3L3}}$ was used to normalize the contrast of all other texture images as shown in Eq. 5.

$$\mathrm{Normalize}\left(\mathrm{TI}_{\mathrm{mask}}\right) = \frac{\mathrm{TI}_{(i,j)^{\mathrm{mask}}}}{\mathrm{TI}_{(i,j)^{\mathrm{L3L3}}}} \tag{5}$$

The resultant normalized TIs were passed to texture energy measurements (TEM) filters which consisted of a moving nonlinear window average of absolute values (Eq. 6).

$$\mathrm{TEM}_{(i,j)} = \sum_{u=-3}^{3} \sum_{v=-3}^{3} \left| \mathrm{TI}_{(i+u, j+v)} \right| \tag{6}$$

Thus, in this feature extraction process, the image under inspection is filtered using these eight masks, and their energies are computed and used as the feature descriptors [18]. A total of eight features were extracted, one using each of the eight masks, denoted by LTE_lEne, etc. A more detailed analysis of applications of Laws texture can be found in the recent book by Mermehdi et al. [19].

Support Vector Machine Classifier

Support vector machine (SVM) [20–22] is a supervised learning-based classifier that uses the input features from the two classes to determine a maximum margin hyperplane that separates the two classes. The hyperplane is determined in

such a way that the distance from this hyperplane to the nearest data points on each side, called the support vectors, is maximal. Consider two-class classification using a linear hyperplane of the form

$$y(x) = w^T \phi(x) + b \tag{7}$$

where $\phi(\bullet)$ denotes the feature transformation kernel, b is the bias parameter, and w is the normal to the hyperplane. The training data consists of the input feature vectors x and the corresponding classes c. $c=-1$ for benign class and +1 for malignant class. At the end of the training, the optimal values for the parameters w and b are determined. During the testing phase, the new feature vector is classified based on the sign of y obtained using Eq. 7. The perpendicular distance to the closest point from the training data set is the margin, and the objective of training an SVM classifier is to determine the maximum margin hyperplane and also to assign a soft penalty to the samples that are on the wrong side of the margin. The problem becomes an optimization problem where we have to minimize

$$\begin{aligned} & C\sum_{i=1}^{N}\xi_i + \frac{1}{2}\| w \|^2 \\ & c_i y(x_i) \geq 1-\xi_i, \quad \xi \geq 0 \end{aligned} \tag{8}$$

where ξ_i are the penalty terms for samples that are misclassified, C is the regularization parameter which controls the tradeoff between the misclassified samples and the margin. The first term in Eq. 8 is equivalent to maximizing the margin. This quadratic programming problem can be solved by introducing Lagrange multipliers a_n for each of the constraints and solving the dual formulation. The Lagrangian is given by

$$\begin{aligned} L(w,,b,,a) = & \frac{1}{2}\| w \|^2 + C\sum_{i=1}^{N}\xi_i \\ & -\sum_{i=1}^{N} a_i \left[c_i y(x_i) - 1 + \xi_i \right] - \sum_{i=1}^{N}\mu_i\xi_i \end{aligned} \tag{9}$$

where a_i and μ_i are the Lagrange multipliers. After eliminating w, b, and ξ_i from the Lagrangian, we obtain the dual Lagrangian which we maximize.

$$\begin{aligned} & \tilde{L}(a) = \sum_{i=1}^{N} a_i - \frac{1}{2}\sum_{i=1}^{N}\sum_{j=1}^{N} a_i a_j c_i c_j k(x_i, x_j) \\ & k(x_i, x_j) = \phi(x_i)^T \bullet \phi(x_j) \\ & 0 \leq a_n \leq C, \quad \sum_{i=1}^{N} a_i c_i = 0 \end{aligned} \tag{10}$$

The predictive model is now given by

$$y(x) = \sum_{i=1}^{N} a_i c_i k(x, x_i) + b \tag{11}$$

and b is estimated as

$$b = \frac{1}{N_M}\sum_{i\in M}\left(c_i - \sum_{J\in S} a_j c_j k(x_i, x_j) \right) \tag{12}$$

M is the set of indices such that $0<a_i<C$. A solution to the quadratic programming problem of maximizing the dual Lagrangian (Eq. 10) is given in [22].

SVM classifiers can be extended to nonlinearly separable data with the help of kernel function application on the data to make them linearly separable [23, 24]. In such a case, every dot product in Eq. 10 is replaced by a nonlinear kernel function. Several standard kernels are often used. We have used the linear kernel, polynomial kernel of order 1, 2, and 3, and the radial basis function (RBF) kernel. The polynomial kernel is defined as

$$k(x_i, x_j) = (1 + x_i \bullet x_j)^p \tag{13}$$

where p is the order of the kernel. The RBF kernel is defined as

$$k(x_i, x_j) = \exp\left(-\| x_i - x_j \|^2 \right) \tag{14}$$

Statistical Test for Feature Selection

We have used Student's *t-test* to select significant features. In this technique, a *t*-statistic, which is the ratio of difference between the means of the feature for two classes to the standard error between class means, is first calculated, and then the corresponding *p*-value is calculated. A *p*-value that is less than 0.01 or 0.05 indicates that the means of the feature are significantly different for the two classes, and hence, the feature is very discriminating.

Classification Process

Usually in classification, a part (mostly 70 %) of the acquired dataset is used for training the classifier, and the remaining samples are used for evaluating the performance of the classifier. However, the performance measures obtained using this holdout technique may depend on which samples are in the training set and which are in the test set, and hence, the measures may be significantly different

depending on how the split is made. In order to get robust results and to address the limitations of the holdout technique, we have adopted stratified *k-fold* cross-validation technique as the preferred data resampling technique. In this technique, the dataset is randomly split into k equal folds, each fold containing the same ratio of non-repetitive samples from both the classes. In iteration one, $(k-1)$ folds of data are used to train the classifier, and the remaining onefold is used to test the classifiers and to obtain the performance measures. This procedure is repeated for $(k-1)$ more times by using a different test set each time. The averages of the performance metrics obtained in all the iterations are reported as the overall performance metrics. In this work, k was taken as 10.

Performance Measures

Sensitivity, specificity, positive predictive value, and accuracy were calculated to evaluate the performance of the classifiers. TN (true-negative) is the number of benign samples identified as benign. TP (true-positive) is the number of malignant images identified as malignant. The number of malignant samples detected as benign is quantified by the FN (false-negative) measure. FP (false-positive) is the number of benign samples identified as malignant. Sensitivity, which is probability that a test will produce a positive result when used on abnormal population, is calculated as TP/(TP + FN), and specificity, which is the probability that a test will produce a negative result when used on normal disease-free population, is determined as TN/(TN + FP). Positive predictive value (PPV), which is the probability that the patient is abnormal when restricted to those patients who test positive, is calculated as TP/(TP + FP), and accuracy, which is the ratio of the number of correctly classified samples to the total number of samples, is calculated as (TP + FP)/(TP + FP + TN + FN).

Results

Selected Features

Table 1 presents the mean ± standard deviation (SD) values of the features for both the benign and malignant classes. The low p-value indicates that all the six LBP features and eight LTE features are significant. Entropy measures randomness of intensity distributions in an image. Complex textures in an image lead to high entropy values. It is evident from Table 1 that all the entropy features (LBP_{18}Ent, LBP_{216}Ent, and LBP_{324}Ent) have higher values for the malignant images, indicating higher randomness in the intensity values of the pixels in the image. This texture difference is also visually evident in the ultrasound images (Fig. 1). In terms of the energy features, most of them are higher for the malignant images.

Classification Results

Since tenfold cross-validation was employed, during each of the 10 iterations, 900 images from each class were used for building the classifier, and the remaining 100 images were used for testing and for determining the performance metrics. Table 2 presents the performance metrics obtained on training the SVM classifier of various kernel configurations using the significant 14 features. All the kernels demonstrate excellent ability in classifying the samples from both classes. The highest accuracy of 99.9 % was registered by the RBF kernel.

Ovarian Cancer Index (OCI)

It is difficult to keep track of and study the variations in the significant features listed in Table 1. Even though the

Table 1 Significant features that had a p-value < 0.0001 and their ranges (mean ± standard deviation) for benign and malignant classes

Feature	Benign	Malignant	p-value
LBP($R=1$, $P=8$) entropy (LBP_{18}Ent)	1.58E+08 ± 0.53E+08	2.17E+08 ± 0.73E+08	0.0000
LBP($R=1$, $P=8$) energy (LBP_{18}Ene)	0.89E+08 ± 0.27E+08	1.33E+08 ± 0.50E+08	0.0000
LBP($R=2$, $P=16$) entropy (LBP_{216}Ent)	3.82E+08 ± 0.69E+08	4.68E+08 ± 1.32E+08	0.0000
LBP($R=2$, $P=16$) energy (LBP_{216}Ene)	0.27E+08 ± 0.09E+08	0.31E+08 ± 0.11E+08	0.0000
LBP($R=3$, $P=24$) entropy (LBP_{324}Ent)	0.22E+08 ± 0.07E+08	0.24E+08 ± 0.11E+08	6.9744e-08
LBP($R=3$, $P=24$) energy (LBP_{324}Ene)	4.19E+08 ± 1.09E+08	3.78E+08 ± 1.19E+08	2.3315e-15
Laws Texture Energy 1 (LTE_1Ene)	0.31E+08 ± 0.10E+08	0.36E+0 ± 0.13E+08	0.0000
Laws Texture Energy 2 (LTE_2Ene)	0.29E+08 ± 0.09E+08	0.31E+08 ± 0.15E+08	1.2659e-05
Laws Texture Energy 3 (LTE_3Ene)	2.8019 ± 0.1963	3.0604 ± 0.1363	0.0000
Laws Texture Energy 4 (LTE_4Ene)	0.2065 ± 0.0495	0.1444 ± 0.0315	0.0000
Laws Texture Energy 5 (LTE_5Ene)	2.5528 ± 0.1203	2.8239 ± 0.1192	0.0000
Laws Texture Energy 6 (LTE_6Ene)	0.2877 ± 0.019	0.2577 ± 0.0139	0.0000
Laws Texture Energy 7 (LTE_7Ene)	2.404 ± 0.0884	2.6327 ± 0.1133	0.0000
Laws Texture Energy 8 (LTE_8Ene)	0.3319 ± 0.0154	0.3232 ± 0.0189	0.0000

Table 2 Classifier performance measures

SVM kernel	TP	TN	FP	FN	Accuracy (%)	Sensitivity (%)	Specificity (%)	PPV (%)
Linear	100	99	0	1	99.8	99.61	100	100
Polynomial (order 1)	100	100	0	0	99.8	99.6	100	100
Polynomial (order 2)	100	100	0	0	99.95	100	99.9	99.9
Polynomial (order 3)	100	100	0	0	99.85	99.9	99.8	99.8
RBF	100	100	0	0	99.9	100	99.8	99.8

TN true-negative, *FN* false-negative, *TP* true-positive, *FP* false-positive

Table 3 Mean ± standard deviation of the *Ovarian Cancer Index* (*OCI*) for both benign and malignant classes

	Benign	Malignant	*p*-value
OCI	2.3959 ± 3.26E-08	2.0502 ± 1.83E-08	<0.0000

implementation of the proposed algorithm in a software application is easy and the software is platform-independent and low cost, there is always an apprehension in the medical community on the reliability of the results predicted by black-box classifiers. This is because the exact operating algorithm and the classifier parameters used are not transparent to the end user. Therefore, we attempted to determine a single index that is a combination of all the 14 features in order to facilitate a quicker, efficient, cost-effective, and more comprehendible diagnosis. This index is nondimensional and, hence, does not have any units. We empirically tried and tested various combinations of the 14 features to develop an index that has unique ranges for both the benign and malignant classes. It is given by,

$$\mathrm{OCI} = \frac{\alpha}{\beta \times 10^{14}} \tag{15}$$

where

$$\alpha = \mathrm{LPB}_{1,8}\mathrm{Ene} \times \mathrm{LPB}_{2,16}\mathrm{Ene} \times \mathrm{LPB}_{3,24}\mathrm{Ene} \times \mathrm{LTE1} \times \mathrm{LTE2} \times \mathrm{LTE3} \times \mathrm{LTE4} \times \mathrm{LTE5} \times \mathrm{LTE6} \times \mathrm{LTE7} \times \mathrm{LTE8}$$
$$\beta = \mathrm{LPB}_{1,8}\mathrm{Ent} \times \mathrm{LPB}_{2,16}\mathrm{Ent} \times \mathrm{LPB}_{3,24}\mathrm{Ent}$$

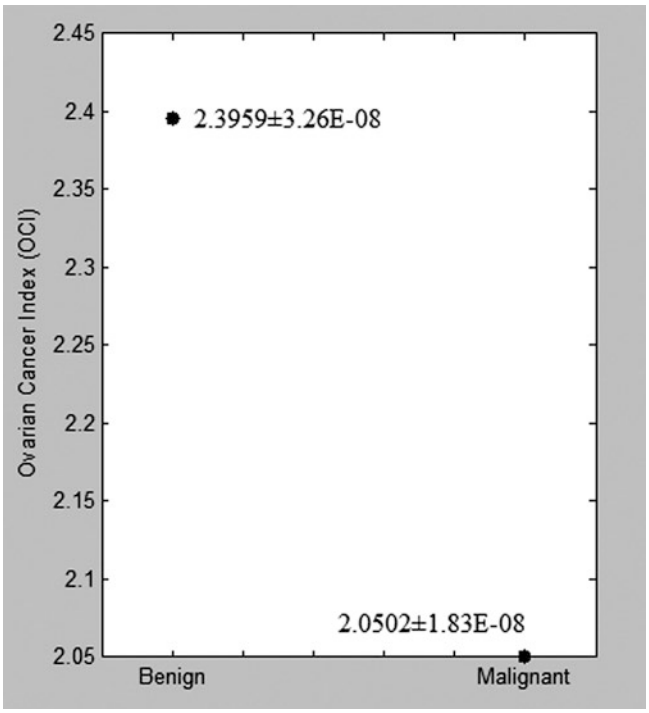

Fig. 4 Plot of mean ± standard deviation of *OCI* for both benign and malignant classes

The range of this index for both the benign and malignant classes is presented in Table 3, and the corresponding plot of the ranges is shown in Fig. 4. It is evident that the index has a significantly distinct range for the two classes as indicated by the *p*-value. Thus, based on the range of the OCI for the given image, the image can be classified into benign or malignant classes. The malignant images have a lower value for this index because of the use of the entropy terms in the denominator of Eq. 15. It can be recalled that the entropy features had a higher value for the malignant cases and their use in the denominator lowers the net index value.

Discussion

There are very few CAD-based studies in the field of ovarian tumor classification. Most of these studies use features based on blood test results or features from mass spectrometry (MS) data. Age and results of 30 blood tests were used as features in a multilayer perceptron classifier in order to classify the patient into one of the three classes, namely, benign, early-stage, and late-stage cancers. On testing 55 cases, an accuracy of 92.9 % was recorded [25]. Assareh et al. [26] attempted to select suitable biomarkers among the high-dimensional input data from protein mass

spectra. Using selected significant three biomarkers in two fuzzy linguistic rules, they have reported a classification accuracy of 100 % for one dataset (91 controls, 162 cancers) and 86.36 % for another dataset (100 normal, 16 benign, 100 cancers). The limitation of this study was the use of holdout technique for data resampling. Holdout technique generally results in less robust results. Using a novel complementary fuzzy neural network on a DNA microarray gene expression dataset (24 normal, 30 cancers), an accuracy of 84.72 % was registered using nine features [27]. In another MS study that evaluated binary images modeled based on the proteomic mass spectrum data (100 normal, 100 cancers), an accuracy of 96.5 % was obtained [28].

Such MS-based classification studies have the key limitation of the curse of dimensionality as they have to process a high-dimensional feature set obtained from a small sample size. Another limitation is the cost associated with and sometimes the nonavailability of the equipment necessary to collect and analyze the MS data. Therefore, in our work, we have used the images from the commonly available and low-cost ultrasound modality and have obtained high classification accuracy. Our proposed algorithm has the following features:

(a) All the steps employed in the CAD algorithm are completely automated, and hence, the results are highly objective.
(b) The feature selection and classifier development have been done using a large dataset of 2,000 samples. Hence, the classifier parameters are generalized enough to accurately handle new patient data. Moreover, the use of stratified cross-validation technique for data resampling has rendered the accuracy to be robust.
(c) Only 16 simple texture features have to be calculated from the images for use in the classifiers. Such a small feature-set reduces the computational load. Unlike MS data, there is no need for complex feature selection techniques for dimensionality reduction.
(d) The technique is low cost as it does not require complicated and expensive specialized software, and also it is based on images obtained through ultrasound which is a commonly used affordable modality.
(e) The algorithm can be implemented as a stand-alone executable software application and can be easily incorporated into existing computers at the physician's office or diagnostic centers.
(f) The physician has to just feed the acquired ultrasound images into the software. The software does all the processing and outputs the class of the image. Hence, there is no need for trained experts for running the software.
(g) The classification accuracy is high (99.9 %), and hence, thus the results give the physician more reliable *information* to make the call of whether the patients needs biopsies or surgeries.
(h) The novel integrated OCI can be easily used by the doctors to determine the class of the image in a quicker, efficient, cost-effective, and comprehendible manner.

Even though we have demonstrated excellent accuracy in this pilot study, we intend to conduct more future studies with larger image databases acquired from multiethnic groups to establish the significance of the results with more confidence.

Conclusion

In this paper, we have presented a CAD technique that uses ultrasound images of the ovary and image mining algorithms to accurately classify benign and malignant ovarian tumor images. We extracted texture features based on LBP and LTE and used them to build and train a SVM classifier. On evaluating the built classifier using 1,000 benign and 1,000 malignant images, we obtained a high accuracy of 99.9 % using a SVM classifier with a RBF kernel. The study is novel with respect to the fact that it uses low-cost ultrasound images and highly discriminating novel combination of simple, easily extractable texture-based features in a most commonly used SVM classifier to obtain the highest accuracy of nearly 100 % in ovarian tumor classification. In order to better improve the transparency of the algorithm for easier comprehension by the end user, we have also formulated a novel integrated index, *Ovarian Cancer Index* (*OCI*), which is a combination of the texture features, and have shown that it has unique ranges for both benign and malignant classes. Even though the results of this pilot study are promising, we intend to establish the clinical applicability of our proposed technique with more studies containing larger image databases.

Conflict of Interest Statement None of the authors have any financial or personal conflict of interest that could inappropriately influence the writing or publication of this manuscript.

Biography U. Rajendra Acharya, PhD, DEng is a visiting faculty in Ngee Ann Polytechnic, Singapore. He is also (i) adjunct professor in University of Malaya, Malaysia, (ii) adjunct faculty in Singapore Institute of Technology, University of Glasgow, Singapore, and (iii) associate faculty in SIM University, Singapore. He received his PhD from National Institute of Technology Karnataka, Surathkal, India, and DEng from Chiba University, Japan.

He has published more than 285 papers, in refereed international SCI-IF journals (178), international conference proceedings (48), textbook chapters (62), books (15 including in Press) with h-index of 24 (h-index = 21 without self-citations, Scopus), and 27 (Google scholar with more than 2,600 citations). He has worked on various funded projects with grants worth more than 2 million SGD. He is in the editorial board of many journals and served as guest editor for many journals. His major interests are in biomedical signal processing, bio-imaging, data mining, visualization, and biophysics for better healthcare design, delivery, and therapy.

M. Muthu Rama Krishnan, PhD received the PhD degree from the Indian Institute of Technology, Kharagpur, India. He is currently a research engineer with Ngee Ann Polytechnic, Singapore. He has published more than 25 papers in peer-reviewed journals. His research interest includes medical image analysis and pattern classification.

Luca Saba, MD, received the MD degree from the University of Cagliari, Italy, in 2002. Today he works in the AOU of Cagliari. Dr. Saba's research fields are focused on neuroradiology, multi-detector row computed tomography, magnetic resonance, ultrasound, and diagnostic in vascular sciences.

His works, as lead author, achieved more than *75* high impact factor, peer-reviewed journals. Dr. Saba has written 7 book chapters, and he presented more than 400 papers in National and International Congress. Dr. Saba is a member of the Italian Society of Radiology (SIRM), European Society of Radiology (ESR), Radiological Society of North America (RSNA), American Roentgen Ray Society (ARRS), and European Society of Neuroradiology (ESNR).

Filippo Molinari, PhD is an assistant professor in biomedical engineering at the Department of Electronics of the Politecnico di Torino (Torino, Italy). His main research interests include biomedical signal processing and medical imaging. He is expert in automated techniques for aiding the diagnostic process in ultrasound imaging. Vascular sonography, atherosclerosis, and tumor detection are Dr. Molinari's main research topics.

He published more than 80 peer-reviewed contributions and 3 collaborative books. Dr. Molinari is a member of the IEEE EMBS, of the European Society for Molecular Imaging (ESMI), and of the American Institute of Ultrasounds in Medicine (AIUM). He is regional associate editor for Europe of the Journal of Medical Imaging and Health Informatics, and he is on the editorial board of other five international journals.

Stefano Guerriero, MD, Born Siracusa (Italy) 10 October 1961. Medical doctor University of Pisa 24 October 1988. Postgraduate in Obstetrics and Gynecology University of Pisa October 1992. His works, as lead author, achieved more than 120 high impact factor, peer-reviewed, Journals as *British Medical Journal, Americal Journal of Obstetrics and Gynecology, Fertility and Sterility, Human Reproduction, Journal of Ultrasound in medicine, Menopause, Maturitas, Ultrasound Obstetrics and Gynecology*. Until now Associate Professor of Obstetrics and Gynecology University of Cagliari. Editor of Ultrasound in Obstetrics and Gynecology from 2011.

Jasjit S. Suri, PhD, MBA is an innovator, visionary, scientist, and an internationally known world leader. Dr. Suri was crowned with Director General's Gold medal in 1980 and the *Fellow of American Institute of Medical and Biological Engineering* (AIMBE), awarded by National Academy of Sciences, Washington DC, in 2004. Dr. Suri has been the chairman of IEEE Denver section and has won over 50 awards during his career and has held executive positions.

References

1. NCI (National Cancer Institute) on ovarian cancer. Information available at http://www.cancer.gov/cancertopics/types/ovarian. Last accessed Aug 2011.
2. Bast Jr RC, Badgwell D, Lu Z, Marquez R, Rosen D, Liu J, Baggerly KA, Atkinson EN, Skates S, Zhang Z, Lokshin A, Menon U, Jacobs I, Lu K. New tumor markers: CA125 and beyond. Int J Gynecol Cancer. 2005;15:274–81.
3. Zaidi SI. Fifty years of progress in gynecologic ultrasound. Int J Gynaecol Obstet. 2007;99:195–7.
4. Menon U, Talaat A, Rosenthal AN, Macdonald ND, Jeyerajah AR, Skates SJ, Sibley K, Oram DH, Jacobs IJ. Performance of ultrasound as a second line test to serum CA125 in ovarian cancer screening. BJOG. 2000;107:165–9.
5. Nossov V, Amneus M, Su F, Lang J, Janco JM, Reddy ST, Farias-Eisner R. The early detection of ovarian cancer: from traditional methods to proteomics. Can we really do better than serum CA-125? Am J Obstet Gynecol. 2008;199:215–23.
6. Kim KA, Park CM, Lee JH, Kim HK, Cho SM, Kim B, Seol HY. Benign ovarian tumors with solid and cystic components that mimic malignancy. AJR Am J Roentgenol. 2004;182: 1259–65.
7. Lenic M, Zazula D, Cigale, B. Segmentation of ovarian ultrasound images using single template cellular neural networks trained with support vector machines. In: Proceedings of 20th IEEE international symposium on Computer-Based Medical Systems, Maribor, 2007, p. 205–12.
8. Hiremath PS, Tegnoor JR. Recognition of follicles in ultrasound images of ovaries using geometric features. In: Proceedings of international conference on Biomedical and Pharmaceutical Engineering, Singapore, 2009, p. 1–8.
9. Deng Y, Wang Y, Chen P. Automated detection of polycystic ovary syndrome from ultrasound images. In: Proceedings of the 30th annual international IEEE Engineering in Medicine and Biology Society conference, Vancouver, 2008, p. 4772–5.
10. Sohail ASM, Rahman MM, Bhattacharya P, Krishnamurthy S, Mudur SP. Retrieval and classification of ultrasound images of ovarian cysts combining texture features and histogram moments. In: IEEE international symposium on Biomedical Imaging: From Nano to Macro, Rotterdam, 2010, p. 288–91.
11. Sohail ASM, Bhattacharya P, Mudur SP, Krishnamurthy S. Selection of optimal texture descriptors for retrieving ultrasound medical images. In: IEEE international symposium on Biomedical Imaging: From Nano to Macro, Chicago, 2011, p. 10–6.
12. Molinari F, Liboni W, Giustetto P, Badalamenti S, Suri JS. Automatic computer-based tracings (ACT) in longitudinal 2-D ultrasound images using different scanners. J Mech Med Biol. 2009;9:481–505.
13. Ojala T, Pietikäinen M, Harwood D. A comparative study of texture measures with classification based on feature distributions. Pattern Recogn. 1996;29:51–9.
14. Ojala T, Pietikäinen M, Maenpaa T. Multiresolution gray-scale and rotation invariant texture classification with local binary patterns. IEEE Trans Pattern Anal. 2002;24:971–87.
15. Liao S, Law MWK, Chung ACS. Dominant local binary patterns for texture classification. IEEE Trans Image Process. 2009; 18:1107–18.
16. Zhang B, Gao Y, Zhao S, Liu J. Local derivative pattern versus local binary pattern: face recognition with high-order local pattern descriptor. IEEE Trans Image Process. 2010;19:533–44.
17. Laws KI. Rapid texture identification. SPIE Conf Series. 1980;238:376–80.
18. Petrou M, Sevilla PG. Image processing – dealing with texture. Chichester: Wiley; 2006.
19. Mirmehdi M, Xie X, Suri JS. Handbook of texture analysis. London: Imperial College Press; 2008.
20. Vapnik V. Statistical learning theory. New York: Wiley; 1998.
21. Burgess CJC. A tutorial on support vector machines for pattern recognition. Data Min Knowl Disc. 1998;2:1–47.
22. Cortes C, Vapnik V. Support-vector networks. Mach Learn. 1995; 20:273–97.
23. David V, Sanchez A. Advanced support vector machines and kernel methods. Neurocomputing. 2003;55:5–20.
24. Muller KR, Mika S, Ratsch G, Tsuda K, Scholkopf B. An introduction to kernel based learning algorithms. IEEE Trans Neural Network. 2001;12:181–201.
25. Renz C, Rajapakse JC, Razvi K, Liang SKC. Ovarian cancer classification with missing data. In: Proceedings of 9th international conference on Neural Information Processing, Singapore, 2002, vol. 2, p. 809–13.
26. Assareh A, Moradi MH. Extracting efficient fuzzy if-then rules from mass spectra of blood samples to early diagnosis of ovarian cancer. In: IEEE symposium on Computational Intelligence and Bioinformatics and Computational Biology, Honolulu, 2007, p. 502–6.
27. Tan TZ, Quek C, Ng GS, Razvi K. Ovarian cancer diagnosis with complementary learning fuzzy neural network. Artif Intell Med. 2008;43:207–22.
28. Meng H, Hong W, Song J, Wang L. Feature extraction and analysis of ovarian cancer proteomic mass spectra. In: 2nd international conference on Bioinformatics and Biomedical Engineering, Shanghai, 2008, p. 668–71.

Ovarian Tumor Characterization and Classification Using Ultrasound: A New Online Paradigm

U. Rajendra Acharya, Luca Saba, Filippo Molinari, Stefano Guerriero, and Jasjit S. Suri

Abstract

Among gynecological malignancies, ovarian cancer is the most frequent cause of death. Image mining algorithms have been predominantly used to give the physicians a more objective, fast, and accurate second opinion on the initial diagnosis made from medical images. The objective of this work is to develop an adjunct Computer-Aided Diagnostic (CAD) technique that uses 3D ultrasound images of the ovary to accurately characterize and classify benign and malignant ovarian tumors. In this algorithm, we first extract features based on the textural changes and higher-order spectra (HOS) information. The significant features are then selected and used to train and evaluate the decision tree (DT) classifier. The proposed technique was validated using 1,000 benign and 1,000 malignant images, obtained from ten patients with benign and ten with malignant disease, respectively. On evaluating the classifier with tenfold stratified cross validation, the DT classifier presented a high accuracy of 97 %, sensitivity of 94.3 %, and specificity of 99.7 %. This high accuracy was achieved because of the use of the novel combination of the four features which adequately quantify the subtle changes and the nonlinearities in the pixel intensity variations. The rules output by the DT classifier are comprehensible to the end user and, hence, allow the physicians to more confidently accept the results. The preliminary results show that the features are discriminative enough to yield good accuracy. Moreover, the proposed technique is completely automated and accurate and can be easily written as a software application for use in any computer.

Keywords

Ovarian tumor • Texture features • Higher-order spectra • Characterization • Classification • Computer-aided diagnosis

U.R. Acharya, PhD, DEng
Department of Electronics and Computer Engineering,
Ngee Ann Polytechnic, Singapore, Singapore

Department of Biomedical Engineering,
Faculty of Engineering, University of Malaya,
Kuala Lumpur, Malaysia

L. Saba, MD
Department of Radiology,
Azienda Ospedaliero Universitaria di Cagliari,
Cagliari, Italy

F. Molinari, PhD
Biolab, Department of Electronics and Telecommunications,
Politecnico di Torino, Torino, Italy

S. Guerriero, MD
Department of Obstetrics and Gynecology,
University of Cagliari, Ospedale San Giovanni di Dio,
Via Ospedale 46, Cagliari 09124, Italy

J.S. Suri, PhD, MBA, Fellow AIMBE (✉)
Department of Biomedical Engineering,
CTO, Global Biomedical Technologies,
Roseville, CA, USA

Department of Biomedical Engineering,
Idaho State University (Aff.), Pocatello, ID, USA
e-mail: jsuri@comcast.net

L. Saba et al. (eds.), *Ovarian Neoplasm Imaging*,
DOI 10.1007/978-1-4614-8633-6_26,

Introduction

In 2011, in the United States, it is estimated that 21,990 new cases will be diagnosed with and 15,460 women would die of ovarian cancer [1]. Ultrasonography and the determination of the levels of a tumor marker called cancer antigen 125 (CA-125) are currently the most commonly used techniques for detecting ovarian cancer. In the case of ultrasonography, the ultrasonographers and radiologists visually inspect the acquired ultrasound images for any subtle changes that differentiate the benign and malignant tumors. Even though this is currently the most common practice, the accuracy and reproducibility of the visual interpretations are most often dependent on the skill of the observer. In the case of evaluation based on serum CA-125, this marker has been found to be elevated only in 50 % of stage 1 cancers [2]. Furthermore, CA-125 can also be raised in other malignancies such as uterine and pancreatic and sometimes in many benign conditions such as fibroids, endometriosis, pelvic inflammatory disease, and benign ovarian cysts [3]. Menon et al. [4] examined women with elevated CA-125 levels and observed that the ultrasound parameters result in varying sensitivity ranging from 84 to l00 %, with a specificity of 97 %, but only a positive predictive value (PPV) of 37.2 %. Other modalities such as computerized tomography, magnetic resonance imaging, and radioimmunoscintigraphy are limited by one or more of these factors: cost, device availability, and radiation exposure. Moreover, preoperative determination of whether an ovarian tumor is malignant or benign, especially when the tumor has both solid and cystic components, has been found to be difficult [5]. Because ultrasound findings of ovarian masses may be inconclusive, on occasion, subsequent surgical removal of the ovary may show that the mass is benign. Such unnecessary procedures not only increase healthcare cost and time but also increase patient anxiety. Owing to the indicated limitations, it is evident that either one of the following solutions is warranted: (a) a stand-alone accurate tumor diagnostic modality, (b) a multimodality-based standardized diagnostic protocol that reliably differentiates benign and malignant tumors, and (c) an adjunct diagnostic modality/technique that accurately classifies the tumors and therefore gives a valuable second opinion to doctors in order to decide further diagnostic protocol for the patient.

The *key objective* of our work is to develop one such adjunct technique for ovarian tumor classification. Medical data mining has become an increasingly popular field of science over the past few decades. Computer-Aided Diagnostic (CAD) techniques developed using data mining framework generally follow these steps: (1) image preprocessing to remove noise, (2) extraction of representative features that quantify the changes in the images (also called the feature extraction phase), (3) selection of significant features (also called the feature selection phase), and (4) classification phase wherein classifiers are built and evaluated using the selected features. Thus, CAD-based techniques can prove to be excellent adjunct techniques, especially for real-time mass screening, because of their ease of use, speed, noninvasiveness, cost-effectiveness, and reliability. Therefore, we have developed a CAD technique that can help the doctors in deciding if the primary diagnosis of whether the tumor is benign or malignant is correct and thus can allow the physicians to make a more confident call with respect to the subsequent treatment protocol.

In the area of ovarian disease management, CAD techniques have been used for automatic follicle segmentation in order to better understand ovarian follicle dynamics [6, 7], for polycystic ovary syndrome detection [8], ovarian cyst classification [9], and ovarian ultrasound image retrieval [10]. There are very few studies in the application of CAD for ovarian cancer detection. Most of these studies use features based on (a) blood test results [11], (b) mass spectrometry (MS) data [12–16], and (c) ultrasound images [17–21]. Such MS-based classification studies are affected by the curse of dimensionality [22] as they have to process a high-dimensional feature set obtained from a small sample size. Moreover, the MS equipment is expensive and not available in most developing and underdeveloped countries. Therefore, in our work, we have proposed the use of images acquired using the commonly available and low-cost ultrasound modality.

Compared to 2D ultrasonography, a 3D ultrasonography approach allows for more objective and quantitative documentation of the morphological characteristics of benign and malignant tumors [23]. Studies have shown that the selective use of 3D ultrasonography and power Doppler ultrasound can improve the diagnostic accuracy of ovarian tumors [24, 25]. Therefore, we have used 3D transvaginal ultrasonography for acquisition of the 2D images used in this work.

Materials and Methods

Figure 1 depicts the block diagram of the proposed real-time image mining CAD technique. It consists of an online classification system (shown on the right side of Fig. 1) which processes an incoming patient's test image. This online system predicts the class label (benign or malignant) based on the transformation of the online grayscale feature vector by the training parameters determined by an off-line learning system (shown on the left side of Fig. 1). The off-line classification system is composed of a classification phase which produces the training parameters using the combination of grayscale off-line training features and the respective off-line ground truth training class labels (0/1 for benign/malignant). The grayscale features for online or off-line training are obtained using the same protocol for feature

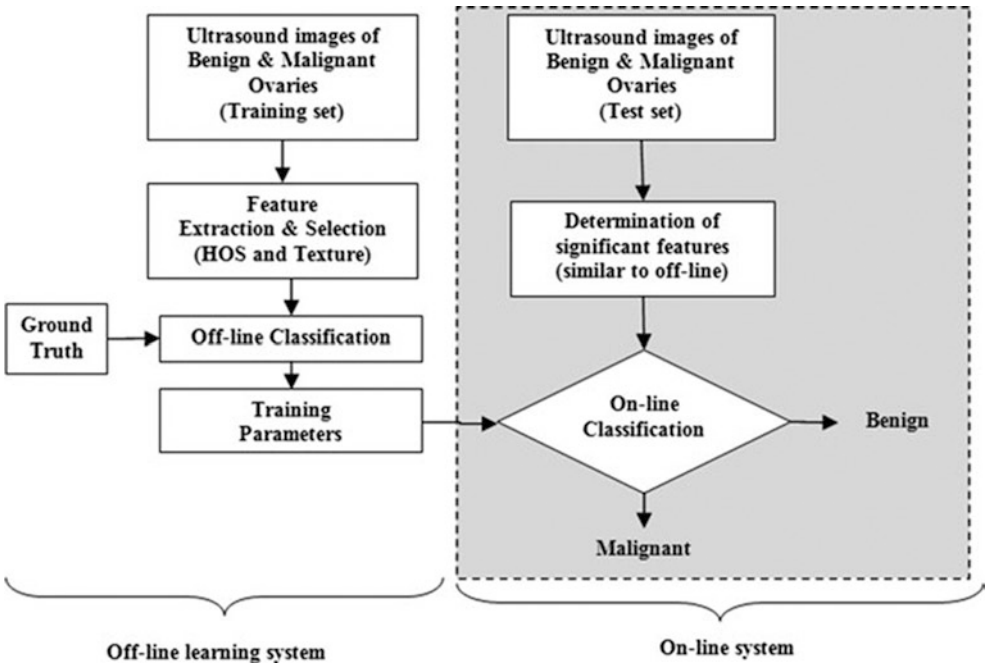

Fig. 1 Block diagram of the proposed system for tumor characterization and classification; the blocks outside the *dotted shaded rectangular box* represent the flow of off-line training system, and the blocks within the *dotted box* represent the online real-time system

extraction: texture features and the higher-order spectra (HOS) features. Significant features among the extracted ones are selected using the *t*-test. We evaluated the decision tree (DT) classifier. The above CAD system was developed using an image database that is split into a training set and a test set. The training set images were used to develop the DT classifier. The built classifier was evaluated using the test set. For evaluation, we used a *k-fold* cross validation protocol. The predicted class labels of the test images and the corresponding ground truth labels (0/1) are compared to determine the performance measures of the system such as sensitivity, specificity, accuracy, and PPV.

In this section, we describe, in detail, the image acquisition procedure and the various techniques used for feature extraction and selection and classification.

Patients and Image Acquisition

Twenty women (age: 29–74 years; mean ± SD = 49.5 ± 13.48) were recruited for this study. The study was approved by the Institutional Review Board. The procedure was explained to each subject and informed consent was obtained. Among these 20 women, 11 were premenopausal and 9 were postmenopausal. All these patients were consecutively selected during presurgical evaluation by one of the authors of this paper (blinded for peer review). Patients with no anatomopathological evaluation were excluded from the study. Biopsies indicated that among the 20 patients, 10 had malignancy in their ovaries and 10 had benign conditions. Postoperative histology results indicated that the benign neoplasms were as follows: 5 endometriomas, 2 mucinous cystadenoma, 1 cystic teratoma, 1 pyosalpinx, and 1 serous cyst. The malignant neoplasms were as follows: 3 primary ovarian cancers (undifferentiated carcinomas), 3 borderline malignant tumors, 1 krukenberg cancer, 1 serous cystadenocarcinoma, 1 serous carcinoma, and 1 carcinosarcoma. All patients were evaluated by 3D transvaginal ultrasonography using a Voluson-I (GE Medical Systems) according to a predefined scanning protocol using 6.5 MHz probe frequency (Thermal Index: 0.6 and Mechanical Index: 0.8). A 3D volume of the whole ovary was obtained. The acquired 3D volumes were stored on a hard disk (Sonoview™, GE Medical Systems). Volume acquisition time ranged from 2 to 6 s depending on the size of the volume box. In cases where a given adnexal mass contained more than one solid area and, hence, had more than one volume stored, only the volume best visualizing the mass was chosen for further analysis. Figure 2 shows typical ultrasound images of benign and malignant classes. We chose the middle 100 images from each volume from each subject. Thus, the evaluated database consisted of 1,000 benign images and 1,000 malignant images.

Feature Extraction

Feature extraction is one of the most important steps in an automated CAD system. It was observed that the type of tumor (tumor-like lesions, benign, tumors of low malignant potential, and malignant) was correlated with lesion diameter, with larger tumors more likely to be malignant [26].

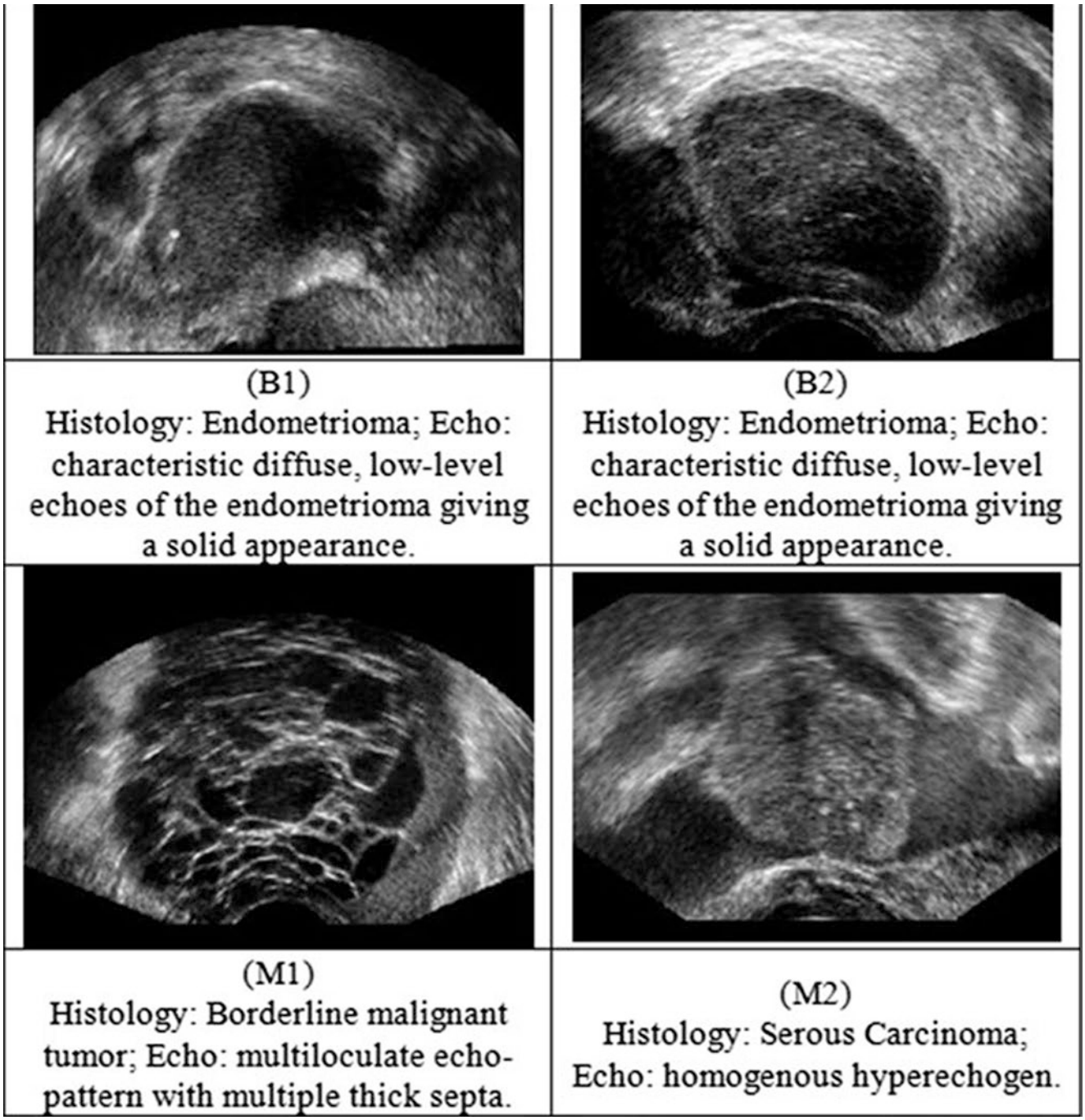

Fig. 2 Ultrasound images of the ovary: (*B1–B2*) benign conditions, (*M1–M2*) malignant tumor

Moreover, there are several morphological changes in the benign and malignant ultrasound images [27, 28]. Usually the histopathologic cytoarchitecture of malignant tumors is different from benign neoplasm with several areas having intra-tumoral necrosis [29]. These changes in lesion diameter and cytoarchitecture variations manifest as nonlinear changes in the texture of the acquired ultrasound images. Therefore, in this work, we have extracted features based on the textural changes in the image and also nonlinear features based on the higher-order spectra information. In this section, we describe these features in detail.

Texture Features

Texture features measure the smoothness, coarseness, and regularity of pixels in an image. The extracted texture descriptors quantify the mutual relationship among intensity

values of neighboring pixels repeated over an area larger than the size of the relationship [30, 31]. There are several texture descriptors available in the literature [31]. We have chosen the following features:

Deviation

Let $f(i)$ where $(i=1,2,\ldots,n)$ be the number of points whose intensity is i in the image and A_x be the area of the image. The occurrence probability of intensity i in the image is given by $h(i)=f(i)/A_x$. The standard deviation is given by

$$\text{Deviation}:\sigma=\sum_{i=1}^{n}(i-\mu)^2 h(i) \tag{1}$$

where $\mu=$mean of intensities.

Fractal Dimension (FD)

Theoretically, shapes of fractal objects remain invariant under successive magnification or shrinking of objects. Since texture is usually a scale-dependent measure [32], using fractal descriptors can alleviate this dependency. A basic parameter of a fractal set is called the fractal dimension (FD). FD indicates the roughness or irregularity in the pixel intensities of the image. Visual inspection of the benign and malignant images in Fig. 2 shows that there are differences in the regularity of pixel intensities in both classes. We have hence used FD as a measure to quantify this irregularity. The larger the FD value, the rougher the appearance of the image. Consider a surface S in Euclidean n-space. This surface is self-similar if it is the union of N_r nonoverlapping copies of itself scaled up or down by a factor of r. Mathematically, FD is computed [33, 34] using the following formula:

$$FD=\frac{\log N_r}{\log\left(\frac{1}{r}\right)} \tag{2}$$

In this work, we used the modified differential box counting with sequential algorithm to calculate FD [34]. The input of the algorithm is the grayscale image where the grid size is in the power of 2 for efficient computation. Maximum and minimum intensities for each (2×2) box are obtained to sum their difference, which gives the M and r by

$$r=\frac{s}{M} \tag{3}$$

where $M=\min(R, C)$, s is the scale factor, and R and C are the number of rows and columns, respectively. When the grid size gets doubled, R and C reduce to half of their original value and above procedure is repeated iteratively until $\max(R, C)$ is greater than 2. Linear regression model is used to fit the line from plot $\log(N_r)$ vs. $\log(1/r)$ and the slope gives the FD as

$$\log N_r = FD\log\left(\frac{1}{r}\right) \tag{4}$$

Gray-Level Co-occurrence Matrix (GLCM)

The elements of a Gray-Level Co-occurrence Matrix (GLCM) are made up of the relative number of times the gray-level pair (a, b) occurs when pixels are separated by the distance $(a, b)=(1, 0)$. The GLCM of an $m\times n$ image can be defined by [35]

$$C_d(i,j)=\left|\begin{Bmatrix}(a,b),(a+\Delta x,b+\Delta y):I(a,b)=i,\\ I(a+\Delta x,b+\Delta y)=j\end{Bmatrix}\right| \tag{5}$$

where $(a,b),(a+\Delta x,b+\Delta y)\in M\times N$, $d=(\Delta x,\Delta y)$. $|\cdot|$ denotes the cardinality of a set. The probability of a pixel with a gray-level value i having a pixel with a gray-level value j at a $(\Delta x,\Delta y)$ distance away in an image is

$$P_d(i,j)=\frac{C_d(i,j)}{\sum_i\sum_j C_d(i,j)} \tag{6}$$

We calculated the following features:

$$\text{Entropy}(\text{E})=-\sum_i\sum_j P_d(i,j)\times\ln\left[P_d(i,j)\right] \tag{7}$$

$$\text{Fourth moment}(m_4)=\sum_i\sum_j(i-j)^4 P_d(i,j) \tag{8}$$

Run Length Matrix

The run length matrix $P_\theta(i,j)$ contains the number of elements where gray level "i" has the run length "j" continuous in direction θ [36]. In this work, run length matrices of $\theta=0°, 45°, 90°$, and 135° were calculated to get the following feature: [37]

$$\text{Run length non-uniformity}(\text{RLNU})=\sum_j\left\{\sum_i P_\theta(i,j)\right\}^2\Big/\sum_i\sum_j P_\theta(i,j) \tag{9}$$

Higher-Order Spectra (HOS)

Second-order statistics can adequately describe minimum-phase systems only. Therefore, in many practical cases, higher-order correlations of a signal have to be studied to

extract information on the phase and nonlinearities present in the signal [38–41]. Higher-order statistics denote higher-order moments (order greater than two) and nonlinear combinations of higher-order moments, called the higher-order cumulants. In the case of a Gaussian process, all cumulant moments of order greater than two are zero. Therefore, such cumulants can be used to evaluate how much a process deviates from Gaussian behavior. Prior to the extraction of HOS-based features, the preprocessed images are first subjected to Radon transform [42]. This transform determines the line integrals along many parallel paths in the image from different angles θ by rotating the image around its center. Hence, the intensities of the pixels along these lines are projected into points in the resultant transformed signal. Thus, the Radon transform converts a 2D image into a 1D signal at various angles in order to enable calculation of HOS features. This 1D signal is then used to determine the bispectrum, $B(f_1, f_2)$, which is a complex valued product of three Fourier coefficients given by

$$B(f_1, f_2) = E\left[A(f_1)A(f_2)A^*(f_1 + f_2)\right] \qquad (10)$$

where $A(f)$ is the Fourier transform of a segment (or windowed portion) of a single realization of the random signal $a(nT)$, n is an integer index, T is the sampling interval, and $E[\cdot]$ stands for the expectation operation. $A^*(f_1+f_2)$ is the conjugate at frequency (f_1+f_2). The function exhibits symmetry and is computed in the nonredundant/principal domain region Ω as shown in Fig. 3. We calculated the H parameters that are related to the moments of bispectrum. The sum of logarithmic amplitudes of bispectrum H_1 is

$$H_1 = \sum_{\Omega} \log\left(\left|B(f_1, f_2)\right|\right) \qquad (11)$$

The weighted center of bispectrum (WCOB) is given by

$$WCOB_x = \frac{\sum_{\Omega} iB(i,j)}{\sum_{\Omega} B(i,j)}, \quad WCOB_y \frac{\sum_{\Omega} jB(i,j)}{\sum_{\Omega} B(i,j)} \qquad (12)$$

where i and j are frequency bin index in the nonredundant region.

We extracted H_1 and two weighted center of bispectrum features for every one degree of Radon transform between 0° and 180°. Thus, the total number of extracted features would be 724 (181×3). To summarize, the following are the steps to calculate the HOS features from the ultrasound image [36]: (1) The original image is first converted to 1D signal at every 1° angle using Radon transform. (2) The 256 point FFT is performed with 128 point overlapping to maintain the continuity. (3) The bispectrum of each Fourier spectrum is computed using the Eq. (9). Similarly, the bispectrum is determined for every 256 samples. (4) The average of all

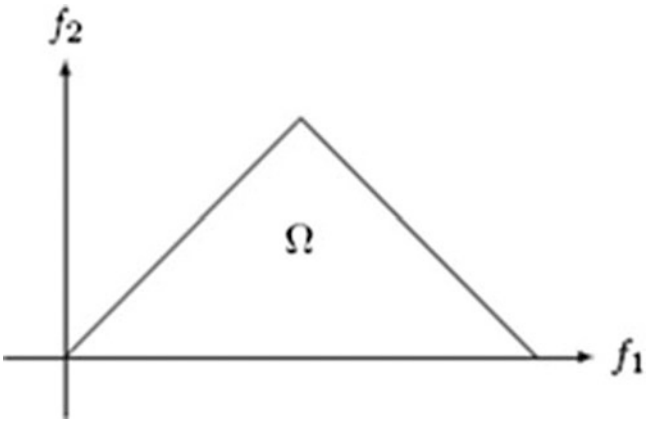

Fig. 3 Principal domain region (**Ω**) used for the computation of the bispectrum for real signals

these bispectra gives one bispectrum for every ultrasound image. (5) From this average bispectrum, the moments of bispectrum and weighted center of bispectrum features given in Eqs. (11) and (12) are calculated.

Feature Selection

After the feature extraction process, there were a total of 729 features (5 texture based and 724 HOS based). Most of these features would be redundant in information they retain, and using them to build classifiers would result in the curse of dimensionality problem [22] and over fitting of classifiers. Therefore, feature selection is done to ensure that only unique and informative features are retained. In this work, we have used Student's *t-test* [43] to select significant features. Here, a *t*-statistic, which is the ratio of difference between the means of the feature for two classes to the standard error between class means, is first calculated, and then the corresponding *p*-value is calculated. A *p*-value that is less than 0.01 or 0.05 indicates that the means of the feature are *statistically* significantly different for the two classes, and hence, the feature is very discriminating. On applying the *t*-test, we found that many features had a *p*-value less than 0.01. However, on evaluating several combinations of these significant features in the classifier, we found that only the four features listed in Table 1 presented the highest accuracy. Therefore, the entire dataset is now represented by a set of these four features for every patient.

Classifier Used

In the case of decision trees (DT), the input features are used to construct a tree, and then a set of rules for the

Table 1 Classifier performance measures

SVM kernel	TP	TN	FP	FN	Accuracy (%)	Sensitivity (%)	Specificity (%)	PPV (%)
Linear	100	99	0	1	99.8	99.61	100	100
Polynomial (order 1)	100	100	0	0	99.8	99.6	100	100
Polynomial (order 2)	100	100	0	0	99.5	100	99.9	99.9
Polynomial (order 3)	100	100	0	0	99.85	99.9	99.8	99.8
RBF	100	100	0	0	99.9	100	99.8	99.8

TN true negative, *FN* false negative, *TP* true positive, *FP* false positive

different classes are derived from the tree [44]. These rules are used for determining the class of an incoming new image.

Classification Process

Usually in classification, the holdout technique is a technique wherein a part (mostly 70 %) of the acquired dataset is used for training the classifier and the remaining samples are used for evaluating the performance of the classifier. However, the performance measures obtained using this technique may depend on which samples are in the training set and which are in the test set, and hence, the final resultant performance measures may be significantly different depending on how the split is made. In order to get robust results, we have adopted stratified *k-fold* cross validation technique as the preferred data resampling technique in this work. In this technique, the dataset is randomly split into k equal folds, each fold containing the same ratio of non-repetitive samples from both the classes. In iteration one, $(k-1)$ folds of data are used to train the classifier, and the remaining one fold is used to test the classifiers and to obtain the performance measures. This procedure is repeated for $(k-1)$ more times by using a different test set each time. The averages of the performance metrics obtained in all the iterations are reported as the overall performance metrics. In this work, k was taken as 10. Due to this iterative technique, the trained classifier will be more robust. In Jackknifing, similar to onefold cross validation method, instead of estimating the performance metrics over all the folds like in k-fold cross validation, we compute and study the bias of some statistic of interest in each fold of the data. In this work, we are interested in the generalization capability of the classifier, and hence, we used k-fold cross validation method.

Performance Measures

Sensitivity, specificity, positive predictive value, and accuracy were calculated to evaluate the performance of the classifiers. TN (true negative) is the number of benign samples identified as benign. TP (true positive) is the number of malignant images identified as malignant. The number of malignant samples detected as benign is quantified by the FN (false negative) measure. FP (false positive) is the number of benign samples identified as malignant. Sensitivity, which is the proportion of actual positives (malignant cases) which are correctly identified, is calculated as TP/(TP + FN), and specificity, which is the proportion of actual negatives (benign cases) which are correctly identified, is determined as TN/(TN + FP). Positive predictive value (PPV), which is the ratio of true positives to combined true and false positives, is calculated as TP/(TP + FP), and accuracy, which is the ratio of the number of correctly classified samples to the total number of samples, is calculated as (TP + TN)/(TP + FP + TN + FN).

Results

Selected Features

Table 1 presents the mean ± standard deviation (SD) values of the selected features for both the benign and malignant classes. The low p-value indicates that the listed features are significant. Even though the means of the features between the two classes appear to be close valued in Table 1, the *t-test* does not determine the significance based on the overall mean values. As previously indicated, the *t-test* judges the difference between their means relative to the spread or variability of their data. In this perspective, the listed features were found to be significant.

Classification Results

Since tenfold cross validation was employed, during each of the 10 iterations, 900 images from each class (a total of 1,800 images) were used for building the classifier and the remaining 100 images from each class (a total of 200 images) were used for testing and for determining the performance metrics. The averages of the performance measures obtained in the tenfolds are reported in Table 2. It is evident that the simple decision tree classifier presented the high accuracy of 97 %, sensitivity of 94.3 %, and specificity of 99.7 %. The advantage of the DT classifier over the other classifiers is that this classifier uses rules to classify a new image. These

Table 2 Significant features that had a p-value <0.0001 and their ranges (mean ± standard deviation) for benign and malignant classes

Feature	Benign	Malignant	p-value
LBP(R = 1, P = 8) entropy (LBP_{18} *Ent*)	1.58E + 08 ±0.53E + 08	2.17E + 08 ± 0.73E + 08	0.0000
LBP(R = 1, P = 8) energy (LBP_{18} *Ene*)	0.89E + 08 ±0.27E + 08	1.33E + 08 ± 0.50E + 08	0.0000
LBP(R = 2, P = 16) entropy (LBP_{216} *Ent*)	3.82E + 08 ±0.69E + 08	4.68E + 08 ± 1.32E + 08	0.0000
LBP(R = 2, P = 16) energy (LBP_{216} *Ene*)	0.27E + 08 ±0.09E + 08	0.31E + 08 ± 0.11E + 08	0.0000
LBP(R = 3, P = 24) entropy (LBP_{324} *Ent*)	0.22E + 08 ±0.07E + 08	0.24E + 08 ± 1.11E + 08	6.9744e-08
LBP(R = 3, P = 24) energy (LBP_{324} *Ene*)	4.19E + 08 ± 1.09E + 08	3.78E + 08 ± 1.19E + 08	2.3315e-15
Laws texture energy 1(LTE_1Ene)	0.31E + 08 ± 0.10E + 08	0.36E + 0 ± 0.13E + 08	0.0000
Laws texture energy 2(LTE_2Ene)	0.29E + 08 ± 0.09E + 08	0.31E + 08 ± 0.15E + 08	1.2659e-05
Laws texture energy 3(LTE_3Ene)	2.8019 ± 0.1963	3.0604 ± 0.1363	0.0000
Laws texture energy 4(LTE_4Ene)	0.2065 ± 0.0495	0.1444 ± 0.0315	0.0000
Laws texture energy 5(LTE_5Ene)	2.5528 ± 0.1203	2.8239 ± 0.1192	0.0000
Laws texture energy 6(LTE_6Ene)	0.2877 ± 0.019	0.2577 ± 0.0139	0.0000
Laws texture energy 7(LTE_7Ene)	2.404 ± 0.0884	2.6327 ± 0.1133	0.0000
Laws texture energy 8(LTE_8Ene)	0.3319 ± 0.0154	0.3232 ± 0.0189	0.0000

rules are comprehensible to the end user and, hence, allow the physicians to more confidently accept the result from the classifier. This is not the case with classifiers such as the artificial neural networks which, in most cases, behave like black boxes by not being transparent in the way in which they determine the class label.

Discussion

There are very few CAD-based studies in the field of ovarian tumor classification. Age and results of 30 blood tests were used as features in a multilayer perceptron classifier in order to classify the patient into one of the three classes, namely, benign, early-stage, and late-stage cancers. On testing 55 cases, an accuracy of 92.9 % was recorded [11]. Assareh et al. [12] selected three significant biomarkers among the high-dimensional input data from protein mass spectra and used them in two fuzzy linguistic rules. On using these rules for classification, they have reported a classification accuracy of 100 % for one dataset (91 controls, 162 cancers) and 86.36 % for another dataset (100 normal, 16 benign, 100 cancers). The limitation of this study was the use of holdout technique for data resampling. As indicated earlier, holdout technique generally results in less robust results due to the dependence of the dataset split made for selecting training and test sets. On using a complementary fuzzy neural network on a DNA microarray gene expression dataset (24 normal, 30 cancers), Tan et al. [13] reported an accuracy of 84.72 % using nine features. In another mass spectra-based study, binary images were first modeled based on the proteomic mass spectrum data from 100 normal and 100 cancers. On evaluation using these models, an accuracy of 96.5 % was obtained [14]. Tang et al. [15] proposed a novel approach for dimensionality reduction in mass spectrometry data and tested it using high-resolution SELDI-TOF data for ovarian cancer (95 normal, 121 cancers). Four statistical moments were used in a kernel partial least squares classifier, and sensitivity of 99.5 %, specificity of 99.16 %, and accuracy of 99.35 % were achieved. Petricoin et al. [16] used a genetic algorithm with self-organizing cluster analysis for detecting ovarian cancer. They used spectra derived from analysis of serum from 50 normal women and 50 patients with ovarian cancer to identify a proteomic pattern that completely discriminated cancer from normal conditions. They identified pattern was used to evaluate 50 malignant and 66 benign conditions. A sensitivity of 100 % and specificity of 95 % were observed. Even though the accuracies obtained using MS data are high, the use of these techniques is limited by the availability and cost of the necessary equipment for data analysis.

Tailor et al. [17] used variables such as age, menopausal status, maximum tumor diameter, tumor volume, locularity, the presence of papillary projections, the presence of random echogenicity, the presence of analyzable blood flow velocity waveforms, the peak systolic velocity, time-averaged maximum velocity, the pulsatility index, and resistance index obtained from 52 benign and 15 malignant transvaginal B-mode ultrasonography images. Using a variant of the back-propagation method, they obtained a sensitivity and specificity of 100 and 98.1 %. Bruning et al. [18] developed a knowledge-based system called ADNEXPERT that used histopathologic and sonographic data for computer-assisted ultrasound diagnosis of adnexal tumors. On evaluation using 69 new adnexal tumor cases, ADNEXPERT achieved an accuracy of 71 %. Biagiotti et al. [19] used variables such as age, papillary projections, random echogenicity, peak systolic velocity, and resistance index obtained from 175 benign and 51 malignant transvaginal B-mode ultrasonography images. Using a three-layer back-propagation network, they obtained 96 % sensitivity. All these three studies [17–19] used features based on evaluations made by the operator, and

hence, these features may be subjective in nature. Zimmer et al. [20] proposed an automatic analysis of the B-mode ultrasound images by quantification of gray-level intensity variations (mean, standard deviation, etc.). Using a segmented region of interest, their algorithm classified the tumor into three main categories (cyst, solid, and semi-solid) and obtained a low accuracy of 70 % for tumors containing solid portions. Lucidarme et al. [21] used the Ovarian HistoScanning (OVHS, Advanced Medical Diagnostics, Waterloo, Belgium) technique for tumor classification. This technique registered 98 % sensitivity, 88 % specificity, and 91.73 % accuracy. HistoScanning is an automatic scoring system based on the quantification of tissue disorganization induced by malignant processes in backscattered ultrasound waves before image processing. Recently, we extracted texture features based on Local Binary Patterns (LBP) and Laws Texture Energy (LTE) and used them to build and train a Support Vector Machine (SVM) classifier. On evaluating 1,000 benign and 1,000 malignant images using the developed system, we obtained a high accuracy of 99.9 % [45]. We tested only texture features in [45] whereas we evaluated a novel combination of HOS and texture features in this present study.

Our study is along the lines of Zimmer et al. [20] wherein we have quantified the gray-level intensity variations in the ultrasound images using texture and HOS-based features. Zimmer et al. [20] employed segmentation algorithms to determine the region of interest (ROI) of the ovarian mass in B-mode ultrasound images. In our technique, we use the whole 2D image and not any segmented portions. We have taken the Radon transform for every 1° circularly around the image to acquire all the possible information within the image. Our results show that all the four selected nonlinear features have unique ranges (with low p-values). The structural features outside the lesion like noise or other changes do not contribute to our results because nonlinear features like HOS are robust to noise and capture the nonlinear interaction of the pixels in the frequency domain and also capture phase coupling. Therefore, the changes outside the lesion do not influence our features or classification results. Using the DT classifier, we have achieved a high accuracy of 97 % due to the use of the novel combination of the four features in the classifier. The time taken to obtain the diagnosis prediction was less than 1 min. Our proposed algorithm has the following features:

(a) The proposed system uses the whole ultrasound image (not any specific ROI), automatically extracts features, and uses them in the DT classifier to predict the class (benign/malignant) of the patient. Since no user interaction is necessary, the end results are more objective and reproducible compared to manual interpretations of ultrasound images which can at times result in interobserver variations.

(b) Because of the use of the stratified cross validation data resampling technique, the system is generalized to accurately predict the class of new ultrasound images, and hence, the proposed technique is robust.

(c) Only four simple and easily determinable powerful features have to be calculated from the images for use in the classifiers. This significantly reduces the computational load and time. Unlike MS data, there is no need for complex techniques for dimensionality reduction.

(d) Since we use images acquired using commonly available and affordable ultrasound modality, there is no additional cost for image acquisition. Moreover, the algorithm can be easily written as a software application that can be installed and used in any radiologists' or physicians' office at no extra cost.

(e) The physician has to just run the software on the acquired B-mode ultrasound images. The software does all the processing and outputs classified image after characterization of the tissue. Hence, there is no need for trained experts for running the software.

On the limitations side, the robustness of such CAD techniques depends on the determination of good features that well discriminate the classes, in this case, benign and malignant tumors. Moreover, for medical-legal concerns, the radiologists have to store all CAD findings and images which increase digital storage requirements. When we use such CAD tools, we tend to rely on the CAD results, leading to a lower performance in detecting cancers than when we do not use CAD. Thus, using CAD may degrade human decision making. Hence, clinical success of such CAD tools depends on these tools having a high sensitivity and a reasonable specificity and also good reproducibility of the results [46]. In this study, we have obtained a high sensitivity of 94.3 % and specificity of 99.7 %. However, we believe that there is more room for improvement in accuracy. Therefore, as part of our future studies, we intend to analyze other texture features to determine more discriminating features. Moreover, the clinical applicability of our proposed technique has to be established with more studies containing larger image databases from multiethnic groups. We also intend to extend the study protocol to 3D, wherein we would include the spatial information of the 3D slices taken from a single patient for analysis.

Conclusion

We have presented a CAD technique for ovarian tumor classification in this paper. A novel combination of four texture and HOS-based features that adequately quantify the nonlinear changes in both benign and malignant ovarian ultrasound images was used to develop classifiers. Our study shows that the decision tree classifier is capable of classifying benign and malignant conditions with a high accuracy of 97 %, sensitivity of 94.3 %, and specificity of 99.7 %. The developed classifier is robust

as it was evaluated with 1,000 benign and 1,000 malignant samples using tenfold stratified cross validation. The preliminary results obtained using the system show that the features are discriminative enough to yield good classification accuracy of 97 %. Moreover, the CAD tool would be a more objective alternative to manual analysis of ultrasound images which might result in interobserver variations. The system can be installed as a stand-alone software application in the physician's office at no extra cost. However, the system has been tested only on 20 cases and further clinical validation will be required to assess the diagnostic accuracy of proposed method.

References

1. NCI (National Cancer Institute) on ovarian cancer. Information website http://www.cancer.gov/cancertopics/types/ovarian. Accessed 4 Oct 2011.
2. Bast Jr RC, Badgwell D, Lu Z, et al. New tumor markers: CA125 and beyond. Int J Gynecol Cancer. 2005;15:274–81.
3. Zaidi SI. Fifty years of progress in gynecologic ultrasound. Int J Gynaecol Obstet. 2007;99:195–7.
4. Menon U, Talaat A, Rosenthal AN, et al. Performance of ultrasound as a second line test to serum CA125 in ovarian cancer screening. BJOG. 2000;107:165–9.
5. Kim KA, Park CM, Lee JH, et al. Benign ovarian tumors with solid and cystic components that mimic malignancy. AJR Am J Roentgenol. 2004;182:1259–65.
6. Lenic M, Zazula D, Cigale B. Segmentation of ovarian ultrasound images using single template cellular neural networks trained with support vector machines. In: Proceedings of 20th IEEE international symposium on Computer-Based Medical Systems, Maribor, 2007, 205–12.
7. Hiremath PS, Tegnoor JR. Recognition of follicles in ultrasound images of ovaries using geometric features. In: Proceedings of international conference on Biomedical and Pharmaceutical Engineering, Singapore, 2009, 1–8.
8. Deng Y, Wang Y, Chen P. Automated detection of polycystic ovary syndrome from ultrasound images. In: Proceedings of the 30th annual international IEEE Engineering in Medicine and Biology Society conference, Vancouver, 2008, p. 4772–5.
9. Sohail ASM, Rahman MM, Bhattacharya P, Krishnamurthy S, Mudur SP. Retrieval and classification of ultrasound images of ovarian cysts combining texture features and histogram moments. In: IEEE international symposium on Biomedical Imaging: From Nano to Macro, Rotterdam, 2010, p. 288–91.
10. Sohail ASM, Bhattacharya P, Mudur SP, Krishnamurthy S. Selection of optimal texture descriptors for retrieving ultrasound medical images. In: IEEE international symposium on Biomedical Imaging: From Nano to Macro, Chicago, 2011, p. 10–6.
11. Renz C, Rajapakse JC, Razvi K, Liang SKC. Ovarian cancer classification with missing data. In: Proceedings of 9th international conference on Neural Information Processing, Singapore, 2002, vol. 2, p. 809–13.
12. Assareh A, Moradi MH. Extracting efficient fuzzy if-then rules from mass spectra of blood samples to early diagnosis of ovarian cancer. In: IEEE symposium on Computational Intelligence and Bioinformatics and Computational Biology, Honolulu, 2007, p. 502–6.
13. Tan TZ, Quek C, Ng GS, Razvi K. Ovarian cancer diagnosis with complementary learning fuzzy neural network. Artif Intell Med. 2008;43:207–22.
14. Meng H, Hong W, Song J, Wang L. Feature extraction and analysis of ovarian cancer proteomic mass spectra. In: 2nd international conference on Bioinformatics and Biomedical Engineering, Shanghai, 2008, p. 668–71.
15. Tang KL, Li TH, Xiong WW, Chen K. Ovarian cancer classification based on dimensionality reduction for SELDI-TOF data. BMC Bioinformatics. 2010;11:109.
16. Petricoin F. Use of proteomic patterns serum to identify ovarian cancer. Lancet. 2002;359:572–7.
17. Tailor A, Jurkovic D, Bourne TH, Collins WP, Campbell S. Sonographic prediction of malignancy in adnexal masses using an artificial neural network. Br J Obstet Gynaecol. 1999;106:21–30.
18. Brüning J, Becker R, Entezami M, Loy V, Vonk R, Weitzel H, et al. Knowledge-based system ADNEXPERT to assist the sonographic diagnosis of adnexal tumors. Methods Inf Med. 1997;36:201–6.
19. Biagiotti R, Desii C, Vanzi E, Gacci G. Predicting ovarian malignancy: application of artificial neural networks to transvaginal and color Doppler flow US. Radiology. 1999;210:399–403.
20. Zimmer Y, Tepper R, Akselrod S. An automatic approach for morphological analysis and malignancy evaluation of ovarian masses using B-scans. Ultrasound Med Biol. 2003;29:1561–70.
21. Lucidarme O, Akakpo JP, Granberg S, et al. A new computer-aided diagnostic tool for non-invasive characterisation of malignant ovarian masses: results of a multicentre validation study. Eur Radiol. 2010;20:1822–30.
22. Bellman RE. Dynamic programming. Mineola: Courier Dover Publications; 2003.
23. Hata T, Yanagihara T, Hayashi K, Yamashiro C, et al. Three-dimensional ultrasonographic evaluation of ovarian tumours: a preliminary study. Hum Reprod. 1999;14:858–61.
24. Laban M, Metawee H, Elyan A, Kamal M, Kamel M, Mansour G. Three-dimensional ultrasound and three-dimensional power Doppler in the assessment of ovarian tumors. Int J Gynaecol Obstet. 2007;99:201–5.
25. Cohen LS, Escobar PF, Scharm C, Glimco B, Fishman DA. Three-dimensional power Doppler ultrasound improves the diagnostic accuracy for ovarian cancer prediction. Gynecol Oncol. 2001;82:40–8.
26. Okugawa K, Hirakawa T, Fukushima K, Kamura T, Amada S, Nakano H. Relationship between age, histological type, and size of ovarian tumors. Int J Gynaecol Obstet. 2001;74:45–50.
27. Webb JAW. Ultrasound in ovarian carcinoma. In: Reznek R, editor. Cancer of the ovary. Cambridge: Cambridge University Press; 2006. p. 94–111.
28. Guerriero S, Alcazar JL, Pascual MA, Ajossa S, Gerada M, Bargellini R, Virgilio B, Melis GB. Intraobserver and interobserver agreement of grayscale typical ultrasonographic patterns for the diagnosis of ovarian cancer. Ultrasound Med Biol. 2008;34:1711–6.
29. Testa AC, Gaurilcikas A, Licameli A, Mancari R, Di Legge A, Malaggese M, Mascilini F, Zannoni GF, Scambia G, Ferrandina G. Sonographic features of primary ovarian fibrosarcoma: a report of two cases. Ultrasound Obstet Gynecol. 2009;33:112–5.
30. Park SB, Lee JW, Kim SK. Content-based image classification using a neural network. Pattern Recogn Letters. 2004;25:287–300.
31. Gonzalez C, Woods RE. Digital image processing. Upper Saddle River: Prentice Hall; 2001.
32. Fortin C. Fractal dimension in the analysis of medical images. IEEE Eng Med Biol. 1992;11:65–71.
33. Mandelbrot BB. The fractal geometry of nature. New York: WH Freeman Ed; 1982.
34. Biswas MK, Ghose T, Guha S, Biswas PK. Fractal dimension estimation for texture images: a parallel approach. Pattern Recogn Letters. 1998;19:309–13.

35. Haralick RM, Shanmugam K, Dinstein I. Textural features for image classification. IEEE Trans Syst Man Cybern. 1973;SMC-3:610–21.
36. Ramana KV, Ramamoorthy B. Statistical methods to compare the texture features of machined surfaces. Pattern Recogn. 1996;29: 1447–59.
37. Galloway MM. Texture classification using gray level run length. Comput Graph Image Process. 1975;4:172–9.
38. Nikias C, Petropulu A. Higher-order spectral analysis. Englewood Cliffs: Prentice-Hall; 1997.
39. Chua KC, Chandran V, Acharya UR, Lim C. Application of higher order spectra to identify epileptic EEG. J Med Syst. 2011;35(6): 1563–71. doi:10.1007/s10916-010-9433-z.
40. Acharya UR, Chua KC, Lim TC, Dorithy DL, Suri JS. Automatic identification of epileptic EEG signals using nonlinear parameters. J Med Mech Biol. 2009;9:539–53.
41. Chua KC, Chandran V, Acharya UR, Lim CM. Analysis of epileptic EEG signals using higher order spectra. J Med Eng Technol. 2009;33:42–50.
42. Ramm A, Katsevich A. The radon transform and local tomography. Boca Raton: CRC Press; 1996.
43. Box JF. Guinness, gosset, fisher, and small samples. Stat Sci. 1987;2:45–52.
44. Larose DT. Decision trees. In: Discovering knowledge in data: an introduction to data mining. Hoboken: Wiley Interscience; 2004. p. 108–26.
45. Acharya UR, Sree SV, Krishnan MM, Saba L, Molinari F, Guerriero S, Suri JS. Ovarian tumor characterization using 3D ultrasound. Technol Cancer Res Treat. 2012;11(6):543–52.
46. Philpotts LE. Can computer-aided detection be detrimental to mammographic interpretation? Radiology. 2009;253(1):17–22.

Evolutionary Algorithm-Based Classifier Parameter Tuning for Automatic Ovarian Cancer Tissue Characterization and Classification

U. Rajendra Acharya, Muthu Rama Krishnan Mookiah, S. Vinitha Sree, Ratna Yanti, Roshan Martis, Luca Saba, Filippo Molinari, Stefano Guerriero, and Jasjit S. Suri

Abstract

Purpose: Ovarian cancer is one of the most common gynecological cancers in women. It is difficult to accurately and objectively diagnose benign and malignant ovarian tumors using ultrasound and other tests. Hence, there is an imperative need to develop a computer-aided diagnostic (CAD) system for ovarian tumor classification in order to reduce patient anxiety and cost of unnecessary biopsies. In this paper, we present an automatic CAD system for the detection of benign and malignant ovarian tumors using advanced image processing and data mining techniques.

Materials and Methods: In the proposed system, Hu's invariant moments, Gabor transform parameters, and entropies are first extracted from the acquired ultrasound images. Significant features are then used to train a probabilistic neural network (PNN) classifier for classifying the images into benign and malignant categories. The model parameter (σ) for which the PNN classifier performs the best is identified using genetic algorithm (GA).

Results: The proposed system was validated using 1,300 benign and 1,300 malignant images obtained from ten patients with benign and ten with malignant disease, respectively. We used 23 statistically significant ($p<0.0001$) features. On evaluating the classifier using tenfold cross-validation technique, we were able to achieve an average classification accuracy of 99.8 %, sensitivity of 99.2 %, and specificity of 99.6 % with the σ of 0.264.

Conclusion: The proposed automated system is automated and hence is more objective, can be easily deployed in any computer, fast, accurate, and can act as an adjunct tool in helping the physicians make a confident call on the nature of the ovarian tumor under evaluation.

Keywords

Ovarian cancer • Hu's invariant moments • Gabor transform • Probabilistic neural network • entropy • Computer-aided diagnosis

U.R. Acharya, PhD, DEng • M.R.K. Mookiah, PhD
R. Yanti • R. Martis
Department of Electronics and Computer Engineering,
Ngee Ann Polytechnic, Singapore, Singapore

S.V. Sree, PhD (✉)
Global Biomedical Technologies Inc., 208 Otter Glen CT,
Roseville, CA 95661, USA
e-mail: vinitha.sree@gmail.com

L. Saba, MD
Department of Radiology, Azienda Ospedaliero Universitaria
di Cagliari, Cagliari, Italy

F. Molinari, PhD
Biolab, Department of Electronics and Telecommunications,
Politecnico di Torino, Torino, Italy

S. Guerriero, MD
Department of Obstetrics and Gynecology, University of Cagliari,
Ospedale San Giovanni di Dio, Via Ospedale 46,
09124 Cagliari, Italy

J.S. Suri, PhD, MBA, Fellow AIMBE
CTO, Global Biomedical Technologies, Roseville, CA USA

Department of Electrical Engineering,
Idaho State University (Aff.), Pocatello, ID, USA
e-mail: jsuri@comcast.net

L. Saba et al. (eds.), *Ovarian Neoplasm Imaging*,
DOI 10.1007/978-1-4614-8633-6_27,

Introduction

Early detection of ovarian cancer continues to be a difficult challenge. Ovarian cancer is the fifth most common cause of cancer death overall in women and one of the leading causes of death due to gynecologic cancers [1]. This pathology causes more than 13,000 deaths each year in the US [2]. The risk of a woman developing ovarian cancer is 1 in 71 [3]. Different conditions are associated with the risk to develop an ovarian cancer, in particular the age [3] and the presence of BRCA1 or BRCA2 genes [4, 5].

Several imaging modalities can be used for the detection and characterization of ovarian cancer [6, 7], and since the introduction of female pelvis ultrasound evaluation, the sonographic appearances of the ovary (normal and pathologic) have been extensively studied [8–10]. The use of ultrasound evaluation as first-line exam for the study of the ovaries relies on the fact that this analysis can be performed without the administration of radiation and contrast materials. With the introduction of transvaginal ultrasonography and 3D ultrasonography, the sensitivity and specificity of ultrasonography further improved [11, 12]. Even though ultrasonography is currently the most common practice, the accuracy and reproducibility of the visual interpretations of the images are often dependent on the skill of the ultrasonographers and thus ultrasonography is limited by interobserver variabilities. Other modalities such as computerized tomography, magnetic resonance imaging, and radioimmunoscintigraphy are limited by cost or device availability and/or radiation exposure. Furthermore, preoperative determination of whether an ovarian tumor is malignant or benign, especially when the tumor has both solid and cystic components, has been found to be difficult [13]. Due to such inconclusive findings, sometimes, surgical procedures such as bilateral oophorectomy with or without hysterectomy have been offered to patients with benign ovarian tumor. Such procedures increase healthcare cost and time and also increase patient anxiety. Therefore, there is an imperative need for an adjunct modality or technique that could provide a valuable second opinion to the physicians on the nature of the imaged tumor thereby enabling them to decide necessary treatment protocols.

In the past few years in the imaging field, new software dedicated to the automated identification (computer-aided detection) and characterization (computer-aided diagnosis (CAD)) of specific pathologies (thyroid cancer, atherosclerosis) have been introduced to help radiologists in the diagnosis of the pathologies [14, 15]. These CAD techniques generally process the acquired images to remove noise. Subsequently, they extract representative features that quantify the changes in pixel intensities in the images. Significant features are then used to train classifiers to develop them to accurately classify new images into benign and malignant classes. CAD-based techniques can prove to be excellent adjunct techniques because of their ease of use, speed, noninvasiveness, cost-effectiveness, and reliability. In the literature, there are very few studies in the application of CAD for ovarian cancer detection. Most of these studies use features based on (a) blood test results [16], (b) mass spectrometry (MS) data [17– 21], and (c) ultrasound images [22–26]. MS-based classification studies are affected by the curse of dimensionality [27] as they have to process a high-dimensional feature set obtained from a small sample size. Also, the MS equipment is expensive and not easily available. Therefore, the CAD technique proposed in this work uses images acquired using the commonly available and low-cost ultrasound modality. A literature review on these techniques (presented in brief in the discussion section of this paper) indicates that there is a need for CAD algorithms that use the ultrasound images and less number of significant features to predict benign and malignant tumors with high accuracy. Therefore, the key objective of this work is to present one such CAD technique for ovarian tumor classification and evaluate the performance of the technique using training and test ovarian tumor image databases. Compared to 2D ultrasonography, a 3D approach allows for more objective and quantitative study of the morphological characteristics of benign and malignant tumors [28]. Studies have shown that the selective use of 3D ultrasonography and power Doppler ultrasound can improve the diagnostic accuracy of ovarian tumors [29, 30]. Therefore, we have used 3D transvaginal ultrasonography images in our work.

Experimental Data

For this study, 20 women (age range: 29–74 years) were recruited. Eleven were premenopausal and nine were postmenopausal. As the first step, the patients were offered B-mode ultrasonography to characterize the morphology of the adnexal masses. These masses were then classified into one of the following classes: unilocular, multilocular, unilocular solid, multilocular solid, or solid. Subsequently, 2D Doppler was used to assess tumor vascularization. Since low-velocity flow without noise had to be detected, the power Doppler settings were tuned such that a maximum sensitivity was achieved. Before surgery, all the participants in the study were subjected to a 3D transvaginal ultrasonography evaluation. 3D volumes of the suspicious areas were obtained from the scans. The time of acquisition of whole volumes ranged from 2 to 6 s. The variation in acquisition time depended on the size of the volume box. If an adnexal mass had more than one volume stored, only the first of the stored volumes was used for further processing. Among the participants, ten had malignant tumors in the ovary while the remaining ten had benign conditions. The middle 100 images were selected from the volume from each subject, and thus, the evaluated

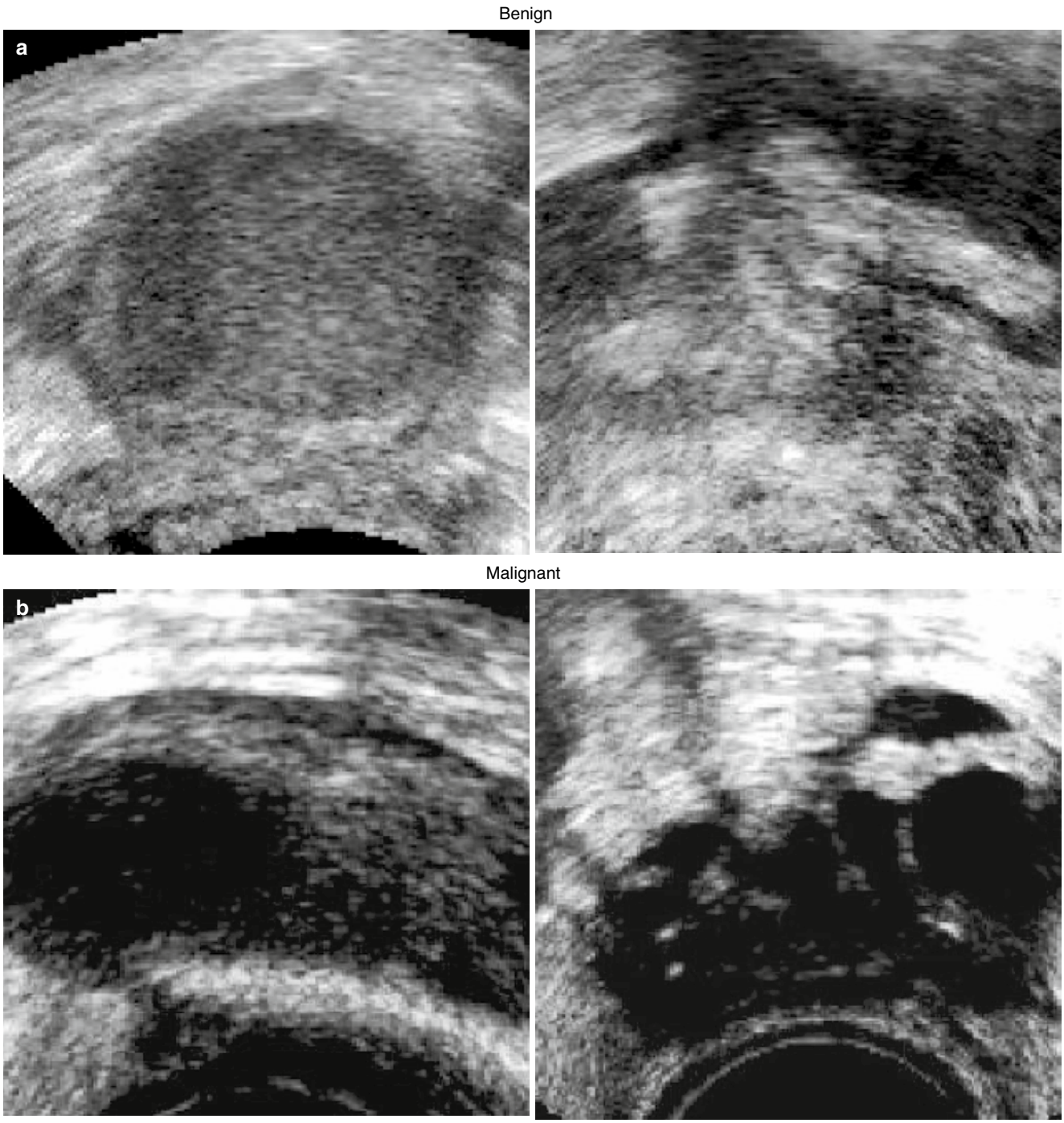

Fig. 1 Typical ultrasound images of (**a**) benign tumors (**b**) malignant tumors

database consisted of 1,300 benign images and 1,300 malignant images. To extract the region of interest (ROI), the ultrasound image was first automatically cropped by utilizing the vertical and horizontal gradients to detect the boundaries of the black frame border surrounding the image. Subsequently, a gynecologist and radiologist were employed to mark out the squared ROI from the cropped image. Images of size 256×256 were considered in our study. A typical set of benign and malignant ultrasound images is depicted in Fig. 1.

Methods

Our proposed system for ovarian tumor classification is presented in Fig. 2. It consists of an online classification system (shown on the right side of Fig. 2) which processes a test image. This online system predicts the class label (benign or malignant) of the test image based on the transformation of the online gray scale feature vector by the training parameters determined by an off-line learning system (shown on the left

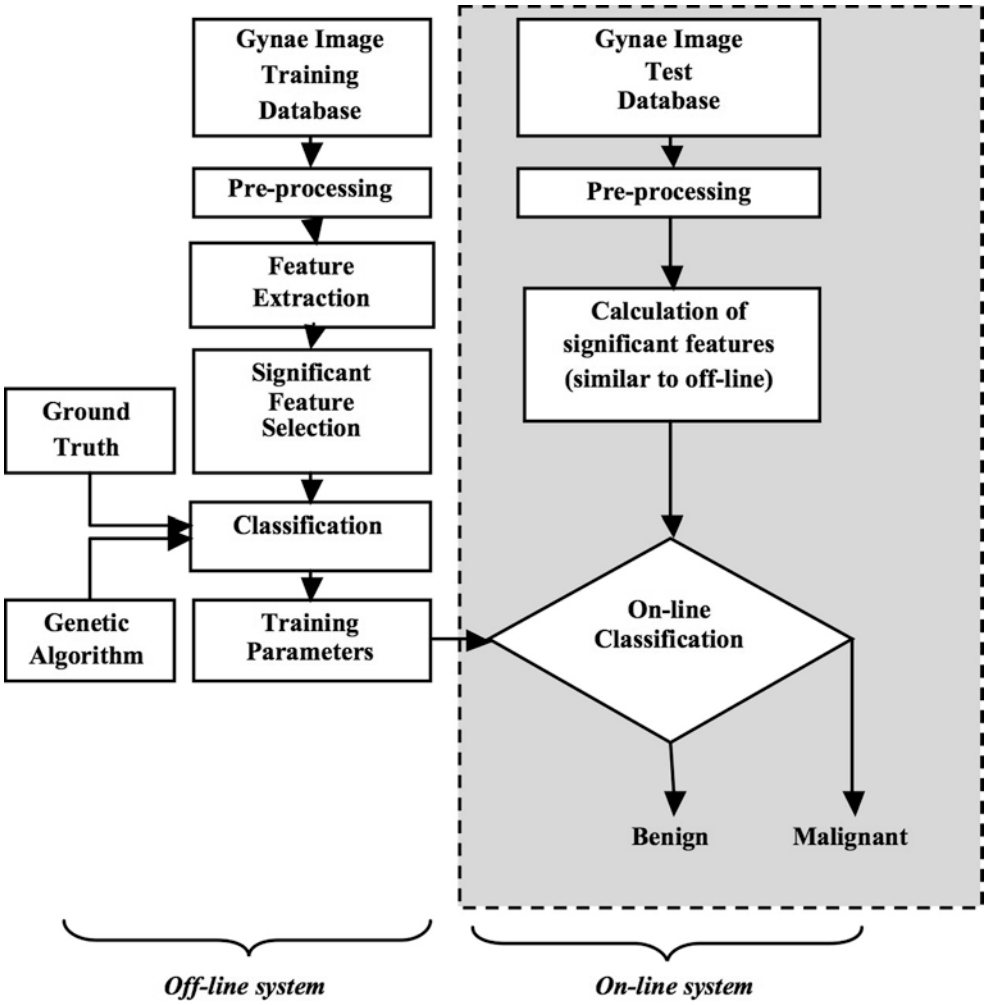

Fig. 2 The proposed system for the ovarian tumor classification

side of Fig. 1). The off-line classification system is composed of a classification phase which produces the training parameters using the combination of gray scale off-line training features and the respective off-line ground truth training class labels (0/1 for benign/malignant). The gray scale features for online or off-line training are the same: Hu's invariant moments, Gabor wavelet transform parameters, and entropies. Significant features among the extracted ones are selected using the *t*-test. We evaluated the probabilistic neural network (PNN) classifier. The best model parameter (σ) for which the PNN classifier performs the best is identified using genetic algorithm. The classifier robustness is evaluated using tenfold cross-validation. The predicted class labels of the test images and the corresponding ground truth labels (0/1) are compared to determine the performance measures of the system such as sensitivity, specificity, accuracy, and PPV.

In the remainder of this section, we describe the features, Gabor wavelet transform and entropy features, the PNN classifier, and the feature selection test (*t*-test) used in this work.

Feature Extraction

In this work, we have extracted seven Hu's invariant moments, mean and standard deviation values of coefficients of Gabor wavelet transform at different angles and slices, and Yager and Kapur entropies. These features are briefly explained in this section.

Hu's Invariant Moments

Moments and the related invariants have been extensively analyzed to characterize the patterns in images in a variety of applications. 2D moment of an image $f(x, y)$ is defined by

$$m_{pq} = \sum_x \sum_y x^p y^q f(x,y) \tag{1}$$

For $p, q = 0, 1, 2\ldots$, the central moment is defined as

$$\mu_{pq} = \sum_x \sum_y (x-\bar{x})^p (y-\bar{y})^q f(x,y) \tag{2}$$

where $\bar{x} = m_{10}/m_{00}$ and $\bar{y} = m_{01}/m_{00}$ are the centroid of the image. Here, we consider binary image. In a binary image, m_{00} is the area of the image. The normalized central moment of order $(p+q)$ is defined as

$$\eta_{pq} = \frac{\mu_{pq}}{\mu_{00}^{\gamma}} \tag{3}$$

For $p, q = 0, 1, 2, 3 \ldots$, where $\gamma = \frac{p+q}{2} + 1$. From this normalized central moment Hu [31] defined seven values through order three that are invariant to object scale, position, and orientation. These seven moments are defined as:

$$M_1 = \eta_{20} + \eta_{02} \tag{4}$$

$$M_2 = (\eta_{20} - \eta_{02})^2 + 4\eta_{11}^2 \tag{5}$$

$$M_3 = (\eta_{30} - 3\eta_{12})^2 + (3\eta_{21} - \eta_{03})^2 \tag{6}$$

$$M_4 = (\eta_{30} + \eta_{12})^2 + (\eta_{21} + \eta_{03})^2 \tag{7}$$

$$\begin{aligned} M_5 = {} & (\eta_{30} - 3\eta_{12})(\eta_{30} + \eta_{12})\left[(\eta_{30} + \eta_{12})^2 \right. \\ & \left. - 3(\eta_{21} - \eta_{03})^2\right] + (3\eta_{21} - \eta_{03})(\eta_{21} + \eta_{03}) \\ & \left[3(\eta_{30} + \eta_{12})^2 - (\eta_{21} + \eta_{03})^2\right] \end{aligned} \tag{8}$$

$$\begin{aligned} M_6 = {} & (\eta_{20} - \eta_{02})\left[(\eta_{30} + \eta_{12})^2 - (\eta_{21} + \eta_{03})^2\right] \\ & + 4\eta_{11}(\eta_{30} + \eta_{12})(\eta_{21} + \eta_{03}) \end{aligned} \tag{9}$$

$$\begin{aligned} M_7 = {} & (3\eta_{21} - \eta_{03})(\eta_{30} + \eta_{12}) \\ & \left[(\eta_{30} + \eta_{12})^2 - 3(\eta_{21} + \eta_{03})^2\right] \\ & + (3\eta_{12} - \eta_{30})(\eta_{21} + \eta_{03}) \\ & \left[3(\eta_{30} + \eta_{12})^2 - (\eta_{21} + \eta_{03})^2\right] \end{aligned} \tag{10}$$

Gabor Wavelet Transform

Among various wavelet bases, Gabor function provides the optimal resolution in both the time (spatial) and frequency domains. It has both multi-resolution and multi-orientation properties and can effectively capture the local spatial frequencies [32]. Two-dimensional Gabor function [33] is a Gaussian modulated complex sinusoid and can be written as

$$\psi_{i,k}(m,n) = \frac{1}{2\pi\sigma_m\sigma_n} \exp\left(-\frac{1}{2}\left(\frac{m^2}{\sigma_m^2} + \frac{n^2}{\sigma_n^2}\right) + 2\pi j\omega m\right) \tag{11}$$

Here, ω is frequency of the sinusoid and σ_m and σ_n are the standard deviations of the Gaussian envelopes. 2D Gabor wavelets are obtained by dilation and rotation of the mother Gabor wavelet $\psi(m,n)$ using

$$\begin{aligned} \psi_{i,k}(m,n) = {} & a^{-l}\psi\left[a^{-l}(m\cos\theta + n\sin\theta),\right. \\ & \left. a^{-l}(-m\sin\theta + n\cos\theta)\right],\ a > 1 \end{aligned} \tag{12}$$

where a^{-1} is a scale factor, l and k are integers, the orientation θ is given by $\theta = k\pi/K$, and K is the number of orientations. The parameters σ_m and σ_n are calculated according to the design strategy proposed by Manjunath et al. [33]. Given an image $I(m,n)$, its Gabor wavelet transform is obtained as

$$\begin{aligned} x_{l,k}(m,n) = {} & I(m,n) * \psi_{l,k}(m,n) \\ & for\ \ l = 1,2,\ldots,S \ \text{ and } \ k = 1,2,\ldots,K \end{aligned} \tag{13}$$

where $*$ denotes the convolution operator. The parameters K and S denote the number of orientations and number of scales, respectively. The mean and the standard deviation of the coefficients are used as features and given by

$$\begin{aligned} \mu_{l,k}(m,n) = {} & \frac{1}{M \times N}\sum_{m=1}^{M}\sum_{n=1}^{N}\left|x_{l,k}(m,n)\right| \ \text{ and} \\ \sigma_{l,k} = {} & \left(\frac{1}{M \times N}\sum_{m=1}^{M}\sum_{n=1}^{N}\left(\left|x_{l,k}(m,n)\right| - \mu_{l,k}\right)^2\right)^{\frac{1}{2}} \end{aligned} \tag{14}$$

The feature vector is then constructed using mean ($\mu_{l,k}$) and standard deviation (std) ($\sigma_{l,k}$) as feature components, for $K = 6$ orientations and $S = 4$ scales, resulting in a feature vector of length 48, given by

$$f = \{\mu_{11}, \sigma_{11}, \ldots, \mu_{48}, \sigma_{48}\} \tag{15}$$

In this work, we extracted 2D Gabor wavelet features at 0º, 30º, 60º, 90º, 120º, and 150º.

Entropy

Entropy is widely used to measure of uncertainty associated with the system. In this work, we have used Yager's measure and Kapur's entropy to estimate the subtle variation in the pixel intensities. Let $f(x,y)$ be the image with $N_i (i = 0, 1, 2, 3, 4 \ldots\ldots\ldots\ldots L-1)$ distinct gray levels. The normalized histogram for a particular region of interest of size $(M \times N)$ is given by

$$H_i = \frac{N_i}{M \times N} \tag{16}$$

Then, *Yager's measure* [34] can be defined as

$$Y = 1 - \frac{\sum_{i=0}^{L-1}\left|2H_i - 1\right|}{\left|M \times N\right|} \tag{17}$$

Kapur's entropy [34] can be defined as

$$K_{\alpha,\beta} = \frac{1}{\beta-\alpha}\log_2 \frac{\sum_{i=0}^{L-1} H_i^{\alpha}}{\sum_{i=0}^{L-1} H_i^{\beta}} \tag{18}$$

where $\alpha \neq \beta,\ \alpha > 0,\ \beta > 0$

In this experiment, we considered $\alpha = 0.5$ and $\beta = 0.7$

Feature Selection

Student's *t*-test [35] is used to assess whether the means of a feature in two groups are statistically different from each other. The result of this test is the *p*-value. Lower *p*-value indicates that the two groups are well separated. Typically, features with *p*-values less than 0.05 are regarded as clinically significant.

Classification

The probabilistic neural network (PNN) model [36–38] is based on Parzen's results on probability density function estimators [37]. PNN is a three-layer feed forward network consisting of an input layer, a pattern layer, and a summation layer. A radial basis function and a Gaussian activation function can be used for the pattern nodes. In this work, PNN model was implemented using radial basis function (RBF) mentioned below.

$$Q = f(x) = \exp\left[-\frac{\| w - p \|^2}{2\sigma^2}\right] \tag{19}$$

where σ is an smoothing parameter.

The net input to the radial basis transfer function is the vector distance between its weight vector w and the input vector p, multiplied by the bias b. The RBF has a maximum of 1 when its input is 0. As the distance between w and p decreases, the output increases. Thus, a radial basis neuron acts as a detector, which produces 1 whenever the input p is identical to its weight vector.

PNN is a variant of radial basis network. When an input is presented, the first layer computes distances d from the input vector to the training input vectors and produces a vector whose element indicates how close the input is to a training input. The second layer sums these contributions for each class of inputs to produce probabilities as its net output vector. Finally, a compete transfer function on the output of the second layer picks the maximum of these probabilities and produces a 1 for that class and a 0 for the other classes [37].

PNN Smoothing Parameter Tuning

The smoothing parameter (σ) which controls the scale factor of the exponential activation function should be chosen appropriately to get the highest accuracy of classification. The decision boundary of the classifier varies continuously from a nonlinear hyperplane when $\sigma \to 1$ and when $\sigma \to 0$ represents the nearest neighbor classifier. For each value of σ, there will be a value for accuracy. The classifier provides highest accuracy only for a particular σ depending on data characteristics [36]. The value of σ has to be evaluated experimentally. One solution is to use brute force technique which requires lot of runs each for the possible σ. Another solution is to define the overall accuracy of the classifier for an initial σ as the fitness function in an evolutionary algorithm and the algorithm can be iterated over generations with a fixed population. In this work, we have used genetic algorithm (GA) [39, 40] which uses principles from natural genetics.

Genetic Algorithm (GA)

Genetic algorithm [37, 39, 40] is a global optimization strategy used in this experiment to tune the smoothing parameter of PNN and to obtain the highest possible accuracy. GA operates in binary-coded string space rather than in the original real feature space. Therefore, the features and its solution are to be encoded into binary strings which are called chromosomes, and finally they are decoded into the real numbers. The algorithm consists of three basic operations, reproduction, crossover, and mutation. A given population size is defined; in our experiment we have assumed population size of 20. Initially, 20 different random σs are assumed and the corresponding average accuracy over 10-folds is computed. The fitness function is made equal to the reciprocal of average accuracy over 10-folds. The problem is to maximize the average accuracy which reflects into minimization of the fitness function. In the 20 initial instances with different σs, the fittest solutions with higher fitness value are selected and reproduced in the next generation. A given crossover probability is defined (in our case we chose 0.8), and the proportion of population are chosen (in our case it will be 80 % of population size of 20 which is equal to 16). Randomly a given crossover site is taken and the chromosome (or bit string) is broken into two parts for each population. Two such strings belonging to different populations are joined at crossover site and new population is obtained. Also a given mutation probability is defined (in our case it is 0.05). Generally it is kept very low in comparison with natural genetics, and the corresponding proportion of bits of binary string is flipped. The three operations are continued in every generation. If there is no change in fitness function over iterations, the algorithm is terminated and the corresponding best fitness is the solution of the problem.

Table 1 Mean ± standard deviation values of the various features for the benign and malignant classes

Features	Benign	Malignant	*p*-value
Entropy			
Yager	0.9962 ± 0.0002	0.9961 ± 0.0001	<0.0001
Kapur	7.829 ± 0.1747	7.8624 ± 0.1262	<0.0001
Gabor transform			
Mean (0° scale 1)	0.0281 ± 0.0083	0.0293 ± 0.0061	<0.0001
Std (0° scale 1)	0.0289 ± 0.0062	0.0308 ± 0.0057	<0.0001
Mean (30° scale 1)	0.0245 ± 0.0068	0.0251 ± 0.0051	0.0162
Std (60° scale 1)	0.0192 ± 0.0038	0.0189 ± 0.0033	0.0312
Mean (90° scale 1)	0.0197 ± 0.005	0.0203 ± 0.0043	0.0026
Mean (120° scale 1)	0.0199 ± 0.0051	0.0204 ± 0.0041	0.0044
Mean (150° scale 1)	0.0243 ± 0.0068	0.0254 ± 0.005	<0.0001
Std (150° scale 1)	0.0225 ± 0.0048	0.0239 ± 0.0038	<0.0001
Mean (0° scale 2)	0.0221 ± 0.0058	0.0227 ± 0.005	0.0043
Std (0° scale 2)	0.0206 ± 0.0042	0.0214 ± 0.0038	<0.0001
Std (30° scale 2)	0.0136 ± 0.0028	0.0134 ± 0.0021	0.0227
Std (60° scale 2)	0.0105 ± 0.0019	0.0104 ± 0.0016	0.0427
Mean (90° scale 2)	0.014 ± 0.0031	0.0143 ± 0.0028	0.0362
Std (150° scale 2)	0.0131 ± 0.0027	0.0136 ± 0.002	<0.0001
Std (120° scale 3)	0.006 ± 0.001	0.0059 ± 0.0009	<0.0001
Std (150° scale 3)	0.0077 ± 0.0012	0.0078 ± 0.0008	0.0385
Std (0° scale 4)	0.0077 ± 0.0025	0.0074 ± 0.0023	0.011
Hu's invariant moments			
M_3	22.2667 ± 2.0598	22.8391 ± 1.9571	<0.0001
M_5	47.4946 ± 4.4118	48.2743 ± 4.5054	<0.0001
M_6	32.0567 ± 2.9685	32.4667 ± 3.0605	0.0005
M_7	46.6377 ± 4.5537	47.1105 ± 4.4465	0.0075

Results

Selected Features

Table 1 shows the mean ± standard deviation values of the various significant features for the benign and malignant classes. Since the *p*-value is less than 0.05, these features can be used to discriminate the two classes with higher accuracy. It can be seen from our results that the mean value of Gabor wavelet coefficients and Hu's invariant moments are higher for malignant images than the benign images. This may be because the malignant images have a relatively complex texture marked by increased randomness in the intensity distributions which lead to higher mean Gabor and Hu's invariant moment values.

Classification Results

Good performance comparison for classifiers can be achieved with huge test data. If the number of data available is less, data swapping may be performed to generate more test vectors. In this work, we have used tenfold cross-validation technique to evaluate the classifier. In this technique, the entire dataset (2,600 images) is divided into ten sets each having similar proportion of samples in both classes. Nine sets (2,340 images) are used for training the classifier, and the remaining one set (260 images) is used for testing and to determine the performance measures. This procedure is repeated nine more times by using a new test set each time. The average of all the ten performance measures is taken as the final value. Performance of the PNN classifier was assessed by measuring sensitivity, specificity, diagnostic accuracy, and positive predictive value (Table 2). It can be seen from Fig. 3 that the mean fitness value decreases as progression of generation increases.

Table 2 Results of average accuracy, sensitivity, specificity, and PPV for the PNN classifier

Classifier	Accuracy	PPV	Sensitivity	Specificity
PNN (σ=0.254)	99.81 %	99.69 %	99.92 %	99.69 %

The PNN classifier presented an average accuracy of 99.81 %, sensitivity of 99.92 %, specificity of 99.69 %, and PPV of 99.69 % with the σ of 0.264 (Table 2). Figure 4 shows a plot of average performance (sensitivity, specificity, and accuracy) for PNN classifier.

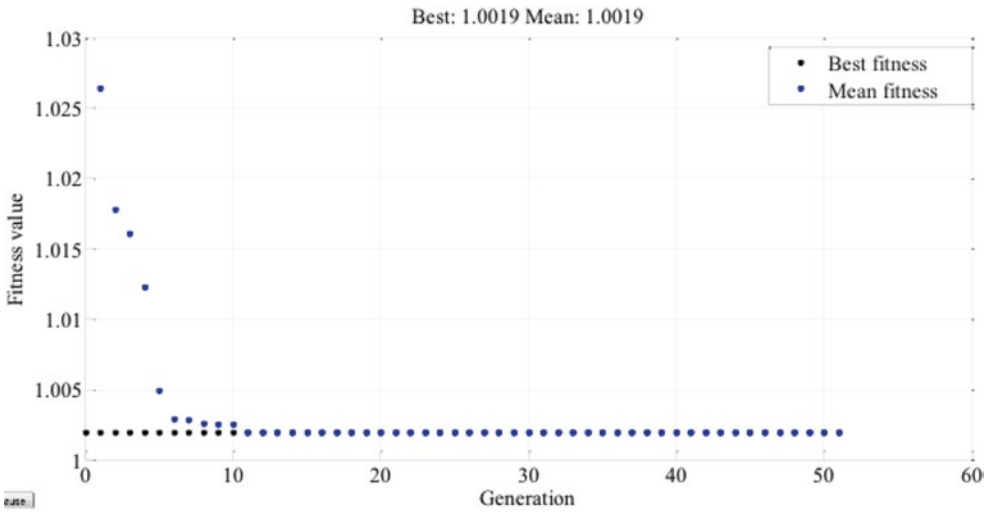

Fig. 3 Best and mean fitness for every generation decreasing with generations

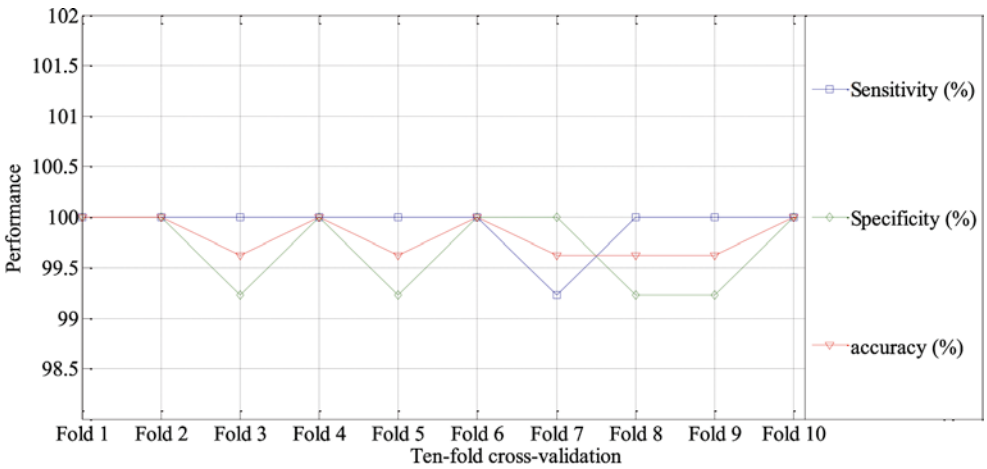

Fig. 4 Plot of average performance (sensitivity, specificity, and accuracy) for PNN classifier

Discussion

Ultrasonography and the determination of the levels of a tumor marker called cancer antigen 125 (CA 125) are currently the most commonly used techniques for detecting ovarian cancer. CA 125 marker has been found to be elevated only in 50 % of stage 1 cancers [41]. Furthermore, CA 125 can also be raised in other malignancies such as uterine and pancreatic, and sometimes in many benign conditions such as fibroids, endometriosis, pelvic inflammatory disease, and benign ovarian cysts [42]. Menon et al. [43] examined women with elevated CA 125 levels and observed that the ultrasound parameters result in varying sensitivity ranging from 84 to l00 %, with a specificity of 97 % but only a PPV of 37.2 %. Standardized blood test data and age were used as features for the classification of benign, early stage, and late stage cancers using multilayer perceptron classifier [16]. The proposed system was able to distinguish between early and late stage cancers with an accuracy of up to 92.9 %.

Three significant biomarkers among the high-dimensional input data from protein mass spectra were used them in two fuzzy linguistic rules [17]. Their proposed method provided an accuracy of 100 % for one dataset (91 controls and 162 cancers) and 86.36 % for another dataset (100 normal, 16 benign, and 100 cancers). Features from a deoxyribonucleic acid (DNA) microarray gene expression dataset were used in a complementary learning neural network (CLNN) [18]. This method yielded an accuracy of 84.72 % [18]. In another study [19], proteomic mass spectrum data

Table 3 Summary of studies that presented various CAD techniques for ovarian tumor classification

Literature	Features	Classifier	Performance
Renz et al. [16]	Standardized blood test data	Multilayer perceptron	Accuracy: 92.9 %
Assareh and Moradi [17]	Protein mass spectra	Fuzzy rule-based classifier	Dataset 1 accuracy: 100 % Dataset 2 accuracy: 86.36 %
Tan et al. [18]	Deoxyribonucleic acid microarray and proteomics data	Complementary fuzzy neural network	Accuracy: 84.72 %
Meng et al. [19]	Energy curves of binary images modeled based on the proteomic mass spectrum data	Similarity analysis	Sensitivity: 98 % Specificity: 95 %
Tang et al. [20]	Four statistical moments (mean, variance, skewness, and kurtosis) obtained from mass spectroscopy	Kernel partial least square classifier	Accuracy: 99.35 % Sensitivity: 99.5 % Specificity: 99.16 %
Petricoin [21]	Proteomic spectra	Genetic algorithm with self-organizing cluster analysis	Sensitivity: 100 % Specificity: 95 %
Tailor et al. [22]	Age, menopausal status, and parameters from transvaginal B-mode ultrasonography images	Back propagation neural network	Sensitivity: 100 % Specificity: 98.1 %
Bruning et al. [23]	Histopathologic and sonographic data	Knowledge-based system called ADNEXPERT	Accuracy: 71 %
Biagiotti et al. [24]	Age and parameters from transvaginal B-mode ultrasonography images	Three-layer back propagation network	Sensitivity: 96 %
Zimmer et al. [25]	Gray level intensity variations in B-mode ultrasound images	Custom developed algorithm	Accuracy: 70 %
Lucidarme et al. [26]	Quantification of tissue disorganization in backscattered ultrasound waves	Ovarian HistoScanning (OHS) system	Sensitivity: 98 % Specificity: 88 % Accuracy: 91.73 %
Acharya et al. [44]	Local Binary Pattern + Law's Mask Energy	Support vector machine	Sensitivity: 100 % Specificity: 99.8 % Accuracy: 99.9 %
Proposed Method	Hu's invariant moments + Gabor wavelet features + entropies	Probabilistic neural network	Sensitivity: 99.9 % Specificity: 99.6 % Accuracy: 99.8 %

after preprocessing were first wrapped into information images that were mapped to binary images under adaptive threshold. The energy curves of binary images were used to classify cancer samples from non-cancer ones using similarity analysis. They reported a sensitivity of 98 %, a specificity of 95 %, and a positive predictive value of 95.15 %. Nowadays, proteomics technologies such as SELDI-TOF mass spectrometry have shown immense promise in the early detection of cancers. In a study [20], four statistical moments (mean, variance, skewness, and kurtosis) were calculated for each interval and used as features in a kernel partial least square classifier. This method achieved an average sensitivity of 99.5 %, specificity of 99.16 %, accuracy of 99.35 %, and a correlation coefficient of 0.9869. The proteomic mass spectra were obtained from the samples of affected or unaffected women [21]. Using these spectra in a genetic algorithm coupled with self-organizing map-based technique, a sensitivity of 100 % and specificity of 95 % was obtained. Even though the accuracies obtained using MS data are high, the use of these techniques is limited by the availability and cost of the necessary equipment for data analysis.

Using features such as age, menopausal status, maximum tumor diameter, tumor volume, locularity, the presence of papillary projections, the presence of random echogenicity, the presence of analyzable blood flow velocity waveforms, the peak systolic velocity, time-averaged maximum velocity, the pulsatility index, and resistance index obtained from 52 benign and 15 malignant transvaginal B-mode ultrasonography images, a sensitivity and specificity of 100 and 98.1 % using a variant of back propagation method was reported [22]. A knowledge-based system called ADNEXPERT was developed using histopathologic and sonographic data from 2,290 adnexal tumors [23]. After an ultrasound examination, the gynecologist interacts with the system posing a maximum of 15 questions before the system arrives at the decision. ADNEXPERT accurately assessed pathology in 49 cases (71 %). The performance of artificial neural networks

(ANNs) with multiple logistic regression (MLR) models for predicting ovarian malignancy in patients with adnexal masses by using transvaginal B-mode and color Doppler flow ultrasonography (US) were compared [24]. A sensitivity of 96 % was obtained using three-layer back propagation classifier using the three-layer neural network using variables such as age, papillary projections, random echogenicity, peak systolic velocity, and resistance index obtained from transvaginal B-mode ultrasonography images. All these three studies [22–24] used features based on evaluations made by the operator, and hence, these features may be subjective in nature.

An automated technique based on the morphological analysis of ovarian masses for malignancy detection was presented [25]. The method follows two stages: (1) initial classification of mass (cyst, semisolid, solid) and (2) detailed analysis of mass. An accuracy of 70 % was reported for tumors containing solid portions. An innovative computer-aided diagnostic technology (ovarian HistoScanning technique) to quantify the characteristic features of transvaginal sonography (TVS) was proposed to discriminate benign from malignant adnexal masses [26]. Preoperative three-dimensional (3D) TVS, serum CA 125 levels, and the TVS-based diagnosis were used as features. Their method showed a sensitivity, specificity, and accuracy of 98, 88, and 91.73 %, respectively. Recently, Acharya et al. [44] proposed an automatic CAD system to classify the benign and malignant ovarian tumors using texture features based on local binary patterns (LBP) and laws texture energy (LTE) extracted from ultrasound images in a support vector machine (SVM) classifier [44]. An average classification accuracy of 99.9 %, sensitivity of 100 %, and specificity of 99.8 % were obtained using 2,000 ultrasound images. Table 3 provides a summary of the above described studies.

Our present study is along the lines of Zimmer et al. [25] and Acharya et al. [44] wherein we have quantified the gray level intensity variations in the ultrasound images using a combination of Hu's invariant moments, Gabor transform parameters, and entropy features. In our technique, we use the entire 3D transvaginal ultrasonography image directly for classification. Our proposed system is able to classify the benign and malignant ovarian tumors with an average accuracy of 99.8 %, sensitivity of 99.9 %, and specificity of 99.6 % using 2,600 ultrasound images. Our proposed algorithm has the following features:

1. The proposed system uses the whole ultrasound image, automatically extracts features and uses them in the PNN classifier to predict the class (benign/malignant). Since the technique is completely automated, the diagnosis is more objective and reproducible compared to manual interpretations.
2. Because of the use of stratified cross-validation data resampling technique to train and test the PNN classifier, the system is generalized to accurately predict the class of new ultrasound images, and hence, the proposed technique is robust.
3. The algorithm can be easily written as a software application that can be installed and used in the doctors' office at no extra cost.

On the limitations side, the robustness of such CAD techniques depends on the determination of good features that well discriminate the benign and malignant tumors. Even though the performance measures obtained in this preliminary study are adequately high, as part of our future studies, we intend to analyze other texture features to determine more discriminating features. Furthermore, we intend to establish the clinical applicability of our proposed technique by validating it using larger image databases from multiethnic groups. We also intend to extend the study protocol to 3D, wherein we would include the spatial information of the 3D slices taken from a single patient for analysis.

Conclusion

A novel CAD system to automatically classify benign and malignant ovarian tumors in ultrasound images is presented. The algorithm extracts features based on image texture, entropies, and Gabor wavelet transform parameters from an input ultrasound image and uses significant features in a PNN classifier to determine the nature of the tumor. Clinical success of such CAD tools depend on these tools having a high sensitivity and a reasonable specificity, and also good reproducibility of the results. Our technique was developed and evaluated on a huge database of 2,600 ultrasound images using tenfold stratified cross-validation. We have obtained an average classification accuracy of 99.81 %, sensitivity of 99.92 %, and specificity of 99.69 % with the σ (value of smoothing parameter in the PNN classifier) of 0.264 that was determined using genetic algorithm. These performance measures are adequate enough for clinical deployment. However, we intend to validate the proposed technique on more large databases in future.

Biography U Rajendra Acharya, PhD, DEng, is a visiting faculty in biomedical engineering department at the Ngee Ann Polytechnic, Singapore. He is also adjunct professor at the University of Malaya, Malaysia, adjunct faculty at Singapore Institute of Technology - University of Glasgow, Singapore, and associate faculty at Singapore Institute of Management University, Singapore. He received his Ph.D. from National Institute of Technology Karnataka, Surathkal, India and DEng from Chiba University, Japan. He has published more than 285 papers, including 178 papers in refereed international SCI-IF (Science Citation Index- Impact Factor) journals, as well as international conference proceedings (48), textbook chapters (62), and books (16). The h-index of Dr. Acharya's work in SCOPUS is 25 without self-citations. He has worked on various funded projects with grants worth more than 2million SGD. He is an editorial board member of many journals, and has served as Guest Editor for numerous journals. His major interests are biomedical signal processing, bio-imaging, data mining, visualization and biophysics for improved healthcare design, delivery and therapy.

Vinitha Sree S, PhD, received her doctoral degree in Biomedical Engineering from Nanyang Technological University (NTU) in 2010. Her PhD research was on breast cancer detection using skin surface electropotentials. She received her Masters degree in Biomedical Engineering from NTU in 2006 and her Bachelors degree in Electronics and Communication Engineering from P.S.G. College of Technology, India in 2004. She was a software engineer at Infosys Technologies Limited, Chennai, India in 2005. In 2010, she worked from NTU as a research associate for First Warning Systems (FWS), and used data mining strategies to analyze FWS data. Her areas of interest include Medical Data Mining, Breast Imaging Systems, Clinical Decision Support Systems, Translational and Clinical Research, and Healthcare Systems and Management. She has published 79 articles in refereed international journals (52), international conference proceedings (14), and book chapters (13). She is the co-editor of the book *Diagnostic and Therapeutic Applications of Breast Imaging* published by SPIE, USA, 2012. She was awarded the MSc. certificate of excellence award for her commendable performance in her Masters degree. She is a reviewer for several international journals, and is the associate editor of the journal of medical imaging and health informatics (JMIHI).

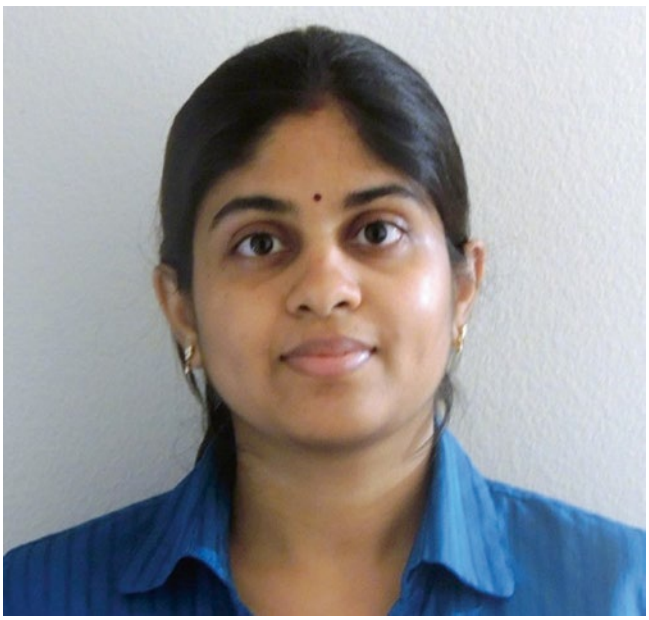

Luca Saba, MD received the MD degree from the University of Cagliari, Italy, in 2002. Today he works in the AOU of Cagliari. Dr. Saba's research fields are focused on neuroradiology, multi-detector row computed tomography, magnetic resonance, ultrasound, and diagnostic in vascular sciences.

His works, as lead author, achieved more than *75* high-impact factor, peer-reviewed, journals. Dr. Saba has written 7 book chapters and he presented more than 400 papers in National and International Congress. Dr. Saba is member of the Italian Society of Radiology (SIRM), European Society of Radiology (ESR), Radiological Society of North America (RSNA), American Roentgen Ray Society (ARRS). and European Society of Neuroradiology (ESNR).

Filippo Molinari, PhD is assistant professor in biomedical engineering at the Department of Electronics of the Politecnico di Torino (Torino, Italy). His main research interests include biomedical signal processing and medical imaging. He is expert in automated techniques for aiding the diagnostic process in ultrasound imaging. Vascular sonography, atherosclerosis, and tumor detection are Dr. Molinari's main research topics.

He published more than 80 peer-reviewed contributions and 3 collaborative books. Dr. Molinari is member of the IEEE EMBS of the European Society for Molecular Imaging (ESMI) and of the American Institute of Ultrasounds in Medicine (AIUM). He is regional associate editor for Europe of the Journal of Medical Imaging and Health Informatics and he is on the editorial board of other five international journals.

Jasjit S. Suri, PhD, MBA, Fellow AIMBE is an innovator, visionary, scientist, and an internationally known world leader and has spent over *25* years in the field of biomedical engineering/sciences and its management. During his career in biomedical industry/imaging, he has had an upstream growth and responsibilities from scientific engineer, scientist, manager, director R&D, Sr. director, vice president to chief technology officer (CTO) level positions in industries like *Siemens Medical Systems*, *Philips Medical Systems*, *Fisher Imaging Corporation*, *Eigen Inc*., *and Biomedical Technologies*, respectively and managed up to 100 people. Dr. Suri has written over *300* publications covering US/European patents, peer-reviewed journals, proceedings, and book chapters. His major contributions are in the area of diagnosis and therapeutic devices covering heart, brain, spine, thyroid, eye, vasculature, breast, and prostate. He has championed the field of image segmentation and registration for image-guided surgical applications. During his leadership, he has released over six different products along with the FDA approvals such as Voyager, SenoScan, and Artemis.

He received his masters from University of Illinois, Chicago, Doctorate from University of Washington, Seattle, and Executive Management from Weatherhead School of Management, Case Western Reserve University (CWRU), Cleveland. Dr. Suri has been board member of several international journals and conference committees. Dr. Suri was crowned with President's Gold medal in 1980 and the *Fellow of American Institute of Medical and Biological Engineering* (AIMBE) awarded by National Academy of Sciences, Washington, DC, in 2004. Dr. Suri has been the chairman of IEEE Denver section and has won over 50 awards during his career.

Stefano Guerriero is Associate Professor of Obstetrics and Gynecology at the Department of Obstetrics and Gynecology of University of Cagliari, Italy and published more than 130 peer reviewed papers. Prof Stefano Guerriero is Editor of Ultrasound in Obstetrics and Gynecology one of the leading journals in this field (Impact Factor: 3.557; 8/77 in Obstetrics & Gynecology) and member of Board of the Italian Society of Ultrasound in Obstetrics and Gynecology (SIEOG) and is involved in the International Ovarian Tumor Analysis (IOTA) studies from several years. He is AD HOC REFEREE FOR Human Reproduction, Human Reproduction Update, Gynecologic Oncology, Ultrasound in Obstetrics & Gynaecology, European Journal of Obstetrics, Gynaecology and Reproductive Biology and several other journals

Muthu Rama Krishnan Mookiah, PhD is a Research Engineer in Ngee Ann Polytechnic, Singapore. He received his B.E from Sethu Institute of Technology in 2002 and M.Tech in Biomedical Signal Processing and Instrumentation from SASTRA University in 2005 and PhD from Indian Institute of Technology Kharagpur in 2012. He has published more than 25 papers in international journals and conferences. His major research interests are in Medical Image Analysis, and Pattern Classification.

Ratna Yanti has completed her diploma in Biomedical Engineering from Ngee Ann Polytechnic, Singapore. Currently pursuing undergraduate degree in National University Singapore, Singapore.

Roshan Joy Martis completed his Bachelors of Engineering and Masters of Technology both from Manipal Institute of Technology, Manipal, India in 2004 and 2008 respectively. He received a PhD from Indian Institute of Technology, Kharagpur, India in 2012. Currently he is working as research and development engineer at Ngee Ann Polytechnic, Singapore. His research interests include physiological signal monitoring, biomedical signal processing and pattern analysis. He also serves as a reviewer in several peer-reviewed journals.

References

1. Jemal A, Siegel R, Ward E. Cancer statistics, 2010. CA Cancer J Clin. 2010;60:277–300.
2. NIH Consensus Development Panel on Ovarian Cancer. NIH consensus conference. Ovarian cancer. Screening, treatment, and follow-up. JAMA. 1995;273:491–7.
3. Horner MJ, Ries LAG, Krapcho M, Neyman N, Aminou R, Howlader N, Altekruse SF, Feuer EJ, Huang L, Mariotto A, Miller BA, Lewis DR, Eisner MP, Stinchcomb DG, Edwards BK, editors. SEER cancer statistics review, 1975–2006, National Cancer Institute, Bethesda. SEER Website. seer.cancer.gov/csr/1975_2006. Based on November 2008 SEER data submission. Published 29 May 2009.
4. Predanic M, Vlahos N, Pennisi JA, Moukhtar M, Alee FA. Color and pulsed Doppler sonography, gray-scale imaging, and serum CA 125 in the assessment of adnexal disease. Obstet Gynecol. 1996;88:283–8.
5. Wu CC, Lee CN, Chen TM, Lai JI, Hsieh CY, Hwieh FJ. Factors contributing to the accuracy in diagnosing ovarian malignancy by color Doppler ultrasound. Obstet Gynecol. 1994;84:605–8.
6. Iyer VR, Lee SI. MRI, CT, and PET/CT for ovarian cancer detection and adnexal lesion characterization. AJR Am J Roentgenol. 2010;194:311–21.
7. Sohaib SA, Reznek RH. MR imaging in ovarian cancer. Cancer Imaging. 2007;7 Spec No A:S119–29.
8. Frangioni JV. New technologies for human cancer imaging. J Clin Oncol. 2008;26:4012–21.
9. Anderiesz C, Quinn MA. Screening for ovarian cancer. Med J Aust. 2003;178:655–6.
10. Jeong YY, Outwater EK, Kang HK. Imaging evaluation of ovarian masses. Radiographics. 2000;20:1445–70.
11. Pascual MA, Graupera B, Hereter L, Rotili A, Rodriguez I, Alcázar JL. Intra-and interobserver variability of 2D and 3D transvaginal sonography in the diagnosis of benign versus malignant adnexal masses. J Clin Ultrasound. 2011;39:316–21.
12. Guerriero S, Alcazar JL, Pascual MA, Ajossa S, Gerada M, Bargellini R, Virgilio B, Melis GB. Intraobserver and interobserver agreement of greyscale typical ultrasonographic patterns for the diagnosis of ovarian cancer. Ultrasound Med Biol. 2008;34:1711–6.
13. Kim KA, Park CM, Lee JH, Kim HK, Cho SM, Kim B, Seol HY. Benign ovarian tumors with solid and cystic components that mimic malignancy. AJR Am J Roentgenol. 2004;182:1259–65.
14. Acharya UR, Vinitha Sree S, Krishnan MM, Molinari F, Garberoglio R, Suri JS. Non-invasive automated 3D thyroid lesion classification in ultrasound: a class of ThyroScan™ systems. Ultrasonics. 2012;52:508–20.
15. Saba L, Gao H, Acharya UR, Sannia S, Ledda G, Suri JS. Analysis of carotid artery plaque and wall boundaries on CT images by using a semi-automatic method based on level set model. Neuroradiology. 2012;54(11):1207–14. PubMed PMID: 22562690.
16. Renz C, Rajapakse JC, Razvi K, Liang SKC. Ovarian cancer classification with missing data. In: Proceedings of 9th international conference on Neural Information Processing, Singapore, 2002, vol. 2, p. 809–13.
17. Assareh A, Moradi MH. Extracting efficient fuzzy if-then rules from mass spectra of blood samples to early diagnosis of ovarian cancer. In: IEEE symposium on Computational Intelligence and Bioinformatics and Computational Biology, Honolulu, 2007, p. 502–6.
18. Tan TZ, Quek C, Ng GS, Razvi K. Ovarian cancer diagnosis with complementary learning fuzzy neural network. Artif Intell Med. 2008;43:207–22.
19. Meng H, Hong W, Song J, Wang L. Feature extraction and analysis of ovarian cancer proteomic mass spectra. In: 2nd international conference on Bioinformatics and Biomedical Engineering, Shanghai, 2008, p. 668–71.
20. Tang KL, Li TH, Xiong WW, Chen K. Ovarian cancer classification based on dimensionality reduction for SELDI-TOF data. BMC Bioinformatics. 2010;11:109.
21. Petricoin F. Use of proteomic patterns serum to identify ovarian cancer. The Lancet. 2002;359:572–7.
22. Tailor A, Jurkovic D, Bourne TH, Collins WP, Campbell S. Sonographic prediction of malignancy in adnexal masses using an artificial neural network. Br J Obstet Gynaecol. 1999;106:21–30.
23. Brüning J, Becker R, Entezami M, Loy V, Vonk R, Weitzel H, Tolxdorff T. Knowledge-based system ADNEXPERT to assist the sonographic diagnosis of adnexal tumors. Methods Inf Med. 1997;36:201–6.
24. Biagiotti R, Desii C, Vanzi E, Gacci G. Predicting ovarian malignancy: application of artificial neural networks to transvaginal and color Doppler flow US. Radiology. 1999;210:399–403.
25. Zimmer Y, Tepper R, Akselrod S. An automatic approach for morphological analysis and malignancy evaluation of ovarian masses using B-scans. Ultrasound Med Biol. 2003;29:1561–70.
26. Lucidarme O, Akakpo JP, Granberg S, Sideri M, Levavi H, Schneider A, Autier P, Nir D, Bleiberg H, Ovarian HistoScanning Clinical Study Group. A new computer-aided diagnostic tool for non-invasive characterisation of malignant ovarian masses: results of a multicentre validation study. Eur Radiol. 2010;20:1822–30.

27. Bellman RE. Dynamic programming. Mineola: Courier Dover Publications; 2003.
28. Hata T, Yanagihara T, Hayashi K, Yamashiro C, Ohnishi Y, Akiyama M, Manabe A, Miyazaki K. Three-dimensional ultrasonographic evaluation of ovarian tumours: a preliminary study. Hum Reprod. 1999;14:858–61.
29. Laban M, Metawee H, Elyan A, Kamal M, Kamel M, Mansour G. Three-dimensional ultrasound and three-dimensional power Doppler in the assessment of ovarian tumors. Int J Gynaecol Obstet. 2007;99:201–5.
30. Cohen LS, Escobar PF, Scharm C, Glimco B, Fishman DA. Three-dimensional power Doppler ultrasound improves the diagnostic accuracy for ovarian cancer prediction. Gynecol Oncol. 2001;82:40–8.
31. Hu M. Visual pattern recognition by moment invariants. IRE Trans Info Theory. 1962;8:179–87.
32. Shen L, Bai L. A review of Gabor wavelets for face recognition. Patt Anal Appl. 2006;9:273–92.
33. Manjunath BS, Ma WY. Texture features for browsing and retrieval of image data. IEEE Trans Pattern Anal Mach Intell. 1996;18: 837–42.
34. Pharwaha APS, Singh B. Shannon and non-shannon measures of entropy for statistical texture feature extraction in digitized mammograms. Proceedings of the World Congress on Engineering and Computer Science (WCECS). San Francisco, USA. 2009, Vol 2. p. 2179.
35. Box JF. Guinness, gosset, fisher, and small samples. Statist Sci. 1987;2:45–52.
36. Specht DF. Probabilistic neural networks. Neural Networks. 1990;3:109–18.
37. Raghu PP, Yegnanarayana B. Supervised texture classification using a probabilistic neural network and constraint satisfaction model. IEEE Trans Neural Netw. 1998;9:516–22.
38. Ng EYK, Acharya UR, Keith LG, Lockwood S. Detection and differentiation of breast cancer using neural classifiers with first warning thermal sensors. Inform Sciences. 2007;177:4526–38.
39. Goldberg DE. Genetic algorithms in search, optimization, and machine learning. Reading: Addison Wesley Professional Publishers, Boston, MA, USA. 1989.
40. Deb K. Multi-objective optimization using evolutionary algorithms. Chichester/New York: Wiley; 2009.
41. Bast Jr RC, Badgwell D, Lu Z, Marquez R, Rosen D, Liu J, Baggerly KA, Atkinson EN, Skates S, Zhang Z, Lokshin A, Menon U, Jacobs I, Lu K. New tumor markers: CA125 and beyond. Int J Gynecol Cancer. 2005;15:274–81.
42. Zaidi SI. Fifty years of progress in gynecologic ultrasound. Int J Gynaecol Obstet. 2007;99:195–7.
43. Menon U, Talaat A, Rosenthal AN, Macdonald ND, Jeyerajah AR, Skates SJ, Sibley K, Oram DH, Jacobs IJ. Performance of ultrasound as a second line test to serum CA125 in ovarian cancer screening. BJOG. 2000;107:165–9.
44. Acharya UR, Sree SV, Krishnan MRM, Saba L, Molinari F, Guerriero S, Suri JS. Ovarian tumor characterization using 3D ultrasound. Technol Cancer Res Treat. 2012;11(6):543–52.

FDG-PET/CT Imaging of Ovarian Cancer

Lin Ho

Abstract

Ovarian cancer is the second most common gynecologic malignancy (after cervical cancer), with a lifetime risk of 1.7 %. Although its incidence has decreased slightly over the past 30 years, it is currently the most common cause of death among women with gynecologic malignancies.

Imaging, especially ultrasound and CT, has become a critical part of the evaluation of patients with ovarian cancer. As for many other malignancies, the role of FDG-PET and PET/CT is being extensively studied for the evaluation of ovarian malignancy, and the goals of oncologic imaging with PET/CT are to help differentiate benign from malignant disease, to determine the extent of malignant disease, to detect residual and recurrent disease, and to monitor and guide therapy. In this chapter the PET/CT application in oncologic imaging will be reviewed.

Keywords

Positron emission tomography • PET/CT • Standardized uptake values (SUV) • FDG • Uptake of FDG • Staging

Ovarian cancer is the second most common gynecologic malignancy (after cervical cancer), with a lifetime risk of 1.7 %. Although its incidence has decreased slightly over the past 30 years, it is currently the most common cause of death among women with gynecologic malignancies [1]. There were estimated 225,500 new cases of ovarian cancer and 140,200 deaths from ovarian cancer expected in 2011 worldwide [1]. Imaging, especially ultrasound and CT, has become a critical part of the evaluation of patients with ovarian cancer. As for many other malignancies, the role of FDG-PET and PET/CT is being extensively studied for the evaluation of ovarian malignancy. According to the American College of Radiology guidelines, the goals of oncologic imaging with PET/CT are to help differentiate benign from malignant disease, to determine the extent of malignant disease, to detect residual and recurrent disease, and to monitor and guide therapy [2].

Positron Emission Tomography/Computed Tomography (PET/CT)

Positron emission tomography (PET) is a functional imaging technique, which provides unique information about the molecular and metabolic changes associated with disease. A range of radiolabeled tracers are currently available for visualization, characterization, and quantification of biological processes in vivo. These include the noninvasive assessment of glucose metabolism, cell proliferation, perfusion, hypoxia, and cell receptor expression. The amounts of PET

L. Ho, MD
PET Imaging Science Center,
Keck School of Medicine,
Los Angeles, CA, USA
e-mail: linhho@usc.edu

L. Saba et al. (eds.), *Ovarian Neoplasm Imaging*,
DOI 10.1007/978-1-4614-8633-6_28,

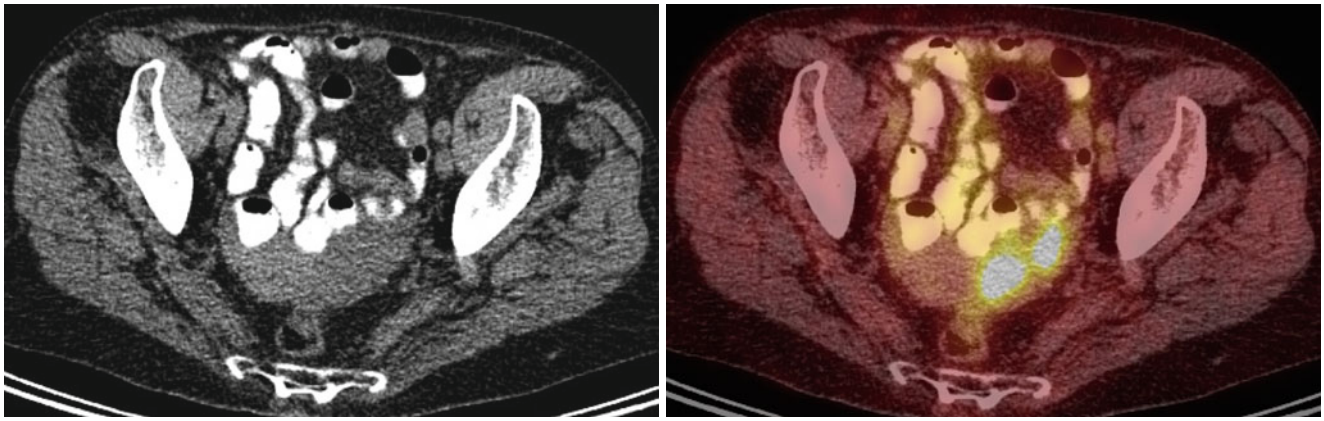

Fig. 1 A 83-year-old woman with newly diagnosed left ovarian cancer (SUV max 8.7)

radiotracers administered are extremely small, generally in the pico- and nanomolar range and have essentially no pharmacologic effect. Glucose metabolism is often increased following malignant transformation resulting in increased cellular accumulation of the glucose analog F-18 fluorodeoxyglucose (FDG). Transport of FDG through the cell membrane via glucose transport proteins (GLUT) and subsequent intracellular phosphorylation by hexokinase (HK) are key steps for cellular accumulation [3]. As FDG-6-phosphate is a poor substrate for glucose-6-phosphate isomerase, and levels of glucose-6-phosphatase are generally low in tumors, FDG-6-phosphate accumulates within cells in proportion to the level of glucose consumption.

Imaging the metabolic activity of tumors provides both more sensitive and specific information about the extent of disease compared with anatomic imaging alone [4]. Combined positron emission tomography and computed tomography (PET/CT) acquire concurrent and co-registered PET and CT images, merging the functional information from PET with the anatomical information from CT [5]. The use of FDG-PET/CT has been shown to improve the diagnostic accuracy compared to either imaging procedure alone by localizing areas of increased FDG uptake with improved anatomic specificity and by providing better characterization of suspicious morphologic abnormalities [6].

Malignant lesions typically present as visually detectable areas of focally increased FDG uptake, whereas most benign tumors do not have increased tracer uptake. False-positive findings (increased FDG uptake in noncancerous tissue) are most commonly due to infection, inflammation, or post radiotherapy changes. It is therefore recommended to wait at least 8 weeks after external beam radiation to evaluate the irradiated area for residual disease [7]. It is important to note that false-positive findings can also occur in benign conditions such as Paget's disease, Grave's disease, adrenal and villous adenomas, healing fractures, and other benign tumors.

Standardized uptake values (SUV) provide a semiquantitative measure of tissue FDG accumulation. SUVs are calculated by normalizing the tissue radioactivity concentration measured with PET to the injected administered activity and patient's body weight [8]. Previous studies have demonstrated that measurements of SUVs provide highly reproducible parameters of tumor glucose utilization [9, 10]. Although SUVs have been shown to be important for monitoring treatment effects, visual image analysis is generally sufficient for staging and restaging of cancer patients (Fig. 1).

Technique for PET/CT

Proper patient preparation and scanning protocol are needed for optimal diagnostic accuracy. Considerations that are unique to FDG-PET/CT systems include bowel preparation techniques, reduction of FDG activity in the urinary bladder, and reconstruction techniques to minimize metallic artifacts.

Bowel definition can be enhanced by using low-density barium for oral contrast material at CT, which does not cause significant artifacts at FDG-PET [11]. Oral hydration is recommended as long as the fluids do not contain glucose.

It is also important to reduce FDG accumulation within the urinary bladder. The patient is asked to void completely immediately prior to the start of scanning and by imaging the pelvis early in the study.

Metallic prostheses can cause foci of apparent increased FDG uptake due to attenuation correction [12]. This artifact can be reduced by minimizing patient motion. When CT is used for attenuation correction, an attenuation-weighted iterative reconstruction technique can also be used to minimize this artifact, although more studies are needed to optimize reconstruction factors such as segmentation, number of iterative steps, and preprocessing of attenuation date [12]. At our institution, an ordered subset expectation maximum iterative

Table 1 Technique used at the author's institution for FDG-PET/CT

Patient preparation
Make sure the patient has ingested no food or drink for at least 4 h prior to scanning
Check blood glucose level prior to radiotracer injection
One hour prior to scanning, inject a weight-based dose of FDG (0.22 mCi/kg [8.1 MBq/kg]) and administer 450 mL of low-density barium orally for the patient to drink as a glucose-free solution
Place the patient in a quiet, dimly lit room with instructions not to talk or move
Immediately prior to scanning, have the patient void completely
Place the patient head first into the gantry with both arms above the head
CT scanning
Scanner: 64-section multidetector[a]
Scan coverage: skull base to midthigh
Detector row configuration: 2×2 mm
kVp = 120
Weight-adjusted milliampere-second mean = 200 mAs
Gantry rotation speed: 0.5 s per revolution
Pitch: 1.75
Image reconstruction: 512×512 matrix, 70-cm field of view (FOV)
PET scanning
Scanner: 64-section multidetector[a]
Scan coverage: skull base to midthigh in a caudal-to-cranial direction
Coverage per table position: 17.0 cm
Number of table positions: 5–7
Acquisition time: 3 min per table position
Section thickness: 2 mm
Image reconstruction: 168×168 matrix, ordered subset expectation maximum iterative reconstruction algorithm (three iterations, 21 subsets), 5-mm Gaussian filter, 70-cm FOV

[a]Siemens Biograph Duo PET/CT system

reconstruction algorithm with three iterations and 21 subsets is used. Examination of non-attenuation-corrected images is also very helpful in avoiding this pitfall.

Imaging technique at our institution for FDG-PET/CT is described in the following paragraphs and summarized in Table 1.

Patient Preparation

The patient is asked to take nothing by mouth for at least 4 h prior to examination. Upon the patient's arrival at the radiology department, his or her weight and height are obtained and a weight-based (0.22 mCi/kg [8.1 MBq/kg]) dose of FDG is prepared. A 22- or 24-gauge intravenous line is placed, usually in the upper extremity contralateral to any prior surgery (e.g., lymph node resection) to ensure proper distribution of radiotracer. The patient's blood glucose is determined to ensure that he or she is not hyperglycemic. At our institution, a serum glucose level of 200 mg/dL is used as a maximum cutoff point. One hour prior to imaging, the FDG dose is injected and 450 mL of low-density barium (Read-Cat 2.1 % weight/volume barium sulfate suspension; E-Z EM, Lake Success, NY) is administered orally for the patient to drink as a glucose-free solution. The patient is then placed in a quiet, dimly lit room for the remainder of the uptake phase. To minimize skeletal muscle uptake during this period, the patient is instructed not to talk and to keep the arms at the sides and the legs uncrossed. Just prior to the start of scanning, the patient is asked to void completely to minimize bladder activity.

Scanning Protocol

For scanning, the patient is positioned supine and head first on a PET/CT system with a single gantry and table. The arms are raised above the head (if the patient can tolerate this position), and he or she is allowed to breathe quietly. CT is performed first. At our institution, a 64-section multidetector Siemens Biography PET/CT system is used with the following parameters: detector row configuration of 2×2 mm, 120 kVp, weight-adjusted milliampere-second mean 200 mAs, gantry rotation speed of 0.5 s per revolution, and pitch of 1.75. A tomogram is used to adjust the FOV so that it extends from the skull base to the midthigh. The images are reconstructed on a 512×512 matrix with a 70-cm FOV.

After CT is completed, the table is moved into the PET scanner. The images are acquired in a caudal-to-cranial direction from the midthigh to the skull base to minimize

bladder filling. Three-minute emission acquisitions per FOV are obtained in three-dimensional mode. Transverse PET scans are obtained per FOV, with a section thickness of 2 mm. Five to seven table positions are usually needed, with each position allowing coverage of 17.0 cm. The PET scans are reconstructed on 168×168 matrix, with an ordered subset expectation maximum iterative reconstruction algorithm (three iterations, 21 subsets), a 5-mm Gaussian filter, and a 70-cm FOV.

The CT transmission map is used for attenuation correction. Attenuation correction accounts for differences in activity due to location within the body (i.e., photons from deep sites are attenuated to a greater degree than photons from superficial sites). Attenuation-corrected and uncorrected PET scans, along with the CT and PET/CT scans, are reviewed on a workstation.

Normal FDG Activity

FDG, an analog of glucose, is distributed via the bloodstream after being glycolytically active tissues. Imaging is typically started at least 60 min after injection to allow sufficient blood pool clearance, thereby improving the target-to-background ratio. Normal physiologic uptake is seen in the brain and myocardium and, to a lesser extent, in the liver, spleen, bone marrow, gastrointestinal tract, testes, and skeletal muscles. Myocardial uptake is variable in fasting patients but often intense in nonfasting individuals. Skeletal muscle uptake is dependent on recent use of the muscle group. Activity within the blood pool, particularly in the mediastinum, can also be seen [13]. Other less frequent sites of uptake include the endometrium, breast, major and minor salivary glands, and brown fat in the supraclavicular and paraspinal regions [13–16]. Because FDG is excreted by the kidneys, intense activity is normally seen in the renal collecting system, ureters, and bladder [13] (Fig. 2).

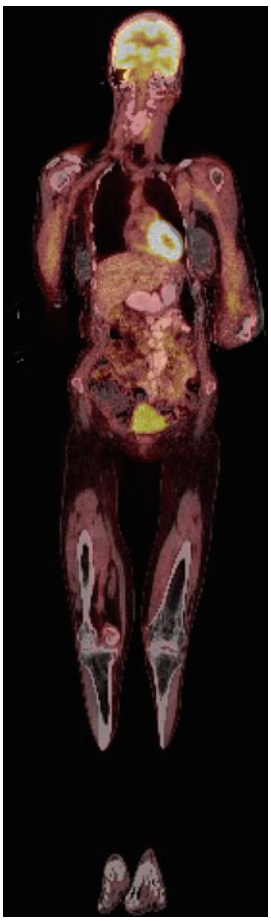

Fig. 2 Normal FDG physiologic activity

Increased FDG uptake can also be seen in many benign processes. Increased uptake has been reported in healing fractures, granulomatous diseases, inflammatory/infectious processes, and foci of wound healing and repair such as ostomy sites [13] (Figs. 3, 4, and 5).

Imaging Features

Physiologic Versus Pathologic Uptake

Ovarian cancer generally appears as a focal FDG-positive area but many other benign lesions or physiologic conditions may have a similar appearance: benign cystadenomas, teratomas, schwannomas, endometriosis, inflammatory processes, normal ovaries in menstruating women (follicular cysts and corpus luteal cysts between days 10 and 25 of the menstrual cycle), as well as normal physiologic activity in bowel, bladder diverticula, pelvic kidney, and focal retained activity in ureters [17]. In this setting, the anatomic correlation provided by the CT images help establish the correct diagnosis.

In premenopausal women, the amount of FDG uptake in the ovaries varies with the phase of menstrual cycle, with physiologic uptake particularly present in the early luteal phase (Fig. 6 – corpus luteal cyst). This can be avoided by performing the scan just subsequent to menstruation. Moreover, the typical appearance of physiologic uptake in the spherical or discoid with smooth margins and is located above the urinary balder or around the uterus, which can be used to distinguish it from pathologic changes. Characteristic CT appearance of normal benign ovarian tissue include the observance of a small rim enhancing cyst, the absence of any lymph nodes, and concordance with the appropriate stage of menstrual cycle are also helpful in recognizing the benign nature of the uptake [18]. In postmenopausal ovaries, however, any ovarian uptake is pathologic, whether benign or malignant (Figs. 7 and 8).

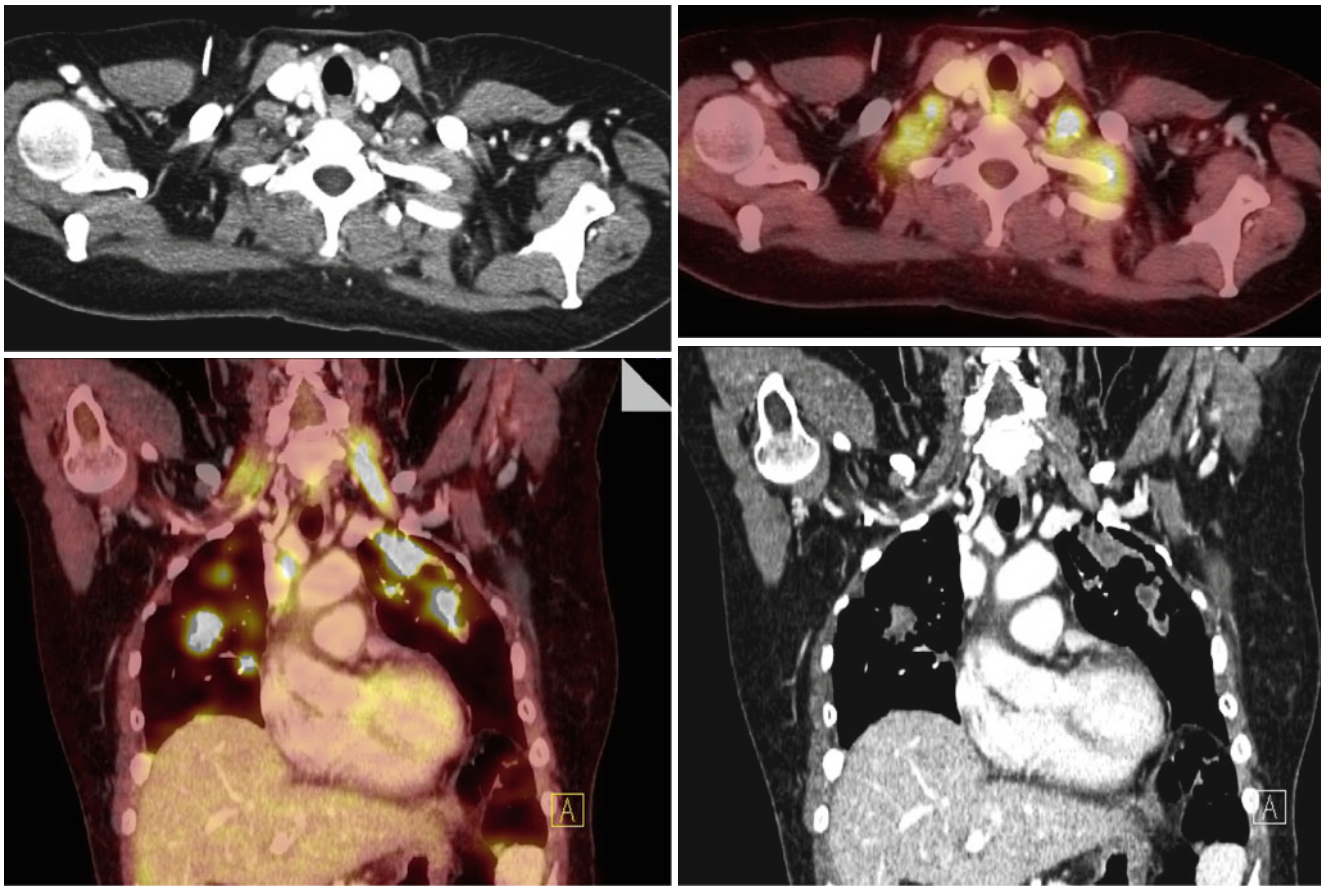

Fig. 3 A 47-year-old woman with history of ovarian cancer. Restaging PET/CT shows extensive hypermetabolic pulmonary metastases. Diffuse physiologic muscular activity is also noted in bilateral scalene muscles

Benign Versus Malignant Lesions

Studies evaluating the role of PEt alone for early diagnosis of ovarian cancer have reported a low sensitivity (58 %) and specificity (76 %) [19]. The advent of combined structural and metabolic data acquired contiguously with PET/CT helps to precisely localize suspicious areas of increased FDG uptake and assess incidental ovarian findings. Ovarian lesions will show variable increase in FDG uptake on PET/CT. Castellucci et al. demonstrated a sensitivity of 87 % and specificity of 100 % for differentiating benign from malignant ovarian cancer [20]. These results were achieved in part by characterizing a focal increased standardized uptake value (SUV) of 3 or higher in the ovary as positive for ovarian malignancy, whereas an SUV of 2.7 or lower was considered benign. Benign and malignant ovarian FDG uptake on PET were also differentiated using concurrently acquired CT, the pattern of FDG uptake and absence of lymphadenopathy in patients with benign lesions.

In another study, PET/CT was found to have a sensitivity of 80 % and specificity of 97 % for diagnosis of synchronous malignancy in the contralateral ovary in patients with primary ovarian cancer [21]. Although PET/CT has a high specificity for lesions greater than 5 mm in size, its sensitivity is much lower than that of sonography for the assessment of small lesions (<5 mm). Therefore, PET/CT has not replaced sonography for the screening of ovarian cancer. However, given its high specificity, FDG-PET/CT is used to assess for occult metastases before the patients undergo surgical treatment.

A study performed by Karantanis et al. showed that FDG-PET/CT is unable to distinguish tumor grade and histologic type among epithelial ovarian carcinoma. There is no statistically significant relationship between SUVmax value and tumor grading or between SUVmax value and histologic type (particularly for serous endometrioid subtypes). However, there is a significant correlation between FDG uptake, SUV mean, tumor grade, clinical stage, cell proliferation index, and GLUT-1 expression in epithelial ovarian cancer [22].

Some pathologic conditions may be missed due to the lack of FDG uptake as in borderline ovarian tumors and

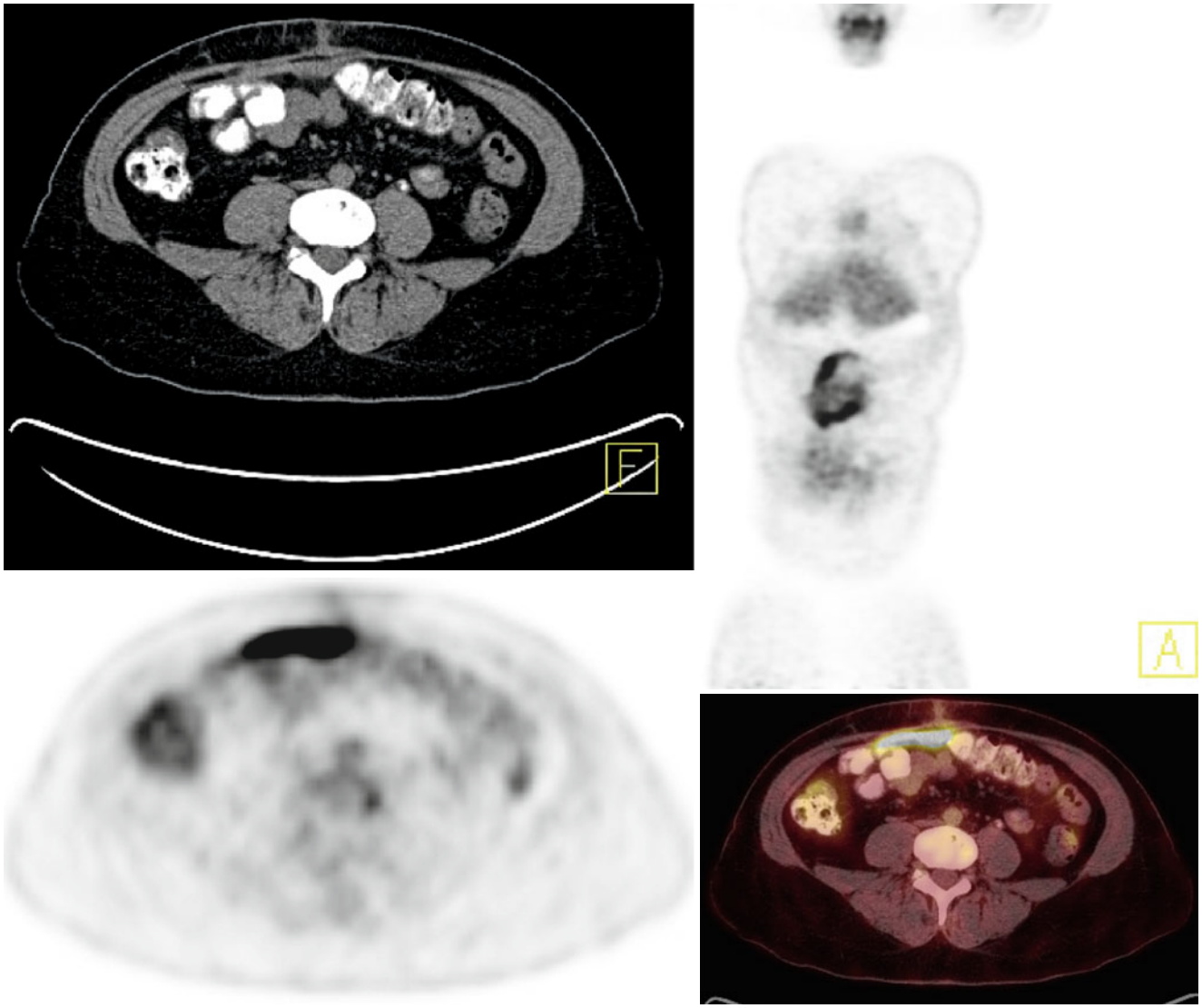

Fig. 4 A 54-year-old woman with history of ovarian cancer. Restaging PET/CT shows new moderately intense activity in the anterior abdomen (SUV max up to 5.7), corresponding to new ventral hernia mesh-related inflammation. This finding could mimic peritoneal metastasis

mucinous adenocarcinoma [23]. A definite diagnosis of a pelvic mass requires a surgical specimen. FDG-PET/CT is a useful noninvasive tool to characterize adnexal lesions in case of inconclusive transvaginal ultrasound in the presurgical phase [20, 23, 24]. In addition, FDG-PET/CT also has a great value in staging.

FDG-PET for Primary Diagnosis of Ovarian Cancer

Currently, the initial investigations of ovarian masses include physical examination, biochemical analysis of tumor markers such as CA-125, and transvaginal ultrasound (TVUS). TVUS is the preferred imaging modality for initial evaluation because of its availability, high resolution, and lack of ionizing radiation. Using ultrasound, a wide range of sensitivities (87–100 %) and specificities (57–90 %) have been reported for detection of ovarian malignancies [19, 20, 25–27]. A systemic review revealed a sensitivity of 87 % and a specificity of 90 % for ultrasound combined with color Doppler in the diagnosis of ovarian cancer [28]. Magnetic resonance imaging (MRI) is often used for further characterization of indeterminate adnexal masses, with a sensitivity and specificity of 100 and 94 %, respectively [29]. Although MRI can be helpful in cancer detection, the major contribution of MRI in adnexal mass evaluation is its ability to provide a confident diagnosis in many common benign adnexal abnormalities [30].

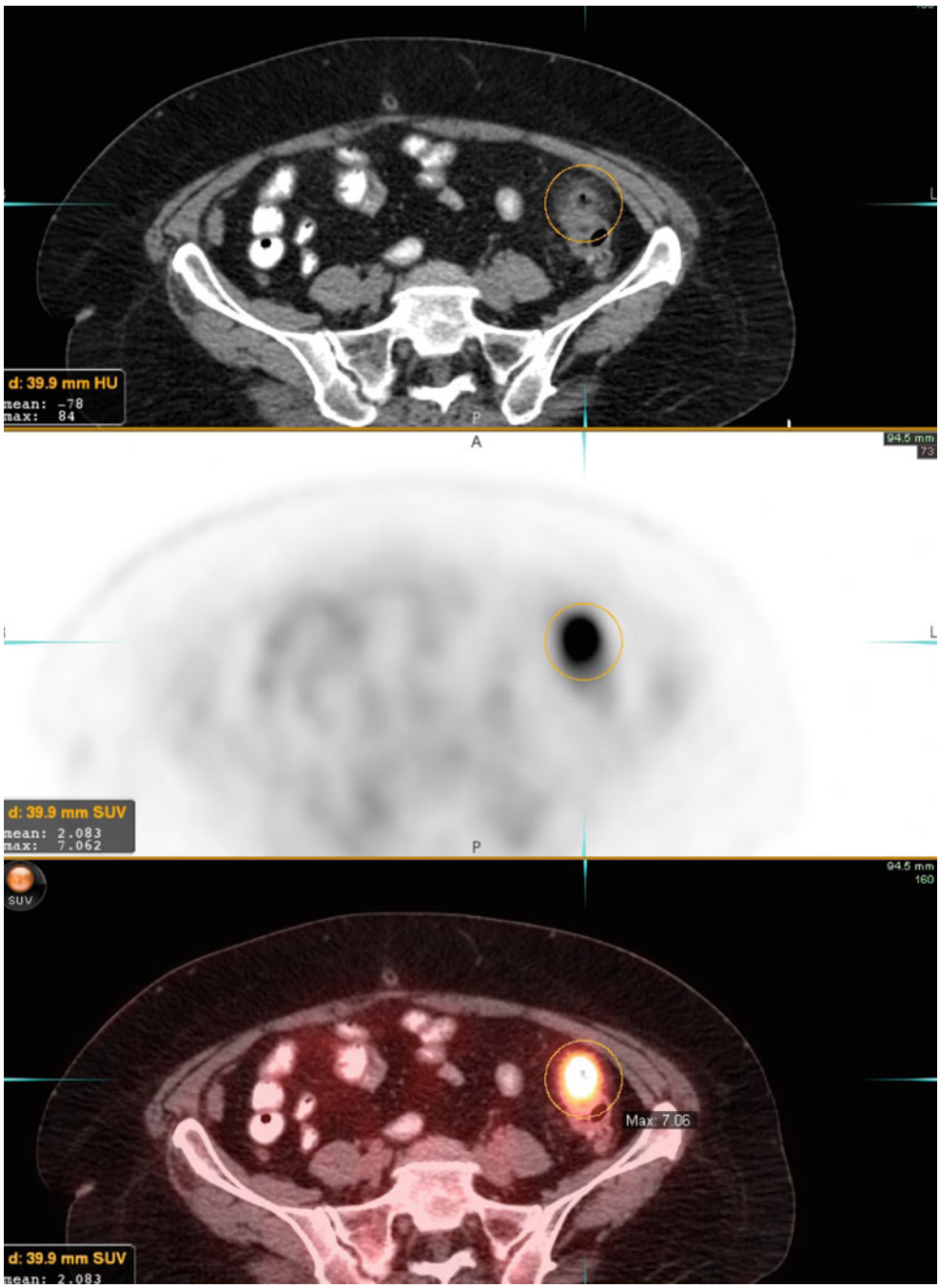

Fig. 5 A 58-year-old woman with history of ovarian cancer. Restaging PET/CT images demonstrate intensely active wall thickening of the distal descending colon (SUV max 7.1) with perifat stranding, consistent with diverticulitis

The role of FDG-PET in the detection of primary ovarian cancer has been evaluated for almost two decades. Ovarian cancer is typically characterized by increased glucose metabolism and therefore demonstrates increased FDG uptake, whereas benign tumors are usually negative on PET imaging. Early studies were predominantly undertaken with 1st-generation whole-body PET scanners, which had a lower sensitivity and spatial resolution compared to the latest PET/CT technology. Nevertheless, results are still comparable to more recent reports using PET/CT. In 2000 and 2002, two studies assessing women with asymptomatic adnexal masses found FDG-PET to have a sensitivity of 58 % and specificity of 76–80 % [19, 25]. Similarly, two further studies evaluated FDG-PET for characterization of a suspicious pelvic mass and found sensitivities and specificities to range from 58 to 78 % and 78 to 87 %, respectively [26, 31]. Despite the relatively low sensitivity of FDG-PET in the detection of primary ovarian cancer, all of the false negative results were either small invasive stage I tumors or lesions of low malignant potential.

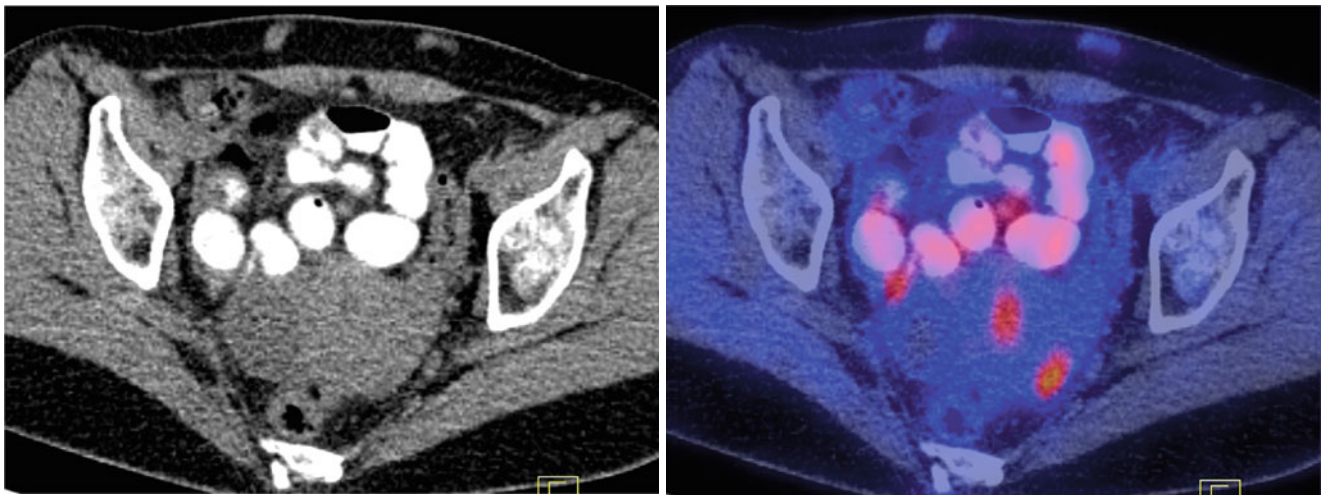

Fig. 6 A 42-year-old premenopausal woman with breast cancer. Axial images show presence of physiologic PET activity in the left ovary, corresponding to corpus luteal cyst on concurrent CT. A few small, mildly active subcutaneous densities in the abdominal wall represent sites of Lovenox injection

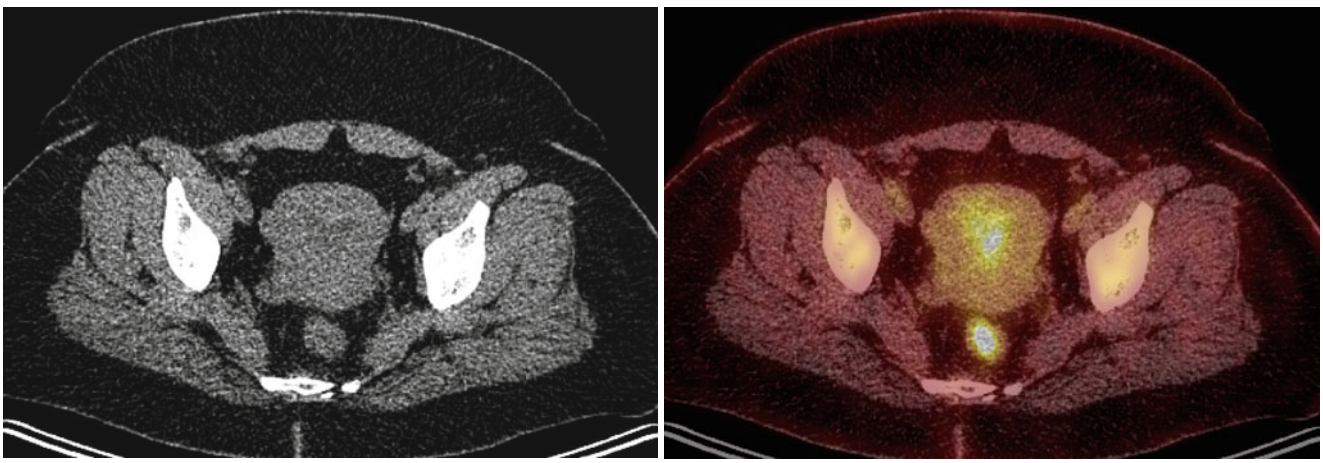

Fig. 7 A 37-year-old premenopausal woman with history of lymphoma. Endometrial activity consistent with menstrual-cycle-related changes

Data with fusion of anatomic and functional imaging using PET/CT resulted in more precise localization of suspicious areas of increased FDG uptake and enabled a better assessment of incidental ovarian findings. In 97 patients, FDG-PET/CT demonstrated areas of abnormally increased metabolic activity in 60 patients, whereas lesions were considered benign in 37 patients [32]. The sensitivity and specificity for FDG-PET/CT were 100 % (57/57) and 92.5 % (37/40), respectively. This was higher than all other imaging modalities including US, CT, MRI, and FDG-PEt alone. The group from Bologna found in 50 consecutive patients a sensitivity, specificity, and accuracy of 87, 100, and 92 %, respectively, compared with 90, 61, and 89 %, respectively, for TVUS. The authors concluded that FDG-PET/CT provides additional information to TVUS for differentiating benign from malignant pelvic lesions as well as to CT for the staging of ovarian cancer patients. These findings were further supported by a prospective study of 133 women with suspected ovarian cancer [24]. Histopathology showed benign tumors in 25 patients, borderline tumors in 13 patients, and malignant tumors in 95 patients. The accuracy of FDG-PET/CT (0.92) was higher compared to pelvic ultrasound (0.83) and contrast-enhanced CT or pelvic MRI (0.75; $p=0.013$).

FDG-PET and FDG-PET/CT, however, do have certain limitations, which also need to be considered. FDG-PET is often not able to detect small tumor deposits (less than 5 mm in size) [20]. Ovarian cancer shows variable levels of increased FDG uptake depending on the cellular composition. Abdominal or pelvic masses containing large cystic

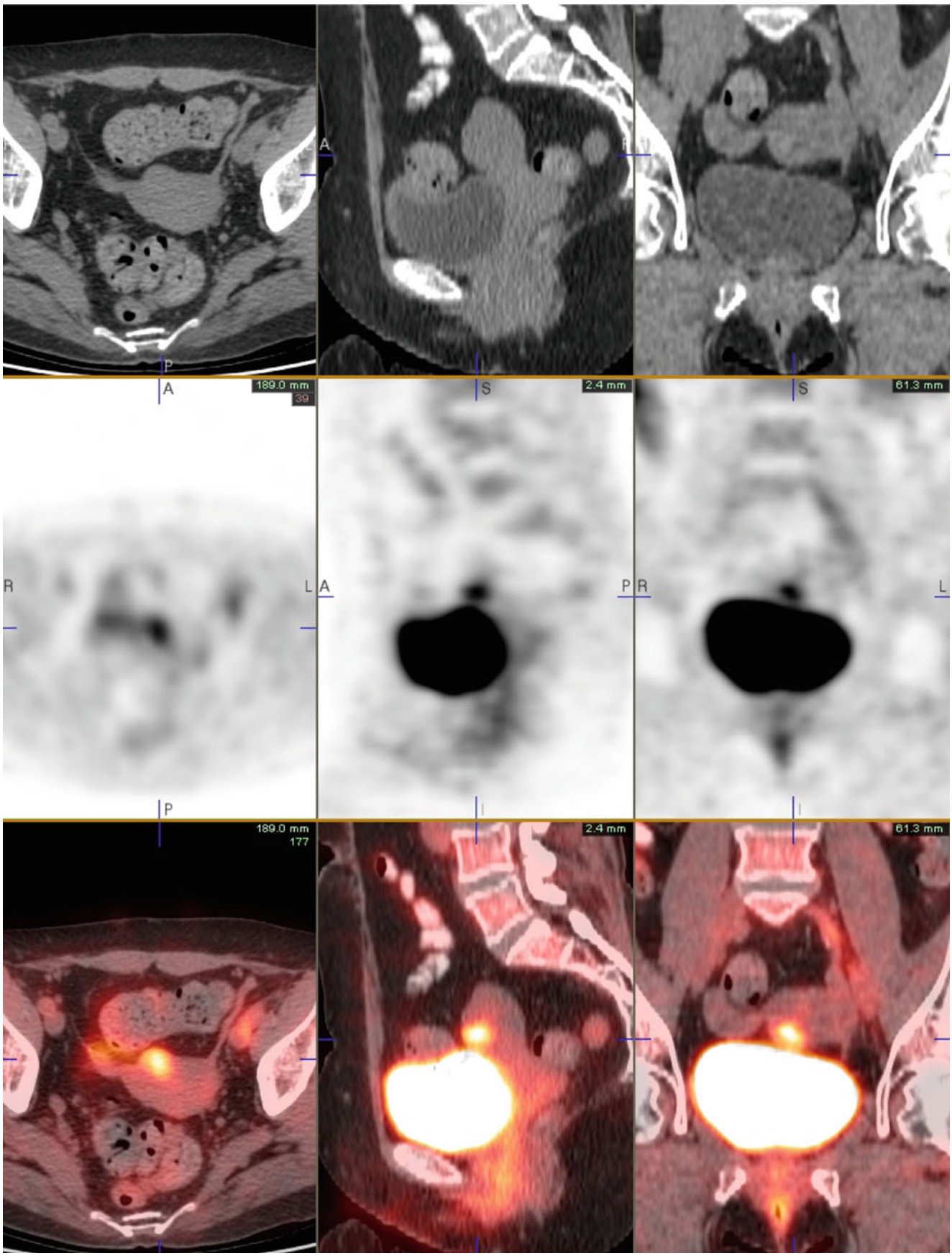

Fig. 8 A 41-year-old woman with history of lymphoma, currently in remission. Restaging PET/CT shows moderately active exophytic fibroid in the right anterior aspect of the uterus which appears less intense on the subsequent follow-up study. No evidence of malignancy is present

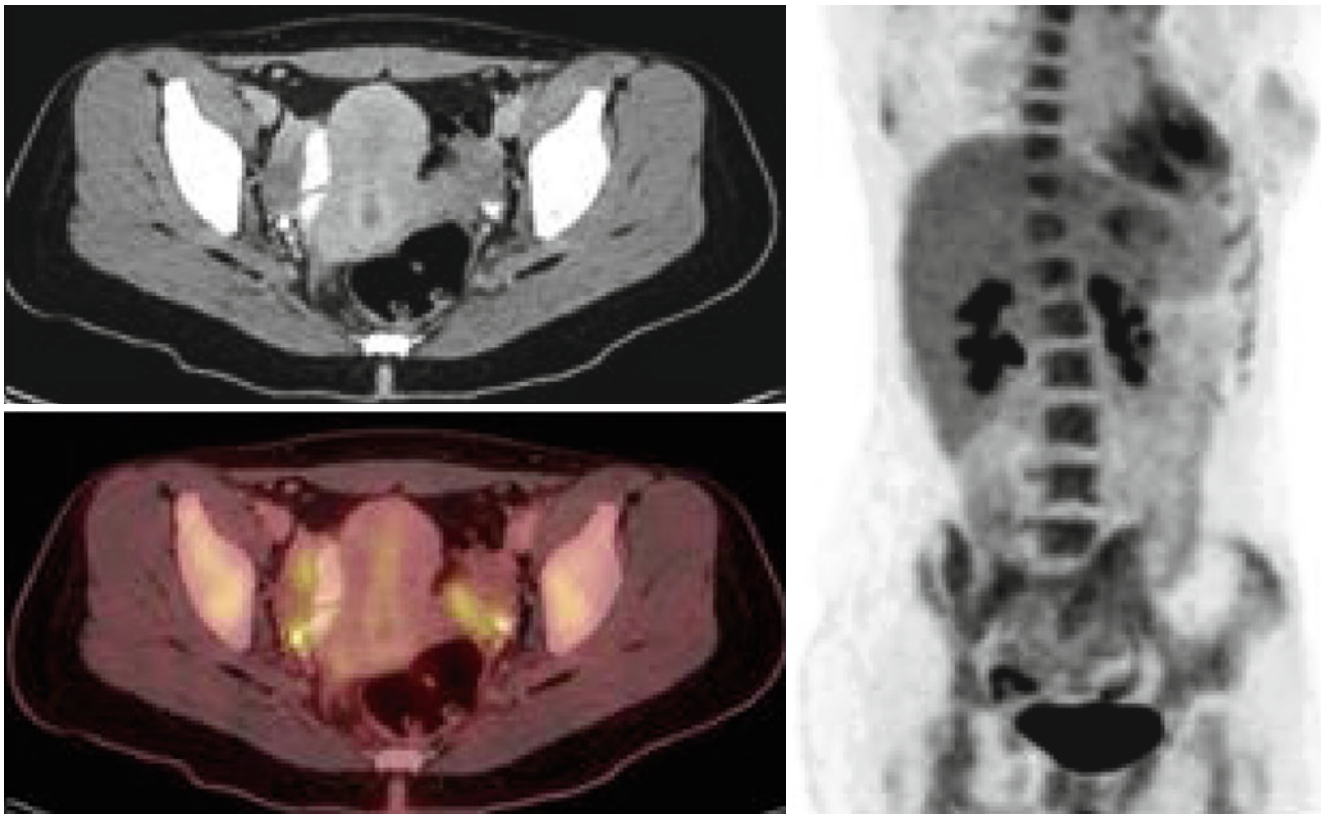

Fig. 9 Bilateral tubo-ovarian activity in a patient with history of breast cancer and chronic salpingitis

components as well as mucinous tumors will often not be metabolically active. False negative results are also seen in borderline ovarian tumor and cystadenocarcinoma of the ovary [19, 31, 33]. In particular, differentiating benign from borderline ovarian tumors is often difficult on FDG-PET. Even though borderline ovarian tumors demonstrate low-grade malignancy, they can be associated with aggressive biologic behavior in the form of peritoneal deposits and lymphadenopathy. However, borderline ovarian tumors are often non-FDG avid or demonstrate low-grade FDG uptake due to their mucinous and serous cellular composition [32].

Although generally false-positive findings in the abdomen and pelvis are rare, early studies showed that in patients with pelvic masses a number of benign conditions can cause increased FDG uptake. These include benign cystadenomas, dermoid tumors, teratomas, schwannomas, endometriosis, and inflammatory process [19, 31, 33] (Fig. 9 – bilateral salpingitis). Increased FDG uptake in normal ovaries is found in premenopausal women; this is related to the time point of ovulation. Two studies reported increased FDG uptake in the ovary and uterine endometrium in the late follicular and early luteal phases of the menstrual cycle [34, 35].

In order to reduce errors in interpretation, specific emphasis needs to be directed towards a good technique when undertaking pelvic PET/CT imaging. Ideally, the bladder should be empty to avoid artifacts on PET images from a high concentration of radioactivity in the bladder. It is suggested that the patient is scanned in a caudal-to-cranial direction, thus imaging the pelvis at the beginning of the study. The CT portion of PET/CT is often helpful to identify bladder diverticula and focal retained activity in ureters. Pelvic imaging can be improved by intravenous injection of furosemide (20–40 mg) to reduce tracer retention in the urinary system. The CT portion of PET/CT is also helpful in identifying normal physiologic activity in bowel, endometrium, and blood vessels. Bowel preparation can be performed with oral hydration as well and some groups recommend the use of oral contrast [36]. The administration of butylscopolamine (20–40 mg) at the time FDG injection has been reported to reduce FDG uptake in the bowel [37].

FDG-PET for Initial Staging of Ovarian Cancer

The most important prognostic factor for ovarian cancer patients is the tumor stage: the 5-year survival rate is 93, 70, 37, and 25 % for stage I, stage II, stage III, and stage IV, respectively [38]. Ovarian cancer is typically staged by exploratory laparotomy at the time of primary debulking in

accordance with the recommendations of the International Federation of Gynecology and Obstetrics (FIGO) [39]. Debulking surgery followed by adjuvant chemotherapy is considered the standard approach in newly diagnosed ovarian cancer. Studies have shown that when using platinum-based chemotherapy in patients with advanced ovarian disease, maximal cytoreduction, correlated to the minimal residual tumor mass after surgery, is one of the most powerful determinants of survival [40].

For preoperative staging of ovarian cancer, CT and MRI have been accepted as being the most useful imaging techniques. Studies evaluating performance of CT in preoperative staging of ovarian cancer have found sensitivities and specificities ranging from 72 to 82 % and 53 to 81 %, respectively [41, 42]. Recent studies have shown that, when used in conjunction with CT, FDG-PET is beneficial in evaluating distant metastases and equivocal lesions [20, 21, 42].

An initial study of 15 patients found that the addition of FDG-PET to CT improved the accuracy in preoperative staging of ovarian cancer from 53 to 87 % [42]. In a later study, 40 ovarian cancer patients underwent FDG-PET/CT with intravenous contrast-enhanced CT for staging prior to primary debulking surgery [21]. An increase in sensitivity, specificity, and accuracy was found for combined FDG-PET/CT compared to CT alone from 37.6 to 69.4 %, 97.1 to 97.5 %, and 89.7 to 94.0 %, respectively. FDG-PET/CT findings and the final pathological staging were in concordance in 75 % of cases.

More recent data has shown that using FDG-PET/CT can result in a stage migration in a significant number of patients. Out of 66 ovarian cancer patients, 64 were initially stage III and 2 were stage IV [43]. However, after PET/CT, 51 % (39/66) were restaged as stage III and 41 % (27/66) as stage IV (Fig. 10).

PET/CT Findings of Ovarian Cancer Metastases

Lymph Node Metastases

The presence of metastatic lymph nodes is another important prognostic factor for patients with ovarian cancer. Recognizing the precise location of metastatic nodes is therefore crucial for selecting appropriate treatment and predicting the possibility of optimal resection. A recent meta-analysis compared the diagnostic performances of CT, MRI, and PET or PET/CT for detection of metastatic lymph nodes in patients with ovarian cancer [44]. Eighteen eligible studies were included, with a total of 882 patients. FDG-PET or PET/CT was more accurate with a sensitivity of 73.2 % and a specificity of 96.7 % than CT (sensitivity, 42.6 %; specificity, 95.0 %) or MRI (sensitivity, 54.7 %; specificity, 88.3 %). When interpreting results from imaging studies the reference standard used is important. Generally, FDG-PET or PET/CT excels compared to other imaging modalities; however, when findings are compared to histopathology, the sensitivity tends to be lower. This is often related to the inability of FDG-PET to detect small and microscopic tumor deposits, which applies to all noninvasive imaging techniques.

Lymphatic dissemination to the pelvic and para-aortic lymph nodes is common, particularly in patients with advanced disease (Fig. 11 – retroperitoneal and mesenteric nodal metastases). Spread of disease through the lymphatic channels of the retroperitoneal lymph nodes and diaphragm may lead to dissemination into the supraclavicular or superior mediastinal lymph nodes and pleural space, or rarely, the internal mammary lymph nodes [45]. Furthermore, involvement of the rectosigmoid colon by ovarian carcinoma is associated with a high incidence of mesenteric nodal metastasis [46]. Lymph node metastasis is present in 10–20 % of patients with presumed early-stage ovarian cancer, and it is present in 40–70 % of patients with advanced-stage disease. Because PET/CT has a low negative predictive value in the pelvis and skip metastases may occur in as many as 60 % of patients, the lack of hypermetabolism in pelvic nodes does not preclude the presence of pathologic para-aortic nodes [47, 48].

FDG-PET/CT accurately depicts metastatic disease on the basis of significantly increased metabolic activity, even in normal-sized nodes (Fig. 11 – active normal-sized nodes). However, the evaluation for detection of small or necrotic lymph nodes or early nodal involvement with PET/CT is limited, with high false-negative rates [49].

In a study of 30 women with advanced-stage (IIC–IV) epithelial ovarian cancer, pretreatment FDG-PET/CT was performed and detected supradiaphragmatic lymph node metastases (LNM) in one or more locations in 67 % (20/30) of patients, whereas conventional CT found LNM only in 33 % (10/30) of patients. Fourteen patients had parasternal, 14 cardiophrenic, 8 other mediastinal, 6 axillary, and 1 subclavian LNM. The patients with supradiaphragmatic LNM had significantly more ascites ($p<0.01$), higher CA-125 levels, and more frequent peritoneal carcinomatosis ($p<0.03$) compared to patients without supradiaphragmatic LNM in preoperative FDG-PET/CT. These findings suggest that the route of epithelial ovarian cancer cells from the peritoneal cavity to the lymphatic system permeates the diaphragm mainly to the cardiophrenic and continues to the parasternal lymph nodes [50] (Fig. 12).

Peritoneal Metastases

In newly diagnosed ovarian cancer, laparoscopy is the standard diagnostic tool for the assessment of intraperitoneal

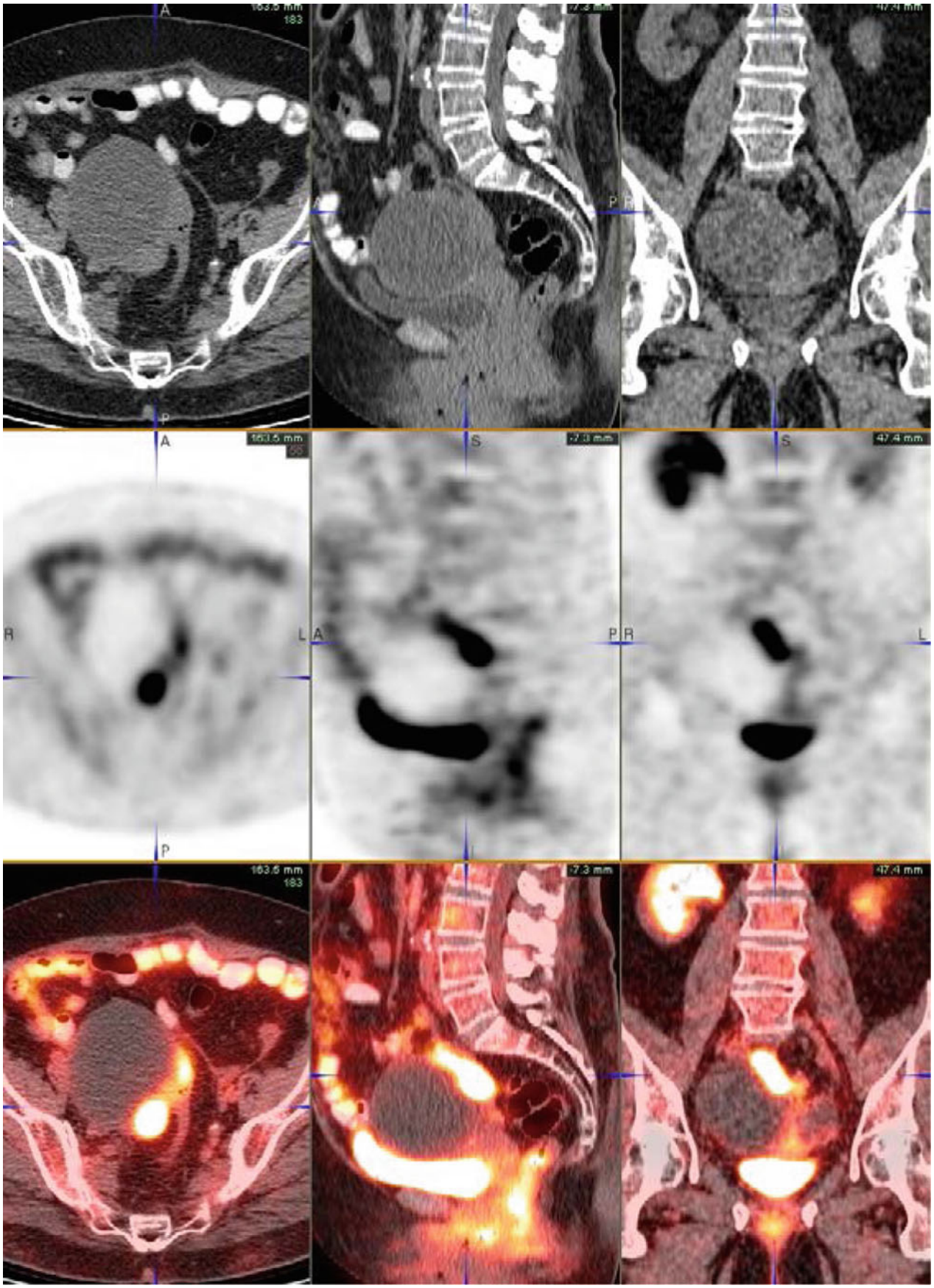

Fig. 10 A 85-year-old woman with newly diagnosed ovarian serous carcinoma. The right adnexal cystic lesion measures approximately 8.2 cm AP × 7.9 cm transverse × 7.8 cm craniocaudal, with intensely active soft tissue component in the superoposterior wall (maximum SUV of 5.9), consistent with primary tumor

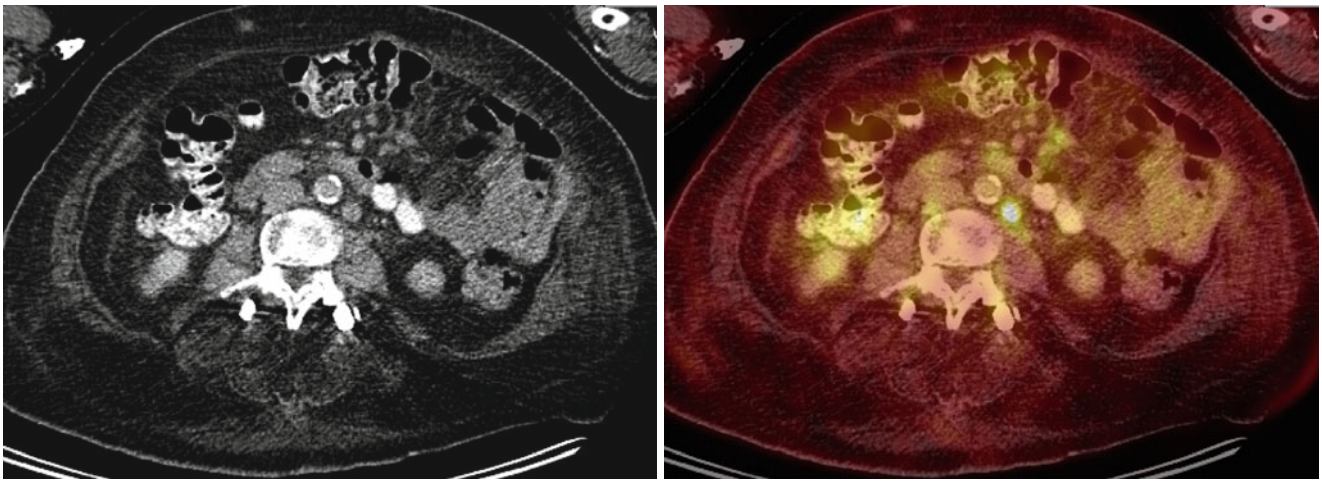

Fig. 11 A 75-year-old woman with history of ovarian cancer. Multiple normal-sized, hypermetabolic retroperitoneal and mesenteric lymph nodes are seen (SUVmax 6.8 in the left para-aortic region), consistent with metastatic disease

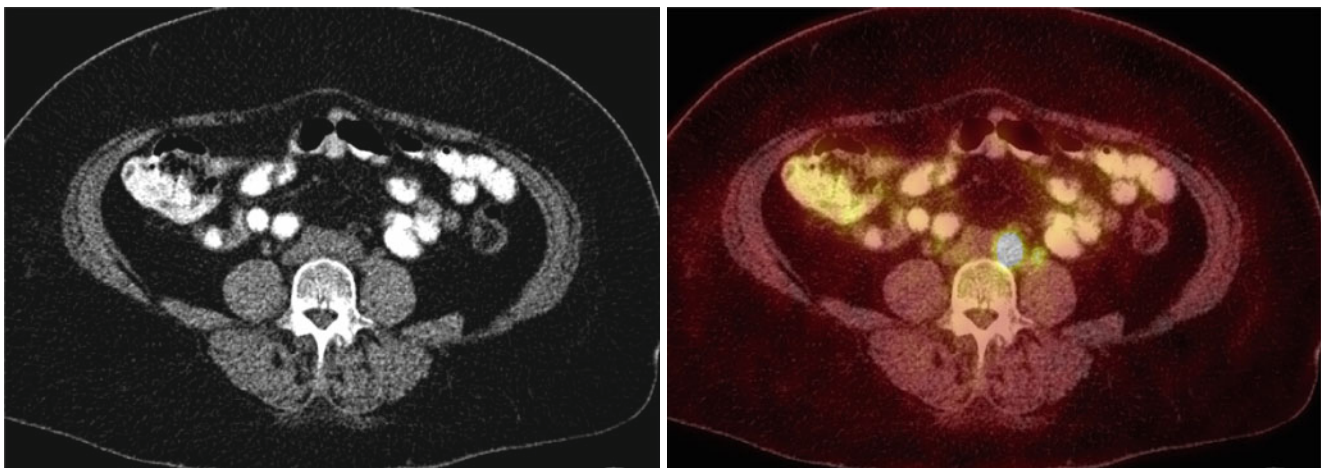

Fig. 12 A 43-year-old woman with history of ovarian cancer. A new intensely active, slightly enlarged left common iliac lymph node (SUV max of 16.7) is noted on the restaging PET/CT scan. Focal urinary stasis is seen in the left ureter

infiltration but it is invasive and requires general anesthesia. The right subphrenic region, the greater omentum, and the pouch of Douglas are the most common locations for peritoneal disease from ovarian carcinoma [51]. In 40 patients with a high suspicion of ovarian cancer, the findings in 9 quadrants of the abdominal-pelvic area (total 346 evaluable quadrants) for FDG-PET/CT and laparoscopy were compared [52]. Tumor deposits were found in 308 quadrants and 38 quadrants were free of disease. PET/CT demonstrated true negative results in 26/346 quadrants (7.5 %) and positive results in 243/346 quadrants (70.2 %). False-positive and negative PET/CT results were found in 12/346 and 65/346 quadrants, respectively. False-positive PET/CT findings were present evenly in all quadrants. False-negative PET/CT findings were noted in 31/109 (28.4 %) upper abdominal quadrants (epigastrium and diaphragmatic areas). A high rate of false-negative results was found in lesions <5 mm. The overall sensitivity and specificity for FDG-PET/CT was 78.9 and 68.4 %, respectively. The authors concluded that PET/CT may be a useful tool for pre-staging of ovarian cancer. From these results it appears that PET/CT is particularly useful in advanced-stage disease but might be best used in conjunction with laparoscopy if identification of small-volume disease is required.

At PET/CT, peritoneal implants appear as nodular soft tissue masses, often with a variable degree of increased metabolic activity. Impaired lymphatic drainage of the peritoneum, a result of blocked diaphragmatic lymphatics, plays an important role in the development of ascites (Fig. 13 – peritoneal implant). Tumor cells tend to follow the circulatory

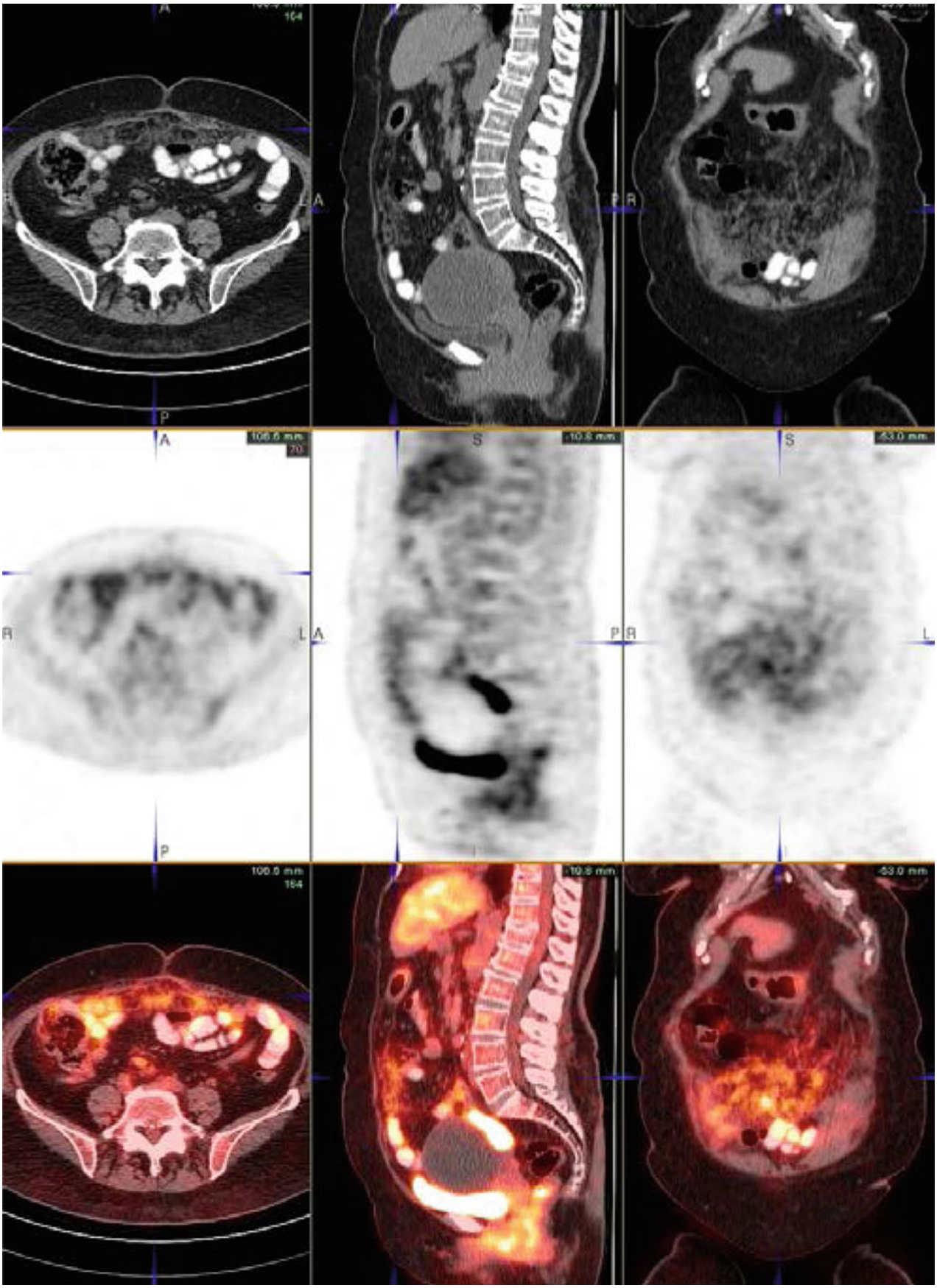

Fig. 13 A 85-year-old woman with newly diagnosed ovarian carcinoma. Extensive peritoneal thickening is seen predominantly in the omentum, with associated hypermetabolic activity (SUVmax up to 3.0), consistent with peritoneal carcinomatosis

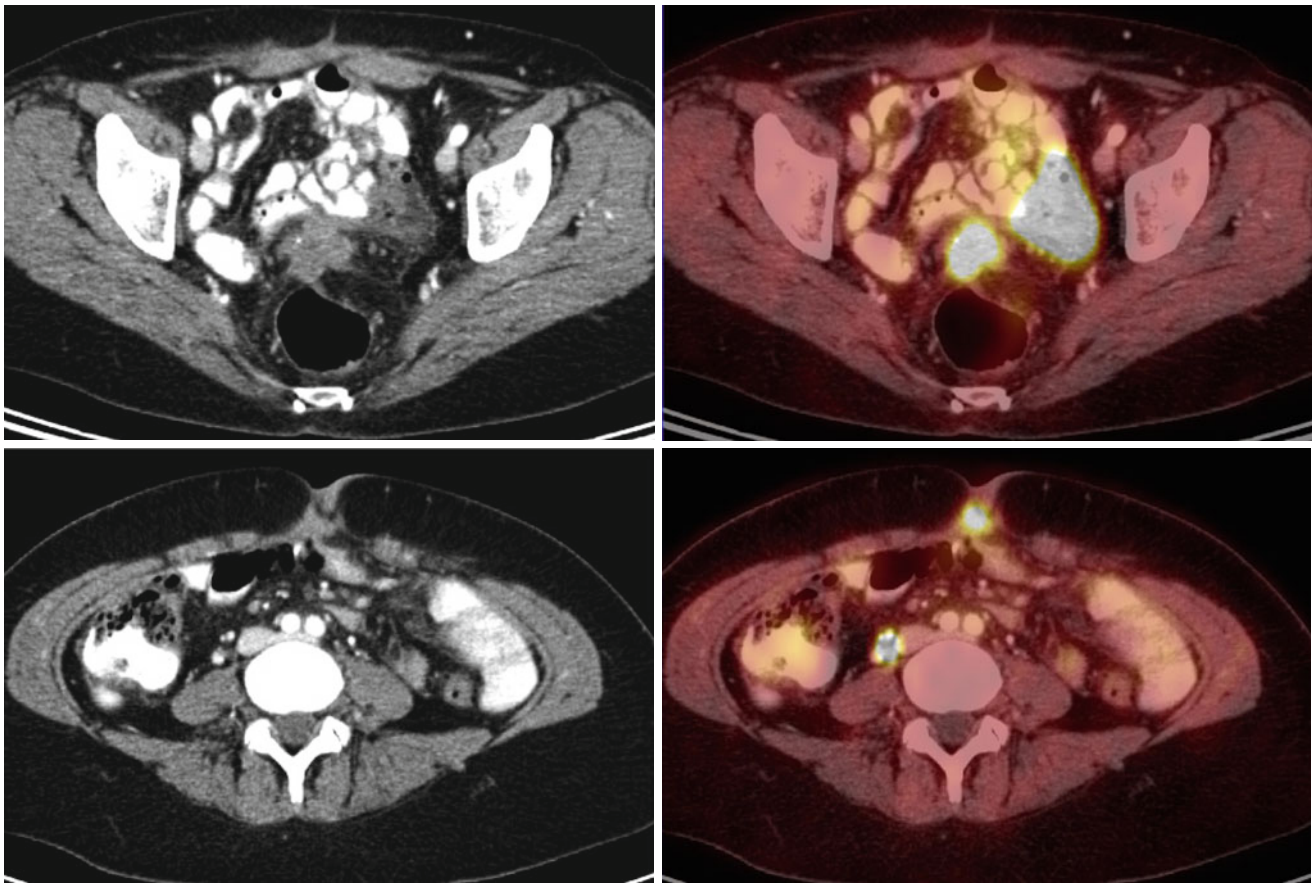

Fig. 14 A 47-year-old woman with history of ovarian cancer, status post debulking surgery and chemotherapy. Restaging PET/CT study shows intensely active implant in the cul-de-sac (SUV max 12.8) (*upper row*) and umbilical implant (SUV max 8.6) (*bottom row*). Urinary stasis is noted in the right ureter at the common iliac level

path of peritoneal fluid, implanting in the pouch of Douglas, paracolic gutters, small bowel mesentery, ileocecal junction, diaphragmatic surface – particularly the right subphrenic space along the convexity of the liver – and the hepatorenal fossa. (Fig. 14 (upper row) – cul-de-sac implant) [53]. The hepatorenal fossa harbors malignant implants by communicating with the right subphrenic space and the right paracolic gutter. In almost 50 % of patients, gravitational accumulation of tumor cells in the mesenteric recesses leads to seeding of malignant cells on small bowel serosal surfaces and in the ileocecal junction [53]. Other sites of involvement include the sigmoid mesocolon, a result of pooling along its superior border, and the right paracolic gutter, a result of cephalic flow. The right hemithorax also may be involved through its communication with the right subphrenic space. Omental thickening and nodularity with diffuse FDG uptake are indicative of omental involvement. However, PET/CT is limited in detecting small-volume disease (lesions < 5–7 mm) and miliary or diffuse peritoneal involvement, even if the disease process is evident on CT [54].

Umbilical metastases (Sister Mary Joseph nodules) are rare and associated with widespread intra-abdominal disease, particularly in patients with serous papillary cystadenocarcinoma (Fig. 14 (bottom row) – umbilical metastasis). This process may be secondary to retrograde lymphatic flow from the peritoneum or to venous spread of disease [55]. The persistence of fetal structures such as the urachus and paraumbilical veins may facilitate the spread of disease to the umbilicus.

Distant Organ Metastases

Hematogeneous dissemination of disease at the time of diagnosis is uncommon; only 2–3 % of patients are found to have pulmonary or hepatic involvement. Pleural effusion is the most common finding of stage IV disease, followed by parenchymal liver metastases (Fig. 15 – hepatic metastases; Fig. 16 – splenic metastasis). Brain metastases are extremely rare. PET/CT has high sensitivity for the depiction of distant metastases, and it may be useful to help determine those patients who are eligible for secondary surgical cytoreduction [56].

In summary, when compared with conventional imaging, most studies found an improvement in diagnostic accuracy

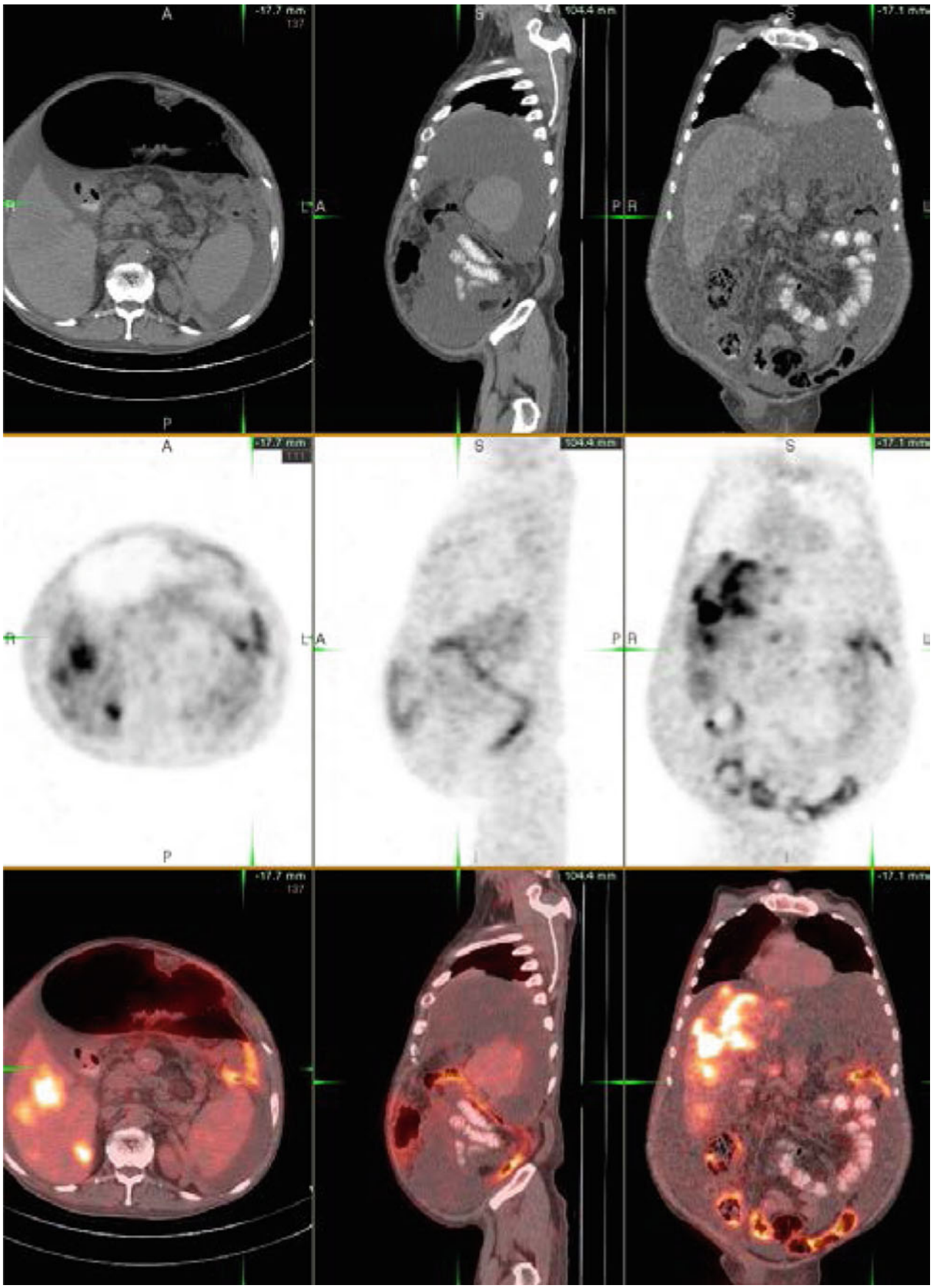

Fig. 15 A 67-year-old woman with history of ovarian cancer with extensive hepatic and peritoneal disease and large ascites. The transverse colon is significantly dilated (measuring up to 10.0 cm) and filled with air, with evidence of obstruction at the splenic flexure where diffuse hypermetabolic serosal implants are seen

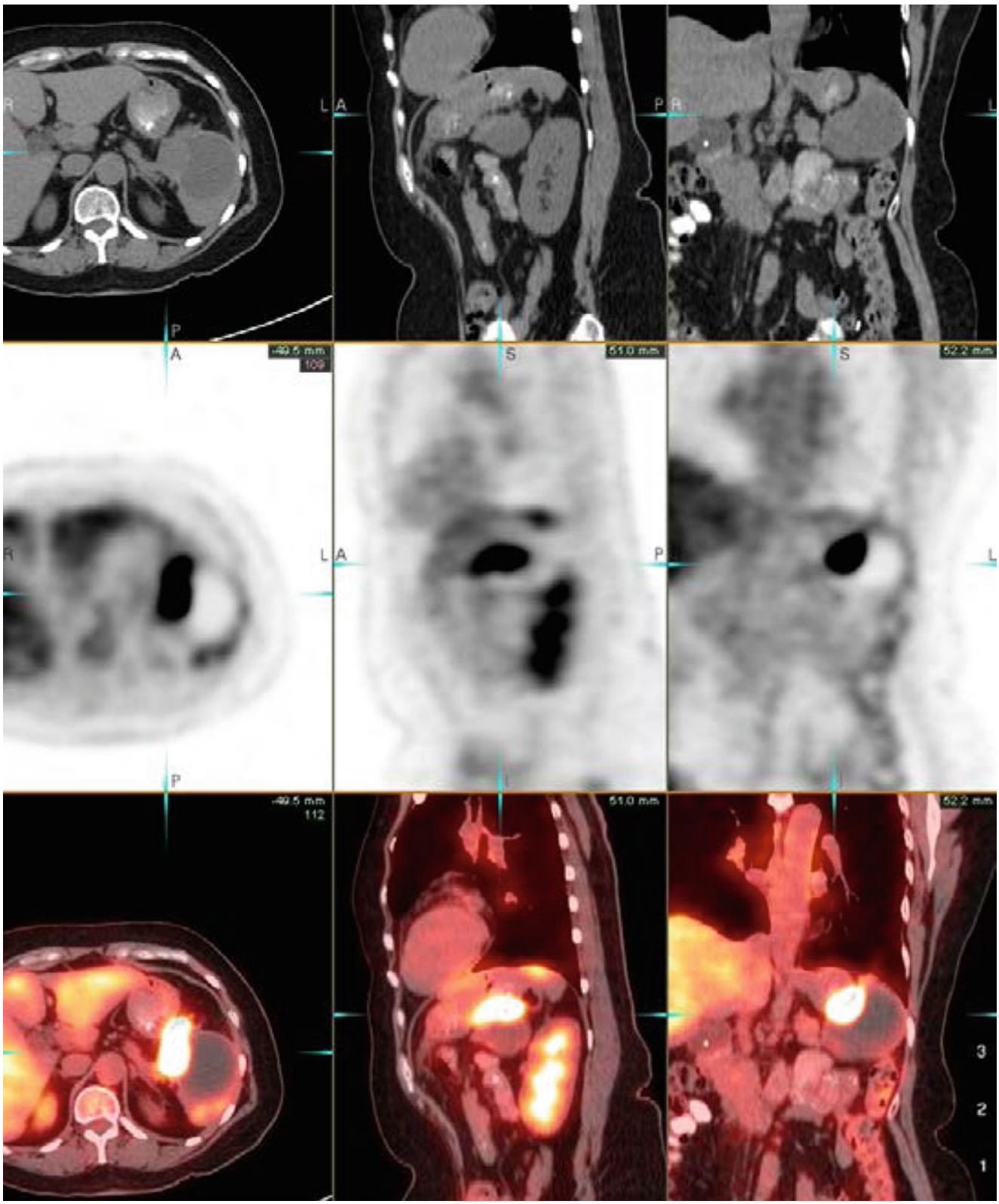

Fig. 16 A 57-year-old woman with history of ovarian cancer. An intensely active soft tissue mass is seen in the anteromedial aspect of the spleen (SUVmax 7.8), which was a biopsy-proven ovarian metastatic disease

using FDG-PET/CT for staging of ovarian cancer prior to surgery. PET/CT provides an accurate assessment of the extent of disease, particularly in areas difficult to assess for tumor deposits by CT and MRI such as the abdomen and pelvis, mediastinum, and supraclavicular region.

Recurrent Ovarian Cancer

The majority of patients with advanced-stage ovarian cancer will have persistent disease or develop recurrent disease, even after a complete clinical response following primary therapy. Clinical follow-up generally includes measurement of serum tumor markers such as CA-125, physical examination, and cross-sectional imaging. Cancer antigen 125 (CA-125) is a membrane-associated mucin protein expressed on female reproductive tract epithelia and is used as a tumor marker in recurrent ovarian cancer. However, CA-125 is not elevated in all patients with persistent or recurrent disease and does not directly reflect the disease burden.

Cross-sectional imaging, predominantly contrast-enhanced CT, is used to localize recurrent ovarian cancer; however, the identification of disease in the abdomen and pelvis is often difficult. A study compared CT to second-look laparotomy in 58 women who were clinically disease-free and found a sensitivity of only 47 % for the detection of recurrent disease with a specificity of 87 % [57]. It is particularly difficult to identify small tumor deposits adjacent to the bowel on CT. MRI has an accuracy equivalent to CT for lesions >2.0 cm and thus CT remains the modality of choice for assessing recurrent disease [58].

The role of FDG-PET in restaging of patients with recurrent ovarian cancer has been studied extensively. In 2001, a study in 24 women reported a diagnostic accuracy of 79.2 % using FDG-PET for detecting recurrent ovarian cancer [59]. The accuracy increased to 94.4 % when combined with conventional imaging modalities. The findings were confirmed by several further studies [60–63].

Various studies have demonstrated the impact of combined functional and structural imaging on the clinical management plan in many patients with suspected recurrent ovarian cancer. In 56 women, the addition of FDG-PET to CT altered the known disease distribution in 61 % of scans leading to a change in management in 57 % of patients [64]. In 32 patients with suspected ovarian cancer recurrence, PET/CT showed a higher sensitivity (91 %) than contrast-enhanced CT (62 %) [63]. With the addition of FDG-PET/CT, 44 % of patients received different treatment; only 2 % of patients were managed expectantly compared to 22 % following CT alone. The percentage of patients who were referred for chemotherapy increased from 31 to 50 % when FDG-PET/CT results were considered. Thrall el al. noted that FDG-PET/CT revealed unsuspected disease either outside the abdomen or in surgically inaccessible areas in 28.6 % of the cases and thus the treatment was changed [61]. In another study, FDG-PET combined with contrast-enhanced CT resulted in a change of management in 39 % of the cases compared to 12 % for contrast-enhanced CT alone and 2 % for FDG-PET combined with a low-dose CT [65].

A study of 51 patients found that combined FDG-PET/CT provided a statistically significant improvement in accuracy from 83 to 92 %, in the diagnosis of ovarian cancer recurrence, compared to CT alone [60]. The co-registered functional and anatomical information from PET/CT is particularly helpful in the abdomen and pelvis. Another study found a sensitivity of 94.5 % and a specificity of 100 % for FDG-PET/CT in the detection of ovarian cancer recurrence [61]. The authors suggested that PET/CT may have the greatest utility in the situation in which CA-125 levels are rising and conventional imaging studies show negative or equivocal findings. In addition, FDG-PET/CT was also found to be valuable imaging technique in the evaluation of suspected recurrent ovarian cancer in the setting of normal CA-125 levels. A study from MD Anderson Cancer Center also concluded that FDG-PET/CT is capable of detecting ovarian cancer recurrence in symptomatic patients with normal CA-125 levels and in this setting, has slightly better sensitivity than contrast-enhanced CT. It can be considered as the frontline modality for all such patients [66]. Thirty-one percent of patients with no indication of malignancy on CT had evidence of disease on FDG-PET/CT which was confirmed on histology.

As discussed earlier, it is important to acknowledge the reference standard used for evaluation of imaging modalities. In a direct comparison with second-look laparotomy in 31 women, the lesion-based sensitivity was 45.3 % for FDG-PEt alone and increased to 58.2 % for FDG-PET/CT [67]. Sironi et al. [54] studied 31 patients prior to second-look laparotomy and found that FDG-PET/CT correctly identified 32 of the 41 lesions that were positive at histological analysis. The overall patient-based sensitivity and specificity were 53 and 86 %, respectively. All lesions missed with PET/CT were equal to or smaller than 0.5 cm in maximum diameter. This study highlights an important limitation of PET imaging for initial evaluation, staging, and restaging in that the metabolic activity of small tumor deposits is often insufficient for positive identification, particularly in areas with higher background activity such as in the abdomen and pelvis.

In 43 patients, FDG-PET/CT had a sensitivity and specificity of 88.4 and 88.2 %, respectively, for detection of recurrent ovarian cancer using histology and clinical follow-up as the reference [62]. More specifically they found a slightly lower sensitivity of 80.9 % for pelvic disease and 93.5 % for extrapelvic disease; specificity was 93.7 % for both. A recent meta-analysis compared FDG-PET, FDG-PET/CT, MRI,

and tumor marker CA-125 for the detection of recurrent disease [68]. PET/CT (sensitivity, 79 %; specificity, 88 %) performed better than CT (sensitivity, 79 %; specificity, 84 %) or MRI (sensitivity, 75 %; specificity, 78 %). The authors concluded that FDG-PEt alone appeared to be useful for the diagnosis of recurrence when CA-125 levels are rising and conventional imaging (CT or MR) is inconclusive or negative.

Monitoring Response to Treatment

Although a substantial number of ovarian cancer patients respond to initial chemotherapy, nonresponding individuals generally have a poor prognosis. The concept of individualizing cancer treatment is very appealing and would involve predicting the response to treatment early in the course of therapy. RECIST (Response Criteria in Solid Tumors) is the widely used method to evaluate response to treatment. In this approach response rate typically based on morphologic criteria and the reduction in tumor size on CT is the most important determinant. However, CT and MRI are limited in detecting the response early after the initiation of therapy because anatomical changes are usually seen months rather than weeks after initiation of therapy.

The use of FDG-PET in this capacity is based on the fact that tumors show early changes in glucose utilization and that changes in uptake closely correlate with response to treatment [7, 10]. In a variety of tumors, it has been shown that changes in glucose metabolism precede changes in tumor size and reflect treatment response. The identification of nonresponders would significantly improve patient management by reducing the use of ineffective therapies, preventing adverse effects, reducing the delay before administering more effective treatment, and hence minimizing costs. To predict treatment response two sequential FDG-PET scans are required; one baseline FDG-PET prior to treatment and a second after initiation of chemotherapy. The change in level of tumor metabolic activity after one or two cycles of chemotherapy can then be compared to treatment response following completion of the treatment course.

There is only limited data available about FDG-PET treatment monitoring studies in ovarian cancer. Thirty-three patients received three cycles of carboplatin-based neoadjuvant chemotherapy, followed by cytoreductive surgery [7]. Quantitative FDG-PET of the abdomen and pelvis was acquired before treatment and after the first and third cycle of chemotherapy. Changes in tumoral FDG uptake, expressed as standardized uptake values (SUVs), were compared with clinical and histopathologic response; overall survival served as a reference. A significant correlation was found between the metabolic response after the first and third cycles of chemotherapy and overall survival using FDG-PET. This was found to be superior to clinical response, CA-125 measurements and histopathology [7]. Median overall survival was higher in those patients found to be metabolic responders after the first and third cycles of chemotherapy. After the first cycle of chemotherapy metabolic responders were defined as having a decrease in SUV by 20 % from baseline. After the third cycle of chemotherapy metabolic responders were defined as having a 55 % decrease in SUV from baseline. Metabolic responders had a median overall survival of 38.3 months compared to 23.1 months in metabolic nonresponders.

Nishiyama et al. demonstrated that the level of tumor FDG uptake prior to and after therapy as well as percentage change have the potential to predict response to chemotherapy or chemoradiotherapy in patients with advanced gynecological malignancies, including eight cases of ovarian cancer [69]. Based on histopathologic analysis of the specimens obtained at surgery, patients were classified as responders ($n=10$) and nonresponders ($n=11$). When an arbitrarily SUV of 3.8 was taken as the cutoff for differentiating between responders and nonresponders after therapy, FDG-PET showed a sensitivity of 90 %, a specificity of 63.6 %, and an accuracy of 76.2 %. When an arbitrary percentage change of 65 % was taken as the cutoff, FDG-PET showed a sensitivity of 90 %, a specificity of 81.8 %, and an accuracy of 85.7 %. There was a statistically significant association between SUV after therapy, percentage change, and pathological findings in ovarian cancer.

A further study by Sironi et al. [54] has shown that FDG-PET/CT has a potential role in assessing response to treatment in ovarian cancer. The authors studied 31 patients with ovarian cancer, almost all papillary serous in stage III. All patients were submitted to primary cytoreductive surgery followed by platinum regimen chemotherapy. After a period of at least 21 days, an FDG-PET/CT scan was acquired for all patients who were scheduled to undergo a second-look procedure, performed soon after imaging examination. PET/CT correctly identified 32 of 41 positive lesions at histologic analysis. All 9 of 41 lesions missed with FDG-PET/CT were ≤5 mm. The absence of persistent tumor lesions was correctly diagnosed with PET/CT in 12 of 14 patients with negative histologic results after second-look surgery. The overall lesion-based sensitivity, specificity, and positive and negative predictive values of PET/CT in the detection of persistent disease were 78, 77, 89, and 57 %, respectively. The accuracy rate for detection of lesions >1 cm in diameter was 90 % [54]. Evidently, the major FDG-PET/CT limitation is the low negative predictive value, which probably depends on the spatial resolution of the technique (about 5 mm). Nevertheless, FDG-PET/CT has shown high positive predictive value. This would help to avoid second-look procedure that, in the future, should be recommended only in apparent responders (Fig. 17).

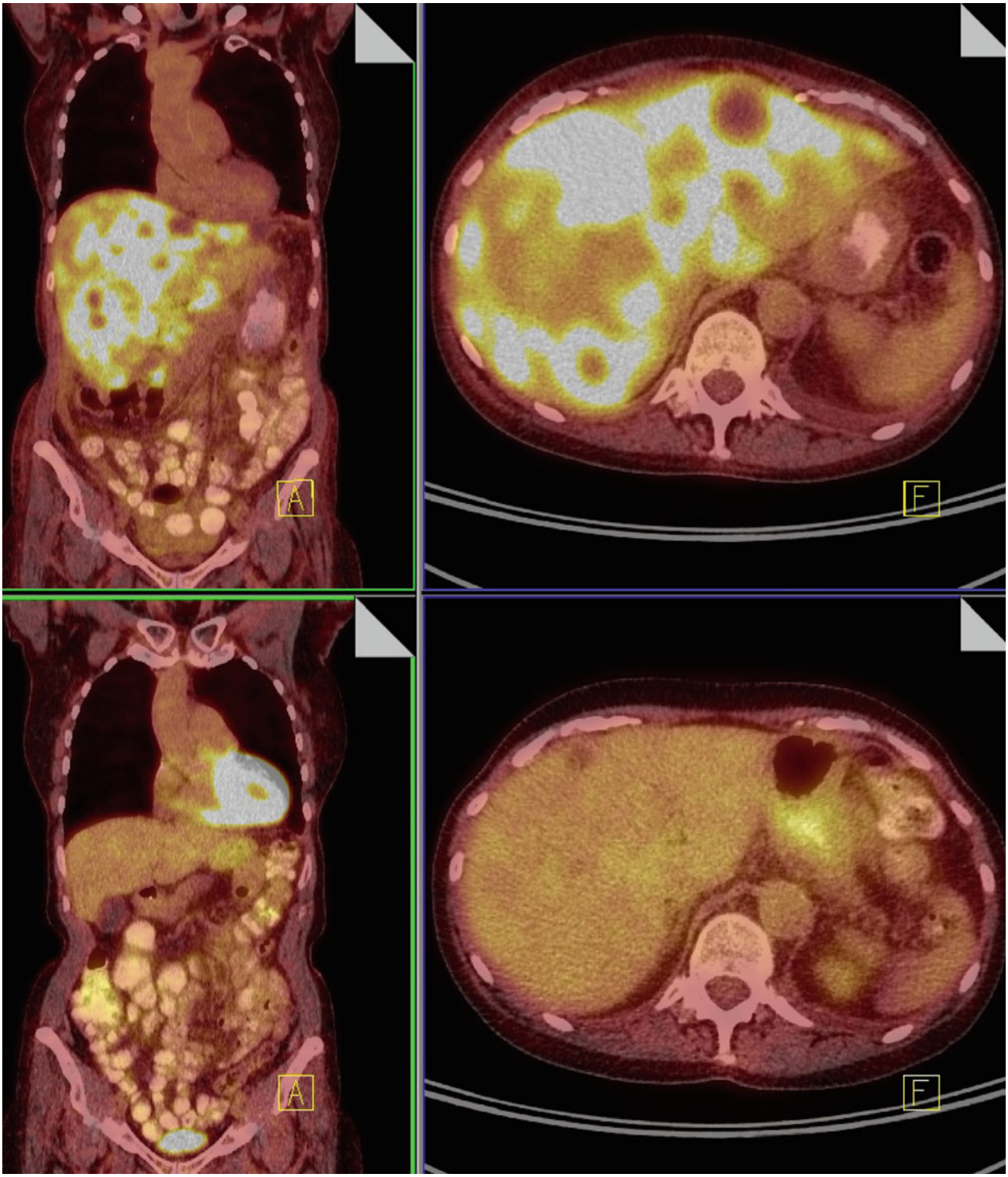

Fig. 17 A 62-year-old woman with history of ovarian cancer and extensive hepatic metastases (SUVmax up to 12.0; *upper row*), currently on chemotherapy. Restaging PET/CT (*bottom row*) shows significant interval improvement to resolution of the previously evident hypermetabolic hepatic metastatic disease

FDG-PET/CT and Radiation Therapy

PET/CT-guided intensity-modulated radiotherapy (IMRT) in recurrent ovarian cancer patients improves the delineation of gross tumor volume (GTV) and reduces the likelihood of geographic misses and therefore improves the clinical outcome. Changes in GTV delineation were found in 35.7 % of patients based on PET/CT information compared with CT data, due to the incorporation of additional lymph node metastases and extension of the metastasis tumor. PET/CT-guided IMRT improves tumor response compared to CT IMRT (complete response 64.3 % vs. 46.7 %, $p=0.021$; partial response 25.0 % vs. 13.3 %, $p=0.036$). The 3-year overall survival is significantly higher in PET/CT IMRT group than control (34.1 % vs. 13.2 %, $p = 0.014$) [70].

PET/MRI Versus PET/CT

PET/CT imaging began a new era of integrated structural and functional imaging. Currently studies are focusing on the development of combined PET/MR systems [71, 72]. This new technology has potential advantages including improved soft tissue visualization and the ability to perform simultaneous rather than sequential acquisitions. It offers the addition of a variety of complex MRI techniques including diffusion and perfusion imaging. Above all, PET/MR would result in a decrease in radiation exposure, which is particularly important for serial follow-up. There is little clinical data available to demonstrate the potential value of PET/MR in patients with gynecological malignancies.

The diagnostic accuracy of PET/CT and PET/MR fusion images were evaluated in 31 patients with uterine and ovarian malignancies. FDG-PET images were fused to CT and T1- and T2-weighted MR images (T1WI, T2WI). PET/MRI fusion was performed semiautomatically. Three types of evaluation were performed: depiction of the uterus and the ovarian lesions on CT or MRI mapping images (first evaluation), additional information for lesion localization with PET and mapping images (second evaluation), and the image quality of fusion on interpretation (third evaluation). For the first evaluation, the score of T2WI (4.68 ± 0.65) was significantly higher than that for CT (3.54 ± 1.02) or T1WI (3.71 ± 0.97) ($p<0.01$). For the second evaluation, the scores for the localization of FDG accumulation showing that T2WI (2.74 ± 0.57) provided significantly more additional information for the identification of anatomical sites of FDG accumulation than did CT (2.06 ± 0.68) or T1WI (2.23 ± 0.61) ($p<0.01$). For the third evaluation, the three-point rating scale for the patient group as a whole demonstrated that PET/T2WI (2.72 ± 0.54) localized the lesion significantly more convincingly than PET/CT (2.23 ± 0.50) or PET/T1WI (2.29 ± 0.53) ($p<0.01$). The authors found PET/T2WI fusion images are superior to PET/CT for the detection and localization of gynecological malignancies [73]. Although PET/MR is promising, further studies need to show the clinical benefit and that PET/MR is cost-effective.

Conclusion

FDG-PET/CT has the potential for a significant impact in staging, restaging, and monitoring of treatment effects in ovarian cancer. For initial staging, FDG-PET/CT has a limited role for assessing primary tumor extent in the pelvis; it provides useful information about lymph node involvement and the presence of distant metastasis. Further evaluation in prospective clinical trials will be required to assess the prognostic value of sequential FDG-PET for treatment monitoring in patients with ovarian cancer.

References

1. Jemal A, Bray F, Center MM, Ferlay J, Ward E, Forman D. Global cancer statistics. CA Cancer J Clin. 2011;61(2):69–90.
2. ACR practice guideline for performing FDG-PET/CT in oncology. http://www.acr.org/SecondaryMainMenuCategories/quality_safety/guidelines/nuc_med.aspx. Accessed 16 May 2012.
3. Avril N. GLUT1 expression in tissue and F-18 FDG uptake. J Nucl Med. 2004;45:930–2.
4. Rohren EM, Turkington TG, Coleman RE. Clinical applications of PET in oncology. Radiology. 2004;231:305–32.
5. Townsend DW, Carney JP, Yap JT, et al. PET/CT today and tomorrow. J Nucl Med. 2004;45:4S–14.
6. Beyer T, Townsend DW, Burn T, et al. A combined PET/CT scanner for clinical oncology. J Nucl Med. 2000;41:1369–79.
7. Avril NE, Weber WA. Monitoring response to treatment in patients utilizing PET. Radiol Clin North Am. 2005;43:189–204.
8. Zasadny KR, Wahl RL. Standardized uptake values of normal tissues at PET with 2-[fluorine-18]-fluoro-2-deoxy-D-glucose: variations with body weight and a method for correction. Radiology. 1993;189:847–50.
9. Minn H, Zasadny KR, Quint LE, et al. Lung cancer: reproducibility of quantitative measurements for evaluating 2-[F-18]-fluoro-2-deoxy-D-glucose uptake at PET. Radiology. 1995;196:167–73.
10. Weber WA, Ziegler SI, Thodtmann R, et al. Reproducibility of metabolic measurements in malignant tumors using FDG PET. J Nucl Med. 1999;40:1771–7.
11. Cohade C, Osman M, Nakamoto Y, et al. Initial experience with oral contrast in PET/CT; phantom and clinical studies. J Nucl Med. 2003;44:412–6.
12. Goerres GW, Ziegler SI, Burger C, et al. Artifacts at PET and PET/CT caused by metallic hip prosthetic material. Radiology. 2003;226:577–84.
13. Shreve PD, Anzai Y, Wahl RL. Pitfalls in oncologic diagnosis with FDG-PET imaging: physiologic and benign variants. Radiographics. 1999;19:61–77.
14. Cohade C, Osman M, Pannu HK, Wahl RL. Uptake in supraclavicular area fat ("USA-Fat"): description on 18F-FDG PET/CT. J Nucl Med. 2003;44:170–6.

15. Chander S, Meltzer CC. McCook Bm. Physiologic uterine uptake of FDG during menstruation demonstrated with serial combined positron emission tomography and computed tomography. Clin Nucl Med. 2002;27:22–4.
16. Nakamoto Y, Tatsumi M, Hammoud D, et al. Normal FDG distribution patterns in the head and neck: PET/CT evaluation. Radiology. 2005;234:879–85.
17. Avril N, Gourtsoyanni S, Reznek R. Gynecological cancers. Meth Mol Biol. 2011;727:171–89.
18. Liu Y. Benign ovarian and endometrial uptake on FDG PET-CT: patterns and pitfalls. Ann Nucl Med. 2009;23:107–12.
19. Fenchel S, Grab D, Nuessle K, et al. Asymptomatic adnexal masses: correlation of FDG PET and histopathologic findings. Radiology. 2002;223:780–8.
20. Castellucci P, Perrone AM, Picchio M, et al. Diagnostic accuracy of 18F-FDG PET/CT in characterizing ovarian lesions and staging ovarian cancer: correlation with transvaginal ultrasonography, computed tomography, and histology. Nucl Med Commun. 2007;28:589–95.
21. Kitajima K, Murakami K, Yamasaki E. Diagnostic accuracy of integrated FDG-PET/contrast-enhanced CT in staging ovarian cancer: comparison with enhanced CT. Eur J Nucl Med Mol Imaging. 2008;35:1912–20.
22. Karantanis D, Allen-Auerbach M, Czernin J. Relationship between glycolytic phenotype, grade and histologic subtype in ovarian carcinoma. Clin Nucl Med. 2012;37:49–53.
23. Musto A, Rampin L, Nanni C, et al. Present and future of PET and PET/CT in gynecologic malignancies. Eur J Radiol. 2011;78:12–20.
24. Nam EJ, Yun MJ, Oh YT, et al. Diagnostic and staging of primary ovarian cancer: correlation between PET/CT, Doppler US, and CT or MRI. Gynecol Oncol. 2010;116:389–94.
25. Grab D, Flock F, Stohr I, et al. Classification of asymptomatic adnexal masses by ultrasound, magnetic resonance imaging, and positron emission tomography. Gynecol Oncol. 2000;77:454–9.
26. Rieber A, Nussle K, Stohr I, et al. Preoperative diagnosis of ovarian tumors with MR imaging: comparison with transvaginal sonography, positron emission tomography, and histologic findings. AJR Am J Roentgenol. 2001;177:123–9.
27. van Trappen PO, Rufford BD, Mills TD, et al. Differential diagnosis of adnexal masses: risk of malignancy index, ultrasonography, magnetic resonance imaging, and radioimmunoscintigraphy. Int J Gynecol Cancer. 2007;17:61–7.
28. Medeiros LR, Rosa DD, da Rosa MI, et al. Accuracy of ultrasonography with color Doppler in ovarian tumor: a systemic quantitative review. Int J Gynecol Cancer. 2009;19:230–6.
29. Adusumilli S, Hussain HK, Caoili EM, et al. MRI of sonographically indeterminate adnexal masses. AJR Am J Roentgenol. 2006;187:732–40.
30. Kinkel K, Lu Y, Mehdizade A, et al. Indeterminate ovarian mass at US: incremental value of second imaging test for characterization-meta-analysis and Bayesian analysis. Radiology. 2005;236:85–94.
31. Kawahara K, Yoshida Y, Kurokawa T, et al. Evaluation of positron emission tomography with tracer 18-fluorodeoxyglucose in addition to magnetic resonance imaging in the diagnosis of ovarian cancer in selected women after ultrasonography. J Comput Assist Tomogr. 2004;24:505–16.
32. Risum S, Hogdall C, Loft A, et al. The diagnostic value of PET/CT for primary ovarian cancer – a prospective study. Gynecol Oncol. 2007;105:145–9.
33. Romer W, Avril N, Dose J, et al. Metabolic characterization of ovarian tumors with positron-emission tomography and F-18 fluorodeoxyglucose. Rofo. 1997;166:62–8.
34. Kim SK, Kang KW, Roh JW, et al. Incidental ovarian 18F-FDG accumulation on PET: correlation with the menstrual cycle. Eur J Nucl Med Mol Imaging. 2005;32:757–63.
35. Nishizawa S, Inubushi M, Okada H. Physiologic 18F-FDG uptake in the ovaries and uterus of healthy female volunteers. Eur J Nucl Med Mol Imaging. 2005;32:549–56.
36. Subhas N, Patel PV, Pannu HK, et al. Imaging of pelvic malignancies with in-line FDG PET-CT: case examples and common pitfalls of FDG PET. Radiographics. 2005;25:1031–43.
37. Stahl A, Weber WA, Avril N, et al. Effect of N-butylscopolamine on intestinal uptake of fluorine-18-fluorodeoxyglucose in PET imaging of the abdomen. Nuklearmedizin. 2000;39:241–5.
38. Pignata S, Vermoken JB. Ovarian cancer in the elderly. Crit Rev Oncol Hematol. 2004;49:77–86.
39. Benedet JL, Bender H, Jones III H, et al. FIGO staging classification and clinical practice guidelines in the management of gynecologic cancers. FIO Committee on Gynecologic Oncology. Int J Gynecol Obstet. 2000;70:209–62.
40. Bristow RE, Tomacruz RS, Armstrong DK, et al. Survival effect of maximal cytoreductive surgery for advanced ovarian carcinoma during the platinum era: a meta-analysis. J Clin Oncol. 2002;20:1248–59.
41. Tempany CM, Zou KH, Silverman SG, et al. Staging of advanced ovarian cancer: comparison of imaging modalities – report from the Radiological Diagnostic Oncology Group. Radiology. 2000;215:761–7.
42. Yoshida Y, Kurokawa T, Kawahara K, et al. Incremental benefits of FDG positron emission tomography over CT alone for the preoperative staging of ovarian cancer. AJR Am J Roentgenol. 2004;182:227–33.
43. Risum S, Hogdall C, Loft A, et al. Does the use of diagnostic PET/CT cause stage migration in patients with primary advanced ovarian cancer? Gynecol Oncol. 2011;116:395–8.
44. Yuan Y, Gu ZX, Tao XF, Liu SY. Computed tomography, magnetic resonance imaging, and positron emission tomography or positron emission tomography/computer tomography for detection of metastatic lymph nodes in patients with ovarian cancer: a meta-analysis. Eur J Radiol. 2012;81(5):1002–6.
45. Kim HJ, Kim JK, Cho KS. CT features of serous surface papillary carcinoma of the ovary. AJR Am J Roentgenol. 2004;183(6):1721–4.
46. Salani R, Diaz-Montes T, Giuntoli RL, Bristow RE. Surgical management of mesenteric lymph node metastasis in patients undergoing rectosigmoid colectomy for locally advanced ovarian carcinoma. Ann Surg Oncol. 2007;14(12):3552–7.
47. Harter P, Gnauert K, Hils R, et al. Pattern and clinical predictors of lymph node metastases in epithelial ovarian cancer. Int J Gynecol Cancer. 2007;17(6):1238–44.
48. Benedetti-Panici P, Greggi S, Maneschi F, et al. Anatomical and pathological study of retroperitoneal nodes in epithelial ovarian cancer. Gynecol Oncol. 1993;51(3):150–4.
49. Choi HJ, Roh JW, Seo SS, et al. Comparison of the accuracy of magnetic resonance imaging and positron emission tomography/computed tomography in the presurgical detection of lymph node metastases in patient with uterine cervical carcinoma: a prospective study. Cancer. 2006;106(4):914–22.
50. Hynninen J, Auranen A, Carpen O, et al. FDG PET/CT in staging of advanced epithelial ovarian cancer: frequency of supradiaphragmatic lymph node metastasis challenges the traditional pattern of disease spread. Gynecol Oncol. 2012;126(1):64–8.
51. Buy JN, Moss AA, Ghossain MA, et al. Peritoneal implants from ovarian tumors: CT findings. Radiology. 1988;169(3):691–4.
52. De Iaco P, Musto A, Orazi L, et al. FDG-PET/CT in advanced ovarian cancer staging: value and pitfalls in detecting lesions in different abdominal and pelvic quadrants compared with laparoscopy. Eur J Radiol. 2011;80(2):e98–103.
53. Meyers MA. Distribution of intra-abdominal malignant seeding: dependency on dynamics of flow of ascitic fluid. Am J Roentgenol Radium Ther Nucl Med. 1973;119(1):198–206.

54. Sironi S, Messa C, Mangili G, et al. Integrated FDG PET/CT in patient with persistent ovarian cancer: correlation with histologic findings. Radiology. 2004;233:433–40.
55. Powell FC, Cooper AJ, Massa MC, Goellner JR, Su WP. Sister Mary Joseph's nodule: a clinical and histologic study. J Am Acad Dermatol. 1984;10(4):610–5.
56. Bristow RE, del Carmen MG, Pannu HK, et al. Clinically occult recurrent ovarian cancer; patient detection for secondary cytoreductive surgery using combined PET/CT. Gynecol Oncol. 2003;90(3):519–28.
57. De Rosa V, Mangoni di Stefano ML, Brunetti A, et al. Computed tomography and second-look surgery in ovarian cancer patients. Correlation, actual role and limitations of CT scan. Eur J Gynecol Oncol. 1995;16:123–9.
58. Javitt MC. ACR Appropriateness Criteria on staging and follow-up of ovarian cancer. J Am Coll Radiol. 2007;4:586–9.
59. Nakamoto Y, Saga T, Ishimori T, et al. Clinical value of positron emission tomography with FDG for recurrent ovarian cancer. AJR Am J Roentgenol. 2001;176:1449–54.
60. Sebastian S, Lee SI, Horowitz NS, et al. PET-CT vs. CT alone in ovarian cancer recurrence. Abdom Imaging. 2008;33:112–8.
61. Thrall MM, DeLoia JA, Gallion H, et al. Clinical use of combined positron emission tomography and computed tomography (FDG-PET/CT) in recurrent ovarian cancer. Gynecol Oncol. 2007;105: 17–22.
62. Iagaru AH, Mittra ES, McDougall IR, et al. 18F-FDG PET/CT evaluation of patients with ovarian carcinoma. Nucl Med Commun. 2008;29:1046–51.
63. Mangili G, Picchio M, Sironi S, et al. Integrated PET/CT as a first-line re-staging modality in patients with suspected recurrence of ovarian cancer. Eur J Nucl Med Mol Imaging. 2007;34:658–66.
64. Simcock B, Neesham D, Quinn M, et al. The impact of PET/CT in the management of recurrent ovarian cancer. Gynecol Oncol. 2006;103(1):271–6.
65. Kitajima K, Murakami K, Yamasaki E, et al. Performance of integrated FDG-PET/contrast-enhanced CT in the diagnosis of recurrent ovarian cancer: comparison with integrated FDG-PET/non-contrast-enhanced CT and enhanced CT. Eur J Nucl Med Mol Imaging. 2008;35:1439–48.
66. Bhosale P, Peungjesada S, Wei W, et al. Clinical utility of positron emission tomography/computed tomography in the evaluation of suspected recurrent ovarian cancer in the setting of normal CA-125 levels. Int J Gynecol Cancer. 2011;20:936–44.
67. Cho SM, Ha HK, Byun JY. Usefulness of FDG PET for assessment of early recurrent epithelial ovarian cancer. AJR Am J Roentgenol. 2002;179:391–5.
68. Gu P, Pan LL, Wu SQ, et al. CA125, PEt alone, PET-CT, CT and MRI in diagnosing recurrent ovarian carcinoma: a systematic review and meta-analysis. Eur J Radiol. 2009;71:164–74.
69. Nishiyama Y, Yamamoto Y, Kanenishi K, et al. Monitoring the neoadjuvant therapy response in gynecological cancer patients using FDG PET. Eur J Nucl Med Mol Imaging. 2008;35:287–95.
70. Du XL, Jiang T, Sheng XG, et al. PET/CT scanning guided intensity-modulated radiotherapy in treatment of recurrent ovarian cancer. Eur J Radiol. 2012;81(11):3551–6.
71. Pichler BJ, Kolb A, Nagele T, et al. PET/MRI: paving the way for the next generation of clinical multimodality imaging applications. J Nucl Med. 2011;51:333–6.
72. Pichler BJ, Wehrl HF, Kolb A, et al. Positron emission tomography/magnetic resonance imaging: the next generation of multimodality imaging? Semin Nucl Med. 2008;38:199–208.
73. Nakajo K, Tatsumi M, Inoue A, et al. Diagnostic performance of fluorodeoxyglucose positron emission tomography/magnetic resonance imaging fusion images of gynecological malignant tumors: comparison with positron emission tomography/computed tomography. Jpn J Radiol. 2010;28(2):95–100.

Contrast-Enhanced Transvaginal Sonography of Ovarian Masses: Potential Role in Early Diagnosis of Ovarian Cancer

Arthur C. Fleischer, Andre Lyshchik, and David A. Fishman

Abstract

The morphologic assessment of ovarian masses using gray scale, 2D/3D, and color Doppler sonography has been shown to be moderately (80–90 %) accurate in distinguishing benign from malignant ovarian masses. The desire to improve the accuracy of early detection of ovarian cancer using sonography has driven to investigate the clinical application of contrast-enhanced transvaginal sonography (CE-TVS). In this chapter will be reviewed the CE-TVS as well as our experience in this field.

Keywords

Ovarian cancer • Ultrasound • Transvaginal ultrasound • Contrast-enhanced transvaginal ultrasound

Introduction

The morphologic assessment of ovarian masses using gray scale, 2D/3D, and color Doppler sonography has been shown to be moderately (80–90 %) accurate in distinguishing benign from malignant ovarian masses [1]. The desire to improve the accuracy of early detection of ovarian cancer using sonography has served as an impetus to investigate the clinical application of contrast-enhanced transvaginal sonography (CE-TVS). This overview will describe and illustrate our clinical experience with this technique as well as the results from several other studies. It will emphasize the potentials and limitations of CE-TVS for distinguishing benign and malignant ovarian masses as well as the potential role of CE-TVS means for early detection of ovarian cancer.

Fundamental Concepts

The basis of improved sonographic detection of ovarian malignancies with microbubbles is the depiction of the tumor microscopic (capillary) vascular network. Beginning with the seminal studies by Folkman, it was shown that tumors require a vascular network derived from the host vasculature for their growth and potential metastatic spread [2]. The vessels that supply nutrients to tumors have irregular branching points and caliber. They form clusters in areas of tumor growth and have numerous arteriovenous malformations. Typically, tumors have rim of vessels, whereas the center of

A.C. Fleischer (✉)
Department of Radiology and Imaging Science,
Vanderbilt University Medical Center,
Nashville, TN 37232, USA

Department of Obstetrics/Gynecology,
Vanderbilt University Medical Center,
Nashville, TN 37232, USA
e-mail: arthur.fleischer@vanderbilt.edu

A. Lyshchik, MD, PhD
Division of Diagnostic Ultrasound,
Department of Radiology,
Thomas Jefferson University,
Philadelphia, PA 19107, USA

D.A. Fishman, MD
Division of Gynecologic Oncology,
Mt. Sinai Medical Center,
New York, NY 10029, USA

L. Saba et al. (eds.), *Ovarian Neoplasm Imaging*,
DOI 10.1007/978-1-4614-8633-6_29,

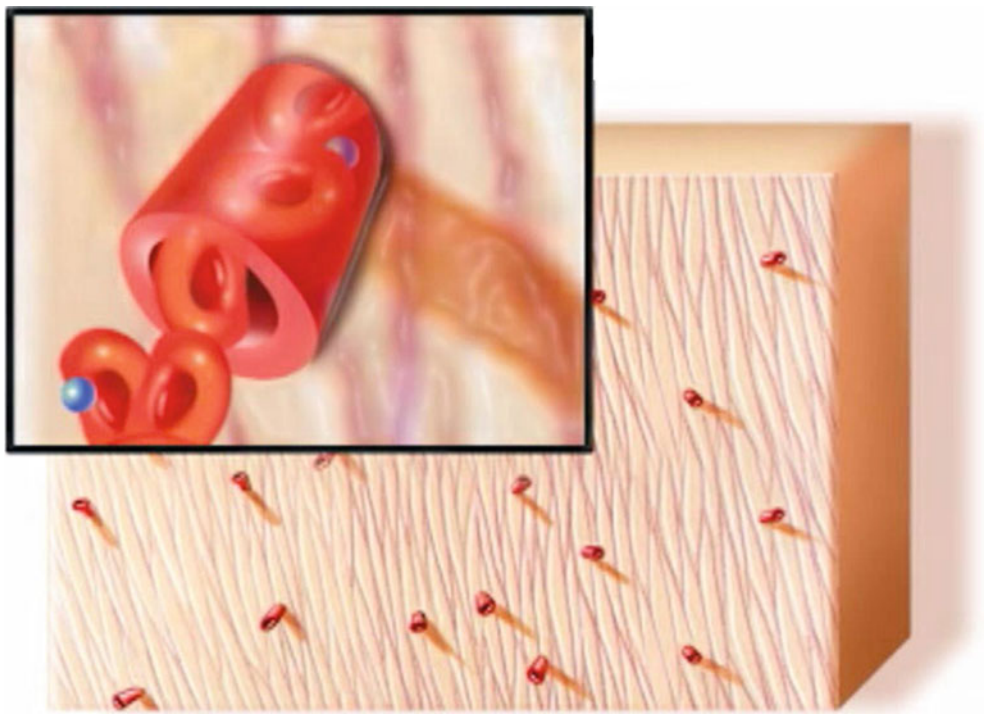

Fig. 1 Drawing depicting the relative size of a Definity® microbubble (in *blue*) compared to an erythrocyte within a large capillary

tumors has areas of relative ischemia. The interstitial pressure within the tumor and its heterogenic vascularity may be factors in not only their detection as malignancies but as factor into the distribution of medications.

Microbubbles used for sonographic enhancement are gas-filled, albumin, phospholipid, lipid, or polymer-coated microspheres that vary from 1/3 to 1/2 the size of an erythrocyte (Figs. 1 and 2). Thus they afford sonographic depiction of the tumor microvessels. The relatively large size of microbubble compared to endothelial gaps limits their distribution into the interstitium. Microbubbles can be imaged with harmonic frequencies due to their oscillations at a multiple of the fundamental. Physiologically microbubbles are expelled after several passes in the respiratory system and have been found to be nontoxic. Implementation of their use is limited primarily involving cost, requirement of intravenous administration, and the additional time required (typically 20–30 min) for their study and cost of additional software. Microbubble-enhanced sonography has been successfully utilized for characterization of liver lesions, based on their enhancement patterns. Malignant liver lesions tend to enhance quickly due to their arterial supply when hemangiomas typically show peripheral interrupted enhancement and focal nodular hyperplasia typically has a central hypovascular scar. Many have advocated the use of contrast-enhanced sonography over CT or MR due to decreased cost, lack of ionizing radiation or nephrotoxicity [3].

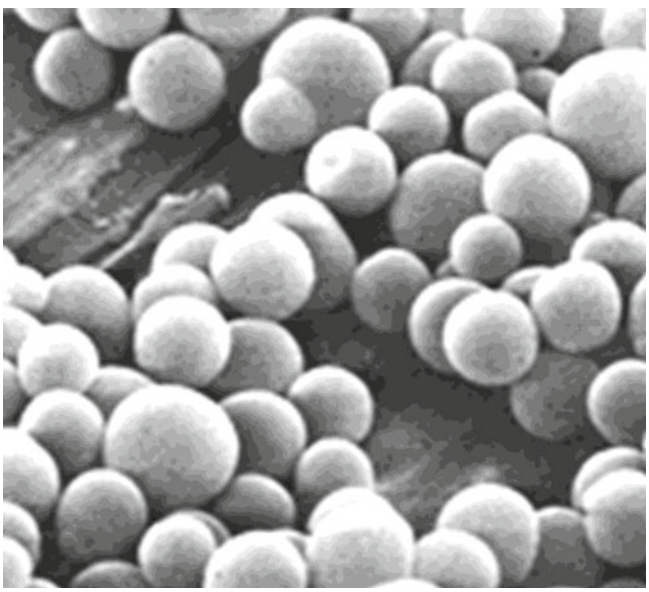

Fig. 2 Picture of Definity® microbubbles showing relative uniformity of size between 2 and 3 μm

Microbubbles have also been routinely utilized in echocardiography and have many other potential applications in vascular disorder such in the evaluations of endovascular stent leaks. In addition, several potential therapeutic applications for microbubbles such as clot lysis and enhanced drug delivery are under active investigation.

Instrumentation and Technique

Contrast-enhanced transvaginal sonography requires the use of microbubble contrast and specialized software for image processing. Most high-end scanners are equipped with various contrast-visualization tools. Additionally, a specialized image processing software is needed for quantification of enhancement kinetics. Scanning and image analysis can be performed within one-half to one hour, making the procedure a reasonable time commitment in a clinical setting.

Before contrast is administered, a complete transvaginal sonogram of the adnexa followed by color and spectral Doppler examination is performed. A detailed morphologic analysis of an adnexa mass for papillary excrescence, irregular wall or septations, as well as any internal content is required prior to contrast administration. This morphologic analysis can be further enhanced using 3D imaging. Following morphologic assessment, color Doppler sonography is performed with particular attention to the vessel distribution and caliber in areas of morphologic abnormality. Color Doppler sonography provides information regarding overall vascularity and vessel distribution. Selected vessels can be interrogated with spectral Doppler for their relative resistance as quantitated by waveform analysis.

Once the preliminary morphologic and color Doppler portions are completed, the contrast-enhanced part of examination can be performed. Microbubble contrast is prepared by either reconstituting lyophilized powder composed of polyethylene glycol, phospholipids, and palmitic acid with normal saline (SonoVue, Bracco Imaging S.p.A.) or activating the contrast by shaking the vial for 45 s using a mechanical agitator (Lantheus Medical Imaging, N. Billerica, MA) (Fig. 3). Using a 3-way stop cock, the contrast is slowly injected into an intravenous line within an antecubital vein, followed by a 10 cc bolus of normal saline. Very tiny amount of contrast (2–3 µl of Definity or 2.4 ml of SonoVue) is needed to provide adequate contrast. Flow of microbubbles within the ovary usually is observed within 30 s of injection.

Harmonic imaging is performed with particular attention to areas of increased vascularity seen on a color Doppler sonography. Once the microbubbles have been injected, a 3-min cine loop is recorded using a dedicated off-line software system specifically designed to quantitate enhancement parameters.

The time-intensity curves that represent enhancement patterns can be quantitated in selected regions of interest. The following parameters can be quantitated:

Wash-in time (s)

Peak enhancement (dB)

Washout time (s)

Area under curve (s^{-1})

The microvascularity of selected region of interest within an ovarian mass can be characterized by enhancement patterns depicted on time-intensity curves. The arrival of contrast to adnexa typically occurs approximately 30 s after IV administration of contrast. Time to peak reflects cardiac output and tone as well as intratumoral pressure, whereas peak intensity and area under curve (AUC) reflect vascular volume. The washout time reflects the complexity of the vascular network which in tumors is characterized by numerous micro- and macroscopic arteriovenous malformations.

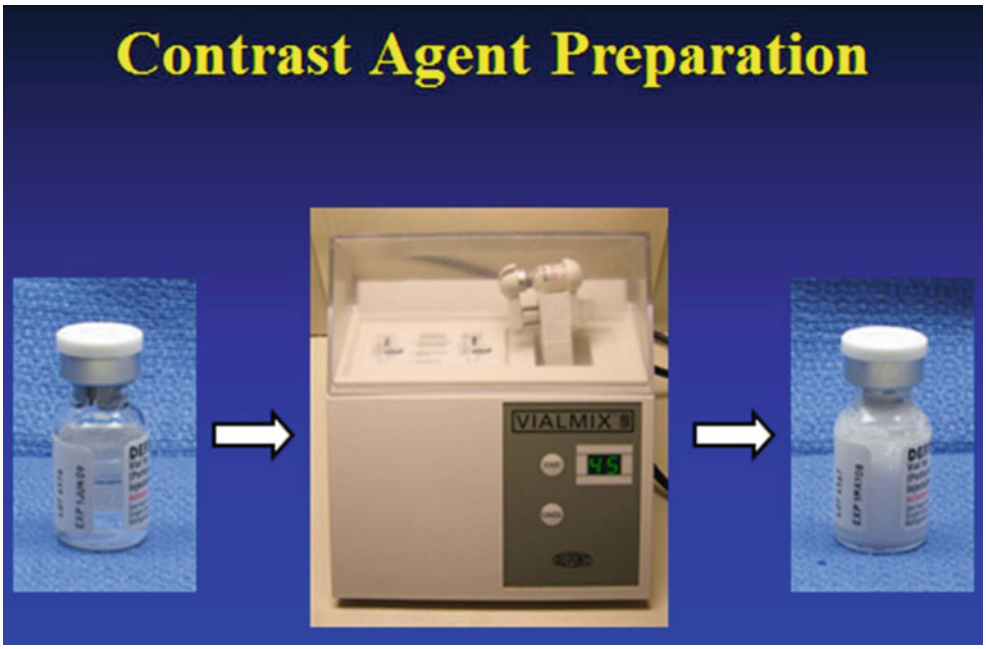

Fig. 3 Picture showing a vial containing microbubbles before (*left*) and after (*right*) their suspension in solution. The fluid appears milky once they are suspended in solution and ready for injection

Our series has utilized Definity® which is a perflutren gas microbubbles with a lipid shell (Lantheus Medical Imaging, N. Billerica, MA) where others have used SonoVue® (Bracco Imaging S.p.A.), which is a sulfur hexafluoride microbubbles with a phospholipid shell. Both sonographic contrast agents have been found to be safe with no reports of significant toxicity after many thousands of patients receiving the pharmaceutical. Although our research is considered "off-label" as conducted with Institutional Review Board approval, it is envisioned that these agents will receive approval for general use soon.

Clinical Studies

The initial reports describing the use of microbubble contrast sonography for ovarian mass evaluation utilized color Doppler sonography [4, 5]. The temporal resolution of color Doppler sonography is limited due to blooming artifacts. Even with this limitation, several initial investigations showed that malignant ovarian masses had greater vascularity than benign ones [4, 5].

The development of harmonic imaging greatly enhanced the accuracy of sonography depiction of tumor vascularity. Marret's study of 101 adnexal masses, 23 malignancies and 78 benign ones, reported a significant difference in the washout times and area under curve with sensitivity between 96 and 100 % and specifically between 83 and 98 %. In a similar study, Testa's initial report described improved accuracy in distinguishing benign from malignant ovarian masses over morphologic analysis [6].

Our group's study of 57 ovarian masses, 13 of which were malignant, focused on difference in enhancement kinetics in benign vs. malignant ovarian lesions [7, 8]. Significant differences are observed in peak enhancement, washout time, and area under curve (Figs. 4, 5, 6, 7, and 8). Even though there was no statistically significant difference in time to peak (wash-in time) 20.2 ± 5.9 s vs. 29.8 ± 13.4 s $p = 0.4$, there were statistically significant differences in greater peak enhancement (21.3 ± 4.7 vs. 8.3 ± 5.7 dB ($p < 0.01$) and one-half washout time (104.2 ± 48.1 vs. 413.8 ± 294.8 s) ($p < 0.001$) in malignancies. After the data was analyzed using receiver-operator curves, it was determined that and AUC > 787 s^{-1} was the most accurate diagnostic criterion for ovarian cancer with 100 % sensitivity and 96.2 % specificity. Similar calculations showed that peak enhancement >17.2 dB had a 90 % sensitivity and 98.3 % specificity and a one-half washout time of 741.0 s had a 100 % sensitivity and 92.3 % specificity (Figs. 9, 10, and 11). In a follow-up study comparing CE-TVS to 2D and 3D color Doppler sonography, CE-TVS was shown to have greater sensitivity and specificity (Fig. 12).

The largest multicenter and most statistically vigorous study on distinguishing ovarian masses using CE-TVS was reported by Testa as part of the International Ovarian Tumor Analysis (IOTA) group [9]. Although they reported that CE-TVS could not reliably distinguish borderline from malignant tumors, their conclusion was that CE-TVS can easily differentiate malignancies from other tumors. This result was also validated by Veyer who found significant differences in enhancement curves in benign vs. malignant tumors [10].

It is hoped that future studies will address how to best integrate the use of contrast-enhanced transvaginal sonography for early detection of ovarian cancer in high-risk and unselected patient population groups [11]. The role of CE-TVS relative to morphologic assessment and Doppler is yet to be determined based on large multicenter prospective studies. Whether or not differences in enhancement pattern are seen in some ovarian cancers and not all remains to be determined.

Present and Future Clinical Roles

The clinical use of CE-TVS for ovarian mass evaluation seems promising for enhancing the early detection of ovarian cancer. Due to its accuracy in distinguishing benign from malignant tumors, its limited ability to discriminate borderline tumors from true malignancies is not envisioned as a major shortcoming since both require surgical removal and pathologic confirmation.

The limitations in use of CE-TVS are mostly related to additional cost and expertise needed for its utilization. This will most likely account for its use as a secondary rather than screening test for patients with an ovarian mass.

Further challenge for CE-TVS may include attempts to label the microbubble for more directed enhancement of tumor cells both within and surrounding the ovary such as in the fallopian tube. It may be possible to attach encapsulated mediation to the labeled microbubbles in order to deliver treatment specifically to tumor.

In summary, the enhanced ability of CE-TVS to detect and differentiate benign from malignant ovarian masses provides significant impetus to stimulate further investigation as a means for early and reliable detection of ovarian cancer. It is hoped that CE-TVS will be included in future multicentered studies for the purpose of enhanced early detection of this dreaded neoplasm.

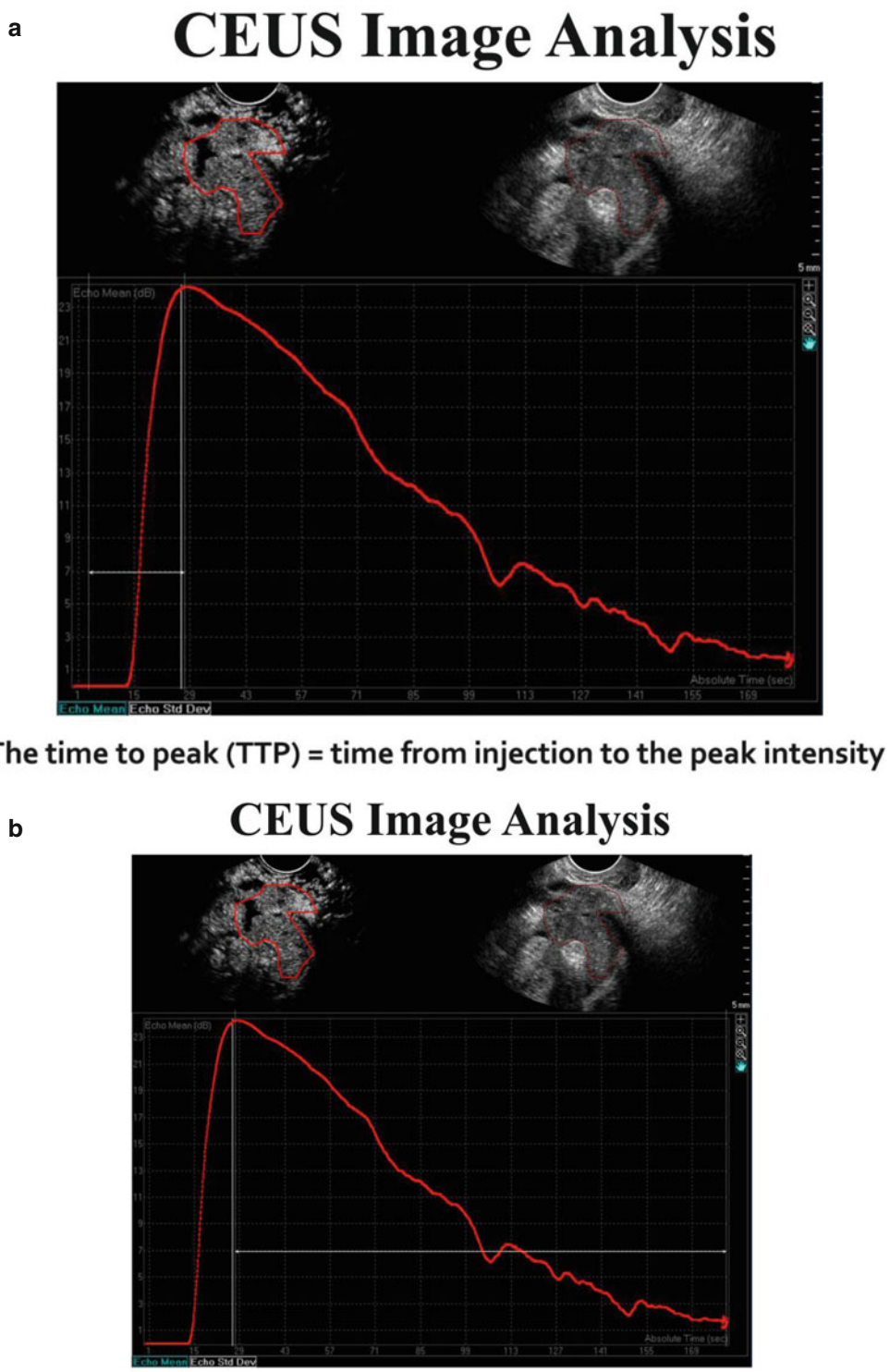

Fig. 4 Quantification of enhancement kinetics with time-intensity curves. The transvaginal sonogram in the *upper right* depicts an ovarian cancer using a scan obtained at the fundamental frequency (3 MHz). The *top left* image shows the same mass with the region of interest outlined in *red* as depicted using harmonic imaging (6 mHz). The time-intensity curve includes the vertical axis as calibrated in dB and the horizontal in seconds. The *red line* shows intensity relative to time during the first 180 s of enhancement. (**a**) Time to peak (*white horizontal line*): This is related to cardiac output and circulation times. (**b**) Washout time (*white horizontal line*) is the time from peak enhancement to complete washout. This reflects flow through the vascular network. (**c**) One-half washout time. (**d**) Area under curve (AUC) (*cross hatched area*) from the beginning of enhancement to washout. This is a reflection of tumor vascular volume

Fig. 4 (continued)

c

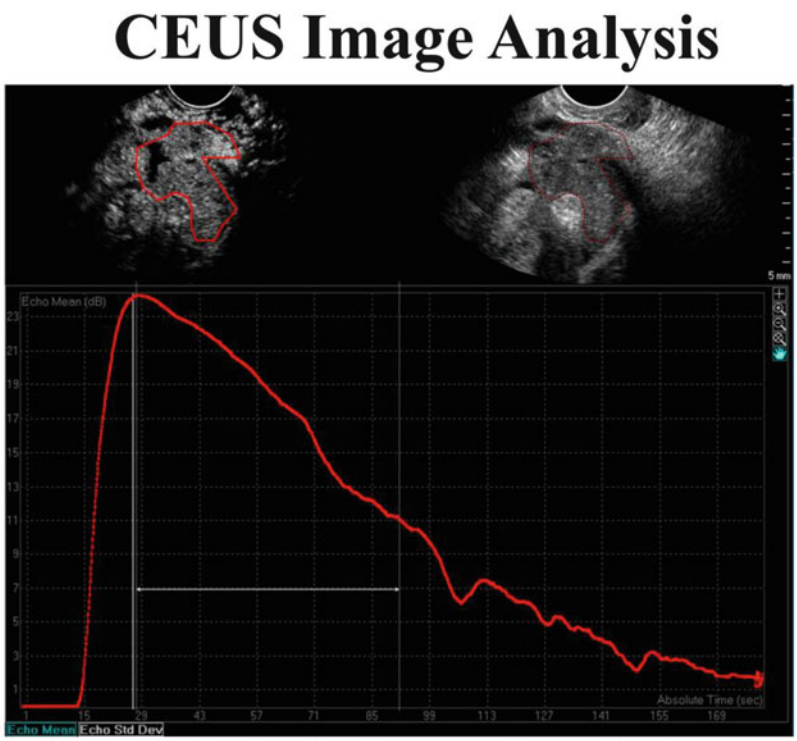

Half wash-out (T 1/2) = the time between the peak enhancement and the time when 50% the enhancement had disappeared

d

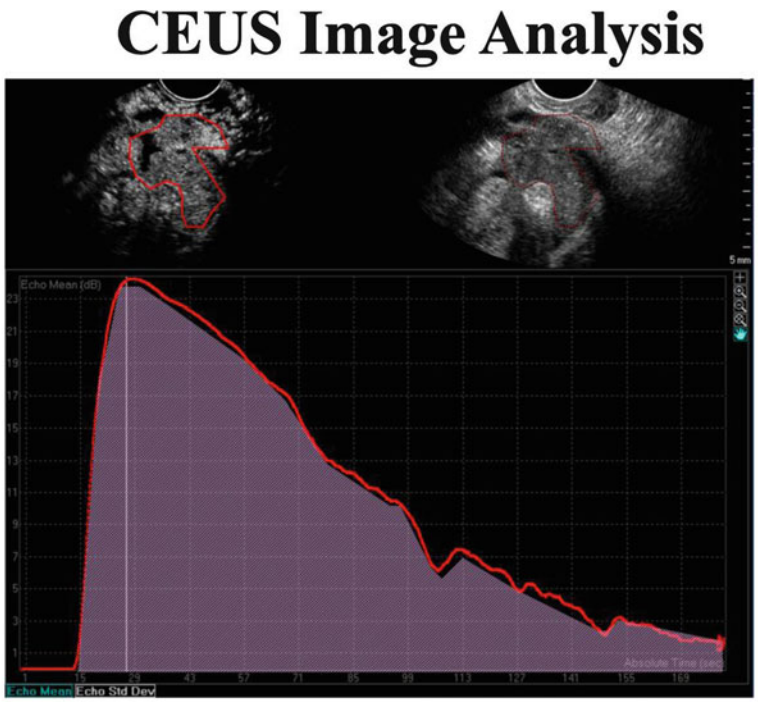

The area under the enhancement curve (AUC) calculated from the arrival of the contrast agent to the end of the wash-out period

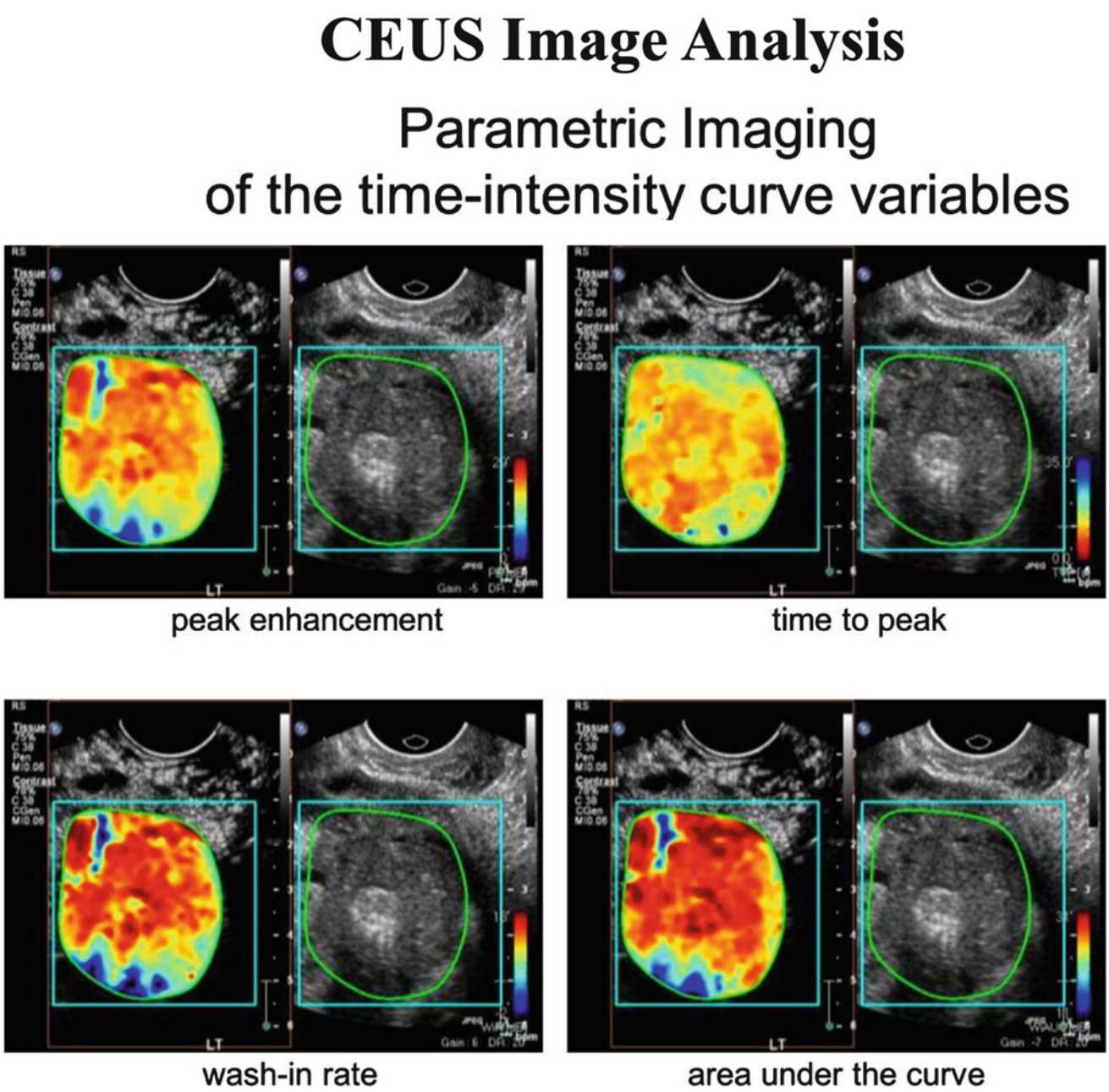

Fig. 5 Parametric mapping of CE-TVS. Colors can be assigned to variables to reflect time to peak, peak enhancement (*top left*), time to peak, (*top right*), wash-in rate (*bottom left*), washout rate, and area under curve. In this tumor, there is heterogeneous enhancement and wash-in rate. The central (*bottom left*) areas have a higher peak enhancement as well as faster time to peak indicating increased malignant potential. The area under curve image (*bottom right*) shows that the tumor is hypervascular

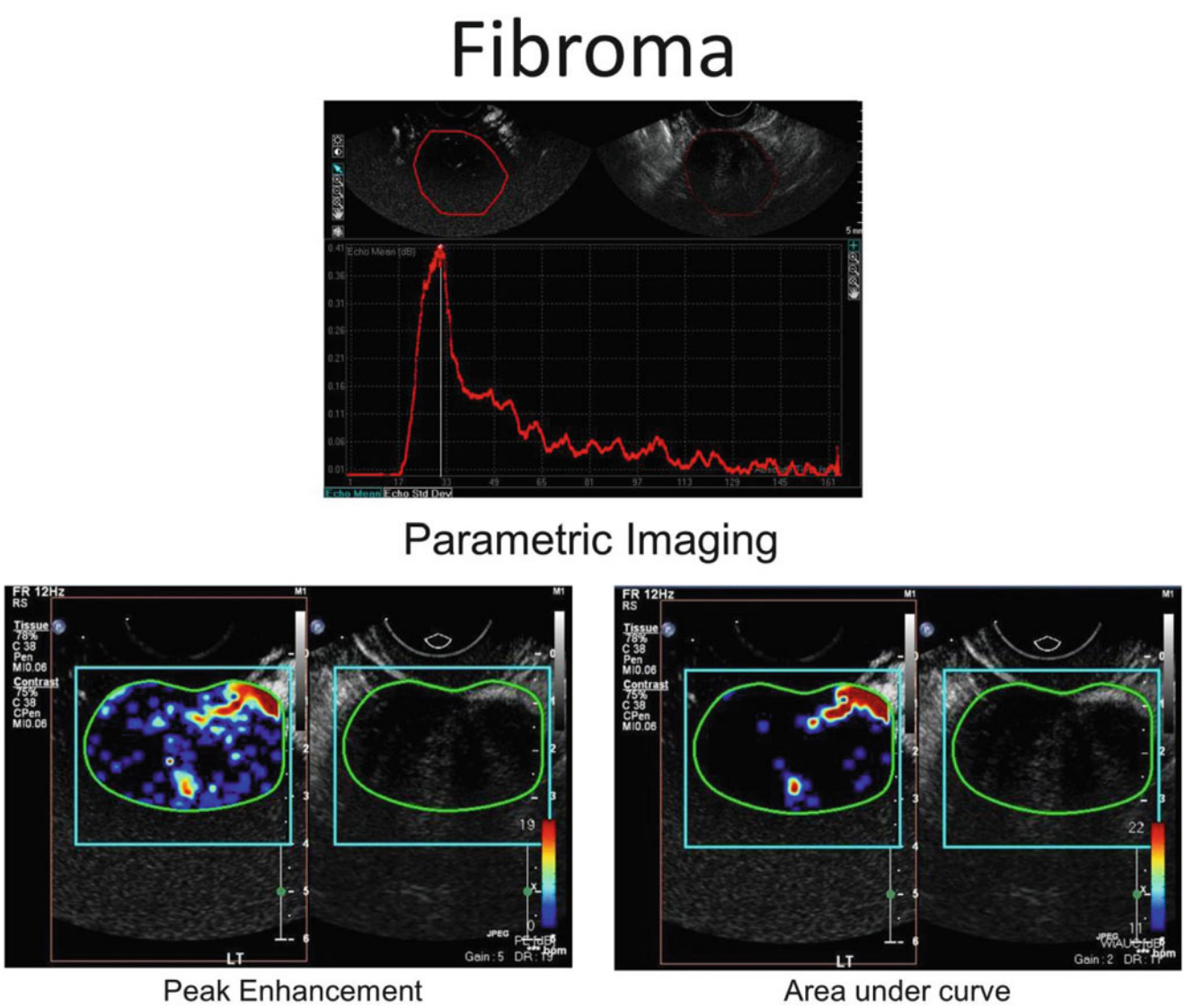

Fig. 6 CE-TVS of a relatively hypovascular solid ovarian mass with demonstrating minimal peak enhancement (0.41 dB), relatively rapid washout (7.5 s), and small AUC (15.3 s^{-1}). This was an ovarian fibroma. (*Top*) Time intensity curve and images of solid, hypovascular mass. (*Bottom*) Parametric imaging of peak enhancement and area under curve

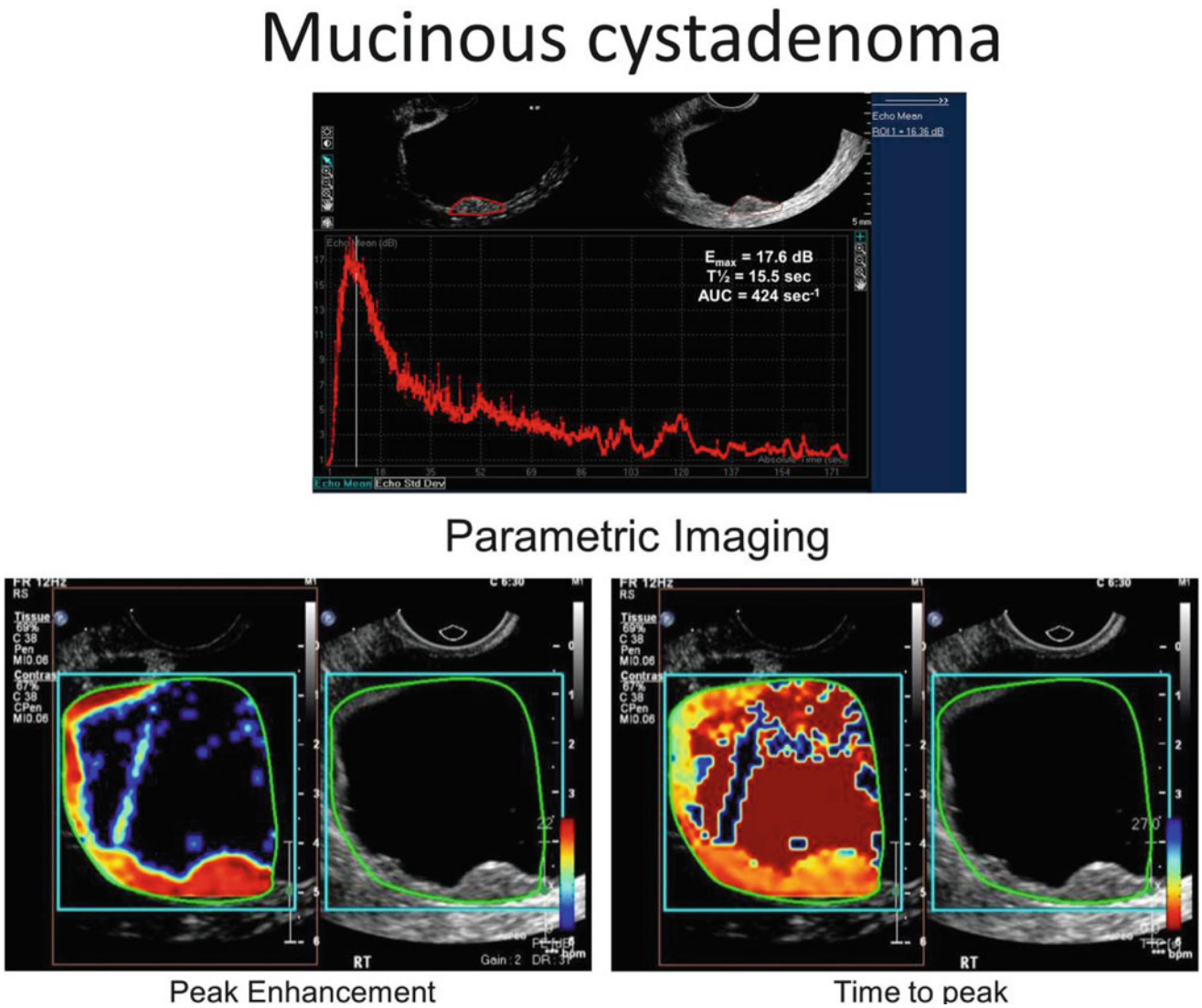

Fig. 7 CE-TVS of a cystic mass with mural nodules showing quick washout 1/2 (15.5 s) and low AUC (47.4 s^{-1}). This was a mucinous cystadenoma. (*Top*) Time intensity curve and images show enhancement of mural module. (*Bottom*) Parametric images showing difference in peak enhancement and time to peak in mural nodule compared to septation

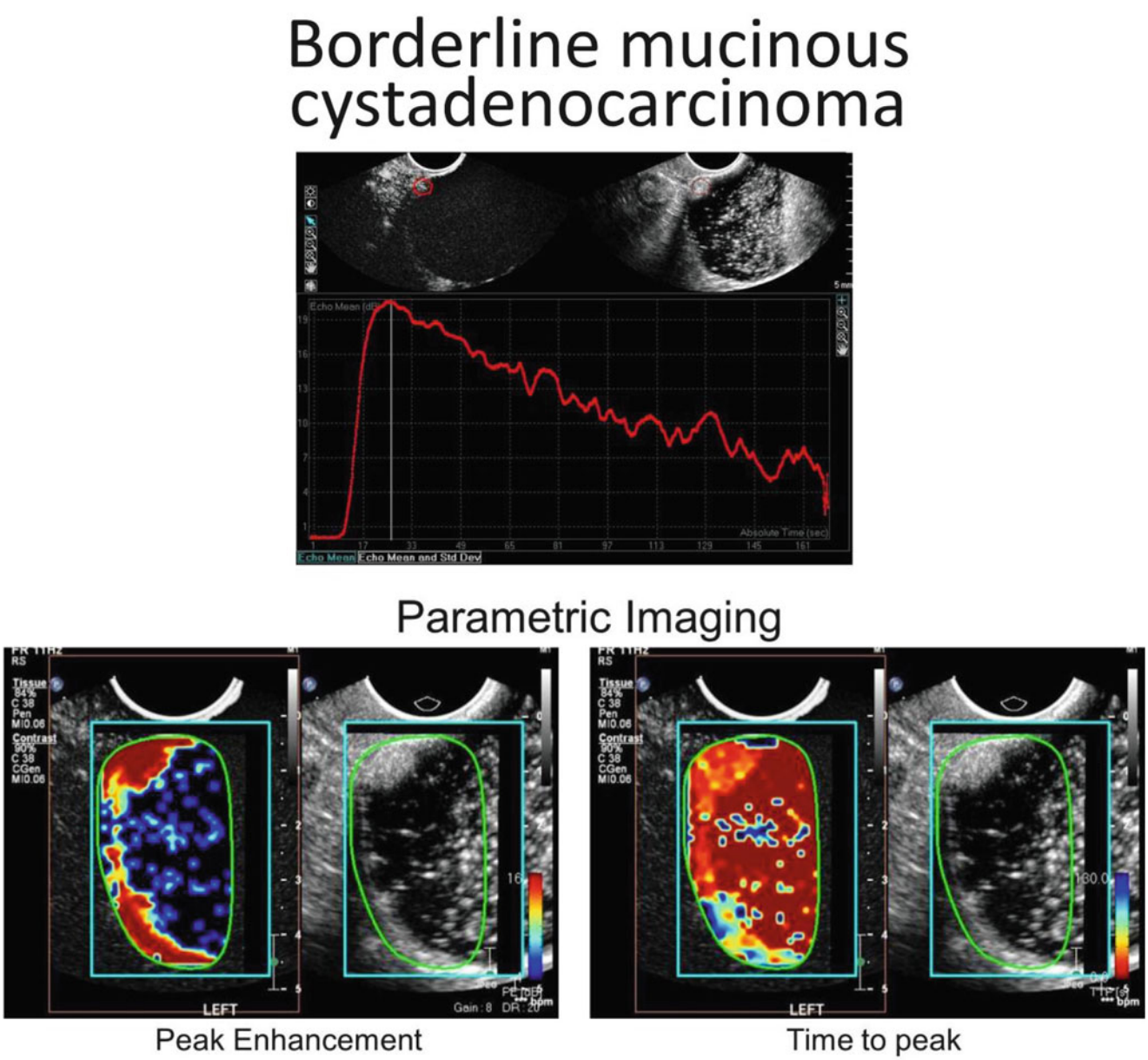

Fig. 8 CE-TVS of a complex mass with mobile echogenic material and a mural nodule (indicated in *red* as region of interest). There is relatively high peak enhancement, long washout, and relatively large area under curve. This was a borderline serous cystadenocarcinoma. (*Top*) Time intensity curve and images shows a cystic mass with a mural module containing echogenic material. (*Bottom*) Parametric images showing focal increased peak enhancement in area of papillary excrescence (*left*) and relatively fast time to peak (*right*)

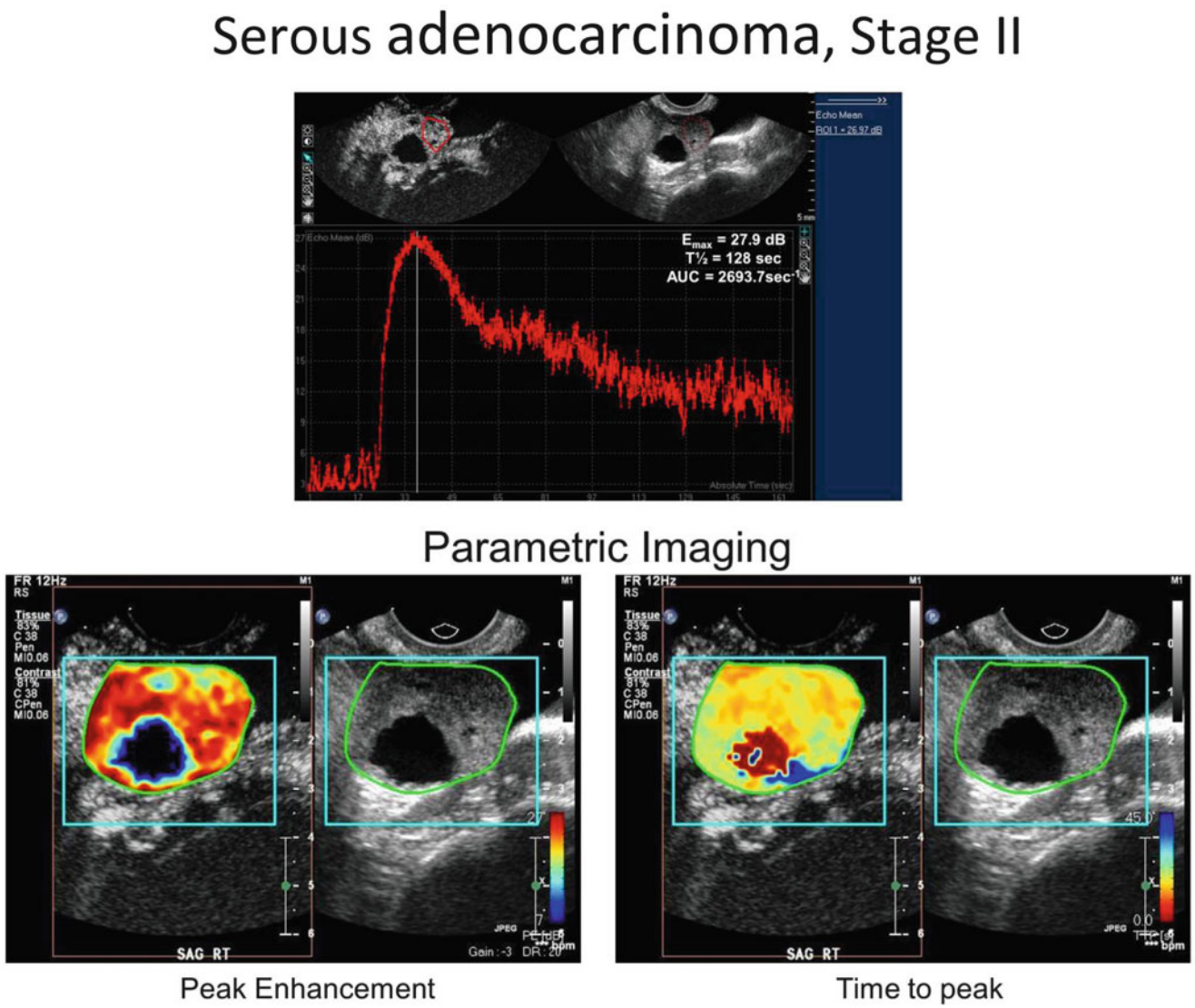

Fig. 9 CE-TVS of a normal-sized ovary containing a small cystic area. Time intensity curve showing high peak enhancement (27 dB), long ½ washout (128 s), and larger area under curve (2,694 s^{-1}). This was a stage II serous cystadenocarcinoma. (*Top*) Time intensity curve and images showing normal-sized ovary containing 1 cm cystic area. (*Bottom*) Parametric map showing high peak enhancement (*left*) and short time to peak (*right*)

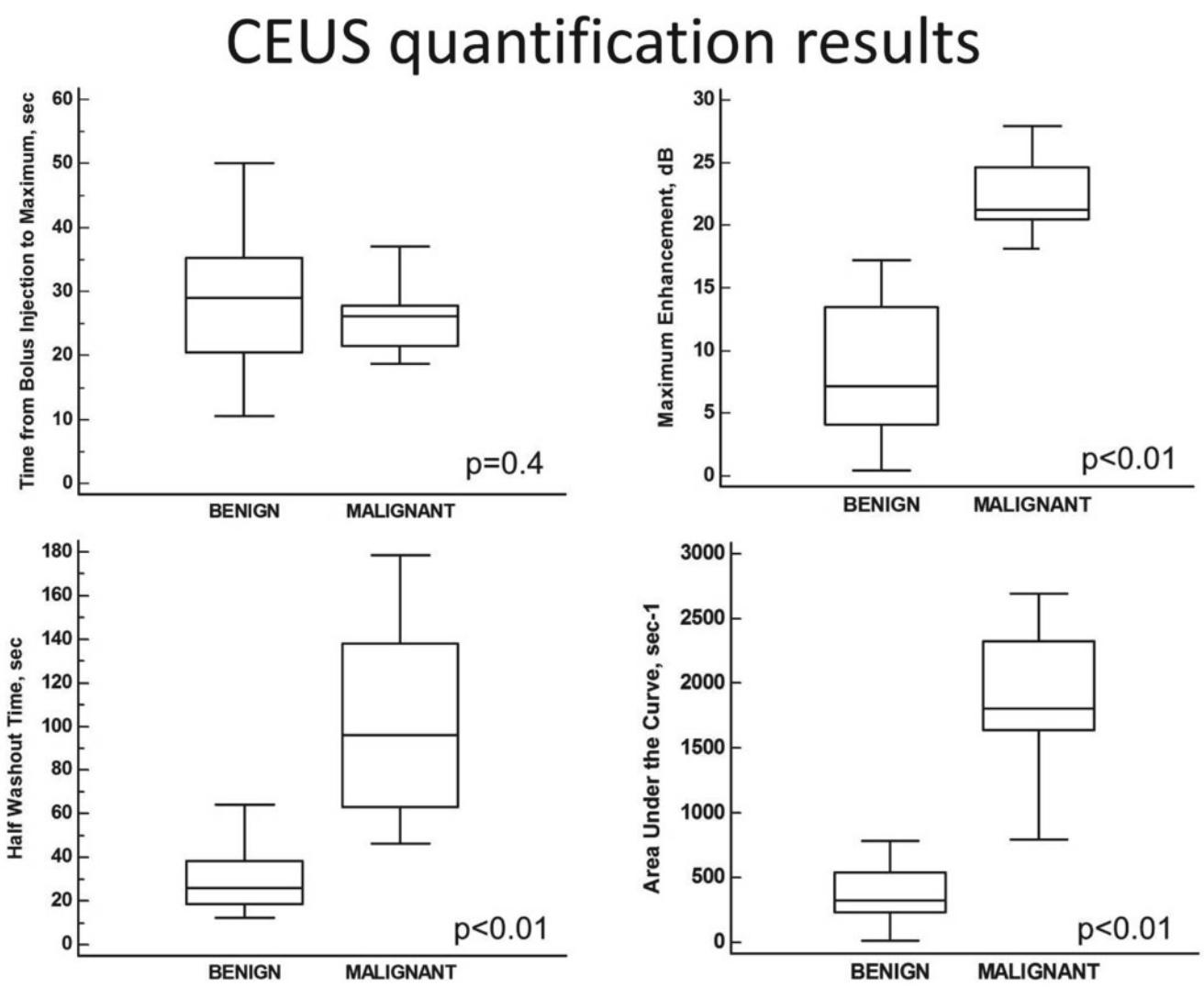

Fig. 10 Bar graphs of mean, range, and standard deviation of enhancement parameters. Differences in time to peak (*top left*), peak enhancement (*top right*), washout time (*bottom left*), and area under curve (*bottom right*) in benign ($n=44$) and malignant ($n=13$) ovarian masses. Except for time to peak ($p=0.4$), peak enhancement, washout, and area under the curve, there were statistically significant ($p<0.01$) differences in the two groups

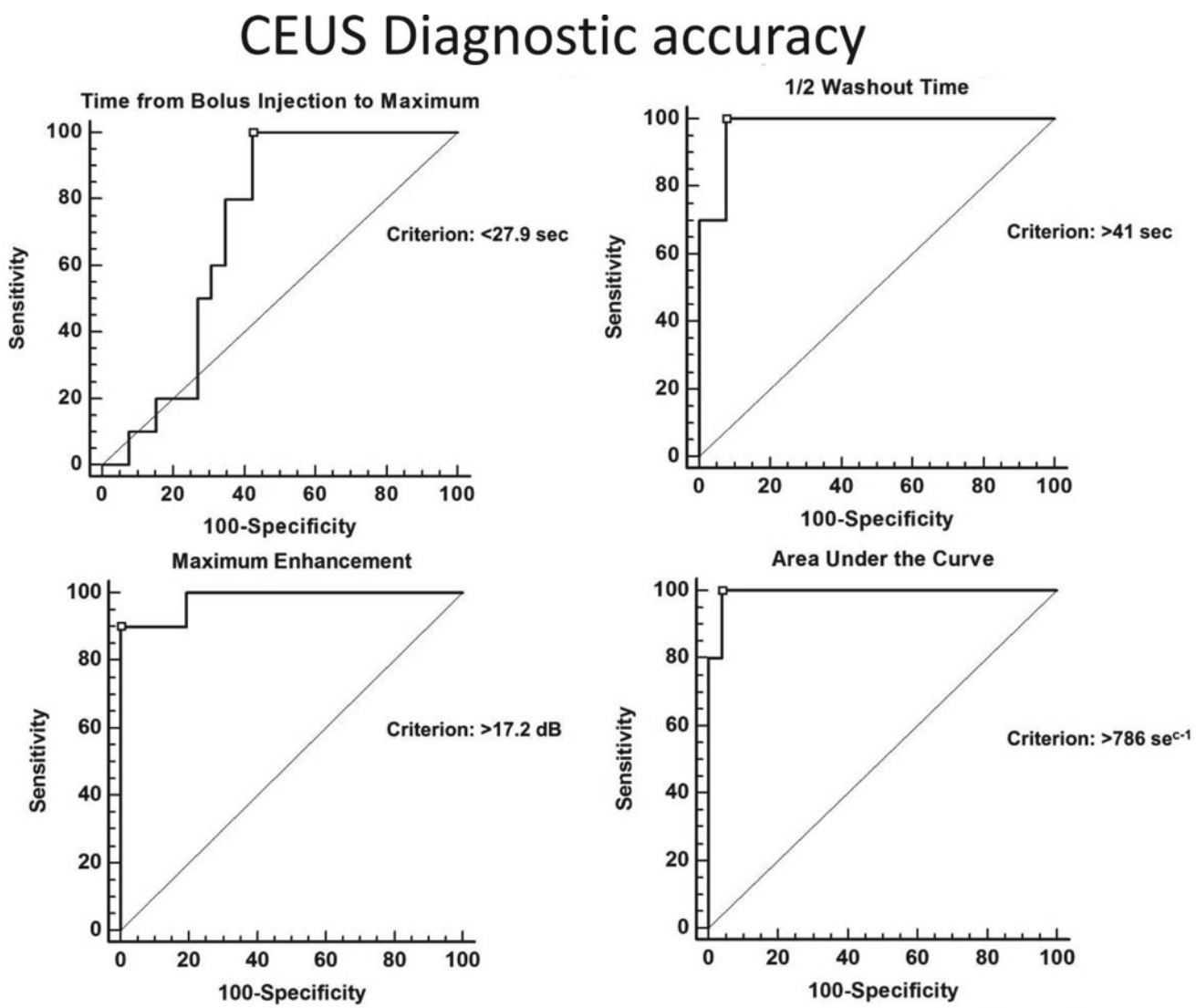

Fig. 11 Receiver operator curves for time to peak (*top left*), maximum enhancement (*bottom left*), washout time (*top right*), and area under curve (*bottom right*). Cutoff values are shown

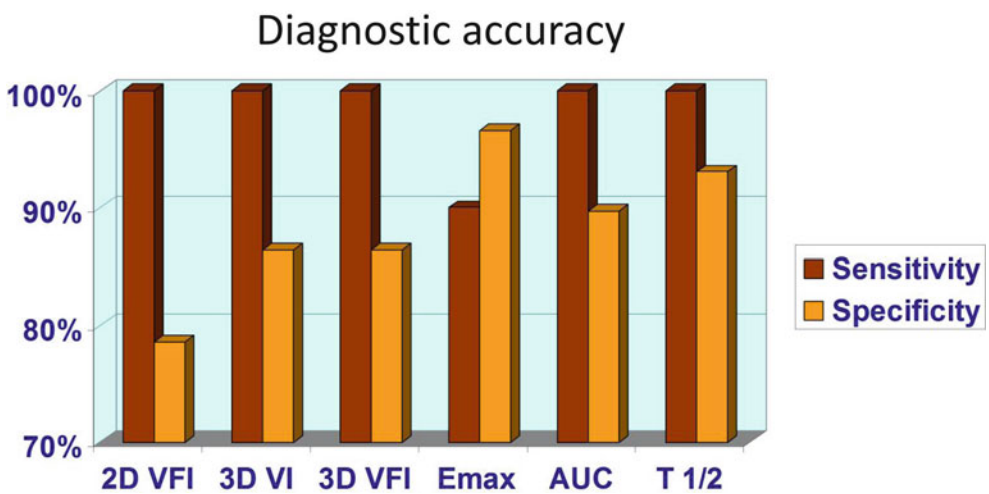

Fig. 12 Comparison of diagnostic accuracy of CE-TVS with 2D/3D color Doppler. CE-TVS has greater specificity

Acknowledgement This study was supported by National Institute of Health/National Cancer Institute, Grant r21 125 227–01

References

1. Valentin L. Prospective cross-validation of Doppler ultrasound examination and gray-scale ultrasound imaging for discrimination of benign and malignant pelvic masses. Ultrasound Obstet Gynecol. 1999;14:273–83.
2. Folkman J, Watson K, Ingber D, Hanahan D. Induction of angiogenesis during the transition from hyperplasia to neoplasia. Nature. 1989;339:58–61.
3. Wilson SR, Greenbaum LD, Goldberg BB. Contrast-enhanced ultrasound: what is the evidence and what are the obstacles? AJR Am J Roentgenol. 2009;193:55–60.
4. Orden MR, Jurvelin JS, Kirkinen PP. Kinetics of a US contrast agent in benign and malignant adnexal tumors. Radiology. 2003;226:405–10.
5. Marret H, Sauget S, Giraudeau B, et al. Contrast enhanced sonography helps in discrimination of benign from malignant adnexal masses. J Ultrasound Med. 2004;23:1629–42.
6. Testa AC, Ferrandina G, Fruscella E, et al. The use of contrasted transvaginal sonography in the diagnosis of gynecologic diseases: a preliminary study. J Ultrasound Med. 2005;24:1267–78.
7. Fleischer AC, Lyshchik A, Jones Jr HW, et al. Contrast-enhanced transvaginal sonography of benign versus malignant ovarian masses: preliminary findings. J Ultrasound Med. 2008;27: 1011–21.
8. Fleischer AC, Lyshchik A, Andreotti RF, et al. Advances in sonography detection of ovarian cancer: depiction of tumor neovascularity with microbubbles. AJR Am J Roentgenol. 2010;194:343–8.
9. Testa AC, Timmerman D, Belle VV, et al. Intravenous contrast ultrasound examination using contrast-tuned imaging (CnTITM) and the contrast medium SonoVue® for discrimination between benign and malignant adnexal masses with solid components. Ultrasound Obstet Gynecol. 2009;34:699–710.
10. Veyer L, Marret H, Bleuzen A, et al. Preoperative diagnosis of ovarian tumors using pelvic contrast-enhanced sonography. J Ultrasound Med. 2010;29:1041–9.
11. Fleischer AC, Lyshchik A, Hirari M, et al. Early detection of ovarian cancer with conventional and contrast-enhanced transvaginal sonography: recent advances and potential improvement. J Oncol. 2012;2012:302858, 11p.

Molecular Imaging of Ovarian Carcinoma

Lucia M.A. Crane, Rick G. Pleijhuis, Marleen van Oosten, and Gooitzen M. van Dam

Abstract

Molecular imaging literally means visualization of molecules but more generally comprises a number of techniques used to visualize single cells or clusters of cells, cell processes and individual receptors and other biomarkers. Its applications are multiple, ranging from imaging of a single biomarker to following tumour growth in time.

In cancer, molecular imaging can be applied in both diagnostics and therapy. The main goal in oncology is to differentiate tumour cells from healthy cells in order to reduce tumour load and, subsequently, morbidity. This will be addressed in this chapter, together with the basic requirements and techniques in molecular imaging, with the focus on the preclinical and clinical application in ovarian cancer.

Keywords

Epidemiology • Epithelial ovarian cancer • Molecular imaging • Bioluminescence imaging • Photoacoustic imaging • Radioguided imaging • Photodynamic therapy

Introduction Molecular Imaging in Cancer

Molecular imaging literally means visualization of molecules but more generally comprises a number of techniques used to visualize single cells or clusters of cells, cell processes and individual receptors and other biomarkers. Its applications are multiple, ranging from imaging of a single biomarker to following tumour growth in time.

L.M.A. Crane, MD, PhD (✉) • R.G. Pleijhuis, MD
M. van Oosten, MD • G.M. van Dam, MD, PhD
Division of Surgical Oncology,
Department of Surgery, BioOptical Imaging Center,
University Medical Center Groningen/University of Groningen,
Hanzeplein 1, 9700 RB Groningen, The Netherlands
e-mail: l.m.a.crane@umcg.nl;
g.m.van.dam@umcg.nl

In cancer, molecular imaging can be applied in both diagnostics and therapy. The main goal in oncology is to differentiate tumour cells from healthy cells in order to reduce tumour load and, subsequently, morbidity. Selective imaging of tumour cells can be beneficial in staging, either laparoscopically or through targeted radioguided imaging. Intraoperative-targeted imaging could aid the surgeon in detecting small metastases and determining resection margins, thus yielding a more complete cytoreduction while leaving healthy tissue relatively unharmed. Intraoperative imaging was previously limited to radioguided techniques such as PET and SPECT, but optical imaging becomes more and more implemented.

Additionally, tumour-targeted chemotherapy would reduce morbidity as healthy cells are left unharmed. Targeted therapy does not require imaging, but identification of tumour-specific targets can lead to multiple targeted strategies, both for imaging and therapy. All the above-mentioned items will be addressed in this chapter, together with the basic requirements and techniques in molecular imaging,

L. Saba et al. (eds.), *Ovarian Neoplasm Imaging*,
DOI 10.1007/978-1-4614-8633-6_30,

with the focus on the preclinical and clinical application in ovarian cancer.

Techniques in Molecular Imaging

Bioluminescence Imaging

One of the first applications to detect tumour cells using light was by using bioluminescence. Bioluminescence imaging (BLI) refers to light produced by living organisms in an enzymatic reaction. Examples from nature in which the emission of light is clearly visible are the common glow-worms (*Lampyridae sp*.; luciferase gene) and more specifically the North American firefly (*Photinus pyralis*) and several types of jellyfish (*Aequorea sp*.).

BLI can be induced in vivo by incorporating a luciferase gene, generally *Fluc* from the *Photinus pyralis*, into the DNA of living cancer cells. Injection of these cells into a laboratory animal will lead to the development of a bioluminescent tumour. Emission of light does not take place until the enzymatic substrate D-luciferin is added. In the presence of ATP and magnesium, luciferase will catalyse oxidation of the luciferin, thus leading to the emission of photons. The signal is generally measured in a small animal imager that provides colour and BLI images superimposed onto each other (Fig. 1). BLI makes it possible to follow tumour growth longitudinally in the same animal, as D-luciferin can be added at any given point in time without the need to sacrifice the animal. Furthermore, the technique yields a high tumour-to-background ratio because non-tumour cells do not express the Fluc gene and therefore do not emit light. However, the need for genetic alterations makes this approach unsuitable for clinical application. Also, the signal imaged at the surface lacks information on the exact size and depth of the tumour, as a small but deeply seated tumour can bring about a much broader but weaker signal on the surface, compared to the stronger but more condensed signal coming from a superficially located tumour (Fig. 2). As penetration of light is limited, imaging of tumour tissue to a depth of >1 cm is problematic, if not impossible.

Fluorescence Imaging

Fluorescence (i.e. optical) imaging (FLI) can be either direct or indirect. Direct FLI is performed by integrating a transporter gene, often that of green fluorescent protein (GFP), into the organism. The fluorescent protein that is produced upon transcription of the gene can subsequently be imaged.

Indirect FLI does not require genetic alterations, as imaging is performed using an externally administered fluorescent substance, such as a fluorescently labelled antibody

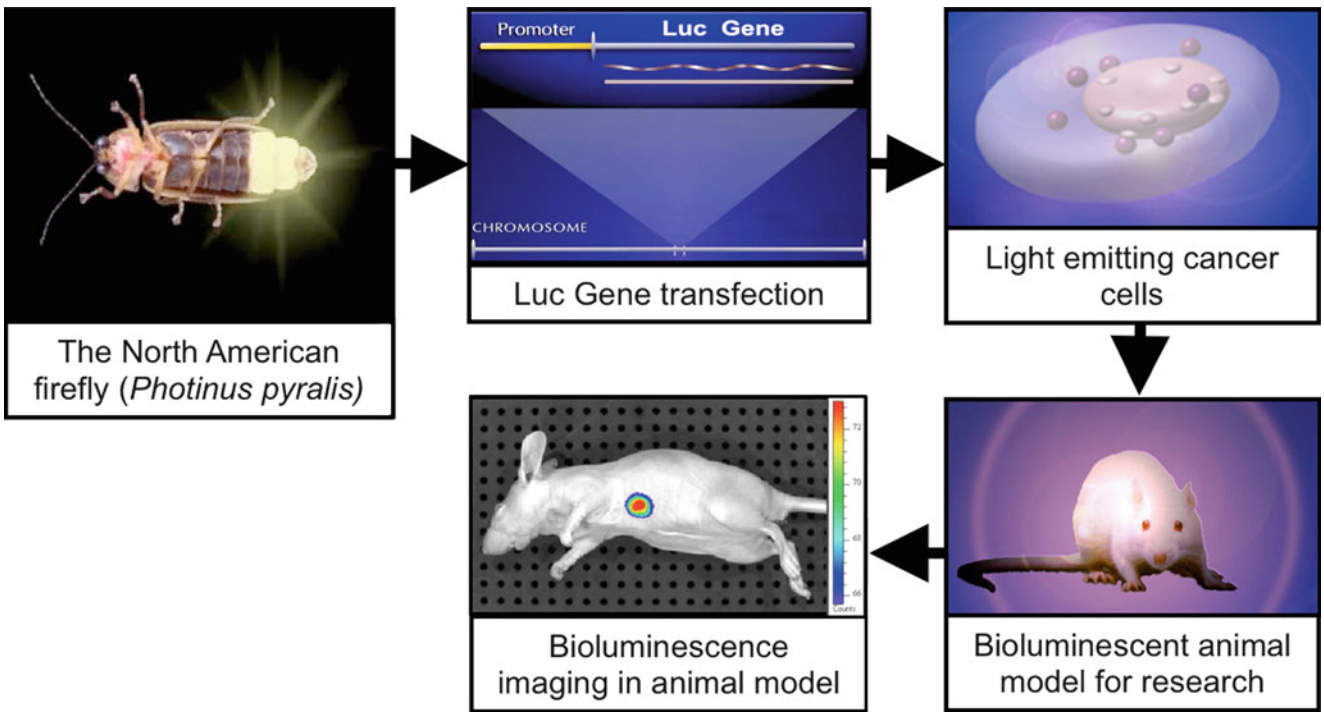

Fig. 1 Principle of BLI

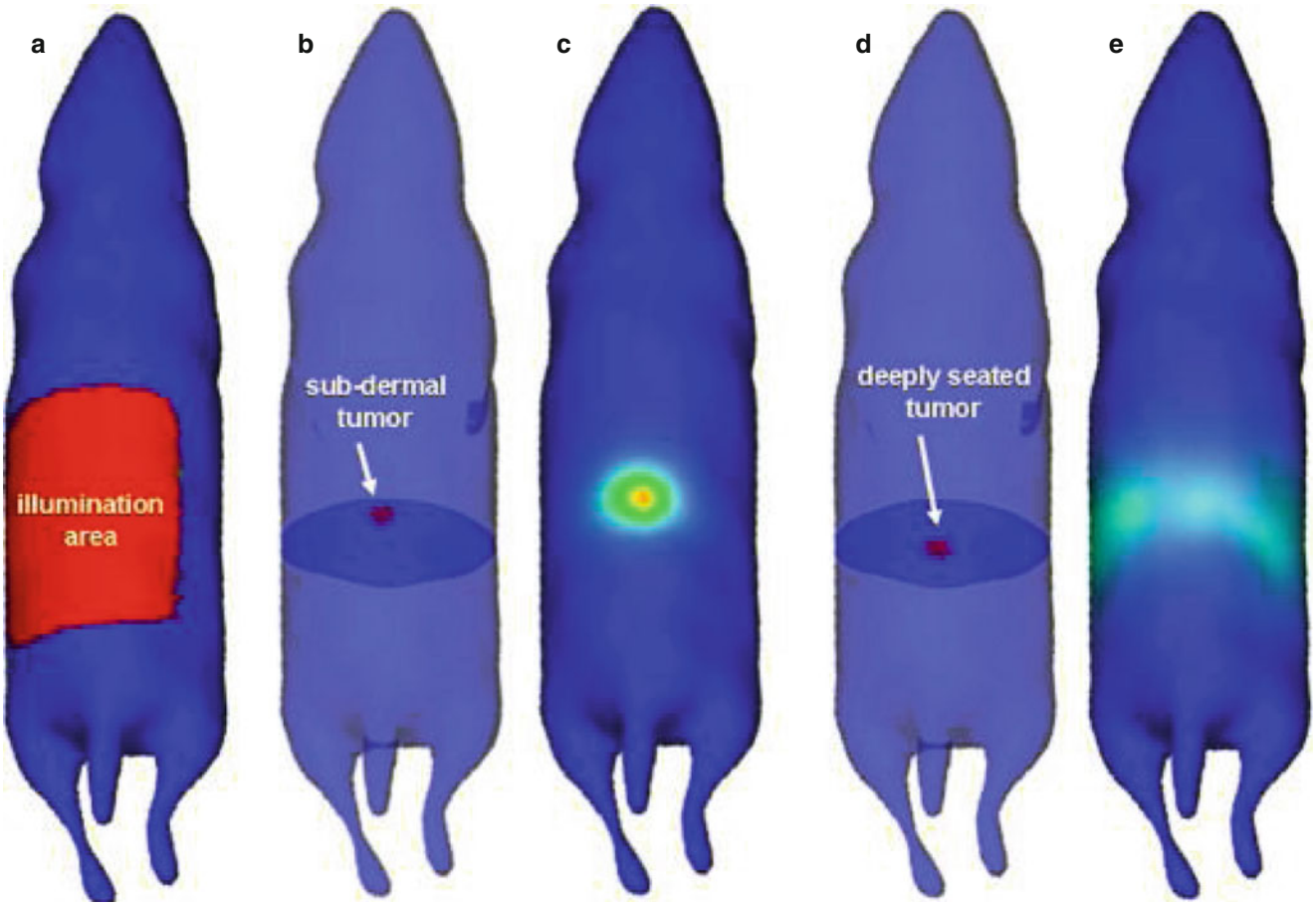

Fig. 2 Non-linear relation between tumour depth and optical signal (Figure from Leblond et al. [114])

or small molecule or simply by injecting solely the fluorescent compound. Upon binding to its target receptor, the fluorescently labelled agent will yield a signal that is specific for cells that carry the target. Nontargeted fluorescent dye such as indocyanine green (ICG) can be used in perfusion studies and to detect the sentinel lymph node in cancer surgery [1–4]. Upon excitation of the fluorescent dye with light of the appropriate wavelength, the electrons shortly reach a higher energy state by absorbance of one or more photons. This phase ends with the emission of a photon with lower energy and thus a slightly higher wavelength and return of the electron into its stable state (Fig. 3). The emitted light can be captured with a fluorescence camera system.

As mentioned above, light in the NIR range is most suitable for in vivo imaging. There are multiple examples of in vitro FLI using an agent that emits in the visible spectrum, mostly based on fluorescein, but results in vivo are far more sensitive when using a NIR fluorescent agent. This light is not visible without sensitive charge-coupled device (CCD) cameras, most of which now combine colour imaging and FLI. Similarly to BLI, both images can be superimposed to help accurately locate the fluorescent signal in the organism (Fig. 4). FLI shares the disadvantages of BLI of having limited tissue penetration and the inability to draw conclusions about tumour size and depth.

Fluorescence Epi-illumination and Transillumination

Most imaging studies are performed using epi-illumination, meaning that the light source for excitation is on the same side of the subject as the CCD camera that translates the emitted signal to an image. Conversely, transillumination refers to a light source opposite from the camera, thus passing the light through the image (Fig. 5) [5]. A shortcoming of the latter is the limited penetration of photons through tissue; adipose tissue in particular, thus making it unsuitable for clinical application. Epi-illumination is often used in preclinical studies because of its simplicity and because scattering and penetration are of limited concern in small animals. In clinical studies in which the subject is located either subcutaneously or in direct view of the CCD camera, for instance, during surgery, epi-illumination is the technique of choice.

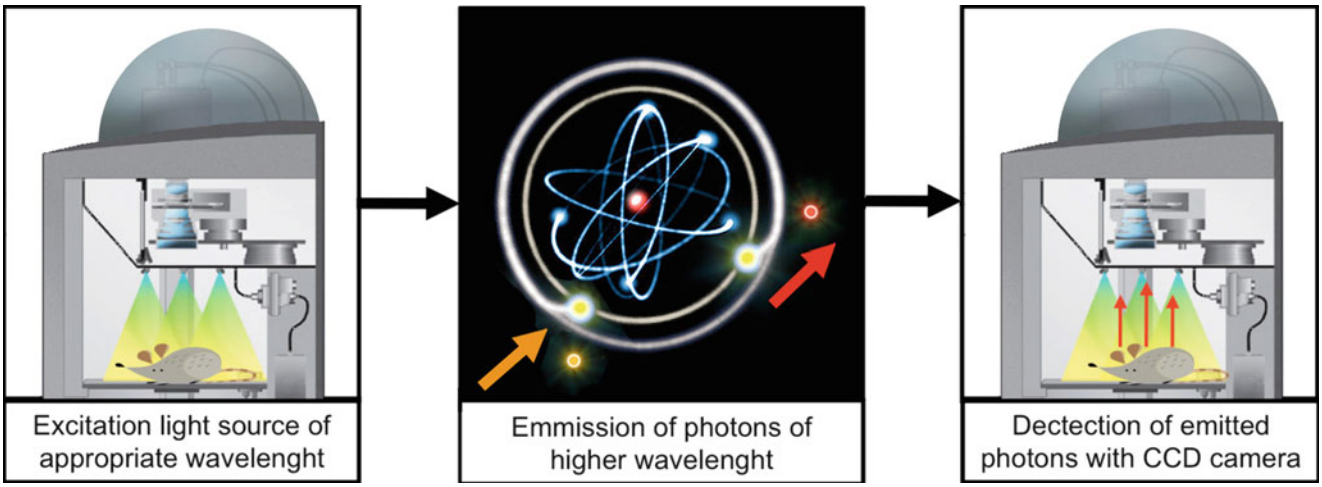

Fig. 3 Principle of FLI

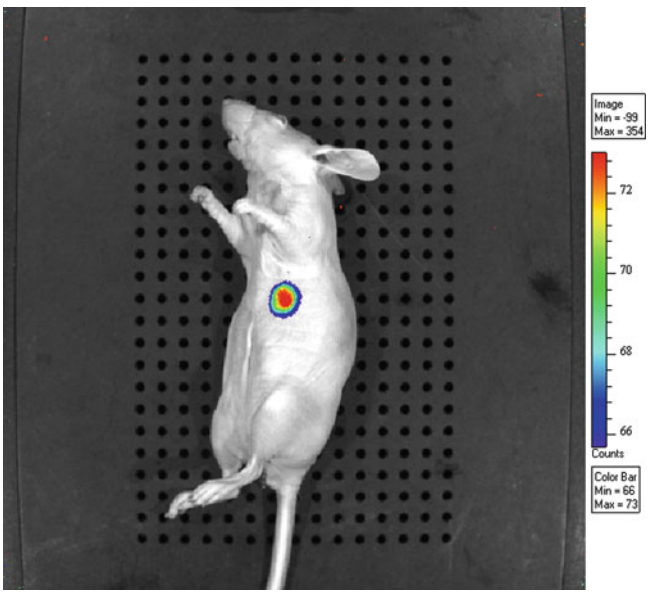

Fig. 4 BLI signal superimposed on color image (depicted in greyscale)

Fluorescence Molecular Tomography

In fluorescence molecular tomography (FMT), the emitted light is measured in different directions. A mathematical calculation transfers this data into a 3D image of the fluorescent or bioluminescent signal within the small animal. Advantages over planar imaging are the ability to calculate volume and depth of the light-emitting tissue of interest. FMT is not used in clinical imaging as light propagation through tissue is limited.

Photoacoustic Imaging

A relatively new technique is photoacoustic imaging, in which the fluorescent agent is excited by light similar to FLI, whereupon thermal expansion causes the emission of ultrasound waves (Fig. 6) [6]. Similar to light propagation, ultrasound waves also suffer from scattering, albeit to a lesser extent. Due to this greater stability of the signal, photoacoustic imaging allows for deeper imaging than FLI, with a current penetration depth of more than 1 cm [7].

Although photoacoustic imaging is an attractive technique for small animal imaging and for imaging of relatively superficial tumours, its value for diagnosis of ovarian cancer is probably low, as tumours and affected lymph nodes are located deep inside the pelvis.

Photodynamic Therapy

The last application of molecular imaging to be mentioned is photodynamic therapy (PDT), in which light is used to induce cell death. This is strictly not an imaging modality but is closely related as light is being used for a tumour-targeted therapeutic approach. A photosensitizer is activated by light of a specific wavelength, whereupon it initiates, in the presence of oxygen, a chemical reaction in which singlet oxygen ($1O_2$) and oxygen radicals are generated. These in turn provoke immediate cell damage in the form of apoptosis or necrosis or indirect cell death through vascular damage, ischemia and inflammatory reactions [8]. A natural photosensitizer is protoporphyrin IX (PPIX), produced by cells during the haem cycle. Synthetic photosensitizers and

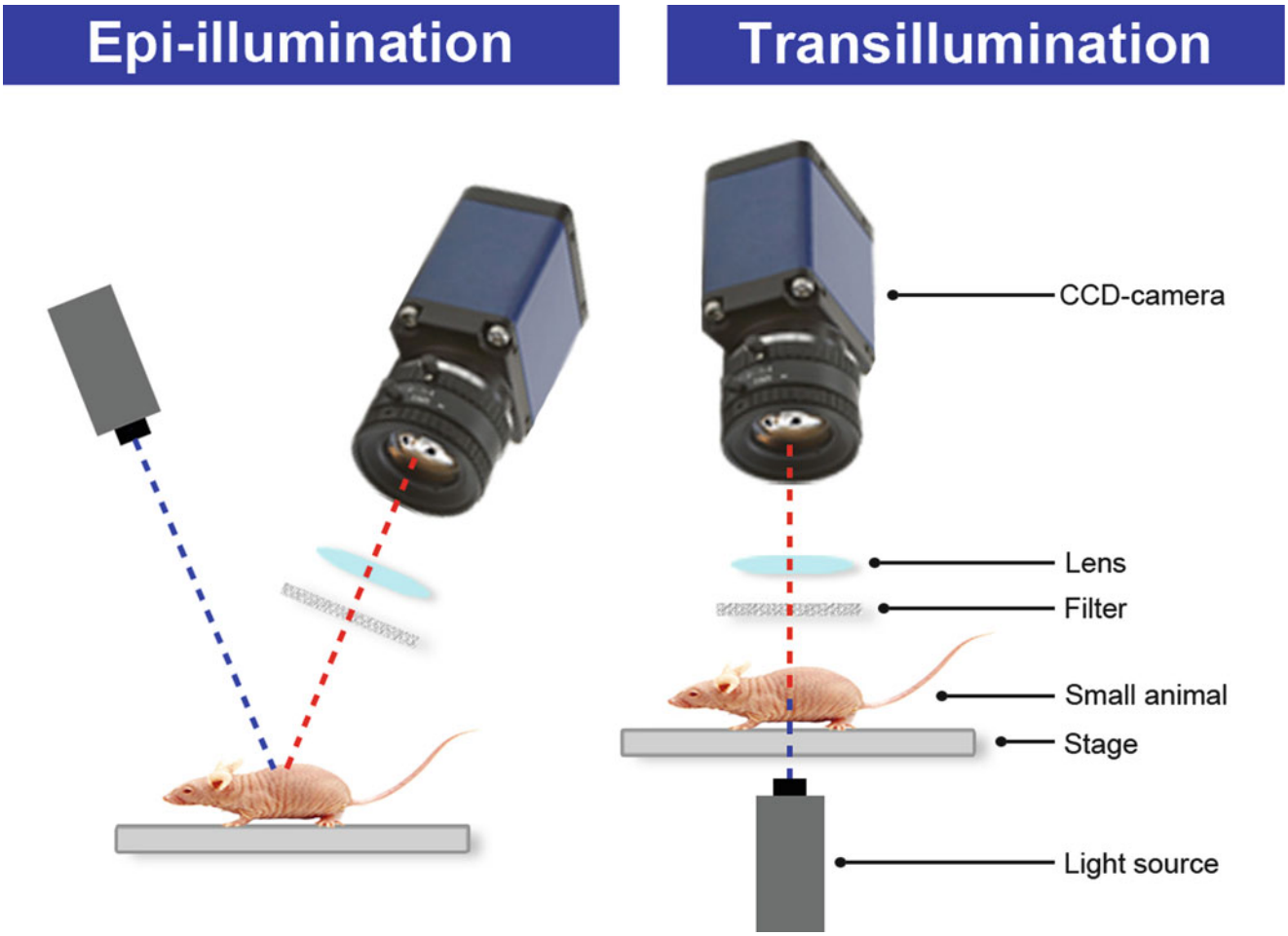

Fig. 5 Epi- and transillumination

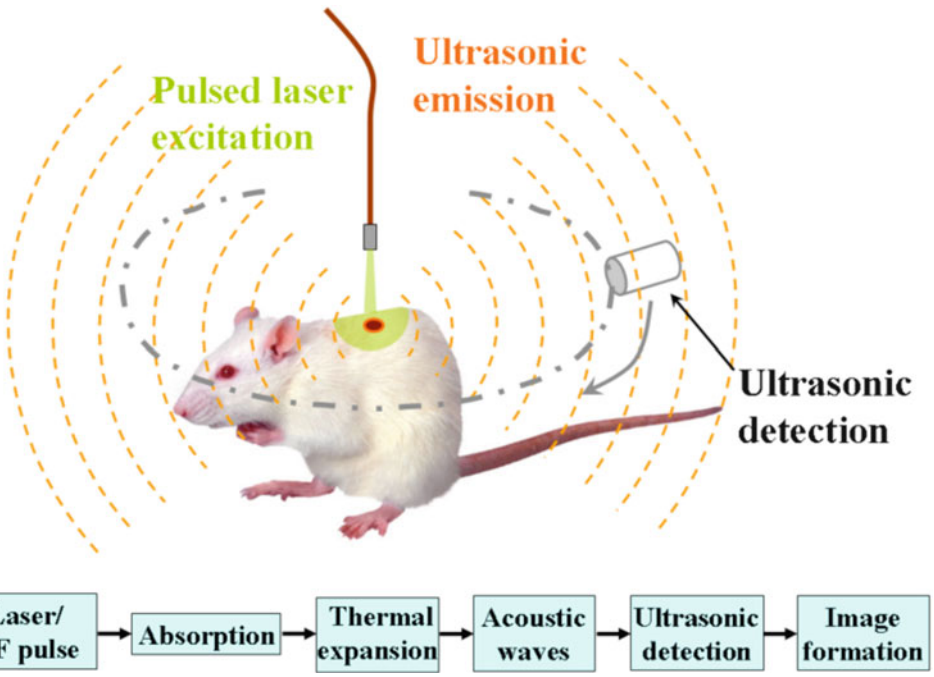

Fig. 6 Principle of photoacoustic imaging (Wikipedia)

prodrugs are increasingly being developed, with favourable characteristics for clinical application. The major disadvantage of PDT is phototoxicity in other tissues than the tumour, leading to strict living rules for patients and requiring a very well-designed illumination area. In case of a sprouting tumour, or a tumour close to vulnerable structures or organs, illumination can easily cause collateral damage, resulting in undesirable side effects.

Photo-immunotherapy (PIT) is a derivative from PDT in which the problem of harming surrounding structures is largely overcome. The photosensitizer is conjugated to a tumour-specific antibody, thus leading to tumour cell death only while leaving healthy tissue unharmed [9]. Unbound photosensitizer does not cause any phototoxicity.

Radioguided Imaging

Imaging plays an important role in cancer diagnosis and treatment follow-up. PET, SPECT, MRI, CT and combinations of these techniques are indispensable in clinical practice, and extensive research is performed to continuously improve sensitivity and specificity rates.

Positron Emission Tomography

In positron emission tomography (PET) scanning, gamma rays are used to detect a radionuclide that is taken up by certain molecules in the body. The most often used tracer is fludeoxyglucose conjugated to fluorine-18 (^{18}F-FDG), which is a derivative of glucose that enables visualization of metabolically active cells and cell processes. Tumours and metastases require large amounts of glucose to support their high expansion rate; however, glucose uptake is not cancer specific. Tumour-specific PET scanning, using an antibody bound to a radioactive label, is now increasingly being performed in order to discriminate healthy tissue from malignant processes [10].

Single-Photon Computed Tomography

Similar to PET, single-photon emission computed tomography (SPECT) makes use of gamma rays to visualize the distribution of a radioisotope within the body. Its resolution of 1 cm performs worse than PET; however, the technique is significantly less expensive. Targeted SPECT can be performed similar to targeted PET, by using radiolabelled antibodies. Both PET and SPECT are often coupled to a CT scan for assessment of exact anatomical localization of lesions.

Magnetic Resonance Imaging

Magnetic resonance imaging (MRI) produces a large magnetic field that forces protons (H^+; abundantly present in water molecules) in the body to align in the same direction. Short exposure with an electromagnetic field makes the protons flip and then realign, in which electromagnetic radiation is produced that is measured and processed into an image. MRI contrast agents, most based on gadolinium, are used to improve the signal from tumours, blood vessels or other specific tissues or structures. For several years, the use of iron oxide particles was considered feasible for imaging of solid tumours; however, most tracers are no longer produced because of safety matters.

Conjugation of ligands to gadolinium with the use of a chelator, often DTPA, yields tumour-specific MRI contrast agents that are likely to improve diagnostic accuracy [11].

Requirements for Molecular Imaging

In molecular imaging, the use of a sensitive detection system is essential to obtain adequate signal-to-noise ratios. Moreover, except in the case of bioluminescence and intrinsic fluorescence, a fluorescent agent with or without a target is required as well as an excitation light source of the appropriate wavelength.

Fluorescent Agent

The fluorescent agent can be either naturally expressed by a cell or organism or exogenously administered. Indirect fluorescence can range from staining of cells in vitro with, for instance, DAPI, in order to detect nuclei by fluorescence microscopy, to intraoperative detection of metastases in patients.

Virtually all objects emit fluorescent light to a certain level, albeit not visible by the naked eye because the signal is by far not strong enough to compete with the visible light. Fluorescence in the visible light spectrum (400–750 nm) is less suitable for imaging purposes, as background fluorescence is high. In contrary, imaging in the near-infrared (NIR) spectrum (750–1000 nm) yields a high signal-to-background ratio, as autofluorescence is minimized (Fig. 7). In living organisms, light <700 nm is to a great extent absorbed by haemoglobin, while wavelengths longer than 950 nm suffer from absorption by water (Fig. 8). Fluorescent agents that emit light in the NIR range are therefore most suitable for in vivo application [5]. Lower wavelengths cause damage in DNA and are therefore not used.

There are three types of fluorescent agents. First, non-specific fluorescent dyes that do not bind to cells but flow along with bodily fluids (blood, lymph or gall). These can be used for perfusion studies or to identify the sentinel lymph node in cancer. Second, targeted agents are fluorescent dyes that are conjugated to a small molecule or antibody that is directed at a certain biomarker. This allows for tissue-specific or tumour-specific imaging. Third, activatable probes do not emit light until cleaved by the appropriate enzyme (Fig. 9). Currently, only three fluorophores are approved for clinical

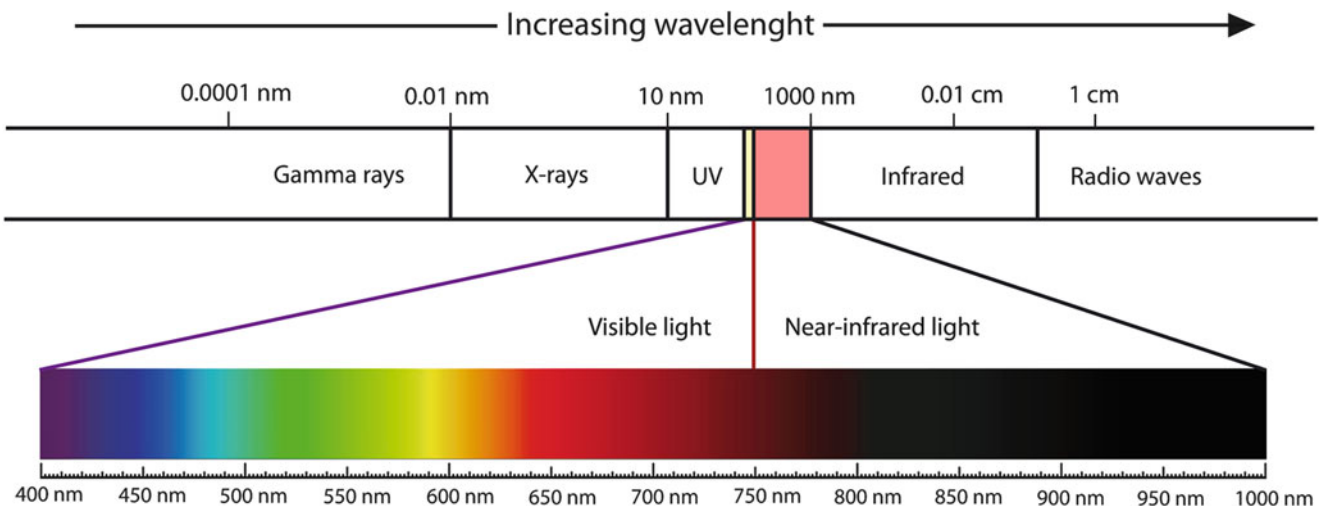

Fig. 7 NIR spectral range

Fig. 8 Absorption in NIR spectral range

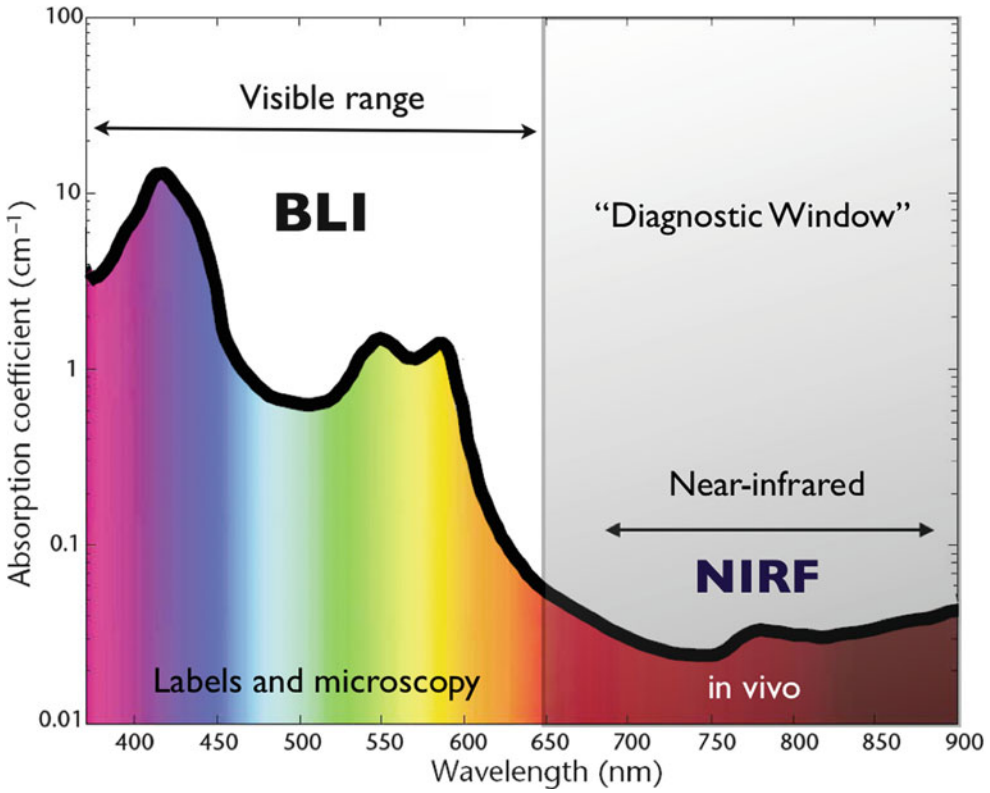

use: indocyanine green (ICG), fluorescein isothiocyanate (FITC) and IRDye800CW [12].

Light Source and Imaging System

Because the human eye is incapable of detecting NIR light, a specialized imaging system is needed to transfer the fluorescence data into an image. Generally, the imaging system consists of one or multiple laser beams of a specific wavelength for excitation. The subsequently emitted signal is captured by a series of lenses and filters and processed by a sensitive charge-coupled device (CCD) camera. With the help of mathematical algorithms and software, most systems provide both a colour image and a fluorescence image. Some, but not all, are capable of superimposing the two, yielding an accurate representation of the fluorescent signal in the background. The list of

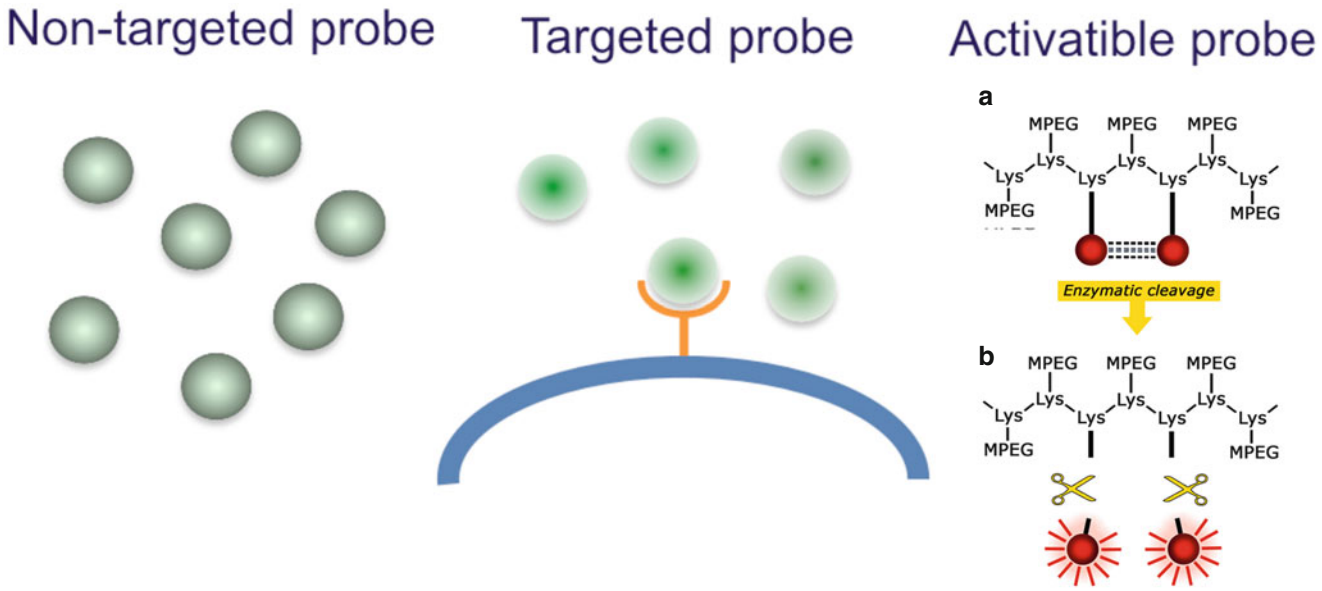

Fig. 9 Fluorescent agents: non-specific, targeted, activatable

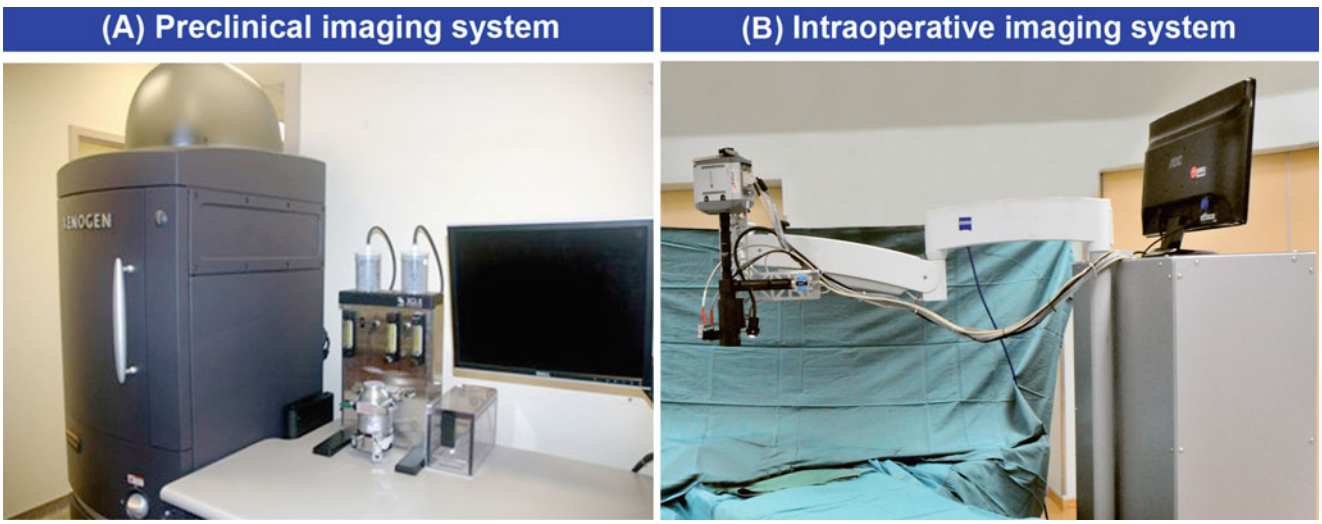

Fig. 10 Preclinical (**a**) and clinical (**b**) imaging systems

imaging systems is long, with both preclinical and clinical cameras on the market (Fig. 10). In the following sections on preclinical and clinical imaging, the relevant systems will be mentioned.

Targeted Imaging in Ovarian Cancer

Target Selection

In cancer treatment, the goal is to differentiate tumour cells from healthy cells. This requires the identification of tumour-specific biomarkers that can serve as targets for either fluorescent agents or targeted (chemo)therapy.

No validated system to select biomarkers has been designed yet, but a number of favourable characteristics can be mentioned [13]. (I) Tumour selectivity can only be achieved if the biomarker is present on malignant cells and absent or only weakly expressed by healthy cells, thus yielding a high tumour-to-normal ratio. (II) Both targeted imaging and (chemo)therapy require the majority of tumour cells to express the biomarker in a diffuse pattern (III). Although cell death can induce apoptosis in neighbouring cells, heterogeneous expression can lead to parts of the tumour being

missed because overall expression is not sufficient. From an economical perspective, biomarkers that are present on the majority of tumours (i.e. in a majority of patients) are preferable. (IV) An extracellular or transmembraneous localization facilitates binding, while internalization (V) leads to accumulation and thus a higher fluorescent signal or a stronger chemotherapeutic effect. (VI) Enzymatic activity is needed when using activatable probes. (VII) For imaging purposes, a biomarker that has already been used in vivo and has shown no toxicity is favourable, as this may shorten the road to clinical application.

Targets in Ovarian Cancer

In ovarian cancer, numerous targets have been described for molecular imaging. However, most are far from implementation in the clinical setting due to lack of toxicity data. A small number of targets have been validated in either preclinical or clinical studies. In this section, only the biomarkers that are suitable for imaging are discussed.

CA-125

Tumour marker CA-125, or MUC16, is expressed in more than 95 % of non-mucinous stage III–IV epithelial ovarian tumours and is used for diagnosis as well as for treatment evaluation and follow-up [14]. Oregovomab is a monoclonal antibody directed at both membrane-bound and soluble CA-125 and has been studied in a number of preclinical and clinical pilot studies. Although the toxicity profile shows that the antibody is safe in the short term and after a 5-year follow-up, no clinical survival benefits can be shown, leaving the exact value of oregovomab unclear [15]. However, an antibody approved for clinical use with a target that is overexpressed in 95 % of tumours may have potential value as a fluorescent agent when conjugated to a near-infrared dye. In the case of oregovomab, this is still entirely theoretic but plausible.

Carbonic Anhydrase IX

Carbonic anhydrase IX (CA-IX) is a hypoxia-related transmembrane protein that is present in several solid tumours and upregulated in ovarian cancer [16, 17]. Staining studies show mainly upregulation in hypoxic areas. Although CA-IX inhibitors have been used as PET imaging agents [18], the focal expression may hamper intraoperative optical imaging as non-hypoxic areas may be overlooked. Nonetheless, CA-IX could turn out to be a feasible target in other diseases, such as vulvar cancer, in which lymph node metastases were found to overexpress the marker [19]. Molecular targeting of CA-IX has already been performed in a mouse model [20]. A number of monoclonal antibodies are now available for preclinical testing; possibly one of these will find its way to the clinic for both therapeutic and imaging purposes.

CXC Chemokine Receptor 4

Chemokine receptor pairs play an important role in tumour metastasis, which is thought to start with the loss of adhesion molecules and degradation of the extracellular matrix. The CXC chemokine receptor 4 (CXCR4) and its chemokine CXCL12 or stromal cell-derived factor 1 (SDF-1) are known to be involved in dissemination of several solid tumours [21–23]. Although not specific for ovarian cancer, MMP and CXCR4-CXCL12 are indicative of metastatic tissue and are therefore worth exploring as targets for imaging, as complete cytoreduction includes removal of metastatic tumour nodules.

The CXCR4-CXCL12 pair seems to be more important than other chemokine receptor pairs in ovarian cancer and is associated with a worse prognosis [24]. This pathway promotes chemotaxis of tumour cells to the metastatic site, where it subsequently facilitates hatching and proliferation. Upon binding to CXCR4, CXCL12 is internalized, after which the receptor is recycled and transported back to the cell membrane within 15 min. Staining studies in ovarian cancer showed CXCR4 staining in 59 % of tumour cells and CXCL12 staining in 91 % of tumour cells, whereas no expression was found in healthy cells [25]. CXCL12 is also found in ascites, where it contributes to peritoneal dissemination.

Imaging of the CXC receptor has been performed by using a CXCR4-directed fluorophore in in vitro models [26, 27]. In vivo imaging in a brain tumour mouse model showed tumour uptake of a CXCR4-radiolabelled monoclonal antibody [28]. Furthermore, the CXCR4 antagonist ADM3100 conjugated to either ^{99m}Tc or ^{64}Cu proved useful in PET localization of tumour xenografts in mice [29, 30]. Due to favourable dosimetry results, introduction into the clinic may be close. As described above, optical imaging requires conjugation of a biomarker to a fluorescent agent and is more likely to be successful once the marker has already been used for imaging. The CXCR4-CXCL12 axis may therefore be an interesting target for fluorescence imaging in the (near) future.

Epidermal Growth Factor Receptor

The epidermal growth factor receptor (EGFR; HER1) plays a significant role in ovarian cancer, as most epithelial tumours express EGFR to some extent, leading to low survival rates [31–34]. Upregulation of EGFR leads to cell proliferation, differentiation, migration, adhesion, protection from apoptosis and malignant transformation [35]. HER1 and HER2 are expressed in 35–70 % and 11 % of epithelial ovarian tumours, respectively. HER1 is not only expressed by cancer cells but also by normal epithelial cells. However, expression rates in tumour are a reported 15–20 times higher, yielding a tumour-to-normal ratio that is high enough for tumour-selective imaging.

The anti-HER1 monoclonal antibody cetuximab is approved for chemotherapeutic treatment of metastatic colorectal cancer, while the anti-HER2 trastuzumab is being used for breast cancer treatment and for metastatic gastric cancer and panitumumab is approved for metastatic colorectal cancer. Dual-labelled radioactive/fluorescent trastuzumab showed comparable uptake in an ovarian cancer mouse model, indicating a possible role for clinical application [10]. Panitumumab-800CW was used for imaging of primary tumours and lymph node metastases smaller than 1 mm in a head-and-neck squamous cell cancer model, showing improved detection compared to panitumumab conjugated to non-specific IgG [36]. Furthermore, panitumumab-800CW and trastuzumab-ICG have been evaluated in an orthotopic breast cancer model [37]. Cetuximab and panitumumab imaging has been described in animal models, but none of these antibodies have been tested in a clinical imaging setting yet [38, 39]. The fact that there are at least three FDA-approved antibodies targeting EGFR, some with promising preclinical imaging data, may lead to faster translation of fluorescent agents into the clinic, for optical imaging of possibly both breast and ovarian tumours.

Epithelial Cell Adhesion Molecule

The epithelial cell adhesion molecule (EpCAM) is a cell surface receptor involved in cell adhesion and is expressed on most epithelial cells. Several solid tumours overexpress EpCAM. Primary epithelial ovarian tumours, metastases and recurrent tumours all show a significantly higher expression than normal ovarian tissue, in which expression on metastatic tumour cells is significantly higher than on malignant cells of the primary tumour [40]. High EpCAM expression is associated with increased tumour cell migration and portends poor survival [41].

Preclinical imaging has been described using an antibody fragment targeting EpCAM conjugated to a radionuclide for PET imaging, as well as near-infrared EpCAM-directed probes in breast and prostate cancer [42–44]. Even more interestingly, two FDA-approved monoclonal antibodies targeting EpCAM are now available; edrecolomab and catumaxomab. Although edrecolomab showed no clinical benefit in colorectal cancer, it has proven safe in clinical application. Both of these monoclonal antibodies bear potential for intraoperative imaging application, as the overexpression of EpCAM yields a high tumour-to-normal ratio. The value in vivo needs yet to be studied.

Folate Receptor

The folate receptor has been identified as a promising target in epithelial ovarian cancer (EOC), as 72–97 % of the tumours overexpress the alpha-isoform of the receptor (Fig. 11) [45, 46]. Furthermore, it is known that expression of FR-α is not influenced by adjuvant chemotherapy, allowing for FR-targeted imaging during primary as well as interval debulking surgery [47]. Its substrate folate, the natural form of folic acid in the body, is a small molecule that is suitable to deliver either imaging agents or chemotherapeutic drugs into the cell. Folate has a very high affinity for FR-α rather than for physiologic folate carriers on healthy cells, and the folate conjugate is easily internalized into the cell where it stays stable for hours in an endosome, before being broken down. Further advantages are that folate is inexpensive, nontoxic and easily to conjugate.

A number of radioactive and chemotherapeutic agents targeting the FR-α have been developed [48–50]. Nuclear imaging with ^{111}In-DTPA-folate shows uptake of the tracer in ovarian cancer and in the kidneys, where FR-α is physiologically expressed [51, 52]. A second nuclear tracer, ^{99m}Tc-folate, has also shown clear uptake in FR-α-positive tumour tissue [53, 54]. The FR-α-targeted monoclonal antibody farletuzumab is now in phase III trials and seems to be safe and effective in the treatment of platinum-resistant tumours [55, 56]. As FR-α is not only overexpressed by ovarian cancer cells but also by other malignancies, FR-targeted optical imaging is increasingly being studied. Several groups have reported the use of nanobodies to either visualize tumour cells or transport drugs into the tumour; however, this is still limited to preclinical research [57].

The only clinical study using FR-targeted optical imaging was presented in 2011 [58]. In this study, folate conjugated to fluorescein isothiocyanate (FITC) was used as a fluorescent agent. Patients with suspected ovarian cancer received an injection of folate-FITC 2 h prior to surgery, allowing for the agent to be taken up by the tumour. During the procedure, a custom-built intraoperative camera system was used to visualize FR-positive tumour cells. Peritoneal metastases as small as 1 mm were found with the aid of fluorescence (Fig. 12). All fluorescent tissue was proven to contain tumour cells, whereas nonfluorescent tissue did not contain malignant cells, and healthy tissue did not emit any fluorescence. This study shows the potential of intraoperative fluorescence imaging, as a significantly higher number of tumour spots were found based on fluorescence compared to surgery without optical imaging. The dye used, FITC, has an emission wavelength that lies just within the visible spectrum, and imaging is to a certain amount hampered by background fluorescence. FR-targeted agents using a NIR dye is expected to yield even better results.

Integrins

The integrin family comprises a great number of cell adhesion molecules including transmembrane glycoproteins that bind to a large variety of ligands, usually containing the RGD tripeptide (Arg-Gly-Asp). Multiple pathways can be activated upon binding: regulating cell proliferation, differentiation, apoptosis and migration. Almost all cells express

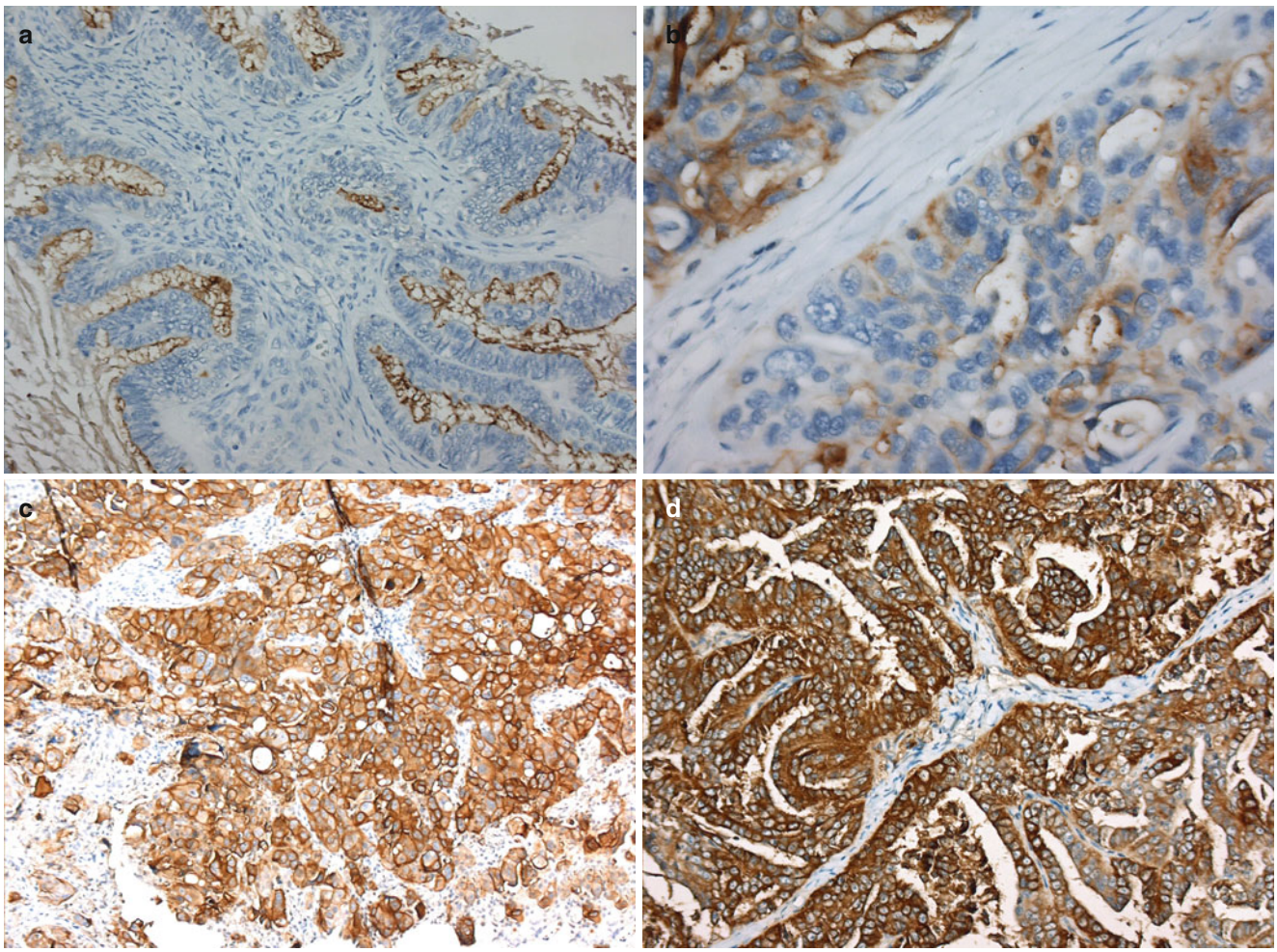

Fig. 11 Folate receptor-alpha expression in serous ovarian cancer. (**a**) No expression (negative), (**b**) weak expression, (**c**) moderate expression, (**d**) strong expression (Crane et al. [47])

integrins but generally not more than a few subtypes. In the normal ovary, integrins are thought to play an important role in follicular development and cell differentiation [59]. In tumorigenesis, integrins and matrix metalloproteinases (see next) activate and regulate each other, thus creating a positive feedback loop towards extracellular matrix degradation and metastasis. In the last decade, the importance of integrin subtype and vitronectin receptor αvβ3 has become clear, as it binds a specific metalloproteinase containing an RGD-sequence and as such creates a clear pathway for dissemination. Subsequently, an alternative pathway of cell migration is activated in which cell adhesion is disrupted and tumour cell invasion is facilitated. Furthermore, αvβ3 promotes angiogenesis, essential for tumour growth.

Integrins, and especially αvβ3, are increasingly being used for imaging purposes. Several studies report of αvβ3-specific binding in vitro and in vivo, some using a dual-labelled optical and PET imaging probe, some using only a near-infrared optical agent [60–64]. A few attempts have been made to target αvβ3 in humans, mainly with PET and SPECT tracers, in which tumours were clearly detected in contrast to liver and bone lesions [64–66]. The monoclonal antibody etaracizumab was shown in clinical phase 0/I studies to have an acceptable toxicity profile and might have potential as an imaging agent [67, 68].

Matrix Metalloproteinase

Matrix metalloproteinases (MMPs) facilitate tumour dissemination by degrading the extracellular matrix. Several MMP subtypes are overexpressed in ovarian cancer, among which MMP1, MMP2, MMP7 and MMP9 [69–71]. CXCL12 activates MMP2 and MMP9 in ovarian tumours, thus directly and indirectly promoting metastasis.

Near-infrared fluorescence imaging of MMP activity can be performed using ‘smart activatable probes’ that are non-fluorescent in their inactive state but become fluorescent upon activation by enzymatic activity of the target. None of these probes have become available for clinical use, but good

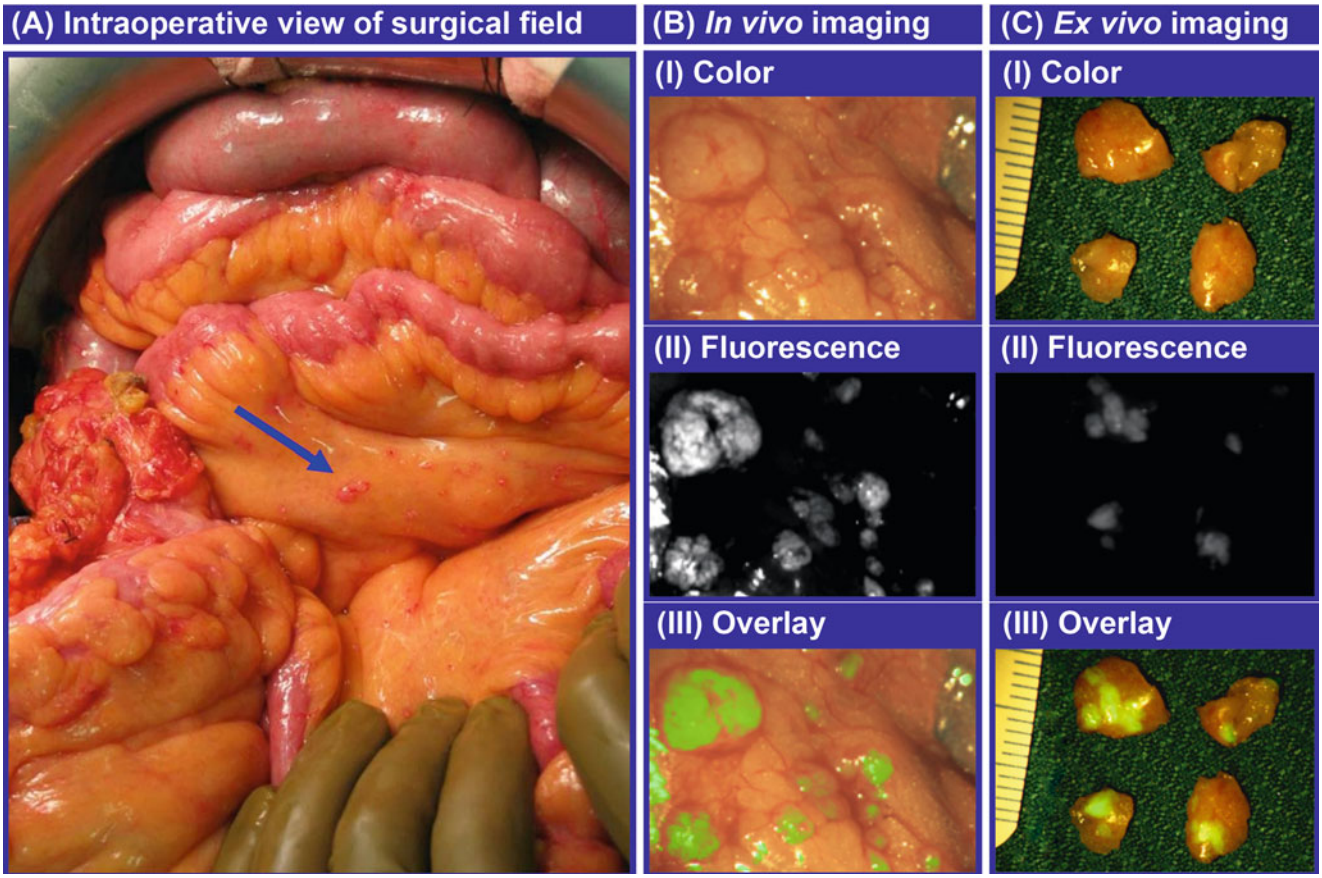

Fig. 12 Intraoperative fluorescence imaging in ovarian cancer. (**a**) The *arrow* points towards a tumor deposit of 1 mm that was detected with fluorescence imaging, (**b**) a close-up image of a tumor nodule, showing the color image (I), the fluorescence image (II) and the fluorescence image superimposed on the color image (III), (**c**) a close-up image of four excised tumor nodules, showing the clear distinction between healthy tissue (no fluorescence) and tumor deposits (fluorescent) with a resolution of <1 mm

results were obtained in in vivo studies of several cancer types [61, 72, 73].

Mucin1

Cell surface associated mucin 1 (MUC1) is a transmembrane glycoprotein that is overexpressed in several types of cancer. Physiologically, mucins are thought to protect the body against infection. However, MUC1 overexpression in cancer is not yet entirely understood. The current idea is that MUC1 protects the cancer cells against the immune system and against chemotherapeutic drugs. Furthermore, it has been shown that MUC1 is able to bind growth factors, which help the tumour cells proliferate [74]. A number of studies have been described using radiolabelled anti-MUC1 antibodies for intraoperative tumour detection and anti-MUC1 antibodies in chemotherapy, reporting beneficial effects. The humanized monoclonal antibody AS1402 is now being studied in a group of patients with recurrent breast cancer and may be an interesting compound for intraoperative imaging when conjugated to a fluorescent agent. Again, this remains speculative, as no experiments in this direction have been reported yet.

Vascular Endothelial Growth Factor

Vascular endothelial growth factor (VEGF) is an important regulator of angiogenesis, playing a role in normal ovarian function as well as in carcinogenesis [75, 76]. Tumour angiogenesis is essential for proliferation, cell survival and dissemination and is promoted through VEGF-related growth factors and receptors. VEGF has several subtypes, of which VEGF-A seems to play the most prominent role in ovarian cancer [77]. By activating two high-affinity tyrosine kinase cell surface receptors, VEGFR-1 and VEGFR-2, intracellular signalling pathways are stimulated leading to endothelial cell recruitment, vascular permeability, proliferation and survival [75].

VEGF is overexpressed in approximately 60–70 % of serous ovarian tumours and is associated with a poor prognosis [78–80]. The anti-VEGF-A monoclonal antibody bevacizumab has shown to improve progression-free survival in both advanced and platinum-resistant ovarian cancer by binding to and neutralizing VEGF-A, preventing its association with endothelial receptors and thus inhibiting angiogenesis [81–84].

Apart from acting as a chemotherapeutical, bevacizumab can be conjugated to radioactive tracers for application in PET imaging, to a fluorescent agent for optical imaging, or

both. Radioactive-labelled bevacizumab for detection of tumours has been shown feasible in patients [85, 86]. In a number of animal studies, including intraperitoneal ovarian cancer xenografts, dual-labelled bevacizumab shows similar and persistent uptake in the tumour in both PET and fluorescence imaging [10].

A clinical trial using bevacizumab-IRDye800CW for imaging of VEGF-A-positive breast cancers is currently underway. The next step is to test the value of this fluorescent agent for intraoperative imaging in ovarian cancer. Advantages compared to folate-FITC are that IRDye800CW has excitation and emission wavelengths in the near-infrared range, yielding higher tumour-to-background ratios. A possible disadvantage is the longer distribution time, meaning that the agent needs to be administered approximately 4 days prior to surgery. Furthermore, the specificity in advanced ovarian cancer may be limited by the fact that VEGF is scavenged in fluids, thus also in ascites, which may hamper the detection of small tumour nodules. However, this remains a theoretical problem as preclinical studies report tumour-to-background ratios high enough to detect even submillimeter metastases [10].

Preclinical and Clinical Imaging in Ovarian Cancer

Preclinical Imaging of Ovarian Neoplasms

Preclinical imaging is always the golden standard to evaluate feasibility before introducing a new technique or agent into the clinic. When it comes to fluorescent agents, the toxicity profile needs to be fully completed before moving into human pilot studies. Below, results from preclinical optical imaging are put forward, focusing mainly on studies on ovarian cancer.

Bioluminescence Imaging

A number of studies are reported in which BLI is used to either follow tumour growth in time or to evaluate the therapeutic effect of chemotherapeutic drugs in murine models for ovarian cancer [26, 87, 88]. BLI is increasingly used as a golden standard when evaluating new fluorescent or dual-labelled agents in a preclinical stadium. After selecting a region of interest (ROI), the overlap between the bioluminescence and the fluorescence or PET signals is calculated. A high overlap means excellent tumour specificity of the fluorescent agent. Similarly, overlap between PET and fluorescence in dual-labelled probes gives an indication on the applicability and sensitivity.

Fluorescence Molecular Tomography

Ovarian tumour localization, growth and response to therapy have been visualized by fluorescence molecular tomography (FMT) with a panel of molecular probes [61]. Even though not many studies have focused on FMT in ovarian cancer, other studies show that this approach may well be suitable for this disease [89].

Photoacoustic Imaging

Although several studies have been performed in which photoacoustic imaging (PAI) was applied to detect cancer, there is not much evidence for this technique in ovarian cancer. An ex vivo study showed that malignant ovaries take up a significantly higher amount of light, leading to a sensitivity and specificity of both 83 % for combined ultrasound and PAI [90]. Visualization of angiogenesis and thus selection of potentially malignant areas have been reported in murine models using an endoscope suitable for PAI. Furthermore, targeting of αvβ3 with a photoacoustic agent seems to be successful in tumour-bearing mice [91]. It seems feasible to translate these approaches to ovarian cancer; however, little can be said regarding effectivity.

Photodynamic Therapy

PDT in ovarian cancer was described as early as 1985, with improvements being made over the following years [92, 93]. PDT has been used to induce tumour shrinkage in rat and mouse models of ovarian cancer using either aminolevulinic acid (ALA) or hexylester aminolevulinic acid (HAL) [94]. ALA promotes synthesis of protoporphyrin IX (PPIX), a natural photosensitizer, but can also function as a photosensitizer in itself.

A number of studies report targeted PDT, either with the use of peptide-conjugated micelles or nanobodies [95, 96]. In photo-immunotherapy (PIT), tumours are targeted with a photosensitizer coupled to an antibody, leading to tumour-specific cell death. This concept was proven in subcutaneous planocellular carcinoma, with a photosensitizer-antibody complex targeting EGFR [9]. No results for PIT in ovarian cancer have been reported yet.

Radioguided Imaging

Targeted PET and SPECT imaging proved feasible in both ovarian cancer cell lines and animal models for ovarian neoplasms. A number of biomarkers have already been evaluated, including EGFR, VEGF, HER2 and folate [10, 97–99].

The evidence for targeted MRI in ovarian cancer mostly stems from animal models in which iron oxide nanoparticles are used [100, 101]. As mentioned above, there are some doubts regarding safety of these compounds, which is why they are not widely used in humans. A possibly interesting development is the synthesis of progesterone receptor-targeted MRI probes for hormone-dependent tumours [102].

Clinical Imaging in Ovarian Cancer

Ovarian neoplasms are often not diagnosed until the tumour has progressed into an advanced stage, due to late onset and

aspecificity of symptoms. This leads to a poor prognosis, with 5-year survival rates in stage III/IV of less than 30 %. The main pillars of treatment are surgery and chemotherapy, either neoadjuvant or as adjuvant therapy following surgical cytoreduction. The combination of cytoreduction with immediate intraperitoneal chemotherapy (HIPEC) has shown to improve prognosis [103, 104].

The goal of surgery is always optimal debulking. The term 'optimal' was initially referred to as residual tumour lesions <2 cm, but the general opinion is now shifting towards full debulking of all visible tumour mass. However, often complete cytoreduction is impossible because of consequent serious morbidity and mortality and sometimes because of massive dissemination. Residual tumour tissue is known to worsen the prognosis.

Chemotherapy is increasingly being administered at neoadjuvant therapy, in order to reduce tumour mass prior to debulking surgery.

It is clear that both surgery and chemotherapy can benefit from targeted molecular imaging and therapy. In the following paragraphs, the (few) clinical applications of optical imaging in ovarian cancer are discussed.

Fluorescence Imaging

The only study thus far reporting of tumour-targeted intraoperative fluorescence imaging in humans is described above under section "Folate receptor". By using an FR-α-directed fluorescent agent, folate-FITC, surgeons were able to discriminate tumour lesions as small as 0.5 mm (Fig. 12). Detection of metastases was significantly higher using fluorescence compared to white light vision (naked eye) [58]. It is expected that new fluorescent agents based on antibodies will be used for ovarian cancer imaging in the near future. An example is VEGF-A targeting bevacizumab conjugated to IRDye800CW, which is now being evaluated in a clinical pilot study in breast cancer patients. The concentration of tracer used for fluorescence imaging is in the microdosing range (<4.5 μg; 30 nmol), which is more than 100-fold lower than the therapeutic dose, thus preventing or greatly reducing side effects.

Nontargeted fluorescence imaging was described for sentinel lymph node detection in other gynaecological cancers [1, 105].

Photoacoustic Imaging

Although PAI has not been applied in humans yet, preparations are well underway. Several systems have been developed, some of which integrate ultrasound and PAI with other modalities such as optical coherence tomography. Tests using ex vivo ovarian tissue yield promising results [106–108].

Photodynamic Therapy

PDT has already been applied in humans, in which ALA was administered intraperitoneally prior to surgery, resulting in a sensitivity of 92 % and specificity of 95 % [109]. Intraperitoneal PDT was further illustrated in a few larger studies by administering porfimer sodium (PHOTOFRIN®, Pinnacle Biologics) 2 days prior to surgery. Although this led to a reduction of the number of lesions with acceptable toxicity levels, no difference was observed in time to recurrence or recurrence rates [110–112]. Another approach was to use a micro-endoscope together with a PDT agent capable of optical imaging and of inducing cell damage. This yielded adequate sensitivity rates of 86 %, but the specificity of 53 % was still insufficient [113]. Targeted PDT is expected to improve the specificity rate. However, neither targeted PDT nor photo-immunotherapy has yet been applied in humans.

Radioguided Imaging

A number of biomarkers have been evaluated for targeted PET/SPECT scanning in humans. Folate is one of the obvious targets, due to its overexpression on epithelial ovarian cancer. A study applying SPECT scanning with ^{111}In-DTPA-folate showed that corresponding CT images were necessary to yield adequate sensitivity rates [52]. However, this probe may help in discriminating benign from malignant adnexal masses.

Targeted SPECT and MRI have not yet been used in a clinical setting.

Summary and Future Perspectives

Molecular imaging is gaining more and more interest, and it is expected that new developments will follow each other rapidly in the coming decade (Fig. 13). The focus will most likely be on tumour targeting, as this enables a patient-tailored diagnostic and therapeutic approach, thus hopefully reducing morbidity and improving the prognosis. Antibodies that are already FDA approved may be translated into the clinic faster than completely novel probes. Microdosing prevents or greatly reduces the risk of side effects. It is not unthinkable that in the future more than one probe will be used in imaging in order to visualize different parts of the tumour. Targeted chemotherapy or photodynamic therapy will lead to a more localized reaction with less morbidity. Finally, molecular imaging techniques will be improved, both in detection accuracy and quantification of the signal, leading to a higher tumour-to-normal ratio.

Conclusion

Molecular imaging comprises several techniques, all based on the use of small molecules emitting light or sound waves (caused by thermal expansion). Tumour-targeted approaches cause less morbidity and yield stronger tumour-to-background signals. When looking into tumour-targeted imaging in ovarian cancer, FR-α, EGFR and VEGF-A seem currently the most promising targets as translation into the clinic has already happened or is close.

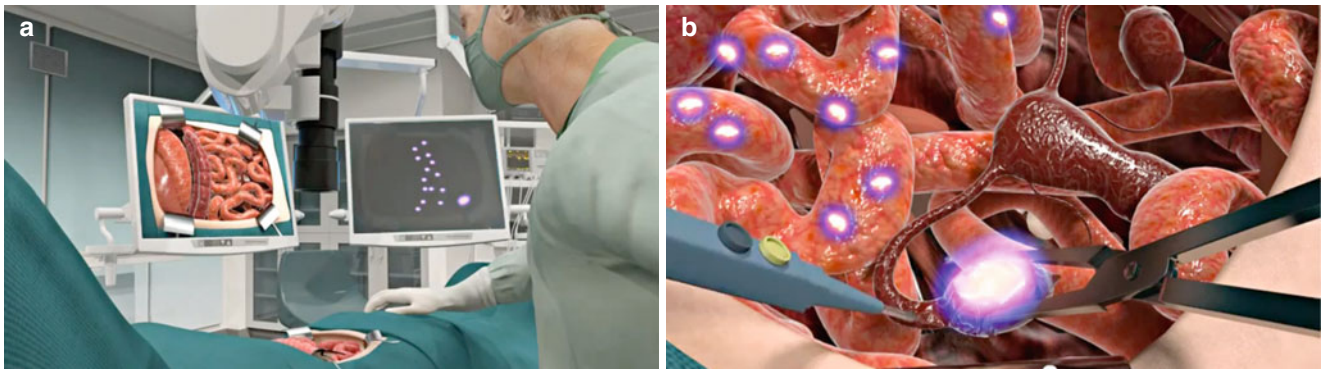

Fig. 13 Artist's impression of intraoperative imaging applications. (**a**) The surgeon sees the color image and the fluorescence image on the monitors in the OR. (**b**) the fluorescence provides guidance for the surgeon

Biography Lucia M.A. Crane (1983) attended medical school at the State University of Groningen, the Netherlands, graduating in 2008. Her PhD thesis finished in early 2011, reports of the first clinical studies applying intraoperative fluorescence imaging in patients with gynaecologic cancer. Crane has worked as a resident in obstetrics and gynaecology. Currently, she works as postdoc in the group of prof. Van Dam on further translation of optical imaging to the clinic.

References

1. Crane LM, Themelis G, Arts HJ, Buddingh KT, Brouwers AH, Ntziachristos V, et al. Intraoperative near-infrared fluorescence imaging for sentinel lymph node detection in vulvar cancer: first clinical results. Gynecol Oncol. 2011;120(2):291–5.
2. Hirche C, Murawa D, Mohr Z, Kneif S, Hunerbein M. ICG fluorescence-guided sentinel node biopsy for axillary nodal staging in breast cancer. Breast Cancer Res Treat. 2010;121(2):373–8.
3. Schubert GA, Seiz-Rosenhagen M, Ortler M, Czabanka M, Scheufler KM, Thomé C. Cortical indocyanine green videography for quantification of acute hypoperfusion after subarachnoid hemorrhage: a feasibility study. Neurosurgery. 2012;71(2 Suppl Operative):ons260–7
4. Yamamoto M, Orihashi K, Nishimori H, Wariishi S, Fukutomi T, Kondo N, et al. Indocyanine green angiography for intra-operative assessment in vascular surgery. Eur J Vasc Endovasc Surg. 2012;43(4):426–32.
5. Ntziachristos V. Fluorescence molecular imaging. Annu Rev Biomed Eng. 2006;8:1–33.
6. Ntziachristos V, Razansky D. Molecular imaging by means of multispectral optoacoustic tomography (MSOT). Chem Rev. 2010;110(5):2783–94.
7. Taruttis A, Ntziachristos V. Translational optical imaging. AJR Am J Roentgenol. 2012;199(2):263–71.
8. Agostinis P, Berg K, Cengel KA, Foster TH, Girotti AW, Gollnick SO, et al. Photodynamic therapy of cancer: an update. CA Cancer J Clin. 2011;61(4):250–81.
9. Mitsunaga M, Ogawa M, Kosaka N, Rosenblum LT, Choyke PL, Kobayashi H. Cancer cell-selective in vivo near infrared photoimmunotherapy targeting specific membrane molecules. Nat Med. 2011;17(12):1685–91.
10. Terwisscha van Scheltinga AG, van Dam GM, Nagengast WB, Ntziachristos V, Hollema H, Herek JL, et al. Intraoperative near-infrared fluorescence tumor imaging with vascular endothelial growth factor and human epidermal growth factor receptor 2 targeting antibodies. J Nucl Med. 2011;52(11):1778–85.
11. Foltz WD, Jaffray DA. Principles of magnetic resonance imaging. Radiat Res. 2012;177(4):331–48.
12. Alford R, Simpson HM, Duberman J, Hill GC, Ogawa M, Regino C, et al. Toxicity of organic fluorophores used in molecular imaging: literature review. Mol Imaging. 2009;8(6):341–54.
13. van Oosten M, Crane LM, Bart J, van Leeuwen FW, van Dam GM. Selecting potential targetable biomarkers for imaging purposes in colorectal cancer using TArget Selection Criteria (TASC): a novel target identification tool. Transl Oncol. 2011;4(2):71–82.

14. Gundogdu F, Soylu F, Erkan L, Tatli O, Mavi S, Yavuzcan A. The role of serum CA-125 levels and CA-125 tissue expression positivity in the prediction of the recurrence of stage III and IV epithelial ovarian tumors (CA-125 levels and tissue CA-125 in ovarian tumors). Arch Gynecol Obstet. 2011;283(6):1397–402.
15. Bellati F, Napoletano C, Gasparri ML, Visconti V, Zizzari IG, Ruscito I, et al. Monoclonal antibodies in gynecological cancer: a critical point of view. Clin Dev Immunol. 2011;2011:890758.
16. Woelber L, Mueller V, Eulenburg C, Schwarz J, Carney W, Jaenicke F, et al. Serum carbonic anhydrase IX during first-line therapy of ovarian cancer. Gynecol Oncol. 2010;117(2):183–8.
17. Hynninen P, Vaskivuo L, Saarnio J, Haapasalo H, Kivela J, Pastorekova S, et al. Expression of transmembrane carbonic anhydrases IX and XII in ovarian tumours. Histopathology. 2006;49(6):594–602.
18. Poulsen SA. Carbonic anhydrase inhibition as a cancer therapy: a review of patent literature, 2. Expert Opin Ther Pat. 2010;20(6): 795–806.
19. Kowalewska M, Radziszewski J, Kulik J, Barathova M, Nasierowska-Guttmajer A, Bidzinski M, et al. Detection of carbonic anhydrase 9-expressing tumor cells in the lymph nodes of vulvar carcinoma patients by RT-PCR. Int J Cancer. 2005;116(6): 957–62.
20. Carlin S, Khan N, Ku T, Longo VA, Larson SM, Smith-Jones PM. Molecular targeting of carbonic anhydrase IX in mice with hypoxic HT29 colorectal tumor xenografts. PLoS One. 2010;5(5):e10857.
21. Barbieri F, Bajetto A, Florio T. Role of chemokine network in the development and progression of ovarian cancer: a potential novel pharmacological target. J Oncol. 2010;2010(1687–8469):426956.
22. Kajiyama H, Shibata K, Terauchi M, Ino K, Nawa A, Kikkawa F. Involvement of SDF-1alpha/CXCR4 axis in the enhanced peritoneal metastasis of epithelial ovarian carcinoma. Int J Cancer. 2008;122(1):91–9.
23. Scotton CJ, Wilson JL, Scott K, Stamp G, Wilbanks GD, Fricker S, et al. Multiple actions of the chemokine CXCL12 on epithelial tumor cells in human ovarian cancer. Cancer Res. 2002; 62(20):5930–8.
24. Jiang YP, Wu XH, Xing HY, Du XY. Role of CXCL12 in metastasis of human ovarian cancer. Chin Med J (Engl). 2007;120(14):1251–5.
25. Jiang YP, Wu XH, Shi B, Wu WX, Yin GR. Expression of chemokine CXCL12 and its receptor CXCR4 in human epithelial ovarian cancer: an independent prognostic factor for tumor progression. Gynecol Oncol. 2006;103(1):226–33.
26. Ray P, Lewin SA, Mihalko LA, Schmidt BT, Luker KE, Luker GD. Noninvasive imaging reveals inhibition of ovarian cancer by targeting CXCL12-CXCR4. Neoplasia. 2011;13(12):1152–61.
27. Nomura W, Tanabe Y, Tsutsumi H, Tanaka T, Ohba K, Yamamoto N, et al. Fluorophore labeling enables imaging and evaluation of specific CXCR4-ligand interaction at the cell membrane for fluorescence-based screening. Bioconjug Chem. 2008;19(9): 1917–20.
28. Nimmagadda S, Pullambhatla M, Pomper MG. Immunoimaging of CXCR4 expression in brain tumor xenografts using SPECT/CT. J Nucl Med. 2009;50(7):1124–30.
29. Zhang J, Tian J, Li T, Guo H, Shen L. 99mTc-AMD3100: a novel potential receptor-targeting radiopharmaceutical for tumor imaging. Chin Chem Lett. 2010;21(4):461–3.
30. Weiss ID, Jacobson O, Kiesewetter DO, Jacobus JP, Szajek LP, Chen X, et al. Positron emission tomography imaging of tumors expressing the human chemokine receptor CXCR4 in mice with the use of 64Cu-AMD3100. Mol Imaging Biol. 2012;14(1): 106–14.
31. Noske A, Schwabe M, Weichert W, Darb-Esfahani S, Buckendahl AC, Sehouli J, et al. An intracellular targeted antibody detects EGFR as an independent prognostic factor in ovarian carcinomas. BMC Cancer. 2011;11:294.
32. Zeineldin R, Muller CY, Stack MS, Hudson LG. Targeting the EGF receptor for ovarian cancer therapy. J Oncol. 2010; 2010(1687–8469):414676.
33. Gui T, Shen K. The epidermal growth factor receptor as a therapeutic target in epithelial ovarian cancer. Cancer Epidemiol. 2012;36(5):490–6.
34. Lin CK, Chao TK, Yu CP, Yu MH, Jin JS. The expression of six biomarkers in the four most common ovarian cancers: correlation with clinicopathological parameters. APMIS. 2009;117(3):162–75.
35. Salomon DS, Brandt R, Ciardiello F, Normanno N. Epidermal growth factor-related peptides and their receptors in human malignancies. Crit Rev Oncol Hematol. 1995;19(3):183–232.
36. Heath CH, Deep NL, Sweeny L, Zinn KR, Rosenthal EL. Use of panitumumab-IRDye800 to image microscopic head and neck cancer in an orthotopic surgical model. Ann Surg Oncol. 2012;19(12): 3879–87.
37. Sano K, Mitsunaga M, Nakajima T, Choyke PL, Kobayashi H. In vivo breast cancer characterization imaging using two monoclonal antibodies activatably labeled with near infrared fluorophores. Breast Cancer Res. 2012;14(2):R61.
38. Nayak TK, Garmestani K, Baidoo KE, Milenic DE, Brechbiel MW. PET imaging of tumor angiogenesis in mice with VEGF-A targeted (86)Y-CHX-A″-DTPA-bevacizumab. Int J Cancer. 2011;128(4): 920–6.
39. Ogawa M, Kosaka N, Choyke PL, Kobayashi H. In vivo molecular imaging of cancer with a quenching near-infrared fluorescent probe using conjugates of monoclonal antibodies and indocyanine green. Cancer Res. 2009;69(4):1268–72.
40. Bellone S, Siegel ER, Cocco E, Cargnelutti M, Silasi DA, Azodi M, et al. Overexpression of epithelial cell adhesion molecule in primary, metastatic, and recurrent/chemotherapy-resistant epithelial ovarian cancer: implications for epithelial cell adhesion molecule-specific immunotherapy. Int J Gynecol Cancer. 2009;19(5):860–6.
41. Shim HS, Yoon BS, Cho NH. Prognostic significance of paired epithelial cell adhesion molecule and E-cadherin in ovarian serous carcinoma. Hum Pathol. 2009;40(5):693–8.
42. Sun Y, Shukla G, Pero SC, Currier E, Sholler G, Krag D. Single tumor imaging with multiple antibodies targeting different antigens. Biotechniques. 2012;0(0):1–3.
43. Tavri S, Jha P, Meier R, Henning TD, Muller T, Hostetter D, et al. Optical imaging of cellular immunotherapy against prostate cancer. Mol Imaging. 2009;8(1):15–26.
44. Eder M, Knackmuss S, Le Gall F, Reusch U, Rybin V, Little M, et al. 68Ga-labelled recombinant antibody variants for immuno-PET imaging of solid tumours. Eur J Nucl Med Mol Imaging. 2010;37(7):1397–407.
45. Kalli KR, Oberg AL, Keeney GL, Christianson TJ, Low PS, Knutson KL, et al. Folate receptor alpha as a tumor target in epithelial ovarian cancer. Gynecol Oncol. 2008;108(3):619–26.
46. Markert S, Lassmann S, Gabriel B, Klar M, Werner M, Gitsch G, et al. Alpha-folate receptor expression in epithelial ovarian carcinoma and non-neoplastic ovarian tissue. Anticancer Res. 2008; 28(6):3567–72.
47. Crane LM, Arts HJ, van Oosten M, Low PS, van der Zee AG, van Dam GM, et al. The effect of chemotherapy on expression of folate receptor-alpha in ovarian cancer. Cell Oncol (Dordr). 2012;35(1): 9–18.
48. Low PS, Henne WA, Doorneweerd DD. Discovery and development of folic-acid-based receptor targeting for imaging and therapy of cancer and inflammatory diseases. Acc Chem Res. 2008;41(1):120–9.
49. Jackman AL, Theti DS, Gibbs DD. Antifolates targeted specifically to the folate receptor. Adv Drug Deliv Rev. 2004;56(8): 1111–25.
50. Reddy JA, Dorton R, Westrick E, Dawson A, Smith T, Xu LC, et al. Preclinical evaluation of EC145, a folate-vinca alkaloid conjugate. Cancer Res. 2007;67(9):4434–42.

51. Mathias CJ, Wang S, Waters DJ, Turek JJ, Low PS, Green MA. Indium-111-DTPA-folate as a potential folate-receptor-targeted radiopharmaceutical. J Nucl Med. 1998;39(9):1579–85.
52. Siegel BA, Dehdashti F, Mutch DG, Podoloff DA, Wendt R, Sutton GP, et al. Evaluation of 111In-DTPA-folate as a receptor-targeted diagnostic agent for ovarian cancer: initial clinical results. J Nucl Med. 2003;44(5):700–7.
53. Fisher RE, Siegel BA, Edell SL, Oyesiku NM, Morgenstern DE, Messmann RA, et al. Exploratory study of 99mTc-EC20 imaging for identifying patients with folate receptor-positive solid tumors. J Nucl Med. 2008;49(6):899–906.
54. Vaitilingam B, Chelvam V, Kularatne SA, Poh S, Ayala-Lopez W, Low PS. A folate receptor-alpha-specific ligand that targets cancer tissue and not sites of inflammation. J Nucl Med. 2012;53(7): 1127–34.
55. Jelovac D, Armstrong DK. Role of farletuzumab in epithelial ovarian carcinoma. Curr Pharm Des. 2012;18(25):3812–5.
56. Teng L, Xie J, Teng L, Lee RJ. Clinical translation of folate receptor-targeted therapeutics. Expert Opin Drug Deliv. 2012;9(8): 901–8.
57. Wang X, Morales AR, Urakami T, Zhang L, Bondar MV, Komatsu M, et al. Folate receptor-targeted aggregation-enhanced near-IR emitting silica nanoprobe for one-photon in vivo and two-photon ex vivo fluorescence bioimaging. Bioconjug Chem. 2011;22(7): 1438–50.
58. van Dam GM, Themelis G, Crane LM, Harlaar NJ, Pleijhuis RG, Kelder W, et al. Intraoperative tumor-specific fluorescence imaging in ovarian cancer by folate receptor-alpha targeting: first in-human results. Nat Med. 2011;17(10):1315–9.
59. Monniaux D, Huet-Calderwood C, Le Bellego F, Fabre S, Monget P, Calderwood DA. Integrins in the ovary. Semin Reprod Med. 2006;24(4):251–61.
60. Beer AJ, Lorenzen S, Metz S, Herrmann K, Watzlowik P, Wester HJ, et al. Comparison of integrin alphaVbeta3 expression and glucose metabolism in primary and metastatic lesions in cancer patients: a PET study using 18F-galacto-RGD and 18F-FDG. J Nucl Med. 2008;49(1):22–9.
61. Hensley HH, Roder NA, O'Brien SW, Bickel LE, Xiao F, Litwin S, et al. Combined in vivo molecular and anatomic imaging for detection of ovarian carcinoma-associated protease activity and integrin expression in mice. Neoplasia. 2012;14(6):451–62.
62. Themelis G, Harlaar NJ, Kelder W, Bart J, Sarantopoulos A, van Dam GM, et al. Enhancing surgical vision by using real-time imaging of alphavbeta3-integrin targeted near-infrared fluorescent agent. Ann Surg Oncol. 2011;18(12):3506–13.
63. Cao J, Wan S, Tian J, Li S, Deng D, Qian Z, et al. Fast clearing RGD-based near-infrared fluorescent probes for in vivo tumor diagnosis. Contrast Media Mol Imaging. 2012;7(4):390–402.
64. Zhu L, Guo N, Li Q, Ma Y, Jacboson O, Lee S, et al. Dynamic PET and optical imaging and compartment modeling using a dual-labeled cyclic RGD peptide probe. Theranostics. 2012;2(8): 746–56.
65. Zhu Z, Miao W, Li Q, Dai H, Ma Q, Wang F, et al. 99mTc-3PRGD2 for integrin receptor imaging of lung cancer: a multicenter study. J Nucl Med. 2012;53(5):716–22.
66. Axelsson R, Bach-Gansmo T, Castell-Conesa J, McParland BJ, Study Group. An open-label, multicenter, phase 2a study to assess the feasibility of imaging metastases in late-stage cancer patients with the alpha v beta 3-selective angiogenesis imaging agent 99mTc-NC100692. Acta Radiol. 2010;51(1):40–6.
67. Moschos SJ, Sander CA, Wang W, Reppert SL, Drogowski LM, Jukic DM, et al. Pharmacodynamic (phase 0) study using etaracizumab in advanced melanoma. J Immunother. 2010;33(3): 316–25.
68. Delbaldo C, Raymond E, Vera K, Hammershaimb L, Kaucic K, Lozahic S, et al. Phase I and pharmacokinetic study of etaracizumab (Abegrin), a humanized monoclonal antibody against alphavbeta3 integrin receptor, in patients with advanced solid tumors. Invest New Drugs. 2008;26(1):35–43.
69. Roomi MW, Monterrey JC, Kalinovsky T, Rath M, Niedzwiecki A. In vitro modulation of MMP-2 and MMP-9 in human cervical and ovarian cancer cell lines by cytokines, inducers and inhibitors. Oncol Rep. 2010;23(3):605–14.
70. Moss NM, Barbolina MV, Liu Y, Sun L, Munshi HG, Stack MS. Ovarian cancer cell detachment and multicellular aggregate formation are regulated by membrane type 1 matrix metalloproteinase: a potential role in I.p. metastatic dissemination. Cancer Res. 2009;69(17):7121–9.
71. Naylor MS, Stamp GW, Davies BD, Balkwill FR. Expression and activity of MMPS and their regulators in ovarian cancer. Int J Cancer. 1994;58(1):50–6.
72. Xie BW, Mol IM, Keereweer S, van Beek ER, Que I, Snoeks TJ, et al. Dual-wavelength imaging of tumor progression by activatable and targeting near-infrared fluorescent probes in a bioluminescent breast cancer model. PLoS One. 2012;7(2):e31875.
73. Keereweer S, Mol IM, Vahrmeijer AL, Van Driel PB, Baatenburg de Jong RJ, Kerrebijn JD, et al. Dual wavelength tumor targeting for detection of hypopharyngeal cancer using near-infrared optical imaging in an animal model. Int J Cancer. 2012;131(7): 1633–40.
74. Hollingsworth MA, Swanson BJ. Mucins in cancer: protection and control of the cell surface. Nat Rev Cancer. 2004;4(1):45–60.
75. Harris AL. Hypoxia – a key regulatory factor in tumour growth. Nat Rev Cancer. 2002;2(1):38–47.
76. Mor G, Visintin I, Lai Y, Zhao H, Schwartz P, Rutherford T, et al. Serum protein markers for early detection of ovarian cancer. Proc Natl Acad Sci U S A. 2005;102(21):7677–82.
77. Trinh XB, Tjalma WA, Vermeulen PB, Van den Eynden G, Van der Auwera I, Van Laere SJ, et al. The VEGF pathway and the AKT/mTOR/p70S6K1 signalling pathway in human epithelial ovarian cancer. Br J Cancer. 2009;100(6):971–8.
78. Koukourakis MI, Limberis V, Tentes I, Kontomanolis E, Kortsaris A, Sivridis E, et al. Serum VEGF levels and tissue activation of VEGFR2/KDR receptors in patients with breast and gynecologic cancer. Cytokine. 2011;53(3):370–5.
79. Wang M, He Y, Shi L, Shi C. Multivariate analysis by Cox proportional hazard model on prognosis of patient with epithelial ovarian cancer. Eur J Gynaecol Oncol. 2011;32(2):171–7.
80. Crasta JA, Mishra S, Vallikad E. Ovarian serous carcinoma: relationship of p53 and bcl-2 with tumor angiogenesis and VEGF expression. Int J Gynecol Pathol. 2011;30(6):521–6.
81. Perren TJ, Swart AM, Pfisterer J, Ledermann JA, Pujade-Lauraine E, Kristensen G, et al. A phase 3 trial of bevacizumab in ovarian cancer. N Engl J Med. 2011;365(26):2484–96.
82. Burger RA. Antiangiogenic agents should be integrated into the standard treatment for patients with ovarian cancer. Ann Oncol. 2011;22 Suppl 8:viii65–8.
83. Burger RA, Brady MF, Bookman MA, Fleming GF, Monk BJ, Huang H, et al. Incorporation of bevacizumab in the primary treatment of ovarian cancer. N Engl J Med. 2011;365(26):2473–83.
84. Itamochi H, Kigawa J. Clinical trials and future potential of targeted therapy for ovarian cancer. Int J Clin Oncol. 2012; 17(5):430–40.
85. Nagengast WB, Hooge MN, van Straten EM, Kruijff S, Brouwers AH, den Dunnen WF, et al. VEGF-SPECT with (111) In-bevacizumab in stage III/IV melanoma patients. Eur J Cancer. 2011;47(10):1595–602.
86. Scheer MG, Stollman TH, Boerman OC, Verrijp K, Sweep FC, Leenders WP, et al. Imaging liver metastases of colorectal cancer patients with radiolabelled bevacizumab: lack of correlation with VEGF-A expression. Eur J Cancer. 2008;44(13): 1835–40.

87. Cordero AB, Kwon Y, Hua X, Godwin AK. In vivo imaging and therapeutic treatments in an orthotopic mouse model of ovarian cancer. J Vis Exp 2010;(42). pii: 2125. doi:10.3791/2125.
88. Richards FM, Tape CJ, Jodrell DI, Murphy G. Anti-tumour effects of a specific anti-ADAM17 antibody in an ovarian cancer model in vivo. PLoS One. 2012;7(7):e40597.
89. Zhao Q, Jiang H, Cao Z, Yang L, Mao H, Lipowska M. A hand-held fluorescence molecular tomography system for intraoperative optical imaging of tumor margins. Med Phys. 2011; 38(11):5873–8.
90. Aguirre A, Ardeshirpour Y, Sanders MM, Brewer M, Zhu Q. Potential role of coregistered photoacoustic and ultrasound imaging in ovarian cancer detection and characterization. Transl Oncol. 2011;4(1):29–37.
91. de la Zerda A, Bodapati S, Teed R, May SY, Tabakman SM, Liu Z, et al. Family of enhanced photoacoustic imaging agents for high-sensitivity and multiplexing studies in living mice. ACS Nano. 2012;6(6):4694–701.
92. Molpus KL, Kato D, Hamblin MR, Lilge L, Bamberg M, Hasan T. Intraperitoneal photodynamic therapy of human epithelial ovarian carcinomatosis in a xenograft murine model. Cancer Res. 1996;56(5):1075–82.
93. McCaughan Jr JS, Schellhas HF, Lomano J, Bethel BH. Photodynamic therapy of gynecologic neoplasms after presensitization with hematoporphyrin derivative. Lasers Surg Med. 1985;5(5):491–8.
94. Guyon L, Ascencio M, Collinet P, Mordon S. Photodiagnosis and photodynamic therapy of peritoneal metastasis of ovarian cancer. Photodiagnosis Photodyn Ther. 2012;9(1):16–31.
95. Yoon HY, Koo H, Choi KY, Lee SJ, Kim K, Kwon IC, et al. Tumor-targeting hyaluronic acid nanoparticles for photodynamic imaging and therapy. Biomaterials. 2012;33(15):3980–9.
96. Master AM, Livingston M, Oleinick NL, Sen Gupta A. Optimization of a Nanomedicine-Based Silicon Phthalocyanine 4 Photodynamic Therapy (Pc 4-PDT) Strategy for Targeted Treatment of EGFR-Overexpressing Cancers. Mol Pharm. 2012. [Epub ahead of print].
97. Nayak TK, Regino CA, Wong KJ, Milenic DE, Garmestani K, Baidoo KE, et al. PET imaging of HER1-expressing xenografts in mice with 86Y-CHX-A″-DTPA-cetuximab. Eur J Nucl Med Mol Imaging. 2010;37(7):1368–76.
98. Oude Munnink TH, Korte MA, Nagengast WB, Timmer-Bosscha H, Schroder CP, Jong JR, et al. (89)Zr-trastuzumab PET visualises HER2 downregulation by the HSP90 inhibitor NVP-AUY922 in a human tumour xenograft. Eur J Cancer. 2010;46(3):678–84.
99. Heskamp S, Laverman P, Rosik D, Boschetti F, van der Graaf WT, Oyen WJ, et al. Imaging of human epidermal growth factor receptor type 2 expression with 18F-labeled affibody molecule ZHER2:2395 in a mouse model for ovarian cancer. J Nucl Med. 2012;53(1):146–53.
100. Quan G, Du X, Huo T, Li X, Wei Z, Cui H, et al. Targeted molecular imaging of antigen OC183B2 in ovarian cancers using MR molecular probes. Acad Radiol. 2010;17(12):1468–76.
101. Klostergaard J, Parga K, Raptis RG. Current and future applications of magnetic resonance imaging (MRI) to breast and ovarian cancer patient management. P R Health Sci J. 2010;29(3): 223–31.
102. Sukerkar PA, MacRenaris KW, Townsend TR, Ahmed RA, Burdette JE, Meade TJ. Synthesis and biological evaluation of water-soluble progesterone-conjugated probes for magnetic resonance imaging of hormone related cancers. Bioconjug Chem. 2011;22(11):2304–16.
103. Di Giorgio A, Naticchioni E, Biacchi D, Sibio S, Accarpio F, Rocco M, et al. Cytoreductive surgery (peritonectomy procedures) combined with hyperthermic intraperitoneal chemotherapy (HIPEC) in the treatment of diffuse peritoneal carcinomatosis from ovarian cancer. Cancer. 2008;113(2):315–25.
104. Deraco M, Kusamura S, Virzi S, Puccio F, Macri A, Famulari C, et al. Cytoreductive surgery and hyperthermic intraperitoneal chemotherapy as upfront therapy for advanced epithelial ovarian cancer: multi-institutional phase-II trial. Gynecol Oncol. 2011;122(2):215–20.
105. Crane LM, Themelis G, Pleijhuis RG, Harlaar NJ, Sarantopoulos A, Arts HJ, et al. Intraoperative multispectral fluorescence imaging for the detection of the sentinel lymph node in cervical cancer: a novel concept. Mol Imaging Biol. 2011;13(5):1043–9.
106. Aguirre A, Guo P, Gamelin J, Yan S, Sanders MM, Brewer M, et al. Coregistered three-dimensional ultrasound and photoacoustic imaging system for ovarian tissue characterization. J Biomed Opt. 2009;14(5):054014.
107. Yang Y, Li X, Wang T, Kumavor PD, Aguirre A, Shung KK, et al. Integrated optical coherence tomography, ultrasound and photoacoustic imaging for ovarian tissue characterization. Biomed Opt Express. 2011;2(9):2551–61.
108. Kamath SD, Ray S, Mahato KK. Photoacoustic spectroscopy of ovarian normal, benign, and malignant tissues: a pilot study. J Biomed Opt. 2011;16(6):067001.
109. Loning M, Diddens H, Kupker W, Diedrich K, Huttmann G. Laparoscopic fluorescence detection of ovarian carcinoma metastases using 5-aminolevulinic acid-induced protoporphyrin IX. Cancer. 2004;100(8):1650–6.
110. Hahn SM, Fraker DL, Mick R, Metz J, Busch TM, Smith D, et al. A phase II trial of intraperitoneal photodynamic therapy for patients with peritoneal carcinomatosis and sarcomatosis. Clin Cancer Res. 2006;12(8):2517–25.
111. Hahn SM, Putt ME, Metz J, Shin DB, Rickter E, Menon C, et al. Photofrin uptake in the tumor and normal tissues of patients receiving intraperitoneal photodynamic therapy. Clin Cancer Res. 2006;12(18):5464–70.
112. Wilson JJ, Jones H, Burock M, Smith D, Fraker DL, Metz J, et al. Patterns of recurrence in patients treated with photodynamic therapy for intraperitoneal carcinomatosis and sarcomatosis. Int J Oncol. 2004;24(3):711–7.
113. Zhong W, Celli JP, Rizvi I, Mai Z, Spring BQ, Yun SH, et al. In vivo high-resolution fluorescence microendoscopy for ovarian cancer detection and treatment monitoring. Br J Cancer. 2009;101(12):2015–22.
114. Leblond F, et al. Pre-clinical whole-body fluorescence imaging: Review of instruments, methods and applications. J Photochem Photobiol B. 2010;98(1):77–94.

Author Index

L. Saba et al. (eds.), *Ovarian Neoplasm Imaging*,
DOI 10.1007/978-1-4614-8633-6, © Springer Science+Business Media New York 2013

B

E

H

M

Q

S

U

Z

Subject Index